insects

Special Issue Reprint

Research on Insect Molecular Biology

Edited by
Shunhua Gui and Yan Shi

mdpi.com/journal/insects

MDPI

Research on Insect Molecular Biology

Research on Insect Molecular Biology

Guest Editors

Shunhua Gui
Yan Shi

MDPI

Basel • Beijing • Wuhan • Barcelona • Belgrade • Novi Sad • Cluj • Manchester

Guest Editors

Shunhua Gui
College of Agriculture
Guizhou University
Guiyang
China

Yan Shi
College of Plant Health and Medicine
Qingdao Agricultural University
Qingdao
China

Editorial Office

MDPI AG
Grosspeteranlage 5
4052 Basel, Switzerland

This is a reprint of the Special Issue, published open access by the journal *Insects* (ISSN 2075-4450), freely accessible at: https://www.mdpi.com/journal/insects/special_issues/33769T30S5.

For citation purposes, cite each article independently as indicated on the article page online and as indicated below:

Lastname, A.A.; Lastname, B.B. Article Title. *Journal Name* **Year**, *Volume Number*, Page Range.

ISBN 978-3-7258-9233-4 (Hbk)
ISBN 978-3-7258-9234-1 (PDF)
https://doi.org/10.3390/books978-3-7258-9234-1

© 2026 by the authors. Articles in this reprint are Open Access and distributed under the Creative Commons Attribution (CC BY) license. The reprint as a whole is distributed by MDPI under the terms and conditions of the Creative Commons Attribution-NonCommercial-NoDerivs (CC BY-NC-ND) license (https://creativecommons.org/licenses/by-nc-nd/4.0/).

Contents

Xingcheng Xie, Yakun Zhang, Heyuan Peng and Zhongyuan Deng
Sex Chromosome Dosage Compensation in Insects
Reprinted from: *Insects* **2025**, *16*, 160, https://doi.org/10.3390/insects16020160 . . . . . **1**

Alfayo Ombuya, Jianyang Guo and Wanxue Liu
Insect Mating Behaviors: A Review of the Regulatory Role of Neuropeptides
Reprinted from: *Insects* **2025**, *16*, 506, https://doi.org/10.3390/insects16050506 . . . . . **20**

Davide Banfi, Tommaso Bianchi, Maristella Mastore and Maurizio Francesco Brivio
The Role of Heat Shock Proteins in Insect Stress Response, Immunity, and Climate Adaptation
Reprinted from: *Insects* **2025**, *16*, 741, https://doi.org/10.3390/insects16070741 . . . . . **46**

Shengli Jing, Jing Yang, Yali Liu, Feifei Wang, Fang Zheng, Aobo Ren, et al.
Functional Analysis of CPSF30 in *Nilaparvata lugens* Using RNA Interference Reveals Its Essential Role in Development and Survival
Reprinted from: *Insects* **2024**, *15*, 860, https://doi.org/10.3390/insects15110860 . . . . . **57**

Sohaib Shahid, Muhammad Bilal Amir, Tian-Bo Ding, Tong-Xian Liu, Guy Smagghe and Yan Shi
RNAi of Neuropeptide CCHamide-1 and Its Receptor Indicates Role in Feeding Behavior in the Pea Aphid, *Acyrthosiphon pisum*
Reprinted from: *Insects* **2024**, *15*, 939, https://doi.org/10.3390/insects15120939 . . . . . **72**

Guofeng Yang, Xuetao Yu, Yan Zhang, Jinhua Luo, Xiaofei Li, Li Zhu, et al.
Screening and Validation of Stable Reference Genes for qRT-PCR Analysis in *Epicauta gorhami* (Coleoptera: Meloidae)
Reprinted from: *Insects* **2024**, *15*, 942, https://doi.org/10.3390/insects15120942 . . . . . **88**

Shao-Ping Chen, Xue-Mei Chu, Mei-Xiang Chi, Jian Zhao and Rong-Zhou Qiu
Transcriptomic Characterization of Phototransduction Genes of the Asian Citrus Psyllid *Diaphorina citri* Kuwayama
Reprinted from: *Insects* **2024**, *15*, 966, https://doi.org/10.3390/insects15120966 . . . . . **101**

Connor J. Tyler, Shubhangi Mahajan, Lena Smith, Haruko Okamoto and Herman Wijnen
Adult Diel Locomotor Behaviour in the Agricultural Pest *Plutella xylostella* Reflects Temperature-Driven and Light-Repressed Regulation Rather than Coupling to Circadian Clock Gene Rhythms
Reprinted from: *Insects* **2025**, *16*, 182, https://doi.org/10.3390/insects16020182 . . . . . **113**

Lingling Li, Wenmeng Li, Jing Liao, Junhong Fu, Changgeng Dai, Yang Hu and Hongbo Li
Ultrastructure and Transcriptome Analysis of the Larval Integument in Solitary and Gregarious Phases of *Mythimna separata*
Reprinted from: *Insects* **2025**, *16*, 190, https://doi.org/10.3390/insects16020190 . . . . . **131**

Marianna Varone, Paola Di Lillo, Katerina Nikolouli, Ayca Eda Özel, Francesca Lucibelli, Gennaro Volpe, et al.
The Early Sex-Specific Expression of the Fruitless Gene in the Asian Tiger Mosquito *Aedes albopictus* (Skuse) and Its Functional Conservation in Male Courtship
Reprinted from: *Insects* **2025**, *16*, 280, https://doi.org/10.3390/insects16030280 . . . . . **149**

Alfonso Cacace, Giovanna De Leva, Ilaria Di Lelio and Andrea Becchimanzi
Immune-Related Genes in the Honey Bee Mite *Varroa destructor* (*Acarina, Parasitidae*)
Reprinted from: *Insects* **2025**, *16*, 356, https://doi.org/10.3390/insects16040356 . . . . . **169**

Chenkai Ma, Fang Xu, Chengjie Hu, Chunguang Cui, Xin Du, Jine Chen, et al.
MPF Regulates Oocyte and Embryo Development During Parthenogenesis Induction in Silkworm, *Bombyx mori*
Reprinted from: *Insects* **2025**, *16*, 361, https://doi.org/10.3390/insects16040361 . . . . . **194**

Zhengwen Yu, Chenju Yang, Lian Xie, Feng Yang and Yuyu Yuan
Physiological and Biochemical Mechanisms of *Aoria nigripes* (Coleoptera, Chrysomelidae) Adaption to Flavonoid-Rich Plant *Nekemias grossedentata*
Reprinted from: *Insects* **2025**, *16*, 399, https://doi.org/10.3390/insects16040399 . . . . . **207**

Rui-Han Lu, Xu-Dong Pang, Shuang-Qin Wen, Guy Smagghe, Tong-Xian Liu and Shun-Hua Gui
Adipokinetic Hormones and Their Receptor Regulate the Locomotor Behavior in *Tribolium castaneum*
Reprinted from: *Insects* **2025**, *16*, 407, https://doi.org/10.3390/insects16040407 . . . . . **222**

Hyuk-Jin Moon, Hyun-Jung Kim, Dong-Hyun Lee, Seo-Yeong Mun and Soo-Dong Woo
Rapid and Economic Baculovirus Titer Determination Using a Novel Transgenic Sf9-QE Cell Line
Reprinted from: *Insects* **2025**, *16*, 426, https://doi.org/10.3390/insects16040426 . . . . . **235**

Hui Li, Sheng Qiao, Xiwen Hong and Yangyang Wei
Deciphering the Olfactory Mechanisms of *Sitotroga cerealella* Olivier (Lepidoptera: *Gelechiidae*): Insights from Transcriptome Analysis and Molecular Docking
Reprinted from: *Insects* **2025**, *16*, 461, https://doi.org/10.3390/insects16050461 . . . . . **248**

Katherine S. Bell, Sebastian Ko, Sam Ali, Brett Bognar, Michael Khmelkov, Nick Rau, et al.
Tissue-Specific Fluorescent Protein Turnover in Free-Moving Flies
Reprinted from: *Insects* **2025**, *16*, 583, https://doi.org/10.3390/insects16060583 . . . . . **271**

Mercè Merayo, Kenia M. Delgado, David Salguero and Dorcas J. Orengo
Chromosomal Inversions in Chromosome U of *Drosophila subobscura*: A Story from Population Studies to Molecular Level
Reprinted from: *Insects* **2025**, *16*, 586, https://doi.org/10.3390/insects16060586 . . . . . **287**

Pedro Lorite, José M. Rico-Porras, Teresa Palomeque, Mª Ángeles Marcos-García, Diogo C. Cabral-de-Mello and Pablo Mora
Cytogenetic and Molecular Characterization of *Sphaerophoria rueppellii* (Diptera, Syrphidae)
Reprinted from: *Insects* **2025**, *16*, 604, https://doi.org/10.3390/insects16060604 . . . . . **304**

Bi-Yue Ding, Qin-Qin Xu, Yu-Jing Liu, Yu-Hong Zhong and Yan Zhou
Development of an Experimental Method Using a Portable Photosynthesis-Monitoring System to Measure Respiration Rates in Small-Sized Insects
Reprinted from: *Insects* **2025**, *16*, 616, https://doi.org/10.3390/insects16060616 . . . . . **323**

Yang Wang, Stine Slotsbo, Steffen Y. Bak, Christopher J. Martyniuk and Martin Holmstrup
Proteomic Responses of the Springtail *Folsomia candida* to Drought
Reprinted from: *Insects* **2025**, *16*, 707, https://doi.org/10.3390/insects16070707 . . . . . **336**

Inzamam Ul Haq, Abdul Basit, Moazam Hyder, Mirza Naveed Shahzad, Asim Abbasi, Yasir Sharif, et al.
Genome-Wide Analysis and Functional Correlation of Tomato *JAZ* Genes Under *Tuta absoluta* Infestation and Nanoparticle-Induced Defense
Reprinted from: *Insects* **2025**, *16*, 1046, https://doi.org/10.3390/insects16101046 . . . . . **351**

Yanting Chen, Xiaomin Zhao, Chenyu Lv, Jianwei Zhao, Mengzhu Shi, Jianwei Fu and Jianyu Li
The Mitochondrial Hsp90 Homolog *PmTRAP1* Mediates Thermal Tolerance in the Papaya Mealybug, *Paracoccus marginatus*
Reprinted from: *Insects* **2025**, *16*, 1064, https://doi.org/10.3390/insects16101064 . . . . . **378**

Xinyu Liu, Yanyan Bai, Yu Qi, Baozhi Liu, Yingying Zhao, Yuting Wu, et al.
Transcriptome Characterization and Identification of Chemosensory Genes in the Egg Parasitoid *Anastatus orientalis*, Along with Molecular Cloning, Sequence Analysis, and Prokaryotic Expression of the Odorant Binding Protein 8 (*AoOBP8*) from *A. orientalis*
Reprinted from: *Insects* **2025**, *16*, 1117, https://doi.org/10.3390/insects16111117 . . . . . **392**

Wei Cen, Ting Yang, Jia-Wen Li, Dan-Na Yu, Kenneth B. Storey and Jia-Yong Zhang
Comparative Mitogenomics of *Pedetontus* and *Pedetontinus* (Insecta: Archaeognatha) Unveils Phylogeny, Divergence History, and Adaptive Evolution
Reprinted from: *Insects* **2025**, *16*, 1194, https://doi.org/10.3390/insects16121194 . . . . . **412**

Jingyun Zhu, Hongran Li, Yan Peng, Minghui Jin, Kaikai Mao and Yutao Xiao
High-Humidity Incubation Improves Post-Microinjection Viability and Larval Performance of CRISPR/Cas9-Edited *Helicoverpa armigera* Embryos
Reprinted from: *Insects* **2025**, *16*, 1257, https://doi.org/10.3390/insects16121257 . . . . . **433**

insects

MDPI

Review

Sex Chromosome Dosage Compensation in Insects

Xingcheng Xie [1,2,†], Yakun Zhang [2,†], Heyuan Peng [1] and Zhongyuan Deng [1,2,*]

[1] School of Agricultural Sciences, Zhengzhou University, Zhengzhou 450001, China; xingchengxie@126.com (X.X.); pengheyuan123@outlook.com (H.P.)
[2] State Key Laboratory for Biology of Plant Diseases and Insect Pests, Institute of Plant Protection, Chinese Academy of Agricultural Sciences, Beijing 100193, China; zhangyakun7@126.com
* Correspondence: dengzhongyuan@outlook.com
† These authors contributed equally to this work.

Simple Summary: The dosage compensation effect is one of the most common mechanisms by which the organisms with sexual dimorphism balance the genes expression. In insects, there mainly exist four types of sex determination, including the male heterogamety XY/X0 and the female heterogamety WZ/Z0. Although there has been a wide variety of studies on the dosage compensation effect, there is still a lack of systematic review. Moreover, some studies are even controversial. Therefore, it is essential to carry out a comprehensive and systematic analysis of previous studies. In this review, we summarized the research progress, analyzed the existing problems, and explored future study prospects. The purpose of this review is to provide references for the future work on sex chromosome dosage compensation in insects.

Abstract: Dosage compensation (DC) is of crucial importance in balancing the sex-linked gene expression between males and females. It serves to guarantee that the proteins or other enzymatic products encoded by the sex chromosome exhibit quantitative parity between the two genders. During the evolutionary process of achieving dose compensation, insects have developed a wide variety of mechanisms. There exist two primary modes of dosage compensation mechanisms, including the up-regulation of heterogametic sex chromosomes in the heterogamety and down-regulation of homogametic sex chromosomes in the homogamety. Although extensive investigations have been conducted on dosage compensation in model insects, many questions still remain unresolved. Meanwhile, research on non-model insects is attracting increasing attention. This paper systematically summarizes the current advances in the field of insect dosage compensation with respect to its types and mechanisms. The principal insects involved in this study include the *Drosophila melanogaster*, *Tribolium castaneum*, *Bombyx mori*, and other lepidopteran insects. This paper analyzes the controversial issues about insect dosage compensation and also provides prospects for future research.

Keywords: dosage compensation; dosage compensation complex; sex determination; sex chromosome; gene expression

1. Introduction

There are numerous methods of sex determination in organisms, and diverse species of organisms have distinguishable types of sex determination [1]. Sex determination refers to the developmental program that determines whether an embryo will follow either the

male or the female pathway [2]. In individuals that reproduce sexually, sex determination is based on the homotypic (such as XX) or heterotypic (such as XY) sex chromosomes [3]. For the XY-type sex determination observed in mammals and fruit flies, males have XY sex chromosomes, whereas females have XX sex chromosomes [4]. However, in the WZ-type sex determination system of many lepidopteran insects, birds, fish, reptiles, and amphibians, the ZZ and WZ sex chromosomes determine males and females, respectively [5]. In organisms in which gender is determined by one sex being homomorphic and the other heteromorphic with regard to the sex chromosomes, a process has evolved to equalize the output of products encoded by the genes located on these chromosomes [6]. This process is known as dosage compensation, and the phenomenon associated with this process is called the dosage compensation effect [7,8]. Dosage compensation is extremely common in bisexual eukaryotes. In 1932, Muller discovered a regulatory mechanism that balances the expression of X-linked gene between male (XY) and female (XX) in *Drosophila melanogaster*, after studying the eye pigment level of individuals with X-linked gene deletion mutations [9]. This mechanism was named as the "dosage compensation mechanism" [9]. Subsequently, achievements were obtained in mammals and *Caenorhabditis elegans*, which revealed three possible dosage compensation mechanisms [10,11]: doubling the expression of a single X chromosome in males (*D. melanogaster*), inactivating one of the female X chromosomes (mammals), and halving the expression of the female's two X chromosomes (*C. elegans*). The evolutionary strategies of dosage compensation across species, such as *D. melanogaster*, mammals, and *C. elegans*, have also been compared [12].

The acquisition of male-specific lethal (MSL) mechanisms in *Drosophila* and the successful identification of the dosage-compensating MSL complex have outlined the molecular basis for the mechanism of dosage compensation in *Drosophila* [13]. The MSL complex is a nucleoprotein RNA-containing protein complex that consists of at least five specific proteins and two non-coding RNAs. It is the core of the *Drosophila* dosage compensation machinery [14]. The functional factors, patterns, and mechanisms of *Drosophila* dosage compensation are thoroughly understood.

Unlike *Drosophila*, mammals obtain the dosage compensation by inactivating one of the X chromosomes in females. Although the composition of the mammalian MSL complex has been determined, its function remains largely unknown [15,16]. So far, research on the dosage compensation types and mechanisms of insects remains in the initial stage. There still exist some controversies regarding the dosage compensation types of insects. However, significant progress has been made in the research on model insects. Drawing on the literature reports and experimental studies, this paper undertakes a review of research on dosage compensation types and mechanisms. It also discusses the causes and issues surrounding the controversial dosage compensation. Additionally, it provides prospects for the further study of dosage compensation in insects.

2. Sex Determination and Differentiation

The evolution of sex determination in organisms has been widely investigated over the years. However, the origin of sex chromosomes in insects is currently not fully understood. Typically, sex chromosomes are postulated to originate from a pair of ancestral autosomes that have evolved a sex-determining locus [17]. Accompanied by the sex-biased segregation of sex chromosomes, a proto-X or Y chromosome is also defined in female or male heterogametic organisms, respectively [18,19]. In accordance with the diversity and flexibility in the evolutionary process, sex differentiation has become increasingly distinct and complex [20]. For the organisms exhibiting sexual dimorphism, sex determination is a crucial step in developmental differentiation [21]. This process is essential for normal

development and survival of individuals, as well as the genetic basis that enables the continuation of species reproduction.

Generally speaking, there exist two main sex determination mechanisms, namely, genetic sex determination (GSD) and environmental sex determination (ESD) [22]. Although sex determination is particularly crucial for the sexual fate of organisms, it remains one of the variable developmental pathways that is influenced by the living environment and chromosomes of the organisms [23]. The sex determination by chromosomes is particularly universal and closely related to the dosage compensation effect. Furthermore, sex chromosome determination mainly presents in the following types [24]: males with the heterogamety XY and X0 and females with the heterogamety WZ and Z0 (Figure 1).

1. WZ-type sex determination: The sex determination of birds, some lepidopteran insects like silkworms and bollworms, as well as crustaceans is of WZ type. WZ type is also common in snakes and some lizards, turtles, amphibians, and fish [25]. This type of female is heterogametes (namely, WZ), while males are homogametes (namely, ZZ) [26]. During the process of gamete formation, females generate female gametes of Z and W types, whereas males only produce male gametes of Z type. When a male gamete Z binds to a female gamete Z, the fertilized egg can develop into a male. If a male gamete Z combines with a female gamete W, the heterozygote continues to grow into a female. Therefore, the ratio of males to females is 1:1 [27].
2. Z0-type sex determination: As a specific type of the WZ sex determination, it is commonly referred to as Z0 sex determination [28,29]. This particular type of sex determination is mainly observed in certain species of butterflies and moths [3]. In these organisms, males have two homomorphic sex chromosomes (ZZ) and only produce one type of gamete, namely, Z [30]. However, females only have an odd sex chromosome (Z) [30]. In this case, due to the absence of maternal W sex chromosome, offspring with ZZ embryos develop into males, while those with Z0 embryos develop into females. For example, a moth of Psychidae, *Talaeporia tubulosa*, employs ambient temperature to govern sex determination in the absence of the W chromosome [31]. During the meiosis process of female individuals, environmental factors may occasionally affect the distribution of Z chromosomes in *T. tubulosa* [31]. At high temperatures, more eggs will carry Z chromosomes, thereby resulting in a higher proportion of males. In contrast, at low temperatures, fewer eggs contain the Z chromosome, which leads to more female offspring [31].
3. XY-type sex determination: It is quite prevalent among animals, encompassing most insects, mollusks, amphibians, and mammals. There exist multiple differences between XY-type and WZ-type sex determination. The female is of the homogametic type (namely, XX), whereas the male is of the heterogametic type (namely, XY). The size and morphology of Y and X chromosomes are different. During meiosis, the female produces only one type of gamete (X), while the male produces two kinds of gametes (X or Y). When the female gamete combines with X sperm, the fertilized egg develops into a female. If it is integrated with Y sperm, the egg develops into a male. Therefore, the sex ratio is generally 1:1 [32].
4. X0-type sex determination: A particular kind of XY sex determination is X0-type sex determination [33], which is analogous to the Z0 type. Insects of this type primarily consist of locusts, crickets, and scorpionflies [33]. The X (or Z) chromosome is generally larger than the Y (or W) chromosome. In nematodes, sex is determined with high fidelity based on the tallying of X-chromosome number in relation to ploidy and the sets of autosomes (referred to as the X:A signal). This process is carried out through a precise strategy. Embryos with ratios of 1X:2A (0.5) or 2X:3A (0.67) develop into

fertile males. In contrast, embryos with ratios of 3X:4A (0.75) or 2X:2A (1.0) develop into self-fertile hermaphrodites [34].

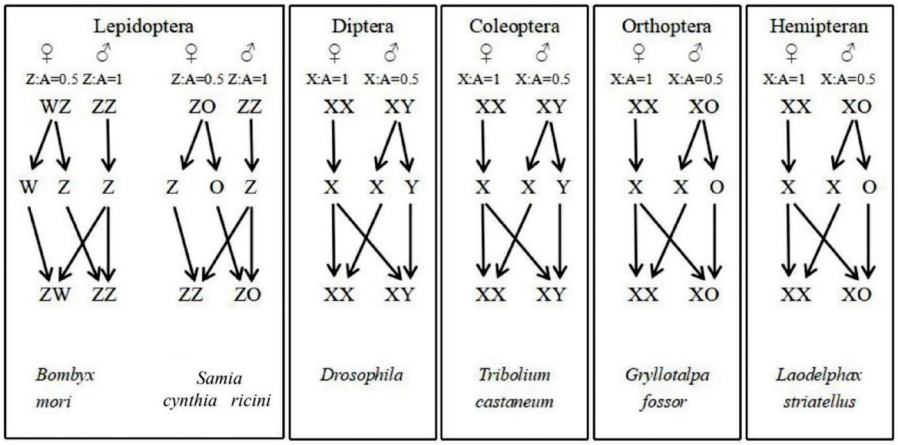


Figure 1. Sex determination types in different insects. The representative insects used for sex determination analysis are *Bombyx mori* [35], *Samia cynthia ricini* [30], *Drosophila* [36], *Tribolium castaneum* [37], *Gryllotalpa fossor* [38], and *Laodelphax striatellus* [39], respectively.

In general, the composition of sex chromosomes determines the gene doses on sex chromosomes. Nevertheless, there is no difference in the performance of biological X (or Z)-linked traits among males. In some organisms with heterotypic sex chromosomes, such as birds having WZ sex chromosomes, it is not always necessary to compensate the gene dose. However, the differences in gene sets may affect gene expression from the same copy as in the homogametic sex [40]. There should be a mechanism to maintain the consistent gene expression levels between the two sexes, and this was later confirmed as the dosage compensation.

3. The Dosage Compensation Effect

3.1. Research on the Dosage Compensation Effect

Sex determination occurs after conception as the result of XX or XY chromosomes pairing [41]. Nevertheless, sex chromosomes have evolved repeatedly. When chromosomes exist in different copy numbers between males and females, they are likely to be subject to different selection pressures compared to the autosomes [42]. Subsequently, this leads to a faster rate of evolution, increased accumulation of sexually antagonistic alleles, and the evolution of dosage compensation [42]. Through the comparison of closely related species, research indicates that heterotypic sex chromosomes evolved from a pair of common chromosomes carrying sex-determining factors [43]. Moreover, the existence of a dosage compensation mechanism was firstly proven at the experimental level in *D. melanogaster*, and the results demonstrated that the amount of H^3 uracil in a single X chromosome of the male fly involved was equal to the number of H^3 uracil inserted into the two X chromosomes of the female fly by the method of autoradiography [44]. Therefore, it was concluded that the amount of RNA produced on the X chromosome of males is approximately twice as much as that on a single X chromosome of females. This above-mentioned phenomenon was subsequently confirmed in mammals and nematodes.

The dosage compensation effect of three model organisms, including the nematodes, insects, and mammals, has also been investigated [45]. For these representative species with distant genetic relationships, there are distinct dosage compensation mechanisms. However, most dosage compensation is achieved by regulating the expression of homotypic

chromosomal-linked genes [34]. Dosage compensation strategies vary from worms to mammals. Nevertheless, there still remains a regulatory complex that can integrate with the X chromosomes of one sex to regulate the transcription along the entire chromosome. For mammalian females, there are two X chromosomes, but the X inactivation-specific transcript (Xist) functions to inactivate one of the X chromosomes, thereby achieving dosage compensation by imprinted and random X-chromosome inactivation [44,46]. In other words, dosage compensation is obtained through inactivating one X chromosome in females [43,47].

The dosage compensation effect in fruit flies is achieved by increasing the gene transcription amount on the X chromosome in males, so that it is approximately equal to the gene transcription number on the two X chromosomes in females [45,47]. *C. elegans* has male (X0) and facultative (XX) forms. The XX facultative individuals can achieve dosage compensation by halving the transcription efficiency of two active X chromosomes [45,48,49]. Gene expression along X chromosomes is regulated by dosage compensation and, simultaneously, histone modifications as well as chromosome structure are also employed to modulate gene expression across X chromosomes [34].

Studies on aneuploid organisms have demonstrated that the gene dosage effect on gene expression is considered variable because of the dosage changes in chromosome fragments. This can be further classified into two effects. The first effect is the positive gene dosage effect. Namely, the gene expression level shows a positive correlation with its dosage. The other one is the inverse dosage effect, which refers to an inverse relationship between gene expression and the copy number of a trans region. This implies that there is a reduction in gene expression when the dosage of another chromosome fragment is increased. The inverse dosage effect is predominant in aneuploid organisms such as *Arabidopsis*, maize, *Datura*, *Drosophila*, and human beings. Dosage compensation ensures the equal expression of different dosages of X chromosomes between females and males, which is conducted by a two-fold up-regulation of the gene expression on the single X chromosome in males to match the gene expression level of the two chromosomes in females. This phenomenon is a consequence of the simultaneous action of the positive and inverse dosage effects [50].

However, studies on dosage compensation are sometimes conflicting [51]. There may also exist complete, partial, and incomplete dosage compensation mechanisms. In these mechanisms, the up-regulation of sex-related genes occurs on a gene-by-gene basis [52]. Incomplete dosage compensation refers to sex-linked expression in the heterogametic sex that is reduced in comparison to ancestral expression, which leads to an expression imbalance and sex-biased gene expression on the sex chromosome between male and female individuals [53]. Incomplete dosage compensation occurs in XY species, which is much more common than that in WZ species. The dosage compensation pattern of orthopteran insects is similar to that of the mammals. Similar to the XY type, however, orthopteran insects only have one sex chromosome. In Orthoptera, there are two genders: male (X0) and female (XX). A study demonstrated that phosphoglucomutase (PGM) is an X-linked gene in orthopteran insects. PGM inhibits the gene expressions on one X chromosome in female individuals, thereby making the gene dosage of PGM roughly equal between males and females [54]. In addition, some studies have also indicated that the dosage compensation exhibits different patterns depending on different somatic tissues. For instance, the evolution of the X chromosome was characterized in five species of *Timema* stick insects [42]. Through whole-genome sequencing, the type of sex determination was identified as XX:X0 [42]. It was concluded that there was almost complete dosage compensation in somatic tissues (heads and legs), whereas the reproductive tracts were lacking in dosage compensation effect [42]. Furthermore, a complete dosage compensation mechanism was also

discovered in a WZ species known as *Manduca sexta*, which is similar to the genome-wide sex gene expression pattern [55]. This finding indicated that the tobacco hornworm balances the key genes in the genome-wide network through full dosage compensation.

In birds, the Z chromosome is partially up-regulated in females, but partially or randomly down-regulated in males. Incomplete dosage compensation in chicken is achieved by up-regulated genes on the Z chromosome in females. The dosage compensation effect of silkworms and Coleopteran insects has also been investigated. For example, *Tribolium castaneum*, the red flour beetle belonging to Coleoptera, shows incomplete dosage compensation [56,57]. However, for the silkworm, which is one of the most deeply studied model insects of Lepidoptera, there are still some controversies regarding its dosage compensation mechanism [58]. Therefore, the dosage compensation mechanism of insects, particularly those with the ZW sex system, needs further comprehensive and more in-depth research.

Generally speaking, the dosage compensation effect occurs only in the sex chromosomes [59]. However, this effect can also be observed in individuals with certain autosomal abnormalities like aneuploidy, as well as in those with only specific autosomal segments [60]. For example, the alcohol dehydrogenase-1 (*ADH1*) gene on the long arm of maize chromosome one (1L) [61] and *α*-glycerophosphate dehydrogenase (*α-GPDH*) genes located on the left arm of *Drosophila* chromosome 2 (2L) [62] both show a dosage compensation effect. However, the dosage compensation mechanism of autosomes need further investigation.

Due to the diversity of sex determination mechanisms in insects, although some insects exhibit strong homology in morphology and biological habits, research on dosage compensation in insects remains challenging and progresses slowly. For some insects, genetic differences can determine the sex of females and males [63]. However, for other insects, environmental conditions may also determine the sex [63]. Even within a single sex chromosome, there is a possibility of the coexistence of two distinct sex chromosome dosage compensation (SCDC) patterns [64]. For instance, in the monarch butterfly, different dosage compensation modes have been observed on the two Z segments, namely, the neo-Z and anc-Z segments [65]. Therefore, so far, only *D. melanogaster* among Diptera species has a clear dosage compensation mechanism [66]. Further research on dosage compensation in *Bombyx mori*, *M. sexta*, and *T. castaneum* is necessary considering that there are many controversies and a lack of sufficient studies on the dosage compensation of these three insects. To better study the dosage compensation of insects, we have summarized the currently known mechanisms of dosage compensation in different insects (Table 1).

Table 1. Dosage compensation indifferent insects.

Order	Species	Sex Mechanism (Female/Male)	Sex Chromosome Dosage Compensation Patterns	Reference
Diptera	*Drosophila melanogaste*	XX/XY	Complete	[36,67]
	Diopsidae	XX/XY		[68]
	Lucilia cuprina	XX/XY		[69]
	Anopheles gambiae	XX/XY		[70–72]
	Anopheles stephensi	XX/XY		[73]
Coleoptera	*Triboliumcastaneum*	XX/XY	Complete	[37,74]
Strepsiptera	*Xenos vesparum*	XX/XY	Complete	[74]
Hemiptera	*Halyomorpha halys*	XX/XY	Complete	[75]
	Homalodisca vitripennis	XX/XY		
	Oncopeltus fasciatus	XX/XY		
	Acyrthosiphon pisum	XX/X0		[76]
	Laodelphax striatellus	XX/X0	Complete (in somatic tissues)	[39]

Table 1. *Cont.*

Order	Species	Sex Mechanism (Female/Male)	Sex Chromosome Dosage Compensation Patterns	Reference
Phasmida	*Timema*	XX/X0	Complete (in heads and legs)	[42]
Orthoptera	*Gryllotalpa fossor*	XX/X0	Complete	[38,77]
	Acheta domesticus	XX/X0		
Lepidoptera	*Bombyx mori*	WZ/ZZ	Complete	[58,78–80]
	Manduca sexta	WZ/ZZ	Complete	[55]
	Cydia pomonella	WZ/ZZ	Complete	[25]
	Plodia interpunctella	WZ/ZZ	Incomplete dosage compensation with balance	[81]
	Heliconius	WZ/ZZ	Complete	[82]
	Papilio xuthus	WZ/ZZ	Complete (excluding sex-biased genes)	[80]
	Papilio machaon	WZ/ZZ	Complete (excluding sex-biased genes)	
	Helicoverpa armigera	WZ/ZZ	Complete	[83,84]
	Leptidea sinapis	WZ/ZZ	Complete	[85]
	Samia cynthia ricini	Z0/ZZ	None	[30]
Hymenoptera	*Apis mellifera*	2N/N	Single-locus complementary sex determination	[86]

3.2. The Dosage Compensation Mechanism of the Fruit Fly

As a representative organism, *Drosophila* achieves dosage compensation by up-regulating the genes on the male X chromosome and doubling the gene expression [87,88]. In somatic cells of *Drosophila*, the dosage compensation mechanism is accomplished when the dosage compensation complex (DCC) directly binds to the X chromosome, acetylates the X chromosome, and causes X-linked genes to be hypertranscribed [89,90]. Several subunits of MSL in DCC are not expressed in male germline cells, but there is still partial dosage compensation [89]. In somatic cells, all DCC condenses and SDC (sex determination and dosage compensation) subunits bind to X chromosomes, followed by starting about the 30-to-40-cell stage of embryogenesis. DCC binding is maintained throughout the adulthood [34]. Currently, this mechanism is the one best understood [24,66] (Figure 2).

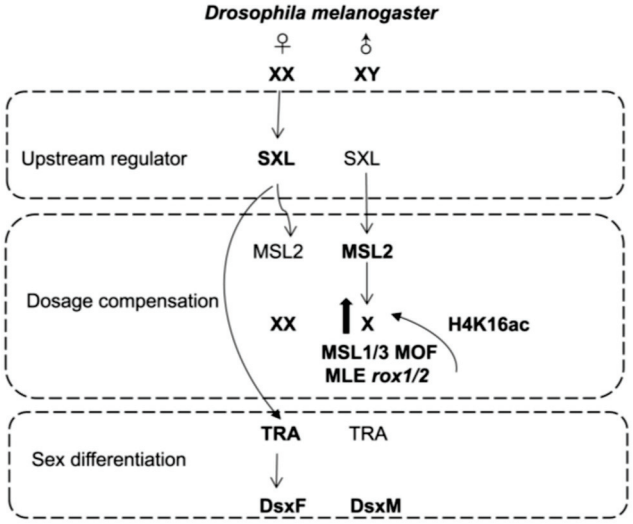


Figure 2. Schematic diagram of the dosage compensation mechanisms involved in *Drosophila* [24,66]. See text for details.

3.2.1. Upstream Regulatory Signals of Drosophila Dosage Compensation

Drosophila dosage compensation is regulated by the alternative splicing of upstream gene *sex lethal* (*Sxl*), which results in its specific expression in males and females [36,91,92]. In males, the *Sxl* transcript retains exon 3 with a stop codon, which makes the *Sxl* gene translate into a short and non-functional SXL protein. In females, exon 3 is spliced out, and the *Sxl* gene is transcribed completely. The intact open reading frame of the transcript is responsible for encoding a functional SXL protein [93]. The female SXL protein binds to the sites in the 5′UTR and 3′UTR of the *msl2* gene and prevents the translation of *msl2* gene [94]. Males have non-functional SXL protein and allow for the *msl2* gene to translate into active MSL2 protein along with other components, which subsequently initiate the dosage compensation effect [95,96]. In females, the *Sxl* gene regulates the splicing of *doublesex* (*dsx*) genes by activating *transformer* (*tra*) genes through accurate splicing [97]. Subsequently, Tra-2 acts as a cofactor to generate the female isoform DsxF, a female-specific Dsx [98]. However, in males, due to the non-functional SXL protein and the absence of Tra protein, *dsx* pre-mRNA is spliced to generate the male-specific Dsx (DsxM). These two proteins, DsxF and DsxM, induce the sex-specific phenotypic changes [99]. Moreover, the existence or absence of Tra protein is crucial for determining sex differentiation [50].

3.2.2. The *Drosophila* DCC

The components of *Drosophila* MSL complex were identified through screening in the *male-specific lethal* (*msl*) genes. Subsequently, genes carrying this mutation were cloned and characterized [57]. The dosage compensation complex of *Drosophila* is encoded by five genes, namely, *msl1*, *msl2*, *msl3*, *maleless* (*mle*), and *males absent on the first* (*mof*), as well as two non-coding RNAs, namely, *roX1* (*RNA on the X1*) and *roX2* (*RNA on the X2*), which is also known as MSL complex [66,100]. Chromatin proteins, such as JIL-1 tandem kinase, Megator (Mtor), Chromatin-linked adapter for MSL proteins (CLAMP), Topoisomerase II (TopoII), and other proteins, may represent additional components of the MSL complex. These chromatin proteins have been shown to co-immunoprecipitate with the core MSL subunits [89]. The genes of *msl1*, *msl3*, *mof*, *mle*, and non-coding RNA can be expressed in both males and females. However, the *msl2* gene is only expressed in males [101]. These components of the MSL complex collaborate at hundreds of discrete affinity sites on the X chromosome of male *Drosophila* but not those of other chromosomes [50]. The MSL complex is a crucial determinant for the survival of male flies, and the absence of any components is specifically lethal to male flies [50,102,103]. Therefore, it is indicated that the MSL complex is essential for insects in the dosage compensation mechanism [10,104].

The assembly sequence of the MSL complex and the interaction site of each component have invariably been the focal points of researchers. Although the reported sequence of MSL complex assembly may vary slightly (possibly due to the different tissues examined or the different cell lines in cell culture), it is definite that MSL1 and MSL2 function as substrates and provide a platform for the assembly of other proteins and *roX* RNAs. Moreover, the interaction between MSL1 and MSL2 is required for the binding of MSL complex to chromosomal entry sites (CESs) on the X chromosome. The addition of MSL3, MOF, and MLE is essential for the extension of the complete MSL complex. *roX* RNAs also play a key role in the localization of the MSL complex [50].

In general, MSL1 serves as a platform for assembling the MSL complex [95,105]. How does MSL1 bind to MSL2 and initiate the assembly of the MSL complex? Experiments have demonstrated that the amino terminus of the MSL1 protein recognizes the X chromosome [106,107]. At the carboxyl terminus, there exists a relatively conserved region known as the PEHE structure. Because of its characteristic amino acid composition, the PEHE

structure functions as the binding region with MSL3 and MOF [108]. MSL1 and MSL2 form a core protein complex, which initiates the assembly of the dosage compensation complex [109]. As a crucial factor in dosage compensation [110], MSL2 is a RING-finger protein with a RING-finger at its amino terminus for binding to MSL1 [111]. Owing to the lack of MSL2 protein, the dosage compensation complex fails to be formed in females of *Drosophila* [112].

However, how do the other components of the complex successively bind to the MSL1/MSL2 platform? The conserved proline domain in MSL2 is *roX* RNA, which is necessary for the efficient incorporation of MSL complex and stabilization of *roX* RNA [113,114]. The condensing characteristic of the roX-MSL2^{CTD} determines the segmentation of the *Drosophila* X chromosome. After specific recruitment by the X chromosome, the C-terminal domain (CTD) of MSL2 is sensitive to *roX* non-coding RNA. Functional analysis of *Drosophila* and mammalian cells reveals that *roX* non-coding RNA and MSL2 CTD assemble into a stable condensation state, and the interaction between them is essential for the dosage compensation in vivo [109]. The conserved cysteine CXC domain of MSL2 enables MSL2 to target the X chromosome instead of the autosomes, and the core protein complex consisting of MSL1 and MSL2 can also bind to the male X chromosome through the CXC domain [115,116]. The CD domain located at the N-terminus of MSL3 is the region that binds to nucleosomes, nucleic acids, and histone H3, whereas the C-terminus is the binding region for two non-coding RNAs [117]. MSL3 is involved in the diffusion of the MSL complex from the binding site on the X chromosome to other sites [118,119]. Inactivation of the MSL3 protein results in the binding of the incomplete MSL1-MSL2 complex to approximately 200 sites on the X chromosome, which are referred to as chromatin entry sites (CESs) or high-affinity sites (HASs) [116].

A histone acetyltransferase MOF is part of the non-specific lethal (NSL) complex. MOF acetylates the sixteenth lysine (H4K16) on male histone H4 by combining with housekeeping genes throughout the whole genome, which neutralizes the positive charge and weakens the inhibition of the internucleosomal structure, thereby enhancing the transcription of the X chromosome [120,121]. Moreover, MOF is the only acetylase that utilizes histone modifications to achieve decondensation of the entire chromatin [122]. Although MLE is an RNA/DNA helicase with an ATPase domain, MLE does not bind to any of these proteins [123,124]. Instead, only RNA via *roX* RNA is assembled into the MSL complex [125]. *roX1* and *roX2* are non-coding RNAs with specific secondary structures on X chromatin [126,127] that primarily bind to MSL complexes and carry out specific mediating functions [128,129]. The low-complexity CTD of MSL2 makes its recruitment to the X chromosome sensitive to *roX* non-coding RNAs. *roX* non-coding RNAs and the CTD of MSL2 form a solidly condensed state, and function analysis further indicates that their interactions are essential for dosage compensation in *Drosophila* and mammalian cells [109]. In addition to these core dosage compensation complexes, there still exist many accessory factors involved in the dosage compensation effect. These factors also facilitate the targeted localization and extension of the MSL complex on the X chromosome [130,131].

The current model, which illustrates the delivery of the MSL complex to nearly all expressed genes on the male X chromosome, mainly consists of two steps [14,132]. Firstly, the MSL complex binds to approximately 200 HAS/CES on the X chromosome [116]. Subsequently, the MSL complex spreads from HAS/CES to the nearby expressed genes due to the association of MSL3 subunit with Lysine 36 of histone H3 (H3K36me3) modification over these genes [133]. There exist one to several copies of a 21-bp GA-rich sequence motif in each HAS/CES [89]. This motif is called the MSL recognition element (MRE) [134]. However, only a small number of all MREs are localized within HAS/CES [89]. The

DNA-binding protein CLAMP has the ability to recognize MREs and is beneficial for the recruitment of MSL to HAS/CES. In consideration of the physical interaction between MSL2 and CLAMP, the CXC and CLAMP-binding domains are essential for the MSL complex to target the X chromosome [89]. More precisely, the first zinc-finger C2H2 domain at the N-terminus of CLAMP interacts with the unstructured highly conserved CLAMP-binding domain (within the *Drosophila* genus) of MSL2 [116]. The structural basis for the interaction between the CLAMP and MSL2 proteins is obtained by the methods of NMR techniques and mutagenic screening experiments [116]. Further study shows that the amino acid residues employed for the above interaction are different from those commonly used for DNA recognition [116]. Moreover, CLAMP is capable of opening the chromatin, and its recognition of MREs may enhance the binding of MSL2 [89].

The MSL complex can specifically bind to the X chromosome. How does the MSL complex precisely localize the X chromosome and initiate dosage compensation? The intensity of CES on the X chromosome determines the affinity of the MSL complex for the X chromosome. Some studies have demonstrated that the MSL complex can specifically bind to the X chromosome and enhance its transcription. Furthermore, the MSL complex number is also crucial for accurate localization on the X chromosome. Although low levels of MSL complex can bind to the X chromosome, the binding sites are significantly diminished. In contrast, high levels of MSL complex may lead to abnormal binding to the chromocenter and the fourth chromosome [13,135]. When the number of MSL complex reaches a critical value, the dosage compensation effect occurs. Otherwise, even if a small number of MSL complex bind to the sex chromosome, the gene transcription does not increase [136]. However, it remains unclear how this doubled precision is accomplished. Recent studies have shown that a nuclear pore component, Mtor, determines the appropriate transcription levels from the male X chromosome [104]. Both Mtor and the components of MSL complex are involved in regulating the levels of dosage-compensated expression [104]. The effects of genomic imbalance on MSL complex and sex chromosome aneuploidy have been further investigated. The results indicate that most X chromosome genes still exhibit dosage compensation compared with normal diploid females [50].

Although the dosage compensation mechanisms in *Drosophila* have been widely studied, many questions still remain unanswered. For example, what is the kinetic basis for the binding of the MSL complex to the X chromosome? What is the specific molecular mechanism by which the MSL complex recognizes the X chromosome and targets the target genes? Are there any other DNA sequence elements that promote the assembly or disassembly of the MSL complex? These problems need further exploration by researchers in future work.

3.3. The Dosage Compensation Mechanism of the Red Flour Beetle

The red flour beetle, *T. castaneum* (Coleoptera; Tenebrionidae), is a major pest of stored grains and is widely distributed in temperate zones around the word [137]. Nevertheless, the dosage compensation mechanism of *T. castaneum* remains controversial. Prince *et al.* pointed out that the mechanism of the red flour beetle is an incomplete dosage compensation mechanism [37]. In the red flour beetle, the expression of male sex chromosomes consistently increases along with autosomes, whereas the expression of female sex chromosomes also shows an increase [37]. Compared with the DCC of *D. melanogaster*, *T. castaneum* has the *msl2*, *msl3*, *mof*, and *mle* genes, but lacks the *msl1* gene [138]. Analysis of the larval RNAi experiment showed that after the knockdown of the *mof* gene, in contrast to the male lethality observed in *D. melanogaster*, the mortality for both females and males of *T. castaneum* was 100% [138]. Further study also revealed that there was no

obvious male-lethal effect for the other three DCC genes, namely, *msl2*, *msl3*, and *mle* [56]. Therefore, these results indicate that there may be no dosage compensation mechanism in *T. castaneum*, or at the very least that the DCC genes of *msl2*, *msl3*, *mof*, and *mle* are not involved in male-specific dosage compensation. In contrast, the DCC of *T. castaneum* is composed of the non-specific lethal complex and plays a role in regulating a large number of critical genes related to the growth, development, and reproduction in both females and males [56]. Single-cell sequencing reveals that the escape from meiotic sex chromosome inactivation and postmeiotic reactivation of the X chromosome may be mediated by the dosage compensation machinery in *T. castaneum* [139].

3.4. The Dosage Compensation Mechanism of the Silkworm

B. mori, also known as the silkworm, is a lepidopteran model insect of great economic importance [140]. Several studies on WZ-bearing species indicate that dosage compensation is either lacking or incomplete in most lineages except for butterflies and moths, where the expression of the Z chromosome (chZ) in males (ZZ) is reduced by half to equal that in females (WZ). However, it is still unknown whether one chZ is inactivated (as in mammals) or both are partially repressed (as in *C. elegans*) [141]. Silkworms are organisms with female heterogamety (male ZZ, female WZ), and the main application of silkworms is the efficient production of silk proteins [141]. A Z-linked gene of the silkworm, named *T15.180a*, was firstly reported by Suzuki et al. in 1998, and the mRNA expression of this gene in males was twice as much as that in females [142]. The second gene, *Bmkettin*, located on the Z chromosome, also exhibited the same expression pattern as *T15.180a* [143]. In 2003, 13 genes surrounding the *Bmkettin* locus were identified, and most of these genes had higher mRNA expression levels in males compared to females [144]. Therefore, it is reasonable to speculate that the silkworms do not have dosage compensation [58]. Until 2011, studies found that the overall male/female expression ratio was not distinguishable from that of the Z chromosome to autosomes [145]. The total expression of the Z chromosome in males was significantly lower than that of the autosomes in males, which is an unexpected dosage compensation pattern [145].

Numerous analyses of experimental data reveal that the silkworm is likely to have a complete dosage compensation mechanism [145]. However, a recent study employing next-generation RNA sequencing technology to analyze the embryos and larval heads of silkworms at different stages found that dosage compensation occurred at 120 h in embryos, and additionally, the expression level of sex chromosomes in silkworms was lower than that of autosomes. Therefore, on the basis of these findings, the authors proposed that the dosage compensation in the silkworm is complete, yet it is different from the classical complete dosage compensation mechanism [79,146]. The homozygous sex chromosomes should have a transcriptional expression level that is nearly equal to that of the autosomes [79,146]. Another study discovered that somatic tissues of silkworms exhibited complete dosage compensation. However, it is not clear in gonadal tissue, and mixing gonad with somatic tissues may also obscure the identification of the dosage compensation types [80].

In the male silkworms, two copies of the Z chromosome were condensed and folded in a similar manner as revealed by the combination of fluorescence in situ hybridization (FISH) assay and genomics [141]. This finding supported the model of regulating Z-linked gene expression by partially or on average suppressing these two copies of the Z chromosome in males [141]. It also demonstrated that the suppression of the Z chromosome in males may emerge before the middle embryonic stage, which is earlier than previously thought [141]. Researchers recently visualized the autosomes and chZ chromosomes in somatic cells of both sexes by the Oligopaint DNA FISH assay, and they discovered that the chromosomes

of *B. mori* are more compacted than those in *Drosophila*. This finding indicated that in the male silkworms, both chZs exhibit similarity in size and shape and are more compact than autosomes or the female chZ chromosome after DC establishment, suggesting that both male chZs are partially and equally down-regulated [141]. Another research revealed that a *Wolbachia* protein named Oscar can mainly target the Masculinizer (Masc) protein and this interaction thus leads to the male killing by a failure of dosage compensation in *B. mori* embryos [147]. There is a wide variety of research on the dosage compensation mechanism of silkworms. However, it remains controversial. The research methods vary, and so do the conclusions [148]. It is not difficult to envisage that for other lepidopteran insects, such as *M. sexta* [55], codling moth [149], *Plodia interpunctella* [81], and other species that have been researched on dosage compensation yet are seldom thoroughly studied, the dosage compensation mechanism theories may also be somewhat controversial.

3.5. The Dosage Compensation Mechanism of the Tobacco Hornworm

Complete dosage compensation was also discovered in *M. sexta* [55]. As another commonly used model organism in Lepidoptera, this insect is extensively employed in biomedical and biological science research. Gene expression in head tissues of males and females was acquired through high-throughput sequencing technology [55]. In general, dosage compensation was complete on the Z chromosome in both male and female tobacco hornworms. It seems likely that the dosage compensation in the *M. sexta* (WZ) species is achieved through the doubling of Z chromosome expression in females, rather than silencing one Z chromosome in males [55]. After filtering out the genes with extremely low expression levels, the average expression level of autosomal chromosomes was highly similar to that of the Z chromosome [55]. This indicated that for most genes in the tobacco hornworm, a complete dosage compensation effect exists [55]. Moreover, this compensation is associated with sex-specific gene expression and is essential for sexual dimorphisms [55].

4. Conclusions and Outlook

The dosage compensation mechanism compensates for the disparities in gene expression resulting from sex differences in organisms and plays an essential role in bisexual eukaryotes. Researchers have extensively conducted investigations into the dosage compensation effects in three phylogenetically distant model organisms, namely, *C. elegans*, *Drosophila*, and humans. Although diverse mechanisms evolve to perform dose compensation across species, the core mechanism is accomplished through the regulation of the X-linked gene expressions. To achieve dose compensation, the nematodes halve expression of both X chromosomes in females. In *Drosophila*, the X chromosome expression is doubled only in males. In contrast, one of the two X chromosomes is inactivated in mammalian females. Understanding the dosage compensation mechanisms across species can provide fundamental insights into the evolutionary conservation and divergence.

Dosage compensation is of crucial importance for the sex differentiation of insects. There exist certain trends in the patterns and mechanisms underlying dosage compensation in insects. However, a strictly universal principle has yet to be established. In some insect species, the regulation of dosage compensation is chromosome-wide. On the contrary, dosage compensation exhibits a more gene-specific trait in other insects rather than affecting the entire chromosome. In insect species with heteromorphic sex chromosomes, the expression of sex-linked genes is at least partially equalized between the two sexes. Moreover, the ultimate objective of dosage compensation in insects and other organisms shares a common characteristic, which is to balance the expression of sex-linked genes between different sexes, thereby ensuring the normal growth and development of organisms.

Nevertheless, the mechanisms and regulatory molecules of dosage compensation differ among insect species.

Although certain key genes associated with insect sex determination have been identified, the manner in which these genes collaborate as well as their upstream and downstream regulators remain unclear. Therefore, it is necessary to conduct in-depth studies on the functions and interrelationships of these genes. Subsequently, a more comprehensive regulatory network for sex determination should be constructed. Given the limited number of known dosage compensation patterns and mechanisms, additional investigations are essential to fully reveal their molecular diversity and to identify whether certain mechanisms are more widespread or have undergone repeated evolution. Environmental factors also have an impact on insect sex determination and sometimes interact with the genetic factors. Further research on how environmental factors influence the sex determination gene expressions and dosage compensation will strengthen our understanding of how insects maintain the balance of sex ratios under diverse environmental conditions.

Differences also exist in the mechanisms of dosage compensation between male heterogamety (XX/XY) and female heterogamety (WZ/ZZ). For example, in the process of XY-type sex determination, fruit flies employ the *Sxl* gene as a key switch. This process is mediated by the MSL complex, which is responsible for dosage compensation by doubling the expression of the X chromosome specifically in males. In contrast, silkworms utilize *Feminizer* (*Fem*) gene as the upstream regulators for WZ-type sex determination. This regulation is mediated by the Masc protein, which plays a role in dosage compensation by suppressing the expression of both male Z chromosomes. However, in both the fruit flies and silkworms, the terminal genes within the sex determination cascade are the constant *doublesex*, which encode male- and female-specific protein products and govern the expression of downstream sex-related genes.

To better elucidate the mechanism of dosage compensation and gene regulation in insects, we can utilize gene editing technology to precisely alter the sex of insects and guide their sex determination to develop in a direction beneficial to humans. In this case, we can also employ the strategy of sex determination and differentiation to control the pest population and expand the scale of natural enemies, for instance, by obtaining sterilized male pests by the radiation sterility method and subsequently releasing them into the wild to mate with other normal females, thereby achieving the goal of controlling the pest population. Furthermore, for some resource insects with economic importance, such as the silkworm, research on its sex determination mechanism can provide technical support for sex control in sericulture of males.

For the evolution from *Drosophila* to humans, dosage compensation has evolved various mechanisms, characterized by the diversity of its components. *D.* melanogaster is the representative insect of Diptera, the dosage compensation mechanism of which is thoroughly understood. *Sciara ocellaris* is another Dipteran insect with an X0 sex determination system: females are XX and males are X0. However, homologous proteins between *Drosophila* and *Sciara* perform different functions. For example, the *Sxl* gene of *Sciara* has no discriminative function in governing sex determination and dosage compensation. Additionally, the *doublesex* gene of *Sciara* is implicated in sex determination but lacks the discriminatory role. In comparison with *Drosophila*, there exist homologous proteins of MLE, whereas MSL2 is absent in *Sciara*. Thus, investigating the functional differences between species is of great significance for understanding the evolution mechanism and environmental adaptation of species.

In recent years, high-throughput sequencing technologies have become increasingly prominent in research on dosage compensation mechanisms. Single-cell sequencing can be employed for transcriptome analysis of insect cells of different genders and developmental stages. This novel approach inevitably contributes to illustrating the cell heterogeneity

and dynamic changes in gene expression during the processes of sex determination and dose compensation. However, except for *Drosophila*, the sex determination and dosage compensation mechanisms in other insects remain unclear. The mechanism in Lepidoptera is even controversial, which also demonstrates the complexity and diversity in dosage compensation processes. Additionally, the mechanisms of various insects also show remarkable differences. In the future, through the integration of multi-omics joint analysis, the expression profiles, protein interaction networks, and epigenetic modifications of insects with different genders will be fully utilized for comprehensively uncovering the mechanism of gender balance and the evolution of dosage compensation in insects.

Author Contributions: X.X., Y.Z. and Z.D. conceived and designed the experiments. X.X., Y.Z. and H.P. analyzed the data. X.X., Y.Z., H.P. and Z.D. wrote the manuscript. All authors have read and agreed to the published version of the manuscript.

Funding: This research was funded by the Henan Province Science and Technology Research Project (No. 242102111100) and the Beijing Natural Science Foundation in China (No. 7224356).

Data Availability Statement: Data contained within the article.

Conflicts of Interest: The authors declare no conflicts of interest.

References

1. Bachtrog, D.; Kirkpatrick, M.; Mank, J.E.; McDaniel, S.F.; Pires, J.C.; Rice, W.; Valenzuela, N. Are all sex chromosomes created equal? *Trends Genet.* **2011**, *27*, 350–357. [CrossRef] [PubMed]
2. Martín, I.; Ruiz, M.F.; Sánchez, L. The gene *transformer-2* of *Sciara* (Diptera, Nematocera) and its effect on *Drosophila* sexual development. *BMC Dev. Biol.* **2011**, *11*, 19. [CrossRef] [PubMed]
3. Blackmon, H.; Ross, L.; Bachtrog, D. Sex determination, sex chromosomes, and karyotype evolution in insects. *J. Hered.* **2017**, *108*, 78–93. [CrossRef] [PubMed]
4. Zhu, Z.X.; Younas, L.; Zhou, Q. Evolution and regulation of animal sex chromosomes. *Nat. Rev. Genet.* **2025**, *26*, 59–74. [CrossRef] [PubMed]
5. Irwin, D.E. Sex chromosomes and speciation in birds and other ZW systems. *Mol. Ecol.* **2018**, *27*, 3831–3851. [CrossRef]
6. Birchler, J.A. Parallel universes for models of X chromosome dosage compensation in *Drosophila*: A review. *Cytogenet. Genome Res.* **2016**, *148*, 52–67. [CrossRef]
7. Charlesworth, B. The evolution of chromosomal sex determination and dosage compensation. *Curr. Biol.* **1996**, *6*, 149–162. [CrossRef]
8. Ruiz, M.F.; Esteban, M.R.; Doñoro, C.; Goday, C.; Sánchez, L. Evolution of dosage compensation in Diptera: The gene *maleless* implements dosage compensation in *Drosophila* (Brachycera Suborder) but its homolog in Sciara (Nematocera Suborder) appears to play no role in dosage compensation. *Genetics* **2000**, *156*, 1853–1865. [CrossRef]
9. Muller, H.J. Further studies on the nature and causes of gene mutations. In Proceeding of the Sixth International Congress Genetics, Ithaca, NY, USA, September 13–18 1932; pp. 213–255.
10. Deng, X.X.; Hiatt, J.B.; Nguyen, D.K.; Ercan, S.; Sturgill, D.; Hillier, L.W.; Schlesinger, F.; Davis, C.A.; Reinke, V.J.; Gingeras, T.R.; et al. Evidence for compensatory upregulation of expressed X-linked genes in mammals, *Caenorhabditis elegans* and *Drosophila melanogaster*. *Nat. Genet.* **2011**, *43*, 1179–1185. [CrossRef]
11. Ferrari, F.; Alekseyenko, A.A.; Park, P.J.; Kuroda, M.I. Transcriptional control of a whole chromosome: Emerging models for dosage compensation. *Nat. Struct. Mol. Biol.* **2014**, *21*, 118–125. [CrossRef]
12. Duan, J.Y.; Larschan, E.N. Dosage compensation: How to be compensated. . .or not? *Curr. Biol.* **2019**, *29*, R1229–R1231. [CrossRef] [PubMed]
13. Demakova, O.V.; Kotlikova, I.V.; Gordadze, P.R.; Alekseyenko, A.A.; Kuroda, M.I.; Zhimulev, I.F. The MSL complex levels are critical for its correct targeting to the chromosomes in *Drosophila melanogaster*. *Chromosoma* **2003**, *112*, 103–115. [CrossRef] [PubMed]
14. Keller, C.I.; Akhtar, A. The MSL complex: Juggling RNA-protein interactions for dosage compensation and beyond. *Curr. Opin. Genet. Dev.* **2015**, *31*, 1–11. [CrossRef] [PubMed]
15. Deng, X.X.; Berletch, J.B.; Nguyen, D.K.; Disteche, C.M. X chromosome regulation: Diverse patterns in development, tissues and disease. *Nat. Rev. Genet.* **2014**, *15*, 367–378. [CrossRef]
16. Galupa, R.; Heard, E. X-chromosome inactivation: New insights into *cis* and *trans* regulation. *Curr. Opin. Genet. Dev.* **2015**, *31*, 57–66. [CrossRef]

17. Westergaard, M. The mechanism of sex determination in dioecious flowering plants. *Adv. Genet.* **1958**, *9*, 217–281.
18. Blackmon, H.; Demuth, J.P. Genomic origins of insect sex chromosomes. *Curr. Opin. Insect Sci.* **2015**, *7*, 45–50. [CrossRef]
19. Saunders, P.A.; Muyle, A. Sex chromosome evolution: Hallmarks and question marks. *Mol. Biol. Evol.* **2024**, *41*, msae218. [CrossRef]
20. Ah-King, M.; Nylin, S. Sex in an evolutionary perspective: Just another reaction norm. *Evol. Biol.* **2010**, *37*, 234–246. [CrossRef]
21. Toyota, K.; Miyakawa, H.; Hiruta, C.; Sato, T.; Katayama, H.; Ohira, T.; Iguchi, T. Sex determination and differentiation in decapod and cladoceran crustaceans: An overview of endocrine regulation. *Genes* **2021**, *12*, 305. [CrossRef]
22. Gamble, T.; Zarkower, D. Sex determination. *Curr. Biol.* **2012**, *22*, R257–R262. [CrossRef] [PubMed]
23. Capel, B. Vertebrate sex determination: Evolutionary plasticity of a fundamental switch. *Nat. Rev. Genet.* **2017**, *18*, 675–689. [CrossRef] [PubMed]
24. Kalita, A.I.; Keller Valsecchi, C.I. Dosage compensation in non-model insects—Progress and perspectives. *Trends Genet.* **2025**, *41*, 76–98. [CrossRef] [PubMed]
25. Gu, L.Q.; Walters, J.R.; Knipple, D.C. Conserved patterns of sex chromosome dosage compensation in the Lepidoptera (WZ/ZZ): Insights from a moth Neo-Z chromosome. *Genome Biol. Evol.* **2017**, *9*, 802–816. [CrossRef]
26. Van't Hof, A.E.; Whiteford, S.; Yung, C.J.; Yoshido, A.; Zrzavá, M.; de Jong, M.A.; Tan, K.L.; Zhu, D.T.; Monteiro, A.; Brakefield, P.M.; et al. Zygosity-based sex determination in a butterfly drives hypervariability of *Masculinizer*. *Sci. Adv.* **2024**, *10*, eadj6979. [CrossRef]
27. Yang, X.; Chen, K.; Wang, Y.H.; Yang, D.H.; Huang, Y.P. The sex determination cascade in the silkworm. *Genes* **2021**, *12*, 315. [CrossRef]
28. Livernois, A.M.; Waters, S.A.; Deakin, J.E.; Marshall Graves, J.A.; Waters, P.D. Independent evolution of transcriptional inactivation on sex chromosomes in birds and mammals. *PLoS Genet.* **2013**, *9*, e1003635. [CrossRef]
29. Traut, W.; Sahara, K.; Marec, F. Sex chromosomes and sex determination in Lepidoptera. *Sex. Dev.* **2007**, *1*, 332–346. [CrossRef]
30. Yoshido, A.; Marec, F. Deviations in the Z:A ratio disrupt sexual development in the eri silkmoth, *Samia cynthia ricini*. *Genetics* **2023**, *224*, iyad023. [CrossRef]
31. Seiler, J. Geschlechtschromosomen-Untersuchungen an Psychiden. I. Experimentelle Beeinflussung der geschlechtsbestimmenden Reifeteilung bei Talaeporia tubulosa Retz. *Arch Zellforsch* **1920**, *15*, 249–268.
32. Moore, E.C.; Roberts, R.B. Polygenic sex determination. *Curr. Biol.* **2013**, *23*, 510–512. [CrossRef] [PubMed]
33. Lasne, C.; Elkrewi, M.; Toups, M.A.; Layana, L.; Macon, A.; Vicoso, B. The scorpionfly (*Panorpa cognata*) genome highlights conserved and derived features of the peculiar Dipteran X chromosome. *Mol. Biol. Evol.* **2023**, *40*, msad245. [CrossRef] [PubMed]
34. Meyer, B.J. Mechanisms of sex determination and X-chromosome dosage compensation. *Genetics* **2022**, *220*, iyab197. [CrossRef] [PubMed]
35. Fujii, T.; Shimada, T. Sex determination in the silkworm, *Bombyx mori*: A female determinant on the W chromosome and the sex-determining gene cascade. *Semin. Cell Dev. Biol.* **2007**, *18*, 379–388. [CrossRef] [PubMed]
36. Gupta, V.; Parisi, M.; Sturgill, D.; Nuttall, R.; Doctolero, M.; Dudko, O.K.; Malley, J.D.; Eastman, P.S.; Oliver, B. Global analysis of X-chromosome dosage compensation. *J. Biol.* **2006**, *5*, 3. [CrossRef]
37. Prince, E.G.; Kirkland, D.; Demuth, J.P. Hyperexpression of the X chromosome in both sexes results in extensive female bias of X-linked genes in the flour beetle. *Genome Biol. Evol.* **2010**, *2*, 336–346. [CrossRef]
38. Rao, S.R.V.; Padmaja, M. Mammalian-type dosage compensation mechanism in an insect—*Gryllotalpa fossor* (Scudder)—Orthoptera. *J. Biosci.* **1992**, *17*, 253–273. [CrossRef]
39. Hu, Q.L.; Ye, Y.X.; Zhuo, J.C.; Huang, H.J.; Li, J.M.; Zhang, C.X. Chromosome-level assembly, dosage compensation and sex-biased gene expression in the small brown planthopper, *Laodelphax striatellus*. *Genome Biol. Evol.* **2022**, *14*, evac160. [CrossRef]
40. Bellott, D.W.; Skaletsky, H.; Cho, T.J.; Brown, L.; Locke, D.; Chen, N.; Galkina, S.; Pyntikova, T.; Koutseva, N.; Graves, T.; et al. Avian W and mammalian Y chromosomes convergently retained dosage-sensitive regulators. *Nat. Genet.* **2017**, *49*, 387–394. [CrossRef]
41. Turano, A.; Osborne, B.F.; Schwarz, J.M. Sexual differentiation and sex differences in neural development. *Curr. Top. Behav. Neurosci.* **2019**, *43*, 69–110.
42. Parker, D.J.; Jaron, K.S.; Dumas, Z.; Robinson-Rechavi, M.; Schwander, T. X chromosomes show relaxed selection and complete somatic dosage compensation across *Timema* stick insect species. *J. Evol. Biol.* **2022**, *35*, 1734–1750. [CrossRef] [PubMed]
43. Ohno, S. Evidence indicating that the X and the Y or the Z and the W were originally an homologous pair of ordinary chromosomes. In *Sex Chromosomes and Sex-linked Genes*; Springer: Berlin/Heidelberg, Germany, 1966; pp. 5–13.
44. Mukherjee, A.S.; Beermann, W. Synthesis of ribonucleic acid by the X-chromosomes of *Drosophila melanogaster* and the problem of dosage compensation. *Nature* **1965**, *207*, 785–786. [CrossRef] [PubMed]
45. Conrad, T.; Akhtar, A. Dosage compensation in *Drosophila melanogaster*: Epigenetic fine-tuning of chromosome-wide transcription. *Nat. Rev. Genet.* **2012**, *13*, 123–134. [CrossRef] [PubMed]

46. Malcore, R.M.; Kalantry, S. A comparative analysis of mouse imprinted and random X-chromosome inactivation. *Epigenomes* **2024**, *8*, 8. [CrossRef]
47. Lentini, A.; Cheng, H.T.; Noble, J.C.; Papanicolaou, N.; Coucoravas, C.; Andrews, N.; Deng, Q.L.; Enge, M.; Reinius, B. Elastic dosage compensation by X-chromosome upregulation. *Nat. Commun.* **2022**, *13*, 1854. [CrossRef]
48. Lucchesi, J.C. On the origin of sex chromosomes. *BioEssays* **1999**, *21*, 188–190. [CrossRef]
49. Chauhan, P.; Swaegers, J.; Sánchez-Guillén, R.A.; Svensson, E.I.; Wellenreuther, M.; Hansson, B. Genome assembly, sex-biased gene expression and dosage compensation in the damselfly *Ischnura elegans*. *Genomics* **2021**, *113*, 1828–1837. [CrossRef]
50. Zhang, S.; Qi, H.Z.; Huang, C.; Yuan, L.J.; Zhang, L.D.; Wang, R.X.; Tian, Y.; Sun, L. Interaction of Male Specific Lethal complex and genomic imbalance on global gene expression in *Drosophila*. *Sci. Rep.* **2021**, *11*, 19679. [CrossRef]
51. Bachtrog, D.; Mank, J.E.; Peichel, C.L.; Kirkpatrick, M.; Otto, S.P.; Ashman, T.L.; Hahn, M.W.; Kitano, J.; Mayrose, I.; Ming, R.; et al. Sex determination: Why so many ways of doing it? *PLoS Biol.* **2014**, *12*, e1001899. [CrossRef]
52. Chen, J.B.; Wang, M.H.; He, X.L.; Yang, J.R.; Chen, X.S. The evolution of sex chromosome dosage compensation in animals. *J. Genet. Genomics* **2020**, *47*, 681–693. [CrossRef]
53. Gu, L.Q.; Walters, J.R. Evolution of sex chromosome dosage compensation in animals: A beautiful theory, undermined by facts and bedeviled by details. *Genome Biol. Evol.* **2017**, *9*, 2461–2476. [CrossRef] [PubMed]
54. Hebbert, D.R. Dosage compensation of the sex-linked enzyme phosphoglucomutase in the orthoptera. *Heredity* **1984**, *53*, 361–369. [CrossRef]
55. Smith, G.; Chen, Y.R.; Blissard, G.W.; Briscoe, A.D. Complete dosage compensation and sex-biased gene expression in the moth *Manduca sexta*. *Genome Biol. Evol.* **2014**, *6*, 526–537. [CrossRef] [PubMed]
56. Wang, Y.Y. Identification and RNAi Analysis of *Tribolium Castaneum* Dosage Compensation Related Genes. Master's Thesis, Nanjing Normal University, Nanjing, China, 2013.
57. Ramesh, B. Elucidating the Evolution of Sex Chromosome Dosage Compensation Using Beetles. Ph.D. Thesis, The University of Texas at Arlington, Arlington, TX, USA, 2021.
58. Zha, X.F.; Xia, Q.Y.; Duan, J.; Wang, C.Y.; He, N.J.; Xiang, Z.H. Dosage analysis of Z chromosome genes using microarray in silkworm, *Bombyx mori*. *Insect Biochem. Mol. Biol.* **2009**, *39*, 315–321. [CrossRef] [PubMed]
59. Disteche, C.M. Dosage compensation of the sex chromosomes. *Annu. Rev. Genet.* **2012**, *46*, 537–560. [CrossRef]
60. Disteche, C.M. Dosage compensation of the sex chromosomes and autosomes. *Semin. Cell Dev. Biol.* **2016**, *56*, 9–18. [CrossRef]
61. Birchler, J.A. The genetic basis of dosage compensation of alcohol dehydrogenase-1 in maize. *Genetics* **1981**, *97*, 625–637. [CrossRef]
62. Devlin, R.H.; Holm, D.G.; Grigliatti, T.A. Autosomal dosage compensation *Drosophila melanogaster* strains trisomic for the left arm of chromosome 2. *Proc. Natl. Acad. Sci. USA* **1982**, *79*, 1200–1204. [CrossRef]
63. Hopkins, B.R.; Kopp, A. Evolution of sexual development and sexual dimorphism in insects. *Curr. Opin. Genet. Dev.* **2021**, *69*, 129–139. [CrossRef]
64. Mora, P.; Hospodářská, M.; Voleníková, A.C.; Koutecký, P.; Štundlová, J.; Dalíková, M.; Walters, J.R.; Nguyen, P. Sex-biased gene content is associated with sex chromosome turnover in Danaini butterflies. *Mol. Ecol.* **2024**, *33*, e17256. [CrossRef]
65. Gu, L.Q.; Reilly, P.F.; Lewis, J.J.; Reed, R.D.; Andolfatto, P.; Walters, J.R. Dichotomy of dosage compensation along the neo Z chromosome of the monarch butterfly. *Curr. Biol.* **2019**, *29*, 4071–4077. [CrossRef] [PubMed]
66. Lucchesi, J.C.; Kuroda, M.I. Dosage compensation in *Drosophila*. *Cold Spring Harb. Perspect. Biol.* **2015**, *7*, a019398. [CrossRef] [PubMed]
67. Witt, E.; Shao, Z.T.; Hu, C.; Krause, H.M.; Zhao, L. Single-cell RNA-sequencing reveals pre-meiotic X-chromosome dosage compensation in *Drosophila* testis. *PLoS Genet.* **2021**, *17*, e1009728. [CrossRef] [PubMed]
68. Wilkinson, G.S.; Johns, P.M.; Metheny, J.D.; Baker, R.H. Sex-biased gene expression during head development in a sexually dimorphic stalk-eyed fly. *PLoS ONE* **2013**, *8*, e59826. [CrossRef] [PubMed]
69. Linger, R.J.; Belikoff, E.J.; Scott, M.J. Dosage compensation of X-linked muller element F genes but not X-linked transgenes in the Australian sheep blowfly. *PLoS ONE* **2015**, *10*, e0141544. [CrossRef]
70. Rose, G.; Krzywinska, E.; Kim, J.; Revuelta, L.; Ferretti, L.; Krzywinski, J. Dosage compensation in the African malaria mosquito *Anopheles gambiae*. *Genome Biol. Evol.* **2016**, *8*, 411–425.
71. Valsecchi, C.I.K.; Marois, E.; Basilicata, M.F.; Georgiev, P.; Akhtar, A. Distinct mechanisms mediate X chromosome dosage compensation in *Anopheles* and *Drosophila*. *Life Sci. Alliance* **2021**, *4*, e202000996. [CrossRef]
72. Krzywinska, E.; Ribeca, P.; Ferretti, L.; Hammond, A.; Krzywinski, J. A novel factor modulating X chromosome dosage compensation in *Anopheles*. *Curr. Biol.* **2023**, *33*, 4697–4703. [CrossRef]
73. Jiang, X.F.; Biedler, J.K.; Qi, Y.M.; Hall, A.B.; Tu, Z.J. Complete dosage compensation in *Anopheles stephensi* and the evolution of sex-biased genes in mosquitoes. *Genome Biol. Evol.* **2015**, *7*, 1914–1924. [CrossRef]

74. Mahajan, S.; Bachtrog, D. Partial dosage compensation in Strepsiptera, a sister group of beetles. *Genome Biol. Evol.* **2015**, *7*, 591–600. [CrossRef]
75. Pal, A.; Vicoso, B. The X chromosome of Hemipteran insects: Conservation, dosage compensation and sex-biased expression. *Genome Biol. Evol.* **2015**, *7*, 3259–3268. [CrossRef] [PubMed]
76. Richard, G.; Legeai, F.; Prunier-Leterme, N.; Bretaudeau, A.; Tagu, D.; Jaquiéry, J.; Le Trionnaire, G. Dosage compensation and sex-specific epigenetic landscape of the X chromosome in the pea aphid. *Epigenetics Chromatin* **2017**, *10*, 30. [CrossRef] [PubMed]
77. Rao, S.R.; Ali, S. Insect sex chromosomes. VI. A presumptive hyperactivation of the male X chromosome in *Acheta domesticus* (L.). *Chromosoma* **1982**, *86*, 325–339. [CrossRef] [PubMed]
78. Kiuchi, T.; Koga, H.; Kawamoto, M.; Shoji, K.; Sakai, H.; Arai, Y.; Ishihara, G.; Kawaoka, S.; Sugano, S.; Shimada, T.; et al. A single female-specific piRNA is the primary determiner of sex in the silkworm. *Nature* **2014**, *509*, 633–636. [CrossRef]
79. Gopinath, G.; Srikeerthana, K.; Tomar, A.; Sekhar, S.M.C.; Arunkumar, K.P. RNA sequencing reveals a complete but an unconventional type of dosage compensation in the domestic silkworm *Bombyx mori*. *R. Soc. Open Sci.* **2017**, *4*, 170261. [CrossRef]
80. Huylmans, A.K.; Macon, A.; Vicoso, B. Global dosage compensation is ubiquitous in Lepidoptera, but counteracted by the masculinization of the Z chromosome. *Mol. Biol. Evol.* **2017**, *34*, 2637–2649. [CrossRef]
81. Harrison, P.W.; Mank, J.E.; Wedell, N. Incomplete sex chromosome dosage compensation in the indian meal moth, *Plodia interpunctella*, based on de novo transcriptome assembly. *Genome Biol. Evol.* **2012**, *4*, 1118–1126. [CrossRef]
82. Walters, J.R.; Hardcastle, T.J.; Jiggins, C.D. Sex chromosome dosage compensation in *Heliconius* Butterflies: Global yet still incomplete? *Genome Biol. Evol.* **2015**, *7*, 2545–2559. [CrossRef]
83. Zhang, Y.K.; Deng, Z.Y.; Gu, S.H.; Li, X.C. Identification and functional analysis of the dosage compensation related gene *Hamsl1* in *Helicoverpa armigera* (*Lepidoptera*: *Noctuidae*). *Acta Entomol. Sin.* **2019**, *62*, 799–813.
84. Deng, Z.Y.; Zhang, Y.K.; Xie, X.C.; Li, H.H.; Guo, H.; Ni, X.Z.; Li, X.C. Transcriptomic and proteomic elucidation of Z chromosome dosage compensation in *Helicoverpa armigera*. *Insect Mol. Biol.* **2024**, *33*, 744–755. [CrossRef]
85. Höök, L.; Leal, L.; Talla, V.; Backström, N. Multilayered tuning of dosage compensation and Z-chromosome masculinization in the wood white (*Leptidea sinapis*) butterfly. *Genome Biol. Evol.* **2019**, *11*, 2633–2652. [CrossRef] [PubMed]
86. Gempe, T.; Hasselmann, M.; Schiøtt, M.; Hause, G.; Otte, M.; Beye, M. Sex determination in honeybees: Two separate mechanisms induce and maintain the female pathway. *PLoS Biol.* **2009**, *7*, e1000222. [CrossRef] [PubMed]
87. Baker, B.S.; Belote, J.M. Sex determination and dosage compensation in *Drosophila melanogaster*. *Annu. Rev. Genet.* **1983**, *17*, 345–393. [CrossRef] [PubMed]
88. Gorman, M.; Baker, B.S. How flies make one equal two: Dosage compensation in *Drosophila*. *Trends Genet.* **1994**, *10*, 376–380. [CrossRef]
89. Shevelyov, Y.Y.; Ulianov, S.V.; Gelfand, M.S.; Belyakin, S.N.; Razin, S.V. Dosage compensation in *Drosophila*: Its canonical and non-canonical mechanisms. *Int. J. Mol. Sci.* **2022**, *23*, 10976. [CrossRef]
90. Lakhotia, S.C. Dosage compensation in *Drosophila* in the 1960s: A personal historical perspective. *J. Genet.* **2021**, *100*, 70. [CrossRef]
91. Seong, K.H.; Kang, S. Noncanonical function of the Sexlethal gene controls the protogyny phenotype in *Drosophila melanogaster*. *Sci. Rep.* **2022**, *12*, 1455. [CrossRef]
92. Oliver, B.; Kim, Y.J.; Baker, B.S. Sex-lethal, master and slave: A hierarchy of germ-line sex determination in *Drosophila*. *Development* **1993**, *119*, 897–908. [CrossRef]
93. Bell, L.R.; Maine, E.M.; Schedl, P.; Cline, T.W. *Sex-lethal*, a *Drosophila* sex determination switch gene, exhibits sex-specific RNA splicing and sequence similarity to RNA binding proteins. *Cell* **1988**, *55*, 1037–1046. [CrossRef]
94. Bashaw, G.J.; Baker, B.S. The *msl-2* dosage compensation gene of *Drosophila* encodes a putative DNA-binding protein whose expression is sex specifically regulated by Sex-lethal. *Development* **1995**, *121*, 3245–3258. [CrossRef]
95. Copps, K.; Richman, R.; Lyman, L.M.; Chang, K.A.; Rampersad-Ammons, J.; Kuroda, M.I. Complex formation by the *Drosophila* MSL proteins: Role of the MSL2 RING finger in protein complex assembly. *Embo J.* **1998**, *17*, 5409–5417. [CrossRef] [PubMed]
96. Deshpande, N.; Meller, V.H. Chromatin that guides dosage compensation is modulated by the siRNA pathway in *Drosophila melanogaster*. *Genetics* **2018**, *209*, 1085–1097. [CrossRef] [PubMed]
97. McKeown, M.; Belote, J.M.; Baker, B.S. A molecular analysis of transformer, a gene in *Drosophila melanogaster* that controls female sexual differentiation. *Cell* **1987**, *48*, 489–499. [CrossRef] [PubMed]
98. Belote, J.M.; Baker, B.S. Sex determination in *Drosophila melanogaster*: Analysis of transformer-2, a sex-transforming locus. *Proc. Natl. Acad. Sci. USA* **1982**, *79*, 1568–1572. [CrossRef]
99. Baker, B.S.; Wolfner, M.F. A molecular analysis of *doublesex*, a bifunctional gene that controls both male and female sexual differentiation in *Drosophila melanogaster*. *Genes Dev.* **1988**, *2*, 477–489. [CrossRef]
100. Gelbart, M.E.; Kuroda, M.I. *Drosophila* dosage compensation: A complex voyage to the X chromosome. *Development* **2009**, *136*, 1399–1410. [CrossRef]

101. Bashaw, G.J.; Baker, B.S. The regulation of the *Drosophila msl-2* gene reveals a function for *Sex-lethal* in translational control. *Cell* **1997**, *89*, 789–798. [CrossRef]
102. Belote, J.M.; Lucchesi, J.C. Male-specific lethal mutations of *Drosophila melanogaster*. *Genetics* **1980**, *96*, 165–186. [CrossRef]
103. Belote, J.M.; Lucchesi, J.C. Control of X chromosome transcription by the maleless gene in *Drosophila*. *Nature* **1980**, *285*, 573–575. [CrossRef]
104. Aleman, J.R.; Kuhn, T.M.; Pascual-Garcia, P.; Gospocic, J.; Lan, Y.; Bonasio, R.; Little, S.C.; Capelson, M. Correct dosage of X chromosome transcription is controlled by a nuclear pore component. *Cell Rep.* **2021**, *35*, 109236. [CrossRef]
105. Gu, W.; Szauter, P.; Lucchesi, J.C. Targeting of MOF, a putative histone acetyl transferase, to the X chromosome of *Drosophila melanogaster*. *Dev. Genet.* **1998**, *22*, 56–64. [CrossRef]
106. Wu, L.P.; Zee, B.M.; Wang, Y.M.; Garcia, B.A.; Dou, Y.L. The RING finger protein MSL2 in the MOF complex is an E3 ubiquitin ligase for H2B K34 and is involved in crosstalk with H3 K4 and K79 methylation. *Mol. Cell* **2011**, *43*, 132–144. [CrossRef] [PubMed]
107. Hallacli, E.; Lipp, M.; Georgiev, P.; Spielman, C.; Cusack, S.; Akhtar, A.; Kadlec, J. Msl1-mediated dimerization of the dosage compensation complex is essential for male X-chromosome regulation in *Drosophila*. *Mol. Cell* **2012**, *48*, 587–600. [CrossRef] [PubMed]
108. Kadlec, J.; Hallacli, E.; Lipp, M.; Holz, H.; Sanchez-Weatherby, J.; Cusack, S.; Akhtar, A. Structural basis for MOF and MSL3 recruitment into the dosage compensation complex by MSL1. *Nat. Struct. Mol. Biol.* **2011**, *18*, 142–149. [CrossRef]
109. Valsecchi, C.I.K.; Basilicata, M.F.; Georgiev, P.; Gaub, A.; Seyfferth, J.; Kulkarni, T.; Panhale, A.; Semplicio, G.; Manjunath, V.; Holz, H.; et al. RNA nucleation by MSL2 induces selective X chromosome compartmentalization. *Nature* **2021**, *589*, 137–142. [CrossRef]
110. Babosha, V.A.; Georgiev, P.G.; Maksimenko, O.G. Mutations of phosphorylation sites in MSL1 protein do not affect dosage compensation in *Drosophila melanogaster*. *Dokl. Biochem. Biophys.* **2021**, *499*, 225–227. [CrossRef]
111. Scott, M.J.; Pan, L.L.; Cleland, S.B.; Knox, A.L.; Heinrich, J. MSL1 plays a central role in assembly of the MSL complex, essential for dosage compensation in *Drosophila*. *EMBO J.* **2000**, *19*, 144–155. [CrossRef]
112. Kelley, R.L.; Solovyeva, I.; Lyman, L.M.; Richman, R.; Solovyev, V.; Kuroda, M.I. Expression of Msl-2 causes assembly of dosage compensation regulators on the X chromosomes and female lethality in *Drosophila*. *Cell* **1995**, *81*, 867–877. [CrossRef]
113. Gelbart, M.E.; Larschan, E.; Peng, S.Y.; Park, P.J.; Kuroda, M.I. *Drosophila* MSL complex globally acetylates H4K16 on the male X chromosome for dosage compensation. *Nat. Struct. Mol. Biol.* **2009**, *16*, 825–832. [CrossRef]
114. Franke, A.; Baker, B.S. The *rox1* and *rox2* RNAs are essential components of the compensasome, which mediates dosage compensation in *Drosophila*. *Mol. Cell* **1999**, *4*, 117–122. [CrossRef]
115. Fauth, T.; Müller-Planitz, F.; König, C.; Straub, T.; Becker, P.B. The DNA binding CXC domain of MSL2 is required for faithful targeting the Dosage Compensation Complex to the X chromosome. *Nucleic Acids Res.* **2010**, *38*, 3209–3221. [CrossRef] [PubMed]
116. Tikhonova, E.; Mariasina, S.; Efimov, S.; Polshakov, V.; Maksimenko, O.; Georgiev, P.; Bonchuk, A. Structural basis for interaction between CLAMP and MSL2 proteins involved in the specific recruitment of the dosage compensation complex in *Drosophila*. *Nucleic Acids Res.* **2022**, *50*, 6521–6531. [CrossRef] [PubMed]
117. Hilfiker, A.; Hilfiker-Kleiner, D.; Pannuti, A.; Lucchesi, J.C. mof, a putative acetyl transferase gene related to the Tip60 and MOZ human genes and to the SAS genes of yeast, is required for dosage compensation in *Drosophila*. *EMBO J.* **1997**, *16*, 2054–2060. [CrossRef] [PubMed]
118. Morales, V.; Regnard, C.; Izzo, A.; Vetter, I.; Becker, P.B. The MRG domain mediates the functional integration of MSL3 into the dosage compensation complex. *Mol. Cell. Biol.* **2005**, *25*, 5947–5954. [CrossRef] [PubMed]
119. Gorman, M.; Franke, A.; Baker, B.S. Molecular characterization of the *male-specific lethal-3* gene and investigations of the regulation of dosage compensation in *Drosophila*. *Development* **1995**, *121*, 463–475. [CrossRef]
120. Uebbing, S.; Konzer, A.; Xu, L.H.; Backström, N.; Brunström, B.; Bergquist, J.; Ellegren, H. Quantitative mass spectrometry reveals partial translational regulation for dosage compensation in chicken. *Mol. Biol. Evol.* **2015**, *32*, 2716–2725. [CrossRef]
121. Lindehell, H.; Glotov, A.; Dorafshan, E.; Schwartz, Y.B.; Larsson, J. The role of H3K36 methylation and associated methyltransferases in chromosome-specific gene regulation. *Sci. Adv.* **2021**, *7*, eabh4390. [CrossRef]
122. Sharma, G.G.; So, S.; Gupta, A.; Kumar, R.; Cayrou, C.; Avvakumov, N.; Bhadra, U.; Pandita, R.K.; Porteus, M.H.; Chen, D.J.; et al. MOF and histone H4 acetylation at lysine 16 are critical for DNA damage response and double-strand break repair. *Mol. Cell. Biol.* **2010**, *30*, 3582–3595. [CrossRef]
123. Gorman, M.; Kuroda, M.I.; Baker, B.S. Regulation of the sex-specific binding of the maleless dosage compensation protein to the male X chromosome in *Drosophila*. *Cell* **1993**, *72*, 39–49. [CrossRef]
124. Kuroda, M.I.; Kernan, M.J.; Kreber, R.; Ganetzky, B.; Baker, B.S. The *maleless* protein associates with the X chromosome to regulate dosage compensation in *Drosophila*. *Cell* **1991**, *66*, 935–947. [CrossRef]
125. Schiemann, A.H.; Weake, V.M.; Li, F.; Laverty, C.; Belikoff, E.J.; Scott, M.J. The importance of location and orientation of male specific lethal complex binding sites of differing affinities on reporter gene dosage compensation in *Drosophila*. *Biochem. Biophys. Res. Commun.* **2010**, *402*, 699–704. [CrossRef] [PubMed]

126. Meller, V.H.; Rattner, B.P. The *roX* genes encode redundant *male-specific lethal* transcripts required for targeting of the MSL complex. *EMBO J.* **2002**, *21*, 1084–1091. [CrossRef] [PubMed]
127. Ilik, I.A.; Quinn, J.J.; Georgiev, P.; Tavares-Cadete, F.; Maticzka, D.; Toscano, S.; Wan, Y.; Spitale, R.C.; Luscombe, N.; Backofen, R.; et al. Tandem stem-loops in *roX* RNAs act together to mediate X chromosome dosage compensation in *Drosophila*. *Mol. Cell* **2013**, *51*, 156–173. [CrossRef] [PubMed]
128. Brockdorff, N.; Turner, B.M. Dosage compensation in mammals. *Cold Spring Harb. Perspect. Biol.* **2015**, *7*, a019406. [CrossRef]
129. Maenner, S.; Müller, M.; Becker, P.B. Roles of long, non-coding RNA in chromosome-wide transcription regulation: Lessons from two dosage compensation systems. *Biochimie* **2012**, *94*, 1490–1498. [CrossRef]
130. Bell, O.; Conrad, T.; Kind, J.; Wirbelauer, C.; Akhtar, A.; Schübeier, D. Transcription-coupled methylation of histone H3 at lysine 36 regulates dosage compensation by enhancing recruitment of the MSL complex in *Drosophila melanogaster*. *Mol. Cell. Biol.* **2008**, *28*, 3401–3409. [CrossRef]
131. Morra, R.; Smith, E.R.; Yokoyama, R.; Lucchesi, J.C. The MLE subunit of the *Drosophila* MSL complex uses its ATPase activity for dosage compensation and its helicase activity for targeting. *Mol. Cell. Biol.* **2008**, *28*, 958–966. [CrossRef]
132. Hosey, A.M.; Brand, M. Chromodomain-mediated spreading on active genes. *Nat. Struct. Mol. Biol.* **2009**, *16*, 11–13. [CrossRef]
133. Makki, R.; Meller, V.H. When down is up: Heterochromatin, nuclear organization and X upregulation. *Cells* **2021**, *10*, 3416. [CrossRef]
134. Ramírez, F.; Lingg, T.; Toscano, S.; Lam, K.C.; Georgiev, P.; Chung, H.R.; Lajoie, B.R.; de Wit, E.; Zhan, Y.; de Laat, W.; et al. High-affinity sites form an interaction network to facilitate spreading of the MSL complex across the X chromosome in *Drosophila*. *Mol. Cell* **2015**, *60*, 146–162. [CrossRef]
135. Schauer, T.; Ghavi-Helm, Y.; Sexton, T.; Albig, C.; Regnard, C.; Cavalli, G.; Furlong, E.E.; Becker, P.B. Chromosome topology guides the *Drosophila* Dosage Compensation Complex for target gene activation. *EMBO Rep.* **2017**, *18*, 1854–1868. [CrossRef] [PubMed]
136. Ilik, I.; Akhtar, A. roX RNAs: Non-coding regulators of the male X chromosome in flies. *RNA Biol.* **2009**, *6*, 113–121. [CrossRef] [PubMed]
137. Campbell, J.F.; Athanassiou, C.G.; Hagstrum, D.W.; Zhu, K.Y. *Tribolium castaneum*: A model insect for fundamental and applied research. *Annu. Rev. Entomol.* **2022**, *67*, 347–365. [CrossRef] [PubMed]
138. Wang, Y.Y.; Li, C.J.; Sang, M.; Li, B. *Tcmof* regulates larval/pupal development and female fecundity in red flour beetle, *Tribolium castaneum*. *Arch Insect Biochem Physiol* **2015**, *88*, 111–122. [CrossRef]
139. Robben, M.; Ramesh, B.; Pau, S.; Meletis, D.; Luber, J.; Demuth, J. scRNA-seq reveals novel genetic pathways and sex chromosome regulation in *Tribolium* spermatogenesis. *Genome Biol. Evol.* **2024**, *16*, evae059. [CrossRef]
140. Ashraf, H.; Qamar, A. Silkworm *Bombyx mori* as a model organism: A review. *Physiol. Entomol.* **2023**, *48*, 107–121. [CrossRef]
141. Rosin, L.F.; Chen, D.H.; Chen, Y.; Lei, E.P. Dosage compensation in *Bombyx mori* is achieved by partial repression of both Z chromosomes in males. *Proc. Natl. Acad. Sci. USA.* **2022**, *119*, e2113374119. [CrossRef]
142. Suzuki, M.G.; Shimada, T.; Kobayashi, M. Absence of dosage compensation at the transcription level of a sex-linked gene in a female heterogametic insect, *Bombyx mori*. *Heredity* **1998**, *81*, 275–283. [CrossRef]
143. Suzuki, M.G.; Shimada, T.; Kobayashi, M. *Bm kettin*, homologue of the *Drosophila* kettin gene, is located on the Z chromosome in *Bombyx mori* and is not dosage compensated. *Heredity* **1999**, *82*, 170–179. [CrossRef]
144. Koike, Y.; Mita, K.; Suzuki, M.G.; Maeda, S.; Abe, H.; Osoegawa, K.; de Jong, P.J.; Shimada, T. Genomic sequence of a 320-kb segment of the Z chromosome of *Bombyx mori* containing a kettin ortholog. *Mol. Genet. Genom.* **2003**, *269*, 137–149. [CrossRef]
145. Walters, J.R.; Hardcastle, T.J. Getting a full dose? Reconsidering sex chromosome dosage compensation in the silkworm, *Bombyx mori*. *Genome Biol. Evol.* **2011**, *3*, 491–504. [CrossRef] [PubMed]
146. Tomihara, K.; Kawamoto, M.; Suzuki, Y.; Katsuma, S.; Kiuchi, T. Masculinizer-induced dosage compensation is achieved by transcriptional downregulation of both copies of Z-linked genes in the silkworm, *Bombyx mori*. *Biol. Lett.* **2022**, *18*, 20220116. [CrossRef] [PubMed]
147. Fukui, T.; Kiuchi, T.; Tomihara, K.; Muro, T.; Matsuda-Imai, N.; Katsuma, S. Expression of the *Wolbachia* male-killing factor Oscar impairs dosage compensation in lepidopteran embryos. *FEBS Lett.* **2024**, *598*, 331–337. [CrossRef] [PubMed]
148. Mongue, A.J.; Hansen, M.E.; Walters, J.R. Support for faster and more adaptive Z chromosome evolution in two divergent lepidopteran lineages. *Evolution* **2022**, *76*, 332–345. [CrossRef]
149. Catalán, A.; Macias-Muñoz, A.; Briscoe, A.D. Evolution of sex-biased gene expression and dosage compensation in the eye and brain of *Heliconius* butterflies. *Mol. Biol. Evol.* **2018**, *35*, 2120–2134. [CrossRef]

Disclaimer/Publisher's Note: The statements, opinions and data contained in all publications are solely those of the individual author(s) and contributor(s) and not of MDPI and/or the editor(s). MDPI and/or the editor(s) disclaim responsibility for any injury to people or property resulting from any ideas, methods, instructions or products referred to in the content.

insects

MDPI

Review

Insect Mating Behaviors: A Review of the Regulatory Role of Neuropeptides

Alfayo Ombuya [1,2,3], Jianyang Guo [1,2,*] and Wanxue Liu [1,2,*]

[1] State Key Laboratory for Biology of Plant Diseases and Insect Pests, Institute of Plant Protection, Chinese Academy of Agricultural Sciences, Beijing 100193, China; alfayoombuya@yahoo.com
[2] Key Laboratory of Invasive Alien Species Control of Ministry of Agriculture and Rural Affairs, Chinese Academy of Agricultural Sciences, Beijing 100193, China
[3] Kenya Plant Health Inspectorate Service (KEPHIS), Mombasa Regional Office, Mombasa P.O. Box 80126-80100, Kenya
* Correspondence: guojianyang@caas.cn (J.G.); liuwanxue@caas.cn (W.L.)

Simple Summary: Mating is a fundamental behavior of animals in perpetuating species. The mating behaviors of insects are complex and primarily regulated by small molecules called neuropeptides. Here, we highlight what is already known about insect mating behaviors and the role played by neuropeptides. In our findings, we note that the mating process of insects entails mate attraction, courtship, copulation, and post-mating behaviors. The 18 neuropeptides discussed in this review are known to regulate mating behaviors and greatly vary among insects. The Neuropeptides vary in mechanistic aspects, and some work closely with other physiological and neurocircuit systems. Moreover, many details about neuropeptides remain unknown, especially in many economically important insects. Given their significance in successful mating and reproduction, neuropeptides remain potential targets for developing safe and sustainable pest control products.

Abstract: Insect mating behaviors are complex, diverse, and primarily regulated by neuropeptides and their receptors. Neuropeptides are peptide signaling molecules mainly secreted by insects' central nervous system (CNS) to reach target organs. A substantial body of research on the role of neuropeptides in regulating mating behaviors in insects has been undertaken. This review aims to (1) synthesize existing knowledge on insect mating behaviors, (2) elucidate the neuropeptidergic mechanisms governing these behaviors, and (3) identify knowledge gaps and propose future research directions. The mating process, covering mate attraction, courtship rituals, copulation, and post-mating behaviors, was elucidated with appropriate examples. Additionally, specific neuropeptides involved at each stage of the mating process, their functions, and mechanistic aspects were discussed as demonstrated in research. The review highlights that insects display behavioral dimorphism in the mating process driven by a complex underlying neuropeptidergic mechanism. While previous publications have generally addressed the role of neuropeptides in insect behavior, none has intensively and methodically examined their role in mating behaviors. In this review, we synthesized 18 neuropeptides that we found to regulate mating behaviors in insects. We note that some of the neuropeptides are malfunctional in their regulatory roles, while others are specific. We also note that these neuropeptides execute their regulatory functions through the G protein-coupled receptor (GPCR) signaling pathway but may take different routes and messengers downstream to effect behavioral change. Neuropeptides also interact with other regulatory systems, such as the endocrine system, to discharge their functions. Given their significance in mediating mating and reproduction, targeted manipulation of the signaling system of neuropeptides could serve as viable targets in the production of ecologically friendly pest management tools. Tools that could disrupt the mating process

would be applied in crop production systems to reduce the population pressure of destructive pests, consequently reducing the urge to use chemical pesticides that are ecologically unfriendly. Our findings not only advance the understanding of neuropeptide-mediated mating regulation but also highlight their potential as eco-friendly pest control targets.

Keywords: mating behavior; neuropeptides; courtship; copulation; post-mating behavior

1. Introduction

Insect mating behavior is a cornerstone of species survival and evolutionary success. Deciphering its regulatory mechanisms not only deepens our understanding of insect biology but also opens avenues for neurobiological innovation and sustainable pest control strategies. Insect mating involves several behavioral and physiological regulations that are evolutionarily pressured to promote successful reproduction. The wide range of mating behaviors is known to vary significantly across various species. Neuropeptides—small peptide molecules secreted by neurosecretory cells—regulate insect physiology through G protein-coupled receptors (GPCRs) [1]. These tiny peptide molecules are crucial for growth, nutrition, reproduction, metabolism, and many other processes (Figure 1) [1,2]. Neuropeptides regulate various aspects of insect life by functioning as neurotransmitters, neuromodulators, hormones, or growth factors [1]. They coordinate intricate behaviors responding to internal and external signals by interacting with specific receptors in the central nervous system and other peripheral tissues. In insect reproduction, neuropeptides are crucial modulators of mating behaviors [3].

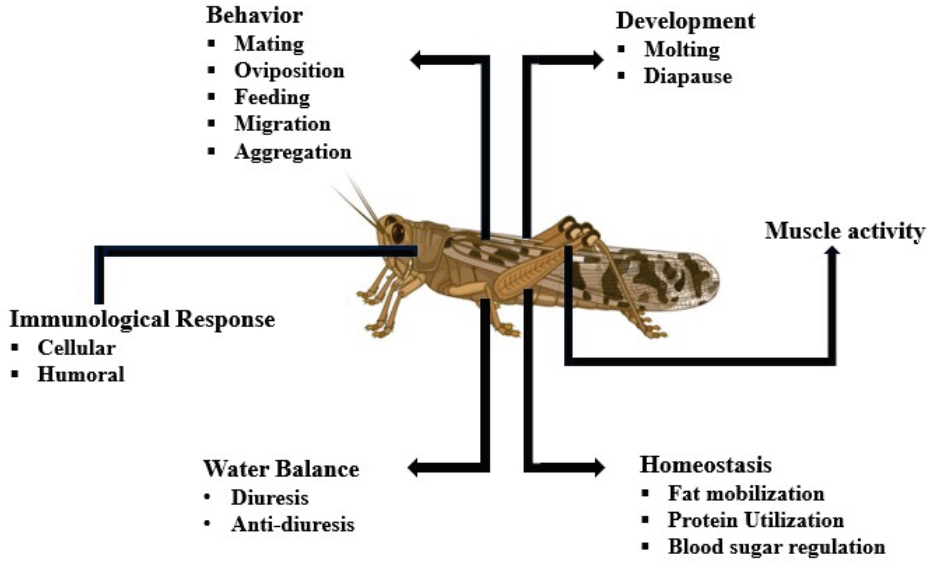


Figure 1. Nearly every physiological function in insects, including immunological responses, pheromone production, diuresis, ecdysis, and muscle activity regulation, is mediated by insect neuropeptides [1,4], Created in BioRender. guo, j. (2025) https://BioRender.com/zeb0u85 (accessed on 28 April 2025).

In addition to expanding our understanding of insect biology, the understanding of how neuropeptides regulate mating behavior in insects is pivotal in the creation of novel tools and approaches in neurobiology and pest control. Researchers have examined the role of neuropeptides in the mating behaviors of various insect species. Their findings have

revealed both conserved and species-specific mechanisms. While previous publications have addressed the role of neuropeptides in insect behavior, none has intensively and methodically examined their role in mating behaviors. In this review, we aim to provide an overview of how insects engage in mating behavior and how neuropeptides regulate them. We begin by highlighting the mating process, ranging from mate attraction, courtship rituals, and copulation to post-mating behaviors, with appropriate examples. Next, we review specific neuropeptides involved at each stage of the mating process with relevant examples as demonstrated in research, and we conclude by discussing applications in pest control. Lastly, we point out knowledge gaps with suggestions on the new directions for neuropeptide research.

2. How Insects Are Adapted to Mating Behavior

Insect mating encompasses mate attraction, courtship rituals, copulation, and post-mating behaviors (Figure 2).

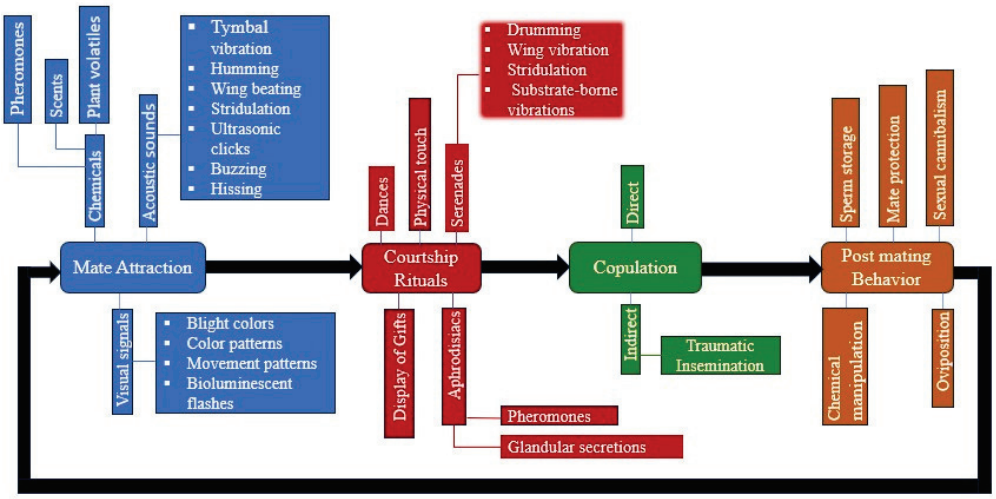


Figure 2. Insects exhibit a complex continuum of mating behaviors, encompassing mate attraction, courtship rituals, copulation, and post-mating activities. These behaviors are evolutionarily ingrained, uniquely adapted for survival, and vary across species. While some insects use chemical cues to attract mates, others utilize enticing songs. Some engage in intricate dances, while others present gifts to "sweep her off her feet". Created in BioRender. guo, j. (2025) https://BioRender.com/0lismvv (accessed on 28 April 2025).

2.1. Attraction of Mates

Insects utilize multimodal sensory cues, including chemical (pheromones), acoustic, and visual signals, to locate and attract mates.

2.1.1. Chemical Communication (Pheromones)

Insects utilize a variety of chemical signals to attract mates, with pheromones being particularly important for long-distance communication [5]. Female moths and butterflies release sex pheromones capable of attracting males from several kilometers away. The pheromones are released from specialized glands in the females, and males can detect them using highly sensitive antennae. Female silkworm moths (*Bombyx mori*) are known to release bombykol pheromone, a volatile 16-carbon alcohol to attract male mates [6], while female gypsy moths (*Lymantria dispar* (L.)) release a sex pheromone identified as (Z)-7,8-epoxy-2-methyloctadecane (synthetic; disparlure) [7]. Male monarch butterflies (*Danaus plexippus*) employ a unique strategy to attract females by producing specific scents. The specific scents are released by specialized

structures called hair-pencils located at the tip of the abdomen, and they are used to communicate the readiness and desirability of a mate [8]. The Colorado potato beetle (*Leptinotarsa decemlineata*) exhibits an intriguing chemical communication strategy by releasing both aggregation and sex pheromones. The male Colorado potato beetle produces an aggregation pheromone (S)-3,7-dimethyl-2-oxo-oct-6-ene-1,3-diol (also referred to as (S)-CPB I), which attracts both males and females to specific locations for feeding and mating activities [9]. Male Fruit flies emit pheromones to entice virgin females and other males to mate [10]. To attract females, the male fruit flies (*Drosophila melanogaster*) use cuticular hydrocarbons (CHCs) as a crucial part of mating behaviors, i.e., mate selection and female receptivity [11]. Queen honeybees (*Apis mellifera*) produce the queen mandibular pheromone (QMP), which attracts drones during the queen's mating flights [12]. German cockroach females (*Blattella germanica*) use volatile and contact sex pheromones to attract males. Pygidial glands of the females release the volatile pheromone called blattellaquinone, which can draw males in from a far distance [13,14]. Volatile pheromones are also employed by female Tsetse flies (*Glossina* spp.) to attract and select mates [15]. Methyl palmitoleate (MPO), methyl oleate, and methyl palmitate compounds are among the chemicals identified as responsible for promoting rapid mating behavior in male tsetse flies [15].

Plant volatiles play a significant role in the process of mate-finding in numerous insect species, including herbivores, pollinators, and parasitoids [16]. The release of these plant-derived volatiles from leaves, flowers, and fruits serves as rendezvous sites for mate-seeking insects and may elicit the release of pheromones. According to Xu and Turlings [16], certain insects can locate mates quickly and effectively by combining pheromones and plant volatiles. The aggregation pheromones released by female bark beetles (*Dendroctonus ponderosae*) draw males and females to appropriate host trees for feeding and mating. The trans-verbenol released by females (*D. ponderosae*) is very attractive to both sexes when combined with volatiles from the host tree [17,18].

2.1.2. Acoustic Signals (Sounds)

Some insect families and orders use acoustic signals to attract mates from long distances. Different mechanisms, including tymbal vibration, wing beating, and stridulation, are used to produce the sounds. Orthopterans, i.e., grasshoppers, crickets, and katydids, make sounds to attract mates. Male crickets (*Gryllus* spp.) and katydids (*Tettigonia viridissima*) stridulate or rub their forewings together to make seductive chirping species-specific songs to attract females over long distances [19]. Male grasshoppers also produce sounds by rubbing their hind legs against their wings to attract mates. Cicadas (Hemiptera: Cicadidae) use tymbals to produce loud mating call sounds [20]. Periodical cicadas (*Magicicada* spp.) and annual cicadas (*Tibicen* spp.) produce some of the loudest insect sounds. These sounds can be heard over long distances, which can be hundreds of meters [21]. Certain Coleopterans of the families Scarabaeidae (scarab beetles) and Cerambycidae (longhorn beetles) make sounds by tapping on objects or rubbing body parts together (stridulation) to attract mates. Both male and female longhorn beetles (Cerambycidae) produce sounds through stridulatory organs, which include a scraper on the pronotum and a file on the mesoscutum [22]. The humming sound produced by the wing vibrations of the female mosquitoes helps males locate the females for mating [23]. *D. melanogaster* males use wing vibrations to produce unique acoustic signals to attract females, with recent studies revealing up to three different patterns of acoustic songs [24]. The male tiger moths (*Bertholdia trigona*) utilize ultrasonic clicks to attract females and jam bat signals to avoid predation [25]. When digging from their underground nests to the soil surface, females of digger wasps (*Bembix rostrata*) and solitary bees (*Colletes cunicularius*) emit volatile odors and buzzing

sounds that serve as cues for patrolling males to estimate the approximate location of the digging virgin females [26]. To attract females, male Madagascar hissing cockroaches (*Gromphadorhina portentosa*) produce hissing sounds [27]. Moreover, features of the hisses vary on the dominant frequency, duration, and rate [27].

2.1.3. Visual Displays

Visual displays play a significant role in the mating behavior of certain insects. Bright colors, patterns, or particular movements are displayed to entice mates. In signaling males about their readiness to mate, the female firefly flashes its bioluminescent backside light to attract a suitable mate who responds by specific flash patterns [28]. Dragonflies and damselflies perform aerial acrobatics to attract mates. In calling and enticing females, male dragonflies (*Sympetrum* spp.) engage in flight displays [29]. The mating behavior of the rhinoceros beetle (*Xylotrupes gideon*) is characterized by aggressive male competition intertwined with specific displays to attract receptive females. To enhance their chances of mating, males show their power and desirability by using their horns to force competitors off branches or out of their territory [30]. Upon overcoming rivals, a successful male uses its horns to perform visual displays that may attract the female into mating with him [30]. Virgin mantis females, *Hierodula patellifera* (Dictyoptera: Mantidae), exhibit a characteristic calling posture [31]. To attract males, a female flexes the abdomen away from the wings and exposes the dorsal surface by curling it ventrally when holding the body beneath a branch or leaf with pumping movements accompanying the curling [31].

2.2. Courtship Rituals

Insect courtship entails elaborate behaviors designed to attract females, and these behaviors are species-specific. Courtship behaviors are numerous, entailing serenades, dances, physical touch, displays of gifts, and aphrodisiacs depending on the species [23].

2.2.1. Serenades

Serenades are vibrational songs or acoustic signals that insects produce to entice potential mates. Insects also use serenades to evaluate the quality of their mates and to coordinate mating habits [32]. Drumming, wing vibrations, substrate-borne vibrations, and stridulation are the forms of serenades [33–35]. Courtship behaviors of the silkworm moth (*B. mori*) are a complex interplay of olfactory cues and specific motor actions. Upon recognizing sex pheromones from a receptive female, the male silkworm moth (*B. mori*) flies towards the female and performs a series of courtship displays. Firstly, the male will produce a wing song by flapping their wings to enhance the auditory aspect of the courtship [36]. The male will then use its forelegs to touch or grasp the female's abdomen in attempted copulation, signaling an intention to mate [36]. Males of the house cricket (*A. domesticus*) call females from a distance through chirping (stridulation), which is performed by rubbing wings together. Each male has a distinctive way of advertising his presence and mating fitness by singing a unique courtship song [37]. At times, males may engage in singing rivalry where they want to outdo each other in singing to attract females. According to studies, females frequently base their partner selection on the wooing song's qualities, such as its length and output [37,38]. The courtship behavior of cicadas combines sound production, visual displays, and tactile interactions that vary in complexity and style [39]. Male cicadas use tymbals, which are unique drum-like structures on their abdomens, to make loud calls to attract females. The pattern of these calls and their intensity can draw in females from a distance and reveal a male's level of fitness [40]. Each species of cicada has a unique song to prevent cross-species mating. Some species, such as the periodical

cicadas (*Magicicada* spp.), can have thousands of males calling simultaneously in large choruses varying in duration and frequency [39]. Female cicadas do not sing but respond to calling males by using soft wing flicks and distinguishing calls from different males, normally preferring those with complex patterns and higher frequency [39]. Upon hearing the soft wing flicks, males adjust their courtship calls accordingly while moving closer to the receptive female. Males of some species of cicadas also engage in body movements and visual signals. Larger males with stronger calls are generally more attractive to females.

2.2.2. Dances

Courtship dances in insects feature complex motions, patterns, or displays intended to woo mates, show off physical prowess, or create pair bonds. The courtship behavior of the dragonfly (*Pachydiplax longipennis*) is a combination of aggressive pursuit and stunning aerial displays [41]. Courtship occurs both in-flight and while perched. Males actively search for receptive females and engage in aerial chase [41]. Chasing involves impressive flight displays that demonstrate agility and fitness. Upon successful reception by a female, the male will grasp the female to copulate [42]. The honeybee (*A. mellifera*) engages in courtship during nuptial flights. Queens mate during specific periods of their lives shortly after emerging as adults. To mate, drones gather in designated areas known as drone congregation areas (DCAs), where they perform aerial dances to attract virgin-receptive queens [43]. When a queen enters a DCA, she is competitively pursued by drones and impressed through flight dances. A successful drone mates with the queen but dies in the mating process due to the rupture of his genitalia, leaving his endophallus bearing the sperm inside the queen [43].

2.2.3. Physical Touch

Insects employ physical touch to assess potential mates, synchronize mating moods, and stimulate reproductive readiness [44]. This tactile communication can involve the antennae, legs, wings, or specialized body structures. The courtship behavior of the Japanese beetle (*P. japonica*) is defined by a mix of mating tactics, male competition, and specific rituals. The beetle displays promiscuous mating, where both males and females can mate with multiple partners in a phenomenon commonly referred to as "scramble competition" [45]. To gain access to females, males actively compete with one another through behavioral and physical contests, where larger males are more likely to succeed in taking receptive females [45]. Successful males engage in particular courtship activities, including tactile behavior, mounted courtship, and attentiveness to the female, to win mating acceptance [45,46]. The male German cockroach (*B. germanica*) combines the use of pheromones and tactile behaviors to court females. A male initiates courtship by following a female and coming up behind her, occasionally tapping her with their forelegs or antennae to stimulate her response [47]. Receptive females release contact sex pheromones that influence male behavior during courtship [48]. Males may also exhibit particular postures and motions that indicate their interest and preparedness for mating [49].

2.2.4. Display of Gifts

Certain male insects offer nuptial gifts to females during courtship or mating. Nuptial gifts can be in the form of food, body parts, or secretions from glands intended to attract females and maximize sperm transfer [50]. Increasing female receptivity, extending copulation, or improving reproductive output are some of the ways nuptial gifts enhance mating success. During mating, the male of some cricket and bush-cricket (Orthoptera; Ensifera) species gives the female an elaborate spermatophore containing spermatophylax (a nutrient-rich edible portion) to keep the female occupied while sperm transfer occurs [51].

Dance flies (Diptera: Empididae) exhibit complex mating behavior that involves offering nuptial gifts. This species' males court females by presenting them with prey items, which can influence the choice of mate and the success of copulation [52]. The likelihood of mating is frequently increased by the size of the gift [53].

2.2.5. Aphrodisiacs

To increase receptivity in a potential mate, certain male insects produce chemical compounds or other substances referred to as aphrodisiacs. Aphrodisiacs can be in the form of pheromones or glandular secretions. Studies have revealed that during courtship, male butterflies of different species release aphrodisiac compounds. The male of the queen butterfly (*Danaus gilippus*) produces an aphrodisiac secretion from the abdominal hair-pencils, which they apply in dusting potential mates via the female's antennae [34]. If the dusted female becomes receptive, the male again releases the compound to reinforce her readiness. Once she is fully prepared, they fly together to a suitable location to mate. Male *D. melanogaster* uses a mix of vibrational cues, sex pheromones, and visual signals to court females [54]. Males vibrate their wings to produce a courtship song, and they frequently tap the female's body with their forelegs to express their interest [54]. Moreover, the males release a pheromone to signal the females their readiness to mate [11].

2.3. Copulation

Copulation is the actual mating process that involves the transfer of sperm from the male to the female. The majority of species practice direct copulation, while in other species, copulation occurs through indirect means. Direct sperm transfer is the most common among species. In direct copulation, male insects transfer sperm into the female's reproductive tract through the aedeagus (equivalent to a penis) [55]. The sperm may be transferred directly to the spermatheca for storage or indirectly through a spermatophore [55]. During copulation, male beetles insert their aedeagus directly into the female's bursa copulatrix to transfer sperm cells [56]. In butterflies, copulation involves sperm transfer via a spermatophore from the male into the female genital tract. Some insects practice indirect copulation, which occurs without physical contact between sexes. The males of silverfish and springtail place a spermatophore on a surface, and the female later picks it up via her genital opening [57]. In bedbugs (*Cimex* spp.), copulation occurs via a unique technique known as traumatic insemination, in which the male injects sperm directly into the female's body cavity by piercing her abdomen with his aedeagus [58]. Traumatic insemination bypasses the conventional process of transferring sperm cells through the genital opening, and bedbugs' mating behavior lacks typical courtship rituals. Depending on the insect species, copulation can last anywhere from a few seconds to several hours. Several variables, including mate-guarding behavior, sperm competition, and nutrient transfer, may be the causes that affect the duration of copulation.

2.4. Post-Mating Behaviors

To maximize reproduction success, insects display a variety of post-mating activities after copulation. Sperm storage, mate protection, chemical manipulation, oviposition, and occasionally sexual cannibalism are examples of post-mating activities undertaken by various species of insects.

Some female insects store sperm in the spermatheca and use it over time to fertilize eggs. Honeybee (*A. mellifera*) queens can store and maintain the viability of sperm for many years, enabling them to fertilize thousands of eggs without needing to mate again [59]. Sperm selection and utilization processes in butterflies and moths enable females to control which male's sperm

fertilizes their eggs [60]. In certain species, males stay with the female after mating to prevent other males from mating with her. The male may guard the female physically or may engage in prolonged copulatory contact with her. Male dragonflies and damselflies remain attached to the female while she lays eggs to guard her from mating with other males [61]. Certain insect species create mating plugs inside the female reproductive tract to block reproduction with competitors. For example, in *D. melanogaster*, the male seminal fluid creates a mating plug inside the female bursa, preventing sperm entry or the female from remating [62]. Some insects employ sperm competition tactics to reduce reproduction success with rival males. Male damselflies (*Hemiphlebia mirabilis*), for example, use specialized structures to remove a rival's sperm from the female genitalia before depositing their own [63]. Certain male insects transfer chemical substances that affect female behavior, making her less interested in mating. A study by Denis and Claisse [64] revealed that male *D. melanogaster* produce proteins in their semen to suppress female receptivity and remating. Studies have also shown that due to some chemical compounds passed by the male, mated female butterflies and moths of polyandrous species frequently show a period of non-receptivity [65]. In certain species, the male is consumed by the female either during or after mating to supply nutrients for the generation of eggs. Female praying mantises (*Hierodula membranacea*) and spiders have been observed to consume their male companions during or after mating [66,67]. The primary concern of insects after mating is to place eggs in an area where they are not vulnerable to predators. Egg-laying techniques and patterns vary greatly and are unique among species, but typically, females lay their eggs in, on, or next to the juvenile stage's diet. For example, mosquitoes lay eggs in standing waters to enhance larval development time [68].

3. Role of Neuropeptides in the Mating Process

Insect behaviors, whether basic or complex, are regulated by neuropeptides [4].

3.1. Role in Choice of Mates, Attraction, and Courtship

Neuropeptides have been shown to affect receptivity, courtship displays, and mate appeal in insects. The various neuropeptides mediating these processes are discussed.

3.1.1. Effect on Receptivity

Pheromone Biosynthesis-Activating Neuropeptide (PBAN)

Pheromone biosynthesis-activating neuropeptide (PBAN) is crucial in mating behavior and is primarily found in lepidopteran insects (like moths). PBAN is specific to females and regulates the release of sex pheromones to attract mates [69,70]. It promotes calling behavior and receptive postures in female moths and ensures species-specific pheromone blends to avoid cross-species mating, thus promoting mating success [71]. PBAN is a 33-amino acid neuropeptide member of the PBAN/pyrokinin peptide family, which is distinguished by the conserved C-terminal motif of FXPRLamide, which is essential for its role [72]. PBAN is produced in the subesophageal ganglion (SEG) of the insect brain and released into the hemolymph through the neurosecretory cells [73]. PBAN neurons are found in the SEG and project to either the corpora allata or the corpora cardiaca, which are neurohemal organs. The signal transduction of sex pheromone synthesis is by PBAN acting on the pheromone gland epidermal cells located at the posterior abdomen of the female insect and binding to a G-protein coupled receptor (PBAN-R) on these cells [71]. The binding of PBAN to PBAN-R activates signaling cascades via an influx of extracellular Ca^{2+}, which stimulates enzymatic pathways that lead to sex pheromone biosynthesis [74]. PBAN neurons in the SEG are influenced by circadian signals. The release of PBAN is synchronized with the circadian clock, thus aligning sex pheromone production with the time of day when mating is likely to happen, usually during

scotophase [72]. The release of PBAN production significantly decreases after mating, which contributes to the loss of female receptivity [72]. Some studies have also shown that PBAN production is tied to the nutritional and hormonal states of the insect. For instance, the juvenile hormone (JH) upregulates PBAN expression [72,75]. Studies have also shown that PBAN sequences and functions in lepidopteran species are highly conserved despite divergence in pheromone chemical structures, suggesting strong evolutionary pressure to retain their function in mating behavior [76]. Male attraction is curtailed, and pheromone production is reduced or eliminated when PBAN or its receptor is knocked down. A study on *P. xylostella* found that RNAi of the PBAN receptor (Plx-PBANr) significantly reduced the biosynthesis of sex pheromones, resulting in a decrease in male attraction and a cessation of mating behavior [77]. Additionally, when the PBAN gene was edited via CRISPR/Cas9-mediated editing, females were found to be less attractive to males, which resulted in the disruption of mating activities. Similarly, in another study on the fall armyworm (*S. frugiperda*), females were found to be less attractive to males when the PBAN gene was altered using CRISPR/Cas9-mediated editing, which also disrupted mating activities [78].

Tachykinin-Related Peptides (TRPs)

Tachykinin-related peptides (TRPs) are a family of neuropeptides found in invertebrates. Functionally and structurally, TRPs are analogous to the vertebrate tachykinins. TRPs are produced in the CNS (brain regions, thoracic ganglia, and abdominal ganglia) and peripheral tissues and are characterized by a conserved motif, C-terminal pentapeptide FX_1GX_2Ramide [79, 80]. In locusts (*Locusta migratoria*) and cockroaches (*Leucophaea maderae*), midgut endocrine cells additionally secrete TRPs as circulating hormones [81,82]. TRPs are multifunctional, modulating locomotion, aggression, feeding, circadian cycles, and, most importantly, sexual behavior. In crickets, TRPs initiate mating calls and modulate sex pheromone release [83]. Studies have demonstrated the role of TRPs in suppressing insect courtship. In fruit flies (*D. melanogaster*) females, TRPs released from a cluster of eight to ten cells located in the *c929*-labeled SEZ region within the subesophageal zone regulate the detection of gustatory pheromone required in the suppression of pheromone-triggered courtship [84]. TRPs also induce the release of adipokinetic hormone (AKH) from the corpora cardiaca in locusts [82]. AKH is critical in mobilizing lipids, carbohydrates, and proline from stores during energy-demanding activities like mating [85]. TRPs specifically interact with a subfamily of structurally related G protein-coupled receptors to produce biological effects [80]. In *D. melanogaster*, the signaling pathway involves TRPs binding to Tachykinin Receptor 86C (TkR86C). TkR86C activation triggers G-protein-coupled signaling, which in turn activates phospholipase C (PLC), raises intracellular Ca^{2+} and second messengers like Inositol trisphosphate (IP_3), and modulates ion channels and neurotransmitter release. The changes trigger neuronal excitability downstream, influencing behavioral decisions. TRPs are widely conserved in insects, including cockroaches, ants, locusts, flies, beetles, and moths. The FX_1GX_2Ramide signature is conserved in all the insect TRPs [79]. Consequently, reproductive strategies could differ, but the TRP neuromodulatory system in many insects remains functionally conserved.

Natalisin (NTL)

Natalisin (NTL) is unique to insects and crustaceans and is a member of the tachykinin-like peptide superfamily that modulates insect reproduction and sexual behavior [49]. It is named NTL because of its significant role in natal functions, especially mating and reproduction. Like TRPs, NTL also has a conserved C-terminal motif FxGxRamide but differs in certain specific sequence features. NTL is highly expressed in mature adults because of its role in mating and is produced within the central nervous system, particularly in the brain, ventral nerve cord, and

the SEG [49,86]. The expressing neurons of NTL are located in the neuromodulatory centers of the insect brain, pars intercerebralis, SEZ, and abdominal ganglia. NTL has been shown to modulate receptivity. In a study, when NTL was silenced in both males and females of *S. frugiperda* via RNAi, a significant reduction in sexual activities was observed, attributable to the reduced calling rate of females and the declined courtship rate of males [49]. Besides promoting receptivity, NTL modulates fecundity. In a study, fecundity was significantly reduced upon NTL knockdown on *T. castaneum* [87]. NTL's transduction signal is via a specific GPCR-natalisin receptor (NTLR) [87]. The binding of NTL to NTLR triggers G-protein-coupled signaling, which triggers changes in Ca^{2+} mobilization, cAMP levels, and MAPK (Mitogen-Activated Protein Kinase) pathway activation. The changes in these pathways influence neuronal excitability and hormonal regulation, resulting in changes in behavior. NTL and its function of promoting mating behavior are highly conserved in insects and crustaceans, implying that it could be an arthropod-only survival innovation. The fact that RNAi silencing of NTL or its receptor consistently results in impaired mating behavior across several insect orders suggests that there is a strong evolutionary selection to keep its function.

3.1.2. Courtship Rituals

Neuropeptide F (NPF)

Neuropeptide F (NPF) is a key neuropeptide in insects that plays a significant role in sexual behavior and reproduction. NPF is an insect homolog of vertebrate neuropeptide Y, produced in the CNS, particularly the brain and the ventral nerve cord [3,88]. The pars intercerebralis, lateral protocerebrum, and mushroom body output neurons (MBONs) are a particular subset of neurons in the brain and ventral nerve cord that express NPF. NPF is short, conserved, and characterized by a C-terminal end with an RPRFamide motif and regulates a variety of neuromodulatory functions, including feeding, stress management, and sexual behavior [89]. NPF affects courtship intensity and sexual drive in *D. melanogaster*, especially in males [90]. Even when deterrents are present, males of *D. melanogaster* with higher NPF levels exhibit improved courtship and a greater desire to mate. In a study on desert locusts (*Schistocerca gregaria*), NPF was also observed to promote courtship, among other physiological behaviors [91]. When given daily injections of trNPF, the adult males showed courtship behavior earlier, whereas RNAi knockdown of the Schgr-NPF precursor transcript prevented or postponed the courtship behavior [91]. NPF and PDF neurons work together to promote prolonged mating duration in male *D. melanogaster* [92]. In a study, the males were also observed to extend their mating period when other males were present, a phenomenon called rival-induced longer mating duration (LMD). The signaling of NPF and PDF with their receptors was critical for LMD to occur [92]. The mechanistic aspects of NPF entail particular biochemical interactions through its G-protein-coupled receptor, NPFR1 [89]. When NPF binds to NPFR1, adenylate cyclase is inhibited, lowering cyclic adenosine monophosphate (cAMP) levels, which in turn affect downstream effectors, causing neuronal excitability and behavioral expression. This NPF-NPFR signaling axis is lauded as one of the most functionally and structurally conserved neuropeptide systems in invertebrates [93].

Diuretic Hormone 31 (DH 31)

Similar in structure and function to vertebrate calcitonin gene-related peptide (CGRP), Diuretic Hormone 31 (DH31) is a 31-amino acid peptide with a highly conserved C-terminal amide group. DH31 traditionally regulates water balance, but recent studies show that DH31 mediates mating and reproduction behaviors [94]. In a study, DH31 was identified as key in promoting the transition of male *D. melanogaster* from feeding to courtship [95]. In males that

were starving, it was observed that feeding took precedence over courtship. However, the order quickly reversed within a few minutes when the males consumed protein-rich foods. DH31 was found to be responsible for the molecular mechanism behind the transition from feeding to courtship. Besides, DH31 also plays a key role in triggering reproductive dormancy during unfavorable conditions, and during this period, egg development is halted. In a study on the female *D. melanogaster*, low temperatures and short days caused reproductive dormancy by reducing the production of juvenile hormone (JH) in the corpus allatum (CA), an action mediated by DH31 [96]. DH31 is expressed in the small and large lateral ventral neurons of the circadian clock circuit, the ventral nerve cord, the enteric ganglia, and the male accessory gland-innervating neurons. The molecular mechanism of DH31 involves binding to its receptor DH31-R, a G-protein-coupled receptor [94]. DH31-R activation increases intracellular cAMP, and the downstream effects of the cAMP-PKA cascade lead to neuronal excitability in clock neurons, visceral muscles, and the sensory processing centers, resulting in behavioral expression. DH31 has been seen to be conserved across insects, with its homolog peptides characterized in nematodes and vertebrates. Functionally, DH31 is evolutionarily deeply conserved to modulate reward signaling, circadian timing of mating, and sexual satiety to inhibit remating [94].

Proctolin (Proc)

Proctolin (Proc) was first characterized in the American cockroach (*Periplaneta americana*) in the 1970s and is a pentapeptide with the Arg-Tyr-Leu-Pro-Thr sequence [97,98]. It is unique to the arthropods, though together with its receptor, it is absent in the genomes of Hymenopterans, Lepidopterans, and the yellow fever mosquito (*Aedes aegypti*) [97,99]. The primary role of Proc in arthropods is to control muscle movements, enhance gut motility and sexual behavior, and act both as a neurotransmitter, neuromodulator, and hormone [97,100–102]. In locusts, Proc also serves as a releasing factor of juvenile hormone (JH) and adipokinetic hormone (AKH) [99], which are critical in the mating process. In addition, studies also suggest that Proc modulates fecundity. The ovipositor muscles of the female tobacco hornworm (*Manduca sexta*) were shown to contain Proc, suggesting its role in promoting egg-laying [103]. Similarly, a study on locusts demonstrated the role of Proc in improving muscle contractions that are pivotal in sustaining the oviposition digging rhythm in locusts [104]. Copulation also requires meticulous coordination of muscle movements enabled through proctolin [97]. Proc is produced in the central nervous system, including the brain and ventral ganglia, and is widely expressed in the visceral and skeletal muscles, including the reproductive tissues [105,106]. To execute its function, Proc binds to its receptor ProcR, which is a GPCR. ProcR activates the phospholipase C pathway and protein kinase C, which increases IP_3, diacylglycerol (DAG), and intracellular Ca^{2+}, leading to increased muscle contraction, neuron excitability, and behavior expression [98,107]. In a study, the injection of phorbol ester into the Proc-sensitive neural sites of the male grasshopper (*Chorthippus biguttulus)* triggered courtship singing [98]. The finding suggests its role in insect courtship in addition to the modulation of mating. In the male kissing bug (*Rhodnius prolixus*), Proc causes muscle contractions of reproductive structures, which facilitate the transfer of seminal fluid and sperm ejaculation during copulation [108]. Proc occurs across many insect orders, with structurally similar peptides occurring in some members of crustaceans (lobsters and crabs) and myriapods (centipedes). However, Proc appears to be an evolutionary innovation of the invertebrates performing analogous functions like oxytocin in the vertebrates.

SIFamide (SIFa)

SIFamide (SIFa) is a highly conserved neuropeptide in arthropods, secreted by the CNS specifically in four highly specialized neurons, pars intercerebralis (PI) of the brain, with its axons projecting into the mushroom body, lateral protocerebrum, and the central

complex [109,110]. It comprises four conserved amino acids at its C-terminal end, thus its name SIFamide (Ser-Ile-Phe-NH_2). It is precise and powerful in modulating sexual behavior, feeding, sleep, and circadian rhythms in insects [109,111,112]. The signaling pathway of SIFa involves binding with its receptors (SIFR), which is a GPCR. SIFR activation initiates the Gq signaling pathway, which stimulates the increase in cAMP levels, IP_3, DAG, and intracellular Ca^{2+}, leading to neuronal excitability, synaptic plasticity, and behavior expression [110]. SIFa affects pheromone detection and sexual attraction in fruit flies (*D. melanogaster*), which in turn affects male courtship behavior [113]. When SIFa is knocked down, males that lack SIFa or its receptor exhibit bisexual tendencies, implying that SIFa is essential for distinguishing appropriate mates [113]. In addition, males also exhibit male-to-male courtship behavior if neurons carrying a SIFaR-gal4 transgene express SIFamide receptor RNAi or are destroyed by the apoptotic protein reaper [113]. SIFa is also essential for integrating several internal and external cues to coordinate multiple tasks, including mating duration [114,115]. For instance, in *D. melanogaster*, SIFa neurons and sNPF neurons work together in a feedback loop to modify behaviors like shorter mating duration (SMD) and longer mating duration (LMD) [114,115]. Mating duration is shortened in males when SIFa neurons are activated [115]. SIFa is extremely conserved among many species of arthropods, and the evolutionary strategy to deploy a small number of neurons to modulate broad behavioral outcomes points to the crucial role of the neuropeptide [109].

Orcokinin (OK)

First identified in the crustacean *Orconectes limosus* (thus the name), OKs are a family of myotropic neuropeptides that have more recently been found in insects, arachnids, and annelids [116]. OK genes produce two distinct mature peptides, orcokinin-A (OK-A) and orcokinin-B (OK-B); however, OK-A is generally longer than OK-B. OK are characterized by a conserved N-terminal Asn-Phe-Asp (NFD) sequence. They are produced in the CNS and the midgut and modulate a variety of physiological processes, including ecdysteroidogenesis, locomotion, and reproduction [116,117]. OK is expressed in the abdominal ganglia, brain-optic lobe interface, neurosecretory cells, and the enteric nervous system. The signaling mechanism of OK is not well understood but is presumed to be through GPCRs coupled with Ca^{2+} signaling pathways. OK is confirmed as essential in the courtship behavior of insects. In a study, male-to-male courtship, which is even uncommon in the wild *D. melanogaster*, was shown to be rampant when the OK gene was knocked down via RNAi [117]. Besides its role in courtship, OK promotes fecundity by regulating vitellogenin transcription, as observed in the cockroach (*B. germanica*) [118]. Similarly, silencing the OK gene in female *D. melanogaster* decreases egg production [117]. The evolutionary conservation of OK across various invertebrates points to its significance in mediating physiological functions.

Leucokinin (LK)

Leucokinins (LKs) are tiny neuropeptides initially characterized in cockroaches (*Leucophaea maderae*) [119]. LKs are found in many insect orders and are distinguished by the highly conserved C-terminal pentapeptide motif, FXSWGamide. LKs are produced in the lateral horn (projecting to the mushroom body and protocerebrum), subesophageal zone (SEZ), and the ventral nerve cord (CNC) and expressed in the Malpighian tubules. Its signaling mechanism entails LK binding to Leucokinin Receptor (LKR), a GPCR, which initiates the Gq signaling pathway, which stimulates the increase in IP_3 and intracellular Ca^{2+}, leading to neuronal excitability and behavior depending on the state [120]. In dehydration or starvation, LK inhibits mating to conserve energy, while in hydrated and fed

states, LK enhances arousal to encourage mating behavior. They are multifunctional, modulating various physiological processes and behaviors in insects and other invertebrates. LK neurons in *D. melanogaster* regulate water homeostasis, feeding, sleep, metabolism, and memory formation [119,121]. LK is an essential modulator of the balance between a courtship touch and defense against body contact [122,123]. When a male courted virgin females in a study on *D. melanogaster*, the females' defensive response to stimuli was compromised; however, after mating, the response improved. The study revealed that the switch between defensive reaction and receptivity to a courtship touch is mediated by the activation of uterine neurons, which consequently activate an LK-dependent pathway [122]. Across insect orders, LK is conserved, and the C-terminal motif (FXSWGamide) is nearly constant, suggesting a strong evolutionary selection due to its vital function in modulating homeostasis and behavior.

3.1.3. Mate Appeal

Pigment-Dispersing Factor (PDF)

The pigment dispersing factor (PDF) is a highly conserved 18-amino-acid, α-amidated neuropeptide [124]. PDF is essential for the modulation of numerous physiological processes, including circadian rhythms, locomotor activity, courtship behavior, and the production of male sex pheromones [92,125,126]. PDF's role in modulating circadian timekeeping is well studied and understood. However, it is shown that PDF affects sex pheromone biosynthesis and mating behavior, aligning it with the circadian clock. In a study by Krupp and Billeter [127] on *D. melanogaster*, it was revealed that disruption of the PDF signaling pathway reduced male sex pheromone production, consequently affecting mate appeal. For insects that mate at certain peak times, for instance, at dawn or dusk, PDF sets this behavioral timing for maximized reproduction success. PDF is also necessary for the copulation process by enabling the critical coordination of muscles necessary for the successful transfer of sperm cells. PDF is produced in the CNS, particularly in the small and large ventrolateral neurons of the brain projecting to the dorsal protocerebrum, mushroom bodies, and neuroendocrine centers. Its signaling mechanism involves the PDF receptor (PDFR), a class B GPCR [128]. When PDF binds to PDFR, it triggers the increase in cAMP, which activates PKA (protein Kinase A), which also triggers the CREB (cAMP Response Element-Binding protein) pathway to modulate circadian clock genes, ion channel activities and mating-related channels [128]. Depending on the time of the day, the CREB pathway may signal sexual receptivity, discrimination of a mate, or the release of JH or Ecdysis Triggering Hormone (ETH) hormones. PDF sequence and its receptor architecture are strongly conserved in many insect orders and crustaceans, suggesting its vital role in circadian and behavioral integration for the reproduction and perpetuation of species.

3.2. Role in Copulation

3.2.1. Adipokinetic Hormone (AKH)

Adipokinetic hormone (AKH) is a neuropeptide critical in the energy mobilization in insects and is dubbed a "hormone of all seasons" [129]. Structurally, it is a small peptide comprising 8–10 amino acids. Functionally similar to vertebrates' glucagon, AKH mobilizes energy stores during high metabolic demand, like flight, starvation, or reproduction activities such as copulation. Critically, mating requires the mobilization of energy stores, which is triggered by AKH [85]. AKH is produced from special neurons found in the corpora cardiaca, and its secretion is triggered by nutritional status, circadian rhythms, and environmental stress [129]. It is expressed in the fat body and various neurons [130].

AKH functions by binding to its receptor, AKHR, a GPCR that triggers the Gq pathway to mobilize energy substrates such as lipids [131]. The Gq pathway mediates the activation of phospholipase C (PLC), which cleaves PIP2 into IP_3, which induces Ca^{2+} release, and DAG, which activates PKC. Ca^{2+} and PKC stimulate energy mobilization. Moreover, AKHR triggers cAMP/PKA signaling via the Gs pathway, leading to lipase activation. AKH is conserved across arthropods and bears structural similarity with the gonadotropin-releasing hormone (GnRH) in vertebrates, suggesting a shared ancestry.

3.2.2. Corazonin (Crz)

Corazonin (Crz) is an 11-amino-acid neuropeptide occurring in arthropods [132]. It is a homolog of the mammalian Gonadotropin-Releasing Hormone (GnRH) produced in the CNS, specifically in the neurosecretory cells of the brain and ventral nerve cord [132]. The Crz neurons are expressed in the pars lateralis, lateral protocerebrum, median neurosecretory cells, and abdominal ganglia, projecting into centers of sexual behavior, hormone production, and motor and courtship centers of the ventral nerve cord. Crz is highly conserved, regulating a diversity of physiological roles, including sexual drive. Studies have shown that Crz modulates the duration of copulation, ejaculation, and reward behaviors [132,133]. Crz binds to a G-protein-coupled receptor (CRZR), which is a rhodopsin-like GPCR [134]. CRZR triggers the Gq proteins signaling pathway, which activates phospholipase C (PLC), resulting in intracellular accumulation of Ca^{2+} mobilization, consequently triggering the PKC (Protein Kinase C) pathway, which initiates behavior change expression [134]. Crz interacts with hormones, including JH and ecdysone, to modulate behavior. Crz is highly conserved across insects, with the pQTFQYSRGWTNamide core being maintained across species, suggesting its functional importance.

3.2.3. Short Neuropeptide F (sNPF)

Short neuropeptide F (sNPF) is a versatile neurohormone regulating several insect physiological functions, including feeding, reproduction, development, and circadian rhythms [3,135]. sNPF is generated in the CNS, primarily in the brain and ventral nerve cord, released by specific interneurons and neurosecretory cells, and widely expressed in the olfactory processing centers, mushroom bodies, lateral protocerebrum, and the abdominal ganglia [136,137]. Crucial for its functions, sNPF has a C-terminal motif (X-X-X-X-RFamide) with a highly conserved amidated RF. sNPF occurs in a wide range of species, and its precursor molecule can have anywhere from one to four isoforms [135]. To function, sNPF binds to its G-protein-coupled receptor (sNPFR). Typically, sNPFR activates the Gq signaling pathway, which activates PLC/IP3/Ca^{2+} cascades, leading to downstream behavior decisions. However, sNPFR may also activate the Gi/o protein pathway, which inhibits cAMP production and downregulation of PKA while regulating ion channels and other effectors responsible for behavior change. Moreover, the sNPF signaling pathway involves interactions with other neuropeptides and hormonal pathways, including PDFs, SIFa, ILPs, JH, and ecdysteroids, to regulate various physiological processes [135]. sNPF is key in modulating sex drive, copulatory persistence, and sexual satiety. Male *D.melanogaster* exhibit a shorter mating duration based on sexual satiety, a phenomenon referred to as shorter mating duration (SMD) that is dependent on sNPF signaling [138]. The structural motif RFamide of sNPF is evolutionarily conserved in coleopterans, dipterans, hymenopterans, and hemipterans, pointing to its critical modulatory role.

3.3. Role in Post-Mating Behaviors

Neuropeptides play a role in controlling the reproductive physiology and behavior of females after mating, including oviposition and decreased susceptibility to remating. Peptides transferred in the seminal fluid cause post-mating responses (PMR) in many female insects, including a sharp rise in egg-laying and a decrease in mating receptivity [139].

3.3.1. Sex Peptide (SP)

Sex Peptide (SP) is a small 36-amino-acid peptide found in *D. melanogaster*. It is produced in the male accessory glands and transferred from males to females via seminal fluid during copulation to inhibit remating as PMR and to stimulate a switch from mating to feeding and oviposition [85,140–143]. After mating, SP triggers an array of behavioral, physiological, and hormonal changes and is widely expressed in the female reproductive tract, specific sensory neurons, and central brain circuits. SP exerts its effects through multiple pathways, including its receptor, SPR, and interaction with other pathways. SP may elicit short or long PMR (also called "sperm effect") in female *D. melanogaster*, depending on the availability of sperm [139]. For sperm retention in storage, SP binds to a sperm cell with its C-terminal end and is gradually released by cleavage at the trypsin cleavage site inside the female reproductive tract, thus initiating or prolonging PMR [139]. SPR (GPCR receptor) activation may trigger the Gi/o signaling pathway that mediates the inhibition of cAMP and downregulation of PKA, leading to downstream changes in gene expression [144]. Inside the female uterus (uterine epithelium), SP may also bind to SPR on the sex peptide sensory neurons (SPSNs) that project into the abdominal ganglion and the brain, leading to the alternation of NPF, octopamine, and ILP signaling, resulting in behavior change, hormonal modulation, and egg maturation. SPR receptor structure and PMR pathway are highly conserved across *D. melanogaster* species, suggesting a strong evolutionary pressure geared towards maintaining its role in reproduction.

3.3.2. Diuretic Hormones (DH44)

Diuretic hormone DH44 is structurally composed of 44 amino acids, is homologous to vertebrate Corticotropin-Releasing Factor (CRF), and is central to modulating body fluid homeostasis, metabolic processes, and sleep–wake cycles (circadian rhythms), including reproduction and mating behaviors [94,145]. It is widely studied in *D. melanogaster*; however, its homologs occur in a range of other insect orders. DH44 modulates oviposition and fluid regulation in reproductive tissues, particularly coordinating with SP and JH to regulate fluid homeostasis during oviposition. The DH 44 neuronal circuit comprises six neurosecretory cells in the pars intercerebralis projecting to the corpus cardiacum, ventral nerve cord, and abdominal ganglia. It is released from median neurosecretory cells (MNCs) in the brain and acts on malpighian tubules, gut, and brain centers to exert its functions [145]. Its mechanistic aspects involve two receptors, DH44-R1 and DH44-R2. Both are GPCRs, but they differ in expression patterns [146]. When DH44 binds to its receptor, it triggers the Gs pathway, which leads to an increase in cAMP, which activates the PKA pathway, consequently stirring downstream effects [145]. In some tissues, DH44 may bind to its receptor, triggering Gq pathway, which leads to Ca^{2+} accumulation that activates the PKC pathway and stirs downstream effects. However, it is not known how DH44 interacts with sex-specific circuits to modulate post-mating behaviors. In female *D. melanogaster*, DH44 influences the ejection and storage of sperm in the uterus [146]. In a study, it was observed that in 1–6 h, female *D. melanogaster* ejected male ejaculates from the uterus, and the action was controlled by a brain-signaling system made up of DH44. It was further observed that whereas DH44 signal enhancement delayed sperm expulsion, DH44 signal suppression

in the brain accelerated sperm ejection from the uterus, leading to a significant drop in sperm in the storage organs, thus lowering fecundity [146]. DH 44 and its receptors are conserved across insect orders, including Diptera, Coleoptera, Hemiptera, and Lepidoptera, indicating a strong evolutionary pressure to maintain the tradeoff between reproduction and survival in insects.

3.3.3. Insulin-like Peptides (ILPs)

Insulin-like peptides (ILPs) are essential for insect metabolism, development, reproduction, and aging [147]. They function through a conserved insulin signaling mechanism and influence several physiological processes (oogenesis, ovulation, and sperm storage) necessary for egg production [148–151]. ILPs are analogous to vertebrate insulin and insulin-like growth factors (IGFs) both structurally and functionally. ILPs are produced in the insulin-producing cells (IPCs) located in the pars intercerebralis and project to mushroom bodies, GnRH-like centers, and circadian centers [152]. ILP binds to its receptor (InR) to activate downstream signaling cascades, including PI3K/Akt (Phosphoinositide 3-Kinase/Protein Kinase B), MAPK, and TOR pathways that are responsible for promoting different responses [152]. ILP signaling also interacts with endocrine factors, including JH, AKH, and ecdysteroids, to exert its function [152]. To ascertain ILPs' functions, a study by Chen and Dou [153] revealed that ILPs interacting with ovary ecdysteroidogenic hormone (OEH) promoted egg development and food storage in *Aedes aegypti* mosquitoes. Similarly, injecting bovine insulin into female adults of green lacewing (*Chrysopa septempunctata*) resulted in increased protease activity, ovarian development, Vg protein abundance, and elevated reproductive performance [147]. ILPs, together with tyrosine kinase receptor (InR), are highly conserved across insects, crustaceans, nematodes, and vertebrates, with conserved downstream signaling cascades pointing to evolutionary pressure to maintain their role for survival.

3.3.4. Ion Transport Peptide (ITP)

Ion transport peptide (ITP) and its variant ITP-like (ITPL) have a variety of functions in the physiology of insects and crustaceans, including osmotic balance, feeding, and reproductive physiology [154,155]. In a study on mosquitoes (*A. aegypti*), the knockdown of ITP and ITPL led to a decrease in blood feeding, egg laying, and egg viability, indicating their significance in reproductive physiology and behavior [156]. Similarly, a knockdown of ITP in the female adults of the red flour beetle (*T. castaneum*) was shown to cause a decrease in egg production [157]. ITP is secreted in the median neurosecretory cells in the brain and projects to neurohemal organs, e.g., corpora cardiaca, digestive tract, Malpighian tubules, and the reproductive tissues. To exert its function, ITP binds to corticotropin-releasing factor (CRF)-like receptor, a Class B1 family of GPCRs. For instance, in locusts, ITP binds to ITPR to trigger the increase in cAMP/PKA, consequently activating ion transporters downstream, targeting V-ATPase for ion secretion in the Malpighian tubules and Na^+/K^+-ATPase to maintain electrochemical gradients [158]. During stress-induced diuresis, ITP also synergizes with DH44 to stabilize osmotic balance, and during favorable conditions, it also synergizes with AKH to streamline reproductive behavior [155]. ITP is widely and functionally conserved in insects for osmoregulation and reproductive support.

3.3.5. Sulfakinin (SK)

Sulfakinin (SK) is primarily found in insects but is analogous to cholecystokinin (CCK) in vertebrates, both in structure and function [159]. SKs are highly conserved with a characteristic C-terminal tyrosine residue (Y(SO_3H)) and FMRFamide heptapeptide core [160]. It exists in two

primary forms, short sulfakinin (sSK) and long sulfakinin (lSK), which differ in their peptide lengths. The key function of SK is to regulate feeding and digestion in insects [160]. Upon mating, insects switch into foraging mode to find food to enhance their survival. The switching from mating to foraging is mediated by SK [123,161]. In a study, the Oriental fruit flies (*B. dorsalis*) were shown to suppress their response to opposite-sex pheromones while increasing their sensitivity to food odors. Even though the flies (*B. dorsalis*) were starved, their antennal responses changed to mating mode when the gene encoding SK receptor 1 (SkR1) was knocked out, suggesting that SkR1 suppressed mating but promoted foraging [161]. Similarly, SK was found to suppress mating behavior in *D. melanogaster* through its receptor CCKLR-17D3 [123,162]. SK is produced in the CNS, particularly the brain, and expressed in the various parts of the CNS and peripheral tissues, including the midgut and fat body. In *D. melanogaster*, SK is expressed in a small number of SK-expressing neurons (SKNs) in the subesophageal zone (SEZ) and pars intercerebralis [159]. The modulation function of SK is mediated through the G-protein-coupled receptor signaling system. SK binds to the GCPRs, SKR1 and SKR2, the two types that occur in *D. melanogaster*. Binding activates the Gq signaling pathway downstream, which triggers PLC/IP_3/Ca^{2+} second messenger pathways, consequently affecting behavioral expression [160]. In some other contexts, the Gq signaling pathway triggers the cAMP/PKA second messenger pathway [161]. SK is widely conserved in insects, with its presence in coleopterans, hemipterans, dipterans, orthopterans, and hymenopterans, striking a parallel function with its homology CCK in vertebrates [160]. Its role of trading mating to feeding points to an evolution strategy that prioritizes survival over reproduction during unfavorable conditions.

4. Discussion of Findings

Insect mating is a continuum of behaviors that range from mate attraction and courtship rituals to copulation and post-mating actions. The complex behaviors vary amongst species, propelled by an intricate underlying neuropeptidergic mechanism. Insects possess a variety of neuropeptides that drive the mating process. Whether it is the release of sex pheromones by moths, the stunning courtship displays of dragonflies, the beautiful melodies of cicadas and crickets, the amazing indirect copulation of springtails, or the prolonged copulatory contact of damselflies, these diverse mating behaviors are all modulated by the neuropeptides. In this review, we highlight 18 neuropeptides that we found to influence behavior in the different stages of insect mating, as elaborated in Figure 3.

As demonstrated (Figure 3), some neuropeptides are multifunctional, while others are specific. For instance, NTL influences mate attraction and courtship in the fall armyworm (*S. frugiperda*) and increases mating appetite in the oriental fruit fly (*B. dorsalis*) and egg-laying in the red flour beetle (*T. castaneum).* Hence, it is the most versatile neuropeptide [49,163], unlike PBAN, which regulates the production of sex pheromones in moths only [70].

Most neuropeptides are produced in the CNS, primarily the brain and the ventral nerve cord. However, some neuropeptides, for instance, TRP, can be released as a circulating hormone from midgut endocrine cells of locusts and cockroaches during fight or flight stress [82]. SP is also produced in the male accessory glands and delivered into the female reproductive system, while AKH is partly produced in the corpus cardiacum (CC). Neuropeptides execute their regulatory functions through the G protein-coupled receptor (GPCR) signaling pathway, which comprises receptors (GPCRs), heterotrimeric G proteins, downstream effectors, and messengers, as shown in Figure 4.

Heterotrimeric G Proteins are the Guanine nucleotide-binding proteins Gα, Gβ, and Gγ subunits. Insects, however, largely utilize Gα in the signaling process comprising Gs, Gi/o, and Gq subunits, as shown in the illustration (Figure 4). The subunits activate downstream effectors, including Adenylate Cyclase (AC) and Phospholipase C (PLC). However, unlike

other neuropeptides using the Gq pathway, ILPs utilize P13K as the downstream effector. The messengers in the Gq pathway comprise cAMP, which activates Protein Kinase A (PKA), and Ca^{2+} and DAG, which activate Protein Kinase C (PKC). As shown, the majority of the neuropeptides reviewed in our work exploit the Gq signaling pathway; however, NTL is capable of exploiting any of the three pathways, possibly the reason behind the ability to mediate more than one activity in the insect mating process. Neuropeptides activate signaling pathways that cause changes in neuronal activity, while others regulate the production of hormones responsible for a certain physiological function [135]. TRPs induce the release of AKH in locusts, while PBAN induces the production of sex pheromones in moths [70,82]. In certain situations, neuropeptides work together to modulate a certain function. For instance, SIFa and sNPF neurons work together in a signaling mechanism that modulates the mating duration to modify behaviors like SMD and LMD.

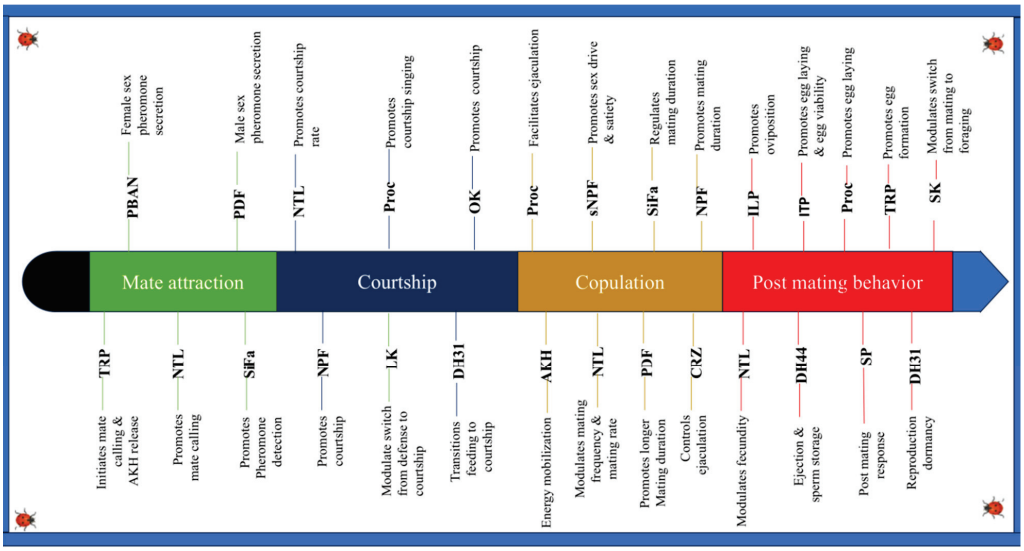


Figure 3. Neuropeptides play a crucial role in driving insect mating behaviors. Without TRPs, the distinctive, loud chorus of cicadas—heralding the start of summer—might be absent from nature. Similarly, without AKH, which mobilizes energy reserves for mating, many insect species could have faced extinction by now. Created in BioRender. guo, j. (2025) https://BioRender.com/hggt62j (accessed on 28 April 2025).

To modulate some mating behaviors, neuropeptides work with other systems, including the endocrine system [164]. In female *D. melanogaster*, DH31 suppresses the production of JH, triggering reproductive dormancy when conditions are not favorable [96]. Reproductive dormancy is critical in prioritizing feeding over reproduction for enhanced survival. In addition, ILPs, in conjunction with JH and ecdysteroids, influence physiological processes like oogenesis, ovulation, and sperm storage that are necessary for egg production [150]. Based on such interactions, the neuropeptide signaling systems on physiological processes can be interrupted to form suitable targets for sustainable pest management tools.

In response to the varied and sometimes fluctuating ecological environments, insects evolve to maximize reproductive and survival success. Pressures, including mate competition, predation, harsh environments, limited resources, and reproductive methods, all influence these evolutionary adaptations. Neuropeptides play a critical role in maintaining critical functions necessary for survival and the perpetuation of species. The neuropeptides reviewed in our work consistently show conserved motifs in their structures responsible for certain behaviors. For instance, the C-terminal motif of FXPRLamide in PBAN is structurally conserved in the lepidopteran females to maintain its mate attraction function across the species [72].

Although their processes, effects, and evolutionary adaptations differ greatly, insect neuropeptides play similar roles as other neuropeptides, including their homologs in vertebrates. For instance, in *D. melanogaster*, SP is essential in modulating post-mating behaviors by discouraging females from remating and promoting transition into oviposition [139]. In long-term relationships, neuropeptides such as vasopressin and oxytocin control sexual receptivity and pair bonding in higher animals [165].

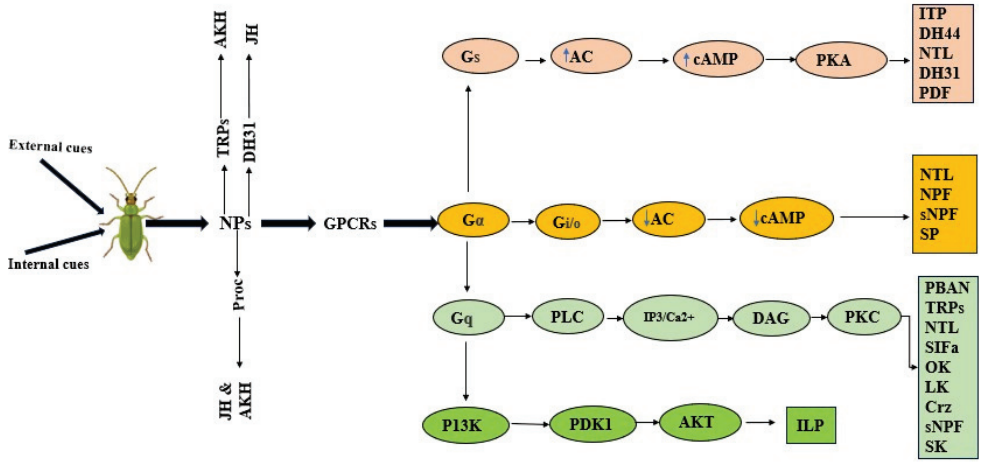


Figure 4. The illustration shows the GPCR signaling pathway exploited by neuropeptides in insects to transmit signals regulating various physiological processes, including the mating behaviors. Neuropeptides are triggered by internal or external cues, and they act either by binding to the GPCRs, triggering heterotrimeric G protein signaling pathways and downstream effectors that cause behavioral expression or via the endocrine system to trigger hormonal responses for regulating specific behavior. Created in BioRender. guo, j. (2025) https://BioRender.com/jnf64vj (accessed on 28 April 2025).

5. Conclusions and Future Perspectives

As incredibly varied creatures, insects display a range of mating behaviors meticulously regulated by neuropeptides. The 18 neuropeptides synthesized in this review play a critical role in the mating process of various insects. Their interaction with hormones and neurotransmitters ensures successful reproduction and perpetuation of the species. The mechanisms, routes, and evolutionary adaptations underlying the regulation of mating behavior in many insects remain largely unknown despite the notable advancements in identifying important neuropeptides and their roles. From this review, we note that most of what is known about these important neuropeptides is based largely on research on fruit flies (*D. melanogaster*). There is a wide range of mating behaviors in many other species whose neuropeptidergic regulatory mechanisms remain unknown. There is a need to replicate research in other species, especially on insects emerging as invasive and destructive globally.

We also note that the research conducted on the functions of neuropeptides, as elucidated in this review, is largely based on RNAi knockdown in conjunction with behavioral assays. Neuronal circuit analysis based on the latest and more robust tools could provide a deeper understanding of the currently unknown mechanistic aspects. Electron microscopy (EM) is potentially a powerful tool in the construction of connectomes that can precisely unravel neuronal pathways, specific targets, and the synaptic architectures involved in mediating mating behavior. For instance, using EM connectomes, expressing neurons of OK can be traced, including the downstream targets and feedback loops, to provide an understanding of the signaling mechanism that is currently not well understood. After mating in *D. melanogaster*, male-derived SP triggers an array of changes in the female to prevent remating [139]. Synaptic

changes after mating that block receptivity can be established based on EM connectomes. EM has previously been applied in *D. Melanogaster* to identify the neuronal circuit in the visual system that computes motion signals [166]. Functional imaging using genetically encoded calcium indicators (e.g., GCaMP) could also be deployed to study the neuronal circuits of neuropeptides in real time. For instance, the blocked remating phenomenon in *D. melanogaster* females could be studied in real time, such as how SP silences the pickpocket ion (ppk+) sensory neurons in females to cut the responses to courtship songs. Single-cell RNA-sequencing (scRNA-seq) could be deployed to compare species and provide evolutionary insights. Neuropeptides, for instance, PBAN, are highly conserved in the lepidopteran species, performing a similar function in mate attraction. scRNA-seq could be deployed in studies to identify receptor expression differences that prevent cross-species courtship and mating. With its chemical specificity, sensitivity, and quantitative precision, mass spectrometry (MS) is a robust tool for researching neuropeptide dynamics in insect mating behavior. Firstly, MS could be critical in characterizing new neuropeptides that are yet to be known to mediate insect mating behavior. This is specifically important because the current research on neuropeptides has been conducted on the model insect *D. melanogaster*, with many insects not yet touched. MS could also be critical in the study of how neuropeptide quantity levels in the insect hemolymph relate to mating behaviors. For instance, MS could be deployed to study how the quantity of SP in the female *D. menologaster* affects receptivity to remating versus time after the completion of initial mating.

Neuropeptides are potential targets for novel insect control techniques because of their significance in reproduction and survival [4]. Targeted manipulation of the signaling system of the neuropeptides will disrupt mating behaviors and other physiological processes that sustain the reproduction and survival of some economically disruptive pests. Tools applied to disrupt the signaling system in the mating process would be applied in crop production systems to reduce the population pressure of destructive pests, thus offering ecologically friendly substitutes to the conventional use of chemical pesticides. Our findings in this review not only advance the understanding of neuropeptide-mediated mating regulation but also highlight their potential as eco-friendly pest control targets.

Author Contributions: Conceptualization, A.O. and J.G.; methodology, A.O. and J.G.; software, A.O. and J.G; validation, J.G. and W. L; formal analysis, A.O. and J.G., investigation, A.O. and J.G.; resources, J.G. and W.L.; data curation, A.O. and J.G.; writing—original draft preparation, A.O.; writing—review and editing, J.G. and W.L; visualization, A.O.; supervision, J.G. and W.L.; funding acquisition, J.G. and W.L. All authors have read and agreed to the published version of the manuscript.

Funding: This study was supported by the National Key R&D Program of China (Grant No. 2024YFC2607600) and the Key R&D Project of Tibet Autonomous Region (XZ202401ZY0001).

Conflicts of Interest: The authors declare no conflicts of interest.

References

1. Schoofs, L.; De Loof, A.; Van Hiel, M.B. Neuropeptides as regulators of behavior in insects. *Annu. Rev. Entomol.* **2017**, *62*, 35–52. [CrossRef] [PubMed]
2. Altstein, M.; Nässel, D.R. Neuropeptide signaling in insects. In *Neuropeptide Systems as Targets for Parasite and Pest Control*; Springer: Boston, MA, USA, 2010; pp. 155–165.
3. Cui, H.-Y.; Zhao, Z.-W. Structure and function of neuropeptide F in insects. *J. Integr. Agric.* **2020**, *19*, 1429–1438. [CrossRef]
4. Scherkenbeck, J.; Zdobinsky, T. Insect neuropeptides: Structures, chemical modifications and potential for insect control. *Bioorg. Med. Chem.* **2009**, *17*, 4071–4084. [CrossRef] [PubMed]
5. Roelofs, W.L. Chemistry of sex attraction. *Proc. Natl. Acad. Sci. USA* **1995**, *92*, 44–49. [CrossRef]
6. Sandler, B.H.; Nikonova, L.; Leal, W.S.; Clardy, J. Sexual attraction in the silkworm moth: Structure of the pheromone-binding-protein–bombykol complex. *Chem. Biol.* **2000**, *7*, 143–151. [CrossRef]

7. Bierl, B.A.; Beroza, M.; Collier, C. Potent sex attractant of the gypsy moth: Its isolation, identification, and synthesis. *Science* **1970**, *170*, 87–89. [CrossRef]
8. Pliske, T.E. Courtship behavior of the monarch butterfly, *Danaus plexippus* L. *Ann. Entomol. Soc. Am.* **1975**, *68*, 143–151. [CrossRef]
9. Dickens, J.C.; Oliver, J.E.; Hollister, B.; Davis, J.C.; Klun, J.A. Breaking a paradigm: Male-produced aggregation pheromone for the Colorado potato beetle. *J. Exp. Biol.* **2002**, *205*, 1925–1933. [CrossRef]
10. Sivinski, J.M.; Calkins, C. Pheromones and parapheromones in the control of tephritids. *Fla. Entomol.* **1986**, *69*, 157–168. [CrossRef]
11. Everaerts, C.; Farine, J.-P.; Cobb, M.; Ferveur, J.-F. Drosophila cuticular hydrocarbons revisited: Mating status alters cuticular profiles. *PLoS ONE* **2010**, *5*, e9607. [CrossRef]
12. Kocher, S.D.; Richard, F.-J.; Tarpy, D.R.; Grozinger, C.M. Queen reproductive state modulates pheromone production and queen-worker interactions in honeybees. *Behav. Ecol.* **2009**, *20*, 1007–1014. [CrossRef] [PubMed]
13. Tokro, P.; Brossut, R.; Sreng, L. Mise en evidence de la pheromone sexuelle chez les femelles de *Blattella germanica* L. *Int. J. Trop. Insect Sci.* **1993**, *14*, 115–126. [CrossRef]
14. Nojima, S.; Schal, C.; Webster, F.X.; Santangelo, R.G.; Roelofs, W.L. Identification of the sex pheromone of the German cockroach, *Blattella germanica*. *Science* **2005**, *307*, 1104–1106. [CrossRef] [PubMed]
15. LeMieux, J. Tsetse Fly Volatile Pheromones Could Treat Diseases They Spread. *Genetic Engineering and Biotechnology News*, 21 February 2023.
16. Xu, H.; Turlings, T.C. Plant volatiles as mate-finding cues for insects. *Trends Plant Sci.* **2018**, *23*, 100–111. [CrossRef]
17. Blomquist, G.J.; Tittiger, C.; MacLean, M.; Keeling, C.I. Cytochromes P450: Terpene detoxification and pheromone production in bark beetles. *Curr. Opin. Insect Sci.* **2021**, *43*, 97–102. [CrossRef]
18. Pitman, G.; Vité, J. Aggregation behavior of *Dendroctonus ponderosae* (coleoptera: Scolytidae) in response to chemical messengers[1]. *Can. Entomol.* **1969**, *101*, 143–149. [CrossRef]
19. Montealegre-Z, F.; Jonsson, T.; Robert, D. Sound radiation and wing mechanics in stridulating field crickets (Orthoptera: Gryllidae). *J. Exp. Biol.* **2011**, *214*, 2105–2117. [CrossRef]
20. Nahirney, P.C.; Forbes, J.G.; Douglas Morris, H.; Chock, S.C.; Wang, K. What the buzz was all about: Superfast song muscles rattle the tymbals of male periodical cicadas. *FASEB J.* **2006**, *20*, 2017–2026. [CrossRef]
21. Oberdörster, U.; Grant, P.R. Acoustic adaptations of periodical cicadas (Hemiptera: Magicicada). *Biol. J. Linn. Soc.* **2007**, *90*, 15–24. [CrossRef]
22. Wei, J.-Q.; Wang, X.-Y.; Zheng, X.-L.; Tong, X. Stridulatory Organs and Sound Recognition of Three Species of Longhorn Beetles (Coleoptera: Cerambycidae). *Insects* **2024**, *15*, 849. [CrossRef]
23. Smithsonian Institution. *Mating in Insects*; Smithsonian Institution: Washington, DC, USA, 1996.
24. Clemens, J.; Coen, P.; Roemschied, F.A.; Pereira, T.D.; Mazumder, D.; Aldarondo, D.E.; Pacheco, D.A.; Murthy, M. Discovery of a new song mode in Drosophila reveals hidden structure in the sensory and neural drivers of behavior. *Curr. Biol.* **2018**, *28*, 2400–2412.e6. [CrossRef] [PubMed]
25. Fernández, Y.; Dowdy, N.J.; Conner, W.E. Extreme duty cycles in the acoustic signals of tiger moths: Sexual and natural selection operating in parallel. *Integr. Org. Biol.* **2020**, *2*, obaa046. [CrossRef] [PubMed]
26. Larsen, O.N.; Gleffe, G.; Tengö, J. Vibration and sound communication in solitary bees and wasps. *Physiol. Entomol.* **1986**, *11*, 287–296. [CrossRef]
27. Clark, D.C.; Moore, A.J. Social communication in the Madagascar hissing cockroach: Features of male courtship hisses and a comparison of courtship and agonistic hisses. *Behaviour* **1995**, *132*, 401–417. [CrossRef]
28. National Geographic Society. *Inside the Wild World of Bug Courtship and Mating Rituals*; National Geographic: Washington, DC, USA, 2025.
29. Horváth, G.; Malik, P.; Kriska, G.; Wildermuth, H. Ecological traps for dragonflies in a cemetery: The attraction of *Sympetrum species* (Odonata: Libellulidae) by horizontally polarizing black gravestones. *Freshw. Biol.* **2007**, *52*, 1700–1709. [CrossRef]
30. Metters, D. Common Rhinoceros Beetle—Land for Wildlife. 2017. Available online: https://www.lfwseq.org.au/author/deborah-metters/page/22/ (accessed on 24 March 2025).
31. Perez, B. Calling behaviour in the female praying mantis, *Hierodula patellifera*. *Physiol. Entomol.* **2005**, *30*, 42–47. [CrossRef]
32. Pervez, A. Courtship. In *Reproductive Strategies in Insects*; CRC Press: Boca Raton, FL, USA, 2022; pp. 119–142.
33. Baker, C.A.; Clemens, J.; Murthy, M. Acoustic pattern recognition and courtship songs: Insights from insects. *Annu. Rev. Neurosci.* **2019**, *42*, 129–147. [CrossRef]
34. O'woma, O.O.; Chigozirim, U.P.; Emmanuel, O.; Chukwuebuka, E.M. Reproductive and survival strategies utilized by insect. A review. *Am. J. Zool. Res.* **2016**, *4*, 1–6.
35. Virant-Doberlet, M.; Cokl, A. Vibrational communication in insects. *Neotrop. Entomol.* **2004**, *33*, 121–134. [CrossRef]

36. Xu, J.; Liu, W.; Yang, D.; Chen, S.; Chen, K.; Liu, Z.; Yang, X.; Meng, J.; Zhu, G.; Dong, S.; et al. Regulation of olfactory-based sex behaviors in the silkworm by genes in the sex-determination cascade. *PLoS Genet.* **2020**, *16*, e1008622. [CrossRef]
37. Rebar, D.; Bailey, N.W.; Zuk, M. Courtship song's role during female mate choice in the field cricket *Teleogryllus oceanicus*. *Behav. Ecol.* **2009**, *20*, 1307–1314. [CrossRef]
38. Gray, D.A. Female house crickets, *Acheta domesticus*, prefer the chirps of large males. *Anim. Behav.* **1997**, *54*, 1553–1562. [CrossRef] [PubMed]
39. Cooley, J.R.; Marshall, D.C. Sexual signaling in periodical cicadas, *Magicicada* spp. (Hemiptera: Cicadidae). *Behaviour* **2001**, *138*, 827–855. [CrossRef]
40. Ávila, G.R.; Deneubourg, J.-L.; Guisset, J.-L.; Wessel, N.; Kurths, J. Firefly courtship as the basis of the synchronization-response principle. *Europhys. Lett.* **2011**, *94*, 60007.
41. Wise, T. Blue Dasher—Life on CSG Pond. 2021. Available online: https://www.lifeoncsgpond.com/blue-dasher (accessed on 24 March 2025).
42. Dragonflywoman. Pachydiplax longipennis—The Dragonfly Woman. 2011. Available online: https://thedragonflywoman.com/tag/pachydiplax-longipennis/ (accessed on 24 March 2025).
43. Heidinger, I.M.M.; Meixner, M.D.; Berg, S.; Büchler, R. Observation of the mating behavior of honey bee (*Apis mellifera* L.) queens using radio-frequency identification (RFID): Factors influencing the duration and frequency of nuptial flights. *Insects* **2014**, *5*, 513–527. [CrossRef]
44. Uzsák, A.; Dieffenderfer, J.; Bozkurt, A.; Schal, C. Social facilitation of insect reproduction with motor-driven tactile stimuli. *Proc. R. Soc. B Biol. Sci.* **2014**, *281*, 20140325. [CrossRef]
45. Kruse, K.C.; Switzer, P.V. Physical contests for females in the Japanese beetle, Popillia japonica. *J. Insect Sci.* **2007**, *7*, 34. [CrossRef]
46. Barrows, E.M.; Gordh, G. Sexual behavior in the Japanese beetle, *Popillia japonica*, and comparative notes on sexual behavior of other scarabs (Coleoptera: Scarabaeidae). *Behav. Biol.* **1978**, *23*, 341–354. [CrossRef]
47. Wada-Katsumata, A.; Schal, C. Antennal grooming facilitates courtship performance in a group-living insect, the German cockroach *Blattella germanica*. *Sci. Rep.* **2019**, *9*, 2942. [CrossRef]
48. Feng, H.Y.; Zhao, Y.Q.; Yang, T.; Zhou, Y.Y.; Gong, L.L.; Zhang, M.Q.; Ma, Y.F.; Hull, J.J.; Dewer, Y.; Zhang, F.; et al. Female contact sex pheromone recognition in the German cockroach (*Blattella germanica*) is mediated by two male antennae-enriched sensory neuron membrane proteins. *Pest Manag. Sci.* **2025**, *81*, 572–584. [CrossRef]
49. Gong, L.; Zhang, M.Q.; Ma, Y.F.; Feng, H.Y.; Zhao, Y.Q.; Zhou, Y.y.; He, M.; Smagghe, G.; He, P. RNAi of yellow-y, required for normal cuticle pigmentation, impairs courtship behavior and oviposition in the German cockroach (*Blattella germanica*). *Arch. Insect Biochem. Physiol.* **2024**, *115*, e22114. [CrossRef] [PubMed]
50. Vahed, K. The function of nuptial feeding in insects: A review of empirical studies. *Biol. Rev.* **1998**, *73*, 43–78. [CrossRef]
51. Vahed, K. The Evolution and Function of the Spermatophylax in Bushcrickets (Orthoptera: Tettigoniidae). Ph.D. Thesis, University of Nottingham, Nottingham, UK, 1994.
52. Cumming, J.M. Sexual selection and the evolution of dance fly mating systems (Diptera: Empididae; Empidinae). *Can. Entomol.* **1994**, *126*, 907–920. [CrossRef]
53. LeBas, N.R.; Hockham, L.R.; Ritchie, M.G. Sexual selection in the gift-giving dance fly, *Rhamphomyia sulcata*, favors small males carrying small gifts. *Evolution* **2004**, *58*, 1763–1772.
54. Iftikhar, H.; Johnson, N.L.; Marlatt, M.L.; Carney, G.E. The role of miRNAs in *Drosophila melanogaster* male courtship behavior. *Genetics* **2019**, *211*, 925–942. [CrossRef]
55. Gapon, D. An instance of intergeneric copulation in the family Rhopalidae (Heteroptera): Structure, functioning and congruence of the genitalia in two different species from the standpoint of the lock-and-key hypothesis. *Zoosyst. Ross.* **2019**, *28*, 3–18. [CrossRef]
56. Matsumura, Y.; Kovalev, A.E.; Gorb, S.N. Penetration mechanics of a beetle intromittent organ with bending stiffness gradient and a soft tip. *Sci. Adv.* **2017**, *3*, eaao5469. [CrossRef]
57. Blomqvist, D.; Hoi, H.; Weinberger, I. S13-1 To see or not to see: The role of habitat density on the occurrence of extra-pair paternity and paternity assurance behaviors. *Acta Zool. Sin.* **2006**, *52*, 229–231.
58. Benoit, J.B.; Jajack, A.J.; Yoder, J.A. Multiple traumatic insemination events reduce the ability of bed bug females to maintain water balance. *J. Comp. Physiol. B* **2012**, *182*, 189–198. [CrossRef]
59. Wu, W.L.; Peng WenJun, P.W.; Hu FuLiang, H.F. Sperm storage of queen honeybee. *Chin. Bull. Entomol.* **2008**, *45*, 323–327.
60. Mongue, A.J.; Hansen, M.E.; Gu, L.; Sorenson, C.E.; Walters, J.R. Nonfertilizing sperm in Lepidoptera show little evidence for recurrent positive selection. *Mol. Ecol.* **2019**, *28*, 2517–2530. [CrossRef] [PubMed]
61. Buskirk, R.E.; Sherman, K.J. The influence of larval ecology on oviposition and mating strategies in dragonflies. *Fla. Entomol.* **1985**, *68*, 39–51. [CrossRef]

62. McDonough-Goldstein, C.E.; Pitnick, S.; Dorus, S. Drosophila female reproductive glands contribute to mating plug composition and the timing of sperm ejection. *Proc. R. Soc. B* **2022**, *289*, 20212213. [CrossRef] [PubMed]
63. Cordero-Rivera, A. Sperm removal during copulation confirmed in the oldest extant damselfly, *Hemiphlebia mirabilis*. *PeerJ* **2016**, *4*, e2077. [CrossRef]
64. Denis, B.; Claisse, G.; Le Rouzic, A.; Wicker-Thomas, C.; Lepennetier, G.; Joly, D. Male accessory gland proteins affect differentially female sexual receptivity and remating in closely related Drosophila species. *J. Insect Physiol.* **2017**, *99*, 67–77. [CrossRef]
65. Wedell, N. Female receptivity in butterflies and moths. *J. Exp. Biol.* **2005**, *208*, 3433–3440. [CrossRef]
66. Birkhead, T.; Lee, K.; Young, P. Sexual cannibalism in the praying mantis *Hierodula membranacea*. *Behaviour* **1988**, *106*, 112–118. [CrossRef]
67. Burke, N.W. Sexual cannibalism as a female resistance trait: A new hypothesis. *Evolution* **2024**, *78*, 612–623. [CrossRef]
68. Su, J.; Zhao, J.; Li, Y.; Lu, Y. Breeding sites, migration paths and phylogenetic relationships of mosquitoes in seven cities in northern and southern China. *Trop. Biomed.* **2024**, *41*, 471–480.
69. Hanin, O.; Azrielli, A.; Applebaum, S.W.; Rafaeli, A. Functional impact of silencing the Helicoverpa armigera sex-peptide receptor on female reproductive behaviour. *Insect Mol Biol.* **2012**, *21*, 161–167. [CrossRef]
70. Zhang, B.; Zhang, Y.; Guan, R.; Du, M.; Yin, X.; Zhao, W.; An, S. Trehalase is required for sex pheromone biosynthesis in Helicoverpa armigera. *Insect Mol Biol.* **2022**, *31*, 334–345. [CrossRef] [PubMed]
71. Cha, W.H.; Kim, B.; Lee, D.-W. Functional Analysis of Pheromone Biosynthesis Activating Neuropeptide Receptor Isoforms in Maruca vitrata. *Cells* **2023**, *12*, 1410. [CrossRef] [PubMed]
72. Rafaeli, A. Pheromone biosynthesis activating neuropeptide (PBAN): Regulatory role and mode of action. *Gen. Comp. Endocrinol.* **2009**, *162*, 69–78. [CrossRef]
73. Shiomi, K. Pheromone biosynthesis activating neuropeptide. In *Handbook of Hormones*; Elsevier: Amsterdam, The Netherlands, 2021; pp. 725–727.
74. Matsumoto, S.; Ohnishi, A.; Lee, J.M.; Hull, J.J. Unraveling the pheromone biosynthesis activating neuropeptide (PBAN) signal transduction cascade that regulates sex pheromone production in moths. *Vitam. Horm.* **2010**, *83*, 425–445.
75. Bober, R.; Azrielli, A.; Rafaeli, A. Developmental regulation of the pheromone biosynthesis activating neuropeptide-receptor (PBAN-R): Re-evaluating the role of juvenile hormone. *Insect Mol. Biol.* **2010**, *19*, 77–86. [CrossRef]
76. Jurenka, R.; Nusawardani, T. The pyrokinin/pheromone biosynthesis-activating neuropeptide (PBAN) family of peptides and their receptors in Insecta: Evolutionary trace indicates potential receptor ligand-binding domains. *Insect Mol. Biol.* **2011**, *20*, 323–334. [CrossRef]
77. Lee, D.-W.; Shrestha, S.; Kim, A.Y.; Park, S.J.; Yang, C.Y.; Kim, Y.; Koh, Y.H. RNA interference of pheromone biosynthesis-activating neuropeptide receptor suppresses mating behavior by inhibiting sex pheromone production in *Plutella xylostella* (L.). *Insect Biochem. Mol. Biol.* **2011**, *41*, 236–243. [CrossRef]
78. Ashok, K.; Bhargava, C.N.; Asokan, R.; Pradeep, C.; Pradhan, S.K.; Kennedy, J.S.; Balasubramani, V.; Murugan, M.; Jayakanthan, M.; Geethalakshmi, V.; et al. CRISPR/Cas9 mediated editing of pheromone biosynthesis activating neuropeptide (PBAN) gene disrupts mating in the Fall armyworm, *Spodoptera frugiperda* (JE Smith) (Lepidoptera: Noctuidae). *3 Biotech* **2023**, *13*, 370. [CrossRef]
79. Nässel, D.R. Tachykinin-related peptides in invertebrates: A review. *Peptides* **1999**, *20*, 141–158. [CrossRef]
80. Van Loy, T.; Vandersmissen, H.P.; Poels, J.; Van Hiel, M.B.; Verlinden, H.; Vanden Broeck, J. Tachykinin-related peptides and their receptors in invertebrates: A current view. *Peptides* **2010**, *31*, 520–524. [CrossRef]
81. Winther, Å.M.; Nässel, D.R. Intestinal peptides as circulating hormones: Release of tachykinin-related peptide from the locust and cockroach midgut. *J. Exp. Biol.* **2001**, *204*, 1269–1280. [CrossRef] [PubMed]
82. Miyashita, A.; Adamo, S.A. Stayin'alive: Endocrinological stress responses in insects. In *Advances in Invertebrate (Neuro) Endocrinology*; Apple Academic Press: Palm Bay, FL, USA, 2020; pp. 283–323.
83. Pascual, N.; Maestro, J.L.; Chiva, C.; Andreu, D.; Bellés, X. Identification of a tachykinin-related peptide with orexigenic properties in the German cockroach. *Peptides* **2008**, *29*, 386–392. [CrossRef] [PubMed]
84. Shankar, S.; Chua, J.Y.; Tan, K.J.; Calvert, M.E.; Weng, R.; Ng, W.C.; Mori, K.; Yew, J.Y. The neuropeptide tachykinin is essential for pheromone detection in a gustatory neural circuit. *eLife* **2015**, *4*, e06914. [CrossRef] [PubMed]
85. Yeoh, J.G.; Pandit, A.A.; Zandawala, M.; Nässel, D.R.; Davies, S.-A.; Dow, J.A. DINeR: Database for insect neuropeptide research. *Insect Biochem. Mol. Biol.* **2017**, *86*, 9–19. [CrossRef]
86. Gui, S.H.; Jiang, H.B.; Liu, X.Q.; Xu, L.; Wang, J.J. Molecular characterizations of natalisin and its roles in modulating mating in the oriental fruit fly, *Bactrocera dorsalis* (Hendel). *Insect Mol. Biol.* **2017**, *26*, 103–112. [CrossRef]
87. Jiang, H.; Lkhagva, A.; Daubnerová, I.; Chae, H.-S.; Šimo, L.; Jung, S.-H.; Yoon, Y.-K.; Lee, N.-R.; Seong, J.Y.; Žitňan, D.; et al. Natalisin, a tachykinin-like signaling system, regulates sexual activity and fecundity in insects. *Proc. Natl. Acad. Sci. USA* **2013**, *110*, E3526–E3534. [CrossRef]

88. Lee, G.; Bahn, J.H.; Park, J.H. Sex-and clock-controlled expression of the neuropeptide F gene in Drosophila. *Proc. Natl. Acad. Sci. USA* **2006**, *103*, 12580–12585. [CrossRef]
89. Huang, Y.C.; Shi, M.; Chen, X.X. Advances in research on the insect neuropeptide F. *Chin. J. Appl. Entomol.* **2015**, *52*, 1315–1325.
90. Liu, W.; Ganguly, A.; Huang, J.; Wang, Y.; Ni, J.D.; Gurav, A.S.; Aguilar, M.A.; Montell, C. Neuropeptide F regulates courtship in Drosophila through a male-specific neuronal circuit. *eLife* **2019**, *8*, e49574. [CrossRef]
91. Van Wielendaele, P.; Wynant, N.; Dillen, S.; Zels, S.; Badisco, L.; Broeck, J.V. Neuropeptide F regulates male reproductive processes in the desert locust, *Schistocerca gregaria*. *Insect Biochem. Mol. Biol.* **2013**, *43*, 252–259. [CrossRef]
92. Kim, W.J.; Jan, L.Y.; Jan, Y.N. A PDF/NPF neuropeptide signaling circuitry of male *Drosophila melanogaster* controls rival-induced prolonged mating. *Neuron* **2013**, *80*, 1190–1205. [CrossRef] [PubMed]
93. Rohwedder, A.; Selcho, M.; Chassot, B.; Thum, A.S. Neuropeptide F neurons modulate sugar reward during associative olfactory learning of *Drosophila larvae*. *J. Comp. Neurol.* **2015**, *523*, 2637–2664. [CrossRef] [PubMed]
94. Lee, G.; Jang, H.; Oh, Y. The role of diuretic hormones (DHs) and their receptors in Drosophila. *BMB Rep.* **2023**, *56*, 209. [CrossRef] [PubMed]
95. Lin, H.-H.; Kuang, M.C.; Hossain, I.; Xuan, Y.; Beebe, L.; Shepherd, A.K.; Rolandi, M.; Wang, J.W. A nutrient-specific gut hormone arbitrates between courtship and feeding. *Nature* **2022**, *602*, 632–638. [CrossRef]
96. Kurogi, Y.; Imura, E.; Mizuno, Y.; Hoshino, R.; Nouzova, M.; Matsuyama, S.; Mizoguchi, A.; Kondo, S.; Tanimoto, H.; Noriega, F.G.; et al. Female reproductive dormancy in Drosophila is regulated by DH31-producing neurons projecting into the corpus allatum. *Development* **2023**, *150*, dev201186. [CrossRef]
97. Zhou, Y.; Nagata, S. Proctolin. In *Handbook of Hormones*; Elsevier: Amsterdam, The Netherlands, 2021; pp. 789–790.
98. Vezenkov, S.R.; Danalev, D.L. From molecule to sexual behavior: The role of the neuropentapeptide proctolin in acoustic communication in the male grasshopper *Chorthippus biguttulus*. *Eur. J. Pharmacol.* **2009**, *619*, 57–60. [CrossRef]
99. Tanaka, Y. Proctolin. In *Handbook of Hormones*; Elsevier: Amsterdam, The Netherlands, 2016; pp. 438–439.
100. Chiang, R.G.; Martens, J.D.; O'donnell, M.J. The vagina muscles of the blood-sucking insect *Rhodnius prolixus* as a model for exploring the physiological effects of proctolin. *Physiol. Entomol.* **2010**, *35*, 154–159. [CrossRef]
101. Taylor, C.A.; Winther, Å.M.; Siviter, R.J.; Shirras, A.D.; Isaac, R.E.; Nässel, D.R. Identification of a proctolin preprohormone gene (Proct) of *Drosophila melanogaster*: Expression and predicted prohormone processing. *J. Neurobiol.* **2004**, *58*, 379–391. [CrossRef]
102. Ormerod, K.G.; LePine, O.K.; Bhutta, M.S.; Jung, J.; Tattersall, G.J.; Mercier, A.J. Characterizing the physiological and behavioral roles of proctolin in *Drosophila melanogaster*. *J. Neurophysiol.* **2016**, *115*, 568–580. [CrossRef]
103. Eaton, J.L. Morphology of abdominal segments eight and nine of the female tobacco hornworm, *Manduca sexta* (Lepidoptera: Sphingidae). *Ann. Entomol. Soc. Am.* **1986**, *79*, 629–635. [CrossRef]
104. Belanger, J.H.; Orchard, I. The locust ovipositor opener muscle: Proctolinergic central and peripheral neuromodulation in a centrally driven motor system. *J. Exp. Biol.* **1993**, *174*, 343–362. [CrossRef]
105. Nässel, D.R.; O'shea, M. Proctolin-like immunoreactive neurons in the blowfly central nervous system. *J. Comp. Neurol.* **1987**, *265*, 437–454. [CrossRef] [PubMed]
106. Orchard, I.; Lee, D.H.; Da Silva, R.; Lange, A.B. The proctolin gene and biological effects of proctolin in the blood-feeding bug, *Rhodnius prolixus*. *Front. Endocrinol.* **2011**, *2*, 59. [CrossRef] [PubMed]
107. Orchard, I.; Belanger, J.H.; Lange, A.B. Proctolin: A review with emphasis on insects. *J. Neurobiol.* **1989**, *20*, 470–496. [CrossRef]
108. Lange, A.B.; Kisana, A.; Leyria, J.; Orchard, I. The Male Reproductive System of the Kissing Bug, *Rhodnius prolixus* Stål, 1859 (Hemiptera: Reduviidae: Triatominae): Arrangements of the Muscles and the Myoactivity of the Selected Neuropeptides. *Insects* **2023**, *14*, 324. [CrossRef]
109. Verleyen, P.; Huybrechts, J.; Schoofs, L. SIFamide illustrates the rapid evolution in Arthropod neuropeptide research. *Gen. Comp. Endocrinol.* **2009**, *162*, 27–35. [CrossRef]
110. Lismont, E.; Mortelmans, N.; Verlinden, H.; Vanden Broeck, J. Molecular cloning and characterization of the SIFamide precursor and receptor in a hymenopteran insect, Bombus terrestris. *Gen. Comp. Endocrinol.* **2018**, *258*, 39–52. [CrossRef]
111. Ayub, M.; Hermiz, M.; Lange, A.B.; Orchard, I. SIFamide influences feeding in the Chagas disease vector, *Rhodnius prolixus*. *Front. Neurosci.* **2020**, *14*, 134. [CrossRef]
112. Arendt, A.; Neupert, S.; Schendzielorz, J.; Predel, R.; Stengl, M. The neuropeptide SIFamide in the brain of three cockroach species. *J. Comp. Neurol.* **2016**, *524*, 1337–1360. [CrossRef]
113. Sellami, A.; Veenstra, J.A. SIFamide acts on fruitless neurons to modulate sexual behavior in *Drosophila melanogaster*. *Peptides* **2015**, *74*, 50–56. [CrossRef]
114. Song, Y.; Zhang, T.; Zhang, X.; Ryu, T.H.; Wong, K.; Wu, Z.; Wei, Y.; Schweizer, J.; Nguyen, K.-N.H.; Kwan, A.; et al. Peptidergic neurons with extensive branching orchestrate the internal states and energy balance of male *Drosophila melanogaster*. *bioRxiv* **2024**. bioRxiv:2024.2006.2004.597277.

115. Wong, K.; Schweizer, J.; Nguyen, K.-N.H.; Atieh, S.; Kim, W.J. Neuropeptide relay between SIFa signaling controls the experience-dependent mating duration of male Drosophila. *bioRxiv* **2019**. bioRxiv:819045.
116. Tanaka, Y. Orcokinins. In *Handbook of Hormones*; Elsevier: Amsterdam, The Netherlands, 2021; pp. 791–793.
117. Silva, V.; Palacios-Muñoz, A.; Volonté, M.; Frenkel, L.; Ewer, J.; Ons, S. Orcokinin neuropeptides regulate reproduction in the fruit fly, *Drosophila melanogaster*. *Insect Biochem. Mol. Biol.* **2021**, *139*, 103676. [CrossRef] [PubMed]
118. Ons, S.; Bellés, X.; Maestro, J.L. Orcokinins contribute to the regulation of vitellogenin transcription in the cockroach *Blattella germanica*. *J. Insect Physiol.* **2015**, *82*, 129–133. [CrossRef] [PubMed]
119. Nässel, D.R.; Wu, S.-F. Leucokinins: Multifunctional neuropeptides and hormones in insects and other invertebrates. *Int. J. Mol. Sci.* **2021**, *22*, 1531. [CrossRef]
120. Zandawala, M.; Yurgel, M.E.; Texada, M.J.; Liao, S.; Rewitz, K.F.; Keene, A.C.; Nässel, D.R. Modulation of Drosophila post-feeding physiology and behavior by the neuropeptide leucokinin. *PLoS Genet.* **2018**, *14*, e1007767. [CrossRef]
121. Nässel, D.R. Leucokinin and associated neuropeptides regulate multiple aspects of physiology and behavior in Drosophila. *Int. J. Mol. Sci.* **2021**, *22*, 1940. [CrossRef]
122. Liu, C.; Zhang, B.; Zhang, L.; Yang, T.; Zhang, Z.; Gao, Z.; Zhang, W. A neural circuit encoding mating states tunes defensive behavior in Drosophila. *Nat. Commun.* **2020**, *11*, 3962. [CrossRef]
123. Nässel, D.R. A brief history of insect neuropeptide and peptide hormone research. *Cell Tissue Res.* **2024**, *399*, 129–159. [CrossRef]
124. Shafer, O.T.; Yao, Z. Pigment-dispersing factor signaling and circadian rhythms in insect locomotor activity. *Curr. Opin. Insect Sci.* **2014**, *1*, 73–80. [CrossRef]
125. Nagata, S. Pigment dispersing hormone. In *Handbook of Hormones*; Elsevier: Amsterdam, The Netherlands, 2021; pp. 861–862.
126. Wei, H.; Yasar, H.; Funk, N.W.; Giese, M.; Baz, E.-S.; Stengl, M. Signaling of pigment-dispersing factor (PDF) in the Madeira cockroach *Rhyparobia maderae*. *PLoS ONE* **2014**, *9*, e108757. [CrossRef] [PubMed]
127. Krupp, J.J.; Billeter, J.-C.; Wong, A.; Choi, C.; Nitabach, M.N.; Levine, J.D. Pigment-dispersing factor modulates pheromone production in clock cells that influence mating in Drosophila. *Neuron* **2013**, *79*, 54–68. [CrossRef] [PubMed]
128. Iga, M.; Nakaoka, T.; Suzuki, Y.; Kataoka, H. Pigment dispersing factor regulates ecdysone biosynthesis via Bombyx neuropeptide G protein coupled receptor-B2 in the prothoracic glands of *Bombyx mori*. *PLoS ONE* **2014**, *9*, e103239. [CrossRef]
129. Lee, G.; Park, J.H. Hemolymph sugar homeostasis and starvation-induced hyperactivity affected by genetic manipulations of the adipokinetic hormone-encoding gene in *Drosophila melanogaster*. *Genetics* **2004**, *167*, 311–323. [CrossRef]
130. Wicher, D.; Agricola, H.-J.; Söhler, S.; Gundel, M.; Heinemann, S.H.; Wollweber, L.; Stengl, M.; Derst, C. Differential receptor activation by cockroach adipokinetic hormones produces differential effects on ion currents, neuronal activity, and locomotion. *J. Neurophysiol.* **2006**, *95*, 2314–2325. [CrossRef]
131. Marco, H.G.; Gäde, G. Adipokinetic hormone: A hormone for all seasons? In *Advances in Invertebrate (NEURO) Endocrinology*; Apple Academic Press: Palm Bay, FL, USA, 2020; pp. 129–175.
132. Khan, Z.; Tondravi, M.; Oliver, R.; Vonhoff, F.J. Drosophila corazonin neurons as a hub for regulating growth, stress responses, ethanol-related behaviors, copulation persistence and sexually dimorphic reward pathways. *J. Dev. Biol.* **2021**, *9*, 26. [CrossRef]
133. Tayler, T.D.; Pacheco, D.A.; Hergarden, A.C.; Murthy, M.; Anderson, D.J. A neuropeptide circuit that coordinates sperm transfer and copulation duration in Drosophila. *Proc. Natl. Acad. Sci. USA* **2012**, *109*, 20697–20702. [CrossRef]
134. Yang, J.; Huang, H.; Yang, H.; He, X.; Jiang, X.; Shi, Y.; Alatangaole, D.; Shi, L.; Zhou, N. Specific activation of the G protein-coupled receptor BNGR-A21 by the neuropeptide corazonin from the silkworm, *Bombyx mori*, dually couples to the Gq and Gs signaling cascades. *J. Biol. Chem.* **2013**, *288*, 11662–11675. [CrossRef]
135. Cholewiński, M.; Chowański, S.; Lubawy, J.; Urbański, A.; Walkowiak-Nowicka, K.; Marciniak, P. Short neuropeptide F in integrated insect physiology. *J. Zhejiang Univ. Sci. B* **2024**, *25*, 389–409. [CrossRef]
136. Chen, W.; Shi, W.; Li, L.; Zheng, Z.; Li, T.; Bai, W.; Zhao, Z. Regulation of sleep by the short neuropeptide F (sNPF) in *Drosophila melanogaster*. *Insect Biochem. Mol. Biol.* **2013**, *43*, 809–819. [CrossRef]
137. Nässel, D.R.; Wegener, C. A comparative review of short and long neuropeptide F signaling in invertebrates: Any similarities to vertebrate neuropeptide Y signaling? *Peptides* **2011**, *32*, 1335–1355. [CrossRef] [PubMed]
138. Kim, W.J.; Lee, S.G.; Auge, A.-C.; Jan, L.Y.; Jan, Y. Sexually satiated male uses gustatory-to-neuropeptide integrative circuits to reduce time investment for mating. *bioRxiv* **2016**. bioRxiv:88724.
139. Peng, J.; Chen, S.; Büsser, S.; Liu, H.; Honegger, T.; Kubli, E. Gradual release of sperm bound sex-peptide controls female postmating behavior in Drosophila. *Curr. Biol.* **2005**, *15*, 207–213. [CrossRef] [PubMed]
140. Tsuda, M.; Aigaki, T. Evolution of sex-peptide in Drosophila. *Fly* **2016**, *10*, 172–177. [CrossRef]
141. Chen, P.S.; Stumm-Zollinger, E.; Aigaki, T.; Balmer, J.; Bienz, M.; Böhlen, P. A male accessory gland peptide that regulates reproductive behavior of female *D. melanogaster*. *Cell* **1988**, *54*, 291–298. [CrossRef]

142. Smith, D.; Hosken, D.; Ffrench-Constant, R.; Wedell, N. Variation in sex peptide expression in *D. melanogaster*. *Genet. Res.* **2009**, *91*, 237–242. [CrossRef]
143. Carvalho, G.B.; Kapahi, P.; Anderson, D.J.; Benzer, S. Allocrine modulation of feeding behavior by the sex peptide of Drosophila. *Curr. Biol.* **2006**, *16*, 692–696. [CrossRef]
144. Yapici, N.; Kim, Y.-J.; Ribeiro, C.; Dickson, B.J. A receptor that mediates the post-mating switch in Drosophila reproductive behaviour. *Nature* **2008**, *451*, 33–37. [CrossRef]
145. Johnson, E.C.; Bohn, L.M.; Taghert, P.H. Drosophila CG8422 encodes a functional diuretic hormone receptor. *J. Exp. Biol.* **2004**, *207*, 743–748. [CrossRef]
146. Lee, K.-M.; Daubnerová, I.; Isaac, R.E.; Zhang, C.; Choi, S.; Chung, J.; Kim, Y.-J. A neuronal pathway that controls sperm ejection and storage in female Drosophila. *Curr. Biol.* **2015**, *25*, 790–797. [CrossRef]
147. Zhang, T.; Zhang, G.; Zeng, F.; Liu, C.; Mao, J. Insulin-like peptides regulate vitellogenesis and oviposition in the green lacewing, *Chrysopa septempunctata*. *Bull. Entomol. Res.* **2017**, *107*, 148–154. [CrossRef] [PubMed]
148. Chen, H.-Y.; Toullec, J.-Y.; Lee, C.-Y. The crustacean hyperglycemic hormone superfamily: Progress made in the past decade. *Front. Endocrinol.* **2020**, *11*, 578958. [CrossRef] [PubMed]
149. Lange, A.B.; Leyria, J.; Orchard, I. The hormonal and neural control of egg production in the historically important model insect, *Rhodnius prolixus*: A review, with new insights in this post-genomic era. *Gen. Comp. Endocrinol.* **2022**, *321*, 114030. [CrossRef] [PubMed]
150. Leyria, J. Endocrine factors modulating vitellogenesis and oogenesis in insects: An update. *Mol. Cell. Endocrinol.* **2024**, *587*, 112211. [CrossRef]
151. Weger, A.A.; Rittschof, C.C. The diverse roles of insulin signaling in insect behavior. *Front. Insect Sci.* **2024**, *4*, 1360320. [CrossRef]
152. Nässel, D.R.; Broeck, J.V. Insulin/IGF signaling in Drosophila and other insects: Factors that regulate production, release and post-release action of the insulin-like peptides. *Cell. Mol. Life Sci.* **2016**, *73*, 271–290. [CrossRef]
153. Chen, K.; Dou, X.; Eum, J.H.; Harrison, R.E.; Brown, M.R.; Strand, M.R. Insulin-like peptides and ovary ecdysteroidogenic hormone differentially stimulate physiological processes regulating egg formation in the mosquito *Aedes aegypti*. *Insect Biochem. Mol. Biol.* **2023**, *163*, 104028. [CrossRef]
154. Yu, B.; Li, D.T.; Wang, S.L.; Xu, H.J.; Bao, Y.Y.; Zhang, C.X. Ion transport peptide (ITP) regulates wing expansion and cuticle melanism in the brown planthopper, *Nilaparvata lugens*. *Insect Mol. Biol.* **2016**, *25*, 778–787. [CrossRef]
155. Gáliková, M.; Klepsatel, P. Ion transport peptide regulates energy intake, expenditure, and metabolic homeostasis in Drosophila. *Genetics* **2022**, *222*, iyac150. [CrossRef]
156. Sajadi, F.; Paluzzi, J.-P.V. Molecular characterization, localization, and physiological roles of ITP and ITP-L in the mosquito, *Aedes aegypti*. *Front. Insect Sci.* **2024**, *4*, 1374325. [CrossRef]
157. Begum, K.; Li, B.; Beeman, R.W.; Park, Y. Functions of ion transport peptide and ion transport peptide-like in the red flour beetle *Tribolium castaneum*. *Insect Biochem. Mol. Biol.* **2009**, *39*, 717–725. [CrossRef] [PubMed]
158. Audsley, N.; Jensen, D.; Schooley, D.A. Signal transduction for *Schistocerca gregaria* ion transport peptide is mediated via both cyclic AMP and cyclic GMP. *Peptides* **2013**, *41*, 74–80. [CrossRef] [PubMed]
159. Nässel, D.R.; Wu, S.-F. Cholecystokinin/sulfakinin peptide signaling: Conserved roles at the intersection between feeding, mating and aggression. *Cell. Mol. Life Sci.* **2022**, *79*, 188. [CrossRef] [PubMed]
160. Zels, S.; Verlinden, H.; Dillen, S.; Vleugels, R.; Nachman, R.J.; Broeck, J.V. Signaling properties and pharmacological analysis of two sulfakinin receptors from the red flour beetle, Tribolium castaneum. *PLoS ONE* **2014**, *9*, e94502. [CrossRef]
161. Li, H.-F.; Dong, B.; Peng, Y.-Y.; Luo, H.-Y.; Ou, X.-L.; Ren, Z.-L.; Park, Y.; Wang, J.-J.; Jiang, H.-B. The Neuropeptide Sulfakinin, a peripheral regulator of insect behavioral switch between mating and foraging. *bioRxiv* **2024**. bioRxiv:2024.2007.2030.605941.
162. Wu, S.; Guo, C.; Zhao, H.; Sun, M.; Chen, J.; Han, C.; Peng, Q.; Qiao, H.; Peng, P.; Liu, Y.; et al. Drosulfakinin signaling in fruitless circuitry antagonizes P1 neurons to regulate sexual arousal in Drosophila. *Nat. Commun.* **2019**, *10*, 4770. [CrossRef]
163. Gui, S.-H.; Pei, Y.-X.; Xu, L.; Wang, W.-P.; Jiang, H.-B.; Nachman, R.J.; Kaczmarek, K.; Zabrocki, J.; Wang, J.-J. Function of the natalisin receptor in mating of the oriental fruit fly, *Bactrocera dorsalis* (Hendel) and testing of peptidomimetics. *PLoS ONE* **2018**, *13*, e0193058. [CrossRef]
164. Bloch, G.; Hazan, E.; Rafaeli, A. Circadian rhythms and endocrine functions in adult insects. *J. Insect Physiol.* **2013**, *59*, 56–69. [CrossRef]
165. Hammock, E.A.; Young, L.J. Oxytocin, vasopressin and pair bonding: Implications for autism. *Philos. Trans. R. Soc. B Biol. Sci.* **2006**, *361*, 2187–2198. [CrossRef]
166. Takemura, S.-Y. Connectome of the fly visual circuitry. *Microscopy* **2015**, *64*, 37–44. [CrossRef]

Disclaimer/Publisher's Note: The statements, opinions and data contained in all publications are solely those of the individual author(s) and contributor(s) and not of MDPI and/or the editor(s). MDPI and/or the editor(s) disclaim responsibility for any injury to people or property resulting from any ideas, methods, instructions or products referred to in the content.

insects

MDPI

Review

The Role of Heat Shock Proteins in Insect Stress Response, Immunity, and Climate Adaptation

Davide Banfi, Tommaso Bianchi, Maristella Mastore and Maurizio Francesco Brivio *

Laboratory of Applied Entomology and Parasitology, Department of Theoretical and Applied Sciences (DiSTA), University of Insubria, 21100 Varese, Italy; davide.banfi@uninsubria.it (D.B.); tbianchi1@studenti.uninsubria.it (T.B.); maristella.mastore@uninsubria.it (M.M.)
* Correspondence: maurizio.brivio@uninsubria.it; Tel.: +39-0332-421-404

Simple Summary: Heat shock proteins (HSPs) are critical for insect resilience, protecting cellular integrity, and regulating immune responses against abiotic and biotic stresses. This review illustrates the functions of HSPs in insects, including protein stabilization and their role in innate immunity. The expression of HSPs reflects evolutionary adaptations to stressors such as changes in temperature, chemicals, and pathogens. Given the drastic temperature changes associated with global climate change, knowledge about HSPs may become essential to fully understand their role as potential biomarkers for environmental monitoring and
pest management.

Abstract: Heat shock proteins (HSPs) play a key role in enhancing insect resilience to abiotic and biotic stresses by preserving cellular integrity and modulating immune responses. This review summarizes the main functions of HSPs in insects, including protein stabilization, interaction with antioxidant systems, and involvement in the innate immune response. The expression of HSPs under environmental conditions reflects their evolutionary adaptation to various stressors, including thermal changes, chemical exposure, and pathogens. Future research should focus on the interaction between HSPs and other stress response systems to improve our understanding of insect adaptation. Furthermore, in the context of global climate change, HSPs emerge as a crucial resilience factor and potential biomarkers for environmental monitoring.

Keywords: HSP; insects; abiotic stress; biotic stress; climate change; immunity

1. Introduction

Insects depend on external environmental conditions to regulate their body temperature, making them highly susceptible to changes in temperature, humidity, or toxicant exposure that can disrupt critical cellular processes. This reliance on ambient temperatures to control metabolism heightens their vulnerability to thermal extremes, which can lead to protein denaturation, enzymatic dysfunction, and loss of membrane integrity [1]. The extensive ecological and taxonomic diversity exhibited by insects, which includes species adapted to an array of habitats and life strategies, makes them exceptionally valuable models for investigating the functions of HSPs across diverse environmental conditions and biological contexts. This diversity is increasingly important as climate change intensifies thermal extremes, amplifying the importance of HSPs for insect survival. Global warming

introduces unprecedented pressures, accelerating metabolic rates, increasing dehydration, altering reproductive cycles, and reshaping ecological interactions [2]. Together with anthropogenic stressors like pesticides and habitat fragmentation [3], these factors create a complex stress landscape that tests insect resilience. This review aims to summarize current knowledge on the induction of heat shock proteins (HSPs) under various stressors, elucidate their roles in stress tolerance and immune responses, and underscore their broad relevance in the context of ongoing environmental changes.

Heat shock proteins (HSPs), first identified in *Drosophila melanogaster* through heat-induced chromosomal puffing [4,5], serve as key molecular chaperones that maintain protein integrity under such stressors. These proteins, encompassing ATP-independent small HSPs (sHSPs, 12–43 kDa) and ATP-dependent families like HSP60, HSP70, and HSP90, perform specialized roles facilitating the folding of nascent polypeptides, preventing aggregation of denatured proteins during stress, and aiding cellular recovery post-exposure [6,7]. The induction of HSPs is orchestrated by heat shock factors (HSFs), which bind to heat shock elements (HSEs) within promoter regions of target genes. These HSEs are specific DNA sequences recognized by HSFs, functioning as transcriptional activators that upregulate HSP gene expression in response to various stress stimuli, particularly thermal stress [8] (Figure 1).

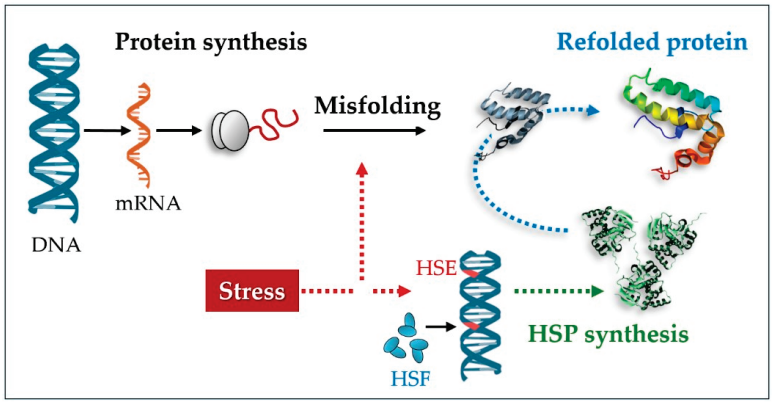


Figure 1. An illustrative scheme of the function of HSPs. Stressors can induce alterations in the molecular architecture of proteins by affecting their functionality; the presence of HSPs controls or restores proper folding while maintaining their functionality.

HSFs, in particular HSF1, are the primary drivers of heat shock protein (HSP) gene transcription [9]. However, HSFs are not the sole regulators of HSP expression since other transcription factors contribute significantly in a context-dependent manner. Feedback loops and crosstalk integrate HSP expression into broader cellular responses. For instance, DREF may be involved in the modulation of Hsp70 expression via DNA replication-related elements during development [10], the GAGA factor enhances chromatin accessibility and directly regulates Hsp70 and Hsp26 through (GA)n sequences [11], and STATs are able to modulate HSP70 and HSP90 gene promoters, playing an important role in HSPs gene activation [12]. Epigenetic mechanisms, including histone acetylation by CBP/p300 [13] and chromatin remodeling by the SWI/SNF homolog BAP [14], further regulate HSP gene accessibility. Thus, while HSF1 is central, a complex network of transcription factors and epigenetic regulators ensures precise, context-specific HSP expression.

The induction of HSPs is not confined to stress exposure [15]; instead, they can be constitutively expressed at basal levels to maintain protein homeostasis. Many of these factors are also present during normal physiological states, where they function as normal regulators of protein activity. HSPs could also be encoded by constitutive gene pathways,

known as Heat Shock Cognates (HSC70 family), which are expressed under non-stress conditions and assist in post-translational protein folding and membrane integration. In contrast, inducible HSPs, e.g., HSP27, HSP70, HSP90, produced in response to cellular stress, help fold and stabilize partially denatured proteins, thereby preserving proteostasis. For example, in *Bombyx mori*, *Bemisia tabaci*, and various *Drosophila* species, both inducible (HSP70s) and constitutive (HSC70s) forms of molecular chaperones are present. Their expression patterns vary depending on developmental stage and tissue type across different body regions [16–19].

Recent studies suggest that HSPs also play a role beyond stress response, contributing significantly to key immunological and developmental processes. For instance, several investigations in *Aspongopus chinensis* have identified 25 HSP genes with distinct expression patterns between diapause and non-diapause stages; notably, the significant downregulation of HSP70-5 during diapause highlights a critical link between endocrine regulation and immune readiness [20]. Moreover, evidence from *Bombyx mori* indicates that 16 sHSPs exhibit tissue-specific expression with differential peaks in the midgut during feeding and in the gonads during pupation, suggesting developmental roles that extend beyond immediate stress responses [21]. By changing the normal physiological level, under abiotic (thermal or chemical) or biotic stress conditions, HSP90 increases significantly, enabling insects to withstand environmental challenges.

HSPs play a crucial role in immune responses, integrating into the sophisticated signaling networks that underpin insect immunity. Three primary immune pathways, the IMD, Toll, and Jak/STAT pathways (Figure 2) govern the recognition of pathogens and the orchestration of immune defenses [22]. The IMD pathway, targeting Gram-negative bacteria, activates a cascade involving proteins such as IMD, FADD, and Dredd, leading to the transcription of antimicrobial peptides (AMPs) like defensins and cecropins [23,24]. The Toll pathway specializes in defense against Gram-positive bacteria and fungi [22], employing receptors like Toll and Spätzle to initiate downstream signaling through MyD88, Tube, and Pelle, culminating in the production of AMPs via transcription factors Dorsal and Dif [25]. Meanwhile, the Jak/STAT pathway is essential for the innate immune system, playing a crucial role in not only defending insects against bacterial, fungal, and viral pathogens but also in tissue repair, relying on cytokines or stress signals to activate Jak kinases and STAT transcription factors that regulate genes encoding AMPs and stress-response proteins [26,27].

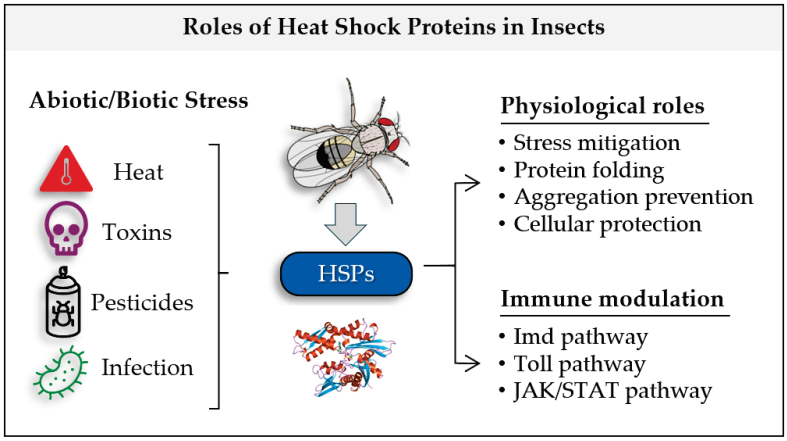


Figure 2. Physiological and immunological role of insects' HSPs.

Emerging research highlights the potential interactions between HSPs and these immune pathways. HSPs, such as HSP70 and HSP90, may modulate immune pathway

activity by stabilizing key signaling proteins, enhancing transcription factor activation, or facilitating the rapid turnover of immune components. These interactions suggest that HSPs contribute not only to stress tolerance but also to immune resilience, underscoring their dual protective role in the face of environmental and biological challenges.

2. Thermal Stress and Heat Shock Proteins

Insects are routinely exposed to extreme thermal conditions that can disrupt protein structure, elevate oxidative stress, and impair cellular homeostasis. With climate change intensifying, these challenges are becoming more severe and rising global temperatures with increasingly uneven weather patterns exacerbate thermal stress, impacting insect survival, reproduction, and ecosystem functions; in this context, HSPs are pivotal in mounting rapid and coordinated defenses against such abiotic challenges. For instance, studies on the locust bean moth, *Ectomyelois ceratoniae*, demonstrate that exposure to extreme temperatures, whether intense heat or severe cold, stimulates the production of these proteins. Interestingly, HSP70 is mainly expressed during cold stress, whereas HSP90 shows higher expression levels under heat, indicating their specialized roles in handling distinct thermal challenges in this insect [28]. In the bumblebee *Bombus terrestris*, thermal stress at temperatures of 9 °C or 38 °C leads to a three-fold increase in HSC (HSP70 family) and its co-chaperone Aha. Remarkably, this upregulation occurs without compromising immune function, suggesting that HSP expression can be precisely modulated to address both thermal and immunological demands [29]. The nocturnal moth *Spodoptera litura*, part of the family Noctuidae, exhibits broad-spectrum thermal protection through the induction of SlHSP20.4 under both heat (42 °C) and cold (5 °C) stresses. This response likely operates under the regulation of distinct isoforms of HSFs, enabling the organism to withstand diverse stress conditions [30]. Similarly, in the bloodsucking bug *Rhodnius prolixus*, HSP70 expression significantly increases at both 0 °C and 40 °C, supporting vital physiological functions such as digestion and molting. RNAi-mediated silencing of HSP70 in this species results in a 60% reduction in survival, underscoring the indispensability of this protein in thermal tolerance [31]. In contrast, the brown planthopper *Nilaparvata lugens* exhibits a biphasic response to thermal stress, HSP70 levels remain stable between 28 °C and 40 °C, dropping significantly during cold stress at 5 °C, only to rebound at 25 °C; this pattern suggests a sophisticated adaptive mechanism that may involve post-translational modifications and interactions with co-chaperones like HSP40. Furthermore, this response to temperature changes seems to correlate with increased resistance to insecticides such as imidacloprid [32].

Specifically considering heat shock-induced stress, in the aquatic chironomid *Prodiamesa olivacea*, exposure to 35 °C results in a dramatic 128-fold increase in HSP70 expression; this remarkable upregulation stabilizes denatured proteins, making HSP70 a sensitive biomarker for thermal stress in freshwater habitats, where increased temperatures exacerbate oxygen depletion and metabolic demands [33]. Similarly, in larvae of *Glyphodes pyloalis*, heat stress at 40 °C induces multiple HSPs that act synergistically with antioxidant enzymes, such as superoxide dismutase (SOD) and catalase, to counteract oxidative damage [34]. Prolonged exposure to 40 °C in this lepidopteran species significantly upregulates GpHSP71.3 and GpHSP82.4; indeed, following RNAi-mediated silencing of GpHSP82.4, mortality increases by 70%, underscoring its critical protective function under heat stress [35].

In *D. melanogaster*, heat stress at 37 °C rapidly induces HSP70 in a tissue-specific manner, with peak expression within two hours. This response also exhibits significant sex-specific differences, highlighting the fine regulation of thermotolerance mechanisms [36,37].

Moreover, in the springtail *Orchesella cincta*, delayed but sustained HSP70 induction correlates strongly with survival during gradual temperature shifts, confirming the adaptive advantage of prolonged HSP expression under slowly changing environmental conditions [38]. Studies on pest species further elucidate the multifaceted roles of HSPs in thermal stress adaptation. In *Mamestra brassicae*, pre-exposure to 37 °C increases the expression of HSP70, HSP90, and HSP60 by five- to eight-fold, enhancing fungal infection survival by 40% through improved phagocytosis [39]. In *Aedes aegypti*, acute heat stress dramatically upregulates small HSPs, emphasizing the species' sensitivity to elevated temperatures [40]. Likewise, in *Grapholita molesta*, pupal exposure to 38 °C for four hours enhances HSP70 and HSP21 expression by 15-fold, boosting adult survival by 25% and reproductive output by 30%, a hormetic effect that highlights the adaptive benefits of HSPs under heat stress [41]. In *Galleria mellonella*, heat shock at 40 °C not only increases the abundance of antimicrobial peptides such as cecropin by four-fold, enhancing survival by 50%, but also boosts antifungal activity by 70% when combined with short-term heat shocks [42,43]. Similarly, in *Agasicles hygrophila*, the heat shock factor AhHSF regulates the transcription of AhHSP70 and AhHSP21 between 36 °C and 39 °C, with RNAi silencing of AhHSF reducing survival by 60% [44]. Finally, in *Spodoptera exigua*, HSPs such as SexHSP74 and SexHSP83 play distinct roles in short- and long-term recovery from heat stress [45]. Heat stress also influences the effects of pesticides; for instance, in *Anopheles sinensis*, AsHSP90AB, upregulated eight-fold under heat stress, interacts with cytochrome P450 enzymes to confer pyrethroid resistance [46]. High levels of HSP expression following thermal shock result from the effectiveness of their promoter. For instance, in *Aedes albopictus*, the use of a *Drosophila* HSP70 promoter increases transfection efficiency ten-fold at 41 °C, demonstrating the value of HSP regulatory elements in genetic research [47]. HSPs are also involved in the regulation of hormonal interactions after heat shock. For example, in *Helicoverpa armigera*, HSP90 phosphorylation mediated by protein kinase C facilitates hormonal interactions between 20-hydroxyecdysone and juvenile hormone signaling under heat stress [48].

Considering only low temperatures, studies in *D. melanogaster* have revealed that under cold stress conditions (0 °C), heat shock proteins (HSPs) function as damage-associated molecular patterns (DAMPs), activating the JAK/STAT immune pathway [49]. Similarly, research on *Ostrinia furnacalis* demonstrates that exposure to 8 °C results in six-fold upregulation of small HSPs and HSP90, alongside immune genes. This finding underscores their dual role in facilitating cold adaptation and promoting immune responses [50]. Furthermore, investigations into *Pyrrhocoris apterus* highlight the critical involvement of HSP70 in recovery from chilling injuries at 0 °C. RNAi-mediated knockdown of HSP70 significantly impairs this recovery process, confirming its essential role in cold stress tolerance [51].

3. Dehydration Stress and Heat Shock Proteins

Climate change intensifies droughts worldwide, driven by rising global temperatures and altered precipitation patterns, all of which reduce water availability. These environmental shifts severely affect insect biodiversity, threatening the essential roles insects play in ecosystems such as pollination, population control, and decomposition. HSPs are recognized as critical molecular tools in insect responses to dehydration and anhydrobiosis. Studies on the Antarctic midge *Belgica antarctica* reveal that HSPs (sHSP, HSP70, HSP90) are rapidly upregulated under dehydration and overhydration, helping maintain cellular homeostasis [52]. The sleeping chironomid *Polypedilum vanderplanki* undergoes anhydrobiosis, a survival mechanism in which HSPs such as Pv-HSP90, Pv-HSP70, Pv-HSC70, Pv-HSP60, Pv-HSP20, and Pv-p23, along with Pv-HSF1, are highly expressed during

desiccation. This demonstrates their role in protecting cellular structures and metabolic functions [53]. Additional research, including RNAi studies on mosquitoes (*Aedes aegypti*, *Anopheles gambiae*, and *Culex pipiens*), highlights species-specific variations in HSP expression during dehydration, underscoring their role in water balance [54]. In bed bugs (*Cimex lectularius*), HSP70 and HSP90 are critical for managing dehydration stress, with HSP90 playing a dominant role during recovery [55]. Collectively, these findings underline the importance of HSPs in enabling insect resilience to extreme dehydration, providing key insights into adaptations crucial for survival in changing environments.

4. Biotic Stresses and Heat Shock Proteins

HSPs are critical for insect survival because, in addition to maintaining cellular proteostasis, they orchestrate complex immune responses against various pathogenic challenges. Indeed, studies in insects indicate that HSPs play an essential role in immune defense mechanisms [56]; for instance, their expression may be significantly affected by pathogen exposure. In the Chinese oak tussar moth *Antheraea pernyi*, the expression of sHSP21 (*ApsHSP21*) was analyzed in immune tissues using qRT-PCR following different pathogen challenges, including lipopolysaccharide (LPS), peptidoglycan (PGN), glucan, and nucleopolyhedrovirus (NPV). The results showed that *ApsHSP21* expression varied depending on the infecting pathogen. In response to LPS, its expression significantly increased, reaching peak levels at 6 and 12 h after injection. PGN exposure led to an earlier peak at 3 h, with glucan treatment also causing a similar early peak at 3 h post-injection. When challenged with NPV, *ApsHSP21* exhibited a substantial increase, peaking at 36 h post-injection. These findings indicate that sHSP21 plays a dynamic role in immune defense, responding differently depending on the nature of the pathogen [57]. Complementary research on the ApsHSP21.4 isoform reveals its capacity to modulate immune-related gene expression after NPV challenge, with eicosanoid signaling mediated by lipid-derived molecules, such as prostaglandins and leukotrienes, serving as a pivotal regulatory mechanism in this crosstalk [58]. In the red flour beetle *Tribolium castaneum*, exposure to LPS elicits coordinated upregulation of HSPs alongside immune effectors, including defensins and thaumatins, the latter of which disrupt microbial membranes and may have evolved through horizontal gene transfer to enhance antifungal protection [59].

Further complexity is evident in *D. melanogaster*, wherein exposure to viral agents causes context-dependent modulation of heat shock protein (HSP) expression. For example, infection with Drosophila C virus leads to upregulation of HSP levels, a response that may result from differential activation or targeting of HSFs. Viral infections, therefore, appear to act as modulators of HSP synthesis. In cases of upregulation, this response may facilitate viral replication and spread through HSP-mediated assembly of molecular complexes such as viral replicases [60–62]. Consistently, inhibition of HSPs has been shown to impair viral replication by disrupting virus-HSP interactions [63]. In contrast, infection of *D. melanogaster* cells with cricket paralysis virus (CrPV) has been reported to suppress HSP expression by approximately 50% [64].

Another study conducted by Zhang and colleagues investigates the interaction between destruxins (DA) and heat shock proteins (HSPs) in silkworm cells; DA induces the up-regulation of Bm*HSP70-3*, Bm*HSP75*, Bm*HSP83*, and Bm*HSCP* genes. Interestingly, the higher expression levels of the HSP70 family (Bm*HSP70-3* and Bm*HSCP*) under DA stress suggest a stronger response compared to the HSP90 family (Bm*HSP75* and Bm*HSP83*) [65]. Another organism widely used in research in this field is *G. mellonella*; for instance, Wojda and colleagues infected this insect with *Bacillus thuringiensis* [66]. The infection induces a five-fold increase in HSP90 expression. More interestingly, the subsequent application

of the HSP90 binding compound DMAG-17 results in higher antimicrobial defense due to the enhanced production of antimicrobial peptides (AMPs), improving larval survival. The binding of 17-DMAG to HSP90 disrupts its interaction with associated chaperone proteins, including HSF-1. The latter is a transcription factor that becomes active under heat shock or stress conditions, dissociating from its inactive complex with HSP90 to enable the transcription of stress-related genes. This process is mimicked by 17-DMAG, as it induces the dissociation of Hsf-1 from HSP90 [66].

Regarding biotic stresses caused by organisms other than bacteria, infection with the nematode *Steinernema carpocapsae* deprived of its cuticle modulates HSP90 expression by four-fold, while the untreated and dead nematodes lead respectively to slightly increased and unchanged HSP90 expression, highlighting the direct involvement of HSPs in nematode-induced biotic stress [67]. Another study conducted on *G. mellonella* larvae investigated the role of several HSPs' responses after infection by the fungus *Conidiobolus coronatus* [68]. HSP60 and HSP90 were prevalent in healthy larvae, while HSP70 and HSP27 were present in trace amounts; upon infection, the levels of HSP60 and HSP27 increased at both 24 h and 48 h, while that of HSP90 increased only at 48 h; no changes were observed in HSP70 levels. These findings highlight the specific roles of HSPs in insects during fungal infection, offering insights into the interplay between insect immunity and pathogens.

Together, these findings highlight the pivotal role of HSPs as adaptable molecular chaperones, seamlessly integrating innate immune signaling with cellular repair mechanisms. This enables insects to thrive in pathogen-rich environments. HSPs are essential for insect survival, ensuring cellular stability while driving adaptive immune responses to diverse pathogens. Research across various insect models has revealed the dynamic and context-dependent expression of HSPs, emphasizing their critical flexibility in addressing specific immune challenges. These studies underscore the importance of HSPs in shaping insect immune defenses, offering profound insights for fundamental research and practical advancements in pest management and immunity studies.

The following Table 1 provides a summary of the stressors and roles of the main HSPs.

Table 1. Stressors and functions of major HSPs.

HSP	Stressors	Functions
HSP 90	• Heat and cold • Dehydration • Rehydration • Insecticides • Toxins • Microorganisms • Parasites • Starvation	• Enhances survival under thermal stress, infections, and insecticide challenges • Facilitates protein folding of misfolded proteins during stress, preventing aggregation • Prevents aggregation of denatured proteins • Stabilizes proteins during stress responses • Supports proteostasis under water stress • Stabilizes signaling kinases and stress-signal transduction pathways under stress • Modulates host-pathogen interactions
HSP 60/70	• Heat and cold • Dehydration • Rehydration • Insecticides • Toxins • Microorganisms • Parasites	• Enhances survival under thermal stress, infections, and insecticide challenges • Facilitates protein folding of misfolded proteins during stress, preventing aggregation • Stabilizes proteins under stress conditions • Prevents aggregation of denatured proteins • Improves thermotolerance and aids recovery after stresses • Supports water-loss tolerance, aiding survival after dehydration and anhydrobiosis • Promotes stress-signal transduction • Exhibits anti-apoptosis effects • Play a role in immune regulation

Table 1. *Cont.*

HSP	Stressors	Functions
HSPs small	• Heat and cold • Dehydration • Rehydration • Microorganisms • Virus	• Enhances survival under thermal stress and infections • Facilitates protein folding of misfolded proteins during stress, preventing aggregation • Stabilizes proteins under stress conditions • Protects against oxidative stress • Promotes innate immune signaling and modulates immune-related genes • Stabilizes the cytoskeleton
Detailed information on the HSPs summarized in this table can be found in supplementary material		

5. Conclusions

In summary, our mini review underscores the integral role of HSPs in enhancing insect resilience against both abiotic and biotic stressors. The literature cited in this article clearly outlines the multifaceted role of HSPs in physiological control in response to stress. By stabilizing proteins, coordinating with antioxidant defenses, and engaging with various cellular stress response mechanisms, HSPs preserve cellular integrity and enhance resilience against environmental fluctuations.

In the context of global climate change, their roles are increasingly significant, offering insights into adaptive mechanisms that may inform broader strategies for understanding biological resilience. HSPs not only maintain cellular integrity by facilitating protein folding and repair but also actively modulate immune responses through pathways such as Toll/NF-κB and integrin-mediated phagocytosis. The remarkable plasticity in their expression, varying across developmental stages, tissues, and environmental conditions, demonstrates a finely tuned system evolved to withstand thermal extremes, chemical exposures, and pathogen attacks. Furthermore, the dual role of HSPs as protectors of cellular homeostasis and as indicators of environmental change positions them as promising biomarkers for assessing ecosystem health in the context of global climate change. Their potential application in pest management, particularly through RNA interference strategies, highlights the translational relevance of these proteins in developing sustainable control measures while minimizing ecological disruption. Future research is critical to further investigate the complex interactions between HSP networks and other stress response systems, including co-chaperone interactions and cross-tolerance mechanisms. These studies are essential for improving our ability to predict insect responses in the context of increasingly variable climatic conditions, as well as for optimizing strategies that concurrently promote agricultural productivity and biodiversity conservation.

Supplementary Materials: The following supporting information can be downloaded at https://www.mdpi.com/article/10.3390/insects16070741/s1. Table S1: HSP full table.

Author Contributions: Conceptualization D.B., T.B. and M.F.B.; writing—original draft preparation, D.B., T.B. and M.F.B.; writing—review and editing D.B., T.B., M.M. and M.F.B.; supervision D.B. and M.F.B.; funding acquisition M.F.B. All authors have read and agreed to the published version of the manuscript.

Funding: This research was funded by FAR 2024 from the University of Insubria.

Data Availability Statement: No new data were created or analyzed in this study. Data sharing is not applicable to this article.

Acknowledgments: We are grateful to Elisa Broggio for her critical reading of the manuscript.

Conflicts of Interest: The authors declare no conflicts of interest.

References

1. Grgac, R.; Rozsypal, J.; Des Marteaux, L.; Stetina, T.; Kostal, V. Stabilization of Insect Cell Membranes and Soluble Enzymes by Accumulated Cryoprotectants during Freezing Stress. *Proc. Natl. Acad. Sci. USA* **2022**, *119*, e2211744119. [CrossRef] [PubMed]
2. Shrestha, S. Effects of Climate Change in Agricultural Insect Pest. *Acta Sci. Agric.* **2019**, *3*, 74–80. [CrossRef]
3. Sánchez-Bayo, F.; Wyckhuys, K.A.G. Worldwide Decline of the Entomofauna: A Review of Its Drivers. *Biol. Conserv.* **2019**, *232*, 8–27. [CrossRef]
4. Ritossa, F. A New Puffing Pattern Induced by Temperature Shock and DNP in *Drosophila*. *Experientia* **1962**, *18*, 571–573. [CrossRef]
5. Ritossa, F. Discovery of the Heat Shock Response. *Cell Stress Chaperones* **1996**, *1*, 97–98. [CrossRef] [PubMed]
6. Tutar, L.; Tutar, Y. Heat Shock Proteins; An Overview. *Curr. Pharm. Biotechnol.* **2010**, *11*, 216–222. [CrossRef] [PubMed]
7. Hu, C.; Yang, J.; Qi, Z.; Wu, H.; Wang, B.; Zou, F.; Mei, H.; Liu, J.; Wang, W.; Liu, Q. Heat Shock Proteins: Biological Functions, Pathological Roles, and Therapeutic Opportunities. *MedComm* **2022**, *3*, e161. [CrossRef] [PubMed]
8. Alagar Boopathy, L.R.; Jacob-Tomas, S.; Alecki, C.; Vera, M. Mechanisms Tailoring the Expression of Heat Shock Proteins to Proteostasis Challenges. *J. Biol. Chem.* **2022**, *298*, 101796. [CrossRef] [PubMed]
9. Åkerfelt, M.; Morimoto, R.I.; Sistonen, L. Heat Shock Factors: Integrators of Cell Stress, Development and Lifespan. *Nat. Rev. Mol. Cell Biol.* **2010**, *11*, 545–555. [CrossRef] [PubMed]
10. Matsukage, A.; Hirose, F.; Yoo, M.A.; Yamaguchi, M. The DRE/DREF Transcriptional Regulatory System: A Master Key for Cell Proliferation. *Biochim. Biophys. Acta Gene Regul. Mech.* **2008**, *1779*, 81–89. [CrossRef] [PubMed]
11. Wilkins, R.C.; Lis, J.T. GAGA Factor Binding to DNA via a Single Trinucleotide Sequence Element. *Nucleic Acids Res.* **1998**, *26*, 2672–2678. [CrossRef] [PubMed]
12. Stephanou, A.; Latchman, D.S. Transcriptional Regulation o f the Heat Shock Protein Genes by STAT Family Transcription Factors. *Gene Expr.* **2018**, *7*, 311.
13. Westerheide, S.D.; Anckar, J.; Stevens, S.M.; Sistonen, L.; Morimoto, R.I. Stress-Inducible Regulation of Heat Shock Factor 1 by the Deacetylase SIRT. *Science* **2009**, *323*, 1063–1066. [CrossRef] [PubMed]
14. Sullivan, E.K.; Weirich, C.S.; Guyon, J.R.; Sif, S.; Kingston, R.E. Transcriptional Activation Domains of Human Heat Shock Factor 1 Recruit Human SWI/SNF. *Mol. Cell. Biol.* **2001**, *21*, 5826–5837. [CrossRef] [PubMed]
15. Chen, B.; Feder, M.E.; Kang, L. Evolution of Heat-Shock Protein Expression Underlying Adaptive Responses to Environmental Stress. *Mol. Ecol.* **2018**, *27*, 3040–3054. [CrossRef] [PubMed]
16. Fang, S.M.; Zhang, Q.; Zhang, Y.L.; Zhang, G.Z.; Zhang, Z.; Yu, Q.Y. Heat Shock Protein 70 Family in Response to Multiple Abiotic Stresses in the Silkworm. *Insects* **2021**, *12*, 928. [CrossRef] [PubMed]
17. Wang, X.-R.; Wang, C.; Ban, F.-X.; Zhu, D.-T.; Liu, S.-S.; Wang, X.-W. Genome-Wide Identification and Characterization of HSP Gene Superfamily in Whitefly (*Bemisia tabaci*) and Expression Profiling Analysis under Temperature Stress. *Insect Sci.* **2019**, *26*, 44–57. [CrossRef] [PubMed]
18. Pauli, D.; Arrigo, A.-P.; Tissières, A. Heat Shock Response in Drosophila. *Experientia* **1992**, *48*, 623–629. [CrossRef] [PubMed]
19. Jagla, T.; Dubińska-Magiera, M.; Poovathumkadavil, P.; Daczewska, M.; Jagla, K. Developmental Expression and Functions of the Small Heat Shock Proteins in Drosophila. *Int. J. Mol. Sci.* **2018**, *19*, 3441. [CrossRef] [PubMed]
20. Ma, X.; Yin, Z.; Li, H.; Guo, J. HSP Gene Superfamily in *Aspongopus chinensis* Dallas: Unravelling Identification, Characterisation and Expression Patterns during Diapause and Non-Diapause Stages. *Bull. Entomol. Res.* **2024**, *114*, 260–270. [CrossRef] [PubMed]
21. Li, J.; Moghaddam, S.H.H.; Du, X.; Zhong, B.X.; Chen, Y.Y. Comparative Analysis on the Expression of Inducible HSPs in the Silkworm, *Bombyx mori*. *Mol. Biol. Rep.* **2012**, *39*, 3915–3923. [CrossRef] [PubMed]
22. Zhang, W.; Tettamanti, G.; Bassal, T.; Heryanto, C.; Eleftherianos, I.; Mohamed, A. Regulators and Signalling in Insect Antimicrobial Innate Immunity: Functional Molecules and Cellular Pathways. *Cell. Signal.* **2021**, *83*, 110003. [CrossRef] [PubMed]
23. Müller, U.; Vogel, P.; Alber, G.; Schaub, G. The Innate Immune System of Mammals and Insects. *Contrib. Microbiol.* **2008**, *15*, 21–44. [PubMed]
24. Nishide, Y.; Kageyama, D.; Yokoi, K.; Jouraku, A.; Tanaka, H.; Futahashi, R.; Fukatsu, T. Functional Crosstalk across IMD and Toll Pathways: Insight into the Evolution of Incomplete Immune Cascades. *Proc. R. Soc. B Biol. Sci.* **2019**, *286*, 20182207. [CrossRef] [PubMed]
25. Roh, K.B.; Kim, C.H.; Lee, H.; Kwon, H.M.; Park, J.W.; Ryu, J.H.; Kurokawa, K.; Ha, N.C.; Lee, W.J.; Lemaitre, B.; et al. Proteolytic Cascade for the Activation of the Insect Toll Pathway Induced by the Fungal Cell Wall Component. *J. Biol. Chem.* **2009**, *284*, 19474–19481. [CrossRef] [PubMed]
26. Bang, I.S. JAK/STAT Signaling in Insect Innate Immunity. *Entomol. Res.* **2019**, *49*, 339–353. [CrossRef]
27. Ding, B.; Zhang, C.; He, L.; Zeng, Q.; Zhang, S.; Yang, H.; Yang, H. JAK/STAT Signaling Pathway Is Involved in Antibacterial Immunity in the Green Peach Aphid *Myzus persicae* (Sulzer). *Pestic. Biochem. Physiol.* **2024**, *205*, 106168. [CrossRef] [PubMed]

28. Farahani, S.; Bandani, A.R.; Alizadeh, H.; Goldansaz, S.H.; Whyard, S. Differential Expression of Heat Shock Proteins and Antioxidant Enzymes in Response to Temperature, Starvation, and Parasitism in the Carob Moth Larvae, *Ectomyelois ceratoniae* (Lepidoptera: Pyralidae). *PLoS ONE* **2020**, *15*, e0228104. [CrossRef] [PubMed]
29. Blasco-Lavilla, N.; García-Reina, A.; De la Rúa, P. Mild Thermal Stress Does Not Negatively Affect Immune Gene Expression in the Bumblebee *Bombus terrestris*. *Apidologie* **2021**, *52*, 163–173. [CrossRef]
30. Shen, Y.; Gu, J.; Huang, L.H.; Zheng, S.C.; Liu, L.; Xu, W.H.; Feng, Q.L.; Kang, L. Cloning and Expression Analysis of Six Small Heat Shock Protein Genes in the Common Cutworm, *Spodoptera litura*. *J. Insect. Physiol.* **2011**, *57*, 908–914. [CrossRef] [PubMed]
31. Paim, R.M.M.; Araujo, R.N.; Leis, M.; Sant'anna, M.R.V.; Gontijo, N.F.; Lazzari, C.R.; Pereira, M.H. Functional Evaluation of Heat Shock Proteins 70 (HSP70/HSC70) on *Rhodnius prolixus* (Hemiptera, Reduviidae) Physiological Responses Associated with Feeding and Starvation. *Insect Biochem. Mol. Biol.* **2016**, *77*, 10–20. [CrossRef] [PubMed]
32. Lu, K.; Chen, X.; Liu, W.; Zhang, Z.; Wang, Y.; You, K.; Li, Y.; Zhang, R.; Zhou, Q. Characterization of Heat Shock Protein 70 Transcript from *Nilaparvata lugens* (Stål): Its Response to Temperature and Insecticide Stresses. *Pestic. Biochem. Physiol.* **2017**, *142*, 102–110. [CrossRef] [PubMed]
33. Llorente, L.; Aquilino, M.; Herrero, Ó.; de la Peña, E.; Planelló, R. Characterization and Expression of Heat Shock and Immune Genes in Natural Populations of *Prodiamesa olivacea* (Diptera) Exposed to Thermal Stress. *Ecotoxicol. Environ. Saf.* **2023**, *263*, 115359. [CrossRef] [PubMed]
34. Liu, Y.; Su, H.; Li, R.; Li, X.; Xu, Y.; Dai, X.; Zhou, Y.; Wang, H. Comparative Transcriptome Analysis of *Glyphodes pyloalis* Walker (Lepidoptera: Pyralidae) Reveals Novel Insights into Heat Stress Tolerance in Insects. *BMC Genom.* **2017**, *18*, 974. [CrossRef] [PubMed]
35. Ding, J.H.; Zheng, L.X.; Chu, J.; Liang, X.H.; Wang, J.; Gao, X.W.; Wu, F.A.; Sheng, S. Characterization, and Functional Analysis of Hsp70 and Hsp90 Gene Families in *Glyphodes pyloalis* Walker (Lepidoptera: Pyralidae). *Front. Physiol.* **2021**, *12*, 753914. [CrossRef] [PubMed]
36. Dahlgaard, J.; Loeschcke, V.; Michalak, P.; Justesen, J. Induced Thermotolerance and Associated Expression of the Heat-Shock Protein Hsp70 in Adult *Drosophila melanogaster*. *Funct. Ecol.* **1998**, *12*, 786–793. [CrossRef]
37. Krebs, R.A.; Feder, M.E. Tissue-Specific Variation in Hsp70 Expression and Thermal Damage in *Drosophila melanogaster* Larvae. *J. Exp. Biol.* **1997**, *200*, 2007–2015. [CrossRef] [PubMed]
38. Bahrndorff, S.; Mariën, J.; Loeschcke, V.; Ellers, J. Dynamics of Heat-Induced Thermal Stress Resistance and Hsp70 Expression in the Springtail, *Orchesella cincta*. *Funct. Ecol.* **2009**, *23*, 233–239. [CrossRef]
39. Richards, E.H.; Dani, M.P.; Lu, Y.; Butt, T.; Weaver, R.J. Effect of Stress on Heat Shock Protein Levels, Immune Response and Survival to Fungal Infection of *Mamestra brassicae* Larvae. *J. Insect Physiol.* **2017**, *96*, 53–63. [CrossRef] [PubMed]
40. Zhao, L.; Becnel, J.J.; Clark, G.G.; Linthicum, K.J. Expression of AeaHsp26 and AeaHsp83 in *Aedes aegypti* (Diptera: Culicidae) Larvae and Pupae in Response to Heat Shock Stress. *J. Med. Entomol.* **2010**, *47*, 367–375. [CrossRef] [PubMed]
41. Su, Y.; Li, X.; Zhang, W.; Zhang, B.; Ma, C. Sen Dynamics of Heat Shock Protein Responses to Thermal Stress Changes after Metamorphosis in a Lepidopteran Insect. *Arch. Insect Biochem. Physiol.* **2021**, *107*, e21791. [CrossRef] [PubMed]
42. Wojda, I.; Kowalski, P.; Jakubowicz, T. Humoral Immune Response of *Galleria mellonella* Larvae after Infection by *Beauveria bassiana* under Optimal and Heat-Shock Conditions. *J. Insect Physiol.* **2009**, *55*, 525–531. [CrossRef] [PubMed]
43. Wojda, I.; Taszłow, P. Heat Shock Affects Host-Pathogen Interaction in *Galleria mellonella* Infected with *Bacillus thuringiensis*. *J. Insect Physiol.* **2013**, *59*, 894–905. [CrossRef] [PubMed]
44. Jin, J.; Li, Y.; Zhou, Z.; Zhang, H.; Guo, J.; Wan, F. Heat Shock Factor Is Involved in Regulating the Transcriptional Expression of Two Potential Hsps (AhHsp70 and AhsHsp21) and Its Role in Heat Shock Response of *Agasicles hygrophila*. *Front. Physiol.* **2020**, *11*, 562204. [CrossRef] [PubMed]
45. Xu, Q.; Zou, Q.; Zheng, H.; Zhang, F.; Tang, B.; Wang, S. Three Heat Shock Proteins from *Spodoptera exigua*: Gene Cloning, Characterization and Comparative Stress Response during Heat and Cold Shocks. *Comp. Biochem. Physiol. B Biochem. Mol. Biol.* **2011**, *159*, 92–102. [CrossRef] [PubMed]
46. Si, F.L.; Qiao, L.; He, Q.Y.; Zhou, Y.; Yan, Z.T.; Chen, B. HSP Superfamily of Genes in the Malaria Vector *Anopheles sinensis*: Diversity, Phylogenetics and Association with Pyrethroid Resistance. *Malar. J.* **2019**, *18*, 132. [CrossRef] [PubMed]
47. Gerenday, A.; Park, Y.-J.; Lan, Q.; Fallon, A.M. Expression Of A Heat-Inducible Gene In Transfected Mosquito Cells. *Insect Biochem.* **1989**, *19*, 679–686. [CrossRef]
48. Liu, W.; Zhang, F.X.; Cai, M.J.; Zhao, W.L.; Li, X.R.; Wang, J.X.; Zhao, X.F. The Hormone-Dependent Function of Hsp90 in the Crosstalk between 20-Hydroxyecdysone and Juvenile Hormone Signaling Pathways in Insects Is Determined by Differential Phosphorylation and Protein Interactions. *Biochim. Biophys. Acta Gen. Subj.* **2013**, *1830*, 5184–5192. [CrossRef] [PubMed]
49. El-Saadi, M.I.; MacMillan, H.A.; Ferguson, L.V. Cold-Induced Immune Activation in Chill-Susceptible Insects. *Curr. Opin. Insect Sci.* **2023**, *58*, 101054. [CrossRef] [PubMed]

50. Chen, K.; Tang, T.; Song, Q.; Wang, Z.; He, K.; Liu, X.; Song, J.; Wang, L.; Yang, Y.; Feng, C. Transcription Analysis of the Stress and Immune Response Genes to Temperature Stress in *Ostrinia furnacalis*. *Front. Physiol.* **2019**, *10*, 1289. [CrossRef] [PubMed]
51. Koštál, V.; Tollarová-Borovanská, M. The 70 KDa Heat Shock Protein Assists during the Repair of Chilling Injury in the Insect, *Pyrrhocoris apterus*. *PLoS ONE* **2009**, *4*, e4546. [CrossRef] [PubMed]
52. Lopez-Martinez, G.; Benoit, J.B.; Rinehart, J.P.; Elnitsky, M.A.; Lee, R.E.; Denlinger, D.L. Dehydration, Rehydration, and Overhydration Alter Patterns of Gene Expression in the Antarctic Midge, *Belgica antarctica*. *J. Comp. Physiol. B* **2009**, *179*, 481–491. [CrossRef] [PubMed]
53. Gusev, O.; Cornette, R.; Kikawada, T.; Okuda, T. Expression of Heat Shock Protein-Coding Genes Associated with Anhydrobiosis in an African Chironomid *Polypedilum vanderplanki*. *Cell Stress Chaperones* **2011**, *16*, 81–90. [CrossRef] [PubMed]
54. Benoit, J.B.; Lopez-Martinez, G.; Phillips, Z.P.; Patrick, K.R.; Denlinger, D.L. Heat Shock Proteins Contribute to Mosquito Dehydration Tolerance. *J. Insect Physiol.* **2010**, *56*, 151–156. [CrossRef] [PubMed]
55. Benoit, J.B.; Lopez-Martinez, G.; Teets, N.M.; Phillips, S.A.; Denlinger, D.L. Responses of the Bed Bug, *Cimex lectularius*, to Temperature Extremes and Dehydration: Levels of Tolerance, Rapid Cold Hardening and Expression of Heat Shock Proteins. *Med. Vet. Entomol.* **2009**, *23*, 418–425. [CrossRef] [PubMed]
56. Pockley, A.G. Heat Shock Proteins as Regulators of the Immune Response. *Lancet* **2003**, *362*, 469–476. [CrossRef] [PubMed]
57. Liu, Q.-N.; Liu, Y.; Xin, Z.-Z.; Zhu, X.-Y.; Ge, B.-M.; Li, C.-F.; Wang, D.; Bian, X.-G.; Yang, L.; Chen, L.; et al. A Small Heat Shock Protein 21 (SHSP21) Mediates Immune Responses in Chinese Oak Silkworm *Antheraea pernyi*. *Int. J. Biol. Macromol.* **2018**, *111*, 1027–1031. [CrossRef] [PubMed]
58. Zhang, C.; Dai, L.; Wang, L.; Qian, C.; Wei, G.; Li, J.; Zhu, B.; Liu, C. Inhibitors of Eicosanoid Biosynthesis Influencing the Transcripts Level of SHSP21.4 Gene Induced by Pathogen Infections, in *Antheraea pernyi*. *PLoS ONE* **2015**, *10*, e0121296. [CrossRef] [PubMed]
59. Altincicek, B.; Knorr, E.; Vilcinskas, A. Beetle Immunity: Identification of Immune-Inducible Genes from the Model Insect *Tribolium castaneum*. *Dev. Comp. Immunol.* **2008**, *32*, 585–595. [CrossRef] [PubMed]
60. Lyupina, Y.V.; Dmitrieva, S.B.; Timokhova, A.V.; Beljelarskaya, S.N.; Zatsepina, O.G.; Evgen'ev, M.B.; Mikhailov, V.S. An Important Role of the Heat Shock Response in Infected Cells for Replication of Baculoviruses. *Virology* **2010**, *406*, 336–341. [CrossRef] [PubMed]
61. Alam, S.B.; Rochon, D. Cucumber Necrosis Virus Recruits Cellular Heat Shock Protein 70 Homologs at Several Stages of Infection. *J. Virol.* **2016**, *90*, 3302–3317. [CrossRef] [PubMed]
62. Merkling, S.H.; Overheul, G.J.; Van Mierlo, J.T.; Arends, D.; Gilissen, C.; Van Rij, R.P. The Heat Shock Response Restricts Virus Infection in Drosophila. *Sci. Rep.* **2015**, *5*, 12758. [CrossRef] [PubMed]
63. Wu, S.; Zhao, Y.; Wang, D.; Chen, Z. Mode of Action of Heat Shock Protein (HSP) Inhibitors against Viruses through Host HSP and Virus Interactions. *Genes* **2023**, *14*, 792. [CrossRef] [PubMed]
64. Moore, N.F.; Pullin, J.S.K.; Reavy, B. Inhibition of the Induction of Heat Shock Proteins in *Drosophila melanogaster* Cells Infected with Insect Picornaviruses. *FEBS Lett.* **1981**, *128*, 93–96. [CrossRef] [PubMed]
65. Zhang, H.; Hu, W.; Xiao, M.; Ou, S.; Hu, Q. Destruxin A Induces and Binds HSPs in *Bombyx mori* Bm12 Cells. *J. Agric. Food Chem.* **2017**, *65*, 9849–9853. [CrossRef] [PubMed]
66. Wojda, I.; Kowalski, P. Galleria mellonella Infected with *Bacillus thuringiensis* Involves Hsp90. *Open Life Sci.* **2013**, *8*, 561–569. [CrossRef]
67. Banfi, D.; Mastore, M.; Bianchi, T.; Brivio, M.F. The Expression Levels of Heat Shock Protein 90 (HSP90) in *Galleria mellonella* Following Infection with the Entomopathogenic Nematode *Steinernema carpocapsae* and Its Symbiotic Bacteria *Xenorhabdus nematophila*. *Insects* **2025**, *16*, 201. [CrossRef] [PubMed]
68. Wrońska, A.K.; Boguś, M.I. Heat Shock Proteins (HSP 90, 70, 60, and 27) in *Galleria mellonella* (Lepidoptera) Hemolymph Are Affected by Infection with *Conidiobolus coronatus* (Entomophthorales). *PLoS ONE* **2020**, *15*, e0228556. [CrossRef] [PubMed]

Disclaimer/Publisher's Note: The statements, opinions and data contained in all publications are solely those of the individual author(s) and contributor(s) and not of MDPI and/or the editor(s). MDPI and/or the editor(s) disclaim responsibility for any injury to people or property resulting from any ideas, methods, instructions or products referred to in the content.

insects

MDPI

Article

Functional Analysis of CPSF30 in *Nilaparvata lugens* Using RNA Interference Reveals Its Essential Role in Development and Survival

Shengli Jing [1], Jing Yang [1], Yali Liu [1], Feifei Wang [1], Fang Zheng [1], Aobo Ren [1], Bingbing Yu [1], Yue Zhao [1], Bing Jia [1], Ruixian Chen [1], Bin Yu [1], Qingsong Liu [1,2] and Jingang Xu [1,*]

[1] College of Life Sciences, Xinyang Normal University, Xinyang 464000, China; shljing@xynu.edu.cn (S.J.); jingyang202409@163.com (J.Y.); liuyali_020601@163.com (Y.L.); ffwang202203@163.com (F.W.); zf15837634522@163.com (F.Z.); renaobo202202@163.com (A.R.); yubingbing2021@163.com (B.Y.); zhaoyue040721@126.com (Y.Z.); jia825285@163.com (B.J.); chenruixian2002@163.com (R.C.); yubin_2015@126.com (B.Y.); qingsongliu@henu.edu.cn (Q.L.)

[2] State Key Laboratory of Cotton Bio-Breeding and Integrated Utilization, State Key Laboratory of Crop Stress Adaptation and Improvement, Key Laboratory of Plant Stress Biology, School of Life Sciences, Henan University, Kaifeng 475004, China

* Correspondence: xujg@xynu.edu.cn; Tel.: +86-376-6393582

Simple Summary: The brown planthopper (*Nilaparvata lugens*) is a major pest threatening rice crops, especially in Asia and Africa, causing damage and transmitting harmful viruses. Current control strategies, such as the use of chemical pesticides, are becoming increasingly ineffective due to the development of resistance in pest populations. RNA interference (RNAi) is a promising alternative for silencing essential genes in pests. This study focuses on the *NlCPSF30* gene (homolog of mammalian CPSF30), which is crucial for mRNA processing in brown planthoppers. By using RNAi to knock down the *NlCPSF30* gene, we observed marked reductions in survival rates and notable developmental defects in the pests. These findings highlight the potential of targeting *NlCPSF30* for developing RNAi-based pest control strategies.

Abstract: The brown planthopper (*Nilaparvata lugens*) is a major pest threatening global rice production, significantly reducing yields annually. As *N. lugens* increasingly develops resistance to conventional control methods, such as chemical pesticides, there is an urgent need for innovative and sustainable pest management strategies. Cleavage and Polyadenylation Specificity Factor 30 (CPSF30) is a key protein involved in mRNA 3′ end processing, yet its function in *N. lugens* remains poorly understood. This study aims to elucidate the role of CPSF30 in the growth and development of *N. lugens* and evaluate its potential as a target for RNA interference (RNAi)-based pest control strategies. We cloned and characterized the cDNA sequence of *NlCPSF30*, which encodes a protein of 341 amino acids containing five CCCH zinc-finger domains and two CCHC zinc-knuckle domains. Sequence alignment revealed that NlCPSF30 is highly conserved among insect species, particularly in the zinc-finger domains essential for RNA binding and processing. Phylogenetic analysis showed that NlCPSF30 is closely related to CPSF30 proteins from other hemipteran species. Expression analysis indicated that *NlCPSF30* is most highly expressed in the fat body and during the adult stage, with significantly higher expression in females than in males. RNAi-mediated silencing of *NlCPSF30* in third-instar nymphs resulted in severe phenotypic abnormalities, including disrupted molting and increased mortality following injection of double-stranded RNA (dsRNA) targeting *NlCPSF30*. Moreover, it influenced the expression of genes associated with hormone regulation, namely *NlHry*, *NlE93*, and *NlKr-h1*. These results suggest that *NlCPSF30* is integral to critical physiological processes, with its disruption leading to increased mortality. Our findings identify *NlCPSF30* as an essential gene for *N. lugens*' survival and a promising target for RNAi-based pest management strategies. This study provides a valuable molecular target and theoretical insights for developing RNAi-based control methods against *N. lugens*.

Keywords: *Nilaparvata lugens*; *NlCPSF30*; gene function; lethal phenotypes; RNA interference

1. Introduction

Rice (*Oryza sativa*) is a vital staple crop, particularly in Asia and Africa, but its production is severely threatened by pests such as the brown planthopper (*Nilaparvata lugens*, BPH), a member of the Hemiptera order. This insect is a major pest that causes direct damage to rice plants and transmits viruses like rice stripe virus and rice grassy stunt virus [1–3]. Conventional control methods, including chemical pesticides and resistant crop varieties, are becoming less effective due to the pest's rapid adaptation and the development of pesticide resistance and virulence of this pest [4]. Therefore, developing innovative and sustainable pest management strategies is imperative.

RNA interference (RNAi) has emerged as a promising approach for pest control due to its ability to specifically silence target genes with high precision [5]. This technique harnesses the power of double-stranded RNA (dsRNA), which is introduced into the cells of target organisms. This leads to the effective suppression of gene function, either by completely silencing the gene or significantly reducing its activity. It is worth noting that RNAi serves as a natural regulatory mechanism against viral infections and gene expression in numerous eukaryotic organisms [6]. Therefore, artificial synthesis of dsRNA of specific genes of pests can be used to introduce them into their cells and hinder their growth even though it can result in death. Based on the origin of dsRNA synthesis, two main strategies for pest control are sprayable dsRNA biopesticides and plant-mediated RNAi strategies. The first sprayable dsRNA biopesticide product, Ledprona [7], was approved by the United States Environmental Protection Agency (EPA) in 2023 (U.S. EPA, 2023). Similarly, the first plant-mediated RNAi product, MON87411, was approved by the U.S. EPA in 2017 (U.S. EPA, 2017) [8]. Ledprona is a long dsRNA that targets the *proteasome subunit beta 5* (ds*PSMB5*) of the Colorado potato beetle [7]. MON87411, on the other hand, is a transgenic maize variety that expresses a dsRNA targeting *sucrose non-fermenting 7* (*DvSnf7*) of the western corn rootworm [8]. These commercially available products represent a novel class of RNAi-based biopesticides for pest control. As a result, numerous studies have focused on investigating the gene functions of various agricultural pests using RNAi approaches, particularly Hemiptera pests. For instance, *Sogatella furcifera* exhibited *chitin deacetylase* [9] and *vitellogenin-like1* [10] genes, *N. lugens* displayed *peroxisomal factor NlPEX14* [11], *groucho* and *groucho1-like* [12] genes, *Megoura viciae* possessed the *tyrosine hydroxylase* [13] gene, and *Diaphorina citri* contained the *hexokinase* [14] gene. Silencing these genes led to abnormal development, increased mortality, and impaired reproduction, thus indicating their potential as target genes for controlling Hemiptera pests. Consequently, it is crucial to screen and identify target genes with significant functions and high RNAi efficiency to enhance pest control measures.

In eukaryotes, the proper processing of precursor mRNA (pre-mRNA) is critical for generating mature mRNA, involving multiple protein complexes responsible for 5′ capping, 3′ polyadenylation, and RNA splicing [15,16]. The 3′ end processing, involving cleavage and polyadenylation, is essential for mRNA stability and function [17]. Key proteins, including cleavage and polyadenylation specificity factor (CPSF), cleavage stimulation factor (CstF), cleavage factors (CFI and CFII), and poly(A) polymerase (PAP), coordinate these processes. These factors recognize the polyadenylation signal, cleave the pre-mRNA, and add a poly-A tail, enhancing mRNA stability and translation efficiency [18,19].

The Cleavage and Polyadenylation Specificity Factor 30 (CPSF30) is essential for 3′ end mRNA processing, as it recognizes specific sequences within mRNA to facilitate pre-mRNA cleavage and polyadenylation, thereby influencing mRNA stability and translational efficiency [20,21]. In various organisms, including humans, *Arabidopsis*, and yeast, CPSF30 possesses three to five CCCH zinc-finger (ZF) domains at the N-terminal. Among these domains, two ZF domains specifically recognize the AAUAAA poly(A) signal and bind to RNA. The C-terminal of CPSF30 may or may not contain a CCHC zinc-knuckle domain, which is responsible for recognizing and binding to polyuracil RNA [22–25]. In model

organisms like yeast [26], *Drosophila* [17,27], and *Arabidopsis thaliana* [28], CPSF30 has been established as a critical regulator of gene expression. Loss of CPSF30 function in these organisms often leads to abnormal development and even death. However, the role of CPSF30 in agricultural pests, such as the brown planthopper, remains largely unexplored.

Given the fundamental role of CPSF30 in these organisms, this study hypothesizes that NlCPSF30 (homolog of mammalian CPSF30) is also vital for the brown planthopper and investigates its potential as an RNAi target. We cloned the coding region of the *NlCPSF30* gene from the brown planthopper, conducted bioinformatics analyses, and examined the spatiotemporal expression patterns of *NlCPSF30* using quantitative real-time PCR. Subsequently, we employed RNAi to silence the *NlCPSF30* gene in the brown planthopper and investigated its role in the growth and development of the pest. Our findings provide new insights into the molecular mechanisms of brown planthopper biology and identify *NlCPSF30* as a potential target for RNAi-based pest control strategies.

2. Materials and Methods

2.1. Insects

The *N. lugens* used in this study was originally sourced from Wuhan University, Hubei, China. The insects were reared on TN1 (Taichung Native 1), a rice variety susceptible to brown planthopper. The rearing conditions were as follows: a temperature of 26 ± 2 °C, a photoperiod of 16 h of light and 8 h of darkness, and a relative humidity of approximately 65 ± 5%.

2.2. Total RNA Extraction and cDNA Synthesis

To clone the *NlCPSF30* gene sequence, total RNA was extracted from thirty fourth-instar nymphs of *N. lugens* using the RNAiso Plus Kit (Takara, Dalian, China), according to the manufacturer's protocol. RNA integrity was assessed by 1% agarose gel electrophoresis, and the RNA concentration and purity were measured using a Nanodrop 2000 spectrophotometer (Thermo Fisher Scientific, Waltham, MA, USA). cDNA was synthesized via reverse transcription using the PrimeScript™ RT Reagent Kit with gDNA Eraser (Takara, Dalian, China), following the manufacturer's instructions [29].

2.3. Cloning and Sequencing of the NlCPSF30 Gene

The *NlCPSF30* gene (a homolog of mammalian CPSF30) sequence (XM_022344588) was retrieved from the *N. lugens* genome database on the National Center for Biotechnology Information (NCBI) website (http://www.ncbi.nlm.nih.gov/) (accessed on 15 August 2024). Gene-specific primers were designed using Primer Premier 5.0 software based on the downloaded sequence (Table 1). The cDNA was amplified via polymerase chain reaction (PCR) using La Taq (Takara, Dalian, China) and gene-specific primers. The PCR conditions consisted of an initial denaturation step at 95 °C for 5 min, followed by 35 cycles of denaturation at 95 °C for 30 s, annealing at 55 °C for 30 s, and extension at 72 °C for 1 min. The amplification process concluded with a final extension step at 72 °C for 10 min. PCR products were ligated into the pMD-18T vector (Takara, Dalian, China) for cloning. The recombinant plasmid was transformed into competent cells, and positive clones were selected for sequencing by Wuhan HeTaiQing Biological Company. The complete coding sequence of the *NlCPSF30* gene was then obtained.

Table 1. Primers related to cloning and functional studies of *NlCPSF30* gene.

Primer Name	Sequence (5′–3′)	Purpose	T_a (°C)	Length (bp)
NlCPSF30-F	TTAGTCAAGATTCCAGGTT	gene cloning	55	1614
NlCPSF30-R	CATCCCATTCATCAGTTT			
q*NlCPSF30*-F	TTACAAAGGGCACTACGC	qRT-PCR	60	97
q*NlCPSF30*-R	CTGTTGCTGCTGCTGGTT			
q*18S rRNA*-F	CGCTACTACCGATTGAA		60	131
q*18S rRNA*-R	GGAAACCTTGTTACGACTT			

Table 1. *Cont.*

Primer Name	Sequence (5′–3′)	Purpose	T_a (°C)	Length (bp)
ds*NlCPSF30*-F	TAATACGACTCACTATAGGGCGTGGCGACAGGACAATA	dsRNA synthesis	55	342
ds*NlCPSF30*-R	TAATACGACTCACTATAGGGAGTAGCAGGAAGTTCAAAA			
ds*GFP*-F	TAATACGACTCACTATAGGGAGAATGAGTAAAGGAGAAGAACTTTTC		55	495
ds*GFP*-R	TAATACGACTCACTATAGGGAGATTTGTATAGTTCATCCATGCCATGT			

T_a: annealing temperatures; length: amplicon length.

2.4. Sequence and Phylogenetic Analysis

Homologous CPSF30 proteins from other insect species were retrieved from the NCBI database (https://www.ncbi.nlm.nih.gov/protein) (accessed on 20 August 2024). The structural domains of these homologous proteins were predicted using the SMART online tool (http://smart.embl-heidelberg.de/) (accessed on 20 August 2024). A phylogenetic tree was constructed using the neighbor-joining (NJ) method in MEGA5.0 software [30], based on the NlCPSF30 protein sequence and homologous CPSF30 sequences from 42 plant, mammal, and insect species. Bootstrap analysis was performed with 1000 replicates, and the results were expressed as percentages. The accession numbers of the sequences used for the multiple sequence alignment and phylogenetic analysis are listed in Table S1.

2.5. Expression Pattern Analysis of NlCPSF30

The spatial and temporal expression of *NlCPSF30* was assessed using quantitative real-time PCR (qRT-PCR). For temporal expression analysis, samples were collected at different developmental stages: eggs (n = 240), first-instar (n = 180), second-instar (n = 120), third-instar (n = 60), fourth-instar (n = 30), fifth-instar (n = 15), and female (n = 5) and male adults (n = 10) at 3 days post-emergence. For spatial expression analysis, at least 20 female and 20 male adults (1–3 days post-emergence) were collected. Antennae, salivary glands, gut, leg, ovaries, and fat body were dissected from the female adults, while testes were dissected from the male adults. All samples were collected in triplicate for biological replication. Total RNAs were extracted from all developmental stages and tissues and reverse-transcribed into cDNA. Specific primers for qRT-PCR were designed based on the cloned gene sequence of *NlCPSF30* using Primer Premier 5.0 software (Table 1). The *18S ribosomal RNA* gene (*18S rRNA*, JN662398) served as the internal reference. qRT-PCR was performed using the CFX96™ Real-Time PCR Detection System (Bio-Rad, Philadelphia, PA, USA), and each assay included three technical replicates. Expression differences of *NlCPSF30* across the developmental stages and tissues were analyzed using one-way ANOVA and quantified using the $2^{-\Delta\Delta Ct}$ (Ct: cycle threshold) method [31].

2.6. Double-Stranded RNA (dsRNA) Synthesis

The dsRNAs were synthesized to achieve the knockdown of *NlCPSF30*. To ensure reliable detection of the target gene at the transcriptional level, the fragment used for dsRNA synthesis was designed to avoid overlapping with the qRT-PCR detection region. The dsRNA-specific primers containing T7 promoter sequences were designed based on the cloned sequence of the *NlCPSF30* gene, with the *green fluorescent protein* (*GFP*, GenBank accession number: MN114103) gene serving as a control (Table 1). The cloned segments of *NlCPSF30* and *GFP* were inserted into plasmids, which were purified using the Plasmid Mini-Extraction Kit (Biotek, Guangzhou, China) according to the manufacturer's instructions. The purified products were then used to synthesize ds*NlCPSF30* and ds*GFP* using the MEG Ascript T7 High Yield Transcription Kit (Ambion, Austin, TX, USA) following the manufacturer's guidelines. The quality and concentration of the synthesized dsRNAs were assessed via 1% agarose gel electrophoresis and a Nanodrop 2000 spectrophotometer (Thermo Fisher Scientific, USA). The final dsRNA concentration was adjusted to 1000 ng/μL using DEPC-treated water.

2.7. RNAi

Approximately 140 third-instar nymphs of the brown planthopper were selected for microinjection in each experimental replicate. Specifically, 80 nymphs were injected with ds*NlCPSF30* and 60 with ds*GFP*. The injections were performed using a Nanoliter 2020 injector (World Precision Instrument, Sarasota, FL, USA) following carbon dioxide (CO_2) anesthesia for 10–15 s. Each nymph was injected with 23 nL of dsRNA (1000 ng/μL) at the mid-line of the thorax [32]. Two hours after injection, the planthoppers were transferred to fresh TN1 rice seedlings for feeding.

To confirm the silencing efficiency of RNAi, five planthoppers were randomly collected from each group at 24 h and 72 h post-injection. The experiment was conducted in four biological replicates to ensure robust data collection. Total RNA was extracted and reverse-transcribed into cDNA. qRT-PCR was conducted to determine the silencing efficiency of *NlCPSF30* following dsRNA injection. Differences in gene silencing efficiency were analyzed using the Student's *t*-test.

2.8. Survival Phenotype Analysis of BPH After RNAi

In each experimental replicate, approximately 140 third-instar nymphs were injected with ds*NlCPSF30* and ds*GFP*, following the procedure outlined above. Survival rates and death phenotypes were observed every 24 h for 10 days. Nearly all planthoppers injected with ds*NlCPSF30* died within this period. Each group included three biological replicates. The proportion of survival planthoppers was calculated, and the data were processed and analyzed accordingly. The mortality phenotypes were photographed using a Leica S8APO stereomicroscope (Leica Microsystems, Wetzlar, Germany).

2.9. Effects of NlCPSF30 Knockdown on the Expression of Hormone-Related Genes

To assess the impact of *NlCPSF30* knockdown on hormone-related gene expression, third-instar nymphs were injected with ds*NlCPSF30* and ds*GFP* as the control. After six days post-injection, RNA was extracted from the insects and converted into cDNA through reverse transcription. The expression levels of hormone-related genes (*NlKr-h1*, *NlHry*, and *NlE93*) were conducted using qRT-PCR. To ensure statistical robustness, three biological replicates were performed for each gene.

2.10. Data Analysis

Statistical analyses were conducted using SPSS 22.0 software (IBM, New York, NY, USA). Data were presented as means ± SEM. The statistical significance of gene silencing efficiency and the survival rate was assessed using the Student's *t*-test (* $p < 0.05$; ** $p < 0.01$; *** $p < 0.001$). A one-way ANOVA was followed by Fisher's least significant difference (LSD) multiple comparison test, and a *p*-value of less than 0.05 was considered statistically significant. The images were captured with a stereomicroscope (Leica S8APO, Wetzlar, Germany).

3. Results

3.1. Sequence Analysis of NlCPSF30

Using cDNA from BPH nymphs as a template, we amplified a segment of the *NlCPSF30* gene via PCR and sequenced the resulting positive clones. The cloned sequence contained a coding sequence (CDS) of 1026 base pairs (bp) spanning six exons located on chromosome 3. This CDS is predicted to encode a 341-amino acid protein. Sequence analysis revealed that NlCPSF30 contains five zinc-finger domains (amino acids 35–168) at the N-terminus and two zinc-knuckle domains (amino acids 87–203 and 284–300) at the C-terminus (Figure 1). Alignment of the NlCPSF30 protein with homologous CPSF30 proteins from six insect orders demonstrated a high degree of sequence conservation (Figure 1B). While most domains were highly conserved, zinc finger 1 (ZF1) and zinc knuckle 1 (ZK1) exhibited lower conservation than their respective counterparts. Among the insects included in our study, NlCPSF30 showed the highest amino acid identity

(62.07%) with the hemipteran insect *Halyomorpha halys*. Conversely, the lowest amino acid identity of 51.45% was observed with the dipteran insect *Drosophila melanogaster* (Table S2). These findings suggest that NlCPSF30 is highly conserved across various insect species.

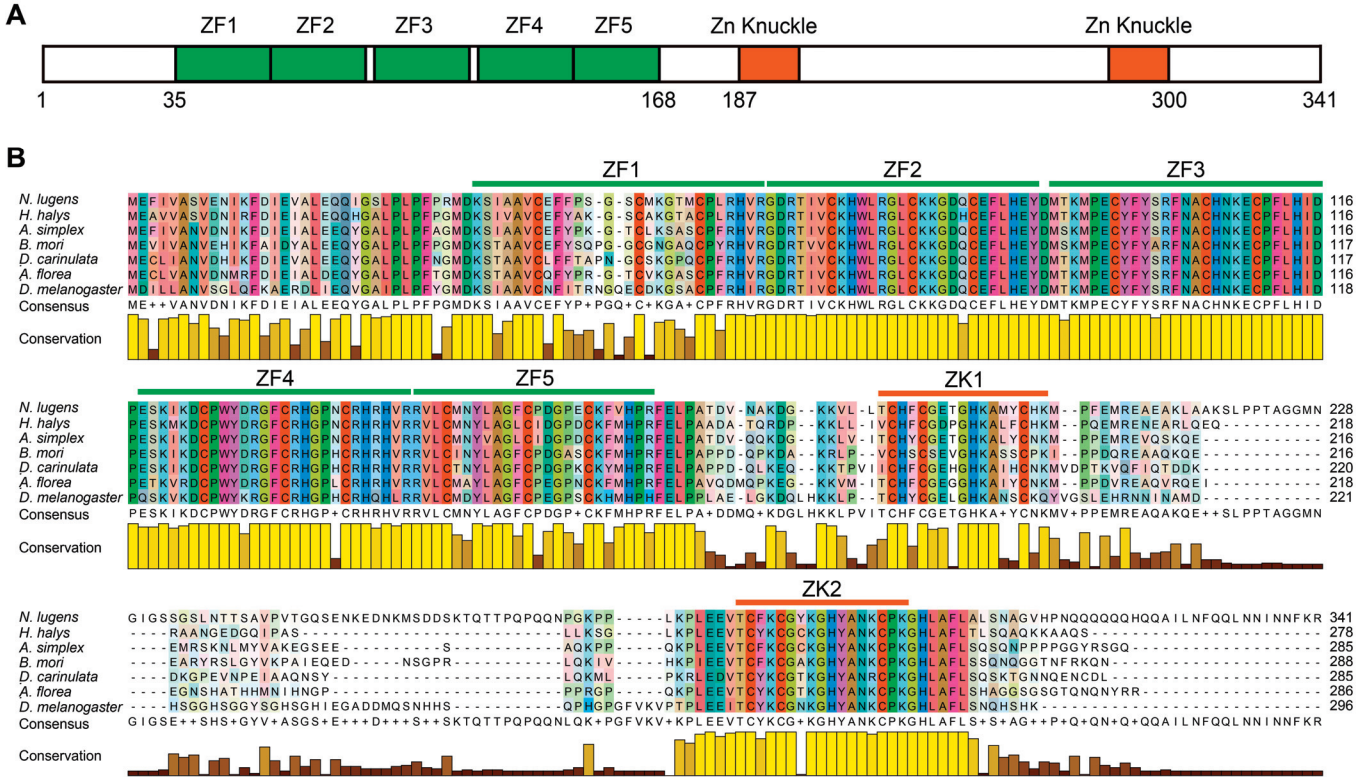


Figure 1. The structures and alignments of amino acid sequences of NlCPSF30 protein. (**A**) Schematic representation of the domain organization in the NlCPSF30 protein. (**B**) Amino acid sequences alignment across six insect orders: *Halyomorpha halys* (Hemiptera), *Anabrus simplex* (Orthoptera), *Bombyx mori* (Lepidoptera), *Diorhabda carinulata* (Coleoptera), *Apis florea* (Hymenoptera), and *Drosophila melanogaster* (Diptera). The green and orange lines represent five CCCH zinc-finger (ZF) domains and two CCHC zinc-knuckle (ZK) domains, respectively.

3.2. Phylogenetic Analysis of NlCPSF30

To elucidate the evolutionary relationship of the NlCPSF30 protein, we conducted an analysis of its amino acid sequence in comparison with orthologs from other species. The sequence was compared with the CPSF30 proteins from 42 species spanning three groups: mammals, insects, and plants (Figure 2). The proteins from the same orders or classes predominantly clustered together in the phylogenetic analysis. Notably, the CPSF30 protein of *N. lugens* exhibited a closer evolutionary relationship with those of other insects than with those of mammals and plants, specifically clustering within the Hemiptera order of insects. The analysis indicated that *N. lugens* is most closely related to *Halyomorpha halys*, another member of the Hemiptera order, with both species clustering within the same clade (Figures 2 and S1).

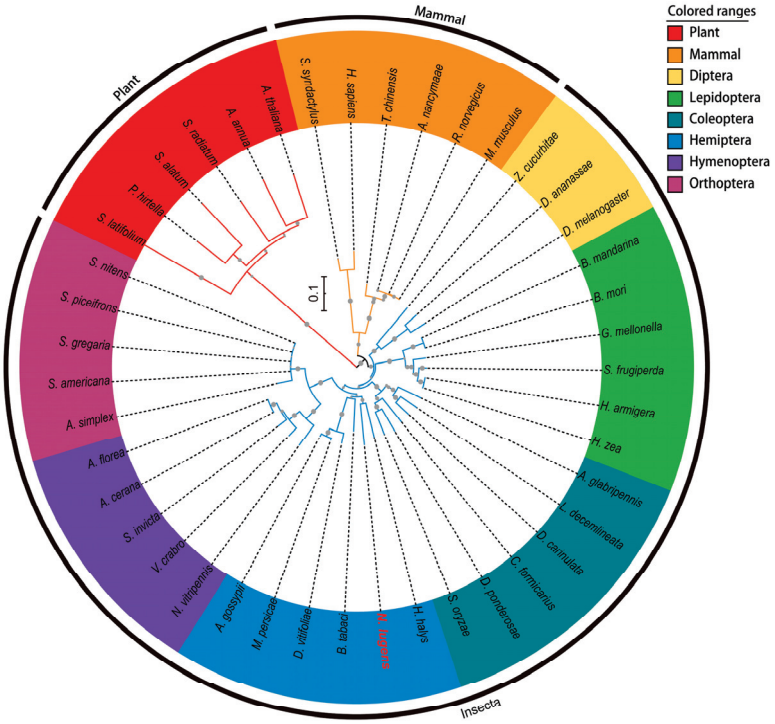


Figure 2. A phylogenetic tree was constructed with NlCPSF30 and 42 orthologs. Different color backgrounds represent the species from specific orders of insects, plants, and mammals. The NlCPSF30 protein of *N. lugens* is indicated in red font.

3.3. Spatial and Temporal Expression Analyses of NlCPSF30

To investigate the expression levels of *NlCPSF30* across different developmental stages of *N. lugens*, we performed qRT-PCR using the total RNA extracted from whole bodies of first- to fifth-instar nymphs, as well as 1- to 3-day-old male and female adults. The results demonstrated that *NlCPSF30* is expressed throughout all developmental stages (Figure 3A). Notably, the highest expression level was observed in female adults, while the lowest was detected in second-instar nymphs.

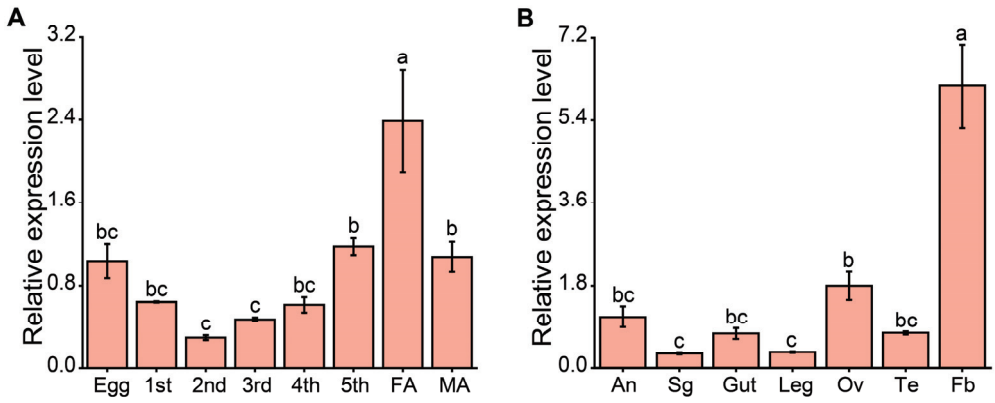


Figure 3. Temporal and spatial expression analyses of *NlCPSF30*. (**A**) Expression analysis of *NlCPSF30* across the developmental stages of the brown planthopper, including eggs, nymphs (first–fifth instars), adult females (FA), and adult males (MA). (**B**) Tissue-specific expression analysis of *NlCPSF30* in different tissues of the brown planthopper: antenna (An), salivary glands (Sg), gut, leg, ovaries (Ov), testes (Te), and fat body (Fb). Data are presented as mean ± standard error of the mean (SEM), with $n = 4$. Different letters indicate statistically significant differences (one-way ANOVA, LSD, $p < 0.05$).

For tissue-specific expression analysis, qRT-PCR was conducted on RNA extracted from various tissues, including the antennae, salivary glands, gut, legs, ovaries, and fat body of female adults, as well as the testes of male adults. The analysis revealed that *NlCPSF30* is expressed in multiple tissues of *N. lugens* (Figure 3B). The highest transcript level was detected in the fat body, while the salivary glands and legs exhibited the lowest expression among the tissues examined. These spatiotemporal expression patterns suggest that *NlCPSF30* plays a crucial role in the growth and development of *N. lugens*.

3.4. Effect of NlCPSF30 by RNAi on the Survival of BPH

To evaluate the effect of the *NlCPSF30* gene knockdown on the viability of the brown planthopper, we employed an RNAi approach via microinjection in third-instar nymphs. After 24 and 72 h of ds*NlCPSF30* injection, the expression levels of *NlCPSF30* were significantly reduced to 30.36% and 27.43%, respectively, compared to the ds*GFP* control group (Figure 4A). These results demonstrate that ds*NlCPSF30* effectively suppressed *NlCPSF30* expression relative to the control.

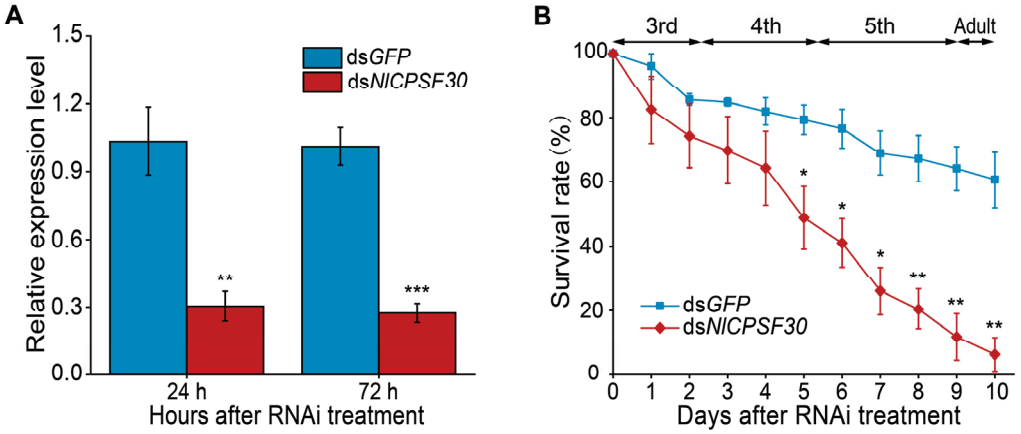


Figure 4. Effects of ds*NlCPSF30* interference on brown planthopper survival. (**A**) Assessment of RNAi efficiency following ds*NlCPSF30* injection. (**B**) Survival rates of third-instar brown planthopper nymphs post-microinjection of ds*NlCPSF30*. The progression from the third-instar to the adult stage in the ds*GFP* control group is illustrated in (**B**). Notably, compared to the ds*GFP* control group, BPH treated with ds*NlCPSF30* exhibited a slower developmental rate during the fifth-instar stage and did not reach adulthood before dying. Experiments were performed in triplicate, and data are presented as the mean ± standard error of the mean (SEM). Statistical significance is indicated as follows: * $p < 0.05$; ** $p < 0.01$; *** $p < 0.001$, determined using Student's *t*-test.

Following the silencing of *NlCPSF30*, we monitored the survival of brown planthoppers every 24 h (Figure 4B). The survival rate of the brown planthoppers treated with ds*NlCPSF30* dropped sharply from 82.54% on day 1 to 6.48% on day 10. In contrast, the survival rate of the nymphs injected with ds*GFP* declined more gradually, from 96.08% to 60.65%. From day 5 onward, the survival rate of the ds*NlCPSF30*-treated brown planthoppers was significantly lower than that of the ds*GFP* control group, with the disparity between the two groups progressively increasing. Notably, the majority of mortality in the brown planthoppers treated with ds*NlCPSF30* occurred during the late fourth-instar and fifth-instar developmental stages (Figure 4B). Additionally, none of the nymphs were able to successfully undergo the transition into adults.

Following the microinjection of ds*NlCPSF30*, two distinct lethal phenotypes were observed: normal death and defective molting (Figure 5). Among the dead BPHs, more than half exhibited normal death, while the remainder displayed defective molting. In the case of normal death, the ds*NlCPSF30*-treated fourth-instar nymphs exhibited smaller body sizes, particularly a reduced abdomen size, compared to the ds*GFP* control group (Figure 5, indicated by green arrows). However, no significant difference in body size

was observed between the ds*NlCPSF30*-treated fifth-instar nymphs and the ds*GFP* control group. Regarding the defective molting, two distinct phenotypes were identified. Firstly, there was a splitting of the old cuticles at the notum, resulting in the exposure of the underlying notum (Figure 5, indicated by red arrows). Secondly, the old cuticle remained attached to the BPH's abdomen and hind legs, leading to unsuccessful molting (Figure 5, indicated by blue arrows). These observations collectively indicate that the knockdown of *NlCPSF30* severely disrupts the development of *N. lugens*.

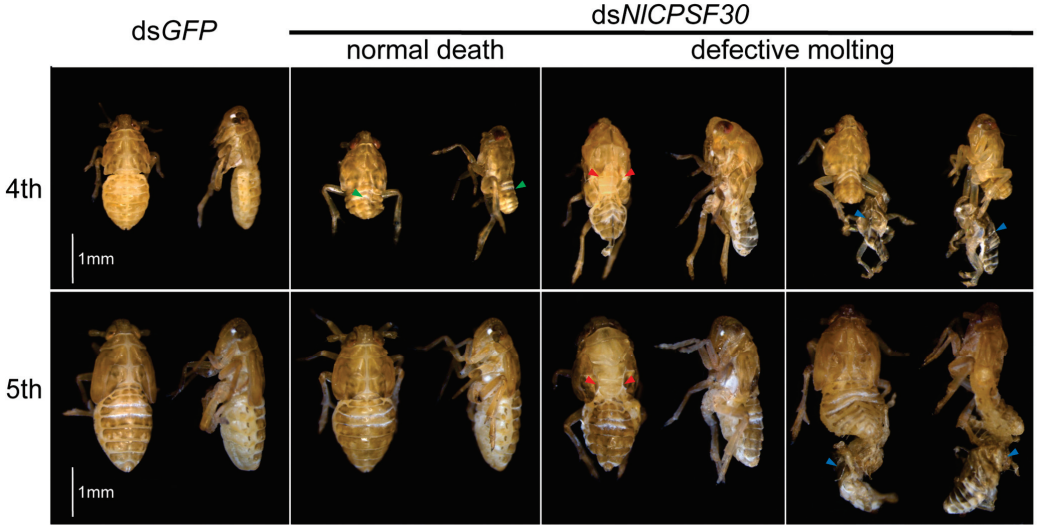


Figure 5. Observation of lethal phenotypes in *N. lugens* following dsRNA microinjection. Third-instar *N. lugens* nymphs were injected with ds*NlCPSF30* (treatment group) and ds*GFP* (control group), and the mortality phenotypes were recorded daily. In the treatment group, some nymphs exhibited molting failure, with varying degrees of molting difficulty observed from the fourth- to the fifth-instar stages. In the fourth-instar stage, the green arrows were used to denote normal death characterized by abnormal abdomen size. Additionally, two distinct defective molting phenotypes are illustrated by the red and blue arrows. The red arrows indicate the splitting of old cuticles at the notum, thereby exposing the underlying notum. Meanwhile, the blue arrows highlight instances where the old cuticle remains attached to the BPH's abdomen and hind legs. Scale bars: 1 mm.

3.5. The Impact of NlCPSF30 Knockdown on the Expression of Hormone-Related Genes

In order to investigate the underlying molecular mechanisms behind the observed mortality and developmental defects in *N. lugens* resulting from silencing *NlCPSF30* expression, we focused on the hormonal pathways that regulate molting and metamorphosis. These processes are tightly controlled by ecdysone and juvenile hormone (JH), which are key hormones in insect development. To assess the impact of *NlCPSF30* knockdown on these pathways, we examined the expression levels of three important hormonal regulatory genes: *NlHry* and *NlE93*, both of which are ecdysone-responsive genes [33,34], and *NlKr-h1*, a juvenile hormone-responsive gene [35]. Six days after injecting third-instar nymphs with dsRNA, *NlCPSF30* expression was found to be reduced by 81% in the ds*NlCPSF30* treatment compared to the ds*GFP* control (Figure 6A), confirming the effectiveness of the knockdown. Similarly, the expression levels of the genes involved in the ecdysone signaling pathway, specifically *NlHry* (Figure 6B) and *NlE93* (Figure 6C), were reduced by 41% and 43%, respectively. These findings suggest that the molting process may be impaired. The downregulation of these two genes correlates with the observed molting defects in ds*NlCPSF30*-treated nymphs. Conversely, the expression of the JH pathway gene, *NlKr-h1*, was upregulated by 62% (Figure 6D), indicating that the development stage remains in the nymph state. This finding is consistent with the observation that none of the nymphs were able to successfully undergo the transition into adulthood. Overall, these results provide further insight into the molecular mechanisms affected by *NlCPSF30* knockdown, shedding

light on the connection between *NlCPSF30* and the hormonal pathways governing molting and metamorphosis in *N. lugens*.

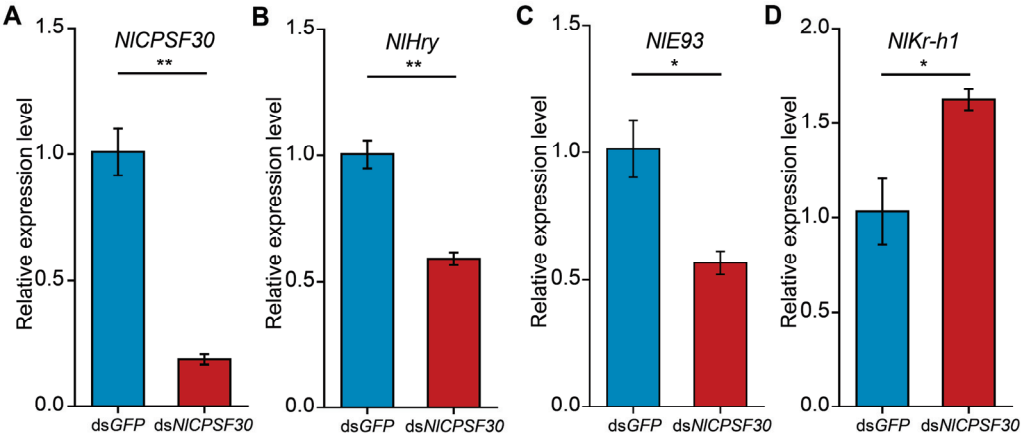


Figure 6. The change in expression hormone-related genes following *NlCPSF30* knockdown. The relative expression levels of *NlCPSF30* (**A**), *NlHry* (**B**), *NlE93* (**C**), and *NlKr-h1* (**D**) at 6 days post-injection of dsRNA. Third-instar nymphs were injected with ds*NlCPSF30* or ds*GFP* (control group). Experiments were performed in triplicate, and data are presented as the mean ± standard error of the mean (SEM). Statistical significance is indicated as follows: * $p < 0.05$; ** $p < 0.01$, determined using Student's *t*-test.

4. Discussion

In this study, we identified and characterized the *NlCPSF30* gene based on its homology with the mammalian CPSF30 and the brown planthopper genome. The NlCPSF30 protein is highly conserved across various organisms, containing five CCCH zinc-finger domains and two CCHC zinc-knuckle domains, critical for recognizing RNA substrates and processing pre-mRNA [21]. The RNAi-mediated knockdown of *NlCPSF30* resulted in increased mortality and impaired development in the nymphs of *N. lugens*. Additionally, it influenced the expression of genes related to hormone regulation, suggesting its involvement in RNA processing and gene regulation in this insect species.

CPSF30 is a zinc-finger protein with conserved zinc-finger and zinc-knuckle motifs, essential for its pre-mRNA 3′ end processing function. However, the number of zinc-finger and zinc-knuckle motifs varies among organisms. For instance, plants like *Arabidopsis thaliana* (AtCPSF30) possess three zinc-finger motifs [23], while five CCCH zinc-finger motifs are predominantly found in eukaryotic CPSF30 homologs, including the *Drosophila melanogaster* clipper (CLP) [17], yeast Yth1 [36], zebrafish Nar [37], and human CPSF30 [38]. Functional and structural studies indicate that the ZF2-ZF3 motifs of human CPSF30 are involved in recognizing the AAUAAA polyadenylation signal (PAS), while the ZF4-ZF5 motifs interact with hFip1, another CPSF subunit, with ZF4 showing a higher affinity for hFip1 [21,22,25]. In this study, ZF2-ZF4 of NlCPSF30 demonstrated high conservation across different insect orders (Figure 1), suggesting similar functions in RNA binding and pre-mRNA 3′ end processing.

The number of zinc-knuckle motifs also varies among CPSF30 homologs. Plant and yeast homologs lack zinc-knuckle motifs [23,36], while mammalian homologs possess one [25], and insect homologs, including CLP [17] and NlCPSF30 (this study), contain two. Zinc knuckles preferentially bind to the U-rich sequences within pre-mRNA, facilitating CPSF30's association with PAS [21,25,39]. Thus, the zinc-finger and zinc-knuckle motifs of CPSF30 provide dual RNA recognition capabilities, crucial for its complex gene regulatory roles.

Our phylogenetic analysis demonstrated that NlCPSF30 is most closely related to the *Halyomorpha halys* CPSF30, aligning with their close taxonomic relationship within Hemiptera. This evolutionary proximity suggests functional similarities between CPSF30

proteins in these hemipteran pests, offering insights for developing RNAi-based pest control strategies.

The expression analysis at different developmental stages revealed that the highest levels of *NlCPSF30* were observed in adult females. This finding is consistent with previous studies in *D. melanogaster*, where the mRNA of the *CLP* gene was predominantly abundant in adult females [17,27]. Furthermore, a tissue-specific expression pattern demonstrated that *NlCPSF30* exhibited high expression in the fat body, a multifunctional tissue involved in molting regulation, hormone synthesis, energy metabolism, and reproduction. Silencing the expression of *NlCPSF30* led to defective molting, as shown in Figure 5. Moreover, our experimental observations revealed that nymphs treated with ds*NlCPSF30* displayed decreased movement activity in comparison to the ds*GFP* control group. In previous studies on the functional characterization of genes related to the BPH, it was found that *NlML1* (*myeloid differentiation factor 2 (MD-2)-related lipid-recognition 1*) [40] and *NlSPARC* (*Secreted protein*, *Acidic and Rich in Cysteine*) [41] were highly expressed in the fat body. Knockdown of these genes resulted in defective molting and increased mortality, which is consistent with the phenotypic effects observed upon silencing *NlCPSF30* expression. These results strongly suggest that *NlCPSF30* plays a crucial role in the development and regulation of essential physiological processes.

The evaluation of RNAi efficiency in gene function research is of utmost importance. It has been observed that the expression levels of the target gene exhibit variation over time after dsRNA injection and also vary with different doses of injected dsRNA. In our study, the expression levels of *NlCPSF30* were found to decrease by 70% and 73% at 24 h and 72 h post-injection with ds*NlCPSF30*, respectively (Figure 4A). A similar trend was observed in the investigation of the *lipophorin receptor* (*NlLpR*) gene, with expression levels decreasing by approximately 50% and 70% at 24 h and 72 h post-injection, respectively [42]. These findings suggest that the reduction in expression levels is more significant with a longer duration of post-injection dsRNA. Additionally, when the doses of ds*NlCPSF30* were adjusted to 11.5 ng, 23 ng, and 46 ng per insect, the expression levels of *NlCPSF30* decreased by 66%, 70%, and 77% at 24 h post-injection, respectively (Figure S2A). A similar pattern was observed in the examination of the autophagy-related gene *NlATG3* [29]. These results indicate that the effectiveness of RNAi is influenced by the dosage of dsRNA.

The knockdown of *NlCPSF30* resulted in a significant increase in mortality among *N. lugens*, particularly affecting normally developed insects (as shown in Figure 5). This effect was most prominent in fourth-instar nymphs, which exhibited smaller body sizes. Interestingly, this phenotype resembled the consequences of silencing certain genes from the fatty acid elongases (*ELOs*) family [43]. Additionally, the knockdown of *NlCPSF30* led to a defective molting phenotype, a characteristic observed in other RNAi-mediated injection experiments involving genes such as the chitinase-like gene family [44] and hormone-related [33–35] genes of BPH. Notably, the phenotypes resulting from the knockdown of five chitinase-like gene family genes (*NlCht1*, *NlCht5*, *NlCht7*, *NlCht9*, and *NlCht10*) [44] resembled those observed after injecting ds*NlCPSF30* (as depicted in Figure 5). To explore the underlying mechanisms, the expression of hormone-related genes like *NlHry* [33], *NlE93* [34], and *NlKr-h1* [35] were examined after injecting ds*NlCPSF30* in this study (as depicted in Figure 6). Previous studies have reported that knockdown of these genes resulted in defective molting, suggesting that changes in hormone-related genes, particularly *NlHry*, *NlE93*, and *NlKr-h1*, may be associated with the function of *NlCPSF30*.

The high mortality rate observed following the *NlCPSF30* knockdown underscores its potential as a target for RNAi-based pest management strategies. As discussed in the introduction, two strategies have been employed for utilizing RNAi-based pest control. Previous studies on plant-mediated RNAi in rice for controlling BPH have reported significant reductions in survival rates of BPH when using dsRNA transgenic rice plants that introduced the *ecdysone receptor* (*NlEcR*) [45] and *salivary protein 1* (*NlSP1*) [46] genes of BPH. Additionally, a novel delivery method for dsRNA of *chitin synthetase A* (*CHSA*) [47] has been successfully applied against BPH. These findings suggest that *NlCPSF30* holds great

potential for practical use in controlling BPH in the future. However, before utilizing the *NlCPSF30* gene for BPH control, it is crucial to consider the dose-response effect, potential off-target and non-target effects, and potential resistance development.

Firstly, the dose-response effect plays a crucial role in RNAi efficacy [48]. In our study investigating the dosage of dsRNA administered to BPH, we observed a wide range of injection doses, spanning from a maximum of 3000 ng [49] to a minimum of 10 ng [50] per BPH. For our study, we opted for a relatively low dose, using a concentration of 1000 ng/μL and injecting 23 nL per BPH, resulting in a total dose of 23 ng. Additionally, we conducted supplementary experiments using injection doses of 11.5 ng (ds*NlCPSF30* 500 ng/μL) and 46 ng (ds*NlCPSF30* 2000 ng/μL) to assess the impact of different ds*NlCPSF30* doses on BPH survival (Figure S2). The results of these experiments showed a significant reduction in *NlCPSF30* gene expression across all three concentrations, and similar trends in mortality were observed, with higher concentrations leading to a more rapid decline in survival rates (Figure S2). These findings were consistent with the studies on BPH *NlATG3* [29] and the egg-specific gene *Nllet1* [50]. Overall, these findings make a valuable contribution to our understanding of the dose-response effects of dsRNA on BPH and offer valuable insights into the potential field applications of dsRNA for effective pest management.

Secondly, it is essential to address the potential off-target and non-target effects that can significantly impact the efficacy of RNAi in pest management applications. It is crucial to consider these effects and prevent any adverse consequences before implementing RNAi on a larger scale [51–54]. To achieve this, we conducted a multiple alignment by comparing the *NlCPSF30* nucleotide sequence with homologous sequences from other insect species. The alignment results revealed that the nucleotide sequence corresponding to the ZF domains exhibited a higher sequence identity compared to other regions. To minimize potential off-target and non-target effects of the *NlCPSF30* gene, it is recommended to select unique or BPH-specific regions of *NlCPSF30* as the target for dsRNA. However, it is important to note that further research is necessary to gain a more comprehensive understanding of these potential off-target and non-target effects.

Finally, resistance development has the potential to impact the efficiency of RNAi. While there have been no reported instances of resistance against RNAi in hemipteran pests, the establishment of the first dsRNA-resistant insect population through laboratory selection in western corn rootworm serves as evidence that resistance to dsRNA can potentially evolve after prolonged and extensive application of RNAi biopesticides [55]. This finding highlights the challenges associated with RNAi-based insect control for hemipteran pests and other pest orders. In the case of sap-feeding hemipteran pests, there are three identified potential mechanisms for resistance development: target modification, mutations in the core RNAi machinery, and physiological mutations [52]. These mechanisms further underscore the need for a comprehensive understanding of resistance development to develop effective strategies for RNAi-based pest control.

5. Conclusions

This study demonstrates that *NlCPSF30* is essential for the survival and development of brown planthoppers. RNAi-mediated knockdown of *NlCPSF30* resulted in a significant decrease in survival rates and the occurrence of molting defects, particularly during the late fourth-instar and fifth-instar developmental stages. Furthermore, it had an influence on the expression of the genes associated with hormone regulation. These results suggest that *NlCPSF30* is a promising target for RNAi-based pest control strategies. Future studies should focus on the development of transgenic rice expressing dsRNA targeting *NlCPSF30* or explore the feasibility of utilizing sprayable ds*NlCPSF30* biopesticides. Such innovations could provide a durable and environmentally friendly solution for managing brown planthopper infestations. Consequently, disrupting the expression of this key gene holds the potential to offer a sustainable alternative to conventional pest control measures.

Supplementary Materials: The following supporting information can be downloaded at: https://www.mdpi.com/article/10.3390/insects15110860/s1, Table S1: List of orthologs of CPSF30 protein in multiple sequence alignment and phylogenetic analysis. Table S2: List of orthologs showing the amino acid identity of NlCPSF30 protein in multiple sequence alignment. Figure S1: A phylogenetic tree was constructed using NlCPSF30 and 30 orthologs from six different insect orders. The species from each insect order were represented by curved frames of different colors. Specifically, the curved frames colored in red, orange, pink, green, blue, and purple represented species from the Hymenoptera, Orthoptera, Hemiptera, Lepidoptera, Coleoptera, and Diptera orders, respectively. Figure S2: Effects of different concentrations of ds*NlCPSF30* on the survival rate of *N. lugens*. (**A**) Relative expression levels of *NlCPSF30* were measured 24 h after the injection of ds*NlCPSF30* at three different concentrations: ds*NlCPSF30* (500 ng/μL), ds*NlCPSF30* (1000 ng/μL), and ds*NlCPSF30* (2000 ng/μL) into third-instar nymphs. As a control, ds*GFP* (1000 ng/μL) treatment was used. The relative expression levels of the gene were normalized using *Nl18S* as the reference gene. (**B**) Survival rates of the nymphs were assessed following the injection with ds*GFP* (1000 ng/μL), ds*NlCPSF30* (500 ng/μL), ds*NlCPSF30* (1000 ng/μL), and ds*NlCPSF30* (2000 ng/μL). Each treatment was replicated three times, with 30–40 brown planthoppers in each replicate. The data are presented as mean ± SEM from three independent experiments. Statistical analysis was performed using a two-sided Student's *t*-test to determine significant differences (* $p < 0.05$; ** $p < 0.01$; *** $p < 0.001$).

Author Contributions: Conceptualization, S.J., Q.L. and J.X.; methodology, J.Y., Y.L., F.W., A.R., F.Z., B.Y. (Bingbing Yu) and J.X.; validation, S.J. and J.X.; formal analysis, B.Y. (Bin Yu) and J.Y.; investigation, Y.Z. and B.J.; validation, F.W., A.R., F.Z., B.Y. (Bingbing Yu), J.X., Y.L. and R.C.; resources, B.Y. (Bingbing Yu) and Y.Z.; data curation, B.Y. (Bin Yu) and Q.L.; writing—original draft preparation, S.J., J.Y., Y.L. and J.X.; writing—review and editing, S.J., B.Y. (Bin Yu) and J.X.; visualization, S.J., J.Y., Y.L. and J.X.; supervision, S.J. and J.X.; project administration, S.J. and Q.L.; funding acquisition, S.J. and Q.L. All authors have read and agreed to the published version of the manuscript.

Funding: This research was funded by the National Natural Science Foundation of China (grants U1704111, 32372548, and 31401732), Zhongyuan Yingcai Jihua (ZYYCYU202012165), the Open Project Funding of the State Key Laboratory of Crop Stress Adaptation and Improvement (2023KF10), and the Joint Fund Project of Science and Technology Research and Development Program of Henan Province (232301420121).

Data Availability Statement: The data presented in this study are available in the article.

Acknowledgments: We thank Guangcun He (Wuhan University) for kindly providing the insects and plants and suggestions from anonymous reviewers for this article.

Conflicts of Interest: The authors declare no conflicts of interest.

References

1. Piyaphongkul, J.; Pritchard, J.; Bale, J. Heat stress impedes development and lowers fecundity of the brown planthopper *Nilaparvata lugens* (Stål). *PLoS ONE* **2012**, *7*, e47413. [CrossRef] [PubMed]
2. Shi, S.; Wang, H.; Zha, W.; Wu, Y.; Liu, K.; Xu, D.; He, G.; Zhou, L.; You, A. Recent advances in the genetic and biochemical mechanisms of rice resistance to brown planthoppers (*Nilaparvata lugens* Stål). *Int. J. Mol. Sci.* **2023**, *24*, 16959. [CrossRef] [PubMed]
3. Younas, M.U.; Wang, G.; Du, H.; Zhang, Y.; Ahmad, I.; Rajput, N.; Li, M.; Feng, Z.; Hu, K.; Khan, N.U.; et al. Approaches to reduce rice blast disease using knowledge from host resistance and pathogen pathogenicity. *Int. J. Mol. Sci.* **2023**, *24*, 4985. [CrossRef] [PubMed]
4. Yang, M.; Cheng, L.; Yan, L.; Shu, W.; Wang, X.; Qiu, Y. Mapping and characterization of a quantitative trait locus resistance to the brown planthopper in the rice variety IR64. *Hereditas* **2019**, *156*, 22. [CrossRef]
5. Agrawal, N.; Dasaradhi, P.V.; Mohmmed, A.; Malhotra, P.; Bhatnagar, R.K.; Mukherjee, S.K. RNA interference: Biology, mechanism, and applications. *Microbiol. Mol. Biol. Rev.* **2003**, *67*, 657–685. [CrossRef]
6. Pallis, S.; Alyokhin, A.; Manley, B.; Rodrigues, T.B.; Buzza, A.; Barnes, E.; Narva, K. Toxicity of a novel dsRNA-based insecticide to the Colorado potato beetle in laboratory and field trials. *Pest Manag. Sci.* **2022**, *78*, 3836–3848. [CrossRef]
7. Rodrigues, T.B.; Mishra, S.K.; Sridharan, K.; Barnes, E.R.; Alyokhin, A.; Tuttle, R.; Kokulapalan, W.; Garby, D.; Skizim, N.J.; Tang, Y.-W.; et al. First sprayable double-stranded RNA-based biopesticide product targets *Proteasome* subunit beta type-5 in colorado potato beetle (*Leptinotarsa decemlineata*). *Front. Plant Sci.* **2021**, *12*, 728652. [CrossRef]
8. Liu, F.; Yang, B.; Zhang, A.; Ding, D.; Wang, G. Plant-mediated RNAi for controlling *Apolygus lucorum*. *Front. Plant Sci.* **2019**, *10*, e21400. [CrossRef]

9. Yang, X.-B.; Zhou, C.; Gong, M.-F.; Yang, H.; Long, G.-Y.; Jin, D.-C.; Chiu, J. Identification and RNAi-based functional analysis of four chitin deacetylase genes in *Sogatella furcifera* (Hemiptera: Delphacidae). *J. Insect Sci.* **2021**, *21*, 9. [CrossRef]
10. Xu, C.; Li, F.; Hou, M.; Liu, Y.; Ons, S. Molecular characterization of Vitellogenin-like1 gene in *Sogatella furcifera* (Hemiptera: Delphacidae), and its function on reproduction. *J. Insect Sci.* **2024**, *24*, 17. [CrossRef]
11. Liu, Y.; Dai, H.; Bamu, A.; Lin, X. Peroxisome biogenesis factor PEX14 is crucial for survival and fecundity of female brown planthopper, *Nilaparvata lugens* (Stål). *Insect Biochem. Mol. Biol.* **2024**, *170*, 104139. [CrossRef] [PubMed]
12. Gao, H.; Jiang, X.; Zheng, S.; Li, Y.; Lin, X. Role of *Groucho* and *Groucho1-like* in regulating metamorphosis and ovary development in *Nilaparvata lugens* (Stål). *Int. J. Mol. Sci.* **2022**, *23*, 1197. [CrossRef] [PubMed]
13. Wang, X.X.; Feng, Z.J.; Chen, Z.S.; Zhang, Z.F.; Zhang, Y.; Liu, T.X. Use of tyrosine hydroxylase RNAi to study Megoura viciae (Hemiptera: Aphididae) sequestration of its host's l-DOPA for body melanism. *J. Insect Physiol.* **2019**, *114*, 136–144. [CrossRef] [PubMed]
14. Yang, S.; Zou, Z.; Xin, T.; Cai, S.; Wang, X.; Zhang, H.; Zhong, L.; Xia, B. Knockdown of hexokinase in *Diaphorina citri* Kuwayama (Hemiptera: Liviidae) by RNAi inhibits chitin synthesis and leads to abnormal phenotypes. *Pest Manag. Sci.* **2022**, *78*, 4303–4313. [CrossRef] [PubMed]
15. Edmonds, M. A history of poly A sequences: From formation to factors to function. *Prog. Nucleic Acid Res. Mol. Biol.* **2002**, *71*, 285–389.
16. Boreikaitė, V.; Passmore, L.A. 3′-end processing of eukaryotic mRNA: Machinery, regulation, and impact on gene expression. *Annu. Rev. Biochem.* **2023**, *92*, 199–225. [CrossRef]
17. Bai, C.; Tolias, P.P. *Drosophila* clipper/CPSF 30K is a post-transcriptionally regulated nuclear protein that binds RNA containing GC clusters. *Nucleic Acids Res.* **1998**, *26*, 1597–1604. [CrossRef]
18. Christofori, G.; Keller, W. 3′ cleavage and polyadenylation of mRNA precursors in vitro requires a poly(A) polymerase, a cleavage factor, and a snRNP. *Cell* **1988**, *54*, 875–889. [CrossRef]
19. Takagaki, Y.; Ryner, L.C.; Manley, J.L. Four factors are required for 3′-end cleavage of pre-mRNAs. *Genes Dev.* **1989**, *3*, 1711–1724. [CrossRef]
20. Thomas, P.E.; Wu, X.; Liu, M.; Gaffney, B.; Ji, G.; Li, Q.Q.; Hunt, A.G. Genome-wide control of polyadenylation site choice by CPSF30 in *Arabidopsis*. *Plant Cell* **2012**, *24*, 4376–4388. [CrossRef]
21. Pritts, J.D.; Oluyadi, A.A.; Huang, W.; Shimberg, G.D.; Kane, M.A.; Wilks, A.; Michel, S.L.J. Understanding RNA binding by the nonclassical zinc finger protein CPSF30, a key factor in polyadenylation during pre-mRNA processing. *Biochemistry* **2021**, *60*, 780–790. [CrossRef] [PubMed]
22. Sun, Y.; Zhang, Y.; Hamilton, K.; Manley, J.L.; Shi, Y.; Walz, T.; Tong, L. Molecular basis for the recognition of the human AAUAAA polyadenylation signal. *Proc. Natl. Acad. Sci. USA* **2018**, *115*, e1419-28. [CrossRef] [PubMed]
23. Addepalli, B.; Hunt, A.G. A novel endonuclease activity associated with the *Arabidopsis* ortholog of the 30-kDa subunit of cleavage and polyadenylation specificity factor. *Nucleic Acids Res.* **2007**, *35*, 4453–4463. [CrossRef] [PubMed]
24. Chakrabarti, M.; Hunt, A.G. CPSF30 at the interface of alternative polyadenylation and cellular signaling in plants. *Biomolecules* **2015**, *5*, 1151–1168. [CrossRef]
25. Pritts, J.D.; Hursey, M.S.; Michalek, J.L.; Batelu, S.; Stemmler, T.L.; Michel, S.L.J. Unraveling the RNA binding properties of the iron-sulfur zinc finger protein CPSF30. *Biochemistry* **2020**, *59*, 970–982. [CrossRef]
26. Tacahashi, Y.; Helmling, S.; Moore, C.L. Functional dissection of the zinc finger and flanking domains of the Yth1 cleavage/polyadenylation factor. *Nucleic Acids Res.* **2003**, *31*, 1744–1752. [CrossRef]
27. Bai, C.; Tolias, P.P. Cleavage of RNA hairpins mediated by a developmentally regulated CCCH zinc finger protein. *Mol. Cell. Biol.* **1996**, *16*, 6661–6667. [CrossRef]
28. Hou, Y.; Sun, J.; Wu, B.; Gao, Y.; Nie, H.; Nie, Z.; Quan, S.; Wang, Y.; Cao, X.; Li, S. CPSF30-L-mediated recognition of mRNA m(6)A modification controls alternative polyadenylation of nitrate signaling-related gene transcripts in *Arabidopsis*. *Mol. Plant* **2021**, *14*, 688–699. [CrossRef]
29. Ye, C.; Feng, Y.; Yu, F.; Jiao, Q.; Wu, J.; Ye, Z.; Zhang, P.; Sun, C.; Pang, K.; Hao, P.; et al. RNAi-mediated silencing of the autophagy-related gene *NlATG3* inhibits survival and fecundity of the brown planthopper, *Nilaparvata lugens*. *Pest Manag. Sci.* **2021**, *77*, 4658–4668. [CrossRef]
30. Ren, Z.W.; Zhuo, J.C.; Zhang, C.X.; Wang, D. Characterization of *NlHox3*, an essential gene for embryonic development in *Nilaparvata lugens*. *Arch. Insect Biochem. Physiol.* **2018**, *98*, e21448. [CrossRef]
31. Livak, K.J.; Schmittgen, T.D. Analysis of relative gene expression data using real-time quantitative PCR and the the $2^{-\Delta\Delta CT}$ method. *Methods* **2001**, *25*, 402–408. [CrossRef]
32. Shangguan, X.; Zhang, J.; Liu, B.; Zhao, Y.; Wang, H.; Wang, Z.; Guo, J.; Rao, W.; Jing, S.; Guan, W.; et al. A mucin-like protein of planthopper is required for feeding and induces immunity response in plants. *Plant Physiol.* **2018**, *176*, 552–565. [CrossRef] [PubMed]
33. Mao, Y.; Li, Y.; Gao, H.; Lin, X. Krüppel homologue 1 interacts directly with Hairy and regulates ecdysis in the brown planthopper. *Insect Mol. Biol.* **2020**, *29*, 293–300. [CrossRef] [PubMed]
34. Mao, Y.; Li, Y.; Gao, H.; Lin, X. The direct interaction between E93 and Kr-h1 mediated their antagonistic effect on ovary development of the brown planthopper. *Int. J. Mol. Sci.* **2019**, *20*, 2431. [CrossRef] [PubMed]

35. Jiang, J.; Xu, Y.; Lin, X. Role of *Broad-Complex* (Br) and *Krüppel homolog* 1 (Kr-h1) in the ovary development of *Nilaparvata lugens*. *Front. Physiol.* **2017**, *8*, 1013. [CrossRef]
36. Barabino, S.M.; Hübner, W.; Jenny, A.; Minvielle-Sebastia, L.; Keller, W. The 30-kD subunit of mammalian cleavage and polyadenylation specificity factor and its yeast homolog are RNA-binding zinc finger proteins. *Genes Dev.* **1997**, *11*, 1703–1716. [CrossRef]
37. Gaiano, N.; Amsterdam, A.; Kawakami, K.; Allende, M.; Becker, T.; Hopkins, N. Insertional mutagenesis and rapid cloning of essential genes in zebrafish. *Nature* **1996**, *383*, 829–832. [CrossRef]
38. Hamilton, K.; Tong, L. Molecular mechanism for the interaction between human CPSF30 and hFip1. *Genes Dev.* **2020**, *34*, 1753–1761. [CrossRef]
39. Barabino, S.M.; Ohnacker, M.; Keller, W. Distinct roles of two Yth1p domains in 3′-end cleavage and polyadenylation of yeast pre-mRNAs. *EMBO J.* **2000**, *19*, 3778–3787. [CrossRef]
40. Wang, W.; Ma, Y.; Yang, R.R.; Cheng, X.; Huang, H.J.; Zhang, C.X.; Bao, Y.Y. An MD-2-related lipid-recognition protein is required for insect reproduction and integument development. *Open Biol.* **2021**, *11*, 210170. [CrossRef]
41. Wang, W.; Zhu, T.; Wan, P.; Wei, Q.; He, J.; Lai, F.; Fu, Q. SPARC plays an important role in the oviposition and nymphal development in *Nilaparvata lugens* Stål. *BMC Genom.* **2022**, *23*, 682. [CrossRef] [PubMed]
42. Lu, K.; Chen, X.; Li, Y.; Li, W.; Zhou, Q. Lipophorin receptor regulates *Nilaparvata lugens* fecundity by promoting lipid accumulation and vitellogenin biosynthesis. *Comp. Biochem. Physiol. A Mol. Integr. Physiol.* **2018**, *219–220*, 28–37. [CrossRef] [PubMed]
43. Li, D.-T.; Chen, X.; Wang, X.-Q.; Moussian, B.; Zhang, C.-X. The fatty acid elongase gene family in the brown planthopper, *Nilaparvata lugens*. *Insect Biochem. Mol. Biol.* **2019**, *108*, 32–43. [CrossRef] [PubMed]
44. Xi, Y.; Pan, P.L.; Ye, Y.X.; Yu, B.; Xu, H.J.; Zhang, C.X. Chitinase-like gene family in the brown planthopper, *Nilaparvata lugens*. *Insect Mol. Biol.* **2014**, *24*, 29–40. [CrossRef] [PubMed]
45. Yu, R.; Xu, X.; Liang, Y.; Tian, H.; Pan, Z.; Jin, S.; Wang, N.; Zhang, W. The insect ecdysone receptor is a good potential target for RNAi-based pest control. *Int. J. Biol. Sci.* **2014**, *10*, 1171–1180. [CrossRef]
46. Huang, J.; Zhang, N.; Shan, J.; Peng, Y.; Guo, J.; Zhou, C.; Shi, S.; Zheng, X.; Wu, D.; Guan, W.; et al. Salivary protein 1 of brown planthopper is required for survival and induces immunity response in plants. *Front. Plant Sci.* **2020**, *11*, 571280. [CrossRef]
47. Lyu, Z.; Xiong, M.; Mao, J.; Li, W.; Jiang, G.; Zhang, W. A dsRNA delivery system based on the rosin-modified polyethylene glycol and chitosan induces gene silencing and mortality in *Nilaparvata lugens*. *Pest Manag. Sci.* **2023**, *79*, 1518–1527. [CrossRef]
48. List, F.; Tarone, A.M.; Zhu-Salzman, K.; Vargo, E.L. RNA meets toxicology: Efficacy indicators from the experimental design of RNAi studies for insect pest management. *Pest Manag. Sci.* **2022**, *78*, 3215–3225. [CrossRef]
49. Si, H.R.; Sun, S.S.; Liu, Y.K.; Qiu, L.Y.; Tang, B.; Liu, F.; Fu, Q.; Xu, C.D.; Wan, P.J. Roles of *GFAT* and *PFK* genes in energy metabolism of brown planthopper, *Nilaparvata lugens*. *Front. Physiol.* **2023**, *14*, 1213654. [CrossRef]
50. Lu, J.B.; Wang, S.N.; Ren, P.P.; He, F.; Li, Q.; Chen, J.P.; Li, J.M.; Zhang, C.X. RNAi-mediated silencing of an egg-specific gene *Nllet1* results in hatch failure in the brown planthopper. *Pest Manag. Sci.* **2023**, *79*, 415–427. [CrossRef]
51. Arora, A.K.; Chung, S.H.; Douglas, A.E. Non-target effects of dsRNA molecules in hemipteran insects. *Genes* **2021**, *12*, 407. [CrossRef] [PubMed]
52. Jain, R.G.; Robinson, K.E.; Asgari, S.; Mitter, N. Current scenario of RNAi-based hemipteran control. *Pest Manag. Sci.* **2021**, *77*, 2188–2196. [CrossRef] [PubMed]
53. Chen, J.; Peng, Y.; Zhang, H.; Wang, K.; Zhao, C.; Zhu, G.; Reddy Palli, S.; Han, Z. Off-target effects of RNAi correlate with the mismatch rate between dsRNA and non-target mRNA. *RNA Biol.* **2021**, *18*, 1747–1759. [CrossRef] [PubMed]
54. Palli, S.R. RNA interference in Colorado potato beetle: Steps toward development of dsRNA as a commercial insecticide. *Curr. Opin. Insect Sci.* **2014**, *6*, 1–8. [CrossRef]
55. Khajuria, C.; Ivashuta, S.; Wiggins, E.; Flagel, L.; Moar, W.; Pleau, M.; Miller, K.; Zhang, Y.; Ramaseshadri, P.; Jiang, C.; et al. Development and characterization of the first dsRNA-resistant insect population from western corn rootworm, *Diabrotica virgifera virgifera* LeConte. *PLoS ONE* **2018**, *13*, e0197059. [CrossRef]

Disclaimer/Publisher's Note: The statements, opinions and data contained in all publications are solely those of the individual author(s) and contributor(s) and not of MDPI and/or the editor(s). MDPI and/or the editor(s) disclaim responsibility for any injury to people or property resulting from any ideas, methods, instructions or products referred to in the content.

insects

MDPI

Article

RNAi of Neuropeptide CCHamide-1 and Its Receptor Indicates Role in Feeding Behavior in the Pea Aphid, *Acyrthosiphon pisum*

Sohaib Shahid [1,2,3], Muhammad Bilal Amir [1], Tian-Bo Ding [1], Tong-Xian Liu [1,4], Guy Smagghe [4,5,6] and Yan Shi [1,*]

[1] Shandong Engineering Research Center for Environment-Friendly Agricultural Pest Management, College of Plant Health and Medicine, Qingdao Agricultural University, Qingdao 266109, China; sohaibshahid90@hotmail.com (S.S.); dr.mbilalamir@outlook.com (M.B.A.); tbding@qau.edu.cn (T.-B.D.); txliu@qau.edu.cn (T.-X.L.)
[2] State Key Laboratory of Integrated Management of Pest Insects and Rodents, Institute of Zoology, Chinese Academy of Sciences, Beijing 100101, China
[3] University of Chinese Academy of Sciences, Beijing 100049, China
[4] Institute of Entomology, Guizhou University, Guiyang 550025, China; guysma9@gmail.com
[5] Cellular and Molecular Life Sciences, Department of Biology, Vrije Universiteit Brussel (VUB), 1050 Brussels, Belgium
[6] Department of Plants and Crops, Ghent University, 9000 Ghent, Belgium
* Correspondence: shiyanyuanyi@aliyun.com

Simple Summary: G protein-coupled receptors (GPCRs) are responsible for the activity of neuropeptides, and interestingly, a number of GPCRs are well-known as pharmaceutical targets, and some are currently being considered as potential pest insect control targets. The purpose of this study is to investigate the function of *CCHamide-1* (abbreviated as *CCHa1*) and its receptor *CCHamide1-receptor* (abbreviated as *CCHa1R*), which belongs to the GPCR superfamily in pea aphid, *Acyrthosiphon pisum*. The pea aphid is a serious agricultural pest and serves as a biological model for various studies. The silencing of *CCHa1* significantly reduced the aphid feeding behavior and reproduction, but not its survival.

Abstract: Neuropeptide *CCHamide-1* (abbreviated as *CCHa1*) is a recently discovered peptide that is present in many arthropods and is the ligand of the *CCHa1R*, a member of the G protein-coupled receptors (GPCRs) superfamily, which plays a regulatory role in diverse physiological processes such as feeding, circadian rhythm, insulin production, lipid metabolism, growth, and reproduction. However, the function of this gene in aphids is still unknown. Here, we characterized and determined the potential role of *CCHa1*/*CCHa1R* signaling in the pea aphid, *Acyrthosiphon pisum*, which is a notorious pest in agriculture. The docking analysis revealed that the *CCHa1* peptide binds to its receptor *CCHa1R* through specific amino acid residues, which are critical for maintaining the structural and functional integrity of the peptide–receptor complex. Quantitative real-time reverse transcription-PCR (qRT-PCR) revealed the expression levels of *CCHa1*/*CCHa1R* transcripts in different development stages and different tissues, indicating that the *CCHa1* expression was high in the first nymphal instar compared to the upcoming nymphal instars and adults, and was predominantly high in the brain. The *CCHa1*/*CCHa1R* transcript levels were significantly upregulated in starved aphids compared to fed aphids. Moreover, RNAi knockdown by the injection of dsRNA-*CCHa1* and dsRNA-*CCHa1R* significantly reduced the corresponding expression of the target gene and reduced their food intake in adult aphids, as revealed by the electrical penetration graph results. *CCHa1*/*CCHa1R*-silencing also reduced the reproduction, but not the survival, in *A. pisum*. Our data demonstrated that *CCHa1*/*CCHa1R* play a role in the regulation of feeding in *A. pisum*, suggesting a role of the *CCHa1* signaling pathway in the aphids relating to their nutritional status.

Keywords: *Acyrthosiphon pisum*; neuropeptide; *CCHamide-1*; feeding behavior; parthenogenetic reproduction

1. Introduction

Neuropeptides regulate physiological, developmental, and behavioral processes throughout the life cycle of animals by acting as neuroactive signaling molecules [1–3]. They exert their function by binding as ligands with ligand-binding pockets of cognate G protein-coupled receptors (GPCRs), which are the largest superfamily of cell surface membrane receptors and are encoded by approximately 1000 genes, sharing conserved seven-transmembrane (7TM) helices connected by three intra- and three extracellular loops [4–7]. This binding initiates the signaling transduction, which triggers a cascade of events within the cell, leading to the activation of G proteins and subsequent downstream signaling pathways. Subsequently, they modulate intercellular interaction and initiate biological effects that influence various physiological functions and behaviors. Several GPCRs are well-known as pharmaceutical targets, and some are currently being considered as potential pest insect control targets [8–10].

The *CCHamide* gene was initially identified within the genome of the silk worm, *Bombyx mori*, as a novel neuropeptide in 2008 [11]. These authors proposed the nomenclature "*CCHa*" for this newly identified neuropeptide, since this proposal is based on the observation that the peptide contains two conserved cysteine residues and a C-terminal amidated histidine residue (XCXXXXXXCXXXHamide), which are features observed in a majority of the analyzed species [11]. Subsequently, in 2010, two *CCHa* genes, which encode two precursors, namely *CCHa1* and *CCHamide-2* (*CCHa2*), were identified in the pea aphid, *Acyrthosiphon pisum* [12]. Moreover, in 2011 and 2012, initial deorphanization in the fruit fly, *Drosophila melanogaster*, of two GPCRs, encoded by CG14593 and CG30106, showed these as the first *CCHa* receptors, and this was reported together with the isolation of *CCHa1* and *CCHa2* precursors [13,14]. In insects, two *CCHa* receptors exist, *CCHa1R* and *CCHa2R*. In *D. melanogaster*, activation of the *CCHa* receptors is triggered by either *CCHa1* or *CCHa2* precursors, suggesting that these neuropeptide signaling systems have different functions [13].

The function of *CCHa2* and its receptor, *CCHa2-R*, has been elucidated in various insects, including the regulation of feeding behaviors observed in the black blowfly (*Phormia regina*), fruit fly (*D. melanogaster*), and pea aphid (*A. pisum*) [14–17]. For *CCHa1*, it has been reported to localize within the olfactory neurons of the CNS and the endocrine cells of the midgut in *D. melanogaster*. These endocrine cells have the appearance of sensory cells, projecting processes close to or into the gut lumen [17,18]. The silencing of *CCHa1* in Or59b-expressing olfactory neurons abolished the starvation effect in *D. melanogaster* [16]. Given its documented presence in the CNS and midgut of insect species, *CCHa1* has also been termed the brain–gut peptide, or enteroendocrine peptide [13,14,19–23]. Furthermore, *CCHa1* and *CCHa2* have been detected in the midgut and brain of male and female mosquitoes of *Aedes aegypti* [23]. The *dsCCHa2*-mediated knockdown revealed its role in regulating the feeding in female mosquitoes, as studied by a capillary feeder bioassay [23]. Despite the research on the *CCHa1* signaling system in *D. melanogaster* and *A. aegypti*, information regarding the functional roles and localization of *CCHa1* and its receptor, *CCHa1R*, in aphids is lacking.

Plant phloem-feeding insects like aphids are characterized by their soft bodies and hemimetabolous life cycle, and are notorious for causing significant damage to a wide range of horticultural crops [24]. They have a remarkable ability to reproduce rapidly and adapt to diverse environments, which is the primary reason behind their devastating impact, causing significant crop losses through both direct sap-feeding and the transmission of viral diseases [25,26]. *A. pisum* has emerged as a valuable model organism for a wide range of scientific investigations. The completion of its whole-genome sequence has facilitated the development of new molecular tools for aphid control [24]. The International Aphid Genomic Consortium has selected *A. pisum* as the model aphid species for developing genomic resources such as ESTs or genome sequencing [25,26]. Hence, elucidating the physiology and behavior modulated by neuropeptides in *A. pisum* presents promising avenues that can be extrapolated to other aphid species, facilitating a comprehensive understanding of mechanisms and the development of effective control measures.

Our research investigates the expression and functional role of *CCHa1/CCHa1R* in *A. pisum*. Firstly, the relative expression of *CCHa1/CCHa1R* in different developmental stages and tissues of *A. pisum* was assessed using qRT-PCR. Moreover, we tested what the effect was of starvation and feeding on the expression of *CCHa1/CCHa1R*. In addition to elucidate the potential role of *CCHa1* in regulating the feeding behavior in *A. pisum*, we employed RNA interference (RNAi) to silence the transcripts of *CCHa1/CCHa1R*, and subsequently analyzed feeding behavior using the electrical penetration graph (EPG) technique. The results revealed that silencing *CCHa1/CCHa1R* significantly impacted probing behavior and phloem feeding, ultimately inhibiting food consumption and lowering reproductive rates in *A. pisum*.

2. Materials and Methods

2.1. Insect Rearing

Wingless pea aphid populations were established on potted broad bean plants (*Vicia faba*) at the Laboratory of Insect Ecology and Molecular Biology, College of Plant Health and Medicine, Qingdao Agricultural University, Shandong, China, and the pea aphid colonies were propagated asexually at 21 ± 2 °C with 70 ± 5% relative humidity and exposed to 16 h of light followed by 8 h of darkness daily, as reported previously [17]. In brief, a low-density rearing strategy, with about 5 aphids per plant, was employed to prevent the development of a winged population and competition. To ensure synchronicity generation for experiments, nymphs aged 0–12 h were carefully collected and meticulously transferred onto fresh broad bean leaves.

2.2. Primers, Sequences, and Phylogenetic Analysis

We designed the optimal primers required for quantitative polymerase chain reaction (qPCR) assays using Primer 3 (https://bioinfo.ut.ee/primer3-0.4.0/ accessed on 19 December 2023), and these primers were subsequently synthesized by Sangon Biotech (Shanghai, China). The primer sequence used in this study is mentioned in Table S1. From the published literature on *A. pisum*, neuropeptide and neurohormone precursors [12], as well as GPCRs [27], cDNA sequences encoding *CCHa1/CCHa1R*, were obtained. The open reading frame (ORF) for the precursor and receptor were confirmed through the ORF finder (https://www.ncbi.nlm.nih.gov/orffinder/ accessed on 10 January 2024). For the precursor, the signal peptides were predicted using the SignalP-5.0server (http://www.cbs.dtu.dk/services/SignalP/ accessed on 22 January 2024), and the sequence logo of the C-terminal motif of *CCHa1* was made using Weblogo [28]. To visualize the evolutionary relationships between *CCHa1/CCHa1R* in *A. pisum* and other insects, we constructed a neighbor-joining tree with 1000 bootstrap replicates. The phylogenetic analysis was executed in MEGA 5.2, following the method outlined by [29,30]. The chosen model was P-distance, and pairwise deletion was employed for gaps and missing data treatment [29,30]. The accession number of the sequences used to visualize the evolutionary relationship of *CCHa1* with other insects is mentioned in Table S2, and *CCHa1R* is mentioned in Table S3. To predict the transmembrane domains of *CCHa1R*, we employed TMHMM version 2.0 (http://www.cbs.dtu.dk/services/TMHMM/ accessed on 15 February 2024), ensuring accuracy in our structural analysis.

2.3. Modeling CCHa1R Docked with Mature Peptide CCHa1

Despite utilizing the SWISS-MODEL platform for homology modeling, we were unable to identify suitable templates with amino acid sequence similarity exceeding 30%. In response to the initial challenges, we adopted an alternative strategy, employing a folded gender approach via the iTASSER platform. This methodology is particularly adept at addressing the challenges posed by proteins with minimal sequence homology and a dearth of appropriate templates. We employed the GPCR I-TASSER (Iterative Threading ASSEmbly Refinement) server to construct the structural model of the *CCHa1R*. Model reliability was evaluated using TM-score values, a structural similarity coefficient ranging from 0 to

1. Scores exceeding 0.5 indicate correct topological structure and reliability, while scores below 0.17 suggest a random, unreliable model. The homology model of the *CCHa1R*, with its C-terminal region excised, served as the basis for docking studies with the *CCHa1* mature peptide. We employed a two-step docking approach, first utilizing the Induced Fit Docking (IFD) method to generate preliminary results, followed by refinement using the QM-Polarized Ligand Docking method. We executed the docking simulations using the Maestro software platform. The previously established docking model of the *CCHa1* mature peptide and *CCHa1R* served as the foundation for our subsequent simulation studies. The docking model of the receptor-mature peptide complex was integrated into a lipid bilayer using the CHARMM-GUI platform. The system was balanced by the addition of chloride ions, ensuring overall charge neutrality. Molecular docking studies, focusing on the interaction between *CCHa1* and *CCHa1R* binding sites, were executed using PyMOL.

2.4. RNA Extraction and cDNA Synthesis

We isolated RNA using the TRIzol® reagent (Invitrogen, Carlsbad, CA, USA), adhering strictly to the manufacturer's recommended protocol. To ensure RNA quality and quantify concentrations accurately, we utilized a NanoDrop 2000 spectrophotometer (Thermo Fisher, Waltham, MA, USA) for quality checks. For the elimination of genomic DNA contamination, RNA from each sample was subjected to treatment with gDNA Eraser and 5X gDNA Eraser Buffer, a protocol meticulously followed according to the guidelines provided by Takara in Dalian, China. Subsequently, cDNA synthesis was achieved using the PrimeScript™ RT Reagent Kit with gDNA Eraser from Takara (Dalian, China), following the manufacturer's recommended procedure. To prepare the cDNA for quantitative Reverse Transcription Polymerase Chain Reaction (qRT-PCR), a 10-fold dilution procedure was implemented to ensure optimal concentrations for subsequent analyses.

2.5. Real-Time Quantitative PCR Analysis

We processed samples to quantify the mRNA expression levels of target genes *CCHa1*/*CCHa1R*. Aforementioned protocols were followed to isolate total RNA and generate first-strand cDNA. qRT-PCR was conducted using an Mx3000P Light Cycler® 96 system from Roche (Indianapolis, IN, USA). We prepared the reaction mixture using 5 μL of TB GreenTM Premix Ex TaqTM 11 (Takara), 1 μL of cDNA (≈200 ng/μL), 1 μL of each primer (10 μM), and 2 μL of nuclease-free water. We used the following PCR protocol: 3 min at 95 °C for initial denaturation, then 35 cycles of 10 s at 95 °C and 30 s at 60 °C. Sample integrity was assessed through a melting curve analysis, with temperatures ranging from 55 to 95 °C. The primer sequences utilized for qRT-PCR analysis are documented in (Table S1). For the reference gene, we chose ribosomal protein RPL7 (NM_001135898.1) [31] and analyzed the relative quantification of expression by using the $2^{-\Delta Ct}$ procedure. To verify primer specificity, we conducted melting curve analyses, seeking solitary peaks that signified exclusive amplification of target genes. The equation E = 10 − 1/slope was employed to calculate the amplification efficiency (E-value) from the linear standard curve. The efficiency of the reaction was found to be superior to 90%, validating our experimental setup. The qRT-PCR analysis was conducted using three biological replicates to ensure the reliability and robustness of the obtained results.

2.6. CCHa1/CCHa1R Expression Profiles Across Developmental Stages and Different Tissues

We assessed *CCHa1*/*CCHa1R* transcription across different developmental stages of *A. pisum* by sampling 20–30 individuals from each nymphal instar (first–fourth) and the adult stage. We performed this with three biological replicates for each stage. The aforementioned protocols were followed to isolate total RNA and generate first-strand cDNA. We dissected tissues from synchronized wingless adult aphids to measure *CCHa1*/*CCHa1R* transcription levels. Tissue samples included antennae (200 aphids), gut (100 aphids), brain (90–100 aphids), cuticle (15–20 aphids), and embryos (10 aphids), and all samples were prepared in 0.1 M PBS (pH 7.4) under a stereoscopic microscope. Following the previously

described protocols, we performed total RNA extraction and first-strand cDNA synthesis. The experimental protocol maintained consistency by using three independent biological replicates throughout all procedures and analyses.

2.7. Profiling CCHa1/CCHa1R Expression in Response to Feeding and Starvation

The transcriptional profiles of the neuropeptide *CCHa1/CCHa1R* in adults (full body) and in the brains of *A. pisum* were measured following starvation and feeding treatment for 3 and 6 h. We adapted the previously described feeding protocol with minor adjustments for our experimental needs [17,32]. In brief, aphids assigned to the "starved" group received no food, while those in the "fed" group were provided with food. For treatment durations of 3 and 6 h, we employed fifteen adult aphids, utilizing five aphids for each individual replication under both the starvation and feeding conditions. Likewise, when focusing on the brain tissues, we dissected 50 brains for each biological replication after 3 and 6 h of starvation and feeding. In total, three biological replicates were prepared for both the 3 and 6 h treatments of starved and fed aphids. The dissections and subsequent experiments were carried out in a controlled environment using 0.1 M PBS (pH 7.4) under a stereoscopic microscope (Olympus). The processes for total RNA extraction and first-strand cDNA synthesis were conducted as mentioned above. The experimental protocol maintained consistency by using three independent biological replicates throughout all procedures and analysis.

2.8. Synthesis and Injection of dsRNA

Double-stranded RNA for *CCHa1* (259 bp) and *CCHa1R* (384 bp) was produced using adult aphid cDNA and the Transcript Aid T7 High Yield Transcription Kit (Thermo Fisher Scientific), adhering to the supplier's instructions. We appended the T7 RNA polymerase promoter sequence (5′-TAATACGACTCACTATAGGG-3′) to both forward and reverse primers to enable dsRNA synthesis, as listed in Table S1. The PCR process involved an initial step at 95 °C for 3 min, followed by 35 cycles at 95 °C for 30 s, 60 °C for 30 s, and 72 °C for 45 s, concluding with a final polymerization step at 72 °C for 10 min. Following amplification, the amplicons were purified using the SteadyPure PCR DNA Purification Kit (Accurate Biotechnology in Changsha, Hunan, China). For dsRNA purification, we employed a phenol (pH 4.7) chloroform extraction and ethanol precipitation method, subsequently eluting the purified dsRNA in diethylpyrocarbonate (DEPC)-treated nuclease-free water. We synthesized a 714 bp *GFP* dsRNA fragment as a control, employing the aforementioned conditions and primers listed in Table S1. To assess dsRNA quantity, we employed a NanoDrop 2000 spectrophotometer from Thermo Fisher, while the integrity of the dsRNA was verified through gel electrophoresis using a 1% agarose gel prior to injection. A clear and singular band observed during gel electrophoresis confirmed the high quality of the dsRNA, indicating its suitability for injection into *A. pisum* for RNAi. We diluted the dsRNA to the desired concentration and preserved it at −80 °C until needed.

We administered dsRNA using an M3301 Nanoliter20 microinjector (World Precision Instruments, Sarasota, FL, USA). To facilitate the immobilization of aphids, a 1% agarose solution was prepared, allowed to cool until solid, and then formed into a petri dish. To secure the aphids, we etched two intersecting grooves into the agarose. Concurrently, we fabricated glass capillaries using 3.5-inch 3-000-203-G/X micropipettes (Drummond Scientific) and a PC-100 Dual-Stage Glass Micropipette Puller (Narishige). Prior to the micro-injection, aphids were immobilized by a brief 5 min incubation on ice. Subsequently, they were positioned on the agarose plate, and approximately 300 nL of dsRNA (at a concentration of approximately 2.8 μg/μL), targeting *dsCCHa1*, *dsCCHa1R*, and *dsGFP* as a control. The injection was delivered to the lateral thorax of adult aphids, specifically between the middle and posterior leg pairs, following the methodology described by [33]. Adult aphids, aged 24 h, were selected for dsRNA injection. To visualize the distribution of injected material, we combined food dye with *dsGFP*, *dsCCHa1*, and *dsCCHa1R* before administering them to the aphids. Each treatment group consisted of 25 injected aphids.

Following injection, the aphids were transferred to clip-caged *V. faba* leaves. Aphids were collected after 24 and 48 h.

2.9. Feeding Behavior Assay

We employed the EPG technique to analyze *A. pisum* feeding behavior across three groups: *dsCCHa1*, *dsCCHa1R* treatments, and *dsGFP* as a control [34], following the recently used protocol for *A. pisum* [35]. Fourteen hours post-injection, we attached a gold wire electrode (2 cm × 18 µm) to the dorsum of eight randomly selected aphids, securing it with electrically conductive silver glue. A Giga-8 DC EPG system served as the recording platform for the connected electrodes [34]. Stylet+, an integrated hardware–software solution from EPG Systems (Wageningen, The Netherlands), was employed to record EPG output. We established the plant connectivity by inserting an electrode into the potted plant's soil, then shielded the entire experimental apparatus within a Faraday cage to mitigate electromagnetic interference. We conducted 8 h EPG recordings of aphids placed on the abaxial surface of a mature leaf from a 2-week-old faba bean plant. Each plant was used once in each replication, ensuring data accuracy and reducing potential biases. EPG waveforms were analyzed using the Stylet+ analysis module [36]. Waveforms were divided into two phases: the first phase was from the initiation of EPG to reaching the phloem, and the second phase related to phloem activity. In phloem-related activity, two waves, E1 and E2, mainly represent the feeding duration. The E2 wave represents the feeding duration and the E1 wave represents the pre-feeding duration. Further analysis was performed using the Excel Workbook for automatic parameter calculation of EPG data 4.3 [37]. Twenty replications were conducted to compare the feeding behavior of treated and control *A. pisum*.

2.10. Survival and Reproduction Assay

Following the injection of *dsCCHa1*, *dsCCHa1R*, and *dsGFP*, we performed a reproductive performance assessment. Non-injected aphids used a control. After dsRNA injection, the aphids were reared on fresh leaves inside the clip cage, and we recorded the fecundity and mortality of adults continuously after a 12 h duration from the beginning of the RNAi assay. To assess viability, 20 aphids per treatment group were subjected to a parallel survival assay. Following dsRNA injection, aphids were transferred to clip-caged *V. faba* leaves, where adult mortality was recorded daily.

2.11. Statistical Analysis

Different developmental stages and body tissue data were analyzed by one-way ANOVA, and post hoc comparisons of the means were performed using the Tukey test at the $p < 0.05$ level. Starvation, feeding, gene silencing, and EPG recording data were analyzed using Excel 2016 and SPSS 20 for comprehensive data evaluation. Statistical comparisons between the treatment and control groups were conducted using independent Student's *t*-tests. Kaplan–Meier survival log rank analysis was applied to mortality data, and reproduction results were examined via independent Student's *t*-tests.

3. Results

3.1. Characterization of CCHa1/CCHa1R and Molecular Docking Analysis

The amino acid and nucleotide sequences of the *CCHa1* ORF are depicted in (Figure 1A). The multi-species alignment of *CCHa1* peptides is presented in (Figure 1B), highlighting a shared [CLSYGHSCWGAH-amide] consensus motif at the C-terminus of the *CCHa1* neuropeptide family. The *A. pisum* genome database (https://bipaa.genouest.org/is/aphidbase/ accessed on 11 January 2024) was used to identify transcripts of the *CCHa1*-R, which has the GenBank accession number ACYPI071161. Characterized as a typical GPCR, the *A. pisum CCHa1R* features seven TM and encodes a protein consisting of 413 amino acids. Analysis of evolutionary relationships demonstrated that *A. pisum CCHa1/CCHa1R* are phylogenetically close to their homologs in various insect species (Figure 1C,D).

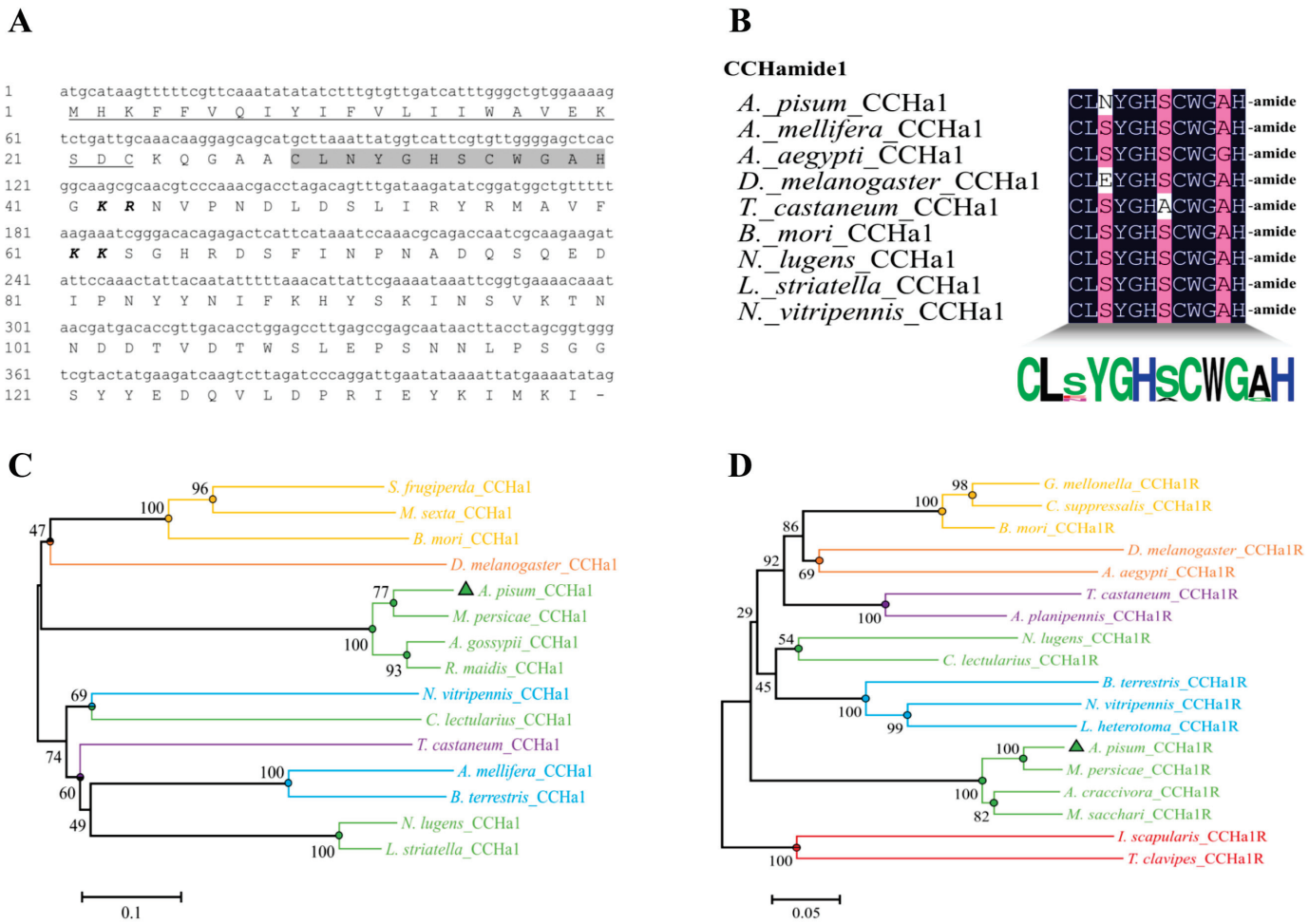


Figure 1. Bioinformatics analysis of *CCHa1*/*CCHa1R* from *A. pisum*. (**A**) Nucleotide and amino acid sequences of *CCHa1* cDNA. The underlined letters are predicted signal peptides, grey background amino acids represent mature peptides, and italic and bold letters are the dibasic cleavage sites. (**B**) Amino acid sequence alignment of *CCHa1* with other insect species; at the bottom, there is a consensus logo. (**C**,**D**) Phylogenetic tree of *CCHa1*/*CCHa1R* in different insects was constructed in MEGA 5.2 with 1000 bootstrap replicates. The model chooses P-distance and the Gaps/Missing DATA Treatment chooses Pairwise deletion. Numbers at branches are percent bootstrap support values. Accession numbers of *CCHa1*/*CCHa1R* are mentioned in Tables S2 and S3.

An alignment was conducted between *A. pisum CCHa1R* and the mRNA sequences of nine other *CCHa1R* insects. *A. pisum CCHa1R* showed identity with other receptors, such as the four *CCHa1R* hemipterans (*Aphis craccivora* 69.84%; *Diaphorina citri* 42.41%; *Bemisia tabaci* 34.05%; *Nilaparvata lugens* 41.25%), three coleopterans (*Tribolium castaneum* 37.94%; *Agrilus planipennis* 37.16%; *Tilloclytus clavipes* 29.77%), two dipterans (*D. melanogaster* 39.11%; *Aedes aegypti* 38.91%), one hymenopteran (*Nasonia vitripennis* 40.08%), one lepidopteran (*B. mori* 38.91%), and one ixodidae (*Ixodes scapularis* 31.13%). The most conserved portions of these GPCRs were predominantly found within their transmembrane segments (Figure S1). The *A. pisum CCHa1* mature peptide (CLNYGHSCWGAH) was docked to the *CCHa1R* target protein. Our molecular docking simulations revealed strong peptide–protein interactions, evidenced by a high binding energy of −8.149 kcal/mol. The *CCHa1R* protein binds the *CCHa1* mature peptide using the following residues: ARG-129, LYS-139, GLN-61, ASN-64, ALA-132, LEU-140, and MET-62. For the *CCHa1* mature peptide, the following residues are involved in the binding: HIS-12, SER-7, ASN-3, LEU-2, CYS-8, and TYR-4 (Figure 2).

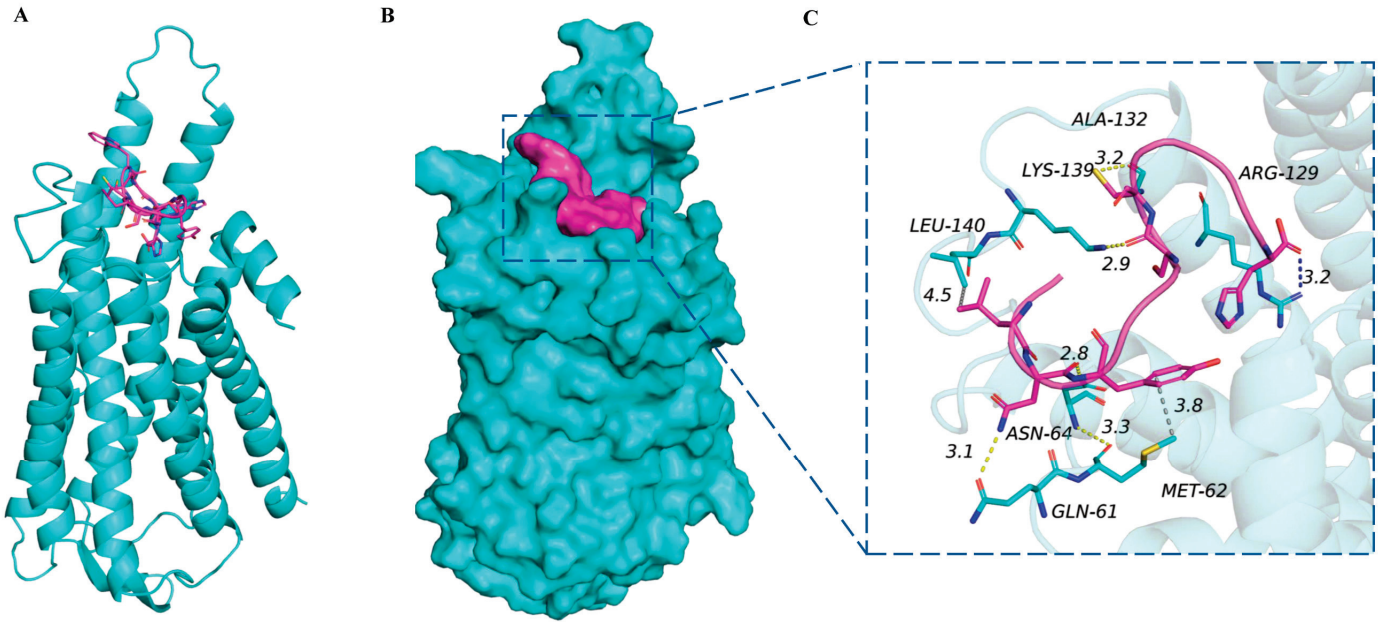


Figure 2. Docking analysis of *CCHa1* mature peptide and its receptor *CCHa1R*. (**A**) Ribbon diagram represents the *CCHa1R* protein bound to the *CCHa1* peptide (shown in purple), illustrating the overall docking pose and spatial orientation within the receptor's binding pocket. (**B**) Surface representation of the *CCHa1R* protein with the *CCHa1* peptide (highlighted in purple) positioned within the binding pocket. The interaction interface between the receptor and peptide. (**C**) Close-up view of the binding interactions between the *CCHa1* peptide and key residues within the receptor's binding site. Hydrogen bonds and distances between critical amino acids (e.g., ARG-129, ALA-132, LYS-139) are indicated, highlighting the molecular contacts involved in the docking. Yellow dash represents hydrogen bond distance.

3.2. Transcriptional Expression of CCHa1/CCHa1R During Developmental Stages and in the Body Tissues of A. pisum

Transcript abundance of *CCHa1/CCHa1R* was quantified across various developmental stages and body tissues using qRT-PCR. First-instar nymphs exhibited the highest expression level, while *CCHa1R* was detected as high in the 2nd-instar nymphs (Figure 3B,D). *A. pisum*'s antennae, brains, cuticles, embryos, and midguts exhibited diverse expression levels for *CCHa1/CCHa1R*, indicating tissue-specific regulation (Figure 3A,C). The brain exhibited the highest expression of both *CCHa1/CCHa1R*, while *CCHa1* was notably absent in the antennae, cuticles, and guts (Ct values $\geq$ 29). Low expression levels were recorded in embryo samples, possibly due to the diluting effect of the included head tissue.

3.3. Transcriptional Expressional Levels of CCHa1/CCHa1R Under Starvation and Feeding Conditions of A. pisum

We measured the transcript expression of *CCHa1/CCHa1R* in both fed and starved aphids, revealing significant disparities between the two groups. Remarkably, our findings showed a substantial upregulation of *CCHa1/CCHa1R* gene expression in starved aphids as compared to their fed counterparts (Figure 4A,B).

Moreover, the transcripts for *CCHa1/CCHa1R* were primarily localized in the brain (Figure 3A,C); our investigation also focused on the relative expression within the brains of fed and starved aphids. Intriguingly, our observations revealed a similar upregulated expression pattern for *CCHa1/CCHa1R* in starved aphids as compared to the control groups (Figure 4C,D). Furthermore, the transcript expression levels of both *CCHa1/CCHa1R* displayed increases in response to prolonged starvation stress.

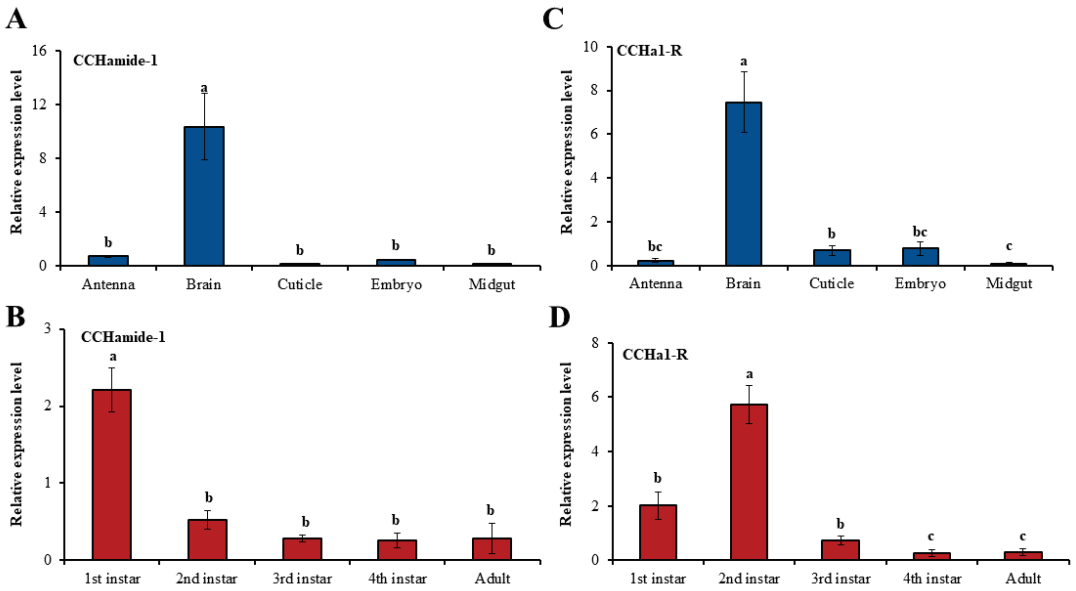


Figure 3. Relative expression levels of *CCHa1*/*CCHa1R* in different body parts during different developmental stages. (**A**–**C**) Relative expression levels of *CCHa1*/*CCHa1R* transcript in different body parts. (**B**–**D**) Relative expression levels of *CCHa1*/*CCHa1R* transcript at different developmental stages. (**A**–**D**) For each sample, the transcript level was measured via qRT-PCR and normalized against RPL7. The bars correspond to the average of three independent replicates. Results are shown as means ± S.E. The data were statistically analyzed by one-way ANOVA followed by Tukey test. Different lowercase letters indicate significant differences at the 0.05 level.

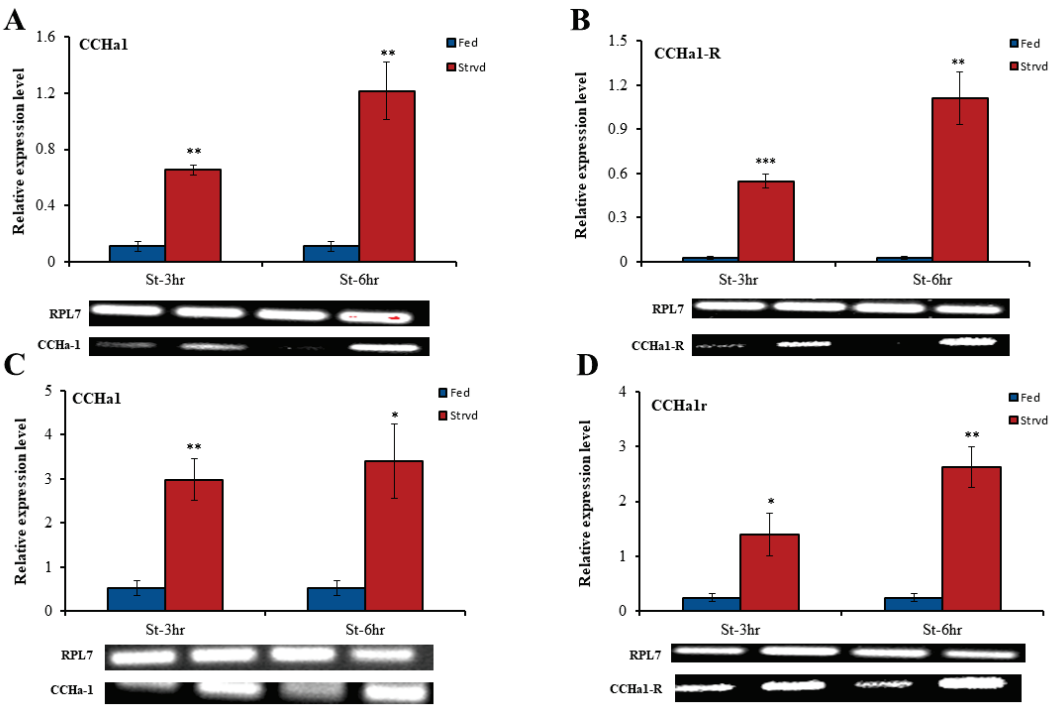


Figure 4. Effect of starvation on the transcriptional expression of *CCHa1*/*CCHa1R* in adults and brain samples. (**A**,**B**) Transcriptional expression of *CCHa1*/*CCHa1R* after starvation in adults. (**C**,**D**) Transcriptional expression of *CCHa1*/*CCHa1R* after starvation in brain. (**A**–**D**) Data were generated from three independent biological replications. Results are shown as means ± S.E. The asterisk on each bar represents the significant difference compared to fed aphids, calculated by statistical analysis (independent student t test, * $p < 0.05$, ** $p < 0.01$, *** $p < 0.001$, respectively).

3.4. RNAi-Based Silencing of CCHa1/CCHa1R via dsRNA Injection

One-day-old adult aphids were subjected to dsRNA injection. At the point of injection, living aphids exhibited cuticular melanization. Significant silencing of *CCHa1/CCHa1R* after dsRNA injection was achieved by 300 nL (~3 μg/μL) of *dsCCHa1* and *dsCCHa1R* compared to *dsGFP* as a control. At 24 and 48 h after dsRNA injection, the expression of *dsCCHa1* and *dsCCHa1R* was downregulated (Figure 5A,B).

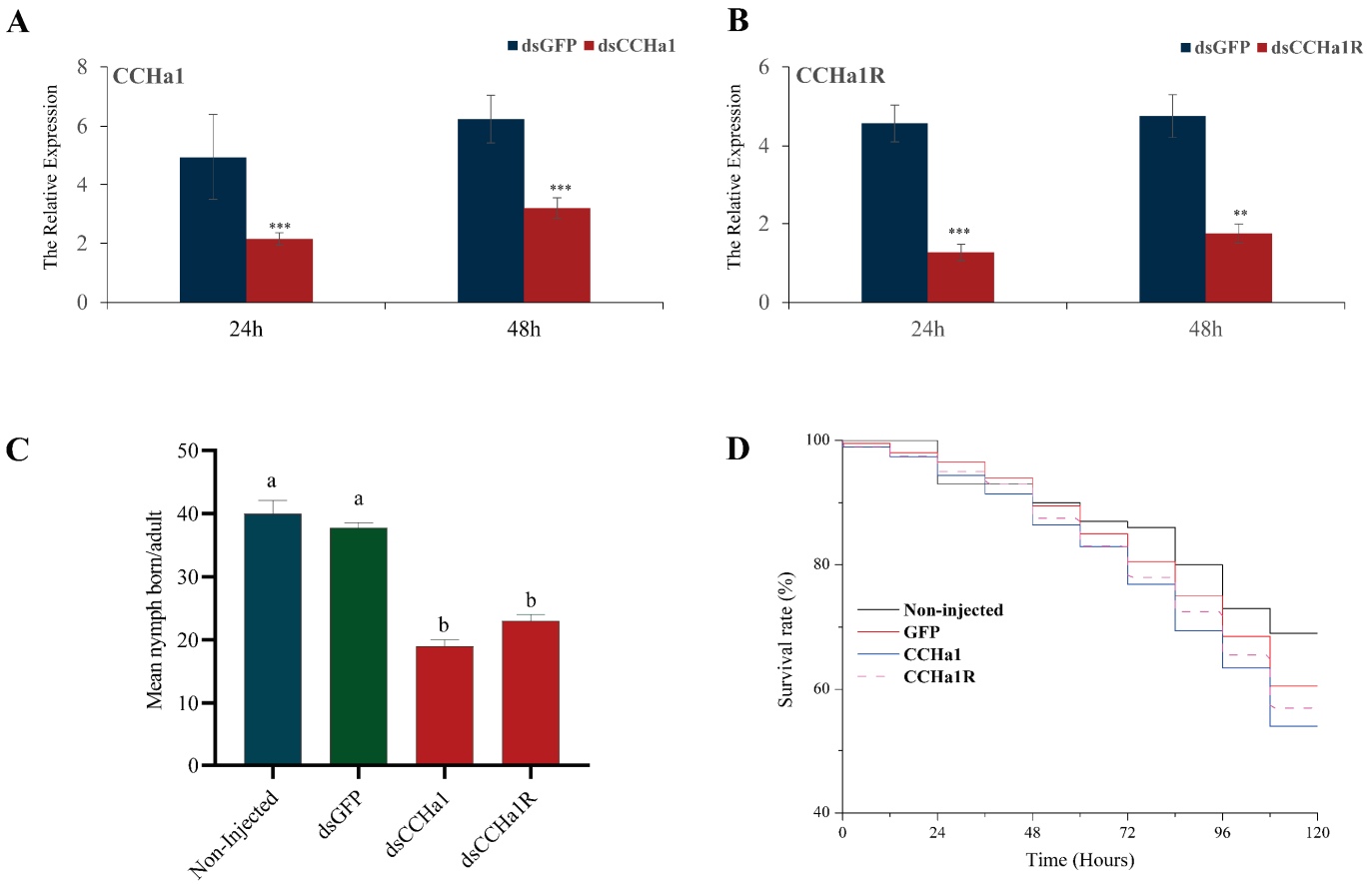


Figure 5. RNAi mediated knockdown of *CCHa1/CCHa1R* expression levels in *A. pisum*. (**A**,**B**) Gene silencing efficiency was detected at different sampling time-points (24 and 48 h) after injection of *dsCCHa1*, *dsCCHa1R* as treatment, and *dsGFP* as a control. (**C**) Effect of *CCHa1/CCHa1R* gene silencing on reproduction of *A. pisum* after injection of ds*CCHa1*, ds*CCHa1R*, and *dsGFP*, as well as in non-injected controls, respectively. (**D**) Influence of *dsCCHa1* and *dsCCHa1R* gene silencing on *A. pisum* survival. Kaplan–Meier survival log-rank analysis shows no significant difference in survival between the ds*CCHa1* and ds*CCHa1R* treatments and the *dsGFP*-injected control ($p < 0.05$). (**A**–**C**) Each treatment contained three biological replicates analyzed by qRT-PCR. The asterisk on each bar represents a significant difference compared to injected *dsGFP*, calculated by statistical analysis (independent Student's *t* test, ** $p < 0.01$, *** $p < 0.001$, respectively).

3.5. CCHa1/CCHa1R Knockdown Effects on A. pisum Feeding Behavior

EPG analysis was employed to examine changes in probing and feeding durations following RNAi-mediated silencing of *dsCCHa1* and *dsCCHa1R*, with *dsGFP* serving as a control. Our analysis focused on 27 EPG parameters: 11 for probing activities and 16 for plant phloem-related behaviors (Table 1). Regarding stylet activity before phloem access, measured by the first probe duration, it showed a marked reduction from 7 h (*dsGFP* control) to 5.6 h (*dsCCHa1*) and 6.1 h (*dsCCHa1R*). ($p = 0.021$). Similarly, both the number of probes and the overall duration of probing exhibited significant decreases across the two groups ($p = 0.012$ and $p = 0.027$). Simultaneously, the total and mean durations of

C and np waves remained statistically similar across the groups (p = 0.066, 0.305 and p = 0.22, 0.490, respectively).

Table 1. Comparison of probing and feeding behaviors of *Acyrthosiphon pisum* in the *dsCCHa1*, *dsCCHa1R* treatment, and *dsGFP* control groups on broad bean seedlings based on EPG recordings.

Tissue Specificity	Parameters		*dsGFP*	*dsCCHa1*	*dsCCHa1R*	*p*
		N	Mean [s] ± SE	Mean [s] ± SE	Mean [s] ± SE	
(From Initiation of EPG to Reaching Phloem)						
Epidermis	Duration of 1st probe	20	24915 ± 1294 a	20,443.21 ± 1105 b	21,985 ± 912 ab	0.021
Epidermis and mesophyll	Time from 1st probe to 1st E	20	6595 ± 1101 b	11,256 ± 1636 a	10,040 ± 1443 ab	0.029
All tissues	Time from start of EPG to 1st sustained E2 (>10 min)	20	8647 ± 1107 b	14,304.79 ± 2066 a	13,925.73 ± 1904 ab	0.044
All tissues	Number of probes	20	4.35 ± 0.76 a	2.3 ± 0.19 b	2.95 ± 0.26 b	0.012
All tissues	Total probing time	20	27,635 ± 447 a	25,839 ± 486 b	26,197 ± 523 b	0.027
All tissues	Number of C	20	9.75 ± 4.24 a	7.58 ± 2.21 b	7.65 ± 2.53 b	0.035
All tissues	Total duration of C	20	21,222 ± 1005 b	24,078 ± 713 ab	24,272 ± 1247 a	0.066
All tissues	Mean duration of C	20	4806 ± 501 a	3896 ± 337 a	3993 ± 340 a	0.22
All tissues	Number of np	20	2.15 ± 0.29 b	3.1 ± 0.31 a	2.95 ± 0.23 a	0.042
All tissues	Total duration of np	20	466 ± 90 a	666 ± 91 a	553 ± 92 a	0.305
All tissues	Mean duration of np	20	132 ± 26 a	176 ± 25 a	153 ± 27 a	0.490
(Related to Phloem Activity)						
Epidermis and mesophyll	Time from start of EPG to 1st E	20	7096 ± 994 b	12,379 ± 1866 a	11,248 ± 1640 ab	0.046
All tissues	Time from start of EPG to 1st E2	20	7600 ± 1091 b	13,544 ± 1322 a	11,472 ± 1397 ab	0.006
All tissues	Time from 1st probe to 1st sustained E2 (>10 min)	20	7862 ± 815 b	13,813 ± 1871 a	13,012 ± 2145 ab	0.034
Phloem	Total duration of E1 followed by E2 and E2	20	12,159 ± 770 a	8139 ± 1025 b	8671 ± 1011 b	0.007
Phloem	Number of single E1	20	0.6 ± 0.2 b	2.55 ± 0.7 a	2.15 ± 0.5 ab	0.043
Phloem	Number of E1	20	7.5 ± 0.7 a	5.35 ± 0.5 b	5.5 ± 0.4 b	0.015
Phloem	Number of E2	20	6.15 ± 0.5 a	4.1 ± 0.2 b	4.65 ± 0.3 b	0.003
Phloem	Number of sustained E2 (longer than 10 min)	20	4.15 ± 0.3 a	2.8 ± 0.3 b	3.01 ± 0.3 b	0.016
Phloem	Total duration of E	20	11,598 ± 638 a	7036 ± 922 b	8340 ± 936 b	0.001
Phloem	Total duration of E1	20	495 ± 103 a	378 ± 62.1 a	414 ± 60.9 a	0.560
Phloem	Total duration of E2	20	10,320 ± 817 a	6707 ± 963 b	7175 ± 969 b	0.014
Phloem	Mean duration of E1	20	98.3 ± 9.2 a	88.0 ± 8.4 a	90.3 ± 8.3 a	0.682
Phloem	Mean duration of E2	20	2610 ± 330 a	1270 ± 182 b	1491 ± 252 b	0.001
Phloem	Duration of 1st E	20	3254 ± 430 a	1335 ± 291 b	1492 ± 299 b	0.001
Phloem	Duration of the longest E2	20	6763 ± 759 a	3867 ± 441 b	4136 ± 481 b	0.001
Phloem	% of probing spent in E2	20	31.73 ± 3.3 a	18.98 ± 3.3 b	21.26 ± 2.3 b	0.010

The two means with the same lowercase letters in the same row are not significantly different (Independent sample t-test $p > 0.05$).

As aphids are plant phloem-sucking insects, the initial insertion of the stylet in the phloem was delayed from ~1.9 h (*dsGFP* group) to 3.4 h and 3.1 h in the *dsCCHa1* and *dsCCHa1R* groups, respectively, as mentioned by "Time from start of EPG to 1st E" (p = 0.046). While E and E2 waveforms showed reduced total durations (p = 0.001 and p = 0.014), respectively, the non-phloematic phase exhibited a significant prolonged time (p = 0.036). However, a significant decrease was observed in the frequency of both E1 and E2 waveforms (p = 0.015 and p = 0.003, respectively), and in the mean duration of the E1 or total duration of E1, no significant differences were observed (p = 0.682 and p = 0.560, respectively). Compared to the *dsGFP* control, both *dsCCHa1* and *dsCCHa1R* treatments showed significant decreases in multiple E2 waveform metrics: mean duration, longest duration, frequency of sustained events, and percentage of probing time (p = 0.001, p = 0.001, p = 0.016, and p = 0.010, respectively).

4. Discussion

In this study, we identified the sequences of *CCHa1/CCHa1R* in the pea aphid, *A. pisum*, revealing significant similarities with the corresponding precursors and receptors from other insect species. Notably, the transmembrane domain regions of *CCHa1R* exhibited significant conservation across different species. Phylogenetic analysis of *CCHa1R* revealed a higher degree of similarity with receptors from other insects compared to the sequence identity observed in the alignment. The reason for this difference is that identity quantifies the exact matches of residues—either nucleotide or amino acid—between two sequences, while similarity indicates the extent of resemblance based on functional, structural, or evolutionary connections [17]. The docking analysis revealed that the *CCHa1* peptide binds to its receptor *CCHa1R* through specific amino acid residues, which are critical for maintaining the structural and functional integrity of the peptide–receptor complex. Residues such as HIS-12, SER-7, ASN-3, LEU-2, CYS-8, and TYR-4 in the peptide, as well as ARG-129, LYS-139, GLN-61, ASN-64, ALA-132, LEU-140, and MET-62 in the receptor, show strong interaction patterns, suggesting a high degree of specificity and affinity in the binding process (Figure 2). Moreover, in the peach–potato aphid, the binding of *AKH* and *AKHR* has been demonstrated and the binding between the receptor and 2271 analog has been predicted to be more stable than the binding with the natural *AKH* [38].

The relative expression levels of *CCHa1/CCHa1R* transcript varied across different developmental stages in *A. pisum*, with a significantly higher expression observed in the first and second nymphal instars compared to the other stages (Figure 3B,D). It is important to note that the low expression levels of the receptor in the later nymphal instars make it difficult to detect any changes in expression through qRT-PCR, which may explain the lack of significant variations across different developmental stages. It was remarkable that neuropeptide receptors other than *CCHa1R* that are involved in feeding regulation in *A. pisum*, such as *CCHa2-R*, neuropeptide F receptor (NPFR), and short neuropeptide F receptor (sNPFR), also displayed consistent expression levels across different developmental stages [17,32,35].

CCHa1/CCHa1R mRNA levels were significantly upregulated in the brains of *A. pisum*, implying that cells located in the guts, antennae, and cuticles of the aphids are not the primary sites of *CCHa1/CCHa1R*. Our findings were similar with previously reported data on receptors in *A. pisum*, showing that *CCHa2-R* expression is more pronounced in the brain compared to the gut and other body tissues [17]. Our findings corroborate the preexisting observations from other insect species and show that in *D. melanogaster*, both *CCHa1* and *CCHa2* are primarily synthesized and secreted in the brain and midgut endocrine cells [15,18,39], and so in turn, these peptides are named "brain-gut peptides" (enteroendocrine peptides). *A. aegypti* transcript expression of *CCHa1* was found to be higher in the head, midgut, and carcass (cuticle, fat body, and skeletal muscle) [23]. Particularly, when assessing sex differences, the transcript of *CCHa1* exhibited increased levels in the midgut of male mosquitoes as compared to the head [23]. However, comparable expression of *CCHa1* was observed in the female head and midgut [23]. Moreover, the immunomapping of *CCHa1* in *A. aegypti* detected neurons in the brain, the ventral nerve cord, and enteroendocrine cells in the posterior midgut close to the midgut/hindgut junction, confirming the expression profiles of these transcripts [23]. Considering the differences in *CCHa1* transcript levels between the heads and midguts of male and female *A. aegypti*, we speculate that the exclusive presence of *CCHa1/CCHa1R* only in the brain may be related to the parthenogenetic characteristics of *A. pisum*.

Starvation influences the expression levels of *CCHa1/CCHa1R* in adults and in the brains of *A. pisum* (Figure 4A–D). The *CCHa1* signaling cascade has documented functions closely related to the feeding and nutritional statuses of diverse insect species. Therefore, we set specific time points to monitor changes in the expression levels of *CCHa1/CCHa1R* in *A. pisum* under conditions of starvation stress and feeding. Simultaneous collection of aphids across all experimental groups was performed to prevent the circadian rhythm from influencing *CCHa1R* transcript expression levels. In *A. pisum*, starvation induced an upreg-

ulation of *CCHa1/CCHa1R* transcript levels, whereas feeding triggered a downregulation, irrespective of quantitative differences between time points. Our findings demonstrated that the expression of *CCHa1/CCHa1R* transcripts in *A. pisum* is influenced by the organism's feeding state. Moreover, our findings were consistent with other feeding-modulated neuropeptides in hemipterans, including *sNPF* and *NPF*, where the transcript expression of precursors and receptors is downregulated under starvation stress and returns to baseline following refeeding [40]. However, in chewing mouthparts insects, including *Schistocerca gregaria* and *B. mori*, starvation-induced stress downregulates the transcript expression of *sNPF* (documented role in feeding in both species) [41]. The correlation between starvation stress and transcript expression may stem from the species-specific physiology of feeding behavior [35]. Taken together, our observations suggest that the *CCHa1* signaling pathway is implicated in the nutritional response of wingless parthenogenetic aphids, particularly through the regulation of *CCHa1R* expression.

The putative functions of *CCHa1/CCHa1R* in regulating *A. pisum* feeding were analyzed using RNAi. Effective target gene silencing requires the incorporation of dsRNA molecules into the insect body, leading to reduced gene expression at the transcription stage [42]. In *A. pisum*, the brain exhibits a higher expression level of *CCHa1/CCHa1R* than other tissues (Figure 3A,C). Following RNAi injection, we observed up to a 50% reduction in *CCHa1/CCHa1R* mRNA levels across the whole aphid body (Figure 5A,B). The significant reduction in gene expression at 24 and 48 h after *CCHa1/CCHa1R* silencing prompted us to analyze alterations in *A. pisum* feeding behavior following dsRNA injection. Ultimately, we employed the EPG technology to investigate changes in *A. pisum* feeding behavior following *CCHa1/CCHa1R* knockdown. Our findings showed that suppressing *CCHa1/CCHa1R* expression in *A. pisum* inhibited the appetite and reduced the food intake of the aphids (Table 1). This suggests that silencing these genes regulates the aphid's appetite, potentially involving *NPF*, *sNPF/sNPFR*, and *CCHa2R* pathways, which consequently modifies feeding behavior and effectively decreases food consumption [17,32,35]. The appearance and length of the E waveform in EPG studies generally reflected the aphid's prioritization of phloem sap feeding [36]. Consequently, the observed delay in phloem activity among *A. pisum* treated with *dsCCHa1* and *dsCCHa1R* indicated a reduced appetite. Corroborating this, *dsCCHa1*-treated aphids also showed a reduced duration of initial probing and overall probing time. Primarily, the reduced appetite and shortened phloem ingestion duration contribute to the decrease in food intake observed in *dsCCHa1*-silenced aphids (Table 1). Our findings revealed a correlation between *CCHa1/CCHa1R* transcript abundance and feeding behavior in *A. pisum*; however, the precise downstream signaling mechanism is yet to be elucidated. Nonetheless, considering the high level of *CCHamide-1* and *CCHa1R* mRNA in the brain of *A. pisum*, we speculate that the brain synthesizes and releases a signal to the *CCHa1R* to stimulate food intake.

The suppression of *CCHa1/CCHa1R* expression has been observed to influence the reproductive process in aphids. The reproduction assay showed a significant decline in aphid fecundity following injection of *dsCCHa1* and *dsCCHa1R*, although survival was not notably influenced by the *CCHa1/CCHa1R* knockdown. The results suggested that aphids might compromise their reproductive capacity to maintain survival in response to nutrient scarcity [43]. Previous studies on *CCHa2R*, *NPF*, and *sNPF/sNPFR* also showed that the survival rate of *A. pisum* remained unaffected, showing no significant changes [17,32,35]. An additional factor potentially contributing to the significant decrease in reproduction after RNAi of *CCHa1/CCHa1R* might be a consequence of *CCHa1*'s indirect involvement in the lipid metabolic process. Indeed, reproductive success is closely tied to lipid availability, as these compounds serve as the main energy source, with reduced levels leading to diminished reproductive output [44]. As this effect has not been previously reported in *A. pisum*, further investigation into the impact of *CCHa1* on lipid metabolism is needed.

In conclusion, in *A. pisum*, the *CCHa1/CCHa1R* transcripts were found to be highly expressed in the brain. Our findings suggest that *CCHa1/CCHa1R* play a role in modulating aphid feeding patterns and food consumption, with subsequent effects on reproduction,

but not on survival. Furthermore, the addition of *CCHa1/CCHa1R* to the existing *A. pisum* "feeding toolkit" represents a valuable contribution to our understanding of insect feeding behavior, particularly in *A. pisum*. While our study centered on wingless *A. pisum*, it is important to note that aphids exhibit wing dimorphism—a trait that allows them to adapt to environmental changes. Winged and wingless aphids display distinct morphological, physiological, and behavioral characteristics [45]. Nutrient availability is believed to be a pivotal factor in orchestrating the wingless-to-winged transition in aphids [46]. Therefore, we believe that investigation into the role of *CCHa1/CCHa1R* in winged *A. pisum* feeding behavior would provide valuable insights.

Supplementary Materials: The following supporting information can be downloaded at https://www.mdpi.com/article/10.3390/insects15120939/s1, Figure S1: Amino acid sequence alignment of the *A. pisum CCHa1R* with other related GPCRs. Seven transmembrane domains are highlighted with black lines (TM1–TM7). Table S1: PCR primers for qRT-PCR and dsRNA synthesis. Table S2: *CCHa1* Accession number of genes used for phylogenetic analysis. Table S3: *CCHa1R* Accession number of genes used for phylogenetic analysis.

Author Contributions: Conceptualization, S.S., Y.S. and T.-X.L.; methodology, S.S.; Y.S. and G.S.; software, S.S., M.B.A. and T.-B.D.; validation, S.S., Y.S. and T.-X.L.; formal analysis, S.S., M.B.A., T.-B.D., T.-X.L., G.S. and Y.S., investigation, S.S. and M.B.A.; resources, Y.S. and T.-X.L.; data curation, S.S. and M.B.A.; writing—original draft preparation, S.S. and M.B.A.; writing—review and editing, Y.S., G.S. and T.-X.L.; visualization, S.S.; supervision, Y.S.; funding acquisition, Y.S. All authors have read and agreed to the published version of the manuscript.

Funding: This study was supported by Qingdao Science and Technology Benefiting the People Demonstration Project (23-2-8-1-xdny-12-nsh), the Science and Technology Supporting Program for Young Innovative Teams in Higher Education of Shandong Province (2023KJ164) and National Key R&D Program (2022YFD2300105).

Institutional Review Board Statement: Not applicable.

Informed Consent Statement: Not applicable.

Data Availability Statement: The data presented in this study are available upon request from the corresponding author.

Acknowledgments: All authors are very thankful to the anonymous reviewers for improving the manuscript.

Conflicts of Interest: The authors declare no conflicts of interest.

References

1. Altstein, M.; Nässel, D.R. Neuropeptide signaling in insects. *Adv. Exp. Med. Biol.* **2010**, *692*, 155–165. [CrossRef]
2. Toprak, U. The role of peptide hormones in insect lipid metabolism. *Fron. Physiol.* **2020**, *11*, 434. [CrossRef] [PubMed]
3. Nässel, D.R.; Zandawala, M. Recent advances in neuropeptide signaling in *Drosophila*, from genes to physiology and behavior. *Prog. Neuro.* **2019**, *179*, 101607. [CrossRef]
4. Jékely, G. Global view of the evolution and diversity of metazoan neuropeptide signaling. *Proc. Natl. Acad. Sci. USA* **2013**, *110*, 8702–8707. [CrossRef] [PubMed]
5. Eichel, K.; Von, Z.M. Subcellular organization of GPCR signaling. *Trends Pharmacol Sci.* **2018**, *39*, 200–208. [CrossRef]
6. Rosenbaum, D.M.; Rasmussen, S.G.; Kobilka, B.K. The structure and function of G-protein-coupled receptors. *Nature* **2009**, *459*, 356–363. [CrossRef] [PubMed]
7. Zhang, M.; Chen, T.; Lu, X.; Lan, X.; Chen, Z.; Lu, S. G protein-coupled receptors (GPCRs): Advances in structures, mechanisms, and drug discovery. *Signal Transduct. Target. Ther.* **2024**, *9*, 88. [CrossRef] [PubMed]
8. Shi, Y.; Nachman, R.J.; Gui, S.H.; Piot, N.; Kaczmarek, K.; Zabrocki, J.; Dow, J.A.T.; Davies, S.A.; Smagghe, G. Efficacy and biosafety assessment of neuropeptide CAPA analogues against the peach-potato aphid (*Myzus persicae*). *Insect Sci.* **2022**, *29*, 521–530. [CrossRef]
9. Rozengurt, E. Signal transduction pathways in the mitogenic response to G protein-coupled neuropeptide receptor agonists. *J. Cell. Physiol.* **1998**, *177*, 507–517. [CrossRef]
10. Wu, F.; Song, G.; de Graaf, C.; Stevens, R.C. Structure and function of peptide-binding G protein-coupled receptors. *J. Mol. Biol.* **2017**, *429*, 2726–2745. [CrossRef]

11. Roller, L.; Yamanaka, N.; Watanabe, K.; Daubnerová, I.; Žitňan, D.; Kataoka, H.; Tanaka, Y. The unique evolution of neuropeptide genes in the silkworm *Bombyx mori*. *Insect Biochem. Mol. Biol.* **2008**, *38*, 1147–1157. [CrossRef] [PubMed]
12. Huybrechts, J.; Bonhomme, J.; Minoli, S.; Prunier-Leterme, N.; Dombrovsky, A.; Abdel-Latief, M.; Robichon, A.; Veenstra, J.A.; Tagu, D. Neuropeptide and neurohormone precursors in the pea aphid, *Acyrthosiphon pisum*. *Insect Mol. Biol.* **2010**, *19*, 87–95. [CrossRef] [PubMed]
13. Hansen, K.K.; Hauser, F.; Williamson, M.; Weber, S.B.; Grimmelikhuijzen, C.J.P. The *Drosophila* genes CG14593 and CG30106 code for G-protein-coupled receptors specifically activated by the neuropeptides *CCHamide-1* and *CCHamide-2*. *Biochem. Biophys. Res. Commun.* **2011**, *404*, 184–189. [CrossRef] [PubMed]
14. Ida, T.; Takahashi, T.; Tominaga, H.; Sato, T.; Sano, H.; Kume, K.; Ozaki, M.; Hiraguchi, T.; Shiotani, H.; Terajima, S.; et al. Isolation of the bioactive peptides *CCHamide-1* and *CCHamide-2* from drosophila and their putative role in appetite regulation as ligands for G protein-coupled receptors. *Front. Endocrinol.* **2012**, *3*, 177. [CrossRef] [PubMed]
15. Ren, G.R.; Hauser, F.; Rewitz, K.F.; Kondo, S.; Engelbrecht, A.F.; Didriksen, A.K.; Schjøtt, S.R.; Sembach, F.E.; Li, S.; Søgaard, K.C.; et al. *CCHamide-2* is an orexigenic brain-gut peptide in *Drosophila*. *PLoS ONE* **2015**, *10*, e0133017. [CrossRef]
16. Sano, H. Coupling of growth to nutritional status: The role of novel periphery-to-brain signaling by the *CCHa2* peptide in *Drosophila melanogaster*. *Fly* **2015**, *9*, 183–187. [CrossRef] [PubMed]
17. Shahid, S.; Shi, Y.; Yang, C.; Li, J.; Ali, M.Y.; Smagghe, G.; Liu, T.-X. CCHamide2-receptor regulates feeding behavior in the pea aphid, *Acyrthosiphon pisum*. *Peptides* **2021**, *143*, 170596. [CrossRef]
18. Li, S.; Torre-Muruzabal, T.; Søgaard, K.C.; Ren, G.R.; Hauser, F.; Engelsen, S.M.; Pødenphanth, M.D.; Desjardins, A.; Grimmelikhuijzen, C.J.P. Expression patterns of the *Drosophila* neuropeptide *CCHamide-2* and its receptor may suggest hormonal signaling from thegut to the brain. *PLoS ONE* **2013**, *8*, e76131. [CrossRef]
19. Farhan, A.; Gulati, J.; Groe-Wilde, E.; Vogel, H.; Hansson, B.S.; Knaden, M. The CCHamide 1 receptor modulates sensory perception and olfactory behavior in starved *Drosophila*. *Sci. Rep.* **2013**, *3*, 2765. [CrossRef] [PubMed]
20. Veenstra, J.A.; Ida, T. More *Drosophila* enteroendocrine peptides: Orcokinin B and the CCHamides 1 and 2. *Cell Tiss. Res.* **2014**, *357*, 607–621. [CrossRef] [PubMed]
21. Fujiwara, Y.; Hermann-Luibl, C.; Katsura, M.; Sekiguchi, M.; Ida, T.; Helfrich-Förster, C.; Yoshii, T. The CCHamide1 neuropeptide expressed in the anterior dorsal neuron 1 conveys a circadian signal to the ventral lateral neurons in *Drosophila melanogaster*. *Front. Physiol.* **2018**, *9*, 1276. [CrossRef] [PubMed]
22. Kuwano, R.; Katsura, M.; Iwata, M.; Yokosako, T.; Yoshii, T. Pigment-dispersing factor and CCHamide1 in the *Drosophila* circadian clock network. *Chron. Int.* **2023**, *40*, 284–299. [CrossRef]
23. Tan, J.; Neupert, S.; Paluzzi, J.-P. Functional characterization of CCHamides and deorphanization of of their receptors in the yellow fever mosquito, *Aedes aegypti*. *Gen. Comp. Endocrinol.* **2024**, *359*, 114618. [CrossRef] [PubMed]
24. Richards, S.; Gibbs, R.A.; Gerardo, N.M.; Moran, N.; Nakabachi, A.; Stern, D.; Tagu, D.; Wilson, A.C.C.; Muzny, D.; Kovar, C.; et al. Genome sequence of the pea aphid *Acyrthosiphon pisum*. *PLoS Biol.* **2010**, *8*, e1000313. [CrossRef]
25. Sabater-Muñoz, B.; Legeai, F.; Rispe, C.; Bonhomme, J.; Dearden, P.; Dossat, C.; Duclert, A.; Gauthier, J.P.; Ducray, D.G.; Hunter, W.; et al. Large-scale gene discovery in the pea aphid *Acyrthosiphon pisum* (Hemiptera). *Gen. Biol.* **2006**, *7*, R21. [CrossRef]
26. Gauthier, J.P.; Legeai, F.; Zasadzinski, A.; Rispe, C.; Tagu, D. AphidBase: A database for aphid genomic resources. *Bioinformatics* **2007**, *23*, 783–784. [CrossRef] [PubMed]
27. Li, C.; Yun, X.; Hu, X.; Zhang, Y.; Sang, M.; Liu, X.; Wu, W.; Li, B. Identification of G protein-coupled receptors in the pea aphid, *Acyrthosiphon pisum*. *Genomics* **2013**, *102*, 345–354. [CrossRef] [PubMed]
28. Crooks, G.E.; Hon, G.; Chandonia, J.M.; Brenner, S.E. WebLogo: A sequence logo generator. *Genome Res.* **2004**, *14*, 1188–1190. [CrossRef] [PubMed]
29. Kumar, S.; Nei, M.; Dudley, J.; Tamura, K. MEGA: A biologist-centric software for evolutionary analysis of DNA and protein sequences. *Brief. Bioinf.* **2008**, *9*, 299–306. [CrossRef] [PubMed]
30. Thompson, J.D.; Higgins, D.G.; Gibson, T.J. improving the sensitivity of progressive multiple sequence alignment through sequence weighting, position-specific gap penalties and weight matrix choice. *Nucleic Acids Res.* **1994**, *22*, 4673–4680. [CrossRef]
31. Nakabachi, A.; Shigenobu, S.; Sakazume, N.; Shiraki, T.; Hayashizaki, Y.; Carninci, P.; Ishikawa, H.; Kudo, T.; Fukatsu, T. Transcriptome analysis of the aphid bacteriocyte, the symbiotic host cell that harbors an endocellular mutualistic bacterium, Buchnera. *Proc. Natl. Acad. Sci. USA* **2005**, *102*, 5477–5482. [CrossRef] [PubMed]
32. Li, X.; Qu, M.J.; Zhang, Y.; Li, J.W.; Liu, T.X. Expression of neuropeptide F gene and its regulation of feeding behavior in the pea aphid, *Acyrthosiphon pisum*. *Front. Physiol.* **2018**, *9*, 87. [CrossRef] [PubMed]
33. Sapountzis, P.; Duport, G.; Balmand, S.; Gaget, K.; Jaubert-Possamai, S.; Febvay, G.; Charles, H.; Rahbé, Y.; Colella, S.; Calevro, F. New insight into the RNA interference response against cathepsin-L gene in the pea aphid, *Acyrthosiphon pisum*: Molting or gut phenotypes specifically induced by injection or feeding treatments. *Insect Biochem. Mol. Biol.* **2014**, *51*, 20–32. [CrossRef] [PubMed]
34. Tjallingii, W.F. Electronic recording of penetration behavior by aphids. *Entomol. Exp. Appl.* **1978**, *24*, 521–530. [CrossRef]
35. Amir, M.B.; Shi, Y.; Cao, H.; Ali, M.Y.; Ahmed, M.A.; Smagghe, G.; Liu, T.X. Short Neuropeptide F and its receptor regulate feeding behavior in pea aphid (*Acyrthosiphon pisum*). *Insects* **2022**, *13*, 282. [CrossRef]
36. Prado, E.; Tjallingii, W.F. Aphid activities during sieve element punctures. *Entomol. Exp. Appl.* **1994**, *72*, 157–165. [CrossRef]
37. Sarria, E.; Cid, M.; Garzo, E.; Fereres, A. Excel Workbook for automatic parameter calculation of EPG data. *Comput. Electron. Agric.* **2009**, *67*, 35–42. [CrossRef]

38. Shi, Y.; Li, H.; Nachman, R.; Liu, T.X.; Smagghe, G. Insecticidal efficacy and risk assessment of different neuropeptide analog combinations against the peach-potato aphid following topical exposure. *Pest Manag. Sci.* **2022**, *79*, 226–233. [CrossRef] [PubMed]
39. Titos, I.; Rogulja, D. A gut-secreted peptide controls arousability through modulation of dopaminergic neurons in the brain. *BioRxiv* **2020**, 275552. [CrossRef]
40. Nagata, S.; Matsumoto, S.; Nakane, T.; Ohara, A.; Morooka, N.; Konuma, T.; Nagai, C.; Nagasawa, H. Effects of starvation on brain short neuropeptide F-1, -2, and -3 levels and short neuropeptide F receptor expression levels of the silkworm, *Bombyx mori*. *Front. Endocrinol.* **2012**, *3*, 3. [CrossRef] [PubMed]
41. Dillen, S.; Verdonck, R.; Zels, S.; Van Wielendaele, P.; Vanden Broeck, J. Identification of the short neuropeptide F precursor in the desert locust: Evidence for an inhibitory role of sNPF in the control of feeding. *Peptides* **2014**, *53*, 134–139. [CrossRef]
42. Ullah, F.; Gul, H.; Wang, X.; Ding, Q.; Said, F.; Gao, X.; Desneux, N.; Song, D. RNAi-mediated knockdown of chitin synthase 1 (CHS1) gene causes mortality and decreased longevity and fecundity in *Aphis gossypii*. *Insects* **2020**, *11*, 22. [CrossRef]
43. Will, T.; Vilcinskas, A. The structural sheath protein of aphids is required for phloem feeding. *Insect Biochem. Mol. Biol.* **2015**, *57*, 34–40. [CrossRef] [PubMed]
44. Hansen, M.; Flatt, T.; Aguilaniu, H. Reproduction, fat metabolism, and life span: What is the connection? *Cell Metab.* **2013**, *17*, 10–19. [CrossRef]
45. Braendle, C.; Davis, G.K.; Brisson, J.A.; Stern, D.L. Wing dimorphism in aphids. *Heredity* **2006**, *97*, 192–199. [CrossRef] [PubMed]
46. Müller, C.B.; Williams, I.S.; Hardie, J. The role of nutrition, crowding and interspecific interactions in the development of winged aphids. *Ecol. Entomol.* **2001**, *26*, 330–340. [CrossRef]

Disclaimer/Publisher's Note: The statements, opinions and data contained in all publications are solely those of the individual author(s) and contributor(s) and not of MDPI and/or the editor(s). MDPI and/or the editor(s) disclaim responsibility for any injury to people or property resulting from any ideas, methods, instructions or products referred to in the content.

insects

MDPI

Article

Screening and Validation of Stable Reference Genes for qRT-PCR Analysis in *Epicauta gorhami* (Coleoptera: Meloidae)

Guofeng Yang [1,†], Xuetao Yu [1,†], Yan Zhang [1], Jinhua Luo [2], Xiaofei Li [1], Li Zhu [1], Huanhuan Zhang [3], Lin Jin [4], Gang Wu [1], Xiaohong Yan [1,*] and Chenhui Shen [1,*]

[1] Key Laboratory of Agricultural Genetically Modified Organisms Traceability, Oil Crops Research Institute of Chinese Academy of Agricultural Science/Supervision and Test Center (Wuhan) for Plant Ecological Environment Safety, Ministry of Agriculture and Rural Affairs, Wuhan 430062, China; yangguofeng8866@163.com (G.Y.); xuetao.yu@outlook.com (X.Y.); zy18736825518@163.com (Y.Z.); lixiaofei@caas.cn (X.L.); zhuli49751@163.com (L.Z.); wugang@caas.cn (G.W.)

[2] Enshi Tujia and Miao Autonomous Prefecture Academy of Agricultural Sciences, Enshi 445000, China; chw63@126.com

[3] Institute of Vegetable, Tibet Academy of Agricultural and Animal Husbandry Sciences, Lhasa 850032, China; 15365182126@163.com

[4] Department of Entomology, College of Plant Protection, Nanjing Agricultural University, Nanjing 210095, China; jinlin@njau.edu.cn

* Correspondence: yanxiaohong@caas.cn (X.Y.); shenchenhui@caas.cn (C.S.)

† These authors contributed equally to this work.

Simple Summary: The reverse transcription-quantitative polymerase chain reaction (qRT-PCR) is often employed to examine the gene expressions under diverse treatments. Screening optimal reference genes are necessary for obtaining reliable expression results of qRT-PCR. Here, the stability of 10 selected reference genes in *Epicauta gorhami* was assessed under three conditions (adult ages, tissues/organs and temperatures). These findings displayed that the best suitable reference genes were as follows: *SOD* and *RPS18* for different adult ages and various temperatures and *RPS18* and *RPS28* for adult tissues. The relative expression patterns of uridine diphosphate (UDP)-N-acetylglucosamine-pyrophosphorylase (*EgUAP*) in diverse adult tissues was employed to verify the results. Our study will lay a vital basis for future functional gene expressions in *E. gorhami*.

Abstract: *Epicauta gorhami* is a hypermetamorphic insect that mainly forage soybeans during the adult stage. However, the lack of appropriate references hinders our studying of the gene function in *E. gorhami*. In this study, referring to five computational tools (Ct value, geNorm, NormFinder, BestKeeper and RefFinder), the stability of 10 housekeeping genes (*GAPDH*, *ACT*, *RPL4*, *RPL27*, *α-TUB*, *RPS18*, *EF1α*, *RPS28*, *RPL13* and *SOD*) was assessed by qRT-PCR under three different conditions (adult ages, tissues/organs and temperatures). The findings suggested that *SOD* and *RPS18* were the most ideal references for examine gene transcripts among diverse adult ages and at various temperatures; a pair of *RPS18* and *RPS28* was the most reliable genes to assess gene expressions in diverse adult tissues. Finally, the relative expression levels of *EgUAP* were computed after normalization *RPS18* and *RPS28* with across diverse adult tissues. As expected, *EgUAP* expression was abundant in the foregut, trachea and antenna and scarce in the midgut, hindgut and epidermis. These findings will lay a solid foundation for analyzing the gene expression of *E. gorhami*.

Keywords: *Epicauta gorhami*; *Glycine max*; reference genes; qRT-PCR; RefFinder

1. Introduction

The bean blister beetle, *Epicauta gorhami* (Coleoptera: Meloidae) is a hypermetamorphic insect that can forage soybeans (*Glycine max*) during the adult stage [1–4]. It poses potential threats to soybean production, which is a crucial oilseed, protein and biodiesel

crop [5,6]. The adults of this species mainly feed on leaves of *G. max* [1–4]. Previous studies on *E. gorhami* have traditionally placed a strong emphasis on diapause [1,3], seasonal adaptation [2], mitogenomic sequencing [7] and the phylogenetic relationship [4,7]. However, there is currently no research on gene functions in *E. gorhami*. In order to further explore molecular mechanisms of target genes, it is imperative to screen the suitable reference genes.

The reverse transcription-quantitative polymerase chain reaction (qRT-PCR) has advantages of high sensitivity, specificity and accuracy, which is widely employed to analyze the target gene transcripts [8,9]. For accurately measuring the mRNA levels of target genes by qRT-PCR, selecting the most optimal references to conduct normalization is essential [10,11]. If unstable reference genes are employed, the results of gene transcripts will be inaccurate [9,10]. Hence, selecting appropriate reference genes should be assessed under various experimental conditions [12–14].

As usual, housekeeping genes (HKGs), such as actin (*ACT*), ribosomal protein (*RPL* and *RPS*) and elongation factor 1α (*EF1α*), are widely employed as references in insect species, due to relative stable expression levels. However, the stability of internal genes may not always constant under diverse experimental treatments [14,15]. In the potato ladybird *Henosepilachna vigintioctomaculata*, *RPL6* and *RPL13* are the suitable references in different developmental stages, whereas *RPS18* and *EF1α* are more optimal among diverse tissues [14]. In the sugarcane stem borer *Chilo sacchariphagus*, *β-ACT* and *RPL7* show the best stable expression in different tissues, whereas *EF1α* and *SDHA* exhibit stability between sexes [15]. Hence, evaluating reference genes at different backgrounds is necessary.

Currently, important advances have been made in the study of reference genes selection in numerous insect species, such as *Mylabris sibirica* (*RPL6* and *RPL13*) [12], *Phthorimaea operculella* (*EF1α* and *RPL13*) [13], *H. vigintioctomaculata* (*RPS18* and *RPL13*) [14] and *C. sacchariphagus* (*β-ACT* and *RPL7* across various tissues and at distinct temperatures; *EF1α* and *SDHA* between sexes) [15]. To sum up, each experimental condition needs at least two reference genes to measure the target gene transcripts in insect species.

In this paper, we selected 10 potential reference genes from the full-length transcriptome of *E. gorhami* adults (unpublished data), which were *ACT*, *EF1α*, *GAPDH* (glyceraldehyde-3-phosphate dehydrogenase), *α-TUB* (α-tubulin), *RPL4*, *RPL13*, *RPL27*, *RPS18*, *RPS28* and *SOD* (superoxide dismutase). The stability of these genes was assessed at diverse adult ages, across different adult tissues and at various temperatures of *E. gorhami*. In addition, the expression pattern of *E. gorhami* uridine diphosphate (UDP)-N-acetylglucosamine (UDP-GlcNAc) pyrophosphorylase (*EgUAP*) across different adult tissues was used to evaluate the results. These findings will lay a vital basis for further research on gene functions in *E. gorhami*.

2. Materials and Methods

2.1. Insect Rearing and Treatment Methods

E. gorhami adults used in this study were obtained in August 2024 from *G. max* plants in Enshi Tujia and Miao Autonomous Prefecture, Hubei Province, China (coordinates: 30°19′43″ N, 109°38′48″ E). The adults were fed under suitable conditions (25 ± 2 °C, 16 h:8 h photoperiod and 50–60% relative humidity) in the insectary for one week.

Adult ages: Four newly emerged adults (two males and two females) were sampled for one biological replicate, every day for a continuous period of 3 days (1-day-old adults, 2-day-old adults and 3-day-old adults). Three biological replicates were conducted.

Adult tissues: These tissues (foregut, midgut, hindgut, antenna, trachea and epidermis) were collected from the 5-day-old adults. Ten adults (5 males and 5 females) were dissected for one biological replicate. Three biological replicates were conducted.

Temperature: The newly emerged adults were reared at three temperatures (4 °C, 25 °C and 37 °C) for 6 h. Four newly emerged adults (2 males and 2 females) were treated for one biological replicate. Three biological replicates were prepared.

2.2. Total RNA Isolation and cDNA Synthesis

Total RNA of each sample was extracted by the TRIzol reagent (YiFeiXue Tech, Nanjing, China), referring to the manufacturer's instructions. The RNA's purity and concentration were detected by a NanoDrop ND-1000 spectrophotometer. Subsequently, 1000 ng of total RNA was used to synthesize cDNA using the HiScript III RT SuperMix with gDNA wiper (Vazyme Biotech Co., Ltd., Nanjing, China). The reaction mixtures were subjected to incubation at 37 °C for 15 min, followed by 85 °C for 5 s. The resultant cDNA samples were diluted 3-fold for the pursuant PCR and qRT-PCR.

2.3. Selection of Candidate References and Primer Design

Based on the full-length transcriptome of *E. gorhami* adults, the BioEdit software (version 7.1.3.0) was employed to conduct a TBLASTN search by using the amino acid sequence of ten candidate reference genes as the queries from *M. sibirica* [12] and *P. operculella* [13]. This resulted in the identification of ten reference genes in *E. gorhami*. These genes included *EF1α*, *ACT*, *RPL4*, *α-TUB*, *RPL13*, *RPL27*, *RPS18*, *GAPDH*, *RPS28* and *SOD*, all of which are commonly utilized as reference genes in other insects [16].

The correctness of the reference gene sequences was substantiated by polymerase chain reaction (PCR) using primers in Table S1. Primer pairs were designed to verify the complete open reading frames of reference genes by Primer Premier 5.0 software (version 5.00), based on the RT-PCR primer design principles [15]. After the amplicons of RT-PCR were confirmed by Sanger sequencing, the sequences of amplicons were uploaded to GenBank, with the accession numbers of PQ497541-PQ497541 (Table S1).

2.4. Quantitative Real-Time PCR (qRT-PCR)

The primers for qRT-PCR were performed by Primer3web version 4.1.0 (https://primer3.ut.ee/, accessed on 12 September 2024) and are presented in Table 1. The products of qRT-PCR were verified by Sanger sequencing. The qRT-PCR experiment was executed by a CFX96 Real-Time System (Bio-Rad Laboratories, Hercules, CA, USA) and ChamQ Universal SYBR qPCR Master Mix (Vazyme Biotech Co., Ltd.). Each reaction consisted of a final volume of 20 μL, containing 10 μL of 2 ChamQ Universal SYBR qPCR Master Mix, 0.4 μL of reverse primer (10 μM), 1 μL of cDNA template and 8.2 μL of RNase-free water. The thermocycling procedure consisted of an initial step of 95 °C for 30 s, followed by 40 cycles of 95 °C for 5 s and annealing at 60 °C for 34 s. After the reaction, a melting curve analysis was conducted for one cycle of 95 °C for 15 s, 60 °C for 60 s and 95 °C for 1 s, which was used to confirm the specificity of the amplified product. The amplification efficiency (E) was computed using a series of 3-fold dilutions of a cDNA template, referring to the equation $E = (10^{[-1/\text{slope}]} - 1) \times 100\%$ [17]. All experiments were conducted in triplicate.

Table 1. Primers of 10 candidate house-keeping genes used in qRT-PCR.

Gene	Primer Sequences (5′to 3′)	Length (bp)	Slope	R^2	Efficiency (%)
EF1α	F-ATCATTGACGCACCTGGACA R-ACCAGTACCAGCAGCAACAA	99	−3.435	0.999	95.50
GAPDH	F-ACAGTACATGCCACCACAGC R-TGGTACACGGAAGGCCATAC	180	−3.351	0.999	98.82
RPL4	F-TCGATGAACCACCGTCAACC R-CGACCGGTACCCCATGATTC	80	−3.308	0.993	100.60
RPL13	F-AAGCCGCCGGTATTAACAGC R-TCACCAGGACGCAACTTCTT	172	−3.318	0.998	100.16
RPL27	F-TCGTATTGGTCTTGGCAGGC R-TCAATGCCGGCAACAATAGC	112	−3.373	0.999	98.03
SOD	F-AGTTGTCCATGCTGATCCGG R-TAACACCACAGGCCAAACGT	95	−3.32	0.998	100.08

Table 1. *Cont.*

Gene	Primer Sequences (5′to 3′)	Length (bp)	Slope	R^2	Efficiency (%)
ACT	F-TACGTGTGGCACCTGAAGAA R-CCAGTTGTACGACCAGAAGCA	169	−3.284	0.997	101.60
α-TUB	F-ATGGGCACGTCTTGATCACA R-TCATTTTCACCTTCGCCCGA	174	−3.258	0.999	102.73
RPS18	F-AGGTGTTGGTCGTCGTTACTC R-TCTAAGGTAGCCGATGTGAGC	210	−3.323	0.999	99.96
RPS28	F-GGTGAGCAAAACCGTCAGATC R-TGCTTCACGTTCAGACTCCA	90	−3.347	0.997	98.97

Note: ACT, actin; SOD, superoxide dismutase; α-TUB, α-tubulin; GAPDH, glyceraldehyde-3-phosphate dehydrogenase; EF1α, elongation factor 1α; RPL4, RPL13, RPL27, RPS18 and RPS28, ribosomal protein.

2.5. Assessment of Reference Gene Stability

The raw Ct values were required for the BioRadCFXManager software (version 3.1.1517.0823). The stability of 10 reference genes under different backgrounds were assessed using a range of algorithms, including BestKeeper [18], Normfinder [19], geNorm [10] and the ΔCt method [20]. In addition, the suitable number of reference genes under different conditions was confirmed by pairwise variation (Vn/n + 1), required for the GeNorm method. In general, a Vn/n + 1 value below the threshold of 0.15 suggests that the starting n reference genes are suitable to normalize gene expression. Finally, the RefFinder [21,22] was applied to analyze the comprehensive ranking of each experimental condition.

2.6. Validation of Selected Reference Genes in Diverse Adult Tissues

The transcription level of uridine diphosphate (UDP)-N-acetylglucosamine-pyrophosphorylase (*UAP*, GenBank: PQ497551) in *E. gorhami* was utilized to assess the stability of selected reference genes across various adult tissues. The primer sequence of *UAP* was as follows: Forward: CGCTACAACGTAACGCCATC, Reverse: CCCCACAATCGCTACGTTTC. The relative transcription level of *EgUAP* in adult tissues were computed by the $2^{-\Delta\Delta Ct}$ method [23], based on *RPS18* and *RPS28*. The SPSS Statistics 29 software (version 29.0.2.0) package was then used to evaluate the variance in expression levels of *EgUAP* among different adult tissues through one-way ANOVA analysis followed by Tukey's test for multiple comparisons.

3. Results

3.1. Selection of Candidate Reference Genes

According to the full-length transcriptome of *E. gorhami*, we applied the BioEdit software (version 7.1.3.0) to perform a TBLASTN search by using the amino acid sequence of ten candidate reference genes as the queries from *M. sibirica* [12] and *P. operculella* [13]. This enabled the identification of ten cDNAs, which we named *ACT*, *GAPDH*, *RPL4*, *EF1α*, *RPL13*, *RPL27*, *RPS18*, *RPS28*, *α-TUB* and *SOD* in *E. gorhami*. We used the Primer Premier 5.0 software to design the primers, with the lengths of 18–22 bp. After the amplification round and then Sanger sequencing, the sequencing results of amplicons were uploaded to GenBank under these accession numbers: PQ497541-PQ497541 (Table S1).

The Primer3web version 4.1.0 (https://primer3.ut.ee/, accessed on 12 September 2024) was used to design the qRT-PCR primers, with the amplification product length ranging from 80 bp to 250 bp. The products of qRT-PCR were verified by sequencing. The melting curve analysis confirmed the specificities of each primer pair for qRT-PCR. As expected, the efficiency (*E*) of 10 primer pairs were between 95.50% (*EF1α*) and 102.73% (*α-TUB*), with the correlation coefficients (R^2) varying from 0.993 to 0.999 (Table 1). These results demonstrated that efficiency of primers reached the standards of traditional qRT-PCR [24].

3.2. Expression Levels of Reference Genes

The threshold-cycle (Ct) of ten reference genes under various testing conditions were presented (Figure 1, Table S2). Among diverse adult ages, *SOD* exhibited smaller gene expression variations, whereas *GAPDH* and *EF1α* demonstrated greater fluctuations (Figure 1A). Across different adult tissues and under different temperature treatments, the expression fluctuations were lower in *RPS18* and *RPS28* and higher in *ACT* and *GAPDH* (Figure 1B,C). A combination of above results indicated that the expression difference was small in all reference genes except for *ACT* and *GAPDH* (Figure 1D).

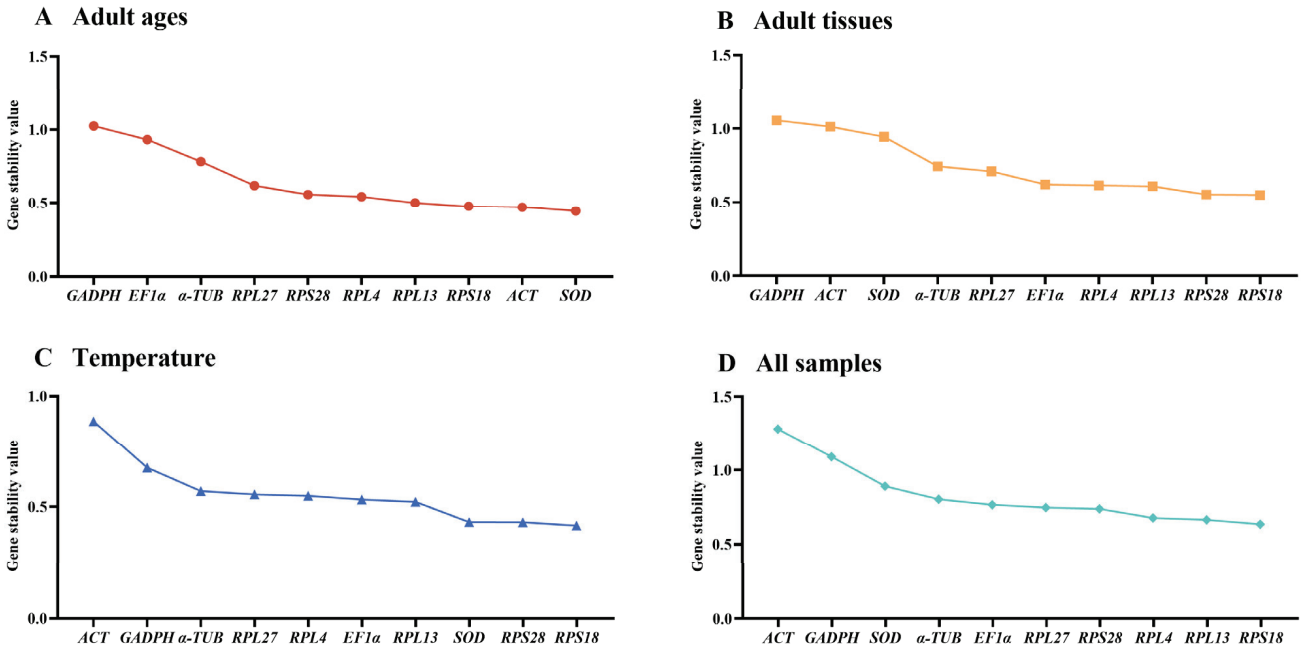


Figure 1. Stability rankings of the ten candidate reference genes in *Epicauta gorhami* computed by the ΔCt method in different samples. The stability values are showed from the least (**left**) to the most stable gene (**right**). Abbreviation: ACT, actin; SOD, superoxide dismutase; α-TUB, α-tubulin; GAPDH, glyceraldehyde-3-phosphate dehydrogenase; EF1α, elongation factor 1α; RPL4, RPL13, RPL27, RPS18 and RPS28, ribosomal protein. The abbreviations are exactly the same as Figures 2–5.

3.3. Stability of the Ten HKGs Among Adult Ages

Based on average expression stability (M-values) and pairwise variation (V-values), the geNorm algorithm evaluates gene stability. These results exhibited that *ACT*, *RPS18* and *SOD* were the most suitable, with M-values below 0.20 (Figure 2A, Table 2). Moreover, V-values suggested that V2/3 to V9/10 values were below 0.15, showing that two diverse references were equal for assessing the gene transcript among adult ages (Figure 2B).

The NormFinder algorithm indicated that the stable ranking of ten reference genes from the most to the least stable were as follows: *SOD*, *RPS18*, *ACT*, *RPL13*, *RPL4*, *RPS28*, *RPL27*, *α-TUB*, *EF1α* and *GAPDH*, with the *p*-value of 0.091, 0.143, 0.172, 0.243, 0.268, 0.329, 0.458, 0.651, 0.849 and 0.954, respectively (Figure 2C, Table 2). The BestKeeper analysis showed that RPL4, RPS28 and SOD were the top three stable genes (Figure 2D, Table 2).

Referring to the results of RefFinder, the ranking of 10 reference genes at adult ages were as follows: *SOD* > *RPS18* > *ACT* > *RPL4* > *RPS28* > *RPL13* > *EF1α* > *RPL27* > *α-TUB* > *GAPDH* (Figure 5A). Therefore, the combination of SOD and RPS18 are the most appropriate for gene transcript analysis by qRT-PCR among various adult ages (Table 3).

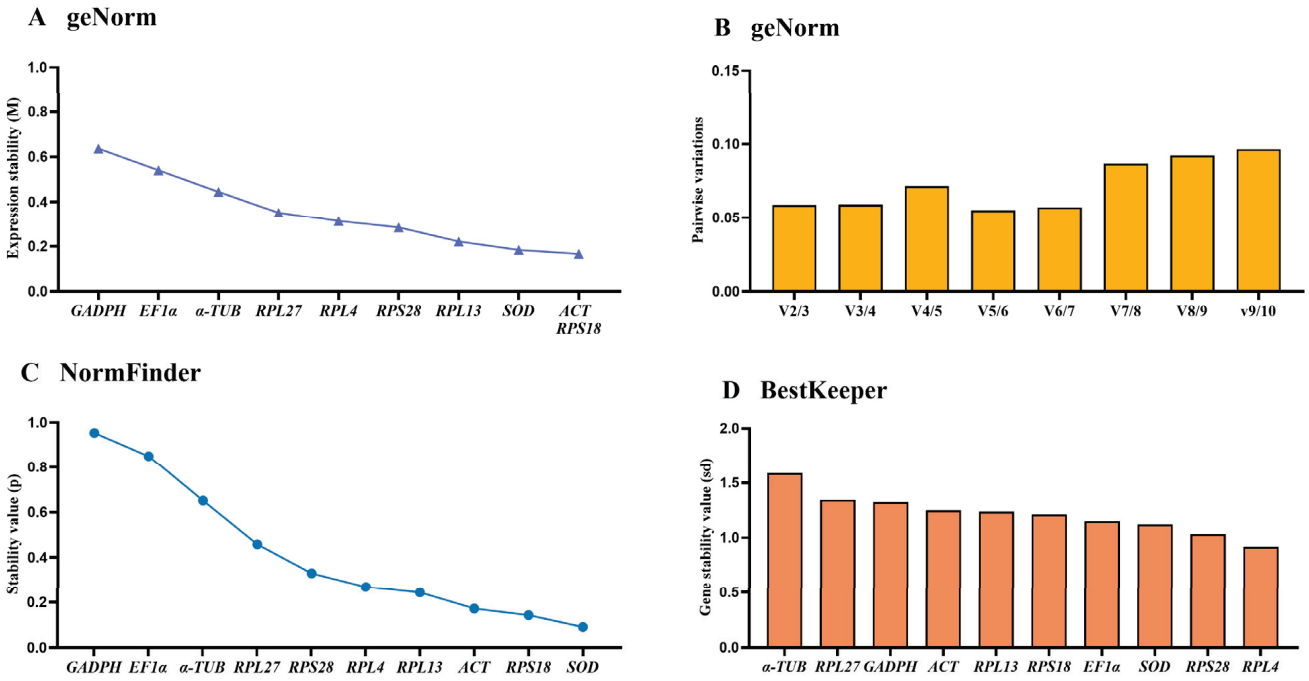


Figure 2. Stability rankings of the ten candidate reference genes in *Epicauta gorhami* computed by geNorm, NormFinder and BestKeeper at various adult ages. Diverse ages of *Epicauta gorhami* adults were sampled (collected on the first to third days of the newly emerged adults). The stability values are showed from the least stable (**left**) to the most stable gene (**right**). (**A**,**B**) geNorm, (**C**) NormFinder and (**D**) BestKeeper.

Table 2. Stability rankings of the ten reference genes under diverse experimental backgrounds.

Conditions	CRGs *	geNorm		Normfinder		BestKeeper		ΔCt	
		M-Value	Rank	*p*-Value	Rank	Stability	Rank	Stability	Rank
Adult ages	*EF1α*	0.540	8	0.849	9	1.149	4	0.931	9
	GADPH	0.636	9	0.954	10	1.325	8	1.024	10
	RPL4	0.313	5	0.268	5	0.920	1	0.543	5
	RPL13	0.221	3	0.243	4	1.236	6	0.500	4
	RPL27	0.351	6	0.458	7	1.344	9	0.619	7
	SOD	0.184	2	0.091	1	1.121	3	0.443	1
	ACT	0.166	1	0.172	3	1.249	7	0.469	3
	α-TUB	0.444	7	0.651	8	1.589	10	0.782	8
	RPS18	0.166	1	0.143	2	1.209	5	0.476	2
	RPS28	0.284	4	0.329	6	1.033	2	0.557	6
Adult tissues	*EF1α*	0.239	1	0.384	5	0.828	2	0.621	5
	GADPH	0.741	9	0.933	10	1.326	9	1.055	10
	RPL4	0.277	2	0.347	4	1.051	7	0.614	4
	RPL13	0.372	4	0.220	3	0.989	6	0.608	3
	RPL27	0.414	5	0.496	6	0.700	1	0.710	6
	SOD	0.563	7	0.815	8	0.971	4	0.944	8
	ACT	0.663	8	0.889	9	1.389	10	1.012	9
	α-TUB	0.468	6	0.536	7	1.085	8	0.744	7
	RPS18	0.318	3	0.146	1	0.987	5	0.549	1
	RPS28	0.239	1	0.201	2	0.914	3	0.552	2

Table 2. *Cont.*

Conditions	CRGs *	geNorm		Normfinder		BestKeeper		ΔCt	
		M-Value	Rank	*p*-Value	Rank	Stability	Rank	Stability	Rank
Temperature treatment	*EF1α*	0.346	6	0.334	4	0.58	6	0.532	5
	GADPH	0.474	8	0.547	9	0.976	9	0.675	9
	RPL4	0.246	3	0.446	7	0.357	3	0.549	6
	RPL13	0.188	2	0.395	6	0.317	2	0.522	4
	RPL27	0.261	4	0.468	8	0.278	1	0.555	7
	SOD	0.123	1	0.217	3	0.407	4	0.431	3
	ACT	0.556	9	0.847	10	1.265	10	0.886	10
	α-TUB	0.412	7	0.392	5	0.899	8	0.570	8
	RPS18	0.123	1	0.155	2	0.429	5	0.415	1
	RPS28	0.307	5	0.131	1	0.646	7	0.430	2

∗ Candidate reference gene.

Table 3. The most optimal reference genes in *E. gorhami* for various experimental backgrounds.

Experimental Conditions	The Recommended Reference Genes	
Adult ages	*SOD*	*RPS18*
Adult tissues	*RPS28*	*RPS18*
Temperature	*SOD*	*RPS18*

3.4. Stability of the Ten HKGs Across Various Adult Tissues

The geNorm results displayed that *RPS28*, *EF1α*, *RPL4* and *RPS18* were the top four stable genes (Figure 3A, Table 2). V-values data demonstrated that all values of from V2/3 to V9/10 were below 0.15, showing that two reference genes in various adult tissues were suitable (Figure 3B).

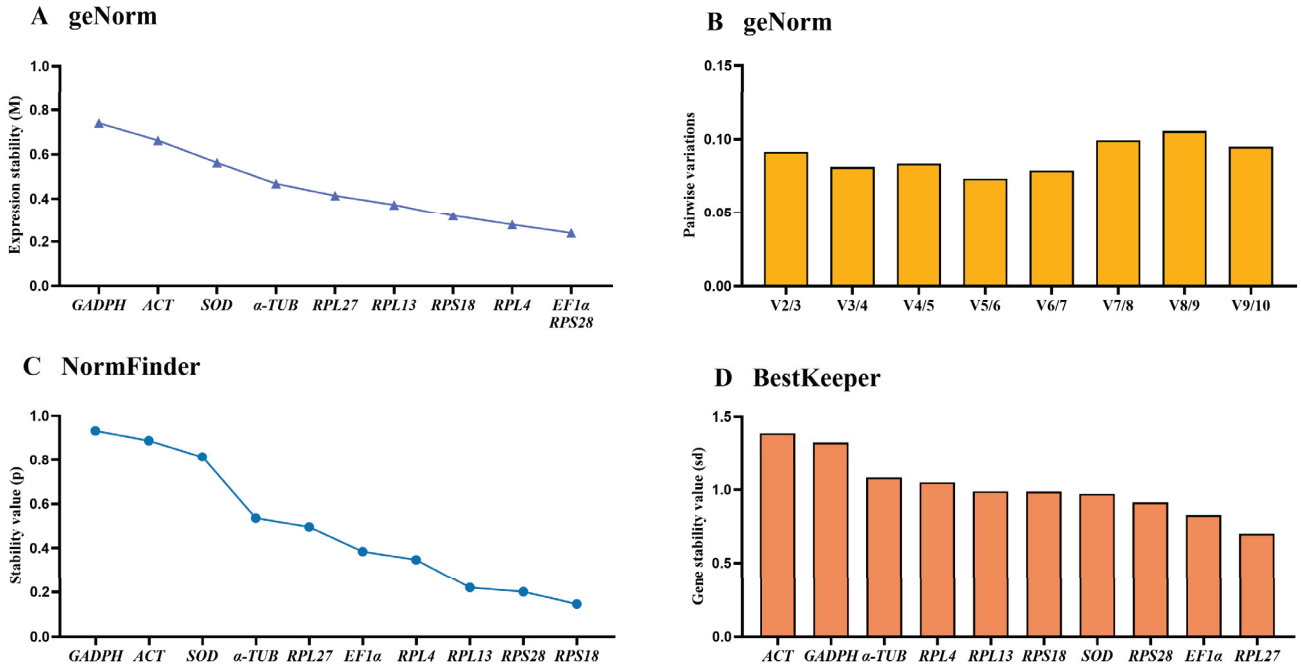


Figure 3. Stability rankings of the ten candidate reference genes in *Epicauta gorhami* calculated by geNorm, NormFinder and BestKeeper among diverse adult tissues. Foregut, midgut, hindgut, epidermis, trachea and antenna were dissected from the 5-day-old adults. The stability values are showed from the least stable (**left**) to the most stable gene (**right**). (**A**,**B**) geNorm, (**C**) NormFinder and (**D**) BestKeeper.

According to the NormFinder data, the rankings of reference genes were as follows: *RPS18* > *RPS28* > *RPL13* > *RPL4* > *EF1α* > *RPL27* > *α-TUB* > *SOD* > *ACT* > *GAPDH* (Figure 3C, Table 2). Moreover, the *p*-values of all reference genes were less than 1.0 (Figure 3C, Table 2). The BestKeeper results indicated that *RPS18* and *RPS28* were the most stable, with the SD values of 0.700 and 0.914, respectively (Figure 3D, Table 2). Furthermore, the SD values of *ACT*, *GADPH*, *α-TUB* and *RPL4* were above 1.0 (Figure 3D, Table 2).

According to RefFinder results, the comprehensive ranking order were as follows: *RPS28* > *RPS18* > *EF1α* > *RPL27* > *RPL13* > *RPL4* > *SOD* > *α-TUB* > *ACT* > *GAPDH* (Figure 5B). Therefore, the pair of *RPS18* and *RPS28* is the most appropriate for qRT-PCR data normalization among diverse adult tissues (Table 3).

3.5. Stability of the Ten HKGs Under Diverse Temperature Conditions

The geNorm results indicated that *RPS18*, *SOD* and *RPL13* were the steadiest references in diverse temperatures, with M-values of 0.123, 0.123 and 0.188, respectively (Figure 4A, Table 2). Moreover, V-values data displayed that all values were below 0.15, showing that two reference genes under various temperature treatments were suitable (Figure 4B).

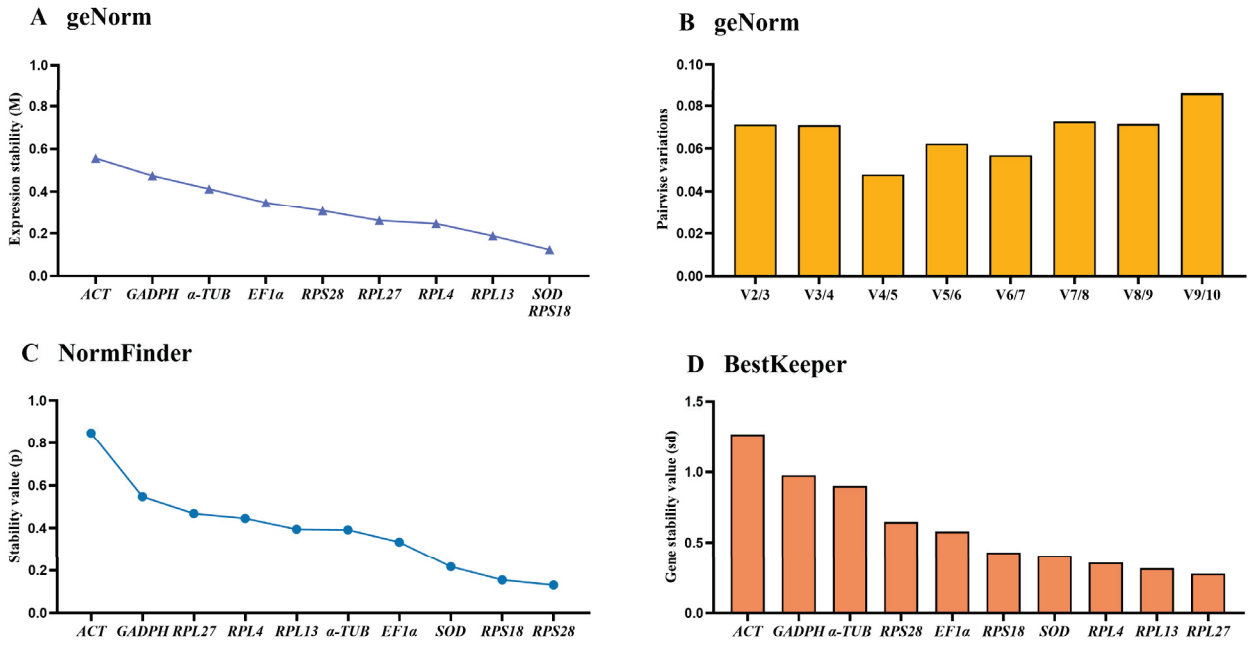


Figure 4. Stability rankings of the ten candidate reference genes in *Epicauta gorhami* assessed by geNorm, NormFinder and BestKeeper at different temperatures. The newly emerged adults reared for 6 h under three temperatures (4 °C, 25 °C and 37 °C) were collected. The stability values are showed from the least stable (**left**) to the most stable gene (**right**). (**A**,**B**) geNorm, (**C**) NormFinder and (**D**) BestKeeper.

The NormFinder results manifested that the steady rankings were *RPS28*, *RPS18*, *SOD*, *EF1α*, *α-TUB*, *RPL13*, *RPL4*, *RPL27*, *GAPDH* and *ACT* (Figure 4C, Table 2). BestKeeper data uncovered that the SD values of these genes were less than 1.0, except for *ACT* (Figure 4D, Table 2).

Refer to the results of RefFinder, the stability orders were as follows: *RPS18* > *SOD* > *RPS28* > *RPL13* > *RPL27* > *RPL4* > *EF1α* > *α-TUB* > *GAPDH* > *ACT* (Figure 5C). To sum up, RPS18 and SOD are the best reference gene pair to evaluate the gene transcript under diverse temperature conditions (Table 3). When combining the three diverse treatments together, the RefFinder results showed that the stability ranking in sequence were *RPS18*, *RPL13*, *RPS28*, *RPL4*, *RPL27*, *EF1α*, *SOD*, *α-TUB*, *GAPDH* and *ACT* (Figure 5D).

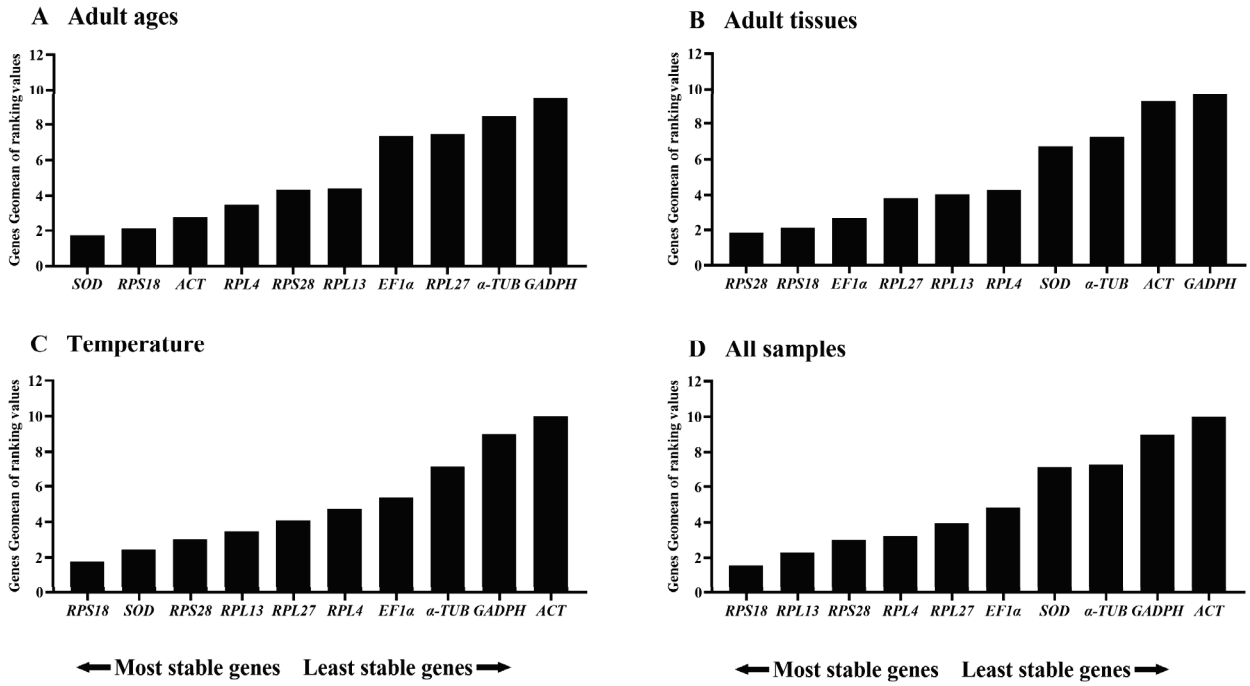


Figure 5. Stability rankings of the ten candidate reference genes in *Epicauta gorhami* computed by the Geomean method of RefFinder in different samples. The stability values are showed from the most stable (**left**) to the least stable gene (**right**). (**A**) adult ages, (**B**) adult tissues, (**C**) temperature and (**D**) all samples.

3.6. Validation of the Selected Reference Genes

To estimate the performance of the recommended reference genes, the relative mRNA level of *EgUAP* in various adult tissues was measured using the most stable references (*RPS18* and *RPS28*) by the $2^{-\Delta\Delta Ct}$ method [23]. Our results indicated that the transcription level of *EgUAP* was high in the foregut, trachea and antenna and low in the midgut, hindgut and epidermis of *E. gorhami* (Figure 6).

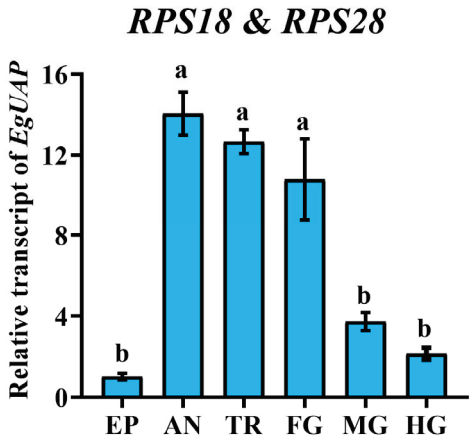


Figure 6. Relative expression level of *EgUAP* among diverse adult tissues of *Epicauta gorhami*. The relative gene expression level of *EgUAP* in the foregut (FG), midgut (MG), hindgut (HG), epidermis (EP), trachea (TR) and antenna (AN) was normalized to the most suitable reference genes (*RPS18* and *RPS28*) by the $2^{-\Delta\Delta Ct}$ method. The relative transcripts are the ratios of copy numbers in different adult tissues relative to the epidermis, which is set at 1. The values are means + SE. Different letters indicate significant differences in gene expression among different tissues ($p < 0.05$).

4. Discussion

In this study, the expression stabilities of ten selected reference genes in *E. gorhami* were estimated to perform qRT-PCR analysis normalization, laying a vital basis for future study of gene functions. Notably, we evaluated the stability of these genes under three different conditions (adult ages, adult tissues/organs and temperatures) for the first time in *E. gorhami*. These findings suggested that *SOD* and *RPS18* were the most ideal reference combination to measure gene transcription levels among different adult ages (Figures 1, 2 and 5 and Tables 2 and 3) and at various temperatures (Figures 1, 4 and 5 and Tables 2 and 3); *RPS18* and *RPS28* was the most reliable genes to assess gene expressions under diverse adult tissues (Figures 1, 3 and 5 and Tables 2 and 3).

Here, we used four programs (geNorm, Normfinder, Bestkeeper and ΔCT) to examine the suitability of reference genes. The findings suggest that different programs' results under different experimental conditions present diverse most stable reference genes (Figures 1–4). For example, in different adult tissues, the geNorm method showed *EF1α* and *RPS28* were the most stable reference genes, and the Normfinder and ΔCT methods identified *RPS18* as the top-ranking reference gene, while the Bestkeeper ranked *RPL27* as the most stable reference gene (Figures 1 and 3, Table 2). These differences may be due to diverse statistical algorithms of each method, which can be found in the publications [10,18–20]. Under such a condition, RefFinder, a web-based tool is widely used to compute the geometric mean of the rankings obtained by the different algorithms, which solves the limitations of operating one single program [21,22].

Ribosomal proteins play a vital function on ribosome assembly, which bind to four ribosomal RNAs (rRNAs) to constitute the ribosomes [25]. Similar to our findings, ribosomal proteins are selected as the most optimal reference genes in insect species, such as Coleopterans *M. sibirica* (*RPL6* and *RPL13*) [12], *Leptinotarsa decemlineata* (*RP18* and *RP4*) [26], *Phaedon brassicae* (*RPL32* and *RPL19*) [27], *Henosepilachna vigintioctopunctata* (*RPL13* and *RPS18*) [16], *Tribolium castaneum* (*RPS6*, *RPL13a*, *RPS3* and *RPL18*) [28], *Ips sexdentatus* (*RPS3*) [29] and *H. vigintioctomaculata* (*RPS18* and *RPL13*) [14]; Hemipterans *Psammotettix striatus* (*RPLP2*) [30], *Rhopalosiphum padi* (*RPL13*, *RPS6* and *RPS18*) [31], *Aphis glycines* (*RPS9*) [32], *Ferrisia gilli* (*RPS8*, *RPL40* and *RPL7*) [33], *Diaphorina citri* (*RPL7*) [34] and *Dichelops melacanthus* (*RPL9* and *RPS23*) [35]; Hymenopterans *Anastatus japonicus* (*RPL13* and *RPS6*) [36]; Lepidopterans *Mythimna loreyi* (*RPL10*, *RPL27* and *RPS3*) [37], *Plutella xylostella* (*RPS13* and *RPS23*) [38], *Spodoptera litura* (*RPS13* and *RPLP0*) [39], *P. operculella* (*RPL13*) [13], *Bombyx mori* (*RPS7*) [40] and *Helicoverpa armigera* (*RPS15* and *RPL27*) [41]; Dipterans *Aphidoletes aphidimyza* (*RPL8* and *RPS3*) [42], *Exorista sorbillans* (*RP49*) [43] and *Chlorops oryzae* (*RPS15*) [44]; Orthopteran *Locusta migratoria* (*RPL32*) [45] and Thysanopterans *Megalurothrips usitatus* (*RPL30*) [46] and *Frankliniella occidentalis* (*RPL32*) [47].

At different adult ages and temperatures, *SOD* was verified to be the most reliable gene (Figures 1, 2, 4 and 5 and Tables 2 and 3). Superoxide dismutase (SOD) is a crucial antioxidant enzyme, catalyzing the conversion of reactive oxygen species into oxygen and hydrogen peroxide [48]. Consistent with our data, SOD is recommended as the most appropriate reference gene in *Spodoptera frugiperda* [49], *Thrips tabaci* [50], *Riptortus pedestris* [51] and *Spodoptera exigua* [52].

In addition, the BestKeeper analysis data indicated that the SD values of *α-TUB*, *EF1α*, *GAPDH* and *ACT* were greater than 1.0 (Table 2), showing that these genes were unaccommodated as reference genes to perform qRT-PCR normalization. Similar results have been verified in other insects, such as *P. operculella* [13], *Ophraella communa* [53], *A. aphidimyza* [42], *Hippodamia convergens* [54], *H. vigintioctomaculata* [14], *Colaphellus bowringi* [55], *H. vigintioctopunctata* [16] and *M. sibirica* [12].

To further validate the accuracy of *RPS18* and *RPS28* in qRT-PCR normalization in *E. gorhami*, we examined the relative transcript level of *EgUAP* in diverse adult tissues. Our results exhibited that *EgUAP* expression was high in the foregut, trachea and antenna and low in the midgut, hindgut and epidermis (Figure 6). The expression pattern is consistent with the fact that UAP catalyzes the formation of UDP-GlcNAc, which is the precursor

of the production of chitin in ectodermally derived epidermal cells, foregut, hindgut and trachea [56–58].

Overall, it is essential to screen and verify the most suitable references to guarantee the accuracy of gene expression. This study would offer a solid basis for further molecular functions of target genes in *E. gorhami*.

5. Conclusions

Ten potential reference genes in *E. gorhami* were assessed for accurate qRT-PCR analysis of *E. gorhami* under three different treatments. These results demonstrated that the steadiest reference genes were as follows: *SOD* and *RPS18* for different adult ages and various temperatures and *RPS18* and *RPS28* for adult tissues. This study is the first one to establish the qRT-PCR normalization analyses in *E. gorhami*, facilitating further research on gene functions of *E. gorhami*.

Supplementary Materials: The following supporting information can be downloaded at: https://www.mdpi.com/article/10.3390/insects15120942/s1, Table S1: A list of primers used for RT-PCR of the genes and Table S2: The overall threshold cycle (Ct) values under different experimental conditions.

Author Contributions: Experiments were designed by G.Y., X.Y. (Xuetao Yu), Y.Z., G.W., X.Y. (Xiaohong Yan) and C.S.; Figures designed and created by G.Y., X.Y. (Xuetao Yu), Y.Z., J.L., G.W., X.Y. (Xiaohong Yan) and C.S.; Statistical analyses were implemented by G.Y., X.Y. (Xuetao Yu), Y.Z., J.L., X.L., L.Z., H.Z., L.J., G.W., X.Y. (Xiaohong Yan) and C.S. All authors have read and agreed to the published version of the manuscript.

Funding: This research was supported by the National Major Special Project of Breeding for Genetically Modified Organisms in China (No. 2016ZX08012-005) and the Innovation Project of Chinese Academy of Agricultural Sciences (No. 2060302-049-091).

Data Availability Statement: The data presented in this study are included in the article and Supplementary Materials; further inquiries can be directed to the corresponding authors.

Conflicts of Interest: The authors declare no conflicts of interest.

References

1. Terao, M.; Hirose, Y.; Shintani, Y. Effects of temperature and photoperiod on termination of pseudopupal diapause in the bean blister beetle, *Epicauta gorhami*. *J. Insect Physiol.* **2012**, *58*, 737–742. [CrossRef] [PubMed]
2. Shintani, Y.; Terao, M.; Tanaka, S. Adaptive significance of precocious pupation in the bean blister beetle, *Epicauta gorhami* (Coleoptera: Meloidae), a hypermetamorphic insect. *J. Insect Physiol.* **2017**, *99*, 107–112. [CrossRef] [PubMed]
3. Terao, M.; Tokuda, M.; Shintani, Y. Geographic variation in photoperiodic response for induction of pseudopupal diapause in *Epicauta gorhami* (Coleoptera: Meloidae). *Environ. Entomol.* **2021**, *50*, 1145–1150. [CrossRef] [PubMed]
4. Zhou, Z.; Liu, Y.; Chen, X. Structural features and phylogenetic implications of three new mitochondrial genomes of blister beetles (Coleoptera: Meloidae). *J. Insect Sci.* **2021**, *21*, 19. [CrossRef] [PubMed]
5. Hina, A.; Razzaq, M.K.; Abbasi, A.; Shehzad, M.B.; Arshad, M.; Sanaullah, T.; Arshad, K.; Raza, G.; Ali, H.M.; Hayat, F.; et al. Genomic blueprints of soybean (*Glycine max*) pathogen resistance: Revealing the key genes for sustainable agriculture. *Funct. Plant Biol.* **2024**, *51*, FP23295. [CrossRef] [PubMed]
6. Vianna, G.R.; Cunha, N.B.; Rech, E.L. Soybean seed protein storage vacuoles for expression of recombinant molecules. *Curr. Opin. Plant Biol.* **2023**, *71*, 102331. [CrossRef] [PubMed]
7. Du, C.; Zhang, L.; Lu, T.; Ma, J.; Zeng, C.; Yue, B.; Zhang, X. Mitochondrial genomes of blister beetles (Coleoptera, Meloidae) and two large intergenic spacers in *Hycleus* genera. *BMC Genom.* **2017**, *18*, 698. [CrossRef]
8. Jozefczuk, J.; Adjaye, J. Quantitative real-time PCR-based analysis of gene expression. *Methods Enzymol.* **2011**, *500*, 99–109.
9. Derveaux, S.; Vandesompele, J.; Hellemans, J. How to do successful gene expression analysis using real-time PCR. *Methods* **2010**, *50*, 227–230. [CrossRef]
10. Vandesompele, J.; De Preter, K.; Pattyn, F.; Poppe, B.; Van Roy, N.; De Paepe, A.; Speleman, F. Accurate normalization of real-time quantitative RT-PCR data by geometric averaging of multiple internal control genes. *Genome Biol.* **2002**, *3*, Research0034. [CrossRef]
11. Valasek, M.A.; Repa, J.J. The power of real-time PCR. *Adv. Physiol. Educ.* **2005**, *29*, 151–159. [CrossRef] [PubMed]
12. Shen, C.H.; Tang, M.; Li, X.F.; Zhu, L.; Li, W.; Deng, P.; Zhai, Q.; Wu, G.; Yan, X.H. Evaluation of reference genes for quantitative expression analysis in *Mylabris sibirica* (Coleoptera, Meloidae). *Front. Physiol.* **2024**, *15*, 1345836. [CrossRef] [PubMed]

13. Shen, C.H.; Peng, L.J.; Zhang, Y.X.; Zeng, H.R.; Yu, H.F.; Jin, L.; Li, G.Q. Reference genes for expression analyses by qRT-PCR in *Phthorimaea operculella* (Lepidoptera: Gelechiidae). *Insects* **2022**, *13*, 140. [CrossRef] [PubMed]
14. Zhang, Y.-X.; Tan, Q.; Shen, C.-H.; Wu, J.-J.; Wu, Y.-K.; Li, W.-Z.; Jin, L.; Li, G.-Q. Reference gene selection for transcriptional profiling by RT-qPCR in the 28-spotted larger potato ladybird. *J. Asia Pac. Entomol.* **2022**, *25*, 101900. [CrossRef]
15. Wang, Z.; Shang, X.; Wei, J.; Tian, X.; Liu, Y.; Zhang, G. Evaluation and validation of reference genes for gene expression analysis using qRT-PCR in the sugarcane stem borer *Chilo sacchariphagus* (Lepidoptera: Pyralidae). *Insects* **2024**, *15*, 594. [CrossRef]
16. Lü, J.; Yang, C.; Zhang, Y.; Pan, H. Selection of reference genes for the normalization of RT-qPCR data in gene expression studies in insects: A systematic review. *Front. Physiol.* **2018**, *9*, 1560. [CrossRef]
17. Pfaffl, M.W. A new mathematical model for relative quantification in real-time RT-PCR. *Nucleic Acids Res.* **2001**, *29*, e45. [CrossRef]
18. Pfaffl, M.W.; Tichopad, A.; Prgomet, C.; Neuvians, T.P. Determination of stable housekeeping genes, differentially regulated target genes and sample integrity: BestKeeper--Excel-based tool using pair-wise correlations. *Biotechnol. Lett.* **2004**, *26*, 509–515. [CrossRef]
19. Andersen, C.L.; Jensen, J.L.; Ørntoft, T.F. Normalization of real-time quantitative reverse transcription-PCR data: A model-based variance estimation approach to identify genes suited for normalization, applied to bladder and colon cancer data sets. *Cancer Res.* **2004**, *64*, 5245–5250. [CrossRef]
20. Silver, N.; Best, S.; Jiang, J.; Thein, S.L. Selection of housekeeping genes for gene expression studies in human reticulocytes using real-time PCR. *BMC Mol. Biol.* **2006**, *7*, 33. [CrossRef]
21. Xie, F.; Xiao, P.; Chen, D.; Xu, L.; Zhang, B. miRDeepFinder: A miRNA analysis tool for deep sequencing of plant small RNAs. *Plant Mol. Biol.* **2012**, *80*, 75–84. [CrossRef] [PubMed]
22. Xie, F.; Wang, J.; Zhang, B. RefFinder: A web-based tool for comprehensively analyzing and identifying reference genes. *Funct. Integr. Genom.* **2023**, *23*, 125. [CrossRef] [PubMed]
23. Livak, K.J.; Schmittgen, T.D. Analysis of relative gene expression data using real-time quantitative PCR and the $2^{-\Delta\Delta CT}$ method. *Methods* **2001**, *25*, 402–408. [CrossRef]
24. Bustin, S.A.; Benes, V.; Garson, J.A.; Hellemans, J.; Huggett, J.; Kubista, M.; Mueller, R.; Nolan, T.; Pfaffl, M.W.; Shipley, G.L.; et al. The MIQE guidelines: Minimum information for publication of quantitative real-time PCR experiments. *Clin. Chem.* **2009**, *55*, 611–622. [CrossRef]
25. Landry-Voyer, A.M.; Mir Hassani, Z.; Avino, M.; Bachand, F. Ribosomal protein uS5 and friends: Protein-protein interactions involved in ribosome assembly and beyond. *Biomolecules* **2023**, *13*, 853. [CrossRef] [PubMed]
26. Shi, X.Q.; Guo, W.C.; Wan, P.J.; Zhou, L.T.; Ren, X.L.; Ahmat, T.; Fu, K.Y.; Li, G.Q. Validation of reference genes for expression analysis by quantitative real-time PCR in *Leptinotarsa decemlineata* (Say). *BMC Res. Notes* **2013**, *6*, 93. [CrossRef] [PubMed]
27. Ma, L.; Jiang, T.; Liu, X.; Xiao, H.; Peng, Y.; Zhang, W. Evaluation of candidate reference genes for gene expression analysis in the brassica leaf beetle, *Phaedon brassicae* (Coleoptera: Chrysomelidae). *PLoS ONE* **2021**, *16*, e0251920. [CrossRef]
28. Toutges, M.J.; Hartzer, K.; Lord, J.; Oppert, B. Evaluation of reference genes for quantitative polymerase chain reaction across life cycle stages and tissue types of *Tribolium castaneum*. *J. Agric. Food Chem.* **2010**, *58*, 8948–8951. [CrossRef]
29. Sellamuthu, G.; Amin, S.; Bílý, J.; Synek, J.; Modlinger, R.; Sen, M.K.; Chakraborty, A.; Roy, A. Reference gene selection for normalizing gene expression in *Ips sexdentatus* (Coleoptera: Curculionidae: Scolytinae) under different experimental conditions. *Front. Physiol.* **2021**, *12*, 752768. [CrossRef]
30. Yuan, F.; Xie, Z.; Li, Z.; Lian, P.; Wei, C. Screening of reference genes for gene expression study in different tissues from the transcriptome data of the vector leafhopper *Psammotettix striatus*. *Gene* **2024**, *927*, 148696. [CrossRef]
31. Li, M.; Li, X.; Wang, C.; Li, Q.; Zhu, S.; Zhang, Y.; Li, X.; Yang, F.; Zhu, X. Selection and validation of reference genes for qRT-PCR analysis of *Rhopalosiphum padi* (Hemiptera: Aphididae). *Front. Physiol.* **2021**, *12*, 663338. [CrossRef] [PubMed]
32. Bansal, R.; Mamidala, P.; Mian, M.A.; Mittapalli, O.; Michel, A.P. Validation of reference genes for gene expression studies in *Aphis glycines* (Hemiptera: Aphididae). *J. Econ. Entomol.* **2012**, *105*, 1432–1438. [CrossRef] [PubMed]
33. Bansal, R.; Haviland, D.R.; Hunter, W.B. Selection and validation of reference genes for quantifying gene expression in the Gill's mealybug. *J. Econ. Entomol.* **2023**, *116*, 2166–2172. [CrossRef] [PubMed]
34. Bassan, M.M.; Angelotti-Mendonc, A.J.; Alves, G.R.; Yamamoto, P.T.; Moura, O.F.F.A.A. Selection of reference genes for expression studies in *Diaphorina citri* (Hemiptera: Liviidae). *J. Econ. Entomol.* **2017**, *110*, 2623–2629. [CrossRef] [PubMed]
35. Pinheiro, D.H.; Moreira, R.O.; Leite, N.A.; Redoan, A.C.; Xavier, A.D.S.; Barros, B.A.; Carneiro, N.P. Suitable reference genes for RT-qPCR analysis in *Dichelops melacanthus* (Hemiptera: Pentatomidae). *Mol. Biol. Rep.* **2020**, *47*, 4989–5000. [CrossRef]
36. Liu, Z.; Xiao, J.; Xia, Y.; Wu, Q.; Zhao, C.; Li, D. Selection and validation of reference genes for RT-qPCR-based analyses of *Anastatus japonicus* Ashmead (Hymenoptera: Helicopteridae). *Front. Physiol.* **2022**, *13*, 1046204. [CrossRef] [PubMed]
37. Wang, L.; Yang, C.; Liu, Q.; Zhang, X.; Mei, X.; Zhang, T.; Ning, J. Validation and evaluation of reference genes for quantitative real-time PCR analysis in *Mythimna loreyi* (Lepidoptera: Noctuidae). *Insects* **2024**, *15*, 185. [CrossRef]
38. Fu, W.; Xie, W.; Zhang, Z.; Wang, S.; Wu, Q.; Liu, Y.; Zhou, X.; Zhou, X.; Zhang, Y. Exploring valid reference genes for quantitative real-time PCR analysis in *Plutella xylostella* (Lepidoptera: Plutellidae). *Int. J. Biol. Sci.* **2013**, *9*, 792–802. [CrossRef]
39. Wu, S.; Luo, Y.; Zeng, Z.; Yu, Y.; Zhang, S.; Hu, Y.; Chen, L. Determination of internal controls for quantitative gene expression of *Spodoptera litura* under microbial pesticide stress. *Sci. Rep.* **2024**, *14*, 6143. [CrossRef]

40. Dalai, M.; Jagota, A. Identification of specific reference gene for normalization of RT-qPCR data in rhythmic gene expression studies of the effect of developmental hormone antagonist in postembryonic development in *Bombyx mori*. *Front. Insect Sci.* **2024**, *4*, 1362473. [CrossRef]
41. Zhang, S.; An, S.; Li, Z.; Wu, F.; Yang, Q.; Liu, Y.; Cao, J.; Zhang, H.; Zhang, Q.; Liu, X. Identification and validation of reference genes for normalization of gene expression analysis using qRT-PCR in *Helicoverpa armigera* (Lepidoptera: Noctuidae). *Gene* **2015**, *555*, 393–402. [CrossRef] [PubMed]
42. Shen, X.X.; Zhang, G.Q.; Zhao, Y.X.; Zhu, X.X.; Yu, X.F.; Yang, M.F.; Zhang, F. Selection and validation of optimal reference genes for RT-qPCR analyses in *Aphidoletes aphidimyza* Rondani (Diptera: Cecidomyiidae). *Front. Physiol.* **2023**, *14*, 1277942. [CrossRef] [PubMed]
43. Yang, J.; Jiang, Z.; Xu, Q.; Liu, X.; Dai, M.; Li, B.; Wei, J. Evaluation of suitable reference genes for expression analysis using quantitative real-time polymerase chain reaction in the parasitoid *Exorista sorbillans* (Diptera: Tachinidae). *Arch. Insect Biochem. Physiol.* **2023**, *113*, e22009. [CrossRef]
44. Tian, P.; Qiu, L.; Zhou, A.; Chen, G.; He, H.; Ding, W.; Li, Y. Evaluation of appropriate reference genes For investigating gene expression in *Chlorops oryzae* (Diptera: Chloropidae). *J. Econ. Entomol.* **2019**, *112*, 2207–2214. [CrossRef]
45. Yang, Q.; Li, Z.; Cao, J.; Zhang, S.; Zhang, H.; Wu, X.; Zhang, Q.; Liu, X. Selection and assessment of reference genes for quantitative PCR normalization in migratory locust *Locusta migratoria* (Orthoptera: Acrididae). *PLoS ONE* **2014**, *9*, e98164. [CrossRef] [PubMed]
46. Hou, Q.; Yuan, L.; Jin, H.; Yan, H.; Li, F.; Wu, S. Identification and validation of reference genes for normalization of gene expression analysis using qRT-PCR in *Megalurothrips usitatus* (thysanoptera: Thripidae). *Front. Physiol.* **2023**, *14*, 1161680. [CrossRef] [PubMed]
47. Zheng, Y.T.; Li, H.B.; Lu, M.X.; Du, Y.Z. Evaluation and validation of reference genes for qRT-PCR normalization in *Frankliniella* occidentalis (Thysanoptera: Thripidae). *PLoS ONE* **2014**, *9*, e111369. [CrossRef]
48. Yamamoto, K.; Yamaguchi, M. Characterization of a novel superoxide dismutase in *Nilaparvata lugens*. *Arch. Insect Biochem. Physiol.* **2022**, *109*, e21862. [CrossRef]
49. Han, S.; Qin, Q.; Wang, D.; Zhou, Y.; He, Y. Selection and evaluation of reference genes for qRT-PCR in *Spodoptera frugiperda* (Lepidoptera: Noctuidae). *Insects* **2021**, *12*, 902. [CrossRef]
50. Singh, S.; Gupta, M.; Pandher, S.; Kaur, G.; Goel, N.; Rathore, P.; Palli, S.R. RNA sequencing, selection of reference genes and demonstration of feeding RNAi in *Thrips tabaci* (Lind.) (Thysanoptera: Thripidae). *BMC Mol. Biol.* **2019**, *20*, 6. [CrossRef] [PubMed]
51. Wang, L.; Liu, Q.; Guo, P.; Gao, Z.; Chen, D.; Zhang, T.; Ning, J. Evaluation of reference genes for quantitative real-time PCR analysis in the bean bug, *Riptortus pedestris* (Hemiptera: Alydidae). *Insects* **2023**, *14*, 906. [CrossRef] [PubMed]
52. Zhu, X.; Yuan, M.; Shakeel, M.; Zhang, Y.; Wang, S.; Wang, X.; Zhan, S.; Kang, T.; Li, J. Selection and evaluation of reference genes for expression analysis using qRT-PCR in the beet armyworm *Spodoptera exigua* (Hübner) (Lepidoptera: Noctuidae). *PLoS ONE* **2014**, *9*, e84730. [CrossRef] [PubMed]
53. Zhang, Y.; Chen, J.; Chen, G.; Ma, C.; Chen, H.; Gao, X.; Tian, Z.; Cui, S.; Tian, Z.; Guo, J.; et al. Identification and validation of reference genes for quantitative gene expression analysis in *Ophraella communa*. *Front. Physiol.* **2020**, *11*, 355. [CrossRef] [PubMed]
54. Yang, C.; Preisser, E.L.; Zhang, H.; Liu, Y.; Dai, L.; Pan, H.; Zhou, X. Selection of reference genes for RT-qPCR analysis in *Coccinella septempunctata* to assess un-intended effects of RNAi transgenic plants. *Front. Plant. Sci.* **2016**, *7*, 1672.
55. Tan, Q.Q.; Zhu, L.; Li, Y.; Liu, W.; Ma, W.H.; Lei, C.L.; Wang, X.P. A de novo transcriptome and valid reference genes for quantitative real-time PCR in *Colaphellus bowringi*. *PLoS ONE* **2015**, *10*, e0118693. [CrossRef] [PubMed]
56. Jiang, L.H.; Mu, L.L.; Jin, L.; Anjum, A.A.; Li, G.Q. Silencing uridine diphosphate N-acetylglucosamine pyrophosphorylase gene impairs larval development in *Henosepilachna vigintioctopunctata*. *Pest. Manag. Sci.* **2022**, *78*, 3894–3902. [CrossRef]
57. Zhang, Z.; Song, X.; Hu, H.; Wang, D.; Chen, J.; Ma, Y.; Ma, X.; Ren, X.; Ma, Y. Knockdown of UDP-N-acetylglucosamine pyrophosphorylase and chitin synthase A increases the insecticidal efficiency of Lufenuron to *Spodoptera exigua*. *Pestic. Biochem. Physiol.* **2022**, *186*, 105178. [CrossRef]
58. Wang, Z.; Long, G.Y.; Zhou, C.; Jin, D.C.; Yang, H.; Yang, W.J. Molecular characterization of UDP-N-acetylglucosamine pyrophosphorylase and its role in the growth and development of the white-backed planthopper *Sogatella furcifera* (Hemiptera: Delphacidae). *Genes* **2022**, *13*, 1340. [CrossRef]

Disclaimer/Publisher's Note: The statements, opinions and data contained in all publications are solely those of the individual author(s) and contributor(s) and not of MDPI and/or the editor(s). MDPI and/or the editor(s) disclaim responsibility for any injury to people or property resulting from any ideas, methods, instructions or products referred to in the content.

insects

MDPI

Article

Transcriptomic Characterization of Phototransduction Genes of the Asian Citrus Psyllid *Diaphorina citri* Kuwayama

Shao-Ping Chen [1,2,†], Xue-Mei Chu [1,2,†], Mei-Xiang Chi [1,2], Jian Zhao [1,2,3] and Rong-Zhou Qiu [1,2,*]

[1] State Key Laboratory of Ecological Pest Control for Fujian and Taiwan Crops, Institute of Plant Protection, Fujian Academy of Agricultural Sciences, Fuzhou 350013, China; fafucsp@163.com (S.-P.C.); 15165546235@163.com (X.-M.C.); cmx895619@163.com (M.-X.C.); zhaojian@faas.cn (J.Z.)
[2] Fujian Key Laboratory for Monitoring and Integrated Management of Crop Pests, Fujian Engineering Research Center for Green Pest Management, Fuzhou 350013, China
[3] Fujian Academy of Agricultural Sciences, Fuzhou 350003, China
* Correspondence: qiurz@faas.cn
† These authors contributed equally to this work.

Simple Summary: Opsin contributes to the phototaxis of Asian citrus psyllid (ACP, *Diaphorina citri*), which is the primary vector of *Candidatus* Liberibacter asiaticus, causing Citrus Huanglongbing (HLB). The objective of this study was to explore the phototransduction pathway of *D. citri* with a view to identifying elicitors that could enhance the phototaxis of *D. citri* in the future. To that end, 87 genes were identified via transcriptome sequencing. Of these genes, 71 were linked to the phototransduction-fly pathway. In addition, when *LW-opsin* gene expression was inhibited, *Gqβ* and *ninaC* were down-regulated. The findings of our study provide a foundation for further research into the phototransduction pathway in ACP, as well as a basis for further investigation into the potential of elicitors to enhance the phototaxis of ACP.

Abstract: Opsin plays a regulatory role in phototaxis of *Diaphorina citri*, functioning as the initial station in the phototransduction cascade. Our study aimed to explore the *D. citri* phototransduction pathway to identify elicitors that may enhance *D. citri* phototaxis in the future. The RNAi technique was employed to inhibit *LW-opsin* gene expression, followed by RNA-Seq analysis to identify phototransduction genes. Finally, RT-qPCR was performed to validate whether genes in the phototransduction pathway were affected by the inhibition of *LW-opsin* expression. A total of 87 genes were identified within the transcriptome as involved in phototransduction based on KEGG functional annotation. Of these, 71 genes were identified as enriched in the phototransduction-fly pathway. These genes encode key proteins in this process, including *Gqα*, *Gqβ*, *Gqγ*, *phospholipase C β* (*PLCβ*), the cation channel *transient receptor potential* (*TRP*), and *TRP-like* (*TRPL*), among others. Moreover, the *LOC103513214* (*Gqβ*) and *LOC103518375* (*ninaC*) genes exhibited reduced expression when *LW-opsin* gene expression was suppressed. Our results provide a basis for further investigation of phototransduction in *D. citri*.

Keywords: Asian citrus psyllid; phototransduction; *LW-opsin*; phototactic behavior; RNA-Seq

1. Introduction

Diaphorina citri Kuwayama (Asian citrus psyllid, Hemiptera, Psyllidae) is one of the most significant pests of citrus. It is the primary vector of *Candidatus* Liberibacter asiaticus, the causal agent of Citrus Huanglongbing (HLB) [1,2]. HLB is a destructive disease, often referred to as the "cancer of the citrus industry", which represents a substantial threat to the global citrus industry and poses a considerable risk to the industry's sustainability [3–5]. The most effective method for controlling HLB is the management of the Asian citrus psyllid through chemical, biological, and physical control measures. Among these, physical control, which leverages the insect's phototactic behavior, is widely employed in field

production due to its high efficacy and environmental compatibility. The Asian citrus psyllid displays positive phototaxis, exhibiting a preference for ultraviolet, blue, and green light [6–8]. It has been demonstrated that opsin regulates phototaxis in ACP [8]; however, the underlying molecular mechanism is not fully understood.

Opsin is a member of the G-protein-coupled receptor family, comprising seven transmembrane domains [9,10]. Based on the type of photoreceptor cell, opsins are classified into two major groups: rhabdomeric-type opsin (r-opsin) and ciliary-type opsin (c-opsin) [11–13]. In general, r-opsin is the main visual pigment in the rhabdomeres of insect compound eyes. Based on the spectral range to which opsins are sensitive, r-opsins of insects are classified into three categories: (1) long-wavelength-sensitive opsin (LW-opsin) with the peak absorbance more than 500 nm; (2) blue-sensitive opsin (BL-opsin) with the peak absorbance at 400–500 nm; and (3) ultraviolet-sensitive opsin (UV-opsin) with the peak absorbance at 300–400 nm [14–16]. *Drosophila* has 7 opsins (Rh1–7), of which Rh1, Rh2, and Rh5 are sensitive to blue light (absorption maxima of 486, 418, and 442 nm), Rh3 and Rh4 are sensitive to UV light (331 and 355 nm), and Rh6 is sensitive to green light (515 nm) [17–20]. Rh7 functions as a light detector and is involved in the regulation of the circadian rhythm [21]. It should be noted that different insect species vary in the number of opsins that they possess. For example, BL-opsin gene loss occurs in some species, such as *Tribolium castaneum* (red flour beetle, Coleoptera: Tenebrionidae), aphids (Aphidoidea), and planthoppers (Fulgoroidea) [22,23].

Opsins form covalent bonds with small molecular chromophores, thereby creating light-sensitive photopigments known as rhodopsins, which act as the primary activators in the phototransduction cascade [24]. The phototransduction pathway in *Drosophila* is most intensively studied. Light activates rhodopsin into metarhodopsin with chromophore conformational change, which initiates the G protein-mediated phototransduction cascade, leading to calcium and sodium ion exchange and the translation of light stimulus into an electrical signal [25–27]. A mutation in *LW-opsin* has been shown to alter gene expression in the phototransduction pathway in *Plutella xylostella* (diamondback moth, Lepidoptera: Plutellidae) [28]. Gene expression associated with the phototransduction pathway in the head of *Mythimna separata* (oriental armyworm, Lepidoptera: Noctuidae) was significantly altered following exposure to various light environments [29]. Thus, it was hypothesized that genes within the phototransduction pathway may enhance the phototaxis of the Asian citrus psyllid, making it essential to understand this pathway in *D. citri*.

Four visual photo-sensing opsins were identified in ACP: Dc-UV (UV-opsin), clustering with *Drosophila* Rh3 and Rh4; Dc-BW (BL-opsin), clustering with Rh5; Dc-LW (LW-opsin), clustering with Rh6; and Dc-UV-like, clustering with Rh7 [8]. The inhibition of *UV-opsin*, BL-opsin, and *LW-opsin* resulted in a reduction in phototactic response rates to the corresponding light source in ACP [8]. The expression of *LW-opsin* was observed to be the highest in ACP adults, in comparison to the other opsins [8]. Furthermore, only the expression of *LW-opsin* was found to be significantly up-regulated in response to white light treatment in comparison to dark treatment in our previous study (data not supplied). Accordingly, *LW-opsin* was selected as the target gene for further experimentation. To investigate the phototransduction pathway in *D. citri*, we first employed the RNA interference (RNAi) technique to inhibit *LW-opsin* gene expression, followed by RNA-Seq analysis to investigate the complete set of genes involved in phototransduction. Ultimately, inhibition of *LW-opsin* expression was observed to influence the mRNA expression levels of specific phototransduction genes, as determined by real-time quantitative PCR (RT-qPCR). This study advances our understanding of the phototransduction pathway in *D. citri* and provides theoretical guidance for identifying elicitors that could enhance *D. citri* phototaxis in the future.

2. Materials and Methods

2.1. Insects

The *D. citri* were reared on healthy *Murraya paniculata* within insect-rearing cages (60 × 40 × 75 cm) in an artificial greenhouse at the Institute of Plant Protection, Fujian

Academy of Agricultural Sciences. The greenhouse was maintained under controlled conditions: temperature 26 ± 1 °C, relative humidity 60% ± 10%, and a 14:10 h (light:dark) photoperiod. To ensure a uniform age of the insects, newly molted adults were collected and placed in a cage (30 × 30 × 35 cm) with a plant for further experiments.

2.2. RNA Extraction and dsRNA Synthesis

The total RNA was extracted using the FreeZol reagent (Vazyme, Nanjing, China), purified with RNA Extraction Buffer (Beyotime, Shanghai, China), and precipitated with isopropanol. Then, 500 ng of total RNA was reverse transcribed into complementary DNA (cDNA) using the HiScript® II 1st Strand cDNA Synthesis Kit (Vazyme), following the manufacturer's protocol. The primers for the synthesis of double-stranded RNA (dsRNA) of *LW-opsin* and *EGFP* were designed according to Li et al. [8] and were synthesized by Sangon Biotech Co., Ltd. (Shanghai, China). The sequence fragment templates of *LW-opsin* and *EGFP* were amplified using the Phanta® Super-Fidelity DNA Polymerase (Vazyme), according to the manufacturer's protocol. The PCR products were purified using a FastPure® Gel DNA Extraction Mini Kit (Vazyme), following the manufacturer's protocol. A total of 2 μg of purified PCR product was employed for dsRNA synthesis in vitro using the T7 Ribomax™ Express large-scale production system (Promega, Madison, WI, USA), according to the manufacturer's protocol.

2.3. RNA Interference of LW-Opsin

Injections of 200 ng of dsRNA were given to 10-day-old female *D. citri* adults using a Nanoject III microsyringe (Drummond Scientific Company, Broomall, PA, USA). After injection, the insects were reared on healthy *M. paniculata* in insect-rearing cages under the same conditions previously described. A total of 30 individuals were collected at 12, 24, 36, and 72 h post-injection, respectively. The dsLW-opsin and dsEGFP treatments were performed in triplicate at each of the four time points. Subsequently, the expression levels of *LW-opsin* were quantified via RT-qPCR to confirm the efficacy of the RNAi. The RT-qPCR amplification was conducted using the GoTaq® qPCR Master Mix (Promega) with an initial step at 95 °C for 10 min, followed by 40 cycles at 95 °C for 15 s and 60 °C for 30 s. A final cycle was carried out at 95 °C for 15 s, 60 °C for 60 s, and 95 °C for 15 s. The gene *β-actin* of *D. citri* was employed as the reference gene. The primers for RT-qPCR were designed following Li et al. [8], and they were synthesized by Sangon Biotech Co.Ltd. (Shanghai, China). The comparative Ct method ($2^{-\Delta\Delta CT}$) was employed for the calculation of the transcript level [30].

2.4. Transcriptome Sequencing

RNA-Seq was conducted on samples collected at time points where *LW-opsin* expression levels were suppressed. The RNA integrity number (RIN) was assessed using an RNA 6000 Nano Lab Chip Kit and Bioanalyzer 2100 (Agilent Technologies, Santa Clara, CA, USA). Samples with an RIN value of 8.0 or higher were submitted to the Shanghai Meiji Biological Company (Shanghai, China) for library construction and sequencing using the Illumina Novaseq 6000 platform (San Diego, CA, USA). Adapter trimming and low-quality filtering of the raw reads were performed using fastp (https://github.com/OpenGene/fastp, accessed on 18 July 2024). The clean reads were then aligned to the *D. citri* genome (https://www.ncbi.nlm.nih.gov/datasets/genome/GCF_000475195.1/, accessed on 18 July 2024) using Bowtie2 (Version 2.4.1) and HISAT2 (http://ccb.jhu.edu/software/hisat2/index.shtml, accessed on 18 July 2024) for sequence analysis. The mapped reads were assembled and spliced with StringTie (http://ccb.jhu.edu/software/stringtie/, accessed on 18 July 2024) in accordance with the *D. citri* genome. New transcripts were identified by comparing them with known transcripts using the Gffcompare tool (Version 0.9.8).

2.5. Gene Function Annotation and Phototransduction Gene Enrichment

A BLASTx search was conducted in protein databases, including NR (non-redundant), Swiss-Prot, Pfam, EggNOG, GO (Gene Ontology), and KEGG (Kyoto Encyclopedia of Genes and Genomes), to determine functional annotation.

A comprehensive search of the transcriptome was performed with the keywords "phototransduction" to identify all genes related to the phototransduction pathway, based on the functional annotation of all protein databases described above. Subsequently, an enrichment analysis of the KEGG pathway was conducted via the Majorbio platform (https://www.majorbio.com/web/www/index, accessed on 31 July 2024). The annotation of the genes' functions within the most enriched pathway was analyzed further.

2.6. Validation of Phototransduction Gene Expression by RT-qPCR

The objective was to validate whether the inhibition of *LW-opsin* expression affects the expression of genes involved in the phototransduction pathway. Accordingly, a subset of phototransduction genes was selected for further analysis. Primers for the selected genes are listed in Table 1. The RT-qPCR amplification was conducted following the previously described protocol.

Table 1. Primers used to validate the expression of phototransduction genes affected by inhibition of *LW-opsin* expression.

Gene ID in NCBI	Homolog Name	Forward Primer Sequence (5′ to 3′)	Reverse Primer Sequence (5′ to 3′)
LOC103507937	*IP3R*	aggcctcgtcagaaagaata	gagctcagcacacttttaca
LOC103507998	*Gqγ*	tccatcatgtaactacccgt	tgttcaggtgacgatcattg
LOC103509434	*PLCβ*	tactcacgggaaagctatgt	cgttttgcagcagtgatttt
LOC103513214	*Gqβ*	agggagaagaaatgtgtcca	ctatctgttgatctgcacgg
LOC103514397	*RK*	caatgaacgacttctccgtt	cattttaccggtatccgctt
LOC103516584	*Gqα*	catatccttggttccagcac	tttgacagcgcagaatacaa
LOC103517132	*PKC*	cagatcggcaaattcaagga	aaatggaggttgtcccacta
LOC103518375	*NINAC*	aagagaggaagacatcaggg	gggcaaatctccttgttgat
LOC103524308	*Arr2*	cgctctgaagaagtcgaaaa	cagttgtttattcgtccggt

2.7. Statistical Analysis

All statistical analyses were performed using the IBM SPSS software (version 22.0, IBM, Armonk, NY, USA). An independent *t*-test was used to assess significant differences in *LW-opsin* gene expression or phototransduction gene expression between the dsEGFP and dsLW-opsin treatment groups.

3. Results

3.1. RNA Interference of LW-Opsin

Following the injection of dsRNA (dsLW-opsin and dsEGFP), the relative expression levels of *LW-opsin* were quantified through RT-qPCR (Figure 1). The expression of *LW-opsin* had decreased by 46.82% at the 36 h time point and by 38.65% at the 72 h time point. Thus, the 36 h time point was considered optimal for conducting further RNA-Seq analysis.

3.2. Illumina Sequencing Analysis

A total of 40.97 Gb of clean data was obtained through transcriptome sequencing, with all samples exceeding 6.33 Gb of clean data. A total of 43,268 expressed genes were detected, comprising 23,604 known genes and 19,664 novel genes. In this paper, novel genes and novel transcripts are designated as "MSTRG". Additionally, 83,232 transcripts were characterized, including 25,321 known transcripts and 57,911 novel transcripts. Approximately 74.38% of the high-quality clean data was retained for assembly and analysis. Furthermore, the percentage of Q_{30} bases exceeded 95.68% (Supplementary Data File S1),

indicating a high level of base accuracy. The sequences of all transcripts were provided as supplementary material (Supplementary Data File S2).

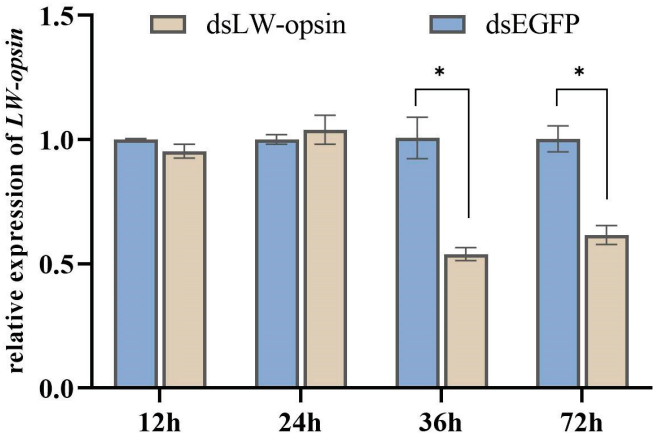


Figure 1. The interference efficiency of RNAi at the transcription level of *LW-opsin*. * indicates $p < 0.05$.

3.3. Phototransduction Genes

A total of 87 genes, including 9 novel genes, were identified within the transcriptome as involved in phototransduction, based on KEGG functional annotation (Table 2). The 87 genes were assigned 19 distinct KO IDs. Of the 87 genes identified, 17 were associated with K08834 (MYO3, myosin III), 15 with K02183 (CALM, calmodulin), 10 with K04255 (Rh2_7, r-opsin), and 6 with K00910 (GRK, G-protein-dependent receptor kinase). Four genes were assigned to K04967 (TRPC4, transient receptor potential cation channel subfamily C member 4), four genes to K05858 (PLCB, phosphatidylinositol phospholipase C, beta), three genes to K02677 (PRKCA, classical protein kinase C alpha type), three genes to K04515 (CAMK2, calcium/calmodulin-dependent protein kinase II), and three genes to K04952 (CNGB1, cyclic nucleotide gated channel beta 1). Two genes belong to K04536 (GNB1, guanine nucleotide-binding protein G(I)/G(S)/G(T) subunit beta-1), two to K13803 (TRPL, transient-receptor-potential-like protein), two genes to K13806 (DAGL, sn1-specific diacylglycerol lipase), one to K04547 (GNG13, guanine nucleotide-binding protein G(I)/G(S)/G(O) subunit gamma-13), and one to K04634 (GNAQ, guanine nucleotide-binding protein G(q) subunit alpha). Additionally, one gene belongs to K04958 (ITPR1, inositol 1,4,5-triphosphate receptor type 1), one to K07972 (GNB, guanine nucleotide-binding protein subunit beta), one to K12322 (GUCY2F, guanylate cyclase 2F), and one to K13805 (ARR2, arrestin2).

Table 2. Genes involved in phototransduction identified through KEGG functional annotation.

KO ID	KO Name	Gene IDs	Gene Number
K00910	GRK	LOC103505361, LOC103505365, LOC103519341, LOC103523400, LOC103524942, LOC103514397	6
K02183	CALM	LOC103505048, LOC103509805, LOC103509868, LOC103510651, LOC103511026, LOC103511569, LOC103511781, LOC103512666, LOC103513726, LOC103514274, LOC103517588, LOC103521078, LOC113468030, LOC103507684, LOC113465625	15
K02677	PRKCA	LOC108253019, LOC108253020, LOC103517132	3
K04255	Rh2_7	LOC103506067, LOC103506845, LOC103516743, LOC103516911, LOC103516912, LOC103517452, LOC103517454, LOC103521071, LOC103524061, LOC113473058	10

Table 2. *Cont.*

KO ID	KO Name	Gene IDs	Gene Number
K04515	CAMK2	LOC103509280, LOC113471771, MSTRG.19456	3
K04536	GNB1	LOC103515883, LOC103515885	2
K04547	GNG13	LOC103507998	1
K04634	GNAQ	LOC103516584	1
K04952	CNGB1	LOC103517837, LOC103522372, LOC103520508	3
K04958	ITPR1	LOC103507937	1
K04967	TRPC4	LOC113472687, LOC108252237, LOC108252236, MSTRG.12236	4
K05858	PLCB	LOC103508056, LOC103513753, LOC103519973, LOC103509434	4
K06636	SMC1	LOC113465618, LOC113466617, LOC113466908, LOC113467623, LOC113467958, LOC113467961, LOC113470296, LOC113473712, LOC113473717, LOC113473739	10
K07972	GNB	LOC103513214	1
K08834	MYO3	LOC103509649, LOC103513890, LOC103514755, LOC103515283, LOC103515285, LOC103515286, LOC103517045, LOC103517041, LOC103517042, LOC103517043, LOC103518375, MSTRG.45354, MSTRG.43624, MSTRG.48618, MSTRG.5326, MSTRG.17197, MSTRG.35405	17
K12322	GUCY2F	LOC103508103	1
K13803	TRPL	LOC103508643, LOC103522058	2
K13805	ARR2	LOC103524308	1
K13806	DAGL	LOC103515251, MSTRG.11676	2

3.4. KEGG Pathway Enrichment of Phototransduction Genes

The phototransduction-fly (map04745, rich factor = 1), phototransduction (map04744, rich factor = 1), and circadian entrainment (map04713, rich factor = 0.26) pathways, which are associated with light perception, were significantly enriched (Figure 2, Supplementary Data File S3). A total of 71 genes were enriched in the phototransduction-fly pathway, 21 genes were enriched in the phototransduction pathway, and 30 genes were enriched in the circadian entrainment pathway.

3.5. Gene Function Annotation Based on Phototransduction-Fly Pathway

A total of 71 genes were found to function in accordance with the phototransduction-fly pathway, as illustrated in Figure 3 and detailed in Table 3. The genes *LOC103516584*, *LOC103513214*, and *LOC103507998* were identified as encoding the α-, β-, and γ-subunits of the heterotrimeric Gq protein, respectively. Four genes were identified as encoding phospholipase C β (PLCβ), four as encoding the cation channel TRP (transient receptor potential), and two as encoding the cation channel TRPL (transient receptor potential like). Three genes were identified as encoding protein kinase C (PKC), fifteen as encoding CaM (calmodulin), and one as encoding Arr2 (arrestin2). Seventeen genes were identified as encoding NINAC (neither inactivation nor afterpotential C), ten as encoding actin, and one as encoding IP3R (inositol 1,4,5-trisphosphate, InsP3). Two genes were identified as encoding DAGL (diacylglycerol lipase), three as encoding CaMKII (CaM kinase II), and six as encoding RK (G protein-coupled receptor kinase 1). To confirm the precise details of these genes, further phylogenetic analysis, gene cloning, and characterization will be required.

It is noteworthy that ten genes (*LOC103506067*, *LOC103506845*, *LOC103516743*, *LOC103516911*, *LOC103516912*, *LOC103517452*, *LOC103517454*, *LOC103521071*, *LOC103524061*, *LOC113473058*) classified within the seven-transmembrane G protein-coupled receptor superfamily were not identified as opsins. Additionally, INAD (inactivation nor afterpotential D) and rdgC (retinal degeneration C) were not identified in our transcriptome.

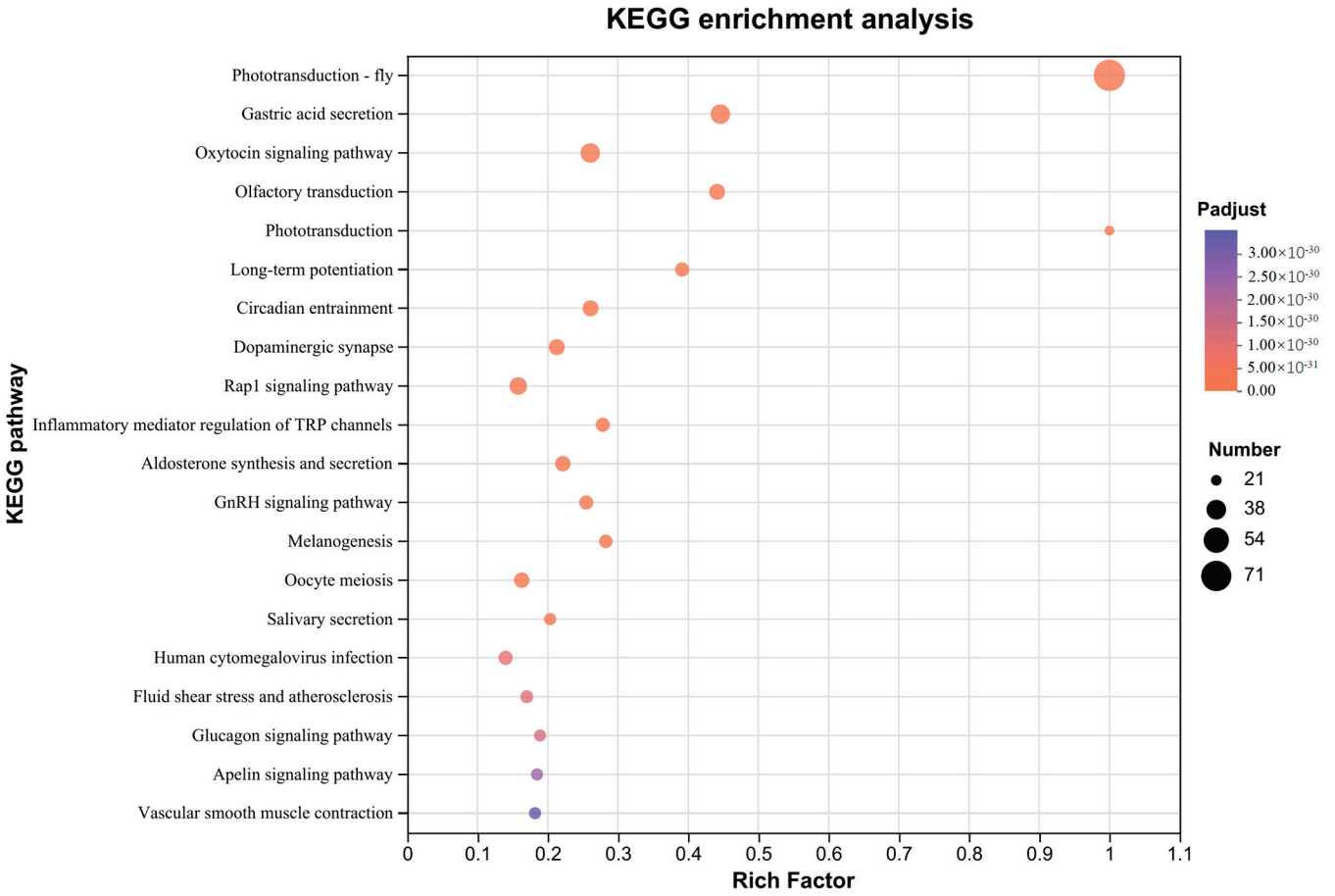


Figure 2. Top 20 of KEGG pathway enrichment of phototransduction genes.

Table 3. Genes associated with the phototransduction-fly pathway.

Gene Name	Gene IDs	Gene Number
Gq	LOC103516584, LOC103513214, LOC103507998	3
PLCβ	LOC103519973, LOC103509434, LOC103513753, LOC103508056	4
TRP	LOC113472687, LOC108252236, LOC108252237, MSTRG.12236	4
TRPL	LOC103508643, LOC103522058	2
PKC	LOC103517132, LOC108253019, LOC108253020	3
CaM	LOC103505048, LOC103509805, LOC103509868, LOC103510651, LOC103511026, LOC103511569, LOC103511781, LOC103512666, LOC103513726, LOC103514274, LOC103517588, LOC103521078, LOC113468030, LOC103507684, LOC113465625	15
Arr2	LOC103524308	1
NINAC	LOC103509649, LOC103513890, LOC103514755, LOC103515283, LOC103515285, LOC103515286, LOC103517045, LOC103517041, LOC103517042, LOC103517043, LOC103518375, MSTRG.5326, MSTRG.17197, MSTRG.35405, MSTRG.43624, MSTRG.45354, MSTRG.48618	17
Actin	LOC113465618, LOC113466617, LOC113466908, LOC113467623, LOC113467958, LOC113467961, LOC113470296, LOC113473712, LOC113473717, LOC113473739	10
IP3R	LOC103507937	1
DAGL	LOC103515251, MSTRG.11676	2
CamKII	LOC113471771, LOC103509280, MSTRG.19456	3
RK	LOC103505361, LOC103505365, LOC103519341, LOC103523400, LOC103524942, LOC103514397	6

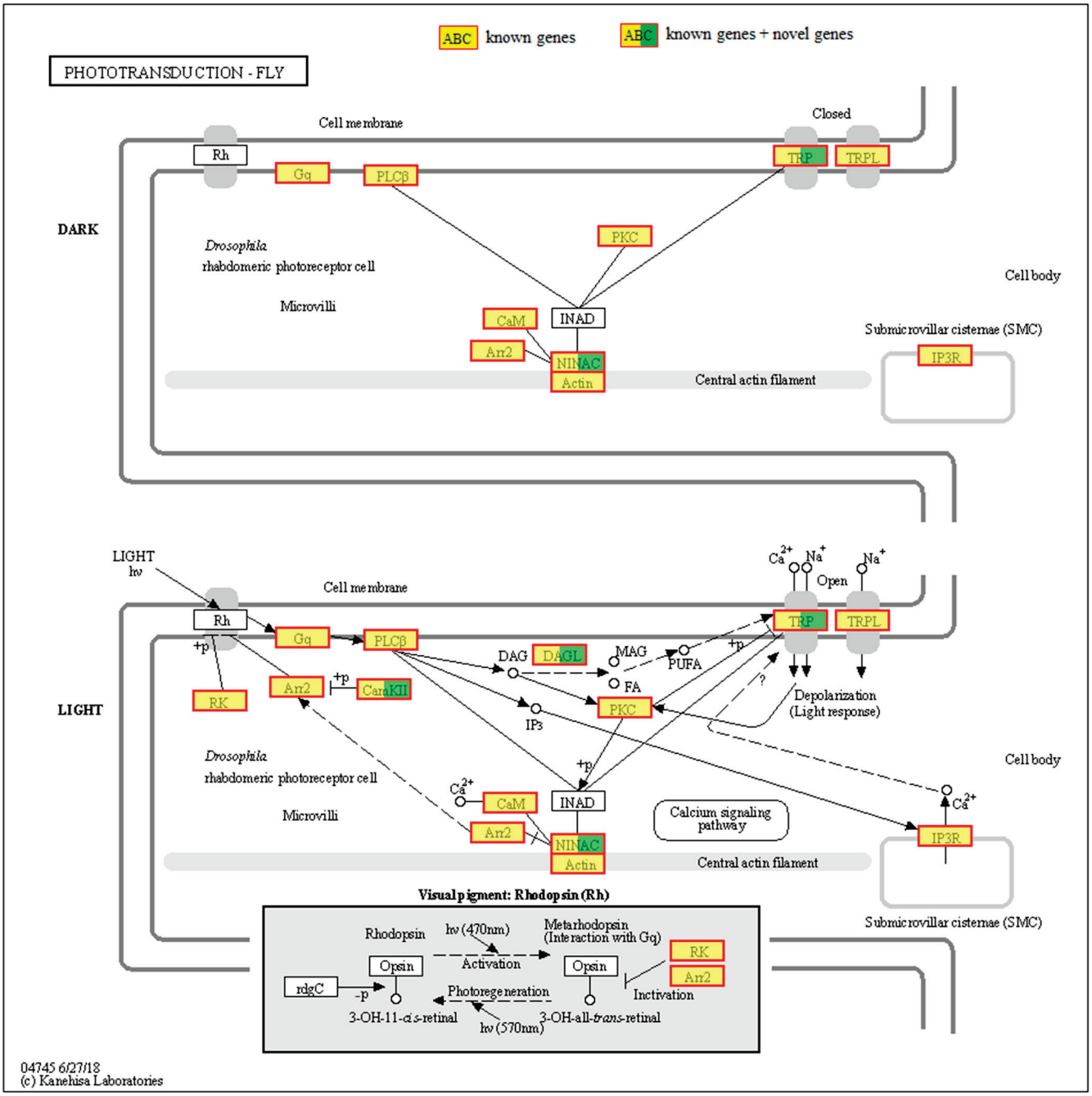


Figure 3. Gene function annotation based on phototransduction-fly pathway. Rh, rhodopsin. Gq, heterotrimeric Gq protein. PLCβ, phospholipase C β. TRP, transient receptor potential. TRPL, transient receptor potential like. PKC, protein kinase C. CaM, calmodulin. Arr2, arrestin2. NINAC, neither inactivation nor afterpotential C. IP3R, inositol 1,4,5-trisphosphate. DAGL, diacylglycerol lipase. CaMKII, CaM kinase II. RK, G protein-coupled receptor kinase 1.

3.6. Knockdown of LW-Opsin Gene Changes the Gene Expression of the Phototransduction Pathway

A total of nine genes were selected for validation to determine whether the knockdown of the *LW-opsin* gene alters the expression of genes involved in the phototransduction pathway. The results demonstrated that only the *LOC103513214* (*Gqβ*) and *LOC103518375* (*ninaC*) genes exhibited a reduction in expression when *LW-opsin* gene expression was inhibited (Figure 4).

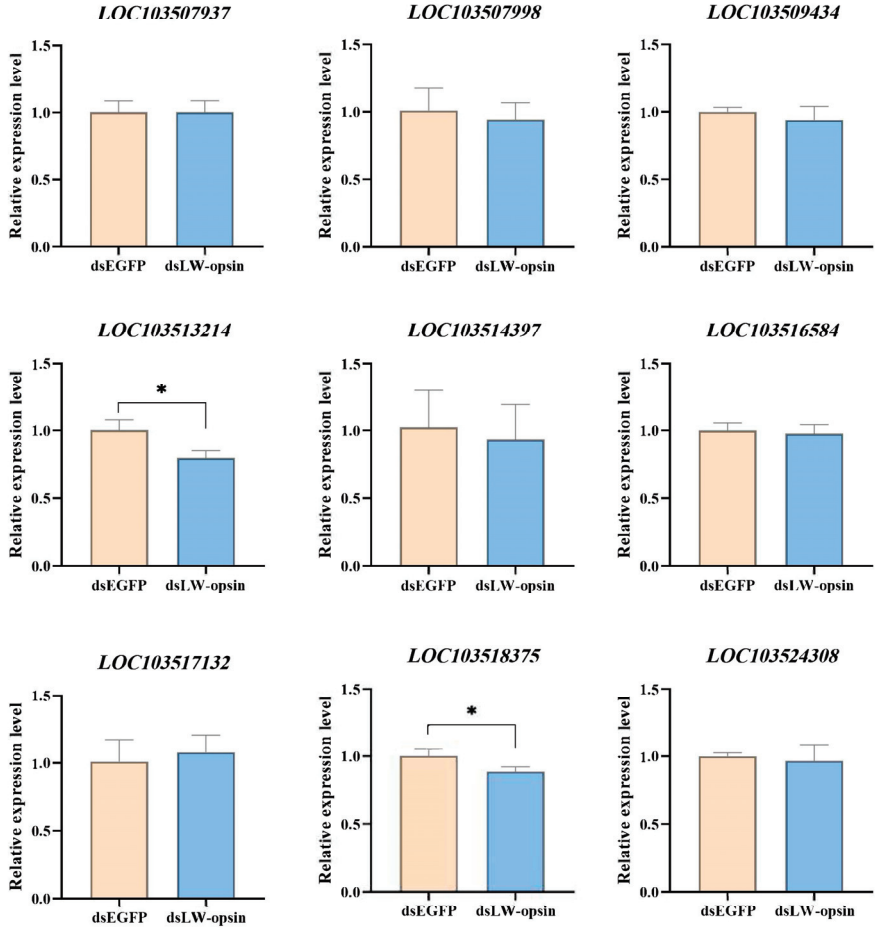


Figure 4. Verification of the 9 phototransduction genes whose expression is influenced by the knockdown of *LW-opsin* gene expression. * indicates $p < 0.05$.

4. Discussion

The *Drosophila* phototransduction pathway (phototransduction-fly) has been extensively studied [13,24–27]. In this study, a total of 71 genes in *D. citri* were identified as enriched in the phototransduction-fly pathway, including *Gqα*, *Gqβ*, *Gqγ*, *Arr2*, *PLCβ*, *TRP*, and *TRPL*, among others, with the exception of *INAD* and *rdgC*. This suggests that the phototransduction pathway in *D. citri* is comparable to that observed in *Drosophila*, although potential variations cannot be ruled out. Furthermore, the phototransduction pathway in non-*Drosophila* insects has been investigated through transcriptome-sequencing techniques. For example, the majority of phototransduction genes were found to be conserved between *D. melanogaster* and Lepidoptera, including *Gqα*, *Gqβ*, *Gqγ*, *Arr1*, *Arr2*, *trp*, *trpl*, and others [31]. In *Ptomaphagus hirtus* (troglobiont beetle, Coleoptera: Leiodidae), approximately 20 genes have been identified, including *LW-opsin*, *arr1*, *arr2*, *trp*, and *trp* [32]. Moreover, studies have demonstrated that gene expression in the phototransduction pathway is altered by environmental stimuli. For instance, eight genes, including *arr2*, *BRh*, and *rdgC*, have been demonstrated to exhibit seasonal adaptations in expression in *Bicyclus anynana* (small brown butterfly, Lepidoptera: Nymphalidae) [33]. Gene expression levels in the phototransduction pathway, including *Gq*, *PLCβ*, *PKC*, *TRP*, *TRPL*, *INAD*, *Arr2*, *NINAC*, and *CamkII*, change when *M. separata* is exposed to different light environments [29]. These studies suggest that the phototransduction pathway is relatively conserved in insects. Furthermore, the expression of the phototransduction genes may be altered in response to changes in the external environment, particularly light.

The functions of phototransduction genes observed in *D. citri* have been well-demonstrated in *Drosophila*. For example, mutations in the α-, β-, or γ-subunits of the

heterotrimeric Gq protein led to reduced light sensitivity [34–36]. Arr2 is a key inhibitory protein responsible for rhodopsin inactivation, which subsequently causes photoreceptor cell inactivation [37]. IP3R, an $InsP_3$ receptor that regulates calcium channels, is linked to retinal degeneration [38,39]. NINAC includes two isoforms, P132 and P174, both of which have a protein kinase structural domain that can bind the myosin head structural domain, but the isoforms have different C-termini, both isoforms are involved in regulating the transport of CaM and Arr2, with P174 mutations resulting in brief reactivation of the photoresponse even after light stimulation ceases [40–42]. In the future, more physiological, behavioural, and mechanistic studies are required to gain a comprehensive understanding of the phototransduction pathway in *D. citri*. With the increasing accessibility of molecular technologies, such as CRISPR/Cas9-based genome editing technology and RNAi technology, research on the function of phototransduction genes in *D. citri* will be a promising area for future exploration.

The functional relationship between opsins and phototactic behavior is firmly established [8,43–46]. Although opsins serve as the initial stage in the phototransduction pathway, few studies have explored changes in downstream genes following opsin gene knockout or knockdown. A recent study has demonstrated that the *LW-opsin* mutation affects the expression of genes involved in the phototransduction pathway in *P. xylostella*, including *NINAC*, *rdgC*, *TRP*, *TRPL*, *INAD*, and others [28]. In our study, only two of the nine validated genes exhibited down-regulated gene expression following the knockdown of the *LW-opsin* gene. This may be due to the fact that entire female bodies were used as samples in our study, as opposed to only the heads used in previous studies [28,29,31–33]. Further validation is required to confirm whether the expression of genes involved in the phototransduction pathway is affected when *LW-opsin* expression is suppressed using only the heads of *D. citri*.

5. Conclusions

In conclusion, a total of 71 genes in *D. citri* were identified as enriched in the phototransduction-fly pathway. These genes encode key proteins in this process, including *Gqα*, *Gqβ*, *Gqγ*, *PLCβ*, *TRP*, and *TRPL*, among others. Moreover, the *LOC103513214* and *LOC103518375* genes exhibited a reduction in expression when *LW-opsin* gene expression was suppressed. Our results contribute to a deeper understanding of the molecular mechanisms underlying *D. citri* vision. This knowledge will facilitate the identification of elicitors that could enhance the understanding of *D. citri* phototaxis moving forward.

Supplementary Materials: The following supporting information can be downloaded at https://www.mdpi.com/article/10.3390/insects15120966/s1, Supplementary Data File S1: Summary of transcriptome-sequencing results generated from *Diaphorina citri*; Supplementary Data File S2: The sequences of all transcripts; Supplementary Data File S3: KEGG pathway enrichment of phototransduction genes.

Author Contributions: Conceptualization, R.-Z.Q., J.Z. and S.-P.C.; methodology, S.-P.C. and X.-M.C.; validation, S.-P.C., X.-M.C. and M.-X.C.; data curation, R.-Z.Q., J.Z. and S.-P.C.; writing—original draft preparation, S.-P.C. and X.-M.C.; writing—review and editing, R.-Z.Q. and J.Z.; visualization, S.-P.C., M.-X.C. and X.-M.C.; supervision, R.-Z.Q.; funding acquisition, R.-Z.Q. and S.-P.C. All authors have read and agreed to the published version of the manuscript.

Funding: This research was funded by the Natural Science Foundation of Fujian Province, grant number 2022J05077, the Free Exploring Research Project of the Fujian Academy of Agricultural Sciences, grant number ZYTS2023009, the Key Project of Natural Science Foundation of Fujian Province, grant number 2023J02009, the National Key R&D Program of China, grant number 2021YFD1400800, and the "5511" Collaborative Innovation Project of High-quality Agricultural Development and Surpassment in Fujian Province (XTCXGC2021011, XTCXGC2021017).

Data Availability Statement: All data are available in publicly accessible repositories (https://dataview.ncbi.nlm.nih.gov/object/PRJNA1178351, accessed on 1 October 2024, Accession: PRJNA1178351).

Conflicts of Interest: The authors declare no conflicts of interest.

References

1. Gottwald, T.R. Current epidemiological understanding of citrus Huanglongbing. *Annu. Rev. Phytopathol.* **2010**, *48*, 119–139. [CrossRef]
2. Grafton-Cardwell, E.E.; Stelinski, L.L.; Stansly, P.A. Biology and management of Asian citrus psyllid, vector of the Huanglongbing pathogens. *Annu. Rev. Entomol.* **2013**, *58*, 413–432. [CrossRef] [PubMed]
3. Bové, J.M. Huanglongbing: A destructive, newly-emerging, century-old disease of citrus. *J. Plant Pathol.* **2006**, *88*, 7–37. [CrossRef]
4. Neupane, D.; Moss, C.B.; Van Bruggen, A.H.C. Estimating citrus production loss due to citrus Huanglongbing in Florida. In Proceedings of the Southern Agricultural Economics Association Annual Meeting, San Antonio, TX, USA, 6–9 February 2016; Available online: https://ageconsearch.umn.edu/bitstream/230093/2/Estimating%20CitrusFinal.pdf (accessed on 28 July 2024).
5. Lee, J.A.; Halbert, S.E.; Dawson, W.O.; Robertson, C.J.; Keesling, J.E.; Singer, B.H. Asymptomatic spread of Huanglongbing and implications for disease control. *Proc. Natl. Acad. Sci. USA* **2015**, *112*, 7605–7610. [CrossRef] [PubMed]
6. Paris, T.M.; Allan, S.A.; Udell, B.J.; Stansly, P.A. Wavelength and polarization affect phototaxis of the Asian citrus Psyllid. *Insects* **2017**, *8*, 88. [CrossRef] [PubMed]
7. Paris, T.M.; Croxton, S.D.; Stansly, P.A.; Allan, S.A. Temporal response and attraction of *Diaphorina citri* to visual stimuli. *Entomol. Exp. Appl.* **2015**, *155*, 137–147. [CrossRef]
8. Li, C.; Tian, F.; Lin, T.; Wang, Z.; Liu, J.; Zeng, X. The expression and function of opsin genes related to the phototactic behavior of Asian citrus psyllid. *Pest Manag. Sci.* **2020**, *76*, 1578–1587. [CrossRef]
9. Terakita, A. The Opsins. *Genome Biol.* **2005**, *6*, 213. [CrossRef]
10. Wang, T.; Montell, C. Phototransduction and retinal degeneration in *Drosophila*. *Pflug. Arch. Eur. J. Physiol.* **2007**, *454*, 821–847. [CrossRef]
11. Arendt, D.; Tessmar-Raible, K.; Snyman, H.; Dorresteijn, A.W.; Wittbrodt, J. Ciliary photoreceptors with a vertebrate-type opsin in an invertebrate brain. *Science* **2004**, *306*, 869–871. [CrossRef]
12. Ullrich-Lüter, E.M.; D'Aniello, S.; Arnone, M.I. C-opsin expressing photoreceptors in echinoderms. *Integr. Comp. Biol.* **2013**, *53*, 27–38. [CrossRef] [PubMed]
13. Yau, K.W.; Hardie, R.C. Phototransduction motifs and variations. *Cell* **2009**, *139*, 246–264. [CrossRef] [PubMed]
14. Briscoe, A.D.; Chittka, L. The evolution of color vision in insects. *Annu. Rev. Entomol.* **2001**, *46*, 471–510. [CrossRef] [PubMed]
15. Feuda, R.; Marletaz, F.; Bentley, M.A.; Holland, P.W.H. Conservation, duplication, and divergence of five opsin genes in insect evolution. *Genome Biol. Evol.* **2016**, *8*, 579–587. [CrossRef]
16. Lebhardt, F.; Desplan, C. Retinal perception and ecological significance of color vision in insects. *Curr. Opin. Insect Sci.* **2017**, *24*, 75–83. [CrossRef]
17. Mcculloch, K.J.; Macias-Muñoz, A.; Briscoe, A.D. Insect opsins and evo-devo: What have we learned in 25 Years? *Philos. Trans. R. Soc. Lond. B Biol. Sci.* **2022**, *377*, 20210288. [CrossRef]
18. Charlton-Perkins, M.; Cook, T.A. Building a fly eye: Terminal differentiation events of the retina, corneal lens, and pigmented epithelia. *Curr. Top. Dev. Biol.* **2010**, *93*, 129–173. [CrossRef]
19. Salcedo, E.; Huber, A.; Henrich, S.; Chadwell, L.V.; Chou, W.H.; Paulsen, R.; Britt, S.G. Blue- and green-absorbing visual pigments of *Drosophila*: Ectopic expression and physiological characterization of the R8 photoreceptor cell-specific Rh5 and Rh6 rhodopsins. *J. Neurosci.* **1999**, *19*, 10716–10726. [CrossRef]
20. Senthilan, P.R.; Helfrich-Förster, C. Rhodopsin 7-The unusual Rhodopsin in *Drosophila*. *PeerJ* **2016**, *4*, e2427. [CrossRef]
21. Ni, J.D.; Baik, L.S.; Holmes, T.C.; Montell, C. A rhodopsin in the brain functions in circadian photoentrainment in *Drosophila*. *Nature* **2017**, *545*, 340–344. [CrossRef]
22. Jackowska, M.; Bao, R.; Liu, Z.; Mcdonald, E.C.; Cook, T.A.; Friedrich, M. Genomic and gene regulatory signatures of cryptozoic adaptation: Loss of blue sensitive photoreceptors through expansion of long wavelength-opsin expression in the red flour beetle *Tribolium castaneum*. *Front. Zool.* **2007**, *4*, 24. [CrossRef] [PubMed]
23. Friedrich, M. Parallel losses of blue opsin correlate with compensatory neofunctionalization of UV-opsin gene duplicates in aphids and planthoppers. *Insects* **2023**, *14*, 774. [CrossRef] [PubMed]
24. Montell, C. *Drosophila* visual transduction. *Trends Neurosci.* **2012**, *35*, 356–363. [CrossRef] [PubMed]
25. Katz, B.; Minke, B. The *Drosophila* light-activated TRP and TRPL channels—Targets of the phosphoinositide signaling cascade. *Prog. Retin. Eye Res.* **2018**, *66*, 200–219. [CrossRef]
26. Landry, C.R.; Castillo-Davis, C.I.; Ogura, A.; Liu, J.S.; Hartl, D.L. Systems-level analysis and evolution of the phototransduction network in *Drosophila*. *Proc. Natl. Acad. Sci. USA* **2007**, *104*, 3283–3288. [CrossRef] [PubMed]
27. Hardie, R.C.; Juusola, M. Phototransduction in *Drosophila*. *Curr. Opin. Neurobiol.* **2015**, *34*, 37–45. [CrossRef]
28. Chen, S.P.; Lin, X.L.; Qiu, R.Z.; Chi, M.X.; Yang, G. An *LW-opsin* mutation changes the gene expression of the phototransduction pathway: A *cryptochrome1* mutation enhances the phototaxis of male *Plutella xylostella* (Lepidoptera: Plutellidae). *Insects* **2023**, *14*, 72. [CrossRef]
29. Duan, Y.; Gong, Z.J.; Wu, R.H.; Miao, J.; Jiang, Y.L.; Li, T.; Wu, X.B.; Wu, Y.Q. Transcriptome analysis of molecular mechanisms responsible for light-stress response in *Mythimna separata* (Walker). *Sci. Rep.* **2017**, *7*, 45188. [CrossRef]
30. Livak, K.J.; Schmittgen, T.D. Analysis of relative gene expression data using real-time quantitative PCR and the $2^{-\Delta\Delta CT}$ method. *Methods* **2001**, *25*, 402–408. [CrossRef]

31. Macias-Muñoz, A.; Rangel Olguin, A.G.; Briscoe, A.D.; Li, W.H. Evolution of phototransduction genes in Lepidoptera. *Genome Biol. Evol.* **2019**, *11*, 2107–2124. [CrossRef]
32. Friedrich, M.; Chen, R.; Daines, B.; Bao, R.; Caravas, J.; Rai, P.K.; Zagmajster, M.; Peck, S.B. Phototransduction and clock gene expression in the troglobiont beetle *Ptomaphagus hirtus* of Mammoth cave. *J. Exp. Biol.* **2011**, *214*, 3532–3541. [CrossRef] [PubMed]
33. Macias-Munoz, A.; Smith, G.; Monteiro, A.; Briscoe, A.D. Transcriptome-wide differential gene expression in *Bicyclus anynana* butterflies: Female vision-related genes are more plastic. *Mol. Biol. Evol.* **2016**, *33*, 79–92. [CrossRef] [PubMed]
34. Scott, K.; Becker, A.; Sun, Y.; Hardy, R.; Zuker, C. Gqα protein function in vivo: Genetic dissection of its role in photoreceptor cell physiology. *Neuron* **1995**, *15*, 919–927. [CrossRef] [PubMed]
35. Dolph, P.J.; Man-Son-Hing, H.; Yarfitz, S.; Colley, N.J.; Deer, J.R.; Spencer, M.; Hurley, J.B.; Zuker, C.S. An eye-specific G beta subunit essential for termination of the phototransduction cascade. *Nature* **1994**, *370*, 59–61. [CrossRef] [PubMed]
36. Schillo, S.; Belusic, G.; Hartmann, K.; Franz, C.; Kühl, B.; Brenner-weiss, G.; Paulsen, R.; Huber, A. Targeted mutagenesis of the farnesylation site of *Drosophila* Gγe disrupts membrane association of the G protein bγ complex and affects the light sensitivity of the visual system. *J. Biol. Chem.* **2004**, *279*, 36309–36316. [CrossRef]
37. Dolph, P.J.; Ranganathan, R.; Colley, N.J.; Hardy, R.W.; Socolich, M.; Zuker, C.S. Arrestin function in inactivation of G protein-coupled receptor rhodopsin in vivo. *Science* **1993**, *260*, 1910–1916. [CrossRef]
38. Srikanth, S.; Wang, Z.; Tu, H.; Nair, S.; Mathew, M.K.; Hasan, G.; Bezprozvanny, I. Functional properties of the *Drosophila melanogaster* inositol 1,4,5-trisphosphate receptor mutants. *Biophys. J.* **2004**, *86*, 3634–3646. [CrossRef]
39. Vázquez-Martínez, O.; Loranca, A.; Palma-Tirado, L.; Wischin-Fuentes, S.; Villalobos-Leal, M.; Antaramián, A.; Riesgo-Escovar, J.; Hernández-Muñoz, R.; Díaz-Muñoz, M. Time course of retinal degeneration associated with the absence of 1, 4, 5-inositol trisphosphate receptor in *Drosophila melanogaster*. *Exp. Biol. Med.* **2010**, *235*, 365–372. [CrossRef]
40. Porter, J.A.; Yu, M.; Doberstein, S.K.; Pollard, T.D.; Montell, C. Dependence of calmodulin localization in the retina on the NINAC unconventional myosin. *Science* **1993**, *262*, 1038–1042. [CrossRef]
41. Li, H.S.; Porter, J.A.; Montell, C. Requirement for the NINAC kinase/myosin for stable termination of the visual cascade. *J. Neurosci.* **1998**, *18*, 9601–9606. [CrossRef]
42. Lee, S.J.; Montell, C. Light-dependent translocation of visual arrestin regulated by the NINAC myosin III. *Neuron* **2004**, *43*, 95–103. [CrossRef] [PubMed]
43. Wakakuwa, M.; Stewart, F.; Matsumoto, Y.; Matsunaga, S.; Arikawa, K. Physiological basis of phototaxis to near-infrared light in *Nephotettix cincticeps*. *J. Comp. Physiol. A* **2014**, *200*, 527–536. [CrossRef] [PubMed]
44. Liu, Y.J.; Yan, S.; Shen, Z.J.; Li, Z.; Zhang, X.F.; Liu, X.M.; Zhang, Q.W.; Liu, X.X. The expression of three opsin genes and phototactic behavior of *Spodoptera exigua* (Lepidoptera: Noctuidae): Evidence for visual function of Opsin in phototaxis. *Insect Biochem. Mol. Biol.* **2018**, *96*, 27–35. [CrossRef] [PubMed]
45. Chen, S.P.; Liu, Z.X.; Chen, Y.T.; Wang, Y.; Chen, J.Z.; Fu, S.; Ma, W.F.; Xia, S.; Liu, D.; Wu, T.; et al. CRISPR/Cas9-mediated knockout of *LW-opsin* reduces the efficiency of phototaxis in the diamondback moth *Plutella xylostella*. *Pest Manag. Sci.* **2021**, *77*, 3519–3528. [CrossRef]
46. Huang, M.; Meng, J.Y.; Zhou, L.; Yu, C.; Zhang, C.Y. Expression and function of opsin genes associated with phototaxis in *Zeugodacus cucurbitae* Coquillett (Diptera: Tephritidae). *Pest Manag. Sci.* **2023**, *79*, 4490–4500. [CrossRef]

Disclaimer/Publisher's Note: The statements, opinions and data contained in all publications are solely those of the individual author(s) and contributor(s) and not of MDPI and/or the editor(s). MDPI and/or the editor(s) disclaim responsibility for any injury to people or property resulting from any ideas, methods, instructions or products referred to in the content.

insects

MDPI

Article

Adult Diel Locomotor Behaviour in the Agricultural Pest *Plutella xylostella* Reflects Temperature-Driven and Light-Repressed Regulation Rather than Coupling to Circadian Clock Gene Rhythms

Connor J. Tyler [1], Shubhangi Mahajan [1], Lena Smith [1], Haruko Okamoto [1,2] and Herman Wijnen [1,*]

[1] SPITFIRE NERC Doctoral Training Partnership, SoCoBio BBSRC Doctoral Training Partnership, School of Biological Sciences and Institute for Life Sciences, University of Southampton, Highfield Campus, Southampton SO17 1BJ, UK; ct13g15@southamptonalumni.ac.uk (C.J.T.); sm6n22@soton.ac.uk (S.M.); ls9g20@soton.ac.uk (L.S.); h.okamoto@sussex.ac.uk (H.O.)

[2] School of Life Sciences, University of Sussex, Brighton BN1 9QG, UK

* Correspondence: hw3a11@soton.ac.uk

Simple Summary: Insect pests such as the diamondback moth, which infests cabbages and related crops, inflict massive amounts of damage to agriculture that costs billions of USD annually. Since the adult diamondback moths spread by migrating, factors controlling their activity and movement are of interest. Daily and seasonal activity rhythms in many animals are regulated by innate daily timekeeping systems termed circadian clocks. In this study, we describe rhythms in the molecular elements of this timekeeping system in diamondback moths and we test if the circadian clock can be held responsible for daily rhythms in moth activity. We found that diamondback moth activity was suppressed by light and regulated by environmental temperature rather than the circadian clock. These insights are helpful in predicting the activity of this agricultural pest.

Abstract: The diamondback moth, *Plutella xylostella,* is arguably the most economically impactful and widespread lepidopteran pest. Though the larval *P. xylostella* life stage is responsible for most of this cost through the consumption of crops, it is the adult form that spreads the pest to fresh crops all around the world, seeking them out in a seasonally expanding range. It is therefore important to understand the activity rhythms of adult *P. xylostella* in response to environmental cues such as light and temperature. We analysed diel rhythms in both adult clock gene expression and locomotor behaviour for the ROTH *P. xylostella* strain. Real-time quantitative PCR analyses of *P. xylostella* demonstrated diel rhythms for transcripts of the clock genes *period* and *timeless* under both entrained and free-running conditions indicating the presence of a functional daily timekeeping mechanism. However, adult locomotor rhythms exhibited temperature-driven and light-repressed regulation rather than circadian control. Thus, our analyses show a lack of coupling between the *P. xylostella* circadian clock and adult locomotor behaviour, which may be relevant in predicting the activity patterns of this agricultural pest.

Keywords: diamondback moth; behavioural rhythm; daily timekeeping; light response; temperature response

1. Introduction

Climate change and an exponentially growing human population are putting pressure on arable land and threatening global famines before the end of the century [1], making food security a priority issue that needs to be addressed [2]. A key factor in the challenge to maintain food production is the control of pest species, with the effects of pests being underestimated [3] and increasing in severity as the climate changes [4–7]. *P. xylostella* (diamondback moth) is a pest species that has taken hold globally, having achieved a cosmopolitan distribution with a seasonally expanding range that covers all but the coldest latitudes [8,9]. *P. xylostella* is a *Brassicaceae* specialist herbivore [10] causing worldwide losses estimated at USD ~5 billion annually [11], up from USD ~1 billion in the 1990s, making *P. xylostella* arguably the world's most costly lepidopteran pest [8]. *P. xylostella* challenges farmers due to rapid proliferation in newly colonised fields and is able to produce 250+ eggs per female [12] and complete multiple life cycles per season [8,13]. *P. xylostella* also shows rapid pesticide resistance gain [14–16], leading to control failures with some regions facing > 90% crop losses [17,18]. Integrated Pest Management (IPM) strategies are being implemented to both diminish pesticide use and *P. xylostella's* impact [19–21]; however, the uptake of these strategies has been limited, with the prohibitive complexity of treatments needed for success causing farmers to fall back onto aggressive pesticide spraying protocols [22–24]. The study of behavioural manipulation as part of control strategies has been gaining increasing attention as these research pathways may complement and help increase the efficacy of IPM [25–27].

The circadian clock acts as an endogenous timekeeping mechanism controlling processes in organisms to best fit the daily rhythms of the planet [28,29]. This clock runs via a series of transcriptional and translational feedback loops (TTFL) that maintain ~24 h rhythms without the need for external stimuli such as light and temperature though it can be entrained by them. The lepidopteran circadian clock differs from that of the model organism *Drosophila melanogaster* [30,31], having two CRYPTOCHROME (CRY) proteins active in the TTFL. CRY2 (vertebrate-like CRY, absent in *Drosophila*) acts as negative regulator in the complex that represses *per, tim* and *cry2* expression [32,33].

Circadian rhythms have a widespread impact on gene expression. For example, ~40% of coding genes were found to exhibit circadian rhythms in mice [34] and ~35% in plants [35]. Synchrony of internal and environmental rhythms is important for health and well-being with circadian clocks exerting a strong influence over organisms' immune systems and anticipation of threats [36–39]. Lepidopteran circadian mechanisms have been shown to influence numerous behaviours including life stage cycles, oviposition [40] and seasonal migrations [41]. *P. xylostella* may better adapt to local environments and rhythmic changes via seasonal migration. In other species, seasonal migration is known to be informed by the clock-dependent detection of relevant changes in the photoperiod [42,43] and temperature [44,45]. Moreover, the way in which *P. xylostella* controls and modulates its behaviour when invading new regions and after invasions have taken place may be important for informing control measures as well as complimenting and improving the efficacy of IPM strategies. *P. xylostella*, which lacks the ability to diapause, migrates seasonally, invading brassica crops grown at higher latitudes as temperatures warm with populations sustained as long as temperatures remain elevated [9,46,47]. The modulating photoperiod in a neotropical *P. xylostella* population had no discernible effect morphology or life history [48]. However, systematic analyses of the impact of changes in both the photoperiod and daily temperature cycles on *P. xylostella* physiology and behaviour remain to be conducted.

It is therefore important to understand both *P. xylostella*'s daily timekeeping mechanisms and the rhythmic behavioural outputs that occur in association with these. Molecular circadian rhythms underlying daily timekeeping were explored by determining transcript profiles of the

P. xylostella clock genes *per* and *tim*. In addition, *P. xylostella* was studied for its diel locomotor activity under a range of environmental light and temperature cycles. Our behavioural analyses of the ROTH *P. xylostella* strain maintained on *Brassica rapa* complement a prior behavioural study using the Geneva 88 *P. xylostella* strain maintained on an artificial diet that identified nocturnal behaviour with relatively weak male-specific circadian behaviour [49].

2. Materials and Methods

2.1. P. xylostella Culture Maintenance

P. xylostella populations were reared within an environmental control room (ECR) at 20 °C in a 12/12 h Light/Dark (L/D) light cycle. W30 × D30 × H30 cm BugDorms (Watkins & Doncaster, Leominster, UK) were used to house mixed-sex populations. The population was acquired from Rothamsted Research, (ROTH strain wild collections during the 1960s) and has been continuously maintained on *Brassica rapa*. A sugar-water source was provided for adults during the egg-laying period, with adults mixed between new cages to prevent genetic isolation.

2.2. P. xylostella Locomotor Activity Assays

In preliminary activity monitor experiments, three different substrates were trialled. Cotton wool saturated with sugar-water or diluted honey versus sugar-agar solid media. As moths often got stuck and/or wet when sugar/honey solution-saturated cotton wool was used, the solid sugar-agar media were used instead. To control fungal growth, this media was prepared with 0.07% methyl 4-hydroxybenzoate. This was added using a 10% methyl 4-hydroxybenzoate w/v stock solution in ethanol after 1% agar and 5% table sugar media had been boiled and cooled down to ~60 °C. During preparation, 25 mm diameter × 95 mm length glass test tubes were filled from the bottom with 2 cm of the media. The media was left to dry before adding individual *P. xylostella* under CO_2 anaesthesia, and the tubes were capped with cellulose acetate to allow gas exchange. Individual *P. xylostella* activity counts were detected with the tubes in horizontal orientation by the TriKinetics LAM25 assay system (TriKinetics, Waltham, MA, USA). Based on the increased mortality at 23 °C in preliminary experiments, assays were conducted at 17 °C or 20 °C.

For individual locomotor assays at a constant temperature, LAM25 monitors were kept inside a black plastic box at 17 °C, with local humidity provided by a tray of water containing algicide and biocide to suppress microbial growth. White LEDs were mounted inside the black plastic tub providing 8 μmol/m^2/s (~400 lux) light for 12/12, 6/6/6/6, 14/10, 16/8, 18/6 and 20/4 h of light (L) and dark (D) cycles or in constant light (L/L) or constant darkness (D/D), shown in Table 1. In parallel, environmental cycles mimicking light and temperature recordings in Kent (51.2874° N, 0.4400° E), UK, in April and June, were set up for individual locomotor activity assays in an Percival incubator, model number: DR-36VL, (Clf Plantclimatics, Wertingen, Germany) based on environmental data from [50], producing the conditions shown in Table 1. The recorded environmental profile in the incubator setups is shown in Supplementary Figure S4, where a programmable LED lamp (FLUVAL14521, Rolf C. Hagen (UK) Ltd. Castleford, UK) was used to create ramping dawn and dusk light, with the incubator maintaining the temperature profile and max light producing 38 μmol/m^2/s (~2000 lux). Gradually ramping temperature cycles in (D/D) and (L/L) conditions were produced in the same incubators, using the four built-in fluorescent lights to provide the light for the latter condition. For each locomotor assay, *P. xylostella* was selected freshly from culturing enclosures and was recorded over 6+ days. The data were collected by a DAM (Drosophila Activity Monitor) system (Trikinetics, Waltham, MA, USA) [51] in 5 min segments and were subsequently exported to ClockLab Analysis Version

6 (Actimetrics, Lafayette, IN, USA) for analysis. DEnM monitors were used to keep track of experimental light, temperature and humidity conditions.

Table 1. Diel environmental conditions for locomotor activity assays. Dawn refers to the phase of increasing light intensity, dusk refers to phase of decreasing light intensity.

Condition	Light Cycle	Temperature
D/D	Constant Dark	17 °C
D/D	Constant Dark	20 °C
12/12	12 h Light, 12 h Dark	17 °C
6/6/6/6	6 h Light, 6 h Dark, 6 h Light, 6 h Dark	17 °C
14/10	14 h Light, 10 h Dark	17 °C
16/8	16 h Light, 8 h Dark	17 °C
18/6	18 h Light, 6 h Dark	17 °C
20/4	20 h Light, 4 h Dark	17 °C
L/L	Constant Light	17 °C
'April'	4 h Light, 5 h dusk, 10 h Dark, 5 h Dawn	10 °C–16 °C
'June'	15.5 h Light, 1.5 h dusk, 5.5 h Dark, 1.5 h dawn	14 °C–20 °C
D/D temp	Constant Dark	14 °C–22 °C
L/L temp	Constant Light	14 °C–22 °C

2.3. P. xylostella RNA Collection and Extraction

Whole adult *P. xylostella* male moths were maintained at 20 °C under 12 h:12 h L/D conditions and then collected every 4 h during the last day of L/D and the first day of subsequent D/D conditions (ZT1-5-9-13-17-21-CT1-5-9-13-17-21). Male moths were used exclusively to avoid confounding effects due to sex ratio fluctuations or female egg load [52]. Adult males were snap-frozen at −80 °C for storage and used to extract RNA using the RNAqueous-4PCR kit (Thermo Fisher Scientific, Loughborough, UK). The isolated RNA was treated with DNase 1 and the resulting RNA samples were tested for concentration and quality using a NanoDrop 1000 spectrophotometer (Thermo Fisher Scientific, Loughborough, UK). Samples were aliquoted into an appropriate working volume (used for specific quantitative polymerase chain reaction (qPCR) plate setups) and were kept at −20 °C for short-term storage.

2.4. qPCR Protocol

RNA samples were used as templates for one-step amplification reverse transcriptase quantitative PCR (qPCR) with the PrecisionPLUS OneStep qRT-PCR Master Mix (Primer Design Ltd., Chandler's Ford, UK), with both a SYBR green florescent dye and ROX dye. qPCR was performed using a StepOnePlus Real-Time PCR System (Thermo Fisher Scientific, Loughborough, UK) to quantify proportional levels of specific RNA transcripts between samples [53]. Amplification thresholds were used to calculate the proportional level of primer-specific transcripts present in each RNA sample using the $2^{-\Delta\Delta CT}$ method [54]. *Elongation factor 1 α* (*Ef1α*) was used as a housekeeping reference gene in order to analyse the relative expression of circadian genes *period* (*per*) and *timeless* (*tim*) shown in Table 2. Primers were designed using Primer-3 and Primer-BLAST [55,56] to amplify desired distinct gene transcripts. Adherence to the MIQE guidelines was submitted along with the research [57].

Table 2. Primer pair sequences and amplicon lengths for *P. xylostella* genes of interest used in qPCR experiments, adapted from [58] and tested using qPCR serial dilution for efficiencies and 5% agarose gel electrophoresis to check expected amplicon lengths.

Primer Pair	Forward Sequence	Reverse Sequence	Amplicon Length (bp)	Efficiencies
Ef1α	5′-GCCTCCCTACAGCGAATC-3′	5′-CCTTGAACCAGGGCATCT-3′	162	98.7%
per	5′-CCGCGAAAGAACGTCTAAGG-3′	5′-GTGCTCGTGGTCGTGGTTA-3′	118	108.7%
tim	5′-ACGCTGCTGAGAAATGGACA-3′	5′-CCGCTATCAGGTCCGATGAC-3′	87	105.9%

2.5. Statistical Analyses

ClockLab Analysis Version 6 software was used to analyse and produce graphical representations of *P. xylostella* locomotor activity data at a 30 min resolution in the form of double-plotted actograms, daily activity profiles and chi-square periodograms and to quantify specific associated parameters of both individual moths and populations. Individual moths were assumed to have died and were excluded from the results if their activity stopped permanently during a 6-day analysis interval. Flies were considered rhythmic if they exhibited a significant ($p <= 0.01$) chi-square periodogram amplitude for a period in the circadian range (15–35 h). Relative rhythmic power (RRP) was calculated as the ratio between that amplitude and the associated significance threshold value. Shapiro–Wilk tests were used to test if data met the assumptions required for parametric testing, e.g., normal distribution of data.

Where the assumption of normality was consistently found to be met, comparisons were performed using t-tests or ANOVA with Tukey's multiple comparisons analysis. In cases where some of the data sets violated this assumption, nonparametric analyses (Mann–Whitney U test, Kruskal–Wallis tests with Dunn's multiple comparison post hoc tests) were used instead. The differences between the light- and dark-phase activity counts of individual moths were assessed using Wilcoxon matched-pairs signed rank test. Simple linear regression was used to describe the relationship between dark-phase length and average dark-phase activity counts. The resulting equation was then compared to models assuming constant daily activity or a constant activity rate during the dark phase. Two-sided permutation t-test estimation statistics [59] were used to illustrate the distribution of activity across two halves of experimental days. The CircaCompare R package 0.1.1 [60] was used for the calculation and comparisons of rhythmic activity and expression profiles using rhythmic features (mesor, amplitude and phase) to compare rhythmic patterns between groups of data through cosinusoidal curve fitting.

3. Results

3.1. P. xylostella Circadian Clock Gene Rhythms

The rhythmic profiles of the clock gene transcripts for *tim* and *per* relative to a reference gene (*Ef1α*) were determined by qPCR from total RNA extracted from adult male moths across a 2-day L/D-D/D time course sampled at a 4 h resolution (Figure 1, Table 3). Significant rhythmicity was observed for each clock gene under each environmental condition using cosinusoidal fitting (Supplementary Figure S1, Supplemental Table S1). The transcript profiles for *per* and *tim* closely matched across the entire time course with no significant difference at any time point (Figure 1, Table 3). Both transcripts exhibited a major increase in association with the onset of dusk or subjective dusk.

Table 3. CircaCompare analysis of *per* and *tim* qPCR L/D-D/D transcript profiles. The Rhythm p value corresponds to the data's cosine fit; mesor represents a rhythm-adjusted mean; amplitude reflects the peak-to-trough difference in the fitted curve; phase peak refers to the daily maximum of the fitted curve.

Condition	Rhythm *p* Value	Mesor	Amplitude	Phase Peak
per	3.19^{-7}	1.11	0.34	16.86
tim	3.89^{-7}	1.14	0.42	17.12

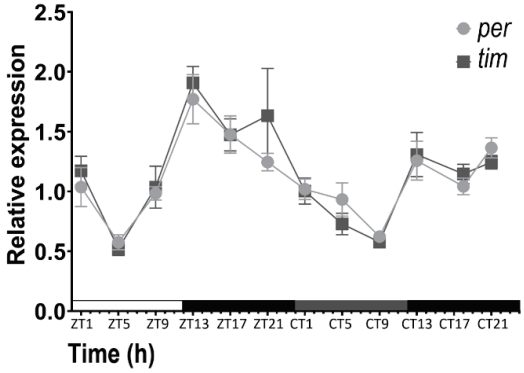


Figure 1. qPCR analysis of *per* and *tim* transcript levels in adult male *P. xylostella* across a 48 h L/D-D/D time course at the indicated L/D (ZT) and D/D (CT) time points. The line graphs show average ± SEM. Relative expression normalised to a reference transcript (*Ef1α*). Six independent biological replicates were used.

3.2. P. xylostella Individual Adult Locomotor Rhythms at Constant Temperature

P. xylostella diel locomotor behaviour was assessed on a sugar/agar substrate using Trikinetics LAM25 monitors at a constant 17 °C for D/D and L/L conditions as well as 12:12, 14:10, 16:8, 18:6 and 20:4 L/D cycles and 6:6:6:6 L/D/L/D cycles (see Figure 2, Supplemental Figures S2 and S3, Table 4, Supplemental Tables S2 and S3). While locomotor behaviour was rhythmic under all L/D cycles, this was not the case for constant D/D or L/L conditions. Moreover, diel activity profiles did not reveal anticipatory features. The activity was increased immediately upon transition from light to dark and then dropped off to a lower level, while the onset of light triggered an immediate and sustained drop in activity. A prior study observed that when placed in 6:6:6:6 L/D/L/D photoperiods, wild-type, but not arrhythmic mutant *Drosophila melanogaster*, exhibited preferential rhythmicity in the circadian range rather than the entrained 12 h L/D cycle [61], such that increased locomotor activity was observed every other 6:6 L/D cycle. However, as is evident from the activity profiles and actograms (see Figure 2, Supplemental Figure S2) as well as comparative analyses of activity levels during the first and second 6:6 L/D phases per cycle (see Supplemental Figure S3), this was not the case for *P. xylostella*. In fact, the differences between the first and second 6:6 L/D phases were no more pronounced than those for the subjective dark versus subjective light phases of the D/D condition, where behaviour was arrhythmic. Thus, no evidence of circadian control of adult locomotor behaviour was uncovered. Instead of clock-mediated rhythmicity, the observed diel locomotor activity patterns exhibited two other regulatory features: (1) light-mediated repression and (2) homeostasis. Beyond the qualitative changes in the activity profiles and actograms, light-mediated repression was demonstrated quantitatively in the significantly reduced activity counts under L/L conditions (Figure 2B, Supplemental Figure S2B) and the preferential activity during the dark phase of L/D cycles versus the subjective dark phases of D/D or L/L cycles (Figure 2D, Supplemental Figure S2D). The data also indicated homeostatic control of diel locomotor activity in the dark as total diel activity was relatively similar across L/D cycles with dark phases varying from 4 to 12 h (Figure 2B, Supplemental Figure S2B), while the dark-phase activity rate was lowest in D/D (Figure 2C, Supplemental Figure S2C). Given very strong light-mediated repression, diel dark-phase activity would be expected to increase proportionally with dark-phase length in the absence of homeostasis. In contrast, homeostatic maintenance of a fixed diel activity level would require proportional decreases in dark-phase activity rates with increasing diel dark-phase length. In fact, the observed adult male and female locomotor activity data were best fit by an intermediate model exhibiting some

level of homeostasis (Figure 3). Though light repression was strong, it was incomplete as the light phase contributed more to total activity in L/D cycles with short dark phases (18:6, 20:4) versus those with equal amounts of light and dark (12:12, 6:6:6:6; Figure 2D, Supplemental Figure S2D).

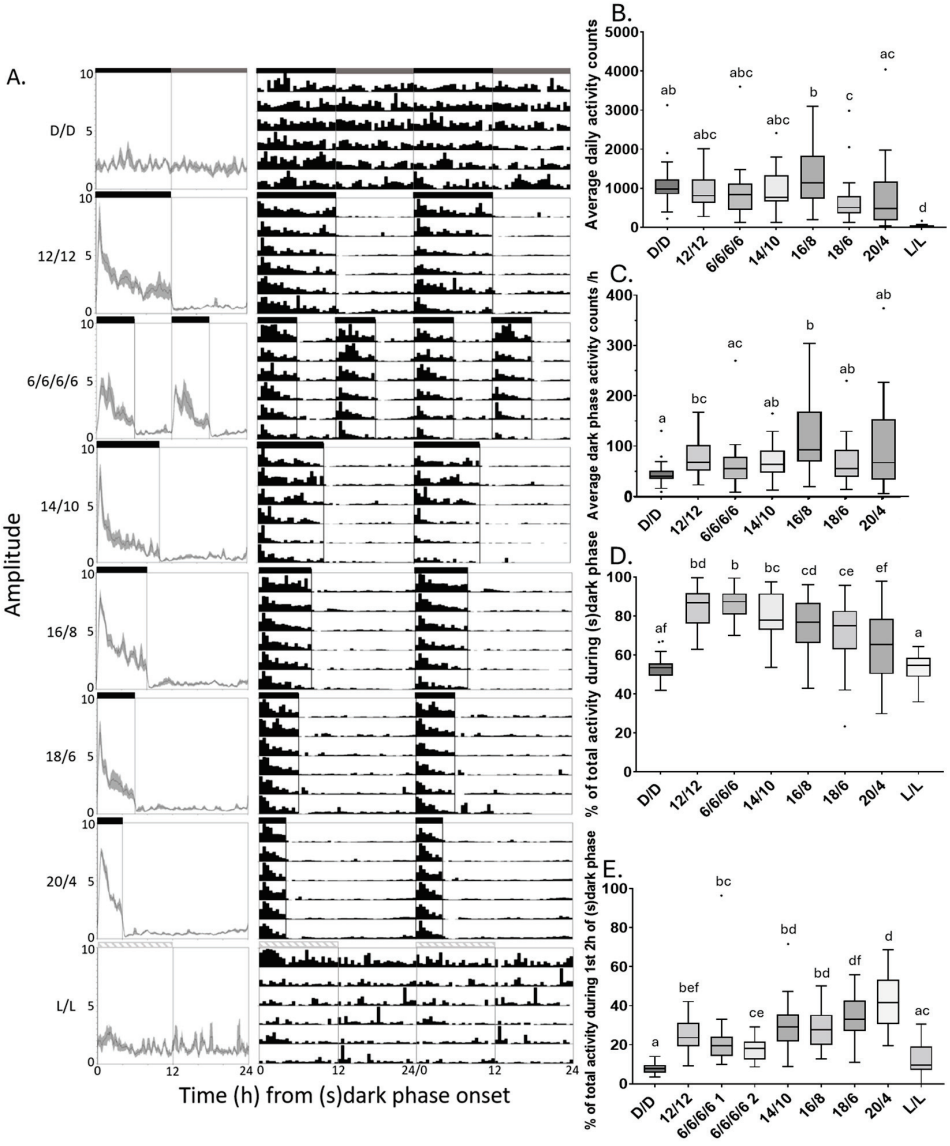


Figure 2. Locomotor behavioural analysis of adult male *P. xylostella* under different lighting conditions. (**A**) Left: normalised average ± SEM daily activity profiles over 6-day intervals for *P. xylostella* adult males. Time is plotted along x-axis in hours (h), starting at the onset of dark or subjective dark phase with normalised activity indicated by the y-axis. Right: double-plotted actograms of normalised average activity of moths over 6 days in 30 min bins. The horizontal bars along the top of individual activity profiles and actograms indicate dark phase (black), subjective dark phase (grey cross hatching), light phase (white) and subjective light phase (grey). (**B**) Total average daily activities, (**C**) average hourly dark-phase activity, (**D**) average % of total activity occurring during (s) dark phase, (**E**) average % of total activity occurring during first 2 h of (s) dark phase. Data points outside Tukey's range (1.5XIQR (Interquartile range)) are shown. Kruskal–Wallis and Dunn's multiple comparison post hoc test results show significant differences from each respective data set through letter grouping system.

Table 4. Periodogram analysis for adult male *P. xylostella* locomotor rhythms. Chi-square periodogram analysis of 6-day data sets for the indicated number (n) of individual males under the indicated conditions. Relative rhythmic power (RRP) was calculated as the ratio between chi-square periodogram amplitude and significance threshold. Condition was found to significantly impact RRP (Kruskal–Wallis test) and Dunn's multiple comparison post hoc test results are annotated in superscript. # indicates that there was only a single rhythmic individual.

Male Condition (n)	% Rhythmic	Period Length (h)	RRP
D/D (23)	4.3	32.5 #	0.85 ±0.02 [a]
12/12 (33)	84.8	23.9 ±0.1	1.31 ±0.05 [bc]
6/6/6/6 (35)	85.7	24.1 ±0.3	1.41 ±0.09 [bc]
14/10 (20)	75.0	23.9 ±0.1	1.22 ±0.07 [b]
16/8 (27)	85.2	24.0 ±0.1	1.41 ±0.09 [bc]
18/6 (33)	87.9	23.8 ±0.2	1.40 ±0.07 [bc]
20/4 (28)	96.4	24.0 ±0.1	1.72 ±0.07 [c]
L/L (26)	11.5	27.2 ±2.1	0.86 ±0.03 [a]

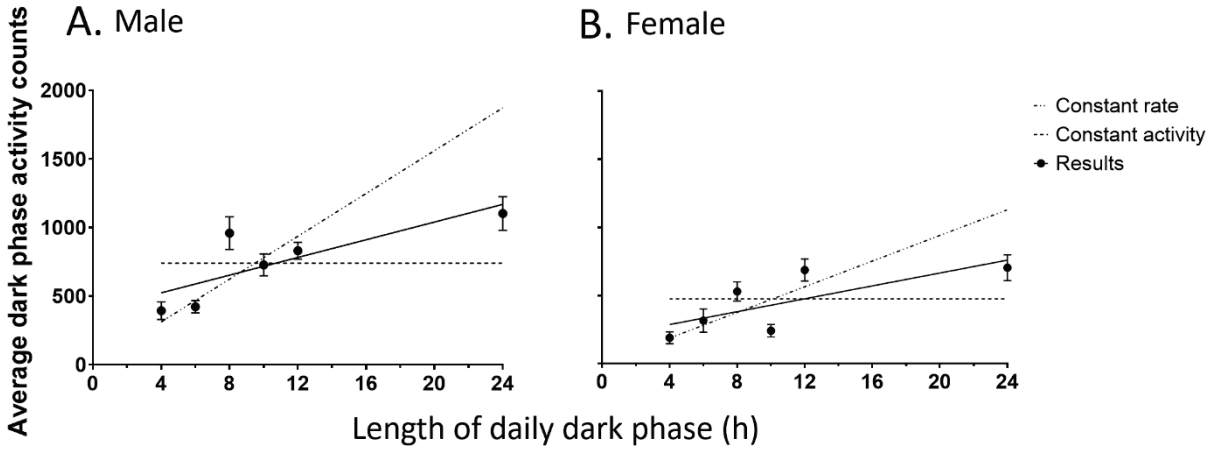


Figure 3. Average dark phase activity as a function of dark-phase duration for *P. xylostella* adult male and female diel locomotor activity. The average ± SEM diel dark-phase activity data are plotted for L/D cycles with 4, 6, 8, 10 and 12 h of dark as well as D/D cycles. The 12 h data represent a combination of the 12:12 L/D and 6:6:6:6 L/D/L/D combinations. A linear regression fit is shown along with theoretical alternatives assuming near-complete light repression representing either a constant dark-phase activity rate or a constant diel activity level.

To follow up on observations by Wang and colleagues [49], who reported weak but significant circadian rhythmicity for the locomotor behaviour of adult male *P. xylostella* of the Geneva 88 strain under 20 °C D/D conditions following prior L/D entrainment, we repeated D/D locomotor analysis for adult male *P. xylostella* of the ROTH strain at 20 °C following L/D entrainment at the same temperature. Again, no behavioural circadian rhythmicity was detected (87.5% arrhythmicity; average RRP 0.82 ± 0.038; Supplemental Figure S4).

3.3. Diel Locomotor Activity Patterns of Individual Adult P. xylostella Males Under Simulated Field Conditions

To better assess diel *P. xylostella* locomotor behaviour under more natural combined light and temperature cycles, we recreated environmental cycles mimicking UK semi-field conditions recorded in Kent in April and June (see [50]). Diel locomotor activity patterns recorded for individual adult males exhibited apparent rhythmicity under both conditions, with both light- and temperature-associated features. Peak activity occurred soon following dark-phase onset, whereas light-phase onset triggered a reduction in activity (Figure 4, Table 5). A significantly larger proportion of diel activity occurred in the dark phase under simulated April conditions, which is consistent with the longer dark phase under these conditions as observed dark-phase activity rates were similar (Figure 4).

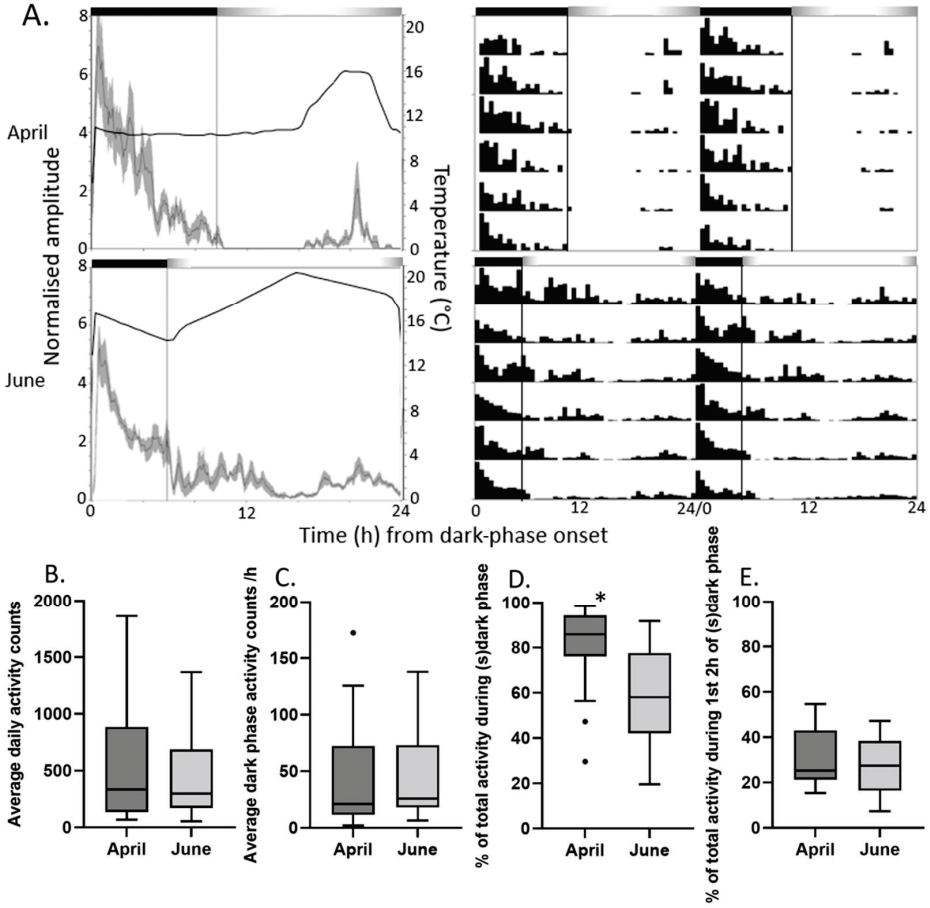


Figure 4. Male adult *P. xylostella* locomotor activity under UK April and June simulation conditions in the lab. (**A**) Left: Average activity profiles show average activity ± SEM (shading) over 24 h of 6-day average activity of 20 *P. xylostella* adult males. Time is plotted along x-axis in hours (h) starting at onset of complete dark phase, with normalised amplitude along y-axis. The black horizontal bar along the top of individual graphs indicates the dark phase with grey-white-grey shaded bars showing the light phase including transitions. A separate line represents the temperature cycle according to the right-hand y-axis. Right: Double-plotted actograms show average activity of moths over 6 days (normalised per 48 h segment) with a 30 min resolution. The environmental light and temperature profiles recorded in the incubators are shown in Supplemental Figure S5B. (**B**) Total average daily counts, (**C**) average hourly dark phase activity, (**D**) average % of total activity occurring during (s) dark phase, (**E**) average % of total activity occurring during first 2 h of (s) dark phase. Data points outside Tukey's range (1.5XIQR (Interquartile range)) are shown. Mann–Whitney U test fresults show significant differences from respective data set through *.

Table 5. Periodogram analysis for *P. xylostella* locomotor rhythms under simulated UK April and June conditions. Chi-square periodogram analysis of 6-day data sets for the indicated number (n) of individual males under the indicated conditions.

Condition (n)	% Rhythmic	Period Length (h)	RRP
April (20)	90%	24.1 ±0.1	1.68 ±0.09
June (20)	80%	24.1 ±0.1	1.56 ±0.13

3.4. Diel Locomotor Activity Behaviour of Individual P. xylostella Males in Response to Temperature Cycles in Constant Light or Constant Dark Conditions

Given the temperature-associated diel locomotor activity features observed under simulated field conditions, we considered the possibility that temperature cycles might induce diel locomotor rhythms in D/D and/or L/L conditions. Significant diel rhythmicity was observed in D/D conditions in the presence of a gradually ramping 14–22 °C temperature cycle, but this was not the case in L/L (see Figure 5, Table 6). Locomotor activity was strongly suppressed by the presence of constant white light and residual activity did not show diel rhythmicity for the large majority of adult male moths. In contrast, in D/D, increased activity was associated with the 12 h phase surrounding peak temperature as well as the 12 h phase associated with rising temperatures.

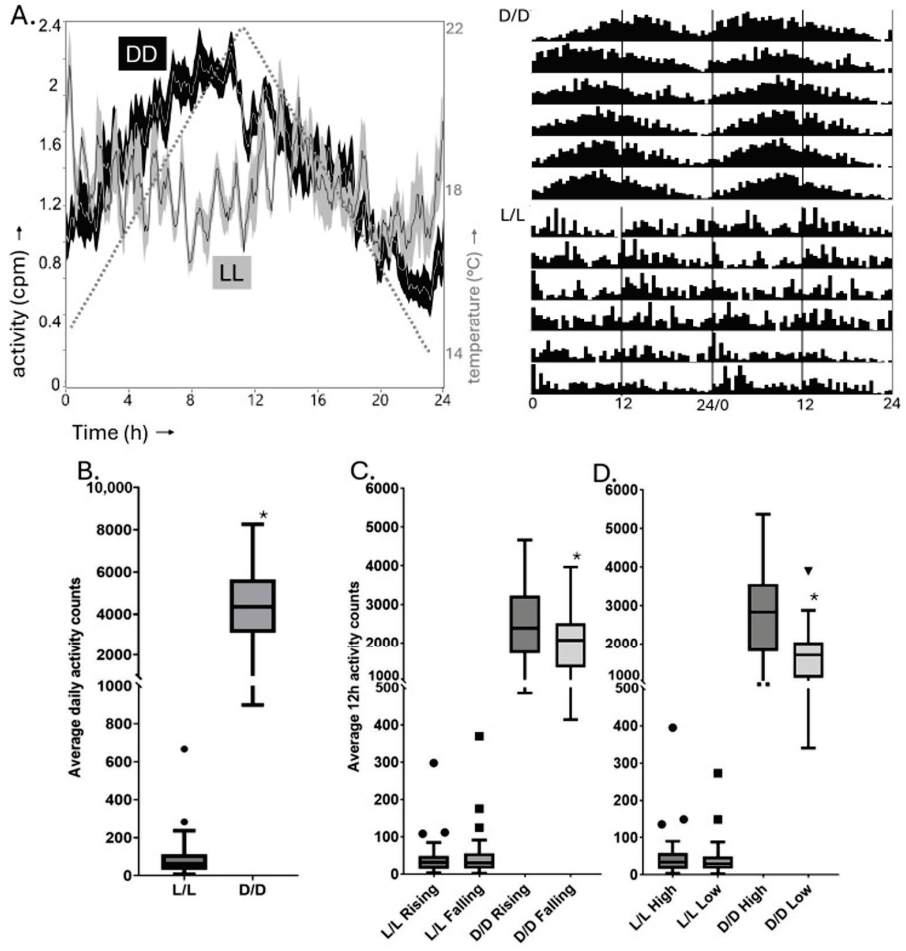


Figure 5. Adult male *P. xylostella* diel locomotor rhythms in D/D or L/L temperature cycle conditions. (**A**) Left: normalised average ± SEM daily activity profiles over 6-day intervals for *P. xylostella* adult

males in D/D (black shading) and L/L (grey shading) conditions. Time is plotted along x-axis in hours (h), starting ~1 h following the temperature cycle trough, with normalised amplitude along y-axis. A separate line represents the temperature cycle according to the right-hand y-axis. Right: double-plotted actograms of normalised average activity of moths over 6 days at a 30 min resolution. (**B**) Total average daily activities, (**C**) average activities during the 12 h intervals of rising and falling temperature, respectively, (**D**) average activities during the 12 h non-overlapping intervals surrounding the temperature high and low points. The Y axes are interrupted to allow inspection of the L/L data at higher resolution. Data points outside Tukey's range (1.5XIQR (Interquartile range)) are shown. Significant differences (Mann–Whitney U test * $p < 0.05$) between conditions in B and between 12 h intervals of the same cycle in (**C**,**D**) are indicated.

Table 6. Constant dark and constant light temperature cycle data. Chi-square periodogram analysis of 6-day data sets for the indicated number (n) of individual males under the indicated conditions. Significant differences in RRP (Mann–Whitney test $p < 0.05$) are annotated ([a] versus [b]).

Condition (n)	% Rhythmic	Period Length (h)	RRP
14–22 D/D (32)	75	24.08 ±0.089	1.36 ±0.090 [a]
14–22 L/L (29)	17	25.80 ±1.98	0.92 ±0.021 [b]

4. Discussion

4.1. Clock Gene Regulation

Our findings that adult *P. xylostella* exhibit rhythmic diel and circadian cycling of *per* and *tim* matches observations of other Lepidopterans [62–65]. Nocturnal moths representing a variety of Lepidopteran families were previously shown to exhibit diel and circadian *per* and *tim* mRNA rhythms with peaks during (subjective) night. This includes the cotton bollworm *Helicoverpa armigera* [65], Mediterranean flour moth *Ephestia kuehniella* [63], Chinese oak silk moth *Antheraea pernyi* [66] and silkworm *Bombyx mori* [67]. We can now add *P. xylostella* as a representative of the superfamily Yponomeutoidea to this list. Moreover, *per* and *tim* transcripts of the day-active monarch butterfly *Danaus plexippus* have also been found to exhibit similar rhythms in L/D and D/D [33,62], confirming that the circadian control of these transcripts is conserved and can be associated with Lepidoptera occupying different temporal niches [68,69]. Under D/D conditions, both *per* and *tim* had lower amplitudes in adult male *P. xylostella* relative expression values compared to L/D, with a significantly reduced rhythmic amplitude for *per* expression. Such damping of clock gene expression in D/D versus L/D conditions has been observed in other Lepidoptera such as *Ephestia kuehniella* [63] and may reflect both a light-mediated enhancement of rhythms as well as a loss of synchrony in peripheral clocks. Tissue-specific studies of molecular circadian rhythms under prolonged free-running conditions may clarify this.

4.2. Absence of Circadian Rhythms in P. xylostella Adult Locomotor Behaviour

Various aspects of Lepidopteran behaviour are known to exhibit control by the circadian clock (as reviewed by [70]). Notably, circadian regulation of adult locomotion or flight has been reported for *Ephestia kuehnellia, Antheraea pernyi, Hyalophoroa cecropia, Samia cynthia ricini*, *Manduca sexta* and *Hyles lineata* [63,71,72]. Though many studied Lepidoptera express rhythms in D/D, there are some that also show a notable weakening of rhythms, including *Hyles lineata* [71] and female *P. interpunctella* [73]. We failed to observe circadian control of adult behaviour in *P. xylostella*. Under constant conditions, adult moths failed to exhibit detectable circadian rhythmicity in their locomotor behaviour. This was true for both males and females at 17 °C in D/D or L/L, as well as males at 20 °C in D/D. Moreover,

there was no evidence of circadian modulation of diel behaviour, which is evidenced by anticipatory increases in activity ahead of light/dark transitions [74] or circadian modulation of non-24 h L/D cycles [61]. In fact, the complete absence of circadian rhythmicity also contrasts with a prior report of weak but significant circadian locomotor rhythms in adult male *P. xylostella* [49]. It should be noted that a number of experimental differences may account for this discrepancy as our work differed in the strain (ROTH versus Geneva 88) and culture method used (culture on *Brassica rapa* versus artificial diet), and there were also subtle differences in the adult setup for locomotor behaviour.

4.3. Light-Mediated Repression of P. xylostella Moth Locomotion

Adaptations to avoid activity under light conditions represent a widely adopted survival strategy [75,76]. Avoiding these activities during light phases is common due to increased risks of predation under light exposure [77]. Moreover, key physiological processes in moths are known to be disrupted by artificial light [78–80]. Light avoidance is particularly well known among nocturnal moths [69] and it has been noted in the study of other behaviours in *P. xylostella* with over 70% of mating and oviposition taking place within the first half of the dark phase in 16/8 conditions [81]. Consistent with these broader principles, our adult moth locomotor activity records demonstrated strong non-circadian responses to changes in lighting conditions with activity levels showing a sudden and sustained decrease upon exposure to light and an immediate temporary increase upon the onset of darkness. Our behavioural analyses under simulated field conditions with dimmable lighting are compatible with *P. xylostella* exhibiting a high level of light sensitivity, with strong activity responses associated with subtle changes in light exposure at the beginning of dawn and the end of dusk. *P. xylostella* may preferentially avoid activity at dawn as predators may use morning light to hunt lingering nocturnal prey, with previous research showing higher predator foraging efficiency around this time [82].

4.4. Homeostatic Regulation of P. xylostella Locomotor Activity

Sleep is known to exhibit a homeostatic component that is independent of circadian control, where the possible accumulation of 'sleep debt' leads to organisms attempting to maintain a certain level of sleep on average [83,84]. Our analyses indicated that homeostasis of diel locomotor activity levels in adult *P. xylostella* at 17 °C across a range of photoperiods with only L/L conditions exhibits a dramatic reduction in activity levels. This phenomenon may at least be in part accounted for by the tendency of adult *P. xylostella* to exhibit a temporary peak in locomotor activity shortly after the onset of darkness.

4.5. Temperature Regulation of diel P. xylostella Adult Locomotor Activity

Our results showed temperature-driven control of adult *P. xylostella* locomotor activity. This may be relevant to impact of both diel and seasonal environmental temperature rhythms. In addition, the impact of temperature on *P. xylostella* activity is relevant in relation to migration across temperature zones [85,86] and the impact of climate change [3]. Notably, the impact of temperature on locomotor activity was abrogated in L/L conditions but appeared to persist in more complex environmental L/D cycles simulating field conditions. This observation could indicate that prolonged light exposure is required for this effect. In many animals prolonged exposure to L/L disrupts the circadian clock and associated behavioural rhythms. In insects such as the monarch butterfly *D. plexippus* [41] and the fruit fly *D. melanogaster* [87], this molecular and behavioural arrhythmicity is mediated via the circadian photoreceptor dCRY. dCRY has an orthologue in *P. xylostella*, which was recently

genetically disrupted [88]. It would be of interest to determine whether *dcry* mutant *P. xylostella* exhibits temperature-mediated modulation of locomotor activity in L/L.

4.6. Disassociation of Locomotor Behaviour Rhythms and Circadian Clock Function

It is unclear why *P. xylostella*'s locomotor activity is governed by light-mediated repression, temperature modulation and homeostatic regulation without exhibiting circadian rhythmicity. One possibility is that the ROTH strain used in this study lost some of its original circadian behaviour after decades of culture under laboratory conditions. Nevertheless, independent observations for the Geneva 88 strain also showed either arrhythmic or weakly circadian behaviour suggesting that *P. xylostella* locomotor behaviour may be largely controlled by alternative means [49]. Perhaps, a homeostatic mechanism in combination with responses to environmental cues is sufficient to drive the onset of temporary peaks in locomotor activity at the onset of darkness. Beyond abiotic time cues such as light and temperature, *P. xylostella* may also respond to rhythmic signals emitted by its host plants. Studies have repeatedly indicated a close relationship between the circadian rhythms of Lepidoptera and host plants [89,90]. Therefore, further research on how *P. xylostella* interacts with its host plants is needed. In this context, it is of interest that *P. xylostella* sexual activity was altered in response to host plant volatiles [81].

It is possible that locomotor activity is an exception and that other relevant rhythmic adult behaviours including feeding, mating and oviposition are circadian clock-controlled [81,91]. Whether migration, which is photoperiodic in a number of insects [92], is controlled by the circadian clock in *P. xylostella* remains to be determined. As noted above, Campos and colleagues found that the modulating photoperiod had no discernible effect on *P. xylostella* morphological and life history traits in a neotropical population [48]. It is possible that temperature rather than photoperiod acts as a migration cue due to its strong effect on the *P. xylostella* life cycle. In *D. plexippus*, a widely researched migratory lepidopteran, migration is triggered via cooling temperatures and is then maintained using circadian clock-assisted compass mechanisms [41,93]. Insensitivity to photoperiodic entrainments may be advantageous to *P. xylostella*, opting for a direct response to light conditions, due to the large changes in light conditions associated with the scale and speed of *P. xylostella* migration [8,94]. Along with temperature, age and affected nutritional quality of host plants may act as a migration cue as it has been shown that older host plants produced *P. xylostella* adults with favourable migratory traits [95].

5. Conclusions

Circadian control of activity rhythms has been described at the behavioural and gene expression levels in both moths and butterflies; however, there can be noticeable species-specific differences between them [62,63,96]. It is therefore unclear how daily timekeeping acts in individual species. We confirmed that light-entrained circadian rhythms of the core clock transcripts *per* and *tim* matched the behaviour of orthologous genes across Lepidoptera [62–65] and other animals [97,98]. This work could be further expanded by determining the circadian transcriptome of *P. xylostella* to further assess the relatedness of its clock mechanisms to those found in other animals. Our findings now provide evidence for the uncoupling of molecular circadian rhythms from adult locomotor behaviour in the economically impactful pest *P. xylostella*. Instead, light-mediated repression, temperature-modulation and homeostasis were identified as important determinants of adult *P. xylostella* diel locomotor behaviour. Our use of simulated field conditions provides new hypotheses regarding the field activity of adult *P. xylostella*. Follow-up studies may link our results to

temporal aspects of integrated pest management strategies for *P. xylostella*, such as those involving chemical treatments and trapping [81,99–102].

Supplementary Materials: The following supporting information can be downloaded at: https://www.mdpi.com/article/10.3390/insects16020182/s1, Figure S1: Comparative analysis of *per* and *tim* L/D and D/D transcript rhythms by cosine fitting; Table S1: Comparative analysis of *per* and *tim* L/D and D/D transcript rhythms by ANOVA; Figure S2: Locomotor behavioural analysis of adult female *P. xylostella* under different lighting conditions; Table S2: Periodogram analysis for adult female *P. xylostella* locomotor rhythms; Table S3: Comparative analysis adult male and female locomotor rhythms by cosine fitting; Figure S3: Phase-associated locomotor activity differences; Figure S4: Adult male *P. xylostella* in 20 °C under 12/12 and D/D light conditions; Figure S5: June and April mimic light and temperature profiles.

Author Contributions: Conceptualization, supervision, project administration, resources and funding acquisition H.W. and H.O.; Author Contributions: methodology, writing—original draft preparation, writing—review and editing, C.J.T., H.W. and H.O.; investigation, software, C.J.T., S.M., L.S. and H.W.; validation, formal analysis, data curation, visualisation C.J.T. and H.W. All authors have read and agreed to the published version of the manuscript.

Funding: C.J.T. and L.S. were funded by the SPITFIRE NERC Doctoral Training Partnership Training Grant NE/L002531/1, while S.M. received funding from the SoCoBio BBSRC Doctoral Training Partnership Training Grant BB/T008768/1.

Institutional Review Board Statement: Not applicable.

Data Availability Statement: All data are available in this paper.

Acknowledgments: We wish to thank the Invertebrate and Plant Growth facilities of the School of Biological Sciences at the University of Southampton as well as the associated technical staff for their support as well as the peer reviewers of our manuscript.

Conflicts of Interest: C.J.T. is presently employed by Syngenta Crop Protection, Bracknell, UK.

References

1. Cribb, J.; De, G. *The Coming Famine: The Global Food Crisis and What We Can Do to Avoid It*, 1st ed.; University of California Press: Berkeley, CA, USA, 2010.
2. Ericksen, P.J.; Ingram, J.S.I.; Liverman, D.M. Food security and global environmental change: Emerging challenges. *Environ. Sci. Policy* **2009**, *12*, 373–377. [CrossRef]
3. Bradshaw, C.J.A.; Leroy, B.; Bellard, C.; Roiz, D.; Albert, C.; Fournier, A.; Barbet-Massin, M.; Salles, J.-M.; Simard, F.; Courchamp, F. Massive yet grossly underestimated global costs of invasive insects. *Nat. Commun.* **2016**, *7*, 12986. [CrossRef]
4. Early, R.; Bradley, B.A.; Dukes, J.S.; Lawler, J.J.; Olden, J.D.; Blumenthal, D.M.; Gonzalez, P.; Grosholz, E.D.; Ibañez, I.; Miller, L.P.; et al. Global threats from invasive alien species in the twenty-first century and national response capacities. *Nat. Commun.* **2016**, *7*, 12485. [CrossRef] [PubMed]
5. Paini, D.R.; Sheppard, A.W.; Cook, D.C.; De Barro, P.J.; Worner, S.P.; Thomas, M.B. Global threat to agriculture from invasive species. *Proc. Natl. Acad. Sci. USA* **2016**, *113*, 7575–7579. [CrossRef]
6. Deutsch, C.A.; Tewksbury, J.J.; Tigchelaar, M.; Battisti, D.S.; Merrill, S.C.; Huey, R.B.; Naylor, R.L. Increase in crop losses to insect pests in a warming climate. *Science* **2018**, *361*, 916–919. [CrossRef]
7. Savary, S.; Willocquet, L.; Pethybridge, S.J.; Esker, P.; McRoberts, N.; Nelson, A. The global burden of pathogens and pests on major food crops. *Nat. Ecol. Evol.* **2019**, *3*, 430–439. [CrossRef]
8. Talekar, N.; Shelton, A. Biology, Ecology, and Management of the Diamondback Moth. *Annu. Rev. Entomol.* **1993**, *38*, 275–301. [CrossRef]
9. Furlong, M.J.; Wright, D.J.; Dosdall, L.M. Diamondback moth ecology and management: Problems, progress, and prospects. *Annu. Rev. Entomol.* **2013**, *58*, 517–541. [CrossRef] [PubMed]
10. Ratzka, A.; Vogel, H.; Kliebenstein, D.J.; Mitchell-Olds, T.; Kroymann, J. Disarming the mustard oil bomb. *Proc. Natl. Acad. Sci. USA* **2002**, *99*, 11223–11228. [CrossRef] [PubMed]

11. Zalucki, M.P.; Shabbir, A.; Silva, R.; Adamson, D.; Shu-Sheng, L.; Furlong, M.J. Estimating the economic cost of one of the world's major insect pests, *Plutella xylostella* (Lepidoptera: Plutellidae): Just how long is a piece of string? *J. Econ. Entomol.* **2012**, *105*, 1115–1129. [CrossRef] [PubMed]
12. Jaleel, W.; Saeed, S.; Saeed, Q.; Naqqash, M.N.; Sial, M.U.; Aine, Q.U.; Yanyuan, L.; Rui, Z.; He, Y.; Lu, L. Effects of three different cultivars of cruciferous plants on the age-stage, two-sex life table traits of *Plutella xylostella* (L.) (Lepidoptera: Plutellidae). *Entomol. Res.* **2019**, *49*, 151–157. [CrossRef]
13. Crafford, J.E.; Chown, S.L. The Introduction and Establishment of the Diamondback Moth (*Plutella xylostella* L., Plutellidae) on Marion Island. In *Antarctic Ecosystems*; Springer: Berlin/Heidelberg, Germany, 1990; pp. 354–358.
14. Tabashnik, B.E.; Liu, Y.B.; Finson, N.; Masson, L.; Heckel, D.G. One gene in diamondback moth confers resistance to four Bacillus thuringiensis toxins. *Proc. Natl. Acad. Sci. USA* **1997**, *94*, 1640–1644. [CrossRef]
15. Xia, X.; Yu, L.; Xue, M.; Yu, X.; Vasseur, L.; Gurr, G.M.; Baxter, S.W.; Lin, H.; Lin, J.; You, M. Genome-wide characterization and expression profiling of immune genes in the diamondback moth, *Plutella xylostella* (L.). *Sci. Rep.* **2015**, *5*, 9877. [CrossRef] [PubMed]
16. Xia, X.; Sun, B.; Gurr, G.M.; Vasseur, L.; Xue, M.; You, M. Gut Microbiota Mediate Insecticide Resistance in the Diamondback Moth, *Plutella xylostella* (L.). *Front. Microbiol.* **2018**, *9*, 25. [CrossRef]
17. Srinivasan, K.; Moorthy, P.N.K. Development and Adoption of Integrated Pest Management for Major Pests of Cabbage Using Indian Mustard as a Trap Crop. In *Management of Diamondback moth and other crucifer pests, Proceedings of the Second International Workshop on Diamondback moth Management, Tainan, Taiwan, 10–14 December 1992*; Asian Vegetable Research and Development Center: Tainan, Taiwan, 1992.
18. Verkerk, R.; Wright, D. Multitrophic interactions and management of the diamondback moth: A review. *Bull. Entomol. Res.* **1996**, *86*, 205–216. [CrossRef]
19. Sayyed, A.H.; Rizvi, M.; Alvi, A.H.K. Management of Diamondback Moth, *Plutella xylostella* (Lepidoptera: Plutellidae): A Lesson from South East Asia for Sustainable Integrated Pest Management. *Pak. J. Biol. Sci.* **2002**, *5*, 234–245. [CrossRef]
20. Birch, A.N.E.; Begg, G.S.; Squire, G.R. How agro-ecological research helps to address food security issues under new IPM and pesticide reduction policies for global crop production systems. *J. Exp. Bot.* **2011**, *62*, 3251–3261. [CrossRef] [PubMed]
21. Philips, C.R.; Fu, Z.; Kuhar, T.P.; Shelton, A.M.; Cordero, R.J. Natural History, Ecology, and Management of Diamondback Moth (Lepidoptera: Plutellidae), With Emphasis on the United States. *J. Integr. Pest Manag.* **2014**, *5*, D1–D11. [CrossRef]
22. Sarfraz, M.; Dosdall, L.M.; Keddie, B.A. Resistance of Some Cultivated Brassicaceae to Infestations by *Plutella xylostella* (Lepidoptera: Plutellidae). *J. Econ. Entomol.* **2007**, *100*, 215–224. [CrossRef]
23. Norton, G.W.; Heinrichs, E.A.; Luther, G.C.; Irwin, M.E. *Globalizing Integrated Pest Management: A Participatory Research Process*; Wiley: Hoboken, NJ, USA, 2008.
24. Uthamasamy; Kannan, M.; Kannan, S.; Arumugam, J. Status, Damage Potential of Diamondback Moth, *Plutella xylostella* (L.) in Tamil Nadu, India. In Proceedings of the Sixth International Workshop on Management of the Diamondback Moth and Other Crucifer Insect Pests, Nakhon Pathom, Thailand, 21–25 March 2011; Asian Vegetable Research and Development Center: Tainan, Taiwan, 2011.
25. Foster, D.L.; Ebling, F.J.; Claypool, L.E. Timing of puberty by photoperiod. *Reprod. Nutr. Dev. (1980)* **1988**, *28*, 349–364. [CrossRef] [PubMed]
26. Cook, S.; Khan, Z.; Pickett, J. The Use of Push-Pull Strategies in Integrated Pest Management. *Annu. Rev. Entomol.* **2007**, *52*, 375–400. [CrossRef]
27. de França, S.M.; Breda, M.O.; Badji, C.A.; de Oliveira, J.V. The Use of Behavioral Manipulation Techniques on Synthetic Insecticides Optimization. In *Insecticides*; Stanislav, T., Ed.; IntechOpen: Rijeka, Yugoslavia, 2013; Ch. 6.
28. Pittendrigh, C.S. Temporal organization: Reflections of a Darwinian clock-watcher. *Annu. Rev. Physiol.* **1993**, *55*, 16–54. [CrossRef]
29. Foster, R.G.; Kreitzman, L. Rhythms of life: The biological clocks that control the daily lives of every living thing. In *Rhythms of Life: The Biological Clocks That Control the Daily Lives of Every Living Thing*; Profile Books: London, UK, 2005; pp. 1–278.
30. Zeng, H.; Qian, Z.; Myers, M.P.; Rosbash, M. A light-entrainment mechanism for the Drosophila circadian clock. *Nature* **1996**, *380*, 129–135. [CrossRef]
31. Huang, R.C. The discoveries of molecular mechanisms for the circadian rhythm: The 2017 Nobel Prize in Physiology or Medicine. *Biomed. J.* **2018**, *41*, 5–8. [CrossRef]
32. Zhu, H.; Yuan, Q.; Briscoe, A.D.; Froy, O.; Casselman, A.; Reppert, S.M. The two CRYs of the butterfly. *Curr. Biol.* **2005**, *15*, R953–R954. [CrossRef]
33. Zhu, H.; Sauman, I.; Yuan, Q.; Casselman, A.; Emery-Le, M.; Emery, P.; Reppert, S.M. Cryptochromes define a novel circadian clock mechanism in monarch butterflies that may underlie sun compass navigation. *PLoS Biol.* **2008**, *6*, e4. [CrossRef] [PubMed]

34. Zhang, R.; Lahens, N.F.; Ballance, H.I.; Hughes, M.E.; Hogenesch, J.B. A circadian gene expression atlas in mammals: Implications for biology and medicine. *Proc. Natl. Acad. Sci. USA* **2014**, *111*, 16219–16224. [CrossRef]
35. Michael, T.P.; McClung, C.R. Enhancer trapping reveals widespread circadian clock transcriptional control in Arabidopsis. *Plant Physiol.* **2003**, *132*, 629–639. [CrossRef] [PubMed]
36. Janszky, I.; Ljung, R. Shifts to and from Daylight Saving Time and Incidence of Myocardial Infarction. *N. Engl. J. Med.* **2008**, *359*, 1966–1968. [CrossRef]
37. Kim, S.-G.; Yon, F.; Gaquerel, E.; Gulati, J.; Baldwin, I.T. Tissue Specific Diurnal Rhythms of Metabolites and Their Regulation during Herbivore Attack in a Native Tobacco, *Nicotiana attenuata*. *PLoS ONE* **2011**, *6*, e26214. [CrossRef]
38. Scheiermann, C.; Kunisaki, Y.; Frenette, P.S. Circadian control of the immune system. *Nat. Rev. Immunol.* **2013**, *13*, 190–198. [CrossRef]
39. Curtis, A.M.; Bellet, M.M.; Sassone-Corsi, P.; O'Neill, L.A. Circadian clock proteins and immunity. *Immunity* **2014**, *40*, 178–186. [CrossRef]
40. Sauman, I.; Hashimi, H. Insect Clocks: What Are They Telling Us Besides Time? *Entomol. Sci.* **1999**, *2*, 589–596.
41. Froy, O.; Gotter, A.L.; Casselman, A.L.; Reppert, S.M. Illuminating the circadian clock in monarch butterfly migration. *Science* **2003**, *300*, 1303–1305. [CrossRef]
42. Robart, A.R.; McGuire, M.M.K.; Watts, H.E. Increasing photoperiod stimulates the initiation of spring migratory behaviour and physiology in a facultative migrant, the pine siskin. *R. Soc. Open Sci.* **2018**, *5*, 180876. [CrossRef] [PubMed]
43. Sockman, K.W.; Hurlbert, A.H. How the effects of latitude on daylight availability may have influenced the evolution of migration and photoperiodism. *Funct. Ecol.* **2020**, *34*, 1752–1766. [CrossRef]
44. Klinner, T.; Schmaljohann, H. Temperature change is an important departure cue in nocturnal migrants: Controlled experiments with wild-caught birds in a proof-of-concept study. *Proc. Biol. Sci.* **2020**, *287*, 20201650. [CrossRef]
45. Burnside, R.J.; Salliss, D.; Collar, N.J.; Dolman, P.M. Birds use individually consistent temperature cues to time their migration departure. *Proc. Natl. Acad. Sci. USA* **2021**, *118*, e2026378118. [CrossRef]
46. Honda, K.-I. Hibernation and Migration of Diamondback Moth in Northern Japan. 2003. Available online: https://www.semanticscholar.org/paper/Hibernation-and-Migration-of-Diamondback-Moth-in-Honda/d349b52cc4c7804254973e79d07150336c5ef947 (accessed on 30 December 2024).
47. Campos, W.G.; Schoereder, J.H.; DeSouza, O.F. Seasonality in neotropical populations of *Plutella xylostella* (Lepidoptera): Resource availability and migration. *Popul. Ecol.* **2006**, *48*, 151–158. [CrossRef]
48. Campos, W.G. Photoperiodism and seasonality in neotropical population of *Plutella xylostella* L. (Lepidoptera: Yponomeutidae). *Neotrop. Entomol.* **2008**, *37*, 365–369. [CrossRef]
49. Wang, D.; Yang, G.; Chen, W. Diel and Circadian Patterns of Locomotor Activity in the Adults of Diamondback Moth (*Plutella xylostella*). *Insects* **2021**, *12*, 727. [CrossRef]
50. Pfeiffenberger, C.; Lear, B.C.; Keegan, K.P.; Allada, R. Locomotor activity level monitoring using the Drosophila Activity Monitoring (DAM) System. *Cold Spring Harb. Protoc.* **2010**, *2010*, pdb.prot5518. [CrossRef]
51. Tahoe, N.M.; Mokhtarzadeh, A.; Curtsinger, J.W. Age-related RNA decline in adult Drosophila melanogaster. *J. Gerontol. A Biol. Sci. Med. Sci.* **2004**, *59*, B896–B901. [CrossRef] [PubMed]
52. Gibson, U.E.; Heid, C.A.; Williams, P.M. A novel method for real time quantitative RT-PCR. *Genome Res.* **1996**, *6*, 995–1001. [CrossRef]
53. Schmittgen, T.D.; Livak, K.J. Analyzing real-time PCR data by the comparative CT method. *Nat. Protoc.* **2008**, *3*, 1101–1108. [CrossRef] [PubMed]
54. Untergasser, A.; Nijveen, H.; Rao, X.; Bisseling, T.; Geurts, R.; Leunissen, J.A. Primer3Plus, an enhanced web interface to Primer3. *Nucleic Acids Res.* **2007**, *35*, W71–W74. [CrossRef] [PubMed]
55. Ye, J.; Coulouris, G.; Zaretskaya, I.; Cutcutache, I.; Rozen, S.; Madden, T.L. Primer-BLAST: A tool to design target-specific primers for polymerase chain reaction. *BMC Bioinform.* **2012**, *13*, 134. [CrossRef] [PubMed]
56. Bustin, S.; Benes, V.; Garson, J.; Hellemans, J.; Huggett, J.; Mueller, R.; Nolan, T.; Shipley, G.; Vandesompele, J.; Wittwer, C. The MIQE Guidelines: Minimum Information for Publication of Quantitative Real-Time PCR Experiments. *Clin. Chem.* **2009**, *55*, 611–622. [CrossRef] [PubMed]
57. Fu, W.; Xie, W.; Zhang, Z.; Wang, S.; Wu, Q.; Liu, Y.; Zhou, X.; Zhou, X.; Zhang, Y. Exploring valid reference genes for quantitative real-time PCR analysis in *Plutella xylostella* (Lepidoptera: Plutellidae). *Int. J. Biol. Sci.* **2013**, *9*, 792–802. [CrossRef] [PubMed]
58. Ho, J.; Tumkaya, T.; Aryal, S.; Choi, H.; Claridge-Chang, A. Moving beyond P values: Data analysis with estimation graphics. *Nat. Methods* **2019**, *16*, 565–566. [CrossRef]
59. Parsons, R.; Parsons, R.; Garner, N.; Oster, H.; Rawashdeh, O. CircaCompare: A method to estimate and statistically support differences in mesor, amplitude and phase, between circadian rhythms. *Bioinformatics* **2019**, *36*, 1208–1212. [CrossRef]

60. Wheeler, D.A.; Hamblen-Coyle, M.J.; Dushay, M.S.; Hall, J.C. Behavior in light-dark cycles of Drosophila mutants that are arrhythmic, blind, or both. *J. Biol. Rhythm.* **1993**, *8*, 67–94. [CrossRef]
61. Shaw, B.; Fountain, M.; Wijnen, H. Control of Daily Locomotor Activity Patterns in Drosophila suzukii by the Circadian Clock, Light, Temperature and Social Interactions. *J. Biol. Rhythm.* **2019**, *34*, 463–481. [CrossRef] [PubMed]
62. Merlin, C.; Gegear, R.J.; Reppert, S.M. Antennal circadian clocks coordinate sun compass orientation in migratory monarch butterflies. *Science* **2009**, *325*, 1700–1704. [CrossRef]
63. Kobelková, A.; Závodská, R.; Sauman, I.; Bazalová, O.; Dolezel, D. Expression of clock genes period and timeless in the central nervous system of the Mediterranean flour moth, Ephestia kuehniella. *J. Biol. Rhythm.* **2015**, *30*, 104–116. [CrossRef] [PubMed]
64. Zhang, J.; Li, S.; Li, W.; Chen, Z.; Guo, H.; Liu, J.; Xu, Y.; Xiao, Y.; Zhang, L.; Arunkumar, K.P.; et al. Circadian regulation of night feeding and daytime detoxification in a formidable Asian pest *Spodoptera litura*. *Commun. Biol.* **2021**, *4*, 286. [CrossRef] [PubMed]
65. Yan, S.; Liu, Y.J.; Zhu, J.L.; Cui, W.N.; Zhang, X.F.; Yang, Y.H.; Liu, X.M.; Zhang, Q.W.; Liu, X.X. Daily expression of two circadian clock genes in compound eyes of *Helicoverpa armigera*: Evidence for peripheral tissue circadian timing. *Insect Sci.* **2019**, *26*, 217–228. [CrossRef]
66. Sauman, I.; Reppert, S.M. Circadian clock neurons in the silkmoth Antheraea pernyi: Novel mechanisms of Period protein regulation. *Neuron* **1996**, *17*, 889–900. [CrossRef]
67. Iwai, S.; Fukui, Y.; Fujiwara, Y.; Takeda, M. Structure and expressions of two circadian clock genes, period and timeless in the commercial silkmoth, Bombyx mori. *J. Insect Physiol.* **2006**, *52*, 625–637. [CrossRef]
68. Kawahara, A.Y.; Breinholt, J.W. Phylogenomics provides strong evidence for relationships of butterflies and moths. *Proc. R. Soc. B Biol. Sci.* **2014**, *281*, 20140970. [CrossRef]
69. Kawahara, A.; Plotkin, D.; Hamilton, C.; Gough, H.; St Laurent, R.; Owens, H.; Homziak, N.; Barber, J. Diel behavior in moths and butterflies: A synthesis of data illuminates the evolution of temporal activity. *Org. Divers. Evol.* **2017**, *18*, 13–27. [CrossRef]
70. Brady, D.; Saviane, A.; Cappellozza, S.; Sandrelli, F. The Circadian Clock in Lepidoptera. *Front. Physiol.* **2021**, *12*, 776826. [CrossRef] [PubMed]
71. Broadhead, G.T.; Basu, T.; von Arx, M.; Raguso, R.A. Diel rhythms and sex differences in the locomotor activity of hawkmoths. *J. Exp. Biol.* **2017**, *220*, 1472–1480. [CrossRef]
72. Truman, J.W.; Riddiford, L.M. Physiology of insect rhythms. 3. The temporal organization of the endocrine events underlying pupation of the tobacco hornworm. *J. Exp. Biol.* **1974**, *60*, 371–382. [CrossRef]
73. Závodská, R.; Fexová, S.; von Wowern, G.; Han, G.B.; Dolezel, D.; Sauman, I. Is the sex communication of two pyralid moths, *Plodia interpunctella* and *Ephestia kuehniella*, under circadian clock regulation? *J. Biol. Rhythm.* **2012**, *27*, 206–216. [CrossRef]
74. Stoleru, D.; Peng, Y.; Agosto, J.; Rosbash, M. Coupled oscillators control morning and evening locomotor behaviour of Drosophila. *Nature* **2004**, *431*, 862–868. [CrossRef]
75. Clark, A.H. Nocturnal animals. *J. Wash. Acad. Sci.* **1914**, *4*, 139–142.
76. Daily, G.C.; Ehrlich, P.R. Nocturnality and species survival. *Proc. Natl. Acad. Sci. USA* **1996**, *93*, 11709–11712. [CrossRef] [PubMed]
77. Longcore, T.; Rich, C. Ecological light pollution. *Front. Ecol. Environ.* **2004**, *2*, 191–198. [CrossRef]
78. Nemec, S.J. Use of Artificial Lighting to Reduce *Heliothis* spp. Populations in Cotton Fields. *J. Econ. Entomol.* **1969**, *62*, 1138–1140. [CrossRef]
79. Sower, L.L.; Shorey, H.H.; Gaston, L.K. Sex Pheromones of Noctuid Moths. XXI. Light: Dark Cycle Regulation and Light Inhibition of Sex Pheromone Release by Females of Trichoplusia ni1,2. *Ann. Entomol. Soc. Am.* **1970**, *63*, 1090–1092. [CrossRef]
80. Svensson, A.M.; Rydell, J. Mercury vapour lamps interfere with the bat defence of tympanate moths (*Operophtera* spp.; Geometridae). *Anim. Behav.* **1998**, *55*, 223–226. [CrossRef] [PubMed]
81. Pivnick, K.A.; Jarvis, B.J.; Gillott, C.; Slater, G.P.; Underhill, E.W. Daily Patterns of Reproductive Activity and the Influence of Adult Density and Exposure to Host Plants on Reproduction in the Diamondback Moth (Lepidoptera: Plutellidae). *Environ. Entomol.* **1990**, *19*, 587–593. [CrossRef]
82. De Kerckhove, D.; Shuter, B.; Abrams, P. Crepuscular Foraging: Do Big Meals Over Small Time Periods Lead to Stable Foraging Rates? 142nd Annual Meeting of the American Fisheries Society: St. Paul, MN, USA, 2012.
83. Cirelli, C.; Bushey, D. Sleep and wakefulness in Drosophila melanogaster. *Ann. N. Y Acad. Sci.* **2008**, *1129*, 323–329. [CrossRef]
84. Deboer, T. Sleep homeostasis and the circadian clock: Do the circadian pacemaker and the sleep homeostat influence each other's functioning? *Neurobiol. Sleep. Circadian Rhythm.* **2018**, *5*, 68–77. [CrossRef] [PubMed]
85. Chapman, J.; Reynolds, D.; Smith, A.; Riley, J.; Pedgley, D.; Woiwod, I. High-altitude migration of the diamondback moth *Plutella xylostella* to the U.K.: A study using radar, aerial netting, and ground trapping. *Ecol. Entomol.* **2002**, *27*, 641–650. [CrossRef]
86. Ke, F.; You, S.; Huang, S.; Chen, W.; Liu, T.; He, W.; Xie, D.; Li, Q.; Lin, X.; Vasseur, L.; et al. Herbivore range expansion triggers adaptation in a subsequently-associated third trophic level species and shared microbial symbionts. *Sci. Rep.* **2019**, *9*, 10314. [CrossRef]

87. Emery, P.; Stanewsky, R.; Hall, J.C.; Rosbash, M. A unique circadian-rhythm photoreceptor. *Nature* **2000**, *404*, 456–457. [CrossRef] [PubMed]
88. Chen, S.P.; Wang, D.F.; Ma, W.F.; Lin, X.L.; Yang, G. Knockout of cryptochrome 1 disturbs the locomotor circadian rhythm and development of *Plutella xylostella*. *Insect Sci.* **2023**, *30*, 1035–1045. [CrossRef] [PubMed]
89. Hoballah, M.E.; Stuurman, J.; Turlings, T.C.; Guerin, P.M.; Connétable, S.; Kuhlemeier, C. The composition and timing of flower odour emission by wild *Petunia axillaris* coincide with the antennal perception and nocturnal activity of the pollinator Manduca sexta. *Planta* **2005**, *222*, 141–150. [CrossRef]
90. Goodspeed, D.; Chehab, E.W.; Min-Venditti, A.; Braam, J.; Covington, M.F. Arabidopsis synchronizes jasmonate-mediated defense with insect circadian behavior. *Proc. Natl. Acad. Sci. USA* **2012**, *109*, 4674–4677. [CrossRef] [PubMed]
91. Lee, S.; Lee, D.-W.; Boo, K.S. Sex Pheromone Composition of the Diamondback Moth, *Plutella xylost el la* (L) in Korea. *J. Asia-Pac. Entomol.* **2005**, *8*, 243–248. [CrossRef]
92. Bradshaw, W.E.; Holzapfel, C.M. What season is it anyway? Circadian tracking vs. photoperiodic anticipation in insects. *J. Biol. Rhythm.* **2010**, *25*, 155–165. [CrossRef] [PubMed]
93. Reppert, S.M.; de Roode, J.C. Demystifying Monarch Butterfly Migration. *Curr. Biol.* **2018**, *28*, R1009–R1022. [CrossRef]
94. Coulson, S.; Hodkinson, I.; Webb, N.; Mikkola, K.; Harrison, J.A.; Pedgley, D. Aerial colonization of high Arctic islands by invertebrates: The diamondback moth *Plutella xylostella* (Lepidoptera: Yponomeutidae) as a potential indicator species. *Divers. Distrib.* **2002**, *8*, 327–334. [CrossRef]
95. Campos, W.; Schoereder, J.; Sperber, C. Does the age of the host plant modulate migratory activity of *Plutella xylostella*? *Entomol. Sci.* **2004**, *7*, 323–329. [CrossRef]
96. Niepoth, N.; Ke, G.; de Roode, J.C.; Groot, A.T. Comparing Behavior and Clock Gene Expression between Caterpillars, Butterflies, and Moths. *J. Biol. Rhythm.* **2018**, *33*, 52–64. [CrossRef] [PubMed]
97. Sehgal, A.; Rothenfluh-Hilfiker, A.; Hunter-Ensor, M.; Chen, Y.; Myers, M.P.; Young, M.W. Rhythmic expression of timeless: A basis for promoting circadian cycles in period gene autoregulation. *Science* **1995**, *270*, 808–810. [CrossRef] [PubMed]
98. Hardin, P.E.; Hall, J.C.; Rosbash, M. Feedback of the Drosophila period gene product on circadian cycling of its messenger RNA levels. *Nature* **1990**, *343*, 536–540. [CrossRef] [PubMed]
99. Furlong, M.J.; Pell, J.K.; Pek Choo, O.; Abdul Rahman, S. Field and laboratory evaluation of a sex pheromone trap for the autodissemination of the fungal entomopathogen Zoophthora radicans (Entomophthorales) by the diamondback moth, *Plutella xylostella* (Lepidoptera: Yponomeutidae). *Bull. Entomol. Res.* **1995**, *85*, 331–337. [CrossRef]
100. Hamby, K.A.; Kwok, R.S.; Zalom, F.G.; Chiu, J.C. Integrating Circadian Activity and Gene Expression Profiles to Predict Chronotoxicity of *Drosophila suzukii* Response to Insecticides. *PLoS ONE* **2013**, *8*, e68472. [CrossRef] [PubMed]
101. Khyati; Malik, I.; Seth, R. Insect clocks: Implication in an effective pest management. *Biol. Rhythm. Res.* **2017**, *48*, 777–788. [CrossRef]
102. Li, P.; Zhu, J.; Qin, Y. Enhanced attraction of *Plutella xylostella* (Lepidoptera: Plutellidae) to pheromone-baited traps with the addition of green leaf volatiles. *J. Econ. Entomol.* **2012**, *105*, 1149–1156. [CrossRef] [PubMed]

Disclaimer/Publisher's Note: The statements, opinions and data contained in all publications are solely those of the individual author(s) and contributor(s) and not of MDPI and/or the editor(s). MDPI and/or the editor(s) disclaim responsibility for any injury to people or property resulting from any ideas, methods, instructions or products referred to in the content.

insects

MDPI

Article

Ultrastructure and Transcriptome Analysis of the Larval Integument in Solitary and Gregarious Phases of *Mythimna separata*

Lingling Li [1,2], Wenmeng Li [3], Jing Liao [1], Junhong Fu [1], Changgeng Dai [1,2], Yang Hu [1,2] and Hongbo Li [1,2,4,*]

[1] Institute of Plant Protection, Guizhou Academy of Agricultural Sciences, Guiyang 550006, China; lilingling2019@163.com (L.L.); liaojing2025@126.com (J.L.); fujunhong231@sina.com (J.F.); ggyydai@163.com (C.D.); huyanggz@126.com (Y.H.)
[2] Guizhou Branch of State Key Laboratory for Biology of Plant Diseases and Insect Pests, Guiyang 550006, China
[3] Key Laboratory of Forest Disaster Warning and Control in Yunnan Province, College of Forestry, Southwest Forestry University, Kunming 650224, China; lwmhbdgh1028@163.com
[4] Key Laboratory of Crop Genetic Resources and Germplasm Innovation in Karst Region, Ministry of Agriculture and Rural Affairs, Guiyang 550006, China
* Correspondence: gzlhb2017@126.com

Simple Summary: Phenotypic plasticity describes the ability of one genotype to produce different phenotypes in response to variable environments. The oriental armyworm, *Mythimna separata*, exhibits phenotypic plasticity in response to changes in population density. Solitary and gregarious phases occur at low and high larval densities, respectively, and lead to morphological, behavioral, and physiological differences. Gregarious larvae generally exhibit a darker body color, but differences in integument ultrastructure and gene expression in the two phases of *M. separata* are largely unknown. In this study, we compared both ultrastructure and differentially expressed genes in the integument of the two larval phases and verified the relevant results. We discovered that gregarious larvae had thicker integuments and more polygonal particles on the cuticle surface than solitary larvae. Many differentially expressed genes were identified relevant to fatty acid synthesis, integument structure, and insecticide detoxification. Our findings provide a valuable resource for understanding the mechanistic basis of behavioral and physiological differences in the two phases of *M. separata*.

Abstract: *Mythimna separata* larvae exhibit both solitary and gregarious phases under low and high population density, respectively; furthermore, differences in morphology, behavior and physiology have been observed in the two phases. The integument plays an essential role in the fitness, general metabolism, communication, and survival of insects; however, differences in the integument ultrastructure and gene expression in the solitary and gregarious phases are largely unknown. In this study, the integument ultrastructure of larvae in the solitary and gregarious phases was compared, and transcriptome analysis was conducted to identify which genes were differentially expressed in the two phases. The results showed that the gregarious larvae had thicker integuments and more polygonal particles on the cuticle surface than solitary larvae. Using the Illumina HiSeq™ sequencing platform, 2774 differentially expressed genes (DEGs) were generated. Among these, many transcripts were identified with roles in the synthesis of fatty acids; structural components of the integument and the insecticide detoxification were differentially expressed in the integument of the two larval phases. qRT-PCR was used to validate expression patterns of the selected transcripts. This study provides a valuable resource for understanding the molecular basis of behavioral and physiological differences in the two phases of *M. separata*.

Keywords: *Mythimna separata*; integument ultrastructure; integument transcriptome; solitary phase; gregarious phase

1. Introduction

Phenotypic plasticity, which describes the ability of one genotype to produce different phenotypes in response to variable environments [1], is a widespread phenomenon in animals. When exposed to different environments, plastic traits will result in altered phenotypes in animals without genetic changes [2]. In general, phenotypes of animals are the outcome of interactions between genetic and environmental factors [3]. More importantly, altered phenotypes in animals are generally associated with higher fitness, which allows the animal to better survive in a rapidly changing environment [4–6]; consequently, phenotypic plasticity has become a hot topic in organismal ecology and evolution.

The oriental armyworm, *Mythimna separata*, is an important polyphagous insect pest that exhibits phenotypic plasticity in response to changes in population density. *M. separata* exhibits solitary and gregarious phases at low and high larval densities, respectively. In the past three decades, obvious differences in *M. separata* morphology, behavior, and physiology have been observed in the solitary and gregarious phases. Gregarious larvae generally exhibit smaller body sizes, a darker body color, and a stronger migratory capability when compared to solitary larvae [7,8]. At the physiological level, gregarious larvae have faster developmental rates, a stronger feeding capability, and a lower food utilization rate as compared to solitary larvae [7]. Most importantly, gregarious larvae display higher immunity and tolerance in response to fungal pathogen ingress [9–11], which may contribute to outbreaks in the field.

The insect integument consists of multiple layers that contain the cuticle and epidermal tissue. This protective outer layer covers the body surface and functions as a physical defense barrier against multiple stressors, including predators [12], pathogens [13], and other environmental stressors [14–16]. The cuticle contains an outer thin epicuticle and an inner thick procuticle. The epicuticle is composed of lipids and lipoproteins, while the procuticle is mostly formed by cuticular proteins and chitin. The epidermal tissue is a cell layer that underlies the insect cuticle and is primarily responsible for the formation of the epidermis and for external morphological changes that occur during insect growth and metamorphosis [12]. To adapt to specific environments, insects have evolved morphologically distinct structural and mechanical properties in their integument. For example, the melanic *Galleria mellonella* larvae have developed different melanin deposition patterns and thicker integuments when compared to non-melanic individuals, which enables them to better resist infection by the entomopathogenic fungus, *Metarhizium brunneum*, at the cuticle interface [13]. Furthermore, pesticide-tolerant insects were shown to develop thicker integument as compared to susceptible ones [14,15]. As described above, the gregarious larvae of *M. separata* exhibit different morphological, behavioral, and physiological traits as compared to solitary ones. However, differences in integument ultrastructure and the accompanying changes in gene expression are largely unknown for the solitary and gregarious phases of *M. separata* larvae.

In this study, the ultrastructure of the integument in solitary and gregarious *M. separata* was compared by scanning electron microscopy (SEM) and transmission electron microscopy (TEM). Furthermore, transcriptome sequencing was performed to identify genes that are differentially expressed in the integument of the two larval phases, and the results were verified by qRT-PCR. Our findings provide a valuable resource for understand-

ing the mechanistic basis of behavioral and physiological differences in the two phases of *M. separata*, and will ultimately be helpful in understanding outbreaks in the field.

2. Materials and Methods

2.1. Insects

The *M. separata* colony used in this study was originally collected in 2014 from corn fields located in Qianxi City, Guizhou, China. The solitary and gregarious phases of *M. separata* were established as described previously [11]. Briefly, solitary larvae were reared individually in a 300 mL cylindrical plastic container, and gregarious larvae were reared in a 1050 mL container at a density of 20 larvae per container. Both larval phases were maintained on a corn-based diet with a 14:10 h light/dark photoperiod at 25 ± 1 °C. After adults emerged, both phases were reared on a 10% honey/water diet.

2.2. Comparison of Larval Integument Properties in the Two Phases of M. separata

The appearance of fifth larval integuments in two phases of *M. separata* was initially photographed with a digital camera (DS-Fi3, Nikon, Tokyo, Japan). For SEM experiments, different integument regions (anterior, middle, and posterior) of the dorsal side were dissected from fifth instar larvae of solitary and gregarious phases. Dissected samples were washed with PBS, placed in fixative for 2 h at room temperature, and maintained at 4 °C until needed. The fixed samples were washed three times in 0.1 M PBS (pH 7.4) for 15 min. Samples were then incubated in 1% OsO_4 in PBS (*v*/*v*) for 1–2 h at room temperature, followed by three more washes in PBS as described above. The fixed cuticles were dehydrated via immersion in a graded series of ethanol (30, 50, 70, 80, 90, and 95%, *v*/*v*) for 15 min each, transferred into 100% ethanol for 15 min (repeated twice), immersed in isoamyl acetate for 15 min, and placed in a critical point dryer. Samples were then attached to metallic stubs using carbon stickers and sputter-coated with gold for 30 s. Samples were then examined with by SEM (TM-1000, Hitachi, Tokyo, Japan). No obvious differences were observed in the ultrastructure of anterior, middle, and posterior regions of integument within the same phase; consequently, we decided to compare the middle regions of integument for differences in the two phases of *M. separata.* Five individuals from each phase were used for SEM analysis.

Integument thickness was compared in fifth instar larvae from the solitary and gregarious phases by TEM as described by Huang et al. [16]. Samples were observed by using a JEM-1210 transmission electron microscope (HT7800, Hitachi, Tokyo, Japan) at 80 kV. Our initial analysis did not reveal any remarkable differences in the cuticles of the two phases of *M. separata*; therefore, cuticular regions were randomly selected for further analysis. Digital images for each sample were recorded and used to measure thickness with Image J software (https://imagej.net/ij/ (accessed on 28 June 2012)). Five areas were selected in each larval integument, and each phase included four individuals.

2.3. RNA Extraction, Library Construction, and Illumina HiSeq™ Sequencing

Samples of both solitary and gregarious integument were collected from three fifth instar larvae. Each sample included three biological replications. Total RNA was extracted using the Eastep® Super Total RNA Isolation Kit according to the manufacturer's instructions (Promega, Madison, WI, USA), and genomic DNA was removed using DNase I (Promega, Madison, WI, USA). RNA quality and concentration were determined by electrophoresis in a 1.2% agarose gel with the Nanodrop Lite Spectrophotometer (Thermo Fisher Scientific, Waltham, MA, USA).

RNA purification, reverse transcription, library construction, and sequencing were conducted by the Bioyigene Sequencing Facility (Wuhan, China). The RNA-seq library was constructed using the NEBNext Ultra RNA Library Prep Kit as recommended by the manufacturer (New England Biolabs, Ipswich, MA, USA). Briefly, mRNA was isolated on oligo(dT) beads and fragmented, and cDNA was synthesized using the SuperScript Double-Stranded cDNA Synthesis Kit (Invitrogen, Carlsbad, CA, USA) with random hexamers (Illumina, San Diego, CA, USA). The synthesized cDNA was repaired, phosphorylated, and adenylated as recommended by Illumina. Libraries were size selected for 200–300 bp cDNA fragments in 2% low-range ultra-pure agarose and were PCR-amplified using Phusion DNA polymerase (New England Biolabs, Ipswich, MA, USA) for 15 cycles. PCR products were quantified with the TBS-380 fluorometer, and the paired-end RNA-seq library was sequenced using the Illumina HiSeq™ platform (HiSeq 2500). The raw paired-end reads were trimmed and the quality was analyzed using SeqPrep (https://github.com/jstjohn/SeqPrep (accessed on 5 October 2016)) and Sickle (https://github.com/najoshi/sickle (accessed on 4 August 2011)) with default parameters. Clean reads were separately aligned to the reference genome of *M. separata* [17] with TopHat v. 2.1.1 (http://tophat.cbcb.umd.edu/ (accessed on 1 April 2010)) [18].

2.4. Differential Expression Analysis and Functional Enrichment

To identify differentially expressed genes (DEGs) in the larval cuticles of the two phases, transcript expression levels were calculated according to the fragments per kilobase of exon per million mapped reads (FPKM). RNA-seq by Expectation-Maximization (RSEM; http://deweylab.biostat.wisc.edu/rsem/ (accessed on 14 February 2020)) was used to quantify gene abundance [19], and the R statistical package EdgeR (http://www.bioconductor.org/packages/2.12/bioc/html/edgeR.html (accessed on 1 January 2010)) was used for differential expression analysis [20]. GO (Gene Ontology) and KEGG (Kyoto Encyclopedia of Genes and Genomes) analyses were performed to identify DEGs significantly enriched in GO terms and metabolic pathways at $p \leq 0.05$. GO functional enrichment and KEGG pathway analysis were conducted using ClusterProfiler (https://github.com/GuangchuangYu/clusterProfiler (accessed on 5 May 2012)) [21].

2.5. Quantitative Real-Time PCR

Quantitative real-time PCR (qRT-PCR) was conducted to verify the reliability of RNA-seq data; this analysis included genes involved in lipid biosynthesis (n = 16), genes encoding cuticular proteins (n = 10), and genes associated with pesticide resistance (n = 9) (Table S1). The first-strand cDNA was synthesized from total RNA of each sample using the protocols included with the iScript cDNA Synthesis Kit (Bio-Rad, Hercules, CA, USA). qRT-PCR was performed with the SsoAdvanced Universal SYBR Green Supermix (Bio-Rad, Hercules, CA, USA) and the CFX96 Real Time PCR System (Bio-Rad, Hercules, CA, USA) using the following parameters: 95 °C for 2 min, followed by 35 cycles of 95 °C for 5 s, and 30 s at 60 °C. Melting curve analysis was conducted to confirm primer specificity, *β-actin* was used as reference gene [22], and expression levels were calculated using the $2^{-\Delta\Delta Ct}$ method [23]. Each sample included three biological replications, and each replication had three technical replications.

2.6. Statistics

Statistical analyses were carried out using the DPS 17.0 statistical package [24]. Datapoints are shown as means ± standard error (SE). Differences in the solitary and gregarious

phases were determined using a two-sample *t*-test with significance levels of $p < 0.05$ (*), $p \leq 0.01$ (**), and $p \leq 0.001$ (***).

3. Results and Discussion

3.1. Comparison of Larval Integument Properties in the Two Phases of M. separata

The integument of gregarious larvae was visibly darker in color than the integument of solitary individuals (Figure 1A,B). SEM analysis showed that more polygonal particles existed in the integument of gregarious larvae than solitary ones, and the edges of polygonal particles in the former was considerably sharper than that in the latter phase. Moreover, the distance between polygonal particles in gregarious individuals was smaller than that in solitary ones (Figure 1C,D). TEM analysis showed that the integument thickness of gregarious larvae (110.13 ± 2.59 μm) was thicker than that of solitary individuals (76.52 ± 7.75 μm) (Figure 2A–C). Similarly, Grizanova et. al. reported that the cuticle of melanic *G. mellonella* larvae was thicker and replete with more melanic spots than that of non-melanic larvae (NM) [13]. These features presumably reduced the ability of conidia to adhere to and germinate on the cuticular surface, which led to lower mortality in melanized larvae when compared to NM individuals [13]. In a previous study, gregarious *M. separata* larvae had higher survival rates than solitary ones when exposed to fungicides [9]. Therefore, we deduced that thicker cuticles in larvae with more particles on the surface contributed to the improved resistance of *M. separata* larvae to pathogens, thereby resulting in the relatively low effectiveness of fungal biopesticides in the field.

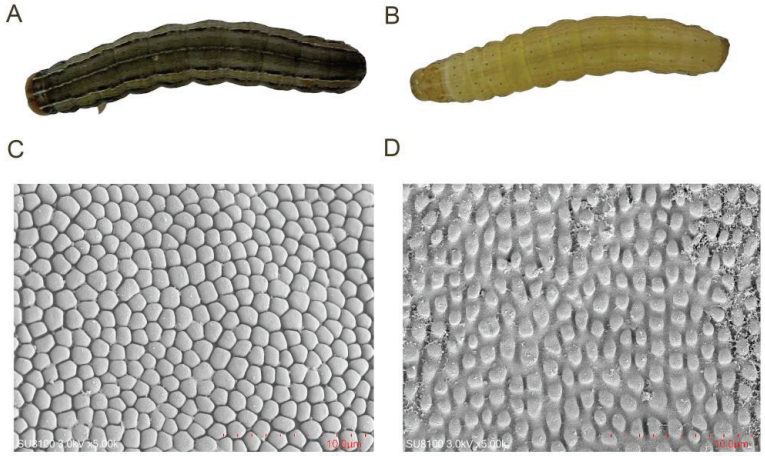


Figure 1. Integument properties in solitary and gregarious *M. separata* larvae. Integument appearance in gregarious (**A**) and solitary (**B**) larvae. Scanning electron microscopy showing differences in the morphology of polygonal particles in gregarious (**C**) and solitary (**D**) larvae.

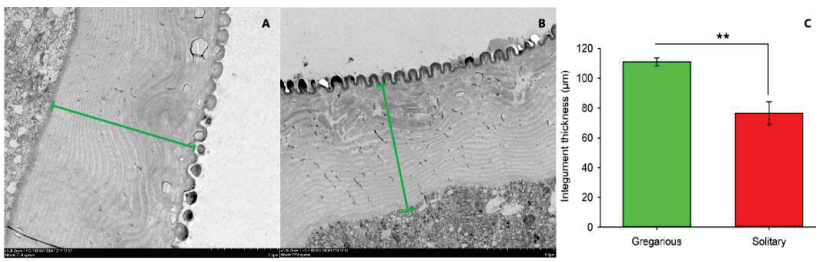


Figure 2. Comparison of integument thickness in different larval phases in *M. separata*. (**A**,**B**) Longitudinal section of the integument in gregarious and solitary larvae, respectively. Images were obtained by scanning electron microscopy. The green line indicates the integument thickness. (**C**) Mean integument thickness in the two phases of larvae using Image J software. Datapoints represent means ($n = 4$) ± standard error (SE). Asterisks indicate significant differences between solitary and gregarious larvae at $p < 0.01$ (**).

3.2. An Overview of the Integument Transcriptome in the Two Phases of M. separata

A total of 47.20 Gb of clean data were acquired using the Illumina HiSeq™ platform. The GC content ranged from 44.82% to 47.25%, and the Q30 rate ranged from 94.64% to 95.40% (Table S2). When these clean data were aligned to the reference genome of *M. separata* [17], a relatively high total mapped ratio (82.09% to 84.72%), multiple mapped ratio (3.61% to 7.20%), and uniquely mapped ratio (75.38% to 79.35%) were observed (Table S3). These results suggest that the quality of the data was high and could be used for further analysis.

3.3. Differential Expression Analysis and Functional Enrichment

Comparative transcriptome analysis revealed that 2774 DEGs were identified in the integument of solitary and gregarious larvae. Among these, 1315 and 1459 genes were upregulated and downregulated in gregarious individuals, respectively (Figure 3).

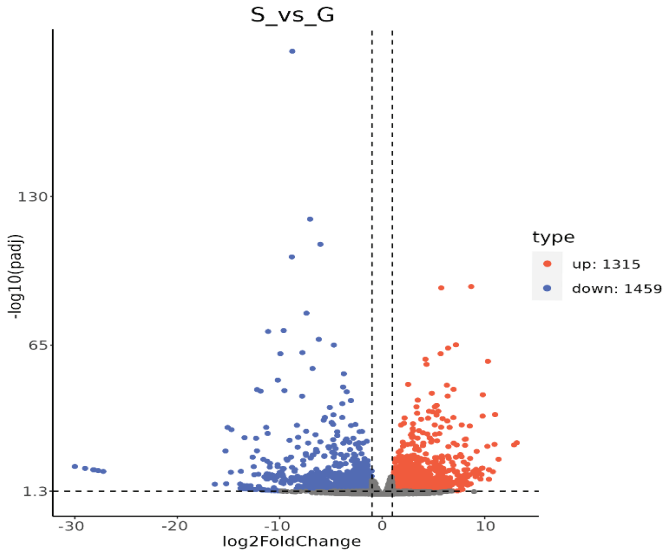


Figure 3. DEGs in the integument of solitary and gregarious *M. separata* larvae. The *x*-axis indicates $\log_2$-fold change and the *y*-axis indicates $-\log_{10}$ significance. Red and green dots represent up- and downregulated unigenes, respectively.

GO functional enrichment analysis of the DEGs was conducted with GOATOOLS (https://github.com/tanghaibao/goatools (accessed on 18 July 2018)), and the 2774 DEGs were classified into three categories, including "biological processes", "molecular functions", and "cellular components". In the biological processes group, DEGs were enriched in "transmembrane transport", "protein folding", and "glycolytic process". In the cellular components group, DEGs were enriched in the "extracellular space" group. With respect to molecular function, DEGs were enriched in "heme binding" and "iron ion binding", followed by "oxidoreductase activity" and "transmembrane transport activity" (Figure 4A).

KEGG analysis showed that the 2774 DEGs could be subdivided into 251 pathways. Among these, gene expression levels in 51 different pathways were significantly changed in the integument of gregarious individuals as compared to solitary ones. These pathways included "biosynthesis of secondary metabolites", "microbial metabolism in diverse environments", "metabolism of xenobiotics by cytochrome P450", "drug metabolism-cytochrome P450", and "carbon metabolism" (Figure 4B). A description of the DEGs and their putative functions in *M. separata* is presented below.

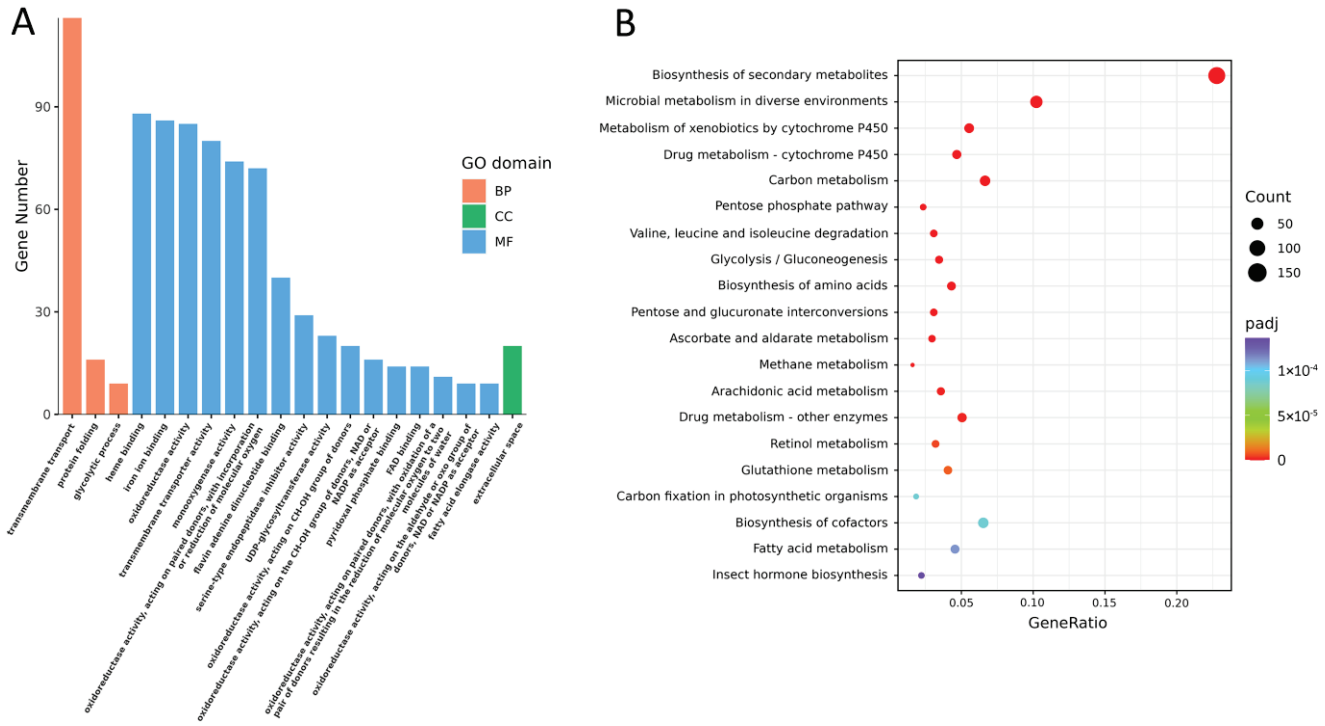


Figure 4. GO functional enrichment and KEGG analysis of DEGs. (**A**) GO analysis of the top 20 enriched pathways in the *M. separata* integument. The *x*-axis indicates the pathways, and the *y*-axis represents the number of DEGs represented in a particular pathway. Abbreviations: BP, biological processes; CC, cellular components; and MF, molecular functions. (**B**) KEGG analysis of the top 20 enriched pathways. The *x*-axis indicates the gene ratio, and the *y*-axis shows the categories. The size of the datapoints reflect a greater level of enrichment. The *q*-values are corrected *p*-values ranging from 0 to 1, with lower values indicating greater enrichment.

3.3.1. Genes Involved in Lipid Biosynthesis and Metabolism

The lipids present in the integument are a complicated mixture of nonpolar chemicals and consist of over 100 compounds, including hydrocarbons (HC), wax esters, fatty alcohols, and free or esterified fatty acids [25]. Among these, the HCs are the most abundant compound in insect lipids. The lipid composition in the integument is variable, and significant differences in composition have been observed among species, different development stages, and between sexes of the same species [26]. Lipid biosynthesis is highly conserved and can be classified into four distinct steps including the synthesis of fatty acid precursors, extension of fatty acid carbon chains, synthesis of very-long-chain fatty aldehydes, and dehydroxylation of very-long-chain fatty aldehydes and synthesis of hydrocarbons [27,28]. Enzymes involved in lipid synthesis include acetyl-CoA carboxylase (ACC), fatty acid synthase (FAS), elongase (ELO), fatty acid desaturase (FAD), fatty acyl-CoA reductase (FAR), and CYP4G (a cytochrome P450 subfamily), which finishes the synthesis of the hydrocarbon chain [25] (Figure 5A).

In this study, 57 transcripts were identified with putative roles in integument lipid metabolism, and 34 genes were associated with lipid biosynthesis pathways. The 34 genes linked to lipid biosynthesis and their relative percentages of the total included 1 gene encoding ACC (1.75%), 3 encoding FAS (5.26%), 9 encoding ELO (15.79%), 10 encoding FAR (17.54%), and 11 encoding FAD (19.39%) (Figure 4B, Table S4). Other genes with potential roles in lipid metabolism were 40.35% of the total number and included genes encoding aldehyde dehydrogenase, 3-hydroxyacyl-CoA dehydrogenase, short-chain 2-methylacyl-CoA dehydrogenase, and alcohol dehydrogenase (AD2) (Figure 5B).

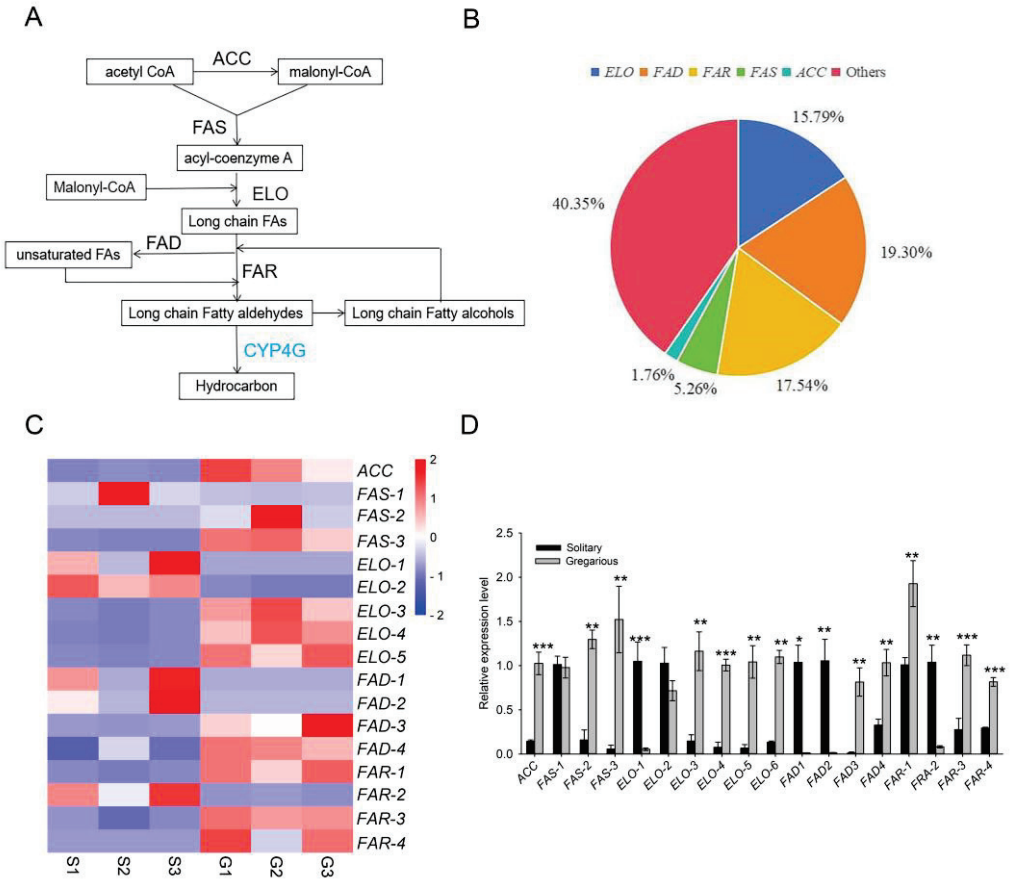


Figure 5. Genes involved in lipid biosynthesis and their expression in the larval integument of solitary and gregarious *M. separata*. (**A**) Diagram of the lipid biosynthesis pathway. Abbreviations: ACC, acetyl-CoA carboxylase; FAS, fatty acid synthase; ELO, elongase; FAD, fatty acid desaturase; and FAR, fatty acyl-CoA reductase. (**B**) Classification of 34 differentially regulated *M. separata* genes with roles in lipid biosynthesis. The pie chart shows relative percentages of the total, and frequencies included *ACC* (1.75%), *FAS* (5.26%), *ELO* (15.79%), *FAR* (17.54%), and *FAD* (19.39%). The other category had a frequency of 40.35% and included genes encoding aldehyde dehydrogenase, 3-hydroxyacyl-CoA dehydrogenase, short-chain 2-methylacyl-CoA dehydrogenase, and alcohol dehydrogenase. RNA-seq (**C**) and qRT-PCR (**D**) analysis of *ACC*, *FAS1–3*, *ELO1–5*, *FAD1–3*, and *FAR1–4* expression in the larval integument of solitary and gregarious *M. separata.* Expression levels in RNA-seq experiments were calculated according to the fragments per kilobase of exon per million mapped reads (FPKM) method. qRT-PCR results were normalized to *β-actin* using the $2^{-\Delta\Delta Ct}$ method. Datapoints represent means (n = 3) ± standard error. Asterisks indicate significant differences between solitary and gregarious larvae at $p < 0.05$ (*); $p < 0.01$ (**); and $p < 0.001$ (***).

3.3.2. Acetyl-CoA Carboxylase

In the de novo hydrocarbon pathway, *ACC* converts acetyl-CoA to malonyl-CoA (Figure 4A), which functions as a substrate for fatty acid synthase [2]. Several studies have shown that *ACC* impacts lipid accumulation, reproduction, and cuticular functions in insects. For example, in *Aedes aegypti*, *ACC*-deficient mosquitoes had lower lipid content and produced defective oocytes that lacked intact eggshells due to *ACC* deficiencies in follicular epithelial cells [29]. In another study, the knockdown of *ACC* transcripts in fat bodies by RNA interference caused a dramatic reduction in triglyceride storage and a concurrent increase in glycogen accumulation in *Drosophila melanogaster* [30]. Furthermore, the mutation of *ACC*-encoding transcripts in oenocytes resulted in oenocyte mortality and caused a failure in the watertightness of spiracles, thus leading to the death of flies [30]. In *Nilaparvata lugens*, Zhang et al. [31] reported that the fungicide jinggangmycin

improved reproduction and upregulated *ACC* transcription, whereas silencing *ACC* eliminated jinggangmycin-enhanced fecundity.

RNA-seq and qRT-PCR analysis confirmed that *ACC* was upregulated in gregarious larvae as compared to solitary individuals (Figure 5C,D). Previous studies showed that the upregulation of *ACC* was associated with insect resistance to selected pesticides [32,33]. Whether the upregulation of *ACC* contributes to enhanced pesticide resistance in gregarious larvae is unknown and warrants further study.

3.3.3. Fatty Acid Synthases

Our results indicated that *FAS*-2 and *FAS*-3 were more highly expressed in the integument of gregarious *M. separata* larvae as compared to solitary individuals (Figure 5C,D). Biochemical experiments have demonstrated that insects contain both microsomal and cytosolic *FAS* [34,35]. The former enzyme is involved in the conversion of methyl-branched precursors to methyl-branched HCs, while the latter is involved in the synthesis and extension of cuticular hydrocarbons (CHCs) [35]. Two or three *FASs* have been reported in Drosophila [36] and related species including *Rhodnius prolixus* [37], *Triatoma infestans* [38], and *Locusta migratoria* [39]. Prior studies showed that Drosophila FAS^{CG3523} was primarily expressed in fat bodies, whereas FAS^{CG3524} and $FAS^{CG17374}$ were predominantly expressed in the integument of oenocytes, suggesting that different *FAS* family members have divergent functions.

FAS function has been studied in several insect species. The RNAi-mediated knockdown of two *L. migratoria FAS* genes led to decreased hydrocarbon levels, reduced desiccation resistance, enhanced cuticular permeability, and increased sensitivity to insecticides [39]. In *R. prolixus* and *Blattella germanica* (L.), *FAS* knockdown reduced fatty acid and hydrocarbon levels in the integument, accelerated water loss, and led to the early death of individuals when subjected to desiccation [40,41]. Cheng et al. [42] showed that *FAS* suppression shortened the lifespan of *Laodelphax striatellus* adult females, inhibited the maturation of oocytes, reduced the expression of genes encoding vitellogenin and vitellogenin receptors, and decreased the production of offspring. In addition, *FAS* participated in cabbage beetle diapause by regulating the lipid accumulation and the expression of stress tolerance genes [43].

In some insects, the composition and amount of fatty acids in the integument contributes to differences in disease resistance [44–47]. We recently demonstrated that gregarious *M. separata* larvae exhibit stronger resistance to entomopathogenic fungi when compared to solitary larvae [9]. In this study, we found that two of the three *M. separata FAS* genes were highly expressed in the integument of gregarious larvae as compared to solitary individuals (Figure 5C,D). It is tempting to speculate that the upregulation of *FASs* contributes to enhanced disease resistance in gregarious larvae, but further evidence is needed to validate this hypothesis.

3.3.4. Fatty Acyl-CoA Elongases

ELO expression in the integument of solitary and gregarious insects was compared by RNA-seq and qRT-PCR. There was variability among the different *ELO* alleles; for example, *ELO1* was upregulated in solitary larvae and downregulated in gregarious larvae. In contrast, there were no significant differences in the expression of *ELO2* in the two phases, whereas *ELO3*, *ELO4*, and *ELO-5* were significantly upregulated in gregarious larvae as compared to solitary larvae (Figure 5C,D).

Fatty acyl-CoA elongases are widely distributed in animals, plants, and microorganisms. In insects, *ELOs* play crucial roles in regulating the biosynthesis of hydrocar-

bons and sex pheromones and affect mating, fecundity, and cuticular functions [48–51]. *ELOs* have been identified in *D. melanogaster*, *Bombyx mori*, *Tribolium castaneum*, *Danaus plexippus*, *Anopheles gambiae*, *Apis mellifera*, *L. migratoria*, *Cyrtotrachelus buqueti*, and *N. lugens* [11,50,52,53]. The number of *ELOs* is variable among species, ranging from seven in *L. migratoria* [52] to 20 in *N. lugens* [54]. *ELO* proteins are characterized by a conserved domain composition, a transmembrane region, and highly conserved HxxHH and YxYY motifs [55].

3.3.5. Fatty Acyl-CoA Reductases

Our RNA-seq and qRT-PCR data consistently indicated that *FAR2* was upregulated in the integument of solitary larvae and significantly downregulated in gregarious larvae (Figure 4C,D). Conversely, *FAR1*, *FAR3,* and *FAR4* were upregulated in gregarious larvae as compared to solitary larvae (Figure 5C,D). The precise roles of the *FAR* orthologs in the two phases are unknown and require further study.

In insects, *FAR* plays an important role in converting carboxylic acids to alcohol during pheromone biosynthesis. The role of *FARs* has been investigated in sex pheromone biosynthesis due to their high specificity and substrate selectivity [56–58]. In *B. mori*, *BmFAR* was specifically expressed in the pheromone gland, and functional experiments showed that *BmFAR* could catalyze the conversion of a sex pheromone precursor to form bombykol [59]. In the Adzuki bean borer, *Ostrinia scapulalis*, a pheromone-specific *FAR,* was involved in converting (Z)-11-tetradecenoic acid to the corresponding alcohol, (Z)-11-tetradecenol [60]. Recently, Cha and Lee found that the knockdown of a pheromone-gland-specific *FAR* reduced the production of a major sex pheromone component and decreased mating in *Maruca vitrata* moths [61].

3.3.6. Fatty Acid Desaturases

FAD1, *FAD2*, *FAD3,* and *FAD4* exhibited contrasting expression patterns. For example, *FAD1* and *FAD2* were highly expressed in the integument of solitary *M. separata* larvae (Figure 5C,D). Interestingly, *FAD3* and *FAD4* were more highly expressed in gregarious larvae. The specific roles of the different *FAD* orthologs in *M. separata* is unknown and warrants further investigation.

FADs catalyze the formation of double bonds in the acyl chains of long-chain fatty acids. One O_2 molecule and two electrons are required for the formation of each double bond, and the number of C atoms in the fatty acyl carbon chain and the position of the desaturated double bond are strictly selected [62,63].

The first insect *FAD* (*desat1*) was identified in *D. melanogaster* [64], and subsequent studies revealed a second allele, *desat2* [65]. Further analysis demonstrated that Desat1 showed specificity to palmitate, whereas Desat2 had substrate specificity for cardamom acid [65]. With the advent of genomic sequencing, large numbers of *FAD*s have been identified and characterized [66–71]. In addition to the fat body and oenocytes, *desat1* was abundant in testes, accessory glands, and ovaries, suggesting that this gene functions in both chemical communication via pheromones and also has a role in reproduction [72]. In soldier beetles, a *FAD* catalyzed the conversion of oleic acid to the 18 carbon precursor of 8 Z-dihydromatricaria acid, a chemical that beetles use to repel avian predators and protect eggs [73]. Collectively, these findings reveal the functional diversity of *FADs* in insects.

3.3.7. Cuticular Proteins

Based on their chitin-binding domains (ChtBD) and conserved motifs, genes encoding cuticular proteins (*CP*) are classified into at least 13 families, including *CPR* (*CP* with Re-

bers and Riddiford (R&R) Consensus), CPAP, TWDL, CPF, CPF-like, CPT, CPLCA, CPLCG, CPLCW, CPLCP, CPCFC, CPG, and apidermin [74]. Many *CPs* have been characterized at the genomic, transcriptomic, or proteomic levels in different insect species and orders [75–79]. The number of characterized *CPs* varies among examined species, ranging from 63 *CPs* in *Pediculus humanuscorporis* to 305 *CPs* in *A. aegypti* [80]; this large range of *CP* genes may be due to differences in insect body sizes and habitats.

Our analysis of the RNA-seq data identified 90 putative *CP* genes in the integument of solitary and gregarious *M. separata*. Based on their deduced amino acid sequence, the 90 *CPs* could be assigned to one of three subfamilies, e.g., *CPRs*, CPH (CP hypothetical), and ungrouped *CPs*. *CPR* was the most abundant subfamily in the larval integument of *M. separata* with 86 genes annotated, and these *CPR*-encoding genes could be further classified into the following subgroups: RR-1 (n = 27), RR-2 (n = 58), and RR-3 (n = 1). In addition to the 86 *CPR* genes, three *CPs* were annotated as CPHs, a family containing presumptive *CPs*. Furthermore, a single *CP* lacking the motifs characteristic of *CPs* was also identified (Figure 6A, Table S5).

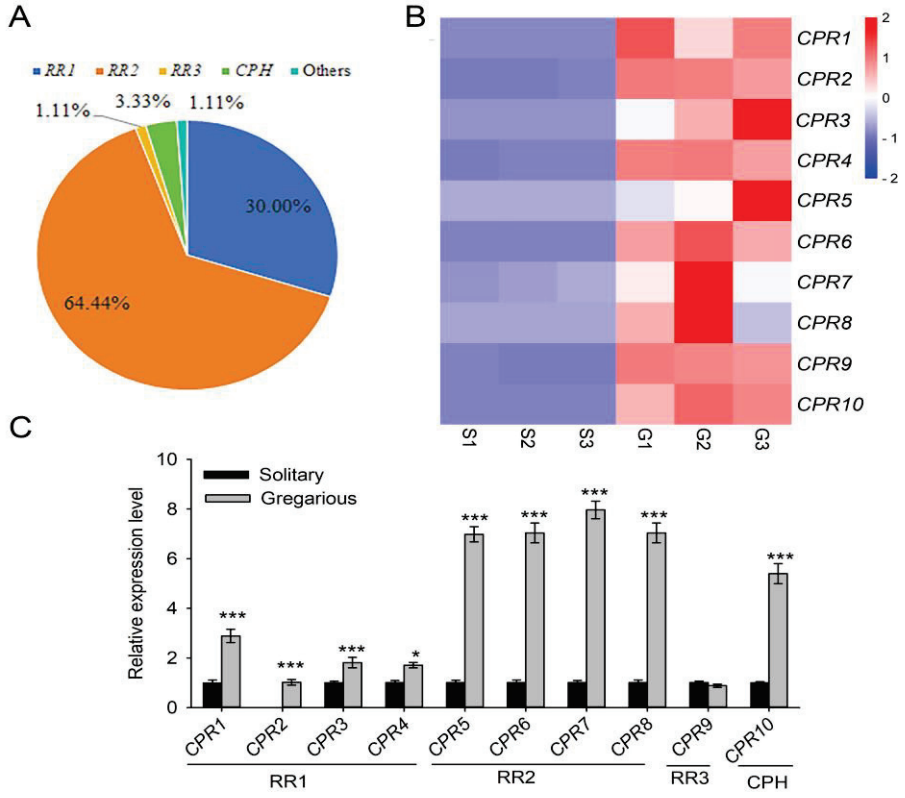


Figure 6. Genes encoding structural cuticular proteins (CPs) and their transcription in the larval integument of solitary and gregarious *M. separata.* (**A**) The classification of the 90 CPs in *M. separata* was based on the presence of the chitin-binding domain (ChtBD) and other conserved motifs. Out of 90 genes, 86 were further categorized into the following *CPRs* (CPs with the Rebers and Riddiford consensus) and included *RR-1* (n = 27), *RR-2* (n = 58), and *RR-3* (n = 1). The remaining *CPs* were categorized as *CPH* (n = 3) and ungrouped *CPs* (n = 1). The diagram shows relative percentages of the total, and frequencies included *RR-1* (30%), *RR-2* (64.4%), *RR-3* (1.11%), *CPH* (3.33%), and ungrouped others (1.11%). RNA-seq (**B**) and qRT-PCR (**C**) analysis of 10 *CPR* genes in the larval integument of solitary and gregarious *M. separata*. The expression level in RNA-seq was calculated as fragments per kilobase of exon per million mapped reads (FPKM). qRT-PCR data points indicate means (n = 3) ± standard error (SE). Asterisks indicated significant differences at $p < 0.05$, (*) and $p < 0.001$ (***).

Based on RNA-seq, we randomly selected 10 genes encoding *CPRs* (*CPR1-10*) and compared their expression profiles in the integument of solitary and gregarious *M. separata* larvae. RNA-seq analysis revealed that all 10 *CPR*s were more highly expressed in the integument of gregarious larvae than in solitary larvae. To verify the reliability of RNA-seq data, the 10 *CPRs* were subjected to qRT-PCR analysis. Our results showed that the expression profiles of *CPR1–8* and *CPR10* were consistent with the RNA-seq results; however, the expression of *CPR9* was not significantly different in the two *M. separata* phases (Figure 6B,C).

In *M. separata*, density-dependent prophylaxis has been observed, and many studies have focused on the immunological and stress response factors responsible for this phenomenon [9,81,82]. Some studies have reported that insects impair the damage caused by pathogen ingress or exposure to chemical pesticides by changing the cuticular structure or thickness [13,14]. Indeed, we found that the exoskeleton of gregarious larvae exhibited different thickness and surface structures than solitary larvae (Figures 1 and 2). Therefore, we hypothesize that larval crowding can cause changes in the cuticular structure of gregarious larvae, and these changes lead to the upregulation of *CPs*, which ultimately enhances resistance to microorganisms in gregarious *M. separata* larvae.

3.3.8. Genes Involved in the Metabolism and Detoxification of Insecticides

Insecticides are widely used to control pests and improve crop yield; however, the extensive use of insecticides has resulted in the development of pesticide-resistant insect populations. The enhanced detoxification and metabolism of insecticides are often the mechanistic basis for resistance, and these processes are often mediated by enzymes such as cytochrome P450s, carboxylesterases, glutathione-S-transferases, and UDP-glucuronosyltransferases [83,84]. Insecticide resistance in field populations of *M. separata* have been observed in China [85,86], but the underlying mechanisms are not completely understood.

In this study, 88 transcripts with putative roles in insecticide resistance were differentially expressed in the solitary and gregarious phases of *M. separata*. Among these, genes encoding cytochrome P450 (*P450*, $n = 46$), UDP-glucuronosyltransferase (*UGT*, $n = 17$), and glutathione-S-transferase (*GST*, $n = 17$) accounted for 51.11%, 19.31, and 19.31% of the total, respectively; other genes accounted for the remaining 9.09% (Figure 7A, Table S6). RNA-seq and qRT-PCR analysis of the nine genes (e.g., *CYP4C1–2*, *GST1–3,* and *UGT1–4*) showed that all were significantly upregulated in the integument of gregarious larvae as compared to that of solitary larvae (Figure 7B,C). The insect integument acts an efficient barrier against adhered pesticide drops, and its role as a penetration factor has been previously reported in several species [15,87,88]. Interestingly, recent studies have demonstrated that several *P450*s were highly expressed in the integument of resistant *Triatoma infestans* nymphs, and the silencing of these genes by RNA interference caused a significant increase in mortality after exposure to deltamethrin [89,90]. Similarly, the knockdown of an integument-enriched esterase gene, *LbEST-inte4*, resulted in a substantial increase in susceptibility to malathion in *Liposcelis bostrychophila* [91]. These results suggest that the insect integument plays an important role in metabolic resistance. Therefore, we hypothesize that upregulation of *P450*s, *GST*s, and *UGT*s might contribute to resistance in the integument tissue of gregarious larvae in *M. separata*. Further functional analysis such as suppression by RNAi is needed to test this hypothesis.

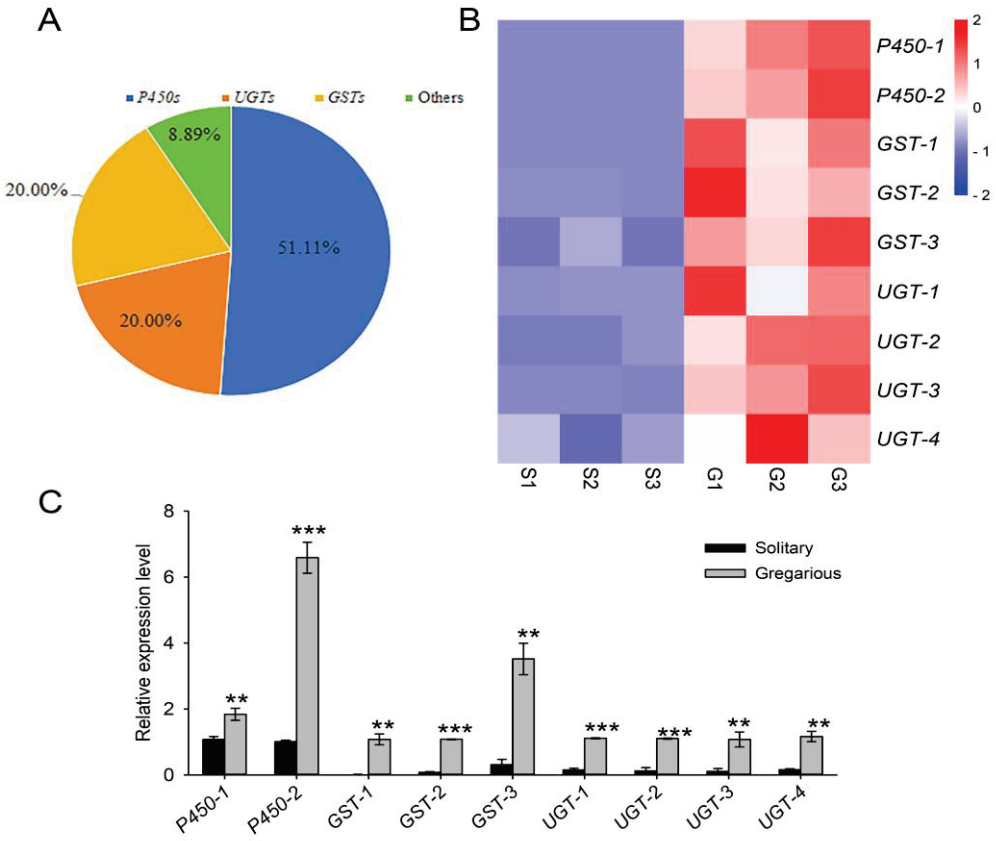


Figure 7. Genes involved in the detoxification and metabolism of insecticides and their expression in the integument of solitary and gregarious *M. separata* larvae. (**A**) Classification of nine genes associated with detoxification and metabolic insecticide resistance. RNA-seq (**B**) and qRT-PCR (**C**) analysis of *CYP4C1–2*, *GST1–3,* and *UGT1–4* in the larval integument of solitary and gregarious *M. separata*. Expression levels in the RNA-seq experiments were calculated according to the FPKM method described above. qRT-PCR results were normalized to *β-actin* expression levels and calculated according to the $2^{-\Delta\Delta Ct}$ method. Datapoints represent means (n = 3) ± standard error (SE). Asterisks indicated significant differences between solitary and gregarious larvae as follows: $p < 0.01$ (**) and $p < 0.001$ (***).

4. Conclusions

In summary, SEM and TEM analysis showed key differences regarding the morphology of the integument in gregarious and solitary *M. separata*. First, the gregarious larval phase exhibited a significantly thicker cuticle than solitary forms. Second, the gregarious phase had a higher density of polygonal particles on the integument surface when compared to solitary larvae. Furthermore, the polygonal particles in gregarious larvae had sharper edges and larger interparticle spaces than solitary larvae. Transcriptome analysis showed that a large number of genes involved in fatty acid synthesis (*ACC*, *FAS*, *ELO*, *FAR*, and *FADs*), integument structure (primarily *CPs*), and insecticide detoxification (*P450s*, *GSTs*, and *UGTs*) were differentially expressed in the integument of solitary and gregarious *M. separata*. These results provide a foundation for future studies focusing on the underlying behavioral and physiological differences in the two phases of *M. separata* larvae.

Supplementary Materials: The following supporting information can be downloaded at https://www.mdpi.com/article/10.3390/insects16020190/s1, Table S1: List of primers used in qRT-PCR experiments. Table S2: Sequencing data obtained from transcriptome analysis of integument in gregarious (G) and solitary (S) *M. separata*. Table S3: Comparison of sequencing data from transcriptome analysis of gregarious (G) and solitary (S) *M. separata* vs. the *M. separata* reference genome. Table S4: List of

differentially expressed genes involved in lipid biosynthesis in the larval integument of solitary and gregarious *M. separata*. Table S5: List of differentially expressed cuticular proteins in the larval integument of solitary and gregarious *M. separata*. Table S6: List of differentially expressed genes associated with pesticide resistance in the larval integument of solitary and gregarious *M. separata*. Sequenced raw reads were deposited in GenBank as accession number PRJNA1171735.

Author Contributions: Conceptualization, L.L. and W.L.; methodology, H.L.; investigation, L.L., W.L., J.L. and J.F.; data curation, L.L., J.L. and C.D.; writing—original draft preparation, L.L.; writing—review and editing, L.L. and H.L.; project administration, Y.H. and H.L.; funding acquisition, Y.H. and H.L. All authors have read and agreed to the published version of the manuscript.

Funding: This work was supported by the National Science Foundation of China (32160641), the Science and Technology Program of Guizhou Province ([2020] IZ022, 2023055), the Post-Foundation for the National Science Foundation of China (202206), the Opening Foundation of the Guizhou Academy of Agricultural Sciences (202403), the Innovation Capacity Construction of Biological Breeding for Specialty Crops in Karst Mountainous Areas (Qianke Hefuqi [2022] 014), The Innovation Capacity Construction of Biological Breeding for Specialty Crops in Karst Mountainous Areas (Qianke Hefuqi [2024] 003-1) and the Construction of Scientific Research Capacity and Conditions for the Provincial Key Laboratory of Biological Breeding of Characteristic Grain and Oil Crops in Karst Mountainous Areas (Qianke Hefuqi [2024] 003-2).

Data Availability Statement: Data are contained within the article.

Acknowledgments: Many thanks are due to Carol Bender for editing the manuscript.

Conflicts of Interest: The authors declare no conflicts of interest.

References

1. Pigliucci, M. *Phenotypic Plasticity, Beyond Nature and Nurture*; JHU Press: Baltimore, MD, USA, 2001.
2. Barber, M.C.; Price, N.T.; Travers, M.T. Structure and Regulation of Acetyl-CoA Carboxylase Genes of Metazoa. *Biochim. Biophys. Acta Mol. Cell Biol. Lipids* **2005**, *1733*, 1–28. [CrossRef] [PubMed]
3. Moffitt, T.E.; Caspi, A. Gene–Environment Interactions in Psychiatry: Joining Forces with Neuroscience. *Nat. Rev. Neurosci.* **2006**, *7*, 583–590.
4. West-Eberhard, M. *Developmental Plasticity and Evolution*; Oxford University Press: Oxford, UK; New York, NY, USA, 2003.
5. Charmantier, A.; McCleery, R.H.; Cole, L.R.; Perrins, C.; Kruuk, L.E.B.; Sheldon, B.C. Adaptive Phenotypic Plasticity in Response to Climate Change in a Wild Bird Population. *Science* **2008**, *320*, 800–803. [CrossRef] [PubMed]
6. Dey, S.; Proulx, S.R.; Teotónio, H. Adaptation to Temporally Fluctuating Environments by the Evolution of Maternal Effects. *PLoS Biol.* **2016**, *14*, e1002388. [CrossRef]
7. Lizhi, L.; Haizhong, X.; Guangbo, L. Effects of Rearing Density on the Food Consumption and Utilization of Larval Oriental Armyworm *Mythimna separata* (Walker). *Acta Entomol. Sin.* **1995**, *38*, 428–435.
8. Bai, Y. *Effects of Larval Density on Growth, Development and Defense Capabilities of the Oriental Army Worm, Mythimna Separata (Lepiotera: Noetuidae)*; Huazhong Agricultural University: Wuhan, China, 2010.
9. Li, H.; Dai, C.; Zhu, Y.; Hu, Y. Larvae Crowding Increases Development Rate, Improves Disease Resistance, and Induces Expression of Antioxidant Enzymes and Heat Shock Proteins in *Mythimna separata* (Lepidoptera: Noetuidae). *J. Econ. Entomol.* **2021**, *114*, 1808–1816. [CrossRef]
10. Kong, H.; Jing, W.; Yuan, L.; Dong, C.; Zheng, M.; Tian, Z.; Hou, Q.; Cheng, Y.; Zhang, L.; Jiang, X.; et al. Bursicon Mediates Antimicrobial Peptide Gene Expression to Enhance Crowded Larval Prophylactic Immunity in the Oriental Armyworm, *Mythimna separata*. *Dev. Comp. Immunol.* **2021**, *115*, 103896. [CrossRef]
11. Li, H.B.; Dai, C.G.; He, Y.F.; Hu, Y.; Shelby, K. Characterization and Expression of Genes Encoding Superoxide Dismutase in the Oriental Armyworm, *Mythimna separata* (Lepidoptera: Noctuidae). *J. Econ. Entomol.* **2019**, *112*, 2381–2388. [CrossRef]
12. Wigglesworth, V. The Physiology of the Cuticle and of Ecdysis in *Rhodnius prolixus* (Triatomidae, Hemiptera); with Special Reference to the Function of the Oenocytes and of the Dermal Glands. *Quart. J. Micr. Sci.* **1933**, *76*, 269–318. [CrossRef]
13. Grizanova, E.V.; Coates, C.J.; Dubovskiy, I.M.; Butt, T.M. Metarhizium Brunneum Infection Dynamics Differ at the Cuticle Interface of Susceptible and Tolerant Morphs of *Galleria mellonella*. *Virulence* **2019**, *10*, 999–1012. [CrossRef]

14. Balabanidou, V.; Grigoraki, L.; Vontas, J. Insect Cuticle: A Critical Determinant of Insecticide Resistance. *Curr. Opin. Insect Sci.* **2018**, *27*, 68–74. [CrossRef] [PubMed]
15. Xu, Y.; Xu, J.; Zhou, Y.; Li, X.; Meng, Y.; Ma, L.; Zhou, D.; Shen, B.; Sun, Y.; Zhu, C. CPR63 Promotes Pyrethroid Resistance by Increasing Cuticle Thickness in *Culex pipiens Pallens*. *Parasites Vectors* **2022**, *15*, 54. [CrossRef]
16. Huang, Y.; Guo, Q.; Sun, X.; Zhang, C.; Xu, N.; Xu, Y.; Zhou, D.; Sun, Y.; Ma, L.; Zhu, C.; et al. *Culex pipiens Pallens* Cuticular Protein CPLCG5 Participates in Pyrethroid Resistance by Forming a Rigid Matrix. *Parasites Vectors* **2018**, *11*, 6. [CrossRef] [PubMed]
17. Tong, D.; Zhang, L.; Wu, N.; Xie, D.; Fang, G.; Coates, B.S.; Sappington, T.W.; Liu, Y.; Cheng, Y.; Xia, J.; et al. The Oriental Armyworm Genome Yields Insights into the Long-Distance Migration of Noctuid Moths. *Cell Rep.* **2022**, *41*, 111843. [CrossRef] [PubMed]
18. Cock, P.J.A.; Fields, C.J.; Goto, N.; Heuer, M.L.; Rice, P.M. The Sanger FASTQ File Format for Sequences with Quality Scores, Based on Profile Hidden Markov Models. *Nucleic Acids Res.* **2010**, *38*, 1767–1771. [CrossRef] [PubMed]
19. Love, M.I.; Huber, W.; Anders, S. Moderated Estimation of Fold Change and Dispersion for RNA-Seq Data with DESeq2. *Genome Biol.* **2014**, *15*, 550. [CrossRef]
20. Robinson Mark, D.; McCarthy Davis, J.; Smyth Gordon, K. EdgeR: A Bioconductor Package for Differential Expression Analysis of Digital Gene Expression Data. *Bioinformatics* **2010**, *26*, 139. [CrossRef]
21. Yu, G.; Wang, L.G.; Han, Y.; He, Q.Y. ClusterProfiler: An R Package for Comparing Biological Themes among Gene Clusters. *Omics A J. Integr. Biol.* **2012**, *16*, 284–287. [CrossRef]
22. Li, H.B.; Dai, C.G.; Zhang, C.R.; He, Y.F.; Ran, H.Y.; Chen, S.H. Screening Potential Reference Genes for Quantitative Real-Time PCR Analysis in the Oriental Armyworm, *Mythimna separata*. *PLoS ONE* **2018**, *13*, e0195096. [CrossRef]
23. Pfaffl, M.W. A New Mathematical Model for Relative Quantification in Real-Time RT–PCR. *Nucleic Acids Res.* **2001**, *29*, e45. [CrossRef]
24. Tang, Q.Y.; Zhang, C.X. Data Processing System (DPS) Software with Experimental Design, Statistical Analysis and Data Mining Developed for Use in Entomological Research. *Insect Sci.* **2013**, *20*, 254–260. [CrossRef] [PubMed]
25. Blomquist, G.J.; Jackson, L.L. Chemistry and Biochemistry of Insect Waxes. *Prog. Lipid Res.* **1979**, *17*, 319–345. [CrossRef] [PubMed]
26. Juárez, M.P.; Fernández, G.C. Cuticular Hydrocarbons of Triatomines. *Comp. Biochem. Physiol. A Mol. Integr. Physiol.* **2007**, *147*, 711–730. [CrossRef]
27. Chung, H.; Carroll, S.B. Wax, Sex and the Origin of Species: Dual Roles of Insect Cuticular Hydrocarbons in Adaptation and Mating. *BioEssays* **2015**, *37*, 822–830. [CrossRef]
28. Blomquist, G.J.; Ginzel, M.D. Chemical Ecology, Biochemistry, and Molecular Biology of Insect Hydrocarbons. *Annu. Rev. Entomol.* **2021**, *66*, 45–60. [CrossRef]
29. Alabaster, A.; Isoe, J.; Zhou, G.; Lee, A.; Murphy, A.; Day, W.A.; Miesfeld, R.L. Deficiencies in Acetyl-CoA Carboxylase and Fatty Acid Synthase 1 Differentially Affect Eggshell Formation and Blood Meal Digestion in *Aedes Aegypti*. *Insect Biochem. Mol. Biol.* **2011**, *41*, 946–955. [CrossRef]
30. Parvy, J.P.; Napal, L.; Rubin, T.; Poidevin, M.; Perrin, L.; Wicker-Thomas, C.; Montagne, J. Drosophila melanogaster Acetyl-CoA-Carboxylase Sustains a Fatty Acid-Dependent Remote Signal to Waterproof the Respiratory System. *PLoS Genet.* **2012**, *8*, e1002925. [CrossRef]
31. Zhang, Y.X.; Ge, L.Q.; Jiang, Y.P.; Lu, X.L.; Li, X.; Stanley, D.; Song, Q.S.; Wu, J.C. RNAi Knockdown of Acetyl-CoA Carboxylase Gene Eliminates Jinggangmycin-Enhanced Reproduction and Population Growth in the Brown Planthopper, *Nilaparvata lugens*. *Sci. Rep.* **2015**, *5*, 15360. [CrossRef]
32. Xi, J.; Pan, Y.; Wei, Z.; Yang, C.; Gao, X.; Peng, T.; Bi, R.; Liu, Y.; Xin, X.; Shang, Q. Proteomics-Based Identification and Analysis Proteins Associated with Spirotetramat Tolerance in Aphis *Gossypii glover*. *Pestic. Biochem. Physiol.* **2015**, *119*, 74–80. [CrossRef]
33. Pan, Y.; Zhu, E.; Gao, X.; Nauen, R.; Xi, J.; Peng, T.; Wei, X.; Zheng, C.; Shang, Q. Novel Mutations and Expression Changes of Acetyl-Coenzyme A Carboxylase Are Associated with Spirotetramat Resistance in Aphis *Gossypii glover*. *Insect Mol. Biol.* **2017**, *26*, 383–391. [CrossRef]
34. Juarez, M.P.; Ayala, S.; Brenner, R.R. Methyl-Branched Fatty Acid Biosynthesis in *Triatoma infestans*. *Insect Biochem. Mol. Biol.* **1996**, *26*, 599–605. [CrossRef]
35. Juárez, P.; Chase, J.; Blomquist, G.J. A Microsomal Fatty Acid Synthetase from the Integument of *Blattella germanica* Synthesizes Methyl-Branched Fatty Acids, Precursors to Hydrocarbon and Contact Sex Pheromone. *Arch. Biochem. Biophys.* **1992**, *293*, 333–341. [CrossRef] [PubMed]
36. St. Pierre, S.E.; Ponting, L.; Stefancsik, R.; McQuilton, P. FlyBase 102—Advanced Approaches to Interrogating FlyBase. *Nucleic Acids Res.* **2014**, *42*, D780–D788. [CrossRef] [PubMed]

37. Majerowicz, D.; Calderón-Fernández, G.M.; Alves-Bezerra, M.; De Paula, I.F.; Cardoso, L.S.; Juárez, M.P.; Atella, G.C.; Gondim, K.C. Lipid Metabolism in *Rhodnius prolixus*: Lessons from the Genome. *Gene* **2017**, *596*, 27–44. [CrossRef]
38. Calderón-Fernández, G.M.; Moriconi, D.E.; Dulbecco, A.B.; Patricia Juárez, M. Transcriptome Analysis of the *Triatoma infestans* (Hemiptera: Reduviidae) Integument. *J. Med. Entomol.* **2017**, *54*, 1531–1542. [CrossRef]
39. Yang, Y.; Zhao, X.; Niu, N.; Zhao, Y.; Liu, W.; Moussian, B.; Zhang, J. Two Fatty Acid Synthase Genes from the Integument Contribute to Cuticular Hydrocarbon Biosynthesis and Cuticle Permeability in *Locusta migratoria*. *Insect Mol. Biol.* **2020**, *29*, 555–568. [CrossRef]
40. Moriconi, D.E.; Dulbecco, A.B.; Juárez, M.P.; Calderón-Fernández, G.M. A Fatty Acid Synthase Gene (FASN3) from the Integument Tissue of *Rhodnius prolixus* Contributes to Cuticle Water Loss Regulation. *Insect Mol. Biol.* **2019**, *28*, 850–861. [CrossRef]
41. Pei, X.J.; Chen, N.; Bai, Y.; Qiao, J.W.; Li, S.; Fan, Y.L.; Liu, T.X. BgFas1: A Fatty Acid Synthase Gene Required for Both Hydrocarbon and Cuticular Fatty Acid Biosynthesis in the German Cockroach, *Blattella germanica* (L.). *Insect Biochem. Mol. Biol.* **2019**, *112*, 103203. [CrossRef]
42. Cheng, J.Y.; Yu, P.H.; Xia, X.; Zhang, R.; Wang, L.H.; Fang, J.C.; Hoffmann, A.A.; Luo, G.H. Identification of a Fatty Acid Synthase Gene (FAS1) from *Laodelphax striatellus* Planthoppers Contributing to Fecundity. *Insect Sci.* **2023**, *30*, 599–610. [CrossRef]
43. Tan, Q.Q.; Liu, W.; Zhu, F.; Lei, C.L.; Wang, X.P. Fatty Acid Synthase 2 Contributes to Diapause Preparation in a Beetle by Regulating Lipid Accumulation and Stress Tolerance Genes Expression. *Sci. Rep.* **2017**, *7*, 40509. [CrossRef]
44. Gołębiowski, M.; Maliński, E.; Boguś, M.I.; Kumirska, J.; Stepnowski, P. The Cuticular Fatty Acids of *Calliphora vicina*, *Dendrolimus pini* and *Galleria mellonella* Larvae and Their Role in Resistance to Fungal Infection. *Insect Biochem. Mol. Biol.* **2008**, *38*, 619–627. [CrossRef] [PubMed]
45. Gołębiowski, M.; Cerkowniak, M.; BoguŚ, M.I.; Włóka, E.; Dawgul, M.; Kamysz, W.; Stepnowski, P. Free Fatty Acids in the Cuticular and Internal Lipids of *Calliphora vomitoria* and Their Antimicrobial Activity. *J. Insect Physiol.* **2013**, *59*, 416–429. [CrossRef] [PubMed]
46. Urbanek, A.; Szadziewski, R.; Stepnowski, P.; Boros-Majewska, J.; Gabriel, I.; Dawgul, M.; Kamysz, W.; Sosnowska, D.; Gołeogonekbiowski, M. Composition and Antimicrobial Activity of Fatty Acids Detected in the Hygroscopic Secretion Collected from the Secretory Setae of Larvae of the Biting Midge *Forcipomyia nigra* (Diptera: Ceratopogonidae). *J. Insect Physiol.* **2012**, *58*, 1265–1276. [CrossRef]
47. Wrońska, A.K.; Boguś, M.I.; Włóka, E.; Kazek, M.; Kaczmarek, A.; Zalewska, K. Cuticular Fatty Acids of *Galleria mellonella* (Lepidoptera) Inhibit Fungal Enzymatic Activities of Pathogenic Conidiobolus Coronatus. *PLoS ONE* **2018**, *13*, e0192715. [CrossRef]
48. Chertemps, T.; Duportets, L.; Labeur, C.; Ueda, R.; Takahashi, K.; Saigo, K.; Wicker-Thomas, C. A Female-Biased Expressed Elongase Involved in Long-Chain Hydrocarbon Biosynthesis and Courtship Behavior in *Drosophila melanogaster*. *Proc. Natl. Acad. Sci. USA* **2007**, *104*, 4273–4278. [CrossRef]
49. Jung, A.; Hollmann, M.; Schäfer, M.A. The Fatty Acid Elongase NOA Is Necessary for Viability and Has a Somatic Role in *Drosophila* Sperm Development. *J. Cell Sci.* **2007**, *120*, 2924–2934. [CrossRef]
50. Zhao, X.; Yang, Y.; Niu, N.; Zhao, Y.; Liu, W.; Ma, E.; Moussian, B.; Zhang, J. The Fatty Acid Elongase Gene LmELO7 Is Required for Hydrocarbon Biosynthesis and Cuticle Permeability in the Migratory Locust, *Locusta migratoria*. *J. Insect Physiol.* **2020**, *123*, 104052. [CrossRef]
51. Pei, X.J.; Fan, Y.L.; Bai, Y.; Bai, T.T.; Schal, C.; Zhang, Z.F.; Chen, N.; Li, S.; Liu, T.X. Modulation of Fatty Acid Elongation in Cockroaches Sustains Sexually Dimorphic Hydrocarbons and Female Attractiveness. *PLoS Biol.* **2021**, *19*, e3001330. [CrossRef]
52. Zuo, W.; Li, C.; Luan, Y.; Zhang, H.; Tong, X.; Han, M.; Gao, R.; Hu, H.; Song, J.; Dai, F.; et al. Genome-Wide Identification and Analysis of Elongase of Very Long Chain Fatty Acid Genes in the Silkworm, *Bombyx mori*. *Genome* **2018**, *61*, 167–176. [CrossRef]
53. Fu, C.; Yang, T.; Liao, H.; Huang, Y.; Wang, H.; Long, W.; Jiang, N.; Yang, Y. Genome-Wide Identification and Molecular Evolution of Elongation Family of Very Long Chain Fatty Acids Proteins in *Cyrtotrachelus Buqueti*. *BMC Genomics* **2024**, *25*, 758. [CrossRef]
54. Li, D.T.; Chen, X.; Wang, X.Q.; Moussian, B.; Zhang, C.X. The Fatty Acid Elongase Gene Family in the Brown Planthopper, *Nilaparvata lugens*. *Insect Biochem. Mol. Biol.* **2019**, *108*, 32–43. [CrossRef] [PubMed]
55. Jakobsson, A.; Westerberg, R.; Jacobsson, A. Fatty Acid Elongases in Mammals: Their Regulation and Roles in Metabolism. *Prog. Lipid Res.* **2006**, *45*, 237–249. [CrossRef] [PubMed]
56. Lassance, J.M.; Groot, A.T.; Liénard, M.A.; Antony, B.; Borgwardt, C.; Andersson, F.; Hedenström, E.; Heckel, D.G.; Löfstedt, C. Allelic Variation in a Fatty-Acyl Reductase Gene Causes Divergence in Moth Sex Pheromones. *Nature* **2010**, *466*, 486–489. [CrossRef]
57. Teerawanichpan, P.; Robertson, A.J.; Qiu, X. A Fatty Acyl-CoA Reductase Highly Expressed in the Head of Honey Bee (*Apis mellifera*) Involves Biosynthesis of a Wide Range of Aliphatic Fatty Alcohols. *Insect Biochem. Mol. Biol.* **2010**, *40*, 641–649. [CrossRef]

58. Antony, B.; Ding, B.J.; Moto, K.; Aldosari, S.A.; Aldawood, A.S. Two Fatty Acyl Reductases Involved in Moth Pheromone Biosynthesis. *Sci. Rep.* **2016**, *6*, 29927. [CrossRef]
59. Moto, K.; Yoshiga, T.; Yamamoto, M.; Takahashi, S.; Okano, K.; Ando, T.; Nakata, T.; Matsumoto, S. Pheromone Gland-Specific Fatty-Acyl Reductase of the Silkmoth, *Bombyx mori*. *Proc. Natl. Acad. Sci. USA* **2003**, *100*, 9156–9161. [CrossRef]
60. Antony, B.; Fujii, T.; Moto, K.; Matsumoto, S.; Fukuzawa, M.; Nakano, R.; Tatsuki, S.; Ishikawa, Y. Pheromone-Gland-Specific Fatty-Acyl Reductase in the Adzuki Bean Borer, *Ostrinia scapulalis* (Lepidoptera: Crambidae). *Insect Biochem. Mol. Biol.* **2009**, *39*, 90–95. [CrossRef]
61. Cha, W.H.; Lee, D.W. Suppression of Pheromone Biosynthesis and Mating Behavior by RNA Interference of Pheromone Gland-Specific Fatty Acyl Reductase in *Maruca vitrata*. *Insect Sci.* **2022**, *29*, 1135–1144. [CrossRef]
62. Guillou, H.; Zadravec, D.; Martin, P.G.P.; Jacobsson, A. The Key Roles of Elongases and Desaturases in Mammalian Fatty Acid Metabolism: Insights from Transgenic Mice. *Prog. Lipid Res.* **2010**, *49*, 186–199. [CrossRef]
63. Haritos, V.S.; Horne, I.; Damcevski, K.; Glover, K.; Gibb, N. Unexpected Functional Diversity in the Fatty Acid Desaturases of the Flour Beetle *Tribolium castaneum* and Identification of Key Residues Determining Activity. *Insect Biochem. Mol. Biol.* **2014**, *51*, 62–70. [CrossRef]
64. Wicker-Thomas, C.; Henriet, C.; Dallerac, R. Partial Characterization of a Fatty Acid Desaturase Gene in *Drosophila melanogaster*. *Insect Biochem. Mol. Biol.* **1997**, *27*, 963–972. [CrossRef] [PubMed]
65. Dallerac, R.; Labeur, C.; Jallon, J.; Knipple, D.; Roelofs, W.; Wicker-Thomas, C. A Delta 9 Desaturase Gene with a Different Substrate Specificity Is Responsible for the Cuticular Diene Hydrocarbon Polymorphism in *Drosophila melanogaster*. *Proc. Natl. Acad. Sci. USA* **2000**, *97*, 9449–9954. [CrossRef] [PubMed]
66. Badouin, H.; Belkhir, K.; Gregson, E.; Galindo, J.; Sundström, L.; Martin, S.J.; Butlin, R.K.; Smadja, C.M. Transcriptome Characterisation of the Ant Formica Exsecta with New Insights into the Evolution of Desaturase Genes in Social Hymenoptera. *PLoS ONE* **2013**, *8*, e68200. [CrossRef] [PubMed]
67. Gu, S.H.; Wu, K.M.; Guo, Y.Y.; Pickett, J.A.; Field, L.M.; Zhou, J.J.; Zhang, Y.J. Identification of Genes Expressed in the Sex Pheromone Gland of the Black Cutworm *Agrotis Ipsilon* with Putative Roles in Sex Pheromone Biosynthesis and Transport. *BMC Genomics* **2013**, *14*, 636. [CrossRef] [PubMed]
68. Falcón, T.; Ferreira-Caliman, M.J.; Franco Nunes, F.M.; Tanaka, É.D.; do Nascimento, F.S.; Gentile Bitondi, M.M. Exoskeleton Formation in *Apis mellifera*: Cuticular Hydrocarbons Profiles and Expression of Desaturase and Elongase Genes during Pupal and Adult Development. *Insect Biochem. Mol. Biol.* **2014**, *50*, 68–81. [CrossRef]
69. Chen, Q.; Cheng, D.; Liu, S.; Ma, Z.; Tan, X.; Zhao, P. Genome-Wide Identification and Expression Profiling of the Fatty Acid Desaturase Gene Family in the Silkworm, *Bombyx mori*. *Genet. Mol. Res.* **2014**, *13*, 3747–3760. [CrossRef]
70. He, P.; Zhang, Y.F.; Hong, D.Y.; Wang, J.; Wang, X.L.; Zuo, L.H.; Tang, X.F.; Xu, W.M.; He, M. A Reference Gene Set for Sex Pheromone Biosynthesis and Degradation Genes from the Diamondback Moth, *Plutella xylostella*, Based on Genome and Transcriptome Digital Gene Expression Analyses. *BMC Genomics* **2017**, *18*, 219. [CrossRef]
71. Qu, C.; Kang, Z.; Zhang, B.; Fang, Y.; Wang, R.; Li, F.; Zhao, H.; Luo, C. Genome-Wide Identification and Expression Profiling of Candidate Sex Pheromone Biosynthesis Genes in the Fall Armyworm (*Spodoptera frugiperda*). *Insects* **2022**, *13*, 1078. [CrossRef]
72. Bousquet, F.; Nojima, T.; Houot, B.; Chauvel, I.; Chaudy, S.; Dupas, S.; Yamamoto, D.; Ferveur, J.F. Expression of a Desaturase Gene, Desat1, in Neural and Nonneural Tissues Separately Affects Perception and Emission of Sex Pheromones in *Drosophila*. *Proc. Natl. Acad. Sci. USA* **2012**, *109*, 249–254. [CrossRef]
73. Haritos, V.S.; Horne, I.; Damcevski, K.; Glover, K.; Gibb, N.; Okada, S.; Hamberg, M. The Convergent Evolution of Defensive Polyacetylenic Fatty Acid Biosynthesis Genes in Soldier Beetles. *Nat. Commun.* **2012**, *3*, 1150. [CrossRef]
74. Willis, J.H. Structural Cuticular Proteins from Arthropods: Annotation, Nomenclature, and Sequence Characteristics in the Genomics Era. *Insect Biochem. Mol. Biol.* **2010**, *40*, 189–204. [CrossRef] [PubMed]
75. Cornman, R.S.; Togawa, T.; Dunn, W.A.; He, N.; Emmons, A.C.; Willis, J.H. Annotation and Analysis of a Large Cuticular Protein Family with the R&R Consensus in *Anopheles gambiae*. *BMC Genomics* **2008**, *9*, 22. [CrossRef]
76. Tang, L.; Liang, J.; Zhan, Z.; Xiang, Z.; He, N. Identification of the Chitin-Binding Proteins from the Larval Proteins of Silkworm, *Bombyx mori*. *Insect Biochem. Mol. Biol.* **2010**, *40*, 228–234. [CrossRef] [PubMed]
77. Dittmer, N.T.; Tetreau, G.; Cao, X.; Jiang, H.; Wang, P.; Kanost, M.R. Annotation and Expression Analysis of Cuticular Proteins from the Tobacco Hornworm, *Manduca sexta*. *Insect Biochem. Mol. Biol.* **2015**, *62*, 100–113. [CrossRef] [PubMed]
78. Dong, Z.; Zhang, W.; Zhang, Y.; Zhang, X.; Zhao, P.; Xia, Q. Identification and Characterization of Novel Chitin-Binding Proteins from the Larval Cuticle of Silkworm, *Bombyx mori*. *J. Proteome Res.* **2016**, *15*, 1435–1445. [CrossRef]
79. Liu, J.; Li, S.; Li, W.; Peng, L.; Chen, Z.; Xiao, Y.; Guo, H.; Zhang, J.; Cheng, T.; Goldsmith, M.R.; et al. Genome-Wide Annotation and Comparative Analysis of Cuticular Protein Genes in the Noctuid Pest *Spodoptera litura*. *Insect Biochem. Mol. Biol.* **2019**, *110*, 90–97. [CrossRef]

80. Ioannidou, Z.S.; Theodoropoulou, M.C.; Papandreou, N.C.; Willis, J.H.; Hamodrakas, S.J. CutProtFam-Pred: Detection and Classification of Putative Structural Cuticular Proteins from Sequence Alone, Based on Profile Hidden Markov Models. *Insect Biochem. Mol. Biol.* **2014**, *52*, 51–59. [CrossRef]
81. Kong, H.; Dong, C.; Jing, W.; Tian, Z.; Zheng, M.; Wang, C.; Hou, Q.; Cheng, Y.; Zhang, L.; Jiang, X.; et al. The Role of Tyramine β-Hydroxylase in Density Dependent Immunityof Oriental Armyworm (*Mythmina separata*) Larva. *Int. J. Mol. Sci.* **2019**, *20*, 1553. [CrossRef]
82. Jiang, S.; Bao, J.; Chen, Y.; Liu, Z.; Liu, R.; Cheng, Y.; Zhang, L.; Jiang, X.; Kong, H. Immunological Regulation by Toll-1 and Spätzle-4 in Larval Density-Dependent Prophylaxis of the Oriental Armyworm, *Mythimna separata*. *Int. J. Biol. Macromol.* **2024**, *264*, 130778. [CrossRef]
83. Li, X.; Schuler, M.A.; Berenbaum, M.R. Molecular Mechanisms of Metabolic Resistance to Synthetic and Natural Xenobiotics. *Annu. Rev. Entomol.* **2007**, *52*, 231–253. [CrossRef]
84. Dimunová, D.; Matoušková, P.; Podlipná, R.; Boušová, I.; Skálová, L. The Role of UDP-Glycosyltransferases in Xenobioticresistance. *Drug Metab. Rev.* **2022**, *54*, 282–298. [CrossRef] [PubMed]
85. Dong, J.; Liu, X.; Yue, J.; Qiao, Y.; Chu, Y.; Wang, P.; Zhang, Q. Resistance of *Mythimna separata* (Lepidoptera: Noctuidae) to Five Different Types of Insecticides in Beijing. *Chinese J. Pestic. Sci.* **2014**, *16*, 687–692.
86. Zhao, Y.Y.; Li, S.U.; Shuai, L.I.; Li, Y.P.; Xu, X.L.; Cheng, W.N.; Wang, Y.; Wu, J.X. xiang Insecticide Resistance of the Field Populations of Oriental Armyworm, *Mythimna separata* (Walker) in Shaanxi and Shanxi Provinces of China. *J. Integr. Agric.* **2018**, *19*, 182–188. [CrossRef]
87. Meng, L.W.; Yuan, G.R.; Chen, M.L.; Zheng, L.S.; Dou, W.; Peng, Y.; Bai, W.J.; Li, Z.Y.; Vontas, J.; Wang, J.J. Cuticular Competing Endogenous RNAs Regulate Insecticide Penetration and Resistance in a Major Agricultural Pest. *BMC Biol.* **2023**, *21*, 187. [CrossRef]
88. Scott, J.; Baker, O.; Dressel, A.; Norris, R.; Burgess IV, E. Isolation and Characterization of the Decreased Cuticular Penetration Mechanism of Fluralaner Resistance in the House Fly, *Musca domestica*. *Pestic. Biochem. Physiol* **2024**, *205*, 106154. [CrossRef]
89. Dulbecco, A.B.; Moriconi, D.E.; Calderón-Fernández, G.M.; Lynn, S.; McCarthy, A.; Roca-Acevedo, G.; Salamanca-Moreno, J.A.; Juárez, M.P.; Pedrini, N. Integument CYP Genes of the Largest Genome-Wide Cytochrome P450 Expansions in Triatomines Participate in Detoxification in Deltamethrin-Resistant *Triatoma infestans*. *Sci. Rep.* **2018**, *8*, 10177. [CrossRef]
90. Dulbecco, A.; Moriconi, D.; Pedrini, N. Knockdown of CYP4PR1, a Cytochrome P450 Gene Highly Expressed in the Integument Ttissue of Triatoma infestans, Increases Susceptibility to Deltamethrin in Pyrethroid-Resistant Insects. *Pestic. Biochem. Physiol* **2021**, *173*, 104781. [CrossRef]
91. Jing, T.; Jiang, S.; Tang, X.; Guo, P.; Wang, L.; Wang, J.; Wei, D. Overexpression of an Integument Esterase Gene LbEST-Inte4 Infers the Malathion Detoxification in *Liposcelis bostrychophila* (Pso-Coptera: Liposcelididae). *J. Agric. Food. Chem.* **2024**, *72*, 11221–11229. [CrossRef]

Disclaimer/Publisher's Note: The statements, opinions and data contained in all publications are solely those of the individual author(s) and contributor(s) and not of MDPI and/or the editor(s). MDPI and/or the editor(s) disclaim responsibility for any injury to people or property resulting from any ideas, methods, instructions or products referred to in the content.

insects

MDPI

Article

The Early Sex-Specific Expression of the Fruitless Gene in the Asian Tiger Mosquito *Aedes albopictus* (Skuse) and Its Functional Conservation in Male Courtship

Marianna Varone [1], Paola Di Lillo [1], Katerina Nikolouli [2], Ayca Eda Özel [2], Francesca Lucibelli [1], Gennaro Volpe [1], Sarah Maria Mazzucchiello [1], Angela Carfora [1], Serena Aceto [1], Giuseppe Saccone [1], Kostas Bourtzis [2] and Marco Salvemini [1,*]

[1] Department of Biology, University of Study of Naples Federico II, 80100 Naples, Italy; marianna.varone@unina.it (M.V.); paola.dilillo@unina.it (P.D.L.); francesca.lucibelli@unina.it (F.L.); gennaro.volpe2@unina.it (G.V.); sarahmaria.mazzucchiello@unina.it (S.M.M.); angela.carfora@unina.it (A.C.); serena.aceto@unina.it (S.A.); giuseppe.saccone@unina.it (G.S.)

[2] Insect Pest Control Laboratory, Joint FAO/IAEA Centre of Nuclear Techniques in Food and Agriculture, Department of Nuclear Sciences and Applications, IAEA Laboratories, 2444 Seibersdorf, Austria; k.nikolouli@iaea.org (K.N.); a.e.ozel@iaea.org (A.E.Ö.); k.bourtzis@iaea.org (K.B.)

* Correspondence: marco.salvemini@unina.it; Tel.: +39-0812535004

Simple Summary: Courtship and mating are key behaviors for the survival and reproductive success of animal populations. In insects, the *fruitless* (*fru*) gene is widely recognized as a central regulator of male mating, orchestrating courtship behavior through sex-specific expression patterns within specialized neural circuits. *fru* orthologs that produce sex-specific isoforms via alternative splicing have been identified across various orders of holo- and hemimetabolous insects, highlighting both the evolutionary conservation of this gene and its ancestral role in courtship regulation within insect taxa. This study focuses on the *fru* ortholog characterization in the Asian tiger mosquito, *Aedes albopictus* (*Aalfru*), and on functional analysis by RNA interference (RNAi)-mediated knockdown to explore its involvement in the genetic control of male courtship behavior.

Abstract: The Asian tiger mosquito, *Aedes albopictus*, is an invasive species and a vector for several significant human pathogens. Gaining a deeper understanding of its reproductive biology offers valuable insights into its evolutionary success and may inform the development of sustainable strategies to control its spread. This study presents a comprehensive structural and functional characterization of the *fruitless* gene in *Ae. albopictus* (*Aalfru*), a pivotal regulator of sexual behavior in insects. Through in silico analysis combined with molecular and functional genetics approaches, we identified a high degree of conservation in the *fru* gene structure and its regulation via sex-specific alternative splicing. Differently from *Drosophila*, *Aedes aegypti*, and other dipteran *fruitless* orthologs, *Aalfru* sex-specific regulation starts in 1-day-old embryos, rather than the late larval stage. Functional analysis using embryonic RNA interference (RNAi) demonstrated that, *Ae. albopictus* males with transiently disrupted *fru* expression at the embryonic stage showed significant deficits in adult mating behavior and failed to produce viable progeny. Our findings elucidate the *Aalfru* gene's molecular organization, developmental regulation, and critical role in courtship behavior, highlighting its importance in male sexual behavior and reproductive success in *Ae. albopictus*.

Keywords: courtship behavior; *fruitless*; *Aedes albopictus*; sex determination; alternative splicing; vector control

1. Introduction

Courtship in the animal kingdom consists of behavioral displays and actions performed by individuals (often males, but not always) to attract a mate and initiate reproductive pairing. These behaviors, which require the evolution of specialized adaptations in neural, sensory, and motor systems, communicate readiness to mate, assess potential mates' suitability, and ensure successful mating between compatible partners [1].

Insects, reflecting their remarkable biodiversity, exhibit an extraordinary range of courtship strategies that rely primarily on innate, stereotyped responses to diverse external stimuli. These courtship behaviors can encompass various sensory modalities, including elaborate visual displays, intricate acoustic signals, specific physical gestures, and complex chemical cues [2]. This reliance on varied and often highly specialized sensory channels underscores insects' evolutionary adaptations in response to selective pressures within their environments, leading to a rich tapestry of species-specific courtship mechanisms across taxa [3,4].

Despite the vast taxonomic diversity of insects, much of our current knowledge regarding the neurogenetic foundations of courtship behavior is derived primarily from studies on *Drosophila melanogaster* [5]. In *Drosophila*, the genes *fruitless* (*fru*) and *doublesex* (*dsx*) are the master regulators in the development and functional activity of neurons that drive sex-specific behaviors. *dsx* is responsible for determining sexual fates in both neural and non-neural cells, contributing to sex-specific physical traits as well as behavior [6]. In contrast, *fru* functions exclusively within the nervous system, shaping the circuits involved explicitly in male courtship and other sexually dimorphic behaviors [7]. *dsx* and *fru* function as terminal regulators within the somatic sex determination cascade of *D. melanogaster*, and their regulation occurs through shared *cis*-regulatory elements. This regulation is achieved for both genes via sex-specific alternative splicing, mediated by a complex containing the serine–arginine-rich female-specific splicing regulator Transformer (TRA) and the non-sex-specific RNA-binding protein Transformer-2 (TRA-2) [8,9].

In *Drosophila*, the functions of *fru* that drive male-specific sexual behavior are primarily mediated by transcripts originating from one of the four identified *fru* promoters, named P1 [2]. *fru*-P1 transcripts undergo sex-specific alternative splicing from the third instar larval stage through adulthood. This results in male-specific transcripts encoding for BTB protein family (Broad-complex, Tramtrack, and Bric-a-brac) transcription factors. Conversely, female-specific transcripts do not produce functional proteins [10]. Transcripts derived from the remaining *fru* promoters (P2, P3, and P4) are present in both sexes but serve distinct roles depending on their timing and tissue of expression. Transcripts produced from promoters P3 and P4 are expressed as early as the embryonic stage and contribute to proper neuronal development [11,12], whereas P2-derived transcripts appear during the pupal stage and are critical for the differentiation of imaginal disc derivatives [10]. These complex promoter and splicing regulations allow *fru* to serve sex-specific and general developmental functions essential to *Drosophila*'s neurogenetic and behavioral systems. Neurogenetic studies have revealed that *fru* helps to establish neurons with sexually dimorphic neurite projections and dendritic branching acting at different levels. At the chromatin regulation level, FRU forms complexes with co-factors, enabling it to function as both an activator or repressor, thereby directing the masculinization or feminization of specific neuronal types [13,14]. At the transcriptional regulation level, genome-wide analyses have identified neuronal development genes directly targeted by FRU, including the *Roundabout* (*Robo*) family, essential for axon pathfinding [15], and *hunchback*, which influences neurite branching [16]. FRU's role also extends to the proteasomal regulation

level, stabilizing the transcription factor Lola in males and preserving male-specific neuron structures and projections [17].

While *Drosophila* provides a valuable model due to its genetic tractability and well-mapped neural circuitry, this focus limits our broader understanding of the molecular and neural mechanisms underlying courtship across other insect taxa. To overcome such limitations, in the past 20 years, orthologs of the *fru* gene have been identified not only in several other dipteran species [18–21] but also in various orders of holometabolous insects, including Hymenoptera [22], Lepidoptera [23], and Coleoptera [24], as well as in hemimetabolous insects, such as Orthoptera [25] and Hemiptera [26]. These studies have revealed insights into the evolution, structure, and function of the *fru* gene, highlighting the conservation of its regulation via sex-specific alternative splicing in holometabolous insects and a more variable situation in hemimetabolous insects and suggesting an ancestral role in sex determination and sexual behavior.

Within Diptera, of particular interest is the functional study of the *fru* gene in the mosquito *Aedes aegypti* by CRISPR-Cas9 technology to generate *fru* mutant individuals [27]. The study demonstrated that mutant males could not mate, thereby confirming the conserved role of the *fru* gene as a key regulator of male courtship and sexual behavior across insect species. Unexpectedly, the researchers also observed that *fru* mutant males exhibited a strong attraction to live human hosts—behavior absent in wild-type males. This surprising result provided the first evidence that male mosquitoes possess the neural circuitry necessary for host-seeking behavior. The findings further indicated that the functional presence of *fruM* transcripts are essential for repressing this trait in males, effectively keeping it latent. These observations underscored an intriguing evolutionary innovation, wherein a master regulator of male-specific sexual behavior has been repurposed to control the female-specific trait of blood-feeding [28].

In this study, we provide an in-depth structural and functional analysis of the *fruitless* gene in *Ae. albopictus* (*Aalfru*), the Asian tiger mosquito (Diptera, suborder Nematocera). Through an integrative approach combining in silico analyses, molecular techniques, and functional genetics, we identified a highly conserved structural element within the *fru* gene. Our findings further elucidate the gene's regulation via sex-specific alternative splicing mechanisms initiated during early embryonic stages. Functional analysis using embryonic RNA interference (RNAi) further revealed that male *Ae. albopictus* individuals with disrupted *fru* expression exhibited marked impairments in mating behavior and could not produce offspring. These findings provide a detailed perspective on the molecular organization, developmental regulation, and functional role of *Aalfru*, underscoring its critical influence on male courtship behavior and reproductive success in this relevant vector species [27] and providing insights that may guide the development of innovative sustainable strategies for controlling its spread.

2. Materials and Methods

2.1. Insect Rearing

Wild-type *Ae. albopictus* used in this study was from Rimini (Italy). Dr. Romeo Bellini established this strain at the Centro Agricoltura Ambiente "Giorgio Nicoli" Srl (CAA, Crevalcore, ITALY), and it has been maintained in the Department of Biology-Federico II University (Naples) since 2019. The mosquitoes were reared under laboratory standard conditions, i.e., 26–27 °C, 60% RH, and 12 h light/12 h dark cycle. Larvae were reared in plastic trays filled with deionized water [29] and provided with TetraMin tropical fish food flakes (Tetra Goldfish granules, Tetra GmbH, Melle, Germany). The adults (sex ratio approximately 1:1) were kept in 32.5 × 32.5 × 32.5 cm or 17.5 × 17.5 × 17.5 cm rearing

cages (Bug Dorm, MegaView Science Co., Ltd., Taichung, Taiwan) with constant access to 10% (*w*/*v*) sucrose and females were blood fed on porcine blood twice a week using the Hemotek system (Hemotek Membrane Feeding Systems, Blackburn, UK). Germination papers were provided in adult cages for oviposition. Laid eggs were collected and stored in plastic containers with sufficient humidity (>90% relative humidity) [30] and then transferred to a larval artificial diet (TetraMin) to obtain the hatching. At the Insect Pest Control Laboratory (IPCL), the *Ae. albopictus* Rimini strain was also used for embryonic microinjections, RT-PCRs, and behavioral experiments. Mosquitoes were reared at 27 ± 1 °C, 80% relative humidity, and a 14/10 h day/night photoperiod. Larvae were fed a 4% liquid diet consisting of tuna meal (50%), bovine liver powder (35%), and brewer's yeast (15%), dissolved in deionized water, while adult mosquitoes were offered a 10% sucrose solution [31]. Blood-feeding was performed twice weekly using porcine blood, and eggs were collected 72 h after the last blood-feeding using moistened oviposition papers (white germination paper, Sartorius Stedium Biotech, Vienna, Austria). The blood used was collected in Himberg, Austria, during the routine slaughtering of pigs in a nationally authorized abattoir, conducted at the highest possible standards strictly following EU laws and regulations.

2.2. Preparation of Double-Stranded RNA (dsRNA) with In Vitro Transcription

Template DNA was amplified with *fruitless* male-specific primers (Table 1: *Aalfru_MB_T7+/Aalfru_MB_T7−)* containing T7 promoter sequence (5′-aatacgactcactataggg-3′) at their 5′ ends. The resulting product, after purification from agarose gels using StrataPrep DNA Gel extraction kit (Agilent, Santa Clara, CA, USA), was used as a template to synthesize dsRNA using the MEGAscript RNAi T7 kit (Invitrogen™, Waltham, MA, USA) according to manufacturer's recommendation. Similarly, a fragment of *GFP* gene was amplified by PCR from the pAct:dCas9 vector (Addgene, Teddington, UK) using *eGFP*-specific primers (Table 1: eGFP_T7+/eGFP_T7−), each containing the T7 promoter sequence at the 5′ end; additionally, dsRNA was synthesized in vitro as previously described.

Table 1. Primers list.

Name	Sequence (5′-3′)	Purpose
Aalrp49+	GACGAAGAAGTTCATCCGCC	cDNA amplification
Aalrp49−	GTTCTGCTGCGAGCGCAG	cDNA amplification
Aalnix+	GTTGTTCGTTACAGACTGATG	cDNA amplification
Aalnix−	CAAAGCTAATGTAAACCATGAC	cDNA amplification
Aalfru_M2+	GAACGGCTACCCTCAGATGA	cDNA amplification and sequencing
Aalfru_C3−	ACCTGCGATTCGTATCCACC	cDNA amplification and sequencing
Aalfru_C5+	ACATGCCTCCGCTGAACGA	cDNA amplification and sequencing
Aalfru_ZnfA−	CCGTTGTTTGTTCCGGGC	cDNA amplification and sequencing
Aalfru_ZnfB−	AGCACTGCTCGACTGGC	cDNA amplification and sequencing
Aalfru_ZnfC−	CGGTAGGTGTCGCCTTGTT	cDNA amplification and sequencing
Aalfru_real+	CGGCAATGCCCATCTACAG	qRT-PCR
Aalfru_real−	GGTCGACACCGTTCATCTGA	qRT-PCR
AalRp49_real+	AGAAGTTCCTGGTCCACAAC	qRT-PCR
AalRp49_real−	GTTCTGCTGCGAGCGCAG	qRT-PCR
Aalfru_MB_T7+	taatacgactcactatagggAGTTCTCAATAGTATGTCATCG	dsRNA synthesis
Aalfru_MB_T7−	taatacgactcactatagggGCGGTGCGATTGCAGTTTTC	dsRNA synthesis
eGFP_T7+	taatacgactcactatagggGGTGAACTTCAAGATCCGCC	dsRNA synthesis
eGFP_T7−	taatacgactcactatagggGCATGGACGAGCTGTACAAG	dsRNA synthesis

2.3. Embryonic Microinjections of dsRNA

Three to four days after blood-feeding, females were placed in *Drosophila* vials (Thermo Scientific™, Wilmington, NC, USA) containing a wet filter paper. Embryos to be injected were collected after allowing females to oviposit for ≤90 min in a dark environment. Light-grey embryos were aligned, transferred on coverslips with double-sided sticky tape, allowed to desiccate briefly, and covered with Halocarbon oil 27 (Sigma-Aldrich Co., Darmstadt, Germany) [32]. Microinjections were performed at the posterior pole of embryos using a mix of 1 µg/µL of dsRNA (dsRNA_*fru*) and injection buffer (5 mM KCl, 0.1 mM sodium phosphate, pH 6.8). Injections were carried out using the XenoWorks® Digital Microinjector (Sutter Instrument Co., Novato, CA, USA) with QUARTZ 0.7 mm needles with filament, which were pulled using a P-2000 Laser-Based Micropipette Puller (Sutter Instrument Co., Novato, CA, USA). The needle pulling specifications were as follows: HEAT = 750, PULL = 200, VEL = 40, DEL = 145, and FIL = 3. A set of control eggs was injected with dsRNA_*GFP* and kept for hatching in parallel with a set of un-injected eggs laid in the same batch. After injections, oil was washed off the embryos, and the coverslips were covered with wet filter paper and allowed to recover under controlled insectary conditions (26–27 °C; 60% RH) for five to six days [32]. Subsequently, the embryos were hatched to a new tray containing larval diet. This experiment was conducted at the IPCL in Seibersdorf (Austria) in accordance with FAO/IAEA guidelines.

2.4. RNA Extraction and cDNA Preparation

Total RNA was isolated from all samples: eggs ($E_{0–24h}$), larvae (L_{I-IV}), pupae (P), and adults (M and F) (N = 10), and different tissues: abdomen (A), heads (H), and carcasses (C) (N = 10), following the TRIzol Reagent (Thermo Fisher Scientific, Waltham, MA, USA) protocol. Total RNA from larvae injected with dsRNA (L_{IV}) (N = 13 or N= 3) was extracted using the RNeasy Micro Kit (Qiagen, Hilden, Germany). RNA quantification measurements were performed using NanoDrop™ 2000/2000c Spectrophotometers (Thermo Scientific™, Wilmington, NC, USA). Extracted RNA (0.5 µg) was retro-transcribed into cDNA using the LunaScript® RT SuperMix Kit (NEB, Ipswich, MA, USA) according to the manufacturer's instructions.

2.5. RT-PCR and RT-qPCR

RT-PCRs were performed using the LongAmp® Taq DNA Polymerase (NEB, Ipswich, MA, USA) according to the manufacturer's instructions. Appropriate annealing temperatures and cycle numbers were adjusted empirically for each primer pair. The primer list is shown in Table 1. The primer pair *Aalrp49+/Aalrp49−* was used as positive control [33]. All gene expression levels in this study were determined using a real-time PCR machine, CFX96 Touch Deep Well Real-Time PCR System (Bio-Rad, Hercules, CA, USA). RT-qPCR was conducted with a reaction volume of 20 µL consisting of 10 µL of 2× iQ SYBR Green Supermix (Bio-Rad, Hercules, CA, USA), 1 µL cDNA template, 0.5 µL forward and reverse primers (10 µmol/L), and 8 µL RNase-Free ddH2O. RT-qPCR was performed under the following conditions: denaturation at 95 °C for 2 min, followed by 40 cycles of dissociation at 95 °C for 15 s, annealing at 58 °C for 30 s, and extension at 72 °C for 30 s. Expression levels were calculated using the $2^{-\Delta\Delta Ct}$ method with a triple technical for each sample [34], all data normalized to the housekeeping gene expression *rp49*.

2.6. Sequence Analysis

Based on the in silico assembled sequence, a set of primers were designed to amplify the complete *Aalfru* gene (*Aalfru_M2+/Aalfru_C3−*; *Aalfru_C3+/Aalfru_ZnfC−*; *Aalfru_C5+/Aalfru_ZnfA−*; and *AalfruC5+/Aalfru_ZnfB−*). The sequence of *Aalfru* was pro-

duced using the Mix2Seq Kit (Eurofins genomics, Ebersberg, Germany). The sequence reactions were assembled into Eurofins tubes using 10 µM *fruitless*-specific primers (see Table 1) and using as a template the RT-PCR gel-purified *Aalfru* product (StrataPrep DNA Gel extraction kit—Agilent, Santa Clara, CA, USA).

2.7. Behavioral Assays

All behavioral experiments were carried out under insectary standards conditions, i.e., 26–27 °C, 60% RH, and 12 h light/12 h dark cycle. To examine whether *Aalfru*-knockdown males exhibited altered mating behavior, 1 male (who had never met a female and had never experienced mating) and 5 virgin females (who originated from the same cohort that emerged on the same day) were crossed (pupae were sexed and separated into individual tubes until emergence to obtain virgin individuals).

A total of three types of crosses were produced:

(a) 1 wild-type male × 5 wild-type females (WT);
(b) 1 *GFP*-knockdown male × 5 wild-type females (*GFP*);
(c) 1 *fru*-knockdown male × 5 wild-type females (*fru*).

Eight replicates were conducted for the WT and *fru* crosses and four replicates for the *GFP* crosses. The crosses were realized in 17.5 cm × 17.5 cm × 17.5 cm cages (BugDorm-4E1515).

The crosses (a), (b), and (c) were observed to analyze the following aspects:

(1) Courtship and mating;
(2) feeding;
(3) fecundity.

(1) The fraction of time spent by the male on various aspects of courtship and mating behavior was recorded through direct observation using manual scoring under controlled laboratory conditions. In each observation session, cages were monitored starting from the moment males and females were introduced, with a total observation time of 30 min per session conducted twice per day, in the early morning and late afternoon.
(2) Following a three-day mating period, the cages were examined for feeding behavior. Mosquitoes had constant access to 10% (*w*/*v*) sucrose, and warm porcine blood was offered at the top of the cages for 30 min. Feeding was assessed based on visual observation of the abdomen of the male and female mosquitoes.
(3) Three days after the blood meal, plastic cups containing deionized water and lined with germination paper were provided in each cage for 48 h. Eggs were counted and examined under an optical stereomicroscope.

2.8. Statistical Analysis

Experimental data were analyzed using GraphPad Prism 9.0 (GraphPad Software, San Diego, CA, USA). The expression pattern analysis was performed by analysis of variance (one-way ANOVA test) followed by Dunnett's multiple comparisons test or Tukey post hoc test). Data collected as a percentage of the total are shown as mean ± SEM. Details of statistical methods are reported in the figure legends.

3. Results and Discussion

3.1. The Molecular Characterization of the Aalfru Gene

In insects, the *fru* gene exhibits a complex genomic organization, generating transcript isoforms by alternative promoters, mutually exclusive terminal exons, and sex-specific alternative splicing [2]. In most species, including mosquitoes, the gene region responsible for sex-specific

alternative splicing, transcribed from the P1 promoter, is located at a large genomic distance from the gene's first exon, C1, which is common to all *fru* transcripts and encodes the DNA-binding BTB domain [2]. As a result, automated gene prediction systems frequently fail to produce a complete *fru* gene model that includes all exons. In the *Ae. albopictus* AaloF1 reference genome, available at the Ensembl Metazoa genome browser https://metazoa.ensembl.org/ (accessed on 2 February 2024), a partial *fru* gene model is present (AALF007440, located in the supercontig JXUM01S001695), including only the first four common exons (Figure 1A). To reconstruct the complete genomic organization of the *fru* gene in *Ae. albopictus*, we conducted a TBLASTN analysis of the AaloF1 genome using as virtual probes the *Ae. aegypti* P1-FRU-ZnF-C male-specific transcript (GenBank acc. Num.: JX186753), and the putative terminal exon sequences encoding the ZnF-A and ZnF-B domains [21]. We identified the following: (1) a sex-specifically regulated exon, located in a different supercontig (JXUM01S000018) and divided into two subregions (male- and female-specific portions); (2) five common exons (C1-C2-C3-C4-C5); (3) three putative alternative zinc finger encoding exons, corresponding to zinc finger type A, B, and C (Figure 1A). Using primer pairs specific for the *Aalfru* exons identified in silico, we performed RT-PCR experiments on RNA samples extracted from adult-sexed mosquitoes, confirming their presence in the transcriptional units of both sexes (Figure 1C,D). At first, we amplified a reference gene, *rp49* (Table 1: *Aalrp49+/Aalrp49−*), as positive control and the male-specific *AalNix* gene (Table 1: *Aalnix+/Aalnix−*) to confirm the genetic sex of mosquitoes (Figure 1B).

Furthermore, RT-PCR analysis using a forward primer located in putative exon M and a reverse primer located in the common exon (*Aalfru*_M2+/*Aalfru*_C3−) produced male-specific (921 bp) and female-specific (2146 bp) cDNA amplification in adults, confirming the regulation of the *fru* gene by sex-specific alternative splicing also in *Ae. albopictus* (Figure 1C). The cDNA products were sequenced (Supplemental Materials File S1) and the alignment of their sequences with the AaloF1 genome led us to define an updated *Aalfru* genomic organization, represented in Figure 1A.

Next, we compared the putative *Aal*FRU protein isoforms with the FRU isoforms of *D. melanogaster*, *An. gambiae*, and *Ae. aegypti* (Figure 2). The alignments revealed the high conservation of the BTB, ZnF-A, ZnF-B, and ZnF-C domains between species (Figure 2B,C), but a very low similarity between the connector and male-specific N-terminal domains (Figure 2A).

3.2. The Developmental Expression Analysis of the Aalfru Gene

In the mosquito *An. gambiae*, the analysis of the sex-specific splicing of the *fru*-P1 transcripts has been conducted exclusively at the adult stage. This analysis revealed, for the first time, the key conservation of the sex-specific alternative splicing mechanism observed in *D. melanogaster*, despite the approximately 250 million years of evolutionary divergence between these two dipteran lineages [18]. In *Ae. aegypti*, the RT-PCR analysis on RNA samples extracted from mixed-sex developmental stages, ranging from embryos to pupae, and on sex-separated adult male and female samples, indicated the presence of sex-specific *fru*-P1 transcripts starting from the third instar larval stage. This is consistent with observations in *D. melanogaster* [21,35]. In the present investigation, we examined the sex-specific expression patterns of *Aalfru*-P1 transcripts in *Ae. albopictus*. To achieve this, we conducted RT-PCR analysis on RNA samples extracted from various sexed developmental stages including embryos (0–24 h), larvae (L_I, L_{II}, L_{III}, and L_{IV}), pupae (P), and adults (M and F). As internal reference markers, we employed the *rp49* gene, which exhibits constitutive expression in *Ae. albopictus* [33], and the male-specific *Aalnix* gene, utilized to identify the sexual karyotype of the developmental samples [36] (Figure 3A).

Our RT-PCR analysis on sexed individuals revealed that the *Aalfru* gene produces sex-specific transcripts already in 0–24 h old embryos and all other developmental stages, (Figure 3A).

This suggests a potential role for the *fru* gene in establishing a dimorphic state in the central nervous system as early as the initial stages of brain development in mosquito larvae. While many dipteran species undertake protracted metamorphosis, during which the adult nervous system forms through the widespread restructuring and substitution of larval neurons, in most mosquitoes, including *Ae. aegypti* and *An. gambiae*, pupae can complete metamorphosis in about one day [26]. Such a rapid metamorphic transition likely limits the extent of neuronal structure reconfiguration, suggesting that a substantial number of larval neurons are conserved into the adult stage in mosquitoes, as observed with some serotonergic neurons that have been shown to persist in *Ae. aegypti* from the larval through to the adult brain [37,38]. We can hypothesize that such an early expression of *fru*-P1 sex-specific isoforms in *Ae. albopictus* may play a role in the development of sex-specific differences in the formation of neural circuits underlying innate behaviors, beginning as early as the larval stage. These differences may then be preserved into the adult stage.

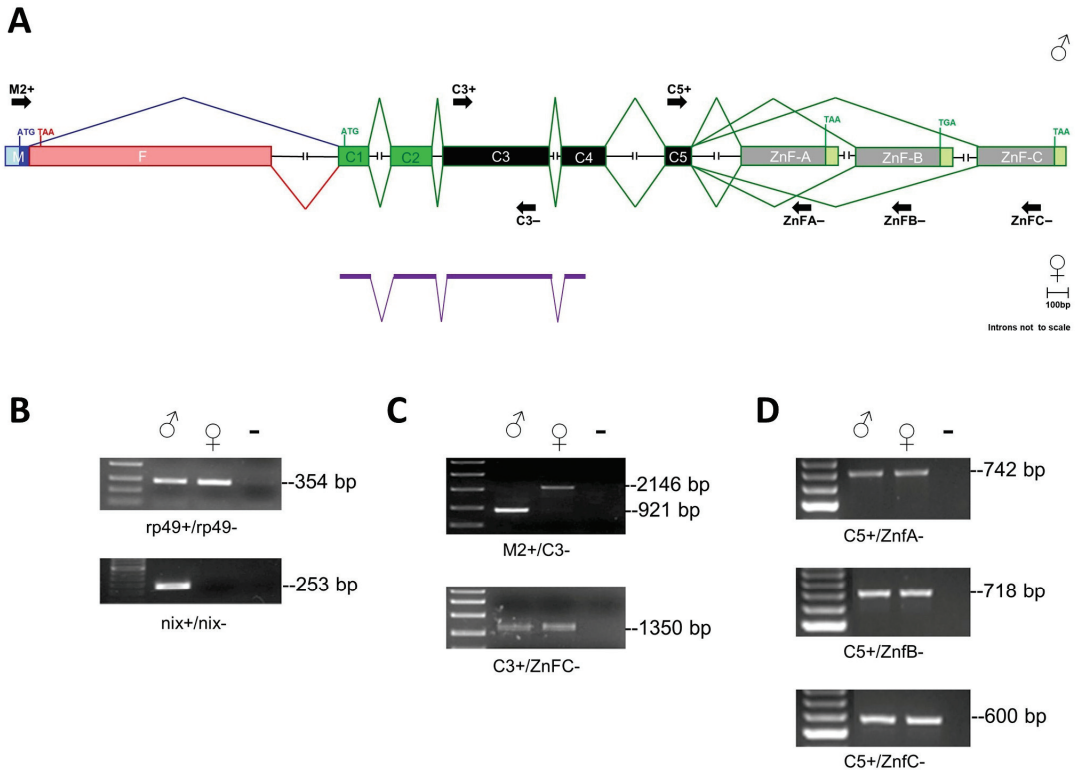


Figure 1. The *Aalfru* gene structure. (**A**) Schematic representation of the *fru* gene in *Ae. albopictus* (introns not to scale). In purple, are the exons belonging to the predicted AALF007440 gene of the *Ae. albopictus* AaloF1 reference genome. The translational start (ATG) and stop (TGA, TAA) sites are indicated. The exons C1 and C2 encode for the BTB domain; the exons C3, C4, and C5 encode for the connecting region; the terminal exons Znf-A, Znf-B, and Znf-C encode for the type A, B, and C zinc finger domains, respectively. The sex-specific region is divided into two sub-regions: male- (M in blue) and female-specific (F in pink) portions, which are alternatively spliced according to sex. (**B**) The RT-PCR amplification with *Aalrp49* and *AalNix* positive controls. The first lane left is a 100-bp ladder (NEB). The *Aalrp49* primer pairs span a 113-bp long intron of the *rp49* gene (genomic amplicon size 467 bp; cDNA amplicon 354 bp). The *Nix* gene is a male-specific positive control. (**C**) The RT-PCR amplifications of *Aalfru* sex-specific and common cDNA fragments on sexed adult *Ae. albopictus* mosquitoes. The first lane left is the High Range ladder (NEB). (**D**) RT-PCR amplifications of *Aalfru* terminal cDNA fragments encoding for zinc finger domains on sexed adult *Ae. albopictus* mosquitoes. The first lane on the left is a 100-bp ladder. Primers used in the PCR amplifications of (**B**–**D**) panels are indicated as short black arrows in (**A**).

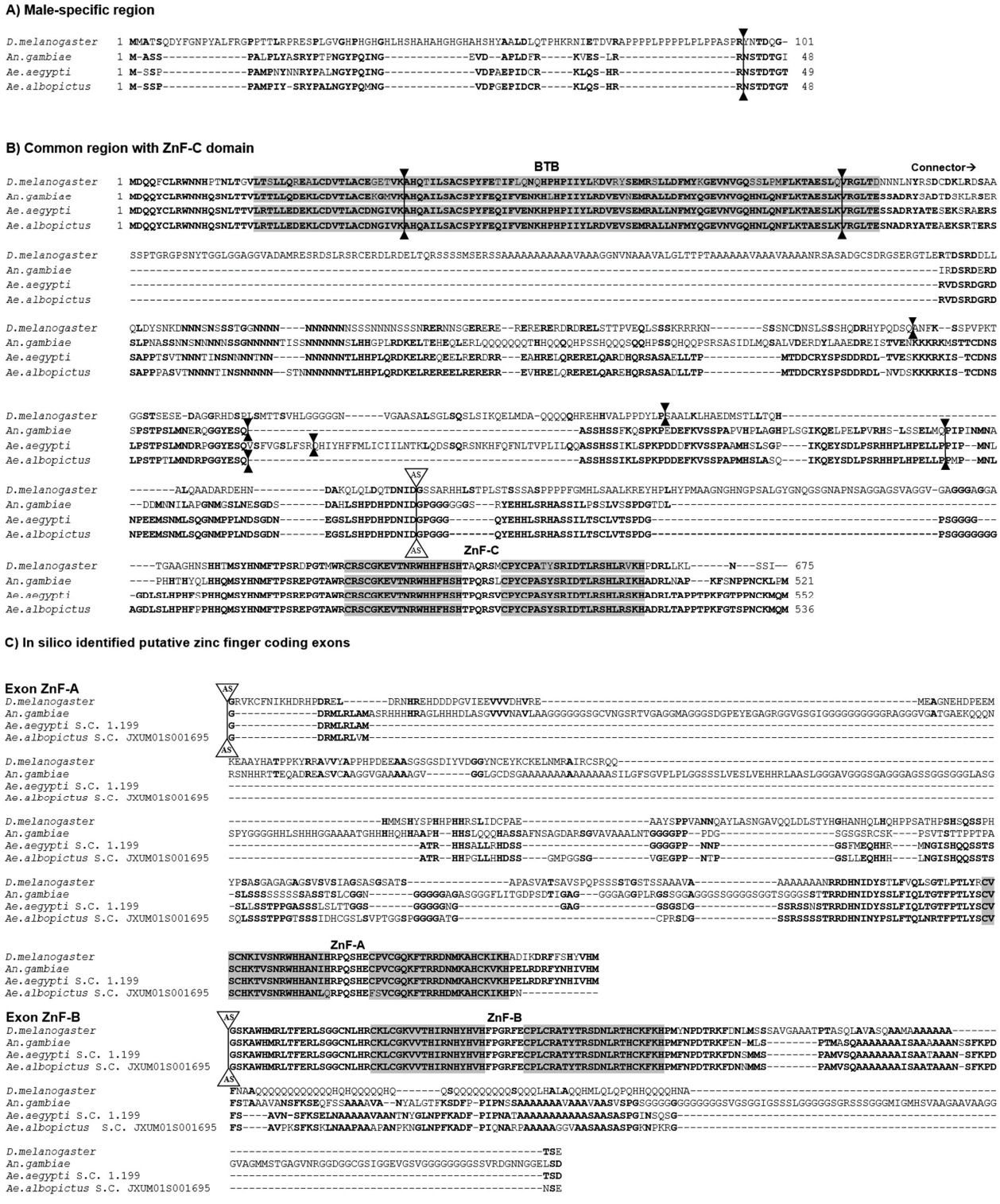


Figure 2. The sequence alignment of the FRU protein isoforms of *D. melanogaster*, *An. gambiae*, *Ae. aegypti*, and *Ae. albopictus*. The conserved BTB domain and zinc finger domains are boxed in grey. The bold letters indicate amino acid identity among at least two species. The intron positions are indicated by solid triangles and the position of the alternative splicing site is indicated by AS white triangles. Gaps were introduced in the alignments to maximize similarity. The sequences are divided into (**A**) male-specific N-terminal portion encoded by P1 transcript; (**B**) common portion of the gene including the BTB domain, the connector region, and the zinc finger type C domain; and (**C**) putative in silico identified zinc finger of type A and B domains of *Ae. albopictus* aligned with the homologous domains of *D. melanogaster*, *An. gambiae*, and *Ae. aegypti*.

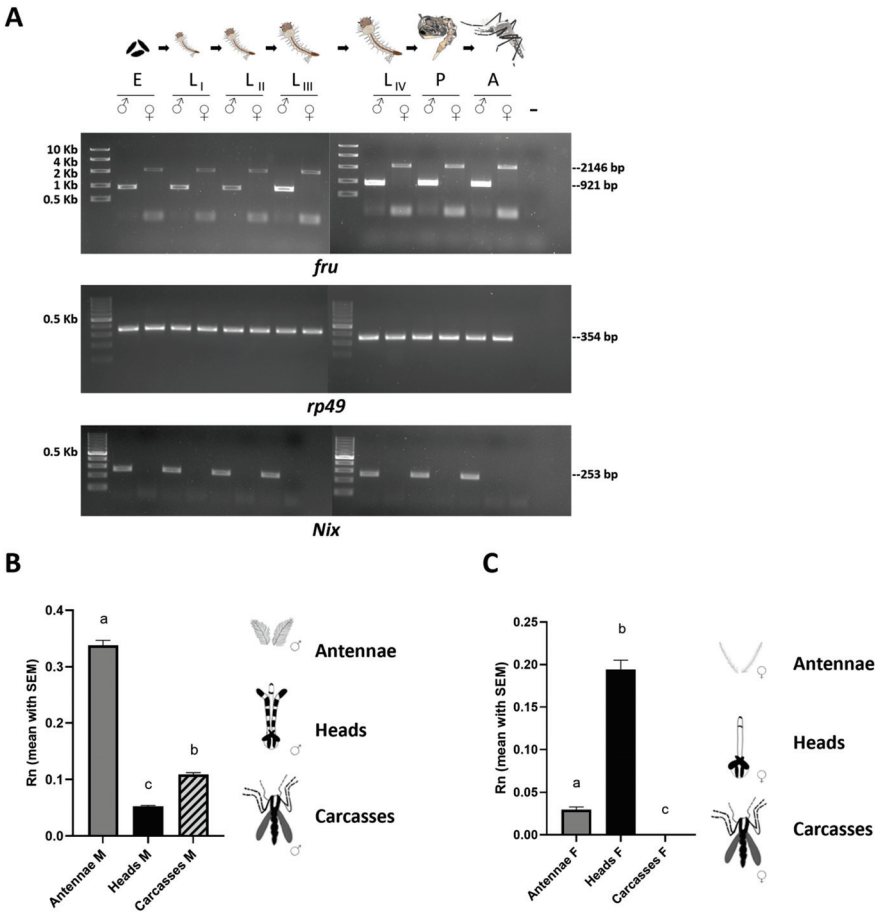


Figure 3. The developmental and spatial expression analyses of the *fru* gene in *Ae. albopictus*. (**A**) The first lane left of each panel is a High-Range ladder or 100-bp ladder (NEB). RT-PCR amplifications of *Aalfru* were performed with M2+/C3− primer pair (for sex-specific adult isoforms) on the following sexed samples: E = 0–24 h embryos; L_I = first instar larvae; L_{II} = second instar larvae; L_{III} = third instar larvae L_{IV} = fourth instar larvae; P = pupae; and A= adults. The *Aalrp49* and *AalNix* were used as a positive control and male-specific control, respectively. (**B**,**C**) The tissue-specific transcription profile of *Aalfru* in males and females. The spatial transcription on male and female antennae, heads, and carcasses (minus heads) sampled by qRT-PCR. The x-axis indicates the sample ID and the y-axis shows the relative expression value obtained by qRT-PCR. The internal reference gene was the *Ae. albopictus* ribosomal protein 49 (*Aalrp49*). (**B**) The error bars represent the SEM (N = 10) (one-way ANOVA test, *p*-Value <0.0001). Tukey post hoc test: 'a' vs. 'c' and 'a' vs. 'b' <0.0001; 'b' vs. 'c' 0,0009); (**C**) The error bars represent the SEM (one-way ANOVA test, *p*-Value <0.0001). Tukey post hoc test: 'a' vs. 'b' and 'a' vs. 'c' <0.0001; 'a' vs. 'c' 0,0482).

We then performed a tissue-specific expression profiling of the *Aalfru* gene in 2-day-old adult males and females by quantitative RT-PCR using a primer pair targeting both male- and female-specific *Aalfru* P1 transcripts (Figure 3B,C). In males, the *fru* transcripts were detectable in the antennae, head, and carcasses with a significantly higher transcription ($p < 000.1$) in the male's antennae and a lower level of transcription in the head and carcasses (Figure 3B). The antennae assume a pivotal role in the olfactory and acoustic behaviors of mosquitoes. In male mosquitoes, the antennae play a crucial role in locating females during mate seeking. Male antennae are highly sensitive to the sound vibrations produced by the wingbeats of females and allow males to detect and amplify these frequencies, facilitating the recognition of and orientation toward a female in flight [39]. Additionally, the antennae are equipped with olfactory sensors that enable males to detect chemical

signals released by females [39]. The specific high transcription of *fru* within the male mosquito's antennae strongly suggests its involvement in the modulation of acoustic and olfactory sexual behavior in the Asian tiger mosquito.

The tissue-specific transcriptional profiling of the *Aalfru* gene in female tissues revealed that there is a significant *Aalfru* ($p < 0.0001$) expression in the heads and a low expression in antennae while no expression at all has been detected in carcasses (Figure 3C). The presence of *Aalfru* P1 transcripts in male carcasses and their complete absence in female carcasses could be linked with the presence of male-specific muscles, such as the Lawrence muscle (MOL), in *Ae. albopictus*. Gailey and colleagues [18] showed the presence of a MOL-like male-specific muscle in the abdomen of *An. gambiae* adult males and that the *An. gambiae* FRUMC isoform is sufficient to induce the formation of the male-specific MOL in *D. melanogaster* transgenic female flies and the rescue of MOL development in mutant males. However, to date, no information about the MOL is available for *Aedes* mosquitoes, representing an interesting topic to be addressed in the future.

3.3. The Conservation of the Aalfru Genomic Organization and Sex-Specific Splicing Regulation

In *Ae. aegypti*, the *fru* gene spans an extensive genomic region of approximately 533 kb, considerably larger than the 130 kb long *fru* gene in *Drosophila* and the 90 kb long *fru* gene in *An. gambiae* [21]. The *Aalfru* gene comprises eight exons and seven introns with substantial length variability. It spans a region of approx. 335 kb in the AaloF1 genome assembly (Figure 4A). We searched in the recently released *Ae. albopictus* AalbF5 chromosome-level genome assembly, available at NCBI website (GCF_035046485.1), and we identified a conserved *fru* locus, with conserved exon–intron organization, located on chromosome 1 and spanning a 587 kb long genomic region (unpub. res.). This highlights how the organization of the *fru* gene within a very large genomic locus is a conserved feature in the *Ae. aegypti* and *Ae. albopictus species*.

To investigate the evolutionary trajectory of *fru* gene organization, we compared the gene structure among *Drosophila*, *Anopheles*, *Ae. aegypti*, and *Ae. albopictus* (Figure 4A). The five non-sex-specific exons in *Aalfru* (C1-C2-C3-C4-C5) show structural similarity to the corresponding exons in *Drosophila*, *An. gambiae*, and *Ae. aegypti fru* genes, with the highest conservation observed in exons C1 and C2, where the encoded amino acid sequences are essentially identical across species. Exons C3, C4, and C5 display greater variability in size and amino acid composition (Figure 2). Additionally, exon P1 encodes a conserved male-specific N-terminal domain and exhibits sex-specific alternative splicing regulation, as seen in the other *fru* orthologues.

We then proceeded to analyze the genomic region where the exon *fru*-P1 is located in *Ae. albopictus* to better understand the structural organization and potential regulatory elements within this region that govern its sex-specific splicing. Exon–intron boundaries were predicted by using the Berkeley BDGP Splice Site Prediction Tool with default parameters http://www.fruitfly.org/seq_tools/splice.html (accessed on 2 February 2024); prediction scores are indicated in red in Figure 4B) and then confirmed by using male- and female-specific *fru*-P1 transcripts vs. genome alignments. The *Aalfru*-P1 transcripts undergo sex-specific alternative splicing from the embryonic stage to adulthood. Similar to what has been observed in *D. melanogaster* and *Ae. aegypti*, the *fru* gene in *Ae. albopictus* features two canonical 5′ donor splice sites (5′ss) in the sex-specifically regulated region [21]. These sites exhibit a conserved sequence matching the eukaryotic 5′ss consensus (MAG/GTRAGT; M = A or C and R = A or G) (Figure 4B). In vivo, these two 5′ss function as alternative sex-specific splicing sites (P1m 5′ss and P1f 5′ss). To assess the intrinsic strength of the two sex-specific 5′ ss, independently of additional flanking regulatory signals, we applied

the MaxEntScan algorithm [21,40]. The results shown in Figure 4B corroborated previous findings in the *Ae. aegypti fru* gene, also indicating that the *Aalfru* female-specific P1f 5′ss (MaxEntScan score = 10.65) seems to be stronger than its male-specific P1m 5′ss counterpart (MaxEntScan score = 9.80) suggesting the existence of a mechanism that represses the P1f 5′ss usage in the male sex.

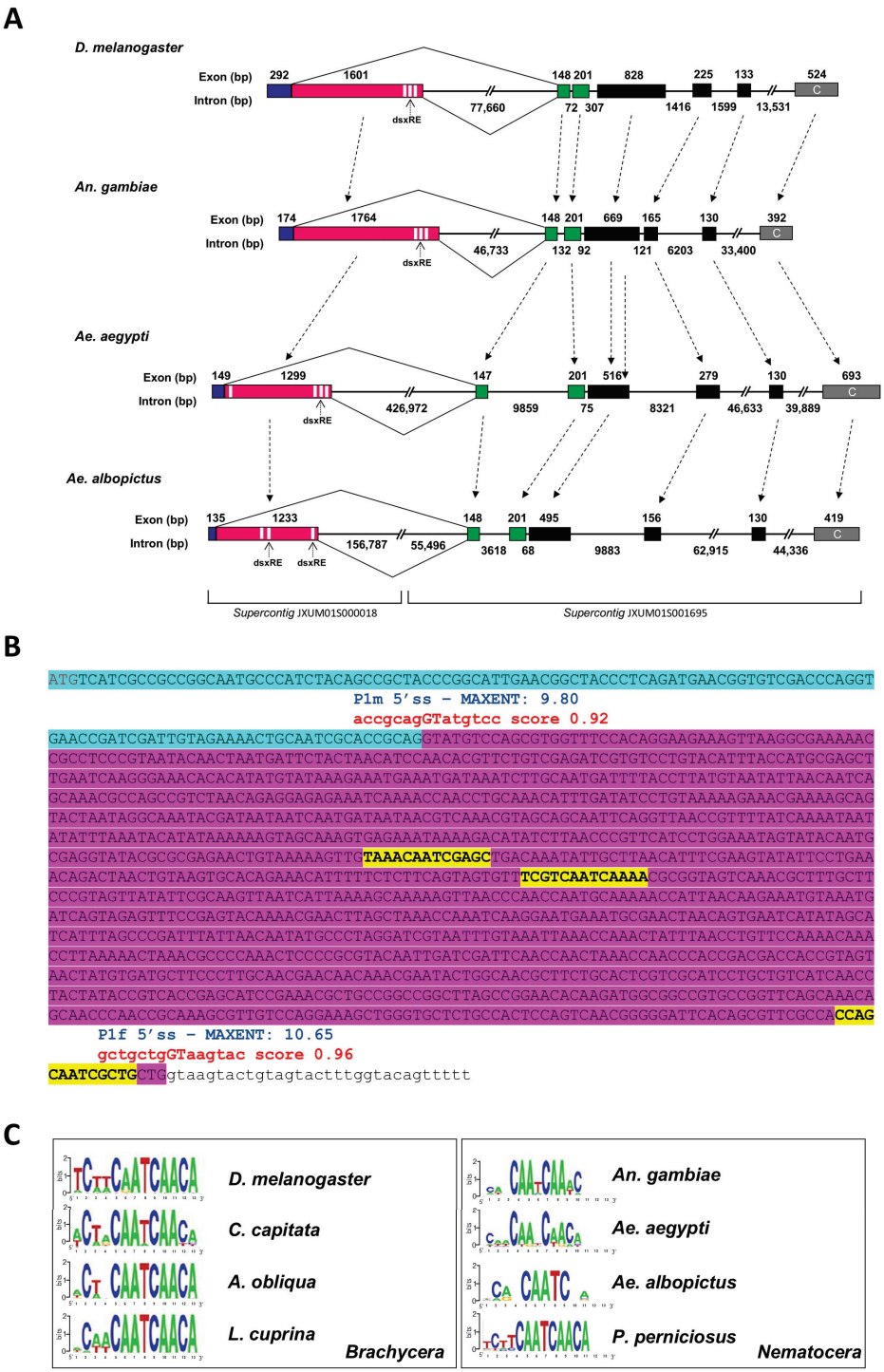


Figure 4. A comparative scheme of *D. melanogaster*, *An. gambiae*, *Ae. Aegypti*, and *Ae. albopictus* gene structures. (**A**) The portions of *fru* genes, starting with the sex-specific regulated region and ending

with the ZnF-C domain encoding exon, are reported. The male-specific and female-specific exons are represented as blue and pink boxes, respectively. The green boxes represent the non-sex-specific exons encoding the BTB domain and the black boxes represent the connector region of FRU proteins. The terminal grey boxes represent the ZnF-C domain encoding exons. The white sequences represent TRA/TRA-2 binding sites. The *Ae. albopictus fru* gene is located in supercontigs JXUM01S001695 and JXUM01S000018 of the AaloF1 reference genome and on chromosome 1 of the AalbF5 genome assembly (GCF_035046485.1). (**B**) The *fru-P1* sex-specific region. The azure sequence indicates the male-specific exon; the purple sequence indicates the female-specific exon. The red are the predicted splicing donor sites. The blue are the P1m 5′ss and P1f 5′ss MAXENT scores. The yellow are the putative TRA/TRA-2 binding sites. (**C**) The WebLogo consensus sequence of the putative TRA/TRA-2 binding sites identified in *dsx* and *fru* genes of Dipteran Brachycera and Nematocera species. Within Nematocera, only in the *P. perniciosus* sand fly species it is possible to define a clear TRA/TRA-2 binding sites consensus sequence.

The sex-specific regulation of *fru* has been extensively studied in *D. melanogaster*, where TRA and TRA-2 splicing regulators play a pivotal role in promoting female-specific splicing. This regulation is mediated by the binding of TRA and TRA-2 proteins to *cis*-regulatory elements, known as TRA/TRA-2 binding sites, which are present in multiple copies within the *fru* and *dsx* mRNAs [41,42]. These binding sites are highly conserved across the *fru* and *dsx* genes of many dipteran species within the Brachycera suborder [8,43]. In contrast, within the Nematocera suborder of Diptera, highly conserved TRA/TRA-2 binding sites have been identified only in the sex-determination genes of sandflies (Figure 4C). This suggests a conserved role for TRA and TRA-2 proteins in regulating sex-specific splicing and controlling sex determination in these species [20,44], and the evolution of different mechanisms and regulators in other Nematocera species, including mosquitoes.

Similar to *Ae. aegypti* and *An. gambiae*, the *fru*-P1 region in *Ae. albopictus* lacks highly conserved TRA/TRA-2 binding sites. Notably, the analysis of this region in *Ae. albopictus* revealed an even greater level of divergence. We identified three putative TRA/TRA-2 binding site sequences with an even higher level of sequence degeneration compared to what has been observed in *Ae. aegypti* and *An. gambiae* (Figure 4A,B). Additionally, while the positions of the putative TRA/TRA-2 binding sites in these two species are conserved relative to *Drosophila*, with three sequences located near the P1f 5′ss, and only in *Ae. aegypti* an additional putative sequence found near the P1m 5′ss, the positions of the three sequences identified in *Ae. albopictus* are also divergent, with two of these sequences located in the center of the female-specific region, and only one found near the P1f 5′ss (Figure 4C). These findings suggest that additional elements, such as the genomic context, flanking intronic sequences, and distinct upstream regulatory proteins, likely play a role in modulating the functional activity of *fru* sex-specific splice sites, thereby enabling their precise sex-specific utilization.

3.4. The In Vivo Functional Analysis of the fru Gene in Ae. albopictus by RNAi Knockdown

To investigate the in vivo function of the *Aalfru* gene, we performed the RNAi knockdown of *fru*-P1 transcripts by microinjecting dsRNA molecules into embryos at the one-hour developmental stage. The dsRNA molecules were specifically designed to target the 5′ region of *fru*-P1 transcripts in both sexes (Figure 5A). Approximately 1400 embryos were injected with these *fru*-specific dsRNAs, while as a negative control, about 500 embryos were injected with dsRNAs targeting the exogenous Green Fluorescent Protein (GFP) gene, absent in the genome of *Ae. albopictus* (Table 2). In both experimental and control groups, we observed high levels of embryo mortality, which we attributed to the microinjection procedure itself and the specific conditions of the *Ae. albopictus* strain utilized for embryo production. Similar mortality rates (98%) were also recorded in additional microinjection tests performed with injection buffer only.

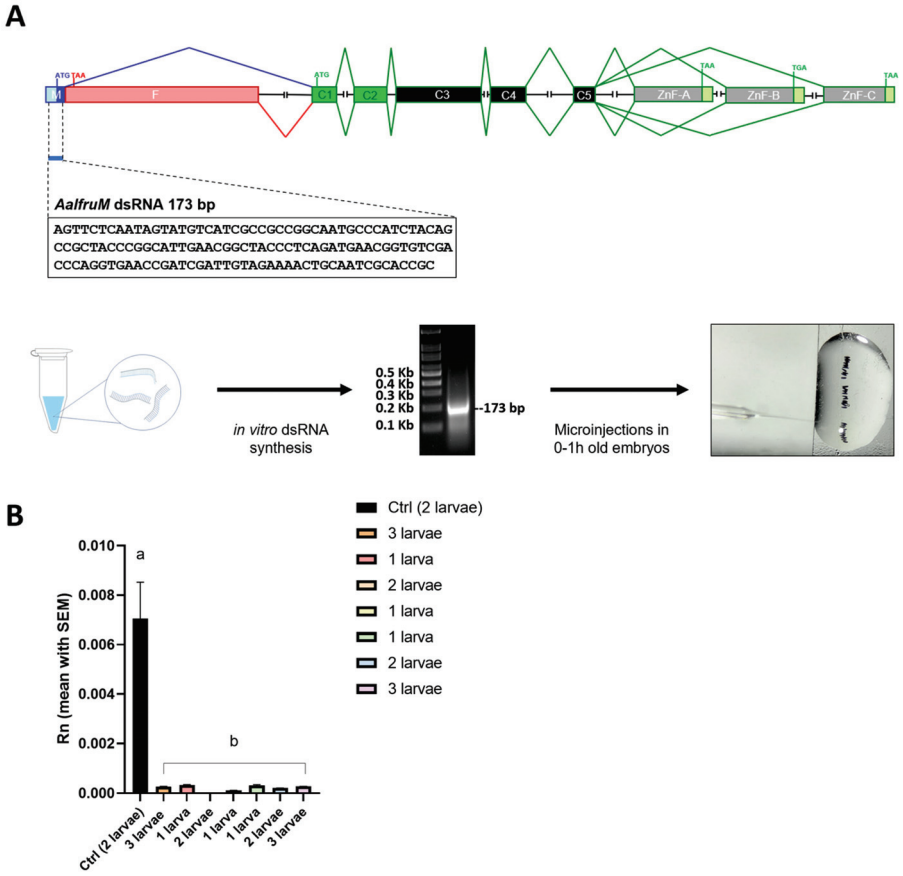


Figure 5. The RNAi knockdown analysis of the *fru* gene in *Ae. albopictus*. (**A**) The schematic representation of the RNAi knockdown analysis. The first lane left is a 100 bp ladder (NEB). The 133 bp long dsRNA synthesized in vitro, targets the M exon of the sex-specifically regulated *Aalfru* gene. This region is present in both the male- and female-specific *Aalfru* transcripts. (**B**) The expression level of the *Ae. albopictus fru* gene in larvae subjected to *AalfruM* interference at the embryonic stage. The larvae were analyzed as single specimens or as a pool of two or three larvae, at the third instar larval stage. The x-axis indicates the sample ID and the y-axis shows the relative expression value obtained by qRT-PCR. The internal reference gene was the *Ae. albopictus* ribosomal protein 49 (*Aalrp49*). The error bars represent the SEM. One-way ANOVA was used to assess differences among the control group and RNAi groups (p-Value < 0.0001), Dunnett's multiple comparisons test: 'a' vs. 'b' <0.0001. Eight wild-type males, four males developed from embryos injected with GFP dsRNA, and eight males developed from embryos injected with *AalfruM* dsRNA were individually crossed with five wild-type females, resulting in a total of twenty mating experiments (Figure 6A). Before cross set-up, all males were visually inspected under a stereomicroscope for abnormalities in sexual phenotypes, including antennae structure, body size, and genitalia. No notable physical abnormalities were observed. To evaluate the effects of the *Aalfru* knockdown on male sexual behavior, we conducted mating assays by observing the formation of mating pairs within each cage and recording the duration of copulation (Figure 6C). A significant difference in mating duration was noted between control males (wild-type and GFP dsRNA-injected) and *Aalfru*-knockdown males when paired with wild-type virgin females. The mating time for *Aalfru*-knockdown males was substantially reduced, averaging approximately 3 s, compared to an average duration of 20 s for the wild-type and GFP control males (Figure 6C). These results suggest that the suppression of *Aalfru* expression profoundly impacts male sexual behavior, likely impairing their ability to sustain normal mating interactions. This highlights the role of *Aalfru* in regulating the key aspects of male reproductive behavior in *Ae. albopictus*.

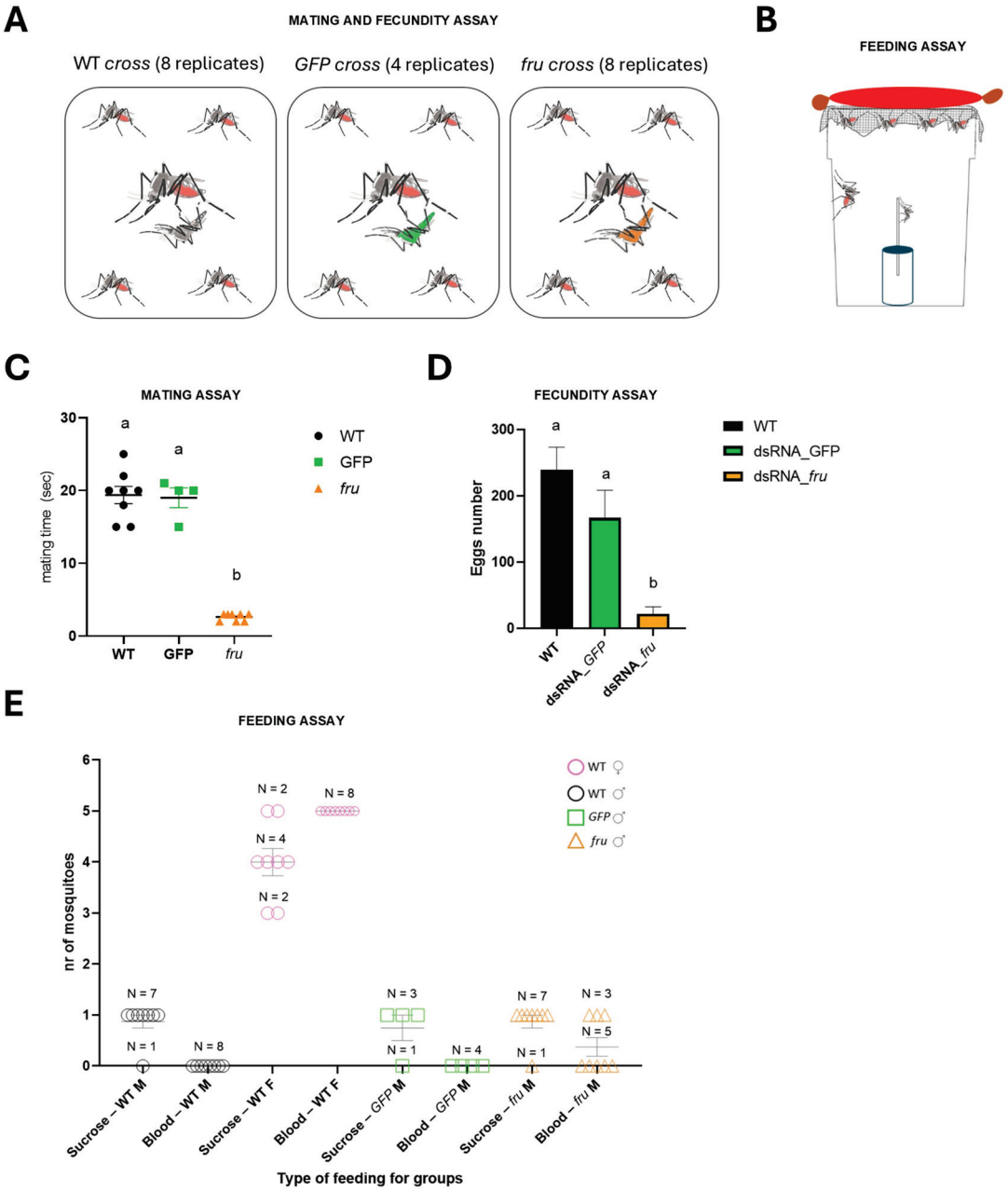


Figure 6. The mating, fecundity, and feeding assays of the RNAi-knockdown *fru* males. (**A**) The mating and fecundity assay schematic. (**B**) The feeding assay schematic. (**C**) The mating time for the three types of crosses is indicated in the A panel. The one-way ANOVA test, *p*-Value < 0.0001. Dunnett's multiple comparisons test: 'a' vs. 'b' < 0.0001. (**D**) The egg numbers for the three types of crosses as indicated in the A panel. The one-way ANOVA test, *p*-Value 0.0004. Dunnett's multiple comparisons test: 'a' vs. 'b' < 0.0001. The different letters above bars ('a' vs. 'b') mean significant differences between the different groups. (**E**) The scatter dot plot shows the number of mosquitoes that fed on sucrose or blood in different groups: wild-type male and female (WT M, WT F), *GFP*, and *fru* males (*GFP* M, *fru* M). Each dot represents an individual cross. The horizontal bars indicate the mean ± standard error of the mean (SEM). N represents the number of crosses (panel A) observed for each group.

A total of 22 *Aalfru* knockdown larvae were obtained following dsRNA injection. Of these, 13 were selected for further analysis to assess the RNAi-mediated reduction in *fru*-P1 transcript levels. From the control group, seven larvae were obtained, and three were

chosen as reference samples for comparison. Using qRT-PCR, we observed a significant reduction ($p < 0.0001$) of more than 90% of *Aalfru* mRNA levels in all larvae tested. This included the individual analysis and pooled analyses of 2–3 larvae at the third instar larval stage, compared to the GFP control group (Figure 5B). These results confirmed the successful knockdown of *fru*-P1 transcripts through embryonic RNAi, demonstrating a significant reduction in expression levels that persists up to the fourth instar larval stage.

Table 2. Number of injected embryos and adult individuals obtained in RNAi knockdown.

Name	Injected Embryos	Larvae	Pupae	Adults	Males	Females	Larval Survival Rate (%)
AalfruM dsRNA	1375	22 *	9	9	8	1	1.60
GFP dsRNA	516	7 †	7	7	4	3	1.36

* Thirteen larvae were used to perform qRT-PCR analysis of *fru* expression level. † Three larvae were used to perform qRT-PCR analysis of *fru* expression level.

In insects, embryonic RNAi is primarily used to study the function of genes involved in early embryonic development and cellular differentiation, rather than genes that play roles in post-embryonic development. This is because the injection of dsRNA into embryos produces a transient effect in the cells, which is not passed on to the next generation. As a result, genes expressed during the later stages of development are generally not easily inactivated using this approach [45,46]. Our developmental expression analysis of the *Aalfru* gene revealed a very early sex-specific expression, starting from the embryonic stage till adulthood. This suggests that this gene may have an early role in establishing sex-specific larval neuron connections in the central nervous system that could persist into adulthood. We tested this hypothesis by analyzing the mating behavior, fertility, and feeding behavior of males developed from dsRNA-injected embryos.

To evaluate mating success, we then measured fecundity by collecting and counting the eggs laid by females from each cross over three days. A statistically significant difference in the average number of eggs was observed between the *Aalfru*-knockdown crosses and the control groups (WT and GFP dsRNA-injected males) with a reduction of more than 90% (Figure 6D). Specifically, females mated with *Aalfru*-knockdown males laid significantly fewer eggs compared to those mated with control males. Notably, none of the eggs from the *Aalfru*-knockdown crosses produced viable larvae, indicating that the eggs were non-viable. This suggests that despite the brief mating interactions observed between *Aalfru*-knockdown males and wild-type females, successful reproduction did not occur. The lack of fertilization in these crosses indicates that the suppression of *Aalfru* impairs the males' ability to effectively fertilize eggs, further underscoring the critical role of *Aalfru* in male reproductive competence and overall mating success.

Basrur et al. (2020) used CRISPR-Cas9 to create *fru* mutant *Ae. aegypti* males, showing they were not only unable to mate, confirming *fru* as a key regulator of male courtship across insects, but also that they were strongly attracted to live human hosts, a behavior not present in wild-type males [28]. This revealed that males possess neural circuits for host-seeking behavior, normally repressed by *fruM*, highlighting an evolutionary adaptation where a male-specific regulator also controls a female-specific trait—blood-feeding [28]. To verify whether in *Ae. albopictus*, the *fru* gene could also be involved in the repression of the female-specific blood-feeding behavior as in *Ae. aegypti*, a feeding assay (Figure 6B) was developed where both male and female mosquitoes were provided with access to either a sucrose solution or a blood meal source. Both *Aalfru*-knockdown and *GFP*-knockdown males exhibited normal feeding behavior on the sucrose source, consistent with the behavior

observed in wild-type males and females. To test blood-feeding responses, a warm blood-filled sausage, which had been rubbed on the operator's arm to transfer odor molecules mimicking human skin scent, was placed atop the cages. Wild-type females fed on the blood sausage, as expected. Interestingly, three out of eight *Aalfru*-knockdown males also exhibited attraction for the blood source, which was completely absent in all *GFP*-knockdown males and wild-type males (Figure 6E). These three *Aalfru*-knockdown males actively explored the area near the sausage, probing the surface of the sausage membrane with their mouthparts, mimicking the blood-feeding behavior typically observed in females. This suggests that *Aalfru* knockdown disrupts the male-specific feeding program, partially inducing female-like blood-feeding behavior.

4. Conclusions

This study underscores the crucial role of the *fruitless* (*fru*) gene in regulating male-specific behaviors in *Ae. albopictus*. Through detailed structural and functional analyses, we revealed a high degree of conservation in *Aalfru* gene organization and its sex-specific alternative splicing mechanisms. In addition, we showed that the *Aalfru* gene exhibits an early sex-specific expression, starting from the embryonic stage, a novel feature not yet reported for any dipteran species.

An open question remains about the upstream splicing regulators of *fru*, as well as of the *dsx* gene in *Aedes* mosquitoes. The absence of evidence of the direct interaction between *AalNix* protein and the pre-mRNA of *Aaldsx*, combined with evidence supporting an indirect regulation of splicing and the presence of potential splicing enhancer elements, strongly suggests the existence of an as-yet unidentified intermediate regulator within the sex determination cascade of *Ae. albopictus* [47]. This hypothetical regulator may act as a mediator between upstream signals, such as those involving *AalNix*, and the downstream splicing machinery responsible for producing sex-specific isoforms of *Aaldsx* and *Aalfru* orthologs. Further investigation into this intermediate factor is essential to fully elucidate the molecular mechanisms driving sex determination in this species, as its identification could bridge critical gaps in our understanding of how upstream genetic signals are translated into the regulation of alternative splicing events.

Our transient embryonic RNA interference-mediated knockdown of *fru* in *Ae. albopictus* demonstrated that its disruption leads to significant impairments in male courtship and mating behavior, ultimately resulting in reproductive failure. Our results suggest an essential role of the *fru* gene in the early formation of sex-specific neuronal connections in mosquitoes. The microinjections performed on embryos immediately affected neurobiological development, and these changes were found to persist in adulthood. Our findings suggest that the neuronal structures formed during the early larval stages are crucial for the sexual behavior and adaptation of adult mosquitoes. Furthermore, the unexpected observation of female-like blood-feeding behavior found in *Ae. aegypti* also seems to be conserved in *fru*-knockdown *Ae. albopictus* males, confirming an intriguing evolutionary repurposing of *fru*, which functions to repress female-specific traits in males. In the future, it would be highly valuable to identify the downstream genes in the pathway of the *fru* gene by utilizing mutant lines generated through CRISPR-Cas9 approaches and combined with transcriptomics. This would provide deeper insights into how this gene contributes to the establishment of sex-specific behavioral patterns.

In conclusion, our findings not only provide insights into the genetic control of determination in *Ae. albopictus* but also open new avenues for developing innovative, gene-targeted strategies for Asian tiger mosquito population management and vector control based on

the interference with the courtship and mating behaviors, as recently proposed for other mosquito species using the *dsx* gene splicing manipulation [48,49].

Supplementary Materials: The following supporting information can be downloaded at https://www.mdpi.com/article/10.3390/insects16030280/s1. File S1: *Aalfru* sequences.

Author Contributions: Conceptualization, M.S. and M.V.; methodology, M.V., P.D.L., F.L., G.V., S.M.M., A.C., K.N. and A.E.Ö.; validation, M.V., P.D.L., F.L., G.V., A.C. and S.M.M.; investigation, M.V., G.S., S.A. and M.S.; resources, K.B., G.S., S.A. and M.S.; data curation, M.S. and M.V.; writing—original draft preparation, M.S. and M.V.; writing—review and editing, M.V., P.D.L., F.L., G.V., S.M.M., A.C., S.A., G.S., K.N., A.E.Ö., K.B. and M.S.; project administration, M.V. and M.S.; funding acquisition, M.S; project supervision, K.B. and M.S. All authors have read and agreed to the published version of the manuscript.

Funding: This research was funded by the EU within the NextGeneration EU-MUR PNRR Extended Partnership initiative on Emerging Infectious Diseases (Project no. PE00000007, INF-ACT) (MS); the University of Naples Federico II and Compagnia di San Paolo, Naples, ITALY, in the frame of the Program STAR2013 (Sostegno Territoriale alle Attività di Ricerca) (STAR2013_25 grant) (MS); and by the POR Campania 2014/2020, Obiettivo specifico 14, Azione 10.4.5, Dottorati di ricerca con caratterizzazione industriale, Regional Agency for the promotion of Research and Innovation, Naples, ITALY, (MV). This study was also financially supported by the Insect Pest Control Subprogramme of the Joint FAO/IAEA Centre of Nuclear Techniques in Food and Agriculture and the United States State Department in the frame of the "Surge Expansion of the Sterile Insect Technique (SIT) to Control Mosquito Populations that Transmit the Zika Virus" project.

Data Availability Statement: Data are contained within the article and Supplementary Materials. The data presented in this study are available in Supplementary File S1.

Acknowledgments: We would like to thank the following students from the University of Naples: Federico II who contributed during their experimental thesis period to the maintenance of *Ae. albopictus* colonies and assisted with experimental procedures; Liliana Tullo; Daniela Carannante; Ciro Rizzo; Michela Schiavo; and Daniela Esposito. We would also like to thank Danilo O. Carvalho for his support during the experimental work carried out at the Insect Pest Control Laboratory.

Conflicts of Interest: The authors declare no conflicts of interest.

References

1. Fuxjager, M.J.; Fusani, L.; Schlinger, B.A. Physiological innovation and the evolutionary elaboration of courtship behaviour. *Anim. Behav.* **2022**, *184*, 185–195. [CrossRef]
2. Salvemini, M.; Polito, C.; Saccone, G. Fruitless alternative splicing and sex behaviour in insects: An ancient and unforgettable love story? *J. Genet.* **2010**, *89*, 287–299. [CrossRef] [PubMed]
3. Brockmann, H.J.; Thornhill, R.; Alcock, J. The Evolution of Insect Mating Systems. *Fla Entomol.* **1984**, *67*, 180. [CrossRef]
4. Shuker, D.; Simmons, L. (Eds.) *The Evolution of Insect Mating Systems*; Oxford University Press: Oxford, UK, 2014.
5. McKelvey, E.G.; Fabre, C.C. Recent neurogenetic findings in insect courtship behaviour. *Curr. Opin. Insect Sci.* **2019**, *36*, 103–110. [CrossRef]
6. Shirangi, T.R.; Taylor, B.J.; McKeown, M. A double-switch system regulates male courtship behavior in male and female *Drosophila melanogaster*. *Nat. Genet.* **2006**, *38*, 1435–1439. [CrossRef] [PubMed]
7. Auer, T.O.; Benton, R. Sexual circuitry in Drosophila. *Curr. Opin. Neurobiol.* **2016**, *38*, 18–26. [CrossRef]
8. Saccone, G.; Salvemini, M.; Polito, L.C. The transformer gene of Ceratitis capitata: A paradigm for a conserved epigenetic master regulator of sex determination in insects. *Genetica* **2011**, *139*, 99–111. [CrossRef]
9. Saccone, G. A history of the genetic and molecular identification of genes and their functions controlling insect sex determination. *Insect Biochem. Mol. Biol.* **2022**, *151*, 103873. [CrossRef]
10. Dornan, A.J.; Gailey, D.A.; Goodwin, S.F. GAL4 enhancer trap targeting of the Drosophila sex determination gene fruitless. *Genesis* **2005**, *42*, 236–246. [CrossRef]

11. Anand, A.; Villella, A.; Ryner, L.C.; Carlo, T.; Goodwin, S.F.; Song, H.J.; A Gailey, D.; Morales, A.; Hall, J.C.; Baker, B.S.; et al. Molecular Genetic Dissection of the Sex-Specific and Vital Functions of the *Drosophila melanogaster* Sex Determination Gene fruitless. *Genetics* **2001**, *158*, 1569–1595. [CrossRef]
12. Song, H.J.; Billeter, J.C.; Reynaud, E.; Carlo, T.; Spana, E.P.; Perrimon, N.; Goodwin, S.F.; Baker, B.S.; Taylor, B.J. The fruitless Gene Is Required for the Proper Formation of Axonal Tracts in the Embryonic Central Nervous System of Drosophila. *Genetics* **2002**, *162*, 1703–1724. [CrossRef] [PubMed]
13. Chowdhury, Z.S.; Sato, K.; Yamamoto, D. The core-promoter factor TRF2 mediates a Fruitless action to masculinize neurobehavioral traits in Drosophila. *Nat. Commun.* **2017**, *8*, 1480. [CrossRef]
14. Ito, H.; Sato, K.; Koganezawa, M.; Ote, M.; Matsumoto, K.; Hama, C.; Yamamoto, D. Fruitless Recruits Two Antagonistic Chromatin Factors to Establish Single-Neuron Sexual Dimorphism. *Cell* **2012**, *149*, 1327–1338. [CrossRef] [PubMed]
15. Ito, H.; Sato, K.; Kondo, S.; Ueda, R.; Yamamoto, D. Fruitless Represses robo1 Transcription to Shape Male-Specific Neural Morphology and Behavior in Drosophila. *Curr. Biol.* **2016**, *26*, 1532–1542. [CrossRef]
16. Goto, J.; Mikawa, Y.; Koganezawa, M.; Ito, H.; Yamamoto, D. Sexually Dimorphic Shaping of Interneuron Dendrites Involves the Hunchback Transcription Factor. *J. Neurosci.* **2011**, *31*, 5454–5459. [CrossRef] [PubMed]
17. Sato, K.; Goto, J.; Yamamoto, D. Sex Mysteries of the Fly Courtship Master Regulator Fruitless. *Front. Behav. Neurosci.* **2019**, *13*, 245. [CrossRef]
18. Gailey, D.A.; Billeter, J.C.; Liu, J.H.; Bauzon, F.; Allendorfer, J.B.; Goodwin, S.F. Functional Conservation of the fruitless Male Sex-Determination Gene Across 250 Myr of Insect Evolution. *Mol. Biol. Evol.* **2006**, *23*, 633–643. [CrossRef]
19. Meier, N.; Käppeli, S.C.; Hediger Niessen, M.; Billeter, J.C.; Goodwin, S.F.; Bopp, D. Genetic Control of Courtship Behavior in the Housefly: Evidence for a Conserved Bifurcation of the Sex-Determining Pathway. *PLoS ONE* **2013**, *8*, e62476. [CrossRef]
20. Petrella, V.; Aceto, S.; Colonna, V.; Saccone, G.; Sanges, R.; Polanska, N.; Volf, P.; Gradoni, L.; Bongiorno, G.; Salvemini, M. Identification of sex determination genes and their evolution in Phlebotominae sand flies (Diptera, Nematocera). *BMC Genom.* **2019**, *20*, 522. [CrossRef]
21. Salvemini, M.; D'Amato, R.; Petrella, V.; Aceto, S.; Nimmo, D.; Neira, M.; Alphey, L.; Polito, L.C.; Saccone, G. The Orthologue of the Fruitfly Sex Behaviour Gene Fruitless in the Mosquito *Aedes aegypti*: Evolution of Genomic Organisation and Alternative Splicing. *PLoS ONE* **2013**, *8*, e48554. [CrossRef]
22. Bertossa, R.C.; van de Zande, L.; Beukeboom, L.W. The Fruitless Gene in Nasonia Displays Complex Sex-Specific Splicing and Contains New Zinc Finger Domains. *Mol. Biol. Evol.* **2009**, *26*, 1557–1569. [CrossRef] [PubMed]
23. Ueno, M.; Nakata, M.; Kaneko, Y.; Iwami, M.; Takayanagi-Kiya, S.; Kiya, T. fruitless is sex-differentially spliced and is important for the courtship behavior and development of silkmoth *Bombyx mori*. *Insect Biochem. Mol. Biol.* **2023**, *159*, 103989. [CrossRef] [PubMed]
24. Nguantad, S.; Chumnanpuen, P.; Thancharoen, A.; Vongsangnak, W.; Sriboonlert, A. Identification of potential candidate genes involved in the sex determination cascade in an aquatic firefly, *Sclerotia aquatilis* (Coleoptera, Lampyridae). *Genomics* **2020**, *112*, 2590–2602. [CrossRef]
25. Boerjan, B.; Tobback, J.; Vandersmissen, H.P.; Huybrechts, R.; Schoofs, L. Fruitless RNAi knockdown in the desert locust, *Schistocerca gregaria*, influences male fertility. *J. Insect Physiol.* **2012**, *58*, 265–269. [CrossRef] [PubMed]
26. Wang, B.; Mao, Z.; Chen, Y.; Ying, J.; Wang, H.; Sun, Z.; Li, J.; Zhang, C.; Zhuo, J. Identification and Functional Analysis of the fruitless Gene in a Hemimetabolous Insect, *Nilaparvata lugens*. *Insects* **2024**, *15*, 262. [CrossRef]
27. Zhang, W.; Wang, J.; Liu, Q.; Gong, Z. A Review of Pathogens Transmitted by the Container-Inhabiting Mosquitoes, *Aedes albopictus*, A Global Public Health Threat. *China CDC Wkly.* **2023**, *5*, 984–990. [CrossRef]
28. Basrur, N.S.; De Obaldia, M.E.; Morita, T.; Herre, M.; von Heynitz, R.K.; Tsitohay, Y.N.; Vosshall, L.B. Fruitless mutant male mosquitoes gain attraction to human odor. *eLife* **2020**, *9*, e63982. [CrossRef]
29. Puggioli, A.; Carrieri, M.; Dindo, M.L.; Medici, A.; Lees, R.S.; Gilles, J.R.L.; Bellini, R. Development of *Aedes albopictus* (Diptera: Culicidae) Larvae Under Different Laboratory Conditions. *J. Med. Entomol.* **2017**, *54*, 142–149. [CrossRef]
30. Bellini, R.; Medici, A.; Puggioli, A.; Balestrino, F.; Carrieri, M. Pilot field trials with *Aedes albopictus* irradiated sterile males in Italian urban areas Urban Areas. *J. Med. Entomol.* **2013**, *50*, 317–325. [CrossRef]
31. Maïga, H.; Yamada, H.; Severin, B.-S.N.; de O. Carvalho, D.; Mamai, W.; Herrero, R.A.; Bourtzis, K.; Bouyer, J. *Guidelines for Routine Colony Maintenance of Aedes Mosquito Species*, 1st ed.; Insect Pest Control Section of the Joint FAO/IAEA Division IAEA, Ed.; Food and Agriculture Organization of the United Nations International Atomic Energy Agency: Vienna, Austria, 2017.
32. Xi, Z.; Dean, J.L.; Khoo, C.; Dobson, S.L. Generation of a novel Wolbachia infection in *Aedes albopictus* (Asian tiger mosquito) via embryonic microinjection. *Insect Biochem. Mol. Biol.* **2005**, *35*, 903–910. [CrossRef]

33. Calle-Tobón, A.; Holguin-Rocha, A.F.; Moore, C.; Rippee-Brooks, M.; Rozo-Lopez, P.; Harrod, J.; Fatehi, S.; Rua-Uribe, G.L.; Park, Y.; Londoño-Rentería, B. Blood Meals With Active and Heat-Inactivated Serum Modifies the Gene Expression and Microbiome of *Aedes albopictus*. *Front. Microbiol.* **2021**, *12*, 724345. [CrossRef]
34. Livak, K.J.; Schmittgen, T.D. Analysis of Relative Gene Expression Data Using Real-Time Quantitative PCR and the $2^{-\Delta\Delta CT}$ Method. *Methods* **2001**, *25*, 402–408. [CrossRef] [PubMed]
35. Lee, G.; Foss, M.; Goodwin, S.F.; Carlo, T.; Taylor, B.J.; Hall, J.C. Spatial, temporal, and sexually dimorphic expression patterns of the fruitless gene in the Drosophila central nervous system. *J. Neurobiol.* **2000**, *43*, 404–426. [CrossRef]
36. Gomulski, L.M.; Mariconti, M.; Di Cosimo, A.; Scolari, F.; Manni, M.; Savini, G.; Malacrida, A.R.; Gasperi, G. The Nix locus on the male-specific homologue of chromosome 1 in *Aedes albopictus* is a strong candidate for a male-determining factor. *Parasites Vectors* **2018**, *11*, 647. [CrossRef] [PubMed]
37. Moffett, S.B.; Moffett, D.F. Comparison of immunoreactivity to serotonin, FMRFamide and SCPb in the gut and visceral nervous system of larvae, pupae and adults of the yellow fever mosquito *Aedes aegypti*. *J. Insect Sci.* **2005**, *5*, 1–12. [CrossRef]
38. Mysore, K.; Flister, S.; Müller, P.; Rodrigues, V.; Reichert, H. Brain development in the yellow fever mosquito *Aedes aegypti*: A comparative immunocytochemical analysis using cross-reacting antibodies from *Drosophila melanogaster*. *Dev. Genes Evol.* **2011**, *221*, 281–296. [CrossRef] [PubMed]
39. Ziemer, T.; Wetjen, F.; Herbst, A. The Antenna Base Plays a Crucial Role in Mosquito Courtship Behavior. *Front. Trop. Dis.* **2022**, *3*, 803611. [CrossRef]
40. Yeo, G.; Burge, C.B. Maximum Entropy Modeling of Short Sequence Motifs with Applications to RNA Splicing Signals. *J. Comput. Biol.* **2004**, *11*, 377–394. [CrossRef]
41. Hoshijima, K.; Inoue, K.; Higuchi, I.; Sakamoto, H.; Shimura, Y. Control of *doublesex* Alternative Splicing by *transformer* and *transformer-2* in *Drosophila*. *Science* **1991**, *252*, 833–836. [CrossRef]
42. Lam, B.J.; Bakshi, A.; Ekinci, F.Y.; Webb, J.; Graveley, B.R.; Hertel, K.J. Enhancer-dependent 5′-Splice Site Control of fruitless Pre-mRNA Splicing. *J. Biol. Chem.* **2003**, *278*, 22740–22747. [CrossRef]
43. Salvemini, M.; Mauro, U.; Lombardo, F.; Milano, A.; Zazzaro, V.; Arcà, B.; Polito, L.C.; Saccone, G. Genomic organization and splicing evolution of the doublesex gene, a Drosophila regulator of sexual differentiation, in the dengue and yellow fever mosquito *Aedes aegypti*. *BMC Evol. Biol.* **2011**, *11*, 41. [CrossRef]
44. Petrella, V.; Aceto, S.; Musacchia, F.; Colonna, V.; Robinson, M.; Benes, V.; Cicotti, G.; Bongiorno, G.; Gradoni, L.; Volf, P.; et al. De novo assembly and sex-specific transcriptome profiling in the sand fly *Phlebotomus perniciosus* (Diptera, Phlebotominae), a major Old World vector of *Leishmania infantum*. *BMC Genom.* **2015**, *16*, 847. [CrossRef] [PubMed]
45. Kennerdell, J.R.; Carthew, R.W. Use of dsRNA-Mediated Genetic Interference to Demonstrate that frizzled and frizzled 2 Act in the Wingless Pathway. *Cell* **1998**, *95*, 1017–1026. [CrossRef] [PubMed]
46. Koo, J.; Palli, S.R. Recent advances in understanding of the mechanisms of RNA interference in insects. *Insect Mol. Biol.* **2024**, 1–14. [CrossRef] [PubMed]
47. Jin, B.; Zhao, Y.; Dong, Y.; Liu, P.; Sun, Y.; Li, X.; Zhang, X.; Chen, X.; Gu, J. Alternative splicing patterns of *doublesex* reveal a missing link between *Nix* and *doublesex* in the sex determination cascade of *Aedes albopictus*. *Insect Sci.* **2021**, *28*, 1601–1620. [CrossRef]
48. Kyrou, K.; Hammond, A.M.; Galizi, R.; Kranjc, N.; Burt, A.; Beaghton, A.K.; Nolan, T.; Crisanti, A. A CRISPR–Cas9 gene drive targeting doublesex causes complete population suppression in caged *Anopheles gambiae* mosquitoes. *Nat. Biotechnol.* **2018**, *36*, 1062–1066. [CrossRef]
49. Larrosa-Godall, M.; Ang, J.X.D.; Leftwich, P.T.; Gonzalez, E.; Shackleford, L.; Nevard, K.; Noad, R.; Anderson, M.A.E.; Alphey, L. Challenges in developing a split drive targeting dsx for the genetic control of the invasive malaria vector *Anopheles stephensi*. *Parasites Vectors* **2025**, *18*, 46. [CrossRef]

Disclaimer/Publisher's Note: The statements, opinions and data contained in all publications are solely those of the individual author(s) and contributor(s) and not of MDPI and/or the editor(s). MDPI and/or the editor(s) disclaim responsibility for any injury to people or property resulting from any ideas, methods, instructions or products referred to in the content.

insects

MDPI

Article

Immune-Related Genes in the Honey Bee Mite *Varroa destructor* (*Acarina, Parasitidae*)

Alfonso Cacace [1], Giovanna De Leva [1], Ilaria Di Lelio [1,2] and Andrea Becchimanzi [1,2,*]

[1] Department of Agricultural Sciences, University of Naples Federico II, 80126 Naples, Italy; alfonso.cacace@unina.it (A.C.); giovanna.deleva@unina.it (G.D.L.); ilaria.dilelio@unina.it (I.D.L.)
[2] BAT Center—Interuniversity Center for Studies on Bioinspired Agro-Environmental Technology, University of Naples Federico II, 80126 Naples, Italy
* Correspondence: andrea.becchimanzi@unina.it

Simple Summary: *Varroa destructor* is a tiny parasitic mite that threatens honey bee populations worldwide by spreading deadly viruses. While efforts to control these mites often rely on chemical treatments, these can harm beneficial insects and lead to resistant mite populations. A promising alternative is using RNA-based treatments to disrupt essential mite functions, such as immunity. However, scientists still know little about how *Varroa* defends itself against infections. In this study, we analyzed the genetic makeup of *Varroa*'s immune system and compared it to that of related species, such as ticks. Our results show that, similar to ticks, *Varroa* lacks certain immune system components found in other arthropods. Its repertoire of antimicrobial peptides is more closely related to that of ticks and spiders than to that of insects. These findings help us better understand how the mite fights infections and provide a foundation for developing new, targeted methods to weaken and control *Varroa* populations. By improving our knowledge of mite immunity, this research contributes to safer and more effective ways to protect honey bee colonies, ensuring their survival and the vital pollination services they provide to ecosystems and agriculture.

Abstract: Despite its ecological and economic importance, many aspects of *Varroa destructor*'s biology remain poorly understood, particularly its defense mechanisms against pathogens. The limited knowledge of *Varroa*'s immunity has hindered the development of RNA interference (RNAi)-based strategies targeting immune-related genes. In this study, we investigated the immune gene repertoire of *V. destructor* by querying its NCBI nr protein database and comparing it to model species of ticks (*Ixodes scapularis*) and mites (*Galendromus occidentalis* and *Tetranychus urticae*). Transcription of candidate immune genes was confirmed by analyzing a de novo assembled transcriptome of *V. destructor*. Our findings reveal that *V. destructor* shares key immunological traits with ticks, including lysozymes, chitinases, and thioester-containing proteins (TEPs), but also shares the absence of transmembrane peptidoglycan recognition proteins (PGRPs), Gram-negative binding proteins, and several lectin families involved in pathogen recognition. Additionally, *Varroa* mites, like ticks, lack homologs of crucial immune signaling components, such as the unpaired ligand (JAK/STAT), Eiger (JNK), and multiple elements of the IMD pathway. They also do not encode canonical antimicrobial peptides (AMPs) like defensins but possess putative homologs of ctenidins, AMPs previously identified in spiders and ticks, which may be adopted as a novel genetic readout for immune response in mites. Our findings lay the groundwork for future functional studies on mite immunity and open new avenues for RNAi-based biocontrol strategies targeting immune pathways to enhance *Varroa* management.

Keywords: chelicerates; immune response; BLASTp; immunity evolution; gene silencing

1. Introduction

Honey bees (*Apis mellifera*) are facing a serious trend of increasing colony losses caused by a multifactorial syndrome in which parasites and pathogens play a major role [1,2]. As indicated by most surveys, colony losses are associated with high levels of *Varroa destructor* and pathogenic viruses, which are vectored by the mites [3,4]. This arthropod is an obligate ectoparasite of honey bees, and has a negative impact on the host, both at the colony and individual level [5,6], since it feeds on liquid tissues through a wound made on the integument of the host [7,8]. This trophic activity has important consequences for the honey bee host, such as the reduction in longevity and weight at emergence [9,10], and the transmission of viral pathogens [11]. In addition, *Varroa* can also impact reproductive fitness, homing, orientation abilities, and also the immune response of bees [12,13].

With a nearly global presence [11,14], *V. destructor* can significantly weaken or even cause the collapse of honey bee colonies if left untreated [15]. Currently, most beekeepers rely heavily on chemical controls to manage the mite [16], despite their detrimental effects on non-target organisms, their residual presence in hive products, and the insurgence of acaricide resistance [17]. This highlights the importance of adopting an Integrated Pest Management (IPM) approach for *Varroa destructor*, which should combine different control methods, including genetic, mechanical, biological, and biotechnical tools, to reduce the impact of treatments with synthetic pesticides [18].

Additional tools for *Varroa* control include "soft" acaricides, such as oxalic acid and thymol, as well as biopesticides like dsRNA [19]. dsRNA works by inducing the degradation of RNA sequences with similar structures, resulting in targeted gene silencing. This process interferes with the synthesis of the encoded protein, enabling selective targeting of specific organismal functions [20].

dsRNA-based control strategies can be classified as either direct killing, targeting vital genes essential for survival, or indirect killing, where lethality occurs only when combined with another treatment. For instance, targeting immune genes with dsRNA combined with a sublethal dose of an entomopathogen-based biopesticide has been proposed as an indirect killing strategy [21].

RNA interference (RNAi) via dsRNA treatments is effective against a wide range of mite species. Since the first application of RNAi through injection in the spider mite *Tetranychus urticae*, silencing the Distal-less gene [22], an increasing number of herbivore and also predator mite species have been shown to be susceptible to RNAi such as *Dermatophagoides pteronyssinus*, *Metaseiulus occidentalis*, *Panonychus citri*, *Phytoseiulus persimilis*, *Sarcoptes scabiei*, *Tetranychus cinnabarinus*, *Tetranychus urticae*, and *Varroa destructor*. The genome sequencing of *T. urticae* allowed research on mites to enter the genome era. A study showed that soaking of mites in the dsRNA solution and mites feeding on dsRNA-coated leaves were the two most efficient methods, and this delivery method may act as a mimic for sprayable dsRNA in future field applications [23].

dsRNA proved to be both (1) deliverable to *V. destructor* by adding it to the artificial diet of adult bees [24,25] or through engineering bees' symbiontic bacteria [26] and (2) effective in controlling mites by targeting several genes. Promising results were observed in the simultaneous silencing of 14 vital genes, including those involved in the cytoskeleton, energy metabolism, and RNA polymerase, significantly reducing mite populations [24,26]. Additionally, salivary genes, which are likely critical for mite feeding, were identified

as vital; their silencing corresponded with reduced mite survival [27,28]. More recently, targeting the *calmodulin* gene to disrupt *Varroa* reproduction led to a significant decrease in mite offspring, though it did not affect mite survival [25]. Despite these advances, the impact of RNAi on many biological functions of *V. destructor* remains unexplored, limiting the potential for indirect strategies such as those that interfere with the mite's immune response.

Arthropods have a more elementary cell-mediated defense system than vertebrates because of the lack of an antigen–antibody complex and memory cells [29]. However, arthropods have evolved effective innate immunity that acts through both cellular and humoral responses directed against invaders [30]. Activation of these responses occurs through the recognition of pathogen-associated molecular patterns (PAMPs) by receptors, known as pattern recognition receptors (PRRs), located on hemocytes (immune cells) and epithelial cells from barrier sites throughout the body [31,32]. Cellular immune responses include phagocytosis, nodulation, encapsulation, and melanization events mediated by hemocytes [33–35]. Humoral responses orchestrated by signaling pathways such as IMD, Toll, JAK/STAT, and JNK lead to the synthesis of various defense enzymes, complement-like proteins, and antimicrobial peptides (AMPs) in response to infection [36–38]. Most of the knowledge about the immunity of the *Acarina* group (mites and ticks) comes from research on the immune responses of ticks, which are structured differently from those of insects and crustaceans. [39]. In ticks and other chelicerates, core intracellular components of the "canonical" IMD pathway, such as the NF-κB transcription factor Relish, are present. However, genome and functional studies indicate that ticks lack key upstream elements, including transmembrane PGRPs and the adapter molecules IMD and FADD [30,40–43].

In this study, we investigated the immune gene repertoire of *V. destructor* by querying its NCBI nr protein database. To place these genes in an evolutionary context, we conducted additional analyses, including comparisons with model species of ticks (*Ixodes scapularis*) and mites (*Galendromus occidentalis* and *Tetranychus urticae*).

2. Materials and Methods

We used a broadly used approach to identify immunity-related genes by inferring protein homology based on sequence similarity through BLASTp searches [44,45]. Immune gene candidates from *D. melanogaster*, reported in Tables 1–3, were used to query the NCBI nr protein database by limiting the target organism to *V. destructor*, *Ixodes scapularis*, *Galendromus occidentalis*, and *Tetranychus urticae*. Only hits with an E-Value less than 1×10^{-5} were considered positive.

To validate the identified candidate immune genes, we used their protein sequences to query a de novo assembled transcriptome of *V. destructor.* The transcriptome was assembled using Illumina reads obtained from a previous study (SRA BioProject ID: PRJNA1097857), in which we analyzed the salivary gland transcriptome of *V. destructor* by comparing it with the transcriptome of the rest of the adult female body [28]. First, reads of all the samples, obtained from more than 140 mites, were cleaned using Trimmomatic [46], merged, and de novo assembled with Trinity [47]. Then, the candidate immune genes were used as the query in tBLASTn searches against the assembled transcriptome. We considered positivity at the transcription level only if the query sequenced had more than 80% identity with the best hit in the transcriptome.

To reconstruct the immune gene phylogeny, putative homologous sequences in other insect species (*Apis mellifera*, *Tribolium castaneum*, and *Bombyx mori*) were identified by sequence similarity searches through BLASTp, using *D. melanogaster* proteins (Tables 1–3) as the query versus the non-redundant NCBI database (nr NCBI db). One best hit per

query was selected and all the protein sequences were aligned using Muscle 3.8 [48], with default settings.

Alignments were automatically trimmed using Gblocks version 0.91b [49] to avoid comparisons of non-conserved regions present only in a subset of the taxa. The best-fit model of amino acid substitution and phylogenetic reconstruction was generated using RAxML 8.2.12 [50]. The maximum likelihood tree was run for 1000 bootstrap replicates and the tree figure was plotted using FigTree v1.4.3. Protein sequences were analyzed with ScanProsite (https://prosite.expasy.org/scanprosite/, accessed on 5 November 2024) and InterProScan [51], in order to identify active sites, conserved patterns, and domains [52]. For PGRPs, we scanned putative homologs for transmembrane helices using DeepTMHMM, which predicts alpha and beta transmembrane proteins using deep neural networks [53].

3. Results and Discussion

3.1. Overview of the Immune Gene Survey

We selected a subset of genes involved in the three phases of the arthropod immune response: recognition, signaling, and response. By using protein sequences from *D. melanogaster*, known to be involved in immunity, as queries in BLASTp searches, we successfully identified putative homologs of *Drosophila* canonical immune genes in *V. destructor*. Specifically, we identified proteins related to recognition, signaling, and response to pathogenic microorganisms (Figure 1).

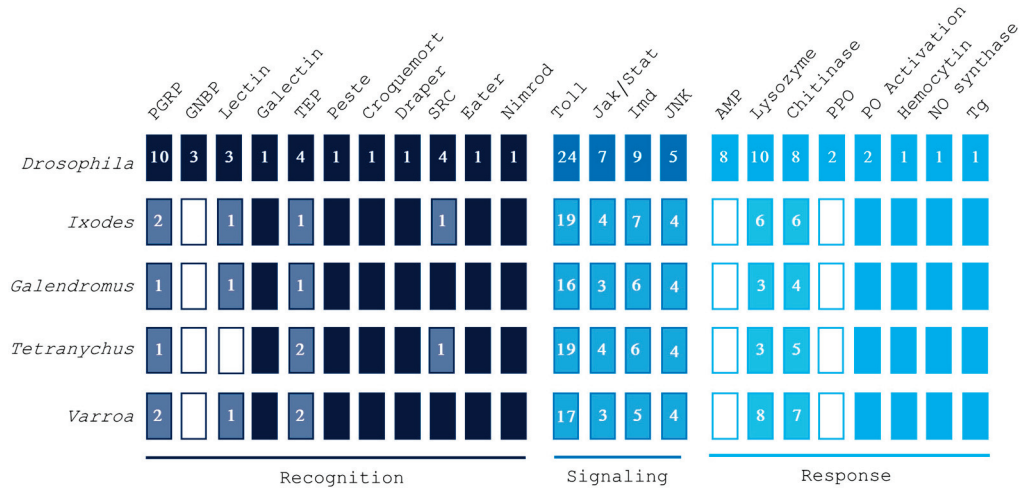


Figure 1. Overview of gene families involved in recognition, signaling, and response pathways in *Varroa destructor*, *Tetranychus urticae*, *Galendromus occidentalis*, and *Ixodes scapularis*. Putative homology was inferred by using *Drosophila melanogaster* queries. Numbers in blocks indicate the amount of different genes identified for each protein family. Filled boxes imply the presence of all the analyzed genes, while empty boxes represent a total absence of them. Abbreviations: peptidoglycan recognition protein (PGRP), Gram-negative binding protein (GNBP), thioester-containing protein (TEP), scavenger receptor class C (SRC), antimicrobial peptide (AMP), pro-phenoloxidase (PPO), phenoloxidase (PO), nitric oxide (NO), transglutaminase (Tg).

3.2. Recognition Genes

Our analysis pointed out the occurrence of proteins encoded by the *V. destructor* genome with significant matches with *Drosophila* genes involved in recognition (Table 1). Among these, only one candidate recognition gene was not transcribed in adult female mites (Supplementary File S1). As occurs in ticks and predatory/phytophagous mites (Tables S1–S3), *V. destructor* lacks transmembrane peptidoglycan recognition proteins (PGRPs), Gram-negative binding proteins, and some members of the c-type lectin family.

Table 1. Immune-related proteins of *Varroa destructor* involved in recognition. Orthologs not found in *V. destructor* are in italics.

Gene Name	Role	*D. melanogaster*	*V. destructor* [1]	E-Value	Identity	Coverage	Transcription
PGRP-LC, peptidoglycan recognition protein	bacterial recognition	AAF50302.3	XP_022660134.1	2×10^{-30}	36.71%	31%	YES
PGRP-LE, peptidoglycan recognition protein	activation of PPO cascade and autophagy	NP_573078.1	XP_022660134.1	5×10^{-25}	31.01%	45%	YES
PGRP-SA, peptidoglycan recognition protein	bacterial recognition	AAF48056.1	XP_022660135.1	9×10^{-34}	32.93%	82%	YES
PGRP-SD, peptidoglycan recognition protein	bacterial recognition	CAD89193.1	XP_022660134.1	5×10^{-27}	33.54%	86%	YES
PGRP-LB, peptidoglycan recognition protein	bacterial recognition	NP_650079.1	XP_022660134.1	2×10^{-31}	35.09%	79%	YES
PGRP-SC1a, peptidoglycan recognition protein	bacterial recognition	CAD89161.1	XP_022660134.1	3×10^{-32}	30.62%	86%	YES
PGRP-SC2, peptidoglycan recognition protein	bacterial recognition	CAD89187.1	XP_022660134.1	3×10^{-35}	31.71%	89%	YES
PGRP-SB1, peptidoglycan recognition protein	PGN degradation and antibacterial activity	CAD89136.1	XP_022660135.1	6×10^{-35}	35.22%	83%	YES
PGRP-LF, peptidoglycan recognition protein	blocking of IMD pathway	NP_648299.3	XP_022660134.1	3×10^{-38}	37.35%	79%	YES
PGRP-LA, peptidoglycan recognition protein	*activation of IMD pathway*	*AAF50304.2*	*Not found*	*Not found*	*Not found*	*Not found*	-
GNBP1, Gram-negative binding protein 1	*bacterial and fungal pattern recognition*	*Q9NHB0.2*	*Not found*	*Not found*	*Not found*	*Not found*	-
GNBP2, Gram-negative binding protein 2	*bacterial and fungal pattern recognition*	*ACU30172.1*	*Not found*	*Not found*	*Not found*	*Not found*	-
GNBP3, Gram-negative binding protein 3	*bacterial and fungal pattern recognition*	*CAJ18910.1*	*Not found*	*Not found*	*Not found*	*Not found*	-
DL1, c-type lectin 1	*bacterial recognition, induction of PPO cascade*	*AAF53793.1*	*Not found*	*Not found*	*Not found*	*Not found*	-

Table 1. *Cont.*

Gene Name	Role	*D. melanogaster*	*V. destructor* [1]	E-Value	Identity	Coverage	Transcription
DL2, c-type lectin 2	*bacterial recognition, induction of PPO cascade*	*NP_001014489.1*	*Not found*	*Not found*	*Not found*	*Not found*	-
DL3, c-type lectin 3 or solute carrier	bacterial recognition, induction of PPO cascade	NP_001014490.1	XP_022646715.1	4×10^{-7}	23.58%	79%	YES
galectin 4	several roles have been hypothesized	ADZ99399.1	XP_022654763.1	1×10^{-9}	34.75%	29%	YES
TEP1, CD109 antigen-like	mark pathogens for phagocytosis	CAB87807.1	XP_022645189.1	0.0	31.32%	98%	YES
TEP2, CD109 antigen-like	mark pathogens	CAB87808.1	XP_022645189.1	0.0	33.79%	98%	YES
TEP3, CD109 antigen-like	mark pathogens	AAL39195.1	XP_022645188.1	0.0	32.35%	97%	YES
TEP4, CD109 antigen-like	mark pathogens	NP_523603.2	XP_022645188.1	0.0	30.90%	98%	YES
Pes, scavenger receptor class B member 1-like	bacterial and fungal recognition	AHN54246.1	XP_022673026.1	4×10^{-61}	29.15%	78%	YES
Crq, croquemort, lysosome membrane protein 2-like	bacterial and fungal recognition	AAF51494.1	XP_022672747.1	5×10^{-70}	28.81%	96%	YES
Drpr, protein draper-like	bacterial and fungal recognition	NP_477450.1	XP_022656525.1	5×10^{-69}	39.01%	72%	YES
sr-CI, scavenger receptor class C, type i	bind to lipoproteins and bacteria	AAW79470.1	XP_022658153.1	3×10^{-24}	28.62%	45%	YES
sr-CII, scavenger receptor class C, type ii	bind to lipoproteins and bacteria	AAF58551.1	XP_022658154.1	4×10^{-23}	27.16%	49%	YES
sr-CIII, scavenger receptor class C, type iii	bind to lipoproteins and bacteria	AAF37564.1	XP_022658154.1	2×10^{-9}	21.00%	90%	YES
sr-CIV, scavenger receptor class C, type iv	bind to lipoproteins and bacteria	AAF51092.1	XP_022658154.1	5×10^{-19}	26.59%	73%	YES
eater	receptor in phagocytosis and microbial binding	AAF56664.5	XP_022668925.1	2×10^{-17}	33.72%	77%	NO
Drp, protein draper-like	receptor in phagocytosis and microbial binding	AAF53364.2	XP_022656529.1	6×10^{-12}	27.66%	62%	YES

[1] Best hit on the E-Value basis obtained by BLASTp searches against the NCBI nr database.

3.2.1. Peptidoglycan Receptor Proteins

Nearly all bacteria have peptidoglycans as crucial components of the cell wall, which are detected by the immune system thanks to pathogen recognition receptors (PRRs). Various families of pattern recognition molecules that identify peptidoglycans have been discovered in insects, and the function of peptidoglycan recognition proteins (PGRPs) in immune defense is relatively well understood in *Drosophila* [54]. Recognition through PGRPs triggers both the Toll and IMD/JNK signaling pathways, resulting in the activation of prophenoloxidase (proPO) or the production of antimicrobial peptides [55]. Most insect species have multiple PGRP genes that vary in both structure and function. For instance, *Drosophila* contains 13 PGRP genes that produce 19 different proteins, whereas *Anopheles gambiae* has 7 PGRP genes that encode 9 distinct proteins [54]. Conversely, our analysis revealed a limited set of PGRPs, identifying only a single putative homolog gene in the species we studied (Figure 2). This gene encodes two isoforms in *V. destructor* and *I. scapularis*, and a single protein in *G. occidentalis* and *T. urticae*. Furthermore, TMHMM analysis indicated that the PGRPs in *V. destructor* lack transmembrane domains, consistent with observations in other mites and ticks [30].

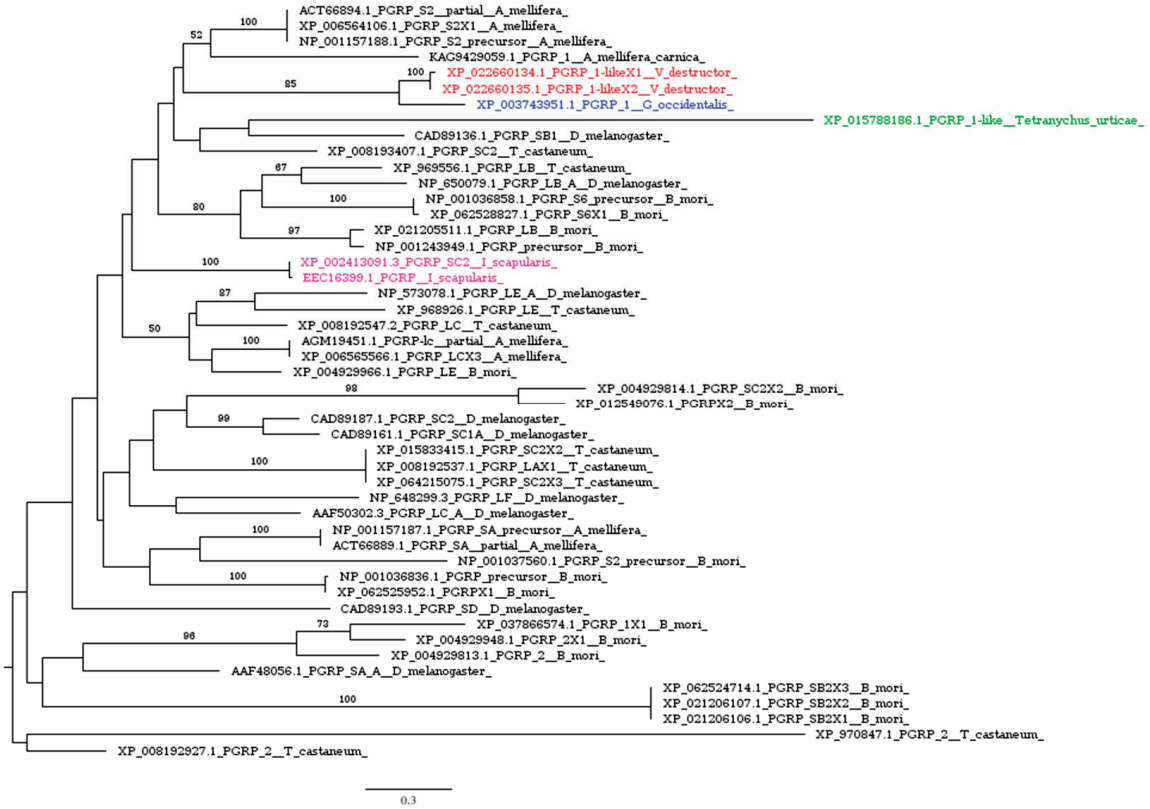


Figure 2. Phylogenetic tree based on maximum likelihood analysis of PGRP putative homologs identified in the genomes of *V. destructor* (in red), *G. occidentalis* (in blue), *T. urticae* (in green), and *I. scapularis* (in purple). The longest branch of the unrooted tree is used as the outgroup. Bootstrap support values > 50% are indicated at each node. The scale bar indicates the number of amino acid substitutions per site.

This lack of transmembrane PGPRs in *Acarina* seems to be associated with the evolution of alternative protein sensors. Indeed, previous works demonstrated that the IMD and JNK pathways of the tick *I. scapularis* are activated by lipid molecular patterns [43], such as 1-palmitoyl-2-oleoyl-sn-glycero-phosphoglycerol (POPG), sensed by the homolog of

croquemort (Crq) [39], a CD36-like protein originally identified in *Drosophila* [56]. Here, we report the presence of the Crq homolog in *V. destructor* (Table 1), which suggests a similar mechanism of recognition in mites.

3.2.2. Gram-Negative Binding Proteins

The structure of Gram-negative binding proteins (GNBPs) is characterized by a carbohydrate-binding module (CBM) at the N-terminus and a glucanase-like domain (Glu) at the C-terminus [57]. The CBM engages with microbial polysaccharides, whereas the Glu domain interacts with subsequent proteases, thus triggering immune signaling pathways [58]. GNBPs detect both bacterial and fungal pathogens, thus activating immune signaling cascades in insects [59]. In *Drosophila*, GNBP1 and peptidoglycan-recognition protein SA (PGRP-SA) work together to trigger the Toll pathway in response to Gram-positive bacterial infections [60], while GNBP3 plays a crucial role in activating the Toll pathway during fungal infections [61].

The comparative study of Palmer and Jiggins (2015) revealed that GNBPs, also known as βGRPs, have been lost from *chelicerates*, likely through a single-loss event [30]. *V. destructor* is no exception and, like other *Acarina* species (Tables S1–S3), shows no similarities to known GNBPs of *D. melanogaster* (Table 1).

3.2.3. Lectins

Lectins, a diverse class of carbohydrate-binding proteins, play a crucial role in the immune defense of numerous insect species. These proteins are recognized for their wide-ranging ability to bind pathogens and their participation in various immune functions, including opsonization, melanization, synthesis of antibacterial peptides, encapsulation, and the direct elimination of bacteria [62,63]. The *Drosophila* c-type lectins (CTLs) DL2 and DL3 agglutinate Gram-negative *Escherichia coli* in a calcium-dependent manner [64]. Our analysis pointed out a reduced CTL repertoire in *Acarina*. *V. destructor* lacks homologs of DL1 and DL2 but possesses a putative homolog of DL3 (Table 1). Notably, no CTLs were detected in the genomes of *I. scapularis*, *G. occidentalis*, and *T. urticae* when using *Drosophila* sequences as the query (Tables S1–S3). However, by using the DL3 putative homolog identified in *V. destructor* as the query, significant hits were obtained for both *I. scapularis* and *G. occidentalis*, though not for *T. urticae* (Table S4), where the best match was with a sushi, von Willebrand factor type A, EGF, and pentraxin domain-containing protein 1. This intriguing reduction in CTLs in *T. urticae* is in line with what was observed after immune challenge in this phytophagous mite by bacteria injection. Indeed, *T. urticae* has lost the capacity to mount an induced immune response against bacteria, in contrast to other mites and chelicerates but similarly to the phloem-feeding aphid *Acyrthosiphon pisum* [65]. The suggested evolutionary link between ecological conditions regarding exposure to bacteria and the architecture of the immune response deserves further studies. Although DL3 is predicted to be a secreted protein, it is detected on the surface of *Drosophila* hemocytes and enhances encapsulation [64]. Similarly, our in silico analysis suggests that the DL3 homolog identified in *V. destructor* is also predicted to be secreted, indicating a potential analogous role in mite immunity.

Galectins, a widely prevalent family of lectins [66], exhibiting thiol group-dependent activity and present in both intracellular and extracellular spaces [67], are upregulated in mosquitoes upon exposure to bacterial infections as well as malaria parasite invasion [68]. Galectins present in the gut of the hematophagous sand fly *Phlebotomus papatasi* facilitate a specific interaction between the insect's midgut and *Leishmania major*, a critical event for parasite survival, and play a role in determining species-specific vector competence [69].

More broadly, insect galectins are believed to participate in pathogen recognition, agglutination, and phagocytosis [66,70]. Variability in galectin transcripts across different insect species has been highlighted by genome-wide studies: 5 transcripts were identified in *Drosophila melanogaster*, 8 in *Anopheles gambiae*, and 12 in *Aedes aegypti* [71], with 4 identified in several *Lepidoptera* species [72]. *Acarina* species (Tables S1–S3), including *V. destructor*, possess putative homologs of galectins (Table 1). Notably, *I. scapularis* shows a significant expansion of galectins, compared to the other target species, which have diversified into three distinct clusters (Figure 3).

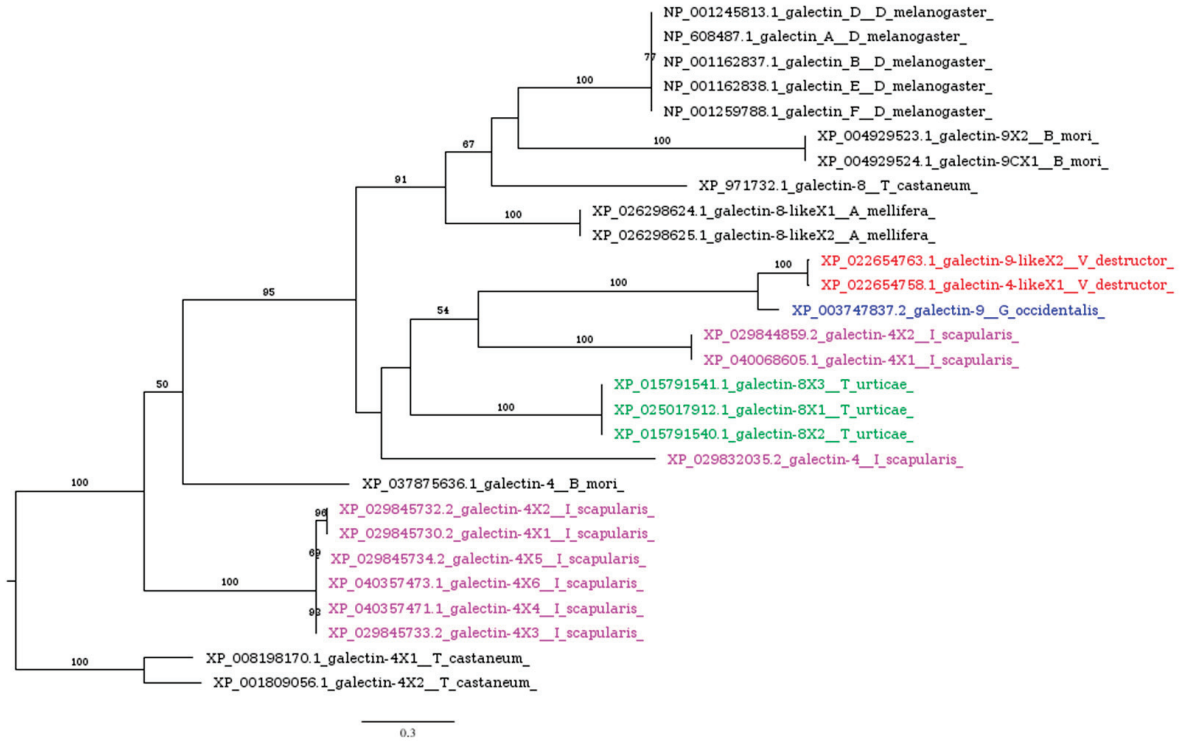


Figure 3. Phylogenetic tree based on maximum likelihood analysis of galectin putative homologs identified in the genomes of *V. destructor* (in red), *G. occidentalis* (in blue), *T. urticae* (in green), and *I. scapularis* (in purple). The longest branch of the unrooted tree is used as the outgroup. Bootstrap support values >50% are indicated at each node. The scale bar indicates the number of amino acid substitutions per site.

3.2.4. Thioester-Containing Proteins

Thioester-containing proteins (TEPs) are a family of proteins that show similarities to vertebrate alpha-2 macroglobulins (A2M) and complement factors [73,74]. Seven members of this family are encoded in the human genome: C3, C4, C5, A2M, pregnancy zone protein (PZP), CD109, and the complement 3 and PZP-like A2M domain-containing 8 (CPAMD8) [75–77]. As seen in complement proteins, certain insect TEPs play a role in the opsonization of microbes and pathogens, effectively "labeling" them for phagocytosis, melanization, and the formation of lytic complexes [78,79]. Given their participation in microbe recognition, TEPs are categorized as pattern recognition receptors (PRRs) [80].

Our phylogenetic analysis revealed a distinct clustering of A2M, CD109, and C3 homologs (Figure 4). All *Acarina* species investigated had at least one representative in each cluster, except for *T. urticae*, which lacks putative homologs of A2M. Notably, the best BLASTp hits of *Drosophila* TEP1, TEP2, TEP3, and TEP4 in the *V. destructor* genome are two isoforms of the same gene (Table 1).

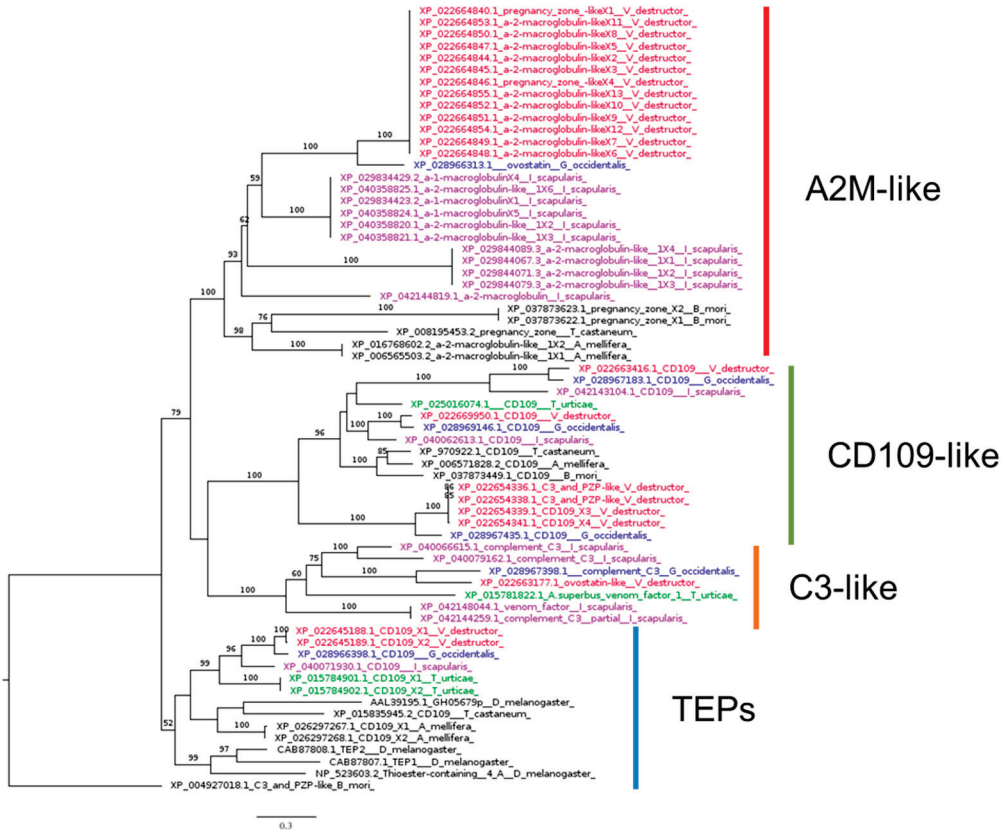


Figure 4. Phylogenetic tree based on maximum likelihood analysis of thioester-containing protein (TEP) identified in the genomes of *V. destructor* (in red), *G. occidentalis* (in blue), *T. urticae* (in green), and *I. scapularis* (in purple). The longest branch of the unrooted tree is used as the outgroup. Bootstrap support values > 50% are indicated at each node. The scale bar indicates the number of amino acid substitutions per site.

3.3. Signaling Pathways

Our analysis revealed the occurrence of protein sequences encoded by the *V. destructor* genome with significant matches with genes of *Drosophila* involved in signaling. Among these, four candidate signaling genes were not transcribed in adult female mites (Supplementary File S1). As occurs in other mites and ticks (Tables S1–S3), the *V. destructor* genome includes a complete Toll pathway, while it lacks some members of IMD (IMD, dFADD, TAB2), JAK/STAT (unpaired), and JNK (Eiger) signaling pathways, which are present in *Drosophila* genomes (Table 2).

Table 2. Immune genes of *Varroa destructor* involved in signaling. Orthologs not found in *V. destructor* are in italics.

Gene Name	Role	*D. melanogaster*	*V. destructor* [1]	E-Value	Identity	Coverage	Transcript
Spz1-1, spätzle 1B	Toll pathway	NP_733188.1	XP_022644257.1	6×10^{-7}	25.32%	62%	NO
Spz1-2, spätzle 1Bii	Toll pathway	NP_001138116.1	XP_022644257.1	2×10^{-7}	25.32%	52%	NO
Spz2, spätzle 2, neurotrophin 1	Toll pathway	NP_001261417.1	XP_022654810.1	3×10^{-15}	27.85%	14%	YES
Spz3, spätzle 3	Toll pathway	NP_609160.2	XP_022643975.1	3×10^{-61}	40.00%	43%	NO
Spz4, spätzle 4	Toll pathway	NP_609504.2	XP_022644415.1	5×10^{-51}	63.55%	17%	YES
Spz5, spätzle 5	Toll pathway	NP_647753.1	XP_022663991.1	1×10^{-14}	38.98%	29%	YES

Table 2. *Cont.*

Gene Name	Role	*D. melanogaster*	*V. destructor* [1]	E-Value	Identity	Coverage	Transcript
Spz6, spätzle 6	Toll pathway	NP_611961.1	XP_022645393.1	2×10^{-30}	63.75%	18%	YES
Toll-1, protein Toll	Toll pathway	NP_524518.1	XP_022664896.1	3×10^{-93}	29.56%	74%	YES
18 wheeler, Toll-2	Toll pathway	NP_476814.1	XP_022651559.1	0.0	38.74%	83%	YES
Toll-6	Toll pathway	NP_001246766.1	XP_022653722.1	0.0	40.50%	77%	NO
Toll-7	Toll pathway	NP_523797.1	XP_022656113.1	0.0	41.21%	82%	YES
Tollo, Toll-8	Toll pathway	NP_524757.1	XP_022651559.1	0.0	40.47%	89%	YES
Tube [2]*, interleukin-1 receptor-associated kinase 4*	Toll pathway	NP_001189164.1	Not found. A putative homolog was found by using the query from the *T. urticae* genome [2].	Not found	Not found	Not found	-
Myd88, myeloid differentiation primary response gene [2]	Toll pathway	AAF58953.1	Not found. A putative homolog was found by using the query from the *T. urticae* genome [2].	Not found	Not found	Not found	-
Pll, pelle	Toll pathway	AAF56686.1	XP_022652064.1	1×10^{-64}	42.48%	60%	YES
Cact, cactus	Toll pathway	AAN10936.1	XP_022667531.1	8×10^{-17}	30.21%	48%	YES
Cactin	Toll pathway	NP_523422.4	XP_022668977.1	0.0	52.09%	82%	YES
Pli, pellino	Toll pathway	NP_524466.1	XP_022668132.1	8×10^{-68}	42.61%	59%	YES
Traf1, TNF-receptor-associated factor 1	Toll pathway	AAD34346.1	XP_022668810.1	8×10^{-101}	46.20%	66%	YES
Traf2,TNF-receptor-associated factor 2	Toll pathway	AAF46338.1	XP_022668812.1	7×10^{-9}	24.84%	30%	YES
Traf3, TNF-receptor-associated factor 3	Toll pathway	NP_727976.1	XP_022687269.1	2×10^{-15}	25.00%	38%	YES
Dl, dorsal	Toll pathway	AAF53611.1	XP_022665229.1	8×10^{-87}	50.37%	39%	YES
Dome, domeless 1, interleukine JAK/STAT receptor	JAK/STAT pathway	CAD12503.1	XP_022659768.1	2×10^{-21}	21.79%	39%	YES
Hops, hopscotch, Janus kinase	JAK/STAT pathway	NP_511119.2	XP_022650171.1	2×10^{-52}	42.59%	61%	YES
STAT92E, signal transducer and activator of transcription, marelle	JAK/STAT pathway	AAX33462.1	XP_022661521.1	1×10^{-129}	36.85%	94%	YES
unpaired 1	*JAK/STAT pathway*	*NP_525095.2*	*Not found*	*Not found*	*Not found*	*Not found*	-
unpaired 2	*JAK/STAT pathway*	*NP_001356882.1*	*Not found*	*Not found*	*Not found*	*Not found*	-
unpaired 3	*JAK/STAT pathway*	*NP_001097014.1*	*Not found*	*Not found*	*Not found*	*Not found*	-
IMD, immune deficiency	*IMD pathway*	*NP_573394.1*	*Not found*	*Not found*	*Not found*	*Not found*	-
dFADD	*IMD pathway*	*NP_651006.1*	*Not found*	*Not found*	*Not found*	*Not found*	-
Dredd, death-related ced-3, caspase-1	IMD pathway	NP_477249.3	XP_022672682.1	2×10^{-17}	28.98%	46%	YES

Table 2. *Cont.*

Gene Name	Role	*D. melanogaster*	*V. destructor* [1]	E-Value	Identity	Coverage	Transcript
Rel, Relish [3]	IMD pathway	NP_477094.1	XP_022656314.1	3×10^{-11}	33.81%	14%	YES
TAB2, TAK1-associated binding protein 2	*IMD pathway*	*NP_611408.2*	*Not found*	*Not found*	*Not found*	*Not found*	-
TAK1, TGF-β-activated kinase 1	IMD pathway	AAF50895.1	XP_022652311.1	8×10^{-81}	41.39%	64%	YES
Key, Kenny	*IMD pathway*	*NP_523856.2*	*Not found*	*Not found*	*Not found*	*Not found*	-
DIAP2/XIAP, death-associated inhibitor of apoptosis 2	IMD pathway	NP_477127.1	XP_022671835.1	2×10^{-59}	31.12%	86%	YES
IRD5, immune response deficiency 5, IK-β, IKKB, I-kappa-B kinase beta	IMD pathway	NP_524751.3	XP_022693386.1	9×10^{-37}	38.05%	31%	YES
Hep, hemipterous	JNK pathway	NP_727661.1	XP_022657489.1	4×10^{-110}	56.25%	25%	YES
Bsk, basket	JNK pathway	P92208.1	XP_022646497.1	0.0	84.72%	96%	YES
Jra, Jun-related antigen	JNK pathway	AAF58845.1	XP_022649508.1	2×10^{-32}	34.36%	78%	YES
Kay, kayak	JNK pathway	NP_001027579.1	XP_022661416.1	2×10^{-10}	41.44%	23%	YES
Egr, Eiger	*JNK pathway*	*AAF58848.2*	*Not found*	*Not found*	*Not found*	*Not found*	-

[1] Best hit on the E-Value basis obtained by BLASTp searches against the NCBI nr database. [2] See Table S5. [3] This sequence does not contain Relish domains and it cannot be considered a Relish homolog (see Section 3.3.3).

3.3.1. The Toll Signaling Pathway

The Toll pathway in *Drosophila* plays a pivotal role in both development and innate immunity. The deletion of its constituent genes enhances susceptibility to a range of pathogens, including Gram-positive bacteria, fungal infections, certain Gram-negative bacteria, and viruses [81]. The Toll pathway appears to be intact in *V. destructor* (Table 2) and other *Acarina* species (Tables S1–S3), according to other studies on *chelicerates* immunity-related genes [30,41]. We found convincing matches for genes encoding the extracellular cytokine spätzle, the transmembrane receptor Toll (Figure 5), the kinase pelle, cactin, pellino, Traf, and the transactivator dorsal (Table 2).

Moreover, our findings include a putative homolog of MyD88 and the *tube* adaptor in the *Acarina* species studied (Table S5). In invertebrates, MyD88 together with the adaptor tube form a complex with the kinase pelle, which in turn leads to the activation of cactus, and ultimately to the activation of the NF-κB ortholog dorsal [82]. Notably, Palmer and Jiggins, in their comparative genomics study, failed to find a tube homolog in any of the species studied, suggesting that the cause might be a lack of the power needed to detect the gene [30]. Indeed, in another comparative study the identification of the tube orthologs in arachnids was possible only by using the tube sequence from the mosquito *A. aegypti*, while no matches were obtained using the *Drosophila* ortholog as the query [41]. Similarly, we found that BLASTp searches using the *Drosophila* tube sequence as the query revealed no hits in *V. destructor* (Table 1), *I. scapularis* (Table S1), and *G. occidentalis* (Table S2) genomes, while a significant match was found in *T. urticae* (Table S3). Using this sequence as an alternative query, we identified significant matches in our target species, suggesting the presence of a tube homolog in the genomes of *Acarina*, including *V. destructor* (Table S5). However, tube and pelle are members of the same gene family, both having a death domain and a kinase domain, and orthology is difficult to infer.

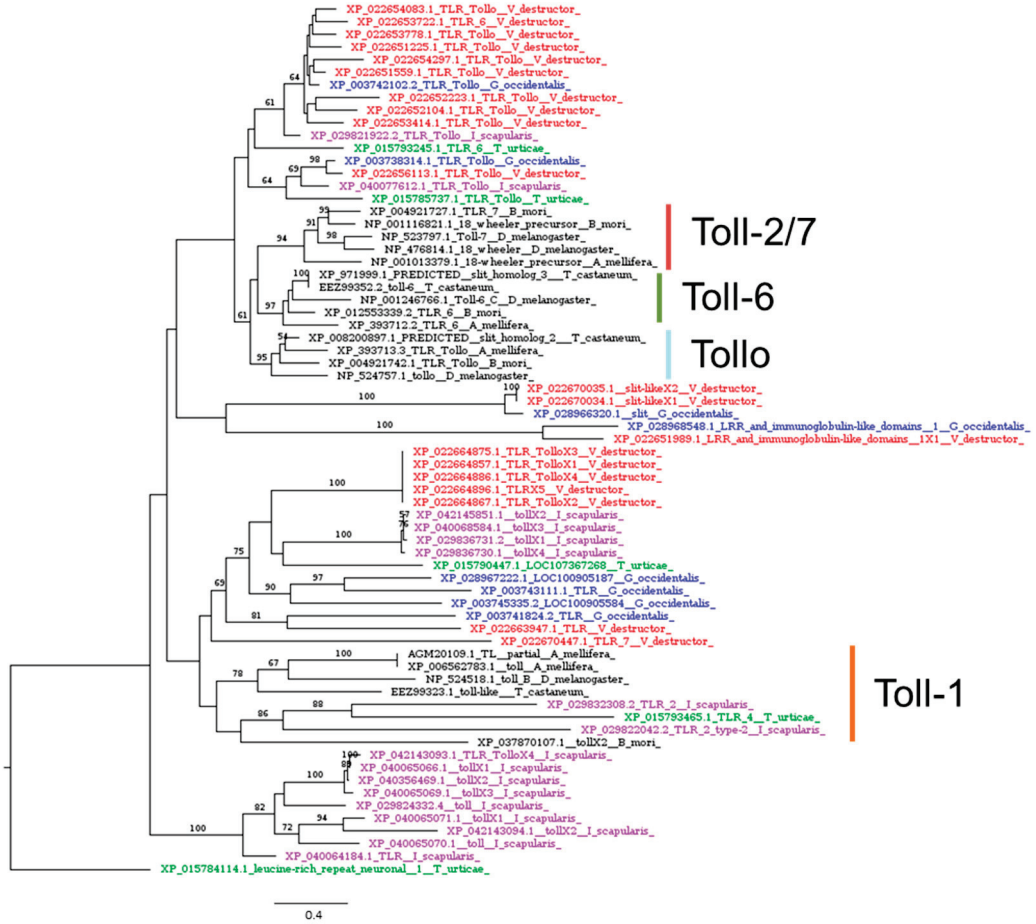


Figure 5. Phylogenetic tree based on maximum likelihood analysis of Toll-1, Toll-6, Toll-7, and Tollo putative homologs identified in the genomes of *V. destructor* (in red), *G. occidentalis* (in blue), *T. urticae* (in green), and *I. scapularis* (in purple). The longest branch of the unrooted tree is used as the outgroup. Bootstrap support values > 50% are indicated at each node. The scale bar indicates the number of amino acid substitutions per site.

Acarina also possess multiple genes encoding Toll receptors (Figure 5), which function as transmembrane receptors in both vertebrates and invertebrates [83,84]. While nine single-copy Toll genes have been identified in *D. melanogaster* (Toll-1 to Toll-9), it appears that Acarina, like other arthropods, lack some of these genes but have multiple isoforms of others. Indeed, *V. destructor* exhibited a highly diversified repertoire of Toll putative homologs (Figure 5). Toll-like sequences in *Acarina* form monophyletic groups (Figure 5), suggesting that diversification of the Toll family occurred after the evolution of the separate lineages of *Acarina* and insects. This is in line with other phylogenetic analyses, which indicated that Toll receptor genes from different phyla fall into separate clusters, showing that they share a common ancestor but evolved independently by gene duplication [85,86]. Our results suggest a functional divergence between *Acarina* and insect Toll receptors, which may be disclosed only by functional data.

3.3.2. The JAK/STAT Signaling Pathway

In *Drosophila*, the JAK/STAT pathway, much like the Toll pathway, plays pivotal roles in both development and immune responses. Although it remains the least detailed among the core insect immune pathways, it appears to be involved in hemocyte overproliferation and antiviral defense [87]. Similar to other *Acarina* species (Tables S1–S3), *V. destructor*

possesses homologs of all core JAK/STAT genes, including those encoding the cytokine receptor domeless, JAK tyrosine kinase (also referred to as hopscotch), and the STAT92E transcription factor (Table 2). However, homologs for upd (unpaired), a crucial ligand for JAK/STAT activation in *Drosophila*, were not identified. This ligand is also absent in other insects, such as *A. mellifera* [88] and *Coccidae* [45]. The presence of the core JAK/STAT components (Table 2) suggests that the JAK/STAT pathway remains functional in *Acarina*, activated by an as-yet-unidentified ligand.

3.3.3. IMD and JNK Signaling Pathways

The immune deficiency (IMD) pathway is critical for fighting Gram-negative bacteria in *Drosophila* [81], and IMD pathway member knockouts influence the susceptibility to some Gram-positive bacteria and fungi as well [89]. In *Drosophila*, the pathway-initiating receptors, PGRPs, engage the adapter proteins IMD and FADD (Fas-associated protein with death domain) [90,91], with FADD subsequently interacting with Dredd (caspase-8) [92], which in turn cleaves IMD. The K63 polyubiquitylation of IMD is facilitated by the E3 ubiquitin ligase IAP2 (inhibitor of apoptosis 2) and the E2-conjugating enzymes Bendless, Uev1a, and Effete [93–95]. This facilitates the binding of Kenny to the inhibitor of NF-κB kinase (IKK)β [92,96]. Additionally, Dredd mediates the cleavage of Relish, leading to the nuclear translocation of its N-terminal fragment, which in turn triggers the expression of antimicrobial peptides (AMPs) [95,97–99]. The resulting signaling scaffold leads to cleavage of the NF-κB signaling molecule Relish, which translocates to the nucleus and promotes antimicrobial peptide (AMP) expression [93,95].

As in other *Acarina* species [100], *V. destructor* appears to be missing many crucial components of the IMD signaling pathway, such as IMD, dFADD, Kenny, and TAB2 (Table 2). However, the Relish search resulted in a positive hit characterized by only 14% coverage (Table 2), which was considered low. Indeed, InterProScan analysis revealed that similarities between the Relish gene in *D. melanogaster* and its putative homolog in *V. destructor* (XP_022656314.1) are only due to the Ankyrin domain's presence in both sequences, while the *V. destructor* sequence lacks canonical Relish domains: the NF-kappa-B/Rel/dorsal domain (IPR011539) and Rel homology dimerization domain (IPR032397) [101,102]. However, the putative Relish homolog identified in I. scapularis includes Relish domains and was used as an alternative query to scan the *V. destructor* genome. This led to the identification of a significantly similar sequence described as proto-oncogene c-Rel-like (XP_022665225.1), showing Relish domains and lacking the Ankyrin domain, that is believed to inhibit its own nuclear translocation [97,102]. However, this loss of the Ankyrin domain, which occurs also in *I. scapularis*, *G. occidentalis*, and *T. urticae*, seems to not alter the functionality of Relish in ticks [103–105].

Using the Dredd protein sequence to search the *V. destructor* genome via BLASTp resulted in a best hit with 46% coverage (Table 2). However, this sequence cannot be considered a true homolog of Dredd (caspase-8) because it lacks the Dredd_N (IPR056259) and Dredd_2nd (IPR056260) domains (Figure 6). These findings align with previous studies reporting the absence of Dredd homologs in ticks and mites [41]. Dredd normally cleaves the loop sequence between the REL and Ankyrin domains of phosphorylated Relish [98,106]. Our results suggest that, in *V. destructor* and *Acarina* in general, the absence of Dredd homologs is likely due to reduced selective pressure on this caspase, stemming from the loss of its substrate: the Ankyrin domain in Relish homologs.

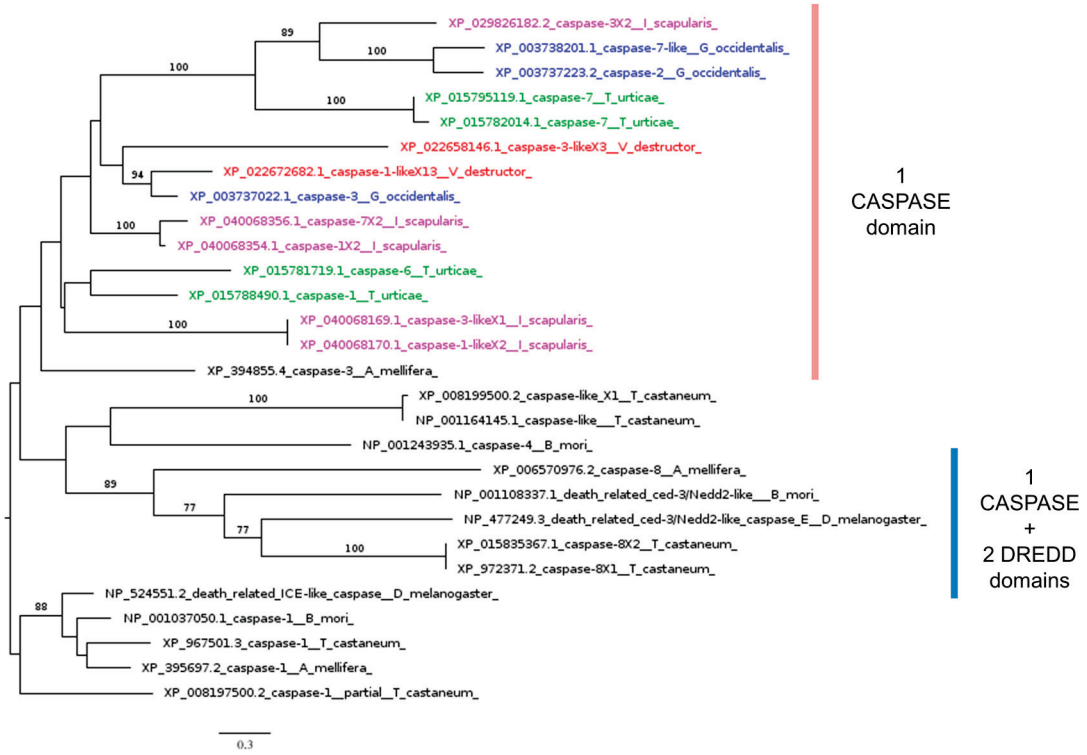


Figure 6. Phylogenetic tree based on maximum likelihood analysis of Dredd putative homologs identified in the genomes of *V. destructor* (in red), *G. occidentalis* (in blue), *T. urticae* (in green), and *I. scapularis* (in purple). The Drice homolog sequences are used as the outgroup. Bootstrap support values > 50% are indicated at each node. The scale bar indicates the number of amino acid substitutions per site.

Despite the absence of upstream regulators, core IMD signaling molecules are active against infection, as reported by several studies on tick IMD pathways [107], which rely on Bendless, Effete, Uev1a, and XIAP (X-linked inhibitor of apoptosis), the homolog of IAP2 [43,108]. Our phylogenetic analysis indicated that all model *Acarina* species studied here, including *V. destructor*, possess homolog genes of the three ubiquitination-conjugating enzymes (UCEs): Bendless, Effete, and Uev1a (Figure 7).

In ticks, once activated, XIAP interacts with the heterodimers Bendless and Uev1a, leading to the ubiquitination of p47 in a K63-dependent manner [43,109]. Ubiquitylated p47 connects to Kenny and induces the phosphorylation of IRD5 and Relish [100]. This mechanism seems well conserved in Acarina. Indeed, we identified putative homologs of XIAP (Table 2) and p47 (Table S6) in our analysis.

Following the initiation of IMD signaling in *Drosophila*, various proteins are recruited to the molecular scaffold within the activated cell, including transforming growth factor-β-activated kinase 1 (TAK1). TAK1, which we identified also in *V. destructor* (Table 2), promotes activation of JNK signaling in parallel to NF-κB signaling [95,110].

In *Drosophila*, the JNK pathway is involved in various developmental processes, along with wound healing, and has been suggested to regulate antimicrobial peptide gene expression and cellular immune responses [81]. The putative homologs identified in *V. destructor* include kay (kayak), hep (hemipterous), bsk (basket), and jra (Jun-related antigen) (Table 2). Searches for homologs to the *Drosophila* Eiger gene found no hits in *Acarina* (Tables S1–S3), including *V. destructor* (Table 2), as observed also for other phyla such as *Coccidae* (*Insecta*, *Hemiptera*) [45].

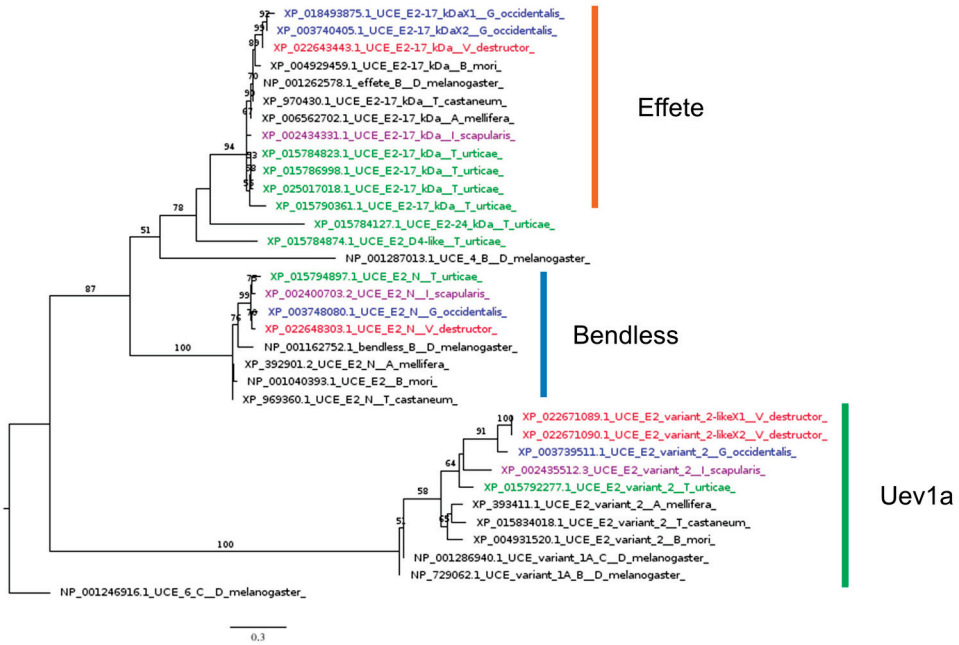


Figure 7. Phylogenetic tree based on maximum likelihood analysis of ubiquitination-conjugating enzymes (UCEs) Bendless, Effete, and Uev1a, identified in the genomes of *V. destructor* (in red), *G. occidentalis* (in blue), *T. urticae* (in green), and *I. scapularis* (in purple). The longest branch of the unrooted tree is used as the outgroup. Bootstrap support values > 50% are indicated at each node. The scale bar indicates the number of amino acid substitutions per site.

3.4. Response Genes

Our analysis revealed the occurrence of several proteins encoded by the *V. destructor* genome with significant matches with genes of *Drosophila* involved in the immune response. Among these, only two candidate response genes were not transcribed in adult female mites (Supplementary File S1). As occurs in ticks and mites (Tables S1–S3), *V. destructor* lacks canonical antimicrobial peptides and prophenoloxidase orthologs, which are present in the *D. melanogaster* genome (Table 3).

Table 3. Immune genes of *Varroa destructor* involved in the immune response. Orthologs not found in *V. destructor* are in italics.

Gene Name	Role	*D. melanogaster*	*V. destructor* [1]	E-Value	Identity	Coverage	Transcript
Att, Attacin	*antimicrobial peptide*	*NP_523745.1*	*Not found*	*Not found*	*Not found*	*Not found*	-
Cec, Cecropin	*antimicrobial peptide*	*C0HKQ7.1*	*Not found*	*Not found*	*Not found*	*Not found*	-
Def, Defensin	*antimicrobial peptide*	*ANY27112.1*	*Not found*	*Not found*	*Not found*	*Not found*	-
Dro, Dosocin	*antimicrobial peptide*	*XP_016946682.1*	*Not found*	*Not found*	*Not found*	*Not found*	-
Mtk, Metchnikowin	*antimicrobial peptide*	*AAO72489.1*	*Not found*	*Not found*	*Not found*	*Not found*	-
Andropin	*antimicrobial peptide*	*P21663.1*	*Not found*	*Not found*	*Not found*	*Not found*	-
Diptericin	*antimicrobial peptide*	*QER92349.1*	*Not found*	*Not found*	*Not found*	*Not found*	-
Drs, Drosomycin	*antimicrobial peptide*	*ANY27466.1*	*Not found*	*Not found*	*Not found*	*Not found*	-
LysX, Lysozyme X, i-type	microbial degradation	CAL85493.1	XP_022671742.1	2×10^{-30}	38.30%	96%	YES

Table 3. *Cont.*

Gene Name	Role	*D. melanogaster*	*V. destructor* [1]	E-Value	Identity	Coverage	Transcript
LysB, Lysozyme B, i-type	microbial degradation	NP_001261245.1	XP_022671739.1	2×10^{-33}	41.01%	97%	YES
LysP, Lysozyme, i-type	microbial degradation	NP_476828.1	XP_022643422.1	4×10^{-37}	43.28%	95%	NO
LysE, Lysozyme E	microbial degradation	CAA80228	XP_022669180.1	3×10^{-32}	43.09%	87%	YES
LysD, Lysozyme D	microbial degradation	NP_476823.1	XP_022671742.1	7×10^{-33}	43.90%	87%	YES
LysE, Lysozyme E	microbial degradation	NP_476827.2	XP_022671742.1	6×10^{-32}	39.42%	97%	YES
LysS, Lysozyme S	microbial degradation	NP_476829.1	XP_022671742.1	1×10^{-34}	44.36%	95%	YES
Lysozyme E, i-type	microbial degradation	ACD99447.1	XP_022648598.1	5×10^{-23}	34.55%	89%	YES
Lysozyme, i-type	microbial degradation	NP_611164.3	XP_022655568.1	6×10^{-19}	35.17%	88%	YES
Lysozyme, i-type	microbial degradation	NP_611163.2	XP_022644325.1	4×10^{-19}	37.30%	73%	YES
Cht2, Chitinase-like protein 4, flocculation protein	fungal degradation	NP_001261282.1	XP_022662471.1	2×10^{-85}	40.37%	73%	YES
Cht4, Chitinase-like protein 2, mucin	fungal degradation	NP_524962.2	XP_022662425.1	9×10^{-112}	38.54%	94%	YES
Cht5, Chitinase-like protein 5, endochitinase	fungal degradation	NP_650314.1	XP_022664603.1	7×10^{-165}	43.43%	95%	YES
Cht7, Chitinase-like protein 7, chitinase 10	fungal degradation	NP_647768.3	XP_022669697.1	0.0	52.05%	99%	NO
Cht6, Chitinase 6	fungal degradation	NP_001245599.1	XP_022662476.1	0.0	49.73%	47%	YES
idgf6	fungal degradation	NP_001286499.1	XP_022662425.1	1×10^{-45}	27.81%	98%	YES
PPO1, Prophenoloxidase 1	*prophenoloxidase response*	*NP_476812.1*	*Not found*	*Not found*	*Not found*	*Not found*	-
PPO2, Prophenoloxidase 2	*prophenoloxidase response*	*NP_610443.1*	*Not found*	*Not found*	*Not found*	*Not found*	-
PAF2, Phenoloxidase-activating factor 2	phenoloxidase activation	AAO24923.1	XP_022659018.1	2×10^{-82}	41.99%	77%	YES
SP, Serine protease-like precursor	phenoloxidase activation	NP_001097766.1	XP_022662993.1	2×10^{-43}	37.84%	56%	YES
Hmct, Hemolectin, hemocytin	cell aggregation	NP_001261809.1	XP_022654008.1	8×10^{-158}	32.23%	66%	YES
Nos, Nitric oxide synthase	production of nitric oxide	NP_001027243.2	XP_022665384.1	6×10^{-68}	29.27%	60%	YES
Tg, Transglutaminase	clotting	NP_609174.1	XP_022666443.1	9×10^{-121}	33.06%	90%	YES

[1] Best hit on the E-Value basis obtained by BLASTp searches against the NCBI nr database.

3.4.1. Antimicrobial Peptides

Antimicrobial peptides (AMPs) are pivotal components of the immune defenses across a broad range of organisms, including insects. These peptides are among the most extensively researched humoral effectors and can be produced either constitutively or in response to specific signaling pathways. Typically composed of 15-to-50 amino acids, AMPs possess an amphipathic structure that enables them to disrupt microbial membrane integrity, thereby inducing alterations in the osmotic equilibrium and ultimately leading to lysis. The activation of the IMD and Toll signaling pathways in *Drosophila* triggers the transcription of distinct antimicrobial peptides [111]. At present, numerous structural families of insect-derived AMPs are identified, such as defensins, cecropins, drosocins, attacins, diptericins, metchnikowins, and melittins, some of which are exclusive to certain taxonomic groups [112]. However, none of these were identified in *V. destructor* and other *Acarina* species studied here by our BLASTp searches (Table 3). In contrast to our findings, defensins were reported from several tick species, including *I. scapularis* [113], suggesting that BLASTp is not the most appropriate method to identify these antimicrobial peptides in our target species. Indeed, we used the defensins identified in *I. scapularis* as alternative queries to scan the *V. destructor* proteome, which again resulted in no significant match. This limitation of BLASTp searches aimed at identifying AMPs was observed by other similar studies. As suggested, the small size of AMPs makes their identification by sequence similarity problematic across large phylogenetic distances [30].

Ctenidins are a family of constitutively expressed, glycine-rich AMPs identified from the spider *Cupiennius salei* that exhibit activity against Gram-negative bacteria [114]. BLASTp using ctenidin-like peptides identified in ticks as queries to scan the *V. destructor* genome led to the identification of putative homologs (Table S7). A similar pattern is observed for *G. occidentalis*, but not in *T. urticae*, where ctenidin putative homologs were not found (Table S7). These findings are particularly significant given the absence of widely adopted genetic readouts for immune pathways in mites [39].

3.4.2. Lysozyme

Lysozymes, enzymes tasked with degrading bacterial cell walls through the cleavage of the polysaccharide component of peptidoglycan, are categorized into two distinct classes in insects: the c-type, which exhibits muramidase activity, and the i-type, which possesses both muramidase and isopeptidase activities [115,116].

In ticks, lysozymes are expressed in the gut, salivary glands, and hemolymph, and are upregulated in response to bacterial challenge, suggesting a possible role of lysozymes: giving innate immunity to ticks against microorganisms [117]. Our analysis identified seven different proteins of *V. destructor* with significant similarity to *Drosophila* lysozymes (Table 3). Among these, only three (XP_022648598, XP_022655568, and XP_022644325) contain the invertebrate (I)-type lysozyme domain profile (LYSOZYME_I). Two of these (XP_022655568 and XP_022644325) also carry the EF hand calcium-binding domain (EF_HAND_1).

By filtering BLASTp results using the same criteria, we identified three lysozyme homologs in *G. occidentalis* and two in *I. scapularis*, carrying both LYSOZYME_I and EF_HAND_1. ScanProsite analysis revealed that among the sequences identified in *T. urticae*, large proteins (>400AA) possess multiple LYSOZYME_Is, while only one sequence (XP_015789674) showed a single LYSOZYME_I and was in the length range of canonical lysozymes (176AA). All these sequences identified in *Acarina* form a monophyletic group that diverges from the lysozymes with LYSOZYME_I and EF_HAND_1 identified in insect species (Figure 8).

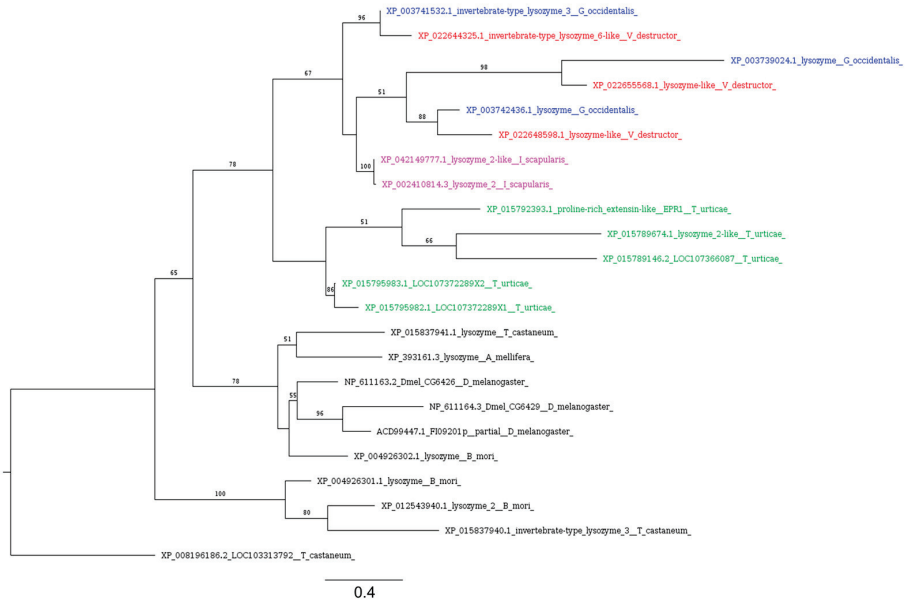


Figure 8. Phylogenetic tree based on maximum likelihood analysis of i-type lysozymes identified in the genomes of *V. destructor* (in red), G. occidentalis (in blue), *T. urticae* (in green), and *I. scapularis* (in purple). The longest branch of the unrooted tree is used as the outgroup. Bootstrap support values > 50% are indicated at each node. The scale bar indicates the number of amino acid substitutions per site.

3.4.3. Melanization and Coagulation

Melanization, a key immune response in arthropods, involves the encapsulation of pathogens with melanin and their subsequent elimination through toxic quinone precursors [55,118]. Central to this melanization process is the enzyme prophenoloxidase (proPO, PPO), which, upon activation, transforms ortho-diphenols such as dopamine into quinones, precursors to melanin that ultimately encase and neutralize the pathogen. It is believed that in the common ancestor of arthropods, the oxygen-carrying molecule hemocyanin likely evolved from a protein resembling PO [119]. While PO has been detected in insects and crustaceans, specific forms of PO have not been identified in the studied chelicerates. Notably, in the horseshoe crab *T. tridentatus*, the oxygen-transporting protein hemocyanin exhibits PO activity upon activation [120]. Similarly, a hemocyanin with PO activity has been observed in the tarantula species *Eurypelma californicum* [121].

There is no evidence of the existence of the PPO cascade in ticks based on the available genomic and transcriptomic data [100]. In line with this, no PPO activity has been reported to be present in the hemolymph of the hard ticks *Amblyomma americanum*, *Dermacentor variabilis*, and *I. scapularis* [122]. Moreover, ticks lack coagulin and hemocyanin, suggesting a unique coagulation system in *Acarina*, which is largely different from that of insects [123]. Our analysis showed that this pattern occurs also in mites, including *V. destructor*, which lack PPO but possess transglutaminase homologs (Table 3). Considering these findings, additional studies are required to characterize melanization and the linked coagulation responses in *Acarina*.

4. Conclusions

Our results shed light on the genetic basis of *Varroa* and *Acarina* immunity, which is important for understanding the evolution of immune response in an economically important group of arthropods. While the genomic resources obtained through different sequencing technologies may result in different genome coverage, introducing bias in comparative analysis, we observed a clear pattern of immune gene loss in *V. destructor*, and

chelicerates in general, supported by previous studies on arthropod immunity. Indeed, the immune gene repertoire of *V. destructor* matches the same pattern that several studies report for ticks, including the lack of transmembrane peptidoglycan recognition proteins (PGRPs), Gram-negative binding proteins, and several lectin families involved in recognition. Regarding signaling pathways, as occurs in ticks, *Varroa* mites lack homologs of the unpaired ligand (JAK/STAT), Eiger (JNK), and many components of IMD. *Varroa* mites also lack homologs of canonical AMPs, such as defensins, while their genome encodes putative homologs of ctenidins, AMPs previously identified in spiders and ticks. The same pattern is consistent in the predatory mite *G. occidentalis*, but not conserved in the phytophagous mite *T. urticae*, for which no canonical lectins nor ctenidins were identified. This suggests a greater degree of immune gene erosion in herbivorous mites, a trend that warrants further investigation.

Although our findings stem from a conservative homology-based approach using canonical insect immune genes, they represent the first comprehensive checklist of immunity-related genes in *V. destructor*. We hope this initial overview will inspire future studies to focus on the functional characterization of these genes, an essential step toward studying immune response in mites and developing novel strategies for pest control based on immunosuppression.

Supplementary Materials: The following supporting information can be downloaded at https://www.mdpi.com/article/10.3390/insects16040356/s1, Supplementary File S1: tBLASTn results using candidate recognition genes as query vs. *Varroa destructor* transcriptome. Table S1: Immune genes involved in recognition, signaling and response in *Ixodes scapularis*. Table S2: Immune genes involved in recognition, signaling and response in *Galendromus occidentalis*. Table S3: Immune genes involved in recognition, signaling and response in *Tetranychus urticae*. Table S4: Results of BLASTp searches against Genbank nr protein database using lectin DL3 putative homolog from *Varroa* as query. Table S5: Results of BLASTp searches against Genbank nr protein database using tube and Myd88 putative homologs from *Tetranychus urticae* as query. Table S6: Results of BLASTp searches against Genbank nr protein database using p47 putative homologs from *Ixodes scapularis* as query. Table S7: Ctenidin-like proteins identified in *V. destructor*, *Galendromus occidentalis* and *Tetranychus urticae*.

Author Contributions: Conceptualization, A.B.; investigation, A.B., A.C. and G.D.L.; formal analysis, A.B. and I.D.L.; data curation, A.B. and G.D.L.; writing—original draft preparation, A.C. and A.B.; writing—review and editing, A.B., I.D.L., and A.C. All authors have read and agreed to the published version of the manuscript.

Funding: This research received no external funding.

Data Availability Statement: All FASTA sequences used, alignments, and tree files are available from Zenodo at https://doi.org/10.5281/zenodo.14837927.

Conflicts of Interest: The authors declare no conflicts of interest.

References

1. Stokstad, E. The Case of the Empty Hives. *Science* **2007**, *316*, 970–972. [CrossRef] [PubMed]
2. Neumann, P.; Carreck, N.L. Honey Bee Colony Losses. *J. Apic. Res.* **2010**, *49*, 1–6.
3. Steinhauer, N.; Kulhanek, K.; Antúnez, K.; Human, H.; Chantawannakul, P.; Chauzat, M.-P.; vanEngelsdorp, D. Drivers of Colony Losses. *Curr. Opin. Insect Sci.* **2018**, *26*, 142–148. [CrossRef]
4. Kielmanowicz, M.G.; Inberg, A.; Lerner, I.M.; Golani, Y.; Brown, N.; Turner, C.L.; Hayes, G.J.R.; Ballam, J.M. Prospective Large-Scale Field Study Generates Predictive Model Identifying Major Contributors to Colony Losses. *PLoS Pathog.* **2015**, *11*, e1004816. [CrossRef]
5. Rosenkranz, P.; Aumeier, P.; Ziegelmann, B. Biology and Control of *Varroa destructor*. *J. Invertebr. Pathol.* **2010**, *103* (Suppl. S1), S96–S119. [CrossRef]

6. Noël, A.; Le Conte, Y.; Mondet, F. *Varroa Destructor*: How Does It Harm *Apis mellifera* Honey Bees and What Can Be Done about It? *Emerg. Top. Life Sci.* **2020**, *4*, 45–57. [CrossRef]
7. Ramsey, S.D.; Ochoa, R.; Bauchan, G.; Gulbronson, C.; Mowery, J.D.; Cohen, A.; Lim, D.; Joklik, J.; Cicero, J.M.; Ellis, J.D.; et al. *Varroa destructor* Feeds Primarily on Honey Bee Fat Body Tissue and Not Hemolymph. *Proc. Natl. Acad. Sci. USA* **2019**, *116*, 1792–1801. [CrossRef]
8. Han, B.; Wu, J.; Wei, Q.; Liu, F.; Cui, L.; Rueppell, O.; Xu, S. Life-History Stage Determines the Diet of Ectoparasitic Mites on Their Honey Bee Hosts. *Nat. Commun.* **2024**, *15*, 725. [CrossRef]
9. De Jong, D.; De Jong, P.H. Longevity of Africanized Honey Bees (Hymenoptera: Apidae) Infested by *Varroa jacobsoni* (Parasitiformes: Varroidae). *J. Econ. Entomol.* **1983**, *76*, 766–768. [CrossRef]
10. Bowen-Walker, P.L.; Gunn, A. The Effect of the Ectoparasitic Mite, *Varroa destructor* on Adult Worker Honeybee (*Apis Mellifera*) Emergence Weights, Water, Protein, Carbohydrate, and Lipid Levels. *Entomol. Exp. Appl.* **2001**, *101*, 207–217. [CrossRef]
11. Traynor, K.S.; Mondet, F.; de Miranda, J.R.; Techer, M.; Kowallik, V.; Oddie, M.A.Y.; Chantawannakul, P.; McAfee, A. *Varroa Destructor*: A Complex Parasite, Crippling Honey Bees Worldwide. *Trends Parasitol.* **2020**, *36*, 592–606. [CrossRef] [PubMed]
12. Kralj, J.; Fuchs, S. Parasitic *Varroa destructor* Mites Influence Flight Duration and Homing Ability of Infested *Apis mellifera* Foragers. *Apidologie* **2006**, *37*, 577–587. [CrossRef]
13. Yang, X.; Cox-Foster, D.L. Impact of an Ectoparasite on the Immunity and Pathology of an Invertebrate: Evidence for Host Immunosuppression and Viral Amplification. *Proc. Natl. Acad. Sci. USA* **2005**, *102*, 7470–7475. [CrossRef] [PubMed]
14. Wilfert, L.; Long, G.; Leggett, H.C.; Schmid-Hempel, P.; Butlin, R.; Martin, S.J.M.; Boots, M. Deformed Wing Virus Is a Recent Global Epidemic in Honeybees Driven by *Varroa* Mites. *Science* **2016**, *351*, 594–597. [CrossRef]
15. Boecking, O.; Genersch, E. Varroosis—The Ongoing Crisis in Bee Keeping. *J. Für Verbraucherschutz Und Leb.* **2008**, *3*, 221–228. [CrossRef]
16. Haber, A.I.; Steinhauer, N.A.; vanEngelsdorp, D. Use of Chemical and Nonchemical Methods for the Control of *Varroa destructor* (Acari: Varroidae) and Associated Winter Colony Losses in U.S. Beekeeping Operations. *J. Econ. Entomol.* **2019**, *112*, 1509–1525. [CrossRef]
17. Lester, P.J. Integrated Resistance Management for Acaricide Use on *Varroa destructor*. *Front. Bee Sci.* **2023**, *1*, 1297326. [CrossRef]
18. Way, M.J.; van Emden, H.F. Integrated Pest Management in Practice—Pathways towards Successful Application. *Crop Prot.* **2000**, *19*, 81–103. [CrossRef]
19. Vilarem, C.; Piou, V.; Vogelweith, F.; Vétillard, A. *Varroa destructor* from the Laboratory to the Field: Control, Biocontrol and IPM Perspectives—A Review. *Insects* **2021**, *12*, 800. [CrossRef]
20. Agrawal, N.; Dasaradhi, P.V.N.; Mohmmed, A.; Malhotra, P.; Bhatnagar, R.K.; Mukherjee, S.K. RNA Interference: Biology, Mechanism, and Applications. *Microbiol. Mol. Biol. Rev.* **2003**, *67*, 657–685. [CrossRef]
21. Caccia, S.; Astarita, F.; Barra, E.; Di Lelio, I.; Varricchio, P.; Pennacchio, F. Enhancement of *Bacillus thuringiensis* Toxicity by Feeding *Spodoptera littoralis* Larvae with Bacteria Expressing Immune Suppressive dsRNA. *J. Pest Sci.* **2020**, *93*, 303–314. [CrossRef]
22. Khila, A.; Grbić, M. Gene Silencing in the Spider Mite *Tetranychus urticae*: dsRNA and siRNA Parental Silencing of the Distal-Less Gene. *Dev. Genes Evol.* **2007**, *217*, 241–251. [CrossRef] [PubMed]
23. Niu, J.; Shen, G.; Christiaens, O.; Smagghe, G.; He, L.; Wang, J. Beyond Insects: Current Status and Achievements of RNA Interference in Mite Pests and Future Perspectives. *Pest Manag. Sci.* **2018**, *74*, 2680–2687. [CrossRef] [PubMed]
24. Garbian, Y.; Maori, E.; Kalev, H.; Shafir, S.; Sela, I. Bidirectional Transfer of RNAi between Honey Bee and *Varroa Destructor*: *Varroa* Gene Silencing Reduces *Varroa* Population. *PLoS Pathog* **2012**, *8*, e1003035. [CrossRef]
25. McGruddy, R.A.; Smeele, Z.E.; Manley, B.; Masucci, J.D.; Haywood, J.; Lester, P.J. RNA Interference as a Next-Generation Control Method for Suppressing *Varroa destructor* Reproduction in Honey Bee (*Apis mellifera*) Hives. *Pest Manag. Sci.* **2024**, *80*, 4770–4778. [CrossRef]
26. Leonard, S.P.; Powell, J.E.; Perutka, J.; Geng, P.; Heckmann, L.C.; Horak, R.D.; Davies, B.W.; Ellington, A.D.; Barrick, J.E.; Moran, N.A. Engineered Symbionts Activate Honey Bee Immunity and Limit Pathogens. *Science* **2020**, *367*, 573–576. [CrossRef]
27. Becchimanzi, A.; Tatè, R.; Campbell, E.M.; Gigliotti, S.; Bowman, A.S.; Pennacchio, F. A Salivary Chitinase of *Varroa destructor* Influences Host Immunity and Mite's Survival. *PLoS Pathog.* **2020**, *16*, e1009075. [CrossRef]
28. Becchimanzi, A.; Cacace, A.; Parziale, M.; De Leva, G.; Iacopino, S.; Jesu, G.; Di Lelio, I.; Stillittano, V.; Caprio, E.; Pennacchio, F. The Salivary Gland Transcriptome of *Varroa destructor* Reveals Suitable Targets for RNAi-Based Mite Control. *Insect Mol. Biol.* **2024**. [CrossRef]
29. Pathak, J.P.N. *Insect immunity*; Springer Science & Business Media: Berlin/Heidelberg, Germany, 2013; ISBN 978-94-011-1618-3.
30. Palmer, W.J.; Jiggins, F.M. Comparative Genomics Reveals the Origins and Diversity of Arthropod Immune Systems. *Mol. Biol. Evol.* **2015**, *32*, 2111–2129. [CrossRef]

31. Wang, X.; Zhang, Y.; Zhang, R.; Zhang, J. The Diversity of Pattern Recognition Receptors (PRRs) Involved with Insect Defense against Pathogens. *Curr. Opin. Insect Sci.* **2019**, *33*, 105–110. [CrossRef]
32. Zhao, L.; Niu, J.; Feng, D.; Wang, X.; Zhang, R. Immune Functions of Pattern Recognition Receptors in Lepidoptera. *Front. Immunol.* **2023**, *14*, 1203061. [CrossRef]
33. Lemaitre, B.; Hoffmann, J. The Host Defense of *Drosophila melanogaster*. *Annu. Rev. Immunol.* **2007**, *25*, 697–743. [CrossRef]
34. Strand, M.R. The Insect Cellular Immune Response. *Insect Sci.* **2008**, *15*, 1–14.
35. Eleftherianos, I.; Heryanto, C.; Bassal, T.; Zhang, W.; Tettamanti, G.; Mohamed, A. Haemocyte-Mediated Immunity in Insects: Cells, Processes and Associated Components in the Fight against Pathogens and Parasites. *Immunology* **2021**, *164*, 401–432. [CrossRef]
36. Medzhitov, R.; Janeway Jr, C.A. Innate Immunity: Impact on the Adaptive Immune Response. *Curr. Opin. Immunol.* **1997**, *9*, 4–9. [CrossRef] [PubMed]
37. Wu, Q.; Patočka, J.; Kuča, K. Insect Antimicrobial Peptides, a Mini Review. *Toxins* **2018**, *10*, 461. [CrossRef] [PubMed]
38. Zhang, W.; Tettamanti, G.; Bassal, T.; Heryanto, C.; Eleftherianos, I.; Mohamed, A. Regulators and Signalling in Insect Antimicrobial Innate Immunity: Functional Molecules and Cellular Pathways. *Cell. Signal.* **2021**, *83*, 110003.
39. O'Neal, A.J.; Singh, N.; Rolandelli, A.; Laukaitis, H.J.; Wang, X.; Shaw, D.K.; Young, B.D.; Narasimhan, S.; Dutta, S.; Snyder, G.A.; et al. Croquemort Elicits Activation of the Immune Deficiency Pathway in Ticks. *Proc. Natl. Acad. Sci. USA* **2023**, *120*, e2208673120. [CrossRef]
40. Smith, A.A.; Pal, U. Immunity-Related Genes in *Ixodes scapularis*—Perspectives from Genome Information. *Front. Cell. Infect. Microbiol.* **2014**, *4*, 116. [CrossRef]
41. Bechsgaard, J.; Vanthournout, B.; Funch, P.; Vestbo, S.; Gibbs, R.A.; Richards, S.; Sanggaard, K.W.; Enghild, J.J.; Bilde, T. Comparative Genomic Study of Arachnid Immune Systems Indicates Loss of Beta-1,3-Glucanase-Related Proteins and the Immune Deficiency Pathway. *J. Evol. Biol.* **2016**, *29*, 277–291. [CrossRef]
42. Rosa, R.D.; Capelli-Peixoto, J.; Mesquita, R.D.; Kalil, S.P.; Pohl, P.C.; Braz, G.R.; Fogaça, A.C.; Daffre, S. Exploring the Immune Signalling Pathway-Related Genes of the Cattle Tick *Rhipicephalus microplus*: From Molecular Characterization to Transcriptional Profile upon Microbial Challenge. *Dev. Comp. Immunol.* **2016**, *59*, 1–14. [CrossRef] [PubMed]
43. Shaw, D.K.; Wang, X.; Brown, L.J.; Chávez, A.S.O.; Reif, K.E.; Smith, A.A.; Scott, A.J.; McClure, E.E.; Boradia, V.M.; Hammond, H.L.; et al. Infection-Derived Lipids Elicit an Immune Deficiency Circuit in Arthropods. *Nat. Commun.* **2017**, *8*, 14401. [CrossRef]
44. Gerardo, N.M.; Altincicek, B.; Anselme, C.; Atamian, H.; Barribeau, S.M.; de Vos, M.; Duncan, E.J.; Evans, J.D.; Gabaldón, T.; Ghanim, M.; et al. Immunity and Other Defenses in Pea Aphids, *Acyrthosiphon pisum*. *Genome Biol.* **2010**, *11*, R21. [CrossRef]
45. Becchimanzi, A.; Nicoletti, R.; Di Lelio, I.; Russo, E. Immune Gene Repertoire of Soft Scale Insects (Hemiptera: Coccidae). *Int. J. Mol. Sci.* **2024**, *25*, 4922. [CrossRef]
46. Bolger, A.M.; Lohse, M.; Usadel, B. Trimmomatic: A Flexible Trimmer for Illumina Sequence Data. *Bioinforma. Oxf. Engl.* **2014**, *30*, 2114–2120. [CrossRef] [PubMed]
47. Haas, B.J.; Papanicolaou, A.; Yassour, M.; Grabherr, M.; Blood, P.D.; Bowden, J.; Couger, M.B.; Eccles, D.; Li, B.; Lieber, M.; et al. De Novo Transcript Sequence Reconstruction from RNA-Seq Using the Trinity Platform for Reference Generation and Analysis. *Nat. Protoc.* **2013**, *8*, 1494–1512. [CrossRef] [PubMed]
48. Edgar, R.C. MUSCLE: Multiple Sequence Alignment with High Accuracy and High Throughput. *Nucleic Acids Res.* **2004**, *32*, 1792–1797. [CrossRef]
49. Castresana, J. Selection of Conserved Blocks from Multiple Alignments for Their Use in Phylogenetic Analysis. *Mol. Biol. Evol.* **2000**, *17*, 540–552. [CrossRef]
50. Stamatakis, A. RAxML-VI-HPC: Maximum Likelihood-Based Phylogenetic Analyses with Thousands of Taxa and Mixed Models. *Bioinformatics* **2006**, *22*, 2688–2690. [CrossRef]
51. Jones, P.; Binns, D.; Chang, H.-Y.; Fraser, M.; Li, W.; McAnulla, C.; McWilliam, H.; Maslen, J.; Mitchell, A.; Nuka, G.; et al. InterProScan 5: Genome-Scale Protein Function Classification. *Bioinformatics* **2014**, *30*, 1236–1240. [CrossRef]
52. de Castro, E.; Sigrist, C.J.A.; Gattiker, A.; Bulliard, V.; Langendijk-Genevaux, P.S.; Gasteiger, E.; Bairoch, A.; Hulo, N. ScanProsite: Detection of PROSITE Signature Matches and ProRule-Associated Functional and Structural Residues in Proteins. *Nucleic Acids Res.* **2006**, *34*, W362–W365. [CrossRef]
53. Hallgren, J.; Tsirigos, K.D.; Pedersen, M.D.; Almagro Armenteros, J.J.; Marcatili, P.; Nielsen, H.; Krogh, A.; Winther, O. DeepTMHMM Predicts Alpha and Beta Transmembrane Proteins Using Deep Neural Networks. *bioRxiv* **2022**.
54. Kurata, S. Peptidoglycan Recognition Proteins in *Drosophila* Immunity. *Dev. Comp. Immunol.* **2014**, *42*, 36–41. [CrossRef]
55. Cerenius, L.; Söderhäll, K. Immune Properties of Invertebrate Phenoloxidases. *Dev. Comp. Immunol.* **2021**, *122*, 104098. [CrossRef] [PubMed]

56. Franc, N.C.; Dimarcq, J.-L.; Lagueux, M.; Hoffmann, J.; Ezekowitz, R.A.B. Croquemort, A Novel Drosophila Hemocyte/Macrophage Receptor That Recognizes Apoptotic Cells. *Immunity* **1996**, *4*, 431–443. [CrossRef] [PubMed]
57. Rao, X.-J.; Zhan, M.-Y.; Pan, Y.-M.; Liu, S.; Yang, P.-J.; Yang, L.-L.; Yu, X.-Q. Immune Functions of Insect βGRPs and Their Potential Application. *Dev. Comp. Immunol.* **2018**, *83*, 80–88. [CrossRef]
58. Takahashi, D.; Garcia, B.L.; Kanost, M.R. Initiating Protease with Modular Domains Interacts with β-Glucan Recognition Protein to Trigger Innate Immune Response in Insects. *Proc. Natl. Acad. Sci. USA* **2015**, *112*, 13856–13861. [CrossRef]
59. Warr, E.; Das, S.; Dong, Y.; Dimopoulos, G. The Gram-Negative Bacteria-Binding Protein Gene Family: Its Role in the Innate Immune System of *Anopheles gambiae* and in Anti-Plasmodium Defence. *Insect Mol. Biol.* **2008**, *17*, 39–51. [CrossRef]
60. Pili-Floury, S.; Leulier, F.; Takahashi, K.; Saigo, K.; Samain, E.; Ueda, R.; Lemaitre, B. In Vivo RNA Interference Analysis Reveals an Unexpected Role for GNBP1 in the Defense against Gram-Positive Bacterial Infection in Drosophila Adults. *J. Biol. Chem.* **2004**, *279*, 12848–12853. [CrossRef]
61. Gottar, M.; Gobert, V.; Matskevich, A.A.; Reichhart, J.-M.; Wang, C.; Butt, T.M.; Belvin, M.; Hoffmann, J.A.; Ferrandon, D. Dual Detection of Fungal Infections in Drosophila via Recognition of Glucans and Sensing of Virulence Factors. *Cell* **2006**, *127*, 1425–1437. [CrossRef]
62. Xia, X.; You, M.; Rao, X.-J.; Yu, X.-Q. Insect C-Type Lectins in Innate Immunity. *Dev. Comp. Immunol.* **2018**, *83*, 70–79. [CrossRef] [PubMed]
63. Wang, W.; Wang, G.; Zhuo, X.; Liu, Y.; Tang, L.; Liu, X.; Wang, J. C-Type Lectin-Mediated Microbial Homeostasis Is Critical for *Helicoverpa armigera* Larval Growth and Development. *PLoS Pathog.* **2020**, *16*, e1008901. [CrossRef]
64. Ao, J.; Ling, E.; Yu, X.-Q. Drosophila C-Type Lectins Enhance Cellular Encapsulation. *Mol. Immunol.* **2007**, *44*, 2541–2548. [CrossRef]
65. Santos-Matos, G.; Wybouw, N.; Martins, N.E.; Zélé, F.; Riga, M.; Leitão, A.B.; Vontas, J.; Grbić, M.; Van Leeuwen, T.; Magalhães, S.; et al. *Tetranychus urticae* Mites Do Not Mount an Induced Immune Response against Bacteria. *Proc. Biol. Sci.* **2017**, *284*, 20170401. [CrossRef]
66. Pace, K.E.; Baum, L.G. Insect Galectins: Roles in Immunity and Development. *Glycoconj. J.* **2002**, *19*, 607–614. [CrossRef]
67. Drickamer, K. Two Distinct Classes of Carbohydrate-Recognition Domains in Animal Lectins. *J. Biol. Chem.* **1988**, *263*, 9557–9560.
68. Dimopoulos, G.; Richman, A.; della Torre, A.; Kafatos, F.C.; Louis, C. Identification and Characterization of Differentially Expressed cDNAs of the Vector Mosquito, Anopheles Gambiae. *Proc. Natl. Acad. Sci. USA* **1996**, *93*, 13066–13071. [CrossRef] [PubMed]
69. Kamhawi, S.; Ramalho-Ortigao, M.; Pham, V.M.; Kumar, S.; Lawyer, P.G.; Turco, S.J.; Barillas-Mury, C.; Sacks, D.L.; Valenzuela, J.G. A Role for Insect Galectins in Parasite Survival. *Cell* **2004**, *119*, 329–341. [CrossRef]
70. Rao, X.-J.; Wu, P.; Shahzad, T.; Liu, S.; Chen, L.; Yang, Y.-F.; Shi, Q.; Yu, X.-Q. Characterization of a Dual-CRD Galectin in the Silkworm *Bombyx Mori*. *Dev. Comp. Immunol.* **2016**, *60*, 149–159. [CrossRef]
71. Waterhouse, R.M.; Kriventseva, E.V.; Meister, S.; Xi, Z.; Alvarez, K.S.; Bartholomay, L.C.; Barillas-Mury, C.; Bian, G.; Blandin, S.; Christensen, B.M.; et al. Evolutionary Dynamics of Immune-Related Genes and Pathways in Disease-Vector Mosquitoes. *Science* **2007**, *316*, 1738–1743. [CrossRef]
72. Lin, Z.; Wang, J.-L.; Cheng, Y.; Wang, J.-X.; Zou, Z. Pattern Recognition Receptors from Lepidopteran Insects and Their Biological Functions. *Dev. Comp. Immunol.* **2020**, *108*, 103688. [CrossRef] [PubMed]
73. Zhu, Y.; Thangamani, S.; Ho, B.; Ding, J.L. The Ancient Origin of the Complement System. *EMBO J.* **2005**, *24*, 382–394. [CrossRef] [PubMed]
74. Sekiguchi, R.; Fujito, N.T.; Nonaka, M. Evolution of the Thioester-Containing Proteins (TEPs) of the Arthropoda, Revealed by Molecular Cloning of TEP Genes from a Spider, Hasarius Adansoni. *Dev. Comp. Immunol.* **2012**, *36*, 483–489. [CrossRef] [PubMed]
75. Sottrup-Jensen, L.; Folkersen, J.; Kristensen, T.; Tack, B.F. Partial Primary Structure of Human Pregnancy Zone Protein: Extensive Sequence Homology with Human Alpha 2-Macroglobulin. *Proc. Natl. Acad. Sci. USA* **1984**, *81*, 7353–7357. [CrossRef]
76. Lin, M.; Sutherland, D.R.; Horsfall, W.; Totty, N.; Yeo, E.; Nayar, R.; Wu, X.-F.; Schuh, A.C. Cell Surface Antigen CD109 Is a Novel Member of the A2 Macroglobulin/C3, C4, C5 Family of Thioester-Containing Proteins. *Blood* **2002**, *99*, 1683–1691. [CrossRef]
77. Li, Z.-F.; Wu, X.; Engvall, E. Identification and Characterization of CPAMD8, a Novel Member of the Complement 3/A2-Macroglobulin Family with a C-Terminal Kazal Domain. *Genomics* **2004**, *83*, 1083–1093. [CrossRef]
78. Lagueux, M.; Perrodou, E.; Levashina, E.A.; Capovilla, M.; Hoffmann, J.A. Constitutive Expression of a Complement-like Protein in Toll and JAK Gain-of-Function Mutants of Drosophila. *Proc. Natl. Acad. Sci. USA* **2000**, *97*, 11427–11432. [CrossRef]
79. Levashina, E.A.; Moita, L.F.; Blandin, S.; Vriend, G.; Lagueux, M.; Kafatos, F.C. Conserved Role of a Complement-like Protein in Phagocytosis Revealed by dsRNA Knockout in Cultured Cells of the Mosquito, *Anopheles Gambiae*. *Cell* **2001**, *104*, 709–718. [CrossRef]

80. Theopold, U.; Schmid, M. Thioester-Containing Proteins: At the Crossroads of Immune Effector Mechanisms. *Virulence* **2017**, *8*, 1468–1470. [CrossRef]
81. Boutros, M.; Agaisse, H.; Perrimon, N. Sequential Activation of Signaling Pathways during Innate Immune Responses in Drosophila. *Dev. Cell* **2002**, *3*, 711–722. [CrossRef]
82. Towb, P.; Sun, H.; Wasserman, S.A. Tube Is an IRAK-4 Homolog in a Toll Pathway Adapted for Development and Immunity. *J. Innate Immun.* **2009**, *1*, 309–321. [CrossRef]
83. Gay, N.J.; Gangloff, M.; Weber, A.N.R. Toll-like Receptors as Molecular Switches. *Nat. Rev. Immunol.* **2006**, *6*, 693–698. [CrossRef] [PubMed]
84. Brennan, J.J.; Gilmore, T.D. Evolutionary Origins of Toll-like Receptor Signaling. *Mol. Biol. Evol.* **2018**, *35*, 1576–1587. [CrossRef]
85. Kanzok, S.M.; Hoa, N.T.; Bonizzoni, M.; Luna, C.; Huang, Y.; Malacrida, A.R.; Zheng, L. Origin of Toll-Like Receptor-Mediated Innate Immunity. *J. Mol. Evol.* **2004**, *58*, 442–448. [CrossRef] [PubMed]
86. Leulier, F.; Lemaitre, B. Toll-like Receptors—Taking an Evolutionary Approach. *Nat. Rev. Genet.* **2008**, *9*, 165–178. [CrossRef] [PubMed]
87. Agaisse, H.; Perrimon, N. The Roles of JAK/STAT Signaling in Drosophila Immune Responses. *Immunol. Rev.* **2004**, *198*, 72–82. [CrossRef]
88. Evans, J.D.; Aronstein, K.; Chen, Y.P.; Hetru, C.; Imler, J.-L.; Jiang, H.; Kanost, M.; Thompson, G.J.; Zou, Z.; Hultmark, D. Immune Pathways and Defence Mechanisms in Honey Bees *Apis mellifera*. *Insect Mol. Biol.* **2006**, *15*, 645–656. [CrossRef]
89. Dionne, M.S.; Schneider, D.S. Models of Infectious Diseases in the Fruit Fly *Drosophila melanogaster*. *Dis. Model. Mech.* **2008**, *1*, 43–49. [CrossRef]
90. Naitza, S.; Rossé, C.; Kappler, C.; Georgel, P.; Belvin, M.; Gubb, D.; Camonis, J.; Hoffmann, J.A.; Reichhart, J.M. The Drosophila Immune Defense against Gram-Negative Infection Requires the Death Protein dFADD. *Immunity* **2002**, *17*, 575–581. [CrossRef]
91. Kaneko, T.; Yano, T.; Aggarwal, K.; Lim, J.-H.; Ueda, K.; Oshima, Y.; Peach, C.; Erturk-Hasdemir, D.; Goldman, W.E.; Oh, B.-H.; et al. PGRP-LC and PGRP-LE Have Essential yet Distinct Functions in the Drosophila Immune Response to Monomeric DAP-Type Peptidoglycan. *Nat. Immunol.* **2006**, *7*, 715–723. [CrossRef]
92. Meinander, A.; Runchel, C.; Tenev, T.; Chen, L.; Kim, C.-H.; Ribeiro, P.S.; Broemer, M.; Leulier, F.; Zvelebil, M.; Silverman, N.; et al. Ubiquitylation of the Initiator Caspase DREDD Is Required for Innate Immune Signalling. *EMBO J.* **2012**, *31*, 2770–2783. [CrossRef] [PubMed]
93. Paquette, N.; Broemer, M.; Aggarwal, K.; Chen, L.; Husson, M.; Ertürk-Hasdemir, D.; Reichhart, J.-M.; Meier, P.; Silverman, N. Caspase Mediated Cleavage, IAP Binding and Ubiquitination: Linking Three Mechanisms Crucial for Drosophila NF-κB Signaling. *Mol. Cell* **2010**, *37*, 172. [CrossRef] [PubMed]
94. Buchon, N.; Silverman, N.; Cherry, S. Immunity in Drosophila Melanogaster—from Microbial Recognition to Whole-Organism Physiology. *Nat. Rev. Immunol.* **2014**, *14*, 796–810. [CrossRef]
95. Kleino, A.; Silverman, N. The Drosophila IMD Pathway in the Activation of the Humoral Immune Response. *Dev. Comp. Immunol.* **2014**, *42*, 25–35. [CrossRef]
96. Kleino, A.; Myllymäki, H.; Kallio, J.; Vanha-aho, L.-M.; Oksanen, K.; Ulvila, J.; Hultmark, D.; Valanne, S.; Rämet, M. Pirk Is a Negative Regulator of the Drosophila Imd Pathway. *J. Immunol. Baltim. Md 1950* **2008**, *180*, 5413–5422. [CrossRef] [PubMed]
97. Stöven, S.; Ando, I.; Kadalayil, L.; Engström, Y.; Hultmark, D. Activation of the Drosophila NF-κB Factor Relish by Rapid Endoproteolytic Cleavage. *EMBO Rep.* **2000**, *1*, 347–352. [CrossRef]
98. Stöven, S.; Silverman, N.; Junell, A.; Hedengren-Olcott, M.; Erturk, D.; Engström, Y.; Maniatis, T.; Hultmark, D. Caspase-Mediated Processing of the Drosophila NF-κB Factor Relish. *Proc. Natl. Acad. Sci. USA* **2003**, *100*, 5991–5996. [CrossRef]
99. Ertürk-Hasdemir, D.; Broemer, M.; Leulier, F.; Lane, W.S.; Paquette, N.; Hwang, D.; Kim, C.-H.; Stöven, S.; Meier, P.; Silverman, N. Two Roles for the Drosophila IKK Complex in the Activation of Relish and the Induction of Antimicrobial Peptide Genes. *Proc. Natl. Acad. Sci. USA* **2009**, *106*, 9779–9784. [CrossRef]
100. Fogaça, A.C.; Sousa, G.; Pavanelo, D.B.; Esteves, E.; Martins, L.A.; Urbanová, V.; Kopáček, P.; Daffre, S. Tick Immune System: What Is Known, the Interconnections, the Gaps, and the Challenges. *Front. Immunol.* **2021**, *12*, 628054. [CrossRef]
101. Müller, C.W.; Rey, F.A.; Sodeoka, M.; Verdine, G.L.; Harrison, S.C. Structure of the NF-κB P50 Homodimer Bound to DNA. *Nature* **1995**, *373*, 311–317. [CrossRef]
102. Dushay, M.S.; Asling, B.; Hultmark, D. Origins of Immunity: Relish, a Compound Rel-like Gene in the Antibacterial Defense of Drosophila. *Proc. Natl. Acad. Sci. USA* **1996**, *93*, 10343–10347. [CrossRef] [PubMed]
103. Naranjo, V.; Ayllón, N.; de la Lastra, J.M.P.; Galindo, R.C.; Kocan, K.M.; Blouin, E.F.; Mitra, R.; Alberdi, P.; Villar, M.; Fuente, J. de la Reciprocal Regulation of NF-kB (Relish) and Subolesin in the Tick Vector, *Ixodes scapularis*. *PLoS ONE* **2013**, *8*, e65915. [CrossRef]

104. Capelli-Peixoto, J.; Carvalho, D.D.; Johnson, W.C.; Scoles, G.A.; Fogaça, A.C.; Daffre, S.; Ueti, M.W. The Transcription Factor Relish Controls *Anaplasma marginale* Infection in the Bovine Tick *Rhipicephalus microplus*. *Dev. Comp. Immunol.* **2017**, *74*, 32–39. [CrossRef]
105. Fongsaran, C.; Verhoeve, V.I.; Jirakanwisal, K.; Harris, E.K.; Macaluso, K.R. Identification and Characterization of a Relish-Type NF-κB, DvRelish, in *Dermacentor variabilis* in Response to Rickettsia Rickettsii Infection. *Front. Cell. Infect. Microbiol.* **2024**, *14*, 1494450. [CrossRef]
106. Jalovecka, M.; Malandrin, L.; Urbanova, V.; Mahmood, S.; Snebergerova, P.; Peklanska, M.; Pavlasova, V.; Sima, R.; Kopacek, P.; Perner, J.; et al. Activation of the Tick Toll Pathway to Control Infection of *Ixodes ricinus* by the Apicomplexan Parasite *Babesia Microti*. *PLoS Pathog.* **2024**, *20*, e1012743. [CrossRef]
107. Oliva Chávez, A.S.; Shaw, D.K.; Munderloh, U.G.; Pedra, J.H.F. Tick Humoral Responses: Marching to the Beat of a Different Drummer. *Front. Microbiol.* **2017**, *8*, 223. [CrossRef]
108. Severo, M.S.; Choy, A.; Stephens, K.D.; Sakhon, O.S.; Chen, G.; Chung, D.-W.D.; Le Roch, K.G.; Blaha, G.; Pedra, J.H.F. The E3 Ubiquitin Ligase XIAP Restricts *Anaplasma phagocytophilum* Colonization of *Ixodes scapularis* Ticks. *J. Infect. Dis.* **2013**, *208*, 1830–1840. [CrossRef]
109. McClure Carroll, E.E.; Wang, X.; Shaw, D.K.; O'Neal, A.J.; Oliva Chávez, A.S.; Brown, L.J.; Boradia, V.M.; Hammond, H.L.; Pedra, J.H.F. P47 Licenses Activation of the Immune Deficiency Pathway in the Tick *Ixodes scapularis*. *Proc. Natl. Acad. Sci. USA* **2019**, *116*, 205–210. [CrossRef]
110. Myllymäki, H.; Valanne, S.; Rämet, M. The Drosophila Imd Signaling Pathway. *J. Immunol. Baltim. Md 1950* **2014**, *192*, 3455–3462. [CrossRef]
111. De Gregorio, E.; Spellman, P.T.; Tzou, P.; Rubin, G.M.; Lemaitre, B. The Toll and Imd Pathways Are the Major Regulators of the Immune Response in Drosophila. *EMBO J.* **2002**, *21*, 2568–2579. [CrossRef]
112. Stączek, S.; Cytryńska, M.; Zdybicka-Barabas, A. Unraveling the Role of Antimicrobial Peptides in Insects. *Int. J. Mol. Sci.* **2023**, *24*, 5753. [CrossRef] [PubMed]
113. Wu, J.; Zhou, X.; Chen, Q.; Chen, Z.; Zhang, J.; Yang, L.; Sun, Y.; Wang, G.; Dai, J.; Feng, T. Defensins as a Promising Class of Tick Antimicrobial Peptides: A Scoping Review. *Infect. Dis. Poverty* **2022**, *11*, 71. [CrossRef] [PubMed]
114. Baumann, T.; Kämpfer, U.; Schürch, S.; Schaller, J.; Largiadèr, C.; Nentwig, W.; Kuhn-Nentwig, L. Ctenidins: Antimicrobial Glycine-Rich Peptides from the Hemocytes of the Spider *Cupiennius salei*. *Cell. Mol. Life Sci.* **2010**, *67*, 2787–2798. [CrossRef]
115. Bachali, S.; Jager, M.; Hassanin, A.; Schoentgen, F.; Jollès, P.; Fiala-Medioni, A.; Deutsch, J.S. Phylogenetic Analysis of Invertebrate Lysozymes and the Evolution of Lysozyme Function. *J. Mol. Evol.* **2002**, *54*, 652–664. [CrossRef]
116. Van Herreweghe, J.M.; Michiels, C.W. Invertebrate Lysozymes: Diversity and Distribution, Molecular Mechanism and in Vivo Function. *J. Biosci.* **2012**, *37*, 327–348. [CrossRef]
117. Tanaka, T.; Kawano, S.; Nakao, S.; Umemiya-Shirafuji, R.; Rahman, M.M.; Boldbaatar, D.; Battur, B.; Liao, M.; Fujisaki, K. The Identification and Characterization of Lysozyme from the Hard Tick *Haemaphysalis longicornis*. *Ticks Tick-Borne Dis.* **2010**, *1*, 178–185. [CrossRef]
118. Cerenius, L.; Lee, B.L.; Söderhäll, K. The proPO-System: Pros and Cons for Its Role in Invertebrate Immunity. *Trends Immunol.* **2008**, *29*, 263–271. [PubMed]
119. Burmester, T. Origin and Evolution of Arthropod Hemocyanins and Related Proteins. *J. Comp. Physiol. B* **2002**, *172*, 95–107. [CrossRef]
120. Nagai, T.; Osaki, T.; Kawabata, S. Functional Conversion of Hemocyanin to Phenoloxidase by Horseshoe Crab Antimicrobial Peptides. *J. Biol. Chem.* **2001**, *276*, 27166–27170. [CrossRef]
121. Voit, R.; Feldmaier-Fuchs, G.; Schweikardt, T.; Decker, H.; Burmester, T. Complete Sequence of the 24-Mer Hemocyanin of the Tarantula Eurypelma Californicum. Structure and Intramolecular Evolution of the Subunits. *J. Biol. Chem.* **2000**, *275*, 39339–39344. [CrossRef]
122. Zhioua, E.; Browning, M.; Johnson, P.W.; Ginsberg, H.S.; LeBrun, R.A. Pathogenicity of the Entomopathogenic Fungus Metarhizium Anisopliae (Deuteromycetes) to *Ixodes scapularis* (Acari: Ixodidae). *J. Parasitol.* **1997**, *83*, 815–818. [CrossRef] [PubMed]
123. Simser, J.A.; Macaluso, K.R.; Mulenga, A.; Azad, A.F. Immune-Responsive Lysozymes from Hemocytes of the American Dog Tick, *Dermacentor variabilis* and an Embryonic Cell Line of the Rocky Mountain Wood Tick, *D. Andersoni*. *Insect Biochem. Mol. Biol.* **2004**, *34*, 1235–1246. [CrossRef] [PubMed]

Disclaimer/Publisher's Note: The statements, opinions and data contained in all publications are solely those of the individual author(s) and contributor(s) and not of MDPI and/or the editor(s). MDPI and/or the editor(s) disclaim responsibility for any injury to people or property resulting from any ideas, methods, instructions or products referred to in the content.

insects

MDPI

Article

MPF Regulates Oocyte and Embryo Development During Parthenogenesis Induction in Silkworm, *Bombyx mori*

Chenkai Ma [1,2,†], Fang Xu [1,2,†], Chengjie Hu [1,2], Chunguang Cui [2], Xin Du [2], Jine Chen [2], Linbao Zhu [2], Shaofang Yu [2], Xingjian He [2], Wei Yu [1], Yongqiang Wang [2,*] and Xia Xu [1,2,*]

[1] College of Life Sciences and Medicine, Zhejiang Sci-Tech University, Hangzhou 310018, China; yuwei@zstu.edu.cn (W.Y.)
[2] Institute of Sericulture and Tea, Zhejiang Academy of Agricultural Sciences, Hangzhou 310021, China
* Correspondence: wangyq@zaas.ac.cn (Y.W.); xuxia@zaas.ac.cn (X.X.)
† These authors contributed equally to this work.

Simple Summary: The unfertilized eggs of silkworm treated in a warm bath (46 °C, 18 min) can induce parthenogenesis, resulting in progeny that are exclusively female and genetically identical. This process involves dynamic changes during oocyte division, which are directly related to the cell cycle. Maturation-promoting factor (MPF) played a crucial role in regulating oocyte meiosis, ensuring normal fertilization and subsequent embryonic development. MPF activity was proportional to the silkworm parthenogenesis induction rate, and the induction rate varied regularly with the change in the activity. Additionally, it was observed that embryonic development was delayed after parthenogenesis induction by the inhibitor interference. These insights hold significant promise for advancing genetic and breeding research.

Abstract: In most species, oocytes are arrested at the prophase or metaphase of meiosis I and require sperm-derived or external stimuli to resume meiosis. Maturation-promoting factor (MPF) is an oocyte maturation factor composing the catalytic subunit Cdc2 and the regulatory subunit CycB that can restart stalled meiosis. In this study, we demonstrated that MPF activity affected parthenogenesis induction in the model lepidopteran insect *Bombyx mori* using activator and inhibitor interference. We found that the upregulation of MPF activity significantly increased the parthenogenesis induction rate, whereas downregulation significantly reduced it. Furthermore, the inhibition of MPF activity also led to a delay in embryonic development. Given its evolutionary conservation, MPF emerges as a potential universal target for manipulating reproductive outcomes, offering broad applications in genetics and selective breeding.

Keywords: MPF; enzyme activity; embryo development; parthenogenesis; *Bombyx mori*

1. Introduction

The silkworm, *Bombyx mori*, serves as a pivotal lepidopteran model organism in genetic and genomic research [1–4]. Under natural conditions, silkworms typically reproduce sexually, although unfertilized eggs may occasionally develop into new individuals through parthenogenesis [4]. However, the natural incidence of parthenogenesis in silkworm is extremely low, at only 0.003% [5,6]. Unfertilized silkworm eggs can be artificially induced to develop using physical or chemical methods. One of the most widely used techniques involves subjecting the eggs to a warm bath (46 °C, 18 min), which induces ameiotic

parthenogenesis (AMP) in silkworm [4]. AMP refers to the absence of allelic recombination during oocyte meiosis, resulting in offspring that are genetically identical to the maternal parent [7]. Although the cytological mechanism of parthenogenesis is well documented, the molecular mechanism of AMP induced by warm bath treatment in silkworm remains to be fully understood.

Oocyte development is arrested at the metaphase of the first meiosis and requires stimulation by sperm or other external factors to resume meiosis in silkworm [8,9]. Interestingly, warm bath induction did not restart the stalled oocyte meiosis in silkworm. Central to cell cycle regulation is maturation-promoting factor (MPF), a heterodimeric complex comprising the catalytic subunit cell division cycle 2 (Cdc2) and the regulatory subunit cyclin B (CycB) [10,11]. Cdc2 is central to the regulation of the G2/M phase transition in the cell cycle [12,13]. It exhibits serine/threonine kinase activity and catalyzes the phosphorylation of various target proteins, thereby ensuring the orderly progression of the cell cycle [14–16]. Cdc2 activity is tightly regulated by CycB, whose expression varies during the cell cycle to further regulate MPF activity [17,18].

MPF is indispensable for meiotic resumption during oocyte maturation [19,20]. In *Xenopus laevis*, MPF accumulated as an inactive complex during oocyte development, and only when CycB reached a certain amount did it switch to an activated state, thus initiating the G2-to-M phase transition and initiating cell meiosis [21,22]. Similarly, in *Sus scrofa*, Cdc2 deficiency led to meiotic failure in small oocytes, and the induction of Cdc2 expression enables the completion of meiotic maturation [23,24]. In *Mus musculus*, phosphatase was decisive for MPF to restore oocyte meiosis [25]. During sexual reproduction, MPF ensures proper oocyte meiosis, fertilization, and embryonic development [26,27]. In mammals, the disruption of Cdc2 activity interferes with MPF function and affected parthenogenesis induction [28]. However, the role of MPF in parthenogenesis induction in insects, such as the silkworm, remains poorly understood and warrants further investigation.

In this study, we investigated the function of MPF in warm-bath-induced parthenogenesis in *B. mori*, a model lepidopteran insect. We found that the mRNA expression levels of *Cdc2* and *CycB* were significantly higher in the parthenogenetic line (Wu14) and corresponding amphigenetic line (54A) following the warm bath treatment of silkworm eggs. MPF activity was found to be directly proportional to the parthenogenesis induction rate, with the induction rate exhibiting a consistent pattern in response to changes in MPF activity. Additionally, embryonic development was delayed after parthenogenesis induction when MPF activity was inhibited, whereas early development was not triggered by MPF activation. Perturbations in MPF activity disrupt oocyte cell cycle regulation, leading to parthenogenesis failure. Phylogenetic analysis further revealed that MPF was highly conserved evolutionarily. These findings not only enhance our understanding of the mechanisms underlying parthenogenesis in silkworms but also provide insights that can be applied to population regulation in other species.

2. Materials and Methods

2.1. Silkworm and Cell Lines

The parthenogenetic line (Wu14) and corresponding amphigenetic line (54A) were bred and provided by Zhejiang Academy of Agricultural Sciences. Wu14 was derived from 54A through warm bath (46 °C, 18 min) induction [6]. Both lines had been bred for over 30 generations, ensuring stable genetic and phenotypic characteristics. The parthenogenetic line Wu14 was derived from the amphigenetic line 54A through warm bath breeding. The amphigenetic line 54A typically reproduces through the fusion of sperm and egg after mating between males and females. We induced unfertilized eggs of 54A using warm bath

treatment and reared the individuals that exhibited pigmentation and successful hatching. After these individuals developed into adults, we continued to apply warm bath treatment to their unfertilized eggs. Through over 30 consecutive generations of selective induction, both the pigmentation rate and hatching rate of Wu14 stabilized at over 80%. In other words, the first generation of Wu14 originated from 54A, and subsequent generations were developed through warm bath induction and selective breeding. Silkworm eggs were incubated at 25 °C and 80% relative humidity (RH) for 10 days. The instar larvae were reared on fresh mulberry leaves at 25 °C and 70% RH. To break diapause and sustain continuous rearing, the eggs were treated with hydrochloric acid. The eggs were immersed in 15% hydrochloric acid at 46 °C for 5 min and then placed at 25 °C and 80% RH until hatching.

2.2. Artificially Induced Parthenogenesis

Next, 12 h after emergence, female moths were dissected the abdomen, and unfertilized eggs were collected for parthenogenesis induction [4]. The unfertilized eggs were soaked in a warm bath at 46 °C for 18 min, followed by rapid cooling in a room temperature water bath at 25 °C for 3 min. After drying, the eggs were placed in an incubator at 16 °C and 80% RH for 3 days. At this stage, the eggs corresponded developmentally to the post-oviposition stage of sexual reproduction. To break diapause, the eggs were immersed in 15% hydrochloric acid at 46 °C for 5 min and then left at 25 °C and 80% RH until hatching. Following parthenogenesis activation, embryonic development was marked by a change in egg color from yellow to dark due to serous pigmentation on the third day [6]. However, not all pigmentated eggs hatched successfully. The pigmentation and hatching rates of eggs in each moth were calculated (n = 42). Pigmentation rate (%) = (number of pigmentated eggs/total number of eggs) × 100%. Hatching rate (%) = (number of hatched eggs/total number of eggs) × 100%.

2.3. Protein Structure and Phylogenetics Analysis

The protein structure was predicted using the online software ProtScale for hydrophobicity (https://web.expasy.org/protscale/ (accessed on 20 January 2025)), Uniprot for sequence annotation (https://www.uniprot.org/ (accessed on 20 January 2025)), Sopma for secondary structure (https://npsa-prabi.ibcp.fr/cgi-bin/npsa_automat.pl?page=/NPSA/npsa_sopma.html (accessed on 20 January 2025)), and Swiss-model for 3D modeling (https://swissmodel.expasy.org/ (accessed on 20 January 2025)) [29]. Evolutionary relationships were inferred using the neighbor-joining (NJ) method. Tests were performed by Bootstrap (1000 replicates). Evolutionary distances were computed using the Poisson correction method. Evolutionary analyses were conducted in MEGA 11 [30].

2.4. RNA Isolation, cDNA Synthesis, and qPCR Analysis

Total RNAs were isolated using Trizol® reagent (Invitrogen, Carlsbad, CA, USA). For complementary DNA (cDNA) synthesis, 1 μg of total RNA was reverse-transcribed using the RevertAid™ First Strand cDNA Synthesis Kit (Thermo Fisher Scientific, Waltham, MA, USA). Quantitative real-time PCR (qRT-PCR) analyses were performed using a SYBR Green Realtime PCR Master Mix (Thermo Fisher Scientific, Waltham, MA, USA). The PCR conditions were as follows: initial incubation at 95 °C for 5 min, 35 cycles at 95 °C for 15 s, and 60 °C for 1 min. *Ribosomal protein 49* (*Bmrp49*) was used as an internal control [31]. A relative quantitative method ($^{\Delta\Delta}$Ct) was used to evaluate quantitative variation. The gene-specific primers used for qRT-PCR are listed in Table 1.

Table 1. Specific primers.

Primer Name	Primer Sequence (5′–3′)
BmCdc2-F	ATGGACTCCCTTGGTTCTGG
BmCdc2-R	CACTGGAACACCGAATGCTC
BmCycB-F	ATGTGCAAACTGGGCTTCTG
BmCycB-R	CTGCTAGTTCTGACGGTCGA
BmRP49-F	TCAATCGGATCGCTATGACA
BmRP49-R	ATGACGGGTCTTCTTGTTGG

2.5. Enzyme Inhibition and Activity Detection

Healthy individuals with consistent pupation times were selected and placed in an incubator at 25 °C and 80% RH. Since Cdc2 is a central component of MPF, we modulated MPF activity by targeting Cdc2 using an activator (HY-129478, MCE, Atlantic City, NJ, USA) and an inhibitor (HY-12529, MCE, Atlantic City, NJ, USA) [32,33]. The activator and inhibitor were separately injected into the pupa using a microsyringe. The needle was injected vertically into the middle of the third abdominal somite. The pupal stage for both the Wu14 and 54A lines was 13 days, and injections were given on the 12th day (one day before emergence). DMSO/corn oil (1:9, v/v) was used to prepare different concentrations of the activator and inhibitor. Based on the properties of the compounds and the preliminary experimental concentration test, three appropriate concentrations were finally set (10 μM, 20 μM, and 40 μM). The administered injection was consistently 5 μL. Eggs were collected 12 h after female emergence, and enzyme activity was detected using ELISA kit (YJ370816, Yuanju, Shanghai, China). MPF is composed of the catalytic subunit Cdc2 and the regulatory subunit CycB. Cdc2 exhibits kinase activity only when bound to CycB. The kinase activity of MPF depends on the binding of Cdc2 to cyclin B and the phosphorylation-activated state of the critical site (Thr161) on Cdc2 [34]. The ELISA kit employed a sandwich immunoassay to measure MPF activity, specifically targeting the Thr161 phosphorylation site of Cdc2, which served as its molecular switch [19,34]. Antibody capture: Antibodies were captured via immobilization on the microplate surface, where they bound to a specific epitope of Thr161-phosphorylated Cdc2, anchoring to the solid phase. Antibody detection: Antibodies were detected via conjugation with horseradish peroxidase (HRP). A spatially distinct epitope was recognized on the same phosphorylated Cdc2 molecule, forming a stable "antibody–antigen–antibody" sandwich complex. Dual-epitope recognition: The requirement for simultaneous binding by both antibodies ensured the detection of intact MPF complexes (Cdc2-CycB with Thr161 phosphorylation) while excluding partially degraded products or nonspecifically phosphorylated proteins. The substrate TMB was added for color development. TMB was converted to a blue color with the catalysis of HRP and subsequently turned yellow in the presence of acid. The intensity of the yellow color was directly proportional to the MPF concentration in the sample. Absorbance was measured at 450 nm with activity proportional to signal intensity.

2.6. Ovariole and Embryo Observation

Female moths 12 h after emergence were dissected, and 8 ovarioles were carefully separated using tweezers in insect phosphate-buffered saline (PBS). Images were captured using a camera (Canon, EOS M3, Tokyo, Japan). We randomly selected and mixed the eggs from 10 female moths and then randomly chose 30 eggs from this mixture for embryo observation. For embryo isolation, 20% KOH solution (100 mL) was heated to boiling in a beaker. Eggs were soaked in KOH solution for 3s and immediately transferred to 60 °C warm water for 3 s. Then, the eggs were placed in a Petri dish with 25 °C water and blown

repeatedly with a plastic glue head dropper until the complete embryos were obtained. We transferred embryos onto a glass slide using a plastic glue head dropper, followed by direct observation under a microscope. Images were captured using microscope (TL3000 Ergo, Leica, Wetzlar, Germany).

2.7. Statistical Analysis

GraphPad Prism 8.3.0 was used for two-tailed Student's *t*-test analysis. Three independent replicates were used for each treatment. Means were determined, and error bars show the means ± SEM (standard error of the mean).

3. Results

3.1. Protein Structures of Cdc2 and CycB

The catalytic subunit Cdc2 (319 aa, pI 7.69) exhibited strong hydrophilicity with predominant polar amino acid composition (Figure 1A). Its kinase domain (aa 4–287) contained three critical phosphorylation sites: Thr-14 and Tyr-15 (inhibitory) and Thr-161 (activating), all located within random coil regions (Figure 1B). The structural prediction of Cdc2 revealed 17 α-helices (38.87%), 11 β-strands (13.48%), and 17 random coils (47.65%) (Figure 1C,D). And the three phosphorylation sites, Thr-14, Thr-15, and Thr-161, were all located within the random coil regions. The regulatory subunit CycB (525 aa, pI 9.27) contained two cyclin-like domains (aa 249–386 and 389–510) that regulate kinase activity (Figure 1A,B). These domains primarily regulate cyclin-dependent protein serine/threonine kinase activity. The secondary structure of CycB comprised 20 α-helices (40.00%) and 18 random coils (57.90%) (Figure 1C,D). The functional MPF complex is formed through Cdc2-CycB interaction, with Thr161 phosphorylation serving as the molecular switch for cell cycle regulation [35,36].

3.2. Phylogenetic Identification of Cdc2 and CycB

Homologous sequences of the Cdc2 and CycB proteins were selected from 20 different species to explore evolutionary conservation. These species were as follows: *B. mori*, *Manduca sexta*, *Trichoplusia ni*, *Ostrinia furnacalis*, *Amyelois transitella*, *Helicoverpa zea*, *Battus philenor*, *Plodia interpunctella*, *Diprion similis*, *Neodiprion lecontei*, *Athalia rosae*, *Hermetia illucens*, *Culicoides brevitarsis*, *Episyrphus balteatus*, *Gryllus bimaculatus*, *Anabrus simplex*, *Schistocerca nitens*, *Homo sapiens*, *Jaculus jaculus*, and *Myxocyprinus asiaticus*. Phylogenetic analysis revealed that the Cdc2 and CycB proteins were moderately conserved across these species (Figure 2). Protein kinase and cyclin-like functional domains were highly specific, further indicating that MPF involved in cell cycle was species-specific. These findings indicated that insights into MPF function in *B. mori* are likely applicable to other species. The sequence numbers of the proteins in the corresponding species are listed in Table 2.

3.3. Differential mRNA Expression in Parthenogenetic and Amphigenetic Lines

The comparative analysis of Wu14 (parthenogenetic) and 54A (amphigenetic) lines revealed striking reproductive differences. The results revealed that the pigmentation rate of Wu14 exceeded 85%, with a hatching rate of over 80%, while 54A exhibited a pigmentation rate of approximately 50% but a significantly lower hatching rate of less than 2% (Figure 3A). We collected unfertilized eggs of 54A and Wu14, including uninduced eggs (UI) and induced eggs (I) in a warm bath. We detected *Cdk2* mRNA expression levels in both UI and I. Subsequently, we examined the mRNA expression levels of *Cdc2* and *CycB* genes in the eggs. The results showed significant differences in *Cdc2* and *CycB* expression between UI and I in parthenogenetic line Wu14, but no such differences were

observed in corresponding amphigenetic line 54A (Figure 3B). These results establish a direct correlation between MPF component expression and parthenogenetic competence.

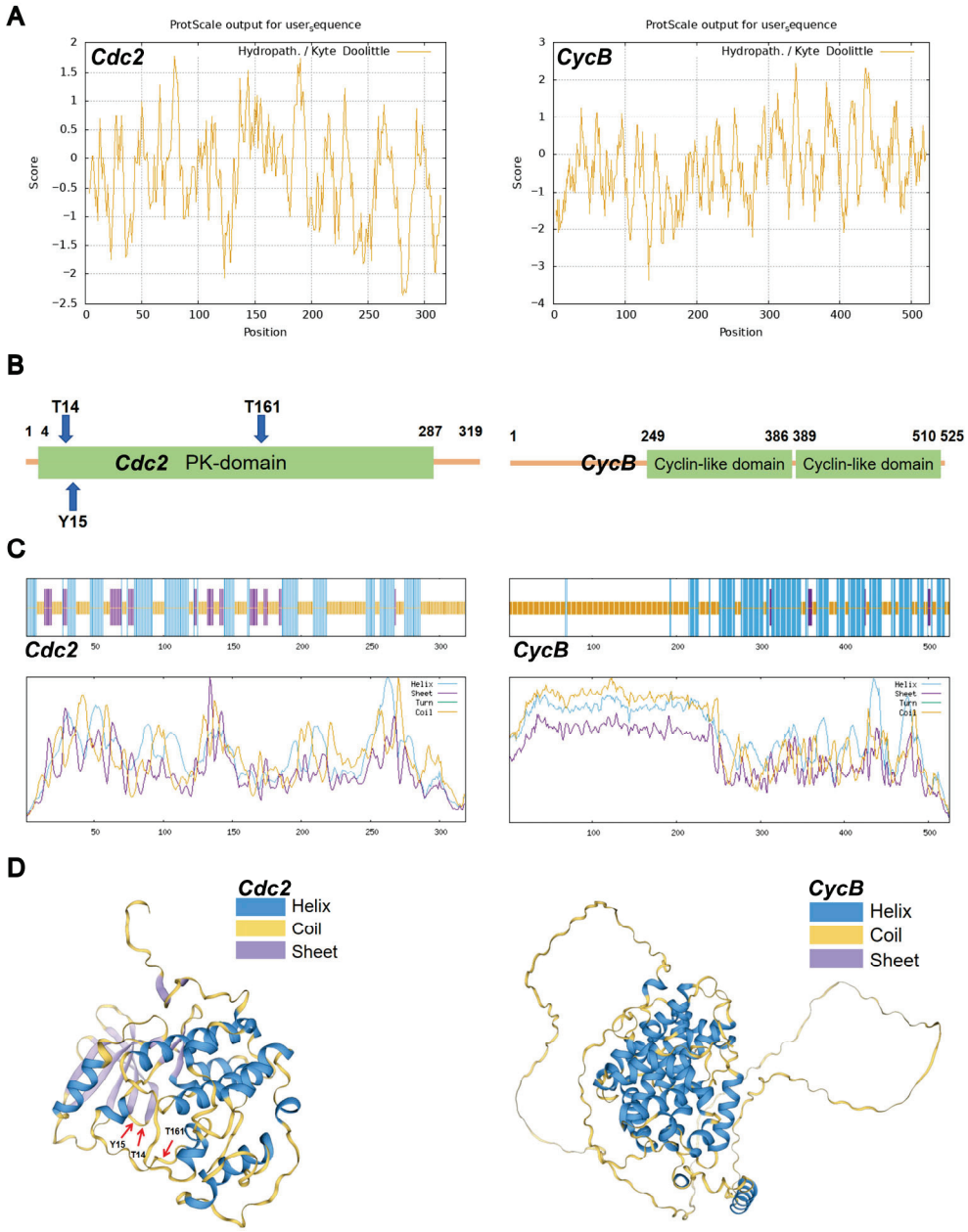


Figure 1. Predicted protein. (**A**) Physicochemical properties of Cdc2 and CycB. The ProtScale was used; a positive score denotes hydrophobic amino acid, and the large value demonstrates strong hydrophobicity; a negative score represents hydrophilic amino acid, and a small value indicates strong hydrophilicity. (**B**) Functional domain of Cdc2 and CycB. Uniprot was used; green is the domain location. (**C**) Secondary structure of Cdc2 and CycB. Sopma was used; blue is the helix; purple is the sheet; green is the turn; yellow is the coil. (**D**) Tertiary structure of Cdc2 and CycB. Swiss-model was used; blue is the helix; purple is the sheet; yellow is the coil.

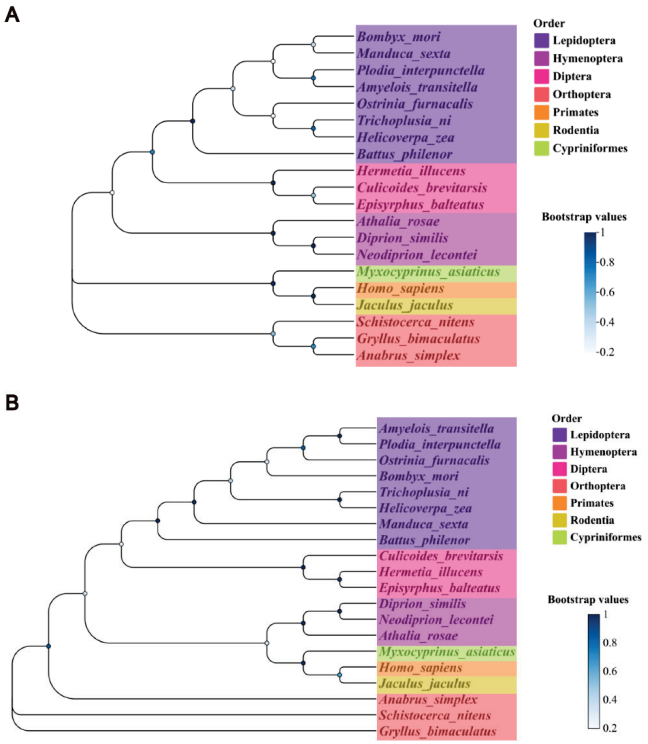


Figure 2. Phylogenetic tree. (**A**) Cdc2. (**B**) CycB. Protein sequences from *B. mori*, *Manduca sexta*, *Trichoplusia ni*, *Ostrinia furnacalis*, *Amyelois transitella*, *Helicoverpa zea*, *Battus philenor*, *Plodia interpunctella*, *Diprion similis*, *Neodiprion lecontei*, *Athalia rosae*, *Hermetia illucens*, *Culicoides brevitarsis*, *Episyrphus balteatus*, *Gryllus bimaculatus*, *Anabrus simplex*, *Schistocerca nitens*, *Homo sapiens*, *Jaculus jaculus*, and *Myxocyprinus asiaticus*.

Table 2. The protein sequence numbers.

Species Name	GenBank Accession Numbers		Order
	Cdc2	CycB	
Bombyx mori	NP_001037512.1	NP_001037343.1	Lepidoptera
Manduca sexta	XP_030037649.1	XP_030029390.1	Lepidoptera
Trichoplusia ni	XP_026740648.1	XP_026731829.1	Lepidoptera
Ostrinia furnacalis	XP_028177540.1	XP_028156235.1	Lepidoptera
Amyelois transitella	XP_013193284.1	XP_013191183.2	Lepidoptera
Helicoverpa zea	XP_047033055.1	XP_047023653.1	Lepidoptera
Battus philenor	XP_068623488.1	XP_068626558.1	Lepidoptera
Plodia interpunctella	XP_053617113.1	XP_053610622.1	Lepidoptera
Diprion similis	XP_046738554.1	XP_046746195.1	Hymenoptera
Neodiprion lecontei	XP_015520372.1	XP_046598379.1	Hymenoptera
Athalia rosae	XP_012254072.1	XP_012254238.2	Hymenoptera
Hermetia illucens	XP_037903055.1	XP_037904258.1	Diptera
Culicoides brevitarsis	XP_063700522.1	XP_063700924.1	Diptera
Episyrphus balteatus	XP_055836824.1	XP_055837226.1	Diptera
Gryllus bimaculatus	GLH05238.1	GLG94543.1	Orthoptera
Anabrus simplex	XP_067015382.1	XP_066990889.1	Orthoptera
Schistocerca nitens	XP_049799429.1	XP_049815951.1	Orthoptera
Homo sapiens	NP_001307847.1	NP_114172.1	Primates
Jaculus jaculus	XP_004657918.1	XP_045016300.1	Rodentia
Myxocyprinus asiaticus	XP_051502898.1	XP_051559981.1	Cypriniformes

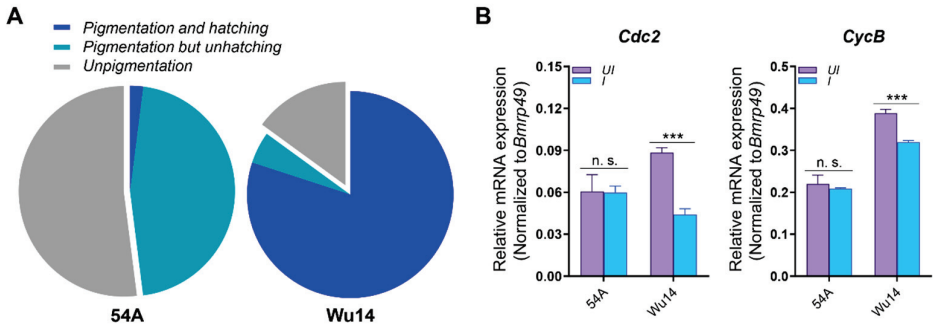


Figure 3. The mRNA expressions in 54A and Wu14. (**A**) Parthenogenesis induction rate. (**B**) mRNA expression. Pigmentation rate is blue and cyan, hatching rate is blue, and unpigmented rate is gray. The mRNA expression level was normalized to *B. mori ribosomal protein 49* (*Bmrp49*), an internal reference. The data shown are means ± S.E.M. (n = 3). Asterisks indicate significant differences with a two-tailed t-test: *** $p < 0.001$; n. s. $p > 0.05$.

3.4. Activator and Inhibitor Effectively Regulated MPF Activity and Were Not Toxic

Then, 12 h after pupae emergence and injection with the activator and inhibitor, unfertilized eggs of female moths were dissected and collected. The activity of MPF was detected at different interference concentrations. We observed that MPF activity increased significantly with higher concentrations of the activator and decreased significantly with higher concentrations of the inhibitor (Figure 4A). Simultaneously, we observed ovariole integrity and egg development at varying concentrations. After both activator and inhibitor interference, the eight ovarioles remained fully arranged on both sides of the abdomen, and there was no significant difference in the development status and shape of the eggs compared with the control (Figure 4B). These results indicated that the activator and inhibitor effectively regulated MPF activity without having toxic effects on egg development.

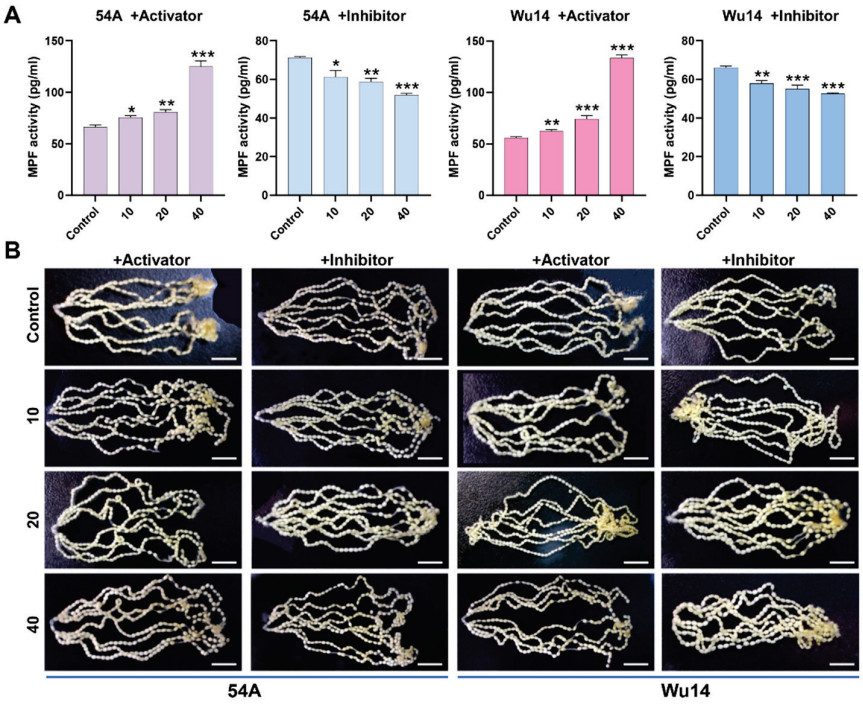


Figure 4. Regulation of MPF activity. (**A**) Enzyme activity. (**B**) Ovariole observation. The unit of concentration was μM. The data shown are means ± S.E.M. (n = 3). Asterisks indicate significant differences with a two-tailed t-test: * $p < 0.05$; ** $p < 0.01$; *** $p < 0.001$. The scale is 1 cm.

3.5. MPF Activity Affected Parthenogenesis Induction

We performed parthenogenesis induction on unfertilized eggs after modulating MPF activity and assessed the rates of pigmentation and hatching. Both the parthenogenetic line Wu14 and corresponding amphigenetic line 54A exhibited significant changes in the rates of pigmentation and hatching in response to alterations in MPF activity (Figure 5). Specifically, the upregulation of MPF activity using the activator led to a marked increase in pigmentation and hatching rates for both 54A and Wu14. Conversely, the downregulation of MPF activity resulted in particularly significant reductions in these rates. These results demonstrated MPF's pivotal role in parthenogenesis initiation, with greater effects observed in the specialized Wu14 line.

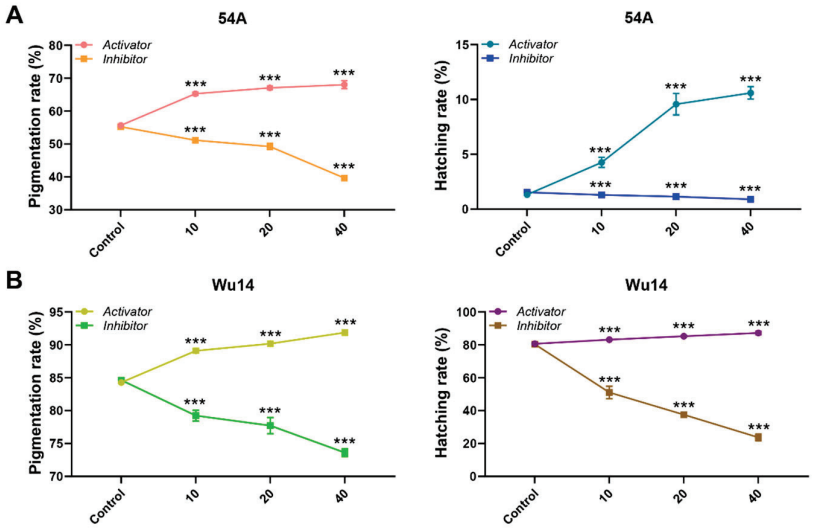


Figure 5. Pigmentation and hatching rates. (**A**) Amphigenetic line 54A. (**B**) Parthenogenetic line Wu14. The unit of concentration was μM. The data shown are means ± S.E.M. (n = 3). Asterisks indicate significant differences with a two-tailed t-test: *** $p < 0.001$.

3.6. Inhibition of MPF Activity Leads to Abnormal Embryonic Development

To systematically evaluate the impact of MPF activity on embryonic development, we conducted detailed morphological analyses of Wu14 embryos under different treatment conditions. The differentiation stage of the tail segment began on the 4th day and reached full development by the 9th day (Figure 6A). On D4 (the differentiation stage of the tail segment), anterior germ segments fused to form head structures; posterior segments developed into a narrow tail region; and a clear distinction between abdominal and tail regions was established. On D5 (the somatic inversion stage), embryonic shortening was observed; ventral curvature in the tail segment was initiated; and the transition from S-shaped to C-shaped morphology took place. On D6 (the epidermis formation stage), complete C-shaped body conformation occurred, and tubercle-like epidermal protrusions emerged. On D7 (the tissue formation stage), the development of body setae (bristle structures) was observed; thoracic hook claws were formed; mandibular serration appeared; and organ pigmentation was initiated. On D8 (the bluish stage), progressive head sclerotization (brown pigmentation) took place, and body pigmentation was initiated but less pronounced. On D9 (the completion stage of full development), full embryonic development was achieved along with preparation for eclosion. Compared to the control, embryos developed synchronously after the activator treatment, while those treated with the inhibitor began to show a developmental delay from day 5 (Figure 6B). This temporal disruption suggests that MPF activity below a critical threshold triggers a progressive developmental delay, ultimately leading

to complete developmental arrest in severe cases. These findings unequivocally establish MPF as both a gatekeeper and pacemaker of successful parthenogenetic development, coordinating multiple checkpoints throughout embryogenesis.

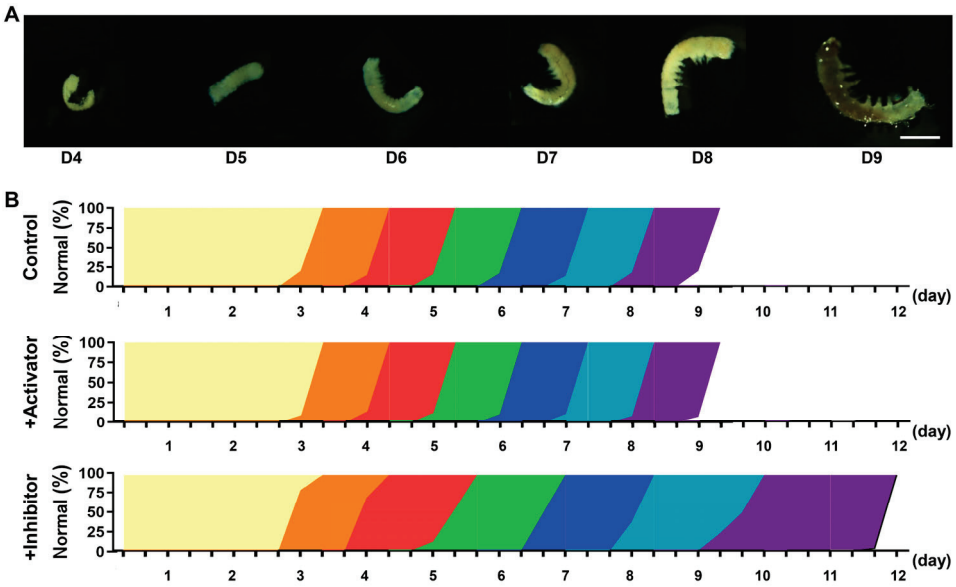


Figure 6. Embryonic development. (**A**) Embryonic morphology. The scale is 1 mm. (**B**) Developmental days. Yellow is D1~D3; orange is D4, the differentiation stage of the tail segment; red is D5, the somatic inversion stage; green is D6, the epidermis formation stage; blue is D7, the tissue formation stage; cyan is D8, the bluish stage; purple is D9, the completion stage of full development.

4. Discussion

Maturation-promoting factor (MPF) serves as a master regulator of oocyte meiosis and cell cycle progression, with its functions well characterized in vertebrate models such as *M. musculus* and *X. laevis* [11,37–39]. However, little is known about parthenogenesis in insects, especially in model lepidopteran insect *B. mori*. Catalytic subunit Cdc2 and regulatory subunit CycB cooperate to form the MPF complex [20]. Random coil regions typically exhibit high structural flexibility, which may facilitate the recognition and phosphorylation of these sites by kinases. Phosphorylation is a critical step in regulating the activity of Cdc2, enabling it to bind with CycB and form the active MPF, thereby driving cell cycle progression. This structural arrangement facilitates kinase recognition and subsequent phosphorylation events that regulate Cdc2 activity, enabling its binding with CycB to form functional MPF complexes capable of driving cell cycle progression. The conserved physicochemical properties and structural features of these subunits across species underscore their fundamental role in maintaining precise control over cellular growth, development, and reproductive processes.

After successive generations of breeding and trait accumulation, the pigmentation and hatching rates ($\geq$85% and $\geq$80%, respectively) of silkworm parthenogenesis induced by warm bath treatment has reached the production application level [40]. The mRNA expression levels of *Cdc2* and *CycB* genes were significantly different between parthenogenetic line Wu14 and corresponding amphigenetic line 54A. In particular, the mRNA expressions of *Cdc2* and *CycB* in Wu14 were significantly downregulated following warm bath induction. Although the mRNA expression levels of Cdc2 and CycB genes significantly decreased after warm bath induction in Wu14, they were higher in Wu14 compared to 54A before induction. This phenomenon may be attributed to the fact that the parthenogenetic line Wu14 has undergone continuous breeding selection for over 30 generations, resulting in

the stabilization of reproductive physiological traits. By the unfertilized egg stage, Wu14 may have already accumulated sufficient mRNA expressions of Cdc2 and CycB. This pre-accumulation allows the encoded proteins to undergo phosphorylation upon warm bath induction, enabling Cdc2 and CycB to form the active MPF. In short, the higher expression levels of Cdc2 and CycB genes in Wu14 before induction may reflect an adaptive mechanism to ensure the rapid activation of MPF after warm bath stimulation, thereby promoting cell cycle progression. The activation of MPF depends on the accumulation of CycB to a threshold level, which triggers the transition of Pre-MPF to its active form (Active-MPF), initiating the G2-to-M phase transition and meiosis [18,41]. The result suggested that MPF was closely related to silkworm parthenogenesis.

Beyond initiation, MPF plays equally critical roles in orchestrating embryonic development through the regulation of cell division and differentiation [42]. The positive correlation between MPF activity and the parthenogenesis induction success was verified by using activator and inhibitor. Furthermore, the inhibition of MPF activity resulted in delayed or even arrested embryonic development. Previous studies in vertebrates have shown that increased MPF activity ensures normal embryonic development, while reduced MPF activity leads to developmental delay [43–45]. These results strongly suggested that the MPF activity directly affected the process of silkworm parthenogenesis. The enhanced MPF activity may provide the necessary molecular drive to initiate the embryonic development program during parthenogenetic development.

In summary, our study establishes MPF activity as a critical determinant of parthenogenetic success in *B. mori*. Phylogenetic sequence analysis showed that the proteins encoded by the *Cdc2* and *CycB* genes are moderately conserved across various species. These findings not only elucidate the molecular mechanism underlying parthenogenesis induced by warm bath treatment but also enhance our understanding of insect reproductive processes. In addition, our study demonstrates that the MPF is potential molecular target for genetic-based population regulation.

Author Contributions: Conceptualization, X.X.; methodology, C.H., C.C., S.Y. and X.H.; software, C.H., C.C. and L.Z.; validation, C.M., F.X., X.D., J.C. and L.Z.; formal analysis, C.M., F.X., X.D., J.C., S.Y., X.H. and X.X.; investigation, C.H., C.C., S.Y. and X.H.; data curation, X.D., J.C. and L.Z.; writing—original draft preparation, C.M. and F.X.; writing—review and editing, W.Y., Y.W. and X.X.; visualization, W.Y.; supervision, W.Y., Y.W. and X.X.; project administration, W.Y., Y.W. and X.X.; funding acquisition, Y.W. and X.X. All authors have read and agreed to the published version of the manuscript.

Funding: This research was funded by the Technological Grant of Zhejiang for Breeding New Agricultural Varieties (2021C02072), National Natural Science Foundation of China (32100377), and Key Scientific and the China Agriculture Research System of MOF and MARA (CARS-18).

Data Availability Statement: The original contributions presented in this study are included in the article. Further inquiries can be directed to the corresponding authors.

Conflicts of Interest: The authors declare no conflicts of interest.

References

1. Mita, K.; Kasahara, M.; Sasaki, S.; Nagayasu, Y.; Yamada, T.; Kanamori, H.; Namiki, N.; Kitagawa, M.; Yamashita, H.; Yasukochi, Y.; et al. The Genome Sequence of Silkworm, *Bombyx mori*. *DNA Res.* **2004**, *11*, 27–35. [CrossRef] [PubMed]
2. Goldsmith, M.R.; Shimada, T.; Abe, H. The genetics and genomics of the silkworm, *Bombyx mori*. *Annu. Rev. Entomol.* **2005**, *50*, 71. [CrossRef] [PubMed]
3. Yang, C.-C.; Yokoi, K.; Yamamoto, K.; Jouraku, A. An update of KAIKObase, the silkworm genome database. *Database* **2021**, *2021*, baaa099. [CrossRef] [PubMed]

4. Klymenko, V.V. Parthenogenesis and cloning in the silkworm *Bombyx mori* L.: Problems and prospects. *J. Insect Biotechnol. Sericol.* **2001**, *70*, 155–165.
5. Wang, Y.; Xu, M.; He, X.; Xia, J. Studies on parthenogenesis of commercial silkworm races. *Acta Sericol. Sin.* **2001**, *27*, 20–23.
6. Liu, P.; Wang, Y.; Du, X.; Yao, L.; Li, F.; Meng, Z. Transcriptome analysis of thermal parthenogenesis of the domesticated silkworm. *PLoS ONE* **2015**, *10*, e0135215. [CrossRef]
7. Strunnikov, V.A. Research on the artificial regulation of sex in animals in the USSR. *Ontogenez* **1978**, *9*, 3–19.
8. Priyadarshini, A.; Basu, D.; Navneet, A.K.; Bhattacharya, A.; Bhattacharya, S.; Maitra, S.; Bhattacharya, S. Activation of both Mos and Cdc25 is required for G2-M transition in perch oocyte. *Mol. Reprod. Dev. Inc. Gamete Res.* **2009**, *76*, 289–300. [CrossRef]
9. Ayeni, J.O.; Varadarajan, R.; Mukherjee, O.; Stuart, D.T.; Sprenger, F.; Srayko, M.; Campbell, S.D. Dual phosphorylation of cdk1 coordinates cell proliferation with key developmental processes in *Drosophila*. *Genetics* **2014**, *196*, 197–210. [CrossRef]
10. Hanna, C.B.; Yao, S.; Patta, M.C.; Jensen, J.T.; Wu, X. WEE2 is an oocyte-specific meiosis inhibitor in rhesus macaque monkeys. *Biol. Reprod.* **2010**, *82*, 1190–1197. [CrossRef]
11. Nishimura, T.; Shimaoka, T.; Kano, K.; Naito, K. Insufficient amount of Cdc2 and continuous activation of Wee1 B are the cause of meiotic failure in porcine growing oocytes. *J. Reprod. Dev.* **2009**, *55*, 553–557. [PubMed]
12. Qiu, G.F.; Liu, P. On the role of Cdc2 kinase during meiotic maturation of oocyte in the Chinese mitten crab, *Eriocheir sinensis*. *Comp. Biochem. Physiol. Part B Biochem. Mol. Biol.* **2009**, *152*, 243–248.
13. Oqani, R.K.; Lin, T.; Lee, J.E.; Kim, S.Y.; Kang, J.W.; Jin, D.I. Effects of CDK inhibitors on the maturation, transcription, and MPF activity of porcine oocytes. *Reprod. Biol.* **2017**, *17*, 320–326. [PubMed]
14. Lim, S.; Kaldis, P. Cdks, cyclins and CKIs: Roles beyond cell cycle regulation. *Development* **2013**, *140*, 3079–3093.
15. Yamashita, M. Toward Modeling of a General Mechanism of MPF Formation during Oocyte Maturation in Vertebrates. *Zool. Sci.* **2000**, *17*, 841–851. [CrossRef]
16. Fattaey, A.; Booher, R.N. Myt1: A Wee1-type kinase that phosphorylates Cdc2 on residue Thr14. *Prog. Cell Cycle Res.* **1997**, *3*, 233–240.
17. Guadagno, T.M.; Newport, J.W. Cdk2 kinase is required for entry into mitosis as a positive regulator of Cdc2–cyclin B kinase activity. *Cell* **1996**, *84*, 73–82.
18. Kuroda, T.; Naito, K.; Sugiura, K.; Yamashita, M.; Takakura, I.; Tojo, H. Analysis of the roles of cyclin B1 and cyclin B2 in porcine oocyte maturation by inhibiting synthesis with antisense RNA injection. *Biol. Reprod.* **2004**, *70*, 154–159.
19. Liu, J.; Lu, X.; Wang, W.; Zhu, J.; Li, Y.; Luo, L.; Zhang, W. Activity of MPF and expression of its related genes in mouse MI oocytes exposed to cadmium. *Food Chem. Toxicol.* **2018**, *112*, 332–341.
20. Li, J.; Qian, W.P.; Sun, Q.Y. Cyclins regulating oocyte meiotic cell cycle progression. *Biol. Reprod.* **2019**, *101*, 878–881.
21. Jessus, C.; Ozon, R. Regulation of cell divisions during oogenesis of vertebrates: The *Xenopus* oocyte paradigm. *Comp. Biochem. Physiol. Part A Physiol.* **1993**, *106*, 431–448.
22. Kobayashi, H.; Minshull, J.; Ford, C.; Golsteyn, R.; Poon, R.; Hunt, T. On the synthesis and destruction of A- and B-type cyclins during oogenesis and meiotic maturation in *Xenopus laevis*. *J. Cell Biol.* **1991**, *114*, 755–765. [PubMed]
23. Kubelka, M.; Anger, M.; Kalous, J.; Schultz, R.M.; Motlík, J. Chromosome condensation in pig oocytes: Lack of a requirement for either cdc2 kinase or MAP kinase activity. *Mol. Reprod. Dev. Inc. Gamete Res.* **2002**, *63*, 110–118. [CrossRef] [PubMed]
24. Kanayama, N.; Miyano, T.; Lee, J. Acquisition of meiotic competence in growing pig oocytes correlates with their ability to activate Cdc2 kinase and MAP kinase. *Zygote* **2002**, *10*, 261–270. [PubMed]
25. Begum, N.; Shen, W.; Manganiello, V. Role of PDE3A in regulation of cell cycle progression in mouse vascular smooth muscle cells and oocytes: Implications in cardiovascular diseases and infertility. *Curr. Opin. Pharmacol.* **2011**, *11*, 725–729.
26. Adhikari, D.; Liu, K. The regulation of maturation promoting factor during prophase I arrest and meiotic entry in mammalian oocytes. *Mol. Cell. Endocrinol.* **2014**, *382*, 480–487.
27. Pei, Z.; Deng, K.; Xu, C.; Zhang, S. The molecular regulatory mechanisms of meiotic arrest and resumption in Oocyte development and maturation. *Reprod. Biol. Endocrinol.* **2023**, *21*, 90. [CrossRef]
28. Phillips, K.P.; Petrunewich, M.A.F.; Collins, J.L.; Booth, R.A.; Liu, X.J.; Baltz, J.M. Inhibition of MEK or cdc2 Kinase Parthenogenetically Activates Mouse Eggs and Yields the Same Phenotypes as $Mos^{-/-}$ Parthenogenotes. *Dev. Biol.* **2002**, *247*, 210–223. [CrossRef]
29. Biasini, M.; Bienert, S.; Waterhouse, A.; Arnold, K.; Studer, G.; Schmidt, T.; Kiefer, F.; Gallo Cassarino, T.; Bertoni, M.; Bordoli, L.; et al. SWISS-MODEL: Modelling protein tertiary and quaternary structure using evolutionary information. *Nucleic Acids Res.* **2014**, *42*, 252–258.
30. Wirawan, I.G.P.; Dewi, N.K.E.S.; Sasadara, M.M.V.; Sunyamurthi, I.G.N.A.; Jawi, I.M.; Wijaya, I.N.; Darmawati, I.A.P.; Suada, I.K.; Krisnandika, A.A.K. Phytochemical Analysis and Molecular Identification of Green Macroalgae *Caulerpa* spp. from Bali, Indonesia. *Molecules* **2022**, *27*, 4879. [CrossRef]

31. Mitsumasu, K.; Azuma, M.; Niimi, T.; Yamashita, O.; Yaginuma, T. Changes in the Expression of Soluble and Integral-Membrane Trehalases in the Midgut During Metamorphosis in *Bombyx mori*. *Zool. Sci.* **2008**, *25*, 693–698.
32. Jang, W.I.; Lin, Z.L.; Lee, S.H.; Namgoong, S.; Kim, N.H. A specific inhibitor of CDK1, RO-3306, reversibly arrests meiosis during in vitro maturation of porcine oocytes. *Anim. Reprod. Sci.* **2014**, *144*, 102–108. [PubMed]
33. Ichikawa, D.; Nakamura, M.; Murota, W.; Osawa, S.; Matsushita, M.; Yanagawa, H.; Hattori, Y. A phenylphthalimide derivative, TC11, induces apoptosis by degrading MCL1 in multiple myeloma cells. *Biochem. Biophys. Res. Commun.* **2020**, *521*, 252–258. [PubMed]
34. Anguita, B.; Jimenez-Macedo, A.R.; Izquierdo, D.; Mogas, T.; Paramio, M.T. Effect of oocyte diameter on meiotic competence, embryo development, p34 (cdc2) expression and MPF activity in prepubertal goat oocytes. *Theriogenology* **2007**, *67*, 526–536.
35. Nagahama, Y.; Yamashita, M. Regulation of oocyte maturation in fish. *Dev. Growth Differ.* **2008**, *50*, 195–219.
36. Zhang, D.X.; Park, W.J.; Sun, S.C.; Xu, Y.N.; Li, Y.H.; Cui, X.S.; Kim, N.H. Regulation of maternal gene expression by MEK/MAPK and MPF signaling in porcine oocytes during in vitro meiotic maturation. *J. Reprod. Dev.* **2011**, *57*, 49–56. [CrossRef]
37. Chesnel, F.; Bazile, F.; Pascal, A.; Kubiak, J.Z. Cyclin B dissociation from CDK1 precedes its degradation upon MPF inactivation in mitotic extracts of *Xenopus laevis* embryos. *Cell Cycle* **2006**, *5*, 1687–1698.
38. Grallert, A.; Patel, A.; Tallada, V.A.; Chan, K.Y.; Bagley, S.; Krapp, A.; Simanis, V.; Hagan, I.M. Centrosomal MPF triggers the mitotic and morphogenetic switches of fission yeast. *Nat. Cell Biol.* **2013**, *15*, 88–95.
39. Cheng, M.; Chen, X.; Han, M.; Luo, X.; Yu, Y.; Lv, Y.; Han, Y.; Cao, L.; Zhang, J.; Wang, M.; et al. miR-155-5p improves oocyte maturation in porcine cumulus cells through connexin 43-mediated regulation of MPF activity. *Theriogenology* **2024**, *214*, 124–133.
40. Liu, P.; Wang, Y.; Du, X.; Shi, F.; Meng, Z. A comparative proteomic analysis of parthenogenetic lines and amphigenetic lines of silkworm. *Biotechnol. Bioprocess Eng.* **2014**, *19*, 641–649.
41. Dutertre, S.; Cazales, M.; Quaranta, M.; Froment, C.; Trabut, V.; Dozier, C.; Mirey, G.; Bouché, J.P.; Theis-Febvre, N.; Schmitt, E.; et al. Phosphorylation of CDC25B by Aurora-A at the centrosome contributes to the G2–M transition. *J. Cell Sci.* **2004**, *117*, 2523–2531. [PubMed]
42. Yu, B.; Wang, Y.; Liu, Y.; Liu, Y.; Li, X.; Wu, D.; Zong, Z.; Zhang, J.; Yu, D. Protein kinase A regulates cell cycle progression of mouse fertilized eggs by means of MPF. *Dev. Dyn.* **2005**, *232*, 98–105. [PubMed]
43. Newport, J.W.; Kirschner, M.W. Regulation of the cell cycle during early *Xenopus* development. *Cell* **1984**, *37*, 731–742. [PubMed]
44. Hashimoto, N.; Kishimoto, T. Cell cycle dynamics of maturation-promoting factor during mouse oocyte maturation. *Tokai J. Exp. Clin. Med.* **1986**, *11*, 471–477.
45. Baek, J.I.; Seol, D.W.; Lee, A.R.; Lee, W.S.; Yoon, S.Y.; Lee, D.R. Maintained MPF Level After Oocyte Vitrification Improves Embryonic Development After IVF, but not After Somatic Cell Nuclear Transfer. *Mol. Cells* **2017**, *40*, 871–879.

Disclaimer/Publisher's Note: The statements, opinions and data contained in all publications are solely those of the individual author(s) and contributor(s) and not of MDPI and/or the editor(s). MDPI and/or the editor(s) disclaim responsibility for any injury to people or property resulting from any ideas, methods, instructions or products referred to in the content.

insects

MDPI

Article

Physiological and Biochemical Mechanisms of *Aoria nigripes* (Coleoptera, Chrysomelidae) Adaption to Flavonoid-Rich Plant *Nekemias grossedentata*

Zhengwen Yu *,†, Chenju Yang †, Lian Xie, Feng Yang and Yuyu Yuan

School of Life Sciences, Guizhou Normal University, Guiyang 550025, China
* Correspondence: gznusky1519@126.com
† These authors contributed equally to this work.

Simple Summary: In recent years, *Aoria nigripes* has inflicted significant damage on *Nekemias grossedentata*. However, the mechanism through which *A. nigripes* overcomes its host's high flavonoid content to survive is still unclear, making it difficult to effectively prevent and control it. The present study is the first to investigate the effects of host plants with different flavonoid levels on the activities of three protective enzymes (SOD, POD, and CAT) and four detoxifying enzymes (CarE, AchE, GST, and CYP450) in *A. nigripes*, which provides important guidance for the further investigation of its adaptive mechanism and the development of pest control strategies. Overall, our findings indicate that the detoxifying enzymes GST and AchE and the protective enzyme POD play a major role in the response of *A. nigripes* to *N. grossedentata*, the "king of plant flavonoids". Meanwhile, dihydromyricetin is an important flavonoid sed in *N. grossedentata* against insect injury stress. Additionally, the major flavonoids of *N. grossedentata* are enriched during digestion and metabolism in insects.

Abstract: This study aimed to explore the physiological and biochemical mechanisms of the interaction between *N. grossedentata* and *A. nigripes*. First, specimens were categorized into low- (6.16% ± 0.66%), medium- (9.23% ± 1.19%), and high-content groups (21.23% ± 1.23%) based on the initial dihydromyricetin concentration in *N. grossedentata*. Subsequently, we assessed the variations in total flavonoids, dihydromyricetin, myricitrin, and myricetin in plants 24, 48, and 72 h post-feeding. Concurrently, we analyzed the impact of plant leaf consumption on the detoxifying [glutathione S-transferase (GST), carboxylesterase (CarE), acetylcholinesterase (AchE), and cytochrome P450 (CYP450)] and protective enzyme [superoxide dismutase (SOD), peroxidase (POD) and catalase (CAT)] activities in *A. nigripes*, along with its metabolic processes. The results demonstrated that *N. grossedentata* enhanced its secondary metabolites, particularly dihydromyricetin, as a defensive response to insect-induced stress. *A. nigripes* utilized its detoxification and protective enzyme systems to mitigate the effects of high flavonoid levels in the host plant, with particular emphasis on the roles of detoxification enzymes (GST, AchE, CYP450, and CarE) in detoxification metabolism, which showed significant correlation ($p < 0.01$) with dihydromyricetin, exhibiting correlation coefficients of 0.689, 0.633, 0.579, and 0.561, respectively. Additionally, key flavonoids in *N. grossedentata* were observed to accumulate with different degrees during digestion and metabolism in insects. These findings lay a theoretical foundation for the further exploration of the molecular mechanisms of *A. nigripes* adaptation to a flavonoid-rich plant *N. grossedentata* and inform the development of novel pest control strategies and the selection of resistant plant varieties.

Keywords: *Aoria nigripes*; *Nekemias grossedentata*; secondary metabolites; detoxifying enzymes; protective enzymes

1. Introduction

Secondary plant metabolites exert deleterious effects on insect feeding behavior, growth, development, as well as reproduction and can be toxic to insects, thereby serving as a defense mechanism against insect herbivory [1]. Flavonoids, the category of the largest group of secondary plant products, are pivotal in plant defenses against pests [2,3]. Their concentration in fresh leaves is significantly enhanced when insects feed on Lingtou Danzong tea [4]. Furthermore, the content of these secondary metabolites can vary across different strains of the same plant [5–8], leading to differences in effects on insects [1]. In response to the detrimental impacts of secondary plant substances, insects adapt to their host plants via various strategies including avoidance of feeding on secondary plant substances and the induction of detoxification metabolism [1]. This involves the secretion of protective enzymes and detoxification enzymes, which is considered a critical adaptive response of insects to plants [9].

Superoxide dismutase (SOD), peroxidase (POD), and catalase (CAT) are essential protective enzymes in insects [10], while glutathione S-transferase (GST), carboxylesterase (CarE), acetylcholinesterase (AchE), and cytochrome P450 (CYP450) are the primary detoxification enzymes [9,11,12]. These enzymes play a significant role in the metabolic adaptation to secondary substances [13,14]. Upon entry into the insect body, secondary substances can stimulate the upregulation of metabolic enzyme gene expression and the production of protective enzymes to neutralize the free radicals produced by harmful substances, thereby safeguarding crucial tissues and organs [13,14]. Concurrently, the elevated activities of detoxification enzymes expedite the detoxification and metabolic processes of secondary substances, facilitating their degradation, utilization, or excretion from the body, thus mitigating or preventing the toxic effects of secondary substances [13,14]. Detoxification and protective enzyme activities in insects are contingent upon the type of host plant [9,15–20], and these activities differ among insects when they feed on various varieties of the same host plant species [9,21]. Investigating the effects of host plants on the activities of protective and detoxifying enzymes in insects can thus provide insights into the adaptive mechanisms of phytophagous insects to their hosts.

Aoria nigripes (Baly, 1860) is a species of Coleoptera, Chrysomelidae, and is widely distributed across China, Vietnam, Laos, Cambodia, Myanmar, Thailand, India, Indonesia, and other regions [22–25]. It is known to cause severe damage to Vitaceae plants, particularly grapes, wild grapes, *Parthenocissus himalayana*, and crystal grapes [23,24,26]. Adults primarily feed on the leaves, petioles, and shoots, as well as the adaxial leaf flesh of leaves and the epidermis of the branches and petioles, creating transparent feeding strips on the leaf blades [26,27]. This feeding weakens the plants and, in severe instances, can lead to plant death, resulting in significant economic losses (Figure 1). Studies on the occurrence and control of *A. nigripes* are limited, although recent research has focused on its biological characteristics and control methods [26–29]. However, no research has been conducted on the protective and detoxifying enzyme activities of this insect.

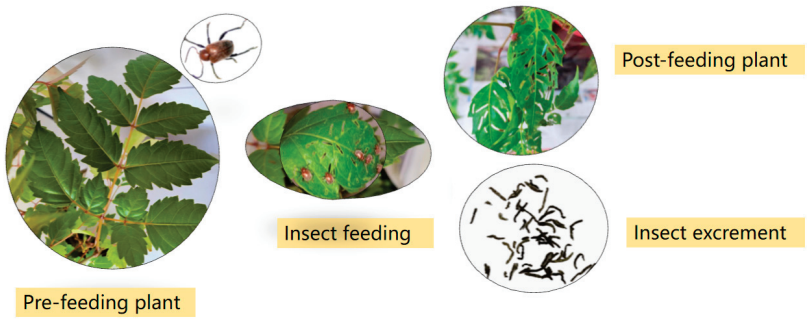


Figure 1. *Aoria nigripes* fetching *N. grossedentata*.

Nekemias grossedentata (Hand.-Mazz.) J. Wen & Z. L. Nie is a perennial woody vine plant in the family Vitaceae, recognized for its high flavonoid content, up to 45% in the dried leaves [30], and is esteemed as the "king of plant flavonoids" [29,31,32]. Its primary medicinal components include dihydromyricetin, myricitrin, and myricetin [33]. To date, research on the insect pests of *N. grossedentata* has been scarce. Our research team has documented damage to *N. grossedentata* caused by *A. nigripes* [29] and determined the complete mitochondrial genome of *A. nigripes* [28]. Adults damage the leaves, creating transparent feeding strips, while larvae target the roots and stems, leading to leaf yellowing or plant death, affecting its quality and yield [29]. As a medicine food homology plant, it holds significant economic value due to its antibacterial, antioxidant, antiviral, and anticancer properties [29,30,34]. The young leaves are primarily processed into products, and feeding by *A. nigripes* results in economic losses. However, on *N. grossedentata*, a plant renowned for its flavonoid content, *A. nigripes* can survive and reproduce without issue. This suggests that the insect has evolved a unique set of mechanisms for detoxifying flavonoids. Consequently, the present study is the first t examined the effects of *N. grossedentata* with varying flavonoid levels (high, middle, and low) on the activities of three protective enzymes (SOD, POD, and CAT) and four detoxifying enzymes (CarE, AchE, GST, and CYP450) in *A. nigripes*, along with changes in their principal flavonoids within the insect. This study also investigated the dynamic changes I the flavonoids in the leaves of the host plant before and after damage by *A. nigripes*. Based on correlation analysis, the physiological and biochemical mechanisms of the interaction between *N. grossedentata* and *A. nigripes* were elucidated. This research serves as a crucial foundation for further investigation into the molecular mechanisms of this insect and the developing novel prevention and control strategies.

2. Materials and Methods

2.1. Insects

The adults of *A. nigripes* were collected Pingba District, Anshun City, Guizhou Province, China (106°45′ E, 26°37′ N, 1244 m above sea level), and reared with crystal grape leaves in the laboratory at a temperature of 25 ± 1 °C, relative humidity of 65 ± 5%, and photoperiod of 14:10 h (L:D). *A. nigripes* adults of uniform size that were healthy and parasite-free were selected and starved for 3 h. At least 150 adults were placed in each cage, and three replicates were set up during the experiment, *N. grossedentata* cultivars with pots were placed in cages, and the leaves did not separate from the plant and the insects fed autonomously. Active *A. nigripes* adults were randomly collected from each group at 24 h, 48 h until 72 h; the elytra were removed, quick-frozen in liquid nitrogen, and then stored at −80 °C for use (the 0 h insect samples were collected after 3 h of starvation).

2.2. Host Plants

N. grossedentata were planted in large quantities in December 2022 at the germplasm resource nursery of Guizhou Normal University (106°63′ E, 26°38′ N) to ensure that the *N. grossedentata* from the cultivars were sufficient and had the same genetic background; they were watered regularly to strive for consistent growth conditions. Based on the content of dihydromyricetin, the most representative compound in *N. grossedentata*, the test plants were grouped as follows: low-content group (6.16% ± 0.66%), medium-content group (9.23% ± 1.19%), and high-content group (21.23% ± 1.23%), with the content approximately doubling in order from low to high. The leaves were collected 0, 24, 48 and 72 h after *A. nigripes* feeding, and the main leaf veins were removed and dried at a constant temperature of 60 °C until constant weight. The dried leaves were ground into powder and used to determine the contents of secondary metabolites.

2.3. Determination of Secondary Metabolite Contents of N. grossedentata

The total flavonoid contents in the leaves were determined by UV spectrophotometry [30], the standard solution was prepared with dihydromyricetin, and the optical density (OD) value was measured at the maximum absorption wavelength to obtain the standard curve. The HPLC method [30] was used to determine the contents of dihydromyricetin, myricitrin, and myricetin. HPLC analyses were carried out with an SHIMADZU LC-20ADXR series system (Shimadzu USA Manufacturing, Inc., Columbia, MD, USA) consisting of two LC-20AD pumps, an SPD-M20A diode array detector, and a SIL-20AC auto sampler. A CAPCELL PAK C18 column (4.6 × 250 mm, 5 μm) was adopted for the analyses. The mobile phase consisted of A (methanol) and B (0.1% phosphoric acid solution). The gradient mode was as follows: 0~20 min, 72% B; 20~21 min, 72~60% B; 21~30 min, 60% B; 30~31 min, 60~58% B; 31~45 min, 58% B; 45~46 min, 58~50% B; 46~50 min, 50% B; 50~51 min, 50~72% B; 51~60 min, 72% B. The flow rate was 1.0 mL/min. The detection wavelength was set at 292 (dihydromyricetin), 254 (myricitrin), and 375 (myricetin) nm. The column temperature was set at 40 °C, and injection volume was set at 10 μL.

2.4. Determination of Flavonoid Compounds in Insect Excreta

A10.00 mg sample was taken, weighed accurately, and put into a 10.0 mL stoppered tube; 5.0 mL of methanol was added; the tube was closed and sonicated for 40 min to obtain the sample solution, which was passed through 0.45 μm microporous filtration membrane; the filtrate was taken for HPLC analysis.

2.5. Measurement of Protective and Detoxifying Enzyme Activities in A. nigripes Adults

The treated adults were randomly sampled at 24, 48 and 72 h after *A. nigripes* feeding, and the number of samples in each experimental group at each time point was 50 individuals. For each enzyme activity assay, 6 adults were taken from each treatment, and 1.0 mL of the corresponding kit extract was added to the homogenate (*A. nigripes* with removed the elytra) in an ice bath. The homogenate was centrifuged for 10 min (12,000 r/min, 4 °C), GST for 15 min, and insect CYP450 at 8000 r/min; the supernatant was placed on ice for the assay.

CAT Assay Kit (product No.: RXWB0478-96), POD Assay Kit (product No.: RXWB0111-96), SOD Assay Kit (product No.: RXWB0482-96), GST Assay Kit (product No.: RXWB0099-96), CarE Assay Kit (product No: RXWB0181-96), AchE Detection Kit (product No.: RXWB0254-96) and Insect CYP450 ELISA Kit (product No.: RX1800390I) were purchased from Quanzhou Ruixin Biological Technology Co. Ltd., Quanzhou, China. The activity of each enzyme was determined according to the manufacturer's instructions.

2.6. Statistical Analysis

The data were analyzed using Excel 2010 and SPSS 25.0 (IBM Corp., Armonk, NY, USA) software. Host secondary metabolite and enzyme activity data were analyzed using one-way analysis of variance (ANOVA), in which differences between means were compared at the $p < 0.05$ significance level using the Waller–Duncan multiple comparison test. Correlation between data were analyzed using Pearson linear correlation analysis. Correlation analyses between the data were carried out using Pearson's linear correlation analysis to correlate the content of each compound at 0, 24, and 48 h of feeding on plants with the values of insect enzyme activities at 24, 48, and 72 h. The correlation analysis were performed using Pearson's linear correlation method. Finally, GraphPad Prism 8.0.2 (GraphPad Software Inc., San Diego, CA, USA) software was used for graphing.

3. Results

3.1. Secondary Metabolites Contents in Host Plant

Feeding *A. nigripes* on *N. grossedentata* exerted a deleterious effect on the plant's growth, resulting in significant weakening. Subsequent analysis revealed variability in the secondary metabolite profiles within the *N. grossedentata* leaves from diverse strains that were characterized by distinct flavonoid levels. Notably, the primary flavonoids in *N. grossedentata* were dihydromyricetin, myricitrin, and myricetin, with elution times of 9.304 min, 28.866 min, and 35.561 min, respectively (Figure 2A,B). Among these, dihydromyricetin (Figure 2C) demonstrated statistically significant differences ($p < 0.05$) in concentration across the three strain types prior to feeding. The high-level strain (21.23% ± 1.23%) exhibited a content that was significantly greater ($p < 0.05$) than that of the low-level (6.16% ± 0.66%) and middle-level (9.23% ± 1.19%) strains, representing a 3.45-fold increase ($p < 0.05$) over the low-level strain. Myricitrin (Figure 2D) showed a significant increase ($p < 0.05$) in low-level leaves (1.50% ± 0.16%) compared to the middle-level (0.53% ± 0.12%) and high-level (0.58% ± 0.06%) strains before feeding. In contrast, myricetin (Figure 2E) exhibited no significant differences ($p > 0.05$) in content among the high-, middle-, and low-level strains before feeding, at 0.05% ± 0.01%, 0.04% ± 0.00%, and 0.04% ± 0.01%, respectively. The total flavonoid content (Figure 2F) was significantly elevated ($p < 0.05$) in the high-level strain (23.62% ± 0.59%) relative to the low-level (11.24% ± 4.89%) and middle-level (14.14% ± 0.66%) strains before feeding, representing a 2.10-fold increase over the low-level strain.

After 24, 48, and 72 h of feeding on *A. nigripes*, the changes in the contents of the primary and secondary metabolites in the host were different. Dihydromyricetin levels were found to rise with increasing feeding duration across all three strain types; compared to the baseline at 0 h, it reached maximum value at 24 h in the low-level and middle-level strains, while significant increases were observed at 48 h in the high-level strain ($p < 0.05$). The content of myricitrin exhibited fluctuations with feeding time, with the low-level strain demonstrating a continuous rise, reaching significance at 72 h ($p < 0.05$). the middle-level and high-level strains showed a pattern of increasing followed by decreasing, with no significant differences observed ($p > 0.05$). The myricetin content decreased uniformly across all strains after feeding, with the differences being non-significant ($p > 0.05$). Similarly, the total flavonoid content exhibited varying trends with the duration of feeding, with the low-level and middle-level strains showing an increase post-feeding, with the low-level strain exhibiting a significant increase at 24 h ($p < 0.05$). The high-level strain exhibited a decrease followed by an increase, with no significant differences observed ($p > 0.05$).

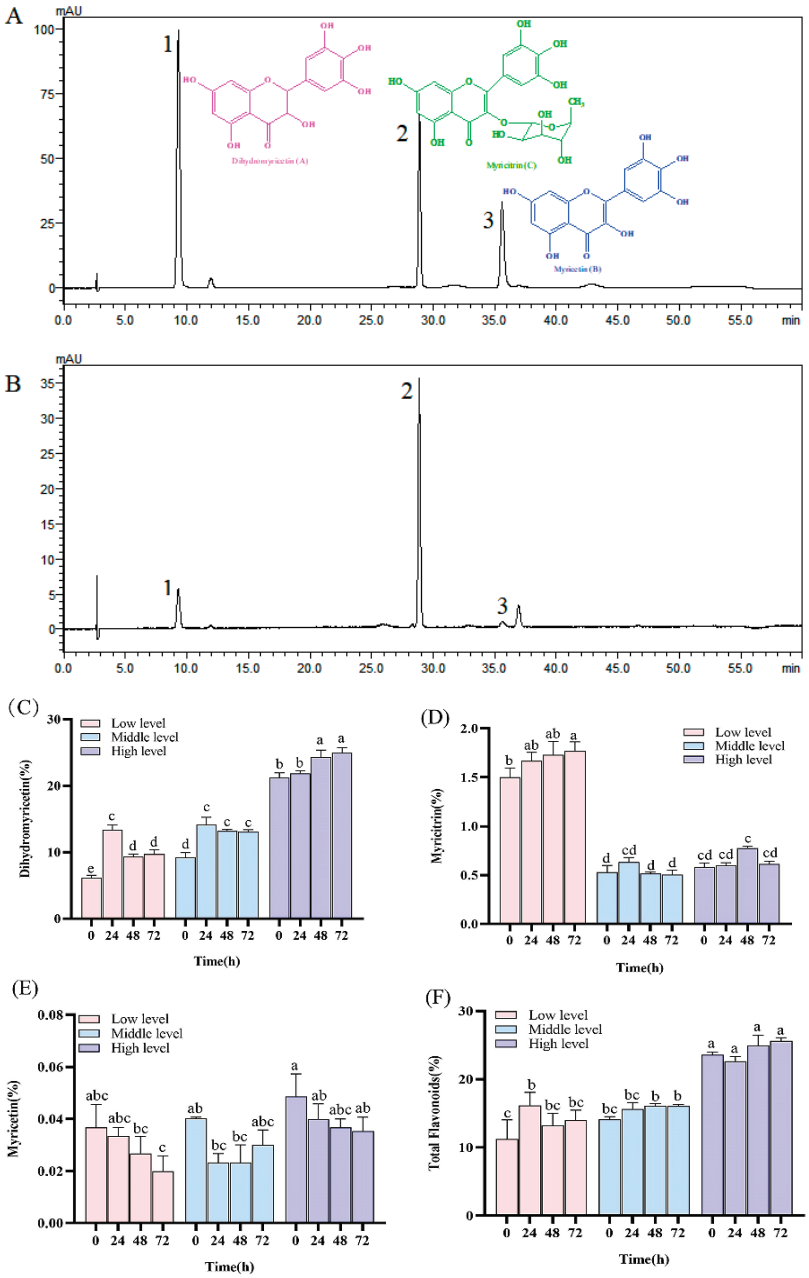


Figure 2. Changes in the content of major flavonoids and total flavonoids in *N. grossedentata*. (**A**) The mixed control, and (**B**) the test sample, where 1 is dihydromyricetin, 2 is myricitrin, 3 is myricetin. The dihydromyricetin content in *N. grossedentata* before insect feeding was used as the basis for grouping, and the content in the test plants was low (6.16% ± 0.66%), medium (9.23% ± 1.19%) and high (21.23% ± 1.23%). Note: The data in the figures are presented as mean ± SE, and different lowercase letters in (**C**–**F**) indicate a significant difference ($p < 0.05$).

3.2. Three Protective and Four Detoxifying Enzyme Activities

Under the influence of high levels of flavonoids in the host, *A. nigripes* exhibited varying degrees of induction in the activities of four detoxifying enzymes (CYP450, CarE, GST, and AchE) and three protective enzymes (CAT, POD, and SOD) (Table 1). The mean values of enzyme activities at 24, 48 and 72 h were compared with the pre-feeding enzyme activities; under low-content stress, the sequence of induction in the detoxification enzyme activities was GST (1.66-fold) > CarE (1.26-fold) > AchE (1.14-fold) > CYP450 (0.98-fold); for protective enzyme activities, the sequence was POD (2.31-fold) > CAT (1.24-fold) > SOD

(1.12-fold). In the context of medium -content stress, the detoxification enzyme activity sequence was AchE (1.80-fold) > CarE (1.61-fold) > GST (1.53-fold) > CYP450 (1.15-fold); for protective enzyme activities, the order of increase was POD (3.09-fold) > CAT (1.49-fold) > SOD (1.08-fold). Under high -content stress, the detoxification enzyme activity sequence was AchE (2.06-fold) ≈ GST (2.06-fold) > CarE (1.93-fold) > CYP450 (1.19-fold); and, for protective enzyme activities, the order was POD (2.88-fold) > CAT (1.36-fold) > SOD (1.10-fold).

Table 1. Effect of *N. grossedentata* with different flavonoids level on the enzymatic activity of *A. nigripes*.

Enzyme	t/h	Host Plant		
		Low Level	Middle Level	High Level
Acetylcholinesterase (U/g), AchE	0	89.76 ± 3.29 ^{e}	89.76 ± 3.29 ^{e}	89.76 ± 3.29 ^{e}
	24	135.98 ± 2.53 ^{d}	160.55 ± 3.32 ^{c}	176.06 ± 3.38 ^{b}
	48	102.17 ± 4.97 ^{e}	182.32 ± 22.22 ^{b}	178.81 ± 2.21 ^{b}
	72	67.96 ± 1.38 ^{f}	141.73 ± 1.56 ^{d}	200.28 ± 1.83 ^{a}
Carboxylesterase (U/g), CarE	0	27.46 ± 1.89 ^{gh}	27.46 ± 1.89 ^{gh}	27.46 ± 1.89 ^{gh}
	24	33.21 ± 2.28 ^{fg}	55.20 ± 4.58 ^{b}	40.83 ± 2.15 ^{de}
	48	49.56 ± 4.14 ^{bc}	39.42 ± 2.80 ^{ef}	47.16 ± 3.38 ^{cd}
	72	20.80 ± 3.36 ^{h}	38.06 ± 6.31 ^{ef}	71.22 ± 4.33 ^{a}
Glutathione S-transferase (U/g), GST	0	722.69 ± 79.50 ^{f}	722.69 ± 79.50 ^{f}	722.69 ± 79.50 ^{f}
	24	1238.20 ± 3.51 ^{cd}	1119.04 ± 3.91 ^{cde}	1475.75 ± 48.71 ^{ab}
	48	1313.40 ± 132.93 ^{bc}	1013.06 ± 92.68 ^{e}	1307.39 ± 146.88 ^{bc}
	72	1043.91 ± 101.74 ^{de}	1183.89 ± 176.17 ^{cde}	1676.28 ± 141.90 ^{a}
Cytochrome P450 (ng/g), CYP450	0	14.95 ± 0.88 ^{d}	14.95 ± 0.88 ^{d}	14.95 ± 0.88 ^{d}
	24	12.47 ± 0.45 ^{e}	16.96 ± 0.81 ^{b}	15.46 ± 0.54 ^{cd}
	48	15.05 ± 0.56 ^{cd}	15.70 ± 1.04 ^{bcd}	18.55 ± 0.21 ^{a}
	72	16.45 ± 1.04 ^{bc}	19.04 ± 0.13 ^{a}	19.38 ± 0.61 ^{a}
Peroxidase (U/g), POD	0	53.92 ± 8.61 ^{g}	53.92 ± 8.61 ^{g}	53.92 ± 8.61 ^{g}
	24	117.47 ± 5.81 ^{f}	182.14 ± 4.34 ^{ab}	173.79 ± 0.46 ^{b}
	48	109.05 ± 9.05 ^{f}	194.12 ± 16.19 ^{a}	137.65 ± 7.48 ^{de}
	72	147.55 ± 6.48 ^{cd}	122.94 ± 2.00 ^{ef}	155.00 ± 6.67 ^{c}
Superoxide Dismutase (U/g), SOD	0	163.03 ± 15.41 ^{c}	163.03 ± 15.41 ^{c}	163.03 ± 15.41 ^{c}
	24	187.58 ± 7.45 ^{ab}	172.05 ± 7.69 ^{bc}	188.42 ± 5.41 ^{ab}
	48	189.68 ± 4.44 ^{ab}	199.36 ± 13.99 ^{a}	162.31 ± 2.72 ^{c}
	72	170.28 ± 12.73 ^{bc}	154.80 ± 18.20 ^{c}	187.44 ± 6.39 ^{ab}
Catalase (U/g), CAT	0	253.18 ± 15.37 ^{c}	253.18 ± 15.37 ^{c}	253.18 ± 15.37 ^{c}
	24	349.05 ± 15.7 ^{b}	404.33 ± 18.86 ^{a}	418.49 ± 17.96 ^{a}
	48	274.96 ± 18.55 ^{c}	396.13 ± 15.45 ^{a}	327.70 ± 0.92 ^{b}
	72	318.82 ± 8.49 ^{b}	331.52 ± 25.78 ^{b}	284.07 ± 3.37 ^{c}

Note: Data in the table are mean ± SD, different lowercase letters indicate significant differences ($p < 0.05$), seven enzyme activities were analyzed separately for differences (data included enzyme activities at 0, 24, 48, and 72 h under the influence of three flavonoid levels of *N. grossedentata*), and enzyme activity at 0 h was pre-feeding.

3.2.1. Superoxide Dismutase Activity

Superoxide dismutase (SOD) activity exhibited variations after *A. nigripes* feeding on three *N. grossedentata* strains with distinct flavonoid levels (Table 1). At 48 h post-feeding, the enzyme activity in the insects sourced from the high-level strain (162.31 ± 2.72 U/g) group was significantly reduced ($p < 0.05$) compared to the low-level (189.68 ± 4.44 U/g) and middle-level (199.36 ± 13.99 U/g) strains. At 72 h, the activity (187.44 ± 6.39 U/g) was significantly elevated ($p < 0.05$) relative to the middle-level strain (154.80 ± 18.20 U/g). The SOD activity in the insects displayed variable changes with extended feeding duration. For the high-level strain, the enzyme activity decreased and then increased, with the 48 h activity differing significantly from both the 24 h and 72 h activities ($p < 0.05$). In the low-level strain, the activity increased and then decreased, and there was no significant

difference among the 24 h, 48 h, and 72 h activities ($p > 0.05$). For the middle-level strain, the activity also increased and then decreased, with the 48 h activity differing significantly from the 24 h and 72 h activities ($p < 0.05$).

3.2.2. Peroxidase Activity

The peroxidase (POD) activity exhibited marked variability following feeding on *N. grossedentata* from three plant strains characterized by distinct flavonoid levels (Table 1). After 24 h of Feeding, insects from the high-level strain group demonstrated a significantly higher POD activity (173.79 ± 0.46 U/g) compared to those from the low-level strain (117.47 ± 5.81 U/g) ($p < 0.05$). At 48 h, the POD activity in *A. nigripes* in the high-level strain (137.65 ± 7.48 U/g) group was also significantly greater than that in the low-level strain (109.05 ± 9.05 U/g) group, which was notably lower than the POD activity in insects from the middle-level strain (194.12 ± 16.19 U/g) ($p < 0.05$). By 72 h, the POD activity in the high-level strain (155.00 ± 6.67 U/g) was found to be significantly higher than in the middle-level strain (122.94 ± 2.00 U/g) ($p < 0.05$). As feeding duration was prolonged, POD activity in the high-level strain decreased and then increased, with significant differences noted between 24 h, 48 h, and 72 h ($p < 0.05$). The low-level strain activity decreased and then increased, with a significant difference between 72 h and both 24 h and 48 h ($p < 0.05$). The middle-level strain activity increased and then decreased, with a significant difference between 72 h and both 24 h and 48 h ($p < 0.05$).

3.2.3. CAT Activity

The catalase (CAT) activity in *A. nigripes* was altered after consuming *N. grossedentata* from three strains with differing flavonoid levels (Table 1). The enzyme activity for the high-level strain was significantly higher ($p < 0.05$) than that of the low-level strain for 24 h and 48 h. The 48-h activity was significantly higher ($p < 0.05$) than that of the low level and middle level strains, which was also significantly lower ($p < 0.05$) than that of the middle level strain. At 72 h, the activity (284.07 ± 3.37 U/g) was significantly lower ($p < 0.05$) than that of the middle-level (331.52 ± 25.78 U/g) and low-level (318.82 ± 8.49 U/g) strains. CAT activities varied with feeding time, with the high-level strain activity continuing to decrease, with significant differences between 24 h, 48 h, and 72 h ($p < 0.05$). The low-level strain activity first decreased and then increased, with significant differences between 48 h and 24 h and 72 h ($p < 0.05$). The middle-level strain activity continued to decrease, with significant differences between 72 h and 24 h and 48 h ($p < 0.05$).

3.2.4. CarE Activity

The Carboxylesterase (CarE) activity in *A. nigripes* was distinct after feeding on *N. grossedentata* from three strains with different flavonoid levels (Table 1). The enzyme activity for the high-level strain at 72 h (71.22 ± 4.33 U/g) was significantly higher ($p < 0.05$) than that of the low-level (20.80 ± 3.36 U/g) and middle-level (38.06 ± 6.31 U/g) strains. The CarE activity of the insects exhibited varying changes with feeding time. The high-level strain activity continued to rise, with significant differences between 72 h and 24 h and 48 h ($p < 0.05$). The low-level strain activity rose and then declined, with significant differences between 24 h, 48 h, and 72 h ($p < 0.05$). The middle-level strain activity continued to fall, with significant differences between 24 h and 48 h and 72 h ($p < 0.05$).

3.2.5. AchE Activity

The acetylcholinesterase (AchE) activity in *A. nigripes* varied following feeding on *N. grossedentata* from three strains with distinct flavonoid levels (Table 1). The enzyme

activities at 24 h, 48 h and 72 h for the high-level strain were significantly higher than those of the low-level strain, which were also significantly higher ($p < 0.05$) than those of the middle-level strain at 72 h. The AchE activity of the insects changed with the duration of feeding. The high-level strain activity continued to increase, with significant differences between 72 h and 24 h and 48 h ($p < 0.05$). The low-level strain activity continued to decrease, with significant differences between 24 h, 48 h, and 72 h ($p < 0.05$). The middle-level strain activity first increased and then decreased, with significant differences between 24 h, 48 h and 72 h ($p < 0.05$).

3.2.6. GST Activity

Glutathione S-transferase (GST) activity in *A. nigripes* displayed variability after feeding on three *N. grossedentata* strains with varying flavonoid levels (Table 1). The 24 h and 72 h enzyme activities for the high-level strain were significantly higher than those for the low-level and middle-level strains, and the high-level strain activity was also significantly higher ($p < 0.05$) than that of the middle-level strain at 48 h. The GST activity varied with feeding time, with the high -level strain activity decreasing and then increasing, with significant differences between 72 h and 48 h ($p < 0.05$). The low-level strain activity increased and then decreased, with significant differences between 72 h and 48 h ($p < 0.05$). The middle-level strain activity decreased and then increased.

3.2.7. CYP450 Activity

Cytochrome P450 (CYP450) enzyme activity in *A. nigripes* was different after feeding on *N. grossedentata* from three strains with distinct flavonoid levels (Table 1). The enzyme activity for the high-level strain was significantly higher ($p < 0.05$) than that of the low-level and middle-level strains at 24 h, 48 h, and 72 h. The activity was significantly higher ($p < 0.05$) at 48 h than that of the middle-level strain, but significantly lower ($p < 0.05$) at 24 h than that of the middle-level strain. The CYP450 activity of the insects changed with feeding time, with the high-level strain activity continuing to increase, with significant differences between 48 h, 72 h, and 24 h ($p < 0.05$). The low-level strain activity continued to increase, with significant differences between 24 h, 48 h and 72 h ($p < 0.05$). The middle-level strain activity first decreased and then increased, with significant differences between 24 h, 48 h and 72 h ($p < 0.05$).

3.3. Relationship Between A. nigripes Enzyme Activity and Secondary Metabolite Content in Host Plant Leaves

Pearson's linear correlation coefficient analysis (Table 2) revealed highly significant positive correlations between the activities of acetylcholinesterase (AchE), carboxylesterase (CarE), glutathione S-transferase (GST), and cytochrome P450 (CYP450) enzymes, as well as the contents of total flavonoids and dihydromyricetin. Conversely, these enzymes and activities exhibited a negative correlation with myricitrin content, with particularly strong negative correlations observed between AchE and CYP450 with myricitrin, and a significant negative correlation between CarE and myricitrin. AchE, CarE, and GST activities also correlated positively with myricetin content, whereas CYP450 activity was negatively correlated with myricetin. Peroxidase (POD) activity positively correlated with total flavonoids, dihydromyricetin, and myricetin content, and negatively and highly significantly correlated with myricitrin content. Superoxide Dismutase (SOD) activity positively correlated with total flavonoids, dihydromyricetin, myricitrin, and myricetin content. Catalase (CAT) activity negatively correlated with total flavonoids, dihydromyricetin, and myricitrin con-

tent, and positively correlated with myricetin content, with the negative correlation with myricitrin being highly significant.

Table 2. Pearson's linear correlation coefficient between the activities of enzymes in *A. nigripes* and the content of secondary metabolites in plant leaves.

Enzyme	Secondary Metabolites			
	Total Flavonoids	Dihydromyricetin	Myricitrin	Myricetin
Acetylcholinesterase (U/g), AchE	0.583 **	0.633 **	−0.797 **	0.251
Carboxylesterase (U/g), CarE	0.563 **	0.561 **	−0.407 *	0.201
Glutathione S-transferase (U/g), GST	0.722 **	0.689 **	−0.143	0.370
Cytochrome P450 (ng/g), CYP450	0.525 **	0.579 **	−0.526 **	−0.047
Peroxidase (U/g), POD	0.178	0.208	−0.527 **	0.121
Superoxide dismutase (U/g), SOD	0.060	0.051	0.189	0.027
Catalase (U/g), CAT	−0.033	−0.123	−0.496 **	0.183

Note: The values in the table are Pearson's correlation coefficient (r), * indicates correlation was significant at the 0.05 level (two-tailed), ** indicates correlation was significant at the 0.01 level (two-tailed).

3.4. Metabolic Accumulation of Major N. grossedentata Flavonoids in Insects

The study findings indicate that *A. nigripes* consumed *N. grossedentata* leaves with varying flavonoid concentrations; following in vivo digestion, the levels of dihydromyricetin, myricetin, and myricitrin were significantly elevated in the insect excreta compared to the raw material (dried leaves of *N. grossedentata*). The content of these flavonoids in the excreta was significantly greater ($p < 0.001$) across all groups except for myricitrin, the content of which was not statistically different ($p > 0.05$) between the medium- and high-content raw materials and the excreta. The alterations in dihydromyricetin content were observed as 0.36-fold, 1.25-fold and 2.31-fold increases in the high-, medium-, and low-flavonoid-content groups, respectively (Figure 3A). And, the contents of myricitrin were 0.11-fold, 0.25-fold and 0.59-fold higher in the high-, medium-, and low-flavonoid-content groups, respectively (Figure 3B). Similarly, the myricetin contents were 1.84-fold, 3.75-fold and 1.35-fold higher in the high-, medium-, and low-flavonoid-content groups, respectively (Figure 3C).

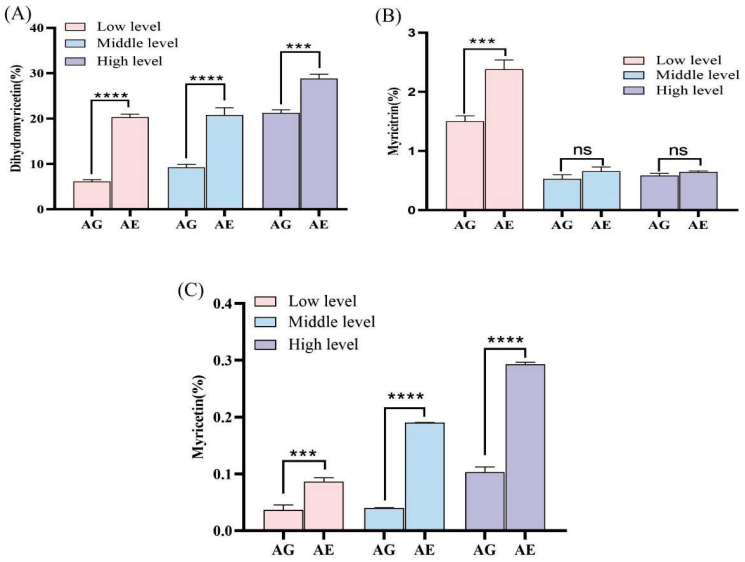


Figure 3. Metabolism of major flavonoids in *N. grossedentata* in *A. nigripes*. AG indicates *N. grossedentata* raw material, AE indicates excreta after insect feeding, *** indicates significant difference at the 0.001 level, **** indicates significant difference at the 0.0001 level, and ns indicates no significant difference. (**A**) Dihydromyricetin content, (**B**) Myricitrin content, (**C**) Myricetin content.

4. Discussion

This study investigated the temporal dynamics of the detoxifying and protective enzymes in *A. nigripes* upon feeding on *N. grossedentata* leaves from three strain types, compared the major flavonoid contents in the leaves of these strains, and analyzed their intercorrelations. These efforts were aimed at providing a theoretical framework for delving into the adaptive mechanisms of *A. nigripes* and establishing a basis for future pest management strategies. It is well established that secondary metabolites serve as the primary line of defense for plants against herbivorous insects [11]. These compounds can impact the activities of protective and detoxifying enzymes in insects [35,36]. Insects have evolved to counteract these various toxins by adjusting the expression of protective and detoxifying enzymes within their bodies [37–39]. Flavonoids, key components of plant secondary metabolites, are crucial in plant defenses against insects and are broadly distributed in plants [40]. Previous research has demonstrated that the activities of POD, SOD, and CAT enzymes are significantly elevated in insects like *Spodoptera frugiperda* when they consume leaves enriched with total phenols, tannins, and flavonoids [41]. Quercetin stress has been shown to induce a marked increase in P450 enzyme activity in the bodies and midguts of adult *Helicoverpa armigera* [42] as well as to stimulate GST activity in silkworms [43].

Plant secondary metabolites induce the production of superoxide radicals in insects, which, in turn, activate protective enzymes to shield the insects from oxidative damage [11,43,44]. When insects are exposed to exogenous compounds, SOD converts superoxide radicals (O^{2-}) into hydrogen peroxide (H_2O_2); CAT then breaks down H_2O_2 into water (H_2O) and oxygen (O_2) when H_2O_2 levels are excessive, while POD acts when H_2O_2 concentrations are low [37,45,46]. This study revealed that the levels of total flavonoids, dihydromyricetin, and myricetin in *N. grossedentata* leaves from high-level and middle-level strains exceeded those from low-level strains, with the myricitrin content being the highest in the low-level strain. At 24 and 48 h post-feeding, the POD and CAT activities in *A. nigripes* consuming high-level and middle-level strain leaves were significantly higher than in those consuming low-level strain leaves, whereas the POD enzyme activities remained unchanged. Over time, the SOD activity exhibited minor fluctuations and positively correlated with several flavonoids; the CAT activity showed a declining trend and negatively correlated with total flavonoids, dihydromyricetin, as well as myricitrin and positively correlated with myricetin; the POD activity showed significant fluctuations and positively correlated with total flavonoids, dihydromyricetin, and myricitrin. Similar findings were observed in *Spodoptera frugiperda*, where the POD, SOD, and CAT activities were significantly increased in the F1 generation larvae fed on potato leaves with high total phenols, tannins, and flavonoids [11,41]. When comparing the mean enzyme activity values at 24, 48, and 72 h post-feeding with pre-feeding values, the order of the increases in protective enzyme activities under stress with low dihydromyricetin content in *N. grossedentata* was POD (2.31-fold) > CAT (1.24-fold) > SOD (1.12-fold); under medium-content stress, the order was POD (3.09-fold) > CAT (1.49-fold) > SOD (1.08-fold); and, under high-content stress, the order was POD (2.88-fold) > CAT (1.36-fold) > SOD (1.10-fold). Among the protective enzymes, POD was found to play a pivotal role in the detoxification and protection of *A. nigripes*, offering a foundation for further in-depth research.

Host plants can affect the detoxification enzyme activities of insects in addition to their protective enzymes. GST, CarE, AchE, and CYP450 are important detoxification enzymes in insects [11,12], which play important roles in the decomposition of exogenous poisons and the maintenance of normal physiological metabolism [36,41,47,48]. The results of this study showed that the CarE enzyme activity of *A. nigripes* fed on the high-level strain was

significantly higher than that of *A. nigripes* feeding on low-level and middle-level strain at 72 h; the AchE enzyme activity at 24 h, 48 h and 72 h of feeding was significantly higher than that of feeding on the low-level strain; the GST enzyme activity at 24 h and 72 h of feeding was significantly higher than that of those feeding on low-level and middle-level strains; the CYP450 enzyme activity at 24 h, 48 h and 72 h of feeding was significantly higher than that of those feeding on the low-level strain. And, all four detoxification enzyme activities were highly significant positively correlated with the total flavonoid and dihydromyricetin contents as well as negatively correlated with the myricitrin content. These results are similar to previous studies, in which GST and CarE activities in the adults of *Monolepta hieroglyphica* increased dramatically after feeding on two host plants, *Lycopersicon esculentum* and *Artemisia selengensis* [49]. *Loxostege sticticalis* larvae showed a rapid increase in detoxification enzyme activity with feeding on unsuitable host plants as feeding time prolonged [19]. Feeding on both potato and tobacco leaves resulted in varying degrees of elevation of GST, CarE, MFO and CYP450 activities in *Spodoptera frugiperda* larvae [41]. These findings indicate that different insect species may have developed their own adaptation mechanisms to their host plants and that different host plants contain different types of secondary metabolites, which lead to differences in enzyme activities [9,50]. The mean values of enzyme activities at 24, 48 and 72 h were compared with pre-feeding enzyme activities; the order of increase in detoxification enzyme activities under *N. grossedentata* stress with a low content of dihydromyricetin was GST (1.66-fold) > CarE (1.26-fold) > AchE (1.14-fold) > CYP450 (0.98-fold); under medium-content stress, the order of increase in detoxification enzyme activities was AchE (1.80-fold) > CarE (1.61-fold) > GST (1.53-fold) > CYP450 (1.15-fold); the order of increase in detoxification enzyme activity under high-content stress was AchE (2.06-fold) ≈ GST (2.06-fold) > CarE (1.93-fold) > CYP450 (1.19-fold.; Among the four detoxification enzymes, GST and AchE play an important role in detoxification of harmful substances in *A. nigripes*, which is of great significance for the subsequent investigation of its detoxification mechanism.

It has been shown that one of the important defense strategies of plants against insects is changing the contents of secondary metabolites [40,51]; among them, flavonoids are one of the largest plant secondary products [52], which are widely found in plants and play an important role in plant defense against pests [40,53]. In the present study, the leaves of three *N. grossedentata* strains were fed to *A. nigripes*, which showed an increasing trend in dihydromyricetin, myricitrin, and total flavonoid contents after feeding, *N. grossedentata* showed different changes for each flavonoid component of the host after insect injury stress, suggesting that they play different roles in defending against insect stress. The content of dihydromyricetin showed the most obvious upward trend during the insect injury process, which was hypothesized to play an important role in the defense of the host against insect injury. Previous studies showed a significant increase in flavonoid content when fresh leaves of Lingtou Danzong tea were fed to *Basilepta melanopus* [4]. Metabolomics data of *Camellia sinensis* after feeding on *Colaspoides femoralis* showed significant enrichment in flavonoids and phenolic acids [3]. However, the impact of the dihydromyricetin content on *A. nigripes* is still unclear, and the molecular mechanisms of the *N. grossedentata* response to insect pests need to be further explored.

5. Conclusions

A. nigripes exhibited the ability to modulate the activities of protective and detoxification enzymes, thereby enhancing its adaptation to the secondary metabolites and toxic substances of *N. grossedentata,* particularly when ingesting leaves with varied flavonoid levels. This study demonstrated that the detoxifying enzymes glutathione S-transferase

(GST) and acetylcholinesterase (AchE), as well as the protective enzyme peroxidase (POD), were particularly efficacious in mitigating the flavonoid-induced stress in *A. nigripes.* Concurrently, the levels of the primary flavonoids dihydromyricetin and myricitrin, which are prominent in *N. grossedentata*, increased following *A. nigripes* consumption, with a trend that closely mirrored that of dihydromyricetin for total flavonoids. This suggests a role of these flavonoids in the host's defense against insect infestation. This research constitutes the first exploration of the interactions between *A. nigripes* and *N. grossedentata*, offering a foundational understanding of their adaptive mechanisms and laying the groundwork for future investigations into pest control strategies.

Author Contributions: C.Y.: conception and design, investigation, data interpretation, writing—original draft, writing—review and editing; L.X.: investigation, data analysis; F.Y.: investigation, data interpretation; Y.Y.: investigation, data interpretation; Z.Y.: conception and design, writing—review and editing, funding acquisition, supervision. All authors reviewed this manuscript. All authors have read and agreed to the published version of the manuscript.

Funding: This work was supported by the National Natural Science Foundation of China [grants No. 32060068 and No. U1812401] and Natural science research project of Guizhou Provincial Department of Education [Qianjiaoji [2022] 009].

Data Availability Statement: The raw data supporting the conclusions of this article will be made available by the authors on request.

Conflicts of Interest: The authors declare no conflicts of interest.

References

1. Chen, C.Y.; Kang, Z.J.; Shi, X.Y.; Gao, X.W. Metabolic adaptation mechanisms of insects to plant secondary metabolites and their implications for insecticide resistance of insects. *Acta Entomol. Sin.* **2015**, *58*, 1126–1130.
2. Li, L.S.; Yuan, Y.F.; Wu, L.; Chen, M. Effects of host plants on the feeding behavior and detoxification enzyme activities in *Hyphantria cunea* (Lepidoptera: Arctiidae) larvae. *Acta Entomol. Sin.* **2018**, *61*, 232–239.
3. Ji, D.Z. Defensive Responses of *Camellia sinensis* to *Colaspoides femoralis* Feeding. Master's Thesis, Guizhou University, Guiyang, China, 2022.
4. Liu, K.B.; Cao, P.R.; Liu, C.Y.; Zhou, Y.H. The effect on the component contents in fresh leaves of Lingtou Danzong tea plant by moderate damage of *Basilepta melanopus*. *J. South China Agric. Univ.* **2005**, *26*, 15–18.
5. Abdel-Aal, E.S.M.; Hucl, P.; Sosulski, F.W.; Graf, R.; Gillott, C.; Pietrzak, L. Screening spring wheat for midge resistance in relation to ferulic acid content. *J. Agric. Food. Chem.* **2001**, *49*, 3559–3566. [CrossRef] [PubMed]
6. Zheng, W.J.; Liu, Z.H.; Zhang, Y.Z.; Liu, X.; Wang, C.H.; Zhao, J.M. Effects of the major nutritional substances and micro-structure of rice plants on the host preference of the small brown plant hopper, *Laodelphax striatellus*. *J. Plant Prot.* **2009**, *36*, 200–206.
7. Wang, Y.; Zhao, M.; Tian, T.W.; Guo, X.R.; Li, W.Z.; Yan, F.M. Study on the relationship between the occurrence quantity of *Rhopalosiphum maidis* (Fitch) and main biochemical substance contents in maize. *J. Henan Agric. Uni.* **2016**, *50*, 364–369.
8. Chen, R.; Gao, H.; Zhang, G.J.; Zhu, K.Y.; Cheng, W.N. Effects of secondary metabolites in wheat kernels on activities of three detoxifying enzymes and related gene expression in *Sitodiplosis mosellena*. *Sci. Agric. Sin.* **2020**, *53*, 4204–4214.
9. Xiang, Y.; Niu, H.; Jin, B.; Zhang, Y.; Yin, P. Effects of Honeysuckle Varieties on Protective and Detoxifying Enzyme Activities in *Heterolocha Jinyinhuaphaga* Chu (Lepidoptera: Geometridae) Larvae. *J. Chem. Ecol.* **2023**, *49*, 205–213. [CrossRef]
10. Yang, Z.D. Studies on Life-History Characteristics of *Plagiodera versicolora* and *Clostera anastomosis* and Their Behavioral Response to the Alkaloids from *Sophora alopecuroids*. Ph.D. Thesis, Nanjing Forestry University, Nanjing, China, 2004.
11. Lu, Z.H.; Chen, Y.P.; Zhou, A.C.; He, S.Q.; Li, H.; Bao, Y.Y.; Cui, F.R. Effects of multi-generation feeding with different host plants on activities of enzyme in *Spodoptera frugiperda* larvae. *J. Environ. Entomol.* **2020**, *42*, 1361–1368.
12. Chertemps, T.; Goff, G.; Maïbèchea, M.; Hilliou, F. Detoxification gene families in Phylloxera: Endogenous functions and roles in response to the environment. *Comp. Biochem. Physiol. Part D Genom. Proteom.* **2021**, *40*, 100867. [CrossRef]
13. Xu, L. Study on effects of three secondary metabolites and cyanobromonamide on P450 and GST in *Lymantria dispar*. Master's Thesis, Northeast Forestry University, Harbin, China, 2021.
14. Li, S.; Ge, Z.; Liu, D.; Cui, X.; Huang, X.; Wang, D. Effects of Host Plants on Activities of Detoxificatoin Enzymes in Different Genotypes of Cereal Aphid Sitobion avenae. *Acta Agric. Boreali-Occident. Sin.* **2018**, *27*, 283–293.

15. Lindroth, R.L. Host plant alteration of detoxification enzyme in *Papilio glaucus glaucus*. *Entomol. Exp. Appl.* **1989**, *50*, 29–35. [CrossRef]
16. Rigsby, C.M.; Showalter, D.N.; Herms, D.A.; Koch, J.L.; Bonello, P.; Cipollini, D. Physiological responses of emerald ash borer larvae to feeding on different ash species reveal putative resistance mechanisms and insect counter-adaptations. *J. Insect Physiol.* **2015**, *78*, 47–54. [CrossRef]
17. Saha, D.; Mukhopadhyay, A.; Bahadur, M. Effect of host plants on fitness traits and detoxifying enzymes activity of *Helopeltis theivora*, a major sucking insect pest of tea. *Phytoparasitica* **2012**, *40*, 433–444. [CrossRef]
18. Wang, K.Y.; Zhang, Y.; Wang, H.Y.; Xia, X.M.; Liu, T.X. Influence of three diets on susceptibility of selected insecticides and activities of detoxification esterases of *Helicoverpa assulta* (Lepidoptera: Noctuidae). *Pestic. Biochem. Phys.* **2010**, *96*, 51–55. [CrossRef]
19. Yin, J.; Feng, H.L.; Li, K.B.; Cao, Y.Z. Effects of host plants on the activities of some detoxification enzymes and protective enzymes in the meadow moth. *Plant Prot.* **2012**, *38*, 35–39.
20. Yang, Y.T.; Shi, C.H.; Cheng, J.X.; Zhang, Y.J. Effects of feeding on different host plants on development, reproduction and protective enzymes of *Bradysia odoriphaga*. *Plant Prot.* **2017**, *43*, 119–123.
21. Liu, Y.K.; Wang, W.X.; Fu, Q.; Lai, F.X.; Luo, J. Effects of host plants on activities of detoxification and protective enzymes in three rice plant hoppers. *Chin. J. Rice Sci.* **2011**, *25*, 659–666.
22. Jacoby, M. Descriptions of new genera and species of phytophagous Coleoptera. *Zoology* **1885**, *53*, 925–929.
23. Hua, L.Z. *List of Chinese Insects: Second Volume*; Zhongshan (Sun Yat-sen) University Press: Guangzhou, China, 2002.
24. Qin, R.H.; Ou, X.H.; Situ, Y.X. *A New Pest Harming Parthenocisus himalayana: Aoria nigripes*; Yunnan Forestry: Kunming, China, 2004.
25. Tan, J.Y.; Wang, S.Y.; Zhou, H.Z. *Fauna Sinica Insects: Fortieth Volume*; Science Press: Beijing, China, 2016; pp. 206–215.
26. Zhou, C.X.; Bai, M.Q.; Ai, Z.X.; Zhao, A.Q. Occurrence rule and green prevention and control technology of *Aoria nigripes* on crystal grape in Sandu county. *Guizhou Agric. Sci.* **2015**, *43*, 62–64.
27. Wang, Z.Y.; Liu, W.W.; Qin, W.T.; Yuan, H.Z.; Yang, S.L.; Li, H. Occurrence and control of the grape pest, *Aoria nigripes*, in Wenshan of Yunnan Province. *Plant Prot.* **2011**, *37*, 178–180.
28. Yang, C.; Jiang, C.; Wu, S.; Feng, X.; Yu, Z. The complete mitochondrial genome of *Aoria nigripes* (Coleoptera, Eumolpidae, Eumolpinae) and its phylogenetic status. *Biodivers. Data J.* **2022**, *10*, e93591. [CrossRef]
29. Zhang, M.; Li, L.; Chen, Q.; Chen, M.; Wei, Y.; Yu, Z. Biological Characteristics and Occurrence of *Aoria nigripes* (Coleoptera: Chrysomelidae) in *Ampelopsis grossedentata*. *J. Henan Agric. Sci.* **2023**, *52*, 94–102.
30. Jiang, C.Y. Effects of Karst Habitat on the Physiological and Biochemical Properties of *Ampelopsis grossedentata* and Its Generalization. Master's Thesis, Guizhou Normal University, Guiyang, China, 2023.
31. Wang, Y.X.; Hong, Z.S.; Yang, K.; Zeng, C.H. Research progress of dihydromyricetin in *Ampelopsis grossedentata*. *J. Shenyang Pharm. Univ.* **2020**, *37*, 569–576.
32. Zheng, Y.K.; Li, J.; Huang, D.; Ou, Y.W.; Yao, R. Research progress on chemical constituents and anti- infective effects of the traditional Chinese medicine vine tea (*Ampelopsis grossedentata*). *Mod. Tradit. Chin. Med. Mater. Medica World Sci. Technol.* **2021**, *23*, 2012–2022.
33. Zheng, X.J.; Xiao, H.; Zeng, Z.; Sun, Z.W.; Lei, C.; Dong, J.Z.; Wang, Y. Composition and serum antioxidation of the main flavonoids from fermented vine tea (*Ampelopsis grossedentata*). *J. Funct. Foods* **2014**, *9*, 290–294. [CrossRef]
34. Liu, H.Y.; Cui, X.M.; Liu, D.Q.; Yang, Y.; Wang, C.X.; Yang, X.Y.; Qu, Y. Research progress of chemical constituents and pharmacological effects of *Ampelopsis grossedentata*. *J. Anhui Agric. Sci.* **2016**, *44*, 135–138.
35. Chen, F.J.; Gao, X.W.; Lei, M.Q.; Zheng, B.Z. Effects of tannic acid on glutathione S-transferases in *Helicoverpa armigera* (Hüb-ner). *Acta Entomol. Sin.* **2003**, *46*, 684–690.
36. Zeng, R.S.; Wen, Z.M.; Niu, G.D.; Schuler, M.A.; Berenbaum, M.R. Allelochemical induction of cytochrome P450 monooxygenases and amelioration of xenobiotic toxicity in *Helicoverpa zea*. *J. Chem. Ecol.* **2007**, *33*, 449–461. [CrossRef]
37. Gao, Y.P.; Luo, M.; Wang, X.Y.; He, X.Z.; Lu, W.; Zheng, X.L. Pathogenicity of *Beauveria bassiana* PfBb and Immune Responses of a Non-Target Host, *Spodoptera frugiperda* (Lepidoptera: Noctuidae). *Insects* **2022**, *13*, 914. [CrossRef]
38. Jiang, X.C.; Shen, Y.D.; Sun, J.C.; Li, X.X.; Huang, Y.; Dong, Y.C.; Cao, H.Q. Effect of chlorantraniliprole and emamectin benzoate on toxicity and detoxification enzymes activity in *Spodoptera frugiperda* larva. *J. Environ. Entomol.* **2019**, *41*, 961–967.
39. Wen, S.F.; Xue, Y.N.; Du, R.S.; Liu, C.; Wang, X.T.; Wang, Y.W.; Liu, C.; Wang, S.; Wang, J.H.; Xia, X.M. Toxicity and sublethal effects of triflumezopyrim on the development and detoxification enzymatic activities in the small brown planthopper (SBPH), *Laodelphax striatellus* (Fallen). *Crop Prot.* **2021**, *150*, 105813. [CrossRef]
40. Deng, Z.; Zhang, Y.; Fang, L.; Zhang, M.; Wang, L.; Ni, X.; Li, X. Identification of the Flavone-Inducible Counter-Defense Genes and Their cis-Elements in *Helicoverpa armigera*. *Toxins* **2023**, *15*, 365. [CrossRef] [PubMed]

41. Lu, Z.; He, S.; Guo, J.; Chen, Y.; Hu, X.; Li, H.; Xie, Q.; Gui, F. Effects of host plants on activities of three groups of enzymes in *Spodoptera frugiperda* (Smith) larvae. *J. South. Agric.* **2020**, *51*, 2461–2469.
42. Giraudo, M.; Hilliou, F.; Fricaux, T.; Audant, P.; Feyereisen, R.; Le Goff, G. Cytochrome P450s from the fall armyworm (*Spodoptera frugiperda*): Responses to plant allelochemicals and pesticides. *Insect Mol. Biol.* **2015**, *24*, 115–128. [CrossRef]
43. Shi, G.Q.; Kang, Z.Y.; Ren, F.; Guo, P. Effects of Quercetin on the Growth and Expression of Immune-Pathway-Related Genes in *Silkworm* (Lepidoptera: Bombycidae). *J. Insect Sci.* **2020**, *20*, 23. [CrossRef]
44. Piskorski, R.; Dorn, S. How the oligophage codling moth *Cydia pomonella* survives on walnut despite its secondary metabolite juglone. *J. Insect Physiol.* **2011**, *57*, 744–750. [CrossRef]
45. Felton, G.W.; Summers, C.B. Antioxidant systems in insects. *Arch. Insect Biochem.* **1995**, *29*, 187–197. [CrossRef] [PubMed]
46. Wang, Y.; Oberley, L.W.; Murhammer, D.W. Antioxidant defense systems of two lipidopteran insect cell lines. *Free Radic. Biol. Med.* **2001**, *30*, 1254–1262. [CrossRef]
47. Li, C.C.; Ning, Q.; Dai, Y.J.; Wang, L.H.; Li, G.Y.; Peng, Y. Cloning and expression analysis of glutathione S-transferase gene in *Pardosa pseudoannulata*. *Jiangsu J. Agric. Sci.* **2019**, *35*, 1068–1074.
48. Lü, C.J.; Han, J.C.; Liu, H.; Ren, Y.X.; Ma, L. Influence of host plants to detoxification enzymes and susceptibilities to insecticides on *Aphis citricola* von der Goot. *J. Plant Prot.* **2007**, *34*, 534–538.
49. Xu, W.; Zhang, J.H.; Bi, J.R.; Ma, Y.X.; Zhang, Y.K.; Shi, S.S. Effects of host plants on digestive enzymes and detoxification enzyme activities in the midgut of *Monolepta hieroglyphica* (Motschulsky). *J. Jilin Agric. Univ.* **2018**, *40*, 551–556.
50. Zhang, A.P.; Song, D.L.; Shi, X.Y.; Liang, P.; Gao, X.W. Effects of three alleochemcals on the carboxylesterase activity and its susceptibility to insecticides in *Bemisia tabaci* Biotype, B. *Chin. J. Pestic. Sci.* **2008**, *10*, 292–296.
51. Erb, M.; Robert, C.A. Sequestration of plant secondary metabolites by insect herbivores: Molecular mechanisms and ecological consequences. *Curr. Opin. Insect Sci.* **2016**, *14*, 8–11. [CrossRef] [PubMed]
52. Gautam, H.; Sharma, A.; Trivedi, P.K. The role of flavonols in insect resistance and stress response. *Curr. Opin. Plant Biol.* **2023**, *73*, 102353. [CrossRef]
53. Simmonds, M.S.J. Flavonoid-insect interactions: Recent advances in our knowledge. *Phytochemistry* **2003**, *64*, 21–30. [CrossRef]

Disclaimer/Publisher's Note: The statements, opinions and data contained in all publications are solely those of the individual author(s) and contributor(s) and not of MDPI and/or the editor(s). MDPI and/or the editor(s) disclaim responsibility for any injury to people or property resulting from any ideas, methods, instructions or products referred to in the content.

insects

MDPI

Article

Adipokinetic Hormones and Their Receptor Regulate the Locomotor Behavior in *Tribolium castaneum*

Rui-Han Lu [1], Xu-Dong Pang [1], Shuang-Qin Wen [1], Guy Smagghe [1], Tong-Xian Liu [1,2] and Shun-Hua Gui [1,2,*]

[1] Guizhou Provincial Key Laboratory for Agricultural Pest Management of the Mountainous Region, Institute of Entomology, College of Agriculture, Guizhou University, Guiyang 550025, China; lrh8032025@163.com (R.-H.L.); jsgz412@163.com (X.-D.P.); 18885644922@163.com (S.-Q.W.); guysma9@gmail.com (G.S.); tx.liu@gzu.edu.cn (T.-X.L.)

[2] Institute of Plant Health and Medicine, Guizhou University, Guiyang 550025, China

* Correspondence: shgui3@gzu.edu.cn

Simple Summary: The insect nervous system regulates locomotor behavior through the use of specialized signaling molecules known as neuropeptides. One such neuropeptide, adipokinetic hormone (AKH), is known to help insects use energy from fats. In this study, we explored how AKH and its receptor (AKHR) affect locomotion in the red flour beetle, Tribolium castaneum, a pest that damages stored grains. We found that AKH strongly activates its receptor, triggering responses at very low concentrations. The genes for AKH were active in the brain, while the receptor was found in the fat-storing tissue. When we reduced AKH or AKHR levels using RNA interference techniques, the beetles moved much less, showing that this signaling pathway is crucial for locomotion. These findings help us understand how insects control their activity, which could lead to better ways to manage pest insects in agriculture and food storage.

Abstract: The regulation of locomotor behavior is essential for insects to perform their life activities. The central nervous system plays a pivotal role in modulating physiological behaviors, particularly movement, with neuropeptides serving as key modulators of these processes. Among these, adipokinetic hormone (AKH) was originally identified in insects as a neurohormone involved in lipid mobilization. This study investigates the functional role of AKHs (AKH1 and AKH2) and their receptor (AKHR) in regulating locomotion in the red flour beetle, *Tribolium castaneum*. Using functional calcium reporter assays, we demonstrated that AKHR is activated by two mature AKH peptides from *T. castaneum*, with half-maximal effective concentrations (EC_{50}) falling within the nanomolar range. Gene expression analysis confirmed the presence of *AKH1* and *AKH2* transcripts in the brain, while *AKHR* expression was localized to the fat body and carcass. The silencing of *AKHs* or *AKHR* through RNA interference resulted in a significant reduction in both movement distance and duration. Collectively, these findings highlight the regulatory influence of AKH/AKHR signaling in locomotor activity in *T. castaneum*, thereby advancing our understanding of the molecular mechanisms underlying locomotor control in this economically important insect species.

Keywords: neuropeptide; RNAi; locomotor behavior; red flour beetle

1. Introduction

The locomotor behavior of insects is fundamental to their survival, impacting essential behaviors such as searching for food, finding mates, escaping predators, and adapting to changing environments. Coordinated movement requires the seamless integration of internal physiological states and external sensory inputs in insects [1,2]. Insect neuropeptides, as small intercellular signaling molecules primarily secreted by the central nervous system, play an integral role in regulating various physiological functions, including locomotion, by interacting with their specific receptors [3,4]. Previous studies have identified neuropeptide–receptor systems being involved in controlling the locomotor behavior in insects. For instance, neuropeptide F had suppressive effects on phase-related locomotor activity in *Locusta migratoria* [5]. Silencing the diuretic hormone receptor resulted in reduced mean velocity in *Drosophila melanogaster* [6]. Moreover, the tachykinin and short neuropeptide F pathways in the central complex have specific roles in the fine-tuning of locomotor activity in adult *D. melanogaster* [7]. Despite these findings, limited attention has been given to the regulatory impact of neuropeptide–receptor systems on locomotor behavior in only a small number of insect species.

Adipokinetic hormone (AKH), a neuropeptide initially isolated from locusts as a neurohormone that facilitates lipid mobilization during flight, is now known to be widespread across insect species [8]. It is documented that AKH plays a vital role in regulating energy mobilization, impacting various physiological processes such as starvation responses, stress adaptation, development, and reproductive capacity [9–13]. These functions are mediated through adipokinetic hormone receptors (AKHRs) that share similarities with vertebrate gonadotropin-releasing hormone receptors [14].

Tribolium castaneum, commonly known as the red flour beetle, is a widespread pest of stored grains, flour, cereals, and other dried food products, causing significant economic damage through contamination. Both the larvae and adults feed on these materials, thriving in warm, dry environments typical of storage facilities. Beyond its role as a pest, *T. castaneum* is a valuable model organism in scientific research. Its short life cycle, ease of lab rearing, and fully sequenced genome make it ideal for studying development, genetics, evolution, and pest control strategies. Notably, it is also used to explore questions in insect biology that complement research on other insects like *D. melanogaster* [15].

In this study, we researched the regulation of the locomotor behavior in *T. castaneum* by AKHs and their receptor. Using molecular profiling and calcium mobilization assays, we comprehensively characterized the *T. castaneum* AKHs (Tc-AKHs) and their receptor (Tc-AKHR), thereby confirming the receptor functional activity of the receptor. Through RNA interference (RNAi), we further demonstrated that silencing the expression of *Tc-AKHs* or their receptor significantly altered locomotor patterns in adult beetles. Collectively, these findings provide valuable insights into the neuromodulatory mechanism underlying insect locomotion.

2. Materials and Methods

2.1. Insect Rearing and Cell Line Maintenance

The *T. castaneum* colony was reared in a controlled growth chamber under specific environmental conditions of 30 ± 1 °C temperature, 70 ± 5% relative humidity, and continuous darkness [16,17]. The insects were provided with a diet consisting of whole wheat flour and brewer's yeast in a 19:1 ratio. Concurrently, the CHO-WTA11 cell line (generously provided by Professor Jiang Hongbo from Southwest University, Chongqing, China) was cultured in a high-glucose Dulbecco's Modified Eagle Medium (DMEM; Sigma, Taufkirchen, Germany) supplemented with 10% fetal bovine serum (FBS; Gibco,

Jenks, OK, USA). The cells were maintained in a 5% CO_2 incubator to ensure optimal growth conditions.

2.2. Sequence Analysis of Tc-AKHR and Its Ligands in T. castaneum

Previous studies enabled the identification of the pre-mRNA sequences of *Tc-AKH1* (NP_001107797.1) and *Tc-AKH2* (NP_001107818.1), as well as the *Tc-AKHR* sequence (NM_001083340.1), through the NCBI database. The transmembrane domains of *Tc-AKHR* were predicted using the TMHMM version 2.0. The corresponding amino acid sequences were derived via ExPASy and subsequently aligned with homologous sequences using NCBI's blastp tool. Phylogenetic analysis was performed using MEGA 5.1, while sequence alignment was conducted with Jalview 2.11. Signal peptides within the *Tc-AKH* precursor were predicted using the SignalP server, and C-terminal motifs were visualized using WebLogo.

2.3. Structural Modeling and Molecular Docking

The amino acid structures of Tc-AKHs were drawn using ChenDraw (v21.0), while homology modeling of Tc-AHKR was conducted via the Alphafold3 tool to generate a three-dimensional structural model. Molecular docking simulations were performed using the CDDOCKER module in Discovery Studio 21.0. The interaction patterns between Tc-AKHs and Tc-AKHR were visualized and analyzed using PyMOL v.3.11.

2.4. Functional Calcium Reporter Assays

The open reading frames (ORFs) of *Tc-AKHR* were cloned into the pcDNA 3.1 (+) expression vector (Tsingke, Beijing, China) for heterologous expression in CHO-WTA11 cells, which served as the reporter system for *Tc-AKH*-induced calcium mobilization. *Tc-AKH* peptides were chemically synthesized based on high-performance liquid chromatography (HPLC) and mass spectrometry (MS) analyses (Zoonbio, Nanjing, China). For GPCR assays, a mixture of expression vectors, containing *Tc-AKHR* (2.5 μg) and apoaequorin in a 1:1 ratio, was transfected into CHO cells using TransIT®-LT1 (Mirus, Madison, WI, USA). The transfected cells were harvested, resuspended in a serum-free high-glucose medium, and incubated with coelenterazine h (Thermo Fisher Scientific, Waltham, MA, USA) under dark conditions. Synthetic *Tc-AKH* peptides, prepared in 10-fold serial dilutions ranging from 2 pM to 20 μM, were added to an opaque 96-well plate. Luminescence was quantified using a SpectraMax L chemiluminescence microplate reader (Molecular Devices, San Jose, CA, USA) [18]. All experiments were conducted in three biological replicates.

2.5. Gene Expression in Different Tissues

Tissue-specific gene expression profiles of *Tc-AKHR* and *Tc-AKHs* were obtained from the Beetle Atlas database (https://motif.mvls.gla.ac.uk/BeetleAtlas/). Origin 2024 was employed to analyze and visualize the differential expression patterns across various tissues.

2.6. Total RNA Isolation and cDNA Synthesis

For total RNA isolation, three adult beetles were placed in RNase-free centrifuge tubes, flash-frozen in liquid nitrogen, and homogenized using a disposable tissue grinding rod under continuous liquid nitrogen cooling. Total RNA was extracted from whole-body samples using the Eastep® Super Total RNA Extraction Kit (Promega, Madison, WI, USA). RNA integrity was assessed on 1% agarose gels, and purity was determined using a Nanodrop 2000 spectrophotometer (Thermo Fisher Scientific, USA). Subsequently, 1 μg of total RNA was reverse-transcribed into cDNA using the StarScript Pro All-in-one RT Mix with gDNA Remover (GenStar, Beijing, China), following the manufacturer's protocol.

2.7. Synthesis of Double-Stranded RNA

The synthesis of double-stranded RNA (dsRNA) targeting specific genes (dsEGFP, dsAKHR, dsAKH1, and dsAKH2) was initiated by generating templates through PCR amplification. Gene-specific primers, incorporating the T7 polymerase promoter sequence at their 5′ ends (Table S1), were used to amplify the target gene fragments. The resulting PCR products were purified and subsequently employed as templates for dsRNA synthesis using the TranscriptAid™ T7 High Yield Transcription Kit (Thermo Fisher Scientific, USA), following the manufacturer's instructions. Post-synthesis, the dsRNA was purified via phenol/chloroform extraction and ethanol precipitation and then resuspended in DEPC-treated water. The concentration of the synthesized dsRNA was quantified using a Nanodrop 2000 spectrophotometer (Thermo Fisher Scientific, USA) at 260 nm, and its integrity was verified via electrophoresis on 1% agarose gels.

2.8. Quantitative Reverse Transcription PCR

Quantitative real-time PCR (qRT-PCR) was conducted using the CFX Opus Real-Time PCR System (Bio-Rad, Hercules, CA, USA). Each reaction mixture consisted of 2 μL of cDNA (200 ng/μL), 1 μL each of forward and reverse gene-specific primers (10 μM), 6 μL of DEPC-treated water, and 10 μL of 2×RealStar Fast SYBR qPCR Mix (GenStar, China). The thermal cycling protocol included an initial denaturation step at 95 °C for 2 min, followed by 39 cycles of 95 °C for 15 s and 60 °C for 30 s. Gene expression levels were quantified in duplicate and normalized to the internal control gene, *T. castaneum* ribosomal protein S3 (*Tcrp3*) [19]. Primer sequences for the target genes are provided in Table S1. Relative gene expression was calculated using the $2^{-\Delta\Delta CT}$ method [20].

2.9. RNA Interference and Movement Analysis

Three-day-old adult *T. castaneum* beetles were anesthetized with CO_2 and immobilized on double-sided tape for microinjection. Approximately 300 ng of dsRNA was injected into the ventral side of the first abdominal segment using a microinjection system (WPI-PV830, World Precision Instruments, Sarasota, FL, USA) equipped with a glass capillary needle [21]. Beetles injected with dsEGFP served as the control group. Following injection, all adults were maintained under identical conditions for 48 h prior to analysis.

For movement assessments, all tests were conducted at room temperature. Groups consisting of three adults each from the treatment (dsAKHR, dsAKH1, and dsAKH2) and control (dsEGFP) groups were transferred to Petri dishes with a diameter of 125 mm. Their motion was recorded for 1 min using a camera (Sony FDR-AX60, Tokyo, Japan) under controlled conditions. The recorded videos were analyzed using the EthoVision XT 17.5 (Noldus, Wageningen, The Netherlands) to quantify movement parameters and generate trajectories. Subject detection was achieved with gray scaling. Thresholds for "moving" and "resting" states were defined as 5 mm/s and 1 mm/s, respectively, based on slight modifications of previously established criteria [17]. For the determination of the active time, the tracking target was divided into a certain number of pixels according to the automatic setting of the software. When 5–60% of the pixels changed, it was considered to be in an active state.

2.10. Statistical Analysis

Statistical analysis began with the Shapiro–Wilk test to evaluate the normality of the datasets. For data conforming to a normal distribution (Shapiro–Wilk test: $p > 0.05$), an independent Student's *t*-test was used to compare mean values of gene expression levels and other parameters between the RNAi-treated and control groups. In cases where data

deviated from normality (Shapiro–Wilk test: $p \leq 0.05$), the nonparametric Mann–Whitney U test was applied. All results are presented as the mean ± SEM from five or more independent experiments. A p-value of <0.05 was considered statistically significant.

3. Results

3.1. Sequence Analysis and Molecular Characterization of AKHs and AKHR in T. castaneum

The full-length pre-mRNA sequences of *Tc-AKH1* and *Tc-AKH2* each consist of two exons. The exons in *Tc-AKH1* are 69 bp and 171 bp in length and encode a protein of 73 amino acids, while those in *Tc-AKH2* are 162 bp and 45 bp in length and encode a 68-amino acid protein, respectively (Figure 1A,C). Notably, the first 19 amino acid residues in both *Tc-AKH1* and *Tc-AKH2* are predicted to function as secretory signal peptides, followed by a conserved mature peptide that ends with a predicted amidation site and a dibasic cleavage signal (GKR) (Figure 1C). When compared to the mature AKH peptide sequences of *T. castaneum*, *D. melanogaster*, *Bombyx mori*, *L. migratoria*, *Acyrthosiphon pisum*, *Spodoptera frugiperda*, *Apis mellifera*, and *Leptinotarsa decemlineata*, it was observed that the AKH peptides are highly conserved and displayed the following characteristic motif: QxxxxxxWamide (Figure 1B).

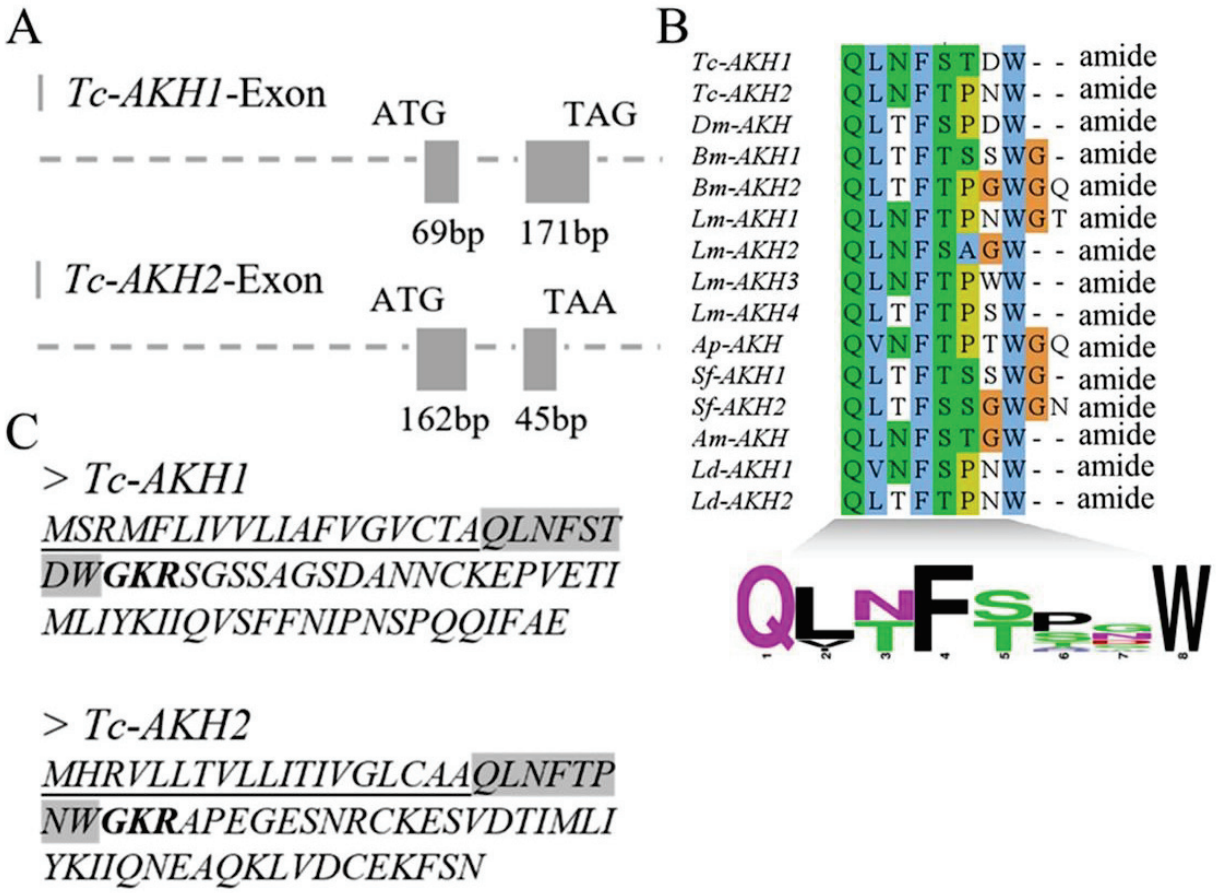


Figure 1. Gene structures and deduced amino acid sequences of *AKHs* in *T. castaneum*. (**A**) Gene structures of *Tc-AKH1* and *Tc-AKH2*. Exons are represented by boxes and introns by lines. (**B**) Sequence alignment of mature *AKH* peptides from *T. castaneum*, *D. melanogaster*, *B. mori*, *L. migratoria*, *A. pisum*, *S. frugiperda*, *A. mellifera* and *L. decemlineata*. The calculated sequence logo is shown at the bottom. (**C**) Deduced amino acid sequences of *Tc-AKHs*. Putative signal peptides are underlined; mature peptides are shaded in gray, and predicted amidation signals with dibasic cleavage sites (KR) are shown in bold.

The *Tc-AKHR* mRNA features a putative ORF of 1137 nucleotides that encodes a protein consisting of 378 amino acids. *Tc-AKHR* is a membrane-bound protein with seven transmembrane domains, consistent with its classification as a G protein-coupled receptor (GPCR). Comparative analysis with AKHR sequences from *D. melanogaster* and *B. mori* revealed a high degree of conservation. The *Tc-AKHR* sequence shares 52.77% similarity with *D. melanogaster AKHR* and 59.73% similarity with *B. mori AKHR*, particularly in the amino acid sequence of the transmembrane domains (Figure 2B).

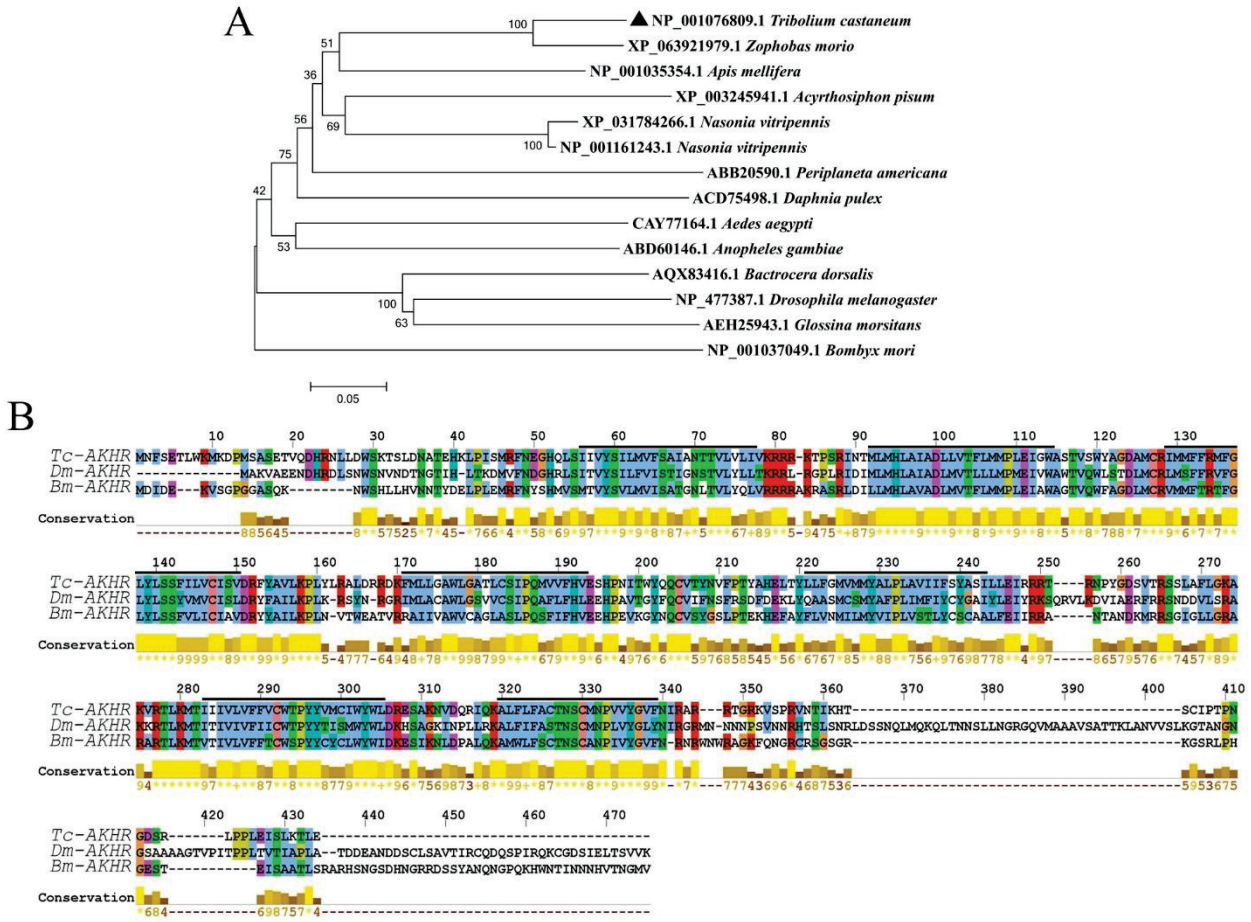


Figure 2. Amino acid sequence alignment and cluster analysis of *AKHR* in *T. castaneum*. (**A**) Evolutionary tree analysis of *Tc-AKHR* (neighbor-joining). The insect *AKHR* protein sequences of *T. castaneum*, *Z. morio*, *A. mellifera*, *A. pisum*, *N. vitripennis*, *P. americana*, *D. pulex*, *A. aegypti*, *A. gambiae*, *B. dorsalis*, *D. melanogaster*, *G. morsitans*, and *B. mori* were selected to construct the evolutionary tree. *Tc-AKHR* was assigned with "▲". (**B**) Comparative amino acid sequence alignment of *T. castaneum*, *D. melanogaster*, and *B. mori AKHR* sequences.

Phylogenetic analysis was further conducted using MEGA5.1 to clarify the evolutionary relationship of *Tc-AKHR* within the arthropod phylum. Using the neighbor-joining method, a gene cluster analysis was performed, which showed that the *Tc-AKHR* from *T. castaneum* (order: Coleoptera) is most closely related to the AKHR from *Zophobas morio* (order: Coleoptera), followed by that from *A. mellifera* (order: Hymenoptera) (Figure 2A).

3.2. Activity Determination of Tc-AKHs on Tc-AKHR

Docking simulations revealed that both Tc-AKH1 and Tc-AKH2 bind to specific docking sites on Tc-AKHR, with each ligand interacting with a distinct set of eight amino

acids on the receptor (Figure 3A,B). These sites are crucial for the binding of Tc-AKHs to Tc-AKHR.

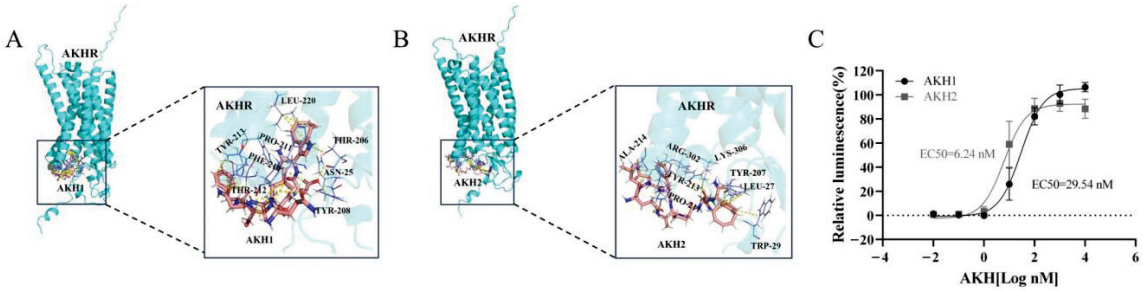


Figure 3. (**A**,**B**) *Tc-AKH1* and *Tc-AKH2* docked to *Tc-AKHR*. The hydrogen bond is represented by a yellow dotted line; the three letters are the abbreviation of the amino acid. and the number is the amino acid number of the receptor. (**C**) Dose–response curves and EC_{50} values of *Tc-AKH1* and *Tc-AKH2*, tested on *Tc-AKHR* expressed in CHO-WTA11 cells.

To evaluate the interaction between *Tc-AKHs* and *Tc-AKHR*, heterologous expression of *Tc-AKHR* was carried out in CHO-WTA11 cells, followed by calcium reporter assays. The results indicated that the CHO cells expressing *Tc-AKHR* were successfully activated by chemically synthesized *Tc-AKHs*. Among the two ligands, *Tc-AKH1* demonstrated a higher sensitivity, with an effective concentration (EC_{50}) of 6.24 nM, compared to *Tc-AKH2*, which exhibited an EC_{50} of 29.54 nM (Figure 3C).

3.3. Expression of Tc-AKHs and Tc-AKHR in Different Tissues of T. castaneum

To investigate the tissue-specific expression patterns of *Tc-AKHR* and *Tc-AKHs*, transcript levels were assessed across various tissues in adult *T. castaneum* according to data from the Beetle Atlas database. The expression of *Tc-AKHR* was found to be higher in the fat body and carcass. The two *Tc-AKHs* exhibited a very high expression in the brain (Figure 4).

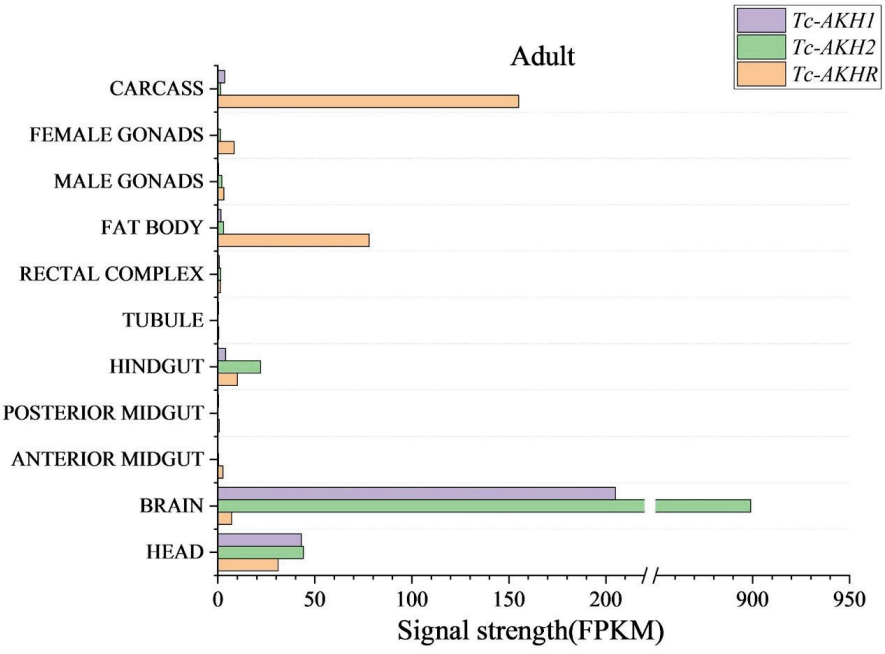


Figure 4. The relative expression of *Tc-AKHR*, *Tc-AKH1*, and *Tc-AKH2* in different adult tissues of *T. castaneum*. Data were obtained from the Beetle Atlas database.

3.4. Effects of Tc-AKH and Tc-AKHR Knockdown on Locomotion

To investigate the role of *Tc-AKHs* and *Tc-AKHR* in locomotor behavior, RNAi was employed to suppress their expression, followed by behavioral analysis in adult beetles. The knockdown efficiency was confirmed through qRT-PCR, revealing significant reductions in mRNA levels: *Tc-AKHR* by 81%, *Tc-AKH1* by 97%, and *Tc-AKH2* by 86% (Figures 5A, 6A and 7A). No cross-regulatory effects were observed between dsAKH1 and dsAKH2 (Figure S1).

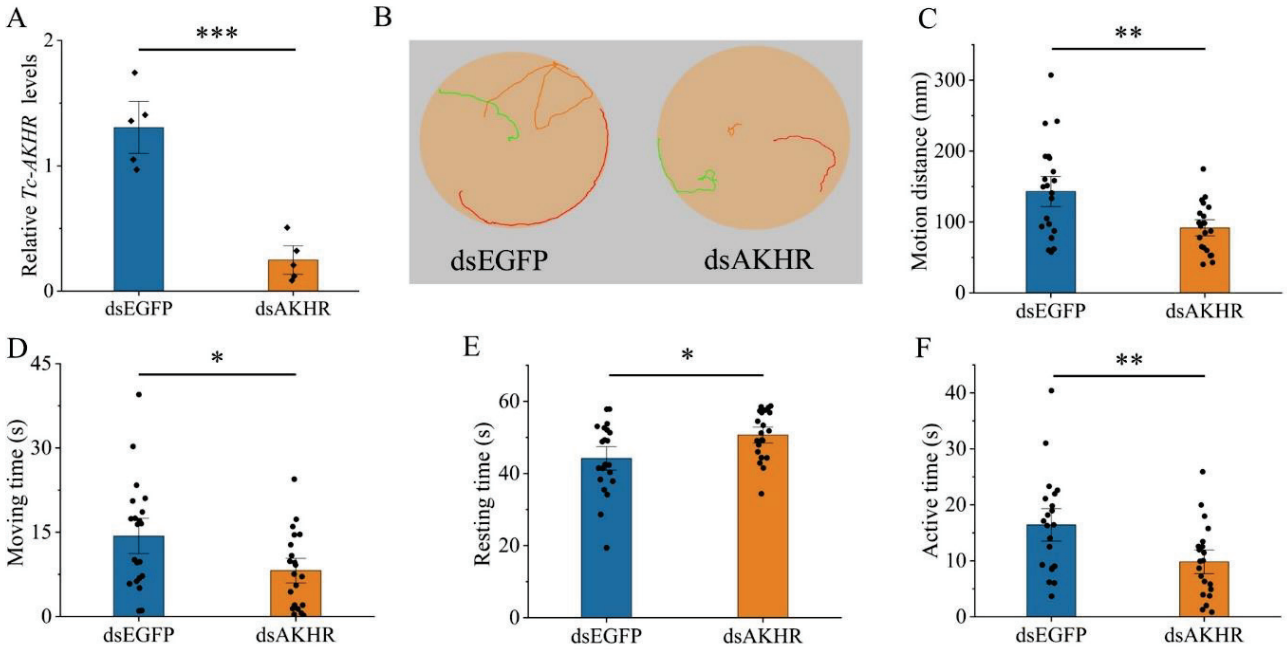


Figure 5. Effect of dsAKHR injected into three-day-old adults on the gene transcript levels and motion situation of *Tc-AKHR*. The data were analyzed using Student's *t*-test or the Mann–Whitney U test. Date are means ± SE. * $p < 0.05$, ** $p < 0.01$, and *** $p < 0.001$. (**A**) Relative expression levels of *Tc-AKHR* at 48 h after injection with dsAKHR; dsEGFP was used as a control. (**B**) Movement trajectory after injection with dsAKHR. (**C**) Changes in motion distance. (**D**) Changes in moving time. (**E**) Changes in resting time. (**F**) Changes in active time.

The subsequent tracking of adult movement behavior demonstrated that the locomotor trajectories of RNAi-treated groups (dsAKHR and dsAKHs) were significantly shorter than those of the control group (dsEGFP) (Figures 5B, 6B and 7B). Further quantitative analysis indicated a marked change in key locomotor parameters, including total motion distance, movement duration, resting time, and active time, across all RNAi groups compared to controls ($p < 0.05$). Specifically, motion distance was significantly reduced with dsAKHR (91.73 mm, $p < 0.01$), dsAKH1 (153.28 mm, $p < 0.01$), and dsAKH2 (99.73 mm, $p < 0.05$) relative to dsEGFP controls (140.62 mm, 244.86 mm, and 134.57 mm, respectively) (Figures 5C, 6C and 7C). Similarly, movement duration was significantly decreased with dsAKHR (8.17 s, $p < 0.05$), dsAKH1 (18.53 s, $p < 0.05$), and dsAKH2 (9.80 s, $p < 0.05$) compared to the control groups (14.33 s, 29.17 s, and 15.30 s, respectively) (Figures 5D, 6D and 7D).

Furthermore, RNAi treatment significantly altered resting and active times. Resting times with dsAKHR (50.66 s, $p < 0.05$), dsAKH1 (39.99 s, $p < 0.05$), and dsAKH2 (48.45 s, $p < 0.05$) were significantly longer than those in controls (44.17 s, 30.64 s, and 42.98 s, respectively) (Figures 5E, 6E and 7E). Active time also exhibited significant reductions

in dsAKHR (9.82 s, $p < 0.01$), dsAKH1 (10.16 s, $p < 0.05$), and dsAKH2 (12.60 s, $p < 0.05$) relative to control values (16.43 s, 17.62 s, and 18.10 s, respectively) (Figures 5F, 6F and 7F).

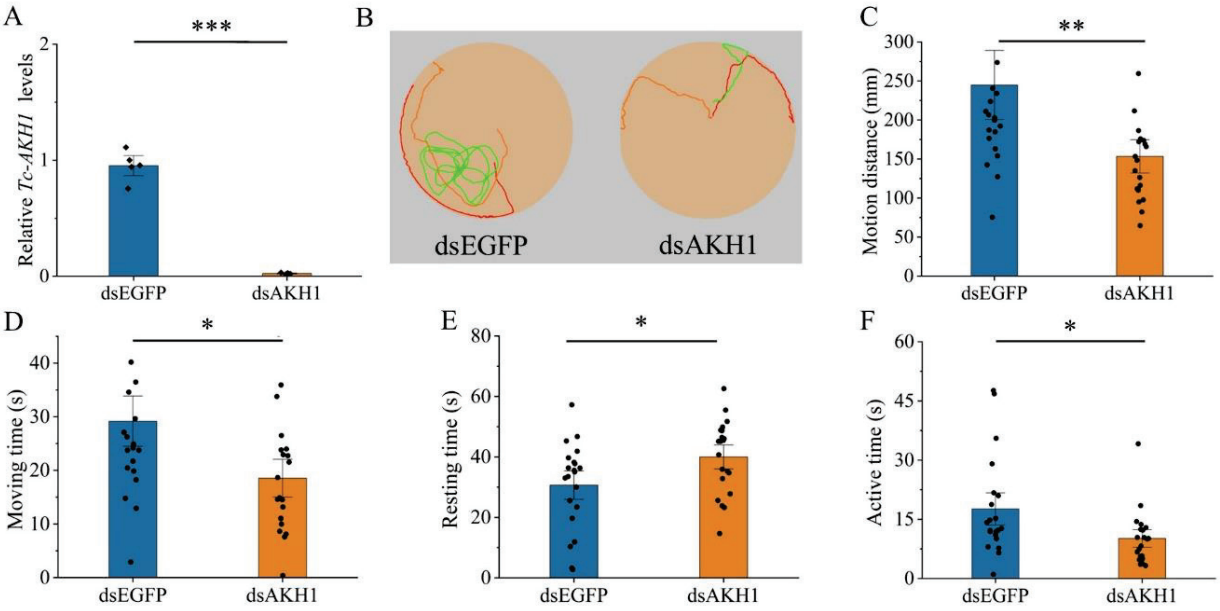


Figure 6. Effect of dsAKH1 injected into three-day-old adults on the gene transcript levels and motion situation of Tc-AKH1. Date are means ± SE. * $p < 0.05$, ** $p < 0.01$, and *** $p < 0.001$. (**A**) Relative expression levels of Tc-AKH1 at 48 h after injection with dsAKH1; dsEGFP was used as a control ($n = 5$). (**B**) Movement trajectory after injection with dsAKH1. (**C**) Changes in motion distance. (**D**) Changes in moving time. (**E**) Changes in resting time. (**F**) Changes in active time. The data in (**A**,**D**,**E**) were analyzed using Student's *t*-test. The data in (**C**,**F**) were analyzed using the Mann–Whitney U test.

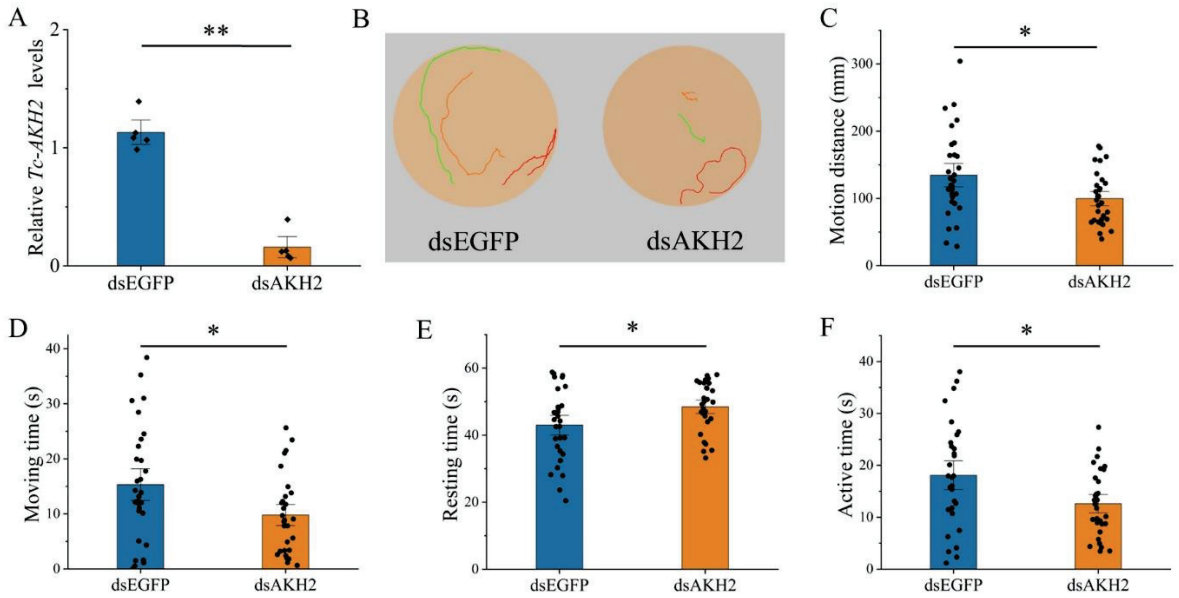


Figure 7. Effect of dsAKH2 injected into three-day-old adults on the gene transcript levels and motion situation of Tc-AKH2. Date are means ± SE. * $p < 0.05$, and ** $p < 0.01$. (**A**) Relative expression levels of Tc-AKH2 at 48 h after injection with dsAKH2; dsEGFP was used as a control ($n = 5$). The data were analyzed using the Mann–Whitney U test. (**B**) Movement trajectory after injection with dsAKH2. (**C**) Changes in motion distance. (**D**) Changes in moving time. (**E**) Changes in resting time. (**F**) Changes in active time. The data in (**C**–**F**) were analyzed using Student's *t*-test.

4. Discussion

In this study, two AKH genes and a single *AKHR* gene were identified in *T. castaneum*. In most insect species, one or two genes that encode AKH precursor genes have been identified, whereas, for instance, in *L. migratoria*, four AKH-encoding genes have been identified. So far, the evolutionary dynamics and functional divergence of AKH genes in regulating species-specific behavioral adaptations remain unknown. Also, it is unclear whether gene duplication leads to functional differentiation in *T. castaneum*. *Tc-AKHR* shares high similarity with AKHRs from other insect orders, including Lepidoptera and Diptera. Phylogenetic analysis confirmed that *T. castaneum AKHR* is orthologous to AKHRs in other insects. Functional calcium reporter assays showed that *Tc-AKHR*-transfected CHO cells responded to two AKH peptides in a concentration-dependent manner, consistent with previous findings in *D. melanogaster*, which confirmed the specificity of receptors for their corresponding ligands [22]. However, the use of CHO cells as a heterologous expression system raises inherent questions regarding the reconstitution of the endogenous cellular milieu of *T. castaneum*, which may bias receptor signal kinetics. Further research could use compatible *T. castaneum* cells. The *Tc-AKH1*, *Tc-AKH2*, and *Tc-AKHR* expressions were assessed in different tissues of adults according to data from the Beetle Atlas database. We found very high levels of *Tc-AKHs* only in the brain, which is not strange for a neuropeptide gene. For *Tc-AKHR*, high levels of expression were found in the fat body, which is the principal insect organ that stores both fat and sugar reserves, consistent with findings in other species [5,23–25]. The fat body is a key organ for lipid storage and energy regulation, and AKHR is known to mobilize lipids from this organ [26]. *Tc-AKHR* was also highly expressed in the carcass, suggesting its involvement in other physiological functions, such as reproduction, muscle tonus, and heart rate [27–29].

RNAi techniques were applied to suppress the expression of *Tc-AKH1*, *Tc-AKH2*, and *Tc-AKHR* in *T. castaneum*, resulting in decreases in locomotor activity. The silencing of *Tc-AKH1* or *Tc-AKH2* produced the same results in locomotion; therefore, we did not find evidence to support the notion that the gene duplication of AKH led to functional differentiation. It is hypothesized that the duplication of the AKH gene resulted in a compensatory effect on locomotion, potentially enhancing its adaptive significance. The influence of AKH on *T. castaneum*'s locomotion is likely attributed to its role in energy regulation. AKH specifically binds to its receptor, triggering enzymatic activation, including glycogen phosphorylase and triglyceride lipases, which facilitate energy mobilization [30,31]. The primary function of AKH is to induce lipid and carbohydrate release from the fat body. The lipid mobilization mechanism is mediated by AKH through triglyceride lipase [32,33]. In parallel, an alternative lipolytic pathway involves Brummer lipase, an enzyme homologous to mammalian adipose triglyceride lipase. *Drosophila* flies deficient in Brummer exhibit impaired lipid mobilization and excessive fat accumulation, while AKH responds to acute lipid demands. Brummer maintains basal lipid homeostasis and contributes to energy supply during metabolic exigencies [34,35]. AKH-mediated lipid mobilization is facilitated by intracellular signaling cascades [36]. One pathway involves calcium release from the endoplasmic reticulum, which acts as a crucial lipid mobilization signal. Another pathway entails AKH binding to its receptor on fat body cells, activating adenylate cyclase and increasing cyclic adenosine monophosphate (cAMP) levels. This cascade activates cAMP-dependent protein kinase A, which subsequently phosphorylates lipid droplets, triglyceride lipase, and perilipin 1/lipid storage droplet-1 protein [37]. Collectively, these findings indicate that AKH regulates peripheral energy reserves and locomotor activity via an intricate signaling network. Further research is necessary to unravel the molecular mechanisms behind this network.

In conclusion, the molecular characteristics of AKHs and AKHR in *T. castaneum*, along with their pharmacological properties, have been described. Through RNAi-mediated suppression of *AKHs* or *AKHR*, the pivotal role of AKH/AKHR signaling in locomotor activity has been confirmed. These findings not only strengthen the established function of AKH in locomotor control but also offer mechanistic insights into the neuromodulatory regulation of insect movement. This contributes to a more comprehensive understanding of neurohormonal pathways related to locomotion.

Supplementary Materials: The following supporting information can be downloaded at: https://www.mdpi.com/article/10.3390/insects16040407/s1. Figure S1. (A) Effect of dsAKH1 injected into three-day-old adults on the gene transcript levels of Tc-AKH2. (B) Effect of dsAKH2 injected into three-day-old adults on the gene transcript levels of Tc-AKH1; Video S1. Motion video after injection with dsAKHR; Video S2. Motion video after injection with dsAKH1; Video S3. Motion video after injection with dsAKH2. Table S1. Primers of this study.

Author Contributions: R.-H.L., X.-D.P., S.-H.G., G.S. and T.-X.L. conceived the study and participated in its design. R.-H.L., X.-D.P. and S.-Q.W. performed the experiments. R.-H.L., X.-D.P. and S.-H.G. analyzed the data. R.-H.L., X.-D.P., S.-H.G., G.S. and T.-X.L. wrote the paper. All authors have read and agreed to the published version of the manuscript.

Funding: This research was funded by Guizhou Provincial Science and Technology Plan Project, grant number Qiankehe Platform Talents-BQW [2024] 008, and Guizhou University Students' Innovation and Entrepreneurship Training Program, grant number gzugc2024034.

Data Availability Statement: The original contributions presented in this study are included in the article and supplementary material. Further inquiries can be directed to the corresponding author.

Conflicts of Interest: The authors declare that the research was conducted in the absence of any commercial or financial relationships that could be construed as potential conflicts of interest.

References

1. Huston, S.J.; Jayaraman, V. Studying sensorimotor integration in insects. *Curr. Opin. Neurobiol.* **2011**, *21*, 527–534. [CrossRef] [PubMed]
2. Dickinson, M.H.; Farley, C.T.; Full, R.J.; Koehl, M.A.; Kram, R.; Lehman, S. How animals move: An integrative view. *Science* **2000**, *288*, 100–106. [CrossRef] [PubMed]
3. Chen, X.; Peterson, J.; Nachman, R.J.; Ganetzky, B. Drosulfakinin activates CCKLR-17D1 and promotes larval locomotion and escape response in *Drosophila*. *Fly* **2012**, *6*, 290–297. [CrossRef] [PubMed]
4. Nässel, D.R.; Zandawala, M. Recent advances in neuropeptide signaling in *Drosophila*, from genes to physiology and behavior. *Prog. Neurobiol.* **2019**, *179*, 101607. [CrossRef]
5. Hou, L.; Yang, P.; Jiang, F.; Liu, Q.; Wang, X.; Kang, L. The neuropeptide F/nitric oxide pathway is essential for shaping locomotor plasticity underlying locust phase transition. *eLife* **2017**, *6*, e22526. [CrossRef]
6. Wang, S.; Li, M.; Wang, N.; Song, Y.; Peng, X.; Chen, M. Functional characterization of two DH44R genes associated with starvation and desiccation in *Rhopalosiphum padi* (Hemiptera: Aphididae). *Pestic. Biochem. Physiol.* **2024**, *201*, 105902. [CrossRef]
7. Kahsai, L.; Martin, J.R.; Winther, A.M. Neuropeptides in the *Drosophila* central complex in modulation of locomotor behavior. *J. Exp. Biol.* **2010**, *213*, 2256–2265. [CrossRef]
8. Stone, J.V.; Mordue, W.; Batley, K.E.; Morris, H.R. Structure of locust adipokinetic hormone, a neurohormone that regulates lipid utilisation during flight. *Nature* **1976**, *263*, 207–211. [CrossRef]
9. Marco, H.G.; Gäde, G. Structure and function of adipokinetic hormones of the large white butterfly *Pieris brassicae*. *Physiol. Entomol.* **2017**, *42*, 103–112. [CrossRef]
10. Kong, X.; Xie, Y.; Cao, Y.; Li, Y.; Zhang, Y.; Zou, Z.; Xia, B.; Xin, T. Expression and functional analysis of adipokinetic hormone reveal its different roles in larval development and female fecundity in *Panonychus citri* (McGregor) (Acari: Tetranychidae). *Insect Mol. Biol.* **2024**, *online ahead of print*. [CrossRef]

11. Hou, Q.L.; Chen, E.H.; Jiang, H.B.; Wei, D.D.; Gui, S.H.; Wang, J.J.; Smagghe, G. Adipokinetic hormone receptor gene identification and its role in triacylglycerol mobilization and sexual behavior in the oriental fruit fly (*Bactrocera dorsalis*). *Insect Biochem. Mol. Biol.* **2017**, *90*, 1–13. [CrossRef] [PubMed]
12. Sajwan, S.; Sidorov, R.; Stašková, T.; Žaloudíková, A.; Takasu, Y.; Kodrík, D.; Zurovec, M. Targeted mutagenesis and functional analysis of adipokinetic hormone-encoding gene in *Drosophila*. *Insect Biochem. Mol. Biol.* **2015**, *61*, 79–86. [CrossRef] [PubMed]
13. Tang, B.; Cheng, Y.; Li, Y.; Li, W.; Ma, Y.; Zhou, Q.; Lu, K. Adipokinetic hormone regulates cytochrome P450-mediated imidacloprid resistance in the brown planthopper, *Nilaparvata lugens*. *Chemosphere* **2020**, *259*, 127490. [CrossRef] [PubMed]
14. Jiang, S.; Marco, H.G.; Scheich, N.; He, S.; Wang, Z.; Gäde, G.; McMahon, D.P. Comparative analysis of adipokinetic hormones and their receptors in Blattodea reveals novel patterns of gene evolution. *Insect Mol. Biol.* **2023**, *32*, 615–633. [CrossRef]
15. Richards, S.; Gibbs, R.A.; Weinstock, G.M.; Brown, S.J.; Denell, R.; Beeman, R.W.; Gibbs, R.; Bucher, G.; Friedrich, M.; Grimmelikhuijzen, C.J.; et al. The genome of the model beetle and pest *Tribolium castaneum*. *Nature* **2008**, *452*, 949–955. [CrossRef]
16. Walski, T.; Van Damme, E.J.M.; Smargiasso, N.; Christiaens, O.; De Pauw, E.; Smagghe, G. Protein N-glycosylation and N-glycan trimming are required for postembryonic development of the pest beetle *Tribolium castaneum*. *Sci. Rep.* **2016**, *6*, 35151. [CrossRef]
17. Pang, X.D.; Li, Y.S.; Lu, R.H.; Smagghe, G.; Liu, T.X.; Gui, S.H. miR-7977 regulates the locomotor behavior by targeting diuretic hormone and SIFamide receptors in *Tribolium castaneum*. *Int. J. Biol. Macromol.* **2025**, *online ahead of print*. [CrossRef]
18. Gui, S.H.; Jiang, H.B.; Liu, X.Q.; Xu, L.; Wang, J.J. Molecular characterizations of natalisin and its roles in modulating mating in the oriental fruit fly, *Bactrocera dorsalis* (Hendel). *Insect Mol. Biol.* **2017**, *26*, 103–112. [CrossRef]
19. Lord, J.C.; Hartzer, K.; Toutges, M.; Oppert, B. Evaluation of quantitative PCR reference genes for gene expression studies in *Tribolium castaneum* after fungal challenge. *J. Microbiol. Methods* **2010**, *80*, 219–221. [CrossRef]
20. Livak, K.J.; Schmittgen, T.D. Analysis of relative gene expression data using real-time quantitative PCR and the 2(-delta delta C(T)) method. *Methods* **2001**, *25*, 402–408. [CrossRef]
21. Noh, M.Y.; Beeman, R.W.; Arakane, Y. RNAi-based functional genomics in *Tribolium castaneum* and possible application for controlling insect pests. *Entomol. Res.* **2012**, *42*, 1–10. [CrossRef]
22. Park, Y.; Kim, Y.J.; Adams, M.E. Identification of G protein-coupled receptors for *Drosophila* PRXamide peptides, CCAP, corazonin, and AKH supports a theory of ligand-receptor coevolution. *Proc. Natl. Acad. Sci. USA* **2002**, *99*, 11423–11428. [CrossRef] [PubMed]
23. Staubli, F.; Jorgensen, T.J.; Cazzamali, G.; Williamson, M.; Lenz, C.; Sondergaard, L.; Roepstorff, P.; Grimmelikhuijzen, C.J. Molecular identification of the insect adipokinetic hormone receptors. *Proc. Natl. Acad. Sci. USA* **2002**, *99*, 3446–3451. [CrossRef] [PubMed]
24. Ziegler, R.; Isoe, J.; Moore, W.; Riehle, M.A.; Wells, M.A. The putative AKH receptor of the tobacco hornworm, *Manduca sexta*, and its expression. *J. Insect Sci.* **2011**, *11*, 40. [CrossRef]
25. Konuma, T.; Morooka, N.; Nagasawa, H.; Nagata, S. Knockdown of the adipokinetic hormone receptor increases feeding frequency in the two-spotted cricket *Gryllus bimaculatus*. *Endocrinology* **2012**, *153*, 3111–3122. [CrossRef]
26. Alves-Bezerra, M.; De Paula, I.F.; Medina, J.M.; Silva-Oliveira, G.; Medeiros, J.S.; Gäde, G.; Gondim, K.C. Adipokinetic hormone receptor gene identification and its role in triacylglycerol metabolism in the blood-sucking insect *Rhodnius prolixus*. *Insect Biochem. Mol. Biol.* **2016**, *69*, 51–60. [CrossRef]
27. Lorenz, M.W. Adipokinetic hormone inhibits the formation of energy stores and egg production in the cricket *Gryllus bimaculatus*. *Comp. Biochem. Physiol. B Biochem. Mol. Biol.* **2003**, *136*, 197–206. [CrossRef]
28. O'Shea, M.; Witten, J.; Schaffer, M. Isolation and characterization of two myoactive neuropeptides: Further evidence of an invertebrate peptide family. *J. Neurosci.* **1984**, *4*, 521–529. [CrossRef]
29. Scarborough, R.M.; Jamieson, G.C.; Kalish, F.; Kramer, S.J.; McEnroe, G.A.; Miller, C.A.; Schooley, D.A. Isolation and primary structure of two peptides with cardioacceleratory and hyperglycemic activity from the corpora cardiaca of *Periplaneta americana*. *Proc. Natl. Acad. Sci. USA* **1984**, *81*, 5575–5579. [CrossRef]
30. Van der Horst, D.J. Insect adipokinetic hormones: Release and integration of flight energy metabolism. *Comp. Biochem. Physiol. B Biochem. Mol. Biol.* **2003**, *136*, 217–226. [CrossRef]
31. Toprak, U. The role of peptide hormones in insect lipid metabolism. *Front. Physiol.* **2020**, *11*, 434. [CrossRef] [PubMed]
32. Arrese, E.L.; Patel, R.T.; Soulages, J.L. The main triglyceride-lipase from the insect fat body is an active phospholipase A (1): Identification and characterization. *J. Lipid Res.* **2006**, *47*, 2656–2667. [CrossRef] [PubMed]
33. Arrese, E.L.; Soulages, J.L. Insect fat body: Energy, metabolism, and regulation. *Annu. Rev. Entomol.* **2010**, *55*, 207–225. [CrossRef]
34. Grönke, S.; Mildner, A.; Fellert, S.; Tennagels, N.; Petry, S.; Müller, G.; Jäckle, H.; Kühnlein, R.P. Brummer lipase is an evolutionary conserved fat storage regulator in *Drosophila*. *Cell Metab.* **2005**, *1*, 323–330. [CrossRef]
35. Grönke, S.; Müller, G.; Hirsch, J.; Fellert, S.; Andreou, A.; Haase, T.; Jäckle, H.; Kühnlein, R.P. Dual lipolytic control of body fat storage and mobilization in *Drosophila*. *PLoS Biol.* **2007**, *5*, e137. [CrossRef]

36. Canavoso, L.E.; Wells, M.A. Role of lipid transfer particle in delivery of diacylglycerol from midgut to lipophorin in larval *Manduca sexta*. *Insect Biochem. Mol. Biol.* **2001**, *31*, 783–790. [CrossRef]
37. Arrese, E.L.; Mirza, S.; Rivera, L.; Howard, A.D.; Chetty, P.S.; Soulages, J.L. Expression of lipid storage droplet protein-1 may define the role of AKH as a lipid mobilizing hormone in *Manduca sexta*. *Insect Biochem. Mol. Biol.* **2008**, *38*, 993–1000. [CrossRef]

Disclaimer/Publisher's Note: The statements, opinions and data contained in all publications are solely those of the individual author(s) and contributor(s) and not of MDPI and/or the editor(s). MDPI and/or the editor(s) disclaim responsibility for any injury to people or property resulting from any ideas, methods, instructions or products referred to in the content.

insects

MDPI

Article

Rapid and Economic Baculovirus Titer Determination Using a Novel Transgenic Sf9-QE Cell Line

Hyuk-Jin Moon [1,2], Hyun-Jung Kim [1], Dong-Hyun Lee [1,2], Seo-Yeong Mun [1] and Soo-Dong Woo [1,2,3,*]

[1] Department of Agricultural Biology, College of Agriculture, Life & Environment Science, Chungbuk National University, Cheongju 28644, Republic of Korea; qlfmzks@chungbuk.ac.kr (H.-J.M.); ajee0216@naver.com (H.-J.K.); 1869oz80@gmail.com (D.-H.L.); msyoung7728@naver.com (S.-Y.M.)
[2] IPBL Inc., Cheongju 28644, Republic of Korea
[3] Biomedical Research Institute, Chungbuk National University Hospital, Cheongju 28644, Republic of Korea
* Correspondence: sdwoo@cbnu.ac.kr; Tel.: +82-43-261-2553

Simple Summary: This study introduces a novel direct titration method for rapidly and economically determining baculovirus titers using a specially engineered Sf9-QE cell line. Sf9-QE transgenic cells were used because they express fluorescence early after viral infection, providing a prompt phenotype; this rapid expression was confirmed to be due to the integration of at least seven copies of the transgene into the cell genome. In addition, the direct titration method was validated using Sf9-QE cells in the three days after subculturing, demonstrating that efficient viral titer quantification is possible between 15 and 30 h after viral infection. Compared to conventional titration methods, similar titer values were obtained, indicating that the time required for protein production using recombinant baculoviruses can be significantly reduced. This new virus quantification method will be very useful in the production of and research into various medically and pharmaceutically useful recombinant proteins using insect viruses.

Abstract: A baculovirus expression system (BES) for the production of recombinant proteins requires rapid and easy virus titer determination. In this study, a novel direct titration method was developed using a novel Sf9-QE cell line to easily and economically determine virus titers in a short time. This direct titration method can determine virus titers by directly counting the initially infected cells. This method requires the rapid identification of the initial virus-infected cells. The genome of Sf9-QE cells, which fluoresce upon virus infection, was found to contain at least seven copy numbers of the enhanced green fluorescent protein (EGFP) transgene. This result suggests that Sf9-QE cells in the early stages of virus infection can be identified by the high expression of EGFP. It was also shown that for accurate virus titration using the direct titration method, Sf9-QE cells should be used within 3 d of subculturing. Additionally, counting fluorescent cells to establish virus infection should be performed within 15 to 30 h after virus infection for reliable virus titration. The direct titration method using Sf9-QE cells provides a rapid, reliable, and cost-effective alternative for determining baculovirus titers in BES research.

Keywords: baculovirus; virus titer; direct titration; Sf9-QE

1. Introduction

The baculovirus expression system (BES), which utilizes entomopathogenic baculoviruses and insect cells, is a highly valuable system for the production of various recombinant pro-

teins [1]. Compared to other host-based expression systems, the BES offers several advantages, including cost-effectiveness, biosafety for researchers, and the ability to provide post-translational modifications of recombinant proteins similar to those found in mammalian expression systems [2]. For the efficient production of target proteins in a BES, it is crucial to establish optimal viral infection conditions [3]; therefore, optimizing the multiplicity of infection (MOI)—the degree of viral infection—is essential to ensure the efficient production of target proteins by maintaining a balance between cell viability and virus production [4].

Accurate virus titration is essential for optimizing the MOI during virus infection. Various virus titration methods, including plaque assays [5], end-point dilution assays involving $TCID_{50}$ (tissue culture infective dose 50) [6], quantitative PCR (qPCR) [7], flow cytometry [8], and enzyme-linked immunosorbent assays (ELISAs) [9], have been developed and are widely used; however, each method has its limitations, such as specific equipment requirements, technical difficulties, or accuracy issues related to experimenter proficiency. Among these methods, the end-point dilution assay involving $TCID_{50}$ is the most commonly used. This method calculates the virus titer by performing serial dilutions of the virus and infecting insect cells, followed by determining the ratio of infected to uninfected wells [10]. This method also allows for accurate virus titer determination even at very low virus concentrations and provides statistically reliable data; however, because this method statistically determines virus titers based on the observation of the cytopathic effect (CPE), it relies on visual observation to determine infection, which introduces subjective interpretation by experimenters, leading to potential variability in the results [6].

To overcome the limitations of the described methods, a transgenic cell line, Sf9-ET, was developed based on the Sf9 insect cell line, which can express enhanced green fluorescent protein (EGFP) upon infection with a baculovirus [11]. This allowed for the relatively easy identification of virus infections under fluorescence microscopy compared to the CPE. Nevertheless, challenges remained, including the long time required for titration due to low fluorescence expression. Hence, the Sf9-QE transgenic cell line was developed to overcome this shortcoming [12]. Sf9-QE cells utilize a combination of regulatory elements, including the homologous region 3 (hr3), *39k* promoter, and *p10* promoter, for a more efficient expression of EGFP. As a result, Sf9-QE cells can complete titration earlier than Sf9-ET cells due to the rapid and strong expression of EGFP; however, the final virus titer determination still requires 6.0 to 6.3 days.

Therefore, in this study, we aimed to develop a new titration method, the direct titration method, with a dramatically reduced time required to determine titers using the Sf9-QE cell line (Figure 1). In the plaque assay, the virus is directly titrated by the number of plaques formed after serial dilution and the inoculation of the virus to be titrated [5]. Using the same principle, our hypothesis was that virus titer determination would be possible if the number of virus-infected cells could be directly counted after serial dilutions of the virus to be titrated; however, unlike the plaque assay, reliable virus titer determination was expected to be possible only if the phenotype identified with EGFP during the primary infection in Sf9-QE cells could be confirmed before the phenotype after the secondary infection of the virus. The observation of EGFP expression in the Sf9-QE cells as early as one day post-infection (d.p.i.) showed the feasibility of such virus titer determination [12]. It has been reported that the budding of baculoviruses occurs from about 17 to 20 h after primary virus infection, with the infection of other cells and the expression of the phenotype occurring after additional time [13]. The rapid and robust expression of the phenotype is required to confirm the phenotype of the primary infection of the virus prior to the expression of the phenotype of the cells after the secondary infection. In the case of Sf9-QE, the early expression of EGFP has already been demonstrated as early as one

day after viral infection by the *39k* promoter, a delayed-early promoter that is activated by the immediately early 1 (IE–1) protein and operates from 3 to 6 h after infection [14,15]. Additionally, although the rapid expression of EGFP at 1 d.p.i. was confirmed, it was believed that the copy number of the transgene present in the transfected cell line would have a major influence on the quantitative expression; therefore, the determination of the copy number of the EGFP transgene in the Sf9-QE cells would further confirm the feasibility of developing a rapid titration method using Sf9-QE cells.

This study presents a new direct titration method that utilizes the distinct properties of the Sf9-QE cell line to overcome the limitations of traditional virus titration techniques through a cost-effective, rapid process while minimizing subjectivity.

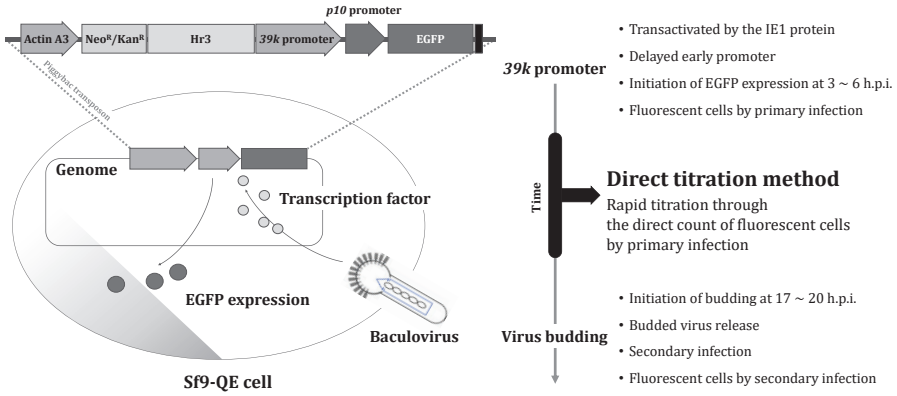


Figure 1. Principle and strategy of the direct titration method for baculovirus titer determination using Sf9-QE cells. Sf9-QE cells fluoresce only upon viral infection. In Sf9-QE cells, the EGFP gene is expressed by the early promoter of the virus, so fluorescence can occur early after viral infection. Secondary viral infection (cell-to-cell infection) can occur from 17 h after the primary viral infection; therefore, theoretically, it would take at least 20 h for the Sf9-QE cells to fluoresce upon secondary viral infection. Virus titers can be determined by directly counting fluorescent cells upon primary infection before fluorescence occurs upon secondary infection.

2. Materials and Methods

2.1. Cells and Viruses

The *Spodoptera frugiperda* cell line Sf9 and the transgenic cell line Sf9-QE were cultured at 27 °C using an Sf–900™ II SFM medium (Gibco, Grand Island, NY, USA) and an Sf–900™ II SFM medium supplemented with G418 (Invitrogen, Carlsbad, CA, USA), respectively. The viruses used consisted of rMultibac, rAc-polh-TEVp, rAc-polh-CVA6-P1, and rAc-polh-RSV-F. rMultibac was generated using Multibac (Geneva Biotech, Geneva, Switzerland), a bacmid derived from *Autographa californica* nucleopolyhedrovirus (AcMNPV-E2, GenBank No. KM667940.1). rAc-polh-TEVP, rAc-polh-CVA6-P1, and rAc-polh-RSV-F are recombinant viruses that express the protease of the tobacco etch virus, the P1 protein of Coxsackievirus A6, and the fusion (F) protein of the respiratory syncytial virus under a *polyhedrin* promoter, respectively (Figure S1).

2.2. Cell Genomic DNA Extraction

Genomic DNA extraction from Sf9-QE cells was performed using an AccuPrep Genomic DNA Extraction Kit (Bioneer, Daejeon, Republic of Korea) according to the manufacturer's instructions. Briefly, cells were collected by centrifugation at 4000 rpm for 5 min, and the supernatant was discarded. The cell pellet was washed with PBS (1 X) and centrifuged under the same conditions. After removing the supernatant, the cell pellet was resuspended in PBS (1 X). Cells were lysed by adding the provided lysis buffer, followed by the addition of absolute ethanol to the lysate. The mixture was transferred to a spin

column and centrifuged at 8000 rpm for 1 min. The column membrane was washed with the provided wash buffer and subjected to a final centrifugation at 13,000 rpm for 1 min to remove the remaining ethanol. The column was then placed into a new microcentrifuge tube, and 50 μL of nuclease-free water was added. The column was centrifuged at 8000 rpm for 1 min to elute the genomic DNA.

2.3. Quantitative Real-Time PCR

To estimate the copy number of the transgene, qPCR was conducted using a QuanStudio1 Real-Time PCR system (Thermo Fisher Scientific, Waltham, MA, USA) with Power SYBR™ Green PCR Master Mix (Thermo Fisher Scientific, Waltham, MA, USA) according to the manufacturer's instructions. Genomic DNA extracted from Sf9-QE cells was serially diluted 2-fold to generate five different concentrations. Each qPCR reaction was performed in a total volume of 20 μL, consisting of 1 μL of template DNA from each concentration, 10 μL of Power SYBR™ Green PCR Master Mix, 1 μL each of forward and reverse primer for the amplification of the EGFP transgene and reference genes, and nuclease-free water to adjust the final volume. Amplification was performed with an initial denaturation at 95 °C for 2 min, followed by 40 cycles of denaturation at 95 °C for 1 s and annealing at 60 °C for 30 s, and a melt-curve analysis was conducted after amplification at 95 °C for 15 s, 60 °C for 1 min, and 95 °C for 15 s. Each reaction was performed in triplicate.

2.4. End-Point Dilution Assay Involving $TCID_{50}$

To perform the end-point dilution assay involving $TCID_{50}$ based on the Reed–Muench method [6], Sf9-QE cells were distributed at a density of 2.0×10^4 cells/90 μL per well in a 96-well cell culture plate. The virus was serially diluted using an Sf–900™ II SFM medium, and 10 μL of the virus at each dilution was inoculated into 8 wells of distributed cells. Then, cells were incubated under the same conditions as described above. Six days after virus inoculation, the number of infected and uninfected wells was counted for each virus dilution using a fluorescence microscope, and the virus titer was calculated using $TCID_{50}$.

2.5. Direct Titration Method

Sf9-QE cells were distributed at a density of 2.0×10^4 cells/90 μL per well in a 96-well cell culture plate. The virus was serially diluted using an Sf–900™ II SFM medium, and 10 μL of the virus at each dilution was inoculated into the 3 wells (for 3 repetitions) of distributed cells. Then, the cells were incubated under the same conditions as described above, and the number of cells expressing EGFP was counted using a fluorescence microscope at specific times after infection. The virus titer was calculated by multiplying the average number of cells counted and the viral dilution ratio.

2.6. Statistical Analysis

All statistical analyses were performed using IBM SPSS Statistics version 25 (IBM Corp., Armonk, NY, USA). Descriptive statistics were calculated for each group, including means and standard deviations. To evaluate the significance of differences between groups, a *t*-test was conducted on triplicate experimental groups. A *p*-value of less than 0.05 was considered statistically significant.

3. Results

3.1. Estimation of Transgene Copy Number in Sf9-QE

To determine the copy number of the EGFP gene integrated into the Sf9-QE cells, glyceraldehyde–3-phosphate dehydrogenase (GAPDH) and elongation factor 1-α (EF1α)

genes were selected as candidate reference genes for qPCR normalization. These genes are known to play housekeeping roles in glycolysis and translation elongation, respectively, and are widely used as reference genes due to their consistent and stable expression in Sf9 cells [16]; however, their exact copy numbers have not been reported. The design and specificity evaluation of qPCR primers for GAPDH (GenBank No. KC262638.1), EF1α (GenBank No. U2013.9.1), and EGFP genes was performed using Primer-BLAST (National Center for Biotechnology Information, https://www.ncbi.nlm.nih.gov/tools/primer-blast/ (accessed on 8 January 2025)), and the sequences of primer pairs are shown in Table S1.

As a result, the reliability of the qPCR was confirmed by amplification-curve and melting-curve analysis (Figure 2A,B). The cycle threshold (Ct) values of the EGFP, GAPDH, and EF1α genes were found to be 18.51 ± 0.91, 20.31 ± 0.89, and 21.31 ± 0.92, respectively (Figure 2C). The copy number ratio of the transgene was calculated using the ΔCt method, where ΔCt is defined as the difference between the Ct values of the transgene and the reference gene. The copy number ratio of the EGFP gene to each reference gene was calculated using the following equation [17]:

$$\text{Copy number ratio} = 2^{-\Delta Ct}$$

$$\Delta Ct = Ct_{\text{transgene}} - Ct_{\text{reference gene}}$$

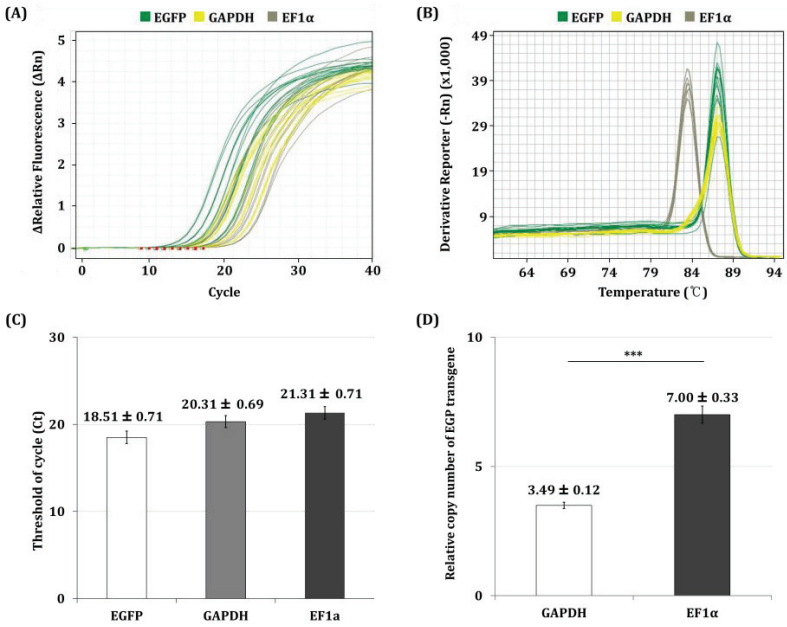


Figure 2. qPCR analysis of the EGFP transgene and reference genes in the Sf9-QE cell genome. To determine the relative copy number of the EGFP transgene in the Sf9-QE cell genome, qPCR was performed using GAPDH and EF1α genes as reference genes. The amplification and melt curves were analyzed to ensure specific and efficient amplification, and the copy number ratio of the EGFP transgene was determined using the ΔCt method. (**A**) Amplification plot of the EGFP transgene and the reference genes in the Sf9-QE cell genome obtained using qPCR. (**B**) Melt curves confirming the specificity of the amplified products. (**C**) Cycle threshold (Ct) values for each gene. (**D**) Calculation of the EGFP transgene copy number ratio relative to the reference genes in the Sf9-QE cell genome. Statistical significance was determined using a *t*-test ($p < 0.05$); *** $p < 0.001$.

Based on the calculations, the copy number ratio of the EGFP gene was determined to be 3.49 ± 0.12 compared to the GAPDH gene and 7.00 ± 0.33 compared to the EF1α gene (Figure 2D). These results indicate that the EGFP transgene is present with approximately

3.5 and approximately 7 times more copies than the respective reference genes, indicating that there are at least seven copies of the EGFP transgene in the Sf9-QE genome; therefore, the high copy number of the EGFP transgene in the Sf9-QE cells suggests that the direct-titration method in this study is likely to be successful due to a large amount of fluorescent protein production.

3.2. Determination of the Cell Condition for the Direct Titration Method

Before determining the virus titer using the direct titration method, the effect of the culture condition of Sf9-QE cells on the level of EGFP expression via virus infection was evaluated. The Sf9-QE cells at one, three, five, and seven days after subculturing were infected with serially diluted viruses, and the number of fluorescent cells was observed at 12 h intervals (Figure 3). The results showed that at 24 h post-infection (h p.i.), EGFP expression was detected in the Sf9-QE cells on all days after subculturing. In particular, fluorescence was observed in cells at one and three days after subculturing, starting at 12 h p.i. The fluorescence intensity increased over time after infection and was most evident at 3 d after subculturing cells.

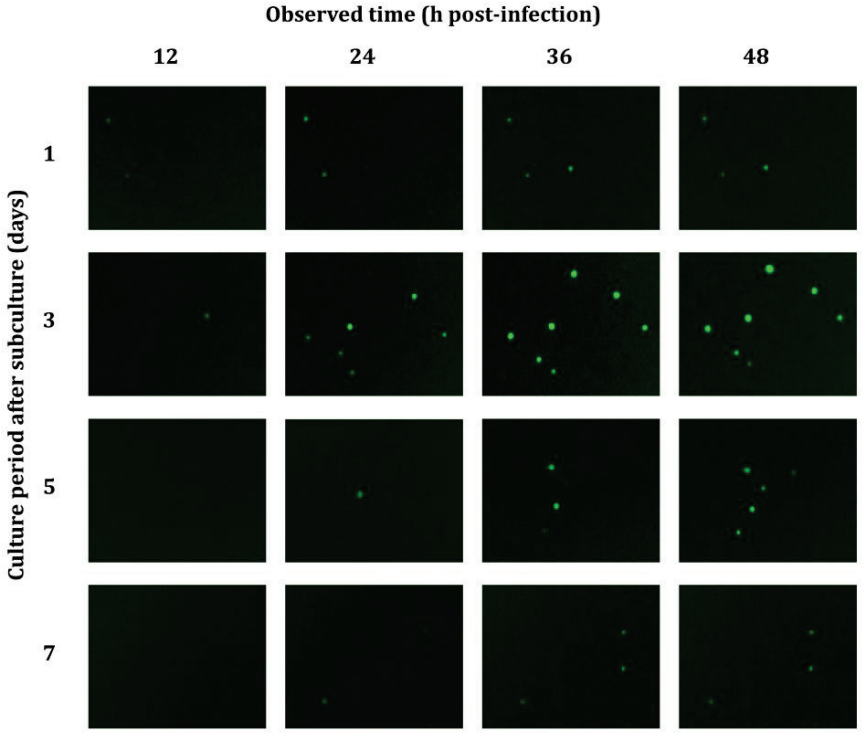


Figure 3. Fluorescence micrographs of Sf9-QE cells via virus infection. Sf9-QE cells were used on days one, three, five, and seven after subculturing. The virus, quantified as 2.39×10^8 PFU/mL by the end-point dilution assay involving the $TCID_{50}$, was diluted to 10–5 and inoculated into Sf9-QE cells. After virus infection, observations were made under a fluorescence microscope at 12 h intervals for up to 48 h.

To determine virus titers via the direct titration method, the number of cells expressing fluorescence was counted. Virus titers were determined based on the following equation using the average number of fluorescent cells counted and the observed dilution ratio:

$$\begin{aligned}\text{Viral titer (number/mL)} &= \mathrm{N} \times 10^{\mathrm{D}} \times 10^{(\text{converted } \mu\text{L to mL})} \times 10^{(\text{ratio of inoculation volume to total volume})} \\ &= \mathrm{N} \times 10^{-\mathrm{D}} \times 10^{3} \times 10^{-1} \\ &= \mathrm{N} \times 10^{-\mathrm{D}+2}\end{aligned}$$

N—average number of fluorescent cells.
10^D—dilution ratio of virus.

The determination of virus titers by the direct titration method showed similar titers when using cells at one and three days after subculturing, but lower virus titers when using cells at five and seven days after subculturing (Figure 4). The virus titer values determined by the direct titration method were compared with the virus titers determined by the end-point dilution assay involving $TCID_{50}$. The results showed that in cells cultured at one and three days after subculturing, the virus titers using each titration method were statistically very similar to each other. Three days after subculturing, the titers in cells were not significantly different when determined at 24 h p.i., whereas one day after subculturing, the titers were not significantly different at any time point, except at 12 h p.i.; however, at five and seven days after subculturing, significant differences in titers determined by each titration method were identified at all time points. These results indicated that the cell condition, i.e., the culture period after subculturing, is very important for the determination of virus titers via the direct titration method using Sf9-QE cells. Additionally, it was shown that there was no significant difference between the virus titer determined by the direct titration method and the PFU titer determined by the end-point dilution assay involving $TCID_{50}$. The direct titration method for virus titration was demonstrated to be feasible using Sf9-QE cells cultured for one or three days after subculturing; however, the time range for virus titer determination by the direct titration method was reevaluated using cells three days after subculturing, which exhibited higher fluorescence intensity, allowing for easier and more accurate counting.

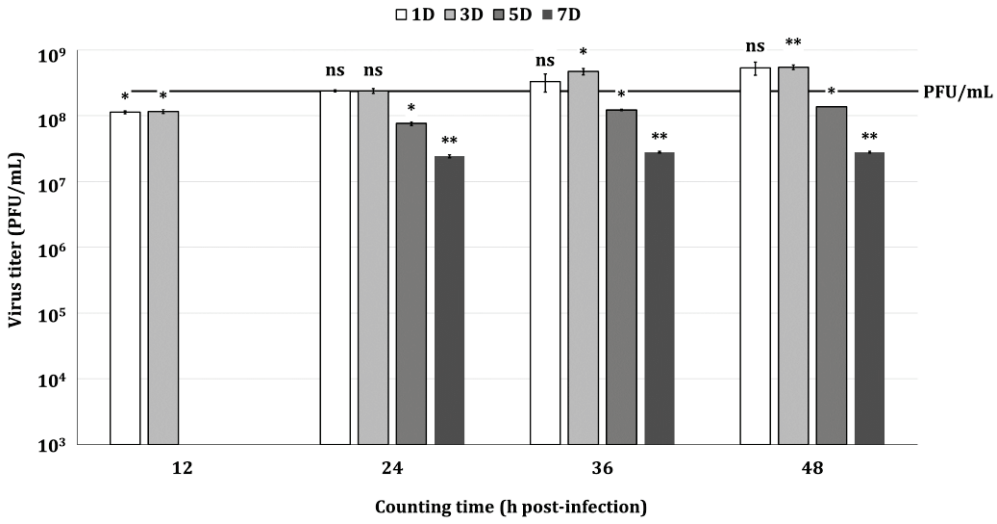


Figure 4. Virus quantification values by the direct titration method using the Sf9-QE cells. Sf9-QE cells were used on days one, three, five, and seven after subculturing. The virus, quantified as 2.39×10^8 PFU/mL (marked as line with PFU/mL) by the end-point dilution assay involving the $TCID_{50}$, was diluted to 10^{-5} and inoculated into the Sf9-QE cells. The number of fluorescent Sf9-QE cells was measured at 12 h intervals for up to 48 h after virus infection. Statistical significance was determined using a *t*-test ($p < 0.05$); ns (not significant, $p \geq 0.05$), * $p < 0.05$, and ** $p < 0.01$.

3.3. Determination of the Optimal Time for the Direct Titration Method

To determine the appropriate observation time range after virus infection for accurate virus titer determination, virus titers were determined by the direct titration method using the Sf9-QE cells three days after subculturing. Virus titers were determined by observing and counting fluorescent cells at 3 h intervals from 12 to 36 h p.i. As a result, the number of fluorescent cells increased over time (Figure 5A). From 15 to 30 h p.i., the virus titers

determined by the direct titration method were not significantly different from those determined by the end-point dilution assay involving $TCID_{50}$ (Figure 5B). In particular, the virus titers determined at 24 h p.i. were the most similar. Thus, it was confirmed that the accurate determination of virus titers by the direct titration method was possible between 15 and 30 h p.i. using the Sf9-QE cells three days after subculturing.

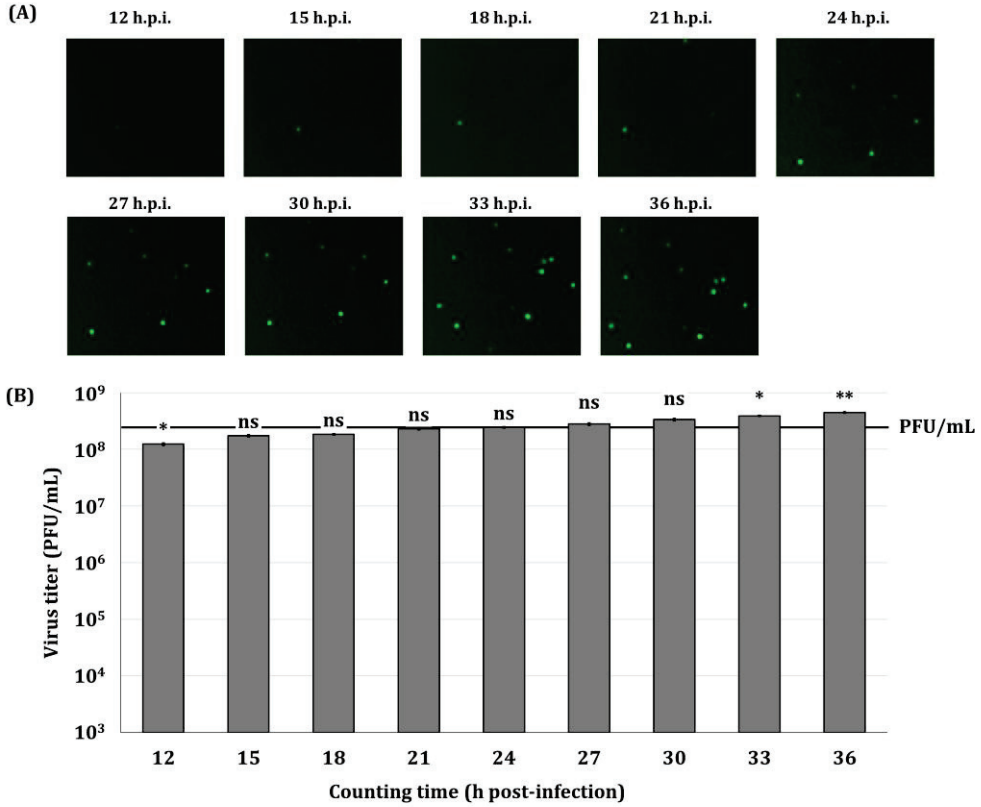


Figure 5. Fluorescence micrographs of Sf9-QE (**A**) with virus infection and virus quantification values (**B**) produced by the direct titration method. Sf9-QE cells at three days after subculturing were used. The virus, quantified as 2.39×10^8 PFU/mL (marked as line with PFU/mL) by the end-point dilution assay involving the $TCID_{50}$, was diluted to 10^{-5} and inoculated into the Sf9-QE cells. Fluorescence observations and cell counting were performed at 3 h intervals from 12 to 36 h after virus infection. Statistical significance was determined using a *t*-test ($p < 0.05$); ns (not significant, $p \geq 0.05$), * $p < 0.05$, and ** $p < 0.01$.

3.4. Viral Titer Values Produced by the Direct Titration Method According to Virus Concentration

Whether the direct titration method for virus titer determination using the Sf9-QE cells was affected by the virus concentration to be titrated was evaluated. After infection of the Sf9-QE cells with viruses showing a 10-fold difference in virus titers and observing fluorescence expression, a higher number of fluorescent cells was observed at lower-virus-dilution concentrations (Figure 6A). Furthermore, the higher the inoculated virus concentration, the more fluorescent cells were observed, indicating that virus titrations using infected cells at higher dilutions are required to accurately count fluorescent cells. In this experiment, when 10^8 PFU/mL of virus was inoculated, counting was easiest in inoculated wells at a 10^{-5} viral dilution, with an average of 24 cells. On the other hand, for the 10^{-4} viral dilution, counting was difficult due to the large number of fluorescent cells, with there being over 200. There was no difference in the virus quantification values between the direct titration method and the end-point dilution assay involving $TCID_{50}$, according to the inoculated virus concentration; therefore, it was confirmed that

virus titer determination using the direct titration method is possible regardless of the concentration of virus to be titrated. However, it appears necessary for the experimenter to select an appropriate virus dilution concentration that is easy to count depending on the concentration of virus to be titrated.

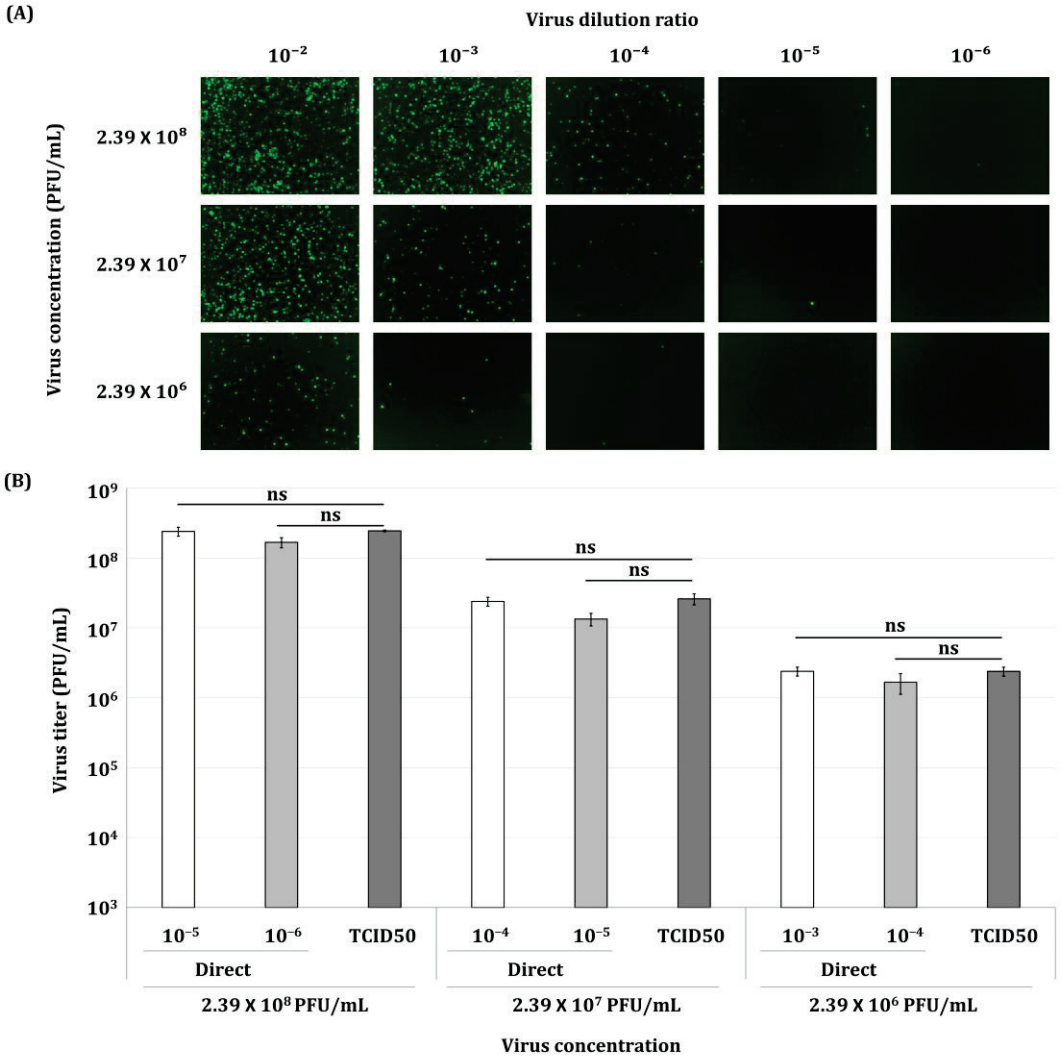


Figure 6. Fluorescence micrographs (**A**) of Sf9-QE cells infected with various concentrations of virus and virus quantification values (**B**) produced by the direct titration method. Sf9-QE cells at three days after subculturing were used. The virus, quantified as 2.39×10^8 PFU/mL by the end-point dilution assay involving the $TCID_{50}$, was diluted 10-fold and 100-fold. Each virus inoculum was serially diluted and then inoculated onto the Sf9-QE cells. Fluorescence observations and cell counting were performed 24 h after virus infection. Virus titers determined by the end-point dilution assay involving the $TCID_{50}$ (TCID50) and the direct titration method (Direct) were compared. The inoculum dilution ratios for each virus used for cell counting in the direct titration method are indicated from 10^{-3} to 10^{-6}. Statistical significance was determined using a *t*-test ($p < 0.05$); ns (not significant, $p \geq 0.05$).

3.5. Titer Determination of Various Viruses Using the Direct Titration Method

The reliability of virus titer determination by the established direct titration method using Sf9-QE cells was evaluated using a variety of recombinant viruses. The titers of all viruses tested showed no significant difference between the results obtained by the direct titration method and the end-point dilution assay involving $TCID_{50}$ (Figure 7). These

results indicate that the titers of various recombinant baculoviruses can be determined quickly and easily using the direct titration method with Sf9-QE cells.

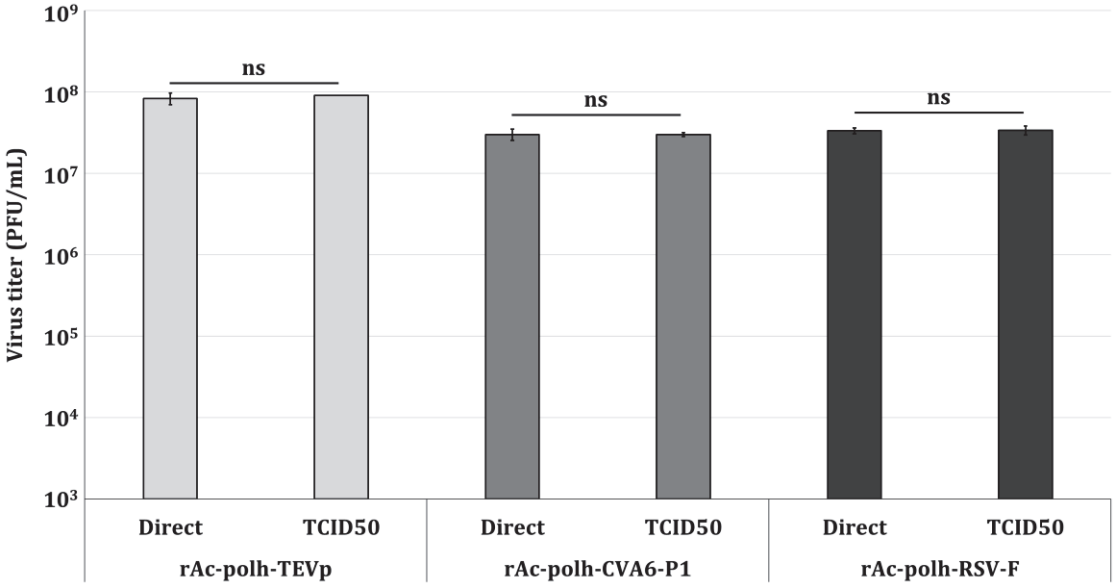


Figure 7. Quantitative titer values of various recombinant viruses produced by the direct titration method. The titers of recombinant viruses producing TEV-protease (rAc-polh-TEVp), CVA6-P1 (rAc-polh-CVA6-P1), and RSV-F proteins (rAc-polh-RSV-F) were determined and compared using the end-point dilution assay involving the $TCID_{50}$ (TCID50) and the direct titration method (Direct). Statistical significance was determined using a *t*-test ($p < 0.05$); ns (not significant, $p \geq 0.05$).

4. Discussion

In this study, a novel direct titration method for virus titer determination was developed that is convenient and enables accurate titration in a short period of time—within 24 h—using unique Sf9-QE cells. Similarly to other existing virus titration methods, the direct titration method showed that virus titers can be determined by serially diluting the virus, inoculating each dilution onto 1 well of a 96-well plate, and counting infected cells before and after 24 h p.i. The reason for this convenient and rapid titration was the use of Sf9-QE cells; transgenic Sf9-QE cells can only express fluorescence upon viral infection, making it convenient to check for viral infection. In addition, the expression of the EGFP gene for fluorescence is achieved by utilizing both the *39k* promoter and strong *p10* promoter, which start to activate about 3 to 6 h p.i., allowing for rapid and high expression. Furthermore, we confirmed the presence of at least seven copies of the EGFP transgene in Sf9-QE cells, indicating that higher levels of EGFP expression may be possible. The production of a specific recombinant protein using a BES typically takes at least four–eight weeks from the generation of the recombinant virus to the identification of the target protein. Various improvements have been made to methods such as recombinant virus generation, isolation, and titration to shorten the time required to produce recombinant proteins [18–20]. In particular, virus titration takes at least 1 to 10 days to complete, depending on the method. Typical titration methods that can be performed in as little as one to two days include qPCR, ELISAs, and flow cytometry [7–9,21,22]; however, these methods have disadvantages, such as the accuracy of titration depending on the experimenter, the complexity of the experimental process, and high cost. Therefore, if it is possible to determine virus titers in a short time with a simple experimental process and low cost, it will make the BES easier and cheaper to use.

The hypothesis for this study was confirmed by the fact that accurate virus titration was possible within 15 to 30 h p.i., and that titration after 33 h p.i. was not accurate. Theoretically, given the formation time of BVs as a secondary infectious agent (17–20 h p.i.) and the early expression time of EGFP (3–6 h p.i.), fluorescence expression by secondary infection could be possible at 20–23 h p.i.; however, in our results, the accurate quantification of virus titers by direct titration was possible up to 30 h p.i. These results are believed to indicate that more time is required for the secondary infection of the virus and for verifiable levels of fluorescence to be visibly expressed. Although the accuracy of the direct titration method for determining virus titers was demonstrated in this study using repeated experiments and a variety of virus samples, it is not clear whether these results are the result of counting only fluorescent cells from primary infection, as we hypothesized.

For the direct counting of fluorescent Sf9-QE cells via primary infection with the virus, the culture status of the cells was determined to be a very important factor. Therefore, we compared the accuracy of virus titer determination by the direct titration method according to the culture period after subculturing, and showed that cells cultured within 3 days should be used. These results not only suggest that the proliferation of viruses is affected by the proliferation status of cells, but also show that a proper cell condition is required for virus titer determination by the direct titration method. According to a previous report, the proliferation of Sf9-QE cells remains in the log phase for about five to six days and then reaches the stationary phase [12]. Therefore, even Sf9-QE cells cultured for three and five days in the log phase have different effects on the proliferation of viruses, resulting in different virus titers determined by the direct titration method. Furthermore, for the direct counting of fluorescent Sf9-QE cells, counting too many cells is not only impractical, but also time-consuming. Therefore, we explored appropriate observation dilution ratios depending on the concentration of virus to be titrated and found that the concentration of virus to be titrated does not affect virus titer determination by the direct titration method. We also found that virus quantification values are reliable even at high virus dilution ratios with a minimum count of 10 or less. These results indicate that virus titer determination by the direct titration method is easier and faster; however, in our experimental experience, the selection of cells to be counted by direct titration requires some judgment on the part of the experimenter as to whether it is more appropriate to count cells at a viral dilution of 10 or less or at the dilution immediately preceding that dilution. In some cases, counting at both dilutions may be a good option.

5. Conclusions

In conclusion, the direct titration method for determining virus titers using Sf9-QE cells offers distinct advantages over existing virus quantification methods. It is a novel method that enables accurate virus titer determination within a short period of time, about 24 h, through a simple experimental process, with the economic advantage of not requiring expensive special equipment and using a very small amount of cells. Through this study, we demonstrated the superiority of the direct titration method for the determination of virus titers using Sf9-QE cells, and expect that this will reduce the effort and time required for BES research.

Supplementary Materials: The following supporting information can be downloaded at: https://www.mdpi.com/article/10.3390/insects16040426/s1: Figure S1: Schematic representation of the recombinant viruses used in this study. Table S1: Sequences of the primer pairs used for qPCR of the transgene and reference genes in the Sf9-QE cells.

Author Contributions: Conceptualization, H.-J.M. and S.-D.W.; methodology, H.-J.M. and D.-H.L.; investigation, H.-J.M. and H.-J.K.; data curation, D.-H.L., H.-J.K. and S.-Y.M.; writing—original draft preparation, H.-J.M.; writing—review and editing, S.-D.W.; supervision, S.-D.W.; funding acquisition, S.-D.W. All authors have read and agreed to the published version of the manuscript.

Funding: This work was supported by the Starting Growth Technological R&D Program (RS-2023-00264948), funded by the Ministry of SMEs and Startups (MSS, Republic of Korea).

Data Availability Statement: The original contributions presented in this study are included in the article/Supplementary Materials; further inquiries can be directed to the corresponding author.

Conflicts of Interest: The authors Hyuk-Jin Moon, Dong-Hyun Lee, and Soo Dong Woo were employed by the company IPBL, Inc. The remaining authors declare that this research was conducted in the absence of any commercial or financial relationships that could be construed as potential conflicts of interest. The authors declare no conflicts of interest.

References

1. Hitchman, R.B.; Possee, R.D.; King, L.A. Baculovirus expression systems for recombinant protein production in insect cells. *Recent Pat. Biotechnol.* **2009**, *3*, 46–54. [CrossRef] [PubMed]
2. Chen, X.; Kong, X.; Zhao, S.; Wu, X. Post-translational modification of baculovirus-encoded proteins. *Virus Res.* **2020**, *279*, 197865. [CrossRef] [PubMed]
3. Radford, K.M.; Cavegn, C.; Bertrand, M.; Bernard, A.R.; Reid, S.; Greenfield, P.F. The indirect effects of multiplicity of infection on baculovirus expressed proteins in insect cells: Secreted and non-secreted products. *Cytotechnology* **1997**, *24*, 73–81. [CrossRef] [PubMed]
4. Wong, K.T.; Peter, C.H.; Greenfield, P.F.; Reid, S.; Nielsen, L.K. Low multiplicity infection of insect cells with a recombinant baculovirus: The cell yield concept. *Biotechnol. Bioeng.* **1996**, *49*, 659–666. [CrossRef]
5. Basak, S.; Kang, H.-J.; Chu, K.-B.; Oh, J.; Quan, F.-S. Simple and rapid plaque assay for recombinant baculoviruses expressing influenza hemagglutinin. *Sci. Prog.* **2021**, *104*, 00368504211004261. [CrossRef]
6. Zhang, Z.; Zhang, X.; Chen, H. TCID50 Assay: A Simple Method to Determine Baculovirus Titer. *Methods Mol. Biol.* **2024**, *2829*, 267–270. [CrossRef]
7. Hitchman, R.B.; Siaterli, E.A.; Nixon, C.P.; King, L.A. Quantitative real-time PCR for rapid and accurate titration of recombinant baculovirus particles. *Biotechnol. Bioeng.* **2007**, *96*, 810–814. [CrossRef]
8. Wu, Q.; Li, Y. Establishment, verification and application of rapid detection of baculovirus infectious titer by flow cytometry. *J. Virol. Methods* **2022**, *303*, 114495. [CrossRef]
9. Wang, W.; Cheng, T.; Ma, K.; Xia, D.; Wang, Y.; Liu, J.; Du, H.; Shih, J.W.K.; Zhang, J.; Zhao, Q. Development of a novel baculovirus titration method using the Enzyme-linked immunosorbent spot (ELISPOT) assay. *J. Virol. Methods* **2013**, *188*, 114–120. [CrossRef]
10. Cresta, D.; Warren, D.C.; Quirouette, C.; Smith, A.P.; Lane, L.C.; Smith, A.M.; Beauchemin, C.A.A. Time to revisit the endpoint dilution assay and to replace the TCID50 as a measure of a virus sample's infection concentration. *PLoS Comput. Biol.* **2021**, *17*, e1009480. [CrossRef]
11. Hopkins, R.F.; Esposito, D. A rapid method for titrating baculovirus stocks using the Sf-9 easy titer cell line. *BioTechniques* **2009**, *47*, 785–788. [CrossRef] [PubMed]
12. Kim, K.-S.; Bae, J.-S.; Moon, H.-J.; Kim, D.-Y.; Woo, S.-D. A novel transgenic Sf9 cell line for quick and easy virus quantification. *Insects* **2024**, *15*, 686. [CrossRef] [PubMed]
13. Rosinski, M.; Reid, S.; Nielsen, L.K. Kinetics of baculovirus replication and release using real-time quantitative polymerase chain reaction. *Biotechnol. Bioeng.* **2002**, *77*, 476–480. [CrossRef]
14. Grose, C.; Putman, Z.; Esposito, D. A review of alternative promoters for optimal recombinant protein expression in baculovirus-infected insect cells. *Protein Expr. Purif.* **2021**, *186*, 105924. [CrossRef]
15. Bruder, M.R.; Aucoin, M.G. Utility of Alternative Promoters for Foreign Gene Expression Using the Baculovirus Expression Vector System. *Viruses* **2022**, *14*, 2670. [CrossRef]
16. Shu, B.; Zhang, J.; Zeng, J.; Cui, G.; Zhong, G. Stability of selected reference genes in Sf9 cells treated with extrinsic apoptotic agents. *Sci. Rep.* **2019**, *9*, 14147. [CrossRef]
17. Maggo, S.; North, L.Y.; Ozuna, A.; Ostrow, D.; Grajeda, Y.R.; Hakimjavadi, H.; Cotter, J.A.; Judkins, A.R.; Levitt, P.; Gai, X. A method for measuring mitochondrial DNA copy number in pediatric populations. *Front. Pediatr.* **2024**, *12*, 1401737. [CrossRef]
18. Scholz, J.; Suppmann, S. A new single-step protocol for rapid baculovirus-driven protein production in insect cells. *BMC Biotechnol.* **2017**, *17*, 83. [CrossRef]

19. Philipps, B.; Rotmann, D.; Wicki, M.; Mayr, L.M.; Forstner, M. Time reduction and process optimization of the baculovirus expression system for more efficient recombinant protein production in insect cells. *Protein Expr. Purif.* **2005**, *42*, 211–218. [CrossRef]
20. Li, J.; Xu, M.; Sun, J.; Li, J.; Chen, J.; Chen, Q.; Chen, J. Rapid titration of recombinant baculoviruses based on NanoLuc secretion in early infection. *J. Virol. Methods* **2022**, *307*, 114565. [CrossRef]
21. Lo, H.-R.; Chao, Y.-C. Rapid titer determination of baculovirus by quantitative real-time polymerase chain reaction. *Biotechnol. Prog.* **2004**, *20*, 354–360. [CrossRef] [PubMed]
22. Yovcheva, M.; Thompson, K.W. Rapid two-day baculovirus titering using flow cytometry. *Methods Mol. Biol.* **2024**, *2829*, 271–275. [CrossRef]

Disclaimer/Publisher's Note: The statements, opinions and data contained in all publications are solely those of the individual author(s) and contributor(s) and not of MDPI and/or the editor(s). MDPI and/or the editor(s) disclaim responsibility for any injury to people or property resulting from any ideas, methods, instructions or products referred to in the content.

insects

MDPI

Article

Deciphering the Olfactory Mechanisms of *Sitotroga cerealella* Olivier (Lepidoptera: *Gelechiidae*): Insights from Transcriptome Analysis and Molecular Docking

Hui Li [1,*], Sheng Qiao [2], Xiwen Hong [1] and Yangyang Wei [3]

[1] School of Food and Strategic Reserves, Henan University of Technology, Zhengzhou 450001, China; xwhong1229@163.com
[2] College of Biological Engineering, Henan University of Technology, Zhengzhou 450001, China; kyla1127@163.com
[3] School of International Education, Henan University of Technology, Zhengzhou 450001, China; 18336538894@163.com
* Correspondence: hli@haut.edu.cn

Simple Summary: This study explores the olfactory mechanisms of *Sitotroga cerealella*, a globally invasive storage pest, by analyzing its antennal transcriptome. We identified 165 presumptive olfactory genes, including odorant-binding proteins, chemosensory proteins, odorant receptors, ionotropic receptors, gustatory receptors, and sensory neuron membrane proteins. These genes show high similarity to orthologs in other insects. qRT-PCR revealed that ScerOBP15 and ScerOBP23 are highly expressed in antennae, particularly in males. Molecular docking showed strong binding affinities of ScerOBP15 to n-heptadecane and ScerOBP23 to geranyl acetone, suggesting roles in host localization. Our findings enhance the understanding of *S. cerealella*'s olfactory processes and provide a foundation for developing targeted pest management strategies.

Abstract: Olfaction is crucial for insect activities such as host seeking, foraging, oviposition, and predator avoidance. While olfactory proteins have been identified across several insect species, their specific functions are largely enigmatic. In this study, we investigated the olfactory proteins of the Angoumois grain moth, *Sitotroga cerealella* Olivier. A total of 165 presumptive olfactory genes were identified in the antennal transcriptome of *S. cerealella*, encompassing 33 odorant-binding proteins (OBPs), 10 chemosensory proteins (CSPs), 58 odorant receptors (ORs), 41 ionotropic receptors (IRs), 21 gustatory receptors (GRs), and 2 sensory neuron membrane proteins (SNMPs). BLASTX and a phylogenetic analysis showed a high similarity of these genes to the orthologs in other model insects. A qRT-PCR analysis demonstrated that ScerOBP15 and ScerOBP23 are specifically and highly expressed in antennae, exhibiting male-biased expression patterns. Moreover, molecular docking revealed their strong binding affinity to the wheat volatiles n-heptadecane and geranyl acetone. Also, the potential active sites within ScerOBP15 and ScerOBP23 that engage with these volatiles have been identified, implying a possible role in host localization. Our findings shed light on the mechanisms underlying the behavioral responses of *S. cerealella* to wheat odors, enhance our comprehension of their olfactory processes, and pave the way for the development of highly specific and sustainable pest management strategies.

Keywords: *Sitotroga cerealella*; olfactory proteins; transcriptome; expression profile; molecular docking

1. Introduction

Insects exhibit a diverse array of behaviors, including courtship, kin recognition, aggregation, foraging for food, and host-plant recognition, all of which are mediated by information from their olfactory and chemosensory systems [1]. Olfaction constitutes a complex network comprising various proteins, including odorant-binding proteins (OBPs), chemosensory proteins (CSPs), odorant receptors (ORs), ionotropic receptors (IRs), gustatory receptors (GRs), sensory neuron membrane proteins (SNMPs), and odorant-degrading enzymes (ODEs) [2]. The olfactory process initiates when odorant molecules diffuse through pores into the sensillum lymph, where they bind to small, amphipathic proteins, specifically OBPs and CSPs. Subsequently, OBPs or CSPs transport the odorant molecules through the sensillum lymph to the ORs, activating the olfactory receptor neurons (ORNs) and converting chemical signals into electrical impulses that are transmitted to the insect brain [3–5]. This intricate process underscores the sophisticated nature of the insect olfactory system and its critical role in mediating essential behaviors.

OBPs, recognized as critical transporters of odorant molecules and pheromones, are specifically concentrated within the sensilla lymph of insect antennae [6,7]. The first OBP, designated as pheromone-binding protein, was identified in the antenna of *Antheraea polyphemus* [8]. Since then, these small (100–300 amino acids) water-soluble globular proteins have been characterized across various insect species through antennal transcriptome analyses [9,10]. These OBPs are classified into several subgroups based on the number of conserved cysteine residues: classic OBPs with six conserved cysteines, Minus-C OBPs with four, Plus-C OBPs with eight, and Dimer OBPs with twelve [10,11]. Ligand-binding assays have demonstrated that pheromone-binding proteins (PBPs) selectively bind pheromones, while general odorant-binding proteins (GOBPs) interact with a broad spectrum of odorants from host plants [12,13]. Similar to OBPs, CSPs are small soluble proteins characterized by four conserved cysteine residues and exhibit greater conservation than OBPs. They are found in the antennal sensillum lymph, as well as in other non-chemosensory organs, suggesting additional roles beyond the transport of odorant molecules [14–16].

In insects, olfactory reception is mediated by two families of olfactory receptors, namely odorant receptors (ORs) and ionotropic receptors (IRs), along with one family of gustatory receptors (GRs). Classical ORs are characterized by the presence of seven conserved transmembrane domains and were first identified in the genome of *Drosophila melanogaster* [14,17]. Pheromone molecules are typically recognized by specific pheromone receptors (PRs). Additionally, insect ORs, in conjunction with the olfactory co-receptor Orco, form an odor-gated ion channel complex that converts chemical signals into electrical signals [16,18,19]. The IR family, first characterized in *D. melanogaster*, possesses a molecular configuration analogous to ionotropic glutamate receptors [20–22]. Compared to ORs, insect IRs are implicated in the detection of acids, amines, and aldehydes within the olfactory system, as well as in various non-chemosensory functions [23,24]. The GR family, expressed in the antennae, proboscis, and palps of insects, plays a crucial role in the detection of CO_2, sugars, and bitter substances [25–28].

Sensory neuron membrane proteins (SNMPs), specifically SNMP1 and SNMP2, are found in the antennae of insects. SNMP1 co-localizes with pheromone receptors in pheromone-specific olfactory sensory neurons (OSNs), whereas SNMP2 is found in the support cells of the sensilla [29–31]. These proteins are hypothesized to play an essential role in pheromone perception.

Molecular docking and molecular dynamics simulation are the leading techniques for probing the interactions between olfactory proteins and ligands [32,33]. A foundational step in molecular docking is obtaining the structural model of the target protein. In the

absence of experimental protein structures, homology modeling uses the tertiary structures of closely related OBPs as templates to predict the three-dimensional structure of OBPs [34]. To date, the three-dimensional structures of over 20 OBPs have been characterized across diverse insect orders, including Lepidoptera, Diptera, and Hemiptera [35,36]. These techniques are widely used to analyze the binding profiles between olfactory proteins and ligands in insects and to compare the binding profiles among different proteins [37,38]. Molecular docking has been applied in virtual screening for insect behavior regulators across various insect orders, such as Coleoptera, Diptera, Hemiptera, Hymenoptera, Lepidoptera, Orthoptera, and Trichoptera [39]. This approach enables the large-scale screening of lead compounds for insect behavior regulators, significantly accelerating their development. It provides a vital theoretical basis for studies on olfactory protein-binding affinities and has substantial implications for the future discovery of novel behavior regulators [37,40].

The Angoumois grain moth, *Sitotroga cerealella* (Olivier) (Lepidoptera: *Gelechiidae*), is a pervasive pest that poses a substantial threat to the storage of grains, such as wheat, rice, and maize. Historically, phosphine fumigation has been the predominant control method. However, a prolonged reliance on pesticides can lead to residues, resistance, and environmental pollution. Recently, modulating olfactory behavior has risen as a promising strategy for pest management. For instance, diallyl trisulfide, a component of garlic, has been shown to disrupt the binding of sex pheromones to PBPs [41]. Thus, elucidating the molecular basis of insect olfaction is essential for devising innovative bio-pesticides and integrated pest management strategies [42]. Despite this, the molecular mechanisms of chemical communication in *S. cerealella* remain largely elusive.

In this study, we performed transcriptome analyses on the antennae of both mated and unmated female and male adults of *S. cerealella*, identifying 165 putative olfactory genes, comprising 33 OBPs, 10 CSPs, 58 ORs, 41 IRs, 21 GRs, and 2 SNMPs. We then conducted sequence alignment and a phylogenetic analysis of these olfactory genes. Furthermore, we evaluated the transcript expression levels of these candidate olfactory genes across various tissues in female and male adults using transcriptome data. The binding affinities of ScerOBP15 and ScerOBP23 to specific wheat volatiles were preliminarily predicted using three-dimensional structural modeling and molecular docking. This research establishes a foundation for future functional studies on these olfactory genes in *S. cerealella* at the molecular level.

2. Materials and Methods

2.1. Insect Rearing and Tissue Collection

The adults of *S. cerealella* were sourced from Zhengzhou (112°42′ E, 34°16′ N), Henan Province, China, and were reared on wheat in 4 L plastic containers under stringent environmental conditions: 28 ± 2 °C, 70 ± 5% relative humidity, and a dark photoperiod. Antennae (At) and bodies with antennae removed (both mated and unmated females and males) were dissected and preserved in 1.5 mL Eppendorf tubes with RNAlater (Ambion, Austin, TX, USA). Thereafter, the samples were rapidly frozen in liquid nitrogen and stored at −80 °C for subsequent analysis.

2.2. RNA-Seq Library Construction and Illumina Sequencing

Total RNA extraction from the antennae of mated and unmated female and male *S. cerealella* was performed using TRIzol reagent (Invitrogen, Carlsbad, CA, USA) following the manufacturer's guidelines. The RNA concentration and purity were determined using a NanoDrop spectrophotometer, and RNA integrity was validated through electrophoresis

on a 1.0% agarose gel and subsequent analysis with an Agilent 2100 Bioanalyzer (Agilent Technologies, Santa Clara, CA, USA). Poly(A) mRNA was purified and enriched from the total RNA using oligo(dT) magnetic beads, fragmented, and subjected to first-strand cDNA synthesis with random hexamer primers. Second-strand cDNA synthesis involved RNase H, buffer, dNTPs, and DNA polymerase I. The double-stranded cDNA underwent end-repair and modification with an A-tailing at the 3′ end and phosphorylation at the 5′ end. Subsequently, PCR amplification generated the library, which was then assessed for quality using the Agilent 2100 Bioanalyzer (Agilent Technologies, Santa Clara, CA, USA). Ultimately, the libraries were sequenced on the MGISEQ-2000 platform (BGI-Shenzhen, China).

2.3. De Novo Assembly and Sequence Annotation

Clean reads for de novo assembly were obtained by removing the adapters and low-quality sequences from the raw reads with SOAPnuke (v2.1.0) [43]. Assembly was conducted using Trinity software (v2.4.0) to produce nonredundant unigenes [43]. Functional annotation of nonredundant unigenes from the *S. cerealella* antennal transcriptome was performed using Diamond blastx against public protein databases: the NCBI nonredundant (NR, e-value < 10^{-5}) database, Gene Ontology (GO, e-value < 10^{-5}), Swiss-Prot (e-value < 10^{-5}), euKaryotic Orthologous Groups/clusters of Orthologous Groups of programs (KOG/COG, e-value < 10^{-3}), and the Kyoto Encyclopedia of Genes and Genomes (KEGG, e-value < 10^{-10}) [44].

2.4. Identification of Olfactory Genes and Phylogenetic Analysis

Candidate olfactory genes in *S. cerealella* were identified through functional annotation results from five publicly available protein databases and validated against the NCBI protein database using BLASTx (https://blast.ncbi.nlm.nih.gov/Blast.cgi, accessed on 23 May 2023). Open reading frames (ORFs) of putative olfactory genes were predicted with the ORF finder (http://www.ncbi.nlm.nih.gov/gorf/gorf.html, accessed on 23 May 2023), and signal peptides were predicted with the SignalP 4.0 program (http://www.cbs.dtu.dk/services/SignalP/, accessed on 28 May 2023). The TMHMM Server 2.0 was employed to predict the transmembrane domains (TMDs) of the olfactory proteins (http://www.cbs.dtu.dk/services/TMHMM, accessed on 28 May 2023) [42].

Phylogenetic trees were constructed with amino acid sequences from *S. cerealella* and other insects' olfactory genes using MEGA7.0 with the maximum-likelihood method, 1000 bootstrap replications, and a poison model. FigTree v.1.4.4 software and Adobe Illustrator CS6 (v5.2.0.17) were used to edit and render the trees. Redundant sequences from other insects were removed to enhance the quality of the phylogenetic trees, except for those from *S. cerealella*.

2.5. Expression Analysis of Olfactory Genes

The FPKM approach was employed to quantify the expression profiles of olfactory genes in the antennae of both female and male *S. cerealella* [45]. Transcriptomic differences among genes were identified using the DEGseq tool with a false discovery rate threshold of less than 0.05, and an absolute value of $|\log2(\text{FoldChange})| > 1$ to determine statistical significance in gene expression [46]. Comparative DEG analysis was conducted to confirm the differential expression of the chemosensory genes between unmated males and females.

Tissues from adult *S. cerealella*, including antennae (At) and body segments devoid of antennae (B), were dissected and preserved in RNase-free tubes (AXYGEN). Total RNA was extracted from these distinct tissues following the manufacturer's protocol using TRIzol reagent (Takara, Dalian, China). cDNA synthesis was performed using the RevertAid First Strand cDNA Synthesis Kit (Thermo Scientific, Waltham, MA, USA). The expression profiles

of the olfactory genes across various adult tissues were validated by qPCR on a Light Cycler 480 System (Rochester, NY, USA) with SYBR Premix EX Taq (Takara, China). A constitutive *S. cerealella* housekeeping gene, glyceraldehyde-3-phosphate dehydrogenase (GAPDH), served as an endogenous control to standardize gene expression and adjust for sample variability [41]. The primers are listed in Table S1. Primers for the target and reference genes were designed with Primer 3 Plus (https://www.primer3plus.com/index.html, accessed on 6 July 2023), with expected amplicon sizes ranging from 100 bp to 200 bp. The qPCRs were set up in 25 μL volumes, comprising 1 μL of each primer (10 μM), 1 μL of cDNA template (200 ng/μL) from tissues such as the antennae and body, 0.375 μL of reference dye (50×), 12.5 μL of 2×SYBR Green QPCR Master Mix (Stratagene, La Jolla, CA, USA), and 9.125 μL sterilized ultrapure H_2O. The thermal-cycling profile consisted of 95 °C for 3 min, followed by 40 cycles of 10 s at 95 °C and 30 s at 55 °C. Dissociation curves were generated by heating the PCR products to 95 °C for 15 s, cooling to 57 °C for 15 s, and then heating to 95 °C for 15 s, with this cycle repeated for 20 min. Each RT-qPCR assay was conducted in triplicate per sample for technical replicates. No-template and no-transcriptase controls were included in each qPCR run to verify specificity. To ensure reproducibility, each qPCR was independently repeated three times for each sample.

The relative quantification $2^{-\Delta\Delta CT}$ approach was applied to evaluate the relative transcript abundance of genes in each tissue (where ΔΔCT = (CTScerOBP − CTScerGAPDH rRNA) Time x − (CTScerOBP – CTScerGAPDH rRNA) Time 0) [47].

2.6. Structure Modeling and Molecular Docking of Ligands

The three-dimensional structure of ScerOBP15 and ScerOBP23 was predicted using the SWISS-model portal at the Expasy tools platform (https://swissmodel.expasy.org/interactive, accessed on 25 July 2023). Assessment of the 3D model quality, including protein geometry, was conducted with UCLA-DOE LAB-SAVES v6.0 (https://saves.mbi.ucla.edu/, accessed on 12 August 2023) [48–50]. Molecular docking studies employed the Auto Dock Vina 1.2.3 software [51,52]. The newly constructed 3D model of ScerOBP15 and ScerOBP23 served as receptors, and ligands were selected from PubChem based on significant experimental affinities. Default settings were applied during the Auto Dock Vina 1.2.3 molecular-docking process, and complexes were identified based on the lowest binding energy. Structural analysis of the visual and docked complexes was performed using the Protein–Ligand Interaction Profiler (https://plip-tool.biotec.tu-dresden.de/plip-web/plip/index, accessed on 27 August 2023) and the PyMOL tool (v2.5.7) [53,54].

3. Results

3.1. Transcriptome Sequencing, Assembly, and Annotation

The antennal transcriptome of unmated male *S. cerealella* produced a total of 25.33 million (SE ± 4.61 million) high-quality reads, achieving a Q20 score of 98.23% (±0.16). The mated male counterpart yielded 23.75 million (SE ± 1.36 million) high-quality reads, also with a Q20 of 98.23% (±0.06). Unmated females produced 26.65 million (SE ± 1.95 million) high-quality reads with a Q20 of 98.23% (±0.16), while mated females generated 26.64 million (SE ± 1.27 million) clean reads, also scoring 98.23% (±0.20) in Q20 (Table 1). Assembly of the *S. cerealella* antennal transcriptome resulted in 142,382 transcripts, with 47,663 (33.48%) being shorter than 500 bp and 33,404 (23.46%) exceeding 2000 bp in length (Table 1). The raw reads from the *S. cerealella* antennal transcriptome have been submitted to the NCBI Short Read Archive (SRA) database under accession number PRJNA877069.

A total of 67,753 (47.59%) transcripts showed sequence similarity to known entries within at least one protein database. Among these, 30,846 (21.67%) genes were classified

into 26 KOG categories, with the 'General function prediction only' category being the most abundant (Figure 1A). An analysis indicated that 17,666 (12.41%) transcripts were associated with three GO categories: biological process, cellular component, and molecular function (Figure 1B). Additionally, 34,591 (24.29%) genes were mapped to five KEGG pathways, encompassing 34 distinct groups (Figure 1C).

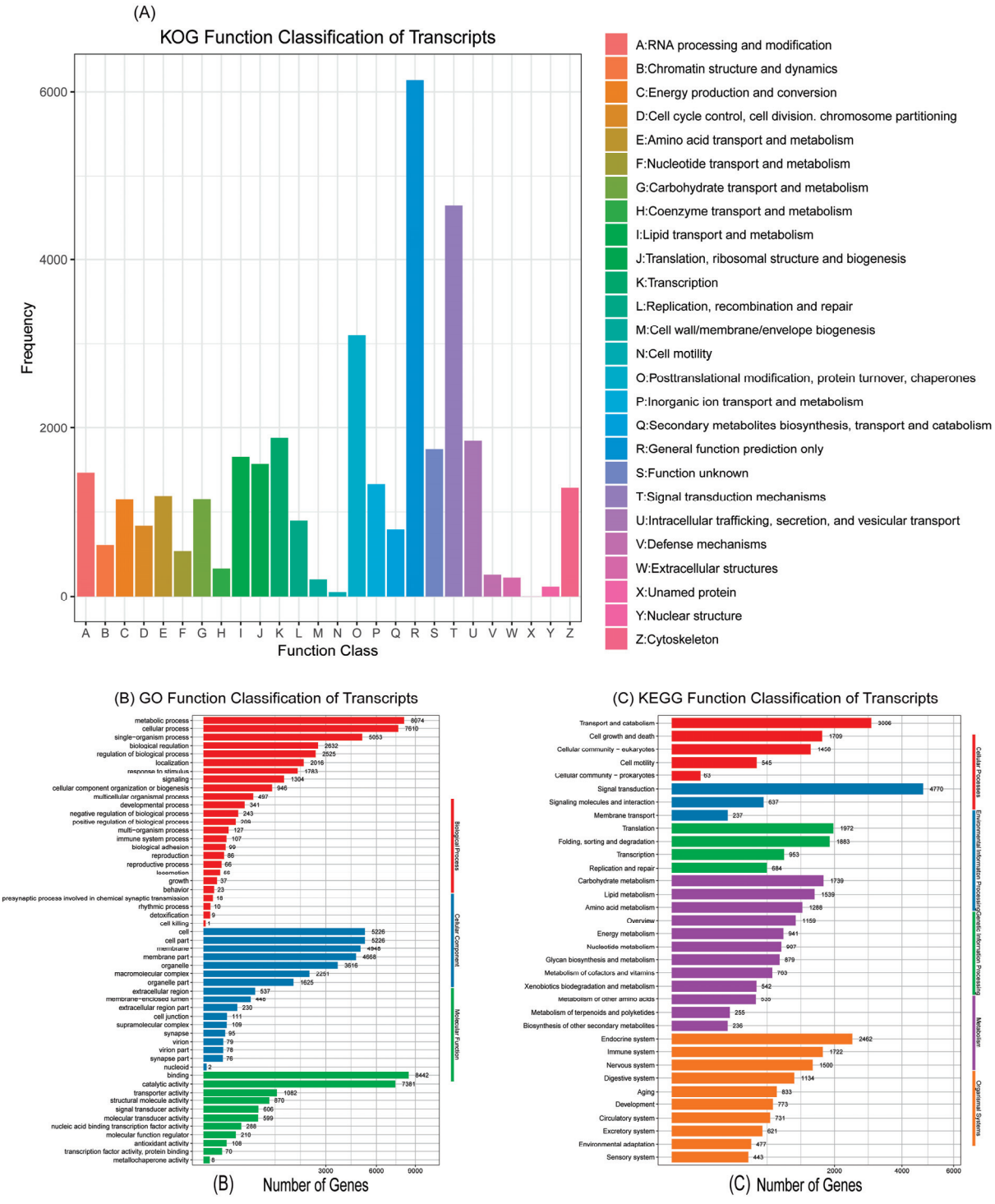


Figure 1. Analyses of the antennal transcriptome of *S. cerealella*. (**A**) Eukaryotic Ortholog Groups of proteins (KOG) annotation of the transcriptome. (**B**) Gene Ontology (GO) annotation of the transcriptomic sequences. (**C**) Kyoto Encyclopedia of Genes and Genomes (KEGG) pathway annotation of the transcriptome. The horizontal axis is logarithmic.

Table 1. Summary of reads and transcripts from the antennal transcriptome of *S. cerealella*.

Category	Unmated Male	Unmated Female	Mated Male	Mated Female
Clean reads (million)	25.33 ± 4.61	26.65 ± 1.95	23.75 ± 1.36	26.64 ± 1.27
Average length (bp)	150	150	150	150
Q20 (%)	98.23 ± 0.16	98.13 ± 0.16	98.23 ± 0.06	98.20 ± 0.20
Q30 (%)	92.60 ± 0.44	92.17 ± 0.23	92.53 ± 0.06	92.53 ± 0.75
GC (%)	45.07 ± 0.38	44.73 ± 1.89	44.70 ± 0.46	45.63 ± 0.70
Transcript length interval	Number of Transcripts		Percentage (%)	
<500 bp	47,663		33.48	
500–1k bp	30,599		21.49	
1k–2k bp	30,716		21.57	
>2k bp	33,404		23.46	
Total Transcripts	142,382		100.00	
Annotated Transcript	Number of Transcripts		Percentage (%)	
Annotated in NR	67,529		47.43	
Annotated in KEGG	34,591		24.29	
Annotated in SwissProt	45,867		32.21	
Annotated in GO	17,666		12.41	
Annotated in KOG	30,849		21.67	
Unknown	74,629		52.41	
Total Transcripts	142,382		100	

3.2. Olfactory-Related Genes in S. cerealella

Following BLAST analysis and functional annotation against five protein databases, we identified a total of 167 putative olfactory genes from the antennal transcriptomes of *S. cerealella*. This set includes 33 OBPs, 10 CSPs, 58 ORs, 41 IRs, 21 GRs, 2 SNMPs, and 2 ODEs.

3.2.1. Identification and Analysis of Putative OBPs

In this investigation, 33 OBPs from the antennal transcriptome of *S. cerealella* were identified, which included 4 PBPs, 3 GOBPs, 1 antennal-binding protein (ABP), and 25 classic OBPs. Three OBP-encoding genes, ScerPBP2, ScerGOBP1, and ScerGOBP2, have been previously reported. Sequence analysis revealed that 18 ScerOBPs had complete ORFs, and 21 ScerOBPs possessed signal peptide sequences. BLAST comparisons indicated that all OBPs exhibited over 51% amino acid sequence identity with their Lepidopteran orthologs, with ScerOBP20 displaying over 96% identity with GOBPs from *Amyelois transitella*. Multiple sequence alignment results demonstrated that 17 ScerOBPs harbored the conserved motif, while 5 ScerOBPs were classified as Minus-C OBPs. A phylogenetic analysis revealed that all ScerPBPs (ScerPBP1–4) grouped with PBPs from other Lepidoptera, and two ScerGOBPs (ScerGOBP1 and ScerGOBP2) fell within the GOBPs clade, whereas ScerGOBP3 clustered with ABPs and OBPs from other Lepidoptera (Figure 2).

3.2.2. Identification and Analysis of Putative CSPs

A total of 10 CSPs were identified in this study. A sequence analysis revealed that nine ScerCSPs possessed complete ORFs with polypeptide lengths varying from 103 to 158 amino acid residues. Additionally, all identified sequences featured an N-terminal signal peptide. Multiple sequence alignment indicated that all ScerCSPs contained a conserved motif with four conserved cysteine residues. A phylogenetic analysis of the ScerCSPs demonstrated the presence of three distinct clades (clades I, II, and III), which is consistent with the patterns observed in other Lepidopteran species. Specifically, ScerCSP6 was found to be monophyletic with CpinCSP16 in clade I, while two ScerCSP

transcripts (ScerCSP2 and ScerCSP9) were associated with the divergent clade II. Clade III was monophyletic, with a large Lepidoptera-specific clade encompassing the remaining seven ScerCSPs (Figure 3).

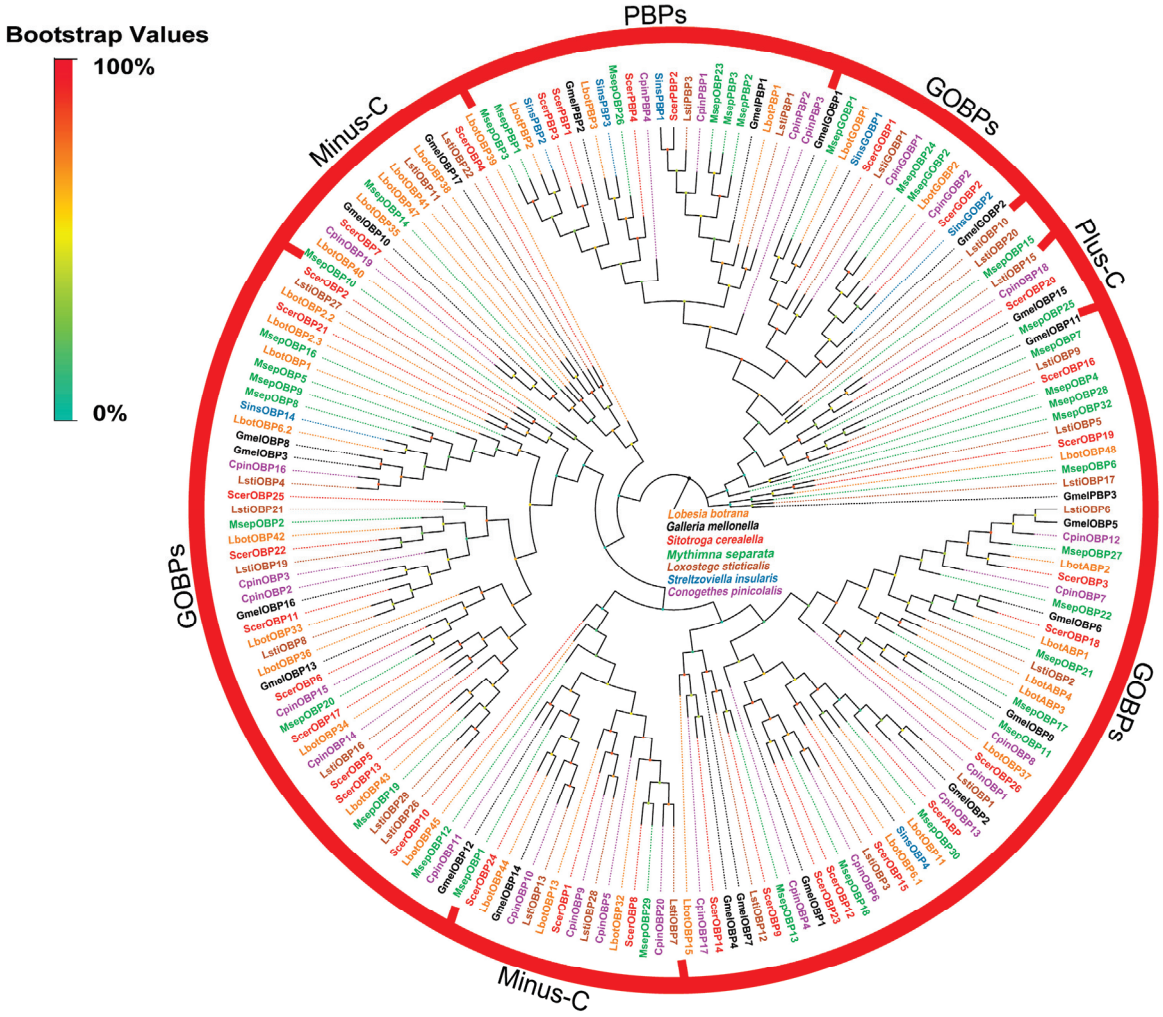


Figure 2. Phylogenetic tree of ScerOBPs. The phylogenetic analysis from OBPs of *S. cerealella* (ScerOBP, highlighted in red) was conducted using reference OBPs of *Streltzoviella insularis* (SinsOBP, highlighted in blue), OBPs of *Conogethes pinicolalis* (CpinOBP, highlighted in purple), OBPs of *Mythimna separata* (MsepOBP, highlighted in green), OBPs of *Galleria mellonella* (GmelOBP, highlighted in black), OBPs of *Loxostege sticticalis* (LstiOBP, highlighted in brown), and OBPs of *Lobesia botrana* (LbotOBP, highlighted in orange). The stability of the nodes was assessed by bootstrap analysis with 1000 replications. Colored dots at nodes represent bootstrap values, and branch colors indicate different species classifications.

3.2.3. Identification and Analysis of Putative ORs

A total of 58 candidate ORs from the antennal transcriptomes of *S. cerealella* were identified based on BLASTx annotation results. Among these, 26 ScerORs possessed complete ORFs, encoding proteins with lengths ranging from 162 to 474 amino acids. Furthermore, three ScerORs (ScerOrco, ScerOR31, ScerOR15) were characterized by the presence of seven transmembrane domains (TMDs). A BLASTx analysis revealed that the majority of ScerORs exhibited low sequence similarity (31.82–78.26%) with orthologs from other insect species, with the exception of ScerOrco. A phylogenetic analysis confirmed that one OR, named ScerOrco, is conserved within the Orco gene family, closely related to

SinsOrco and GmelORco. Additionally, all ScerPRs (ScerPR1–4) were found to be part of the pheromone receptor (PR) family (Figure 4).

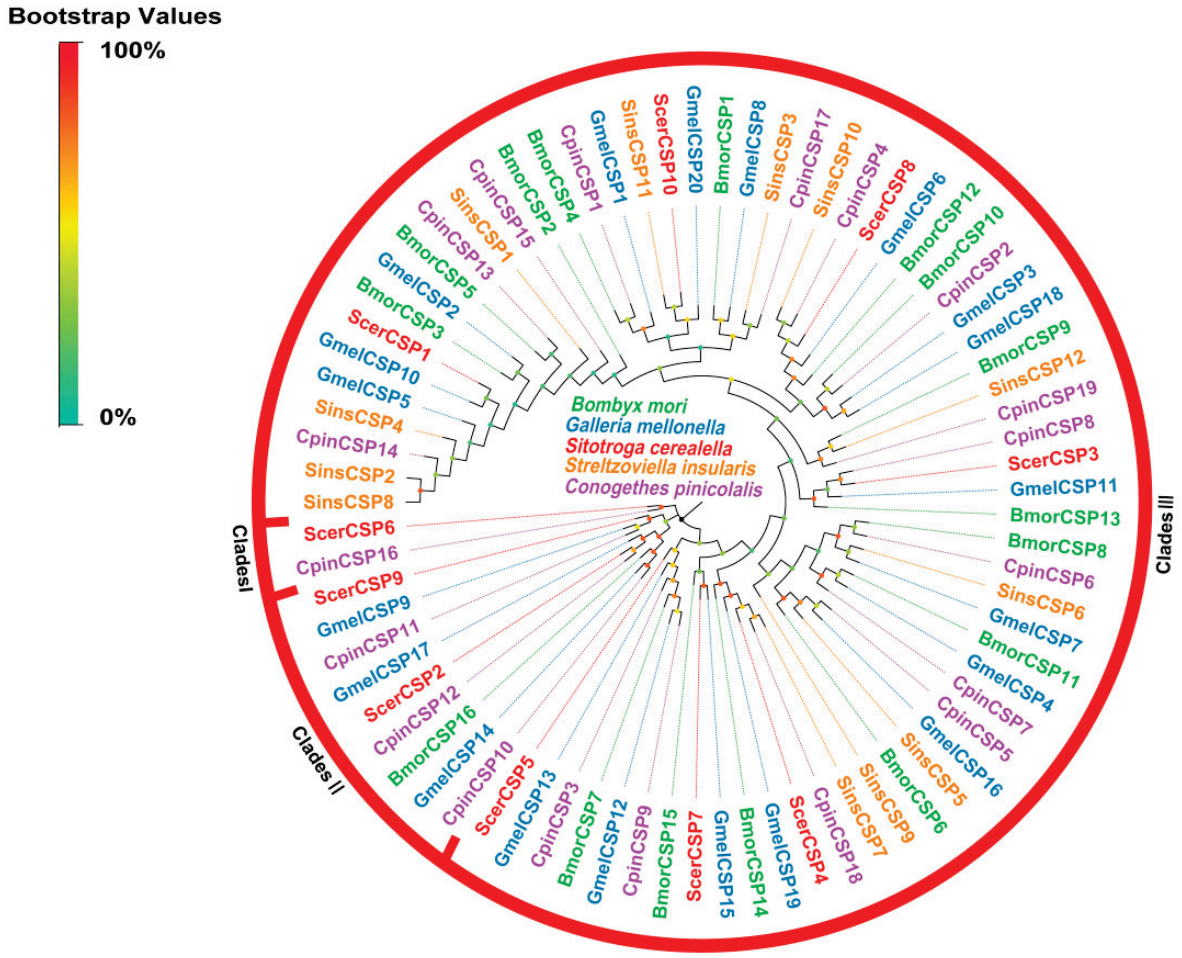


Figure 3. Phylogenetic tree of ScerCSPs. The phylogenetic analysis of CSPs from *S. cerealella* (ScerCSP, highlighted in red) was conducted using reference CSPs of *Galleria mellonella* (GmelCSP, highlighted in blue), CSPs of *Conogethes pinicolalis* (CpinCSP, highlighted in purple), CSPs of *Bombyx mori* (BmorCSP, highlighted in green), and CSPs of *Streltzoviella insularis* (SinsCSP, highlighted in orange). The stability of the nodes was assessed by bootstrap analysis with 1000 replications. Colored dots at nodes represent bootstrap values, and branch colors indicate different species classifications.

3.2.4. Identification and Analysis of Putative IRs

A bioinformatic analysis of the *S. cerealella* antennal transcriptome identified a total of 41 candidate IRs, with 18 ScerIRs exhibiting complete ORFs that spanned 473 to 916 amino acid residues. A phylogenetic analysis, incorporating ScerIRs and IRs from other Lepidopteran insects, revealed that ScerIRs segregated into 11 distinct groups, encompassing IR8a, IR25a, IR21a, IR40a, IR41a, IR64a, IR68a, IR75d, IR75q, IR75p, and IR93a. Notably, ScerIR8a is grouped within the IR8a clade, hypothesized to function as co-receptors with other IRs, and demonstrated a high sequence identity of 98.85% with IR8a from *Athetis lepigone* (Figure 5).

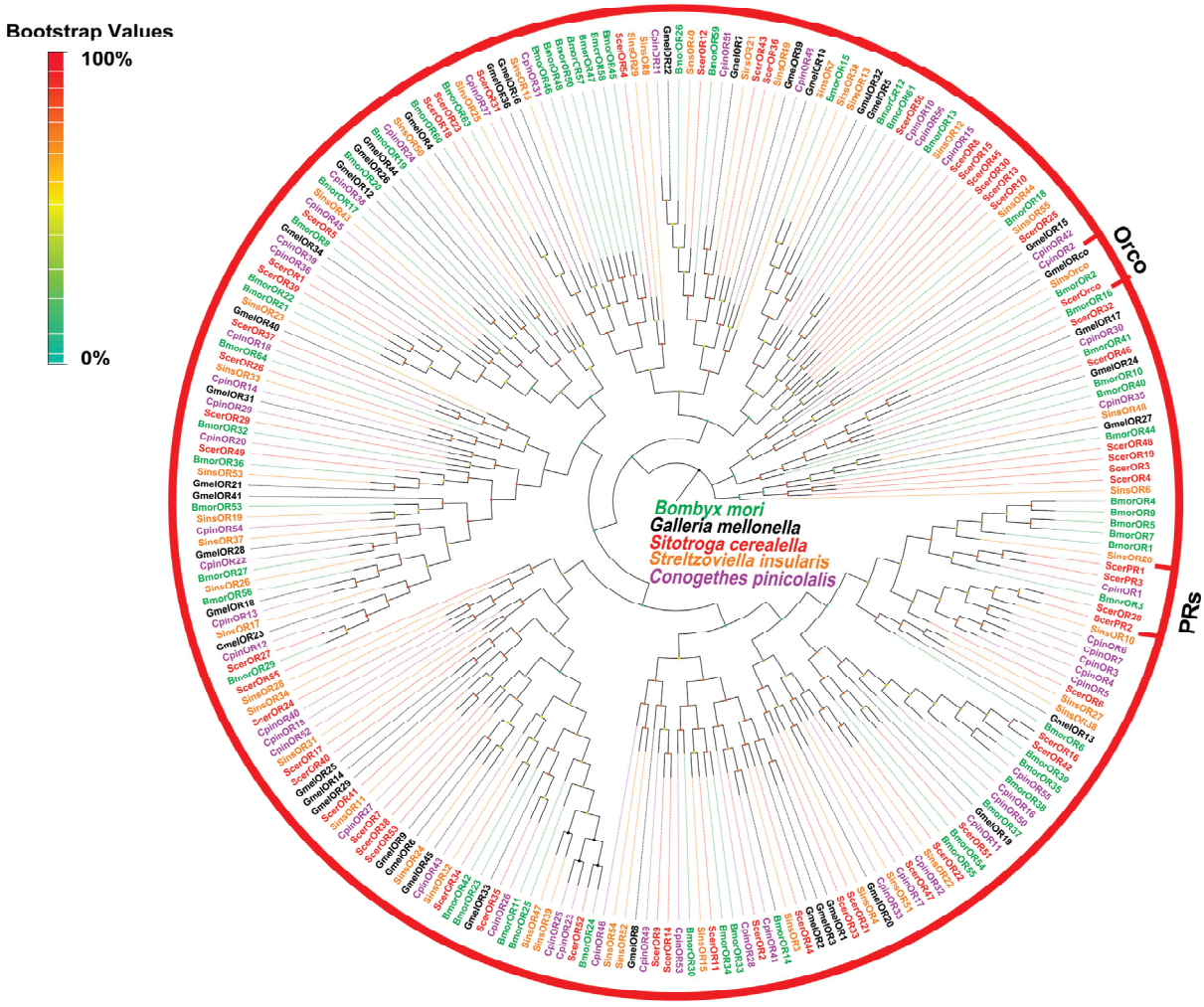


Figure 4. Phylogenetic tree of ScerORs. The phylogenetic analysis of ORs from *S. cerealella* (ScerOR, highlighted in red) was conducted using reference ORs of *Galleria mellonella* (GmelOR, highlighted in black), ORs of *Conogethes pinicolalis* (CpinOR, highlighted in purple), ORs of *Bombyx mori* (BmorOR, highlighted in green), and ORs of *Streltzoviella insularis* (SinsOR, highlighted in orange). The stability of the nodes was assessed by bootstrap analysis with 1000 replications. Colored dots at nodes represent bootstrap values, and branch colors indicate different species classifications.

3.2.5. Identification and Analysis of Putative GRs

In the antennal transcriptome of *S. cerealella*, we identified 22 candidate gustatory receptors (ScerGRs 1–22), with 10 ScerGRs exhibiting incomplete ORFs due to the absence of either a 5′ or 3′ terminus. Of these, nine genes were nearly full-length, possessing complete ORFs that encoded proteins with lengths ranging from 326 to 483 amino acids and featuring 6–8 transmembrane domains. A phylogenetic analysis revealed that all ScerGRs were segregated into four distinct clades: 'CO_2 receptors', 'sugar receptors', 'fructose receptors', and 'bitter receptors'. ScerGR14–16 were classified within the 'CO_2 receptors' clade, alongside BmorGR1N, BmorGR2NJ, and BmorGR3F, which are known carbon dioxide sensors. Seven ScerGRs were found to cluster with sugar-sensing receptors (BmorGR4S, 5NJF, 6P, 7, 8R) from Bombyx mori. Additionally, ScerGR19 and ScerGR20 were grouped with fructose receptors, including BmorGR9R and BmorGR10. The remaining nine ScerGRs were categorized under the 'bitter receptors' clade (Figure 6).

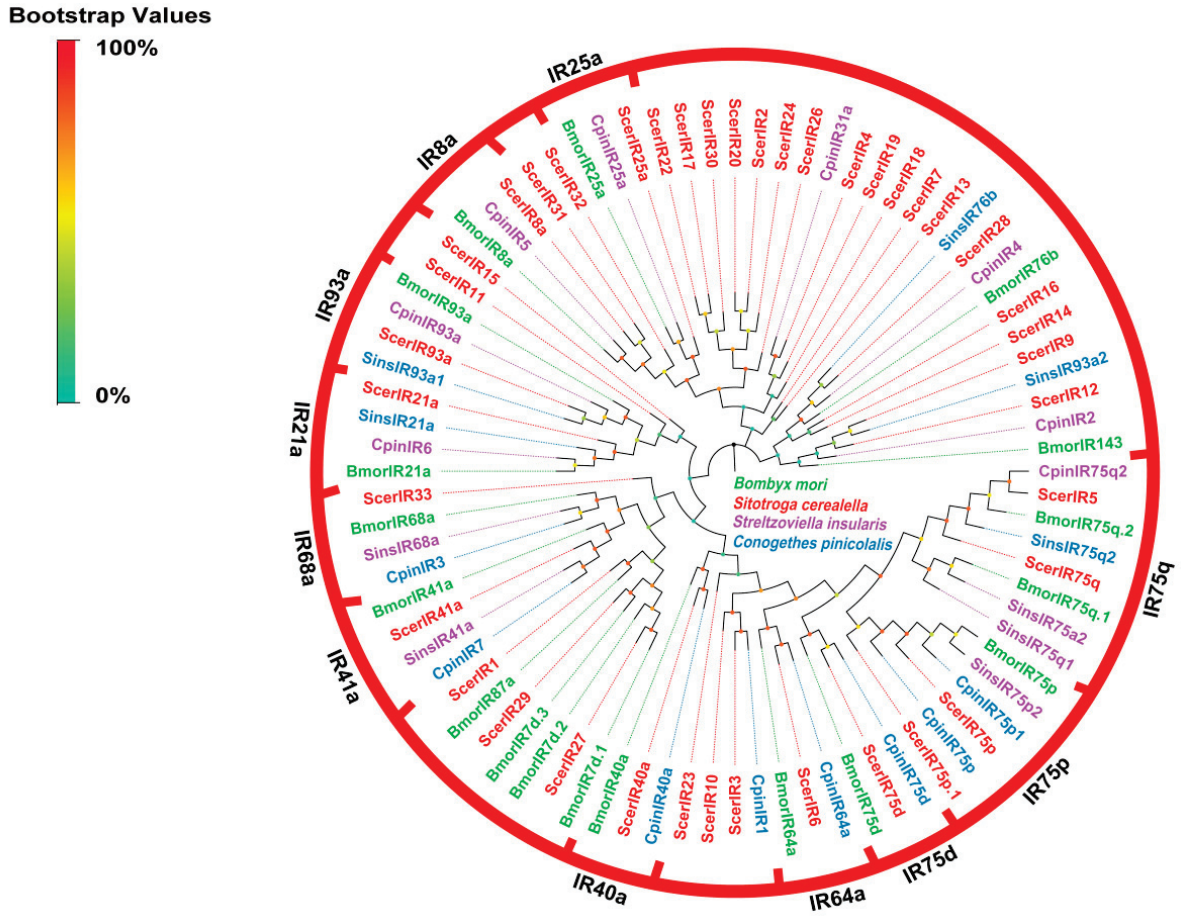


Figure 5. Phylogenetic tree of ScerIRs. The phylogenetic analysis of IRs from *S. cerealella* (ScerIR, highlighted in red) was conducted using reference IRs of *Conogethes pinicolalis* (CpinIR, highlighted in blue), IRs of *Bombyx mori* (BmorIR, highlighted in green), and IRs of *Streltzoviella insularis* (SinsIR, highlighted in purple). The stability of the nodes was assessed by bootstrap analysis with 1000 replications. Colored dots at nodes represent bootstrap values, and branch colors indicate different species classifications.

3.2.6. Identification and Analysis of Putative SNMPs

In the transcriptomes of adult *S. cerealella*, we identified two candidate sensory neuron membrane proteins (SNMPs). Both proteins possessed ORFs, with lengths varying from 521 to 524 amino acid residues, and featured two transmembrane domains (TMDs). A BLASTx analysis indicated that ScerSNMP1 exhibited 82.03% sequence similarity to HkahSNMP1, while ScerSNMP2 showed 71.32% sequence identity to HkahSNMP2. A phylogenetic analysis revealed three distinct groups, with ScerSNMP1 clustering within the SNMP1 clade and ScerSNMP2 within the SNMP2 clade, alongside other Lepidopteran SNMP2s. Notably, both the SNMP1 and SNMP2 clades were prevalent in the antennae of the insects (Figure 7).

3.3. Identification of Sex-Bias Expression Genes Based on Transcriptome

Analysis of the FPKM values derived from the *S. cerealella* antennal transcriptome (Figure 8) revealed that five OBPs, including ScerGOBP2, ScerPBP1, ScerPBP3, ScerOBP15, and ScerOBP23, were markedly expressed in male antennae (FPKM > 10,000). In contrast, two OBPs, ScerGOBP1 and ScerGOBP2, exhibited high expression in female antennae (FPKM > 10,000). ScerCSP8 was identified as the predominant CSP in the antennae of

S. cerealella. ScerOrco and ScerIR25a were the most abundantly expressed OR and IR, respectively, potentially reflecting their specialized roles. ScerGR19 was the predominant GR in the antennae of *S. cerealella*, and ScerSNMP1 was the most highly expressed SNMP. A total of 25 olfactory-related genes, comprising 11 ScerOBPs, 11 ScerORs, 2 ScerSNMPs, and 1 ScerCSP, demonstrated sex-biased expression in mated *S. cerealella*, with a male bias. In virginal *S. cerealella*, 26 olfactory-related genes (11 ScerOBPs, 12 ScerORs, 2 ScerSNMPs, and 1 ScerCSP) showed sex-biased expression, with 23 genes exhibiting a male bias and the remaining 3 showing a female bias.

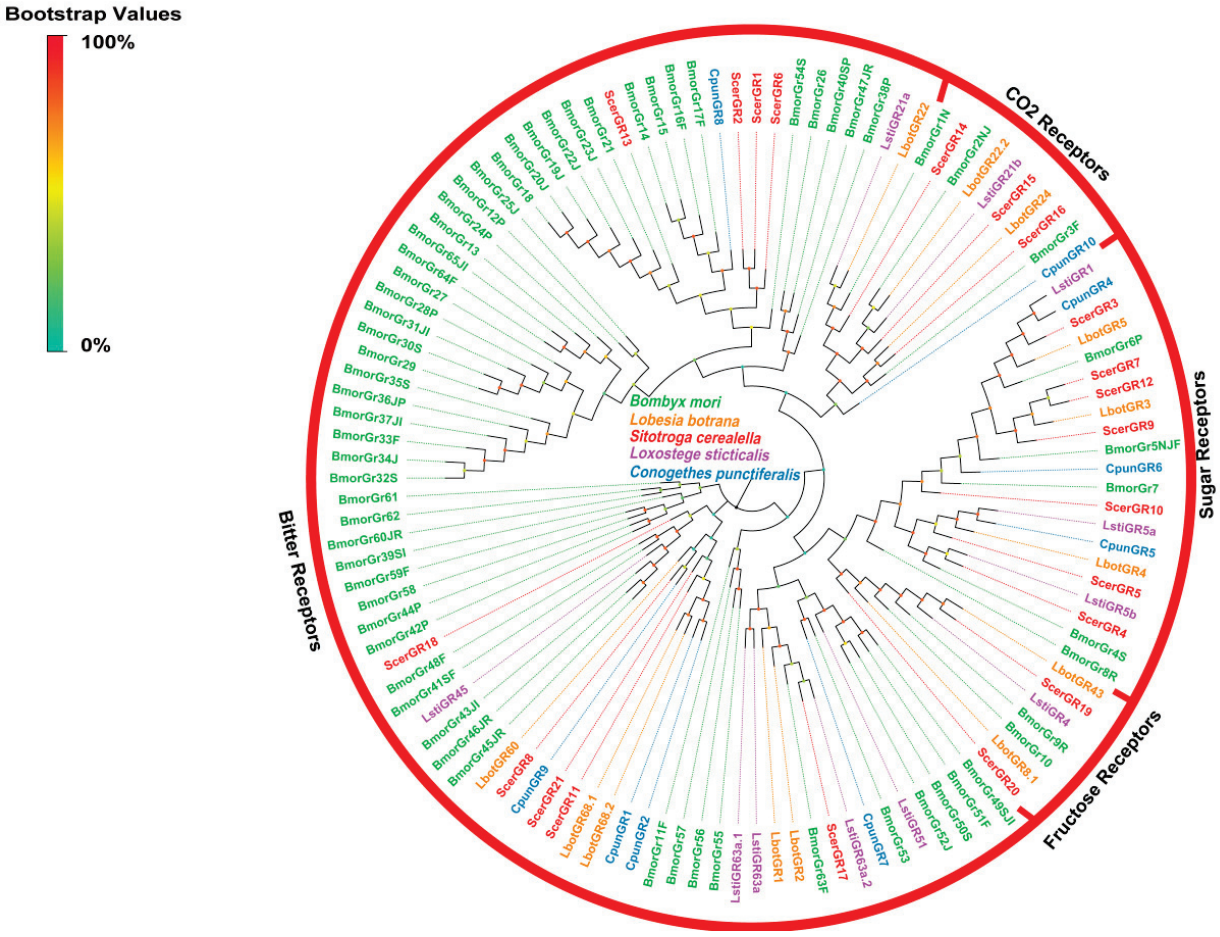


Figure 6. Phylogenetic tree of ScerGRs. The phylogenetic analysis of GRs from *S. cerealella* (ScerGR, highlighted in red) was conducted using reference GRs of *Conogethes punctiferalis* (CpunGR, highlighted in blue), GRs of *Bombyx mori* (BmorGR, highlighted in green), GRs of *Lobesia botrana* (LbotGR, highlighted in orange), and GRs of *Loxostege sticticalis* (LstiGR, highlighted in purple). The stability of the nodes was assessed by bootstrap analysis with 1000 replications. Colored dots at nodes represent bootstrap values, and branch colors indicate different species classifications.

A semi-quantitative reverse transcription quantitative PCR (RT-qPCR) was employed to investigate the expression profiles of ScerOBP15 and ScerOBP23 across the adult tissues of *S. cerealella*, encompassing antennae and bodies devoid of antennae. The RT-qPCR findings revealed significantly elevated expression levels of ScerOBP15 and ScerOBP23 in male antennae relative to other tissues ($p < 0.01$; Figure 9). Additionally, there was no significant variation in the expression levels of ScerOBP15 and ScerOBP23 among the female antennae, female bodies, and male bodies (Figure 9).

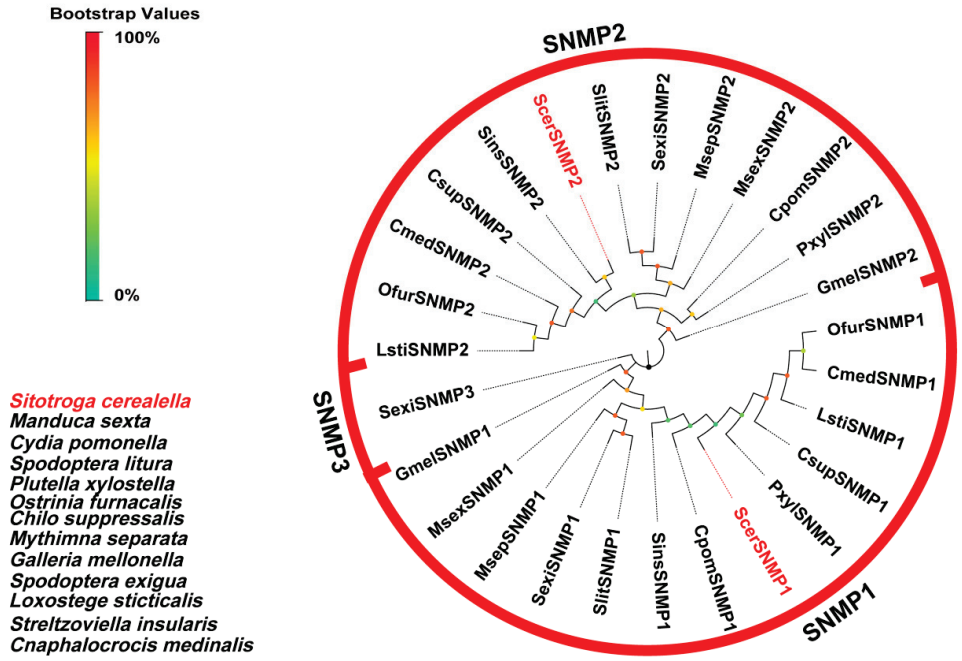


Figure 7. Phylogenetic tree of ScerSNMPs. The phylogenetic analysis of SNMPs from *S. cerealella* (ScerSNMP, highlighted in red) was conducted using reference SNMPs from twelve other insects. The stability of the nodes was assessed by bootstrap analysis with 1000 replications. Colored dots at nodes represent bootstrap values, and branch colors indicate different species classifications.

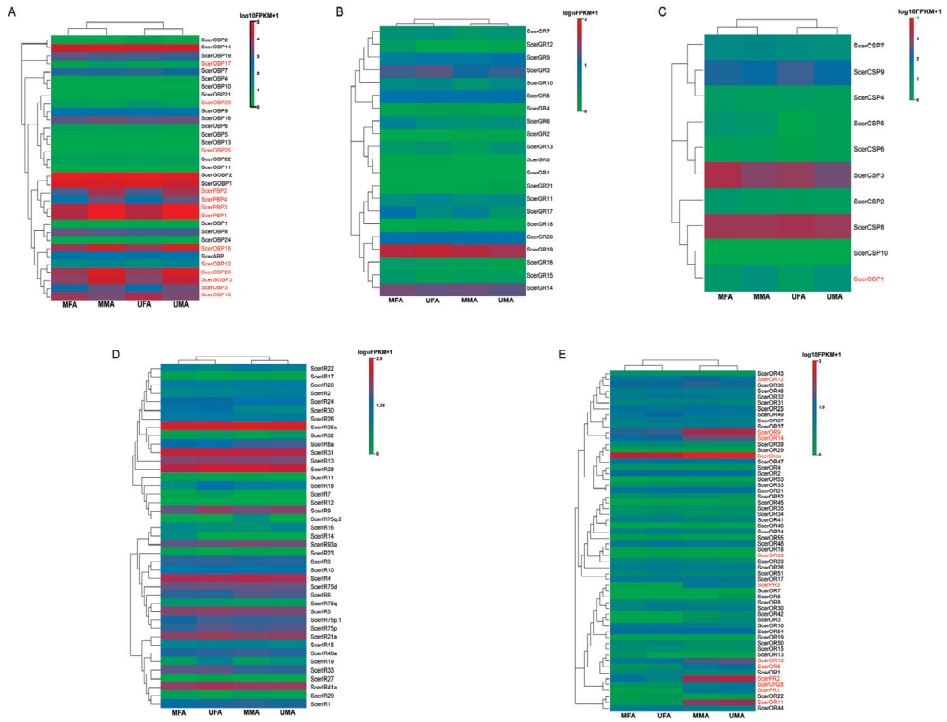


Figure 8. Expression levels (FPKM) of olfactory genes in mated and unmated female and male antennae are displayed behind the gene names (red indicates that there are differences in gene expression levels between male and female antennae). Expression values (FPKM) are shown on a log2 scale. (**A**): ScerOBPs, (**B**): ScerGRs, (**C**): ScerCSPs, (**D**): ScerIRs, (**E**): ScerORs; MFA: mated female antennae, UFA: unmated female antennae, MMA: mated male antennae, UMA: unmated male antennae.

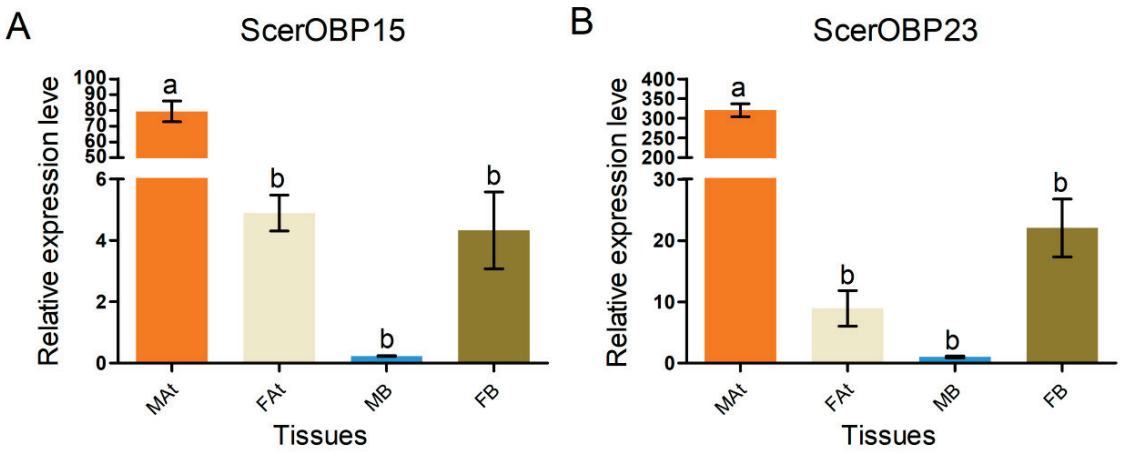


Figure 9. Odorant-binding proteins (OBPs) expression levels of *S. cerealella* in different chemosensory tissues. MAt: male antennae; FAt: female antennae; MB: male bodies; FB: female bodies. Standard errors are represented by the error bar. Different letters (a, b) above each bar denote significant differences ($p < 0.05$). (**A**) ScerOBP15; (**B**) ScerOBP23.

3.4. Protein Structure and Interaction Analysis by 3-Dimensional Docking

To elucidate the interactions between ScerOBP15, ScerOBP23, and the volatiles from the wheat and *S. cerealella*, we modeled the 3D structures of ScerOBP15 and ScerOBP23 using the Swiss-model software. The template details are presented in Table 2. The accuracy of the constructed models was evaluated using ERRAT, Verify-3D, and ProCheck, with the outcomes indicating that the models' structures are plausible (Supplementary Materials: Figures S1–S3). Sequence alignment of the target proteins with their respective templates was conducted using the ESPript 3.0 tool [55]. The analysis revealed that both ScerOBP15 and ScerOBP23 possess six conserved cysteine residues, which can form three disulfide bonds (Supplementary material: Figure S4). Additionally, both proteins feature six α-helices, which is consistent with the typical structural features of OBPs. We accordingly reasoned that the 3D structures of ScerOBP15 and ScerOBP23 were acceptable and could be used for further analysis.

Table 2. Modeling information of ScerOBP15 and ScerOBP23 in *S. cerealella*.

Name	Template	Species/Protein Name	Seq Identify	Coverage
ScerOBP15	2erb.1.A	*Anopheles gambiae*/AgamOBP1	40.37%	0.95
ScerOBP23	3ogn.1.A	*Culex quinquefasciatus*/OBP	31.93%	0.90

An analysis reveals that the binding affinity of ScerOBP15 for 12 ligands spans from −6.201 to −4.406 kcal/mol, as outlined in Table 3. Notably, ScerOBP15 exhibits the strongest binding affinity with geranyl acetone, with a binding energy of −6.201 kcal/mol. Following is oleic acid, with a binding energy of −6.016 kcal/mol, and the interaction with pentadecanoic acid is characterized by a binding energy of −5.721 kcal/mol. The binding energy with eight other volatiles, substantial at −5.00 kcal/mol, indicates a high binding affinity for these substances. Docking experiments conducted with the ScerOBP15 protein model identified several key binding sites (Table 3). Figure 10 illustrates the three-dimensional binding configurations, binding cavities, and two-dimensional interaction diagrams of the docked complexes. Key residues within the ScerOBP15 binding pocket, such as IEU-4, ILE-44, LEU-48, LEU-67, TRP-104, PHE-113, and LEU-114, are primarily involved in ligand interactions, predominantly through hydrophobic interactions.

Table 3. Binding energy of odor compounds and ScerOBPs.

Compounds	Molecular Formula	CAS Number	Binding Energy (kcal/mol)	
			ScerOBP15	ScerOBP23
tetradecane	C14H30	629-59-4	−5.402	−5.392
1-pentadecene	C15H30	13360-61-7	−5.308	−5.349
hexadecane	C16H34	544-76-3	−5.386	−5.293
n-heptadecane	C17H36	629-78-7	−5.685	−5.938
1-iododecane	C10H21I	2050-77-3	−4.406	−4.901
nonylaldehyde	C9H18O	124-19-6	−4.468	−4.595
capric aldehyde	C10H20O	112-31-2	−4.384	−4.608
palmitic acid	C16H32O2	57-10-3	−5.509	−5.37
oleic acid	C18H34O2	112-79-8	−6.016	−5.907
pentadecanoic acid	C15H30O2	1002-84-2	−5.721	−5.632
methylheptenone	C8H14O	110-90-3	−4.638	−4.755
geranyl acetone	C13H22O	689-67-8	−6.201	−5.811

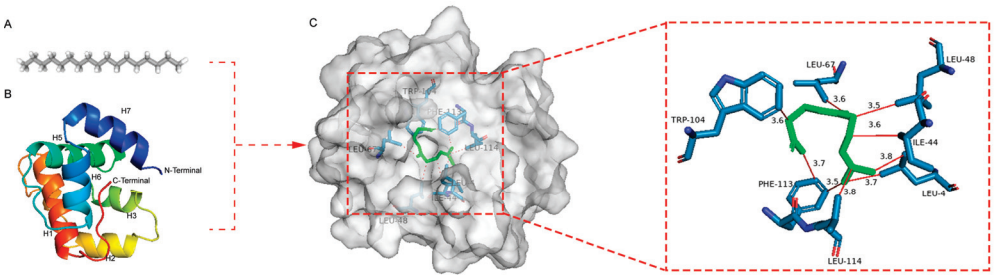


Figure 10. The binding mode and interaction diagram of ScerOBP15 with geranyl acetone (Hydrophobic interactions: red). (**A**) geranyl acetone; (**B**) The 3D model of the target protein ScerOBP15 based on the crystal structure of the template protein of AgamOBP1; (**C**) Three-dimensional structure of the combined model between ScerOBP15 and geranyl acetone.

Molecular-docking analyses revealed that ScerOBP23 exhibits binding affinities of −5.938, −5.907, −5.811, and −5.632 kJ/mol with n-heptadecane, oleic acid, geranyl acetone, and pentadecanoic acid, respectively. This indicates that ScerOBP23 is capable of forming stable complexes with these four ligand molecules. The spatial architecture of the residues and the nature of the interaction forces are pivotal for understanding the key interactions between these amino acid residues and ligands. Figure 11 presents the three-dimensional binding configurations, binding cavities, and two-dimensional interaction diagrams of the docked complexes. Key residues within the ScerOBP23 binding pocket, including ILE-15, IEU-54, IEU-55, ALA-58, LEU-60, LEU-72, LEU-75, ILE-76, VAL-84, VAL-119, and PHE-121, are engaged in ligand interactions. In the n-heptadecane–ScerOBP23 complex, these residues primarily exhibit hydrophobic interactions, with odor molecules largely enveloped by hydrophobic amino acid-rich binding cavities.

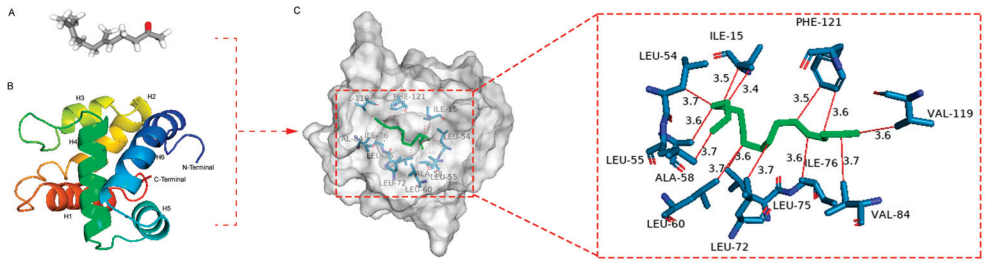


Figure 11. The binding mode and interaction diagram of ScerOBP23 with n-heptadecane (Hydrophobic interactions: red). (**A**) n-heptadecane; (**B**) The 3D model of the target protein ScerOBP23 based on the crystal structure of the template protein of AgamOBP1; (**C**) Three-dimensional structure of the combined model between ScerOBP23 and n-heptadecane.

4. Discussion

In recent years, advancements in high-throughput sequencing technologies have facilitated the identification of numerous olfactory-related genes in various insect species, including *Oxya chinensis* (Thunberg) [56], *Cotesia vestalis* (Haliday) [57], *Locusta migratoria* (L.) [58], *Micromelalopha troglodyta* (Graeser) [59], *Anastatus japonicus* (Ashmead) [60], and *Ceracris nigricornis* (Walker) [42]. Despite these findings, a systematic characterization of the olfactory-related genes in *S. cerealella* remains lacking. To address this gap, we utilized the MGISEQ-2000 platform for sequencing the antennal transcriptome of *S. cerealella*, resulting in the identification of 167 olfactory-related genes, encompassing 33 OBPs, 10 CSPs, 58 ORs, 41 IRs, 21 GRs, 2 SNMPs, and 2 ODEs. Subsequently, we explored the expression profiles, ligand affinities, and binding mechanisms of ScerOBP15 and ScerOBP23. Our mining of olfactory-related genes aims to elucidate the olfactory mechanisms of *S. cerealella* and lays the groundwork for developing eco-friendly control strategies.

Odorant-binding proteins are responsible for transporting odor molecules to olfactory receptor neurons (ORNs), where they activate olfactory receptors (ORs) or ionotropic receptors (IRs), ultimately conveying the signals to downstream effectors within the olfactory system [56]. The antennal transcriptome of *S. cerealella* revealed a number of ScerOBPs comparable to certain species, with 28 identified in *S. insularis* and 32 in *Micromelalopha troglodyta* [16,59], yet surpassing the counts in *Oxya chinensis* (18 OBPs) [56], *Cotesia vestalis* (22 OBPs) [57], *Hylamorpha elegans* (16 OBPs) [61], and *Ceracris nigricornis* (20 OBPs) [42]. Four genes were designated as candidate pheromone-binding proteins due to their clustering with PBPs from other Lepidopteran species in the phylogenetic analysis of *S. cerealella* OBPs. An analysis of the antennal transcriptome data revealed that ScerPBPs are more highly expressed in male antennae than in female antennae, indicating a potential role in mate recognition in *S. cerealella*. Similarly, certain PBPs, such as CpunPBP2, exhibit elevated expression in male antennae, suggesting that PBP genes may serve distinct functions across sexes. Given that PBPs are known to be modulated by sex pheromone release, mating, or oviposition, these genes likely play crucial roles in reproductive behaviors [62]. Additionally, a phylogenetic analysis revealed that ScerGOBP1 formed a distinct clade with GOBPs from various Lepidopteran species, including *G. mellonella*, *M. separata*, *L. botrana*, *S. insularis*, *L. sticticalis*, and *C. pinicolalis*, while ScerGOBP2 clustered with GOBP2 from these species. This suggests a shared evolutionary origin for these GOBPs. An expression analysis indicated that ScerGOBP1 and ScerGOBP2 were highly expressed in both antennal samples, potentially implicating them in the detection of common odors. Considering that several OBPs from *Grapholita funebrana* are highly expressed in the antennae of both male and female moths, and that GfunGOBPs exhibit a dual capacity for selectively binding to sex pheromones and host-plant volatiles [63,64], it is plausible that their *S. cerealella* counterparts may possess analogous functions. However, additional research is necessary to explore the potential evolutionary conservation of these functions.

Based on FPKM values, ScerOBP15 and ScerOBP23 exhibited high levels of expression in both male and female antennae. However, analysis with the DESeq2 program indicated that the expression levels of these genes in male antennae were markedly higher than in female antennae, a finding confirmed by RT-qPCR. Additionally, RT-qPCR revealed no significant difference in the expression levels of ScerOBP15 and ScerOBP23 between male and female bodies lacking antennae. Consistent with these results, Semanotus bifasciatus exhibited similar expression patterns for SbifOBP18 and SbifOBP21 in both sexes' antennae [65].

Within the insect olfactory system, CSPs participate in the transport of odor molecules, akin to OBPs [66,67]. CSPs, characterized by four conserved cysteine residues, exhibit

greater sequence conservation compared to OBPs [68,69]. In our study, ten ScerCSPs were identified in the antennal transcriptome of *S. cerealella*, each featuring a 16–22 amino acid signal peptide. Beyond their chemoreceptive role, CSPs are implicated in a variety of functions. Numerous studies have documented the presence of CSPs in pheromone glands, suggesting their potential involvement in pheromone release. Additionally, CSPs are hypothesized to play a role in insect development and regeneration. For instance, in *Blatta germanica*, a CSP is involved in leg regeneration [70]. OcomCSP12 is specifically expressed in *Ophraella communa* ovaries, and silencing this gene will result in the embryos not developing completely [71]. A similar phenomenon is observed in Apis mellifera [72]. Furthermore, CSPs are engaged in fatty acid biosynthesis and other metabolic pathways [73].

In this research, we identified 58 ORs from the antennal transcriptome of *S. cerealella*, with 26 possessing ORFs. Notably, 12 of these ORs exhibited a significant expression difference in FPKM values. Within *S. cerealella*, ScerPR1–3 were characterized as pheromone receptors (PRs), and an FPKM analysis revealed their specific expression in male antennae. Additionally, eight other ScerORs displayed a male antennae-enriched expression pattern, though their specific functions remain elusive and necessitate further investigation. Functional annotation of the antennal transcriptome revealed the presence of an Orco homolog in *S. cerealella*, and phylogenetic analysis indicated that ScerOrco clusters within a conserved clade with Orco from other Lepidopteran species. In insects, Orco is a highly conserved protein, typically with a single copy present per species. Typically, heterotetrameric odorant-gated ion channels are formed by the association of Orco with a variable OR [18].

A total of 41 IRs were identified in the antennal transcriptome of *S. cerealella*, surpassing the numbers identified in *L. sticticalis* (17) [14], *Hylamorpha elegans* (22) [61], *C. medinalis* (13) [74], *G. mellonella* (22) [75], and *Halyomorpha halys* (24) [76]. A phylogenetic analysis, incorporating ScerIRs with IRs from other Lepidopteran species, revealed 11 distinct clusters, including the IR8a, IR25a, IR21a, IR40a, IR41a, IR64a, IR68a, IR75d, IR75q, IR75p, and IR93a groups. IR8a and IR25a are recognized as co-receptors, as evidenced by their co-expression with other IRs in prior studies [10]. The roles of IRs are more intricate than those of ORs, extending beyond olfaction to include the detection of amines, acids, taste, and temperature sensing. For instance, IR21a and IR93a have been implicated in thermosensation in *Drosophila* [77,78]. IR41a is involved in long-range attraction to the polyamines [79]; and IR64a, specifically activated by acid, is suggested to play a crucial role in acid detection in *Drosophila* [80].

In our analysis of *S. cerealella*, we identified 21 GRs, a count lower than that observed in *B. mori* (65) and *Manduca sexta* (45) [81,82]. This discrepancy could be attributed to the specific expression of certain GRs in non-olfactory tissues [83]. Numerous moth species, including *S. cerealella*, utilize GRs for the detection of sugar, fructose, CO_2, and bitter components [11]. A phylogenetic analysis indicated that ScerGR14–16 grouped with potential CO_2 receptor orthologs (Bmor1N, 2NJ, and 3F) from *B. mori*, implying a potential role in CO_2 detection in *S. cerealella* [82]. Nine GRs (Scer3–5, 7, 9, 10, 12, 19, 20) were classified within the sugar and fructose receptor clades. Empirical evidence supports the crucial role of sugar and fructose in host location and oviposition behavior in female moths, suggesting that these nine GRs may modulate egg-laying behavior [83]. Additionally, nine ScerGRs were identified within the bitter receptor clade, potentially involved in the perception and discrimination of plant-derived toxic secondary metabolites [82].

ScerOBP15 and ScerOBP23 exhibit broad binding spectra for volatile compounds in wheat grains, with 8 out of 12 host volatile compounds demonstrating binding activity. Notably, they exhibit strong binding affinity for n-heptadecan, oleic acid, pentadecanoic

acid, and geranylacetone. ScerOBP15 shows a stronger binding capacity to oleic acid, pentadecanoic acid, and geranyl acetone compared to ScerOBP23, but a slightly weaker affinity for n-heptadecan. This suggests that both ScerOBP15 and ScerOBP23 are capable of selectively recognizing volatile compounds from host plants. In other insects, OBPs have been shown to selectively bind to host volatile compounds or environmental volatile information substances. For instance, HparOBP14 from the Black Gill tortoise beetle can bind to the host-plant volatile compound 6-Methyl-5-hepten-2-one, as well as other volatiles such as p-Xylene, methanol, formaldehyde, α-pinene, and geraniol [84]. DcitOBP2 from the citrus mealybug binds to the host volatile compounds methyl disulfide and D-limonene [85]. SlitOBP34 from Spodoptera litura binds to host-plant volatile compounds, including benzaldehyde, 1-hexanol, and ethyl cis-3-hexenoate [86]. Crystal structure studies of OBPs using NMR have revealed that OBPs typically interact with different ligands through non-polar or polar amino acid residues in their hydrophobic binding cavities, forming hydrogen bonds, hydrophobic interactions, and van der Waals forces [87,88]. For example, AcerOBP2 forms hydrogen bonds with 4-methoxybenzaldehyde and (E)-ethyl cinnamate, while with methyl cinnamate, only hydrophobic interactions and van der Waals forces are observed [89]. This study demonstrates that ScerOBP15 and ScerOBP23 have the strongest binding effects with geranylacetone and n-heptadecan, respectively, with binding energies of -6.201 kcal/mol and -5.938 kcal/mol. Molecular-docking results indicate that geranylacetone is located within a binding cavity formed by six α-helices in ScerOBP15 and stabilizes the protein–ligand complex by forming hydrophobic interactions with seven hydrophobic amino acid residues, including IEU-4, ILE-44, LEU-48, LEU-67, TRP-104, PHE-113, and LEU-114. Similarly, n-heptadecan is situated in the binding cavity of ScerOBP23 and forms hydrophobic interactions with several surrounding hydrophobic amino acid residues, resulting in a tight binding with ScerOBP23. The binding of geranylacetone and n-heptadecan to ScerOBP15 and ScerOBP23, respectively, suggests that these ligands are enclosed by a hydrophobic cavity, leading to a strong receptor–ligand interaction. This binding mode is analogous to that of Apis cerana AcerOBP2 with methyl cinnamate, highlighting the pivotal role of hydrophobic amino acids in OBP–ligand binding [89]. This study predicts the key amino acid residues involved in odor ligand binding by ScerOBP15 and ScerOBP23 using molecular docking. However, molecular docking is often a static and instantaneous simulation, potentially deviating from actual protein-binding scenarios. Therefore, to further elucidate the specific role of these hydrophobic amino acids in the recognition of host volatiles by ScerOBP15 and ScerOBP23, additional approaches, such as site-directed mutagenesis and fluorescence competition binding assays, are required to assess the impact of key amino acid mutations on the ligand-binding capacity of ScerOBP15 and ScerOBP23.

5. Conclusions

The primary objective of this study was to identify the genes underlying olfactory sensation, host localization, feeding behavior, and oviposition preferences in *S. cerealella* through transcriptome sequencing analysis. We annotated a total of 167 chemoreception-related transcripts, comprising 33 OBPs, 10 CSPs, 58 ORs, 41 IRs, 21 GRs, 2 SNMPs, and 2 ODEs. Phylogenetic trees were constructed, and thorough comparative analyses were conducted. Additionally, we conducted preliminary structural and functional analyses of ScerOBP15 and ScerOBP23, focusing on the role of key residues in protein–ligand interactions. This research offers significant insights into the olfactory recognition mechanisms of *S. cerealella* and facilitates the further functional characterization of these genes.

Supplementary Materials: The following supporting information can be downloaded at https://www.mdpi.com/article/10.3390/insects16050461/s1: Figure S1: Error value of ERRAT calculation of modeled ScerOBP15 and ScerOBP23; Figure S2: Verify-3D evaluation of the model of ScerOBP15 and ScerOBP23; Figure S3: Procheck's evaluation of ScerOBP15 and ScerOBP23 model; Figure S4: Sequence alignment of ScerOBP15 and ScerOBP23 with homology modeling templates; Table S1: GenBank accession numbers of genes used in phylogenetic analyses; Table S2: Primers design of selected genes for RT-qPCR; Table S3: Putative Olfactory proteins identified in *S. cerealella* antennae.

Author Contributions: Conceptualization, H.L.; methodology, H.L. and X.H.; validation, X.H., S.Q., and Y.W.; formal analysis, S.Q. and Y.W.; resources, X.H., S.Q., and Y.W.; data curation, X.H. and S.Q.; writing—original draft preparation, X.H. and S.Q.; writing—review and editing, H.L.; visualization, X.H.; supervision, H.L.; funding acquisition, H.L. All authors have read and agreed to the published version of the manuscript.

Funding: This research was funded by the National Natural Science Foundation of China, grant number 31501891, the Key Science and Technology Program of Henan Province, grant number 222102110217, the Henan Provincial Science and Technology Research and Development Plan Joint Fund (application research category) project, grant number 242103810077, and the Cultivation Programme for Young Backbone Teachers at Henan University of Technology, grant number 21420094.

Data Availability Statement: All the sequencing data generated in this study were submitted to the National Genomics Data Center under accession number: PRJNA877069.

Acknowledgments: We would like to thank the staff at FeiSha Company (Wuhan, China) for their technical support.

Conflicts of Interest: The authors declare that this study received funding from FeiSha Company (Wuhan, China). The funder had the following involvement with the study: the construction of the cDNA library and sequencing. The funder was not involved in the study design, analysis, or interpretation of the data, writing of this article, or decision to submit it for publication.

Abbreviations

The following abbreviations are used in this manuscript:

OBPs	Odorant-binding proteins
GOBPs	General odorant-binding proteins
PBPs	Pheromone-binding proteins
CSPs	Chemosensory proteins
ORs	Odorant receptors
IRs	Ionotropic receptors
GRs	Gustatory receptors
SNMPs	Sensory neuron membrane proteins
ODEs	Odorant-degrading enzymes
ORNs	Olfactory receptor neurons
ORFs	Open-reading frames
BLASTx	Basic Local Alignment Search Tool
qRT-PCR	Quantitative Real-Time Reverse Transcription Polymerase Chain Reaction
SOAPnuke	RSOAPaligner nuke
FPKM	Fragments per kilobase of exon model per million mapped fragments
KOG	Eukaryotic Ortholog Groups
GO	Gene Ontology
KEGG	Kyoto Encyclopedia of Genes and Genomes

References

1. Zhang, T.; Coates, B.S.; Ge, X.; Bai, S.; He, K.; Wang, Z. Male-and female-biased gene expression of olfactory-related genes in the antennae of Asian corn borer, *Ostrinia furnacalis* (Guenée) (Lepidoptera: Crambidae). *PLoS ONE* **2015**, *10*, e0128550. [CrossRef]
2. Jing, D.; Zhang, T.; Bai, S.; He, K.; Prabu, S.; Luan, J.; Wang, Z. Sexual-biased gene expression of olfactory-related genes in the antennae of *Conogethes pinicolalis* (Lepidoptera: Crambidae). *BMC Genom.* **2020**, *21*, 244. [CrossRef]
3. Leal, W.S. Odorant reception in insects: Roles of receptors, binding proteins, and degrading enzymes. *Annu. Rev. Entomol.* **2013**, *58*, 373–391. [CrossRef]
4. Zhao, Y.; Ding, J.; Zhang, Z.; Liu, F.; Zhou, C.; Mu, W. Sex-and tissue-specific expression profiles of odorant binding protein and chemosensory protein genes in *Bradysia odoriphaga* (Diptera: Sciaridae). *Front. Physiol.* **2018**, *9*, 107. [CrossRef]
5. Pelosi, P.; Iovinella, I.; Zhu, J.; Wang, G.; Dani, F.R. Beyond chemoreception: Diverse tasks of soluble olfactory proteins in insects. *Bacteriol. Rev.* **2018**, *93*, 184–200. [CrossRef]
6. Pelosi, P.; Zhou, J.J.; Ban, L.P.; Calvello, M. Soluble protein in insect chemical communication. *Cell. Mol. Life Sci.* **2006**, *63*, 1658–1676. [CrossRef]
7. He, P.; Li, Z.Q.; Zhang, Y.F.; Chen, L.; Wang, J.; Xu, L.; Zhang, Y.N.; He, M. Identification of odorant-binding and chemosensory protein genes and the ligand affinity of two of the encoded proteins suggest a complex olfactory perception system in *Periplaneta americana*. *Insect Mol. Biol.* **2017**, *26*, 687–701. [CrossRef]
8. Vogt, R.G.; Riddiford, L.M. Pheromone binding and inactivation by moth antennae. *Nature* **1981**, *293*, 161–163. [CrossRef]
9. Chang, X.Q.; Nie, X.P.; Zhang, Z.; Zeng, F.F.; Lv, L.; Zhang, S.; Wang, M.Q. De novo analysis of the oriental armyworm *Mythimna separata* antennal transcriptome and expression patterns of odorant-binding proteins. *Comp. Biochem. Physiol. Part D Genom. Proteom.* **2017**, *22*, 120–130. [CrossRef]
10. Li, Y.J.; Chen, H.C.; Yan, M.W.; Wang, J.; Shao, Z.M.; Wu, F.A.; Sheng, S.; Wang, J. Identification of chemosensory genes by antennal transcriptome analysis and expression profiles of odorant-binding proteins in parasitoid wasp *Aulacocentrum confusum*. *Comp. Biochem. Physiol. D Genom. Proteom.* **2021**, *40*, 100881. [CrossRef]
11. Gonzalez, F.; Johny, J.; Walker, W.B.; Guan, Q.; Mfarrej, S.; Jakše, J.; Montagné, N.; Jacquin-Joly, E.; Alqarni, A.S.; Al-Saleh, M.A.; et al. Antennal transcriptome sequencing and identification of candidate chemoreceptor proteins from an invasive pest, the American palm weevil, *Rhynchophorus palmarum*. *Sci. Rep.* **2021**, *11*, 8334. [CrossRef] [PubMed]
12. Jiang, X.C.; Liu, S.; Jiang, X.Y.; Wang, Z.W.; Xiao, J.J.; Gao, Q.; Sheng, C.W.; Shi, T.F.; Zeng, H.R.; Yu, L.S.; et al. Identification of olfactory genes from the greater wax moth by antennal transcriptome analysis. *Front. Physiol.* **2021**, *12*, 663040. [CrossRef] [PubMed]
13. Liu, P.; Zhang, X.; Meng, R.; Liu, C.; Li, M.; Zhang, T. Identification of chemosensory genes from the antennal transcriptome of *Semiothisa cinerearia*. *PLoS ONE* **2020**, *15*, e0237134. [CrossRef]
14. Wei, H.S.; Li, K.B.; Zhang, S.; Cao, Y.Z.; Yin, J. Identification of candidate chemosensory genes by transcriptome analysis in *Loxostege sticticalis Linnaeus*. *PLoS ONE* **2017**, *12*, e0174036. [CrossRef] [PubMed]
15. Rojas, V.; Jiménez, H.; Palma-Millanao, R.; González-González, A.; Machuca, J.; Godoy, R.; Ceballos, R.; Mutis, A.; Venthur, H. Analysis of the grapevine moth *Lobesia botrana* antennal transcriptome and expression of odorant-binding and chemosensory proteins. *Comp. Biochem. Physiol. D Genom. Proteom.* **2018**, *27*, 1–12. [CrossRef]
16. Yang, Y.; Li, W.; Tao, J.; Zong, S. Antennal transcriptome analyses and olfactory protein identification in an important wood-boring moth pest, *Streltzoviella insularis* (Lepidoptera: Cossidae). *Sci. Rep.* **2019**, *9*, 17951. [CrossRef]
17. Clyne, P.J.; Warr, C.G.; Freeman, M.R.; Lessing, D.; Kim, J.; Carlson, J.R. A novel family of divergent seven-transmembrane proteins: Candidate odorant receptors in *Drosophila*. *Neuron* **1999**, *22*, 327–338. [CrossRef]
18. Sato, K.; Pellegrino, M.; Nakagawa, T.; Nakagawa, T.; Vosshall, L.B.; Touhara, K. Insect olfactory receptors are heteromeric ligand-gated ion channels. *Nature* **2008**, *452*, 1002–1006. [CrossRef]
19. Trible, W.; Olivos-Cisneros, L.; McKenzie, S.K.; Saragosti, J.; Chang, N.C.; Matthews, B.J.; Oxley, P.R.; Kronauer, D.J. Orco mutagenesis causes loss of antennal lobe glomeruli and impaired social behavior in ants. *Cell* **2017**, *170*, 727–735. [CrossRef]
20. Benton, R.; Vannice, K.S.; Gomez-Diaz, C.; Vosshall, L.B. Variant ionotropic glutamate receptors as chemosensory receptors in *Drosophila*. *Cell* **2009**, *136*, 149–162. [CrossRef]
21. Cao, D.; Liu, Y.; Wei, J.; Liao, X.; Walker, W.B.; Li, J.; Wang, G. Identification of candidate olfactory genes in *Chilo suppressalis* by antennal transcriptome analysis. *Int. J. Biol. Sci.* **2014**, *10*, 846–860. [CrossRef] [PubMed]
22. Raji, J.I.; Melo, N.; Castillo, J.S.; Gonzalez, S.; Saldana, V.; Stensmyr, M.C.; DeGennaro, M. Aedes aegypti mosquitoes detect acidic volatiles found in human odor using the IR8a pathway. *Curr. Biol.* **2019**, *29*, 1253–1262. [CrossRef]
23. Abuin, L.; Bargeton, B.; Ulbrich, M.H.; Isacoff, E.Y.; Kellenberger, S.; Benton, R. Functional architecture of olfactory ionotropic glutamate receptors. *Neuron* **2011**, *69*, 44–60. [CrossRef]

24. Gomez-Diaz, C.; Martin, F.; Garcia-Fernandez, J.M.; Alcorta, E. The two main olfactory receptor families in *Drosophila*, ORs and IRs: A comparative approach. *Front. Cell. Neurosci.* **2018**, *12*, 253. [CrossRef] [PubMed]
25. Montell, C. A taste of the *Drosophila* gustatory receptors. *Curr. Opin. Neurobiol.* **2009**, *19*, 345–353. [CrossRef] [PubMed]
26. Freeman, E.G.; Wisotsky, Z.; Dahanukar, A. Detection of sweet tastants by a conserved group of insect gustatory receptors. *Proc. Natl. Acad. Sci. USA* **2014**, *111*, 1598–1603. [CrossRef]
27. Agnihotri, A.R.; Roy, A.A.; Joshi, R.S. Gustatory receptors in Lepidoptera: Chemosensation and beyond. *Insect Mol. Biol.* **2016**, *25*, 519–529. [CrossRef]
28. Zhang, S.; Wang, X.; Zhang, Y.; Zheng, Y.; Fan, Z.; Zhang, R. Identification of olfactory genes in *Monochamus saltuarius* and effects of *Bursaphelenchus xylophilus* infestation on their expression. *Forests* **2022**, *13*, 258. [CrossRef]
29. Benton, R.; Vannice, K.S.; Vosshall, L.B. An essential role for a CD36-related receptor in pheromone detection in *Drosophila*. *Nature* **2007**, *450*, 289–293. [CrossRef]
30. Forstner, M.; Gohl, T.; Gondesen, I.; Raming, K.; Breer, H.; Krieger, J. Differential expression of SNMP-1 and SNMP-2 proteins in pheromone-sensitive hairs of moths. *Chem. Senses* **2008**, *33*, 291–299. [CrossRef]
31. Cassau, S.; Krieger, J. The role of SNMPs in insect olfaction. *Cell Tissue Res.* **2021**, *383*, 21–33. [CrossRef] [PubMed]
32. Devillers, J. 2D and 3D structure–activity modelling of mosquito repellents: A review. *SAR QSAR Environ. Res.* **2018**, *29*, 693–723. [CrossRef]
33. Liggri, P.G.; Pérez-Garrido, A.; Tsitsanou, K.E.; Dileep, K.V.; Michaelakis, A.; Papachristos, D.P.; Pérez-Sánchez, H.; Zographos, S.E. 2D finger-printing and molecular docking studies identified potent mosquito repellents targeting odorant binding protein 1. *Insect Biochem. Mol. Biol.* **2023**, *157*, 103961. [CrossRef] [PubMed]
34. John, B.; Sali, A. Comparative protein structure modeling by iterative alignment, model building and model assessment. *Nucleic Acids Res.* **2003**, *31*, 3982–3992. [CrossRef]
35. Brito, N.F.; Moreira, M.F.; Melo, A.C.A. A look inside odorant-binding proteins in insect chemoreception. *J. Insect Physiol.* **2016**, *95*, 51–65. [CrossRef]
36. Zheng, J.; Li, J.; Han, L.; Wang, Y.; Wu, W.; Qi, X.; Tao, Y.; Zhang, L.; Zhang, Z.; Chen, Z. Crystal structure of the Locusta migratoria odorant binding protein. *Biochem. Biophys. Res. Commun.* **2015**, *456*, 737–742. [CrossRef]
37. Venthur, H.; Mutis, A.; Zhou, J.J.; Quiroz, A. Ligand binding and homology modelling of insect odorant-binding proteins. *Physiol. Entomol.* **2014**, *39*, 183–198. [CrossRef]
38. Wang, Q.; Wen, X.; Lu, Y.; Wen, J. Comparison and functional analysis of chemosensory protein genes from *Eucryptorrhynchus scrobiculatus* Motschulsky and *Eucryptorrhynchus brandti* Harold. *Front. Physiol.* **2021**, *12*, 661310. [CrossRef] [PubMed]
39. Jin, S.; Qian, K.; He, L.; Zhang, Z. iORandLigandDB: A Website for Three-Dimensional Structure Prediction of Insect Odorant Receptors and Docking with Odorants. *Insects* **2023**, *14*, 560. [CrossRef]
40. Okimoto, N.; Futatsugi, N.; Fuji, H.; Suenaga, A.; Morimoto, G.; Yanai, R.; Ohno, Y.; Narumi, T.; Taiji, M. High-performance drug discovery: Computational screening by combining docking and molecular dynamics simulations. *PLoS Comput. Biol.* **2009**, *5*, e1000528. [CrossRef]
41. Ma, M.; Chang, M.M.; Lei, C.L.; Yang, F.L. A garlic substance disrupts odorant-binding protein recognition of insect pheromones released from adults of the angoumois grain moth, *Sitotroga cerealella* (Lepidoptera: Gelechiidae). *Insect Mol. Biol.* **2016**, *25*, 530–540. [CrossRef] [PubMed]
42. Yuan, H.; Chang, H.; Zhao, L.; Yang, C.; Huang, Y. Sex-and tissue-specific transcriptome analyses and expression profiling of olfactory-related genes in *Ceracris nigricornis* Walker (Orthoptera: Acrididae). *BMC Genom.* **2019**, *20*, 808. [CrossRef] [PubMed]
43. Haas, B.J.; Papanicolaou, A.; Yassour, M.; Grabherr, M.; Blood, P.D.; Bowden, J.; Couger, M.B.; Eccles, D.; Li, B.; Lieber, M.; et al. De novo transcript sequence reconstruction from RNA-seq using the Trinity platform for reference generation and analysis. *Nat. Protoc.* **2013**, *8*, 1494–1512. [CrossRef]
44. Tatusov, R.L.; Fedorova, N.D.; Jackson, J.D.; Jacobs, A.R.; Kiryutin, B.; Koonin, E.V.; Krylov, D.M.; Mazumder, R.; Mekhedov, S.L.; Nikolskaya, A.N.; et al. The COG database: An updated version includes eukaryotes. *BMC Bioinform.* **2003**, *4*, 41. [CrossRef] [PubMed]
45. Trapnell, C.; Williams, B.A.; Pertea, G.; Mortazavi, A.; Kwan, G.; Van Baren, M.J.; Salzberg, S.L.; Wold, B.J.; Pachter, L. Transcript assembly and quantification by RNA-Seq reveals unannotated transcripts and isoform switching during cell differentiation. *Nat. Biotechnol.* **2010**, *28*, 511–515. [CrossRef]
46. Love, M.I.; Huber, W.; Anders, S. Moderated estimation of fold change and dispersion for RNA-seq data with DESeq2. *Genome Biol.* **2014**, *15*, 550. [CrossRef]
47. Livak, K.J.; Schmittgen, T.D. Analysis of relative gene expression data using real-time quantitative PCR and the $2^{-\Delta\Delta CT}$ method. *Methods* **2001**, *25*, 402–408. [CrossRef]

48. Bowie, J.U.; Lüthy, R.; Eisenberg, D. A method to identify protein sequences that fold into a known three-dimensional structure. *Science* **1991**, *253*, 164–170. [CrossRef]
49. Lüthy, R.; Bowie, J.U.; Eisenberg, D. Assessment of protein models with three-dimensional profiles. *Nature* **1992**, *356*, 83–85. [CrossRef]
50. Laskowski, R.A.; MacArthur, M.W.; Moss, D.S.; Thornton, J.M. PROCHECK: A program to check the stereochemical quality of protein structures. *J. Appl. Crystallogr.* **1993**, *26*, 283–291. [CrossRef]
51. Trott, O.; Olson, A.J. AutoDock Vina: Improving the speed and accuracy of docking with a new scoring function, efficient optimization, and multithreading. *J. Comput. Chem.* **2010**, *31*, 455–461. [CrossRef] [PubMed]
52. Eberhardt, J.; Santos-Martins, D.; Tillack, A.F.; Forli, S. AutoDock Vina 1.2. 0: New docking methods, expanded force field, and python bindings. *J. Chem. Inf. Model.* **2021**, *61*, 3891–3898. [CrossRef]
53. DeLano, W.L. Pymol: An Open-Source Molecular Graphics Tool. *CCP4 Newsl. Protein Crystallogr* **2002**, *40*, 82–92.
54. Adasme, M.F.; Linnemann, K.L.; Bolz, S.N.; Kaiser, F.; Salentin, S.; Haupt, V.J.; Schroeder, M. PLIP 2021: Expanding the scope of the protein-ligand interaction profiler to DNA and RNA. *Nucleic Acids Res.* **2021**, *49*, W530–W534. [CrossRef]
55. Robert, X.; Gouet, P. Deciphering key features in protein structures with the new ENDscript server. *Nucleic Acids Res.* **2014**, *42*, W320–W324. [CrossRef]
56. Cui, Y.; Kang, C.; Wu, Z.; Lin, J. Identification and expression analyses of olfactory gene families in the rice grasshopper, *Oxya chinensis*, from antennal transcriptomes. *Front. Physiol.* **2019**, *10*, 1223. [CrossRef] [PubMed]
57. Liu, Y.; Du, L.; Zhu, Y.; Yang, S.; Zhou, Q.; Wang, G.; Liu, Y. Identification and sex-biased profiles of candidate olfactory genes in the antennal transcriptome of the parasitoid wasp Cotesia vestalis. *Comp. Biochem. Physiol. D Genom. Proteom.* **2020**, *34*, 100657. [CrossRef]
58. Zheng, R.; Xia, Y.; Keyhani, N.O. Sex-specific variation in the antennal proteome of the migratory locust. *J. Proteomics* **2020**, *216*, 103681. [CrossRef]
59. Zhang, Y.; Feng, K.; Mei, R.; Li, W.; Tang, F. Analysis of the Antennal Transcriptome and Identification of Tissue-specific Expression of Olfactory-related Genes in *Micromelalopha troglodyta* (Lepidoptera: Notodontidae). *J. Insect Sci.* **2022**, *22*, 8. [CrossRef]
60. Zhan, H.X.; Li, L.; Li, F.Q.; Zang, L.S. Identification and Comparative Expression Profiles of Candidate Olfactory Receptors in the Transcriptomes of the Important Egg Parasitoid Wasp *Anastatus japonicus* Ashmead (Hymenoptera: Eupelmidae). *Plants* **2023**, *12*, 915. [CrossRef]
61. González-González, A.; Rubio-Meléndez, M.E.; Ballesteros, G.I.; Ramírez, C.C.; Palma-Millanao, R. Sex-and tissue-specific expression of odorant-binding proteins and chemosensory proteins in adults of the scarab beetle *Hylamorpha elegans* (Burmeister) (Coleoptera: Scarabaeidae). *PeerJ* **2019**, *7*, e7054. [CrossRef] [PubMed]
62. Jing, D.; Zhang, T.; Prabu, S.; Bai, S.; He, K.; Luan, J.; Wang, Z. PBP genes regulated by the development of the ovaries, sex pheromone release, mating and oviposition behavior in *Conogethes punctiferalis* (Guenée). *Chemoecology* **2021**, *31*, 1–9. [CrossRef]
63. Rihani, K.; Ferveur, J.F.; Briand, L. The 40-year mystery of insect odorant-binding proteins. *Biomolecules* **2021**, *11*, 509. [CrossRef]
64. Li, L.L.; Xu, B.Q.; Li, C.Q.; Li, B.L.; Chen, X.L.; Li, G.W. Different Binding Affinities of Three General Odorant-Binding Proteins in *Grapholita funebrana* (Treitscheke)(Lepidoptera: Tortricidae) to Sex Pheromones, Host Plant Volatiles, and Insecticides. *J. Econ. Entomol.* **2022**, *115*, 1129–1145. [CrossRef] [PubMed]
65. Li, H.; Hao, E.; Li, Y.; Yang, H.; Sun, P.; Lu, P.; Qiao, H. Antennal transcriptome analysis of olfactory genes and tissue expression profiling of odorant binding proteins in *Semanotus bifasciatus* (cerambycidae: Coleoptera). *BMC Genom.* **2022**, *23*, 461. [CrossRef]
66. Zhu, J.; Iovinella, I.; Dani, F.R.; Pelosi, P.; Wang, G. Chemosensory proteins: A versatile binding family. *Olfactory Concepts Insect Control* **2019**, *2*, 147–169.
67. Qiu, L.; He, L.; Tan, X.; Zhang, Z.; Wang, Y.; Li, X.; He, H.; Ding, W.; Li, Y. Identification and phylogenetics of *Spodoptera frugiperda* chemosensory proteins based on antennal transcriptome data. *Comp. Biochem. Physiol. D Genom. Proteom.* **2020**, *34*, 100680. [CrossRef]
68. Picimbon, J.F. Evolution of protein physical structures in insect chemosensory systems. *Olfactory Concepts Insect Control* **2019**, *2*, 231–263.
69. Cui, Z.; Liu, Y.; Wang, G.; Zhou, Q. Identification and functional analysis of a chemosensory protein from *Bactrocera minax* (Diptera: Tephritidae). *Pest Manag. Sci.* **2022**, *78*, 3479–3488. [CrossRef]
70. Kitabayashi, A.N.; Arai, T.; Kubo, T.; Natori, S. Molecular cloning of cDNA for p10, a novel protein that increases in the regenerating legs of *Periplaneta americana* (American cockroach). *Insect Biochem. Mol. Biol.* **1998**, *28*, 785–790. [CrossRef]
71. Ma, C.; Cui, S.; Tian, Z.; Zhang, Y.; Chen, G.; Gao, X.; Tian, Z.; Chen, H.; Guo, J.; Zhou, Z. OcomCSP12, a chemosensory protein expressed specifically by ovary, mediates reproduction in *Ophraella communa* (Coleoptera: Chrysomelidae). *Front. Physiol.* **2019**, *10*, 1290. [CrossRef] [PubMed]

72. Maleszka, J.; Forêt, S.; Saint, R.; Maleszka, R. RNAi-induced phenotypes suggest a novel role for a chemosensory protein CSP5 in the development of embryonic integument in the honeybee (*Apis mellifera*). *Dev. Genes Evol.* **2007**, *217*, 189–196. [CrossRef]
73. Cheng, D.; Lu, Y.; Zeng, L.; Liang, G.; He, X. Si-CSP9 regulates the integument and moulting process of larvae in the red imported fire ant, *Solenopsis invicta*. *Sci. Rep.* **2015**, *5*, 9245. [CrossRef] [PubMed]
74. Zeng, F.F.; Zhao, Z.F.; Yan, M.J.; Zhou, W.; Zhang, Z.; Zhang, A.; Lu, Z.X.; Wang, M.Q. Identification and comparative expression profiles of chemoreception genes revealed from major chemoreception organs of the rice leaf folder, *Cnaphalocrocis medinalis* (Lepidoptera: Pyralidae). *PLoS ONE* **2015**, *10*, e0144267. [CrossRef] [PubMed]
75. Zhao, H.X.; Xiao, W.Y.; Ji, C.H.; Ren, Q.; Xia, X.S.; Zhang, X.F.; Huang, W.Z. Candidate chemosensory genes identified from the greater wax moth, *Galleria mellonella*, through a transcriptomic analysis. *Sci. Rep.* **2019**, *9*, 10032. [CrossRef]
76. Sun, D.; Huang, Y.; Qin, Z.; Zhan, H.; Zhang, J.; Liu, Y.; Yang, S. Identification of candidate olfactory genes in the antennal transcriptome of the stink bug *Halyomorpha halys*. *Front. Physiol.* **2020**, *11*, 876. [CrossRef]
77. Ni, L.; Klein, M.; Svec, K.V.; Budelli, G.; Chang, E.C.; Ferrer, A.J.; Benton, R.; Samuel, A.D.; Garrity, P.A. The ionotropic receptors IR21a and IR25a mediate cool sensing in Drosophila. *eLife* **2016**, *5*, e13254. [CrossRef]
78. Tyrrell, J.J.; Wilbourne, J.T.; Omelchenko, A.A.; Yoon, J.; Ni, L. Ionotropic Receptor-dependent cool cells control the transition of temperature preference in *Drosophila* larvae. *PLoS Genet.* **2021**, *17*, e1009499. [CrossRef]
79. Hussain, A.; Zhang, M.; Üçpunar, H.K.; Svensson, T.; Quillery, E.; Gompel, N.; Ignell, R.; Grunwald Kadow, I.C. Ionotropic chemosensory receptors mediate the taste and smell of polyamines. *PLoS Biol.* **2016**, *14*, e1002454. [CrossRef]
80. Ai, M.; Blais, S.; Park, J.Y.; Min, S.; Neubert, T.A.; Suh, G.S. Ionotropic glutamate receptors IR64a and IR8a form a functional odorant receptor complex in vivo in Drosophila. *J. Neurosci.* **2013**, *33*, 10741–10749. [CrossRef]
81. Koenig, C.; Hirsh, A.; Bucks, S.; Klinner, C.; Vogel, H.; Shukla, A.; Mansfield, J.H.; Morton, B.; Hansson, B.S.; Grosse-Wilde, E. A reference gene set for chemosensory receptor genes of *Manduca sexta*. *Insect Biochem. Mol. Biol.* **2015**, *66*, 51–63. [CrossRef]
82. Wanner, K.W.; Robertson, H.M. The gustatory receptor family in the silkworm moth *Bombyx mori* is characterized by a large expansion of a single lineage of putative bitter receptors. *Insect Mol. Biol.* **2008**, *17*, 621–629. [CrossRef] [PubMed]
83. Li, G.; Du, J.; Li, Y.; Wu, J. Identification of putative olfactory genes from the oriental fruit moth *Grapholita molesta* via an antennal transcriptome analysis. *PLoS ONE* **2015**, *10*, e0142193. [CrossRef]
84. Qu, Y.; Liu, X.; Zhao, X.; Qin, J.; Cao, Y.; Li, K.; Zhou, J.J.; Wang, S.; Yin, J. Evidence of the involvement of a Plus-C odorant-binding protein HparOBP14 in host plant selection and oviposition of the Scarab Beetle *Holotrichia parallela*. *Insects* **2021**, *12*, 430. [CrossRef] [PubMed]
85. Zhang, H.; Chen, J.L.; Lin, J.H.; Lin, J.T.; Wu, Z.Z. Odorant-binding proteins and chemosensory proteins potentially involved in host plant recognition in the Asian citrus psyllid, *Diaphorina citri*. *Pest Manag. Sci.* **2020**, *76*, 2609–2618. [CrossRef]
86. Chen, Y.W.; Yang, H.H.; Gu, N.; Li, J.Q.; Zhu, X.Y.; Zhang, Y.N. Identification of attractants for adult Spodoptera litura based on the interaction between odorant-binding protein 34 and host volatiles. *Pestic. Biochem. Physiol.* **2024**, *203*, 106005. [CrossRef] [PubMed]
87. Li, L.L.; Huang, J.R.; Xu, J.W.; Yao, W.C.; Yang, H.H.; Shao, L.; Zhang, H.R.; Dewer, Y.; Zhu, X.Y.; Zhang, Y.N. Ligand-binding properties of odorant-binding protein 6 in Athetis lepigone to sex pheromones and maize volatiles. *Pest Manag. Sci.* **2022**, *78*, 52–62. [CrossRef]
88. Dong, J.F.; Wang, K.; Sun, Y.L.; Tian, C.H.; Wang, S.L. Antennal transcriptome analysis of odorant-binding proteins and characterization of GOBP2 in the variegated cutworm *Peridroma saucia*. *Front. Physiol.* **2023**, *14*, 1241324. [CrossRef]
89. Zhang, L.; Jiang, H.Q.; Wu, F.; Wen, P.; Qing, J.; Song, X.M.; Li, H.L. Eastern honeybee *Apis cerana* sense cold flowering plants by increasing the static binding affinity of odorant-binding protein to cold floral volatiles from loquats. *Int. J. Biol. Macromol.* **2023**, *232*, 123227. [CrossRef]

Disclaimer/Publisher's Note: The statements, opinions and data contained in all publications are solely those of the individual author(s) and contributor(s) and not of MDPI and/or the editor(s). MDPI and/or the editor(s) disclaim responsibility for any injury to people or property resulting from any ideas, methods, instructions or products referred to in the content.

insects

MDPI

Article

Tissue-Specific Fluorescent Protein Turnover in Free-Moving Flies

Katherine S. Bell [1], Sebastian Ko [1], Sam Ali [1], Brett Bognar [1], Michael Khmelkov [1], Nick Rau [1], Oscar K. Peng [1], Mavi Eyuboglu [1], John Paine [1], Andy Tong [1], Anuj Saria [1], Siddharth Agrawal [1], Kelvin J. A. Davies [2,3] and John Tower [1,*]

[1] Molecular and Computational Biology Section, Department of Biological Sciences, University of Southern California, Los Angeles, CA 90089, USA; bellkath@usc.edu (K.S.B.); kosebast@usc.edu (S.K.); sammiali.usc@gmail.com (S.A.); bognar@usc.edu (B.B.); khmelkov@usc.edu (M.K.); nickrau24@gmail.com (N.R.); oscar.peng@ucsf.edu (O.K.P.); meyubogl@usc.edu (M.E.); johnpain@usc.edu (J.P.); andytong@usc.edu (A.T.); anujsari@usc.edu (A.S.); siddharth.agrawal18@gmail.com (S.A.)

[2] Leonard Davis School of Gerontology, Ethel Percy Andrus Gerontology Center, University of Southern California, Los Angeles, CA 90089, USA; kelvin@usc.edu

[3] Department of Biochemistry & Molecular Medicine, Keck School of Medicine of USC, University of Southern California, Los Angeles, CA 90089, USA

* Correspondence: jtower@usc.edu

Simple Summary: The regulated synthesis and degradation of proteins is called protein turnover, and protein turnover is critical for the removal of damaged proteins and for normal regulation of cell and animal physiology. Defects in protein turnover during aging are implicated in the accumulation of damaged proteins in various tissues and in aging-associated diseases. In the past, protein turnover has typically been assayed by labeling the cells or animal with a radioactive or heavy isotope, followed by quantification by mass spectrometry. One limitation of these assays is that they are invasive and destructive, requiring the sacrifice of the animal. Here, we report the use of fluorescent proteins to assay protein half-life in vivo in adult *Drosophila melanogaster*. The ability to measure turnover without sacrifice of the animal facilitates the study of the effects of drugs and other small molecules.

Abstract: Conditional transgenic systems and multi-copy target transgenes were used to produce transient fluorescent protein expression in adult *Drosophila melanogaster*, with the goal of developing an in vivo assay of protein turnover. Free-moving flies were assayed at multiple time points using video, and decay in fluorescence was used to calculate protein half-life. Additional experiments involved image capture of anesthetized flies. The half-life of eGFP was increased by the proteasome inhibitor bortezomib, both in vivo and in vitro, indicating proteasomal degradation of eGFP. The accumulation of eGFP in vivo was decreased by the protein synthesis inhibitor cycloheximide, without affecting half-life. The half-lives of several fluorescent proteins were determined, using both tissue-general and tissue-specific expression, in flies of both sexes and varying ages. Typical half-life values varied by fluorescent protein. DsRED showed a greater half-life than eGFP, and little if any degradation was detected for mCherry. Half-life also varied by tissue, with greater eGFP half-life observed in muscle relative to other tissues. Increased half-life with age was detected for DsRED but not for eGFP. Limited effects were observed for sex and female mating status. Taken together, the data indicate the in vivo assays are promising tools for the study of protein degradation regulated by protein sequence, subcellular compartment, tissue and small molecules.

Keywords: *Drosophila*; GFP; DsRED; video; turnover; in vivo; degradation; proteasome; bortezomib; cycloheximide

1. Introduction

In the past, protein half-life has typically been assayed by labeling with a radioactive or heavy isotope followed by quantification by mass spectrometry [1]. One limitation of these assays is that they are invasive and destructive, requiring sacrifice of the animal. Here, we report the use of fluorescent proteins to assay protein half-life in vivo in adult *Drosophila melanogaster*.

Flies were engineered to produce transient expression of a fluorescent protein using the conditional transgenic systems Tet-ON or Gene-Switch [2–4]. After removal of the activating drug, synthesis of new protein ceases, and fluorescence declines in a manner proportional to protein degradation, yielding a measurement of protein half-life [1,5]. The conditional transgenic systems also allow for tissue-specific expression of fluorescent proteins, which is important in light of evidence for tissue-specific effects of aging on protein degradation [6–8]. Moreover, the system allows for assay of proteins targeted to organelles.

2. Materials and Methods

2.1. Video Assays

For video assay, flies were gently knocked into 4 dram (~15 mL) glass vials, using 6 flies per vial and 4 vials per group, and each vial was covered with a glass coverslip. Each vial was individually placed in a dark box illuminated using two LED lights, and two synchronized video cameras were used to capture fluorescence in 4-min videos (see Supplementary Figure S1). Prior to recording, flies were transferred to media supplemented with 200 μg/mL mifepristone for the Gene-Switch system or 640 μg/mL doxycycline for the Tet-ON system to initiate fluorescent protein expression and then removed from the drug media after 24 or 48 h, as indicated. Recordings were taken immediately after removal from the drug (day 1) and every day over a period of 5–6 days. Videos were analyzed using FluoreScore version 1 software, which identifies each fly and quantifies pixel intensity in the area of the flies in each frame [9]. The data from the cameras was combined to yield a fluorescence intensity value for each vial at each time point, and average fluorescence intensity values for the 4 vials in each group were averaged. Fluorescence typically peaked at 24 h after cessation of drug treatment for the Gene-Switch system and at 4–5 days after cessation of drug treatment for the Tet-ON system, after which it decreased exponentially. The natural logarithm of each average fluorescence value was taken, the values for each group were plotted as ln(fluorescence) versus time, and the slope of the resulting linear regression from peak to minimum was used to calculate half-life.

2.2. Fly Culture and Strains

Drosophila melanogaster were cultured at 25 °C using a standard agar/dextrose/cornmeal/yeast media [10], and adult flies were passaged to fresh media every other day. *Actin-GS-255B* is previously described and contains the *Actin5C* gene promoter driving tissue-general expression of Gene-Switch [1]. The *repo-GS* strain drives Gene-Switch expression in glial cells and was generously provided by Amita Sehgal [11]. The *5966-GS* strain expresses Gene-Switch in midgut enterocytes and was generously provided by Pankaj Kapahi [12]. *Actin88F-GS* drives expression of Gene-Switch in flight muscle and was generously provided by Jason Karpac [13]. The *w[1118]*; *3xP3-GFP[M1]* strain transgenic construct includes a synthetic promoter containing three binding sites for the Eyeless/PAX6 transcription factor and was generously provided by Ernst Wimmer [14]; the construct drives high-level expression of eGFP specif-

ically in retinal tissue and is abbreviated here as *eyeless-GFP*. Certain strains were obtained from the Bloomington Drosophila Stock Center (BDSC), including strain *y[1] w[*]; P{w[+mC] = elav-Switch.O}GSG301 (BDSC#43642)*, which is abbreviated here as *y; Elav-GS*, strain *y[1] w[*]; P{tubP-GAL4}LL7/TM3* (BDSC#5138), abbreviated here as *tub-GAL4*, strain *y[1] w[*]; wg[Sp-1]/CyO; P{Mhc-Switch.O}GSG314-2* (BDSC#43641), abbreviated here as *Mhc-GS*, strain *w[1118]; P{UAS-MitoTimer}3* (BDSC#57323), abbreviated here as *UAS-MT* [15,16], and strain *y[1] w[*]; wg[Sp-1]/CyO, P{Wee-P.ph0}Bacc[Wee-P20]; P{y[+t7.7] w[+mC] = 20XUAS-6XmCherry-HA}attP2* (BDSC#52268), abbreviated here as *UAS-mCherry*. The *w[1118]* strain (BDSC#5905) is the isogenized version (*w[1118]-iso*; *2-iso*; *3-iso*) that was previously cured of Wolbachia [10]. The *UAS-eGFP* strain employed is abbreviated as *Ultra-GFP* and contains multiple copies of a *UAS-2xeGFP* construct on both the second and third chromosomes and has been previously described [1]. To generate mated females, age-synchronized virgin females at 1–2 days of age were combined with young (3–14 day old) male *w[1118]* flies in regular food vials, with 20 females and 20 males per vial, for 48 h, after which the males were removed.

2.3. Generation of Multi-Copy Strains

Generation of Tet-ON strain REDA: The Tet-ON system driver construct rtTA consists of the *Actin5C* promoter driving expression of the reverse tetracycline trans-activator protein called rtTA [1]. The construct is inserted on the third chromosome, and the insertion strain is named *rtTA(3)E2*. The target construct contains a synthetic promoter consisting of seven Tet-operator (TetO) sequences fused to the core promoter sequences of the *hsp70* gene, driving expression of DsRED [17]. Two independent strains bearing insertions of this *TetO-DsRED* construct on the third chromosome were used, *TetO-DsRED[6]* and *TetO-DsRED[26B]* [17], each in the *w[1118]* genetic background. The target transgenic constructs bear the *mini-white+* marker gene and have light orange-colored eyes resulting from partial rescue of the *w[1118]* mutant phenotype. To increase the copy number of the target constructs, each strain was crossed to *P(ry+,Δ2-3)99B* transposase strain [18], and third chromosomes were isolated that had increased dosage of the *mini-white+* marker, as indicated by a more red eye color, and named *TetO-DsRED[6-7]* and *TetO-DsRED[26B-6]*, respectively. The increased copy number of the constructs was confirmed by crossing to the *rtTA(3)E2* strain, assaying progeny ± DOX treatment, and confirming a total two-fold increase in DsRED signal using fluorescence microscopy. The *TetO-DsRED[6-7]* and *TetO-DsRED[26B-6]* insertions were then recombined onto the same third chromosome, and the increased copy number was confirmed by again crossing to the *rtTA(3)E2* strain, assaying progeny ± DOX treatment, and confirming a total four-fold increase in DsRED signal using fluorescence microscopy. Finally, the chromosome bearing the *TetO-DsRED[6-7]* and *TetO-DsRED[26B-6]* insertions was recombined with *rtTA(3)E2* to generate a chromosome bearing all three insertions on the same third chromosome, balanced over *TM3 Sb* balancer, and in a *y[*] w[*]* genetic background; the resulting strain *y[*] w[*]; TetO-DsRED[6-7], TetO-DsRED[26B-6], rtTA(3)E2/TM3 Sb*, which is abbreviated as "REDA". The yellow mutant body color allows for increased detection of fluorescence from internal tissues relative to a wild-type body color.

Multi-copy mitoGFP strain: The strains *P{UAS-mito-HA-GFP.AP}2* and *P{UAS-mito-HA-GFP.AP}3* [19] were obtained from BDSC (BDSC#8442; BDSC#8443). Each strain was crossed to *P(ry+,Δ2-3)99B* transposase strain, and chromosomes were isolated that had increased dosage of the *mini-white+* marker strain, as indicated by a more red eye color, and named *UAS-mitoGFP[AP2-4]* and *UAS-mitoGFP[AP3-7]*, respectively. The increased copy number of the constructs was confirmed by crossing to the *tub-GAL4* strain and assaying progeny to confirm a two-fold increase in GFP signal us-

ing fluorescence microscopy. *UAS-mitoGFP[AP2-4]* and *UAS-mitoGFP[AP3-7]* were then combined into the same strain using double-balancer crosses to yield strain *y[*] w[*]; UAS-mitoGFP[AP2-4]; UAS-mitoGFP[AP3-7]/TM3 Ser*.

Multi-copy MitoTimer strain: The *UAS-MT* strain was crossed to the *P(ry+,Δ2-3)99B* transposase strain, and a third chromosome was isolated that had an increased dosage of the *mini-white+* marker, as indicated by a more red eye color, and named *UAS-MT[1]*. The increased copy number of the construct was confirmed by crossing to the *tub-GAL4* strain and assaying progeny to confirm a two-fold increase in green and red fluorescence signals using fluorescence microscopy. The *UAS-MT[1]* was crossed to the *P(ry+,Δ2-3)99B* transposase strain, and the third chromosome was isolated that had an increased dosage of the *mini-white+* marker strain, as indicated by a more red eye color, and named *UAS-MT[1-1]*. The increased copy number of the construct was confirmed by crossing to the *tub-GAL4* strain and assaying progeny to confirm a three-fold increase in green and red fluorescence signals using fluorescence microscopy (Figure S5).

2.4. Cameras and Filters

The 3D tracking and quantification of GFP fluorescence were carried out essentially as previously described [9]. Briefly, two video cameras (Grasshopper type GRAS-20S4C, Point Grey Research, Scottsdale, AZ, USA) were directed at the glass vial containing the fly. The vial was illuminated by two LED lights, and video was recorded at 30 fps. For GFP fluorescence tracking, blue LEDs were used as follows: The MF469-35 filters (Thorlabs, Inc., Newton, NJ, USA) were fixed in front of the blue LEDs to limit the light to a range of approximately 452 nm to 486 nm, which overlaps the eGFP absorption peak at approximately 488 nm. The MF525-39 filters were placed in front of the camera lenses to limit the light to the range of approximately 510 nm to 548 nm, which overlaps the emission peak for eGFP at approximately 509 nm. For DsRED tracking, green LEDs were used as follows: The TRITC excitation filters (MF542-20; Thorlabs, Inc.) were fixed in front of the green LEDs to limit the light to a range of approximately 532 nm to 552 nm, which overlaps the DsRED absorption peak at approximately 555 nm. The TRITC/CY3.5 emission filters (Thorlabs MF620-52) were placed in front of the camera lenses to limit the light to the range of approximately 595 nm to 645 nm, which overlaps the emission peak for DsRED at approximately 590 nm.

2.5. Vials, Media and Fly Handling for Video Assays

Assay of tissue-general eGFP in parallel in young and old, male and female flies. Flies were maintained as adults on NutriFly Grape Agar Premix media (Genesee Scientific 47-102), adjusted to 0.5% Casein protein (Sigma/Aldrich, St. Louis, MO, USA); this is to reduce background green fluorescence from the gut that can result from the standard *Drosophila* media. For assay, 6 flies were knocked into an empty 4 dram glass shell vial (Kimble 60965-4, Wayne, PA, USA), without anesthetization, on a foam mouse pad to avoid damage to vials. The bottom of the vial was covered with a round piece of black filter paper to reduce glare, and the top of the vial was covered with a glass coverslip.

Assay of eGFP, mitoGFP and DsRED in various tissue patterns. Clear glass shell vials (4 mL; ThermoFisher, Waltham, MA, USA) were filled with 500 μL media. The media was NutriFly Grape Agar Premix (Genesee Scientific 47-102, San Diego, CA, USA), adjusted to 0.5% Casein protein (Sigma/Aldrich) and adjusted to 0.25% wgt/vol blue dye #1. This media was used to reduce background fluorescence. The media was adjusted to a final concentration of 200 μg/mL mifepristone for the Gene-Switch system or to 640 μg/mL doxycycline for the Tet-ON system. To introduce flies, the flies were lightly anesthetized with CO_2 gas, knocked into the vial, and the vial covered at the top with a small piece

of clear tape (Grey Parrot brand crystal clear office tape) to prevent flies from escaping without compromising visibility. Flies were passaged to fresh vials every other day (using light CO_2 anesthesia). When not being assayed, all flies were kept in an incubator at 25 °C, with the exception of mitoGFP flies, which were maintained at 22 (±0.5) °C.

2.6. In Vivo Bortezomib Treatment

Virgin female progeny of *Actin-GS-255B* x *ultraGFP* cross were placed in vials with media adjusted to a final concentration of 20 μM bortezomib. The control group media received an equal volume of ethanol vehicle. All flies were also exposed to 200 μg/mL mifepristone in the media for 48 h starting from the first day of videos. Videos were taken every day for 11 days. Flies were switched to fresh ± drug vials every 48 h through the end of the experiment.

2.7. In Vivo Cycloheximide Treatment

Virgin female progeny of the *Actin-GS-255B* x *ultraGFP* cross were treated with cycloheximide added to food vials as an aqueous solution. Flies were treated with cycloheximide beginning 7 days before the start of video recordings, at an initial age of 1–3 days. Flies in the low-concentration group were maintained on media adjusted to a final concentration of 5 μM cycloheximide, and the high-concentration group was maintained on media adjusted to a final concentration of 10 μM cycloheximide. Flies in the control group were maintained on vials adjusted with an equal volume of water vehicle. Beginning with the initial video recording, all flies were transferred to vials adjusted to 200 μg/mL mifepristone, in addition to any cycloheximide. Videos were taken every day for 7 days. After 48 h, flies were removed from mifepristone and transferred to new ± cycloheximide vials; flies continued to be switched to fresh drug vials every 48 h through the end of the experiment.

2.8. Microscope Image Capture Assay and Statistical Analysis

Flies with eGFP expression were maintained on NutriFly Grape Agar Premix (Genesee Scientific 47-102), adjusted to 0.5% Casein protein (Sigma/Aldrich). Flies with red fluorescent protein expression were maintained in regular fly media vials. Flies were transferred to fresh vials every other day without anesthetization. For image capture, three flies at a time were anesthetized with CO_2 on a fly pad (Genesee Scientific), positioned on their side, and fluorescence images were generated using the Leica MZFLIII fluorescence microscope and Spot imaging system. Fly fluorescence was quantified using Image J version 1.54 software [20] and selecting the desired fly body regions as ROI using the free-hand drawing tool. For each time point, >10 flies per sample were quantified, and the data average ± standard deviation was calculated. The ln(fluorescence) versus time was plotted and analyzed using Prism 9 to conduct linear regression and generate half-life values.

2.9. In Vitro Proteasome Assay

In vitro degradation of protein by the proteasome was assayed essentially as previously described [10]. Young (3–4 day old) virgin female flies from the eyeless-GFP strain were used to generate extracts containing abundant eGFP. Whole flies were homogenized using a motorized pestle in an extraction buffer composed of 50 mM Tris, 25 mM KCl, 10 mM NaCl, 1 mM $MgCl_2$, and 1 mM DTT at pH 7.5. Three groups of 20 flies each were homogenized in 500 μL of buffer. After homogenization, each sample was subjected to 3 rounds of a freeze/thaw cycle consisting of 5 min in dry ice followed by 5 min in a room-temperature water bath. After 3 cycles the samples were centrifuged for 2 min at 10,000× *g* in a 4 °C cold room. The supernatants from the 3 replicates were pooled and then diluted 1:4 in the buffer solution. Next, 180 μL aliquots of the diluted extract were added

to black 96-well plates (Greiner Bio-One 82050-728, Kremsmünster, Austria), and 20 μL of either pure ethanol (control) or 250 μM Bortezomib (experimental group) was added to each sample. Purified recombinant eGFP (Cell Biolabs STA-201, San Diego, CA, USA) at 1 mg/mL in PBS was diluted 1:5, 1:10 and 1:15 with PBS, and 200 μL of each sample was loaded into the plate in duplicate as controls. This plate was then introduced to the plate reader pre-warmed to 37 °C. GFP fluorescence was quantified using the BioTek Synergy H4 Hybrid Multi-Mode Microplate Reader (Agilent, Santa Clara, CA, USA) in the USC Dornsife NanoBiophysics Core facility (Los Angeles, CA, USA). Readings were taken at 30 s intervals at 395 nm excitation/510 nm emission to detect GFP fluorescence.

2.10. Generation of Partially Purified eGFP Extract

Young virgin female flies of the *eyeless-GFP* strain were anesthetized with CO_2 on the fly pad, and the heads were removed using a razor blade. A total of 80 heads were combined with 1 mL PBS, homogenized and subjected to 3 rounds of freeze/thaw, centrifuged as described above, and the supernatant used as extract. The extract was diluted 1:2, 1:4, 1:8, and 1:16 in PBS and added to the plate at 180 μL per well. Three replicates of each concentration were supplemented with 20 μL of 250 μM bortezomib, and the controls were supplemented with 20 μL of ethanol vehicle. Reads were conducted using a plate reader as described above, at room temperature (23.5 ± 0.5 °C). GFP fluorescence was quantified using a BioTek Synergy H4 Hybrid Multi-Mode Microplate Reader. For all experiments, readings were taken at 30 s intervals at 395 nm excitation/510 nm emission to detect GFP fluorescence.

2.11. Video Analysis Software and Statistical Analysis

Videos were generated and analyzed essentially as previously described [9]. The software SaveImageToAviEx_v142.exe is used to record videos at 30 frames per second. The desired number of frames to capture is input by the user, and the resulting video from each camera is recorded and saved as .avi video files. The FluoreScore suite is next used to process these videos into quantitative data. The software FluoreScoreGUI is used to analyze representative videos, select a fluorescence threshold for fly detection, select the ROI, and create a mask if needed to omit any areas with background fluorescence from the analysis. Next, the software template.bat file is used and can be edited for each experiment to indicate the chosen threshold for fluorescence detection, the coordinates for the ROI, and which mask files to utilize, if any. The template.bat file is the only file the user edits and runs directly. It calls the software FluoreScoreCMDV2.exe, which analyzes the videos and derives fluorescence values for the flies in each frame of video, and calls the software SqueezeData_V1.1.exe, which combines the data from the two cameras and filters out signal below the input threshold. The final output is .csv files with total fly fluorescence for each frame of video. The software Cymito_v5.R uses the data from the .csv files to create plots of average fluorescence versus time for each group in the experiment. This software also generates a summary .csv file, with the data in an easy-to-read format, including columns for the average daily fluorescence for every vial, average across all vials, and standard deviation. The data are then plotted as average ln(fluorescence) versus time using Prism 9 to conduct linear regression and generate half-life values. Linear models were also constructed using values from the replicate vials, rather than a single average for each time point, but demonstrated no advantage in identifying differences between groups or constructing lines with a good fit. To conduct ANOVA, the half-life values along with information about the age and sex of the flies were organized into a table, which was then read into R. The R lm function was used to construct a linear model relating half-life

to age and sex (including interaction), and then the ANOVA function was used to run the statistical test. Both functions are available in base R version 4.4.

3. Results

3.1. In Vivo Assay of eGFP Half-Life Using the Gene-Switch System

eGFP was expressed in free-moving flies using the Gene-Switch system [3]. The driver transgene was Actin-GS-255B, in which the tissue-general Actin5C gene promoter drives expression of the Gene-Switch transcription factor [1]. The target was multiple copies of the UAS-eGFP transgene (the "Ultra-GFP" strain), in which the UAS promoter sequences bind Gene-Switch to drive expression of eGFP [1]. When flies containing this driver and target are fed the trigger drug mifepristone, this activates the Gene-Switch transcription factor to produce high-level, tissue-general induction of eGFP [1]. eGFP expression in the flies was quantified using two video cameras (Figure S1), and analysis of the time course for eGFP induction shows that the level of eGFP expression peaks approximately 24 h after the end of the 48 h period of drug treatment (Figure 1A and Figure S8D). To determine the in vivo eGFP half-life, the period from the peak of expression to the subsequent minimum was transformed to the natural log and analyzed by linear regression (Figure 1D). This yielded an in vivo half-life for eGFP in this experiment of 3.5 days.

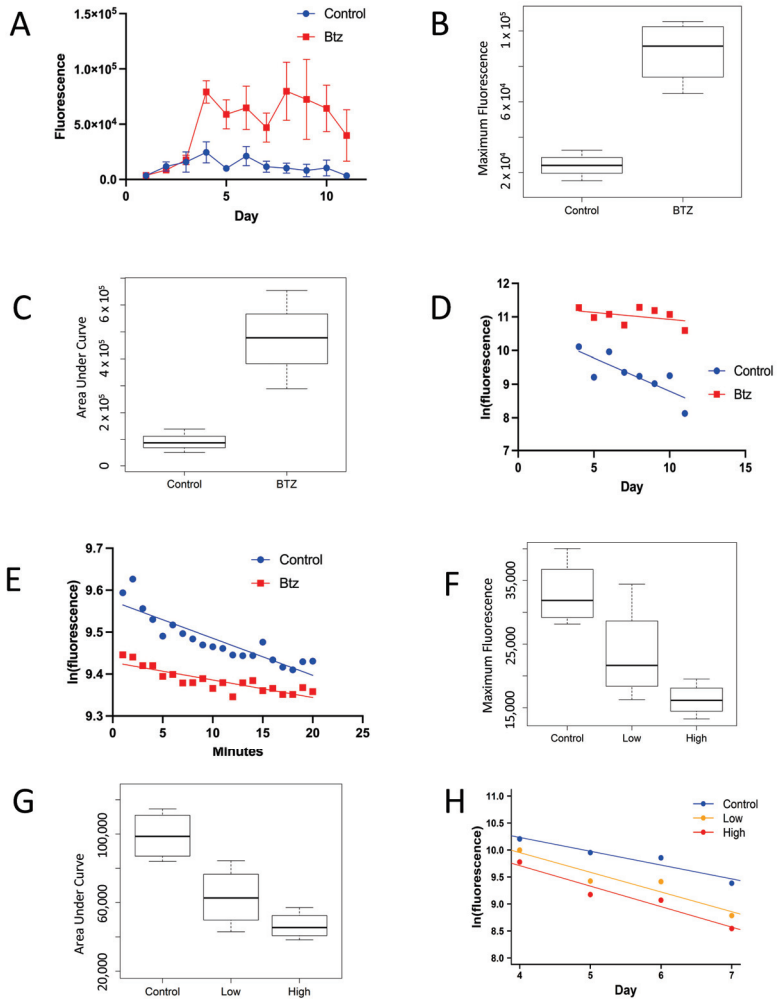


Figure 1. Effect of proteasome inhibitor bortezomib and translation inhibitor cycloheximide. eGFP was expressed in free-moving flies using the Gene-Switch system. The driver transgene is *Actin-GS-255B*, in which the tissue-general *Actin5C* gene promoter drives the expression of the

Gene-Switch transcription factor. The target construct is *UAS-eGFP*, where the UAS promoter sequences bind Gene-Switch to drive the expression of eGFP. (**A**) Fluorescence assay of pulsed eGFP expression in free-moving virgin females (control; blue symbols) and in virgin females treated with 20 μM bortezomib (Btz; red symbols). ID#070722. (**B**) The peak expression level for control and bortezomib-treated flies at day 4, from (**A**). $p = 0.00315$. (**C**) Area under the curve (AUC) quantification of eGFP fluorescence for control and bortezomib-treated flies in (**A**). $p = 0.00239$. (**D**) Fluorescence decay from the peak for control and bortezomib-treated flies in (**A**). The control half-life is 3.5 days, and the Btz half-life is 17 days. $p = 0.0489$. (**E**) In vitro proteasomal degradation assay. Fluorescence decay of eGFP in fly extract (control; blue symbols) and in the presence of 20 μM bortezomib (Btz; red symbols). Control half-life 78 min, Btz half-life 165 min. $p = 0.0004$. ID#072922. Statistical tests are linear regression and ANCOVA; a statistical summary is presented in Table S1. (**F**) Fluorescence assay of pulsed eGFP expression in free-moving virgin females and in females pre-treated with low concentration (5 μM) or high concentration (10 μM) cycloheximide. The peak levels of eGFP fluorescence for control and cycloheximide-treated flies are presented (Experiment ID #081323). Peak levels in the high drug concentration group are significantly lower than the control group ($p = 0.003284$). The low-concentration group did not significantly differ from the control ($p = 0.09583$) or high drug concentration ($p = 0.1586$). (**G**) Area under the curve (AUC) quantification of eGFP fluorescence for control and cycloheximide-treated flies (Experiment ID #081323). Control AUC was significantly different from low drug concentration (5 μM; $p = 0.02091$) and high drug concentration (10 μM; $p = 0.001728$). (**H**) Fluorescence decay of eGFP in control and cycloheximide-treated flies in (Experiment ID #081323). The slope for the control group was −0.2558 (half-life 2.71 days), the slope for low concentration was −0.3648 (half-life 1.90 days), and the slope for high concentration was −0.3801 (half-life 1.82 days). Slopes did not significantly differ ($p = 0.4281776$). Slopes compared with ANCOVA.

3.2. Bortezomib Increases eGFP Half-Life In Vivo and In Vitro

To confirm that the loss of eGFP fluorescence with time is due to protein degradation, the dependence of fluorescence decay on normal proteasome function was assayed. To determine if cytoplasmic eGFP is degraded by the proteasome, the proteasome inhibitor drug bortezomib was employed [21]. Bortezomib was fed to flies at 20 μM in the media, coincident with the induction of eGFP expression by mifepristone. Notably, eGFP expression in flies treated with bortezomib reached maximum levels approximately three times greater than controls, consistent with inhibited degradation due to bortezomib (Figure 1A,B). Quantification of area under the curve (AUC), a measure of total eGFP accumulation, confirmed a 5.6-fold greater eGFP expression in the bortezomib-treated group relative to the control group across the entire assay period (Figure 1C). Consistent with these results, plotting ln(fluorescence) versus time reveals a greater in vivo half-life for eGFP in the bortezomib-treated flies (17 days) relative to controls (3.5 days; Figure 1D; Supplementary Table S1). Increased area under the curve for eGFP accumulation in the presence of bortezomib was confirmed in two additional experiments (Supplementary Figure S2).

To further confirm degradation of eGFP by the proteasome and inhibition by bortezomib, an in vitro proteasome assay was used (Figure 1E) [10]. Extracts prepared from flies expressing eGFP were incubated in the absence and presence of 20 μM bortezomib, and the change over time in eGFP fluorescence was measured using a plate reader. The rate of decay of fluorescence in fly extracts is more rapid than that in living animals, and therefore half-life was measured in minutes rather than days. Plotting ln(fluorescence) versus time again revealed inhibition of eGFP degradation by bortezomib, as indicated by increased eGFP half-life, consistent with proteasome-dependent degradation (Figure 1E; Supplementary Table S1). We note that the absolute eGFP fluorescence detected by plate reader assay was reduced in the presence of bortezomib; however, the magnitude of

the inhibitory effect was roughly equal across different sources and concentrations of eGFP, including dilutions of partially purified eGFP (Supplementary Figure S3A,B), as well as purified recombinant eGFP and the starting extract used for proteasome assay (Supplementary Figure S3C), indicating that half-life calculations are not significantly affected (see Section 4).

3.3. Cycloheximide Decreases eGFP Expression In Vivo

To determine if the in vivo assay could also capture changes in protein synthesis, the translation inhibitor cycloheximide was fed to flies at concentrations of 5 μM and 10 μM in the media. A pulse of eGFP expression was then induced with mifepristone. The peak level of eGFP fluorescence achieved was significantly lower in the drug-treated groups compared to controls (Figure 1F). Consistent with this, quantification of AUC revealed reduced accumulation of eGFP in the cycloheximide-treated groups across the entire assay period (Figure 1G). The half-life of eGFP in the presence and absence of cycloheximide treatment was calculated from the slope of ln(fluorescence) versus time. The eGFP half-life did not differ significantly between the groups, indicating that the decreased eGFP accumulation observed was driven by decreased synthesis (Figure 1H). These results support the conclusion that the in vivo assay provides a relatively accurate measure of in vivo protein half-life.

3.4. Half-Life Values of Different Fluorescent Proteins

Having validated the assay, several different fluorescent proteins were chosen to illustrate this assay's ability to measure the decay rates of proteins whose stabilities might vary and to calculate both longer and shorter half-life values. The fluorescent proteins used in these experiments were eGFP, mitoGFP, DsRED, mCherry, and MitoTimer. Half-life values were calculated under different conditions, including age, sex, and mating status of the flies, as well as targeting different tissues or subcellular compartments.

The first experiments were designed to compare cytoplasmic eGFP degradation rates in males and females, at both younger and older ages, with tissue-general expression. Five independent experiments were conducted comparing young and old virgin males and young and old virgin females, with all four groups assayed in parallel. The young fly starting ages were 5–6 days, and the old fly starting ages were 35–55 days. The average eGFP half-life was 3.9 days in young males, 3.9 days in young females, 4 days in old males, and 3.4 days in old females. No statistically significant relationship between eGFP half-life and age was detected when analyzing the entire dataset using ANOVA (Figure 2A; Supplementary Table S6). It is notable that eGFP half-life in young males and females appears particularly variable (Figure 3A; Supplementary Table S1 and Figure S4A), and this may be one reason a significant effect of age was not detected when analyzing the entire dataset. However, when ANOVA analysis was limited to only the flies >30 days of age, a significant increase with age was detected ($p = 0.039$) (Supplementary Figure S4B). No significant relationship was detected between eGFP half-life and either sex or female mating status (Figure 2B, Supplementary Table S1).

A COX8 mitochondrial targeting sequence fused to the N-terminus of eGFP results in mitoGFP [19]. *UAS-mitoGFP* construct insertions were mobilized to increase copy number and combined into the same strain (Section 2). When crossed to the tissue-general *Actin-GS-255B* driver, this yielded sufficient mitoGFP signal to allow video assay of half-life, giving an average half-life of 2.6 days (Supplementary Figure S6 and Table S3). Interestingly, mitoGFP half-life appeared slightly reduced in old flies relative to young flies (Figure 3A), and mitoGFP in old flies had a shorter half-life than did cytoplasmic eGFP (Figure 3A). No consistent effects of sex or mating status on mitoGFP half-life were observed (Supplementary Table S3).

The half-life of the red fluorescent protein DsRED was assayed using the Tet-ON conditional gene expression system, in which the *actin5C* gene promoter drives tissue-general expression of the doxycycline-activated transcription factor rtTA, targeting the construct *TetO-DsRED* in the presence of the drug (Supplementary Figure S9A,B). Different conditional expression systems were used for eGFP and DsRED in part due to a lack of reagents for Tet-ON. The time course for DsRED induction using Tet-ON revealed a peak of expression approximately 4–5 days after the 48 h period of drug treatment (Figure S8C,E). The average half-life of DsRED in video assays of young virgin males and virgin females was 7.9 days (Figure 2C; Supplementary Table S4). Notably, when analyzed across all video and microscope assays, the half-life of DsRED increased dramatically with age (Figure 3A), and the half-life of DsRED was significantly greater than that of eGFP in flies of comparable age (Figure 3A). No consistently significant difference in DsRED half-life was observed between virgin males and virgin females or between virgin females and mated females (Supplementary Table S4).

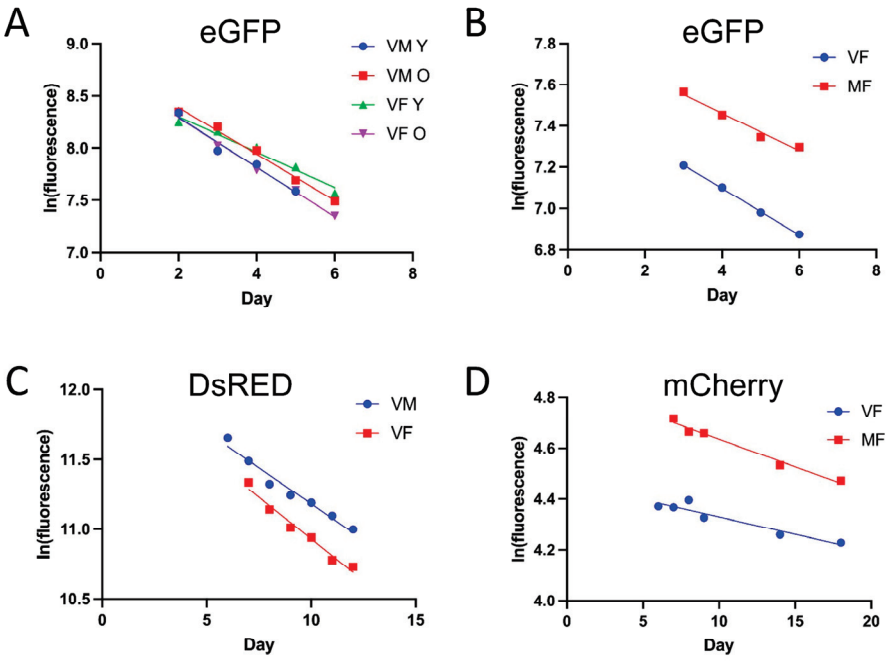


Figure 2. Half-lives of different fluorescent proteins. (**A**,**B**) Tissue-general expression of eGFP. The driver transgene is *Actin-GS-255B*, in which the tissue-general *Actin5C* gene promoter drives expression of the Gene-Switch transcription factor. The target construct is *UAS-eGFP*, where the UAS promoter sequences bind Gene-Switch to drive expression of eGFP. (**A**) Fluorescence decay of eGFP in young (Y; 6 days old) and old (O; 36 days old) virgin males (VM) and virgin females (VF). Half-life values in days: 2.9 (VM Y), 3.1 (VM O), 4.1 (VF Y), 2.9 (VF O). Experiment ID #092619. (**B**) Fluorescence decay in virgin females (VF) and mated females (MF). ID #121720. Half-life values in days: 6.2 (VF) and 7.6 (MF). Statistical summary for eGFP experiments presented in Supplementary Table S1. (**C**) Fluorescence decay of DsRED in free-moving flies, using the Tet-ON system. The driver transgene is *rtTA(3)E2*, in which the tissue-general *Actin5C* promoter drives expression of the rtTA transcription factor. The target transgene is *TetO-DsRED*, where the TetO promoter sequences drive expression of DsRED. Virgin males (VM) and virgin females (VF). $p = 0.2552$. ID #111920. Half-life in days: 6.7 (VM), 5.8 (VF). (**D**) Fluorescence decay of mCherry in flies anesthetized during microscope image capture using the Gene-Switch system. The driver transgene is *Actin-GS-255B*, and the target transgene is *UAS-mCherry*. Virgin females (VF) and mated females (MF). $p = 0.0319$. ID#072221. Half-life in days: 51 (VF), 32 (MF). Statistical summary for mCherry presented in Supplementary Table S5. Statistical tests are linear regression and ANCOVA.

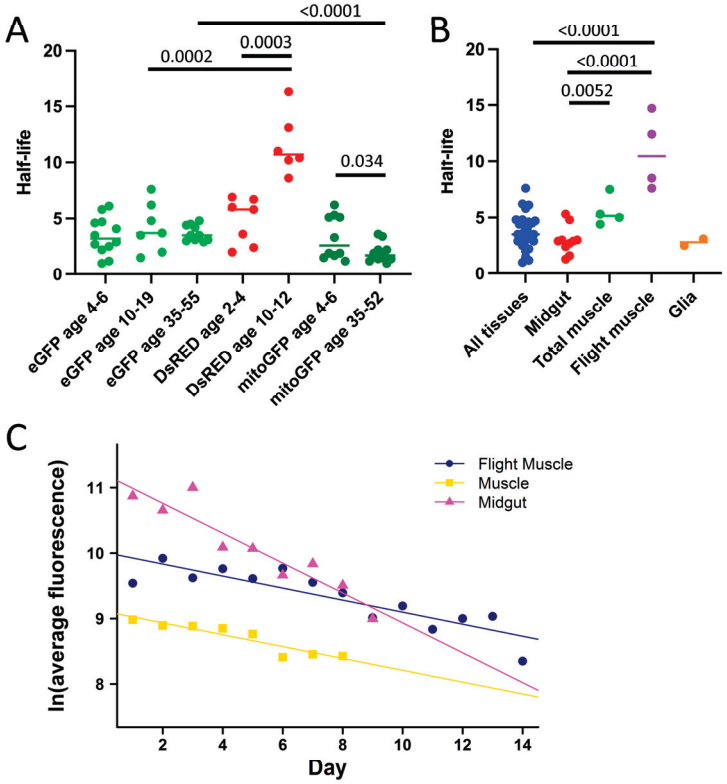


Figure 3. Half-life differences across age and tissue types. (**A**,**B**) Data were analyzed across all video and microscope assays. The statistical test is an unpaired, two-tailed *t*-test, and *p*-values for comparisons are presented above the plots. (**A**) Half-life of fluorescent proteins in flies of different age groups. The fluorescent proteins and the age range of the flies are indicated below the *X*-axis. In each case fluorescent protein expression is tissue-general. Both eGFP and mitoGFP were expressed using the *Actin-GS-255B* driver and the Gene-Switch system, whereas DsRED was expressed using the *rtTA(3)E2G* driver and Tet-ON system. (**B**) Half-life of eGFP expressed in various tissues using the Gene-Switch system. "All tissues" indicates tissue-general expression using the *Actin-GS-255B* driver. Midgut is *5966-GS* driver, total muscle is *Mhc-GS* driver, flight muscle is *88F-GS* driver, and glia is *REPO-GS* driver. (**C**) Examples of fluorescence decay of eGFP targeted to muscle and midgut of mated females. In each case the target construct is *UAS-eGFP*. eGFP fluorescence decay is plotted for flight muscle (using driver *88F-GS*, Experiment ID #100221), total muscle (using driver *Mhc-GS*, Experiment ID #092021), and midgut (using driver *5966-GS*, Experiment ID #111021). The slope of eGFP decay in the midgut (half-life 3.0 days) differed from flight muscle (half-life 7.6 days, $p = 0.003159$) and muscle (half-life 7.5 days, $p = 0.0006211$), whereas no significant difference was detected between flight muscle and total muscle ($p = 0.9671537$). Statistical tests are linear regression and ANCOVA.

Another red fluorescent protein, mCherry, was found to have a particularly long half-life. The Gene-Switch system and the tissue-general *Actin-GS-255B* driver were used to drive expression of mCherry, using a high copy number *UAS-mCherry* strain. Microscope assay yielded a half-life of 51 days in virgin females and 32 days in mated females (Figure 2D; Supplementary Table S5). Induction of mCherry expression using the GeneSwitch system was also observed using the glia-specific *REPO-GS* driver (Supplementary Figure S9C,D), as well as with other drivers. However, the video assays were complicated by high background and poor fit to exponential decay models, and half the assays did not detect any decay in red fluorescence (Supplementary Table S5).

Finally, another red fluorescent protein, the mitochondria-targeted MitoTimer, was also assayed [15,22]. A multi-copy *UAS-MitoTimer* strain was constructed (Supplementary Figure S5), and MitoTimer was expressed in neurons using the *Elav-GS* driver. Robust induction of red

fluorescence was observed in video assays in both virgin males and virgin females, yielding a half-life of 4.8–6.7 days. There was no significant difference in half-life between the sexes (Supplementary Table S5).

3.5. Tissue-Specific Expression of eGFP

Protein half-life can vary by tissue [23,24]. To investigate possible differences in tissue-specific eGFP turnover rates, eGFP was expressed using several tissue-specific drivers, and half-life was assayed in virgin males, virgin females and mated females (Supplementary Table S2). When analyzed across all assays, the half-life of eGFP expressed in total muscle or flight muscle was significantly greater than that in midgut, and the half-life of eGFP in flight muscle was significantly greater than that observed with tissue-general expression (Figure 3B). Specifically, tissue-general expression of eGFP using the *Actin-GS-255B* driver yielded an average eGFP half-life of 3.7 days; targeting eGFP expression to the midgut using the *5966-GS* driver yielded an average half-life of 3.0 days; targeting eGFP to total muscle using the *Mhc-GS* driver yielded an average half-life of 5.6 days; targeting eGFP to flight muscle using the *88F-GS* driver yielded an average half-life of 10.8 days; and finally, targeting eGFP to glia using the *REPO-GS* driver yielded an average half-life of 2.8 days (Figure 3B). No consistent difference in eGFP half-life between virgin and mated females was observed with any driver (Supplementary Table S2).

To enable direct comparison of eGFP decay rates between tissues, data were normalized with regard to time, using the datasets with the largest number of points in the linear range. Consistent with the data presented above, the eGFP half-life in the midgut was smaller than that in total muscle or flight muscle in both mated females (Figure 3C) and virgin females (Supplementary Figure S7).

4. Discussion

Here, methods for measuring the half-life of fluorescent proteins in living flies are presented, which enable measurements of protein turnover under different conditions and in distinct tissues and subcellular locations. This assay captures changes in both protein degradation and synthesis. The half-life of eGFP was increased by the proteasome inhibitor bortezomib, both in vivo and in vitro, indicating proteasomal degradation of eGFP. Consistent with the conclusion that eGFP is degraded by the proteasome, bortezomib has previously been shown to inhibit GFP degradation in cultured human H1299 carcinoma cells [25], and proteasome inhibitors MG132 and Z-L3-VS inhibited GFP degradation in cultured HeLa cells [26]. It was observed that in the plate reader assay, absolute eGFP fluorescence was slightly lower in the presence of bortezomib. The absolute magnitude of this effect was approximately equal across different concentrations of eGFP, with a larger percent change at lower concentrations (Supplementary Figure S3). This indicates that the observed effect, a decrease in half-life in the presence of bortezomib, was unlikely to be an artifact of this inhibition, because a preferential decrease in eGFP fluorescence at lower concentrations would tend to produce a steeper rate of decay, and the effect observed with bortezomib is in the opposite direction. Thus, the presence of this inhibitory effect should not affect our conclusions. The inhibitory effect was not detected in the video experiments. The accumulation of eGFP in vivo was decreased by the protein synthesis inhibitor cycloheximide, without affecting half-life.

DsRED protein was expressed in a tissue-general pattern using the Tet-ON system and *Actin5C* gene promoter and had a generally greater half-life than was observed for tissue-general expression of eGFP using the Gene-Switch system and *Actin5C* gene promoter. For example, the average half-life of eGFP across the video assay experiments was 4.1 days,

whereas the average half-life of DsRED across the video assay experiments was 7.8 days (Supplementary Tables S1, S2 and S4). Consistent with these observations, a previous study of cultured *Drosophila* S2 cells reported a half-life for eGFP of approximately 3.8 days and a half-life for DsRED of approximately 8 days [27]. The similarity between the half-life values previously obtained using cultured *Drosophila S2* cells and the half-life values obtained here for in vivo *Drosophila* assays supports the accuracy of our method for measuring in vivo fluorescent protein half-life, as well as its ability to discern differences in the decay rate between different proteins. Limited degradation of mCherry was detected, and examples of decay rates for eGFP, DsRED and mCherry in young virgin females are plotted from peak to minimum on the same *X*-axis scale for comparison (Supplementary Figure S10).

Differences in the decay rates for fluorescent proteins can be exploited for various uses in research. For example, the Repressible Dual Differential Marker (ReDDM) method for lineage tracing takes advantage of the longer half-life of H2B-RFP (red fluorescent protein) relative to mCD8-GFP (green fluorescent protein) to distinguish stem cells from their differentiated progeny [28]. The half-life of DsRED increased rapidly between eclosion and day 12 of age, with statistically significant increases detected for each of virgin females, mated females, and virgin males. In the future, it may be of interest to ask if the half-life of DsRED continues to increase at greater ages.

Increased transgene copy number resulted in proportionally increased levels of fluorescent protein expression, as expected (for example, see Figure S5). This increased fluorescent protein expression is not expected to affect fluorescent protein stability. This is supported by several experiments in which similar half-life values were calculated for the same fluorescent protein despite differences in the maximum fluorescence value (for example, see Figure 2B). There was no indication of any saturation of the video camera assays or fluorescence microscope assays, such as fluorescence curves that are truncated at the top (for examples, see Supplemental Figure S8), indicating that the assays are within the linear range. Whereas differences in light penetration might yield somewhat lower fluorescence intensity from internal tissues, we were able to reproducibly assay fluorescent protein half-life in internal tissues such as the gut and nervous system (see Tables S2 and S5). In the future, increasing the input light intensity might further increase the ability to assay subsets of internal cells.

Half-life also varied by tissue, with greater eGFP half-life observed in muscle relative to other tissues. Cytoplasmic eGFP had a similar half-life in young flies when expressed in a tissue-general pattern and when targeted to midgut enterocytes and to glial cells (summarized in Figure 3B). In contrast, eGFP half-life was longer in young flies when targeted to muscle tissue (Figure 3B). The relatively longer half-life of eGFP in *Drosophila* muscle tissue may be related to observations that muscle tissue shows preferential accumulation of protein aggregates and induction of hsp70 protein relative to other adult tissues during aging [29,30]. These results appear similar to the mouse, where muscle tissue was reported to exhibit generally slower protein turnover than other tissues such as liver [23]. Limited effects were observed for *Drosophila* sex and female mating status. Taken together, the data indicate the in vivo assays are promising tools for the study of protein degradation regulated by protein sequence, subcellular compartment, tissue and small molecules.

Limitations of this study include some asymmetry of the experiments. For example, eGFP has been assayed only using the Gene-Switch system, and DsRED has been assayed only using the Tet-ON system. One reason for this is the relative lack of reagents for the Tet-ON system. Successful expression of eGFP with Tet-ON has been reported in the past, but the tetO-GFP strains are no longer extant [17]. For both the Gene-Switch and Tet-ON systems, the protein half-life is calculated from the peak of expression to the subsequent minimum. Because the peak in protein expression occurs >24 h after the cessation of

drug treatment, it seems unlikely that the differences in the measured half-lives of eGFP and DsRED are a consequence of using different systems but rather are due to inherent differences in the half-lives of the two proteins. In the future, it may be of interest to generate additional fluorescent protein target constructs for the Tet-ON system to allow for direct comparison of half-life values between different proteins without the possible confounding effects of different transgenic systems.

A limitation of the Gene-Switch system is that the mifepristone used to trigger fluorescent protein expression can have significant physiological effects. In mated females, mifepristone reduces progeny production and midgut size and greatly increases median life span [31]. Limiting mifepristone treatment to 48 h is expected to limit confounding effects. However, it is possible the effects of even brief mifepristone treatment are one reason that differences in eGFP half-life between virgin and mated females were not detected using Gene-Switch. Other conditional gene expression systems each have their own limitations. For example, using heat shock gene promoters and a heat pulse is problematic due to the effects of heat on *Drosophila*. In particular, increased temperature reduces the physiological changes associated with mating in female flies, including eliminating the effect of mating on lifespan and midgut size, making heat shock induction unsuitable for comparisons of virgin and mated females [31]. Moreover, increased temperature shortens lifespan in *Drosophila* and can affect protein turnover, altering both synthesis and degradation [32,33]. The DOX (doxycycline) drug used to trigger the Tet-ON system has been found to have small effects on mitochondrial translation and gene expression [34]. Similarly, the Q-system for conditional gene expression is confounded by the fact that the triggering drug, quinic acid, has pleiotropic effects on aging and life span [35,36]. Therefore, the use of any conditional gene expression system requires careful consideration of the possible side effects of the system activator.

Additional limitations of the video assay include some variability in results, particularly for the youngest flies. Reasons for this likely include some unequal lighting throughout the vial and some unequal coverage of all regions by the video cameras, combined with fly movement, which is greater in young flies. In future experiments, this variability might be reduced by adding a third camera to improve vial coverage, adding additional lighting, and/or by lengthening video recording time to lessen the impact of fly movement.

Supplementary Materials: The following supporting information can be downloaded at https://www.mdpi.com/article/10.3390/insects16060583/s1, Figure S1: Setup of video assay; Figure S2: Effect of bortezomib in vitro, replicate assays; Figure S3: Effect of bortezomib on fluorescence plate reader assay; Figure S4: Summary of half-life values for young and old virgin males and virgin females assayed in parallel; Figure S5: Increased copy number of transgenes produced by P element transposition; Figure S6: Degradation rate of tissue-general mitoGFP; Figure S7: Fluorescence decay of eGFP targeted to muscle and midgut of virgin females; Figure S8: Examples of time course for fluorescent protein expression; Figure S9: Examples of fluorescent protein expression in flies cultured in the absence and presence of drug; Figure S10: Comparison plot for half-life of eGFP, DsRED and mCherry in young virgin female flies; Table S1: Tissue-general eGFP expression in young and old virgin males and virgin females; Table S2: Tissue-general and tissue-specific expression of eGFP; Table S3: Tissue-general expression of mitoGFP; Table S4: Tissue-general expression of DsRED using the Tet-ON system; Table S5: Analysis of mCherry and MitoTimer; Table S6: ANOVA summary.

Author Contributions: Conceptualization, J.T.; methodology, J.T.; software, A.S., S.A. (Siddharth Agrawal) and K.S.B.; validation, J.T. and K.S.B.; formal analysis, J.T. and K.S.B.; investigation, K.S.B., S.K., S.A. (Siddharth Agrawal), B.B., M.K., N.R., O.K.P., M.E., J.P., A.T., A.S., S.A. (Sam Ali) and J.T.; resources, J.T.; data curation, S.A. (Sam Ali), S.K., S.A. (Siddharth Agrawal), B.B., M.K., N.R., O.K.P., M.E., J.P., A.T., A.S., S.A. (Sam Ali) and J.T.; writing—original draft preparation, K.S.B. and J.T.; writing—review and editing, K.S.B. and J.T.; visualization, K.S.B. and J.T.; supervision, J.T. and

K.J.A.D.; project administration, J.T. and K.J.A.D.; funding acquisition, J.T., K.J.A.D., K.S.B. and S.A. (Sam Ali). All authors have read and agreed to the published version of the manuscript.

Funding: National Institute on Aging (AG057741) J.T.; National Institute of General Medical Sciences (T32-GM118289) K.S.B.; National Institute on Aging (T32-AG052374) S.A. (Sam Ali); National Institute on Aging (AG052374) K.J.A.D.

Data Availability Statement: The datasets supporting the conclusions of this article are included within the article/Supplementary Materials and its additional files. Software used for video assays is available upon publication at https://github.com/johntower/Tracking-Paper-2024 (accessed on 27 May 2025).

Conflicts of Interest: The authors declare no conflicts of interest.

Abbreviations

eGFP	enhanced green fluorescent protein
DsRED	*Discosoma* species red fluorescent protein
LED	Light-emitting diode
COX8	cytochrome c oxidase subunit 8
UAS	upstream activating sequence
GS	Gene-Switch
rtTA	reverse tetracycline trans-activator
tetO	Tet-operator

References

1. Bell, H.S.; Tower, J. In vivo assay and modelling of protein and mitochondrial turnover during aging. *Fly* **2021**, *15*, 60–72. [CrossRef] [PubMed]
2. Nicholson, L.; Singh, G.K.; Osterwalder, T.; Roman, G.W.; Davis, R.L.; Keshishian, H. Spatial and temporal control of gene expression in *Drosophila* using the inducible GeneSwitch GAL4 system. I. Screen for larval nervous system drivers. *Genetics* **2008**, *178*, 215–234. [CrossRef] [PubMed]
3. Osterwalder, T.; Yoon, K.S.; White, B.H.; Keshishian, H. A conditional tissue-specific transgene expression system using inducible GAL4. *Proc. Natl. Acad. Sci. USA* **2001**, *98*, 12596–12601. [CrossRef]
4. Ford, D.; Hoe, N.; Landis, G.N.; Tozer, K.; Luu, A.; Bhole, D.; Badrinath, A.; Tower, J. Alteration of *Drosophila* life span using conditional, tissue-specific expression of transgenes triggered by doxycyline or RU486/Mifepristone. *Exp. Gerontol.* **2007**, *42*, 483–497. [CrossRef]
5. Trauth, J.; Scheffer, J.; Hasenjager, S.; Taxis, C. Strategies to investigate protein turnover with fluorescent protein reporters in eukaryotic organisms. *AIMS Biophys.* **2020**, *7*, 90–118. [CrossRef]
6. Sala, A.J.; Bott, L.C.; Morimoto, R.I. Shaping proteostasis at the cellular, tissue, and organismal level. *J. Cell Biol.* **2017**, *216*, 1231–1241. [CrossRef]
7. Jiao, J.; Demontis, F. Skeletal muscle autophagy and its role in sarcopenia and organismal aging. *Curr. Opin. Pharmacol.* **2017**, *34*, 1–6. [CrossRef]
8. Hetz, C. Adapting the proteostasis capacity to sustain brain healthspan. *Cell* **2021**, *184*, 1545–1560. [CrossRef]
9. Tower, J.; Agrawal, S.; Alagappan, M.P.; Bell, H.S.; Demeter, M.; Havanoor, N.; Hegde, V.S.; Jia, Y.; Kothawade, S.; Lin, X.; et al. Behavioral and molecular markers of death in *Drosophila melanogaster*. *Exp. Gerontol.* **2019**, *126*, 110707. [CrossRef]
10. Pomatto, L.C.; Carney, C.; Shen, B.; Wong, S.; Halaszynski, K.; Salomon, M.P.; Davies, K.J.; Tower, J. The Mitochondrial Lon Protease Is Required for Age-Specific and Sex-Specific Adaptation to Oxidative Stress. *Curr. Biol.* **2017**, *27*, 1–15. [CrossRef]
11. Jacobs, J.A.; Sehgal, A. Anandamide Metabolites Protect against Seizures through the TRP Channel Water Witch in *Drosophila melanogaster*. *Cell Rep.* **2020**, *31*, 107710. [CrossRef] [PubMed]
12. Luis, N.M.; Wang, L.; Ortega, M.; Deng, H.; Katewa, S.D.; Li, P.W.; Karpac, J.; Jasper, H.; Kapahi, P. Intestinal IRE1 Is Required for Increased Triglyceride Metabolism and Longer Lifespan under Dietary Restriction. *Cell Rep.* **2016**, *17*, 1207–1216. [CrossRef] [PubMed]
13. Mlih, M.; Khericha, M.; Birdwell, C.; West, A.P.; Karpac, J. A virus-acquired host cytokine controls systemic aging by antagonizing apoptosis. *PLoS Biol.* **2018**, *16*, e2005796. [CrossRef]
14. Horn, C.; Jaunich, B.; Wimmer, E.A. Highly sensitive, fluorescent transformation marker for *Drosophila* transgenesis. *Dev. Genes Evol.* **2000**, *210*, 623–629. [CrossRef]

15. Laker, R.C.; Xu, P.; Ryall, K.A.; Sujkowski, A.; Kenwood, B.M.; Chain, K.H.; Zhang, M.; Royal, M.A.; Hoehn, K.L.; Driscoll, M.; et al. A novel MitoTimer reporter gene for mitochondrial content, structure, stress, and damage in vivo. *J. Biol. Chem.* **2014**, *289*, 12005–12015. [CrossRef]
16. Xu, P.; Damschroder, D.; Zhang, M.; Ryall, K.A.; Adler, P.N.; Saucerman, J.J.; Wessells, R.J.; Yan, Z. Atg2, Atg9 and Atg18 in mitochondrial integrity, cardiac function and healthspan in *Drosophila*. *J. Mol. Cell. Cardiol.* **2019**, *127*, 116–124. [CrossRef]
17. Hoe, N.; Huang, C.M.; Landis, G.; Verhage, M.; Ford, D.; Yang, J.; van Leeuwen, F.W.; Tower, J. Ubiquitin over-expression phenotypes and ubiquitin gene molecular misreading during aging in *Drosophila melanogaster*. *Aging* **2011**, *3*, 237–261. [CrossRef]
18. Robertson, H.M.; Preston, C.R.; Phillis, R.W.; Johnson-Schlitz, D.M.; Benz, W.K.; Engels, W.R. A stable genomic source of P element transposase in *Drosophila melanogaster*. *Genetics* **1988**, *118*, 461–470. [CrossRef]
19. Cox, R.T.; Spradling, A.C. A Balbiani body and the fusome mediate mitochondrial inheritance during *Drosophila* oogenesis. *Development* **2003**, *130*, 1579–1590. [CrossRef]
20. Schneider, C.A.; Rasband, W.S.; Eliceiri, K.W. NIH Image to ImageJ: 25 years of image analysis. *Nat. Methods* **2012**, *9*, 671–675. [CrossRef]
21. Tan, C.R.C.; Abdul-Majeed, S.; Cael, B.; Barta, S.K. Clinical Pharmacokinetics and Pharmacodynamics of Bortezomib. *Clin. Pharmacokinet.* **2019**, *58*, 157–168. [CrossRef] [PubMed]
22. Ferree, A.W.; Trudeau, K.; Zik, E.; Benador, I.Y.; Twig, G.; Gottlieb, R.A.; Shirihai, O.S. MitoTimer probe reveals the impact of autophagy, fusion, and motility on subcellular distribution of young and old mitochondrial protein and on relative mitochondrial protein age. *Autophagy* **2013**, *9*, 1887–1896. [CrossRef] [PubMed]
23. Rolfs, Z.; Frey, B.L.; Shi, X.; Kawai, Y.; Smith, L.M.; Welham, N.V. An atlas of protein turnover rates in mouse tissues. *Nat. Commun.* **2021**, *12*, 6778. [CrossRef]
24. McClatchy, D.B.; Martinez-Bartolome, S.; Gao, Y.; Lavallee-Adam, M.; Yates, J.R., 3rd. Quantitative analysis of global protein stability rates in tissues. *Sci. Rep.* **2020**, *10*, 15983. [CrossRef]
25. Neznanov, N.; Komarov, A.P.; Neznanova, L.; Stanhope-Baker, P.; Gudkov, A.V. Proteotoxic stress targeted therapy (PSTT): Induction of protein misfolding enhances the antitumor effect of the proteasome inhibitor bortezomib. *Oncotarget* **2011**, *2*, 209–221. [CrossRef]
26. Dantuma, N.P.; Lindsten, K.; Glas, R.; Jellne, M.; Masucci, M.G. Short-lived green fluorescent proteins for quantifying ubiquitin/proteasome-dependent proteolysis in living cells. *Nat. Biotechnol.* **2000**, *18*, 538–543. [CrossRef]
27. Verkhusha, V.V.; Kuznetsova, I.M.; Stepanenko, O.V.; Zaraisky, A.G.; Shavlovsky, M.M.; Turoverov, K.K.; Uversky, V.N. High stability of *Discosoma* DsRed as compared to *Aequorea* EGFP. *Biochemistry* **2003**, *42*, 7879–7884. [CrossRef]
28. Antonello, Z.A.; Reiff, T.; Ballesta-Illan, E.; Dominguez, M. Robust intestinal homeostasis relies on cellular plasticity in enteroblasts mediated by miR-8-Escargot switch. *EMBO J.* **2015**, *34*, 2025–2041. [CrossRef]
29. Wheeler, J.C.; Bieschke, E.T.; Tower, J. Muscle-specific expression of *Drosophila hsp70* in response to aging and oxidative stress. *Proc. Natl. Acad. Sci. USA* **1995**, *92*, 10408–10412. [CrossRef]
30. Demontis, F.; Piccirillo, R.; Goldberg, A.L.; Perrimon, N. Mechanisms of skeletal muscle aging: Insights from *Drosophila* and mammalian models. *Dis. Models Mech.* **2013**, *6*, 1339–1352. [CrossRef]
31. Landis, G.N.; Ko, S.; Peng, O.; Bognar, B.; Khmelkov, M.; Bell, H.S.; Tower, J. A screen of small molecule and genetic modulators of life span in female *Drosophila* identifies etomoxir, RH5849 and unanticipated temperature effects. *Fly* **2022**, *16*, 397–413. [CrossRef] [PubMed]
32. Miquel, J.; Lundgren, P.R.; Bensch, K.G.; Atlan, H. Effects of temperature on the life span, vitality and fine structure of *Drosophila melanogaster*. *Mech. Ageing Dev.* **1976**, *5*, 347–370. [CrossRef] [PubMed]
33. Niedzwiecki, A.; Fleming, J.E. Changes in protein turnover after heat shock are related to accumulation of abnormal proteins in aging *Drosophila melanogaster*. *Mech. Aging Dev.* **1990**, *52*, 295–304. [CrossRef] [PubMed]
34. Zhang, L.; Ging, N.C.; Komoda, T.; Hanada, T.; Suzuki, T.; Watanabe, K. Antibiotic susceptibility of mammalian mitochondrial translation. *FEBS Lett.* **2005**, *579*, 6423–6427. [CrossRef]
35. Riabinina, O.; Potter, C.J. The Q-System: A Versatile Expression System for *Drosophila*. *Methods Mol. Biol.* **2016**, *1478*, 53–78. [CrossRef]
36. El Din, R.H.; Thabit, S. Quinic acid protects against the development of Huntington's disease in *Caenorhabditis elegans* model. *BMC Complement. Med. Ther.* **2024**, *24*, 377. [CrossRef]

Disclaimer/Publisher's Note: The statements, opinions and data contained in all publications are solely those of the individual author(s) and contributor(s) and not of MDPI and/or the editor(s). MDPI and/or the editor(s) disclaim responsibility for any injury to people or property resulting from any ideas, methods, instructions or products referred to in the content.

insects

MDPI

Article

Chromosomal Inversions in Chromosome U of *Drosophila subobscura*: A Story from Population Studies to Molecular Level

Mercè Merayo [1], Kenia M. Delgado [1], David Salguero [2,3] and Dorcas J. Orengo [2,3,*]

[1] Faculty of Computer Science, Multimedia and Telecommunications Universitat Oberta de Catalunya, Rambla del Poblenou, 156, 08018 Barcelona, Spain; mmerayo@uoc.edu (M.M.); kenia98@uoc.edu (K.M.D.)
[2] Departament de Genètica, Microbiologia i Estadística, Universitat de Barcelona, 08028 Barcelona, Spain; dsalguero@ub.edu
[3] Institut de Recerca de la Biodiversitat (IRBio), Universitat de Barcelona, 08028 Barcelona, Spain
* Correspondence: dorcasorengo@ub.edu

Simple Summary: *Drosophila subobscura* is a Palearctic species that colonized the west coast of both Americas in the last quarter of the 20th century. This species stands out for its large chromosomal inversion polymorphism that affects its five long chromosomes. Studies of natural populations in these three geographic areas revealed that the inversion polymorphism has an adaptive character. However, there is no information on which genes may be involved in the different climatic adaptations. Characterization of the inversion breakpoints will allow a first approach to the genes included in the inversions and to find candidates to be affected by selection. In this work, we take advantage of the existence of a reference genomic sequence that carries the U_{1+2} arrangement to localize the breakpoints of inversions U_6 and U_8. Our results suggest that the origin of both inversions would have been mediated by transposons and, in the case of U_8, we found a new fold-back-type element characteristic of the subobscura species.

Abstract: *Drosophila subobscura* is a Palearctic species that colonized the west coast of South and North America in the last quarter of the 20th century. This species stands out for its large chromosomal inversion polymorphism that affects its five long chromosomes. Studies of natural populations revealed that the inversion polymorphism has an adaptive character and while the arrangement U_{st} was classified as adapted to cold, other arrangements, such as $U_{\underline{1+2+6}}$ and $U_{\underline{1+8}+2}$, were considered warm adapted. Characterization of the inversion breakpoints will allow a first approach to the genes included in the inversions and to find candidates to be affected by selection. In this work, we take advantage of the existence of a reference genomic sequence carrying the U_{1+2} arrangement to locate the breakpoints of the U_6 and U_8 inversions, mapping paired-end Illumina reads from two homokaryotypic strains to $U_{\underline{1+2+6}}$ and $U_{\underline{1+8}+2}$, respectively. To date, most of the characterized inversion breakpoints in *D. subobscura* have been generated by non-homologous end-joining. In contrast, the U_6 and U_8 inversions seem to have originated by transposons, and, at the distal breakpoint of inversion U_8, we describe a new fold-back-like element characteristic of the suboscura species group that we have named *Ziga-Zaga*.

Keywords: *Drosophila subobscura*; chromosomal inversions; fold-back element

1. Introduction

Chromosomal inversions represent an important structural variation both within species and in speciation processes. They consist of two breaks in a chromosome that leave a fragment free, and, when repaired, the ends are joined so that this fragment is inserted in the opposite direction within the chromosome. Inversions were inferred more than 100 years ago by Sturtevant in *Drosophila* comparing genetic maps built from recombination rates [1] and their existence was later confirmed by cytological studies of polytene chromosomes. Polytene chromosomes are giant chromosomes typical of some Diptera tissues that are made up of numerous DNA replicas that remain together without the cells dividing. In addition, the two homologous chromosomes also remain paired. This means that, when there is a heterozygote for a chromosomal inversion, these polytene chromosomes form inversion loops that are detected cytologically [2]. For this reason, chromosomal inversions have been studied mainly in Diptera and very especially in different species of *Drosophila* [3,4].

In Europe, the study of inversions has been carried out extensively in *Drosophila subobscura* Collin and its twin species *D. madeirensis* Monclús (endemic to Madeira) and *D. guanche* Monclús (endemic to the Canary Islands). The karyotype of this group of species consists of five long acrocentric chromosomes named A (=X), J, U, E and O, and a point-shaped chromosome named dot, and these three species differ from each other by a series of fixed inversions. The most common arrangement of each chromosome in northern European populations was named the standard arrangement and is therefore not necessarily the ancestral arrangement [5]. For example, the ancestral arrangement of chromosome U of *D. subobscura* (B Muller element) corresponds to the U_{1+2} arrangement, which is the only one present in *D. madeirensis* and *D. guanche* and one of the polymorphic variants in *D. subobscura* [6]. This chromosome shows a rich structural polymorphism by inversions that, in most of the Mediterranean natural populations analyzed, consists of five arrangements: U_{st}, U_1, U_{1+2}, $U_{\underline{1+8}+2}$ and $U_{\underline{1+2+6}}$ [5,7]. These arrangements differ by two tandem inversions (U_1 and U_2, which cytologically share a breakpoint) and other overlapping inversions (Figure 1).

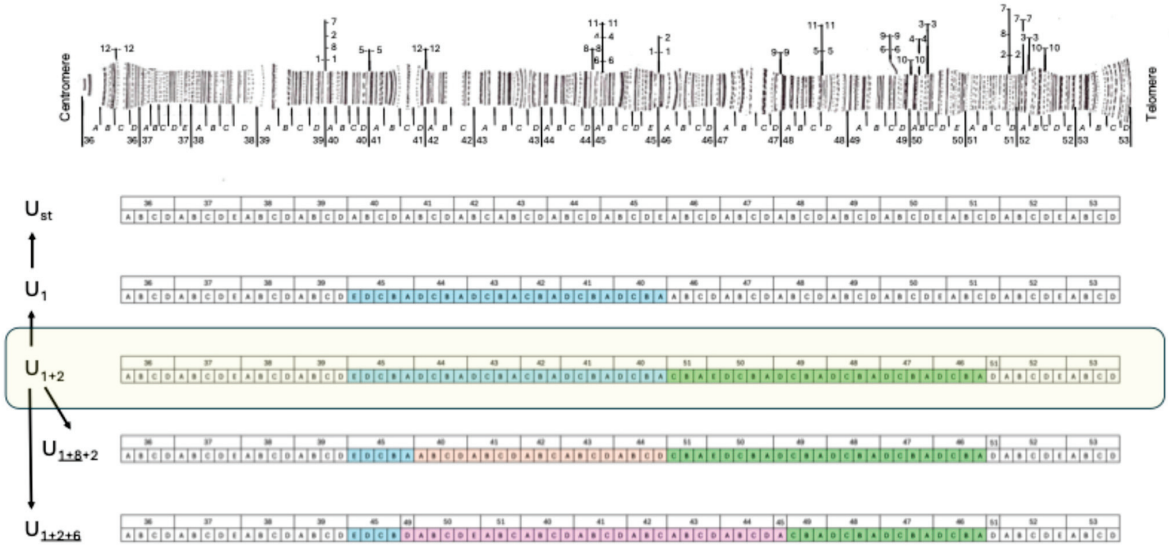


Figure 1. Kunze-Mühl and Müller [8] cytological map of chromosome U_{st} of *D. subobscura* and a schematic representation of four successive inversions on this chromosome. The ancestral character of the U_{1+2} arrangement is indicated by yellow shading and, on the left, the sequential relationship among the arrangements is indicated.

Whereas the endemic species of this group are monomorphic, *D. subobscura* is a species with a large chromosomal polymorphism by inversions affecting its five long acrocentric chromosomes. This species was originally from the Palearctic region with a wide distribution from southern Scandinavia to northern Africa and from the Caucasus to the Macaronesian islands, where its chromosomal inversion polymorphism has been widely studied [5]. The latitudinal clinal variation of this polymorphism in Europe suggested an adaptive origin that would be confirmed when, in the last quarter of the 20th century, the species colonized the Pacific coast of both Chile and North America and rapidly replicated these clines [9]. This adaptive character is also supported by the fact that the variation in chromosomal polymorphism over time correlates with temperature changes in the same direction as the latitudinal clines [7,10,11].

Inversions may affect the fitness of individuals mainly in two ways. On the one hand, inversions could directly break a gene or affect its expression by separating the gene from its regulatory region. On the other hand, since inversions block recombination in heterokaryotypes [12], they can hold together specific combinations of coadapted alleles of the genes included in an inversion [13]. Although several studies point to an adaptive origin of the inversion polymorphism in *D. subobscura*, the genes responsible for the adaptive character of the inversions and their clinal variation are still unknown. A first step in this direction must be the molecular characterization of the breakpoints that delimit the inversions. In the last decade, when the genomic sequence of this species was not yet available, several studies aimed at the molecular characterization of the inversion's breakpoints of chromosomes O, E and A of *D. subobscura*, obtaining probes from a chromosome walking on the genome of *D. pseudoobscura* and performing in situ hybridization [14–19]. Once the genome of *D. guanche* was available [20], a chromosomal walking in this genome sequence was used to characterize the fixed inversions (in chromosomes A, J, E and O) between *D. guanche* and *D. subobscura* [21]. Finally, Karageorgiou and collaborators obtained a genomic sequence for *D. subobscura* from a homokaryotipic line for the arrangements A_{st}, J_{st}, U_{st} E_{st} and $O_{\underline{3+4}}$. These authors performed a whole genome synteny analysis of this genome with that of *D. guanche* and obtained the breakpoints of all the fixed inversions between these two species identified before by more classical methods [21] and for the inversions U_1 and U_2 (that are polymorphic in *D. subobscura*) [22]. Their results for U_1 and U_2 inversions show clear evidence of an origin by staggered breaks that gave rise to duplicated sequences in opposite orientations of 689 and 1007 bp in length, respectively. Furthermore, their results show that these two tandem inversions, which cytologically share a breakpoint, are separated by about 31 kb [22].

The distribution of inversions along chromosomes is not completely random and several of them have some shared breakpoint, at least at the cytological level [8]. Furthermore, many of the molecularly characterized breakpoints have revealed the presence of duplicated sequences in opposite orientation flanking the inverted region [23]. Depending on the nature of these duplicated sequences, two main mechanisms have been proposed for the origin of the inversions. When the duplicated sequences are repetitive sequences, as for example with transposable elements, inversions may have arisen from non-allelic homologous recombination (NAHR) between these repeated sequences. On the other hand, when the duplicated sequences are non-repetitive fragments, and they are duplicated only in one of the two arrangements, the duplicated sequence could be the consequence of a non-homologous end-joining (NHEJ) of two staggered breaks [23]. Both mechanisms seem to act to varying degrees in genome evolution depending on the species. However, in the case of *D. subobscura*, the molecular characterization of several breakpoints has only detected clear examples of NHEJ [21,22]. In addition, other less frequent and/or more

complex mechanisms may occur at the origin of some inversions. In this sense, it has recently been seen that two inversions of *D. subobscura* have required the intervention of two homologous chromosomes at their origin [24,25].

In the last decade, with the growth in next-generation sequencing, several methodologies have been developed to detect structural variants from paired-end sequences [26–28]. In short, clusters of read pairs that do not map to the reference genome in the expected orientation and distance to each other are indicative of the existence of structural variants (SVs). In the present work, we have used this strategy to characterize the breakpoints of two inversions of chromosome U of *D. subobscura* (the U_6 and U_8 inversions). We chose these two inversions to apply this bioinformatic strategy because on chromosome U only inversions U_1 and U_2 had been previously characterized. On the other hand, both U_6 and U_8 are the most common inversions that originate in a U_{1+2} arrangement in the Mediterranean area, and we were able to obtain homokaryotypic strains for these inversions. Furthermore, we can take advantage of the fact that the reference genome of *D. subobscura* [29] carries the U_{1+2} arrangement to find the breakpoints of these two inversions (U_6 and U_8) by directly comparing the reference genomic sequence with those of the U_{1+2+6} and $U_{\underline{1+8}+2}$ arrangements. In the case of the $U_{\underline{1+8}+2}$ arrangement, there are two more very interesting characteristics: (1) it seems to be adapted to warm climates [30,31]; and (2) one of its breakpoints is shared with inversions U_1 and U_2 [8]. Our objective is, therefore, the molecular characterization of the breakpoints of these two inversions. This work will contribute to knowledge of the origin of the inversions and, although it does not focus directly on the adaptation of inversions, it may be a first step to understanding their selective maintenance in nature.

2. Materials and Methods

2.1. Drosophila Strains

The homokaryotypic strains of *D. subobscura* used in this study were obtained through over 13 generations of sibmating from isofemale lines established upon collection in Observatori Fabra (Barcelona, Catalonia, Spain), as reported in [15]. Specifically, the sequenced strains were OF28 and OF58, which are homokaryotypic for the $U_{\underline{1+2+6}}$ and $U_{\underline{1+8}+2}$ chromosomal arrangements, respectively. In addition, strain OF74, which is homokaryotypic for the U_{1+2} arrangement, was also used to validate the bioinformatic results using polymerase chain reactions (PCRs).

2.2. DNA Extraction and Sequencing

For each strain, genomic DNA was extracted from 20 adult individuals using the Puregen Cell kit B (Qiagen, Hilden, Germany). Two and four micrograms of genomic DNA for strains OF28 and OF58, respectively, were sent to CNAG (Barcelona, Spain) for further sample preparation and sequencing. Libraries for paired-end Illumina reads, separated by ~300 bp inserts, were indexed for multiplex sequencing on the same sequencing lane of a HiSeq 2500 flowcell (Illumina Inc., San Diego, CA, USA) and sequenced in PE mode and 2 × 101 nt read length. A total of 41,333,785 and 67,671,844 reads were obtained, respectively.

2.3. Bioinformatics of Sequencing Data

To map the two breakpoints of an inversion (i.e., regions AB and CD in the reference genome and regions AC and BD in the inverted genome, Figure 2), we used a strategy already applied to *D. melanogaster* [26,27], which consists of detecting clusters of discordant

paired-end reads when mapping to the reference genome. It is expected that the reassembling de novo of these discordant reads will recover the inverted points AC and BD.

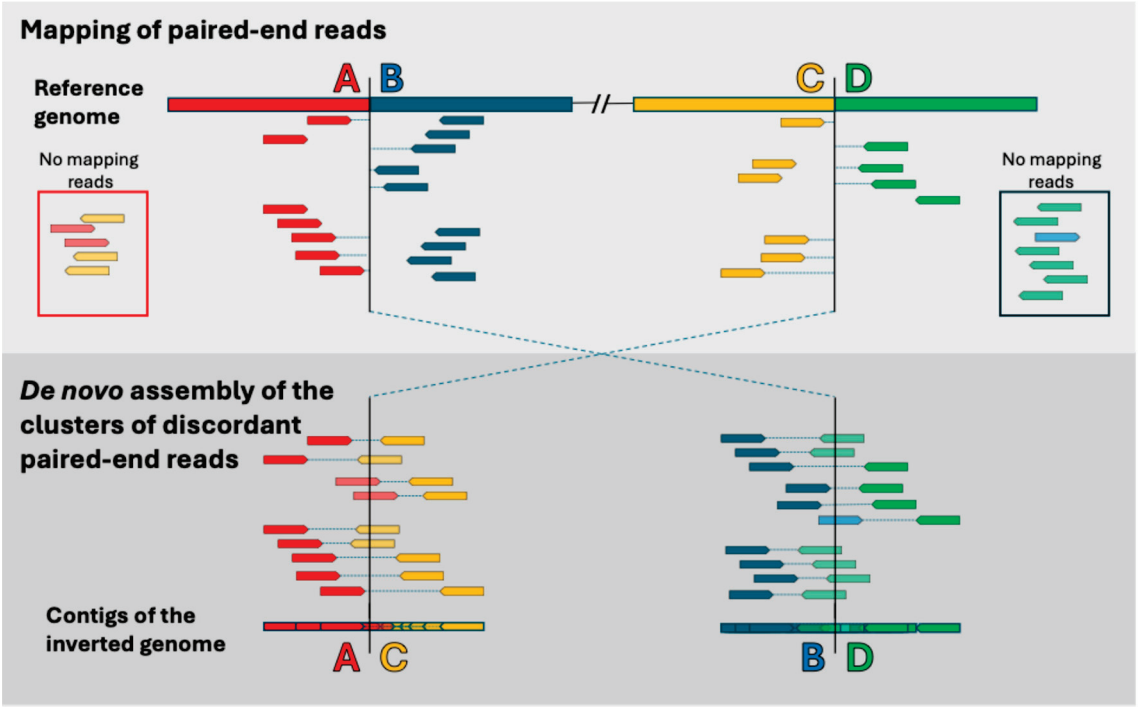


Figure 2. Schematic representation of the paired-end reads mapping around the breakpoints of a chromosomal inversion. Reads from each paired-end are indicated by two colored arrows joined by a dashed line (pairs are red-orange or blue-green, depending on the region where they map). (**Top**) Reads mapping positions on the reference sequence in the AB and CD regions. Around breakpoints in the reference sequence, reads map into clusters of discordant pairs (without the expected orientation and with a mapped distance much larger than the average insert size). In addition, reads spanning breakpoints are not mapped. In the boxes are reads that do not map to any part of the reference genome (in lighter color). (**Bottom**) The inferred positions on the inverted haplotype (regions AC and BD) of the clusters of discordant paired-end reads and the contigs obtained by their de novo assembly.

The bioinformatics workflow followed is presented in Supplementary Materials Figures S1 and S2, and the scripts used are available on https://github.com/mercemerayo/Dsubobscura-inversions; accessed on 30 March 2025. This workflow consists of five main steps: (1) quality control, (2) mapping to a reference genome; (3) detecting of discordant paired-end reads; (4) de novo assembling of the discordant reads; (5) verification of the contigs. The first step of quality control and preprocessing of the reads was performed with fastp [32]. Then, the processed reads were mapped to a "hologenome" of reference consisting of the genomes of *D. subobscura* (UCBerk Dsub 1.0), *Saccaromyces cerevisae* and other possible microbial symbionts or pathogens following the list used by Kapun and collaborators [33], where other possible members of the *Drosophila* microbiome [34,35] have been added (Supplementary Materials Table S1). Mapping to a hologenome allows for the rapid removal of reads corresponding to microorganisms that it includes, avoiding them interfering with the correct mapping of the rest of the reads. The mapping was performed using the software BWA-MEM2 (version 2.2.1) [36] and the duplicated reads were marked using Samtools version 1.19.2 [37]. The mapping of the U chromosome was then analyzed using the BreakDancer program (version 1.4.5) [38]. This software detects paired-end reads that map in a discordant way and returns an output consisting of a list of coordinates where clusters of such discordant reads occur. This list was filtered for

possible inversions expanding through the coordinates of known molecular markers near the cytological breakpoints of the inversion of interest. Table 1 shows the information of the molecular markers used to search for the inversion breakpoints and Figure 3 shows their location on the chromosome U used as the genome of reference.

Table 1. Cytological localization of the breakpoints of U_6 and U_8 inversions in *D. subobscura*, and cytological and genomic localization of molecular markers near these breakpoints.

Inversion	Marker	Band	Reference	BLAST
U_6	Proximal BP.	45B/45A	[8]	¿?
	Ddc	44D	[39]	7,888,695–7,890,041
	dpy	49D	[20]	16,420,251–16,503,087
	Distal BP.	49D/49C	[8]	¿?
U_8	Proximal BP.	45A/44D	[8]	¿?
	Ddc	44D	[8]	7,888,695–7,890,041
	Proximal BP. U_1 (*Dgua6E013454)*	40A	[8,22]	14,589,270–14,593,607
	Distal BP. U_2(*Dgua6E013443*)	51C	[8,22]	14,634,213–14,639,290
	Distal breakpoint	51C/40A	[8]	¿?

Note: ¿? Means unknowns location.

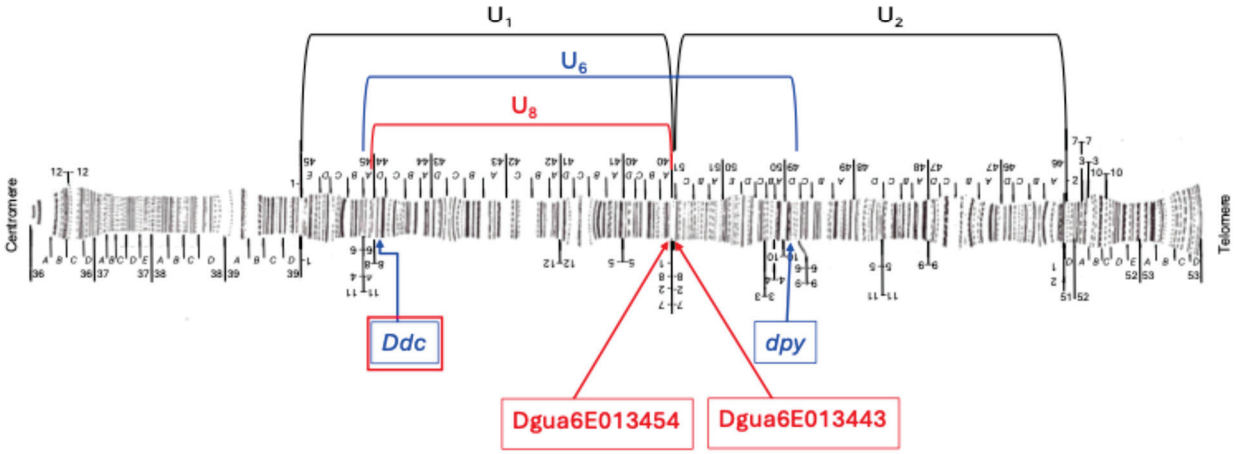


Figure 3. Location of genetic markers near the U_6 (indicated in blue boxes) and U_8 (indicated in red boxes) inversion breakpoints mapped in previous studies on Kunze-Mühl and Müller's cytological map [8] of the *D. subobscura* U chromosome. Note that the U chromosome map has been modified to show the U_{1+2} arrangement. Also, note that the *Ddc* gene was used as a marker for both inversions.

Once the coordinates of the putative inversions were determined, paired-end reads mapping around 5 kb on each side were extracted with Samtools (version 1.19.2) and de novo reassembled using SPAdes (version 4.0.0) [40]. We used two types of read pairs for the assembly. The first type included pairs where both reads were mapped to the target regions. The second included pairs in which one read mapped within 5 kb of either putative breakpoint, while the other read remained unmapped. These unmapped reads are of great interest, as they are expected to cross the breakpoint (Figure 2).

Finally, the recovered contigs were aligned to the *D. subobscura* reference genome [29] using the Basic Local Alignment Search Tool (BLAST) on the webpage of NCBI [41] to assign their relative location in the reference genome and infer their location in the inverted genome (Supplementary Materials Figures S3 and S4).

2.4. PCR Validation and Sanger Sequencing

For each inversion analyzed (U_6 and U_8), we identified putative contigs that crossed the breakpoints in the inverted chromosome, or two concatenated contigs that were ex-

pected to align in the corresponding manner. These contigs were used to design amplification primers for the regions AC and BD, using the Primer-BLAST facility on the NCBI webpage that uses Primer3 (version 2.5.0). Before choosing a primer pair, the presence of each oligo was also tested for also in the reference genome to be sure that a correct combination of the four primers would also obtain amplification for regions AB and CD in a strain with the U_{1+2} arrangement (Supplementary Materials Tables S2 and S3).

A total of eight PCR amplifications were performed for each inversion: AB, CD, AC and BD, both for the OF74 strain carrying the U_{1+2} arrangement and for the strain with the additional inversion (OF28 or OF58, depending on the tested inversion U_6 or U_8, respectively). In the case of the OF74 strain, only two PCRs should be positive (AB and CD) and with an amplification band of known size. In the case of the other strain, only the combinations of primers AC and BD should give an amplification band and, in some cases, their sizes are unknown.

For the BD fragment of the $U_{\underline{1+8}+2}$ arrangement, the bioinformatics approach generated two unconnected contigs. As a result, a primer walking sequencing was initiated to resolve these fragments further. Since the original BD primers generated a faint secondary amplification band (Supplementary Materials Figure S5) and some of the sequencing primers did not work properly, a pair of internal PCR primers (Bi and Di, Supplementary Materials Table S2) were designed to obtain a nested reamplification PCR in an attempt to achieve greater specificity of DNA amplification. In all cases, amplicons were purified with Exo-SapIT (Amersham Biosciences, Piscataway, NJ, USA) prior to their sequencing with the ABI PRISM version 3.2 cycle sequencing kit (Applied Biosystems, Foster City, CA, USA). Sequencing products were separated using an ABI PRISM 3730 sequencer (Perkin-Elmer, Norwalk, CT, USA). Sequences were assembled using the DNASTAR package [42].

The sequences newly obtained for regions AC and BD in the arrangement $U_{\underline{1+8}+2}$ have been deposited in the European Nucleotide Archive (ENA) under project number PRJEB88772.

3. Results

3.1. Inversion U_6

For the OF28 strain ($U_{\underline{1+2+6}}$), the BreakDancer software (version 1.4.5) returned a list of 166 possible inversions in the chromosome U, 92 of which had a score higher than 99. Among these, an inversion at coordinates 7,714,784 and 16,614,075 stands out, which is consistent with the molecular markers we had for the inversion U_6 (Table 1). In addition, this inversion was one of those supported by a higher number of reads (83). The reassembling of the reads that mapped around these coordinates in the reference genome gave a total of 55 contigs with only four of them having a length greater than 5 kb. Contig_1 with a length of 11,791 bp crosses the BD region, while contig_4 with 6421 bp crosses the AC breakpoint in the arrangement $U_{\underline{1+2+6}}$. It should be noted that, when performing BLAST with the obtained contigs, the breakpoints that are recovered are slightly shifted with respect to those indicated by BreakDancer. Thus, the proximal breakpoint would be between positions 7,714,148 and 7,714,441 of chromosome U of the reference genome instead of position 7,714,784 predicted by BreakDancer. On the other hand, the distal breakpoint would be between positions 16,613,602 and 16,613,622 instead of the position 16,614,075. In both cases the recovered points are approximately 400 bp before those predicted (Supplementary Materials Figure S3).

Both breakpoints are in intergenic regions and no clear duplications were found in either the original or inverted arrangements (Figure 4). The proximal breakpoint is near the

LOC117902107 gene, and the distal breakpoint is close to the 3′ end of the LOC117900774 gene. These genes are orthologous to the *hermes* and CG13481 genes in *D. melanogaster,* respectively.

At the proximal breakpoint, there is a partial SGM element [43] and Contig_4 has an initial region (1–489) with a sequence that does not match to any of the original AB or CD regions.

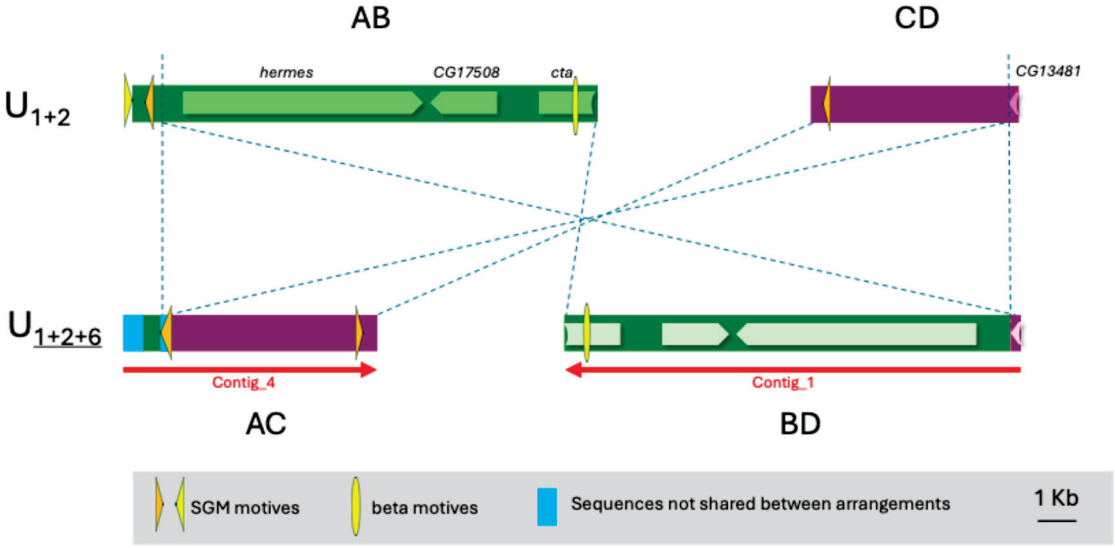


Figure 4. Schematic representation of inversion U_6 breakpoint regions in chromosomal arrangements U_{1+2} and $U_{\underline{1+2+6}}$ and their functional annotation. Red arrows represent the recovered contigs. The names of the genes correspond to the orthologous genes in *D. melanogaster*. Genes on the BD regions are indicated with a fainter color because they are only inferred from the overall sequence similarity. The orange and yellow triangles show the starting and ending sequences of the SGM motif, respectively.

The PCR performed with the primers designed to validate the inversion produced several bands, indicating the possible presence of repetitive sequences in these regions. It is important to keep in mind that, although both Contig_1 and Contig_4 cross the breakpoints in the inverted arrangement, they extend mainly on the internal part of the inversion (regions B and C, respectively). Regions A and D only are covered by 465 and 271 nucleotides, respectively, which makes it difficult to design suitable primers for performing the PCR validation of the breakpoints.

3.2. Inversion U_8

In the case of the OF58 strain ($U_{\underline{1+8+2}}$), the BreakDancer software gave a list of 205 possible inversions in the chromosome U, 90 of which had a score higher than 99. Among these, an inversion at coordinates 7,772,887 and 14,722,269 stands out, which is consistent with the molecular markers we had for the inversion U_8 (Table 1). In addition, this inversion was one of those supported by a higher number of reads (48). The reassembling of the reads that mapped around these coordinates in the reference genome yielded a total of four contigs. The contig_1 with a length of 10,248 bp crosses the AC breakpoint in the inverted arrangement ($U_{\underline{1+8+2}}$) since its first 5334 nucleotides align directly in region A (from 7,767,475 to 7,772,833) of the chromosome U of the reference genome, while its last part aligns in the inverted direction in region C (from 14,716,861 to 14,721,766) of the same chromosome (Figure 5). Contig_2 with 6368 bp aligns only to region B and Contig_3 with 5481 bp aligns only to region D. On the other hand, the BLAST analysis with the Contig_4 of only 314 bp does not return any resemblance with the reference genome. Figure 5 shows

that the three longest contigs cover practically the entire AB and CD regions of the reference genome, leaving only 141 and 12 nucleotides uncovered, respectively. In these uncovered regions (7,772,834–7,772,973 for the proximal point and 14,721,767–14,721,777 for the distal point) must be located the breakpoints in the original arrangement. It should be noted that the proximal point fits well with the BreakDancer prediction, while the distal point was predicted to be ~500 bp more distal. Another point that arises from our results is that the distal breakpoint is ~100 kb more distal than the proximal breakpoint of inversion U_2 (Table 1). Thus, inversions U_1 and U_2 would overlap inversion $U_{8,}$ and the arrangement should be named $U_{\underline{1+2+8}}$.

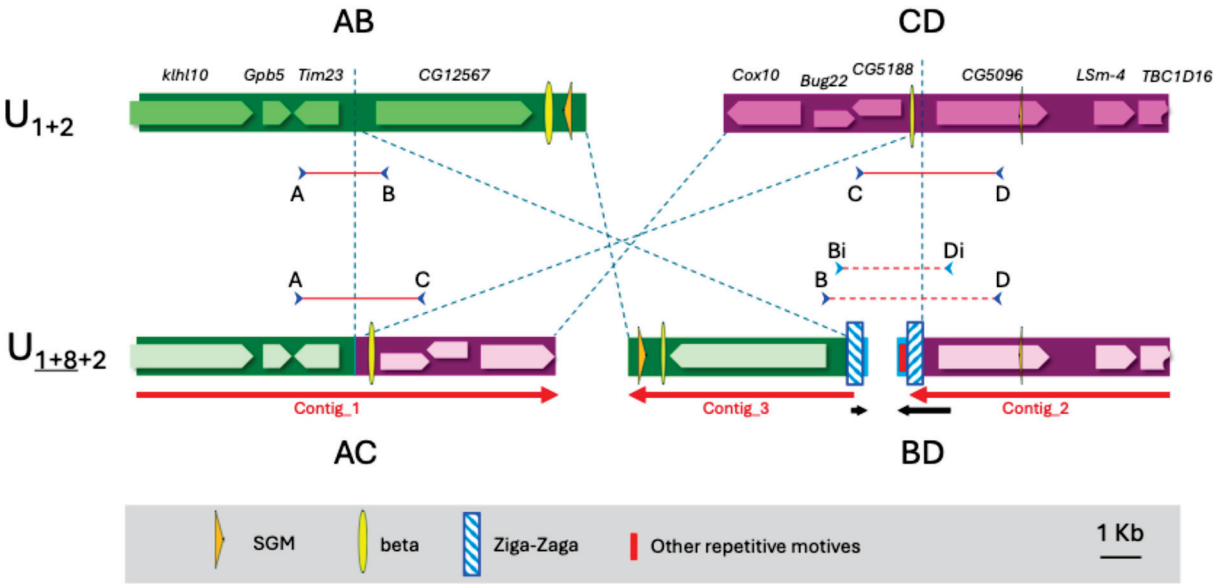


Figure 5. Schematic representation of inversion U_8 breakpoint regions in chromosomal arrangements U_{1+2} and $U_{\underline{1+8}+2}$. Red arrows represent the recovered contigs from Illumina paired-end reads. The black arrows show the sequences obtained by Sanger sequencing. Genes on the inverted arrangement are indicated with a fainter color because they are only inferred from overall sequence similarity. The orange triangles show the starting sequences of the SGM motif. Blue arrowheads show the location of the PCR primers used to validate the breakpoints.

Both breakpoints in the U_{1+2} arrangement are in intergenic regions, but near genes. The proximal point is flanked by the gene *Tim23* and the orthologous to *CG12567* of *D. melanogaster*. The distal point falls between two predicted genes orthologous to *D. melanogaster,* CG5188 and CG5096, respectively.

In the inverted genome, the AC region has been assembled continuously, but the sequence in the BD region is discontinuous and would probably have incorporated new sequences, such as those recovered by Contig_4. In fact, the last ~320 nucleotides of contig_2 and the first ~130 of Contig_3 do not match the original AB or CD regions and have some similarities to multiple sequences in the genome.

Four oligonucleotides, one in each region (A, B, C and D), were designed to test the correct assignment of contigs (Supplementary Materials Table S2 and Figure 5). As expected, the combinations of primers AB and CD only gave an amplification band when using DNA from the strain OF74 that has the original arrangement U_{1+2}. On the other hand, also as expected, the combinations of primers AC and BD only gave an amplification band when using DNA from the strain OF58 that carries the arrangement $U_{\underline{1+8}+2}$ (Supplementary Materials Figure S5). The recovered bands AB, CD and AC have the sizes expected from the known sequences. For its part, the band obtained for the region BD, in the inverted

arrangement, shows a size of approximately 4 kb, indicating that a sequence of ~1.3 kb has been inserted between Contig_2 and Contig_3.

Sequencing of the BD fragment was initiated by primer walking, but several problems were encountered in completing this sequence. To begin with, the PCR band obtained was much weaker than that of the other fragments tested (Supplementary Materials Figure S5). Attempts to improve band intensity by adjusting the annealing temperature and designing reamplification primers (Figure 5) were unsuccessful. In addition, some sequencing primers did not work, and others only allowed obtaining about 300 bp and then the sequence quality suddenly dropped. Therefore, only 436 bp could be added to the sequence of the beginning of Contig_3 (end of subregion B of the BD region) and 269 bp at the end of Contig_2 (beginning of subregion D of the BD region). The BLAST analysis of the complete sequence obtained revealed that subregions B and D of the inverted genome contain repeated fragments in inverted sense. Thus, a 371 bp fragment at the end of subregion B (136 nucleotides at the beginning of Contig_3 and 235 added by Sanger sequencing) and 371 bp at the beginning of subregion D (323 bp at the end of Contig_2 plus 48 added by Sanger sequencing) show a 97% identity in the reversed direction. In addition, part of these inverted sequences gave a BLAST alignment (92% identity) with the sequence close to one of the breakpoints for the fixed inversion Af3 between chromosomes X of *D. subobscura* and *D. guanche* that could not be completely sequenced [21].

Given the impossibility of continuing sequencing towards the interior of the BD region, we changed our strategy and attempted to sequence from the interior of the BD fragment outwards. Assuming that Contig_4 (which did not align anywhere in the original arrangement) had to be found between contigs 3 and 2 in the inverted arrangement, we designed amplification primers that would allow us to check this hypothesis and decide in which direction Contig_4 is located. The PCR results would seem to indicate that Contig_4 is located between the two long contigs in the reverse direction, but the sizes of the bands obtained do not fit our expectations and none of the amplification primers were able to yield a clear sequence.

We also investigated whether the sequences around the breakpoints contained any of the repetitive sequences described in *D. subobscura*, i.e., SGM (Miller et al. 2000 [43]) and α, β or δ motifs [15]. Two fragments of SGM of ~200 and ~60 bp were found in the regions B and D, respectively, and also two small fragments of the β motif of ~130 and ~170 bp were found in the regions B and C, respectively (Figure 5).

3.3. Description of "Ziga-Zaga", a Fold-Back Element in the Subobscura Group

The difficulties that we found in completing the BD sequence led us to find a sequence of 371 bp long that is repeated in an inverted orientation next to the BD breakpoint. This structure, along with the difficulties in obtaining a strong PCR band in this region, suggests that this could be a fold-back element. BLAST analysis of this 371 bp sequence in NCBI revealed that it has no homology to any sequence in the general database. When searched within specific genomes, it is not found in either the *Drosophila melanogaster* or *D. pseudoobscura* genomes, and its occurrence appears to be restricted to the *D. subobscura* group. In this group of species, some TEs and satellite sequences have already been described as SGM [43] and sat290 [44], but the sequence found here has no similarities to them. Therefore, we named this new FB element *Ziga-Zaga*, where each unit of 371 bp will be *Ziga* or *Zaga*, and when they are found together, form the *Ziga-Zaga* element. This sequence of 371 bp seems to correspond to a partial *Ziga* repeat since when using the whole 472 bp of the sequence that we know occurs at the end of the B subregion, the BLAST matches include this additional 101 bp that are not found at the beginning of the subregion

D. On the other hand, BLAST of the initial 592 bp of the D region produces two types of matches: those already expected for its final fragment of 371 bp (222–592) and another collection of matches for the first 221 nucleotides.

When searching for very similar sequences (megablast) with alignments of more than 50 bp, it is found that the modular 371 bp sequence (*Ziga* or *Zaga*) occurs 98 times in the *D. subobscura* genome distributed across all chromosomes. Many of these repeated sequences are paired in the genome and, when this is the case, most (30 pairs) are in inverted orientation and separated by a variable length, ranging from 130 to 5854 bp (Supplementary Materials Table S4).

The genomes of *D. madeirensis* and *D. guanche* also have this *Ziga-Zaga* element on all their chromosomes, indicating that its appearance predates speciation in this group. The number of copies detected by BLAST in the *D. madeirensis* genome is 68 (lower than that of *D. subobscura*), and it has many copies on the O chromosome (Supplementary Materials Table S4) and especially in its last 35 kb where five partial copies (from 124 to 371 bp) are found in tandem orientation and separated by variable lengths no longer than 2.2 kb. In the case of *D. guanche*, the BLASTN was performed on the CNAG website (https://denovo.cnag.cat/dguanche; accessed on 12 April 2025) since the results obtained through NCBI do not correspond to chromosomes but to scaffolds. After filtering for alignments longer than 50 bp, we found 121 matches (Supplementary Materials Table S4). This number is higher than that obtained for *D. subobscura*, but many of these matches (34) correspond to alignments that do not exceed 100 bp. In addition, even considering these short alignments, the fold-back structure was only found in 13 instances. Another observation is that at the extremes of the chromosomes, a higher number of these repeats seem to be concentrated but in the same orientation. This is the case of the chromosome A telomere with three tandem partial copies.

Next to the *Zaga* fragment found in region D of the $U_{\underline{1+8}+2}$ arrangement is a fragment of 221 nucleotides that is also a repetitive sequence. As pointed out above, when doing BLAST for the whole 592 nucleotide sequence at the beginning of subregion D, two collections of different matches are obtained. For the first 221, a total of 56 matches were obtained in the *D. subboscura* genome. All of them are close to a match of the *Ziga* or *Zaga* sequences, but their relative position and orientation is very variable. The same pattern is observed in *D. madeirensis* that has 32 matches for this sequence. It highlights that the telomere of chromosome O seems to be enriched with this sequence alternating with the *Zaga* motifs. As this sequence of 221 bp is always close to a *Ziga* motive, we named it *company* (companion in Catalan).

4. Discussion

Several studies have revealed that the rich chromosomal inversion polymorphism in *D. subobscura* is modeled by natural selection [9] and particularly mediated by thermal adaptation [7,10,11,29,45–49]. However, it is not known which genes are being directly selected along with each inversion. A first step in this direction must be the molecular localization of the inversion breakpoints. In this study, we have focused on the characterization of two U chromosome inversions (U_6 and U_8). The first does not seem to be particularly adapted to certain climatic conditions since its frequency of occurrence in natural populations is low, but the U_8 inversion is considered to be well adapted to warm climates [29,47,50].

4.1. Limitations of the Methods Used to Molecularly Characterize Inversions and Their Breakpoints

Before the genome sequence of *D. subobscura* was available, several studies were carried out using laborious methodologies of chromosome walking and in situ hybridization in order to locate probes that crossed each of the breakpoints of some of its most common chromosomal inversions [14–19]. Once a complete genomic sequence was available, the breakpoints of three more inversions could be found by a synteny analysis comparing two complete genomes, either from related species [22] or from individuals carrying other chromosomal arrangements [25]. The present study adds information in this regard for two inversions of the U chromosome (U_6 and U_8), exploring the utility of a new approach to the problem, mapping paired-read sequences from individuals carrying an inversion with respect to the reference genome.

This approach has been used by Cridland and Thornton in *D. melanogaster* to identify diverse structural variants [26]. Specifically, these authors could differentiate between three kinds of SV: indels, Class 1 events (tandem duplications or translocations) and Class 2 events (inversions or duplications with a change in orientation). Regarding Class 2 events, they state that most of those detected could be artifacts of the sequencing process, reinforcing the importance of having multiple read pairs supporting each event. Lately, Corbett-Detig et al. have presented a method that uses the mapping of multiple samples to detect inversions and their breakpoints in population samples [27]. This approach allowed them to confirm the breakpoints of three previously characterized inversions and localize those of four more. Nevertheless, one of the breakpoints of both inversions *In(2L)t* and *In(3R)P* could not be recovered and it could be due to the presence of repetitive elements adjacent to these breakpoints [51,52]. The only drawback of the method of Corbett-Detig et al. is that inversions present in only one individual will be missed.

We have returned to the original method of searching for clusters of discordant reads by mapping sequences from a single strain using BreakDancer, which is one of several programs that have been developed for this purpose [28]. This methodology has proven to be robust enough to recover the breakpoints of a fixed inversion between *D. subobscura* and *D. guanche* in chromosome J [53]. In this case, the sequences obtained for the de novo assembly of the discordant reads of *D. subobscura* around the predicted breakpoints in *D. guanche* perfectly match the sequences obtained by the traditional method of chromosome walking and in situ hybridization [21]. In the present study, we applied this approach to find the breakpoints of two long polymorphic inversions of the U chromosome and this has allowed the molecular characterization of one of them (U_8). However, our results for the U_6 inversion are inconclusive, as the recovered contigs only partially cross the breakpoints of the inverted genome. The recovery of these "chimeric" contigs (with BLAST alignments of different fragments to one or another region of the reference genome) seems to confirm the location of the breakpoints, but the shortness of the sequence in one of the two regions did not allow us to design suitable primers for PCR validation. Furthermore, the assembling of the reads yielded a high number of small contigs, which may be indicative of the presence of repetitive sequences in the inverted genome. In fact, BLAST of some of these contigs, such as Contig_5 of 3251 bp showed a high similarity of its sequence to multiple sites not only on chromosome U but also on the rest of the chromosomes. This makes it unfeasible to fully conclude the molecular characterization of these breakpoints in this way.

Regarding the U_8 chromosomal inversion, the proposed strategy yielded better results, allowing us to molecularly characterize its breakpoints. The selected reads from the mapping to the reference U chromosome could be assembled into three long contigs covering the two original regions AB and CD (Supplementary Materials Figure S4), and

a short contig of 314 bp with a sequence that does not exist in the ancestral arrangement. In this case, the proximal breakpoint recovered by our sequence fits well with the point predicted by BreakDancer. On the other hand, the distal point is displaced by about 500 bp, which is a distance greater than the expected 95% confidence interval, which would be twice the standard deviation of the insert size [54], which for this sample is 213. The region around the proximal breakpoint in the inverted arrangement (AC) was determined directly from one of the recovered contigs. However, to complete the sequence of the distal breakpoint (BD), PCR amplification and Sanger sequencing of the central region were required. Several problems were encountered in completing this sequence. To begin with, the PCR band obtained was much weaker than that of the other fragments tested (Supplementary Materials Figure S5). Our efforts to obtain a more intense band were futile, both by varying the annealing temperature and by designing reamplification primers. In addition, some sequencing primers did not work; and others only allowed us to obtain a fragment of about 300 bp and then the sequence quality suddenly dropped. The attempt to sequence from Contig 4, which appears to be in the central region of the missing sequence, also yielded no results. The origin of the problem seems to be in the existence of a region duplicated in the inverted orientation that could be hindering both correct amplification and obtaining suitable sequencing primers. This region has similarities to another present near a fixed inversion between *D. subobscura* and *D. guanche* and which also prevented its complete characterization. These observations seem to point to the presence of a fold-back element that could be involved in the origin of the inversion (see below).

Thus, we can conclude that, although the method used allows the recovery of inversion breakpoints, it does not allow the complete molecular characterization of those involving complex repetitive sequences. In these cases, the complete characterization will require the use of long-read sequencing technologies to circumvent the major problems found in repetitive regions (the assembly of short reads or finding good primers to proceed with Sanger sequencing). In the case of the BD region of inversion U_8, the PCR results indicate that a stretch of ~1.3 kb is missing between the two contigs of the Illumina assembly. A long read should allow us to connect these two contigs and decipher if there is any duplicated sequence with respect to the AC region that could clearly indicate the molecular origin of the inversion.

4.2. Origin of the Inversions U_6 and U_8

Two main mechanisms have been proposed as the origin of inversions: non-allelic homologous recombination (NAHR) and non-homologous end-joining (NHEJ).

In the case of NAHR, the inversion arises from recombination between sequences of the same chromatid that are duplicated in an inverted direction and flanking the fragment that undergoes inversion. Thus, both arrangements, the standard and the inverted, carry these flanking inverted sequences. Most of these inverted sequences correspond to transposable elements (TEs). In addition, TEs may generate chromosomal inversions through their transpositional activity, leaving TE inserts at one or both inversion breakpoints [55,56]. In *D. melanogaster*, several instances of the role of transposons have been identified [57,58], and also the origin of inversions in *D. buzzati* appears to be largely mediated by the action of transposons [59,60].

On the other hand, the NHEJ consists in the repair of two breaks in the same chromatid that may be blunt or staggered, and, in which case, will generate a duplication of a fragment of one or both original sequence breakpoints in the inverted arrangement in an inverted direction. This mechanism seems to be prevalent in the melanogaster species group [23] and in the subobscura species group [21]. In some cases, the mechanism of origin has had to

be more complex, involving more than one chromatid, as has been inferred in *D. subobscura* for the E_9 and O_7 inversions [24,25].

In this work, we have analyzed two inversions of the U chromosome of *D. subobscura* at the molecular level. Although for the U_6 inversion, the characterization has not been complete, it seems that there are no duplicated sequences in either the ancestral or the inverted arrangement. On the other hand, the presence of a partial SGM element [43] close to the breakpoint in Contig 4 along with a ~500 bp fragment whose sequence does not match any of the original AB or CD regions could indicate that the origin of this inversion is mediated by a transposable element. In the case of inversion U_8, a new fold-back-like element has been characterized. The BD breakpoint region has not been completely sequenced, but the whole inverted repeat of *Ziga-Zaga* has been obtained and other repetitive sequences seem also to be present. It is interesting to note that the AC region includes an intermediate stretch of 34 nucleotides (5334–5368 in contig_1) that does not correspond to either of the two original subregions A or C (Supplementary Materials Figure S4). This sequence forms an almost perfect palindromic sequence with a high identity to the 21 first nucleotides of the *Ziga* unit (Supplementary Materials Figure S6). Since this stretch of sequence is very short (34 bp), its presence here could be a simple coincidence. However, the fact that it corresponds precisely to the outermost nucleotides of the *Ziga-Zaga* element along with their precise location right in the middle of the sequences where a break and repair has occurred suggests that it could be related to the origin of the inversion (and could be the footprint of the previous presence of a *Ziga-Zaga* element). Our conclusion is that the U_8 inversion could have originated through the mediation of the *Ziga-Zaga* element. In cases where TEs are involved, it is almost impossible to know whether it was produced by NAHR or by the TE transposition process itself. Since the inversion event, the sequences have been able to evolve, preventing us from seeing the traces left by the process that generated it. On the other hand, since the complete sequence of the BD region is unknown, the possibility that the origin of the inversion was by NEHJ cannot be completely ruled out.

5. Conclusions

In this work, we present a bioinformatics pipeline that appears to be a reliable approach for obtaining the breakpoints of inversions in *D. subobscura*. However, sequences cannot be fully recovered when complex repetitive sequences are involved in the origin of the inversions.

To date, most of the inversions characterized at the molecular level in *D. subobscura* have originated from the repair of staggered end breaks generating inverted repeats in the new arrangement. The two inversions studied here show features consistent with a possible origin mediated by transposons, suggesting for the first time in this species that such a mechanism may play a role in inversion origination.

In fact, at the distal breakpoint of the U_8 inversion, there is a folding element that prevented us from completing the sequence of this region. BLAST analysis of this sequence reveals that it is characteristic of the subobscura species group and confirms that this repetitive sequence is mostly present with a folding structure. Thus, we described a new fold-back-like element, which we have named *Ziga-Zaga*.

Supplementary Materials: The following supporting information can be downloaded at: https://www.mdpi.com/article/10.3390/insects16060586/s1, Figure S1: Workflow used to detect the inversion breakpoints.; Figure S2: Workflow used to reconstruct and validate the inversion breakpoints; Figure S3: Schematic representation of inversion U_6 breakpoint regions; Figure S4: Schematic

representation of inversion U_8 breakpoint regions; Figure S5: Agarose gel with the PCR products; Figure S6: Alignment of the intermediate AC sequence of inversion U_8 to the *Ziga-Zaga* element; Table S1: Microorganisms included in the hologenome of reference.; Table S2: PCR primers designed to amplify breakpoint regions of inversion U_8; Table S3: Expected amplification bands; Table S4: Abundance of the *Ziga-Zaga* element in the genome of three species.

Author Contributions: Conceptualization, D.J.O.; methodology, M.M., K.M.D., D.S. and D.J.O.; software, M.M. and K.M.D.; validation, M.M., K.M.D. and D.J.O.; formal analysis, D.J.O.; investigation, M.M., K.M.D., D.S. and D.J.O.; resources, D.S. and D.J.O.; software, M.M. and K.M.D.; data curation, D.J.O.; writing—original draft preparation, D.J.O.; writing—review and editing, M.M., K.M.D. and D.J.O.; visualization, M.M. and D.J.O.; supervision, D.J.O.; project administration, D.J.O.; funding acquisition, D.J.O. All authors have read and agreed to the published version of the manuscript.

Funding: This work was supported by 2021SGR00279 from Agència de Gestió d'Ajuts Universitaris i de Recerca (AGAUR), Generalitat de Catalunya, Spain and The APC was funded by MDPI.

Data Availability Statement: The scripts used are available on https://github.com/mercemerayo/Dsubobscura-inversions (accessed on 30 March 2025). The sequences newly obtained for regions AC and BD in the arrangements $U_{\underline{1+2+6}}$ and $U_{\underline{1+8}+2}$ will be deposited in the European Nucleotide Archive (ENA) under project number PRJEB88772.

Acknowledgments: We thank Serveis Científico-Tècnics from Universitat de Barcelona for automatic sequencing facilities.

Conflicts of Interest: The authors declare no conflicts of interest.

References

1. Sturtevant, A.H. Genetic Factors Affecting the Strength of Linkage in Drosophila. *Proc. Natl. Acad. Sci. USA* **1917**, *3*, 555–558. [CrossRef] [PubMed]
2. Painter, T.S. A New Method for the Study of Chromosome Rearrangements and the Plotting of Chromosome Maps. *Science* **1933**, *78*, 585–586. [CrossRef]
3. Sharakhov, I.V.; Sharakhova, M.V. Chromosomal Inversions and Their Impact on Insect Evolution. *Curr. Opin. Insect Sci.* **2024**, *66*, 101280. [CrossRef]
4. Krimbas, C.B.; Powell, J.R. *Drosophila Inversion Polymorphism*; Krimbas, C.B., Powell, J.R., Eds.; CRC Press: Boca Raton, FL, USA, 1992.
5. Krimbas, C.B.; Loukas, M. The Inversion Polymorphism of *Drosophila subobscura*. In *Evolutionary Biology*; Hecht, H., Steere, W., Wallace, B., Eds.; Plenum Press: New York, NY, USA; London, UK, 1980; pp. 163–234.
6. Krimbas, C.B.; Loukas, M. Evolution of the Obscura Group Drosophila Species. I. Salivary Chromosomes and Quantitative Characters in *D. Subobscura* and Two Closely Related Species. *Heredity* **1984**, *53*, 469–482. [CrossRef]
7. Solé, E.; Balanyà, J.; Sperlich, D.; Serra, L. Long-Term Changes in the Chromosomal Inversion Polymorphism of *Drosophila subobscura*. I. Mediterranean Populations from Southwestern Europe. *Evolution* **2002**, *56*, 830–835.
8. Kunze-Mühl, E.; Müller, E. Weitere Untersuchungen Uber Die Chromosomale Struktur Und Die Natürlichen Strukturtypen von *Drosophila subobscura* Coll. *Chromosoma* **1958**, *9*, 559–570. [CrossRef] [PubMed]
9. Prevosti, A.; Ribó, G.; Serra, L.; Aguadé, M.; Balanyà, J.; Monclús, M.; Mestres, F. Colonization of America by *Drosophila subobscura*: Experiment in Natural Populations That Supports the Adaptive Role of Chromosomal-Inversion Polymorphism. *Proc. Natl. Acad. Sci. USA* **1988**, *85*, 5597–5600. [CrossRef] [PubMed]
10. Orengo, D.J.; Puerma, E.; Aguadé, M. Monitoring Chromosomal Polymorphism in Drosophila Subobscura over 40 Years. *Entomol. Sci.* **2016**, *19*, 215–221. [CrossRef]
11. Orengo, D.J.; Prevosti, A. Temporal Changes in Chromosomal Polymorphism of *Drosophila subobscura* Related to Climatic Changes. *Evolution* **1996**, *50*, 1346–1350. [CrossRef]
12. Sturtevant, A.H.; Beadle, G.W. The Relations of Inversions in the X Chromosome of *Drosophila melanogaster* to Crossing over and Disjunction. *Genetics* **1936**, *21*, 554–604. [CrossRef]
13. Dobzhansky, T. Genetics of Natural Populations. XIX. Origin of Heterosis through Natural Selection in Populations of *Drosophila pseudoobscura*. *Genetics* **1950**, *35*, 288–302. [CrossRef] [PubMed]

14. Papaceit, M.; Segarra, C.; Aguadé, M. Structure and Population Genetics of the Breakpoints of a Polymorphic Inversion in *Drosophila subobscura*. *Evolution* **2013**, *67*, 66–79. [CrossRef] [PubMed]
15. Puerma, E.; Orengo, D.J.; Salguero, D.; Papaceit, M.; Segarra, C.; Aguadé, M. Characterization of the Breakpoints of a Polymorphic Inversion Complex Detects Strict and Broad Breakpoint Reuse at the Molecular Level. *Mol. Biol. Evol.* **2014**, *31*, 2331–2341. [CrossRef] [PubMed]
16. Orengo, D.J.; Puerma, E.; Papaceit, M.; Segarra, C.; Aguadé, M. A Molecular Perspective on a Complex Polymorphic Inversion System with Cytological Evidence of Multiply Reused Breakpoints. *Heredity* **2015**, *114*, 610–618. [CrossRef] [PubMed]
17. Puerma, E.; Orengo, D.J.; Aguadé, M. Multiple and Diverse Structural Changes Affect the Breakpoint Regions of Polymorphic Inversions across the Drosophila Genus. *Sci. Rep.* **2016**, *6*, 36248. [CrossRef]
18. Puerma, E.; Orengo, D.J.; Aguadé, M. The Origin of Chromosomal Inversions as a Source of Segmental Duplications in the Sophophora Subgenus of Drosophila. *Sci. Rep.* **2016**, *6*, 30715. [CrossRef]
19. Puerma, E.; Orengo, D.J.; Aguadé, M. Inversion Evolutionary Rates Might Limit the Experimental Identification of Inversion Breakpoints in Non-Model Species. *Sci. Rep.* **2017**, *7*, 17281. [CrossRef]
20. Puerma, E.; Orengo, D.J.; Cruz, F.; Gómez-Garrido, J.; Librado, P.; Salguero, D.; Papaceit, M.; Gut, M.; Segarra, C.; Alioto, T.S.; et al. The High-Quality Genome Sequence of the Oceanic Island Endemic Species Drosophila Guanche Reveals Signals of Adaptive Evolution in Genes Related to Flight and Genome Stability. *Genome Biol. Evol.* **2018**, *10*, 1956–1969. [CrossRef] [PubMed]
21. Orengo, D.J.; Puerma, E.; Aguadé, M. The Molecular Characterization of Fixed Inversions Breakpoints Unveils the Ancestral Character of the Drosophila Guanche Chromosomal Arrangements. *Sci. Rep.* **2019**, *9*, 1706. [CrossRef]
22. Karageorgiou, C.; Gámez-Visairas, V.; Tarrío, R.; Rodríguez-Trelles, F. Long-Read Based Assembly and Synteny Analysis of a Reference *Drosophila subobscura* Genome Reveals Signatures of Structural Evolution Driven by Inversions Recombination-Suppression Effects. *BMC Genomics* **2019**, *20*, 223. [CrossRef]
23. Ranz, J.M.; Maurin, D.; Chan, Y.S.; Von Grotthuss, M.; Hillier, L.W.; Roote, J.; Ashburner, M.; Bergman, C.M. Principles of Genome Evolution in the *Drosophila melanogaster* Species Group. *PLoS Biol.* **2007**, *5*, e152. [CrossRef] [PubMed]
24. Orengo, D.J.; Puerma, E.; Cereijo, U.; Aguadé, M. The Molecular Genealogy of Sequential Overlapping Inversions Implies Both Homologous Chromosomes of a Heterokaryotype in an Inversion Origin. *Sci. Rep.* **2019**, *9*, 17009. [CrossRef] [PubMed]
25. Karageorgiou, C.; Tarrío, R.; Rodríguez-Trelles, F. The Cyclically Seasonal Drosophila Subobscura Inversion O7 Originated From Fragile Genomic Sites and Relocated Immunity and Metabolic Genes. *Front. Genet.* **2020**, *11*, 565836. [CrossRef]
26. Cridland, J.M.; Thornton, K.R. Validation of Rearrangement Break Points Identified by Paired-End Sequencing in Natural Populations of Drosophila Melanogaster. *Genome Biol. Evol.* **2010**, *2*, 83–101. [CrossRef]
27. Corbett-Detig, R.B.; Cardeno, C.; Langley, C.H. Sequence-Based Detection and Breakpoint Assembly of Polymorphic Inversions. *Genetics* **2012**, *192*, 131–137. [CrossRef] [PubMed]
28. Medvedev, P.; Stanciu, M.; Brudno, M. Computational Methods for Discovering Structural Variation with Next-Generation Sequencing. *Nat. Methods* **2009**, *6*, S13. [CrossRef]
29. Bracewell, R.; Chatla, K.; Nalley, M.J.; Bachtrog, D. Dynamic Turnover of Centromeres Drives Karyotype Evolution in Drosophila. *Elife* **2019**, *8*, e49002. [CrossRef]
30. Menozzi, P.; Krimbas, C.B. The Inversion Polymorphism of *D. Subobscura* Revisited: Synthetic Maps of Gene Arrangement Frequencies and Their Interpretation. *J. Evol. Biol.* **1992**, *5*, 625–641. [CrossRef]
31. Rego, C.; Balanyà, J.; Fragata, I.; Matos, M.; Rezende, E.L.; Santos, M. Clinal Patterns of Chromosomal Inversion Polymorphisms in *Drosophila subobscura* Are Partly Associated with Thermal Preferences and Heat Stress Resistance. *Evolution* **2010**, *64*, 385–397. [CrossRef]
32. Chen, S.; Zhou, Y.; Chen, Y.; Gu, J. Fastp: An Ultra-Fast All-in-One FASTQ Preprocessor. *Bioinformatics* **2018**, *34*, i884–i890. [CrossRef]
33. Kapun, M.; Fabian, D.K.; Goudet, J.; Flatt, T. Genomic Evidence for Adaptive Inversion Clines in Drosophila Melanogaster. *Mol. Biol. Evol.* **2016**, *33*, 1317–1336. [CrossRef]
34. Douglas, A.E. The Drosophila Model for Microbiome Research. *Lab Anim.* **2018**, *47*, 157–164. [CrossRef]
35. Guilhot, R.; Xuéreb, A.; Lagmairi, A.; Olazcuaga, L.; Fellous, S. Microbiota Acquisition and Transmission in Drosophila Flies. *iScience* **2023**, *26*, 107656. [CrossRef]
36. Li, H. Aligning Sequence Reads, Clone Sequences and Assembly Contigs with BWA-MEM. *arXiv* **2013**, arXiv:1303.3997.
37. Danecek, P.; Bonfield, J.K.; Liddle, J.; Marshall, J.; Ohan, V.; Pollard, M.O.; Whitwham, A.; Keane, T.; McCarthy, S.A.; Davies, R.M. Twelve Years of SAMtools and BCFtools. *Gigascience* **2021**, *10*, giab008. [CrossRef]
38. Chen, K.; Wallis, J.W.; Mclellan, M.D.; Larson, D.E.; Kalicki, J.M.; Pohl, C.S.; Mcgrath, S.D.; Wendl, M.C.; Zhang, Q.; Locke, D.P.; et al. BreakDancer: An Algorithm for High Resolution Mapping of Genomic Structural Variation. *Nat. Methods* **2009**, *6*, 677–681. [CrossRef]

39. Papaceit, M.; Aguadé, M.; Segarra, C. Chromosomal Evolution of Elements B and C in the Sophophora Subgenus of Drosophila: Evolutionary Rate and Polymorphism. *Evolution* **2006**, *60*, 768. [CrossRef]
40. Prjibelski, A.; Antipov, D.; Meleshko, D.; Lapidus, A.; Korobeynikov, A. Using SPAdes De Novo Assembler. *Curr. Protoc. Bioinformatics* **2020**, *70*, e102. [CrossRef]
41. Johnson, M.; Zaretskaya, I.; Raytselis, Y.; Merezhuk, Y.; McGinnis, S.; Madden, T.L. NCBI BLAST: A Better Web Interface. *Nucleic Acids Res.* **2008**, *36*, W5–W9. [CrossRef]
42. Burland, T.G. DNASTAR's Lasergene Sequence Analysis Software. *Methods Mol. Biol.* **2000**, *132*, 71–91.
43. Miller, W.J.; Nagel, A.; Bachmann, J.; Bachmann, L. Evolutionary Dynamics of the SGM Transposon Family in the *Drosophila Obscura* Species Group. *Mol. Biol. Evol.* **2000**, *17*, 1597–1609. [CrossRef]
44. Bachmann, L.; Raab, M.; Sperlich, D. Satellite DNA and Speciation: A Species Specific Satellite DNA of Drosophila Guanche. *J. Zool. Syst. Evol. Res.* **1989**, *27*, 84–93. [CrossRef]
45. Balanyà, J.; Solé, E.; Oller, J.M.; Sperlich, D.; Serra, L. Long-Term Changes in the Chromosomal Inversion Polymorphism of *Drosophila subobscura*. II. European Populations. *J. Zool. Syst. Evol. Res.* **2004**, *42*, 191–201. [CrossRef]
46. Rezende, E.L.; Balanyà, J.; Rodríguez-Trelles, F.; Rego, C.; Fragata, I.; Matos, M.; Serra, L.; Santos, M. Climate Change and Chromosomal Inversions in *Drosophila subobscura*. *Clim. Res.* **2010**, *43*, 103–114. [CrossRef]
47. Galludo, M.; Canals, J.; Pineda-Cirera, L.; Esteve, C.; Rosselló, M.; Balanyà, J.; Arenas, C.; Mestres, F. Climatic Adaptation of Chromosomal Inversions in Drosophila Subobscura. *Genetica* **2018**, *146*, 433–441. [CrossRef]
48. Khadem, M.; Arenas, C.; Balanyà, J.; Mestres, F. Long-Term Changes in the Inversion Chromosomal Polymorphism: Drosophila Subobscura Population from Rasht (North of Iran). *J. Genet.* **2022**, *101*, 45. [CrossRef]
49. Zivanovic, G.; Arenas, C.; Mestres, F. Rate of Change for the Thermal Adapted Inversions in *Drosophila subobscura*. *Genetica* **2019**, *147*, 401–409. [CrossRef]
50. Zivanovic, G.; Arenas, C.; Mestres, F. Individual Inversions or Their Combinations: Which Is the Main Selective Target in a Natural Population of Drosophila Subobscura? *J. Evol. Biol.* **2016**, *29*, 657–664. [CrossRef]
51. Andolfatto, P.; Wall, J.D.; Kreitman, M. Unusual Haplotype Structure at the Proximal Breakpoint of *In(2L)t* in a Natural Population of *Drosophila melanogaster*. *Genetics* **1999**, *153*, 1297–1311. [CrossRef]
52. Matzkin, L.M.; Merritt, T.J.S.; Zhu, C.-T.; Eanes, W.F. The Structure and Population Genetics of the Breakpoints Associated with the Cosmopolitan Chromosomal Inversion *In(3R)Payne* in *Drosophila melanogaster*. *Genetics* **2005**, *170*, 1143–1152. [CrossRef]
53. Domínguez, M.I. Localización y Estudio de La Inversión Cromosómica J_1 En *Drosophila subobscura*. Implicaciones Evolutivas y Adaptativas. Master's Thesis, Universitat Oberta de Catalunya, Barcelona, Spain, 2025.
54. Fan, X.; Abbott, T.E.; Larson, D.; Chen, K. BreakDancer: Identification of Genomic Structural Variation from Paired-End Read Mapping. *Curr. Protoc. Bioinformatics* **2014**, *45*, 15.6.1–15.6.11. [CrossRef]
55. Aulard, S.; Vaudin, P.; Ladevèze, V.; Chaminade, N.; Périquet, G.; Lemeunier, F. Maintenance of a Large Pericentric Inversion Generated by the Hobo Transposable Element in a Transgenic Line of *Drosophila melanogaster*. *Heredity* **2004**, *92*, 151–155. [CrossRef]
56. Engels, W.R.; Preston, C.R. Formation of Chromosome Rearrangements by P Factors in Drosophila. *Genetics* **1984**, *107*, 657–678. [CrossRef]
57. Lyttle, T.W.; Haymer, D.S. The Role of the Transposable Element *Hobo* in the Origin of Endemic Inversions in Wild Populations of *Drosophila melanogaster*. *Genetica* **1992**, *86*, 113–126. [CrossRef]
58. Kusakabe, S.; Harada, K.; Mukai, T. The Rare Inversion with a P Element at the Breakpoint Maintained in a Natural Population of Drosophila Melanogaster. *Genetica* **1990**, *82*, 111–115. [CrossRef]
59. Casals, F.; Cáceres, M.; Ruiz, A. The Foldback-like Transposon Galileo Is Involved in the Generation of Two Different Natural Chromosomal Inversions of *Drosophila buzzatii*. *Mol. Biol. Evol.* **2003**, *20*, 674–685. [CrossRef]
60. Cáceres, M.; Ranz, J.M.; Barbadilla, A.; Long, M.; Ruiz, A. Generation of a Widespread Drosophila Inversion by a Transposable Element. *Science* **1999**, *285*, 415–418. [CrossRef]

Disclaimer/Publisher's Note: The statements, opinions and data contained in all publications are solely those of the individual author(s) and contributor(s) and not of MDPI and/or the editor(s). MDPI and/or the editor(s) disclaim responsibility for any injury to people or property resulting from any ideas, methods, instructions or products referred to in the content.

insects

MDPI

Article

Cytogenetic and Molecular Characterization of *Sphaerophoria rueppellii* (Diptera, Syrphidae)

Pedro Lorite [1,*], José M. Rico-Porras [1], Teresa Palomeque [1], Mª Ángeles Marcos-García [2], Diogo C. Cabral-de-Mello [3] and Pablo Mora [3,*]

[1] Department of Experimental Biology, Genetics Area, University of Jaén, Paraje Las Lagunillas s/n, 23071 Jaén, Jaén, Spain; jmrico@ujaen.es (J.M.R.-P.); tpalome@ujaen.es (T.P.)
[2] Unidad Asociada de I+D+i al CSIC "Interrelaciones Insecto-Patógeno-Planta y Sus Agentes de Biocontrol" (IPAB), Research Institute CIBIO (Centro Iberoamericano de la Biodiversidad), Scientific Park, University of Alicante, Ctra. San Vicente Del Raspeig s/n, 03690 San Vicente del Raspeig, Alicante, Spain; marcos@ua.es
[3] Department of General and Applied Biology, Institute of Biosciences/IB, UNESP—São Paulo State University, Rio Claro 13506-900, São Paulo, Brazil; cabral.mello@unesp.br
* Correspondence: plorite@ujaen.es (P.L.); pm.ruiz@unesp.br (P.M.)

Simple Summary: Hoverflies or flower flies (Syrphidae) are a diverse group of dipterans, with more than 6600 species worldwide. This insect group has high relevance to pollination and the regulation of insect pest populations. *Sphaerophoria rueppellii* is a hoverfly widely distributed across the Palearctic region, particularly common in Mediterranean ecosystems and crops. It is already used commercially to control aphid pests and, due to its strong trophic preference for aphids, it is effective without damaging agroecosystems. Because it is native to these areas, its use in biological control avoids the risks associated with introducing non-native species. This study provides new genetic and cytogenetic information on *S. rueppellii*, including its chromosomes and mitochondrial genome, to help improve the understanding of its evolutionary relationships.

Abstract: *Sphaerophoria rueppellii* is a Palearctic hoverfly widely used as a native biocontrol agent against aphid pests in Mediterranean agroecosystems. In this study, we present a cytogenetic analysis and characterization of the mitochondrial genome of this species. Chromosomal preparations, obtained from third-instar larvae, were used for conventional staining, DAPI staining and C-banding techniques, and major ribosomal DNA (rDNA) location by fluorescence in situ hybridization (FISH). Karyotype analysis revealed a diploid number of 2n = 10, with heterochromatic blocks in the pericentromeric regions of all autosomes and rDNA clusters on both sex chromosomes. The complete mitochondrial genome (16,605 bp) was sequenced and annotated using next-generation sequencing and assembly pipelines. It contains the typical 37 mitochondrial genes and a highly A + T-rich control region with tandem repeats. Gene order and codon usage were conserved compared with other Syrphidae. Phylogenetic reconstruction based on mitochondrial protein-coding genes clarifies the species' placement within the Syrphini tribe. Our results contribute valuable genomic and cytogenetic information that supports comparative analyses and may aid in taxonomic clarification within the genus. These findings also offer key data that could guide the genetic optimization of *S. rueppellii* as an efficient, environmentally safe biological control agent in sustainable agriculture.

Keywords: *Sphaerophoria rueppellii*; Syrphidae; mitochondrial genome; cytogenetics; karyotype; phylogeny

1. Introduction

Syrphids (Diptera, Syrphidae), also known as hoverflies or flower flies, are a family with 6674 species and 284 genera distributed worldwide [1], making them one of the largest dipteran families. This diverse family of flies exhibits a striking mimicry to hymenopterans such as bees and wasps, with which they are often mistaken. Adults are frequently found on flowers, feeding on nectar and pollen [2], and in some cases, they can also act as effective pollinators [1,3]. The larvae of syrphids have a very different and highly varied biology compared to the adults, displaying diverse feeding habits. Syrphids are currently classified into four subfamilies [4,5] based on integrated taxonomy (larval and adult morphology, molecular data, and larval feeding habits). The larvae of Eristalinae species are phytophagous and saprophagous, while those of Microdontinae, Pipizinae, and Shyrphinae are predatory. Predatory species mainly feed on soft-bodied Hemiptera species, such as aphids (Aphidoidea) and psyllids (Psylloidea) [6], which makes some of them valuable for biological pest control [7,8].

Sphaerophoria rueppellii Wiedemann, 1820 is widely distributed throughout the Palearctic region, being particularly abundant in Mediterranean natural ecosystems and crops. Because *S. rueppellii* is native to the Mediterranean region where it is applied, its use in biological control avoids the ecological risks typically associated with the introduction of non-native species, such as invasive behavior, the disruption of trophic interactions, or the competitive displacement of endemic fauna. The environmental conditions within its range allow for optimal predatory activity against aphid pests without causing harm to the biocenosis (as seen with invasive species) or leading to ecological imbalances (such as displacement or competition). Currently, this species is commercially available as a biological pest control agent [2,9,10]. The species has also been the focus of detailed studies on larval morphology and aspects of its reproductive biology, highlighting its importance as a well-studied and ecologically significant predator [11–13].

Cytogenetic studies in insects are essential for understanding their genetic diversity, evolutionary relationships, and population dynamics. They provide insights into karyotype evolution, sex determination mechanisms, chromosomal rearrangements, and their impact on species diversification [14]. Chromosomal rearrangements play a significant role in shaping adaptability and resistance to environmental changes, as they can lead to genetic differentiation, reproductive isolation, and even speciation, as observed in model organisms such as *Drosophila pseudoobscura* Frolova, 1929 and *D. persimilis* Dobzhansky and Epling, 1944 [15]. In applied entomology, the study of chromosomal and genomic structures has been fundamental to improving pest control strategies. Cytogenetic research conducted over the past three decades on fruit flies of the family Tephritidae has significantly supported the development of sterile insect techniques (SITs) [16]. More recent genomic analyses, such as those performed on *Ceratitis capitata* Wiedemann, 1824, have identified temperature-sensitive lethal regions that are useful for improving genetic sexing strains and enhancing the efficiency of SIT programs [17]. Additionally, understanding karyotypic diversity in beneficial insects such as butterflies, parasitoids, and pollinators provides critical insights into their evolutionary potential and ecological adaptability. A remarkable example is found in the butterfly genus *Agrodiaetus*, whose species exhibit extraordinary variability in chromosome numbers. This karyotypic diversity has been linked to rapid and effective speciation mechanisms, as chromosomal rearrangements may act as reproductive barriers that promote differentiation among closely related popula-

tions [18]. Collectively, these findings contribute to the optimization of beneficial insect use in sustainable pest management and biodiversity conservation programs.

The analysis of mitochondrial DNA sequences in insect species is essential for phylogenetic studies, molecular identification, and conservation [19–21]. As mitochondrial DNA is maternally inherited and exhibits a relatively high mutation rate, it enables the differentiation of cryptic species and facilitates a more precise assessment of evolutionary relationships [22]. Additionally, studying mitochondrial DNA helps to elucidate genetic variability and ecological adaptation, key factors for improving the effectiveness of insects in biological pest control [23]. Moreover, it provides valuable insights into the demographic history of populations and their resilience to environmental changes [24–26].

Despite its relevance as a biological control agent in Mediterranean agroecosystems, detailed genetic information on *S. rueppellii* remains scarce. Previous studies have provided only basic insights into its karyotype, without thorough analysis of its heterochromatin distribution or ribosomal gene organization. Similarly, its mitochondrial genome has not yet been fully characterized or systematically compared with related species. These knowledge gaps limit our understanding of its genetic diversity and evolutionary placement within Syrphidae. This study aims to provide a cytogenetic and molecular characterization of *S. rueppellii.* The objectives include analyzing its karyotype and heterochromatin distribution, determining the location of its rDNA genes, and sequencing and annotating its complete mitochondrial genome to explore gene organization, codon usage, and structural features. Additionally, the study conducts phylogenetic analyses to clarify the placement of *S. rueppellii* within the Syrphinae subfamily. By generating foundational genetic and cytogenetic data, this research supports the evaluation of genetic diversity, evolutionary stability, and taxonomic consistency within the genus. These insights are essential for developing targeted breeding and conservation strategies, improving mass-rearing efficiency, and ensuring the safe and effective application of *S. rueppellii* as a native, environmentally sustainable biological control agent.

2. Materials and Methods

2.1. Material and Chromosome Preparation

Larvae and pupae of *Sphaerophoria rueppellii* (Syrphidae, Syrphinae, Syrphini) were provided by BioNostrum Pest Control Company® (San Vicente del Raspeig, Spain). The larvae were fed with aphids (*Aphis hederae* Kaltenbach, 1843 and *Aphis fabae* Scopoli, 1763) until adult emergence. Third-stage larvae (L3) were used for chromosome preparations. Their brains were dissected in phosphate-buffered saline (PBS) and incubated in a colchicine solution (0.04% in NaCl 0.9%) for 30 min, before immersion in distilled water for 45 min to induce an osmotic shock, and were then preserved in an absolute ethanol/glacial acetic acid solution (3:1).

For the chromosome preparations, the brains were macerated in a 50% glacial acetic acid solution. The resulting suspension was then dispersed in droplets onto a glass slide and then dried on a heating plate at 42 °C. Afterward, the slides were dehydrated through a graded ethanol series (70%, 80%, and 100%, each for 30 s) and stored at −20 °C until further use. Chromosome spreads were either stained with Giemsa or mounted with VECTASHIELD containing the DAPI (4′-6-diamino-2-phenylindole) fluorochrome (Vector Labs, Burlingame, CA, USA) and examined under an Olympus BX51 fluorescence microscope (Olympus, Hamburg, Germany) equipped with an Olympus DP70 camera. Image acquisition and processing were performed using DP Manager (Olympus) and Adobe Photoshop CS4 software (Adobe Systems, San Jose, CA, USA). Chromosome morphology was determined on the basis of arm ratio, as proposed by Levan et al. [27].

2.2. C-Banding

Heterochromatin blocks were visualized using the C-banding technique, following a modified version of the protocol described by Sumner [28]. The slides were first treated with a 0.2 M hydrochloric acid solution for 10 min at 25 °C. They were then incubated in a 5% barium hydroxide solution at 60 °C for 1 min and 30 s, followed by washing with water. After a brief rinse in the initial hydrochloric acid solution, the slides underwent a final wash in 2 × SSC at 60 °C for 2 min. Finally, the slides were mounted using VECTASHIELD with DAPI.

2.3. DNA Extraction, Probes, and Fluorescence In Situ Hybridization (FISH)

The heads and thoraxes of a pool of five males were used for genomic DNA (gDNA) extraction, employing the NucleoSpin Tissue kit (Macherey-Nagel GmbH & Co., Düren, Germany).

The chromosomal localization of ribosomal DNA (rDNA) was determined by FISH. A fragment of the 18S rDNA was amplified using the primers 18S-965 and 18S-1573R [29], using *S. rueppellii* gDNA as a template. The resulting PCR product was labeled with biotin-16-dUTP (Roche Diagnostics GmbH, Mannheim, Germany) through nick translation, utilizing a DNA Polymerase I/DNase I mix (Invitrogen, San Diego, CA, USA). The labeled DNA was then precipitated and dissolved in a hybridization solution (50% v/v deionized formamide, 10% v/v dextran sulfate, 2 × SSC) to a final concentration of 15 ng/µL.

The fluorescence in situ hybridization (FISH) experiments were performed following the protocol described by Cabral-de-Mello and Marec [30]. Prior to hybridization, the slides were treated with RNase A (100 µg/mL in 2 × SSC) for 60 min at 37 °C and then washed in 2 × SSC. Subsequently, the slides were incubated in a fixation solution containing 3.7% formaldehyde in 4 × SSC, 0.1% v/v Tween-20, and 1% w/v skimmed milk, followed by dehydration in an ethanol series (70%, 90%, and 100%) for 5 min at each concentration. The hybridization solution was denatured at 95 °C for 10 min and then placed on ice for 3–5 min. Hybridization was carried out by applying 25 µL of probe solution to each slide. The slides were heated at 70 °C for 1 min and 30 s and subsequently transferred to a humid chamber for overnight incubation at 37 °C. After hybridization, the coverslips were removed and the slides were washed three times in 2 × SSC at room temperature. Before immunological detection, the slides were incubated for 15 min in Washing/Blocking Buffer (WBB; 4 × SSC, 0.1% v/v Tween-20, 1% w/v skimmed milk). The biotin-labeled probes were detected using Alexa Fluor 488-conjugated streptavidin (Invitrogen) at a concentration of 10 µg/mL in WBB. After incubation for 60 min at 37 °C, the slides were washed three times in WBB at room temperature, air-dried, and mounted with VECTASHIELD containing DAPI.

2.4. Mitogenomic Sequencing and Assembly Strategies

Approximately 4–5 µg of gDNA was sent to Novogen Company Ltd. (Cambridge, UK) for sequencing using the Illumina® Hiseq™ 2000 platform (San Diego, CA, USA). A 350 bp fragment library was constructed, and 151 bp paired-end reads were generated, yielding around 2.6 gigabases (Gb) of sequencing data. To maintain high-quality data, low-quality sequences were removed using Trimmomatic v0.36 [31].

The de novo assembly of the mitogenome was performed with NOVOPlasty v4.3.1 [32], a tool designed for reconstructing organelle genomes from NGS data by extending a seed sequence. In this study, the *Sphaerophoria philanthus* Meigen, 1822 *cox1* gene (GenBank accession number OM372559) served as the seed for mitogenome assembly. Different K-mer values were tested, with 33 providing the most complete mitogenome assembly.

2.5. Mitogenome Annotation and Sequence Analysis

The mitogenome was annotated following the methodology described by Cameron [19], using the MITOS2 web server within the Galaxy platform (accessible at: https://usegalaxy.eu/?tool_id=toolshed.g2.bx.psu.edu/repos/iuc/mitos2/mitos2/2.1.9+galaxy0&version=latest, accessed on 31 March 2025). The annotation of the protein-coding genes (PCGs) was manually refined to ensure the correct identification of the start and stop codons and open reading frames, as well as consistency with other Syrphidae mitogenomes using Geneious R11.1.5 (Biomatters Ltd., Auckland, New Zealand). The annotation of ribosomal RNA (rRNA) genes remains one of the most challenging aspects of mitochondrial genome characterization [19]. In this case, the boundaries of the rRNA genes were extended until adjacent tRNA genes were identified, as per the standard methodology [33]. The large ribosomal subunit (*lrRNA*) was found between the *tRNA-Leu* and *tRNA-Val* genes, and the entire nucleotide stretch between them was designated as part of the *lrRNA* gene. Based on this method, the 3′ boundary of the small subunit rRNA (*srRNA*) was determined by the location of the *tRNA-Val* gene. However, there is no tRNA immediately upstream (5′ end) of the *srRNA* gene, leading to ambiguity in defining its starting point. To improve their accuracy, researchers have utilized secondary structure modeling and the identification of conserved sequence motifs at the 5′ end [19,34]. Because the MITOS annotation tool incorporates secondary structure into its predictions [19], its output was used as the basis for annotating the *srRNA* gene in species of *Sphaerophoria* Lepeletier & Serville, 1828.

Additionally, base composition analysis, mitogenome circularization, and secondary structure predictions were performed using the same software. Codon usage analysis was conducted in MEGA v.11.0.13. The assembled mitogenome with the corresponding annotations was submitted to GenBank under accession number PV660707.

2.6. Comparative Phylogenetics

The available Syrphinae mitogenomes were retrieved from GenBank, comprising a dataset of 80 sequences representing 60 species (Supplementary Table S1). Multiple sequences from the same species were included due to variations in their origins and sizes. In GenBank, mitogenome sequences were available for only two *Sphaerophoria* species: *S. philanthus* and *S. taeniata* Meigen, 1822. The mitogenome of *S. philanthus* (NC_071899) is annotated, whereas that of *S. taeniata* (OX016545) is not. To facilitate comparisons, the genome of *S. taeniata* was annotated, and the annotation of *S. philanthus* was reviewed using the same criteria applied to *S. rueppellii*.

Additionally, as an external outgroup, we included the mitochondrial genome sequences of five Syrphidae species belonging to the subfamily Eristalinae, which is phylogenetically close to the subfamily Syrphinae [5,35] (Supplementary Table S1).

The concatenated PCGs were aligned using MAFFT v7.453 software [36]. Poorly aligned positions and divergent regions were removed using the Gblocks program v.0.91.1 [37] (available at https://ngphylogeny.fr/tools/tool/276/form, accessed on 13 April 2025). Phylogenetic relationships were inferred through the Maximum Likelihood (ML) partitioned model [38] in IQtree2 [39]. We used the GTR + F + I + G4 model as it showed the lowest Bayesian information criterion (BIC) calculated with ModelFinder [40] with 1000 ultrafast bootstrap [41] replicates to assess branch support.

3. Results and Discussion

3.1. Cytogenetic Analysis

The karyotypic analysis shows that the analyzed *S. rueppellii* specimens have a chromosome number of 2n = 10. The karyotype consists of four pairs of large autosomes and

one heteromorphic pair of small chromosomes corresponding to the sex chromosomes (Figure 1A,B). The largest autosomes (pair 1) and the smallest ones (pair 4) are submetacentric, while the intermediate-sized autosomes (pairs 2 and 3) are metacentric. Regarding the sex chromosomes, the X is larger than the Y, and their morphologies cannot be determined in mitotic metaphases due to their small size. However, in prometaphases, where the chromosomes are less condensed, it is possible to observe that the X chromosome is clearly acrocentric (Figure 1C). Even in this phase, the small size of the Y chromosome does not allow for a clear determination of its morphology.

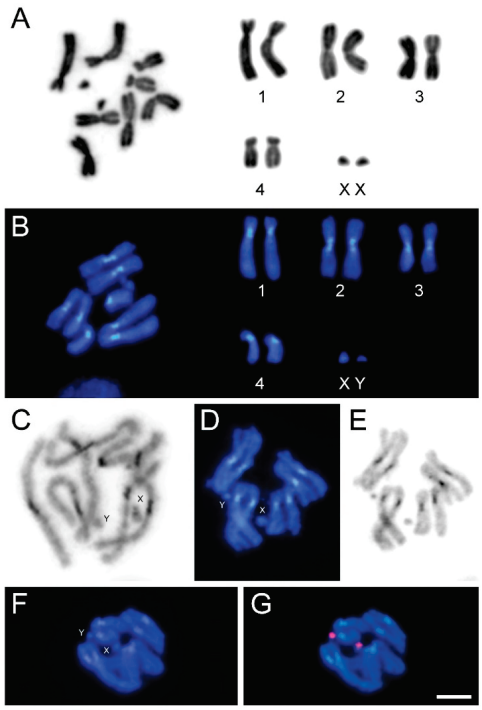


Figure 1. *Sphaerophoria rueppellii*. (**A**) Female mitotic metaphase and karyotype stained with Giemsa. (**B**) Male mitotic metaphase and karyotype stained with DAPI. (**C**) Male mitotic prometaphase stained with DAPI and inverted to grayscale. Male mitotic metaphase stained with DAPI (**D**), and same metaphase after C-banding and staining with Giemsa (**E**), showing coincidence of heterochromatic blocks with DAPI-positive pericentromeric region of autosomes. (**F**) DAPI staining and (**G**) FISH of male mitotic chromosomes using rDNA as probe, showing presence of hybridization signals (in red) on both sex chromosomes. Bar = 5 μm.

Within the Syrphidae family, the chromosomal number and sex chromosome system have been determined for over 700 taxa, primarily due to the extensive work conducted by J. Wallace Boyes, Janny M. van Brink, and their collaborators [42–51]. In the past 45 years, only nine additional species have been analyzed [52–54]. The analyzed species exhibit diploid numbers ranging from 2n = 8 to 2n = 14 and possess an XY sex chromosome system. Within the genus *Sphaerophoria* Lepeletier & Serville, 1828, approximately twenty species have been studied, all of which have a chromosomal number of 2n = 8 [55]. However, chromosomal polymorphisms have been identified in some of them, leading to higher chromosomal numbers [49].

In S. *rueppellii*, populations exhibiting chromosomal counts of 2n = 8 and 2n = 10 have been documented [49]. Populations with 2n = 8 have been identified in northern Italy and the Netherlands, whereas those with 2n = 10 have been reported in northern Italy, Sicily, Portugal, and Ethiopia. In the latter karyotype, the medium-sized chromosomes are metacentric, while the largest and smallest pairs are submetacentric to subtelocen-

tric (Figure 2). Additionally, a population from Biella (Italy) presented individuals with 2n = 12 chromosomes. This karyotype is similar to that of the 2n = 8 individuals, but includes two pairs of microchromosomes of unknown origin [49].

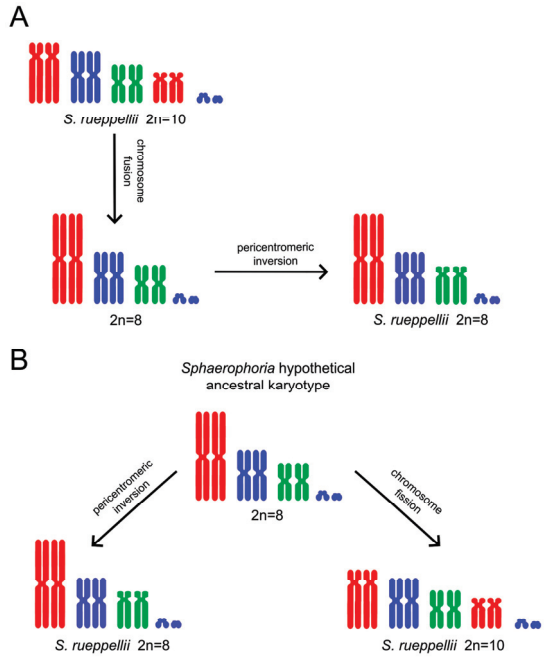


Figure 2. *Sphaerophoria rueppellii* karyotypes. (**A**) Karyotype evolution in *S. rueppellii* according to Boyes et al. [49]. (**B**) Alternative hypothesis. Possible explanation provided in text.

The material analyzed in this study exhibits a karyotype similar to the 2n = 10 configuration described by Boyes et al. [49]. Those authors proposed that the 2n = 8 karyotype arose from 2n = 10 by means of an end-to-end fusion of submetacentric–subtelocentric autosomes, resulting in the formation of a metacentric chromosome (Figure 2A). Subsequently, a pericentric inversion in one of the autosomes would have led to the metacentric chromosome observed in the 2n = 8 karyotype. An alternative explanation could account for the chromosomal polymorphism observed in S. *rueppellii*. The intermediate karyotype proposed by Boyes et al. [49], in which all autosomes are metacentric, was not found in any of the analyzed populations of this species. However, this karyotype is the most common among the *Sphaerophoria* species studied to date. It is therefore plausible to consider this configuration as the ancestral karyotype within the genus, including *S. rueppellii*. The karyotypes observed in *S. rueppellii* could have easily derived from this ancestral form (Figure 2B). The 2n = 8 karyotype may have arisen through a pericentric inversion in one autosome, converting it into a submetacentric–subtelocentric chromosome. The centric fission of the largest metacentric chromosome in the ancestral karyotype could have produced the 2n = 10 configuration.

A recent high-quality, near-chromosome-level de novo genome assembly was generated for *S. rueppellii*, using a hybrid approach that combined PacBio long-read and Illumina short-read sequencing data, followed by super-scaffolding with Hi-C data [56]. This process yielded six chromosome-level scaffolds, suggesting the presence of five pairs of autosomes plus a small sex chromosome (likely the X chromosome), corresponding to a chromosomal number of 2n = 12. However, a karyotype with five pairs of autosomes has not been observed in any of the *S. rueppellii* populations analyzed to date. It is possible that the *S. rueppellii* individuals used for genome sequencing actually possess only four pairs of autosomes (2n = 10). This hypothesis is based on several observations: the relative sizes of

the six largest scaffolds and the chromosome sizes reported by Boyes et al. [49]. Furthermore, scaffold 3 (pseudochromosome 3) does not show a clearly defined centromere. Bailey et al. [56] consider that this is likely due to an incorrect assembly. In addition, scaffold 5 appears to correspond to a small metacentric chromosome not previously identified in *S. rueppellii* (Figure 3). We suggest that scaffold 5 contains the centromere of the largest autosome, while scaffold 3 corresponds to its long arm. This is why a centromere could not be detected in scaffold 3 in the genome assembly. Furthermore, there is a correlation between the relative sizes of the autosomes and the sizes of the scaffolds (Table 1). For instance, chromosome 4 accounts for between 15.9% and 18.0% of the total genome length. This percentage is very close to that of scaffold 4 (16.5%) in relation to the assembled genome (455 Mb). This putative inconsistency between pseudochromosomes obtained from genome assembly and the chromosome number observed reinforces the importance of the complementary analysis of karyotype in genome assembly projects.

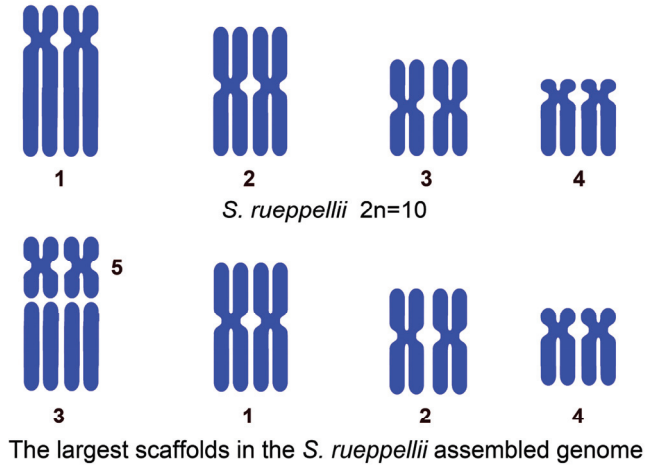


Figure 3. A comparison between the autosomes in the 2n = 10 karyotype and the five largest near-chromosome-level scaffolds (autosomes) obtained from the *S. rueppellii* genome assembly (GCA_920937365.1).

Table 1. A comparison between the relative length of each autosome in the 2n = 10 karyotype of *Sphaerophoria rueppellii* [49] and the relative size of the largest scaffolds obtained from its genome assembly [56].

	Chromosome 1	**Chromosome 2**	**Chromosome 3**	**Chromosome 4**
The relative length of each autosome in the 2n = 10 karyotype.	27.9–28.8%	25.5–27.8%	22.0–24.5%	15.9–18.0%
	Scaffolds 3 + 5	Scaffold 1	Scaffold 2	Scaffold 4
The percentage of each scaffold relative to the total assembled megabases.	31.9% (19.14 + 12.73)	27.6%	22.3%	16.5%

Staining with DAPI reveals the presence of prominent DAPI-positive chromatin blocks in the pericentromeric regions of all autosomes (Figure 1B–D). C-banding confirms the presence of heterochromatin blocks located in the same pericentromeric regions, coinciding with the DAPI + signals (Figure 1E). Both sex chromosomes appear to be euchromatic.

Although the chromosome number and sex chromosome system are known for over 700 taxa within the Syrphidae family, C-banding techniques have been applied to

only a limited number of species, albeit from two different subfamilies: Eristalinae and Syrphinae [52–54]. Despite the scarce data available, the presence of pericentromeric heterochromatin blocks in autosomes appears to be a common feature. However, the presence or absence of heterochromatin in the sex chromosomes is more variable, ranging from heterochromatin in both sex chromosomes (in some cases, completely heterochromatic), to heterochromatin in only one sex chromosome, or its absence from both. Among the species previously studied is *Sphaerophoria scripta* Linnaeus, 1758, which displays pericentromeric heterochromatin in all autosomes and the X chromosome, while its Y chromosome is euchromatic [53]. In *S. rueppellii*, the DAPI+ heterochromatin observed in its autosomes corresponds to pericentromeric heterochromatin. In the X chromosome, a DAPI + pericentromeric region is also visible (Figure 1C), but this region does not produce differential staining after C-banding (Figure 1E).

FISH with the rDNA probe revealed clusters located on both sex chromosomes (Figure 1F,G). To our knowledge, no previous studies have addressed the localization of rDNA genes in Syrphidae. However, their position has been determined in other dipteran groups, with varying results. While it is generally common for major rDNA to be located on the sex chromosomes, there are also groups with additional clusters on autosomes, and even some cases where rDNA is exclusively located on autosomes [57–59]. Further analysis of related species will be necessary to determine whether a specific pattern for rDNA localization is conserved in Syrphidae.

3.2. Mitogenome Analysis, Gene Organization, and Sequence Analysis

The mitogenome of *S. rueppellii* is 16,605 bp in length (Figure 4). GenBank currently contains mitogenome sequences for only two other species of the *Sphaerophoria* genus, with sizes similar to that found in *S. rueppellii*: *S. taeniata* (16,422 bp) [60] and *S. philanthus* (16,036 bp). These sizes fall within the range of other species analyzed within the tribe Syrphini, with mitogenomes ranging from 15,326 bp in *Eupeodes corollae* Fabricius, 1794 [61] to 19,366 bp in *Chrysotoxum bicinctum* Linnaeus, 1758 [62] (Supplementary Table S1). The *S. rueppellii* mitogenome comprises the standard complement of mitochondrial genes: 13 protein-coding genes (PCGs), 2 rRNA genes, 22 tRNA genes, and a non-coding control region rich in adenine and thymine (A + T) (Table 2, Figure 4). The annotation of the mitogenomes of *S. rueppellii*, as well as *S. philanthus* and *S. taeniata*, is provided in Supplementary Table S2. The analysis of mitogenomes across various arthropod groups has allowed for the establishment of the gene order in the ancestral pancrustacean–insect genome [63,64]. There are no gene rearrangements in the mitogenome of *S. rueppellii* compared to this ancestral mitogenome, nor in the other two *Sphaerophoria* species.

Table 2. Annotation of complete mitogenome of *Sphaerophoria rueppellii*. IGN: Intergenic nucleotides. Negative values refer to overlapping nucleotides.

Gene	Strand	Nucleotide Number		Length	IGN	Start Codon	Stop Codon
(I) tRNA-Ile	H	1	66	66	−3		
(Q) tRNA-Gln	L	64	132	69	3		
(M) tRNA-Met	H	136	204	69	0		
nad2	H	205	1237	1033	0	ATT	T–
(W) *tRNA-Trp*	H	1238	1306	69	16		
(C) *tRNA-Cys*	L	1323	1388	66	6		
(Y) *tRNA-Tyr*	L	1395	1460	66	41		
cox1	H	1502	3035	1534	0	TTG	T–
(L1) *tRNA-Leu* (UAA)	H	3036	3101	66	4		
cox2	H	3106	3789	684	0	ATG	TAA
(K) *tRNA-Lys*	H	3790	3860	71	14		
(D) *tRNA-Asp*	H	3875	3944	70	0		

Table 2. *Cont.*

Gene	Strand	Nucleotide Number		Length	IGN	Start Codon	Stop Codon
atp8	H	3945	4106	162	−7	ATT	TAA
atp6	H	4100	4777	678	7	ATG	TAA
cox3	H	4785	5573	789	3	ATG	TAA
(G) *tRNA-Gly*	H	5577	5642	66	0		
nad3	H	5643	5996	354	2	ATT	TAA
(A) *tRNA-Ala*	H	5999	6067	69	−1		
(R) *tRNA-Arg*	H	6067	6130	64	14		
(N) *tRNA-Asn*	H	6145	6211	67	0		
(S1) *tRNA-Ser* (UCU)	H	6212	6278	67	1		
(E) *tRNA-Glu*	H	6280	6346	67	19		
(F) *tRNA-Phe*	L	6366	6433	68	0		
nad5	L	6434	8169	1736	0	ATG	TA–
(H) *tRNA-His*	L	8170	8234	65	0		
nad4	L	8235	9575	1341	−7	ATG	TAA
nad4l	L	9569	9865	297	2	ATG	TAA
(T) *tRNA-Thr*	H	9868	9933	66	0		
(P) *tRNA-Pro*	L	9934	9999	66	2		
nad6	H	10,002	10,526	525	11	ATT	TAA
cob	H	10,538	11,674	1137	3	ATG	TAA
(S2) *tRNA-Ser* (UGA)	H	11,678	11,746	69	16		
nad1	L	11,763	12,710	948	1	TTG	TAA
(L2) *tRNA-Leu* (UAG)	L	12,712	12,776	65	0		
lrRNA	L	12,777	14,111	1335	0		
(V) *tRNA-Val*	L	14,112	14,182	71	0		
srRNA	L	14,183	14,972	790	0		
Control Region		14,973	16,605	1633			

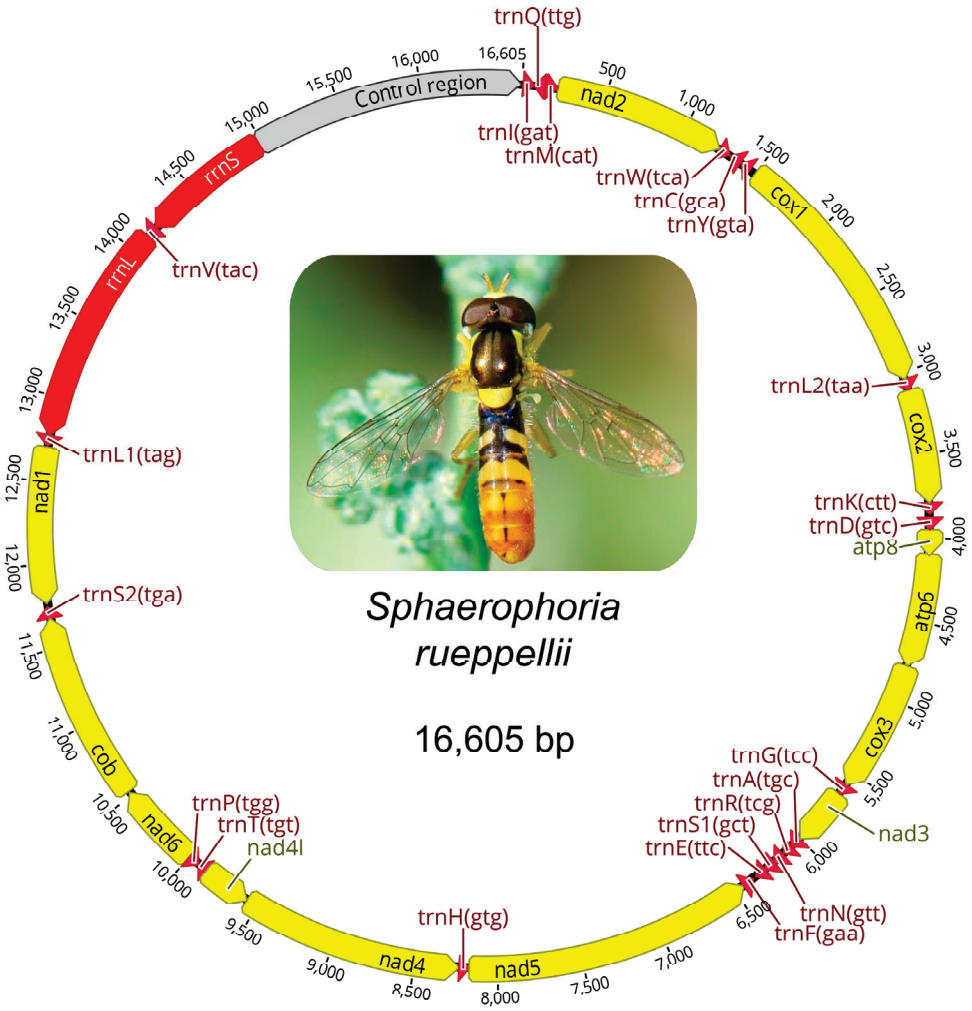


Figure 4. Graphical map of mitogenome of *Sphaerophoria rueppellii*.

In *S. rueppellii*, four protein-coding genes (*nad5*, *nad4*, *nad4l*, and *nad1*) are located on the light (L) strand, while the remaining nine are located on the heavy (H) strand (Table 2). Translation initiation in these genes predominantly occurs with typical ATN start codons, except for *cox1* and *nad1*, which start with the TTG codon. These same start codons are found in all three *Sphaerophoria* species (Supplementary Table S2). In *S. rueppellii*, as well as in *S. taeniata*, ten of the thirteen protein-coding genes end with a complete TAA stop codon, whereas incomplete stop codons (T– or TA–) are found in *nad2*, *cox1*, and *nad5*. In *S. philanthus*, in addition to these three genes, the cob gene also ends with an incomplete stop codon (Supplementary Table S2). Truncated stop codons often result from gene sequences terminating just before the start of a downstream tRNA gene, with the complete stop codon restored post-transcriptionally through polyadenylation [33].

The mitogenome of *S. rueppellii* displays a strong A + T bias, with an A + T content of 80.77%, such as in other Syrphidae species [65], that is typical of insect mitogenomes [19,20,66]. The codon usage also reflects this bias towards A + T codons, with a clear preference for codons rich in A and T. To assess codon usage bias, Relative Synonymous Codon Usage (RSCU) was employed (Table 3). RSCU quantifies how frequently a specific codon is used compared to its expected frequency if all synonymous codons for an amino acid were utilized equally. An RSCU value of 1 indicates no bias, values greater than 1 suggest a codon is used more frequently than expected, and values less than 1 imply under-representation. RSCU is strongly influenced by the nucleotide composition of the genome. In mitochondrial genomes with high A + T contents, such as that of *S. rueppellii*, codons rich in adenine and thymine (e.g., NNA or NNT) exhibit elevated RSCU values, indicating their preferential usage. The most used codons are A + T-rich: TTA (Leu, 14.33%), ATT (Ile, 10.00%), TTT (Phe, 8.66%), and ATA (Met, 7.62%). As a result, the amino acids these codons encode are particularly abundant in the mitochondrial proteome of this species. The A + T bias also extends to termination codons. Within the protein-coding genes (PCGs), TAA, along with its incomplete forms (TA–, T–), is the only stop codon used, appearing 13 times, while TAG is entirely absent.

Table 3. Codon usage of *Sphaerophoria rueppellii* mitogenome protein-coding genes. Total of 3741 codons analyzed. RSCU: Relative Synonymous Codon Usage. * = termination codon.

Codon	n	RSCU	%	Codon	n	%	RSCU	Codon	n	%	RSCU	Codon	n	%	RSCU
UUU(F)	324	1.91	8.66	UCU(S)	124	3.31	3.06	UAU(Y)	184	4.92	1.96	UGU(C)	38	1.02	2
UUC(F)	16	0.09	0.43	UCC(S)	5	0.13	0.12	UAC(Y)	4	0.11	0.04	UGC(C)	0	-	0
UUA(L)	536	5.54	14.33	UCA(S)	96	2.57	2.37	UAA(*)	13	0.35	2	UGA(W)	96	2.57	1.96
UUG(L)	10	0.1	0.27	UCG(S)	0	-	0	UAG(*)	0	-	0	UGG(W)	2	0.05	0.04
CUU(L)	18	0.19	0.48	CCU(P)	81	2.17	2.53	CAU(H)	69	1.84	1.92	CGU(R)	20	0.53	1.43
CUC(L)	0	0	-	CCC(P)	6	0.16	0.19	CAC(H)	3	0.08	0.08	CGC(R)	0	-	0
CUA(L)	16	0.17	0.43	CCA(P)	40	1.07	1.25	CAA(Q)	70	1.87	1.97	CGA(R)	35	0.94	2.5
CUG(L)	0	0	-	CCG(P)	1	0.03	0.03	CAG(Q)	1	0.03	0.03	CGG(R)	1	0.03	0.07
AUU(I)	374	1.98	10.00	ACU(T)	85	2.27	1.85	AAU(N)	210	5.61	1.92	AGU(S)	42	1.12	1.04
AUC(I)	3	0.02	0.08	ACC(T)	2	0.05	0.04	AAC(N)	9	0.24	0.08	AGC(S)	2	0.05	0.05
AUA(M)	285	1.9	7.62	ACA(T)	97	2.59	2.11	AAA(K)	83	2.22	1.8	AGA(S)	55	1.47	1.36
AUG(M)	15	0.1	0.40	ACG(T)	0	-	0	AAG(K)	9	0.24	0.2	AGG(S)	0	-	0
GUU(V)	71	1.75	1.90	GCU(A)	88	2.35	2.32	GAU(D)	63	1.68	1.88	GGU(G)	41	1.10	0.79
GUC(V)	0	0	-	GCC(A)	3	0.08	0.08	GAC(D)	4	0.11	0.12	GGC(G)	0	-	0
GUA(V)	89	2.2	2.38	GCA(A)	60	1.60	1.58	GAA(E)	70	1.87	1.92	GGA(G)	159	4.25	3.07
GUG(V)	2	0.05	0.05	GCG(A)	1	0.03	0.03	GAG(E)	3	0.08	0.08	GGG(G)	7	0.19	0.14

Figure 5 shows the 22 tRNA genes identified in *S. rueppellii*, with lengths ranging from 64 bp (*tRNA-Arg*) to 71 bp (*tRNA-Lys*, *tRNA-Val*). Most of these tRNAs exhibit the expected cloverleaf secondary structure. However, an exception is found in *tRNA-Ser1* (AGN), which lacks a stable DHU arm, a trait commonly reported in many insects and other metazoans [67]. The tRNA sequences are highly conserved among the three *Sphaerophoria* species. In fact, no changes were found in 15 out of the 22 tRNAs. The observed mutations, which affect one or two positions, are located in the loops of the DHU

and TΨC arms, regions where such variations are less likely to impact tRNA structure [68]. The only mutation observed outside these regions occurs in the stem of the anticodon arm of *tRNA-His*; however, this is unlikely to disrupt stability as it results in a U–A to U–G base pair change (or vice versa), which probably does not significantly affect arm pairing stability.

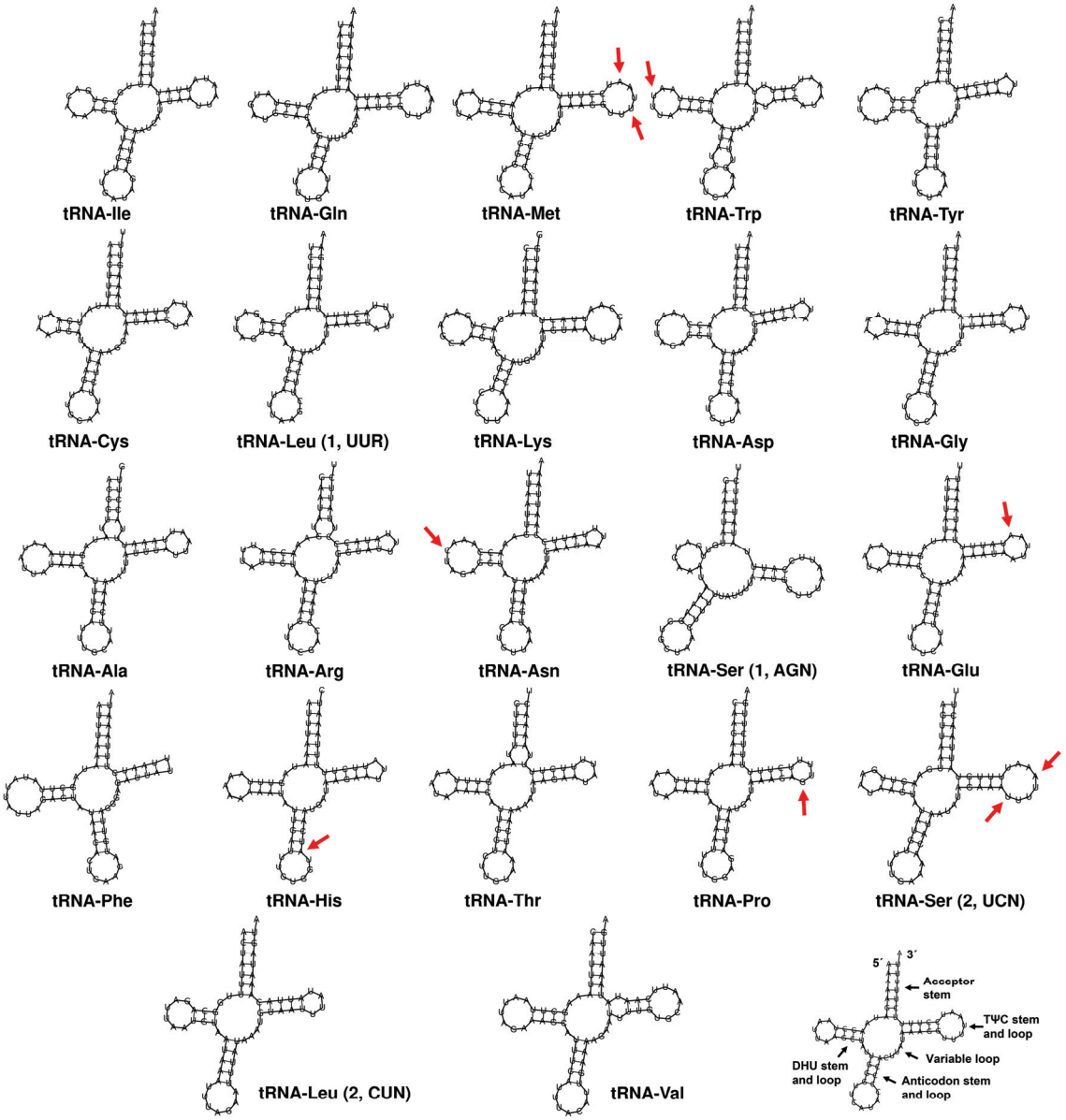


Figure 5. Secondary structures of all tRNAs in *Sphaerophoria rueppellii*. Arrows indicate variable positions in comparison among three *Sphaerophoria* species.

Mitochondrial genomes typically contain two classes of non-coding elements: the control region (CR) and intergenic spacers (IGSs). *S. rueppellii* features 17 IGSs in addition to its CR (Table 2). The most extensive IGS, 41 bp long, is located between the *tRNA-Tyr* and *cox1* genes, while the remaining spacers range from 1 to 19 bp in length. Four gene overlaps are present in the *S. rueppellii* mitogenome: between the *tRNA-Ile* and *tRNA-Gl*n genes (3 bp), *atp8* and *atp6* (7 bp), *tRNA-Ala* and *tRNA-Arg* (1 bp), and between nad4 and *nad4l* (7 bp). The same overlaps, and with identical lengths, are found in the mitogenomes of other *Sphaerophoria* species (Supplementary Table S2). The *atp8–atp6* overlap, which

includes the shared sequence ATGATAA, contains the ATG start codon of *atp6* and the TAA stop codon of *atp8*. The *nad4l–nad4* overlap, with the sequence ATGTTAA (in the L strand), includes the ATG start codon of *nad4* and the TAA stop codon of *nad4l*. These overlaps are known to be conserved features in arthropods [19,69], although some of them are absent in certain hymenopteran groups [70].

In mitochondrial genomes, the CR typically represents the largest segment of non-coding DNA. Located immediately downstream of the small subunit rRNA (*srRNA*) gene, this region is believed to play a key role in the regulation of both replication and transcription processes [71]. Its base composition and length vary widely among species [66,72]. In Syrphidae mitogenomes, the CR exhibits considerable variability and is one of the main contributors to the overall mitogenome length [65,66]. Among *Sphaerophoria* species, differences in CR length are also evident, with *S. rueppellii* showing the longest control region (1633 bp), compared to *S. philanthus* (1059 bp) and *S. taeniata* (1435 bp) (Supplementary Table S2).

Despite differences in overall length, the CR sequences of the three *Sphaerophoria* species exhibit a high degree of conservation at both the 5′ and 3′ ends (Supplementary Figure S1). The increased size of the CR in *S. rueppellii* is due to the presence of a tandemly repeated element with four identical copies of a 215 bp sequence. Tandem repeat structures within the mitochondrial CR have been observed across several insect orders, and as observed in *S. rueppellii*, with a high degree of sequence conservation [66,73–75]. Similar sequences were also identified in the CRs of *S. taeniata* (221 bp) and *S. philanthus* (222 bp), with >84% sequence identity to the repeat unit found in *S. rueppellii*. However, in these two species, the repeated element is not organized in tandem. In *S. philanthus*, the 221 bp sequence is present as a single copy, while in *S. taeniata*, two copies are present, separated by a 154 bp spacer region that partially resembles the repeat. The two 222 bp sequences in *S. taeniata* share 98.64% sequence identity with one another. Notably, these sequences exhibit greater similarity to the *S. philanthus* copy (93.67% and 94.12%) than to that of *S. rueppellii*, potentially suggesting a closer phylogenetic relationship between *S. taeniata* and *S. philanthus*.

In the published genome assembly of *S. rueppellii* [56], the mitochondrial genome was also assembled and reported to be 16,387 bp in length, which differs from the 16,605 bp observed in our assembly. Unfortunately, that publication does not provide any accession number for the mitochondrial sequence, nor does it appear to be deposited in GenBank, making it impossible to determine the exact cause of the size discrepancy. However, the difference in length between the two assemblies, 218 bp, is very close to the 215 bp length of the tandem repeat identified in the CR of our assembly, suggesting that the mitogenome reported by Bailey et al. [56] may contain only three copies of the repeat unit, as opposed to the four observed in our data. Although this difference might also be attributable to the use of distinct assembly methodologies, another plausible explanation is the existence of heteroplasmy in mitogenome size, caused by intraspecific variation in the number of repeat units within the CR. Such heteroplasmy variation has been documented in other insect taxa [66,76,77].

3.3. Phylogenetic Analyses

The classification of the subfamily Syrphinae into tribes has undergone numerous revisions. Recent studies using coding loci [35] support the division of the subfamily into three distinct tribes: Syrphini, Bacchini, and Melanostomini. For phylogenetic analysis, available data from the GenBank database were used for all the currently represented Syrphinae species. The Maximum Likelihood (ML) tree, based on concatenated PCG

sequences, is shown in Figure 6. This analysis clusters Syrphinae sequences into three well-supported clades, with a topology similar to that obtained by Mengual et al. [35], thus supporting the division of the subfamily Syrphinae into three tribes.

The genus *Sphaerophoria* belongs to the tribe Syrphini. The phylogenetic reconstruction of Syrphini species based on mitochondrial genome data reveals that the majority of genera appear to form coherent, well-supported clades, which generally correspond with current taxonomic classifications and support their monophyletic status. However, exceptions exist, and the results also highlight some unresolved taxonomic issues, potential misidentifications, and cases of paraphyly or polyphyly.

A primary observation is that most species from the same genus tend to group together, suggesting that they share a common ancestor and supporting the monophyly of those genera. Genera such as *Eupeodes* Osten Sacken, 1877, *Scaeva* Fabricius, 1805, *Syrphus* Fabricius, 1775, *Dasysyrphus* Enderlein, 1938, and *Chrysotoxum* Meigen, 1803 form distinct and well-resolved clades, consistent with expectations from morphology-based taxonomy.

One illustrative case that underscores the importance of data quality and accurate specimen identification is that of *Eupeodes latifasciatus* Macquart, 1829. Two mitochondrial genome sequences labeled under this species are available in GenBank. One of them (acc. no. OV049928) clusters as expected within the *Eupeodes* clade, alongside *E. luniger* Meigen, 1822 and *E. americanus* Wiedemann, 1830. However, the second *E. latifasciatus* sequence (acc. no. MZ329813) is placed within the *Syrphus* clade, closely related to *S. vitripennis* Meigen, 1822. This suggests a likely misidentification, with the misassigned sequence perhaps belonging to a *Syrphus* species. This example highlights the critical need for the careful taxonomic validation and curation of sequences submitted to public repositories such as GenBank.

Beyond individual misidentifications, the tree reveals deeper evolutionary patterns. Some genus-level groupings appear to be paraphyletic, such as the genera *Ocyptamus* Macquart, 1834 and *Victoriana* Miranda, 2020, both with Neotropical distribution, as well as *Allograpta* Osten Sacken, 1875 and *Sphaerophoria*. Adults and immature stages of the species belonging to the *Allograpta* and *Sphaerophoria* genera also exhibit a significant similarity in their morphological characteristics [11,78]. These findings are consistent with previous phylogenetic studies [79–81], which also identified complex relationships among these genera.

A particularly interesting and problematic case involves the genus *Epistrophe* Walker, 1852, which appears polyphyletic in the tree. Species attributed to *Epistrophe* are distributed across multiple clades, rather than forming a cohesive monophyletic group. This pattern had already been noted by Li et al. [65], and is further confirmed in the present analysis. The taxonomic instability of Epistrophe points to the need for comprehensive revisions incorporating molecular, morphological, and ecological data.

Within the *Sphaerophoria* clade, an unexpected placement occurs with *Epistrophe lamellata* Huo, Ren et Zheng, 2007. This species is nested within the *Sphaerophoria* group rather than with other *Epistrophe* species. The presence of *E. lamellata* in this clade raises two possibilities: it could be a case of mislabeling or incorrect identification, or it may reflect a deeper issue with the species' generic assignment. Unfortunately, due to limited information available for *E. lamellata*, it is difficult to determine the cause with confidence. However, this pattern is not entirely novel because *E. lamellata* was also placed near *Sphaerophoria* in a previous tree published by Guo et al. [82], though no explanation for this was provided. In another phylogenetic reconstruction by Li et al. [65], *E. lamellata* appeared to be closely related to *Allograpta javana* Wiedemann, 1824, suggesting its placement near *Allograpta* + *Sphaerophoria*.

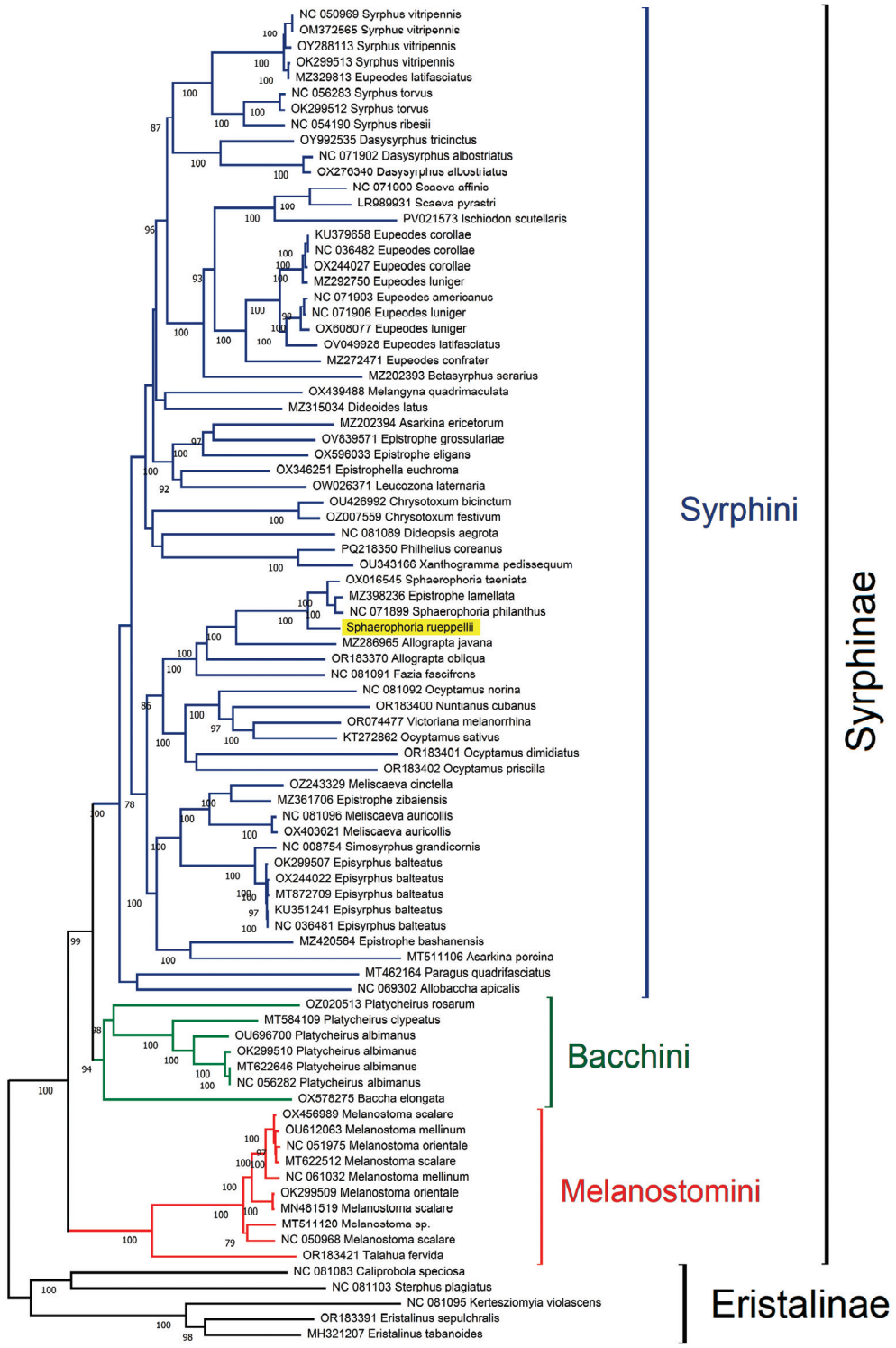


Figure 6. Phylogenetic relationships based on Maximum Likelihood (ML) analysis. Bootstrap values above 70 shown next to branches. *S. rueppellii* highlighted in yellow.

In summary, the phylogenetic analysis confirms the monophyly of several Syrphini genera while also revealing unexpected placements and possible paraphyly in others. These findings emphasize the importance of accurate species identification, proper annotation in genetic databases, and the continued integration of genomic data with traditional taxonomy. Particularly for complex groups like *Epistrophe*, a revision that incorporates

broader sampling and multi-gene approaches may be necessary in order to resolve their evolutionary relationships definitively.

Supplementary Materials: The following supporting information can be downloaded at: https://www.mdpi.com/article/10.3390/insects16060604/s1, Figure S1: Control region analysis; Table S1: Available mitogenomes from Syrphinae subfamily; Table S2: Mitogenome annotations in *Sphaerophoria* species.

Author Contributions: Conceptualization, P.L., J.M.R.-P. and P.M.; methodology; P.L., J.M.R.-P., T.P., D.C.C.-d.-M. and P.M.; investigation; P.L., J.M.R.-P., T.P., D.C.C.-d.-M. and P.M.; resources, M.Á.M.-G.; writing—original draft preparation, P.L., J.M.R.-P. and P.M.; writing—review and editing, P.L., J.M.R.-P., T.P., M.Á.M.-G., D.C.C.-d.-M. and P.M.; funding acquisition, P.L., M.Á.M.-G. and T.P. All authors have read and agreed to the published version of the manuscript.

Funding: This work was supported by Universidad de Jaén (through the program "Plan de Apoyo a la Investigación 2023–2024, Acción 1"). This study is part of the AGROALNEXT program (AGROALNEXT/2022/052-BIOPESTNEW), supported by the Spanish Ministry of Science and Innovation (MCIN), with funding from the European Union, through the NextGenerationEU initiative (PRTR-C17.I1), and the Generalitat Valenciana, Spain. Pablo Mora is supported by the São Paulo Research Foundation (FAPESP), Brazil. Process Number #2024/ 01521-9.

Data Availability Statement: The *Sphaerophoria rueppellii* mitogenome sequence was submitted to NCBI (acc. number PV660707).

Conflicts of Interest: The authors declare no conflicts of interest.

References

1. Dunn, L.; Lequerica, M.; Reid, C.R.; Latty, T. Dual ecosystem services of syrphid flies (Diptera: Syrphidae): Pollinators and biological control agents. *Pest Manag. Sci.* **2020**, *76*, 1973–1979. [CrossRef] [PubMed]
2. Amorós-Jiménez, R.; Pineda, A.; Fereres, A.; Marcos-García, M.Á. Prey availability and abiotic requirements of immature stages of the aphid predator *Sphaerophoria rueppellii*. *BioControl* **2012**, *63*, 17–24. [CrossRef]
3. Pérez-Bañón, C.; Petanidou, T.; Marcos-García, M.Á. Pollination in small islands by occasional visitors: The case of *Daucus carota* subsp. *commutatus* (Apiaceae) in the Columbretes archipelago. *Spain. Plant Ecol.* **2007**, *192*, 133–151. [CrossRef]
4. Mengual, X.; Ståhls, G.; Rojo, S. Phylogenetic relationships and taxonomic ranking of pipizine flower flies (Diptera: Syrphidae) with implications for the evolution of aphidophagy. *Cladistics* **2015**, *31*, 491–508. [CrossRef]
5. Wong, D.; Norman, H.; Creedy, T.J.; Jordaens, K.; Moran, K.M.; Young, A.; Mengual, X.; Skevington, J.H.; Vogler, A.P. The phylogeny and evolutionary ecology of hoverflies (Diptera: Syrphidae) inferred from mitochondrial genomes. *Mol. Phylogenet. Evol.* **2023**, *184*, 107759. [CrossRef]
6. Rojo, S.; Gilbert, F.; Marcos-García, M.Á.; Nieto, J.M.; Mier, M.P. *A World Review of Predatory Hoverflies (Diptera, Syrphidae: Syrphinae) and Their Prey*; Ibero-American Center for Biodiversity (CIBIO): Murcia, Spain, 2003; 319p.
7. Gómez-Polo, P.; Traugott, M.; Alomar, O.; Castañe, C.; Rojo, S.; Agustí, N. Identification of the most common predatory hoverflies of Mediterranean vegetable crops and their parasitism using multiplex PCR. *J. Pest Sci.* **2014**, *87*, 371–378. [CrossRef]
8. Pekas, A.; de Craecker, I.; Boonen, S.; Wäckers, F.L.; Moerkens, R. One stone; two birds: Concurrent pest control and pollination services provided by aphidophagous hoverflies. *BioControl* **2020**, *149*, 104328. [CrossRef]
9. Amorós-Jiménez, R.; Pineda, A.; Fereres, A.; Marcos-García, M.Á. Feeding preference of the aphidophagous hoverfly *Sphaerophoria rueppellii* affects the performance of its offspring. *BioControl* **2014**, *54*, 427–435. [CrossRef]
10. Burgio, G.; Dindo, M.L.; Pape, T.; Whitmore, D.; Sommaggio, D. Diptera as predators in biological control: Applications and future perspectives. *BioControl* **2025**, *70*, 1–17. [CrossRef]
11. Orengo-Green, J.J.; Kanturski, M.; Ricarte, A.; Marcos-García, M.Á. A great little ally: Revealing the morphology of the immature stages of the aphid pest predator *Sphaerophoria rueppellii* (Wiedemann, 1830) (Diptera: Syrphidae). *Eur. Zool. J.* **2022**, *89*, 625–640. [CrossRef]
12. Alba-Tercedor, J.; Marcos-García, M.Á. Revealing the larval anatomy of the hoverfly *Sphaerophoria rueppellii* (Wiedemann, 1820) (Diptera, Syrphidae) using micro-computed tomography. *Sci. Rep.* **2024**, *14*, 28848. [CrossRef] [PubMed]
13. Orengo-Green, J.J.; Casas, J.L.; Marcos-García, M.Á. Effect of abiotic climatic factors on the gonadal maturation of the biocontrol agent *Sphaerophoria rueppellii* (Wiedemann, 1830) (*Diptera: Syrphidae*). *Insects* **2022**, *13*, 573. [CrossRef] [PubMed]

14. Blackmon, H.; Ross, L.; Bachtrog, D. Sex determination, sex chromosomes, and karyotype evolution in insects. *J. Hered.* **2017**, *108*, 78–93. [CrossRef] [PubMed]
15. Fuller, Z.L.; Koury, S.A.; Phadnis, N.; Schaeffer, S.W. How chromosomal rearrangements shape adaptation and speciation: Case studies in *Drosophila pseudoobscura* and its sibling species *Drosophila persimilis*. *Mol. Ecol.* **2019**, *28*, 1283–1301. [CrossRef]
16. Zacharopoulou, A.; Augustinos, A.A.; Drosopoulou, E.; Tsoumani, K.T.; Gariou-Papalexiou, A.; Franz, G.; Mathiopoulos, K.D.; Bourtzis, K.; Mavragani-Tsipidou, P. A review of more than 30 years of cytogenetic studies of Tephritidae in support of sterile insect technique and global trade. *Entomol. Exp. Appl.* **2017**, *164*, 204–225. [CrossRef]
17. Sollazzo, G.; Gouvi, G.; Nikolouli, K.; Aumann, R.A.; Djambazian, H.; Whitehead, M.A.; Berube, P.; Chen, S.H.; Tsiamis, G.; Darby, A.C.; et al. Genomic and cytogenetic analysis of the *Ceratitis capitata* temperature-sensitive lethal region. *G3 Genes Genomes Genet.* **2023**, *13*, jkad074. [CrossRef]
18. Kandul, N.P.; Lukhtanov, V.A.; Pierce, N.E. Karyotypic diversity and speciation in *Agrodiaetus* butterflies. *Evolution* **2007**, *61*, 546–559. [CrossRef]
19. Cameron, S.L. How to sequence and annotate insect mitochondrial genomes for systematic and comparative genomics research. *Syst. Entomol.* **2014**, *39*, 400–411. [CrossRef]
20. Cameron, S.L. Insect mitochondrial genomics: Implications for evolution and phylogeny. *Annu. Rev. Entomol.* **2014**, *59*, 95–117. [CrossRef]
21. Dong, X.; Zhang, H.; Zhu, X.; Wang, K.; Xue, H.; Ye, Z.; Zheng, C.; Bu, W. Mitochondrial introgression and mitonuclear discordance obscured the closely related species boundaries in *Cletus* Stål from China (Heteroptera: Coreidae). *Mol. Phylogenet. Evol.* **2023**, *184*, 107802. [CrossRef]
22. Duque-Gamboa, D.N.; Castillo-Cárdenas, M.F.; Hernández, L.M.; Guzmán, Y.C.; Manzano, M.R.; Toro-Perea, N. Mitochondrial DNA suggests cryptic speciation in *Prodiplosis longifila* Gagné (Diptera: Cecidomyiidae) associated with geographic distance and host specialization. *Bull. Entomol. Res.* **2018**, *108*, 739–749. [CrossRef] [PubMed]
23. Lea, V.; Uroš, S.; Jelena, J.; Sanja, B.; Biljana, S.; Mirko, Đ. Toward the development of the trojan female technique in pest insects: Male-specific influence of mitochondrial haplotype on reproductive output in the seed beetle *Acanthoscelides obtectus*. *Evol. Appl.* **2024**, *17*, e70065. [CrossRef] [PubMed]
24. Breton, S.; Ghiselli, F.; Milani, L. Mitochondrial short-term plastic responses and long-term evolutionary dynamics in animal species. *Genome Biol. Evol.* **2021**, *13*, evab084. [CrossRef] [PubMed]
25. Kang, N.; Hu, H. Adaptive evidence of mitochondrial genes in Pteromalidae and Eulophidae (Hymenoptera: Chalcidoidea). *PLoS ONE* **2023**, *18*, e0294687. [CrossRef]
26. Nanini, F.; Souza, P.G.C.; Soliman, E.P.; Zauza, E.A.V.; Domingues, M.M.; Santos, F.A.; Wilcken, C.F.; da Silva, R.S.; Corrêa, A.S. Genetic diversity, population structure and ecological niche modeling of *Thyrinteina arnobia* (Lepidoptera: Geometridae), a native Eucalyptus pest in Brazil. *Sci. Rep.* **2024**, *14*, 20963. [CrossRef]
27. Levan, A.; Fredga, K.; Sandberg, A.A. Nomenclature for centromeric position on chromosomes. *Hereditas* **1964**, *52*, 201–220. [CrossRef]
28. Sumner, A.T. A simple technique for demonstrating centromeric heterochromatin. *Exp. Cell Res.* **1972**, *75*, 304–306. [CrossRef]
29. Mullin, P.G.; Harris, T.S.; Powers, T.O. Phylogenetic relationships of Nygolaimina and Dorylaimina (Nematoda: Dorylaimida) inferred from small subunit ribosomal DNA sequences. *Nematology* **2005**, *7*, 59–79. [CrossRef]
30. Cabral-de-Mello, D.C.; Marec, F. Universal fluorescence in situ hybridization (FISH) protocol for mapping repetitive DNAs in insects and other arthropods. *Mol. Genet. Genom.* **2021**, *296*, 513–526. [CrossRef]
31. Bolger, A.M.; Lohse, M.; Usadel, B. Trimmomatic: A flexible trimmer for Illumina sequence data. *Bioinformatics* **2014**, *30*, 2114–2120. [CrossRef]
32. Dierckxsens, N.; Mardulyn, P.; Smits, G. NOVOPlasty: De novo assembly of organelle genomes from whole genome data. *Nucleic Acids Res.* **2017**, *45*, e18. [CrossRef] [PubMed]
33. Ojala, D.; Montoya, J.; Attardi, G. tRNA punctuation model of RNA processing in human mitochondria. *Nature* **1981**, *290*, 470–474. [CrossRef] [PubMed]
34. Song, H.; Sheffield, N.C.; Cameron, S.L.; Miller, K.B.; Whiting, M.F. What happens when the phylogenetic assumptions are violated?: The effect of base compositional heterogeneity and among-site rate heterogeneity in beetle mitochondrial phylogenomics. *Syst. Entomol.* **2010**, *35*, 429–448. [CrossRef]
35. Mengual, X.; Mayer, C.; Burt, T.O.; Moran, K.M.; Dietz, L.; Nottebrock, G.; Pauli, T.; Young, A.D.; Brasseur, M.V.; Kukowka, S.; et al. Systematics and evolution of predatory flower flies (Diptera: Syrphidae) based on exon-capture sequencing. *Syst. Entomol.* **2023**, *48*, 250–277. [CrossRef]
36. Katoh, K.; Standley, D.M. MAFFT multiple sequence alignment software version 7: Improvements in performance and usability. *Mol. Biol. Evol.* **2013**, *30*, 772–780. [CrossRef]

37. Talavera, G.; Castresana, J. Improvement of phylogenies after removing divergent and ambiguously aligned blocks from protein sequence alignments. *Syst. Biol.* **2007**, *56*, 564–577. [CrossRef]
38. Chernomor, O.; von Haeseler, A.; Minh, B.Q. Terrace aware data structure for phylogenomic inference from supermatrices. *Syst. Biol.* **2016**, *65*, 997–1008. [CrossRef]
39. Minh, B.Q.; Schmidt, H.A.; Chernomor, O.; Schrempf, D.; Woodhams, M.D.; von Haeseler, A.; Lanfear, R. IQ-TREE 2: New models and efficient methods for phylogenetic inference in the genomic era. *Mol. Biol. Evol.* **2020**, *37*, 1530–1534. [CrossRef]
40. Kalyaanamoorthy, S.; Minh, B.Q.; Wong, T.K.F.; von Haeseler, A.; Jermiin, L.S. ModelFinder: Fast model selection for accurate phylogenetic estimates. *Nat. Methods* **2017**, *14*, 587–589. [CrossRef]
41. Hoang, D.T.; Chernomor, O.; von Haeseler, A.; Minh, B.Q.; Vinh, L.S. UFBoot2: Improving the ultrafast bootstrap approximation. *Mol. Biol Evol.* **2018**, *35*, 518–522. [CrossRef]
42. Boyes, J.W. Somatic chromosomes of some syrphid flies. *Can. J. Genet. Cytol.* **1959**, *1*, 39–48. [CrossRef]
43. Boyes, J.W.; Van Brink, J.M. Chromosomes of Syrphidae. I. Variations in karyotype. *Chromosoma* **1964**, *15*, 579–590. [CrossRef] [PubMed]
44. Boyes, J.W.; Van Brink, J.M. Chromosomes of Syrphidae. II. Karyotypes of five species in the tribe Sericomyiini. *Chromosoma* **1966**, *19*, 399–404. [CrossRef]
45. Boyes, J.W.; Van Brink, J.M. Chromosomes of Syrphidae. III. Karyotypes of some species in the tribes Milesiini and Myoleptini. *Chromosoma* **1967**, *22*, 417–455. [CrossRef]
46. Boyes, J.W.; Van Brink, J.M. Chromosomes of Syrphidae. V. Microchromosomes. *Chromosoma* **1970**, *31*, 207–216. [CrossRef]
47. Boyes, J.W.; Van Brink, J.M. Chromosomes of Syrphidae. VI. The tribe Pipizini. *Genetica* **1972**, *43*, 321–333. [CrossRef]
48. Boyes, J.W.; Van Brink, J.M.; Mehta, R.D. Chromosomes of Syrphidae. IV. Karyotypes of fourteen species in the tribe Chrysotoxini. *Chromosoma* **1968**, *24*, 233–242. [CrossRef]
49. Boyes, J.W.; Van Brink, J.M.; Boyes, B.C. *Chromosomes of Syrphinae (Diptera: Syrphidae)*; Genetics Society of Canada: Ottawa, ON, Canada, 1971; pp. 1–158.
50. Boyes, J.W.; Boyes, B.C.; Van Brink, J.M.; Vockeroth, J.R. Cytotaxonomy of South American Syrphinae (Diptera: Syrphidae). *Genetica* **1973**, *44*, 368–415. [CrossRef]
51. Boyes, J.W.; Van Brink, J.M.; Boyes, B.C.; Vockeroth, J.R. *Chromosomes of Eristalinae and Microdontinae (Diptera: Syrphidae)*; Genetics Society of Canada: Ottawa, ON, Canada, 1980; pp. 1–137.
52. Rozek, M.; Marcos-Garcia, M.Á.; Lachowska, D. C-banding patterns in chromosomes of four species of syrphid flies (Diptera, Syrphidae). *Folia Biol. Krakow* **1995**, *43*, 107–109.
53. Rozek, M.; Lachowska, D.; Marcos-Garcia, M.Á. The C-banded karyotypes of *Syrphis corolla* (Fabr.) and *Sphaerophoria scripta* (L.) (Diptera, Syrphidae). *Folia Biol. Krakow* **1996**, *44*, 11–13.
54. Khajuria, M.; Bhatti, A.A.; Tripathi, N.K. First report on the chromosomal analysis of three species of tribe Eristalini (Diptera: Syrphidae) from outer Himalayas, India. *Biologia* **2019**, *74*, 469–475. [CrossRef]
55. Morelli, M.W.; Blackmon, H.; Hjelmen, C.E. Diptera and Drosophila Karyotype Databases: A useful dataset to guide evolutionary and genomic studies. *Front. Ecol. Evol.* **2022**, *10*, 832378. [CrossRef] [PubMed]
56. Bailey, E.; Field, L.; Rawlings, C.; King, R.; Mohareb, F.; Pak, K.H.; Hughes, D.; Williamson, M.; Ganko, E.; Buer, B.; et al. A near-chromosome level genome assembly of the European hoverfly, *Sphaerophoria rueppellii* (Diptera: Syrphidae), provides comparative insights into insecticide resistance-related gene family evolution. *BMC Genom.* **2022**, *23*, 198. [CrossRef]
57. Marchi, A.; Pili, E. Ribosomal RNA genes in mosquitoes: Localization by fluorescence in situ hybridization (FISH). *Heredity* **1994**, *72*, 599–605. [CrossRef]
58. Brianti, M.T.; Ananina, G.; Recco-Pimentel, S.M.; Klaczko, L.B. Comparative analysis of the chromosomal positions of rDNA genes in species of the *tripunctata* radiation of *Drosophila*. Cytogenet. *Genome Res.* **2009**, *125*, 149–157. [CrossRef]
59. Madalena, C.R.; Díez, J.L.; Gorab, E. Chromatin structure of ribosomal RNA genes in dipterans and its relationship to the location of nucleolar organizers. *PLoS ONE* **2012**, *7*, e44006. [CrossRef]
60. Falk, S.; Sudworth, J.; University of Oxford and Wytham Woods Genome Acquisition Lab; Darwin Tree of Life Barcoding Collective; Wellcome Sanger Institute Tree of Life Programme; Wellcome Sanger Institute Scientific Operations: DNA Pipelines Collective; Tree of Life Core Informatics Collective; Darwin Tree of Life Consortium. The genome sequence of a hoverfly, *Sphaerophoria taeniata* (Meigen, 1822). *Wellcome Open Res.* **2023**, *8*, 474. [CrossRef]
61. Pu, D.Q.; Liu, H.L.; Gong, Y.Y.; Ji, P.C.; Li, Y.J.; Mou, F.S.; Wei, S.J. Mitochondrial genomes of the hoverflies *Episyrphus balteatus* and *Eupeodes corollae* (Diptera: Syrphidae), with a phylogenetic analysis of Muscomorpha. *Sci. Rep.* **2017**, *7*, 44300. [CrossRef]

62. Hawkes, W.; Wotton, K.; Smith, M.; University of Oxford and Wytham Woods Genome Acquisition Lab; Natural History Museum Genome Acquisition Lab; Darwin Tree of Life Barcoding Collective; Wellcome Sanger Institute Tree of Life Programme; Wellcome Sanger Institute Scientific Operations: DNA Pipelines Collective; Tree of Life Core Informatics Collective; Darwin Tree of Life Consortium. The genome sequence of the two-banded wasp hoverfly, *Chrysotoxum bicinctum* (Linnaeus, 1758). *Wellcome Open Res.* **2021**, *6*, 321. [CrossRef]
63. Boore, J.; Lavrov, D.; Brown, W. Gene translocation links insects and crustaceans. *Nature* **1998**, *392*, 667–668. [CrossRef]
64. Sterling-Montealegre, R.A.; Prada, C.F. Variability and evolution of gene order rearrangement in mitochondrial genomes of arthropods (except Hexapoda). *Gene* **2023**, *892*, 147906. [CrossRef] [PubMed]
65. Li, H.; Yan, Y.; Li, J. Eighteen mitochondrial genomes of Syrphidae (Insecta: Diptera: Brachycera) with a phylogenetic analysis of Muscomorpha. *PLoS ONE* **2023**, *18*, e0278032. [CrossRef] [PubMed]
66. Zhang, D.-X.; Hewitt, G.M. Insect mitochondrial control region: A review of its structure, evolution and usefulness in evolutionary studies. *Biochem. Syst. Ecol.* **1997**, *25*, 99–120. [CrossRef]
67. Wolstenholme, D.R. Animal mitochondrial DNA: Structure and evolution. *Int. Rev. Cytol.* **1992**, *141*, 173–216. [CrossRef]
68. Ruiz-Mena, A.; Mora, P.; Rico-Porras, J.M.; Kaufmann, B.; Seifert, B.; Palomeque, T.; Lorite, P. A comparative analysis of mitogenomes in species of the *Tapinoma nigerrimum* complex and other species of the genus *Tapinoma* (Formicidae, Dolichoderinae). *Insects* **2024**, *15*, 957. [CrossRef]
69. Beckenbach, A.T.; Stewart, J.B. Insect mitochondrial genomics 3: The complete mitochondrial genome sequences of representatives from two neuropteroid orders: A dobsonfly (order Megaloptera) and a giant lacewing and an owlfly (order Neuroptera). *Genome* **2009**, *52*, 31–38. [CrossRef]
70. Ruiz-Mena, A.; Mora, P.; Montiel, E.E.; Palomeque, T.; Lorite, P. Complete nucleotide sequence of the mitogenome of *Tapinoma ibericum* (Hymenoptera: Formicidae: Dolichoderinae), gene organization and phylogenetic implications for the Dolichoderinae subfamily. *Genes* **2022**, *13*, 1325. [CrossRef]
71. Taanman, J.W. The mitochondrial genome: Structure, transcription, translation and replication. *Biochim. Biophys. Acta* **1999**, *1410*, 103–123. [CrossRef]
72. Dowton, M.; Cameron, S.L.; Dowavic, J.I.; Austin, A.D.; Whiting, M.F. Phylogenetic approaches for the analysis of mitochondrial genome sequence data in the Hymenoptera—A lineage with both rapidly and slowly evolving mitochondrial genomes. *Mol. Phylogenet. Evol.* **2009**, *52*, 512–519. [CrossRef]
73. Pita, S.; Panzera, F.; Vela, J.; Mora, P.; Palomeque, T.; Lorite, P. Complete mitochondrial genome of *Triatoma infestans* (Hemiptera, Reduviidae, Triatominae), main vector of Chagas disease. *Infect. Genet. Evol.* **2017**, *54*, 158–163. [CrossRef]
74. Morgan, B.; Wang, T.Y.; Chen, Y.Z.; Moctezuma, V.; Burgos, O.; Le, M.H.; Huang, J.P. Long-read sequencing data reveals dynamic evolution of mitochondrial genome size and the phylogenetic utility of mitochondrial DNA in Hercules beetles (*Dynastes*; Scarabaeidae). *Genome Biol. Evol.* **2022**, *14*, evac147. [CrossRef] [PubMed]
75. Yuan, Y.; Zhang, L.; Li, K.; Hong, Y.; Storey, K.B.; Zhang, J.; Yu, D. Nine mitochondrial genomes of Phasmatodea with two novel mitochondrial gene rearrangements and phylogeny. *Insects* **2023**, *14*, 485. [CrossRef] [PubMed]
76. Ji, H.; Xu, X.; Jin, X.; Yin, H.; Luo, J.; Liu, G.; Zhao, Q.; Chen, Z.; Bu, W.; Gao, S. Using high-resolution annotation of insect mitochondrial DNA to decipher tandem repeats in the control region. *RNA Biol.* **2019**, *16*, 830–837. [CrossRef]
77. Anand, R.; Singh, S.P.; Sahu, N.; Singh, Y.T.; Mazumdar-Leighton, S.; Bentur, J.S.; Nair, S. Polymorphisms in the hypervariable control region of the mitochondrial DNA differentiate BPH populations. *Front. Insect Sci.* **2022**, *2*, 987718. [CrossRef]
78. Arcaya, E.; Pérez-Bañón, C.; Mengual, X.; Zubcoff-Vallejo, J.J.; Rojo, S. Life table and predation rates of the syrphid fly *Allograpta exotica*, a control agent of the cowpea aphid *Aphis craccivora*. *BioControl* **2017**, *115*, 74–84. [CrossRef]
79. Mengual, X.; Ståhls, G.; Rojo, S. First phylogeny of predatory flower flies (Diptera, Syrphidae, Syrphinae) using mitochondrial COI and nuclear 28S rRNA genes: Conflict and congruence with the current tribal classification. *Cladistics* **2008**, *24*, 543–562. [CrossRef]
80. Mengual, X.; Ståhls, G.; Skevington, J.H. Life on an island: The phylogenetic placement of Loveridgeana and Afrotropical *Sphaerophoria* (Diptera: Syrphidae) inferred from molecular characters. *Syst. Biodivers.* **2020**, *19*, 22–53. [CrossRef]
81. Zhao, R.; Li, H.; Wu, G.; Wang, Y.F. Codon usage bias analysis in the mitochondrial genomes of five *Rhingia* Scopoli (Diptera, Syrphidae, Eristalinae) species. *Gene* **2024**, *917*, 148466. [CrossRef]
82. Guo, S.; Chen, J.; Song, N. Phylogenomic analysis of Syrphoidea (Diptera: Syrphidae, Pipunculidae) based on the expanded mitogenomic data. *Arch. Insect Biochem. Physiol.* **2023**, *114*, 1–13. [CrossRef]

Disclaimer/Publisher's Note: The statements, opinions and data contained in all publications are solely those of the individual author(s) and contributor(s) and not of MDPI and/or the editor(s). MDPI and/or the editor(s) disclaim responsibility for any injury to people or property resulting from any ideas, methods, instructions or products referred to in the content.

insects

MDPI

Article

Development of an Experimental Method Using a Portable Photosynthesis-Monitoring System to Measure Respiration Rates in Small-Sized Insects

Bi-Yue Ding [1,2,*,†], Qin-Qin Xu [2,†], Yu-Jing Liu [2], Yu-Hong Zhong [2] and Yan Zhou [1]

[1] Instrument and Equipment Sharing Service Center, Academy of Agricultural Sciences, Southwest University, Chongqing 400715, China; zhouyanswu@126.com
[2] Key Laboratory of Entomology and Pest Control Engineering, College of Plant Protection, Southwest University, Chongqing 400715, China; qinqinxu999@163.com (Q.-Q.X.); yjingliu1@163.com (Y.-J.L.); zyz123579@email.swu.edu.cn (Y.-H.Z.)
* Correspondence: dingbiyue302@swu.edu.cn; Tel.: +86-(023)-68253756
† These authors contributed equally to this work.

Simple Summary: Understanding how insects breathe is essential for both ecological research and pest control. However, accurately measuring the respiration rates of small-sized insects has been challenging due to a lack of suitable tools. This study evaluated the use of a portable photosynthesis system, originally developed for plants, to measure insect respiration. The results demonstrated that this method is effective across various insect species and developmental stages. Moreover, factors such as temperature, starvation, and specific chemicals significantly influenced respiration rates. Silencing a mitochondrial protein-coding gene through RNA interference reduced respiration and increased resistance to certain stresses. Overall, this study introduces a novel experimental method for measuring insect respiration, offering insights into their adaptation mechanisms and providing a potential tool for improved pest management. These findings also contribute valuable information to our understanding of how insects interact with their environment and respond to challenges such as climate change.

Abstract: Respiration rates in insects are critical for survival and environmental adaptation, being influenced by developmental stages, environmental conditions, and the regulation of mitochondrial protein-coding genes. However, methods for field-based measurements in small-sized insects remain limited. In this study, we established a portable photosynthesis system to quantify respiration rates in five small-sized insects (body length < 8 mm): *Acyrthosiphon pisum*, *Aphis citricidus*, *Tuta absoluta*, *Tribolium castaneum*, and *Bactrocera dorsalis*. We tested its effectiveness across life stages and under diverse treatments, including light/dark cycles, insecticides, temperature shifts, starvation, mitochondrial inhibitors, and RNA interference. The system exhibited high sensitivity and reproducibility rates, revealing stage-specific respiration patterns. Various treatments, as well as expression changes in mitochondrial protein-coding genes, significantly affected respiration rates. This study validates the portable system as a reliable tool for insect respiration studies and highlights regulatory networks associated with respiratory plasticity. These findings enhance experimental methodologies and advance our understanding of insect adaptation to environmental stressors and pest control strategies.

Keywords: respiration rates; photosynthesis-monitoring system; insects; various treatments; RNAi

1. Introduction

The respiratory system in insects is essential for environmental adaptation, development, and survival [1,2]. To meet their high metabolic demands, insects depend on efficient gas exchange [3]. Respiration rates are influenced by multiple factors, including body size, activity level, food availability, temperature, and oxygen concentration [4,5]. Activities such as flight or mating can substantially increase respiration rates [6]. Temperature has a direct effect on insect respiration by influencing the metabolic rate, thereby affecting thermoregulation and respiratory efficiency under changing conditions [7]. These mechanisms underpin insects' adaptability to environmental fluctuations, particularly in the context of global climate change [8,9]. Understanding insect respiration, therefore, holds ecological relevance and practical value in pest management [3,10]. For instance, strategies that target respiratory processes have led to the development of effective pesticides and control methods [11–14]. The respiration rate is thus a key parameter in studies of insect biology, ecology, and environmental interaction [4,15]. However, current techniques for measuring respiration in small-sized insects (body length < 8 mm) are limited by low sensitivity and poor field operability [16,17].

The portable photosynthesis system has become a widely used tool for quantifying photosynthetic parameters across diverse plant species and environmental conditions owing to its ease of use, standardized protocols, and high degree of experimental reproducibility [18–22]. Applications include studies in rapeseed [20], soybean [23], paper mulberry [24], cotton [25], mulberry [19], poplar [26], and switchgrass [27]. For example, it has been employed to measure the net photosynthesis, transpiration, intracellular CO_2 concentration, and stomatal conductance in a *Brassica napus* variety resistant to Sclerotinia [20], as well as to assess the net photosynthetic rate in *Pakchoi* after seedling treatment with a polymeric hydrogel [28]. This system calculates the photosynthetic efficiency by simultaneously monitoring the CO_2/H_2O gas exchange, light intensity, and leaf temperature via integrated infrared sensors and environmental probes, enabling the precise quantification of photosynthesis and transpiration in field settings [29]. Based on these operational principles, the portable photosynthesis system offers untapped potential for measuring respiration in micro-insects by leveraging its high sensitivity to the CO_2 flux, originally intended for detecting plant stomatal dynamics.

Mitochondria are essential organelles that regulate cellular respiration and energy production in eukaryotes [30]. In insects, mitochondrial genomes and associated genes play critical roles in respiratory function. Complete mitochondrial genome sequences have been reported for several species, including *Leucinodes orbonalis* [31], *Rhyzopertha dominica* [32], *Choroterpes yixingensis* [33], and *Aphis citricidus* [34], revealing 13 mitochondrial protein-coding genes. Although the expression patterns of these genes have been studied under various experimental conditions in some insect species [35–37], the relationship between their expression and respiration rates remains poorly understood in *Acyrthosiphon pisum*.

In this study, we developed a technique to measure respiration in small-sized insects, using a portable photosynthesis system. To validate its applicability, we assessed respiration rates across different life stages in multiple insect species and under various experimental conditions in *Ac. pisum*. This work presents a novel methodology for investigating insect respiration and contributes to a deeper understanding of insect adaptation mechanisms.

2. Materials and Methods

2.1. Insects

Ac. pisum was reared on *Vicia faba* seedlings, *Aphis citricidus* on *Citrus sinensis*, *Tuta absoluta* on *Solanum lycopersicum*, and *Bactrocera dorsalis* on an artificial diet, as previously

described [38]. All the insects were maintained at 25 °C and 75% relative humidity and under a photoperiod of 14 h of light and 10 h of darkness. *Tribolium castaneum* was reared on a mixture of wheat flour and brewer's yeast powder (in a 10:1 ratio) under conditions of 30 °C, 30% relative humidity, and a photoperiod cycle of 16 h of light and 8 h of darkness.

2.2. Sample Collection from Various Developmental Stages and Treatments

Developmental stages. Insects from different developmental stages of *Ac. pisum* and *Ap. citricidus* (first-instar nymphs (N1), second-instar nymphs (N2), third-instar nymphs, fourth-instar nymphs (N3), and three-day-old adults (AD)), *Ap. citricidus* (first-instar nymphs (N1), second-instar nymphs (N2), third-instar nymphs, fourth-instar nymphs (N3), three-day-old wingless adults (AD-WL), and three-day-old winged adults (AD-WL)), *T. absoluta* (eggs (E), larvae (L), pupae (P), and adults (AD)), *B. dorsalis* (eggs (E), first-instar larvae (L1), second-instar larvae (L2), third-instar larvae (L3), pupae (P), female adults (AD-F), and male adults (AD-M)), and *T. castaneum* (eggs (E), larvae (L), pupae (P), female adults (AD-F), and male adults (AD-M)) were collected for respiration rate measurements. For egg stages, 50 individuals were pooled per group; for larvae, pupae, and adults, 10 individuals were pooled. Each treatment included eight biological replicates.

Photoperiod. *Ac. pisum* individuals, maintained under a 14:10 h light–dark cycle, were sampled at two-hour intervals to assess respiration rate variations throughout the photoperiod. Ten aphids were pooled per group, with eight biological replicates.

Temperatures. *Ac. pisum* was exposed to acute thermal stress at 35 °C and 4 °C for 4, 8, or 12 h. Respiratory measurements were taken immediately after treatment. Aphids reared at 25 °C served as controls. Ten individuals were pooled per group, with eight biological replicates.

Insecticides. *Ac. pisum* was treated with LC_{20} concentrations of avermectin, β-cypermethrin, and imidacloprid [39]. Aphids treated with acetone were used as controls. Ten individuals were pooled per group, with eight biological replicates.

Starvation. *Ac. pisum* was starved for 4, 8, or 12 h. After each starvation period, individuals were collected for respiration rate measurements. Normally fed aphids served as controls. Ten insects were pooled per group, with eight biological replicates.

Mitochondrial inhibitors. *Ac. pisum* was treated with mitochondrial inhibitors (rotenone and antimycin A). Aphids treated with acetone were used as controls. Ten insects were pooled per group, with eight biological replicates.

2.3. Measured Respiration Rates

Insect respiration rates were measured using a modified LI-6800 photosynthesis system (Ecotek Technology, Beijing, China), coupled with a custom insect chamber containing a ventilated lid and an artificial feeding device (Figure 1), according to the manufacturer's instructions with slight modifications. Briefly, after assembling the system and performing preheating checks and zeroing calibration through the instrument's startup protocol, we configured the operational parameters as follows: a 500 μmol s^{-1} airflow, a 25 °C temperature control, and 400 μmol mol^{-1} CO_2 levels with active scrubbing. The humidity was maintained between 50 and 75% using the system's water vapor subsystem. The insects were placed in the transparent chamber, which was sealed within the LI-6800 leaf chamber (Ecotek Technology, Beijing, China) and measurements were taken continuously for 10 min, with automatic data collection every 2 min. The insects were given time to reach a stable respiratory state (ΔCO_2 remained within 0.01 μmol mol^{-1}). Respiration rates were calculated as CO_2 emissions per minute, normalized to the insect's body mass (μmol g^{-1} min^{-1}), reflecting gas-exchange dynamics under controlled environmental conditions.

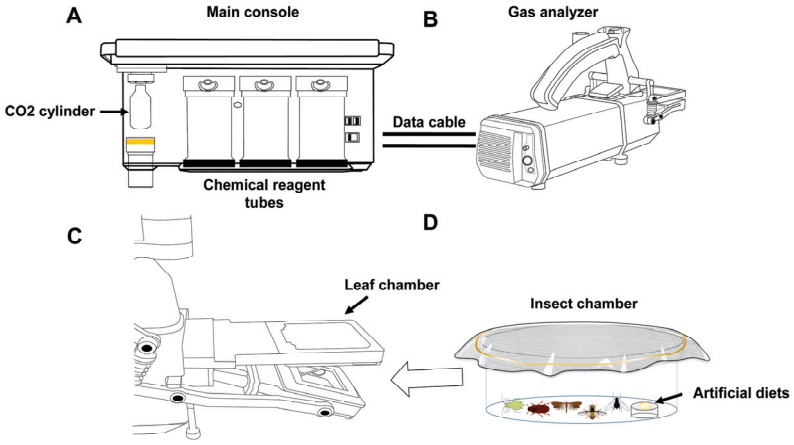


Figure 1. Device for measuring respiration rates of small-sized insects, using the portable photosynthesis system. (**A**) Main console. (**B**) Gas analyzer. (**C**) Position of the leaf chamber on the gas analyzer. (**D**) Insect chamber, equipped with an artificial-diet provision system. The insect chamber is inserted into the leaf chamber for gas-exchange measurements when containing experimental insects.

2.4. RT-qPCR

The primers for 13 mitochondrial protein-coding genes are listed in Table S1. The total RNA was extracted from treated samples using TRIzol reagent (Invitrogen, Carlsbad, CA, USA), and cDNA was synthesized using the PrimeScript RT reagent kit (Takara, Dalian, China). Quantitative PCR (qPCR) analysis was performed with NovoStart SYBR qPCR SuperMix (Novoprotein, Shanghai, China) to quantify target gene expression levels. Standard curves were generated with serial cDNA dilutions to determine the amplification efficiency and CT values. *Apactin* and *ApNADH* were used as reference genes for normalization via qBASE+ [40,41].

2.5. RNA Interference Assay

Double-stranded RNA (dsRNA) was synthesized using the TranscriptAid T7 high-yield kit (Thermo Scientific, Wilmington, DE, USA). Aphids were topically treated with 500 ng/μL dsRNA, with dsGFP as a control. The treated aphids were fed artificial diets for 12 h before respiration rate measurements (Section 2.3). Each group contained ten individuals, with eight replicates.

2.6. Statistical Analyses

Statistical analyses were performed using GraphPad Prism 7.0 (GraphPad Software, San Diego, CA, USA). Multiple group comparisons, including respiration rates among different developmental stages and various treatments and transcriptional patterns of mitochondrial protein-coding genes during light/dark periods and across developmental stages, were analyzed using one-way ANOVA with LSD post hoc tests ($p < 0.05$). Pairwise comparisons, including transcriptional patterns of mitochondrial protein-coding genes in different treatments and the RNAi assay, were assessed using Student's *t*-test (*, $p < 0.05$; **, $p < 0.01$; ***, $p < 0.001$).

3. Results

3.1. Measurement of Respiration Rates in Different Insects, Using a Portable Photosynthesis-Monitoring System

To test the applicability of this method for various small-sized insects, we used a portable photosynthesis-monitoring system to measure the respiration rates of five in-

sect species: *Ac. pisum* and *Ap. citricidus* (Hemiptera: Aphididae), *Tu. absoluta* (Lepidoptera: Gelechiidae), Tr. castaneum (Coleoptera: Tenebrionidae), and B. dorsalis (Diptera: Tephritidae) across different developmental stages or morphs. The results demonstrate that this method offers high sensitivity, ease of use, and excellent reproducibility. The respiration rate profiles revealed that second-instar nymphs exhibited the lowest respiration rates (1.16 μmol g^{-1} min^{-1}), while first-instar nymphs showed the highest (1.93 μmol g^{-1} min^{-1}) in *Ac. pisum* (Figure 2A). In *Tu. absoluta*, pupae had the lowest rates (0.03 μmol g^{-1} min^{-1}), whereas larvae displayed the highest rates (2.58 μmol g^{-1} min^{-1}) (Figure 2B). In *Tr. Castaneum*, eggs had the lowest respiration rates (0.07 μmol g^{-1} min^{-1}), while larvae exhibited the highest (0.74 μmol g^{-1} min^{-1}) (Figure 2C). In B. dorsalis, pupae displayed the lowest rates (0.06 μmol g^{-1} min^{-1}), while first-instar larvae exhibited the highest (23.31 μmol g^{-1} min^{-1}) (Figure 2D). In Ap. citricidus, winged adults (0.63 μmol g^{-1} min^{-1}), wingless adults (0.64 μmol g^{-1} min^{-1}), third-instar nymphs (0.72 μmol g^{-1} min^{-1}), and fourth-instar nymphs (0.79 μmol g^{-1} min^{-1}) had the lowest respiration rates, while first-instar nymphs showed the highest (1.71 μmol g^{-1} min^{-1}) (Figure 2E).

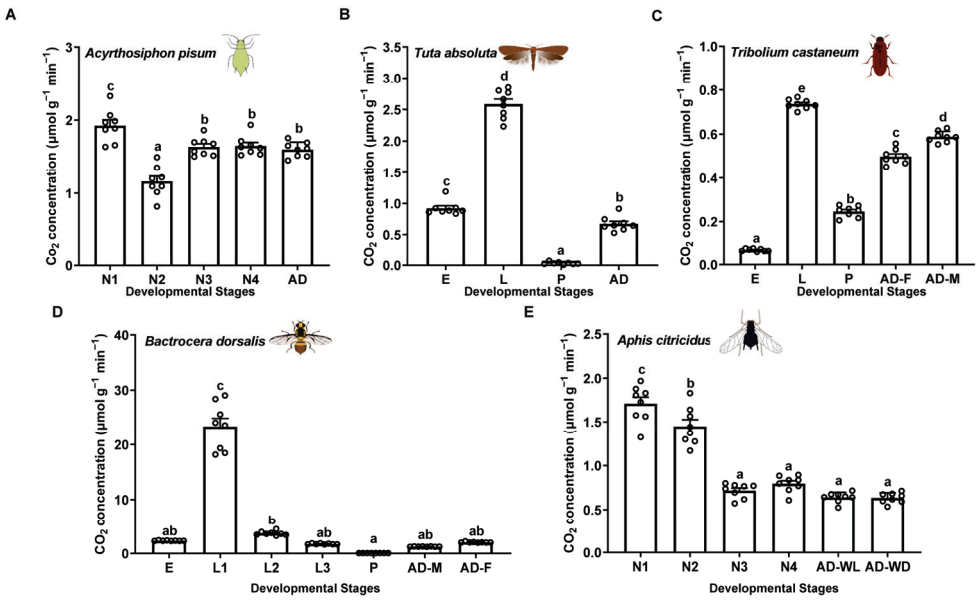


Figure 2. Respiration rates of different insects, using the portable photosynthesis-monitoring system. (**A**) Acyrthosiphon pisum. (**B**) Tuta absoluta. (**C**) Tribolium castaneum. (**D**) Bactrocera dorsalis. (**E**) Aphis citricidus. Values represent the mean ± standard error (SE) of eight biological replicates. Lowercase letters denote statistically significant differences determined through one-way ANOVA with LSD post hoc testing ($p < 0.05$).

3.2. Measurement of Respiration Rates of Ac. pisum Under Various Treatments, Using a Portable Photosynthesis-Monitoring System

To assess the applicability of this method for measuring insect respiration under different conditions, we tested *Ac. pisum* exposed to light/dark cycles over a full photoperiod, insecticides, varying temperatures, starvation periods, and mitochondrial inhibitors at different concentrations. The respiration rates remained stable throughout the photoperiod, with only a slight initial increase followed by a subsequent decrease during light periods (Figure 3A). All three insecticides (imidacloprid, abamectin, and β-cypermethrin) reduced respiration rates (Figure 3B). High temperatures (32 °C) significantly increased the respiration rates, whereas low temperatures (4 °C) markedly decreased them

(Figure 3C). Starvation also reduced respiration rates, with the reduction intensifying over time (Figure 3D). Both mitochondrial inhibitors (rotenone and antimycin A) suppressed respiration rates, with progressive decreases at higher concentrations (Figure 3E).

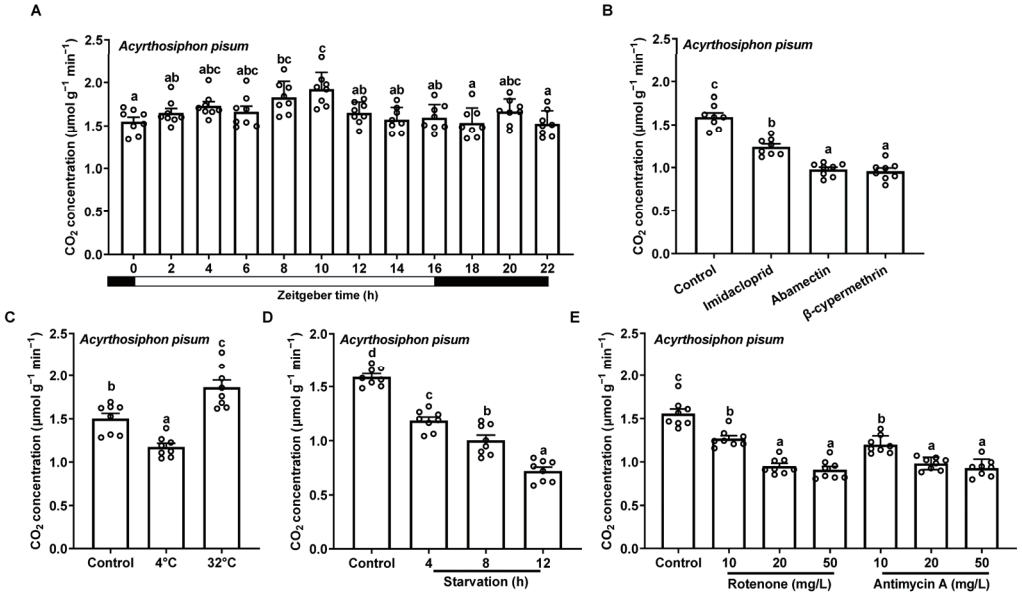


Figure 3. Respiration rates of Acyrthosiphon pisum under different treatments, using the portable photosynthesis-monitoring system. (**A**) Light/dark cycles over a full photoperiod. (**B**) Insecticide exposure. (**C**) Varying temperatures. (**D**) Starvation at various time points. (**E**) Mitochondrial inhibitors. Values represent the mean ± standard error (SE) of eight biological replicates. Lowercase letters denote statistically significant differences determined through one-way ANOVA with LSD post hoc testing ($p < 0.05$).

3.3. Measurement of Respiration Rates of Ac. pisum Under the Silencing of a Key Mitochondrial Protein-Coding Genes, Using a Portable Photosynthesis-Monitoring System

To measure the respiration rates of Ac. pisum under the silencing of a key mitochondrial protein-coding gene, using the portable photosynthesis-monitoring system, we systematically quantified the expression profiles of 13 protein-coding genes. The expression profiles showed stable expression levels during light periods, with lower expression levels later in the light phase and dynamic changes during darkness (zeitgeber times ZT16–ZT22), peaking at ZT18 or ZT22 (Figure S1). Developmental-stage-specific profiles revealed higher gene expression levels in younger nymphs. For example, NAD1, NAD4, NAD5, Cytb, COX1, COX2, COX3, and ATP6 were highly expressed in second-instar nymphs, while NAD2, NAD4L, NAD6, and ATP8 peaked in third-instar nymphs (Figure S2). Larger insects (fourth-instar nymphs and adults) generally showed lower expression levels.

Treatment-induced changes included imidacloprid downregulating NAD2; abamectin reducing NAD5 and ATP8; and β-cypermethrin suppressing NAD2, NAD4, NAD4L, COX1, and ATP8 (Figure 4A). Low temperatures (4 °C) upregulated ATP8, while high temperatures decreased NAD4, NAD6, Cytb, COX3, and ATP6 (Figure 4B). Starvation specifically downregulated ATP8 (Figure 4C). Rotenone reduced NAD1, NAD2, NAD4, NAD4L, NAD5, NAD6, Cytb, and ATP8, whereas antimycin A suppressed NAD1, NAD2, NAD4, NAD4L, NAD6, and ATP8 (Figure 4D).

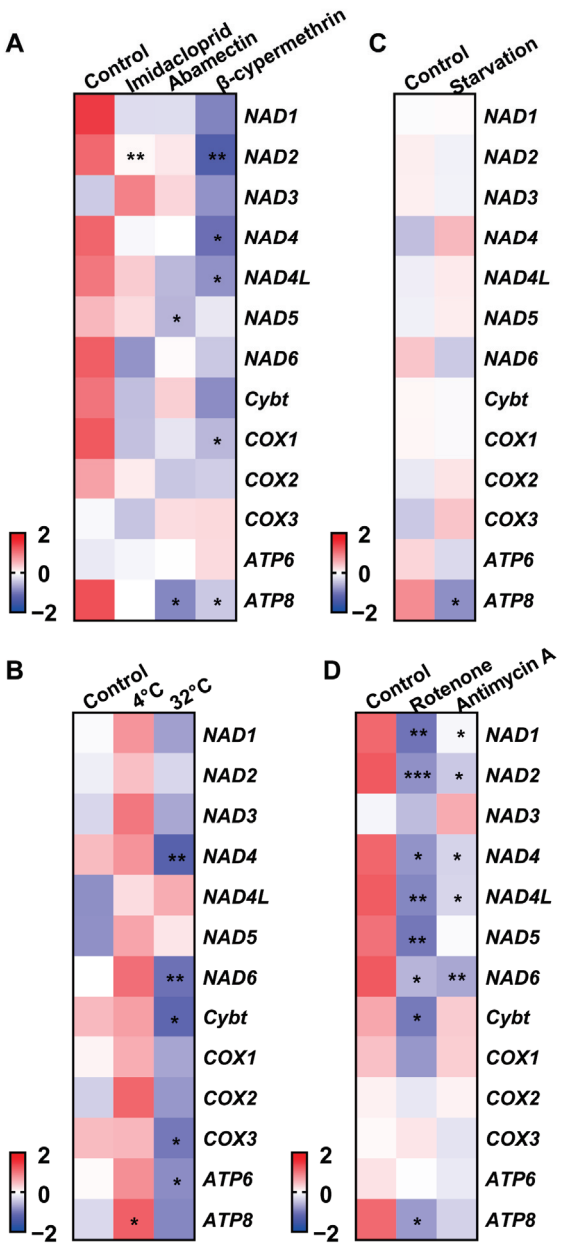


Figure 4. Transcriptional patterns of mitochondrial protein-coding genes in Acyrthosiphon pisum under different treatments. (**A**) Insecticide exposure. (**B**) Varying temperatures. (**C**) Starvation. (**D**) Mitochondrial inhibitors. Values represent the mean ± standard error (SE) of three biological replicates. Asterisks denote statistically significant differences as determined by Student's *t*-test (* $p < 0.05$, ** $p < 0.01$, *** $p < 0.001$).

Given the downregulation of *ATP8* under multiple stresses (abamectin, β-cypermethrin, starvation, and rotenone), this gene was further used to measure the respiration rates of *Ac. pisum* under the silencing of a key mitochondrial protein-coding gene, using the portable photosynthesis-monitoring system. The successful silencing of ATP8 (44.1% efficiency) (Figure 5A) led to significant changes in other mitochondrial genes, with COX1 being significantly upregulated (Figure 5B). The silenced-gene insects exhibited significantly lower respiration rates compared to the dsGFP controls (0.91 vs. 1.34 μmol g^{-1} min^{-1}, Figure 5C). Additionally, the dsATP8-treated groups demonstrated enhanced resistance to abamectin (a 15.2% lower mortality rate, Figure 5D) and β-cypermethrin (a 13.6% lower mortality rate, Figure 5E).

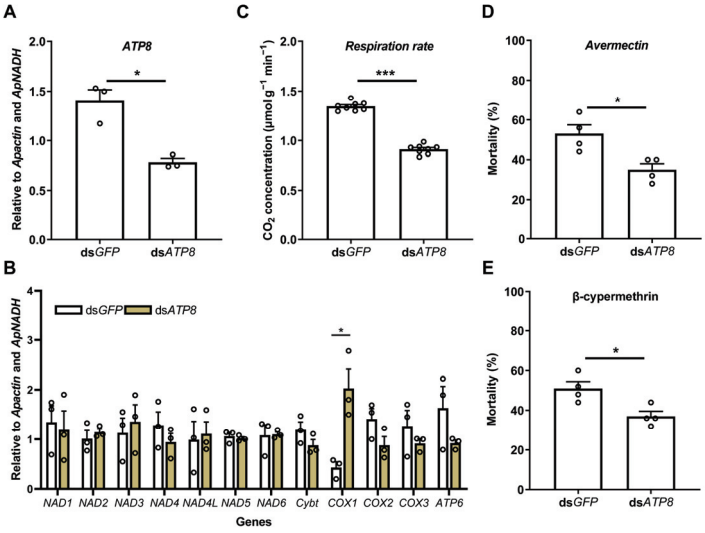


Figure 5. Respiration rates of *Acyrthosiphon pisum* under the silencing of a key mitochondrial protein-coding gene (*ATP8*), using the portable photosynthesis-monitoring system. Effects of ATP8 silencing on the respiration rates and stress resistance of *Acyrthosiphon pisum*. (**A**) Relative expression level of *ATP8* after *ATP8* dsRNA treatment. (**B**) Relative expression levels of other mitochondrial protein-coding genes after *ATP8* dsRNA treatment. (**C**) Respiration rates of *Ac. pisum* after *ATP8* dsRNA treatment. (**D**) Mortality of *Ac. pisum* under avermectin treatment upon feeding dsRNA. (**E**) Mortality of *Ac. pisum* under β-cypermethrin treatment upon feeding dsRNA. Values represent the mean ± standard error (SE) of three biological replicates for gene expression levels, eight for respiration rate, and four for mortality. Asterisks denote statistically significant differences as determined by Student's *t*-test (* $p < 0.05$, *** $p < 0.001$).

4. Discussion

In this study, we demonstrated the feasibility of using a portable photosynthesis system to measure respiration rates in small-sized insects, providing a practical and efficient approach for field-based studies. The results revealed significant variation in respiration rates across developmental stages and species, which aligns with previous reports showing that metabolic demands increase with higher energy requirements for activities such as flight, reproduction, stress resistance, and foraging [7,42]. A prior study indicated that geographic populations of three beetle species from different regions of Brazil exhibited significant differences in respiration rates [14]. Similarly, in *Helicoverpa armigera*, respiration rates fluctuated dynamically across developmental stages, peaking temporarily during interlarval molting and metamorphosis to pupae, sharply declining in the pupal phase, and rising again immediately before eclosion [15]. The high sensitivity and reproducibility rates of the portable photosynthesis system establish it as a valuable tool for future research, particularly in ecological and environmental studies requiring field measurements. Going forward, this system could be used to measure the respiration rates of extremely small insects and assess their stabilities under extreme environmental temperature and humidity conditions to test the detection limits of the system.

The respiration rates of *Ac. pisum* were differentially influenced by environmental and chemical treatments. Light/dark cycles showed minimal effects on metabolic activity, suggesting stable respiratory regulation under variable light conditions. In contrast, significant changes were observed under insecticide exposure, with all the compounds reducing respiration rates, likely due to mitochondrial disruption. High temperatures increased respiration rates, while lower temperatures suppressed them. Starvation similarly reduced respiration, consistent with energy conservation strategies during nutrient deprivation.

Mitochondrial inhibitors further confirmed respiratory suppression through targeted interference. These patterns align with observations in other insects. For example, starvation reduced respiration in *H. armigera* [15], and mitochondrial inhibitors (rotenone, malonate, and antimycin A) decreased respiratory activity in the flight muscles of *Vespula vulgaris*, *Bombus impatiens*, *Apis mellifera*, and *Locusta migratoria* [16]. Similar effects were reported for imidacloprid in *Euschistus heros* males [43], plant-derived compounds (lemongrass essential oil, geranyl acetate, cinnamon terpenoids, clove oils, and citral) in *Sitophilus granarius* and *Ulomoides dermestoides* [44–46], squamocin/tebufenozide in *Anticarsia gemmatalis* larvae [47,48], *Cymbopogon citratus* essential oil in *Podisus nigrispinus* [7], and chlorantraniliprole in *Hypothenemus hampei* [17], collectively demonstrating the broad conservation of metabolic responses across taxa.

Mitochondrial gene expression dynamics reveal key regulatory mechanisms underlying respiratory plasticity during development and in response to environmental stress. Under light–dark cycles, most mitochondrial genes exhibit stable expression levels, with small fluctuations observed at the end of light phases or during periods of darkness. Analyses across developmental stages revealed high expression levels of *NAD1*, *NAD4*, *NAD5*, *Cytb*, *COX1-3*, and *ATP6* in early nymphal stages, reflecting the increased energy demands for growth. Lower expression levels in later nymphs and adults suggest a shift in energy use toward maintenance and reproduction, which aligns with observations of low *ATG5* levels during early diapause, followed by peak expression after 12 weeks of diapause induction [49]. Cold stress was shown to increase *ATP8* expression, likely as a response to maintain energy balance through adaptive processes, while starvation led to a decrease in *ATP8* expression to conserve resources. Additionally, mitochondrial inhibitors generally reduced the expression levels of electron-transport-chain (ETC) genes, indicating the direct suppression of mitochondrial function. These results corroborate those of earlier studies. For example, lower expression levels of *Cytb*, *NAD3*, *NAD5*, *NAD6*, *ATP6*, and *ATP8* were observed in *Cryptolestes ferrugineus* resistant to phosphine [37], contrasting with the higher expression levels of *COX1-3*, *NAD1*, *NAD4*, *NAD5*, *ATP6*, and *Cytb* in *Monochamus alternatus* during pinewood nematode infection [36]. Furthermore, imidacloprid exposure reduces the expression levels of *COX3*, *NAD4*, and *NAD4L* in *Choroterpes yixingensis* [9], while long-term cold stress lowered the expression levels of *NAD1*, *NAD4*, *NAD4L*, *NAD5*, *COX1*, *COX3*, *ATP6*, and *ATP8* in *C. ferrugineus* [9]. These findings suggest both shared and distinct effects of chemical and cold stress on mitochondrial gene networks. Additionally, pyrethroid-resistant *Anopheles sinensis* populations exhibited higher *NAD5* expression and lower *ATP8* expression levels [50], further highlighting the evolutionary conservation of mitochondrial regulatory systems that enable adaptation to different stressors.

RNAi-targeting *ATP8* provided functional evidence for its role in regulating respiration. The silencing of *ATP8* significantly reduced respiration rates, indicating its critical role in maintaining aerobic energy production. Notably, the compensatory upregulation of *COX1* was observed, suggesting the potential mitochondrial complementary mechanisms that help to stabilize respiration rates and energy homeostasis. Interestingly, the ds*ATP8*-treated insects exhibited lower respiration rates and reduced mortality rates under exposure to abamectin and β-cypermethrin, implying that *ATP8* downregulation may reduce metabolic rates, thereby decreasing toxin uptake and insecticide susceptibility. This protective effect could stem from optimized energy allocation to counteract chemical toxicity. Similar patterns have been observed in other mitochondrial genes. For instance, *NAD6* knockdown resulted in increased mortality rates, whereas the suppression of *COX1* reduced mortality rates following exposure to allyl isothiocyanate [51]. Similarly, *NAD4* silencing led to the broad downregulation of mitochondrial genes (including *NAD1*, *NAD2*,

NAD4L, *COX1*, *COX3*, *ATP6*, and *ATP8*) in a manner similar to that of the transcriptional cascade triggered by *COX3* knockdown, which further reduced respiration rates but improved cold tolerance in *C. ferrugineus* [9]. Studies on *B. dorsalis* revealed that avermectin and malathion induced *COX2* expression, and silencing *COX2* increased pesticide-induced mortality rates [11]. These findings align with the idea that metabolic suppression may be linked to toxin tolerance. Reduced energy flux could limit toxin uptake or activate survival pathways, as seen in phosphine-resistant insects and nematodes with impaired mitochondrial function [52,53].

5. Conclusions

In conclusion, the use of a portable photosynthesis system for measuring respiration rates in small-sized insects opens up new possibilities for field-based studies, enabling a better understanding of how climate change and pest control measures affect insect population dynamics. Furthermore, the comprehensive analysis of mitochondrial gene expression, coupled with functional validation through RNAi, not only enhances our understanding of the molecular mechanisms governing respiration but also identifies potential targets for the development of more effective and environmentally friendly pest control strategies.

Supplementary Materials: The following supporting information can be downloaded at https://www.mdpi.com/article/10.3390/insects16060616/s1: Table S1: Primers used in this study. Figure S1: Transcriptional patterns of mitochondrial protein-coding genes in *Acyrthosiphon pisum* during light/dark periods. Figure S2. Transcriptional patterns of mitochondrial protein-coding genes in *Acyrthosiphon pisum* during different developmental stages.

Author Contributions: Conceptualization, B.-Y.D.; methodology, B.-Y.D.; investigation, B.-Y.D., Q.-Q.X., Y.-H.Z., Y.-J.L. and Y.Z.; resources, B.-Y.D.; data curation, B.-Y.D. and Q.-Q.X.; writing—original draft preparation, B.-Y.D.; writing—review and editing, B.-Y.D. and Q.-Q.X.; visualization, B.-Y.D. and Q.-Q.X.; supervision, B.-Y.D.; project administration, B.-Y.D.; funding acquisition, B.-Y.D. All authors have read and agreed to the published version of the manuscript.

Funding: This research was funded by the National Natural Science Foundation of China, grant number 32302338, and the Natural Science Foundation of Chongqing, grant number CSTB2024NSCQ-MSX0794.

Data Availability Statement: The original contributions presented in this study are included in the article/Supplementary Material. Further inquiries can be directed to the corresponding author.

Acknowledgments: We thank the anonymous reviewers for their invaluable comments and suggestions about this manuscript.

Conflicts of Interest: The authors declare no conflicts of interest.

References

1. Westneat, M.W.; Betz, O.; Blob, R.W.; Fezzaa, K.; Cooper, W.J.; Lee, W.K. Tracheal respiration in insects visualized with synchrotron X-ray imaging. *Science* **2003**, *299*, 558–560. [CrossRef] [PubMed]
2. Contreras, H.L.; Bradley, T.J. Metabolic rate controls respiratory pattern in insects. *J. Exp. Biol.* **2009**, *212*, 424–428. [CrossRef]
3. Harrison, J.F.; Greenlee, K.J.; Verberk, W.C.E.P. Functional hypoxia in insects: Definition, assessment, and consequences for physiology, ecology, and evolution. *Annu. Rev. Entomol.* **2018**, *63*, 303–325. [CrossRef] [PubMed]
4. Hetz, S.K.; Bradley, T.J. Insects breathe discontinuously to avoid oxygen toxicity. *Nature* **2005**, *433*, 516–519. [CrossRef]
5. Lalouette, L.; Williams, C.M.; Hervant, F.; Sinclair, B.J.; Renault, D. Metabolic rate and oxidative stress in insects exposed to low temperature thermal fluctuations. *Comp. Biochem. Physiol. A-Mol. Integr. Physiol.* **2011**, *158*, 229–234. [CrossRef]
6. Contreras, H.L.; Bradley, T.J. Transitions in insect respiratory patterns are controlled by changes in metabolic rate. *J. Insect Physiol.* **2010**, *56*, 522–528. [CrossRef] [PubMed]

7. Clissold, F.J.; Simpson, S.J. Temperature, food quality and life history traits of herbivorous insects. *Curr. Opin. Insect Sci.* **2015**, *11*, 63–70. [CrossRef]
8. Verberk, W.C.E.P.; Bilton, D.T. Respiratory control in aquatic insects dictates their vulnerability to global warming. *Biol. Lett.* **2013**, *9*, 20130473. [CrossRef]
9. Yuan, G.-Q.; Chen, M.-Q.; Hou, Q.-L.; Tang, P.-A.; Chen, E.-H. Identification and functional analysis of mitochondrial protein-coding genes associated with the adaptability to cold stress of the rusty grain beetle *Cryptolestes ferrugineus*. *J. Stored Prod. Res.* **2025**, *112*, 102626. [CrossRef]
10. Nayak, M.K.; Daglish, G.J.; Phillips, T.W.; Ebert, P.R. Resistance to the fumigant phosphine and its management in insect pests of stored products: A global perspective. *Annu. Rev. Entomol.* **2020**, *65*, 333–350. [CrossRef]
11. Jiang, S.-D.; Wang, L.; Wang, L.; Sun, J.; Wang, J.J.; Wei, D.D. Mitochondrial coding genes mediate insecticide tolerance in the oriental fruit fly, *Bactrocera dorsalis* (Hendel). *Pest. Biochem. Physiol.* **2024**, *199*, 105763. [CrossRef] [PubMed]
12. Brügger, B.P.; Martínez, L.C.; Plata-Rueda, A.; Castro, B.M.d.C.e.; Soares, M.A.; Wilcken, C.F.; Carvalho, A.G.; Serrão, J.E.; Zanuncio, J.C. Bioactivity of the *Cymbopogon citratus* (Poaceae) essential oil and its terpenoid constituents on the predatory bug, *Podisus nigrispinus* (Heteroptera: Pentatomidae). *Sci. Rep.* **2019**, *9*, 8358. [CrossRef]
13. Plata-Rueda, A.; Martínez, L.C.; Santos, M.H.D.; Fernandes, F.L.; Wilcken, C.F.; Soares, M.A.; Serrão, J.E.; Zanuncio, J.C. Insecticidal activity of garlic essential oil and their constituents against the mealworm beetle, *Tenebrio molitor* Linnaeus (Coleoptera: Tenebrionidae). *Sci. Rep.* **2017**, *7*, 46406. [CrossRef]
14. Sousa, A.H.; Faroni, L.R.D.A.; Guedes, R.N.C.; Tótola, M.R.; Urruchi, W.I. Ozone as a management alternative against phosphine-resistant insect pests of stored products. *J. Stored Prod. Res.* **2008**, *44*, 379–385. [CrossRef]
15. Jiang, T.; Ma, L.; Liu, X.-Y.; Xiao, H.-J.; Zhang, W.-N. Effects of starvation on respiratory metabolism and energy metabolism in the cotton bollworm *Helicoverpa armigera* (Hübner) (Lepidoptera: Noctuidae). *J. Insect Physiol.* **2019**, *119*, 103951. [CrossRef] [PubMed]
16. Teulier, L.; Weber, J.M.; Crevier, J.; Darveau, C.A. Proline as a fuel for insect flight: Enhancing carbohydrate oxidation in hymenopterans. *Proc. R. Soc. B* **2016**, *283*, 20160333. [CrossRef]
17. Plata-Rueda, A.; Martínez, L.C.; Costa, N.C.R.; Zanuncio, J.C.; de Sena Fernandes, M.E.; Serrão, J.E.; Guedes, R.N.C.; Fernandes, F.L. Chlorantraniliprole–mediated effects on survival, walking abilities, and respiration in the coffee berry borer, *Hypothenemus hampei*. *Ecotoxicol. Environ. Saf.* **2019**, *172*, 53–58. [CrossRef] [PubMed]
18. Gao, Q.; Liu, Y.; Liu, Y.; Dai, C.; Zhang, Y.; Zhou, F.; Zhu, Y. Salicylic acid modulates the osmotic system and photosynthesis rate to enhance the drought tolerance of *Toona ciliata*. *Plants* **2023**, *12*, 4187. [CrossRef]
19. Shi, S.; Li, H.; Wang, X.; Wang, Z.; Xu, J.; He, X.; Yang, Z.a. Greater biomass production under elevated CO_2 is attributed to physiological optimality, trade-offs in nutrient allocation, and oxidative defense in drought-stressed mulberry. *Antioxidants* **2025**, *14*, 383. [CrossRef]
20. Yu, M.; Fan, Y.; Li, X.; Chen, X.; Yu, S.; Wei, S.; Li, S.; Chang, W.; Qu, C.; Li, J.; et al. *LESION MIMIC MUTANT 1* confers basal resistance to *Sclerotinia sclerotiorum* in rapeseed via a salicylic aciddependent pathway. *J. Exp. Bot.* **2023**, *74*, 5620–5634. [CrossRef]
21. Zveushe, O.K.; Sajid, S.; Dong, F.; Han, Y.; Zeng, F.; Geng, Y.; Shen, S.; Xiang, Y.; Kang, Q.; Zhang, Y.; et al. Different sex combinations of *Populus cathayana* affect soil respiration and tea litter decomposition by influencing plant growth and soil functional microbial diversity. *Plant Soil* **2023**, *490*, 631–650. [CrossRef]
22. Wang, S.; Wang, T.; Gao, L.; Du, H.; Wang, D.; Ma, M.; Rennenberg, H. Iron addition promotes mercury removal from soil by *Robinia pseudoacacia*-rhizobia symbiosis. *Tree Physiol.* **2025**, *45*, tpae166. [CrossRef] [PubMed]
23. He, S.; Li, X.; Chen, M.; Xu, X.; Zhang, W.; Chi, H.; Shao, P.; Tang, F.; Gong, T.; Guo, M.; et al. Excellent canopy structure in soybeans can improve their photosynthetic performance and increase yield. *Agriculture* **2024**, *14*, 1783. [CrossRef]
24. Zhang, K.; Zhang, F.; Li, H.; Su, Y.; Wu, Y. Stable nitrogen isotopes as an effective tool for estimating the nitrogen demand of *Broussonetia papyrifera* (L.) vent seedlings under variable nitrate concentrations. *Agronomy* **2023**, *13*, 1663. [CrossRef]
25. Kayoumu, M.; Iqbal, A.; Muhammad, N.; Li, X.; Li, L.; Wang, X.; Gui, H.; Qi, Q.; Ruan, S.; Guo, R.; et al. Phosphorus availability affects the photosynthesis and antioxidant system of contrasting Low-P-Tolerant cotton genotypes. *Antioxidants* **2023**, *12*, 466. [CrossRef]
26. Li, Y.; Ruan, S.; Li, D.; Liu, J.; Hu, Q.; Dian, Y.; Yu, Z.; Zhou, J. Photosynthetic difference of six poplar genotypes and estimation of photosynthetic capacities based on leaf hyperspectral reflectance. *For. Res.* **2024**, *4*, e037. [CrossRef]
27. Chieppa, J.; Brown, T.; Giresi, P.; Juenger, T.E.; Resco de Dios, V.; Tissue, D.T.; Aspinwall, M.J. Climate and stomatal traits drive covariation in nighttime stomatal conductance and daytime gas exchange rates in a widespread C4 grass. *New Phytol.* **2021**, *229*, 2020–2034. [CrossRef]
28. Feng, Q.; Luo, Y.; Liang, M.; Cao, Y.; Wang, L.; Liu, C.; Zhang, X.; Ren, L.; Wang, Y.; Wang, D.; et al. Rhizobacteria protective hydrogel to promote plant growth and adaption to acidic soil. *Nat. Commun.* **2025**, *16*, 1684. [CrossRef]

29. Riches, M.; Lee, D.; Farmer, D.K. Simultaneous leaf-level measurement of trace gas emissions and photosynthesis with a portable photosynthesis system. *Atmos. Meas. Tech.* **2020**, *13*, 4123–4139. [CrossRef]
30. Zhao, R.Z.; Jiang, S.; Zhang, L.; Yu, Z.B. Mitochondrial electron transport chain, ROS generation and uncoupling. *Int. J. Mol. Med.* **2019**, *44*, 3–15. [CrossRef]
31. Despabiladeras, J.B.; Bautista, M.A.M. Complete mitochondrial genome of the eggplant fruit and Shoot Borer, *Leucinodes orbonalis* Guenée (Lepidoptera: Crambidae), and comparison with other pyraloid moths. *Insects* **2024**, *15*, 220. [CrossRef] [PubMed]
32. Perkin, L.C.; Smith, T.P.L.; Oppert, B. Variants in the mitochondrial genome sequence of *Rhyzopertha dominica* (Fabricius) (Coleoptera: Bostrycidae). *Insects* **2021**, *12*, 387. [CrossRef] [PubMed]
33. Wang, X.; Zhou, S.; Wu, X.; Wei, Q.; Shang, Y.; Sun, G.; Mei, X.; Dong, Y.; Sha, W.; Zhang, H. High-altitude adaptation in vertebrates as revealed by mitochondrial genome analyses. *Ecol. Evol.* **2021**, *11*, 15077–15084. [CrossRef] [PubMed]
34. Francoso, E.; Zuntini, A.R.; Ricardo, P.C.; Santos, P.K.F.; Araujo, N.d.S.; Silva, J.P.N.; Goncalves, L.T.; Brito, R.; Gloag, R.; Taylor, B.A.; et al. Rapid evolution, rearrangements and whole mitogenome duplication in the Australian stingless bees *Tetragonula* (Hymenoptera: Apidae): A steppingstone towards understanding mitochondrial function and evolution. *Int. J. Biol. Macromol.* **2023**, *242*, 124568. [CrossRef]
35. Guan, J.-Y.; Zhang, Z.-Y.; Cao, Y.-R.; Xu, X.-D.; Storey, K.B.; Yu, D.-N.; Zhang, J.-Y. The complete mitochondrial genome of *Choroterpes* (*Euthralus*) *yixingensis* (Ephemeroptera: Leptophlebiidae) and its mitochondrial protein-coding gene expression under imidacloprid stress. *Gene* **2021**, *800*, 145833. [CrossRef]
36. Zhang, Z.-Y.; Guan, J.-Y.; Cao, Y.-R.; Dai, X.-Y.; Storey, K.B.; Yu, D.-N.; Zhang, J.-Y. Mitogenome analysis of four Lamiinae species (Coleoptera: Cerambycidae) and gene expression responses by *Monochamus alternatus* when infected with the parasitic nematode, *Bursaphelenchus mucronatus*. *Insects* **2021**, *12*, 453. [CrossRef]
37. Chen, E.-H.; Duan, J.-Y.; Song, W.; Wang, D.-X.; Tang, P.-A. RNA-seq analysis reveals mitochondrial and cuticular protein genes are associated with phosphine resistance in the rusty grain beetle (Coleoptera: Laemophloeidae). *J. Econ. Entomol.* **2021**, *114*, 440–453. [CrossRef] [PubMed]
38. Chen, E.-H.; Wei, D.; Wei, D.-D.; Yuan, G.-R.; Wang, J.-J. The effect of dietary restriction on longevity, fecundity, and antioxidant responses in the oriental fruit fly, *Bactrocera dorsalis* (Hendel) (Diptera: Tephritidae). *J. Insect Physiol.* **2013**, *59*, 1008–1016. [CrossRef]
39. Qiang, W.X.; Zhong, L.C.; Tian, X.Y.; Zhou, S. Effects of sublethal dosage of imidacloprid, abamectin and beta-cypermethrin on the development and reproduction of green of the morph of pea aphid (*Acyrthosiphon pisum*). *Acta Prataculturae Sin.* **2014**, *23*, 279–286.
40. Hellemans, J.; Mortier, G.; De Paepe, A.; Speleman, F.; Vandesompele, J. qBase relative quantification framework and software for management and automated analysis of real-time quantitative PCR data. *Genome Biol.* **2007**, *8*, R19. [CrossRef]
41. Yang, C.; Pan, H.; Liu, Y.; Zhou, X. Selection of reference genes for expression analysis using quantitative real-time PCR in the pea aphid, *Acyrthosiphon pisum* (Harris) (Hemiptera, Aphidiae). *PLoS ONE* **2014**, *9*, e110454. [CrossRef] [PubMed]
42. Lebenzon, J.E.; Overgaard, J.; Jørgensen, L.B. Chilled, starved or frozen: Insect mitochondrial adaptations to overcome the cold. *Curr. Opin. Insect Sci.* **2023**, *58*, 101076. [CrossRef] [PubMed]
43. Haddi, K.; Mendes, M.V.; Barcellos, M.S.; Lino-Neto, J.; Freitas, H.L.; Guedes, R.N.C.; Oliveira, E.E. Sexual success after stress? Imidacloprid-induced hormesis in males of the neotropical stink bug *Euschistus heros*. *PLoS ONE* **2016**, *11*, e0156616. [CrossRef] [PubMed]
44. Plata-Rueda, A.; Rolim, G.D.S.; Wilcken, C.F.; Zanuncio, J.C.; Serrão, J.E.; Martínez, L.C. Acute toxicity and sublethal effects of lemongrass essential oil and their components against the Granary weevil, *Sitophilus granarius*. *Insects* **2020**, *11*, 379. [CrossRef]
45. Plata-Rueda, A.; Martínez, L.C.; Rolim, G.d.S.; Coelho, R.P.; Santos, M.H.; Tavares, W.d.S.; Zanuncio, J.C.; Serrão, J.E. Insecticidal and repellent activities of *Cymbopogon citratus* (Poaceae) essential oil and its terpenoids (citral and geranyl acetate) against *Ulomoides dermestoides*. *Crop Prot.* **2020**, *137*, 105299. [CrossRef]
46. Plata-Rueda, A.; Campos, J.M.; da Silva Rolim, G.; Martínez, L.C.; Dos Santos, M.H.; Fernandes, F.L.; Serrão, J.E.; Zanuncio, J.C. Terpenoid constituents of cinnamon and clove essential oils cause toxic effects and behavior repellency response on granary weevil, *Sitophilus granarius*. *Ecotoxicol. Environ. Saf.* **2018**, *156*, 263–270. [CrossRef]
47. Fiaz, M.; Martínez, L.C.; Costa, M.d.S.; Cossolin, J.F.S.; Plata-Rueda, A.; Gonçalves, W.G.; Sant'Ana, A.E.G.; Zanuncio, J.C.; Serrão, J.E. Squamocin induce histological and ultrastructural changes in the midgut cells of *Anticarsia gemmatalis* (Lepidoptera: Noctuidae). *Ecotoxicol. Environ. Saf.* **2018**, *156*, 1–8. [CrossRef]
48. Fiaz, M.; Martínez, L.C.; Plata-Rueda, A.; Gonçalves, W.G.; Shareef, M.; Zanuncio, J.C.; Serrão, J.E. Toxicological and morphological effects of tebufenozide on *Anticarsia gemmatalis* (Lepidoptera: Noctuidae) larvae. *Chemosphere* **2018**, *212*, 337–345. [CrossRef]

49. Lebenzon, J.E.; Denezis, P.W.; Mohammad, L.; Mathers, K.E.; Turnbull, K.F.; Staples, J.F.; Sinclair, B.J. Reversible mitophagy drives metabolic suppression in diapausing beetles. *Proc. Natl. Acad. Sci. USA* **2022**, *119*, e2201089119. [CrossRef]
50. Ding, Y.-R.; Van, Z.-T.; Si, F.-L.; Li, X.-D.; Mao, Q.-M.; Asghar, S.; Chen, B. Mitochondrial genes associated with pyrethroid resistance revealed by mitochondrial genome and transcriptome analyses in the malaria vector *Anopheles sinensis* (Diptera: Culicidae). *Pest Manag. Sci.* **2020**, *76*, 769–778. [CrossRef]
51. Sun, Y.; Jiang, Y.; Wu, H.; Xu, N.; Ma, Z.; Zhang, C. Function of four mitochondrial genes in fumigation lethal mechanisms of Allyl Isothiocyanate against *Sitophilus zeamais* adults. *Pest Biochem. Physiol.* **2021**, *179*, 104947. [CrossRef] [PubMed]
52. Steven, Z.; Jujiao, K.; Paul, E. Mitochondrial modulation of phosphine toxicity and resistance in *Caenorhabditis elegans*. *Toxicol. Sci.* **2008**, *102*, 179–186.
53. Pimentel, M.A.G.; Faroni, L.R.D.A.; Tótola, M.R.; Guedes, R.N.C. Phosphine resistance, respiration rate and fitness consequences in stored-product insects. *Pest Manag. Sci.* **2007**, *63*, 876–881. [CrossRef] [PubMed]

Disclaimer/Publisher's Note: The statements, opinions and data contained in all publications are solely those of the individual author(s) and contributor(s) and not of MDPI and/or the editor(s). MDPI and/or the editor(s) disclaim responsibility for any injury to people or property resulting from any ideas, methods, instructions or products referred to in the content.

insects

MDPI

Article

Proteomic Responses of the Springtail *Folsomia candida* to Drought

Yang Wang [1], Stine Slotsbo [1], Steffen Y. Bak [2], Christopher J. Martyniuk [3] and Martin Holmstrup [1,*]

[1] Department of Ecoscience, Aarhus University, C.F. Møllers Allé 4, 8000 Aarhus, Denmark; wybiology351@gmail.com (Y.W.); stsl@ecos.au.dk (S.S.)
[2] International Flavors & Fragrances Inc., Edwin Rahrs Vej 38, 8220 Brabrand, Denmark; steffen.yde.bak@iff.com
[3] Center for Environmental and Human Toxicology, University of Florida, 2187 Mowry Road, Gainesville, FL 32611, USA; cmartyn@ufl.edu
* Correspondence: martin.holmstrup@ecos.au.dk

Simple Summary: Springtails are small insect-like animals living in the soil almost all over the world. Most springtails are less than 5 mm in length, yet they can have great influence on the fertility of soil because they occur in very high numbers, sometimes in hundreds of thousands per square meter. These animals are adapted to life in moist soil and in many respects have a physiology resembling freshwater animals. Here, we explore the functional proteins in springtails when they are stressed by drought conditions. We find that proteins important for growth and reproduction are becoming less abundant in drought-exposed animals, but on the other hand, we see no strong indication of proteins related to cellular stress handling being more abundant. This suggests that springtails will stop growing and egg laying when they are experiencing drought but will be able to survive until soils become moist again.

Abstract: Springtails are adapted to life in the pore space of soil, where humidity in moist soil is close to saturation. Drought is the most important limiting factor for springtails; however, their molecular and physiological adaptations to low humidity are not well understood. The present study explored the global proteomic drought response of the springtail, *Folsomia candida* (Isotomidae, Collembola). In relatively dry soil (−360 kPa), adult springtails initially lost body water but re-established the normal body water content over the following two weeks. Nano LC–MS/MS analysis identified a total of 1729 unique proteins. Proteomic analysis and pathway enrichment found that the proteome generally did not show a dramatic induction of proteins in response to drought stress. After an initial down-regulation of pathways related to metabolism and growth, these pathways gradually returned to the same levels as in moist soil. Other pathways such as the cytoskeleton pathway, which is important in cell proliferation and differentiation, were predominantly down-regulated throughout the experiment in drought-exposed animals, which correlated with essentially no somatic growth of the springtails in dry soil. This study facilitates the understanding of the consequences of climate change on soil functioning and fertility.

Keywords: Collembola; desiccation; protein regulation; pathway analysis; metabolism

1. Introduction

Springtails are small arthropods living in the soil and leaf litter of most regions of the world [1]. These animals mainly feed on fungal hyphae and bacteria and, to some

extent, on dead organic matter and fine roots [2–4]. Through their feeding habits and high population numbers, springtails can be important drivers of decomposition processes and nutrient cycling in the soil [5–7].

Many springtail species are adapted to life in the soil pore space where humidity is close to saturation most of the time [8]. For this reason, low soil humidity may be an important limiting factor for springtails as well as for many other soil invertebrates [9,10]. The ongoing climatic changes are predicted to escalate the occurrence of summer droughts and generally cause decreasing soil moisture levels on a wide geographical scale [11,12]. Decreasing soil moisture will negatively impact the population dynamics and feeding activities of soil animals, which in turn erodes important decomposition processes in the soil.

The growth, development, and reproduction of springtails are highly dependent on sufficient humidity of the soil, and most species have optimal conditions when soils are close to the field capacity where free water is readily available for these animals [13–15]. Despite the apparent dependence on high soil humidity for optimal performance, springtails can osmoregulate and endure extreme drought in the soil by accumulation of compatible osmolytes such as sugars and sugar alcohols in body fluids [16–18]. This enables them to absorb water vapor from pore air and maintain water balance at soil humidities even below the wilting point of plants (−1.5 MPa) and survive drought for weeks [19–21].

Folsomia candida Willem (a soil dwelling springtail) is capable of water vapor absorption and survives extreme drought conditions in soil with water potentials equivalent to −6 MPa [18]. Recently, we have shown that *F. candida*, despite its remarkable drought resistance, is sensitive to subtle decreases in soil water potential [15]. Thus, reproduction was completely paused when soil water potential decreased from −2 kPa (~field capacity) to −20 kPa, and body growth ceased at −200 kPa. This observation was surprising since such drought levels should not cause evaporative water loss. In fact, the osmotic pressure of body fluids is equivalent to about −900 kPa, creating a water vapor gradient and a net influx of water from the soil and into the body fluids of the animal at these soil water potentials [21].

Currently, we do not know why common somatic traits such as growth and reproduction are ceasing to occur when water balance is, seemingly, not physiologically challenging. To address this question, we employed untargeted proteomic analysis of springtails exposed to moderately dry soil compared to animals subjected to optimal moisture conditions. When the animals are exposed to such environmental contrasts, changes in active peptides, proteins, enzymes and specific pathways can provide critical pieces of evidence for understanding dynamic and real-time responses to realistic drought conditions. Gene expression studies have previously provided some insight into the molecular mechanisms underlying tolerance of severe desiccation stress of springtails [22,23], but very little is known of the proteomic responses to drought [24]. The sequenced genome of *F. candida* provides abundant genetic information in public databases [25], facilitating protein identification and responsive pathway enrichments. Physiological responses can be dynamic over time, and therefore, we expected that the proteomic responses to drought during a 20-day period would capture proteomic responses as much as possible. Transcriptional responses of *F. candida* to drought and other environmental stressors usually take place almost immediately (hours), whereas proteomic and physiological responses often occur on a longer time scale (days) [23,26]. The present study aimed to identify candidate pathways to increase our understanding of the dynamic and real-time responses to realistic drought conditions in *F. candida* as a representative of soil dwelling springtails. We hypothesized that pathways involved in the accumulation of sugars and other drought-protective osmolytes would be

up-regulated in *F. candida* as would be the case with general stress-related pathways (e.g., antioxidant defense mechanisms). In contrast, we expected pathways related to cellular growth and reproduction to be suppressed.

2. Materials and Methods

2.1. Test Animals

The parthenogenetic *Folsomia candida* (Collembola, Isotomidae, reference genome: ASM221717v1) originated from a laboratory culture kept at 20 °C (±1 °C) with a 12:12 h light–dark cycle. The test animals were cultured in Petri dishes with a moistened floor of plaster of Paris mixed with charcoal (8:1 *w*/*w*). The animals were fed dried baker's yeast ad libitum. For the experiment, the springtails were age-synchronized to reduce variation, and only medium-sized adults (25 ± 3 days old) having a dry mass of ca. 40 µg were used for our study.

2.2. Test Soil

Soil from the top 0–20 cm layer was collected in Foulum Experimental Station, Department of Agroecology, Aarhus University, Denmark. The field from which test soil was sampled had been organically cultivated without pesticide application for more than 20 years. This soil was a loamy sand consisting of 32% coarse sand (>200 µm), 48% fine sand (20–200 µm), 9% silt (2–20 µm), 7% clay (<2 µm), and 4% organic matter (determined by loss-on-ignition), and it had a pH of 5.9. The total organic carbon content was 1.6% [15]. The soil was thoroughly homogenized, dried at 105 °C for 24 h, and sieved through a 2 mm mesh prior to use. Soil water content was adjusted to 6% (mild drought) and 20% (control) of dry mass by adding appropriate volumes of deionized water to the soil and mixing it thoroughly. None of these soil water levels cause mortality [15]. The actual soil water contents of test soils were determined by subtracting the soil mass before and after drying at 105 °C for 24 h and showed that the measured water content was 20.3 ± 0.4 g g^{-1} dry mass. Based on a previously published retention curve, the soil water potential of the test soils was −2.4 kPa (control) and −360 kPa (mild drought), respectively [15]. These two levels of soil water potential represent a realistic moisture range in European soils [8,20].

2.3. Drought Exposure Experiment

Springtails were exposed to the two soil humidities in 50 mL glass jars containing 30 g of soil. Thirty adult animals were added to each jar using five jars (replicates) for each soil humidity level and sampling time. A total of 20 mg of dried baker's yeast was sprinkled on the surface of the soil as food source for the springtails, and the jars were closed with tightly fitting screw caps. During the experiment, water evaporation from the beakers was negligible because the lids were only briefly opened for aeration every 3 days, and 20 mg of dried yeast was added after 7 and 14 days. In total, 55 jars with animals were made for each soil humidity (11 sampling times × 5 replicates). Jars with springtails were destructively sampled after 1, 2, 3, 5, 8, 10, 14, 15, 16, 17, and 20 days. Previous experiments have shown that physiological responses of springtails to drought are well captured within 1–3 weeks of exposure [15,21]. On each sampling day, the soil of a replicate was gently spread out in a tray, and animals were recovered using an aspirator. Twenty animals were sampled for proteomic analysis, placed in 2 mL centrifugation tubes, and immediately stored at −80 °C until protein extraction and further analysis. The remaining ten animals in each replicate were sampled for measurement of body mass and body water content.

2.4. Body Mass and Body Water Content of Springtails

Body mass and body water content were measured at all sampling times in 5 replicates. The total fresh mass of ten animals of each replicate was determined using a Sartorius Micro SC 2 balance accurate to ±1 µg (Sartorius AG, Goettingen, Germany). After measuring the fresh mass, the dry mass of adults was obtained by weighing after freeze-drying for 24 h. The average fresh and dry mass per animal was calculated based on the number of adults, and the body water content was calculated as mg water mg^{-1} dry mass. The effects of soil humidity and time on the body mass and body water content of springtails were analyzed using linear regression models. Each model included day, soil humidity (control or drought), and their interaction (day × soil humidity) as predictors. Model assumptions were verified through visual inspection of residuals, and no transformations were required. Analyses were performed in R Studio 2023.12.1 Build 402.

2.5. Sample Preparation for Proteomics

Proteomic analysis of springtails was performed on days 1, 2, 5, 14, and 20, with 3 replicates per sampling time. Total proteins were extracted from springtails using 250 µL lysis buffer (5% sodium dodecyl sulfate (SDS), 100 mM triethylammonium bicarbonate (TEAB), and protease inhibitor (complete, EDTA-free, Roche, Basel, Switzerland)), followed by heating (95 °C for 10 min) and mixing at 900 rpm. Subsequently, homogenization was performed on a Precellys Evolution (Bertin technologies, Cergy-Pontoise, France) using 6000 rpm and a cycle scheme with 20 s ON/30 s OFF in 5 cycles. The homogenized samples were sonicated on a Biorupter Pico (Diagenode, Seraing, Belgium) water bath ultra sonicator at 4 °C for 10 min, followed by centrifugation at 14,000× *g*. Supernatants from each sample were used for protein-concentration measurement by a detergent-compatible Bradford assay (Pierce™ Detergent-Compatible Bradford Assay Kit, Thermo Fischer, Waltham, MA, USA). A volume equal to 100 µg of proteins from each springtail sample was used for protein digestion. Protein digestion was performed using the S-Trap™ digestion protocol (ProtiFi, Plainsboro, NJ, USA) but with a few modifications. Trypsin digestion was prolonged to overnight at 37 °C with a trypsin-to-protein ratio of 1:62.5 [27]. Peptides were dried down using a speed vacuum instrument at 35 °C. Dried peptides were resuspended in 50 µL 0.1% trifluoroacetic acid (TFA). Peptide concentrations were estimated using a peptide specific BCA kit following the manufacturer's protocol (Pierce™ Quantitative Peptide Assays, Thermo Scientific™). Based on peptide concentrations, peptide samples were adjusted to reach the same concentrations. A QC sample was prepared by mixing 10 µL from each sample. All samples were transferred to LC vials and saved at 5 °C until analysis.

2.6. Data Acquisition

LC-MS/MS analysis was carried out using an UltiMate™ 3000 RSLCnano System (Thermo Fisher Scientific, Waltham, MA, USA) interfaced to a Q Exactive™ HF Hybrid Quadrupole-Orbitrap™ Mass Spectrometer (Thermo Fisher Scientific, Waltham, MA, USA) as previously described by Kumar et al. [28]. The dissolved peptide samples were trapped by a 20 mm nano Viper Trap Column (Acclaim™ PepMap™ 100 C18, 3 µm particle size and an inner diameter of 0.075 mm) that was connected to a 400 mm analytical column (PepSep, ReproSil 3 µm C18 beads, pore diameter 120 Å, and an inner diameter of 0.075 mm). Separation was performed at a flow rate of 300 nL min^{-1} through a gradient method of a 40 min gradient of 0–41% Solvent B (100% ACN, 0.1% FA) and eluted into the Nanospray Flex Ion Source (Thermo Scientific™) interfaced to the MS instrument. Data was acquired on the Q Exactive HF instrument in data-dependent MS/MS mode using

HCD fragmentation. The peptide masses were measured in the MS scan by the Orbitrap with a resolution of 60,000 (FWHM) at m/z 200. The top 12 most intense ions were selected and fragmented in the quadrupole using a 1.2 Da width isolation window. MS/MS spectra were recorded in the Orbitrap with a resolution of 30,000 (FWHM) at m/z 200 followed by dynamic exclusion including an exclusion duration of 30 s and an exclusion mass tolerance width of $\pm$10 ppm relative to masses on the list. Sample acquisition was designed with an initiation block of five injections of the QC sample followed with continuous blocks of five samples and one QC sample. All samples were randomly distributed over the blocks to avoid the change in block effects.

2.7. Data Analysis

The raw data was processed (smoothing, background subtraction, and centroiding) by Proteome Discoverer (Version 2.2, Thermo Scientific^{TM}) and submitted to database searching against a UniProt *Folsomia candida* database containing 30,219 sequences using an in-house Mascot server. Trypsin was set as protease with a maximum of two missed cleavages acceptable. S-Carbamidomethyl cysteine was defined as a fixed modification and oxidation of methionine as variable modification. The MS/MS results were searched with a peptide ion mass tolerance of $\pm$10 ppm and a fragment ion mass tolerance of $\pm$0.8 Da. A percolator was used for calculating the false discovery rate (FDR), and only peptides that were identified as rank 1 peptides and with a confidence value of 1% ($q < 0.01$) were considered for further analysis [29].

Data analyses were performed in Expressionist v.12.0.9 (Genedata). Imported raw files were noise-filtered using a chemical noise subtraction. Chromatograms were retention-time-aligned by a pairwise alignment, filtered, and smoothed before peak detection, based on volumes. Detected peaks were subjected to isotopic clustering, and singletons were filtered out. Peak clusters were matched to the identifications from the Proteome Discoverer. Peptides were grouped based on protein identifications. Proteins were quantified based on the three most intense peptides Hi-3 [30]. Quantitative results were exported into Analyst v.12.0.9 (Genedata) for normalization, statistical filtering, and testing. Quantitative abundances were normalized by an intensity drift normalization, where intensities from QC samples were used to correct for drifting in the nano LC-MS/MS performance.

2.8. Differential Abundance Analysis and Pathway Enrichment of Proteomics Data

The differential abundance of proteins in the drought group compared to the control group was normalized and analyzed in Rstudio (4.2.2) with the EdgeR package [31]. Abundance ratios ≥ 1.5 were classified as up-regulated abundances, while those ≤ -1.5 were classified as down-regulated abundances [32]. Abundance ratios between -1.5 and 1.5 (excluding equal to -1.5 and ≤ -1.5) were classified as stable. The fold change (FC) equated to the $\log_2$ of abundance ratios ($\log_2$FC ≤ -0.585 or ≥ 0.585), which was set as a cutoff for the up-regulated and down-regulated expressions of proteins, and the FC values were employed for all differential expressions in proteins in this study. The significant proteins with differential FC were based on a false discovery rate (FDR < 0.05) at each time point. The pathway enrichment approach used the package clusterProfiler 4.0 in R [33], using q value < 0.1 to correct the adjusted p values (FDR < 0.05). The top pathways and molecular events were sorted using the criteria of FDR (FDR < 0.05).

2.9. Heatmap Analysis and Two-Way ANOVA Analysis

MetaboAnalyst 6.0 was used to analyze protein abundance data in each treatment over time. For each biological replicate, relative protein abundance data were normalized

using Quantile normalization, followed by Log transformation (base 10). Auto-scaling (mean-centered divided by the standard deviation of each variable) was then conducted to normalize data. Clustering was generated for the samples using mean centering and the Fast Ward algorithm (distance measure Euclidean) based on results of a two-way ANOVA with soil moisture level and sampling time as factors.

3. Results

3.1. Growth and Body Water Content

Springtails exposed to control soil humidity significantly increased their dry body mass by three times during the 20-day experiment (linear regression, $p < 0.001$, Figure 1). In contrast, animals exposed to drought did not grow, and their dry mass remained stable or slightly declined over time. This was confirmed by a significant negative interaction between day and treatment in the linear model ($p < 0.001$), indicating that drought reduced growth compared to control animals. No mortality occurred during the experiment.

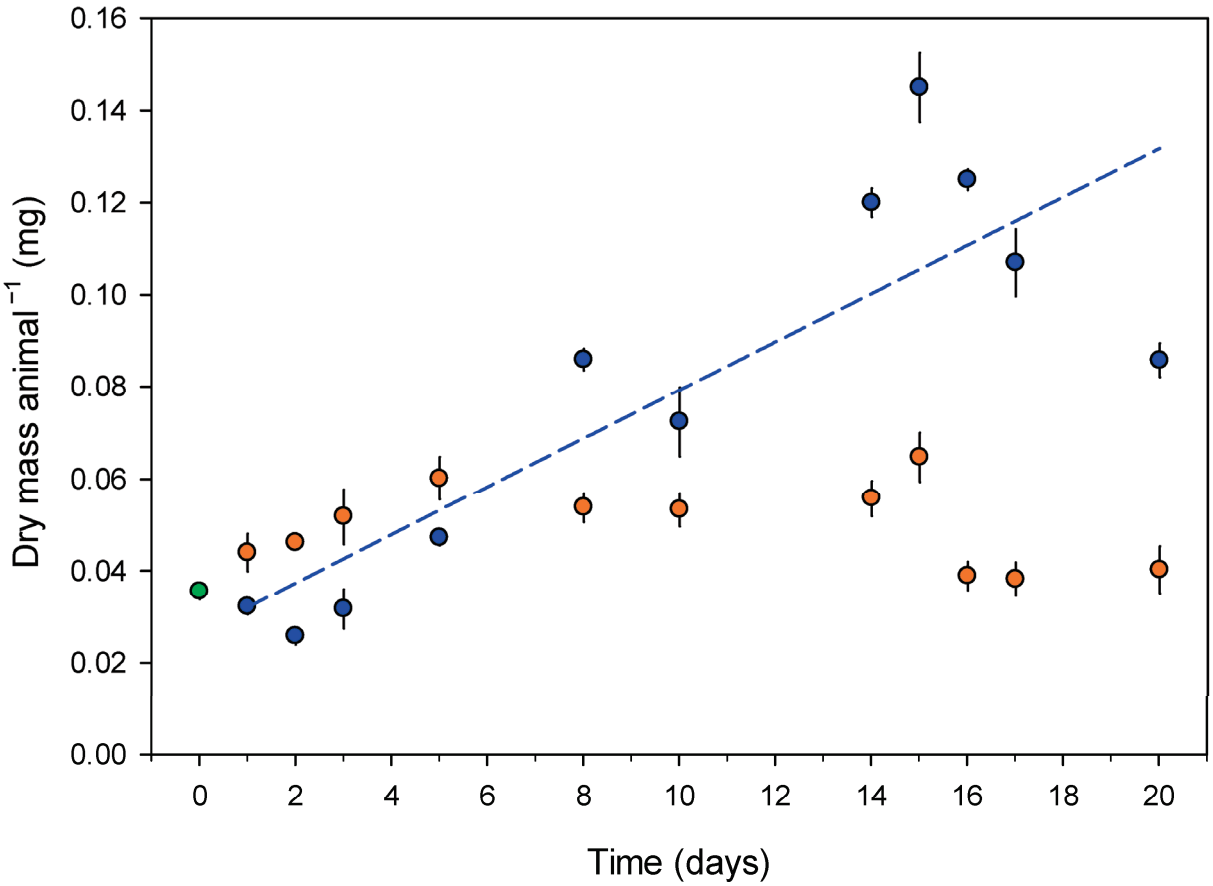


Figure 1. The body dry mass (mean ± SE, n = 5) of *Folsomia candida* throughout the experiment. The green dot indicates the body dry mass at the start of the experiment. Blue points and the line represent animals exposed to control soil humidity (20% of dry mass; −2.4 kPa). Orange points represent animals exposed to dry soil treatment (6% of dry mass; −360 kPa). The body dry mass increased significantly over time in the control treatment ($p < 0.001$).

In the control soil, springtail body water content remained relatively stable, with a slight but non-significant increase over time (linear regression, $p = 0.087$; Figure 2). Springtails exposed to drought had significantly lower water content on day 1 compared to control animals ($p < 0.001$). However, a significant positive interaction between day

and drought treatment ($p = 0.0014$) indicated that the water content in drought-exposed springtails increased more rapidly over time, eventually reaching levels similar to those of the control group by the end of the experiment.

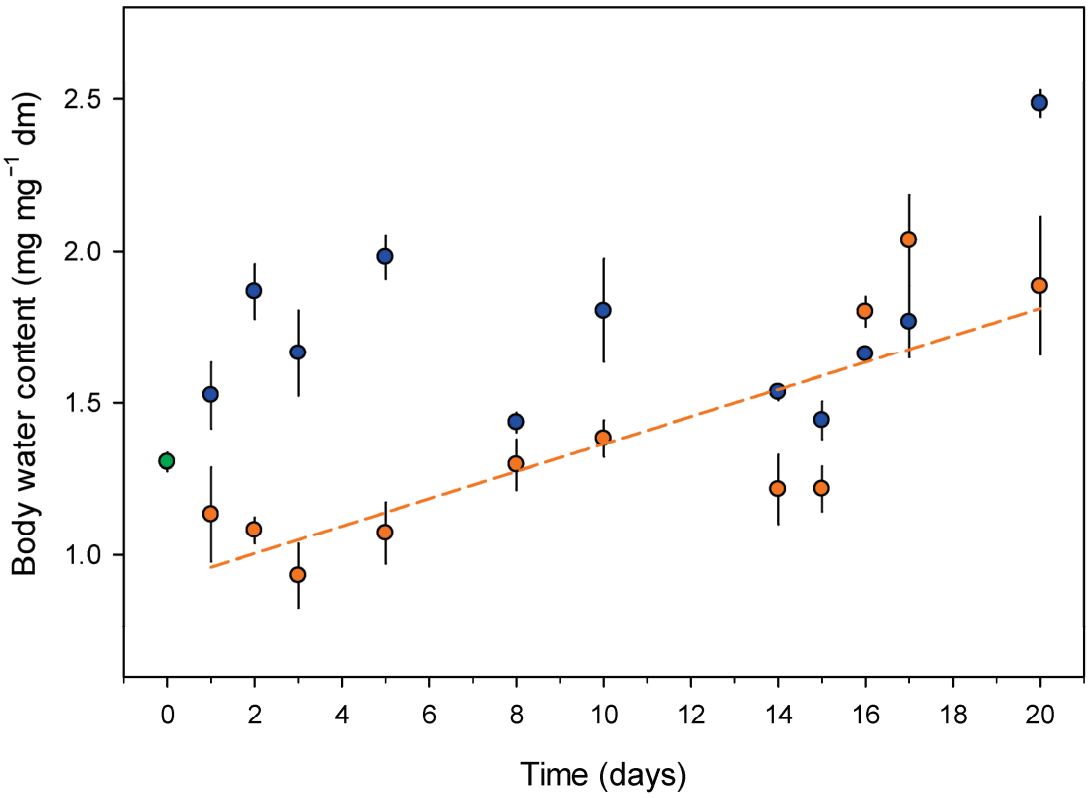


Figure 2. The body water content (mean ± SE, n = 5) of *Folsomia candida* throughout the experiment. The green dot indicates the initial body water content at the start of the experiment. Blue points represent animals exposed to control soil humidity (20% of dry mass; −2.4 kPa), while orange points and the line represent animals exposed to dry soil conditions (6% of dry mass; −360 kPa). Springtails exposed to dry soil initially had lower water content but increased water content more rapidly over time compared to the control group.

3.2. Proteomics

The complete dataset consisted of a total of 115 LC-MS/MS runs and was used in the protein identification and quantification workflow. In total, we identified and quantified 2315 proteins, and across all 115 runs, we had an average of 94.6% of total proteins found, providing an almost complete data matrix. After filtering to optimize the downstream analysis, a total of 1729 proteins (equivalent to ca. 75% of the identified and quantified proteins) in a clean dataset were used for further analysis. We examined the distribution of the abundances and qualities of identified proteins (Supplementary Figure S1). In the heatmap, the changes in all protein abundances have been shown with all replicates at both levels of soil water content (Figure 3). The trends of changes in protein abundances have been mainly divided into two clusters, including a dominant down-to-up trend from day 1 to 14 and, conversely, a dominant up-to-down trend from day 1 to 14 across both SWC groups (Figure 3). Among the two clusters, the protein abundances in the drought group show major responses to drought stress, including down-regulating and up-regulating proteins, compared to the control group on day 20 (Figure 3). A total of 42 proteins were significantly impacted by the factor of soil water content and, twice as many as that, 91 proteins were significantly impacted by the interaction effect of soil water content

and duration of drought exposure (Supplementary Figure S2), suggesting the proteomic responses of *F. candida* attributable to soil water content levels and exposure duration.

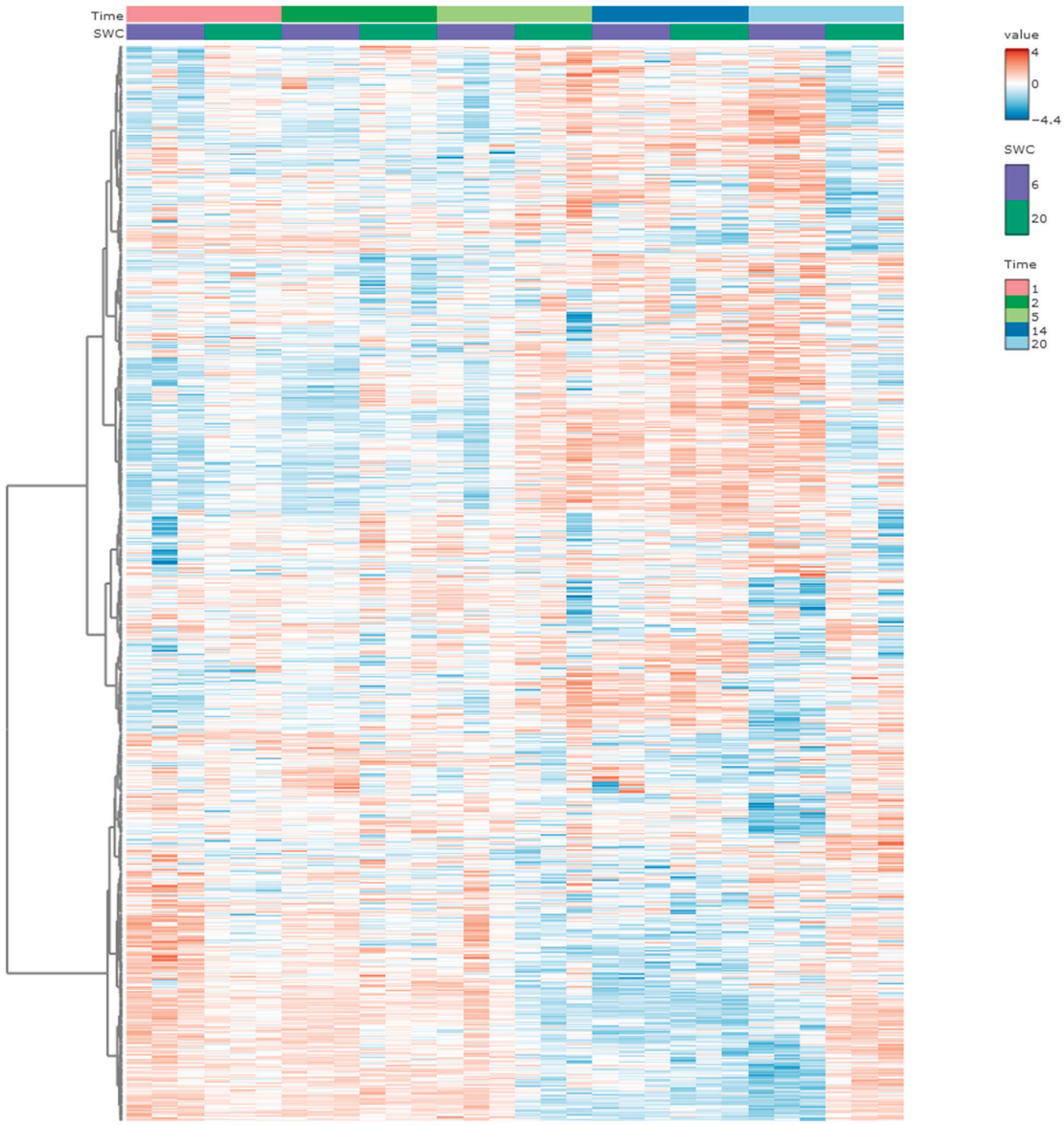


Figure 3. Heatmap of proteomic responses to the two soil water contents in time series. The time bar shows the days 1, 2, 5, 14, and 20 days in 5 different colors. SWC represents soil water content with two levels of 6 and 20 (percent of dry weight) using two colors. The value shows the range of fold changes of proteins in each replicate (down-regulated in blue, up-regulated in red). Each column in the heatmap is one biological replicate. n = three replicates for each treatment at each time point.

Compared to the control SWC on each day, we identified proteins with significantly different abundances in the drought group (Figure 4, Supplementary Dataset 1). In general, we observed a higher proportion of down-regulated than up-regulated proteins in the drought-exposed animals (Figure 4). On the last day of the drought experiment, day 20, we observed a major response in the springtail proteome for the drought group, involving 366 up-regulated proteins and 327 down-regulated proteins (Figure 4).

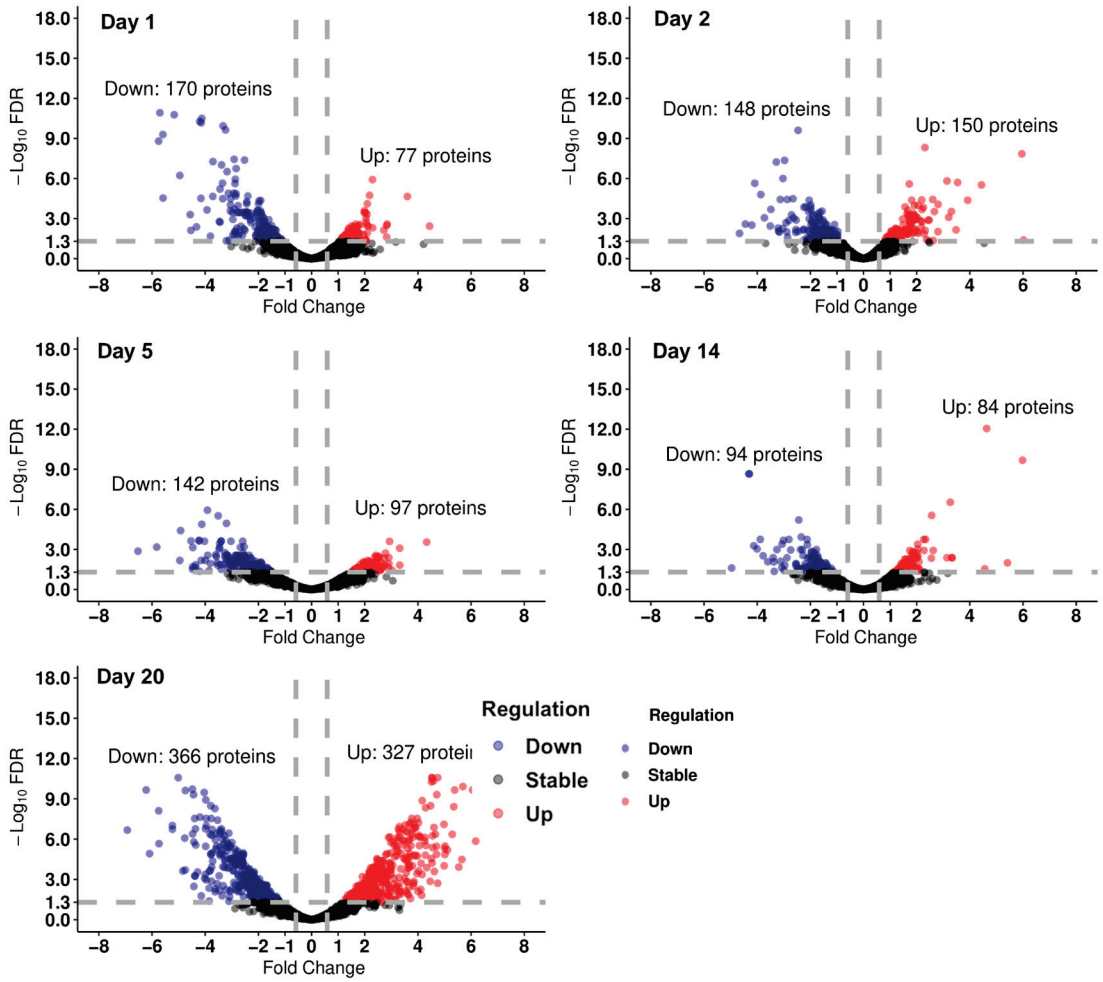


Figure 4. Volcano plots for differential proteins of drought group in time series. The five plots show differential abundances of proteins on days 1, 2, 5, 14, and 20, respectively. The criteria for fold change of proteins range less than $\log_2(-1.5) = -0.585$ and greater than $\log_2(1.5) = 0.585$ (left side of the left vertical dashed line and right side of the right vertical dashed line), and the criteria for $-\log10$ FDR is 1.3 on the *y*-axis (equal and above the horizontal dashed line). The blue dots are down-regulated proteins with criteria (fold change ≤ -0.585, FDR < 0.05) and the red dots are up-regulated proteins with criteria (fold change ≥ 0.585, FDR < 0.05). The black dots are proteins that do not change (FDR > 0.05).

Among the most notable drought-responsive proteins, we identified two types of peritrophin and four types of chitinases in the proteomic data of *F. candida* (Supplementary Dataset 1), which was probably related to the cessation of growth in dry soil.

Vitellogenin proteins, a family of glycolipoproteins that are precursors to the egg yolk proteins found in maturing eggs, were also responsive to soil moisture and down-regulated in dry soil (Supplementary Dataset 1).

We identified four heat shock proteins (HSPs) in this study, but no clear pattern occurred pointing towards a general stress response prompted by exposure to dry soil (Supplementary Dataset 1).

The identified proteins were mainly distributed among 31 pathways out of 119 known for *F. candida* in the KEGG database (Supplementary Dataset 2). In particular, responsive pathways were significantly enriched under drought stress at different time points (Figure 5, FDR < 0.05, Supplementary Dataset 3). Six pathways initially decreased (day 1 to 5) and then significantly increased up to more than five times higher than in controls from then until

day 20 (Figure 5), including glycolysis/gluconeogenesis from −0.16 to 1.4 fold changes (FDR < 0.01), TCA cycle from 0.2 to 1.9 fold changes (FDR < 0.01), pentose phosphate pathway from −0.3 to 1.7 fold changes (FDR < 0.01), butanoate metabolism from −0.4 to 1.7 fold changes (FDR < 0.01), fatty acid degradation from −0.3 to 1.2 fold changes (FDR < 0.01), and amino acid metabolisms from 0.07 to 0.94 fold change (FDR < 0.01). Additionally, the cytoskeleton pathway slightly changed from −0.58 to 0.01 fold change (FDR < 0.01) (Figure 5). Detoxification pathways were, in general, down-regulated in the beginning of the drought exposure but significantly raised at day 20 (FDR < 0.01). However, Glutathione S-transferase, Glutathione S-transferase theta-1, and Glutathione S-transferase 5—enzymes which are involved in Glutathione metabolism for detoxification and oxidative stress elimination—showed significantly increased fold changes of 2.1, 4.7, and 2.5, respectively, under drought stress on days 2, 14, and 20 (Supplementary Dataset 3).

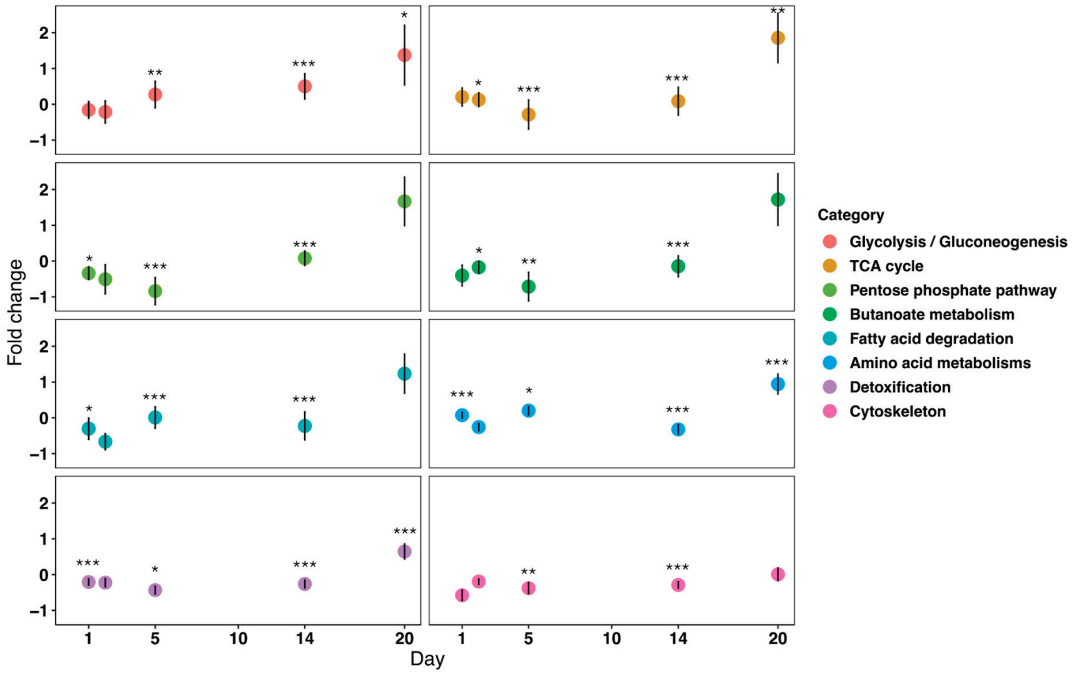


Figure 5. Changes in metabolic pathways in *Folsomia candida* under drought stress from day 1 to 20 with 8 metabolic pathways shown in different colors on days 1, 2, 5, 14, and 20. Each dot shows mean values of the pathway fold change each day. Black bars are standard deviations for fold change derived from differentially abundant proteins measured in each pathway (minimum 7 up to 157 proteins in a pathway). The asterisks represent significant fold changes in a pathway, compared to the control on specific days ("*" for $p < 0.05$, "**" for $p < 0.01$, "***" for $p < 0.001$).

In the Glycolysis/Gluconeogenesis and the TCA cycle, a dozen key enzymes were identified and enriched, and their fold changes were impacted by drought and/or the interaction effect of drought and time (Figure 4 and Supplementary Dataset 4). For example, there was an interaction effect of drought and time on the rate-limiting enzyme Fructose-bisphosphate aldolase (FBA), which was significantly up-regulated from −2.3 to 4.5 fold changes from day 2 to 20 (FDR < 0.01), but not by either drought or time (FDR > 0.05). Moreover, another interaction effect of drought and time on aldehyde dehydrogenase (ALDH) was detected, where the fold change decreased from 1.6 to −2.3 from day 5 to 20 (FDR < 0.01), suggesting probably ethanol accumulated due to the up-regulated alcohol dehydrogenase (ADH), instead of acetate (Figure 4). Although we did not detect more

interaction effects on other enzymes in glycolysis, their changes are important to the sugar accumulations at low soil moisture.

Enzymes for the metabolism of long-chain fatty acids were detected (Figure 6). Most were up-regulated in the drought group compared to the control group (Supplementary Dataset 4). An interaction effect of drought and exposure time on the trifunctional enzyme beta subunit (TP-beta) showed that the fold changes in TP-beta increased from −1.5 to 3.6 from day 2 to 20 (FDR < 0.01), along with effects by drought or/and exposure time (FDR < 0.01). Medium-chain specific acyl-CoA dehydrogenase increased from −1.4 to 3.6 with the effect of exposure time from day 1 to 20 (FDR < 0.05).

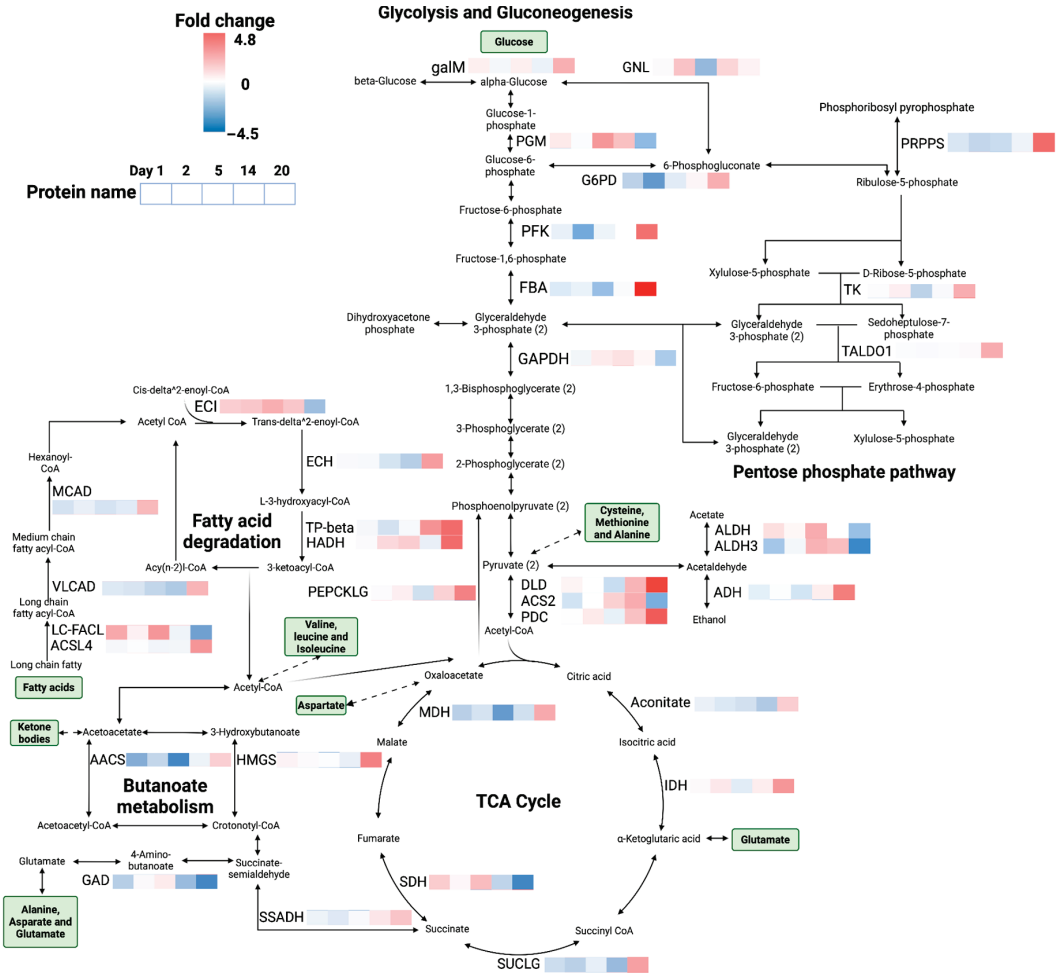


Figure 6. Responsive pathways of *Folsomia candida* exposed to drought. Five essential pathways in this network are shown, including glycolysis/gluconeogenesis, TCA cycle, pentose phosphate pathway, butanoate metabolism, and fatty acid degradation. The five horizontally connected squares next to the protein name represent days 1, 2, 5, 14, and 20, respectively, and different colors in each square show the fold changes of up-regulated or down-regulated proteins in the pathways on each day, ranging from blue to red (−4.5 to 4.5). The green boxes indicate the names of carbohydrates, amino acids, and sugars in the pathways. Unidirectional and bidirectional arrows represent the steps as irreversible or reversible, respectively. The dashed arrows represent multiple steps in these biochemical processes.

We detected interaction effects of drought and exposure time for enzymes in amino acid metabolisms in this study (Figure 6 and Supplementary Dataset 4). For example, S-methyl-5′-thioadenosine phosphorylase (MTAP) in cysteine and methionine biosynthesis increased from −4.2 to 1.1 fold changes with an effect from drought stress (FDR < 0.05)

and an interaction effect of drought and time from day 1 to 20 (FDR < 0.01). Amidophosphoribosyl transferase (PPAT) increased from −1.8 to 2.4 fold changes with an interaction effect of drought and time from day 1 to 20 (FDR < 0.05). More interaction effects of drought and time were detected in the amino acid metabolism, playing important roles in other metabolic pathways, such as Acetoacetyl-CoA synthetase (AACS) in butanoate metabolism that increased from −2.4 to 1.5 fold changes (FDR < 0.01), also impacted by drought (FDR < 0.01) and exposure time (FDR < 0.01), and TP-beta in fatty acid degradation as well.

In detoxification pathways, we mainly identified enzymes in Glutathione metabolism (Supplementary Dataset 4). There was an interaction effect of drought and exposure time from day 1 to 20 on Glutathione S-transferase theta-1 (GSTT1), which increased from −2.8 to 4.7 fold changes (FDR < 0.01). Glutathione S-transferase 1, isoform D (GSTD1), was also significantly impacted by drought and the interaction effect, which increased from −2.1 fold changes on day 1 to 0.3 on day 14 (no data on day 20). Moreover, Gamma-glutamyltranspeptidase 1(GGT) was down-regulated by −1.9 on day 14 and −1.8 on day 20. Glutathione S-transferase Mu 1 (GSTM1) and 5 (GSTM5) showed −2.1 fold changes on day 2. Glutathione S-transferase 1 (GST) showed −3.2 fold changes on day 20. The FC for ornithine decarboxylase (OAZ) was 2.7 on day 20. 1-Cys peroxiredoxin (1-Cys Prx) had −1.7 fold changes on day 5 and 1.9 on day 20. Microsomal Glutathione S-transferase (MGST) showed −2 fold changes on day 5 and 4.5 on day 20. 5-oxoprolinase (OPLAH) showed −1.7 fold changes on day 14 and 3.4 on day 20. Glutamate–cysteine ligase (GSHA) showed 2.5 fold changes on day 20.

4. Discussion

The general proteomic response of *F. candida* when exposed to dry soil was an initial down-regulation of essential pathways related to metabolism and growth. After a depression during the first 5 days, these pathways gradually returned to the same levels as in moist soil. This pattern likely reflects the quick drop in body water content when springtails were transferred to dry soil, followed by a slow increase in hydration until animals, after two weeks, reached the same body water content as the animals in moist soil. Soil invertebrates may respond to dry conditions by becoming less active, or even enter dormancy, characterized by depressed respiratory metabolism [34–36]. Moreover, we observed that animals in the dry soil did not increase their body mass, which is consistent with the depressed metabolic pathways in the first part of the drought exposure.

Drought stress poses a threat to the survival, growth, and reproduction of *F. candida* [15]. These springtails have evolved the ability to tolerate drought stress by accumulating compatible osmolytes that increase body fluid osmolality, thereby countering body water loss and even facilitating water vapor absorption across the skin [16]. A transcriptomic study demonstrated that differentially expressed transcripts of *F. candida* under drought stress are involved in diverse biological processes, such as the glucose catabolic process, carbohydrate transport, the chitin metabolic process, oxidative phosphorylation, and the juvenile hormone metabolic process [23].

In the present study, the proteome did not show a dramatic and rapid induction of proteins in response to drought stress when the body water content dropped. For example, on day 1, there were twice as many down-regulated proteins as up-regulated proteins. This result contrasts with the study by [23], which reported positive and rapid transcriptomic responses to counter drought conditions (relative humidity 98.2%) after 24 h. Altered protein abundance for cellular functions occurs downstream of gene expression and hence displays a delayed response to the environmental changes compared to transcriptomic

levels. Moreover, other studies, such as those by [37], show that molecular responses in organisms can be disparate between gene and protein and are complex due to temporal constraints and multi-dimensional regulation (i.e., microRNA, post-transcriptional, post-translational modifications of proteins, etc.)

Although the immediate overall responses of the proteome were not as expected based on earlier reports on transcriptomic responses to drought [23], the changes in proteins and pathways related to the accumulation of desiccation-protective compatible osmolytes were time-dependent, suggesting that after an initial decrease, these pathways became highly active later (at day 20), where water balance was re-established. Butanoate metabolism and pentose phosphate metabolism became carbon stores for fatty acid degradation and glycolysis, respectively. The ethanol pathway, namely glycolysis and ethanol production, contributed to sugar alcohols for osmoregulation. Noteworthy was that no significant changes in the respiratory chain were detected over the drought exposure. This is hypothesized to be due to accumulated carbohydrates for springtails under drought stress, rather than complete catalysis to the final product CO_2. Here, the results suggest that the transformation of fatty acids to sugars increased the osmolality of the animal hemolymph, facilitating water vapor absorption.

Several other pathways were affected by drought over time. For example, the cytoskeleton pathway, which is important in cell proliferation and differentiation [38], was predominantly down-regulated throughout the experiment in drought-exposed animals, which correlates with absent or negligible somatic growth of the springtails. In addition, the early responses of several enzymes in the beta-oxidation of unsaturated fatty acids and pentose pathways suggested that fatty acid degradation and carbohydrate synthesis were initiated in the first couple of days. This may relate to an altered composition of membrane phospholipid fatty acids of drought-exposed *F. candida* [39]. Detoxification, especially glutathione metabolism, also increased with the increasing beta-oxidation of fatty acids. Moreover, the observed decrease in peritrophin suggests a loss of structural and functional integrity of peritrophic membranes composed of chitin and protein, and the increase in chitinases indicates the breakdown of chitin structure, likely facilitating water absorption by balancing osmolality through thin layers of chitin skeletons and loss of structure of peritrophin within 5–14 days under drought stress. When the body water content in animals from the drought group became higher than the control, peritrophic proteins increased and chitinases decreased on day 20.

In summary, our results suggest that the proteomic response of *F. candida* to drought stress is highly time-dependent. Proteins in pathways related to carbon flux from fatty acids to sugars increased during the exposure to dry soil, and this may relate to gradual body water content increases over time, which eventually reached the same level of hydration as in control animals exposed to moist soil. Furthermore, proteins related to growth were inhibited, and proteins in reproduction were significantly down-regulated. This study contributes to understanding mechanisms related to drought tolerance in springtails and other arthropods. Increased knowledge of the capacities of soil arthropods to tolerate increased intensity and frequency of dry periods is important in order to understand the consequences of climate change for soil functioning and fertility.

Supplementary Materials: The following supporting information can be downloaded at https://www.mdpi.com/article/10.3390/insects16070707/s1, Supplementary Figure S1. Distribution of protein abundances and qualities. Supplementary Figure S2. Interaction effect of drought and time on *Folsomia candida*. Supplementary Dataset 1. Fold changes of proteins at five time points. Supplementary Dataset 2. Enriched pathways in *Folsomia candida*. Supplementary Dataset 3. Sig-

nificantly responsive pathways in *Folsomia candida*. Supplementary Dataset 4. Interaction effect of drought and time on proteins in pathways.

Author Contributions: Conceptualization, Y.W., M.H. and S.S.; Methodology, Y.W., M.H., S.S., S.Y.B. and C.J.M.; Formal Analysis, Y.W., C.J.M., S.Y.B. and S.S.; Investigation, Y.W.; Resources, S.Y.B.; Writing—Original Draft Preparation, Y.W. and M.H.; Writing—Review and Editing, Y.W., M.H., C.J.M., S.Y.B. and S.S.; Visualization, Y.W.; Supervision, M.H., S.Y.B., C.J.M. and S.S.; Funding Acquisition, M.H. All authors have read and agreed to the published version of the manuscript.

Funding: This research was funded by the EU Commission under the Marie Sklodowska-Curie Action—European Training Network (PRORISK; Project No. 859891).

Data Availability Statement: The data presented in this study are available on request from the corresponding author due to restrictions.

Conflicts of Interest: Author Steffen Y. Bak was employed by the International Flavors & Fragrances Inc. The remaining authors declare that the research was conducted in the absence of any commercial or financial relationships that could be construed as a potential conflict of interest.

References

1. Potapov, A.M.; Guerra, C.A.; van den Hoogen, J.; Babenko, A.; Bellini, B.C.; Berg, M.P.; Chown, S.L.; Deharveng, L.; Kováč, Ľ.; Kuznetsova, N.A.; et al. Globally invariant metabolism but density-diversity mismatch in springtails. *Nat. Commun.* **2023**, *14*, 674. [CrossRef]
2. Bødvarsson, H. Alimentary studies of seven common soil-inhabiting Collembola of southern Sweden. *Entomol. Scand.* **1970**, *1*, 74–80.
3. Ngosong, C.; Raupp, J.; Richnow, H.H.; Ruess, L. Tracking Collembola feeding strategies by the natural C-13 signal of fatty acids in an arable soil with different fertilizer regimes. *Pedobiologia* **2011**, *54*, 225–233. [CrossRef]
4. Potapov, A.A.; Semenina, E.E.; Korotkevich, A.Y.; Kuznetsova, N.A.; Tiunov, A.V. Connecting taxonomy and ecology: Trophic niches of collembolans as related to taxonomic identity and life forms. *Soil Biol. Biochem.* **2016**, *101*, 20–31. [CrossRef]
5. Bardgett, R.D.; Chan, K.F. Experimental evidence that soil fauna enhance nutrient mineralization and plant nutrient uptake in montane grassland ecosystems. *Soil Biol. Biochem.* **1999**, *31*, 1007–1014.
6. Filser, J.; Faber, J.H.; Tiunov, A.V.; Brussaard, L.; Frouz, J.; De Deyn, G.; Uvarov, A.V.; Berg, M.P.; Lavelle, P.; Loreau, M.; et al. Soil fauna: Key to new carbon models. *Soil* **2016**, *2*, 565–582. [CrossRef]
7. Peguero, G.; Sol, D.; Arnedo, M.; Petersen, H.; Salmon, S.; Ponge, J.F.; Maspons, J.; Emmett, B.; Beier, C.; Schmidt, I.K.; et al. Fast attrition of springtail communities by experimental drought and richness-decomposition relationships across Europe. *Glob. Change Biol.* **2019**, *25*, 2727–2738. [CrossRef]
8. Vannier, G. The porosphere as an ecological medium emphasized in Professor Ghilarov's work on soil animal adaptations. *Biol. Fertil. Soils* **1987**, *3*, 39–44.
9. Blankinship, J.C.; Niklaus, P.A.; Hungate, B.A. A meta-analysis of responses of soil biota to global change. *Oecologia* **2011**, *165*, 553–565. [CrossRef]
10. Peng, Y.; Penuelas, J.; Vesterdal, L.; Yue, K.; Peguero, G.; Fornara, D.A.; Hedenec, P.; Steffens, C.; Wu, F.Z. Responses of soil fauna communities to the individual and combined effects of multiple global change factors. *Ecol. Lett.* **2022**, *25*, 1961–1973. [CrossRef]
11. EEA. *Climate Change, Impacts and Vulnerability in Europe 2016*; An Indicator-Based Report; European Environment Agency: Copenhagen, Denmark, 2017.
12. IPCC. Impacts, Adaptation, and Vulnerability. Contribution of Working Group II to the Sixth Assessment Report of the Intergovernmental Panel on Climate Change. In *Climate Change 2022*; Pörtner, H.-O., Roberts, D.C., Tignor, M., Poloczanska, E.S., Mintenbeck, K., Alegría, A., Craig, M., Langsdorf, S., Löschke, S., Möller, V., et al., Eds.; Cambridge University Press: Cambridge, UK, 2022.
13. Aupic-Samain, A.; Baldy, V.; Delcourt, N.; Krogh, P.H.; Gauquelin, T.; Fernandez, C.; Santonja, M. Water availability rather than temperature control soil fauna community structure and prey-predator interactions. *Funct. Ecol.* **2021**, *35*, 1550–1559. [CrossRef]
14. Holmstrup, M. Water relations and drought sensitivity of *Folsomia candida* eggs (Collembola: Isotomidae). *Eur. J. Entomol.* **2019**, *116*, 229–234. [CrossRef]
15. Wang, Y.; Slotsbo, S.; Holmstrup, M. Soil dwelling springtails are resilient to extreme drought in soil, but their reproduction is highly sensitive to small decreases in soil water potential. *Geoderma* **2022**, *421*, 115913.
16. Bayley, M.; Holmstrup, M. Water vapor absorption in arthropods by accumulation of myoinositol and glucose. *Science* **1999**, *285*, 1909–1911.

17. Holmstrup, M.; Sjursen, H.; Ravn, H.; Bayley, M. Dehydration tolerance and water vapour absorption in two species of soil-dwelling Collembola by accumulation of sugars and polyols. *Funct. Ecol.* **2001**, *15*, 647–653.
18. Sjursen, H.; Bayley, M.; Holmstrup, M. Enhanced drought tolerance of a soil-dwelling springtail by pre-acclimation to a mild drought stress. *J. Insect Physiol.* **2001**, *47*, 1021–1027.
19. Holmstrup, M. The springtail *Megaphorura arctica* survives extremely high osmolality of body fluids during drought. *J. Comp. Physiol. B* **2018**, *188*, 939–945. [CrossRef]
20. Holmstrup, M.; Bayley, M. *Protaphorura tricampata*, a euedaphic and highly permeable springtail that can sustain activity by osmoregulation during extreme drought. *J. Insect Physiol.* **2013**, *59*, 1104–1110. [CrossRef]
21. Holmstrup, M.; Slotsbo, S.; Rozsypal, J.; Henriksen, P.G.; Bayley, M. Accumulation of free amino acids during exposure to drought in three springtail species. *J. Insect Physiol.* **2015**, *82*, 114–121. [CrossRef]
22. Clark, M.S.; Thorne, M.A.S.; Purac, J.; Burns, G.; Hillyard, G.; Popovic, Z.D.; Grubor-Lajsic, G.; Worland, M.R. Surviving the cold: Molecular analyses of insect cryoprotective dehydration in the Arctic springtail *Megaphorura arctica* (Tullberg). *BMC Genom.* **2009**, *10*, 328. [CrossRef]
23. Timmermans, M.J.; Roelofs, D.; Nota, B.; Ylstra, B.; Holmstrup, M. Sugar sweet springtails: On the transcriptional response of *Folsomia candida* (Collembola) to desiccation stress. *Insect Mol. Biol.* **2009**, *18*, 737–746. [CrossRef]
24. Thorne, M.A.S.; Worland, M.R.; Feret, R.; Deery, M.J.; Lilley, K.S.; Clark, M.S. Proteomics of cryoprotective dehydration in *Megaphorura arctica* Tullberg 1876 (Onychiuridae: Collembola). *Insect Mol. Biol.* **2011**, *20*, 303–310. [CrossRef]
25. Faddeeva-Vakhrusheva, A.; Kraaijeveld, K.; Derks, M.F.L.; Anvar, S.Y.; Agamennone, V.; Suring, W.; Kampfraath, A.A.; Ellers, J.; Le Ngoc, G.; van Gestel, C.A.M.; et al. Coping with living in the soil: The genome of the parthenogenetic springtail *Folsomia candida*. *BMC Genom.* **2017**, *18*, 14. [CrossRef]
26. Bahrndorff, S.; Marien, J.; Loeschcke, V.; Ellers, J. Dynamics of heat-induced thermal stress resistance and Hsp70 expression in the springtail, *Orchesella cincta*. *Funct. Ecol.* **2009**, *23*, 233–239. [CrossRef]
27. Zougman, A.; Selby, P.J.; Banks, R.E. Suspension trapping (STrap) sample preparation method for bottom- up proteomics analysis. *Proteomics* **2014**, *14*, 1006–1010. [CrossRef]
28. Kumar, R.; Kane, H.; Wang, Q.; Hibberd, A.; Jensen, H.M.; Kim, H.S.; Bak, S.Y.; Auzanneau, I.; Bry, S.; Christensen, N.; et al. Identification and characterization of a novel species of genus *Akkermansia* with metabolic health effects in a diet-induced obesity mouse model. *Cells* **2022**, *11*, 2084. [CrossRef]
29. Kall, L.; Canterbury, J.D.; Weston, J.; Noble, W.S.; MacCoss, M.J. Semi-supervised learning for peptide identification from shotgun proteomics datasets. *Nat. Methods* **2007**, *4*, 923–925. [CrossRef]
30. Silva, J.C.; Gorenstein, M.V.; Li, G.Z.; Vissers, J.P.C.; Geromanos, S.J. Absolute quantification of proteins by LCMS^{E}: A virtue of parallel MS acquisition. *Mol. Cell Proteom.* **2006**, *5*, 144–156. [CrossRef]
31. Robinson, M.D.; McCarthy, D.J.; Smyth, G.K. edgeR: A Bioconductor package for differential expression analysis of digital gene expression data. *Bioinformatics* **2010**, *26*, 139–140. [CrossRef]
32. Levin, Y. The role of statistical power analysis in quantitative proteomics. *Proteomics* **2011**, *11*, 2565–2567. [CrossRef]
33. Yu, G.C.; Wang, L.G.; Han, Y.Y.; He, Q.Y. clusterProfiler: An R package for comparing biological themes among gene clusters. *Omics-A J. Integr. Biol.* **2012**, *16*, 284–287. [CrossRef]
34. Barrett, J. Metabolic responses to anabiosis in the 4th stage juveniles of *Ditylenchus dipsaci* (nematoda). *Proc. R. Soc. Ser. B-Biol. Sci.* **1982**, *216*, 159–177. [CrossRef]
35. Bayley, M.; Overgaard, J.; Høj, A.S.; Malmendal, A.; Nielsen, N.C.; Holmstrup, M.; Wang, T. Metabolic changes during estivation in the common earthworm *Aporrectodea caliginosa*. *Physiol. Biochem. Zool.* **2010**, *83*, 541–550. [CrossRef] [PubMed]
36. Crowe, J.H.; Madin, K.A.C.; Loomis, S.H. Anhydrobiosis in nematodes: Metabolism during resumption of activity. *J. Exp. Zool.* **1977**, *201*, 57–64. [CrossRef]
37. Gleason, L.U.; Fekete, F.J.; Tanner, R.L.; Dowd, W.W. Multi-omics reveals largely distinct transcript- and protein-level responses to the environment in an intertidal mussel. *J. Exp. Biol.* **2023**, *226*, jeb245962. [CrossRef]
38. Wasteneys, G.O.; Galway, M.E. Remodeling the cytoskeleton for growth and form: An overview with some new views. *Annu. Rev. Plant Biol.* **2003**, *54*, 691–722. [CrossRef]
39. Holmstrup, M.; Hedlund, K.; Boriss, H. Drought acclimation and lipid composition in *Folsomia candida*: Implications for cold shock, heat shock and acute desiccation stress. *J. Insect Physiol.* **2002**, *48*, 961–970.

Disclaimer/Publisher's Note: The statements, opinions and data contained in all publications are solely those of the individual author(s) and contributor(s) and not of MDPI and/or the editor(s). MDPI and/or the editor(s) disclaim responsibility for any injury to people or property resulting from any ideas, methods, instructions or products referred to in the content.

insects

MDPI

Article

Genome-Wide Analysis and Functional Correlation of Tomato *JAZ* Genes Under *Tuta absoluta* Infestation and Nanoparticle-Induced Defense

Inzamam Ul Haq [1], Abdul Basit [1], Moazam Hyder [1], Mirza Naveed Shahzad [2], Asim Abbasi [3], Yasir Sharif [4], Muhammad Adeel Ghafar [1], Xiangyun Cai [1], Nazih Y. Rebouh [5] and Youming Hou [1,*]

[1] State Key Laboratory of Agricultural and Forestry Biosecurity, Key Laboratory of Biopesticides and Chemical Biology, MOE, College of Plant Protection, Fujian Agriculture and Forestry University, Fuzhou 350002, China
[2] Department of Statistics, University of Gujrat, Gujrat 50700, Pakistan
[3] Department of Entomology, University of Agriculture, Faisalabad 38040, Pakistan; asimuaf95@gmail.com
[4] College of Agriculture, Fujian Agriculture and Forestry University, Fuzhou 350002, China
[5] Department of Environmental Management, Institute of Environmental Engineering, RUDN University, 6 Miklukho-Maklaya St., Moscow 117198, Russia
* Correspondence: ymhou@fafu.edu.cn

Simple Summary: Tomato crops around the world are under serious threat from an insect pest called *Tuta absoluta*, which damages the leaves and reduces crop quality and yield. Traditional pesticides used to control this pest can harm the environment and human health. In this study, we explored a safer and more sustainable way to boost the plant's natural defense system. We focused on a group of genes in tomato plants that help defend against insect attack. We tested the use of mesoporous silica nanoparticles, which can trigger the plant's defense without harming the environment. By studying changes in gene activity and measuring the damage caused by insects, we found that these nanoparticles reduced pest survival and damage on the plants. Certain defense-related genes were strongly linked to better resistance. This research shows that it is possible to use eco-friendly materials to protect crops by strengthening their own defense systems. The findings could help farmers reduce pesticide use and grow healthier crops in a more sustainable way.

Abstract: Tomato (*Solanum lycopersicum*) production is increasingly threatened by *Tuta absoluta*, a destructive pest that compromises yield and quality. To explore sustainable alternatives to conventional insecticides, we investigated the jasmonate-mediated defense pathway by performing a genome-wide characterization of the JAZ gene family in *S. lycopersicum*. A total of 39 *SlJAZ* genes were identified and mapped to 12 chromosomes. Detailed analysis revealed conserved motifs, diverse exon–intron structures, four major phylogenetic groups, and the presence of multiple MeJA- and stress-responsive cis-elements. Synteny analysis indicated gene duplication events and evolutionary conservation with Arabidopsis and potato. Small RNA predictions suggested that 33 *SlJAZ* genes are targeted by 69 microRNAs, implying multilayered regulation. Transcriptome analysis under four treatment conditions—mesoporous silica nanoparticles (MSNs) ± pest infestation—revealed 21 differentially expressed SlJAZ genes. *SlJAZ1*, *SlJAZ19*, *SlJAZ20*, and *SlJAZ22* were notably upregulated under the combined MSN and pest treatment, with expression patterns validated by qRT-PCR (R^2 = 0.92). Phenotypic assessment of leaf damage index, larval survival rate, and number of leaf mines showed reduced pest activity in MSN-treated plants. Regression analysis demonstrated significant negative correlations between expression levels of *SlJAZ20*, *SlJAZ26*, and *SlJAZ29* and pest-related damage traits. These findings indicate that MSNs function as effective elicitors of JA-responsive defense in tomato and modulate

the expression of specific JAZ genes linked to enhanced resistance. The study provides a valuable foundation for integrating nanotechnology with molecular defense strategies to promote sustainable pest management.

Keywords: jasmonate signaling; *SlJAZ* gene family; mesoporous silica nanoparticles; *Tuta absoluta*; tomato defense mechanisms

1. Introduction

Plants have developed complex defense mechanisms to protect themselves from various biotic and abiotic stresses [1]. A central component of these defense mechanisms is the jasmonic acid (JA) signaling pathway, which plays a pivotal role in regulating plant responses to herbivore attacks, pathogen infections, and environmental challenges [2]. Within this pathway, the Jasmonate ZIM-domain (JAZ) family of proteins acts as transcriptional repressors of JA-responsive genes [3]. Under non-stress conditions, JAZ proteins suppress the expression of defense genes by interacting with transcription factors such as MYC2. However, when plants encounter stress, elevated levels of JA trigger the degradation of JAZ proteins through the ubiquitin-proteasome pathway, allowing for the activation of defense-related gene expression [4,5].

The study of the JAZ gene family has garnered considerable attention due to its crucial role in orchestrating plant defense mechanisms [6,7]. *Solanum lycopersicum* (tomato), a crop of significant economic and agricultural importance, serves as an ideal model for investigating these mechanisms [8–10]. Tomatoes are cultivated extensively worldwide, and their susceptibility to various pests and diseases can lead to significant yield losses, directly impacting food security and economic stability in many regions [11,12]. The understanding of defense-related gene families such as the JAZ genes in tomatoes is therefore essential for developing crop varieties with enhanced resistance to stressors [13,14]. In light of growing concerns about the environmental impacts and diminishing efficacy of chemical pesticides, alternative strategies that leverage the plant's innate defense mechanisms are increasingly needed [15–18].

Nanotechnology has emerged as a promising field in agricultural innovation, with various nanoparticles showing potential to enhance crop resilience and reduce the reliance on chemical inputs [19,20]. Mesoporous silica nanoparticles (MSNs) have attracted attention for their ability to modulate plant physiological processes and act as carriers for agrochemicals [21,22]. Their porous structure allows them to be functionalized and used as delivery systems for growth regulators, fertilizers, or pesticides [23]. In addition to enhancing plant growth, MSNs have been shown to improve tolerance to various environmental stresses by influencing gene expression and metabolic processes [24,25]. Despite the growing body of research, the specific molecular mechanisms through which MSNs affect plant defense pathways—particularly transcription factors such as the JAZ family—remain largely unexplored.

One of the most destructive pests to tomato crops is *Tuta absoluta* (Meyrick), commonly known as the tomato leaf miner [26]. Native to South America, this pest has rapidly spread across Europe, Africa, and parts of Asia, where it has caused significant damage to tomato crops in both open fields and greenhouses [27]. The feeding activity of *T. absoluta* severely reduces the photosynthetic capacity of tomato plants, leading to stunted growth, compromised fruit quality, and, in severe cases, total crop loss [28]. *T. absoluta* populations have developed resistance to several widely used insecticides, including pyrethroids and organophosphates [29,30], which has severely limited the effectiveness of conventional chemical control strategies [31]. This situation highlights the urgent need for alternative, sustainable pest control strategies that do

not rely solely on chemical inputs. The use of MSNs as a tool to enhance the plant's natural defenses against *T. absoluta* presents a promising solution. However, little is known about the combined effects of MSNs and pest infestation on gene expression, particularly in relation to defense-related genes like the JAZ gene family.

Tomato plants remain vulnerable to *T. absoluta*, and the reliance on chemical pesticides to manage this pest is becoming unsustainable due to the rapid evolution of insecticide resistance [29]. The environmental consequences of pesticide overuse further underscore the need for innovative and eco-friendly approaches to pest control [32]. Although MSNs offer a promising strategy for boosting plant defense mechanisms [33], there is limited understanding of how these nanoparticles influence the molecular responses of tomato plants, particularly under pest pressure. Specifically, the effects of MSNs on JAZ gene expression in tomatoes infested with *T. absoluta* have not been thoroughly investigated. Addressing this knowledge gap could lead to the development of new approaches that not only mitigate the damage caused by *T. absoluta* but also reduce reliance on harmful pesticides.

The primary aim of this study is to investigate the role of mesoporous silica nanoparticles in modulating the defense responses of tomato plants, with a particular focus on the JAZ gene family under infestation by *T. absoluta*. This study seeks to identify and characterize the JAZ gene family in *S. lycopersicum* through genome-wide analysis, providing a comprehensive understanding of the distribution and structure of these genes. Additionally, this research aims to evaluate the effect of MSNs on JAZ gene expression under both normal and pest-infested conditions, allowing for a comparison of molecular responses between treated and untreated plants.

2. Materials and Methods

2.1. Plant Materials and Growth Conditions

Tomato plants (*S. lycopersicum* cv. Zhefen 202), a cultivar widely grown in southeastern China, were selected for this study based on their availability in our laboratory. Seeds were germinated in sterilized soil and grown under controlled greenhouse conditions at the Plant Protection Institute. The greenhouse was maintained at 25 ± 2 °C during the day and 18 ± 2 °C at night, with a relative humidity of 60–70%. A 16 h light/8 h dark photoperiod was applied using artificial lighting to support optimal plant development. Plants were watered daily, and a standard Hoagland nutrient solution was applied weekly. At the four-leaf stage, seedlings were transplanted into 5 L pots and maintained under the same environmental conditions.

Mesoporous silica nanoparticles (MSNs), characterized by uniform pore sizes (2–50 nm), high surface area, and excellent physicochemical stability, are widely used as carriers in agricultural and biomedical applications. In this study, we utilized unloaded MSNs synthesized via the sol–gel method (see Supplementary Figure S1) to assess their direct impact on plant gene expression, eliminating the confounding effects of loaded bioactive compounds.

2.2. Experimental Design

For the experimental setup, tomato plants were assigned to four treatment groups based on the application of mesoporous silica nanoparticles (MSNs) and *T. absoluta* infestation: (1) WN/WI—without MSNs and without *T. absoluta* (control), (2) WN/I—without MSNs but with *T. absoluta* infestation, (3) N/WI—with MSNs but without *T. absoluta* infestation, and (4) N/I—with both MSNs and *T. absoluta* infestation. Each treatment group consisted of three biological replicates, with twenty plants per replicate, arranged in a completely randomized design.

MSNs were synthesized following the method of Chen et al. [34] and suspended in deionized water at a concentration of 30 mg/L. The suspension was applied to the foliage of N/WI and N/I plants using a handheld sprayer to ensure uniform coverage. Spraying was conducted once per week for a total of four consecutive weeks to the designated MSN treatment groups (N/WI and N/I). After the completion of the fourth spraying, neonate larvae of *T. absoluta* (<24 h old) were gently transferred onto the abaxial surface of tomato leaves using a fine brush. Each plant in the WN/I and N/I groups received 10 larvae to ensure a consistent and uniform infestation. Pest pressure was maintained throughout the experiment, and infestation levels were visually monitored daily across biological replicates to ensure homogeneity. Phenotypic parameters, including leaf damage index (LDI), larval survival rate, and the number of leaf mines, were assessed 5 days after larval infestation, similarly plant material for molecular analyses was collected 5 days after infestation.

2.3. Assessment of Pest-Induced Leaf Damage, Larval Survival, and Leaf Mining

To evaluate the defensive impact of mesoporous silica nanoparticles (MSNs) against *T. absoluta*, phenotypic parameters were measured across the four treatment groups. The scoring of leaf damage index (LDI) using a 0–5 ordinal scale was based on traditional approaches originally described by Hussey & Parr [35], and has been adopted in later studies [36,37]. Leaf mining activity (mines per leaf) was assessed by counting the visible mines under a stereomicroscope, following general quantification practices widely used in leaf-miner ecological studies [38].

Leaf Damage Index (LDI) was visually assessed at 5 days post-infestation on each treated plant. The extent of damage was scored using a modified 0–5 scale, where 0 = no visible damage, 1 = 1–10% leaf area damaged, 2 = 11–25%, 3 = 26–50%, 4 = 51–75%, and 5 $\geq$ 75%. The index for each treatment was calculated using the formula:

$$\text{LDI}\ (\%)\ =\ \left(\frac{\sum(\textit{Scale}\ \times\ \textit{Number of Leaves at Scale})}{\textit{Total}\times\textit{Leaves Observed}\ \times\ 5}\right)\ \times\ 100$$

The average LDI was computed from five randomly selected plants per treatment.

Larval Survival Rate was calculated by counting the number of living larvae recovered from each plant at 5 days post-infestation. The survival rate was expressed as a percentage of the total number of larvae initially introduced (20 larvae per plant):

$$\text{Larval Survival}\ (\%)\ =\ \left(\frac{\textit{Number of Larvae}}{20}\right)\ \times\ 100$$

Leaf Mining Activity was quantified by counting the number of visible mines per leaf under a stereomicroscope. Five infested leaves per plant were randomly selected, and the total number of mines was averaged per leaf.

2.4. Genome-Wide Identification of JAZ Genes

The tomato reference genome (ITAG5.0) sequence was obtained from the Phytozome database (https://phytozome-next.jgi.doe.gov/ (accessed on 9 September 2024)). Candidate JAZ proteins were identified using a combination of Hidden Markov Model (HMM) searches and BLAST searches (https://blast.ncbi.nlm.nih.gov/Blast.cgi, accessed on 9 September 2024). For the HMM search, profile HMMs corresponding to the TIFY domain (Pfam ID: PF06200) and the Jas motif (Pfam ID: PF09425) were retrieved from the Pfam database (https://www.ebi.ac.uk/interpro/set/pfam/, accessed on 9 September 2024) and queried against the tomato proteome using TBtools (version 2.122) [39] with an e-value threshold of 1×10^{-5}. *Arabidopsis* JZA proteins were downloaded from the TAIR (https://www.arabidopsis.org/index.jsp (accessed on 10 September 2024)) database. *Ara-*

bidopsis proteins were used to BLAST against tomato protein sequences. All candidate sequences identified by HMM or BLAST were verified using Pfam, SMART, and NCBI-CDD. Genes containing both the TIFY and Jas domains were classified as canonical JAZ proteins. In line with previous reports in tomato and Arabidopsis, we also retained a subset carrying only one domain but clustering within the JAZ clade; these were designated as non-canonical JAZ-like members. All candidates were cross-checked using PlantTFDB (http://planttfdb.gao-lab.org/ (accessed on 15 September 2024)) to confirm annotation. Genes lacking both domains or those representing incomplete gene models were excluded from further analysis.

2.5. Determination of Physicochemical Properties

The theoretical molecular weight (MW) and isoelectric points (pI) of the proteins were analyzed using the ProtParam tool (https://web.expasy.org/protparam/; accessed on 7 October 2024) [40]. Additionally, predictions for subcellular localization were made using CELLO v2.5 (http://cello.life.nctu.edu.tw/; accessed on 24 September 2024) [41].

2.6. Domain and Motif Analysis

To investigate the conserved domains and motifs within the JAZ protein family in *S. lycopersicum*, a comprehensive in silico analysis was performed. Full-length amino acid sequences of the identified JAZ proteins were retrieved from the Phytozome database. The JAZ domain (Pfam ID: PF06200) and the TIFY domain (Pfam ID: PF06202) were confirmed through domain searches using the Pfam database (https://www.ebi.ac.uk/interpro/set/pfam/, accessed on 12 September 2024). Only sequences containing these domains were retained for further analysis to ensure functional relevance.

For motif discovery, the MEME Suite (v5.5.5) (http://meme-suite.org/ (accessed on 15 September 2024)) [42] was employed, with the maximum number of motifs set to 12, allowing for comprehensive identification of conserved patterns across the JAZ protein family. The identified motifs were analyzed for their distribution and conservation across different JAZ members, contributing to insights into structural variations and potential functional specialization within the family. Each motif was annotated and visualized using the MEME output, and sequences were compared across homologous JAZ proteins from other species to highlight conserved and unique structural features.

2.7. Phylogenetic and Gene Structure Analysis

To analyze the evolutionary relationships of the identified JAZ genes, a phylogenetic tree was constructed. Full-length amino acid sequences of the JAZ proteins from *S. lycopersicum* and homologous JAZ proteins from *Arabidopsis thaliana*, and *Solanum tuberosum* were aligned using ClustalW (version 2.1) (https://www.genome.jp/tools-bin/clustalw, accessed on 17 September 2024), and the Neighbor-Joining phylogenetic tree was generated using Poison model in MEGA X software (version 11.0.13) (https://www.megasoftware.net/, accessed on 18 September 2024) [43]. Bootstrap analysis with 1000 replicates was performed to assess the robustness of the phylogeny. Gene structure analysis was conducted by retrieving the exon-intron information of the JAZ genes from the Phytozome database, and the gene structures were visualized and mapped out on chromosomes using the TBtools software (version 2.122) [39].

2.8. Promoter Cis-Regulatory Elements Analysis

The promoter regions (2 kb upstream of the transcription start site) of each identified JAZ gene were analyzed to identify cis-regulatory elements associated with defense and

stress responses. Promoter sequences were extracted from the *S. lycopersicum* genome. The PlantCARE database (http://bioinformatics.psb.ugent.be/webtools/plantcare/html/ (accessed on 22 September 2024)) was utilized for scanning these promoter sequences to detect putative cis-elements.

The analysis focused on identifying elements known to mediate responses to biotic and abiotic stresses, including the MeJA-responsive elements, abscisic acid-responsive elements, light-responsive elements, and other stress-associated motifs. These elements were annotated and mapped across the promoter regions of each JAZ gene, with special attention given to motifs related to jasmonate signaling, as they are critical in modulating plant defense mechanisms.

2.9. Gene Duplication and Synteny Analysis

The genome and GFF3 annotation files of *S. lycopersicum* were processed through MCScanX to identify duplicated gene pairs. Synonymous (Ks) and non-synonymous (Ka) substitution rates were calculated using a basic Ka/Ks calculator. The divergence time, in million years ago (MYA), was estimated for duplicated gene pairs using the formula 't = Ks/2r' with a neutral substitution rate of r = 6.56×10^{-9} for tomato [44].

Comparative synteny analysis was conducted to investigate genome conservation between *S. lycopersicum*, *S. tuberosum*, and *Arabidopsis*, highlighting evolutionary relationships. The genome and GFF3 files were subjected to McScanX in TBtools software, and the resulting files were used for multiple synteny analysis. Homologous gene pairs were identified using MCScanX software (version 2.0), and collinear blocks were visualized to assess syntenic regions across species. Gene pairs involved in segmental or tandem duplications were highlighted to facilitate identification of duplication patterns.

2.10. Protein–Protein Interaction Analysis

The potential interactions of SlJAZ proteins with other proteins were analyzed by constructing a protein–protein interaction network based on their homologs in Arabidopsis, utilizing the STRING 11.5 tool (https://www.string-db.org/cgi/; accessed on 9 October 2024). Interacting proteins with maximum similarity and an E-value below 10^{-5} were selected. The top 10 interactions, filtered at a high confidence threshold of 0.7, were included in the analysis. MCL clustering was applied with an inflation parameter of 3, and dotted lines were used to represent connections between clusters.

2.11. Prediction of microRNAs

MicroRNA (miRNA) target prediction for JAZ genes in *S. lycopersicum* was conducted to identify potential post-transcriptional regulatory elements. The CDSs of JAZ genes were used as input in psRNATarget (https://www.zhaolab.org/psRNATarget/ (accessed on 29 September 2024)) [45] to predict miRNA binding sites. Default parameters were applied for target accessibility, with the expectation of pairing complementarity, and target sites were screened for high complementarity scores. Identified miRNA binding sites were mapped to both coding sequences (CDS) and untranslated regions (UTRs) of the JAZ genes. Only miRNAs with high predicted binding scores were retained for further analysis.

2.12. Gene Expression Analysis

Total RNA was extracted from tomato leaves of all four treatment groups (WN/WI, WN/I, N/WI, and N/I) using the TRIzol reagent (Invitrogen, Carlsbad, CA, USA) following the manufacturer's protocol. RNA integrity was assessed using the Agilent 2100 Bioanalyzer (Agilent Technologies, Santa Clara, CA, USA), and samples with an RNA

integrity number (RIN) $\geq$ 7.0 were used for library construction. RNA-seq libraries were prepared using the Illumina TruSeq RNA Sample Preparation Kit (Illumina, San Diego, CA, USA), according to the manufacturer's instructions. mRNA was enriched using oligo(dT) magnetic beads, fragmented into ~200 bp fragments, and reverse transcribed into cDNA. After end repair, adaptor ligation, and PCR amplification, libraries were quality checked on the Agilent Bioanalyzer. Sequencing was performed on the Illumina NovaSeq 6000 platform (Illumina, USA), generating 150 bp paired-end reads. Raw reads were quality-checked using FastQC (v0.11.9) and filtered with Trimmomatic (v0.39) to remove adapters and low-quality bases. Clean reads were mapped to the tomato reference genome (ITAG5.0) using HISAT2 (v2.2.1) with default parameters. Transcript abundance was estimated as FPKM (Fragments Per Kilobase of transcript per Million mapped reads) using StringTie (v2.1.5). Differential expression analysis was conducted with DESeq2 (v1.34.0), applying a Benjamini–Hochberg adjusted p-value < 0.05 and $|\log_2$ fold change$| \geq 1$ as the significance threshold. Genes meeting these criteria were considered differentially expressed. Heatmaps of expression patterns were generated using the pheatmap package in R (v4.1.0). Based on the heatmap, we selected the candidate genes to further study their expression by qPCR analysis.

2.13. qPCR-Based Expression Analysis

Total RNA was extracted from leaf samples of the tomato plants using the TRIzol reagent (Invitrogen, USA) according to the manufacturer's instructions. The quality and quantity of RNA were determined using a NanoDrop spectrophotometer (Thermo Fisher Scientific, Waltham, MA, USA), and RNA integrity was verified by gel electrophoresis. First-strand cDNA was synthesized from 1 μg of total RNA using the Evo M-MLV RT Kit (Accurate Biotechnology, Hunan, Co., Ltd., Changsha, China) following the manufacturer's protocol. qRT-PCR was performed with specific primers (Supplementary Table S1) for the selected JAZ genes (designed using Primer3 software), and the specificity of each primer pair was verified through melting curve analysis. qPCR reactions were conducted using the SYBR Green Master Mix (Bio-Rad, Hercules, CA, USA) on a CFX96 Touch Real-Time PCR Detection System (Bio-Rad, USA). The thermal cycling conditions were as follows: initial denaturation at 95 °C for 3 min, followed by 40 cycles of 95 °C for 15 s and 60 °C for 30 s. The expression levels were normalized to the tomato actin gene as an internal control. Relative expression levels were calculated using the $2^{-\Delta\Delta Ct}$ method, and each reaction was performed in triplicate.

2.14. Statistical Analysis

All experimental data were subjected to statistical analysis using R software (version 4.1.0). Data were analyzed using one-way analysis of variance (ANOVA), followed by Tukey's post hoc test to compare differences between treatment groups. For gene expression analysis, DESeq2 was used to identify differentially expressed genes, with significance determined by an adjusted p-value < 0.05. qPCR data were analyzed using the same statistical methods. Regression analysis was conducted to assess the relationship between *SlJAZ* gene expression and pest-related traits (leaf damage index, larval survival rate, and number of leaf mines), with R^2, slope, and p-values calculated using linear models. Results are presented as mean $\pm$ standard error, with statistical significance set at $p < 0.05$.

3. Results

3.1. Identification and Distribution of JAZ Genes

A total of 39 JAZ genes were identified in the *S. lycopersicum* genome and were mapped onto all 12 chromosomes. The chromosomal distribution of these genes is shown in Figure 1.

Chromosome 1 contains the highest number of JAZ genes, with 12 genes (*SlJAZ1*, *SlJAZ2*, *SlJAZ3*, *SlJAZ4*, *SlJAZ5*, *SlJAZ6*, *SlJAZ7*, *SlJAZ8*, *SlJAZ9*, *SlJAZ10*, *SlJAZ11*, *SlJAZ12*) located between 0 Mb and 80 Mb. Chromosome 3 houses 7 genes (*SlJAZ14*, *SlJAZ15*, *SlJAZ16*, *SlJAZ17*, *SlJAZ18*, *SlJAZ19*, *SlJAZ20*), distributed along the chromosome from 10 Mb to 60 Mb.

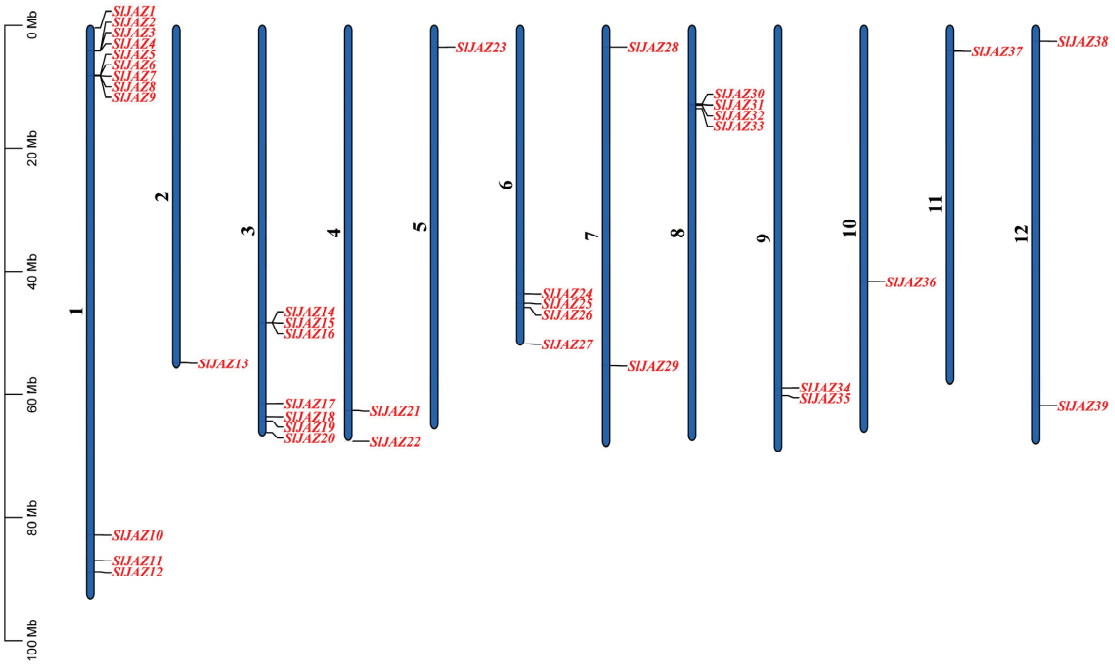


Figure 1. Chromosomal distribution of JAZ genes in *S. lycopersicum*. This figure shows the mapping of 39 identified JAZ genes across the 12 chromosomes of the tomato genome.

Chromosome 4 contains 2 JAZ genes (*SlJAZ21*, *SlJAZ22*), while chromosome 2 (*SlJAZ13*), Chromosomes 5 (*SlJAZ23*), Chromosomes 10 (*SlJAZ36*) and Chromosomes 11 (*SlJAZ37*) harbors only 1 gene each. Chromosome 6 holds 4 JAZ genes (*SlJAZ24*, *SlJAZ25*, *SlJAZ26*, *SlJAZ27*), while chromosome 7 includes 2 JAZ genes (*SlJAZ28*, *SlJAZ29*). Chromosome 8 houses 4 genes (*SlJAZ30*, *SlJAZ31*, *SlJAZ32*, *and SlJAZ33*), spread between 20 Mb and 60 Mb. Finally, chromosomes 12 contains 2 JAZ genes (*SlJAZ38* and *SlJAZ39*). This distribution highlights that while some chromosomes have a higher density of JAZ genes, others have only one or two. Figure 1 and Supplementary Table S2 provides the detailed chromosomal locations of all identified genes.

3.2. Physicochemical Properties of SlJAZ Genes

The *SlJAZ* genes showed diverse physicochemical properties. *SlJAZ5* was the smallest gene comprising 183 bps, while *SlJAZ27* was the most extended gene with 2106 bps. Same genes showed smallest and larges proteins 61 and 702 amino acid residues. Number of exons varied from 24 in SlJAZ4 to 1 in SlJAZ34. Theoretical isoelectric points varied from 5.17 for SlJAZ19 to 10.34 for SlJAZ10. The expected molecular weight ranged between 6989.3 for SlJAZ5 to 78205.24 dalton (Da) for SlJAZ27. Grand Average of Hydropathy (GRAVY) value for protein sequences ranged from −0.954 for SlJAZ13 to 0.514 for SlJAZ22. The subcellular localization prediction showed that SlJAZ proteins are located in nucleus, mitochondria, plasma membrane, and chloroplast. Majority of the proteins were localized in nucleus, while some are located in more than one cell compartments (Supplementary Table S2).

3.3. Phylogenetic Analysis

Figure 2 illustrates the phylogenetic relationships among JAZ proteins from *Arabidopsis thaliana* (AtJAZ), *Solanum lycopersicum* (SlJAZ), and *Solanum tuberosum* (StJAZ), which were grouped into four distinct clades (A–D). Genes are color-coded by species, and background shading highlights the four groups. Group A consisted of 18 members, including *StJAZ15*, *SlJAZ25*, *SlJAZ18*, and *AtJAZ3*, with several clusters supported by high bootstrap values (>80). Members of this clade retained the canonical ZIM and Jas domains, suggesting strong structural conservation. Group B comprised 19 genes, such as *AtTIFY2B*, *SlJAZ20*, and *SlJAZ37*. Compared with Groups A and C, Group B showed longer branch lengths, indicating an earlier divergence. Several members exhibited motif variations, particularly in the Jas domain, and were uniquely predicted to contain miRNA binding sites such as miR164 and miR482.

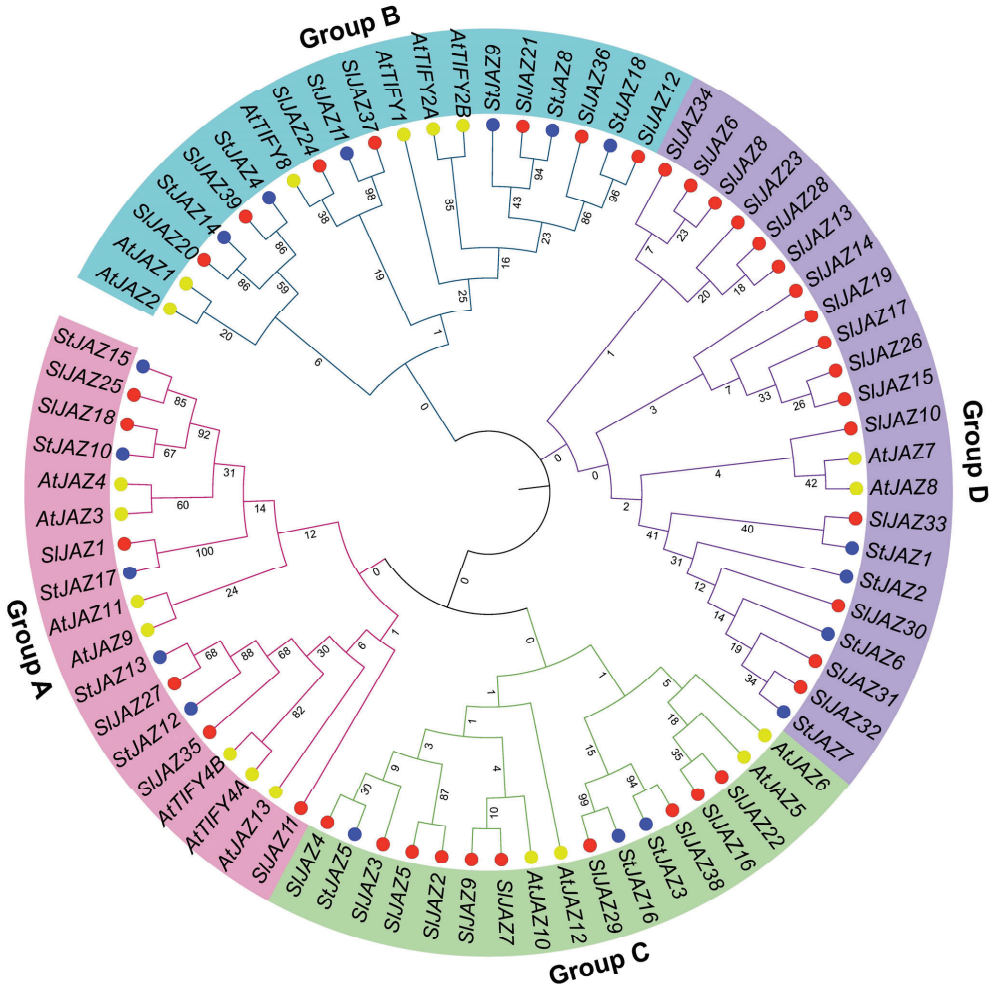


Figure 2. Phylogenetic relationships of JAZ proteins from *Solanum lycopersicum* (SlJAZ), *Arabidopsis thaliana* (AtJAZ), and *Solanum tuberosum* (StJAZ). The tree was constructed using the maximum likelihood method with 1000 bootstrap replicates and classified the 39 *SlJAZ* proteins into four major groups (A–D). Homologous proteins from *A. thaliana* and *S. tuberosum* were included for comparative analysis. Distinct background shading indicates the four groups, while node colors represent species origin: red = *S. lycopersicum*, blue = *S. tuberosum*, and yellow-green = *A. thaliana*. Grouping patterns supported by high bootstrap values highlight conserved evolutionary relationships, species-specific expansions, and functional conservation within the JAZ family.

Group C, containing 17 genes including *SlJAZ4*, *AtJAZ10*, and *StJAZ16*, displayed shorter branch lengths and tight clustering, consistent with a more recent divergence.

Members of this clade carried highly conserved ZIM and Jas domains and were enriched in stress-responsive cis-elements in their promoter regions. Group D was the largest clade, encompassing 22 members, predominantly from tomato. This expansion suggests species-specific duplication within *S. lycopersicum*. While Group D proteins retained both conserved domains, variation in promoter cis-elements and the absence of predicted miR319 target sites in some members indicated potential diversification in regulatory functions.

3.4. Motif, Gene Structure, and Domain Analysis

The motif and gene structure analysis of the 39 identified JAZ genes in *S. lycopersicum* revealed a diverse array of conserved motifs and gene structures associated with their roles in jasmonate signaling (Figure 3, Supplementary Table S3). In total, 12 distinct motifs were detected, with motif 7 being the longest (50 amino acids) and motifs 2 and 4 the shortest (15 amino acids each). Among them, motifs 1 and 2 were the most conserved and were present in the majority of JAZ proteins, underscoring their essential role in maintaining the core structure and function of these proteins. However, a few exceptions were observed: motif 1 was absent in *SlJAZ21*, *SlJAZ19*, and *SlJAZ12*, while motif 2 was missing in *SlJAZ21*, *SlJAZ19*, *SlJAZ12*, and *SlJAZ36*. Motif 1 corresponds to the conserved TIFY/ZIM domain, which is critical for protein–protein interactions and recruitment of the NINJA–TPL complex, whereas motif 2 represents the Jas domain, which mediates binding to the SCFˆCOI1 complex for jasmonate-dependent degradation of JAZ repressors. The absence of these motifs in specific members may reflect functional divergence within the family. Other motifs (3–10) were found in a subset of proteins and may contribute to subgroup-specific specialization.

The gene structure analysis, as shown in Figure 4, revealed considerable variation in exon-intron organization among the JAZ genes. While some genes, such as *SlJAZ6* and *SlJAZ23*, exhibited a relatively simple structure with a few exons and introns, other genes, such as *SlJAZ21* and *SlJAZ36*, displayed more complex gene structures with multiple exons and introns. Additionally, the length of untranslated regions (UTRs) varied significantly among the JAZ genes, which may play a role in the post-transcriptional regulation of these genes under different stress conditions. The domain analysis further highlighted the presence of the TIFY and JAS domains, which are essential for the functioning of JAZ proteins in jasmonate signaling. Figure 4 shows that all 39 JAZ proteins contain the conserved TIFY domain (green) necessary for protein–protein interactions, and most of the JAZ proteins also possess the JAS domain (yellow), which is required for interaction with the COI1 receptor. These domains are highly conserved across the JAZ proteins, reflecting their fundamental role in jasmonate-mediated defense responses. The comparison of gene structures and motifs across the JAZ gene family suggests both conserved functions and potential specialization among the different members.

3.5. Cis-Regulatory Elements

The analysis of the cis-regulatory elements in the promoter regions of the 39 JAZ genes revealed a wide range of elements associated with various stress responses, hormonal regulation, and development. As shown in Figure 5, the promoter regions (2 kb upstream of the transcription start site) contained numerous light-responsive elements, which were the most abundant across all JAZ genes, suggesting that light regulation may play a significant role in the expression of these genes. Additionally, several stress-responsive elements, such as the MeJA-responsive elements, abscisic acid-responsive elements, and defense and stress-responsive elements, were identified in the majority of the JAZ genes.

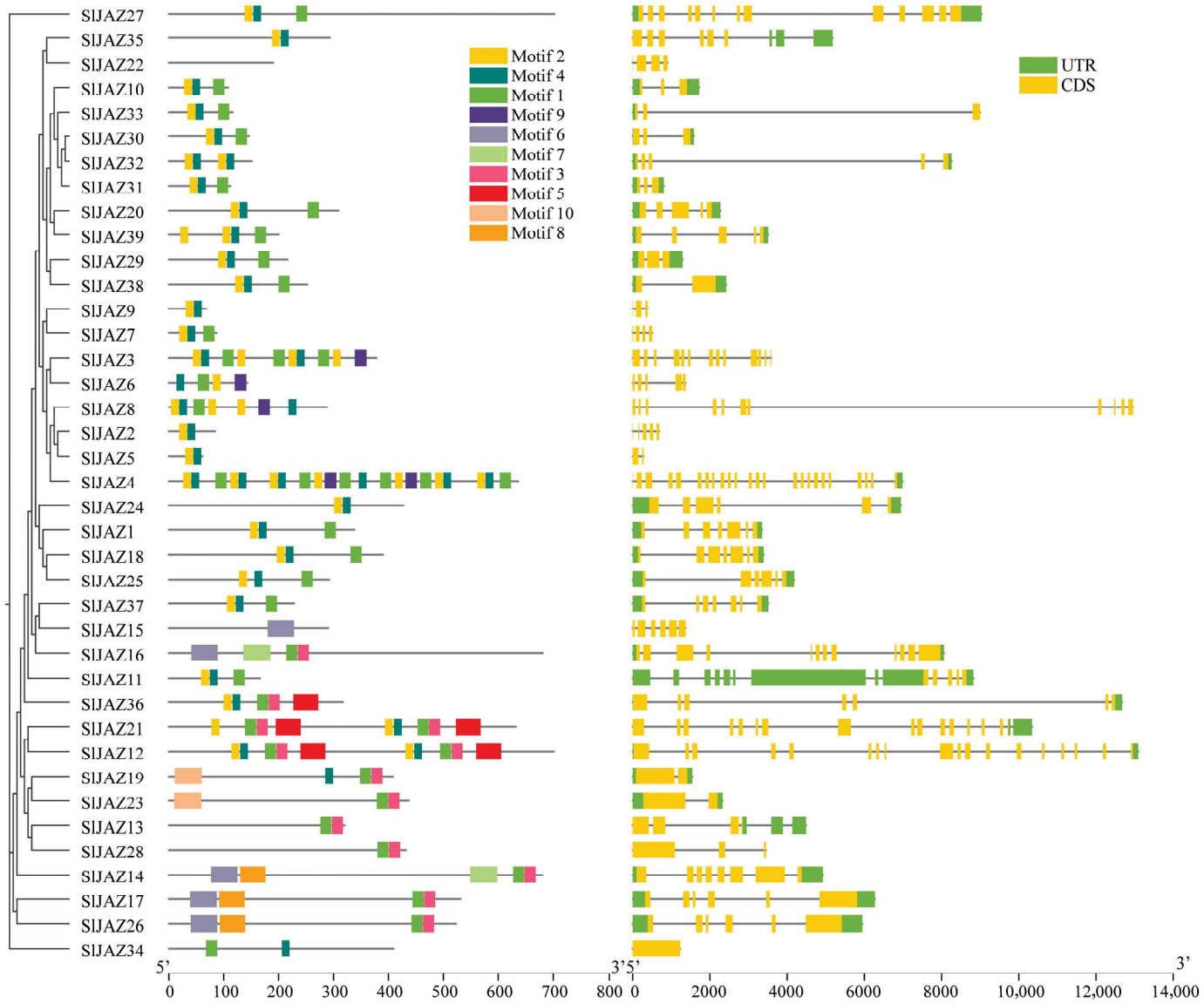


Figure 3. Conserved motifs in JAZ proteins of *S. lycopersicum*. This figure illustrates the distribution of 10 conserved motifs identified across the 39 JAZ proteins in tomato. Motifs 1 and 2, present in nearly all JAZ proteins, highlight their critical roles in maintaining core functions within the jasmonate signaling pathway. Variations in motif composition among JAZ family members suggest functional diversification, contributing to specialized roles within the plant's defense responses.

Salicylic acid-responsive elements, anaerobic induction elements, and auxin-responsive elements were also prevalent, indicating a potential role for these genes in responding to biotic and abiotic stresses through hormonal signaling pathways. Gibberellin-responsive elements, drought-responsive elements, and circadian control elements were present in several JAZ genes, suggesting that these genes might be involved in developmental processes and environmental stress responses. Furthermore, cis-elements related to meristem expression, endosperm expression, and anaerobic induction were less frequent but still observed in a subset of the JAZ genes, indicating specialized regulatory roles in plant growth and development. Overall, the presence of a diverse array of cis-regulatory elements in the promoter regions of the JAZ genes highlights their potential involvement in a wide range of regulatory processes, particularly in response to environmental stimuli and hormonal signals.

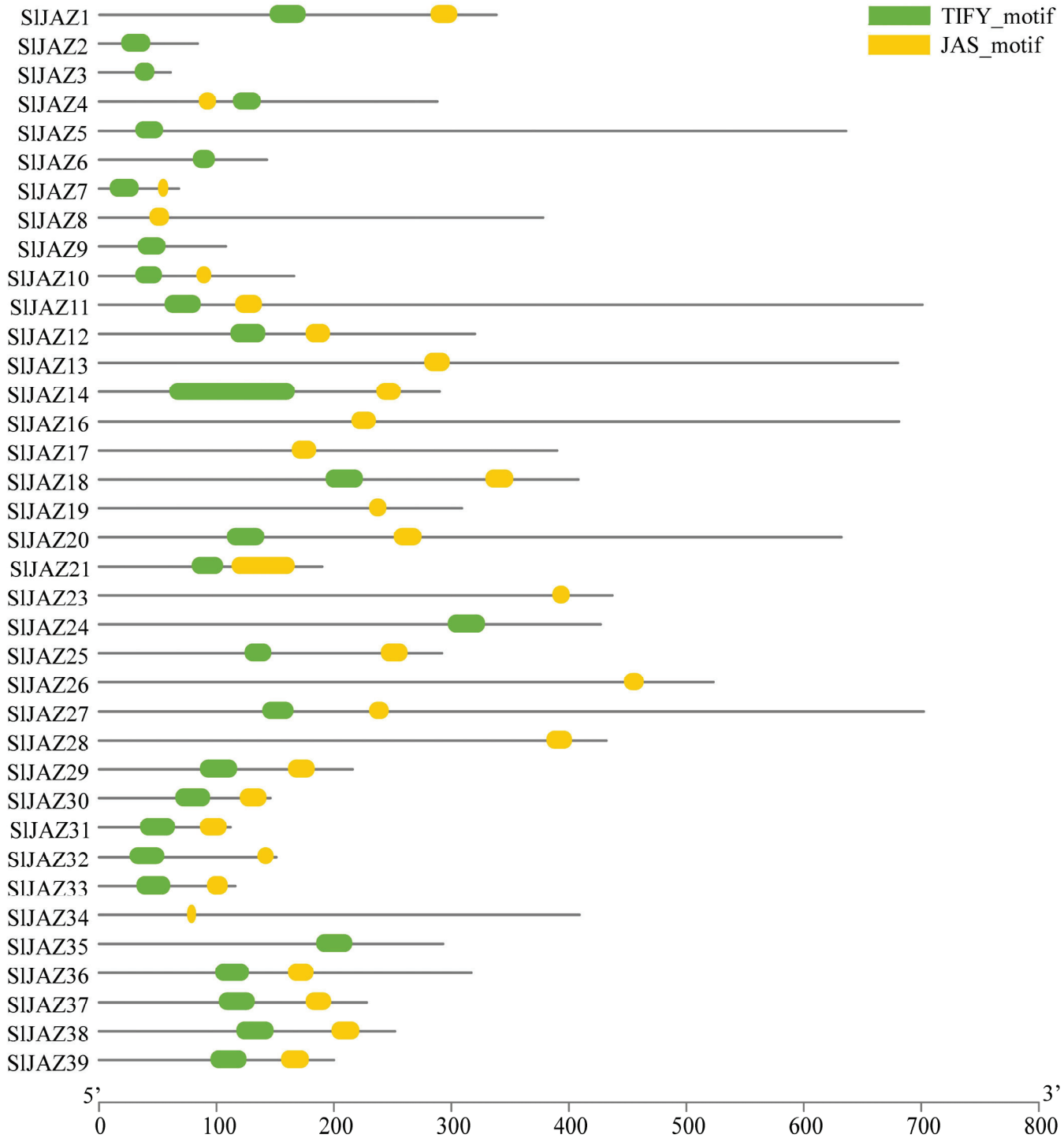


Figure 4. Gene structure and conserved domains of JAZ genes in *S. lycopersicum*. This figure displays the exon-intron organization and conserved domains (TIFY and JAS) within the 39 JAZ genes. Variability in gene structures, with differences in the number and length of exons and introns, suggests functional diversity among JAZ genes. The presence of the conserved TIFY domain (green) across all genes and the JAS domain (yellow) in most genes highlights their essential roles in jasmonate-mediated signaling and protein interactions.

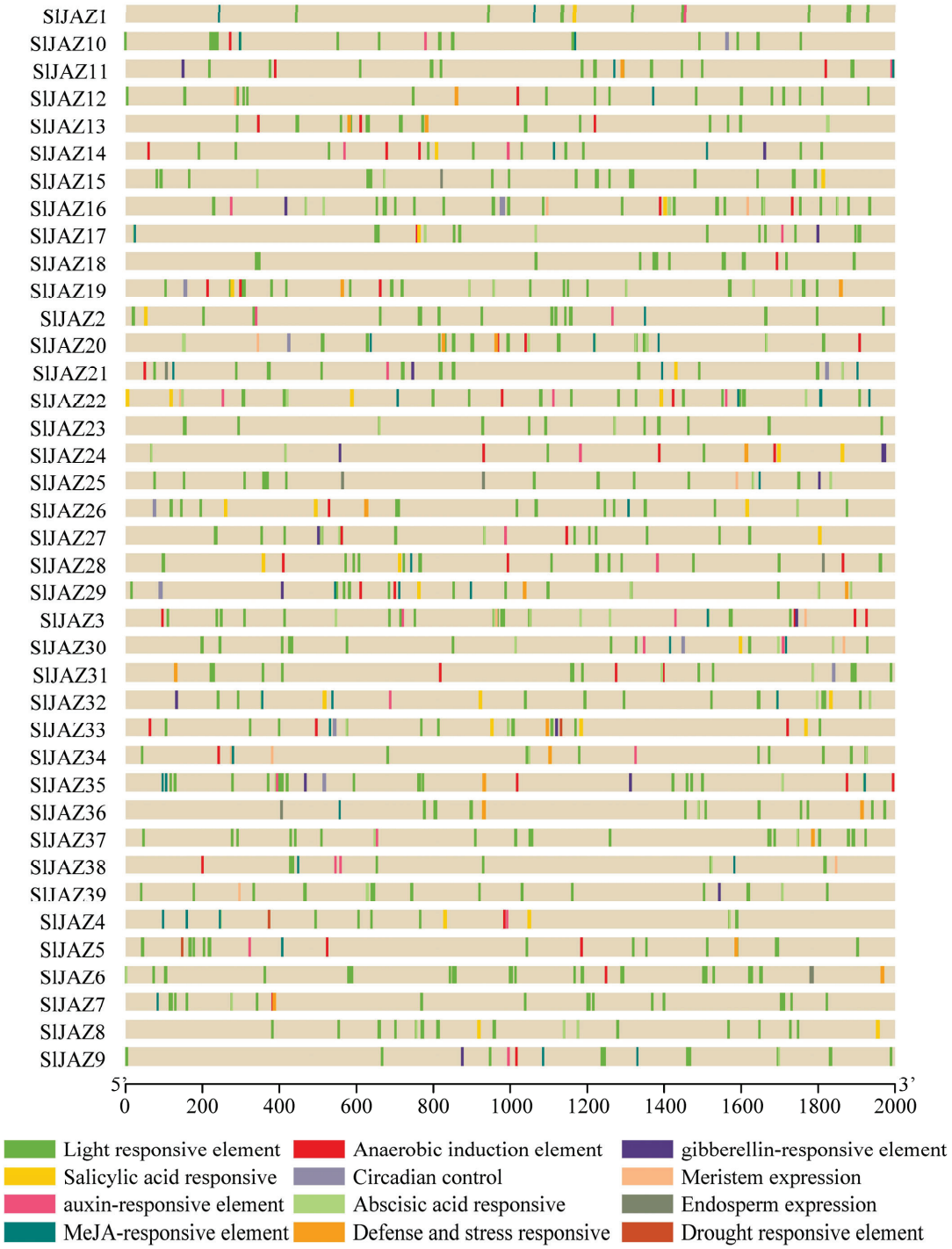


Figure 5. Cis-regulatory elements in promoter regions of JAZ genes in *S. lycopersicum*.

3.6. Duplication and Synteny Analysis

The duplication analysis revealed seven duplicated gene pairs (Table 1, Figure 6) out of 39 *SlJAZ* genes. One gene pair (*SlJAZ19-SlJAZ20*) was tandemly duplicated, while all others showed segmental duplication. These segmental duplications suggest that gene duplication has played a critical role in the expansion of the JAZ gene family in tomato. The Ka/Ks ratios of duplicated *SlJAZ* gene pairs were all less than one, indicating that although duplication events are stochastic in origin, purifying selection has subsequently acted on these gene pairs to preserve their functions and maintain evolutionary stability.

The estimated duplication times ranged from 43.63 million years ago (MYA) for *SlJAZ17-SlJAZ26* to 144.04 MYA for *SlJAZ12-SlJAZ21* (Table 1). Figure 6 shows the duplicated gene pairs on different chromosomes of *S. lycopersicum*; the red lines shows the duplicated genes, while gray lines in the background shows the duplication blocks of whole genome.

Table 1. The duplication events for SlJAZ17-SlJAZ26.

Gene-1	Gene-2	Ka	Ks	Ka_Ks	Selection Pressure	Duplication Type	T = Ks/2r (MYA)
SlJAZ12	*SlJAZ21*	0.480957	1.872467	0.256858	Purifying	Segmental	144.0359
SlJAZ38	*SlJAZ20*	0.521719	N/A	N/A	N/A	Segmental	N/A
SlJAZ38	*SlJAZ29*	0.249556	1.284069	0.194348	Purifying	Segmental	98.77454
SlJAZ19	*SlJAZ20*	0.9835	N/A	N/A	N/A	Tandem	N/A
SlJAZ18	*SlJAZ25*	0.302624	0.860289	0.35177	Purifying	Segmental	66.17609
SlJAZ17	*SlJAZ26*	0.204479	0.567128	0.360552	Purifying	Segmental	43.62523
SlJAZ27	*SlJAZ35*	0.23627	0.725057	0.325864	Purifying	Segmental	55.77358

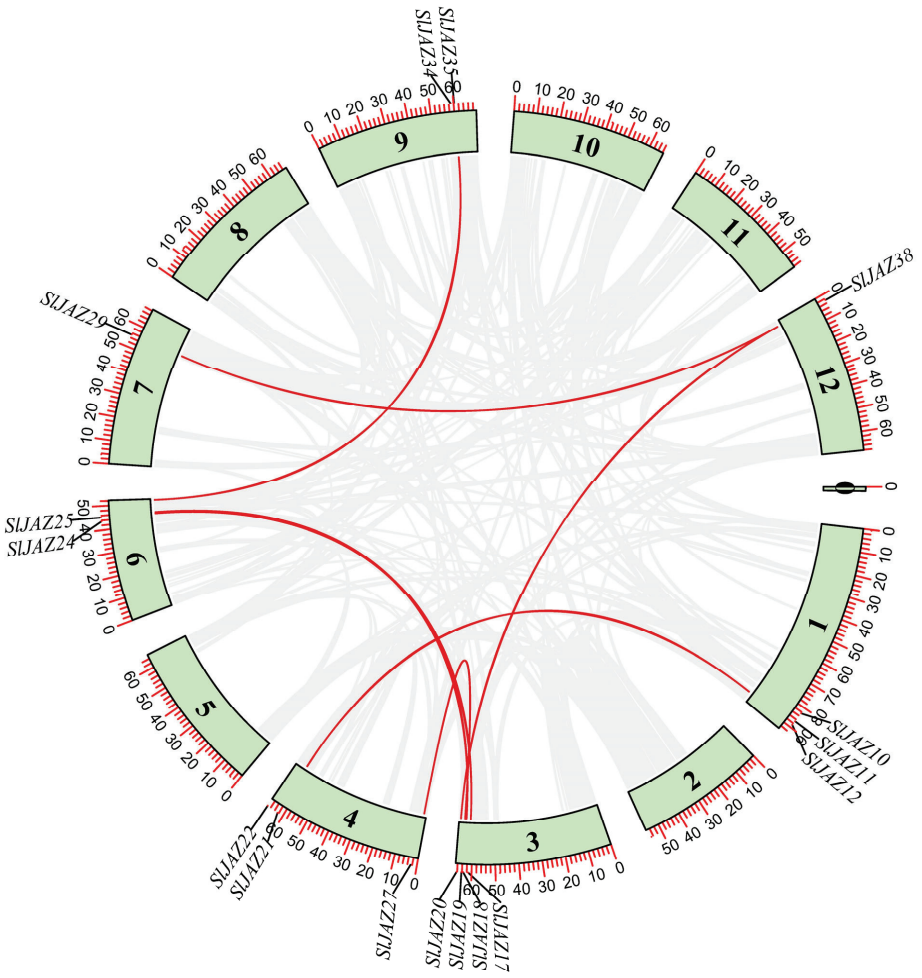


Figure 6. Chromosomal location and duplication events of JAZ genes in *S. lycopersicum*. *SlJAZ* genes predominantly shows segmental duplication.

In addition to the duplication events within *S. lycopersicum*, Figure 7 highlights the synteny relationships of JAZ genes between *S. lycopersicum*, *A. thaliana*, and *S. tuberosum*. Numerous syntenic blocks were observed between *S. lycopersicum* and *S. tuberosum*, and *A.*

thaliana, which is expected due to their shared evolutionary history. *S. lycopersicum* shared 15 syntenic JAZ genes with *Arabidopsis*, while the syntenic genes among *S. lycopersicum* and *S. tuberosum* were 20 (Figure 7). Higher number of syntenic genes among *S. lycopersicum* and *S. tuberosum* showed there more closed evolutionary relationships compared to *Arabidopsis*, which reflects more distant evolutionary relationship between these species. The identification of these syntenic relationships and duplication events is significant in understanding the evolutionary history of the JAZ gene family.

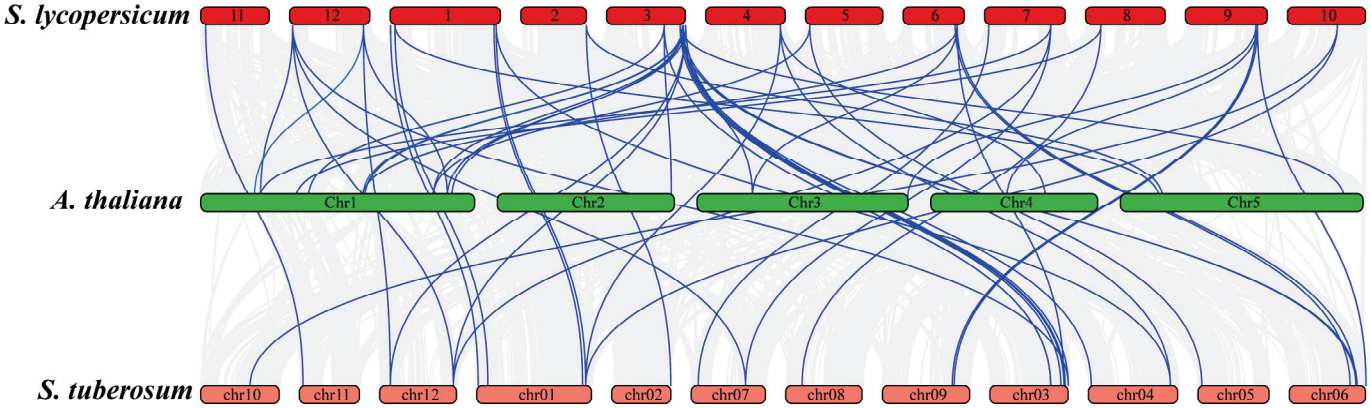


Figure 7. Synteny analysis of JAZ genes between *S. lycopersicum*, *S. tuberosum*, and *A. thaliana*. *S. lycopersicum* and *S. tuberosum* shred more syntenic genes as compared to *S. lycopersicum* and *Arabidopsis*.

3.7. miRNA Prediction

The miRNA prediction analysis identified several miRNAs that may regulate the expression of JAZ genes in *S. lycopersicum*. Overall, 69 miRNAs from 39 families targeted 33 genes (Supplementary Table S4). *SlJAZ25* was targeted by most of the miRNAs, followed by *SlJAZ18*, *SlJAZ12*, and *SlJAZ4*, and so on. Similarly, stu-miR8029, stu-miR8037, stu-miR169f-5p, stu-miR169g, targeted the greatest number of genes (Supplementary Table S4). Schematic representation of miRNAs, target genes, and target sites is given in Figure 8. Specifically, *SlJAZ1*, located on chromosome 1, was predicted to be targeted by two miRNAs: stu-miR8041a-5p and stu-miR5303g. These miRNAs target regions in the coding sequence of *SlJAZ1*, suggesting that they may play a role in post-transcriptional regulation by reducing the stability or translational efficiency of the JAZ transcripts. Similarly, *SlJAZ23*, located on chromosome 5, was also predicted to be targeted by stu-miR8041a-5p, indicating that this miRNA may have multiple regulatory targets within the JAZ gene family. The predicted miRNA binding sites were found in both the 3′ untranslated regions (UTRs) and the coding regions of the JAZ genes, suggesting diverse mechanisms of miRNA-mediated regulation.

3.8. Expression Profiling of SlJAZ Genes Under Different Treatments

The global expression profiles of the 39 *S. lycopersicum* JAZ genes were analyzed across four treatment groups: N/WI (with nanoparticles, without infestation), N/I (with nanoparticles, with infestation), WN/WI (without nanoparticles, without infestation), and WN/I (without nanoparticles, with infestation). The results, visualized in Figure 9 using a heatmap, reveal distinct expression patterns of the JAZ genes in response to the different treatments. Several JAZ genes showed significant upregulation or downregulation under specific treatments. For instance, *SlJAZ9* and *SlJAZ21* exhibited notable downregulation in the N/WI treatment, while *SlJAZ20* and *SlJAZ22* were highly upregulated in the N/I treatment. In the WN/I group, *SlJAZ9* was downregulated, indicating a possible role in

pest stress responses without the influence of nanoparticles. Additionally, *SlJAZ1*, *SlJAZ2*, *SlJAZ3*, *SlJAZ19*, and *SlJAZ22* showed consistent upregulation in response to *T. absoluta* infestation, particularly in the presence of nanoparticles (N/I).

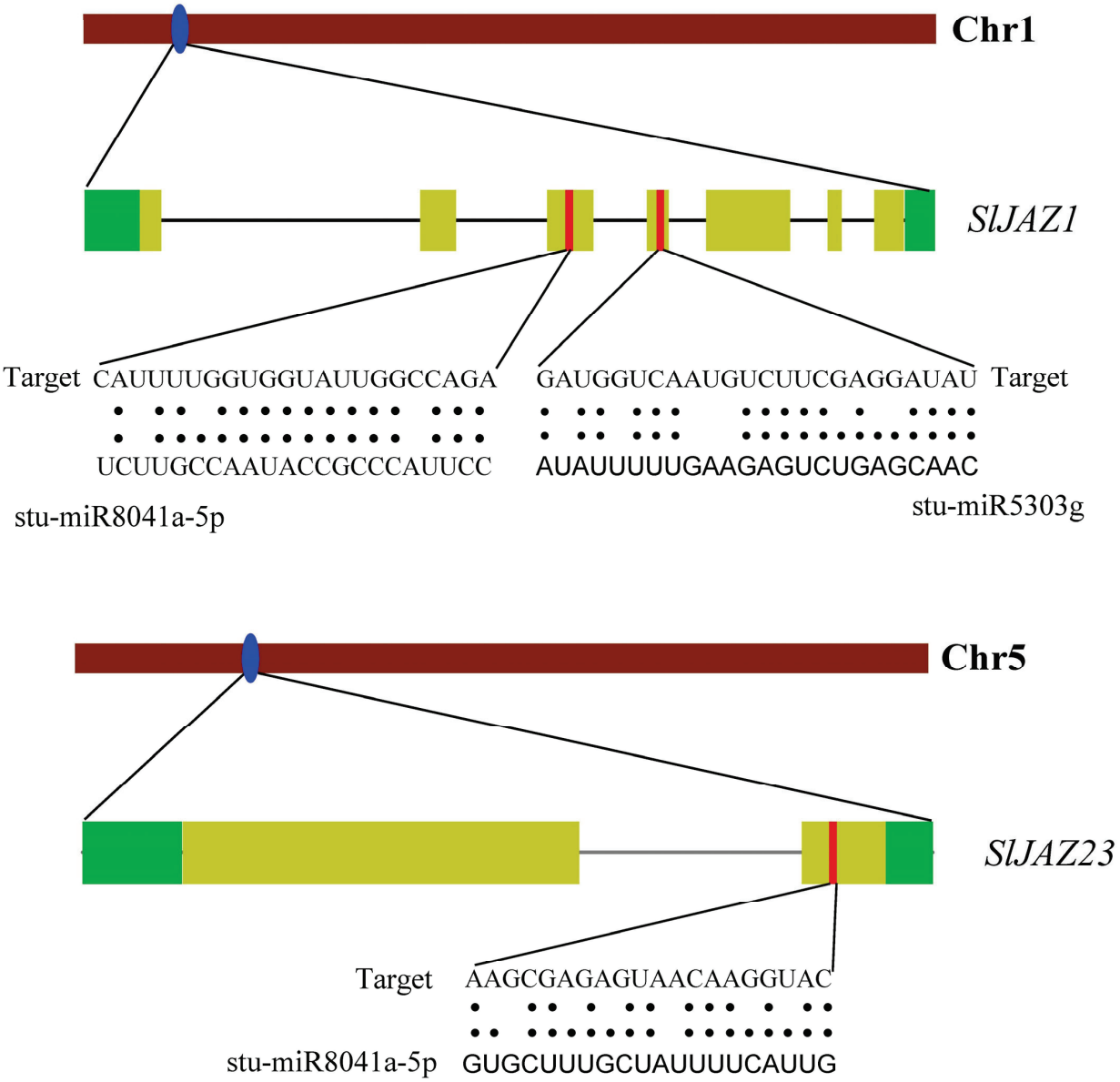


Figure 8. Predicted miRNA target sites in JAZ genes of *S. lycopersicum*. This figure highlights the miRNA binding sites predicted for JAZ genes, focusing on *SlJAZ1* and *SlJAZ23* as potential targets.

SlJAZ1, *SlJAZ19*, *SlJAZ20*, and *SlJAZ22* showed a distinct expression pattern, being significantly upregulated only under the combined treatment of MSNs and *T. absoluta*. This suggests that MSNs may function as priming agents, enhancing the jasmonate pathway to enable a faster or stronger response upon pest attack. The lack of similar upregulation in the MSNs-only or pest-only treatments further indicates that these genes may respond specifically to stress integration rather than individual stimuli. Additionally, the downregulation of *SlJAZ11* and *SlJAZ30* in pest-infested plants without MSNs but not in those pretreated with MSNs implies that nanoparticle exposure may help maintain regulatory homeostasis in jasmonate signalling under biotic stress; however, further studies are warranted to substantiate this role of MSNs and to clarify the underlying regulatory mechanisms.

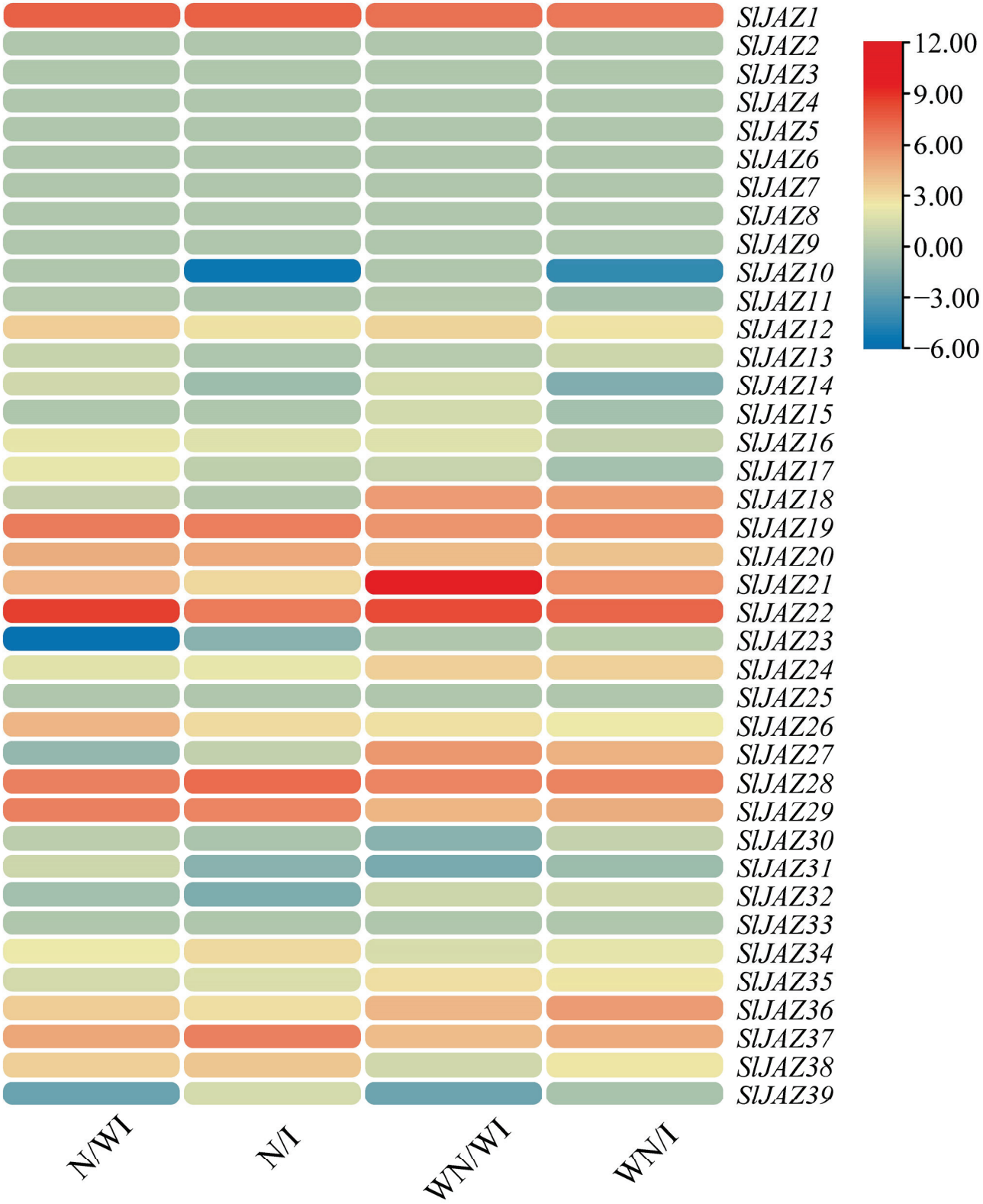


Figure 9. Expression profiling of selected *SlJAZ* genes under different treatments. Heatmaps represent relative expression patterns across the four treatment groups: WN/WI (without MSNs, without infestation), WN/I (without MSNs, with infestation), N/WI (with MSNs, without infestation), and N/I (with MSNs, with infestation). Expression values were $\log_2$-transformed and normalized, with red indicating upregulation and blue indicating downregulation.

3.9. Phenotypic Effects of Tuta absoluta and MSNs on Tomato Plants

To evaluate the role of mesoporous silica nanoparticles (MSNs) in modulating tomato plant resistance against *Tuta absoluta*, we assessed three key phenotypic traits: leaf damage index, larval survival rate, and the number of leaf mines (Table 2). In *T. absoluta*–infested plants without MSN treatment (WN/I), the leaf damage index reached 45.2 ± 4.7%, which was significantly higher than the 20.6 ± 3.8% observed in the MSN-treated infested group (N/I) ($F(3,16) = 92.41$, $p < 0.01$). No visible damage was recorded in the control (WN/WI) or MSN-only (N/WI) groups. Larval survival was also significantly reduced by MSN application. The WN/I group exhibited 84.6 ± 2.9% larval survival, while the N/I treatment led to a marked decrease to 52.3 ± 4.4% ($F(3,16) = 77.86$, $p < 0.01$). The number of leaf mines per leaf declined from 12.4 ± 1.8 in WN/I to 5.1 ± 1.2 in N/I ($F(3,16) = 68.13$, $p < 0.01$), confirming a significant reduction in feeding activity under nanoparticle exposure. No mines were observed in WN/WI or N/WI treatments. Overall, the application of MSNs significantly suppressed pest-induced leaf damage, reduced larval viability, and decreased mining activity, indicating enhanced defense performance under pest pressure.

Table 2. Effects of Mesoporous Silica Nanoparticles (MSNs) and *T. absoluta* Infestation on Leaf Damage, Larval Survival, and Leaf Mining in Tomato Plants.

Treatment Group	Leaf Damage Index (%) (Mean ± SE)	Larval Survival Rate (%) (Mean ± SE)	Number of Leaf Mines per Leaf (Mean ± SE)
WN/WI (Control: No Pest, No MSNs)	0.0 ± 0.0 ^{c}	-	0.0 ± 0.0 ^{c}
WN/I (Pest Only)	45.2 ± 4.7 ^{a}	84.6 ± 2.9 ^{a}	12.4 ± 1.8 ^{a}
N/WI (MSNs Only)	0.0 ± 0.0 ^{c}	-	0.0 ± 0.0 ^{c}
N/I (MSNs + Pest)	20.6 ± 3.8 ^{b}	52.3 ± 4.4 ^{b}	5.1 ± 1.2 ^{b}

Note: Values represent mean ± standard error (SE). Different lowercase letters (a–c) within the same column indicate significant differences among treatments according to one-way ANOVA followed by Tukey's HSD test ($p < 0.05$).

3.10. Regression Analysis of SlJAZ Gene Expression and Pest-Related Parameters

Regression analysis was conducted to evaluate the relationship between the relative expression levels of 13 *SlJAZ* genes and three pest-related phenotypic parameters: leaf damage index, larval survival rate, and number of leaf mines. The analysis revealed gene-specific variations in the strength and direction of association with each trait. For leaf damage index, *SlJAZ20* showed the highest coefficient of determination ($R^2 = 0.831$, $p = 0.090$), followed by *SlJAZ29* ($R^2 = 0.579$, $p = 0.281$) and *SlJAZ26* ($R^2 = 0.462$, $p = 0.365$). Similarly, negative correlations were observed between *SlJAZ20*, *SlJAZ26*, and *SlJAZ29* expression and the number of leaf mines, with *SlJAZ20* again exhibiting the strongest correlation ($R^2 = 0.831$). Regression coefficients for genes such as *SlJAZ31*, *SlJAZ39*, and *SlJAZ10* remained low ($R^2 < 0.2$) across all traits, indicating weak associations. For larval survival rate, valid regression could only be performed for treatments with complete data. Among these, *SlJAZ20* and *SlJAZ29* yielded the highest R^2 values (0.923 and 0.853, respectively), indicating potential associations under specific conditions (Supplementary Table S5).

3.11. qPCR Validation

Quantitative real-time PCR (qPCR) was performed to validate the RNA-seq results for a subset of 12 *SlJAZ* genes that showed significant differential expression across the four treatment groups: WN/WI (without nanoparticles, without infestation), WN/I (without nanoparticles, with infestation), N/WI (with nanoparticles, without infestation), and N/I

(with nanoparticles, with infestation). The relative expression levels (Figure 10) were largely consistent with RNA-seq data and highlighted three distinct trends. The comparison of WN/WI with WN/I revealed transcriptional responses to pest infestation. *SlJAZ21* was strongly downregulated under infestation, while *SlJAZ22* showed moderate induction, suggesting divergent roles in basal defense signaling. Several other genes, including *SlJAZ1*, *SlJAZ19*, and *SlJAZ20*, were also significantly induced by infestation. The comparison of WN/WI with N/WI showed that MSN treatment alone was sufficient to trigger the upregulation of multiple genes, including *SlJAZ21* and *SlJAZ22*. This suggests that nanoparticles may act as priming agents, enhancing the readiness of JA signaling components even in the absence of biotic stress. Under combined treatment (N/I), several genes displayed expression patterns that differed from those observed under either stress or nanoparticle exposure alone. Notably, the downregulation of *SlJAZ21* observed in WN/I was reversed under N/I, while *SlJAZ22* exhibited further induction. Similarly, *SlJAZ27* and *SlJAZ37* showed their highest expression in the N/I group. These results indicate that MSN pretreatment not only modifies the expression of individual JAZ genes but also influences their regulatory behavior under pest challenge.

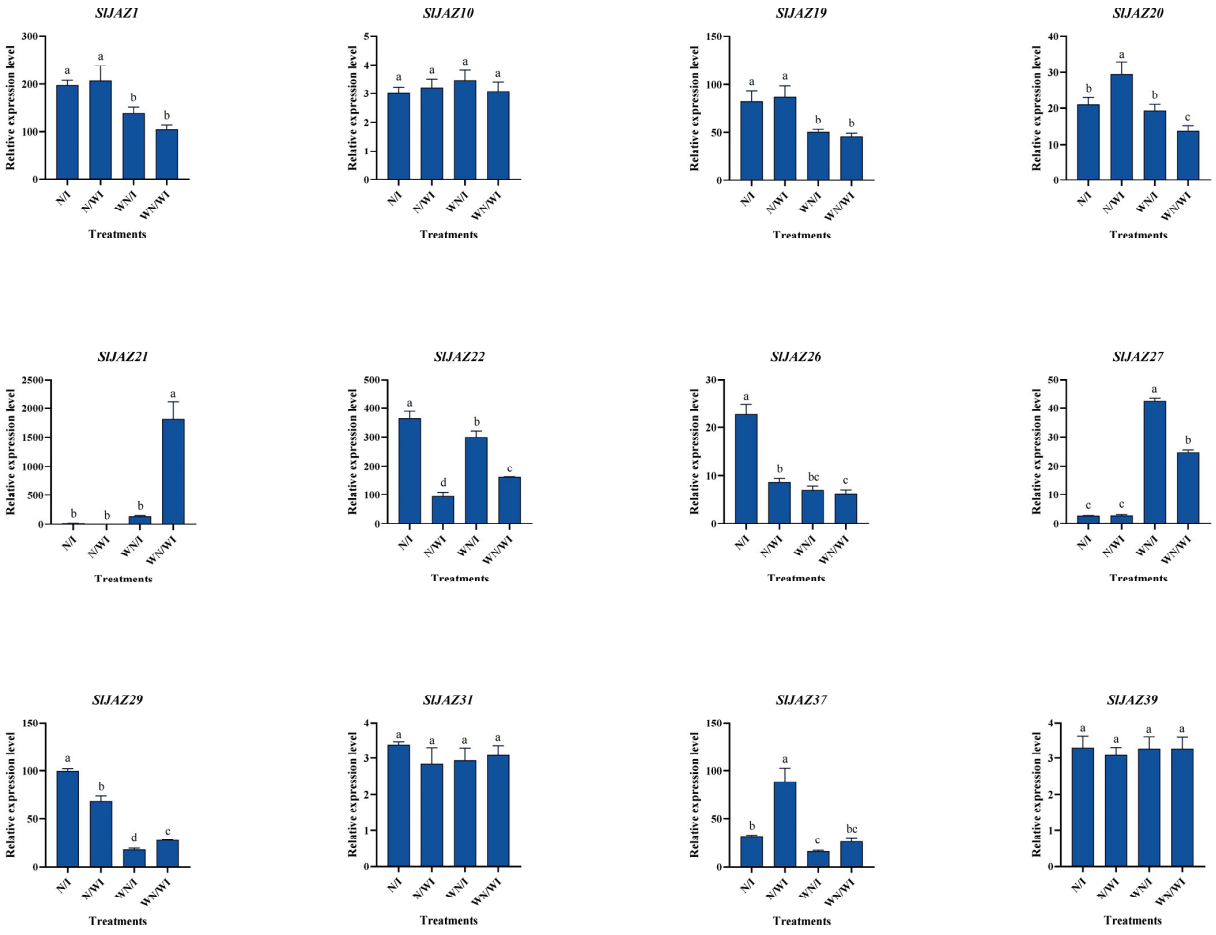


Figure 10. Validation of JAZ gene expression by qPCR in *S. lycopersicum* under different treatments. This figure confirms RNA-seq expression trends for selected JAZ genes across the four treatment groups: N/WI (nanoparticles without infestation), N/I (nanoparticles with infestation), WN/WI (no nanoparticles, no infestation), and WN/I (no nanoparticles, with infestation) using quantitative real-time PCR. Different lowercase letters (a–d) above the bars indicate statistically significant differences among treatments according to one-way ANOVA followed by Tukey's HSD test ($p < 0.05$).

4. Discussion

The JAZ gene family in *S. lycopersicum* is integral to jasmonate (JA) signaling, a pathway critical for coordinating defense responses against a wide range of biotic stresses [5,46]. JAZ proteins act as transcriptional repressors, preventing the activation of JA-responsive genes under normal conditions. When plants encounter stress, JA levels rise, triggering the ubiquitination and degradation of JAZ proteins, thereby relieving their repression on transcription factors like MYC2, which initiates the expression of defense-related genes [4,47]. Our results align with this model, demonstrating that several JAZ genes in tomato, including *SlJAZ1*, *SlJAZ9*, and *SlJAZ19*, respond to pest and nanoparticle treatments through differential expression. These findings mirror observations by Campos et al. [48], who reported that specific JAZ genes in tomato are selectively activated in response to stress, underscoring their specialized roles within the plant's defense network. Compared with the earlier report by Sun et al. [49] which identified 26 *SlJAZ* genes and Thines et al. [50], who reported 17 genes, our analysis revealed 39 members in tomato. This expansion was made possible by the use of updated genome annotation combined with advanced domain- and profile-based searches using the Pfam database, SMART, and HMMER3.0. Integration of these tools allowed us to detect additional low-similarity sequences carrying the conserved TIFY and/or Jas domains, thereby expanding the repertoire of JAZ genes identified in tomato.

Moreover, phylogenetic and structural analyses of JAZ genes suggest that these genes have diversified to fulfill specialized functions across species [51,52]. In tomato, *SlJAZ21* and *SlJAZ22* exhibited contrasting expression responses; *SlJAZ21* was suppressed by infestation but restored under MSN treatment, whereas *SlJAZ22* was consistently induced, suggesting functional divergence between these two closely related members. Similar findings in other plant species, such as *A. thaliana* and *O. sativa*, reveal that JAZ genes have undergone adaptive evolution, equipping plants with finely tuned responses to environmental stressors [3,50]. These comparisons highlight that while the core functions of JAZ proteins in JA signaling are conserved, the gene family's diversity allows for flexible and specific responses, a feature that could be exploited in breeding for enhanced pest resistance.

Nanotechnology has emerged as an innovative approach to enhance plant resilience, and mesoporous silica nanoparticles (MSNs) have shown potential in modulating plant physiology [25,53]. In this study, MSNs were applied to tomato plants to examine their effects on JAZ gene expression, revealing significant upregulation of genes such as *SlJAZ20* and *SlJAZ22*. These results are consistent with previous research by Torabian, Zahedi and Khoshgoftar [25], who found that nanoparticles can induce stress tolerance mechanisms by modulating gene expression, particularly under abiotic stresses such as salinity. MSNs are thought to enhance defense pathways by acting as elicitors, potentially priming the plant's defense machinery through interaction with key regulatory pathways like JA signaling [54]. The upregulation of *SlJAZ20* and *SlJAZ22* suggests that MSNs may influence JA signaling, a mechanism previously observed in studies on nanoparticle-mediated priming of defense responses in wheat and rice [55].

While MSNs have been widely studied for their ability to deliver agrochemicals and enhance nutrient availability [56], their direct influence on transcriptional regulation in defense pathways is relatively novel. Here, MSNs may have induced a "primed" state, wherein the JA pathway is activated upon the onset of pest pressure, providing plants with a rapid and robust defense response. This mechanism aligns with studies on silicon nanoparticles in plants, which have shown that nanoparticles can activate antioxidant and other defense-related genes [57,58]. Consequently, MSNs offer a promising alternative

to traditional chemical pesticides by activating innate defense pathways and enhancing resilience, reducing environmental toxicity concerns [59].

T. absoluta, commonly known as the tomato leaf miner, is a significant pest of tomato crops worldwide, and managing this pest has become increasingly challenging due to its resistance to chemical pesticides [27,60]. The current study shows that *T. absoluta* infestation significantly alters JAZ gene expression in tomato plants, with distinct expression patterns observed in tolerant and susceptible plants. In untreated plants under infestation (WN/I), *SlJAZ9* and *SlJAZ21* were significantly downregulated, suggesting that pest-induced stress can suppress specific components of the JA pathway. Such suppression has been associated with increased susceptibility in previous studies [47]. Conversely, genes such as *SlJAZ1* and *SlJAZ19* were upregulated, potentially reflecting an attempt by the plant to mount a defense response.

Our findings further indicate that MSNs may have a protective effect, as evidenced by higher expression levels of several JAZ genes in MSN-treated plants under infestation (N/I). This observation supports studies by Raliya, Nair, Chavalmane, Wang and Biswas [57] and Sun, Hussain, Yi, Rookes, Kong and Cahill [56], which suggest that nanoparticle application can enhance defense responses under biotic stress conditions. The expression of JAZ genes, particularly *SlJAZ1*, *SlJAZ2*, and *SlJAZ3*, in the presence of MSNs suggests that these nanoparticles might mitigate pest-induced stress, enhancing plant resilience. This response aligns with recent work showing that nanoparticle-treated plants often exhibit upregulated antioxidant and defense pathways [55,58], offering a dual benefit of enhanced pest tolerance and potential growth support under pest pressure.

The combined treatment of MSNs and *T. absoluta* infestation (N/I) resulted in notable upregulation of key *JAZ* genes, suggesting that nanoparticle application primes the plant for an enhanced transcriptional response to pest stress. Such priming effects, where MSNs strengthen defense signaling and mitigate pest-induced suppression, are increasingly recognized in plant defense studies [59,61]. The observed upregulation of *SlJAZ19*, *SlJAZ20*, and *SlJAZ22* indicates that MSNs may enhance JA signaling responsiveness, effectively "priming" the plant for faster and stronger defense activation upon pest encounter. This finding aligns with research by Raliya, Nair, Chavalmane, Wang and Biswas [57], who reported that nanoparticles can trigger priming mechanisms, resulting in a more resilient plant response to subsequent stress.

The differential expression patterns of *SlJAZ* genes under the combined MSNs and *T. absoluta* treatment, as shown in Figure 10, suggest that members of the same gene family can play functionally distinct roles depending on environmental and stress cues. Similar divergence has been reported in other plant species—for instance, in *Arabidopsis*, AtJAZ1 and AtJAZ10 show opposite transcriptional responses under insect herbivory and hormonal treatments, indicating sub-functionalization within the gene family [47,62]. Likewise, in *Oryza sativa*, *OsJAZ* genes exhibit tissue-specific and stimulus-dependent expression divergence [63]. Such variation may arise from differences in promoter cis-regulatory elements, miRNA targeting, or protein–protein interactions within the JA signalling network. In tomatoes, the distinct cis-element profiles and predicted miRNA regulation of *SlJAZ* genes (Figure 6 and Supplementary Table S3) likely contribute to this heterogeneity. Moreover, nanoparticle exposure may alter hormonal sensitivity or redox balance, further influencing gene-specific expression.

Recent studies have highlighted the complexity of JAZ interactions with transcription factors in tomato defence against root-knot nematodes. For instance, Huang et al. [64] demonstrated that *SlWRKY45* physically interacts with multiple *SlJAZ* proteins, notably *SlJAZ1*, *SlJAZ2*, *SlJAZ7*, and *SlJAZ11*, and negatively regulates *Meloidogyne incognita* re-

sistance by repressing JA biosynthesis through inhibition of *SlAOC* transcription. More recently, Huang et al. [65] revealed that *SlVQ15* recruits *SlWRKY30IIc*, which in turn binds the promoters of *SlJAZs* and represses their expression, establishing a regulatory loop in which *SlJAZ5* interferes with this interaction. These findings reflect intricate layers of feedback within JA signalling. Our current study complements these works by demonstrating that specific *SlJAZ* genes—such as *SlJAZ1*, *SlJAZ19*, and *SlJAZ22*—respond dynamically to MSNs and *T. absoluta* stress, suggesting that *JAZ-TF* complexes may also function under abiotic-biotic interaction contexts and could be sensitive to nanoparticle-based elicitors. Priming is a well-established concept in plant defense, typically induced by biological or chemical elicitors that "train" the plant to respond more effectively to future stresses [66]. In this study, MSNs appear to serve as abiotic priming agents, preparing the JA pathway to be more responsive to *T. absoluta* infestation. Such an effect has been documented with silicon nanoparticles, where pre-treated plants exhibit heightened defense responses when challenged by pests or pathogens [25,58,67]. Furthermore, the mitigating effect of MSNs under pest infestation suggests that these nanoparticles can enhance and sustain the plant's innate defenses, thereby reducing the need for high pesticide inputs and offering a sustainable alternative that addresses environmental and health concerns [59]. Compared to previous studies that primarily focused on the structural identification and hormonal response of JAZ family members in tomato [49] or broadly characterized the JAZ role in jasmonate signalling [50], our study provides several novel insights. First, we present an updated and expanded genome-wide identification of 39 *SlJAZ* genes using the latest SL4.0 reference genome and domain-specific HMM profiling. Second, we integrate bioinformatics analyses with transcriptomic profiling under both mesoporous silica nanoparticles (MSNs) and *T. absoluta* stress conditions, offering the first exploration of nanoparticle-induced modulation of JAZ expression in tomato. Third, we report miRNA targeting predictions, protein–protein interaction networks, and syntenic relationships with other species, providing a multi-dimensional view of JAZ gene regulation.

In this study, synteny comparisons were made with *S. tuberosum* as the closest sequenced Solanaceae relative and *A. thaliana* as a widely used reference model. While these comparisons confirmed the expected evolutionary relationships, the inclusion of additional Solanaceae species such as *Capsicum annuum* or *Nicotiana tabacum* in future analyses would provide a more nuanced view of JAZ gene evolution across the family. Another limitation of this study is the absence of detailed phenotypic validation of tomato plants treated with MSNs under *T. absoluta* infestation. While our transcriptomic findings highlight potential roles of specific *SlJAZ* genes in JA-mediated defence, the lack of supporting physiological or agronomic data—such as pest damage assessment, plant growth measurements, or yield performance—prevents a full understanding of the functional impact. Future research should include comprehensive phenotypic analyses to confirm whether the transcriptional responses observed here translate into measurable resistance traits and improved plant performance in field conditions. The ability of MSNs to mitigate the adverse effects of *T. absoluta* infestation highlights their potential as a sustainable component of integrated pest management. By activating and priming natural defense pathways like the JA signaling cascade, MSNs offer a biologically favorable approach to pest control, potentially reducing pesticide reliance. This study's findings contribute to a growing body of evidence suggesting that nanoparticle priming could be strategically implemented to strengthen crop resilience, thus paving the way for sustainable agricultural practices.

5. Conclusions

This study provides a comprehensive genome-wide characterization of the *SlJAZ* gene family in tomato and demonstrates their involvement in jasmonate-mediated defense responses under *T. absoluta* infestation and mesoporous silica nanoparticle (MSN) treatment. A total of 39 *SlJAZ* genes were identified, exhibiting diverse structural features, conserved motifs, and evolutionary conservation with orthologs in Arabidopsis and potato. Transcriptome profiling and qRT-PCR validation revealed that several *SlJAZ* genes, particularly *SlJAZ1*, *SlJAZ19*, *SlJAZ20*, and *SlJAZ22*, were induced under combined MSN and pest stress. Phenotypic assessments confirmed that MSN application reduced leaf damage, larval survival, and mining activity. Notably, regression analysis indicated that the expression of *SlJAZ20*, *SlJAZ26*, and *SlJAZ29* negatively correlated with pest-induced damage, suggesting their regulatory role in defense activation. Together, these findings establish MSNs as eco-compatible elicitors of JA-dependent immunity and identify specific *SlJAZ* genes as candidate markers for breeding insect-resistant tomato cultivars. The integration of nanotechnology, gene expression profiling, and phenotypic validation offers a promising strategy for enhancing plant resilience and reducing reliance on chemical pesticides in sustainable agriculture.

Supplementary Materials: The following supporting information can be downloaded at: https://www.mdpi.com/article/10.3390/insects16101046/s1, Supplementary Figure S1: Schematic of mesoporous silica nanoparticles (MSNs), Supplementary Table S1: Primers Used to study the expression of *SlJAZ* genes, Supplementary Table S2: Identified *JAZ* genes in the *S. lycopersicum* genome and their physicochemical properties, Supplementary Table S3: Top 12 identified conserved motif in SlJAZ proteins, Supplementary Table S4: Predicted miRNAs targeting *SlJAZ* genes, Supplementary Table S5: Regression analysis between the relative expression levels of qRT-PCR–validated *SlJAZ* genes and pest-related phenotypic parameters in tomato under different treatment conditions.

Author Contributions: Conceptualization, I.U.H. and Y.H.; methodology, I.U.H. and A.B.; software, A.B., M.H., M.N.S., Y.S., M.A.G., X.C. and A.A.; validation, I.U.H., N.Y.R., A.B. and Y.S.; formal analysis, A.A., N.Y.R., M.N.S. and I.U.H.; investigation, I.U.H., N.Y.R., M.H. and M.A.G.; resources, X.C. and Y.H.; data curation, M.H., A.A., M.N.S., X.C. and M.A.G.; writing—original draft preparation, I.U.H.; writing—review and editing, A.B., A.A., N.Y.R., M.H., M.N.S., Y.S., M.A.G., X.C. and Y.H.; visualization, Y.S.; supervision, Y.H.; project administration, Y.H.; funding acquisition, Y.H. All authors have read and agreed to the published version of the manuscript.

Funding: This work was supported by the National Natural Science Foundation of China (U22A20489; 32361143791).

Data Availability Statement: The original contributions presented in this study are included in the article/Supplementary Materials. Further inquiries can be directed to the corresponding author.

Acknowledgments: We would like to thank all of the participants who volunteered their time in the study. We appreciate very much the valuable comments and suggestion by the Reviewers and Editors. We acknowledge the use of artificial intelligence tools for language editing and manuscript drafting assistance, while the research, ideas, and conclusions remain solely the authors' work. All authors have reviewed and approved the final version, maintaining full responsibility for its content.

Conflicts of Interest: The authors declare no conflicts of interest.

Abbreviations

The following abbreviations are used in this manuscript:

JA	Jasmonic Acid
JAZ	Jasmonate ZIM-domain
MSNs	Mesoporous Silica Nanoparticles
qRT-PCR	Quantitative Real-Time Polymerase Chain Reaction
DEGs	Differentially Expressed Genes
SlJAZ	*Solanum lycopersicum* JAZ
GO	Gene Ontology
KEGG	Kyoto Encyclopedia of Genes and Genomes
miRNA	MicroRNA
LDI	Leaf Damage Index
LSR	Larval Survival Rate
LMN	Leaf Mine Number
R^2	Coefficient of Determination
FDR	False Discovery Rate
ANOVA	Analysis of Variance

References

1. Apostolova, E.L. Molecular Mechanisms of Plant Defense against Abiotic Stress. *Int. J. Mol. Sci.* **2023**, *24*, 10339. [CrossRef]
2. Wang, Y.; Mostafa, S.; Zeng, W.; Jin, B. Function and mechanism of jasmonic acid in plant responses to abiotic and biotic stresses. *Int. J. Mol. Sci.* **2021**, *22*, 8568. [CrossRef]
3. Pauwels, L.; Goossens, A. The JAZ proteins: A crucial interface in the jasmonate signaling cascade. *Plant Cell* **2011**, *23*, 3089–3100. [CrossRef] [PubMed]
4. Browse, J. Jasmonate passes muster: A receptor and targets for the defense hormone. *Annu. Rev. Plant Biol.* **2009**, *60*, 183–205. [CrossRef]
5. Wasternack, C.; Hause, B. Jasmonates: Biosynthesis, perception, signal transduction and action in plant stress response, growth and development. An update to the 2007 review in Annals of Botany. *Ann. Bot.* **2013**, *111*, 1021–1058. [CrossRef]
6. Kazan, K.; Manners, J.M. JAZ repressors and the orchestration of phytohormone crosstalk. *Trends Plant Sci.* **2012**, *17*, 22–31. [CrossRef]
7. Song, S.; Qi, T.; Wasternack, C.; Xie, D. Jasmonate signaling and crosstalk with gibberellin and ethylene. *Curr. Opin. Plant Biol.* **2014**, *21*, 112–119. [CrossRef]
8. Chen, S.; Zhang, L.; Ma, Q.; Chen, M.; Cao, X.; Zhao, S.; Zhang, X. Jasmonate ZIM Domain Protein (JAZ) Gene SLJAZ15 Increases Resistance to Orobanche aegyptiaca in Tomato. *Plants* **2024**, *13*, 1493. [CrossRef] [PubMed]
9. Liu, W.; Liu, K.; Chen, D.; Zhang, Z.; Li, B.; El-Mogy, M.M.; Tian, S.; Chen, T. *Solanum lycopersicum*, a model plant for the studies in developmental biology, stress biology and food science. *Foods* **2022**, *11*, 2402. [CrossRef] [PubMed]
10. Wasternack, C.; Song, S. Jasmonates: Biosynthesis, metabolism, and signaling by proteins activating and repressing transcription. *J. Exp. Bot.* **2016**, *68*, 1303–1321. [CrossRef]
11. Panno, S.; Davino, S.; Caruso, A.G.; Bertacca, S.; Crnogorac, A.; Mandić, A.; Noris, E.; Matić, S. A review of the most common and economically important diseases that undermine the cultivation of tomato crop in the mediterranean basin. *Agronomy* **2021**, *11*, 2188. [CrossRef]
12. Qi, T.; Huang, H.; Song, S.; Xie, D. Regulation of jasmonate-mediated stamen development and seed production by a bHLH-MYB complex in Arabidopsis. *Plant Cell* **2015**, *27*, 1620–1633. [CrossRef]
13. Zhang, X.; Zhou, Y.; Dhanasekaran, S.; Wang, J.; Zhou, H.; Gu, X.; Li, B.; Zhao, L.; Zhang, H. Insights into the defense mechanisms involved in the induction of resistance against black spot of cherry tomatoes by *Pichia caribbica*. *LWT* **2022**, *169*, 113973. [CrossRef]
14. Song, S.; Qi, T.; Fan, M.; Zhang, X.; Gao, H.; Huang, H.; Wu, D.; Guo, H.; Xie, D. The bHLH subgroup IIId factors negatively regulate jasmonate-mediated plant defense and development. *PLoS Genet.* **2013**, *9*, e1003653. [CrossRef] [PubMed]
15. Zhou, W.; Li, M.; Achal, V. A comprehensive review on environmental and human health impacts of chemical pesticide usage. *Emerg. Contam.* **2024**, *11*, 100410. [CrossRef]
16. Liu, B.; Seong, K.; Pang, S.; Song, J.; Gao, H.; Wang, C.; Zhai, J.; Zhang, Y.; Gao, S.; Li, X. Functional specificity, diversity, and redundancy of Arabidopsis JAZ family repressors in jasmonate and COI1—Regulated growth, development, and defense. *New Phytol.* **2021**, *231*, 1525–1545. [CrossRef] [PubMed]
17. Song, S.; Liu, B.; Song, J.; Pang, S.; Song, T.; Gao, S.; Zhang, Y.; Huang, H.; Qi, T. A molecular framework for signaling crosstalk between jasmonate and ethylene in anthocyanin biosynthesis, trichome development, and defenses against insect herbivores in Arabidopsis. *J. Integr. Plant Biol.* **2022**, *64*, 1770–1788. [CrossRef]

18. Song, J.; Pang, S.; Xue, B.; Rong, D.; Qi, T.; Huang, H.; Song, S. The AMS/DYT1–MYB module interacts with the MED25–MYC–MYB complexes to inhibit jasmonate—Regulated floral defense in Arabidopsis. *J. Integr. Plant Biol.* **2025**, *67*, 408–422. [CrossRef]
19. Mariyam, S.; Upadhyay, S.K.; Chakraborty, K.; Verma, K.K.; Duhan, J.S.; Muneer, S.; Meena, M.; Sharma, R.K.; Ghodake, G.; Seth, C.S. Nanotechnology, a frontier in agricultural science, a novel approach in abiotic stress management and convergence with new age medicine-A review. *Sci. Total Environ.* **2023**, *912*, 169097. [CrossRef]
20. Haq, I.U.; Cai, X.; Ali, H.; Akhtar, M.R.; Ghafar, M.A.; Hyder, M.; Hou, Y. Interactions Between Nanoparticles and Tomato Plants: Influencing Host Physiology and the Tomato Leafminer's Molecular Response. *Nanomaterials* **2024**, *14*, 1788. [CrossRef]
21. Okeke, E.S.; Nweze, E.J.; Ezike, T.C.; Nwuche, C.O.; Ezeorba, T.P.C.; Nwankwo, C.E.I. Silicon-based nanoparticles for mitigating the effect of potentially toxic elements and plant stress in agroecosystems: A sustainable pathway towards food security. *Sci. Total Environ.* **2023**, *898*, 165446. [CrossRef]
22. Haq, I.U.; Liu, H.; Ghafar, M.A.; Zafar, S.; Subhan, M.; Abbasi, A.; Hyder, M.; Basit, A.; Rebouh, N.Y.; Hou, Y. Mesoporous Silica Nanoparticles Impair Physiology and Reproductive Fitness of *Tuta absoluta* Through Plant-Mediated Oxidative Stress and Enzymatic Disruption. *Insects* **2025**, *16*, 877. [CrossRef]
23. Gao, Y.; Gao, D.; Shen, J.; Wang, Q. A review of mesoporous silica nanoparticle delivery systems in chemo-based combination cancer therapies. *Front. Chem.* **2020**, *8*, 598722. [CrossRef]
24. Dilnawaz, F.; Misra, A.N.; Apostolova, E. Involvement of nanoparticles in mitigating plant's abiotic stress. *Plant Stress* **2023**, *10*, 100280. [CrossRef]
25. Torabian, S.; Zahedi, M.; Khoshgoftar, A.H. Effects of foliar spray of nano-particles of FeSO4 on the growth and ion content of sunflower under saline condition. *J. Plant Nutr.* **2017**, *40*, 615–623. [CrossRef]
26. Yang, H.; Zhang, C.; Shen, Y.; Gao, H.; Zhang, G.; Liu, W.; Jiang, H.; Zhang, Y. Life Table Parameters of the Tomato Leaf Miner *Tuta absoluta* (Lepidoptera: Gelechiidae) on Five Tomato Cultivars in China. *Insects* **2024**, *15*, 208. [CrossRef] [PubMed]
27. Desneux, N.; Wajnberg, E.; Wyckhuys, K.A.; Burgio, G.; Arpaia, S.; Narváez-Vasquez, C.A.; González-Cabrera, J.; Catalán Ruescas, D.; Tabone, E.; Frandon, J. Biological invasion of European tomato crops by *Tuta absoluta*: Ecology, geographic expansion and prospects for biological control. *J. Pest Sci.* **2010**, *83*, 197–215. [CrossRef]
28. Mahlangu, L.; Sibisi, P.; Nofemela, R.S.; Ngmenzuma, T.; Ntushelo, K. The differential effects of *Tuta absoluta* infestations on the physiological processes and growth of tomato, potato, and eggplant. *Insects* **2022**, *13*, 754. [CrossRef] [PubMed]
29. Ong'onge, M.A.; Ajene, I.J.; Runo, S.; Sokame, B.M.; Khamis, F.M. Population dynamics and insecticide resistance in *Tuta absoluta* (Lepidoptera: Gelechiidae), an invasive pest on tomato in Kenya. *Heliyon* **2023**, *9*, e21465. [CrossRef] [PubMed]
30. Yalcin, M.; Mermer, S.; Kozaci, L.D.; Turgut, C. Insecticide resistance in two populations of *Tuta absoluta* (Meyrick, 1917) (Lepidoptera: Gelechiidae) from Turkey. *Turk. J. Entomol.* **2015**, *39*, 137–145.
31. Tropea Garzia, G.; Siscaro, G.; Biondi, A.; Zappalà, L. *Tuta absoluta*, a South American pest of tomato now in the EPPO region: Biology, distribution and damage. *EPPO Bull.* **2012**, *42*, 205–210. [CrossRef]
32. Guedes, R.N.C.; Walse, S.S.; Throne, J.E. Sublethal exposure, insecticide resistance, and community stress. *Curr. Opin. Insect Sci.* **2017**, *21*, 47–53. [CrossRef]
33. Hajiahmadi, Z.; Shirzadian-Khorramabad, R.; Kazemzad, M.; Sohani, M.M. Enhancement of tomato resistance to *Tuta absoluta* using a new efficient mesoporous silica nanoparticle-mediated plant transient gene expression approach. *Sci. Hortic.* **2019**, *243*, 367–375. [CrossRef]
34. Chen, S.; Guo, X.; Zhang, B.; Nie, D.; Rao, W.; Zhang, D.; Lü, J.; Guan, X.; Chen, Z.; Pan, X. Mesoporous silica nanoparticles induce intracellular peroxidation damage of Phytophthora infestans: A new type of green fungicide for late blight control. *Environ. Sci. Technol.* **2023**, *57*, 3980–3989. [CrossRef]
35. Hussey, N.; Parr, W. The effect of glasshouse red spider mite (*Tetranychus urticae* Koch) on the yield of cucumbers. *J. Hortic. Sci.* **1963**, *38*, 255–263. [CrossRef]
36. Škaloudová, B.; Křivan, V.; Zemek, R. Computer-assisted estimation of leaf damage caused by spider mites. *Comput. Electron. Agric.* **2006**, *53*, 81–91. [CrossRef]
37. Rocandio-Rodríguez, M.; Torres-Castillo, J.A.; Juárez-Aragón, M.C.; Chacón-Hernández, J.C.; Moreno-Ramírez, Y.d.R.; Mora-Ravelo, S.G.; Delgado-Martínez, R.; Hernández-Juárez, A.; Heinz-Castro, R.T.Q.; Reyes-Zepeda, F. Evaluation of Resistance of Eleven Maize Races (*Zea mays* L.) to the Red Spider Mite (*Tetranychus merganser*, Boudreaux). *Plants* **2022**, *11*, 1414. [CrossRef] [PubMed]
38. Lee, D.H.; Park, J.-J.; Cho, K. Characterization of leaf mining damage of *Liriomyza trifolii* (Diptera: Agromyzidae) in Cherry-Tomato Greenhouse. *J. Asia Pacif. Entomol.* **2004**, *7*, 201–205. [CrossRef]
39. Chen, C.; Chen, H.; Zhang, Y.; Thomas, H.R.; Frank, M.H.; He, Y.; Xia, R. TBtools: An integrative toolkit developed for interactive analyses of big biological data. *Mol. Plant* **2020**, *13*, 1194–1202. [CrossRef] [PubMed]

40. Gasteiger, E.; Gattiker, A.; Hoogland, C.; Ivanyi, I.; Appel, R.D.; Bairoch, A. ExPASy: The proteomics server for in-depth protein knowledge and analysis. *Nucleic Acids Res.* **2003**, *31*, 3784–3788.
41. Yu, C.S.; Chen, Y.C.; Lu, C.H.; Hwang, J.K. Prediction of protein subcellular localization. *Proteins Struct. Funct. Bioinform.* **2006**, *64*, 643–651. [CrossRef]
42. Bailey, T.L.; Johnson, J.; Grant, C.E.; Noble, W.S. The MEME suite. *Nucleic Acids Res.* **2015**, *43*, W39–W49. [CrossRef]
43. Kumar, S.; Stecher, G.; Li, M.; Knyaz, C.; Tamura, K. MEGA X: Molecular evolutionary genetics analysis across computing platforms. *Mol. Biol. Evol.* **2018**, *35*, 1547–1549. [CrossRef]
44. Yuan, Y.; Bayer, P.E.; Scheben, A.; Chan, C.-K.K.; Edwards, D. BioNanoAnalyst: A visualisation tool to assess genome assembly quality using BioNano data. *BMC Bioinform.* **2017**, *18*, 323. [CrossRef] [PubMed]
45. Dai, X.; Zhuang, Z.; Zhao, P.X. psRNATarget: A plant small RNA target analysis server (2017 release). *Nucleic Acids Res.* **2018**, *46*, W49–W54. [CrossRef] [PubMed]
46. Yan, Y.; Christensen, S.; Isakeit, T.; Engelberth, J.; Meeley, R.; Hayward, A.; Emery, R.N.; Kolomiets, M.V. Disruption of OPR7 and OPR8 reveals the versatile functions of jasmonic acid in maize development and defense. *Plant Cell* **2012**, *24*, 1420–1436. [CrossRef] [PubMed]
47. Chini, A.; Fonseca, S.; Fernandez, G.; Adie, B.; Chico, J.M.; Lorenzo, O.; García-Casado, G.; López-Vidriero, I.; Lozano, F.; Ponce, M. The JAZ family of repressors is the missing link in jasmonate signalling. *Nature* **2007**, *448*, 666–671. [CrossRef]
48. Campos, M.L.; De Almeida, M.; Rossi, M.L.; Martinelli, A.P.; Litholdo Junior, C.G.; Figueira, A.; Rampelotti-Ferreira, F.T.; Vendramim, J.D.; Benedito, V.A.; Pereira Peres, L.E. Brassinosteroids interact negatively with jasmonates in the formation of anti-herbivory traits in tomato. *J. Exp. Bot.* **2009**, *60*, 4347–4361. [CrossRef]
49. Sun, Y.; Liu, C.; Liu, Z.; Zhao, T.; Jiang, J.; Li, J.; Xu, X.; Yang, H. Genome-Wide Identification, Characterization and Expression Analysis of the JAZ Gene Family in Resistance to Gray Leaf Spots in Tomato. *Int. J. Mol. Sci.* **2021**, *22*, 9974. [CrossRef]
50. Thines, B.; Katsir, L.; Melotto, M.; Niu, Y.; Mandaokar, A.; Liu, G.; Nomura, K.; He, S.Y.; Howe, G.A.; Browse, J. JAZ repressor proteins are targets of the SCFCOI1 complex during jasmonate signalling. *Nature* **2007**, *448*, 661–665. [CrossRef]
51. Huang, Y.-L.; Zhang, L.-K.; Zhang, K.; Chen, S.-M.; Hu, J.-B.; Cheng, F. The impact of tandem duplication on gene evolution in Solanaceae species. *J. Integr. Agric.* **2022**, *21*, 1004–1014. [CrossRef]
52. Koo, A.J.; Howe, G.A. The wound hormone jasmonate. *Phytochemistry* **2009**, *70*, 1571–1580. [CrossRef]
53. Rossanese, A. Development of Multifunctional Mesoporous Silica Nanoparticles with Antioxidant Properties for Treating Inflammatory-Related Diseases. Ph.D. Thesis, Politecnico di Torino, Torino, Italy, 2023.
54. Ranjan, A.; Sinha, R.; Bala, M.; Pareek, A.; Singla-Pareek, S.L.; Singh, A.K. Silicon-mediated abiotic and biotic stress mitigation in plants: Underlying mechanisms and potential for stress resilient agriculture. *Plant Physiol. Biochem.* **2021**, *163*, 15–25. [CrossRef] [PubMed]
55. Prasad, R.; Gupta, N.; Kumar, M.; Kumar, V.; Wang, S.; Abd-Elsalam, K.A. Nanomaterials act as plant defense mechanism. In *Nanotechnology: Food and Environmental Paradigm*; Springer: Singapore, 2017; pp. 253–269.
56. Sun, D.; Hussain, H.I.; Yi, Z.; Rookes, J.E.; Kong, L.; Cahill, D.M. Mesoporous silica nanoparticles enhance seedling growth and photosynthesis in wheat and lupin. *Chemosphere* **2016**, *152*, 81–91. [CrossRef]
57. Raliya, R.; Nair, R.; Chavalmane, S.; Wang, W.-N.; Biswas, P. Mechanistic evaluation of translocation and physiological impact of titanium dioxide and zinc oxide nanoparticles on the tomato (*Solanum lycopersicum* L.) plant. *Metallomics* **2015**, *7*, 1584–1594. [CrossRef] [PubMed]
58. Siddiqui, M.H.; Al-Whaibi, M.H. Role of nano-SiO2 in germination of tomato (*Lycopersicum esculentum* seeds Mill.). *Saudi J. Biol. Sci.* **2014**, *21*, 13–17. [CrossRef]
59. Guedes, R.; Smagghe, G.; Stark, J.; Desneux, N. Pesticide-induced stress in arthropod pests for optimized integrated pest management programs. *Annu. Rev. Entomol.* **2016**, *61*, 43–62. [CrossRef]
60. Zappala, L.; Biondi, A.; Alma, A.; Al-Jboory, I.J.; Arno, J.; Bayram, A.; Chailleux, A.; El-Arnaouty, A.; Gerling, D.; Guenaoui, Y. Natural enemies of the South American moth, *Tuta absoluta*, in Europe, North Africa and Middle East, and their potential use in pest control strategies. *J. Pest Sci.* **2013**, *86*, 635–647. [CrossRef]
61. Mostofa, M.G.; Rahman, M.M.; Ansary, M.M.U.; Keya, S.S.; Abdelrahman, M.; Miah, M.G.; Phan Tran, L.-S. Silicon in mitigation of abiotic stress-induced oxidative damage in plants. *Crit. Rev. Biotechnol.* **2021**, *41*, 918–934. [CrossRef] [PubMed]
62. Chung, H.S.; Koo, A.J.; Gao, X.; Jayanty, S.; Thines, B.; Jones, A.D.; Howe, G.A. Regulation and function of Arabidopsis JASMONATE ZIM-domain genes in response to wounding and herbivory. *Plant Physiol.* **2008**, *146*, 952–964. [CrossRef]
63. Ye, H.; Du, H.; Tang, N.; Li, X.; Xiong, L. Identification and expression profiling analysis of TIFY family genes involved in stress and phytohormone responses in rice. *Plant Mol. Biol.* **2009**, *71*, 291–305. [CrossRef]

64. Huang, H.; Zhao, W.; Qiao, H.; Li, C.; Sun, L.; Yang, R.; Ma, X.; Ma, J.; Song, S.; Wang, S. SlWRKY45 interacts with jasmonate-ZIM domain proteins to negatively regulate defense against the root-knot nematode Meloidogyne incognita in tomato. *Hortic. Res.* **2022**, *9*, uhac197. [CrossRef]
65. Huang, H.; Ma, X.; Sun, L.; Wang, Y.; Ma, J.; Hong, Y.; Zhao, M.; Zhao, W.; Yang, R.; Song, S. SlVQ15 recruits SlWRKY30IIc to link with jasmonate pathway in regulating tomato defence against root—Knot nematodes. *Plant Biotechnol. J.* **2025**, *23*, 235–249. [CrossRef] [PubMed]
66. Conrath, U.; Beckers, G.J.; Langenbach, C.J.; Jaskiewicz, M.R. Priming for enhanced defense. *Annu. Rev. Phytopathol.* **2015**, *53*, 97–119. [CrossRef] [PubMed]
67. Torabian, S.; Farhangi-Abriz, S.; Zahedi, M. Efficacy of FeSO 4 nano formulations on osmolytes and antioxidative enzymes of sunflower under salt stress. *Indian J. Plant Physiol.* **2018**, *23*, 305–315. [CrossRef]

Disclaimer/Publisher's Note: The statements, opinions and data contained in all publications are solely those of the individual author(s) and contributor(s) and not of MDPI and/or the editor(s). MDPI and/or the editor(s) disclaim responsibility for any injury to people or property resulting from any ideas, methods, instructions or products referred to in the content.

insects

MDPI

Article

The Mitochondrial Hsp90 Homolog *PmTRAP1* Mediates Thermal Tolerance in the Papaya Mealybug, *Paracoccus marginatus*

Yanting Chen [1], Xiaomin Zhao [1], Chenyu Lv [1], Jianwei Zhao [1], Mengzhu Shi [2], Jianwei Fu [2] and Jianyu Li [1,*]

[1] Fujian Key Laboratory for Monitoring and Integrated Management of Crop Pests, Institute of Plant Protection, Fujian Academy of Agricultural Sciences, Fuzhou 350013, China; fafucyt@126.com (Y.C.)
[2] Institute of Quality Standards and Testing Technology for Agro-Products, Fujian Academy of Agricultural Sciences, Fuzhou 350002, China
* Correspondence: roy111999@foxmail.com

Simple Summary: The papaya mealybug, *Paracoccus marginatus*, is a major agricultural pest known for its high-temperature resilience. This study explores the molecular basis of thermal adaptation in this species by focusing on the role of heat shock protein 90 (Hsp90) genes. We cloned and characterized three *Hsp90* genes—*PmHsp90-1*, *PmHsp90-2*, and *PmTRAP1*—and analyzed their expression under heat stress. Functional analysis via RNA interference demonstrated that suppression of *PmTRAP1* significantly reduced survival under extreme high-temperature conditions. Our findings reveal the essential function of a mitochondrial chaperone in insect thermal adaptation and provide new insights into the molecular basis of environmental stress response in insects.

Abstract: The papaya mealybug, *Paracoccus marginatus*, a significant invasive pest in tropical and subtropical regions, exhibits a notable capacity to withstand high-temperature stress. To elucidate the molecular basis of this thermotolerance, we investigated the role of heat shock protein 90 (Hsp90) genes in this species. The full-length cDNA sequences of three *Hsp90* genes—*PmHsp90-1*, *PmHsp90-2*, and *PmTRAP1*—were cloned, subjected to bioinformatic analysis, and their expression profiles under heat stress were detected. RNAi-mediated suppression of *PmTRAP1* was conducted to evaluate survival under extreme high-temperature conditions. The open reading frames (ORFs) of *PmHsp90-1*, *PmHsp90-2*, and *PmTRAP1* are 2175 bp, 2178 bp, and 2085 bp in length, encoding proteins comprising 724, 725, and 694 amino acids, respectively. Phylogenetic and structural analyses confirmed that PmHsp90-1 and PmHsp90-2 are cytosolic isoforms, each containing a characteristic C-terminal MEEVD motif, while PmTRAP1 was identified as the mitochondrial isoform. All three genes were significantly upregulated under heat stress. RNAi-mediated knockdown of *PmTRAP1* markedly reduced the survival rate of *P. marginatus* under extreme high temperature. These findings demonstrate that *PmTRAP1* is essential for heat tolerance in the papaya mealybug. This study provides crucial insights into the molecular mechanisms of thermal adaptation in insects and identifies *PmTRAP1* as a potential target for future research on managing insect responses to environmental stress.

Keywords: papaya mealybug; Hsp90; Hsp75; mitochondrial chaperone TRAP1; heat stress

1. Introduction

The papaya mealybug, *Paracoccus marginatus* Williams and Granara de Willink (Hemiptera: Pseudococcidae), is a highly polyphagous invasive pest species. It infests over 200 host plants including economically important crops such as citrus, papaya, cassava and pepper, as well as numerous ornamentals [1]. Both nymphs and female adults damage plants through pierce-sucking feeding on stems, leaves, and fruits, causing chlorosis, defoliation, twig dieback, and reductions in fruit quality [2]. The papaya mealybug is native to Central America and has subsequently invaded numerous countries across Africa, North America, Oceania, Central and South America, and Asia [3,4]. Its spread is primarily attributed to the movement of infested plant materials and fruits, facilitating its establishment in new territories [5]. As a pest predominantly distributed in tropical and subtropical regions [6], the survival and distribution of *P. marginatus* are intrinsically linked to temperature. Therefore, understanding its molecular mechanisms for coping with high-temperature stress is fundamental to deciphering its environmental adaptability and invasive potential.

Current research on the thermal adaptability of *P. marginatus* has primarily focused on its biological traits—such as development and reproduction—and physiological responses. Studies indicate that the upper temperature threshold for egg hatching is 37 °C, while the optimal and maximum developmental temperatures for adult females are 28.4 °C and 32.1 °C, respectively [7]. Life table analyses further reveal that this pest can establish populations within the temperature range of 20–30 °C, with the highest net reproductive rate observed at 30 °C [8]. Under extreme high-temperature stress (36 °C), the activities of key antioxidant enzymes in *P. marginatus*, including peroxidase (POD), polyphenol oxidase (PPO), catalase (CAT), and superoxide dismutase (SOD), are significantly elevated, indicating an essential physiological mechanism for mitigating thermal damage [9].

Previous molecular studies have identified 12 *PmHsp70* genes in *P. marginatus*, among which *PmHsp70-11* and *PmHsp70-12* were shown to play critical roles in the heat stress response [10]. Heat shock proteins (Hsps) are known to enhance insect tolerance to various biotic and abiotic stressors [11]. Based on molecular weight, Hsps are mainly classified into six families: small heat shock proteins (sHSP), Hsp40, Hsp60, Hsp70, Hsp90, and Hsp110 [12]. Hsp90 is a highly conserved molecular chaperone that maintains protein and cellular homeostasis. Unlike chaperones involved in de novo protein folding, Hsp90 stabilizes metastable client proteins in partially folded states, facilitating their conformational maturation, stability, and assembly into functional complexes [13]. It is estimated that Hsp90 interacts with approximately 10% of the eukaryotic proteome [14]. In most eukaryotes, functional specialization of Hsp90 is achieved through compartment-specific isoforms: cytosolic Hsp90, endoplasmic reticulum (ER)-localized GRP94 (94 kDa glucose-regulated protein), mitochondrial TRAP1 (tumor necrosis factor receptor-associated protein 1), and—in plants—chloroplastic Hsp90C [15].

Accumulating evidence suggests that Hsp90 participates in various insect physiological processes, including development, reproduction, and responses to environmental stressors such as chemical exposure and thermal fluctuation [16–19]. For example, in *Anaphothrips obscurus* (Müller), *AoHsp90* expression was significantly up-regulated following heat shock treatments [20]. Similarly, in *Sitodiplosis mosellana*, *Hsp90* has been implicated in diapause maintenance and thermal stress response [21]. While studies on insect Hsp90 have provided insights into thermal responses, most have centered on cytosolic isoforms. The functions of compartment-specific isoforms, particularly the mitochondrial TRAP1, in insect thermotolerance remain poorly understood. In *Nilaparvata lugens*, *NlGRP94* is essential for oogenesis, fecundity, and late embryogenesis, whereas RNAi knockdown of

NlTRAP1 did not result in obvious phenotypic defects, nor was its expression induced by temperature stress [22]. In *Bombyx mori*, *TRAP1* promotes the proliferation of the *B. mori* nuclear polyhedrosis virus (*BmNPV*) [23]. Structural studies suggest that the N-terminal strap of *TRAP1* regulates a thermosensitive kinetic barrier during conformational cycling, implicating its role in thermal adaptation in higher eukaryotes [24]. Accordingly, the expression of *AgHsp75* (a *TRAP1* homolog) in *Aphis glycines* was induced by high temperature (36 °C) [25]. Nevertheless, the functional role of *TRAP1* in insect thermotolerance remains to be experimentally validated.

In this study, we cloned the full-length cDNA sequences of the *PmHsp90* genes from *P. marginatus* and performed comprehensive bioinformatic analyses. The expression profiles of *PmHsp90s* under different thermal stress conditions were characterized to preliminarily assess its responsiveness to temperature variations. Furthermore, RNA interference (RNAi) was employed to silence *PmTRAP1* to investigate its biological function in mediating thermal tolerance in the papaya mealybug. These results will enhance our understanding of the molecular mechanisms underlying thermal adaptation in *P. marginatus*.

2. Materials and Methods

2.1. Insect Rearing

The laboratory colony of papaya mealybug was established from individuals collected on papaya (*Carica papaya* L.) leaves on the campus of Fujian Agriculture and Forestry University (FAFU), Cangshan District, Fuzhou City, Fujian Province, China, in 2018. Since then, the population has been continuously reared on potato (*Solanum tuberosum* L.) sprouts under controlled conditions in an artificial climate chamber. The rearing conditions were maintained at 26 °C, 75% relative humidity, and a photoperiod of 14 h light/10 h darkness. For all experiments, insects were selected from this long-term colony, which had been maintained for multiple generations under the standard rearing conditions, ensuring their full acclimation to the host and environment.

2.2. Total RNA Extraction and cDNA Synthesis

Approximately 10 adult papaya mealybugs were used for total RNA extraction using the SteadyPure Universal RNA Extraction Kit (AG21024, Accurate Biology, Changsha, China), following the manufacturer's protocol. The concentration and purity (OD_{260}/OD_{280} ratio) of the extracted total RNA were measured using a NanoDrop 2000 spectrophotometer (Thermo Fisher Scientific, Waltham, MA, USA), and its integrity was verified by electrophoresis on a 2% agarose gel.

cDNA templates for full-length gene cloning were synthesized using a reverse transcription kit (R312-02, Vazyme, Nanjing, China) according to the following steps: First, 1000 ng of total RNA was mixed with nuclease-free water to a final volume of 8 μL, incubated at 65 °C for 5 min, and immediately placed on ice for 2 min. Then, 2 μL of 5× gDNA wiper mix was added, and the mixture was incubated at 42 °C for 2 min. Finally, 2 μL of 10× RT mix, 2 μL of Enzyme mix, 1 μL of Oligo dT primer, and 5 μL of nuclease-free water were added. After thorough vortexing and brief centrifugation, the reaction mixture was subjected to thermal cycling under the following conditions: 25 °C for 5 min, 37 °C for 45 min, and 85 °C for 5 s. The synthesized cDNA was stored at −20 °C.

2.3. Identification and Molecular Cloning of PmHsp90 cDNA

2.3.1. Candidate Gene Screening

Members of the Hsp90 gene family were identified through integrated analysis of a previously established papaya mealybug transcriptome dataset. Initial functional annotation of

transcripts was performed using multiple databases, including NCBI NR (Non-Redundant Protein), GO (Gene Ontology), COG (Clusters of Orthologous Groups), KEGG (Kyoto Encyclopedia of Genes and Genomes), Pfam, and Swiss-Prot. Candidate *PmHsp90s* were initially selected based on HSP domain homology. Redundant sequences derived from sequencing artifacts or assembly errors were eliminated via multiple sequence alignment. Subsequent validation included conserved domain identification using NCBI CDD (https://www.ncbi.nlm.nih.gov/cdd, accessed on 9 April 2025); functional module detection with SMART (https://smart.embl.de/smart/change_mode.cgi, accessed on 9 April 2025) and signature motif screening using ScanProsite (https://prosite.expasy.org/scanprosite/, accessed on 9 April 2025). This bioinformatic pipeline confirmed a unique *PmHsp90* sequence containing complete *Hsp90* characteristic domains.

2.3.2. Molecular Cloning of *PmHsp90* Isoforms

Full-length cDNA sequences of three *PmHsp90* isoforms (*PmHsp90-1*, *PmHsp90-2*, and *PmTRAP1*) were amplified from cDNA templates using gene-specific primers (Table 1) designed with Oligo software (version 7.0, Molecular Biology Insights, Inc., Cascade, CO, USA). PCR reactions were conducted in 25 μL volumes containing 12.5 μL 2× Reaction Buffer, 0.5 μL dNTP Mix (10 mM each), 1.0 μL each of forward and reverse primers (10 μM), 0.5 μL DNA polymerase, 7.5 μL nuclease-free water, and 2.0 μL cDNA. Thermocycling comprised initial denaturation (95 °C, 5 min), 35 cycles of denaturation (95 °C, 15 s), isoform-specific annealing (56 °C for *PmHsp90-1*/*PmHsp90-2*; 49 °C for *PmTRAP1*; 20 s each), and extension (72 °C, 130 s), followed by final extension (72 °C, 5 min).

Table 1. Primers used for gene cloning, quantitative real-time PCR (qRT-PCR), and double-stranded RNA (dsRNA) synthesis in this study.

Gene	Forward Primer (5′-3′)	Reverse Primer (5′-3′)	Usage
PmHsp90-1	ATGCCGGAAGACGTAGCTATG	TCAATCGACTTCTTCCATTCT	cDNA sequence cloning
PmHsp90-2	ATGCCTGAAGACGTAGCAATG	TTAATCGACCTCTTCCATTCT	
PmTRAP1	ATGATTAGTTTAATCAGTCGT	TTAATGTTTTTCCAAAGCTAA	
PmHsp90-1	AGACAGAAAGCCGAAGCAGAT	CTGCTTCGGCTTTCTGTCTCA	Fluorescence quantitative PCR
PmHsp90-2	GAAGCCAACTCCGAATTGACCA	GGTATGACGAAAGCCGACCTTG	
PmTRAP1	GGTATGACGAAAGCCGACCTTG	GCTGTAGAAACCGACACCGAAT	
Pmβ-actin	CATCCTGCGTTTGGATTTAG	TCCAAAGCAACATAGCACAAT	
PmTRAP1	TAATACGACTCACTATAGG AAGGAAACGTATCTGAAGAGC	TAATACGACTCACTATAGG CCAATAATACCCCTTTGCTTC	dsRNA synthesis
GFP	AATACGACTCACTATAGGG-CACAAGTTCAGCGTGTCC	TAATACGACTCAC-TATAGGGGGTGCTCAGGTAGTGGTT	

The target PCR product was purified using the Magen Gel Extraction Kit (D2111-03, Magen, Shanghai, China) following the manufacturer's protocol. Purified DNA fragments were ligated into the Hieff Clone® Zero TOPO-BLunt Simple Cloning Kit (10910ES20, YESEN, Shanghai, China) in a 10 μL reaction containing 2 μL insert DNA, 1 μL 10× Enhancer Solution, 1 μL vector, and nuclease-free water. After 4 min incubation on ice, the ligation mixture was transformed into DH5α competent cells (11802ES80, YESEN, Shanghai, China) via heat shock (42 °C, 45 s) following 25 min ice incubation. Transformed cells were recovered in 500 μL antibiotic-free LB medium (37 °C, 200 rpm, 60 min), concentrated by centrifugation (5000× *g*, 1 min), and plated on LB agar containing carbenicillin (100 μg/mL). Positive clones were screened after 12–16 h incubation at 37 °C. Single colonies were cultured overnight in LB-carbenicillin broth and submitted to Tsingke Biotechnology (Beijing, China) for Sanger sequencing.

2.3.3. Bioinformatic Characterization of PmHsp90 Isoforms

Open reading frames (ORFs) of *PmHsp90-1*, *PmHsp90-2*, and *PmTRAP1* were predicted using the NCBI ORF Finder (https://www.ncbi.nlm.nih.gov/orffinder/, accessed on 2 April 2025). Protein properties were analyzed through soelectric point (pI) and molecular weight (Mw) prediction using ExPASy (https://web.expasy.org/compute_pi/, accessed on 3 April 2025), and subcellular localization forecasting with TargetP-2.0 (https://services.healthtech.dtu.dk/services/TargetP-2.0/, accessed on 3 April 2025).

Amino acid sequences of *PmHsp90* genes were aligned with known insect Hsp90 orthologs from *Phenacoccus solenopsis*, *Bombyx mori*, *Drosophila virilis*, *Tribolium castaneum*, *Aphis glycines*, *Spodoptera frugiperda*, and *Trichogramma chilonis* using DNAMAN (version 9.0, Lynnon Corp, Pointe-Claire, QC, Canada).

Phylogenetic analysis was performed using Hsp90 homologs from 14 insect species: *Nilaparvata lugens*, *S. frugiperda*, *T. chilonis*, *Exorista civilis*, *Zeugodacus cucurbitae*, *Cotesia vestalis*, *Pteromalus puparum*, *Loxostege sticticalis*, *Plutella xylostella*, *Mythimna separata*, *Pieris rapae*, *Bombyx mori*, *Apis mellifera*, and *P. solenopsis*. All reference sequences were retrieved from NCBI GenBank (accession numbers provided in Section 3.1). Phylogenetic reconstruction was conducted in MEGA (version 12.0, Mega Limited, Auckland, New Zealand) using the neighbor-joining method with 1000 bootstrap replicates.

2.4. Thermal Stress Response of PmHsp90 Expression

The expression patterns of *PmHsp90s* under high-temperature stress were investigated. Female adults were transferred into Petri dishes (90 mm in diameter) with multiple ventilation holes to ensure adequate air circulation. The dishes containing papaya mealybugs were then exposed to a range of temperature treatments in an artificial climate chamber. Based on preliminary survival assays, the mealybugs were exposed to 38 °C, 42 °C, and 46 °C for 30 min, with a control group maintained at 26 °C. All treatment temperatures were set below the previously determined lethal threshold of 48 °C (unpublished data). Three biological replicates (10 adults per replicate) were maintained per treatment. Samples were immediately flash-frozen in liquid nitrogen post-treatment and stored at −80 °C until RNA extraction.

Total RNA was extracted from samples and reverse-transcribed using the HiScript III 1st Strand cDNA Synthesis Kit (R312, Vazyme Biotech, Nanjing, China). Gene-specific qPCR primers for *PmHsp90* isoforms were designed with Oligo 7.0 (Table 1). *Pmβ-actin* was used as the endogenous control for normalization [26]. Its stability under heat stress conditions in *P. marginatus* has been empirically confirmed by its consistent Cq values in our previous gene expression analysis [10] and was verified again across all samples in the present study. Quantitative real-time PCR was performed in 20 µL reactions containing 10 µL ChamQ Universal SYBR qPCR Master Mix (Q711, Vazyme Biotech, Nanjing, China), 0.4 µL ROX2 Reference Dye, 0.4 µL each of forward/reverse primers, 2 µL cDNA template, and nuclease-free water. Amplification was conducted on a QuantStudio^{TM} 6 Pro Flex real-time PCR system (Thermo Fisher Scientific, Waltham, MA, USA) under the following protocol: 95 °C for 30 s; 40 cycles of 95 °C for 10 s and 60 °C for 30 s (annealing/extension); followed by melt curve analysis (95 °C for 15 s, 60 °C for 60 s, 95 °C for 15 s). All reactions included three technical replicates.

Relative gene expression was calculated via the $2^{-\Delta\Delta Ct}$ method [27]. Statistical significance ($p < 0.05$) was determined by independent samples *t*-test using SPSS (Version 27.0, IBM Corp., Armonk, NY, USA), with data visualization in GraphPad Prism (Version 8.3.0, GraphPad Software, San Diego, CA, USA).

2.5. Functional Validation of PmTRAP1 via RNA Interference

2.5.1. Double-Stranded RNA Synthesis

T7 promoter-containing dsRNA primers targeting *PmTRAP1* (Table 1) were used to amplify template DNA followed by gel purification. Double-stranded RNA (dsRNA) was synthesized using the T7 RNA Transcription Kit (SJ004, BELONGBIO, Chengdu, China). Each 50 μL reaction contained the following components: 5 μL of 10× Transcription Buffer, 8 μL of NTP Mix, 1 μL of linear template DNA, 1 μL of RNase Inhibitor, 1 μL of T7 RNA Polymerase, and nuclease-free water up to the final volume. The reaction was incubated at 37 °C for 2 to 8 h. Subsequently, the synthesized dsRNA was purified and resuspended in DEPC-treated water at a concentration of 10,000 ng/μL.

2.5.2. Microinjection and Sampling

Day-7 female adults were microinjected abdominally with 500 ng dsPmTRAP1 (experimental group) or dsGFP (control) using a Nanoject III microinjector (Drummond Scientific, Broomall, PA, USA; n = 25 adults/group). Following injection, the insects were allowed to recover for 30 min in Petri dishes containing moistened filter paper before being transferred onto fresh potato sprouts. The inoculated sprouts were then maintained under controlled conditions at 26 °C, 75% relative humidity, and a photoperiod of 14 h light/10 h darkness. Samples were collected at 24 h and 72 h post-injection, with five biological replicates per time point, each consisting of five adults. All samples were immediately flash-frozen in liquid nitrogen for subsequent analysis.

2.5.3. Silencing Efficiency Validation

Total RNA extraction and cDNA synthesis were performed as previously described. *PmTRAP1* expression levels were quantified via qRT-PCR following established protocols. Silencing efficiency was calculated as

$$\text{Efficiency (\%)} = [1 - \text{RE}_{\text{dsPmTRAP1}}/\text{RE}_{\text{dsGFP}}] \times 100$$

where RE represents the relative expression of *PmTRAP1* normalized to the reference gene (*Pmβ-actin*), determined by the $2^{-\Delta\Delta Ct}$ method.

2.6. Thermal Tolerance Assay Following PmTRAP1 Silencing

The thermal tolerance of adult female papaya mealybugs was assessed following RNAi. Insects were divided into three groups: a non-injected (untreated) control, a control group microinjected with dsGFP, and an experimental group microinjected with dsPmTRAP1. At 24 h post-injection, each group was subjected to thermal stress at either 44 °C or 45 °C for 2 h in the artificial climate chamber. The selection of these temperatures was based on previous findings, in which the upper lethal temperature (ULT) for this species was determined to be 48 °C after 2 h of exposure. Therefore, 44 °C and 45 °C represent severe sublethal temperatures capable of inducing a measurable heat stress response while avoiding acute mortality in control treatments. Following heat exposure, mealybugs were transferred to fresh potato sprouts and allowed to recover for 24 h under standard rearing conditions. Mortality was assessed by gentle probing of appendages and cephalic regions with a soft brush under a stereomicroscope; individuals showing no voluntary movement were recorded as dead. Each temperature treatment included five biological replicates (10 adults/replicate). Differences in survival rates among the three treatment groups were analyzed using one-way ANOVA followed by Fisher's LSD for post hoc comparisons in SPSS 25.0, with a significance level of $p < 0.05$.

3. Results

3.1. Characterization of PmHsp90 Isoforms in P. marginatus

The ORFs of *PmHsp90-1*, *PmHsp90-2*, and *PmTRAP1* measured 2718 bp, 2712 bp, and 2088 bp, encoding 725, 723, and 695 amino acid residues, respectively. The nucleotide sequences of *PmHsp90-1*, *PmHsp90-2*, and *PmTRAP1* have been deposited in the GenBank database under accession numbers PX400431, PX400432, and PX400433, respectively. Predicted molecular weights were 177.1 kDa, 177.8 kDa, and 172.3 kDa with isoelectric points (pI) of 4.94, 4.91, and 4.98.

TargetP-2.0 subcellular localization predicted cytosolic localization for PmHsp90-1 and PmHsp90-2, while PmTRAP1 localized to mitochondria. This indicates *PmHsp90-1* and *PmHsp90-2* belong to cytosolic Hsp90 family, whereas *PmTRAP1* represents a mitochondrial Hsp (Hsp75/TRAP1).

Amino acid sequence alignment of PmHsp90s with known Hsp90s from other species revealed three highly conserved domains within all PmHsp90 family members: the N-terminal domain (NTD), middle domain (MD), and C-terminal domain (CTD) (Figure 1), despite variations in their genomic organization. Specifically, three conserved family signatures were identified within the NTD: signature 1 (NKEIFLRELISNSSDALDKIR), signature 2 (LGTIAKSGT), and signature 3 (IGQFGVGFYSAYLVAD). Two additional family signatures were located in the MD: signature 4 (IKLYVRRVFI) and signature 5 (GIVDSEDLPLNISRE). Furthermore, the C-terminal domain of both PmHsp90-1 and PmHsp90-2 contained the conserved MEEVD motif, characteristic of cytosolic Hsp90 proteins.

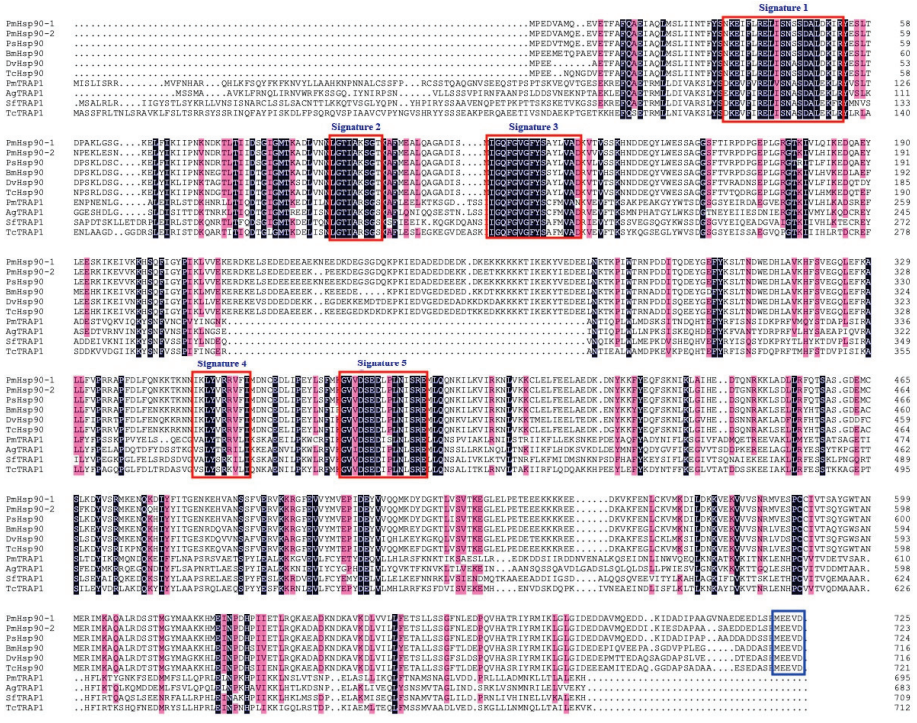


Figure 1. Multiple amino acid sequence alignments of Hsp90 from *Paracoccus marginatus* and other insects. PsHsp90: *Phenacoccus solenopsis*; BmHsp90: *Bombyx mori*; DvHsp90: *Drosophila virilis*; TcHsp90: *Tribolium castaneum*; AgTARP1: *Aphis glycines*; SfTARP1: *Spodoptera frugiperda*; TcTARP1: *Trichogramma chilonis*. The red box highlights conserved signatures diagnostic of the Hsp90 protein family. The blue box highlights the characteristic C-terminal 'MEEVD' motif. Residues shaded with a dark blue background are identical across all sequences; those with a pink background represent similar residues with a consensus level exceeding 75%.

Phylogenetic analysis revealed distinct clustering patterns for PmHsp90 isoforms. The cytoplasmic isoforms PmHsp90-1 and PmHsp90-2 formed a highly supported monophyletic clade with PsHsp90 from *P. solenopsis*. This clade then clustered with NlHsp90b from *N. lugens* and AmHsp90 from *A. mellifera*. In contrast, PmTRAP1, classified within the mitochondrial TRAP1 subfamily based on its grouping with established insect TRAP1 orthologues (SfTRAP1 from *S. frugiperda*, TcTRAP1 from *T. castaneum*, and NlHsp90c (NlTRAP1) from *N. lugens*), was phylogenetically distinct (Figure 2).

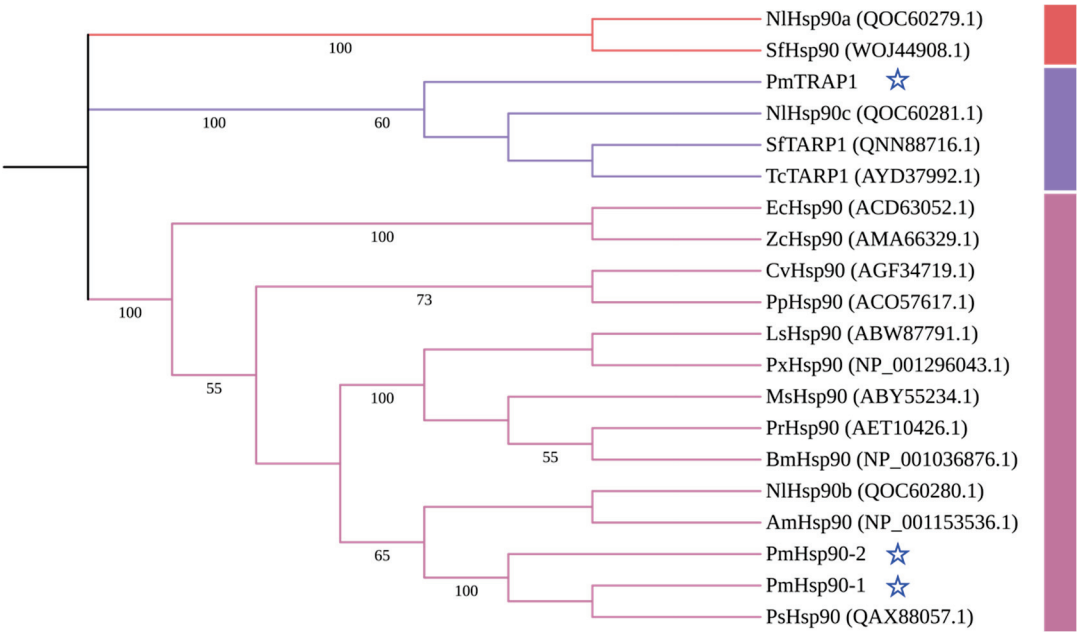


Figure 2. Phylogenetic analysis of Hsp90 proteins from *Paracoccus marginatus* and other insects using the Neighbor-Joining method. PmHsp90 proteins from *P. marginatus* are highlighted with blue stars. Colored bars on the right represent the major gene clades: GRP94, TRAP1, and Hsp90. NlHsp90a (QOC60279.1), NlHsp90b (QOC60280.1), NlHsp90c (QOC60281.1): *Nilaparvata lugens*; SfHsp90 (WOJ44908.1), SfTARP1 (QNN88716.1): *Spodoptera frugiperda*; TcTARP1 (AYD37992.1): *Trichogramma chilonis*; EcHsp90 (ACD63052.1): *Exorista civilis*; ZcHsp90 (AMA66329.1): *Zeugodacus cucurbitae*; CvHsp90 (AGF34719.1): *Cotesia vestalis*; PpHsp90 (ACO57617.1): *Pteromalus puparum*; LsHsp90 (ABW87791.1): *Loxostege sticticalis*; PxHsp90 (NP 001296043.1): *Plutella xylostella*; MsHsp90 (ABY55234.1): *Mythimna separata*; PrHsp90 (AET10426.1): *Pieris rapae*; BmHsp90 (NP 001036876.1): *Bombyx mori*; AmHsp90 (NP 001153536.1): *Apis mellifera*; PsHsp90 (QAX88057.1): *Phenacoccus solenopsis*.

3.2. Thermal Induction of PmHsp90 Isoform Expression

Heat treatments at 38 °C, 42 °C, and 46 °C significantly upregulated *PmHsp90* gene family expression in *P. marginatus*, though with distinct isoform-specific responses (Figure 3). Specifically, *PmHsp90-1* expression exhibited a significant 4.18-fold increase at 38 °C compared to the control ($t = 7.29$, $df = 4$, $p = 0.002$), with more modest yet significant increases of 1.35-fold at 42 °C ($t = -8.090$, $df = 4$, $p = 0.001$) and 1.97-fold at 46 °C ($t = -8.090$, $df = 4$, $p = 0.001$) (Figure 3A). *PmHsp90-2* was significantly induced at 38 °C (2.28-fold; $t = -3.463$, $df = 4$, $p = 0.026$) and 42 °C (3.61-fold; $t = -9.892$, $df = 4$, $p = 0.001$), but remained unchanged at 46 °C (Figure 3B). *PmTRAP1* demonstrated pan-thermal responsiveness with significant upregulation across all temperatures: 2.10-fold at 38 °C ($t = -10.275$, $df = 4$, $p = 0.001$), 2.24-fold at 42 °C ($t = -8.526$, $df = 4$, $p = 0.001$), and 2.06-fold at 46 °C ($t = -15.732$, $df = 4$, $p < 0.001$) (Figure 3C). Given its consistent and substantial induction at all three temperatures tested, *PmTRAP1* was selected for functional validation.

3.3. RNAi Silencing Efficiency of PmTRAP1 in P. marginatus

Female adults injected with dsPmTRAP1 exhibited significant downregulation of target gene expression compared to dsGFP controls at both post-injection timepoints: 38.76% silencing efficiency at 24 h ($t = 3.914$, $df = 4$, $p = 0.017$) and 40.86% at 72 h ($t = 6.472$, $df = 4$, $p = 0.003$), confirming successful and persistent RNAi-mediated suppression (Figure 4).

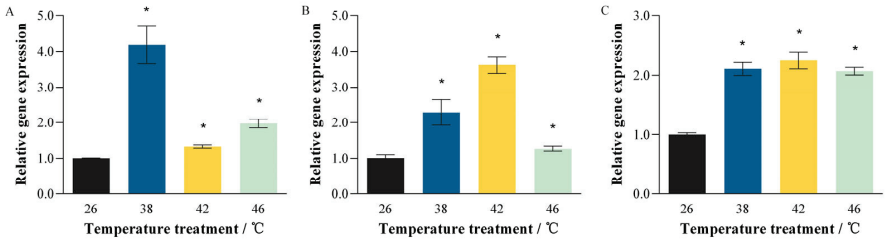


Figure 3. Relative expression levels of *PmHsp90* genes in *Paracoccus marginatus* under heat stress. Expression was quantified at 38 °C, 42 °C, and 46 °C relative to the 26 °C control (set as 1). (**A**) *PmHsp90-1*, (**B**) *PmHsp90-2*, (**C**) *PmTRAP1*. Asterisks indicate significant differences versus control (Student's *t*-test: $p \leq 0.05$). Error bars represent ± standard error (SE).

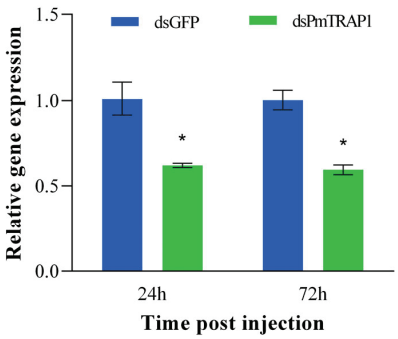


Figure 4. Silencing efficiency of *PmTRAP1* following dsRNA injection. Relative expression levels of *PmTRAP1* at 24 h and 72 h post-injection in dsPmTRAP1-treated groups compared to dsGFP controls. Expression in dsGFP control group was normalized to 1. Asterisks indicate significant differences versus dsGFP control group (Student's *t*-test: $p \leq 0.05$). Error bars represent ± standard error (SE).

3.4. Impact of PmTRAP1 Silencing on Thermal Tolerance

Following RNAi-mediated silencing, all microinjected insects (in both dsGFP and dsPmTRAP1 groups) survived the 24 h recovery period under standard conditions prior to heat exposure. When these insects were subsequently subjected to thermal stress, the dsGFP-injected group exhibited significantly higher mortality than the non-injected untreated control at both temperatures (44 °C: $p = 0.029$, 45 °C: $p = 0.001$; Figure 5). At 44 °C, survival rates did not differ significantly between *PmTRAP1*-silenced and dsGFP-injected control groups ($p = 0.152$; Figure 5). However, exposure to the more severe temperature of 45 °C resulted in significantly reduced survival in the *PmTRAP1*-silenced group compared to both the dsGFP-injected and untreated control groups ($p < 0.001$; Figure 5).

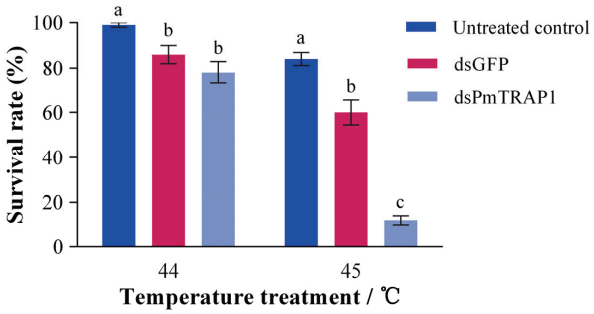


Figure 5. Survival response of *Paracoccus marginatus* to heat stress following RNAi-mediated suppression of *PmTRAP1*. Survival rates of adult mealybugs after 2 h exposure to 44 °C and 45 °C. Insects were either untreated (non-injected control), injected with dsGFP or injected with dsPmTRAP1. Different lowercase letters above bars indicate statistically significant differences among treatments for each temperature (one-way ANOVA followed by Fisher's LSD, $p < 0.05$). Error bars represent ± standard error (SE; n = 5 biological replicates).

4. Discussion

P. marginatus is a major invasive insect species predominantly distributed in tropical and subtropical regions, demonstrating notable thermotolerance. Hsp90 plays a crucial role in mediating insect responses to various biotic and abiotic stresses [28]. The characterization of the Hsp90 gene family in *P. marginatus* reveals a system of compartment-specific chaperones involved in heat stress response. The presence of two cytosolic isoforms (*PmHsp90-1*, *PmHsp90-2*) alongside a mitochondrial homolog (*PmTRAP1*), and the marked upregulation of all three genes under thermal stress shows their involvement in *P. marginatus*' thermal stress response. Furthermore, the role of the mitochondrial gene *PmTRAP1* in thermal adaptation was functionally validated using RNA interference technology.

Based on subcellular localization, *Hsp90* genes can be classified into three categories: cytosolic, endoplasmic reticulum (GRP94), and mitochondrial (TRAP1) [15]. In this study, only the cytosolic and mitochondrial Hsp90 genes were successfully cloned from *P. marginatus*, while the ER-localized GRP94 was not identified. This result is consistent with the number of *Hsp90* genes documented in some insects such as *N. lugens* and *B. mori* [22,23,29,30]. However, the compositional pattern differs; in both *N. lugens* and *B. mori*, one cytosolic *Hsp90*, one *GRP94*, and one *TRAP1* have been reported, whereas in *P. marginatus*, no *GRP94* homolog was detected. In contrast, certain insect species, including *A. obscurus* [20] and *S. frugiperda* [31], have been found to possess only one or two *Hsp90* genes, which may result from gene loss or limitations in transcriptome assembly completeness. Similarly, no *GRP94* homologous gene was identified in the transcriptomic data of *P. marginatus* in this study.

Multiple sequence alignment revealed that all three identified PmHsp90 proteins contain the five signature motifs conserved in the Hsp90 family, as well as the three conserved domains (NTD, MD, and CTD) consistent with the canonical Hsp90 architecture reported in other species [32,33]. Each domain serves a specialized function; the NTD is responsible for ATP binding, the MD facilitates client protein interactions, and the CTD mediates dimerization through specific structural motifs [13]. The two cytosolic isoforms, PmHsp90-1 and PmHsp90-2, possess a C-terminal MEEVD motif, which is typical of cytosolic Hsp90s and consistent with known localization patterns [13]. Phylogenetic analysis further supported their functional classification; PmHsp90-1 and PmHsp90-2 clustered with cytosolic NlHsp90 (NlHsp90b) from *N. lugens*, whereas PmTRAP1 grouped with mitochondrial NlHsp90c (NlTRAP1) from the same species. This independent evolutionary for TRAP1 could explain its significant sequence divergence (e.g., sharing only ~46% identity

with cytosolic Hsp90 in *N. lugens*) [22] and distinct structural features, such as the absence of a charged linker domain between the NTD and MD and a C-terminal EEVD motif, which may account for its specialized role in the mitochondrial environment, including its temperature-sensitive ATPase activity [34]. These findings demonstrate that Hsp90 from distinct subcellular compartments exhibit high evolutionary conservation, reflecting their specialized functions in organelle-specific protein homeostasis.

As ectothermic organisms, insects are highly sensitive to ambient temperature, which profoundly influences their growth, development, lifespan, and reproduction. Current climate change, characterized by increasing global mean temperatures and a rising frequency of extreme heat events, poses substantial challenges to ectothermic insects [35,36]. Heat shock proteins play a crucial role in facilitating the appropriate folding and functional maintenance of proteins under stress conditions, thereby protecting organisms from or mitigating damage [37]. In this study, the expression of three *PmHsp90* genes in *P. marginatus* was up-regulated under thermal stress, indicating that the *PmHsp90* gene family is responsive to high-temperature stress. Notably, *PmHsp90-1* showed significant up-regulation at 46 °C, whereas *PmHsp90-2* did not. This differential expression pattern indicates that even isoforms from the same gene family with the same subcellular compartment can display distinct thermal response thresholds and dynamics The Hsp induction is not triggered by a fixed temperature set point, but rather depends on both stress intensity and duration. Such functional specialization has also been observed in other insects. For example, in *S. frugiperda*, the expression of *SfHsp90s* was significantly elevated after exposure to an extreme temperature of 45 °C, showing a transient expression pattern that increased and then decreased with prolonged treatment time [31]. Moreover, thermal stress significantly induced the expression of *Aohsp90* in *A. obscurus*, although expression declined with further temperature increases [20]. It is noteworthy that the *Hsp90* genes reported in these previous studies are all cytosolic or ER forms. In contrast, the present study demonstrates that the mitochondrial isoform *PmTRAP1* is also up-regulated under heat stress. This finding implies that, in addition to cytosolic and endoplasmic reticulum pathways, the mitochondrial pathway is involved in the heat stress response in insects, thereby expanding our understanding of the regulatory network mediated by the Hsp90 family in insect thermal adaptation.

The consistent upregulation of *PmTRAP1* under high-temperature stress is particularly notable, especially in light of its well-documented functions in other species. In humans, *TRAP1* has been extensively studied and is known to play important roles in tumor cell growth [38,39]; however, its function in insects remains relatively limited. Previous studies have demonstrated that *TRAP1* can protect cells from oxidative stress and apoptosis [40]. In *Drosophila*, knockdown of *TRAP1* resulted in mitochondrial dysfunction and increased sensitivity to heat and drug stress [41], whereas overexpression of *TRAP1* extended healthspan by enhancing stress resistance, locomotor activity, and fertility [42]. Functionally, TRAP1 differs from cytosolic Hsp90s by lacking the charged linker and C-terminal EEVD motif, and its ATPase activity is uniquely modulated by temperature and divalent cations such as Mg^{2+} and Ca^{2+} [34]. Given that mitochondria operate at temperatures approaching 50 °C under physiological conditions, which is significantly higher than that of the surrounding cytosol (37 °C) [43]. The heat-induced expression of *PmTRAP1* suggests it may act as a holdase under thermal stress, maintaining client proteins in a folding-competent state to safeguard mitochondrial proteostasis. However, studies on the response of TRAP1 to thermal stress remains scarce, with available evidence confined to only a few species. For instance, in *N. lugensm*, the expression of NlTRAP1 was not induced by temperature [22]. In contrast, in *A. glycine*, the expression of *AgHsp75* (a TRAP1 homolog) was up-regulated

under both high temperature and imidacloprid exposure [25]. A similar absence of temperature responsiveness was observed in a non-insect species, the mollusk *Chlamys farreri*, where *CfTRAP1* expression showed no temperature dependence [44]. Notably, our findings demonstrated that the expression of *PmTRAP1* is clearly regulated by temperature.

The critical role of *PmTRAP1* in thermotolerance was confirmed through RNAi-mediated knockdown. Under extreme heat stress (45 °C), *PmTRAP1* knockdown individuals exhibited significantly higher mortality compared with both dsGFP-injected and non-injected controls, indicating its essential function. Notably, no significant effect was observed at the sublethal temperature of 44 °C, suggesting that *PmTRAP1* becomes indispensable only under severe thermal stress approaching the organism's physiological limit. Our results imply that under extreme heat, *PmTRAP1* is vital for survival. While the underlying mechanism in papaya mealybug requires further investigation, this essential function may involve maintaining mitochondrial integrity, as TRAP1 deficiency has been shown to cause mitochondrial dysfunction and reduce thermotolerance in *Drosophila melanogaster* [41]. Therefore, *PmTRAP1* serves as a crucial protective component in the papaya mealybug's thermal response under threshold conditions.

5. Conclusions

In conclusion, this study provides the first molecular and functional characterization of the Hsp90 gene family in *P. marginatus*. We successfully identified and cloned two cytosolic isoforms (*PmHsp90-1*, *PmHsp90-2*) and a mitochondrial isoform (*PmTRAP1*). Our results indicate that all three *PmHsp90* genes are responsive to high-temperature stress. Crucially, we have established through RNAi that the mitochondrial isoform, *PmTRAP1*, is indispensable for survival under extreme heat stress. These findings significantly expand our understanding of the molecular mechanisms underpinning thermal adaptation in this invasive pest, highlighting the importance of compartment-specific Hsp90 function. While *PmTRAP1* is a key protector against acute thermal stress, its role under chronic or fluctuating field-relevant temperatures needs further investigation. Furthermore, given the pleiotropic function of *Hsp90* family genes, future studies should explore the roles of *PmHsp90s* in adapting to other stressors, such as insecticide exposure. Overall, this work establishes a solid molecular foundation for understanding environmental adaptation in this significant invasive pest.

Author Contributions: Conceptualization, Y.C. and J.L.; methodology, X.Z. and C.L.; software, J.Z.; validation, M.S. and J.F.; writing—original draft preparation, Y.C., J.Z., and M.S.; writing—review and editing, J.L.; visualization, X.Z.; project administration, Y.C. and J.L. All authors have read and agreed to the published version of the manuscript.

Funding: This research was funded by National Key Research and Development Program of China (2024YFC2607602), Project of Fujian Academy of Agricultural Sciences (YCZX202406), Basic Scientific Research for Public Welfare Research Institutes of Fujian Province (2023R1022001), and "5511" Collaborative Innovation Project (XTCXGC2021017, XTCXGC2021011).

Data Availability Statement: The original contributions presented in this study are included in the article. Further inquiries can be directed to the corresponding author.

Conflicts of Interest: The authors declare no conflicts of interest.

References

1. Miller, D.R.; Miller, G.L. Redescription of *Paracoccus marginatus* Williams and Granara de Willink (Hemiptera: Coccoidea: Pseudococcidae), including descriptions of the immature stages and adult male. *Proc. Entomol. Soc. Wash.* **2002**, *104*, 1–23.

2. Myrick, S.; Norton, G.W.; Selvaraj, K.N.; Natarajan, K.; Muniappan, R. Economic impact of classical biological control of papaya mealybug in India. *Crop Prot.* **2014**, *56*, 82–86. [CrossRef]
3. Seni, A.; Chongtham, S. Papaya mealybug *Paracoccus marginatus* williams & granara de willink (Hemiptera: Pseudococcidae), a current threat to agriculture—A review. *Agric. Rev.* **2013**, *34*, 216–222.
4. CABI. Crop Protection Compendium. Available online: http://www.cabi.org/cpc (accessed on 10 July 2025).
5. Tanwar, R.K. Papaya mealybug and its management strategies. *Technol. Bull (Natl. Cent. Integr. Pest Manag.)* **2010**, *22*, 1–22.
6. Chen, Y.; Shi, M.; Fu, J.; Zhao, Z.; Liu, W.; Li, J. Prediction of potential suitable habitats for *Paracoccus marginatus* in China under climate change conditions. *J. Plant Prot.* **2023**, *50*, 1491–1498.
7. Amarasekare, K.G.; Chong, J.H.; Epsky, N.D.; Mannion, C.M. Effect of temperature on the life history of the mealybug *Paracoccus marginatus* (Hemiptera: Pseudococcidae). *J. Econ. Entomol.* **2008**, *101*, 1798–1804. [CrossRef]
8. Amutha, M.; Dharajothi, B. Life table and population parameters of *Paracoccus marginatus* at varying temperatures on cotton. *Indian J. Plant Prot.* **2016**, *44*, 24–29.
9. Chen, Q.; Liang, X.; Wu, C.-l.; Wang, Y.-r.; Zhao, H.-p.; Chen, Q. Influence of different temperatures on protective enzyme activities of *Paracoccus marginatus* (Hemiptera: Pseudococcidae). *Genom. Appl. Biol.* **2020**, *39*, 241–245.
10. Chen, Y.; Zhao, J.; Shi, M.; Ruan, F.; Fu, J.; Liu, W.; Li, J. Characterization and expression patterns of heat shock protein 70 genes from *Paracoccus marginatus* in response to temperature and insecticide stress. *Agriculture* **2024**, *14*, 2164. [CrossRef]
11. Banfi, D.; Bianchi, T.; Mastore, M.; Brivio, M.F. The role of heat shock proteins in insect stress response, immunity, and climate adaptation. *Insects* **2025**, *16*, 741. [CrossRef]
12. Morimoto, R. Cells in stress: Transcriptional activation of heat shock genes. *Science* **1993**, *259*, 1409–1410. [CrossRef]
13. Abdullah, H.; Marwan, E.S.; Hassan, N. The *Hsp90* family: Structure, regulation, function, and implications in health and disease. *Int. J. Mol. Sci.* **2018**, *19*, 2560. [CrossRef]
14. Zhao, R.; Houry, W.A. Molecular interaction network of the *Hsp90* chaperone system. *Adv. Exp. Med. Biol.* **2007**, *594*, 27–36.
15. Johnson, J.L. Evolution and function of diverse *Hsp90* homologs and cochaperone proteins. *Biochim. Biophys. Acta.* **2012**, *1823*, 607–613. [CrossRef]
16. Ding, J.H.; Zheng, L.X.; Chu, J.; Sheng, S. Characterization, and functional analysis of *Hsp70* and *Hsp90* gene families in *Glyphodes pyloalis* (Walker) (Lepidoptera: Pyralidae). *Front. Physiol.* **2021**, *12*, 753914. [CrossRef]
17. Garcia-Gomez, B.; Sánchez, T.A.; Cano, S.N.; Nascimento, N.A.D.; Bravo, A.; Soberón, M. Insect chaperones *Hsp70* and *Hsp90* cooperatively enhance toxicity of *Bacillus thuringiensis Cry1A* toxins and counteract insect resistance. *Front. Immunol.* **2023**, *14*, 1151943. [CrossRef]
18. Will, T.; Schmidtberg, H.; Škaljac, M.; Vilcinskas, A. Heat shock protein 83 plays pleiotropic roles in embryogenesis, longevity, and fecundity of the Pea Aphid *Acyrthosiphon pisum*. *Dev. Genes Evol.* **2017**, *227*, 1–9. [CrossRef] [PubMed]
19. Xiong, W.; Zhai, M.; Yu, X.; Wei, L.; Mao, J.; Liu, J.; Xie, J.; Li, B. Comparative RNA-sequencing analysis of ER-based HSP90 functions and signal pathways in *Tribolium castaneum*. *Cell Stress Chaperones* **2017**, *23*, 29–43. [CrossRef] [PubMed]
20. Guo, X.J.; Feng, J.N. Comparisons of expression levels of heat shock proteins (*Hsp70* and *Hsp90*) from *Anaphothrips obscurus* (Thysanoptera: Thripidae) in polymorphic adults exposed to different heat shock treatments. *J. Insect Sci.* **2018**, *18*, 15. [CrossRef] [PubMed]
21. Cheng, W.; Li, D.; Wang, Y.; Liu, Y.; Zhu-Salzman, K. Cloning of heat shock protein genes (*hsp70*, *hsc70* and *hsp90*) and their expression in response to larval diapause and thermal stress in the wheat blossom midge, *Sitodiplosis mosellana*. *J. Insect Physiol.* **2016**, *95*, 66–77. [CrossRef]
22. Chen, X.; Li, Z.D.; Dai, Y.T.; Jiang, M.X.; Zhang, C.X. Identification and characterization of three heat shock protein 90 (*Hsp90*) homologs in the Brown planthopper. *Genes* **2020**, *11*, 1074. [CrossRef]
23. Wang, X.; Zhang, Y.; Fei, S.; Awais, M.M.; Sun, J. Heat Shock Protein 75 (*TRAP1*) facilitate the proliferation of the *Bombyx mori* nucleopolyhedrovirus. *Int. J. Biol. Macromol.* **2021**, *175*, 372–378. [CrossRef]
24. Partridge, J.R.; Lavery, L.A.; Elnatan, D.; Naber, N.; Cooke, R.; Agard, D.A. A novel N-terminal extension in mitochondrial *TRAP1* serves as a thermal regulator of chaperone activity. *eLife* **2014**, *3*, e03487. [CrossRef]
25. Wang, X.; Li, S.; Yao, L.; Liu, Y.; Chen, Y.; Yang, H.; Fan, D. The stress-induced expression of the *Aghsp75* gene in *Aphis glycines* in response to imidacloprid and temperature stress. *Chin. J. Biol. Control* **2020**, *36*, 913–919.
26. Liang, X.; Chen, Q.; Wu, C.; Liu, Y.; Han, Z.; Wu, M. Reference gene selection for analyzing the transcription patterns of two fatty *acyl-CoA* reductase genes from *Paracoccus marginatus* (Hemiptera: Pseudococcidae). *J. Insect Sci.* **2021**, *21*, 11.
27. Livak, K.J.; Schmittgen, T.D. Analysis of relative gene expression data using real-time quantitative PCR and the $2^{-\Delta\Delta CT}$ method. *Methods* **2001**, *25*, 402–408. [CrossRef]
28. King, A.M.; Macrae, T.H. Insect heat shock proteins during stress and diapause. *Annu. Rev. Entomol.* **2015**, *60*, 59–75. [CrossRef] [PubMed]

29. Wu, P.; Shang, Q.; Huang, H.; Zhang, S.; Zhong, J.; Hou, Q.; Guo, X. Quantitative proteomics analysis provides insight into the biological role of *Hsp90* in *BmNPV* infection in *Bombyx mori*. *J. Proteom.* **2019**, *203*, 103379. [CrossRef] [PubMed]
30. Lu, Y.; Li, D.; Ai, H.; Xie, X.; Jiang, X.; Afrasiyab; Zhang, H.; Xu, J.; Huang, S. Glucose-regulated protein 94 facilitates the proliferation of the *Bombyx mori* nucleopolyhedrovirus via inhibiting apoptosis. *Int. J. Biol. Macromol.* **2023**, *253*, 127158. [CrossRef] [PubMed]
31. Ruan, H.Y.; Zhou, L.; Yang, L.; Meng, J.Y.; Zhang, C.Y. Functional analysis of two *SfHsp90* genes in response to high temperature and insecticide stress in *Spodoptera frugiperda* (Lepidoptera: Noctuidae). *Eur. J. Entomol.* **2024**, *121*, 54–63. [CrossRef]
32. Li, J.; Buchner, J. Structure, function and regulation of the *Hsp90* machinery. *Biomed J.* **2013**, *36*, 106–117.
33. Schopf, F.H.; Biebl, M.M.; Buchner, J. The *HSP90* chaperone machinery. *Nat. Rev. Mol. Cell Biol.* **2017**, *18*, 345–360. [CrossRef] [PubMed]
34. Joshi, A.; Ito, T.; Picard, D.; Neckers, L. The mitochondrial *HSP90* paralog *TRAP1*: Structural dynamics, interactome, role in metabolic regulation, and inhibitors. *Biomolecules* **2022**, *12*, 880. [CrossRef]
35. Sgrò, C.M.; Terblanche, J.S.; Hoffmann, A.A. What can plasticity contribute to insect responses to climate change? *Annu. Rev. Entomol.* **2016**, *61*, 433–451. [CrossRef] [PubMed]
36. González-Tokman, D.; Córdoba-Aguilar, A.; Dáttilo, W.; Lira-Noriega, A.; Sánchez-Guillén, R.A.; Villalobos, F. Insect responses to heat: Physiological mechanisms, evolution and ecological implications in a warming world. *Biol. Rev.* **2020**, *95*, 802–821. [CrossRef]
37. Zhao, L.; Jones, W.A. Expression of heat shock protein genes in insect stress responses. *Invertebrate. Surviv. J.* **2012**, *9*, 93–101.
38. Nguyen, M.C.; Tu, G.H.; Koprivnikar, K.E.; Gonzalez-Edick, M.; Jooss, K.U.; Harding, T.C. Antibody responses to galectin-8, *TARP* and *TRAP1* in prostate cancer patients treated with a GM-CSF-secreting cellular immunotherapy. *Cancer Immunol. Immunother.* **2010**, *59*, 1313–1323. [CrossRef]
39. Xie, S.; Wang, X.; Gan, S.; Tang, X.; Zhu, S. The mitochondrial chaperone *TRAP1* as a candidate target of oncotherapy. *Front. Oncol.* **2021**, *10*, 585047. [CrossRef]
40. Hua, G.; Zhang, Q.; Fan, Z. Heat shock protein 75 (*TRAP1*) antagonizes reactive oxygen species generation and protects cells from granzyme M-mediated apoptosis. *J. Biol. Chem.* **2007**, *282*, 20553–20560. [CrossRef] [PubMed]
41. Costa, A.C.; Loh, S.H.Y.; Martins, L.M. Drosophila *Trap1* protects against mitochondrial dysfunction in a *PINK1/parkin* model of Parkinson's disease. *Cell Death Dis.* **2013**, *4*, e467. [CrossRef]
42. Baqri, R.M.; Pietron, A.V.; Gokhale, R.H.; Turner, B.A.; Kaguni, L.S.; Shingleton, A.W.; Kunes, S.; Miller, K.E. Mitochondrial chaperone *TRAP1* activates the mitochondrial UPR and extends healthspan in *Drosophila*. *Mech. Ageing Dev.* **2014**, *141–142*, 35–45. [CrossRef] [PubMed]
43. Chrétien, D.; Bénit, P.; Hyung-Ho, H.; Susanne, K.; Riyad, E.K.; Young-Tae, C.; Martin, J.; Jacobs, H.T.; Pierre, R.; Malgorzata, R. Mitochondria are physiologically maintained at close to 50 °C. *PLoS Biol.* **2018**, *16*, e2003992. [CrossRef] [PubMed]
44. Yu, H.; Yang, Z.; Sui, M.; Cui, C.; Hu, Y.; Hou, X.; Xing, Q.; Huang, X.; Bao, Z. Identification and characterization of *hsp90* gene family reveals involvement of *hsp90*, *grp94* and not *TRAP1* in heat stress response in *Chlamys farreri*. *Genes* **2021**, *12*, 1592. [CrossRef] [PubMed]

Disclaimer/Publisher's Note: The statements, opinions and data contained in all publications are solely those of the individual author(s) and contributor(s) and not of MDPI and/or the editor(s). MDPI and/or the editor(s) disclaim responsibility for any injury to people or property resulting from any ideas, methods, instructions or products referred to in the content.

insects

MDPI

Article

Transcriptome Characterization and Identification of Chemosensory Genes in the Egg Parasitoid *Anastatus orientalis*, Along with Molecular Cloning, Sequence Analysis, and Prokaryotic Expression of the Odorant Binding Protein 8 (*AoOBP8*) from *A. orientalis*

Xinyu Liu, Yanyan Bai, Yu Qi, Baozhi Liu, Yingying Zhao, Yuting Wu, Jiating Yang, Yanan Wang and Shouan Xie *

Key Laboratory of National Forestry and Grassland Administration on Management of Forest Bio-Disaster, College of Forestry, Northwest A&F University, Yangling 712100, China; xinyuliu2023@nwafu.edu.cn (X.L.); baiyanyan@nwafu.edu.cn (Y.B.); qiyu427@nwafu.edu.cn (Y.Q.); liubaozhi2024@163.com (B.L.); zhaoyingying@nwafu.edu.cn (Y.Z.); wyt261888@163.com (Y.W.); 15333443128@163.com (J.Y.); wynnnqz@gmail.com (Y.W.)

* Correspondence: shouanxie@163.com; Tel.: +86-15029233960

Simple Summary: *Anastatus orientalis* is an important natural enemy of *Lycorma delicatula* and is being tested as a potential biological control agent for invasive *L. delicatula* around the world. Studying the genes related to chemosensory proteins in parasitic wasps is vital for enhancing their ability to locate hosts and improve parasitism efficiency. In this study, transcriptome sequencing was used to identify 62 chemosensory-related genes in male and female adults from *A. orientalis*. The values for fragments per kilobase per million (FPKM) indicated that the chemosensory protein gene families in *A. orientalis* exhibit different expression levels in male and female adults, with some genes showing significant differences and displaying sex-biased expression. Meanwhile, the nucleotide and amino acid sequences of *AoOBP8* and the physiochemical properties of its encoded protein were clarified. The gene *AoOBP8* was expressed in male and female adults and various tissues of adults, and the highest expression level was detected in the head. The study showed that *AoOBP8* played a significant role in olfactory recognition in *A. orientalis*. These results provide molecular evidence supporting further exploration of chemosensory mechanisms governing host recognition and localization in *A. orientalis*.

Abstract: *Anastatus orientalis*, a prominent egg parasitoid of *Lycorma delicatula*, demonstrates considerable potential for biological control. *A. orientalis* is dependent on host volatiles to identify and locate appropriate hosts for reproduction, with its olfactory system playing a vital role in volatile detection. There is little known about the chemosensory genes in *A. orientalis*. Therefore, here, we conducted a transcriptome analysis of the males and females from *A. orientalis*. Overall, 24 odorant binding proteins (OBPs), 4 chemosensory proteins (CSPs), 26 odorant receptors (ORs), 3 gustatory receptors (GRs), 3 ionotropic receptors (IRs), and 2 sensory neuron membrane proteins (SNMPs) were identified by transcriptome analysis. The values for fragments per kilobase per million (FPKM) indicated that the chemosensory protein gene families in *A. orientalis* exhibit different expression levels in male and female adults, with some genes showing significant differences and displaying sex-biased expression. Furthermore, RACE technology, phylogenetic analysis, and expression analysis were used to investigate the role that *AoOBP8* plays in olfaction in *A. orientalis*. *AoOBP8* was highly expressed in females and the heads of adults, indicating that the gene

has a crucial role to play in the search for hosts and in oviposition in female adults, while the head is crucial in recognizing chemical information. These results contribute to a deeper understanding of the functions of chemosensory protein gene families in *A. orientalis* and offer a reference for developing biocontrol methods for forestry pests.

Keywords: *Anastatus orientalis*; *Lycorma delicatula*; transcriptome analysis; chemosensory-related gene; biological control

1. Introduction

The spotted lanternfly (hereafter SLF), *Lycorma delicatula* (White) (Homoptera: Fulgoridae), is a prevalent garden pest with a broad distribution [1]. It poses a significant threat to economically important tree species and ornamental plants, affecting both domestic and international environments [2]. In regions where the SLF is already established, various control measures have been implemented, including the use of insecticides [3], traps [4], and chipping to destroy egg masses [5]. However, these efforts appear to be insufficient given that the SLF is still spreading rapidly to new regions [6].

Parasitic wasps, as an important type of natural enemy insect in biological control, play a significant role in the green control of agricultural and forestry pests [7]. *Anastatus orientalis*, as the native parasitic wasp of *L. delicatula*, possesses considerable potential for biological control [8,9]. *A. orientalis* is a dominant egg parasitoid wasp of *L. delicatula*. It was first discovered in China in 2013 and was formally described and published in 2015 [8]. In China, the distribution pattern of *A. orientalis* is the same as that of *L. delicatula* [10]. It is a key biological factor in controlling the population of the *L. delicatula*, capable of accurately locating and identifying its egg masses for parasitism [11]. Under natural conditions, the parasitism rate of *A. orientalis* can reach up to 40.2%, and up to 77.3% in laboratory artificial breeding conditions [7]. Moreover, *A. orientalis* is easy to rear in captivity and has strong host-seeking abilities. Bao et al. showed that the parasitism rate of *A. orientalis* decreased with the increase in host densities of *Antherea pernyi* Guérin and Méneville, and the daily maximum parasitism amount on *A. pernyi* was 16.2%, which demonstrated the high biocontrol potential of *A. orientalis* [9]. In other words, *A. orientalis* has demonstrated considerable potential for reducing *L. delicatula* populations, and the research opportunities surrounding this natural enemy are exceptionally promising. Consequently, conducting research on *A. orientalis* is essential.

Chemoreception is critical for the survival of insects. Insects display a variety of behavioral responses, such as mating, host searching and ovipositing, in response to different odor signals detected in their living environment [12–14]. Odorant recognition in insects involves multiple olfactory-related proteins, including odorant binding proteins (OBPs) and chemosensory proteins (CSPs), ionotropic receptors (IRs), odorant receptors (ORs), gustatory receptors (GRs), and sensory neuron membrane proteins (SNMPs) [14,15]. Understanding the molecular mechanisms of insect chemosensory proteins provides valuable insights into their olfactory system, offering potential avenues for regulating insect behavior. Previous studies suggested that the success of parasitic wasps in suppressing pest populations depends on their ability to locate hosts in a complex chemical environment [7,16]. Like most insects, parasitic wasps locate their hosts by foraging, and reproduction occurs through a series of behavioral activities, regulated mainly by chemoreception [17–19]. The identification of chemosensory genes in parasitic wasps is crucial, both to address the mechanisms controlling intraspecific or interspecific chemical communication and for the potential genetic manipulation of parasitoid

behavioral responses via the modification of their ability to discriminate the chemical cues used in biological control strategies [20]. Currently, there are no reports on the molecular mechanisms of chemosensory proteins in *A. orientalis*. Therefore, conducting research on the identification and expression patterns of genes related to chemosensory proteins in *A. orientalis* is crucial.

In recent years, with the advancement of technology, the identification of genes associated with chemosensory proteins in many parasitic wasps has been successfully accomplished using transcriptome sequencing and high-throughput sequencing technologies, such as *Chouioia cunea* [14], *Aulacocentrum confusum* [15], *Cotesia vestalis* [21], *Anastatus japonicus* Ashmead [22], *Sclerodermus* sp. [23], and *Telenomus remus* Nixon [24], providing a foundation for understanding chemosensory protein mechanisms in insects. However, little is known about the transcriptomic studies or the olfactory molecular mechanisms of *A. orientalis*. Therefore, studying the molecular characterization of the odorant sensory mechanisms in *A. orientalis* is of particular importance.

The protection and utilization of native parasitic insects is an important measure for pest control, and *A. orientalis*, as a newly discovered local parasitic insect group in China, plays a significant role in controlling *L. delicatula*. At present, research on *A. orientalis* is mainly focused on its morphology, parasitic efficiency, group rearing techniques and control effectiveness [8,9,25]. However, studying the molecular characterization of the odorant sensory mechanisms in *A. orientalis* is highly significant for improving its parasitism rate in the field. But there is no report on the molecular mechanism of chemical recognition in *A. orientalis*. Therefore, high-throughput sequencing was employed to analyze the transcriptomes of male and female *A. orientalis* adults, and to identify and analyze chemosensory protein genes in this study. These results contribute to our understanding of the olfactory mechanisms in *A. orientalis* and offer a theoretical foundation for formulating sustainable and eco-friendly pest management strategies.

2. Materials and Methods

2.1. Insect Collection

The *A. orientalis* specimens used in this study were collected from parasitized egg masses of *L. delicatula* on 9 December 2023 in Xi Lijiagou Village (34°15′ N, 109°45′ E), Puhua Town, Lantian County, Xi'an City, Shaanxi Province, in China. After the emergence of parasitic wasps, adults were fed with a 10% honey water solution. Male and female adults were separated according to morphological characteristics, and the heads with antennae, thorax, and abdomen of the *A. orientalis* adults were dissected for RNA extraction. For each treatment, there were 3 biological replicates. All collected tissues were placed in 1.5 mL Eppendorf tubes, frozen immediately with liquid nitrogen, and then stored at −80 °C until use.

2.2. RNA Extraction and cDNA Library Construction and Transcriptome Sequencing

To fulfill the sample size requirements for transcriptome sequencing, ensuring that each sample weighed no less than 100 mg, we established three biological replicates for both the female and male adult groups of *A. orientalis*, resulting in a total of six samples, namely, AoF1, AoF2, AoF3, AoM1, AoM2, and AoM3. Each of these samples contained 100–120 individual parasitic wasps. RNA was extracted from the above-mentioned six samples by using the Eastep® Super total RNA Extraction Kit (Cat.# LS1040, Shanghai Promega Trading Co., Ltd., Shanghai, China). Once the concentration and purity of the total RNA extracted from *A. orientalis* adults were verified, construction and sequencing of the cDNA library were performed (Supplementary Document S1) by Wuhan Maiwei Metabolic Biotechnology Co., Ltd. (Wuhan, China).

2.3. Transcriptome Assembly, Gene Annotation, Identification and Sequence Analysis

Once clean and high-quality data was obtained, DIAMOND software (v2.0.4) was used to align the unigene sequences with NR, Swiss-Prot, COG, KOG, eggNOG4.5, and KEGG databases [13,26,27], KEGG orthology results for unigene were obtained using KOBAS, and InterProScan was used to analyze the GO orthology of novel genes via the integrated InterPro database [28–30]. Following the prediction of unigene amino acid sequences, HMMER software (v3.1b2) was utilized to align them with the Pfam database for annotation purposes [31,32].

Regarding the analysis of transcriptome data of *A. orientalis* adults, all candidate OBPs, CSPs, ORs, GRs, IRs, and SNMPs were manually checked using the BLASTx program (https://blast.ncbi.nlm.nih.gov/Blast.cgi, accessed on 6 July 2025), with alignment parameters including species name, gene description, accession number, E-value, and identity, leading to the identification of chemosensory proteins. To compare the differential expression of chemosensory genes in the transcriptomes of male and female *A. orientalis*, the read number for each chemosensory gene between male and female adults was converted to RPKM (Reads Per Kilobase per Million mapped reads) [33,34].

Based on the results of transcriptome data screening and the results of the preliminary experiments, we selected the *AoOBP8* gene for further analysis, as it demonstrated high expression levels in our preliminary experiments.

2.4. Molecular Cloning and Prokaryotic Expression of the Odorant Binding Protein 8 of A. orientalis (AoOBP8)

2.4.1. RNA Isolation and AoOBP8 cDNA Synthesis

First, total RNA was extracted from each sample using the Eastep® Super total RNA Extraction Kit (Cat.# LS1040, Shanghai Promega Trading Co., Ltd., Shanghai, China). Once the concentration and purity of the total RNA extracted from *A. orientalis* had been verified, total RNA was reverse-transcribed using the PrimeScript™ II 1st Strand cDNA Synthesis Kit (Code No. 6110A, Takara Biomedical Technology (Beijing) Co., Ltd., Beijing, China). The detailed method can be found in Supplementary Document S1.

2.4.2. Molecular Cloning

Fragments of the putative *AoOBP8* gene were procured from the transcriptome database for *A. orientalis*. The veracity of the sequences was established by polymerase chain reaction (PCR) using the primers in Table 1. Full-length cDNA was obtained by 5′- and 3′-RACE using the SMARTer® RACE5′/3′ kit (Code No. 634858/59, Takara Biomedical Technology (Beijing) Co., Ltd., Beijing, China) with the specific primers listed in Table 1. We subsequently recovered and purified the PCR product. The purified DNA was ligated onto the PGEM-Teasy Vector (Cat.# A1360, Shanghai Promega Trading Co., Ltd., Shanghai, China) and the dideoxynucleotide method was used for sequencing (Sangon Biotech, Shanghai, China).

Table 1. Primers used in this study.

Primer Names	Primer Sequences	Length of Primer	Primer Usage
AoOBP8-F	GATATTCGTCCTCGTTGG	18 bp	amplification of intermediate fragments
AoOBP8-R	ATCTTTCGGCGTAGCATT	18 bp	
AoOBP8-R1	GCAGCCGTAGCAATCATCTT	20 bp	5′RACE
AoOBP8-R2	ATCAATGGCAGTCTCGTGTA	20 bp	
AoOBP8-F1	CTATTAGCGAGTGCAAGGC	19 bp	3′RACE
AoOBP8-F2	ACAAATGCTACGCCGAAAG	19 bp	

Table 1. *Cont.*

Primer Names	Primer Sequences	Length of Primer	Primer Usage
UPM long	CTAATACGACTCACTATAGGGC AAGCAGTGGTATCAACGCAGAGT	45 bp	Universal Primer
UPM short	CTAATACGACTCACTATAGGGC	22 bp	
NUP	AAGCAGTGGTAACAACGCAGAGT	23 bp	
M13F	GTTGTAAAACGACGGCCAG	19 bp	
M13R	CAGGAAACAGCTATGAC	17 bp	
β-*Actin*-F	GTGCGACGTGGACGTGAGAA	20 bp	RT-qPCR
β-*Actin*-R	AGACGGAGCAAGAGCGGTGA	20 bp	
α-*tubulin*-F	TTTCGACGGAGCTTTGAATGTAG	23 bp	
α-*tubulin*-R	TTGGTGATTTCAGCAACGGATAA	23 bp	
Q-*AoOBP8*-F	CGGCATACCGTACTGAAGTT	20 bp	
Q-*AoOBP8*-R	CTTTCGGCGTAGCATTTGTT	20 bp	

2.4.3. Bioinformatic and Phylogenetic Analyses

The cDNA sequence of *AoOBP8* was translated with the Translate tool (https://web.expasy.org/translate/ (accessed on 6 July 2025)). Amino acid sequences were deduced using ExPASy (http://web.expasy.org/translate (accessed on 6 July 2025)). The molecular weight (MW) and isoelectric point (pI) of the deduced amino acid sequences were predicted with Compute pI/Mw (https://web.expasy.org/protparam/ (accessed on 6 July 2025)). The N-linked glycosylation sites were analyzed using NetNGlyc 1.0 Server (http://www.cbs.dtu.dk/services/NetNGlyc/ (accessed on 6 July 2025)). Sequence comparisons were performed using DNAMAN. Additionally, a phylogenetic tree was constructed using a total of 20 insect TPS protein sequences obtained from NCBI via MEGA7.0 software and Clustal X 1.83 using the maximum likelihood method. Bootstrap values were calculated based on 1000 replicates [35].

2.4.4. Expression of AoOBP8 Gene

cDNA templates derived from different developmental stages of *A. orientalis* were used for temporal expression tests. Primers were designed for quantitative real-time PCR (RT-qPCR) by Prime 5.0 and are listed in Table 1. The expression of the target gene was measured by RT-qPCR and normalized with two stable reference genes (β-Actin and α-tubulin). Detailed reaction systems for each PCR can be found in Supplementary Document S1. The reactions were performed with a StepOnePlus^{TM} Real-Time PCR Instrument (Thermo Fisher Scientific, Singapore). The relative expression level was calculated using the $2^{-\Delta\Delta Ct}$ method [36].

2.4.5. Prokaryotic Expression and Identification of His-AoOBP8

The expression primers corresponding to the gene encoding *AoOBP8* were designed using Prime 5.0 software, and EcoRI and HindIII enzyme cutting sites were introduced at the 5′ and 3′ ends, respectively. The expression fragment of β-enolase was amplified using EX Taq DNA polymerase, and the PCR product was verified by sequencing. The expression fragment and the pET-30a plasmid were double-digested separately and then ligated by T4 DAN ligase, and then the expression plasmid, pET-30a-β-enolase, was constructed successfully. Afterward, the expression plasmid was introduced into *E. coli* DH5α cells for expansion, followed by extraction using the plasmid mass extraction kit (Tiangen, Beijing, China).

The expression plasmid was transformed into *Escherichia coli* Origami (DE3) cells via heat shock, and positive clones were selected for protein expression. *E. coli* Origami (DE3) cells carrying the expression plasmid were incubated at 37 °C for 4 h with shaking until cultures reached an optical density (OD) = 0.6. The synthesis of β-enolase was induced

with the addition of isopropyl β-d-thiogalactoside (IPTG; final concentration of 1 mM) to the cultures, and the cells were collected by centrifugation after incubation at 20 and 37 °C for 4 h, respectively. The cells were disrupted by ultrasonication and subsequently centrifuged to separate the soluble and insoluble fractions. The soluble and insoluble fractions were analyzed by reduced sodium dodecyl sulfate polyacrylamide gel electrophoresis (SDS–PAGE).

About Western blot detection of the expressed fusion protein His-AoOBP8. First, place the PVDF membrane in 200 mL of blocking solution consisting of 5% skim milk powder, and seal it overnight at 4 °C. The following day, wash the membrane with 30 mL of TBST buffer and drain it after washing. Next, soak the membrane in a blocking solution (5% skim milk powder) diluted with mouse anti-6 × His primary antibody at a volume ratio of 1:1000, and incubate it overnight at 4 °C. The next day, wash the membrane six times with 30 mL of TBST buffer, allowing 5 min for each wash. After completing the sixth wash, drain the membrane and soak it in goat anti-mouse IgG secondary antibody diluted with blocking solution at a volume ratio of 1:3000. Incubate at room temperature for 2 h, followed by another six washes with 30 mL of TBST buffer for 5 min each. After washing, take photographs and observe the results after color development using the WTMB color reagent kit.

The crude protein of the His-AoOBP8 fusion protein was purified using a Ni-NTA affinity chromatography column. The equilibrium column was washed with imidazole elution solutions at concentrations of 20, 50, and 500 mmol/L. Subsequently, the protein was eluted through overnight dialysis with Tris HCl buffer at pH 7.4 and 50 mmol/L. Finally, analyze the collected protein samples using 15% SDS-PAGE and validate the purified fusion protein through Western blot.

2.5. Statistical Analysis

The data were summarized as the mean ± SE (standard error) for all data sets. A one-way analysis of variance (ANOVA) was performed on data with more than 3 groups using SPSS 26.0. Differences between means were tested using a Student-Newman-Keuls (S-N-K) test for multiple comparisons. The independent sample *t*-tests were used for data with fewer than 3 groups. All experiments were performed with 3 biological replicates. Each biological replicate was performed with 3 technical repetitions. Differences were considered statistically significant at the 5% level ($p < 0.05$).

3. Results

3.1. Transcriptome Sequencing and Assembly of A. orientalis

We obtained a total of 46.44 Gb of high-quality reads, with each sample yielding more than 6.41 Gb of clean data. The Q30 base percentage exceeded 97.03%, and GC content ranged from 36.03% to 38.01% (Table 2). Transcript assembly using Trinity produced 71,513 transcripts with an N50 length of 2692 bp. The analysis of the assembled sequences yielded 40,182 unigenes, with an N50 length of 2904 bp, reflecting strong assembly integrity (Table 3).

Table 2. Summary of sequencing data of six cDNA libraries of *A. orientalis*.

Sample	Raw Reads	Clean Reads	Clean Base (G)	Error Rate (%)	Q20 (%)	Q30 (%)	GC Content (%)
AoF1	54,635,230	51,945,542	7.79	0.01	99.02	97.03	38.015
AoF2	45,726,002	42,760,376	6.41	0.01	98.78	96.14	37.905
AoF3	54,278,948	51,546,124	7.73	0.01	98.94	96.74	37.775
AoM1	67,109,646	64,403,836	9.66	0.01	98.95	96.93	37.175
AoM2	50,562,262	47,874,422	7.18	0.01	98.87	96.62	36.035
AoM3	54,119,120	51,134,978	7.67	0.01	98.89	96.66	36.675

Table 3. Illumina transcriptome assembly results for female and male *A. orientalis*.

	Length Range	Transcript	Unigene
Transcript length interval	200~500 bp	27,120	5610
	500~1000 bp	14,422	12,008
	1000~2000 bp	13,241	9938
	≥2000 bp	16,728	12,626
Sequencing Statistics	Total Number	71,513	40,182
	Mean Length	1417	1833
	N50	2692	2904
	N90	563	774
	Total Bases	101,331,167	73,664,248

3.2. Functional Annotation of the Unigenes in A. orientalis

The unigene sequences were aligned using Diamond 4.6.8 software against eight major databases: KEGG, NR, Swiss-Prot, TrEMBL, KOG, GO, and Pfam. The transcriptome data of *A. orientalis* adults produced a total of 40,182 annotated unigenes, with the NR and TrEMBL databases providing the highest number (26,113 unigenes, 64.99%, 26,326 unigenes, 65.52%, respectively) (Table 4). Meanwhile, the results indicated that 28,075 of the 40,182 unigenes (69.87%) had been annotated in at least one database.

Table 4. Analysis of annotation of a pooled assembly of female and male *A. orientalis* in different databases.

Database	Number of Genes	Percentage (%)
KEGG	22,709	56.52
NR	26,113	64.99
SwissProt	20,542	51.12
TrEMBL	26,326	65.52
KOG	19,036	47.37
GO	23,074	57.42
Pfam	23,512	58.51
Annotated in at least one Database	28,075	69.87
Total Unigenes	40,182	100

Based on the annotation results from the NR database, a species distribution map of the sequence alignment was drawn. The results showed that 36.38% of the genes were aligned to *Nasonia vitripennis*, 12.4% were aligned to *Ceratosolen solmsi* marchali, 11.84% were aligned to *Trichomalopsis sarcophagae*, 3.18% were aligned to *Copidosoma floridanum*, 1.84% were aligned to *Trichogramma pretiosum*, 0.69% were aligned to *Idotea baltica*, and 33.67% were aligned to other species (Figure 1).

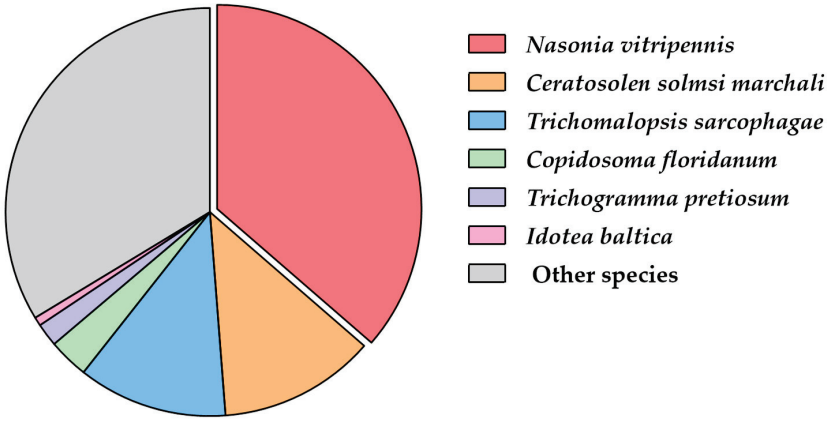


Figure 1. Species distribution of unigenes of *A. orientalis* in NR database.

3.3. Functional Classification of Unigenes in A. orientalis

3.3.1. GO Enrichment Analysis

In the GO database, the gene functions of *A. orientalis* were classified into three categories: biological process (BP), cellular component (CC), and molecular function (MF). Among them, the number of unigenes involved in biological processes was the largest. Cellular and metabolic processes were the two largest groups in both data sets among the biological process category. In molecular function, the number of unigenes involved in binding function and catalytic activity was the highest, with 15,597 and 9786, respectively. In cellular components, the number of unigenes for cell anatomical entities was the largest, at 20,556, followed by protein complexes (6993). In the biological process, the number of unigenes involved in intracellular processes (17,636) and metabolic processes (14,048) was relatively large (Figure 2). These GO annotations provide insights into the global gene expression profile for male and female adults of *A. orientalis*.

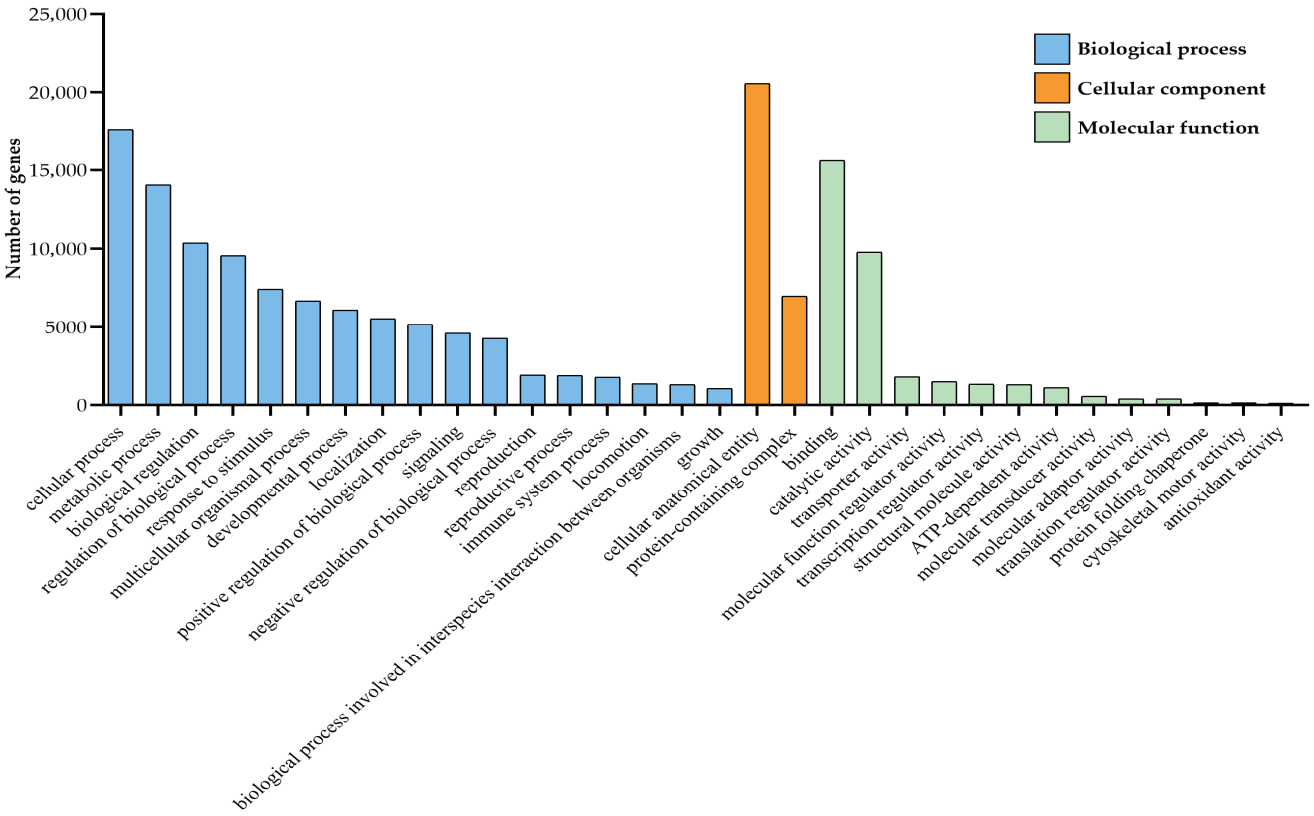


Figure 2. Gene ontology classifications of the *A. orientalis* unigenes.

3.3.2. KEGG Enrichment Analysis

The gender-differentiated expression genes of *A. orientalis* were enriched in six sections, including cellular processes, environmental information processing, genetic information processing, human diseases, metabolism, and organismal systems. A bar chart of enrichment items was drawn, as shown in Figure 3. These pathways include cell cycle (117, 3.14%), ribosome (281, 7.54%), coronavirus disease (300, 8.05%), and carbon metabolism (165, 4.43%), etc. At the same time, the 20 most significantly enriched pathway items were plotted as a scatter plot, as shown in Figure 4. The larger the circle, the higher the abundance. The closer the color is to red, the greater the significance. The trends presented in Figures 3 and 4 are consistent.

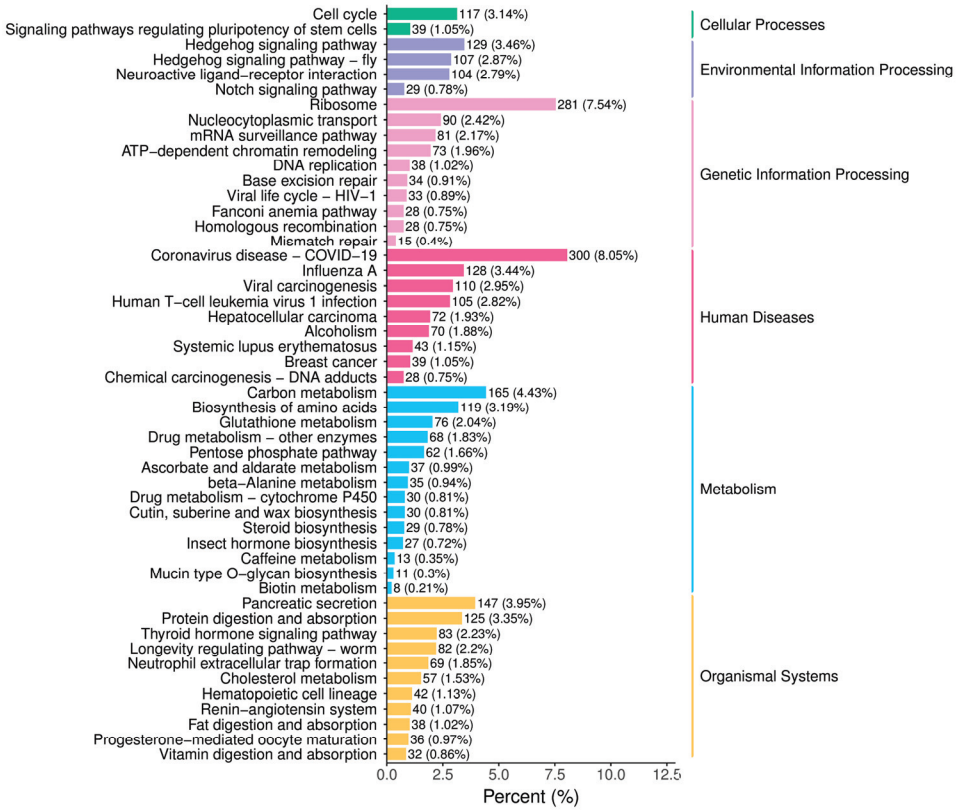


Figure 3. KEGG pathway enrichment column diagram of *A. orientalis*.

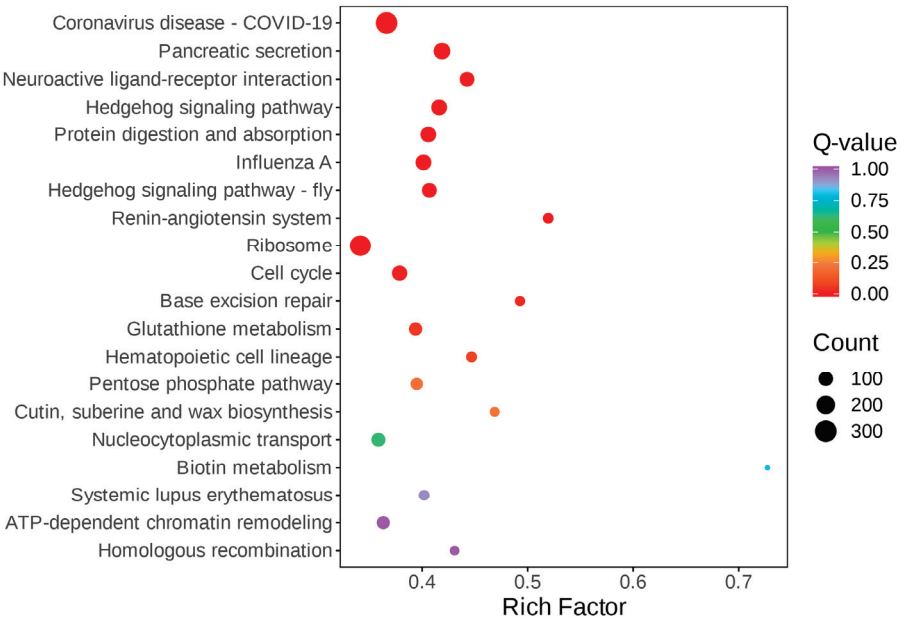


Figure 4. KEGG pathway enrichment scatterplot of *A. orientalis*.

3.4. Analysis of Differentially Expressed Genes and Identification and Analysis of Candidate Chemosensory Protein Genes

By analyzing the differentially expressed genes (DEGs) in female and male adults of *A. orientalis*, a total of 13,747 differentially expressed genes were obtained, among which 4929 were down-regulated genes and 4665 were up-regulated genes (Figure 5). Overall, 62 genes related to chemical perception in *A. orientalis* were screened from the database,

including 24 OBPs, 4 CSPs, 26 ORs, 3 IRs, 3 GRs, and 2 SNMPs. The identified odor-related genes exhibited varying FPKM values between male and female adult insects. For instance, some genes, such as *AoOBP1*, *AoOBP4*, *AoOBP7*, *AoOBP11*, *AoOBP24*, *AoCSP4*, *AoOR12*, *AoOR13*, and *AoSNMP1*, were expressed at higher levels in male adults compared with female adults. There were also two genes that were exclusively expressed in male adults: *AoOR12* and *AoOR13*. Conversely, other olfactory genes, such as *AoOBP5*, *AoOBP14*, *AoOBP17*, *AoOBP18*, and *AoSNMP2*, demonstrated greater expression levels in female adults than in their male counterparts (Table S1).

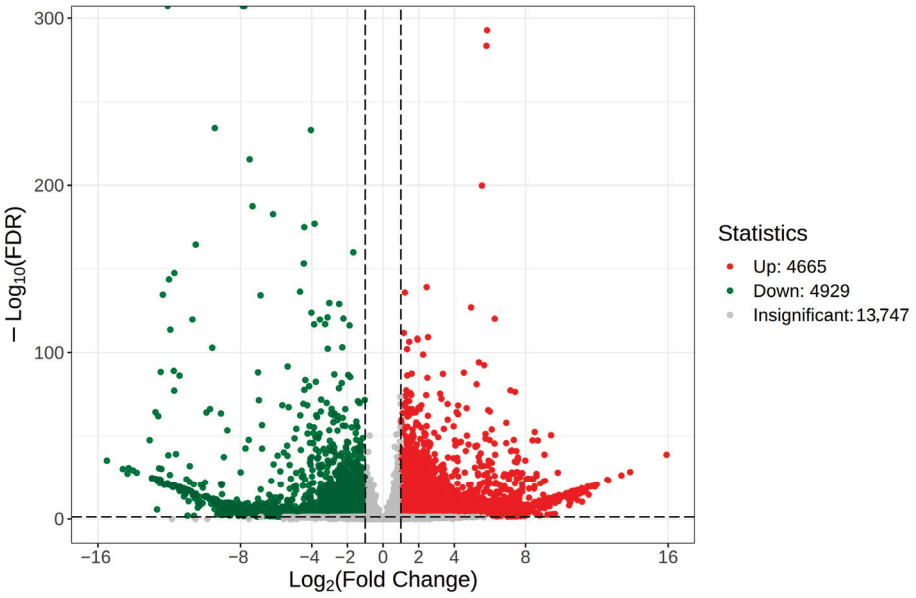


Figure 5. Volcano map of differentially expressed genes of *A. orientalis*.

3.5. Molecular Cloning and Prokaryotic Expression of AoOBP8

3.5.1. Cloning and Sequence Analysis of AoOBP8

The full-length cDNA sequence of *AoOBP8* was cloned and deposited in the GenBank database (GenBank accession number: PQ836618). The product was analyzed by agarose gel electrophoresis (Figure 6). Our results show that the full length of *AoOBP8* from *A. orientalis* was 701 bp, and the ORF of *AoOBP8* was 450 bp, encoding 149 amino acids (Figure 7). The start codon (ATG) was located at 149 bp and the stop codon (TAG) was located at 599 bp. The sequence included a 5′ untranslated region of 148 bp in length and a 3′ untranslated region of 103 bp in length. The 3′UTR region contained the typical polyadenylation signal sequence AATAA and a 31 bp PolyA tail. The NCBI conserved domain online analysis indicated that the amino acids encoded by the *AoOBP8* had a conserved domain of the insect odorant-binding protein family PBP-GOBP superfamily at positions 91 to 420 (E-value: 3.60×10^{-20}). Physicochemical properties of the protein coded by *AoOBP8* were as follows: The molecular formula of its protein was derived as $C_{776}H_{1174}N_{194}O_{219}S_{11}$. The molecular mass was 17.078 kDa, and the isoelectric point (PI) was 7.53. The total number of negatively charged amino acid residues (Asp + Glu) was 14, and the total number of positively charged amino acid residues (Arg + Lys) was 15. The grand average of hydropathicity was −0.074, indicating that the protein was a hydrophilic protein. The aliphatic index was 74.03 and the instability index was 47.01, suggesting that it was an unstable protein.



Figure 6. PCR products of *AoOBP8*. Marker represents DL 2000 DNA Marker; 1 represents the middle segment of *AoOBP8*; 2 represents the 5′ RACE segment of *AoOBP8*; 3 represents the 3′ RACE segment of *AoOBP8*.

```
1                                                                CAGGAAACAGCTATGACCATGATTACGCCAAGCTTGCATGCCTGCAGGTCGACTCTAG
59   ACTCGAGGGATCCAGATCTCCAGTCTTAAGCAGTGGTAACAACGCAGAGTCTAATACGACTCACTATAGGGCAAGCAGTGGTAACAACGC
149  ATGTATTACACGAGACTGCCATTGATATTCGTCCTCGTTGGATTTTTATATCCTGCCGTCCATGCCGGGACGCGGCCAAGCTTCGTATCC
1      M   Y   Y   T   R   L   P   L   I   F   V   L   V   G   F   L   Y   P   A   V   H   A   G   T   R   P   S   F   V   S
239  GACAAGATGATTGCTACGGCTGCCAGCGTCGTGAACGCTTGTCAAATGCAAACGGGCGTGGCCACTGCCGACATCGAATCGGTGAGAAAC
31     D   K   M   I   A   T   A   A   S   V   V   N   A   C   Q   M   Q   T   G   V   A   T   A   D   I   E   S   V   R   N
329  GGCCAGTGGCCCGATACACCGGAATTAAAGTGTTACATGTACTGTCTTTGGGAGCAATTTGGACTGATTGATGAAAAGCGAGAATTGAGC
61     G   Q   W   P   D   T   P   E   L   K   C   Y   M   Y   C   L   W   E   Q   F   G   L   I   D   E   K   R   E   L   S
419  TTAAATGGCATGCTAACTTTCTTCCAAAGAATACCGGCATACCGTACTGAAGTTCAAAAGGCTATTAGCGAGTGCAAGGCCCTTGGTAAA
91     L   N   G   M   L   T   F   F   Q   R   I   P   A   Y   R   T   E   V   Q   K   A   I   S   E   C   K   A   L   G   K
509  TATTTCGCTACCGGCGATACTTGCGAATACGCGTACACGTTTAACAAATGCTACGCCGAAAGATCGCCAAGAACTTACTACCTCTTTTGA
121    Y   F   A   T   G   D   T   C   E   Y   A   Y   T   F   N   K   C   Y   A   E   R   S   P   R   T   Y   Y   L   F   *
599  ACTGGACAAAAACGCTTAAGTCCGAATTAAGAAAAGATATCCGATTTTAGACACCCATTATAATAATGAACGAAAAAAAAAAAAAAAAAA
689  AAAAAAAAAAAAA
```

Figure 7. Nucleotide and amino acid sequences of *AoOBP8*. The start and stop codons are indicated in bold italic font, and "*" represents a stop codon. The conserved cysteines are indicated in a red box.

In the prediction of hydrophobicity results on the ProtScale online platform of ExPASy, hydrophilic amino acids have negative values, while hydrophobic amino acids have positive values. The higher the absolute value, the stronger the hydrophilicity/hydrophobicity. The results are shown in the following figure. The prediction results of the ProtScale online software (https://web.expasy.org/protscale/, accessed on 6 July 2025) indicate that in the amino acid sequence of *AoOBP8*, hydrophilicity and hydrophobicity are evenly distributed in a mixed manner throughout the entire polypeptide chain. The minimum hydrophobicity value is approximately −2.244, and the maximum value is approximately 3.278. Based on this, it can be preliminarily determined that this protein is a hydropathic (Figure S1).

The predicted signal peptide of the deduced protein suggested a VHA-GT cleavage site between pos. 22 and 23 (probability: 0.9563) (Figure S2). Transmembrane prediction using the hidden Markov models (TMHMM) program result showed that *AoOBP8* has

no transmembrane domain (Figure S3). The secondary structure analysis of the SOPMA protein revealed that the secondary structure of the *AoOBP8* protein consists of an alpha helix (65.77%), extended strand (3.36%), and random coil (30.87%). Thus, it can be seen that the alpha helix is the main structural form of the *AoOBP8* protein (Figures S4 and S5).

3.5.2. Sequence Alignment and Phylogenetic Analysis of AoOBP8

Sequence alignment and phylogenetic analysis indicated that the sequence identity of *AoOBP8* from *A. orientalis* with other selected Hymenoptera insect OBPs is 73.03%. The result showed that *AoOBP8* possesses six conserved Cys residues, matching the pattern of classic OBPs (Figure S6). The phylogenetic tree based on OBPs from *A. orientalis* and other species from Hymenoptera was constructed using the neighbor-joining method (Figure S7). The *AoOBP8* in *A. orientalis* was clustered closely with the *NvOBP69a* in *N. vitripennis* with 41% confidence, indicating that the genetic distance between *AoOBP8* and *NvOBP69a* is the shortest. This is consistent with the results of the amino acid sequence homology analysis.

3.5.3. Expression of AoOBP8 in Male and Female Adults and in Various Tissues

The expression pattern of *AoOBP8* was investigated by RT-qPCR (Figure 8). The analysis of the results revealed that the expression level of *AoOBP8* in female adults was slightly higher than that in male adults, but there was no significant difference between them ($p = 0.055$) (Figure 8A). The relative expression level of *AoOBP8* was detected in the head, thorax and abdomen. The relative expression level of *AoOBP8* in various tissues went from high to low in the order of head, thorax and abdomen, with the relative expression level in the head significantly higher than in the thorax and abdomen ($p = 0.001$). The expression levels of *AoOBP8* in the thorax and abdomen were not significantly different ($p = 0.539$) (Figure 8B).

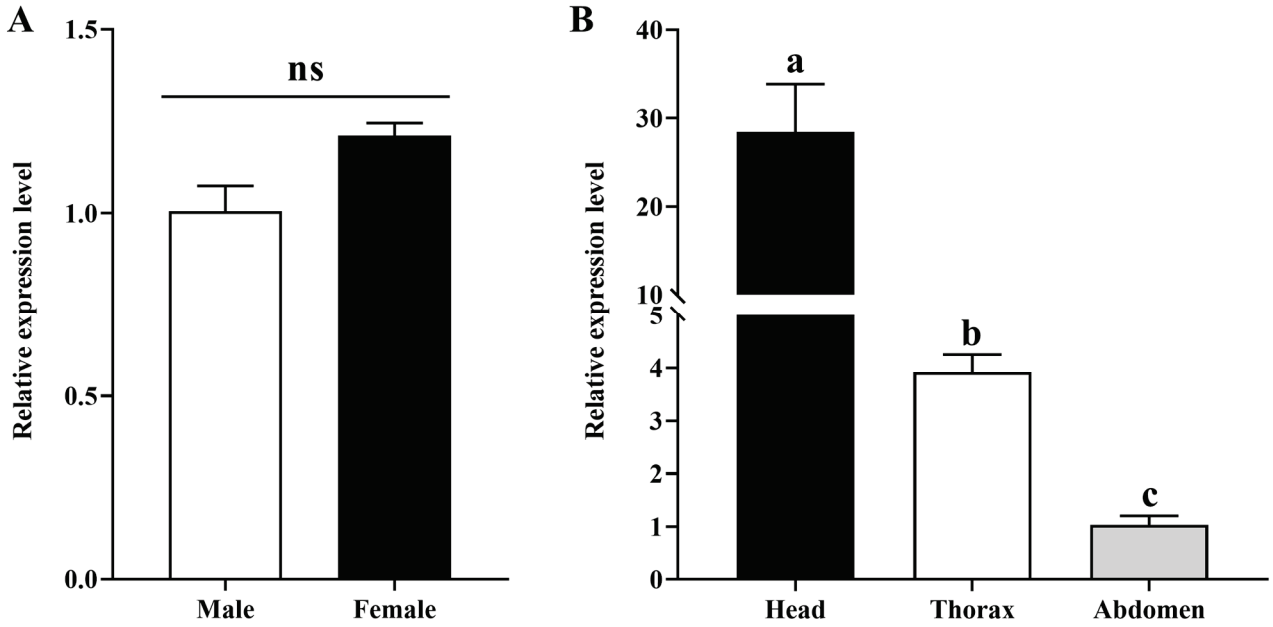


Figure 8. Relative expression level of *AoOBP8*. (**A**) relative expression level in male and female adults, (**B**) relative expression level in different issues (head, thorax and abdomen). The "ns" on the bar chart indicates no significant difference ($p > 0.05$, independent samples *t*-test). While different lowercase letters (a, b, c) on the bar chart indicate significant difference between head, thorax and abdomen ($p < 0.05$, S-N-K test).

3.5.4. Prokaryotic Expression of AoOBP8

The *AoOBP8* protein sequence was constructed into the expression vector and then transformed into competent cells of *E. coli*. The cells were cultured and induced to express, and the bacterial cells were collected. The samples were purified for small-scale experiments. The expression and purification effects of the target protein were verified through SDS-PAGE and Western blot. To further determine whether the target protein was expressed, the TMB color development kit was used for color reaction. Following the Western blot procedure, the labeled antibodies were employed for detection (Figures 9–11). In conclusion, the target protein is expressed with inclusion bodies, and affinity purification can successfully purify the target protein.

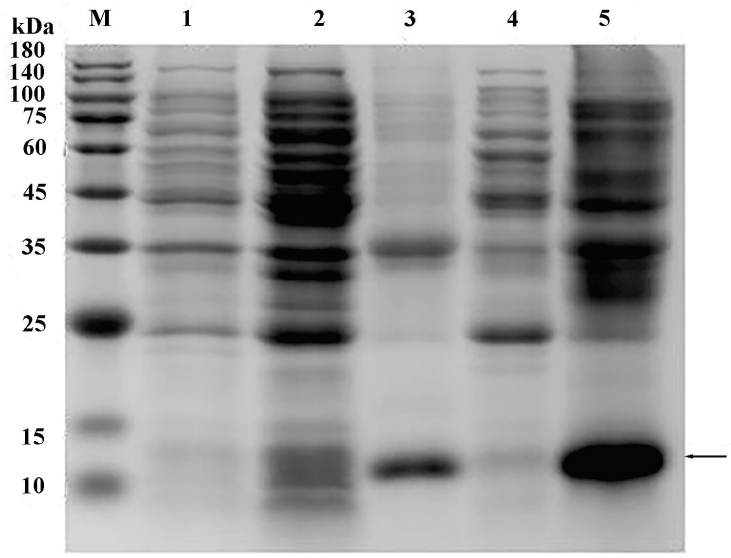


Figure 9. Analysis of SDS-PAGE for the small-scale expression of a fusion protein. M: Protein Marker; 1: Total protein before induction; 2: Supernatant at 20 °C; 3: Precipitate at 20 °C; 4: Supernatant at 37 °C; 5: Precipitate at 37 °C. The black arrow points to the target protein.

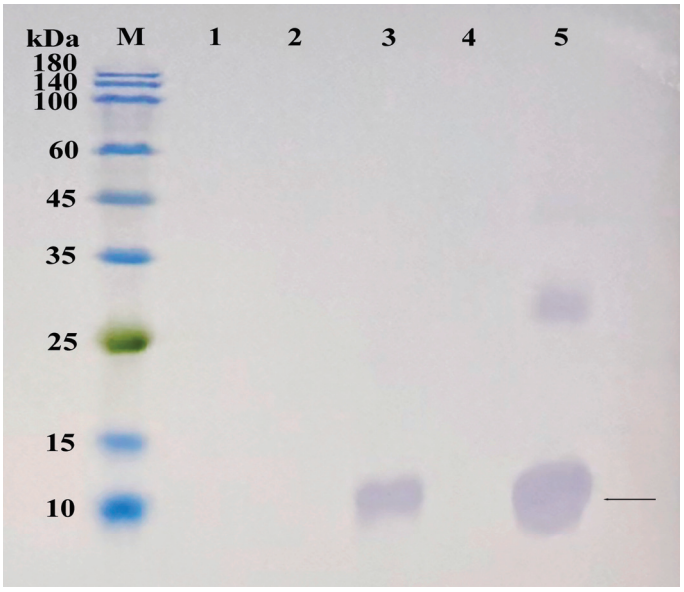


Figure 10. Expression trial of fusion protein Western blot analysis chart. M: Protein marker; 1: Total protein before induction; 2: Supernatant at 20 °C; 3: Precipitate at 20 °C; 4: Supernatant at 37 °C; 5: Precipitate at 37 °C. The black arrow points to the target protein.

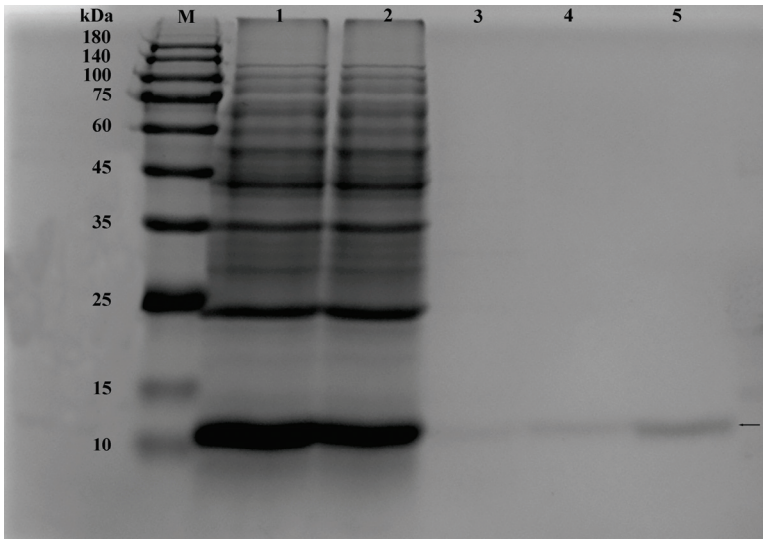


Figure 11. Purification of fusion protein by nickel-affinity agarose chromatography and SDS-PAGE analysis diagram. M: Protein marker; 1: Loading; 2: Flow out; 3: 20 mM Imidazole elution component; 4: 50 mM Imidazole elution component; 5: 500 mM Imidazole elution component. The black arrow points to the target protein.

4. Discussion

A. orientalis, as an efficient and environmentally friendly pest control strategy for *L. delicatula*, has high potential as a biocontrol agent for the suppression of this pest, and it has already been confirmed in the United States, South Korea, and China [9,37–39]. Previous studies have demonstrated that olfaction is the most crucial chemical-sensing pathway for parasitic wasps. These insects rely on their highly sensitive olfactory detection system to regulate various behavioral responses, including mating, host seeking, host location, and host selection [40]. Currently, research on the chemosensory genes of various insect species is advancing rapidly; however, the chemosensory genes in parasitic wasps have received comparatively less attention. In this study, we conducted a transcriptomic analysis of *A. orientalis* using the Illumina NovaSeq 6000 high-throughput sequencing platform (San Diego, CA, USA). We successfully obtained 71,513 transcripts and 40,182 unigenes. This marks the first time we have constructed a transcriptome database from the adults of *A. orientalis*, from which we identified a total of 62 chemosensory protein genes (24 OBPs, 4 CSPs, 26 ORs, 3 IRs, 3 GRs, and 2 SNMPs). The assembled sequence data provides a wealth of information for the functional characterization and identification of the *A. orientalis* transcriptome, as well as for further studies on several critical genes. Previous studies have identified chemosensory membrane genes in several parasitic wasps, namely, *Trichogramma chilonis* (85 genes) [12], *C. cunea* (144 genes) [14], *A. confusum* (84 genes) [15], *A. japonicus* (201 genes) [22], *T. remus* (62 genes) [24], *C. vestalis* (253 genes) [41], *Q. mendeli* (124 genes) [42], *Anagrus nilaparvatae* (163 genes) [43], *Aenasius bambawalei* (324 genes) [44], *Aphidius gifuensis* (100 genes) [45], and *Macrocentrus cingulum* (112 genes) [46], based on transcriptome sequencing. In comparison with the genes identified in other parasitic wasps, *A. orientalis* has a relatively small number of chemosensory-related genes; nonetheless, this quantity remains within a reasonable range. Due to the small size of *A. orientalis*, it is challenging to dissect specific tissues such as the antennae and mouthparts. Consequently, this study conducted transcriptome sequencing on whole individuals, including both female and male adults. As a result, some chemosensory genes with low expression levels in the antennae and mouthparts could not be identified. Additionally, transcripts that were

present in low abundance and those that were too divergent to be identified through a BLAST search may have been missed during the transcriptome analysis [14]. Therefore, it is unlikely that the identified genes encompass the complete set of chemosensory genes in *A. orientalis*. Nevertheless, this study marks the first comprehensive characterization of chemosensory genes in *A. orientalis*. Our findings offer valuable insights into the molecular mechanisms of chemoreception in this species and highlight potential molecular targets for use in biological control strategies. In this study, the wasps we collected emerged from the host eggs as adults within 24 h, so they had finished mating. We assume that these chemosensory genes with female antennal-specific or dominant expression profiles may play important roles in locating suitable hosts and oviposition sites. This, however, should be verified in further experiments.

OBP and OR have important roles to play in the process of olfaction in insects. Odorant molecules entering through pores interact with OBP/PBPs, which then become solubilized, allowing for the transport of odorants to ORs located in the membrane of the ciliated dendrites [12,47]. A total of 24 OBPs were identified in the adult transcriptomes of *A. orientalis*. The number of OBPs of *A. orientalis* identified was smaller than that of *C. cunea* (25 OBPs) [14], *Q. mendeli* (58 OBPs) [42], and *A. bambawalei* (54 OBPs) [44]. However, it was greater than the number found in *T. chilonis* (22 OBPs) [12], *C. vestalis* (22 OBPs) [16,41], *A. confusum* (11 OBPs) [15], *Sclerodermus* sp. (10 OBPs) [23] and *T. remus* (5 OBPs) [24]. More OBPs were not found because, compared with the antennae, RNA obtained from the whole body may result in genes with low expression that cannot be detected [48]. Furthermore, several genes, including *AoOBP1*, *AoOBP4*, *AoOBP7*, *AoOBP11*, *AoOBP24*, *AoCSP4*, *AoOR12*, *AoOR13*, and *AoSNMP1*, exhibited higher expression levels in male adults than in female adults. Additionally, there are two genes, *AoOR12* and *AoOR13*, that are exclusively expressed in male adults. Based on the higher expression levels of those chemosensory-related genes in males than in females, we suggest that these male-enriched OBPs may be involved in sex-specific behaviors, such as by selectively combining with and transporting some pheromones released by females in the process of molecular recognition, and in searching for suitable mates [49,50]. In contrast, several olfactory genes, including *AoOBP5*, *AoOBP14*, *AoOBP17*, *AoOBP18*, and *AoSNMP2*, showed higher expression levels in female adults compared with males. We hypothesize that these genes, which are highly expressed in female insects, may be involved in their search for suitable hosts and egg-laying sites. This hypothesis is further supported by findings related to *T. remus* [24].

Olfactory receptors (ORs) are crucial for insects to detect general odors and sex pheromones. Most ORs in insects are expressed in the antennae [12,51,52]. In our study, a total of 26 ORs were identified in the transcriptome of *A. orientalis*. The number of identified ORs was lower than the number found in *C. cunea* (80 ORs) [14], *T. chilonis* (45 ORs) [12], *A. gifuensis* (62 ORs) [45], and *C. vestalis* (158 ORs) [41]. There may be several explanations for these differences. As OR expressions are modulated by different environmental conditions in which various types of scents exist, lab-reared *A. orientalis* have no opportunity for exposure to such a diversity of odors or volatiles released from host insects or related plants. For this reason, we speculate that some of the olfactory receptor genes may not be expressed well. Previous studies have shown that some OR genes of *M. mediator* were upregulated following contact with host odors [20]. Additionally, parasitoids may also have different expressions of the OR genes under different physiological situations. Some ORs might be specifically expressed at different developmental stages or in other olfactory tissues [46,53]. Overall, the factors mentioned above may affect the number of ORs identified in *A. orientalis*.

CSPs are soluble carrier proteins that may have a function similar to OBPs in insects [54]. In our study, we only identified four CSPs, which were fewer than the number

found in *C. cunea* (11 CSPs) [14], *Sclerodermus* sp. (10 CSPs) [23], *C. vestalis* (11 CSPs) [41], and *A. nilaparvatae* (11 CSPs) [43]. CSPs can be detected in both chemosensory tissues (including the antennae, maxillary palps, labial palps, etc.) and non-chemosensory tissues (including the legs, wings, and pheromone glands) [55]. Our transcriptome analysis showed no significant differences for some CSPs between males and females. This indicates that the CSPs may be involved in odorant detection [55]. However, further experimental verification is needed to determine how this protein functions.

IRs are expressed in sensory neurons with a combinatorial fashion that responds to many distinct odors. In different olfactory neurons, IRs are sufficient to contribute to the responsiveness of ectopic odors [56]. A total of three IRs were identified from the transcriptome in *A. orientalis*. This is less than the amount that was identified in *T. chilonis* (14 IRs) [12], *A. confusum* (19 IRs) [15], and *A. gifuensis* (23 IRs) [45]. The DEG result obtained in our study showed that the expression levels of IR in both male and female adults' libraries are relatively low. This gives us reason to suggest that the IRs identified in both male and female *A. orientalis* could be involved in the processes of searching for food or avoiding harmful substances. For example, certain odor-evoked behaviors have been related to IR pathways in *Drosophila*; the activity of IR64a, which is acid-sensing, has proven to be both necessary and sufficient to promote the behavioral aversion that allows flies to avoid unripe or rotting fruit [57].

Among insect SNMPs (SNMP1 and SNMP2), SNMP1 is usually expressed in the neuron cells that respond to pheromones, whereas SNMP2 is normally expressed in the supporting cells [58]. In this study, two SNMPs were identified in *A. orientalis*. According to the analysis of the transcriptome, SNMP1 was down-regulated in females in comparison with males, while the opposite was true for SNMP2. This suggests that the function of SNMP1 may also be involved in odor or pheromone processing. This is supported by a study showing SNMP1 to be abundantly expressed and localized to the receptor membrane of sex-pheromone-specific olfactory sensory neurons (OSNs) [59].

Gustatory receptors can recognize non-volatile compounds, including sugars, bitter compounds, and the gas carbon dioxide [60]. This study identified a total of three GRs in *A. orientalis*. This is less than the amount that was identified in *C. cunea* (17 GRs) [14], *Q. mendeli* (10 GRs) [42], and *M. cingulum* (20 GRs) [46]. The expression levels of IRs in both male and female adults' libraries are relatively low. We speculate that a possible reason is that GR expression levels are quite low and mainly expressed in gustatory organs [61].

OBPs act in insect olfactory processes, and OBPs are expressed in the olfactory organs and play a role in the binding and transport of hydrophobic odorants through the sensillum lymph to olfactory receptor neurons within the antennal sensilla [62]. The identification of chemosensory genes from the transcriptome database is a vital step in studying the chemosensory perception process of parasitic wasps [41]. In this study, the *AoOBP8* gene was cloned from the transcriptome database of *A. orientalis* by reverse transcription-PCR and RACE-PCR, and recombinant *AoOBP8* was expressed in a prokaryotic expression system. In addition, the relative expression level of *AoOBP8* in the head was significantly higher than in the thorax and abdomen. Our results indicate that the head tissues contain many chemical-sensing genes, which play a crucial role in the behaviors of parasitic wasps, such as searching for hosts and identifying hosts. This hypothesis is further supported by findings related to *T. remus*. Most of the olfactory genes in *T. remus* are highly expressed in the heads of both female and male adults [24]. Furthermore, previous studies have shown that odorant-binding protein 8 of *Orius sauteri (OsauOBP8*) could bind with four common insecticides (phoxim, fenitrothion, chlorpyrifos, deltamethrin), and these results help to better understand the molecular mechanisms of OBPs to insecticides in insects [63].

However, whether *AoOBP8* also has similar functions to *OsauOBP8* remains to be verified through further experiments.

Various inorganic compounds play a crucial regulatory role in the processes by which parasitic wasps search for hosts, identify them, mate, and lay eggs. Consequently, the genes responsible for chemical sensing in these wasps are closely linked to their function in biological control. *A. orientalis*, an important parasitic enemy of the forestry pest *L. delicatula* during its egg stage, has been identified as a candidate gene through transcriptome screening. This research offers valuable genetic resources for investigating the interactions between pests, plants, and parasitic wasps at the molecular level. The findings indicate that the genes associated with chemical perception in *A. orientalis* are expressed differently in female and male insects. This suggests that these genes have distinct roles in host recognition, localization, mating, oviposition, and foraging for food. They can serve as target genes for the development of attractants, providing a reference for future in-depth studies on the molecular mechanisms of chemical ecology in *A. orientalis*. Ultimately, this research aims to enhance the utilization of *A. orientalis* for controlling *L. delicatula*.

5. Conclusions

A. orientalis demonstrates considerable potential for the biological control of *L. delicatula*, which depends on a sensitive olfactory system to identify and locate appropriate hosts for reproduction. The transcriptome database of *A. orientalis* females and males was constructed, and a total of 71,513 transcripts and 40,182 unigenes were identified. Overall, 62 chemosensory genes were screened from the NR database. Phylogenetic analysis showed that these chemosensory genes were most closely related to chemosensory genes found in other Hymenopteran insects. RT-qPCR detection showed that some chemosensory genes showed significant differences and displayed sex-biased expression, indicating that female adults play a key role in the recognition of chemical information for searching for a host and oviposition. In addition, *AoOBP8* was highly expressed in the adult head, indicating that the head plays a key role in the recognition of chemical information. However, further experimental verification is needed to determine how these chemosensory proteins function. The findings herein offer a basis for revealing the chemical–ecological regulatory mechanisms of host finding and oviposition behavior, and provide a reference for developing bio-control methods in forestry.

Supplementary Materials: The following supporting information can be downloaded at: https://www.mdpi.com/article/10.3390/insects16111117/s1, Figure S1: Hydropathy plot of *AoOBP8*; Figure S2. Signal peptide of *AoOBP8*; Figure S3. Transmembrane domain of *AoOBP8*; Figure S4. Secondary structure of *AoOBP8*; Figure S5. Tertiary structure of *AoOBP8*; Figure S6. Multiple sequence alignment among *AoOBP8* with OBPs from other parasitoid wasps; Figure S7. Phylogenetic tree of *AoOBP8*; Table S1: DEG analysis of chemosensory-related genes in *A. orientalis*; Supplementary Document S1: Method of RNA Extraction, cDNA Synthesis, Library Construction and Transcriptome Sequencing.

Author Contributions: Conceptualization, X.L. and S.X.; methodology, X.L. and Y.W. (Yuting Wu); software, X.L.; validation, X.L.; investigation, Y.B., Y.Z., Y.W. (Yanan Wu) and Y.Q.; resources, B.L.; data curation, X.L. and J.Y.; writing—original draft preparation, X.L.; writing—review and editing, S.X.; visualization, X.L.; supervision, X.L.; project administration, X.L. and S.X.; funding acquisition, X.L. and S.X. All authors have read and agreed to the published version of the manuscript.

Funding: This research was supported by the "Green Pollution Control Technology Based on Chemical Pheromone in *Agrilus zanthoxylum*", The National Public Welfare Forestry projects in China (Grant No. 201504324); "Shaanxi Province's Second Batch of Special Support Program for High-Level Talents

Leading Talents Project" (No. Shaanxi Group 2020-44); Xi'an Innovation Strong Foundation Plan-Agricultural technology research and development projects "Lantian County's Development and application technology of pheromone lure for *Agrilus zanthoxylum*" (No. 2022JH-JSYF-0261); The 2024 Shaanxi Forestry Science and Technology Innovation Special Project "Green Control Technology for *Agrilus zanthoxylum* Using Chemical Pheromones" (SXLK2024-0213); Shaanxi Provincial Department of Science and Technology will support Yangling in its innovation and development of science and technology projects in 2025. "Green Control and Demonstration of Pine Wood Borer Pests Based on Chemical Semiochemicals" (2025ZY-QYCXYL-07).

Data Availability Statement: The original contributions presented in this study are included in the article/Supplementary Materials. Further inquiries can be directed to the corresponding author.

Conflicts of Interest: The authors declare no conflicts of interest.

References

1. Lee, D.H.; Park, Y.L.; Leskey, T.C. A review of biology and management of *Lycorma delicatula* (Hemiptera: Fulgoridae), an emerging global invasive species. *J. Asia-Pac. Entomol.* **2019**, *22*, 589–596. [CrossRef]
2. Barringer, L.; Ciafré, C.M. Worldwide feeding host plants of spotted lanternfly, with significant additions from north America. *Environ. Entomol.* **2020**, *49*, 999–1011. [CrossRef]
3. Leach, H.; Biddinger, D.J.; Krawczyk, G.; Smyers, E.; Urban, J.M. Evaluation of insecticides for control of the spotted lanternfly, *Lycorma delicatula*, (Hemiptera: Fulgoridae), a new pest of fruit in the Northeastern US. *Crop Prot.* **2019**, *124*, 104833. [CrossRef]
4. Francese, J.A.; Cooperband, M.F.; Murman, K.M.; Cannon, S.L.; Booth, E.G.; Devine, S.M.; Wallace, M.S. Developing traps for the spotted lanternfly, *Lycorma delicatula* (Hemiptera: Fulgoridae). *Environ. Entomol.* **2020**, *49*, 269–276. [CrossRef] [PubMed]
5. Cooperband, M.F.; Mack, R.; Spichiger, S.E. Chipping to destroy egg masses of the spotted lanternfly, *Lycorma delicatula* (Hemiptera: Fulgoridae). *J. Insect Sci.* **2018**, *18*, 7. [CrossRef]
6. Urban, J.M.; Leach, H. Biology and management of the spotted lanternfly, *Lycorma delicatula* (Hemiptera: Fulgoridae), in the United States. *Annu. Rev. Entomol.* **2023**, *68*, 151–167. [CrossRef]
7. Godfray, H.C.J. *Parasitoids: Behavioral and Evolutionary Ecology*; Princeton University Press: Princeton, NJ, USA, 1994; p. 194.
8. Yang, Z.Q.; Choi, W.Y.; Cao, L.M.; Wang, X.Y.; Hou, Z.R. A new species of *Anastatus* (Hymenoptera: Eulpelmidae) from China, parasitizing eggs of *Lycorma delicatula* (Homoptera: Fulgoridae). *Zool. Syst.* **2015**, *40*, 290–302. [CrossRef]
9. Bao, K.X.; Dang, Y.Q.; Zhuang, Y.T.; Fan, M.X.; Wang, X.Y. Evaluation of parasitic capacity of *Anastatus orientalis* (Hymenoptera: Eupelmidae) on eggs of *Antherea pernyi* (Lepidoptera: Saturniidae) based on functional response Model. *Chin. J. Biol. Control* **2025**, *41*, 260–268.
10. Hou, Z.R. Study on the *Lycorma delicatula* and Egg Parasitoids. Master's Thesis, Chinese Academy of Forestry, Beijing, China, 2013.
11. Bao, K.X. Studies on the Field Lethal Factor of Spotted Lanternfly and Biology of Its Natural Enemy at Egg Stage—*Anastatus orientalis*. Master's Thesis, Agricultural University of Hebei, Baoding, China, 2022.
12. Liu, J.B.; Wu, H.; Yi, J.Q.; Song, Z.W.; Li, D.S.; Zhang, G.R. Transcriptome characterization and gene expression analysis related to chemoreception in *Trichogramma chilonis*, an egg parasitoid. *Gene* **2018**, *678*, 288–301. [CrossRef]
13. Wu, Q.; Zhou, X.; Xu, Z.Y.; Zhang, X.F.; Yuan, H.C.; Guo, J.X. Transcriptome analysis and identification of chemosensory membrane proteins in the head of *Euplatypus parallelus*. *Insects* **2025**, *16*, 504. [CrossRef]
14. Zhao, Y.N.; Wang, F.Z.; Zhang, X.Y.; Zhang, S.H.; Guo, S.L.; Zhu, G.P.; Liu, Q.; Li, M. Transcriptome and expression patterns of chemosensory genes in antennae of the parasitoid wasp *Chouioia cunea*. *PLoS ONE* **2016**, *11*, e0148159. [CrossRef]
15. Li, Y.J.C.; Chen, H.C.; Hong, T.L.; Yan, M.W.; Wang, J.; Shao, Z.M.; Wu, F.A.; Sheng, S.; Wang, J. Identification of chemosensory genes by antennal transcriptome analysis and expression profiles of odorant-binding proteins in parasitoid wasp *Aulacocentrum confusum*. *Comp. Biochem. Physiol. Part D Genom. Proteom.* **2021**, *40*, 100881. [CrossRef]
16. Vinson, S.B. The general host selection behavior of parasitoid Hymenoptera and a comparison of initial strategies utilized by larvaphagous and oophagous species. *Biol. Control* **1998**, *11*, 79–96. [CrossRef]
17. Vet, L.E.M.; Dicke, M. Ecology of Infochemical Use by Natural Enemies in a Tritrophic Context. *Annu. Rev. Entomol.* **1992**, *37*, 141–172. [CrossRef]
18. Turlings, T.C.; Tumlinson, J.H.; Lewis, W.J. Exploitation of herbivore-induced plant odors by host-seeking parasitic wasps. *Science* **1990**, *250*, 1251–1253. [CrossRef] [PubMed]
19. De Moraes, C.M.; Lewis, W.J.; Pare, P.W.; Alborn, H.T.; Tumlinson, J.H. Herbivore-infested plants selectively attract parasitoids. *Nature* **1998**, *393*, 570–573. [CrossRef]

20. Wang, S.N.; Peng, Y.; Lu, Z.Y.; Dhiloo, K.H.; Gu, S.H.; Li, R.J.; Zhou, J.J.; Zhang, Y.J.; Guo, Y.Y. Identification and expression analysis of putative chemosensory receptor genes in *Microplitis mediator* by antennal transcriptome screening. *Int. J. Biol. Sci.* **2015**, *11*, 737–751. [CrossRef] [PubMed]
21. Nishimura, O.; Brillada, C.; Yazawa, S.; Maffei, M.E.; Arimura, G. Transcriptome pyrosequencing of the parasitoid wasp *Cotesia vestalis*: Genes involved in the antennal odorant-sensory system. *PLoS ONE* **2012**, *7*, e50664. [CrossRef]
22. Zhan, H.X.; Li, L.; Li, F.Q.; Zang, L.S. Identification and comparative expression profiles of candidate olfactory receptors in the transcriptomes of the important egg parasitoid wasp *Anastatus japonicus* Ashmead (Hymenoptera: Eupelmidae). *Plants* **2023**, *12*, 915. [CrossRef]
23. Zhou, C.X.; Min, S.F.; Tang, Y.L.; Wang, M.Q. Analysis of antennal transcriptome and odorant binding protein expression profiles of the recently identified parasitoid wasp, *Sclerodermus* sp. *Comp. Biochem. Physiol. D Genom. Proteom.* **2015**, *16*, 10–19. [CrossRef]
24. Zhou, W.; Xu, Z.; Yang, W.J.; Mao, Y.; Sheng, L.Y.; Du, J.L.; Wu, D.G.; Wang, Z.X.; Huang, B.H. Analysis of the transcriptome and chemosensory-related genes of *Telenomus remus* Nixon. *Plant Prot.* **2022**, *48*, 264–277.
25. Seo, M.; Kim, J.H.; Seo, B.Y.; Park, C.; Choi, B.R.; Kim, K.H.; Ji, C.W.; Cho, J.R. Mass-rearing techniques of *Anastatus orientalis* (Hymenoptera: Eupelmidae), as the egg-parasitoid of *Lycorma delicatula* (Hemiptera: Fulgoridae): An using method of *Antheraea pernyi* (Lepidoptera: Saturniidae) and *L. delicatula* eggs in laboratory. *Kor. J. Appl. Entomol.* **2018**, *57*, 243–251. [CrossRef]
26. Buchfink, B.; Xie, C.; Huson, D.H. Fast and sensitive protein alignment using DIAMOND. *Nat. Methods* **2015**, *12*, 59–60. [CrossRef] [PubMed]
27. Kanehisa, M.; Goto, S.; Kawashima, S.; Okuno, Y.; Hattori, M. The KEGG resource for deciphering the genome. *Nucleic Acids Res.* **2004**, *32*, 277–280. [CrossRef] [PubMed]
28. Xie, C.; Mao, X.; Huang, J.; Ding, Y.; Wu, J.; Dong, S.; Kong, S.; Gao, G.; Li, C.Y.; Wei, L.P. KOBAS 2.0: A web server for annotation and identification of enriched pathways and diseases. *Nucleic Acids Res.* **2011**, *39*, 316–322. [CrossRef]
29. Jones, P.; Binns, D.; Chang, H.Y.; Fraser, M.; Li, W.; McAnulla, C.; McWilliam, H.; Maslen, J.; Mitchell, A.; Nuka, G.; et al. InterProScan 5: Genome-scale protein function classification. *Bioinformatics* **2014**, *30*, 1236–1240. [CrossRef]
30. Ashburner, M.; Ball, C.A.; Blake, J.A.; Botstein, D.; Butler, H.; Cherry, J.M.; Davis, A.P.; Dolinski, K.; Dwight, S.S.; Eppig, J.T.; et al. Gene ontology: Tool for the unification of biology. *Nat. Genet.* **2000**, *25*, 25–29. [CrossRef]
31. Eddy, S.R. Profile hidden Markov models. *Bioinformatics* **1998**, *14*, 755–763. [CrossRef]
32. Finn, R.D.; Bateman, A.; Clements, J.; Coggill, P.; Eberhardt, R.Y.; Eddy, S.R.; Heger, A.; Hetherington, K.; Holm, L.; Mistry, J.; et al. Pfam: The protein families database. *Nucleic Acids Res.* **2014**, *42*, 222–230. [CrossRef]
33. Mortazavi, A.; Williams, B.A.; McCue, K.; Schaeffer, L.; Wold, B. Mapping and quantifying mammalian transcriptomes by RNA-Seq. *Nat Methods* **2008**, *5*, 621–628. [CrossRef]
34. Li, R.Q.; Yu, C.; Li, Y.R.; Lam, T.W.; Yiu, S.M.; Kristiansen, K.; Wang, J. SOAP2: An improved ultrafast tool for short read alignment. *Bioinformatics* **2009**, *25*, 1966–1967. [CrossRef]
35. Kumar, S.; Stecher, G.; Tamura, K. MEGA7: Molecular evolutionary genetics analysis version 7.0 for bigger datasets. *Mol. Biol. Evol.* **2016**, *33*, 1870–1874. [CrossRef]
36. Livak, K.J.; Schmittgen, T.D. Analysis of relative gene expression data using real-time quantitative PCR and the $2^{-\Delta\Delta CT}$ method. *Methods Enzymol.* **2001**, *25*, 402–408. [CrossRef] [PubMed]
37. Broadley, H.J.; Sipolski, S.J.; Pitt, D.B.; Hoelmer, K.A.; Wang, X.Y.; Cao, L.M.; Tewksbury, L.A.; Hagerty, T.J.; Bartlett, C.R.; Russell, A.D.; et al. Assessing the host range of *Anastatus orientalis*, an egg parasitoid of spotted lanternfly (*Lycorma delicatula*) using Eastern U.S. non-target species. *Front. Insect Sci.* **2023**, *3*, 1154697. [CrossRef]
38. Kim, I.K.; Koh, S.H.; Lee, J.S.; Choi, W.I.; Shin, S.C. Discovery of an egg parasitoid of *Lycorma delicatula* (Hemiptera: Fulgoridae) an invasive species in South Korea. *J. Asia-Pac. Entomol.* **2011**, *14*, 213–215. [CrossRef]
39. Liu, X.Y.; Bai, Y.Y.; Zhao, Y.Y.; Qi, Y.; Jiang, N.; Liu, B.Z.; Lü, S.J.; Xie, S.A. Morphology and ultrastructure of the antennal sensilla of adult *Anastatus orientalis* (Hymenoptera: Eupelmidae), a parasitoid of *Lycorma delicatula* (Hemiptera: Fulgoridae). *Acta Entomol. Sin.* **2025**, *68*, 123–132.
40. Liu, L.; Wei, K.; Bao, K.X.; Xie, J.Y.; Wang, X.Y. Ultrastructure of antennal sensilla of *Anastatus orientalis* (Hymenoptera: Eupelmidae), an egg parasitoid of the invasive spotted lanternfly, *Lycorma delicatula* (Hemiptera: Fulgoridae). *Ultramicroscopy* **2025**, *276*, 114179. [CrossRef]
41. Liu, Y.P.; Du, L.X.; Zhu, Y.; Yang, S.Y.; Zhou, Q.; Wang, G.R.; Liu, Y. Identification and sex-biased profiles of candidate olfactory genes in the antennal transcriptome of the parasitoid wasp *Cotesia vestalis*. *Comp. Biochem. Physiol. D Genom. Proteom.* **2020**, *34*, 100657. [CrossRef] [PubMed]
42. Huang, Z.Y.; Wang, X.Y.; Lu, W.; Zheng, X.L. Sensory gene identification in the transcriptome of the ectoparasitoid *Quadrastichus mendeli*. *Sci. Rep.* **2021**, *111*, 9726. [CrossRef]

43. Ma, Y.; Guo, Z.X.; Wang, L.Y.; Wang, B.Y.; Huang, T.F.; Tang, B.J.; Zhang, G.R.; Zhou, Q. The genome of the rice planthopper egg parasitoid wasps *Anagrus nilaparvatae* casts light on the chemo- and mechanosensation in parasitism. *BMC Genom.* **2022**, *23*, 541. [CrossRef]
44. Nie, X.P.; Li, Q.L.; Xu, C.; Li, D.Z.; Zhang, Z.; Wang, M.Q.; Zhou, A.M.; Li, S.Q. Antennal transcriptome and odorant binding protein expression profiles of an invasive mealybug and its parasitoid. *J. Appl. Entomol.* **2018**, *142*, 149–161. [CrossRef]
45. Kang, Z.W.; Tian, H.G.; Liu, F.H.; Liu, X.; Jing, X.F.; Liu, T.X. Identification and expression analysis of chemosensory receptor genes in an aphid endoparasitoid *Aphidius gifuensis*. *Sci. Rep.* **2017**, *7*, 3939. [CrossRef] [PubMed]
46. Ahmed, T.; Zhang, T.T.; Wang, Z.Y.; He, K.L.; Bai, S.X. Gene set of chemosensory receptors in the polyembryonic endoparasitoid *Macrocentrus cingulum*. *Sci. Rep.* **2016**, *6*, 24078. [CrossRef]
47. Pelosi, P.; Maida, R. Odorant-binding proteins in insects. *Comp. Biochem. Physiol. B Biochem. Mol. Biol.* **1995**, *111*, 503–514. [CrossRef] [PubMed]
48. Zhang, S.F.; Kong, X.B.; Wang, H.B.; Zhou, G.; Yu, J.X.; Liu, F.; Zhang, Z. Sensory and immune genes identification and analysis in a widely used parasitoid wasp *Trichogramma dendrolimi* (Hymenoptera: Trichogrammatidae). *Insect Sci.* **2016**, *23*, 417–429. [CrossRef]
49. Wu, J.D.; Shen, Z.C.; Hua, H.Q.; Zhang, F.; Li, Y.X. Identification and sex expression profiling of odorant-binding protein genes in *Trichogramma japonicum*, (Hymenoptera: Trichogrammatidae) using RNA-seq. *Appl. Entomol. Zool.* **2017**, *52*, 623–633. [CrossRef]
50. Bonduriansky, R. The evolution of male mate choice in insects: A synthesis of ideas and evidence. *Biol. Rev.* **2001**, *76*, 305–339. [CrossRef]
51. Leal, W.S. Odorant reception in insects: Roles of receptors, binding proteins, and degrading enzymes. *Annu. Rev. Entomol.* **2013**, *58*, 373–391. [CrossRef]
52. Vosshall, L.B.; Amrein, H.; Morozov, P.S.; Rzhetsky, A.; Axel, R. A spatial map of olfactory receptor expression in the *Drosophila* antenna. *Cell* **1999**, *96*, 725–736. [CrossRef] [PubMed]
53. Ahmed, T.; Zhang, T.T.; Wang, Z.Y.; He, K.L.; Bai, S.X. Identification and expression pattern analysis of chemosensory receptor genes in the *Macrocentrus cingulum* (Hymenoptera: Braconidae) antennae. *Eur. J. Entomol.* **2016**, *113*, 76–83. [CrossRef]
54. Poivet, E.; Gallot, A.; Montagné, N.; Glaser, N.; Legeai, F.; Jacquinjoly, E. A comparison of the olfactory gene repertoires of adults and larvae in the noctuid moth *Spodoptera littoralis*. *PLoS ONE* **2013**, *8*, e60263. [CrossRef] [PubMed]
55. Sheng, S.; Liao, C.W.; Zheng, Y.; Zhou, Y.; Xu, Y.; Song, W.M.; He, P.; Zhang, J.; Wu, F.A. Candidate chemosensory genes identified in the endoparasitoid *Meteorus pulchricornis* (Hymenoptera: Braconidae) by antennal transcriptome analysis. *Comp. Biochem. Physiol. D Genom. Proteom.* **2017**, *22*, 20–31. [CrossRef]
56. Benton, R.; Vannice, K.S.; Gomez-Diaz, C.; Vosshall, L.B. Variant ionotropic glutamate receptors as chemosensory receptors in *Drosophila*. *Cell* **2009**, *136*, 149–162. [CrossRef]
57. Ai, M.; Min, S.; Grosjean, Y.; Leblanc, C.; Bell, R.; Benton, R.; Suh, G.B. Acid sensing by the *Drosophila* olfactory system. *Nature* **2010**, *468*, 691–695. [CrossRef]
58. Forstner, M.; Gohl, T.; Gondesen, I.; Raming, K.; Breer, H.; Krieger, J. Differential expression of snmp-1 and snmp-2 proteins in pheromone-sensitive hairs of moths. *Chem. Senses* **2008**, *33*, 291–299. [CrossRef]
59. Rogers, M.E.; Krieger, J.; Vogt, R.G. Antennal SNMPs (sensory neuron membrane proteins) of lepidoptera define a unique family of invertebrate CD36-like proteins. *J. Neurobiol.* **2001**, *49*, 47–61. [CrossRef]
60. Weiss, L.A.; Dahanukar, A.; Kwon, J.Y.; Banerjee, D.; Carlson, J.R. The molecular and cellular basis of bitter taste in *Drosophila*. *Neuron* **2011**, *69*, 258–272. [CrossRef]
61. Scott, K.; Brady, R.; Cravchik, A.; Morozov, P.; Rzhetsky, A.; Zuker, C.; Axel, R. A chemosensory gene family encoding candidate gustatory and olfactory receptors in *Drosophila*. *Cell* **2001**, *104*, 661–673. [CrossRef]
62. Li, G.W.; Zhang, Y.; Li, Y.P.; Wu, J.X.; Xu, X.L. Cloning, expression, and functional analysis of three odorant-binding proteins of the oriental fruit moth, *Grapholita molesta* (busck) (Lepidoptera: Tortricidae). *Arch. Insect Biochem. Physiol.* **2016**, *91*, 67–87. [CrossRef] [PubMed]
63. Wu, Z.R.; Pei, Y.W.; Zhang, X.Q.; Lu, M.; Liu, X.L. Different binding properties of odorant-binding protein 8 to insecticides in *Orius sauteri*. *Pestic. Biochem. Physiol.* **2024**, *200*, 105842. [CrossRef] [PubMed]

Disclaimer/Publisher's Note: The statements, opinions and data contained in all publications are solely those of the individual author(s) and contributor(s) and not of MDPI and/or the editor(s). MDPI and/or the editor(s) disclaim responsibility for any injury to people or property resulting from any ideas, methods, instructions or products referred to in the content.

insects

MDPI

Article

Comparative Mitogenomics of *Pedetontus* and *Pedetontinus* (Insecta: Archaeognatha) Unveils Phylogeny, Divergence History, and Adaptive Evolution

Wei Cen [1,†], Ting Yang [1,†], Jia-Wen Li [1], Dan-Na Yu [1], Kenneth B. Storey [2] and Jia-Yong Zhang [1,3,*]

[1] College of Life Sciences, Zhejiang Normal University, Jinhua 321004, China
[2] Department of Biology, Carleton University, Ottawa, ON K1S5B6, Canada
[3] Key Laboratory of Wildlife Biotechnology, Conservation and Utilization of Zhejiang Province, Zhejiang Normal University, Jinhua 321004, China
* Correspondence: zhang3599533@163.com or zhangjiayong@zjnu.cn
† These authors contributed equally to this work.

Simple Summary: The evolutionary history of the order Archaeognatha has long been a subject of considerable scientific interest and debate. In this study, we utilized 14 mitochondrial genomes from *Pedetontus* and *Pedetontinus* species to investigate the phylogeny and divergence times within Archaeognatha. Integrated analyses of genetic distances, phylogenetic reconstructions, and divergence time estimations suggest that the current morphological classification system for *Pedetontus* may require revision. Furthermore, evidence of positive selection was detected in the mitochondrial protein-coding genes of these species under both temperate and tropical environmental conditions.

Abstract: Archaeognatha is phylogenetically positioned as the basal lineage relative to all extant insect orders and comprises approximately 600 described species. The internal phylogenetic relationships and divergence times within this ancient order have long been a subject of scientific debate. In this study, we assembled 14 mitochondrial genomes from species within the genera *Pedetontus* and *Pedetontinus* to clarify the phylogenetic relationship and estimate divergence times within Archaeognatha. Phylogenetic analyses revealed that both Machilidae and Machilinae are paraphyletic; *Pedetontinus* included in this analysis formed a well-supported monophyletic clade, whereas the sampled *Pedetontus* species were not recovered as a monophyletic clade. Divergence time estimates indicate that Archaeognatha originated during the Late Carboniferous (301.15 Mya, 95% HPD: 298.88–303.67 Mya), with subsequent diversification spanning from the Mesozoic era to the present. The adaptive radiation of epiphytic bryophytes and potential coevolutionary interactions between plants and insects are proposed to have significantly contributed to the diversification of Archaeognatha. Based on multiple lines of evidence, we propose that the current morphological criteria for species delineation within *Pedetontus* (*Pd.*) require revision to better reflect its evolutionary history. In the branch-site model analysis, when *Pd. silvestrii*—collected from temperate regions—was designated as the foreground branch, two positively selected sites were detected at the 66th position of the *Cytb* and the 34th position of *ATP6*. When *Pd. hainanensis* and *Pd. bawanglingensis*—collected from tropical regions—were used as the foreground branches, six positively selected sites were identified at the 622nd position of *Cytb*, the 499th position of *ATP6*, and the 623rd, 873rd, 1106th, and 1141st positions of *COI*.

Keywords: mitogenomes; *Pedetontus*; *Pedetontinus*; phylogeny; divergence time; selective stress analysis

1. Introduction

Archaeognatha occupies a pivotal position at the base of the insect phylogenetic tree and comprises approximately 600 extant species, representing the sister group to all other extant insect lineages [1,2]. The order is currently recognized as comprising two extant families: Machilidae and Meinertellidae [3]. Additionally, several paleoforms, such as *Ditrigoniophthalmus*, *Charimachilis*, and *Mesomachilis*, have been proposed as early-diverging lineages that predate the split between Machilidae and Meinertellidae [4]. Although the precise phylogenetic placement of these paleoforms remains unresolved, multiple studies suggest they may retain key plesiomorphic characteristics, providing important insights into early insect evolutionary [5–8]. To date, 41 species of Archaeognatha have been documented in China [9–30], with 40 species belonging to the family Machilidae. These Machilidae species are distributed across the following genera: *Pedetontinus* (10 species), *Pedetontus* (17 species), *Haslundichilis* (2 species), *Coreamachilis* (2 species), *Metamachilis* (1 species), *Silvestrichilis* (3 species), *Allopsontus* (4 species), and *Songmachilis* (1 species). The remaining species belongs to the family Meinertellidae and is classified within the genus *Machilontus*.

Within this taxonomic framework, the family Machilidae is divided into three distinct subfamilies—Machilinae, Petrobiellinae, and Petrobiinae [31]. The genera *Pedetontus* and *Pedetontinus* are classified within the subfamily Petrobiinae. These genera share the following morphological characteristics: an unscaled antennal flagellum, large contiguous compound eyes, paired shoe-shaped ocelli situated subinferior to the compound eyes, mandibles with four apical teeth, scaled maxillary palps and thoracic legs, meso- and metacoxae each bearing a stylus, and an elongate multi-articulate ovipositor. Specifically, *Pedetontus* is characterized by fore femora that are consistently unswollen, abdominal coxites II–V/VI bearing two pairs of retractile vesicles, and a primary-type ovipositor lacking a terminal claw. In contrast, *Pedetontinus* typically exhibits unmodified fore femora, each coxite of abdominal segments II–VII bearing only one pair of retractile vesicles, and a tertiary-type ovipositor [23,30].

Archaeognatha possesses a mitochondrial genome that exhibits structural conservation patterns commonly found in typical insect taxa. Characterized by matrilineal transmission, accelerated evolutionary dynamics, and non-recombining properties, this genomic system has proven to be a valuable tool for molecular studies aimed at testing and refining phylogenetic hypotheses [32–34]. Evidence indicates that intergenic regions can serve as homologous characters for genus-level classification and frequently form stem-loop or hairpin secondary structures [35,36]. These hairpin motifs are widely distributed in the intergenic spacers between mitochondrial PCGs of diverse metazoan taxa, including insects [37–39]. Guan et al. were the first to identify long hairpin structures located between the *ND1* and *16S rRNA* genes in the subfamilies Petrobiinae and Machilinae, revealing a strong correlation between their spatial arrangement and phylogenetic relationships [36]. These discoveries highlight the functional and evolutionary significance of mitochondrial genome architecture.

In recent years, research on phylogenetic relationships has expanded in both scope and analytical rigor. The majority of phylogenetic studies have consistently supported the monophyly of Hexapoda and Archaeognatha [2,40–44]. However, the internal classification system of Archaeognatha remains complex and continues to be a subject of active scientific debate. Ma et al. demonstrated that both Machilidae and its subfamily Machili-

nae are paraphyletic, whereas Petrobiellinae forms a monophyletic clade together with Meinertellidae. This finding challenges the previous morphological hypothesis of monophyly and provides critical molecular evidence for revising the phylogenetic framework of Archaeognatha [3]. Zhang et al. confirmed the monophyly of Meinertellidae through an integrative analysis of morphological and DNA data from 15 Burmese amber specimens [2]. Montagna subsequently expanded the analysis by incorporating two Triassic fossils and species from Zygentoma, further supporting for the monophyly of Meinertellidae and the paraphyly of the broadly defined Machilidae [45]. Cen et al. built upon previous work by including sequence data from six *Pedetontus* species, yielding preliminary support for the monophyly of this genus and revealing its sister-group relationship with *Pedetontinus* [46]. Palacios-Martinez et al. conducted a Bayesian phylogenetic analysis integrating *COI*, *18S rDNA*, and *ITS2* sequence data across multiple loci, demonstrating that Machilidae and its two subfamilies—Machilinae and Petrobiinae—are non-monophyletic [1]. Collectively, these findings underscore the need for an integrative taxonomic revision that incorporates multi-locus and multidisciplinary evidence to resolve systematic inconsistencies and clarify cladogenetic patterns within this lineage.

Fossil-calibrated molecular clocks have become a widely accepted and effective method for reconstructing the deep phylogeny of insects [33,34,46,47]. However, the evolutionary history of Archaeognatha remains incompletely resolved due to an incomplete and sparse fossil record [46]. While the earliest potential representatives of Archaeognatha are dated to the Devonian period [48,49], definitive crown-group fossils have been found exclusively in Late Carboniferous to Early Permian strata from France and North America, supporting the hypothesis that the order originated during the Late Carboniferous [50,51]. Molecular evidence from Misof et al. suggests that the divergence of Archaeognatha from other insect lineages began approximately 479 million years ago (Mya) [52]. Zhang et al. further demonstrated, through a comprehensive phylogenetic framework combining fossil morphology with biomolecular evidence from Burmese amber specimens, that the two major families within Archaeognatha diverged well before the Cretaceous [2]. Notably, Montagna inferred that the extant family Machilidae was already present during the Middle Triassic—approximately 100 million years earlier than previous estimates [45]. More recently, Cen et al. reported that Machilidae originated in the Middle Triassic (approximately 238.46 Mya), Meinertellidae diverged approximately 127.76 Mya during the Early Cretaceous, and the crown group of Archaeognatha emerged approximately 301.19 Mya during the Late Carboniferous, followed by a prolonged phase of diversification throughout the Mesozoic era [46]. Despite these advances, the evolutionary history of Archaeognatha remains incompletely resolved, underscoring the importance of integrative analyses that combine fossil evidence with molecular datasets to more accurately reconstruct its diversification dynamics.

Although the prevailing view holds that the mitochondrial genome evolves under neutral or nearly neutral conditions [53], accumulating evidence suggests that mitochondrial protein-coding genes (PCGs) associated with environmental adaptation exhibit signatures of significant positive selection [54–56]. Given their essential role in energy metabolism during responses to environmental stressors, mitochondrial genomes provide a critical framework for investigating mechanisms of positive selection and adaptive evolution, particularly under conditions of strong natural selection. Xu et al. conducted a positive selection analysis on Heptageniidae taxa inhabiting cold environments and identified 27 positively selected sites across eight protein-coding genes [56]. Feng et al. performed a similar analysis on *Chionea* in cold environments and detected significant signals of positive selection in the mitochondrial genes *COIII*, *ND6*, and *ND5*, suggesting that the positive

selection of these three genes may represent a key adaptive mechanism enabling *Chionea* species to survive in low-temperature habitats [57]. Faddeeva et al. examined selective pressures across Hexapoda lineages and found that 250 genes exhibited significant positive selection, indicating a potential role for these genes in lineage divergence [58]. Collectively, these studies underscore the importance of comparative mitochondrial genomic analyses across diverse taxa for understanding the functional dynamics of positive selection in adaptation to extreme environments and in shaping evolutionary trajectories.

Building upon the current state of research, this study aims to achieve the following objectives: (1) to compare the mitochondrial genomes of 14 species representing the genera *Pedetontus* and *Pedetontinus*; (2) to reconstruct phylogenetic topology and estimate divergence times within Archaeognatha; and (3) to examine whether the mitochondrial genome of *Pd. silvestrii* from temperate region has undergone positive selection during cold adaptation and whether similar selection signals are present in *Pedetontus* species from the tropical region in response to high-temperature adaptation.

2. Materials and Methods

2.1. Specimen Acquisition and Genomic DNA Extraction

Detailed sample information is presented in Table 1. For simplicity, the generic name *Pedetontus* is abbreviated as *Pd.* and *Pedetontinus* is abbreviated as *Pn.* throughout the text. Following sample collection, morphological examination was conducted on fourteen specimens utilizing a Nikon SMZ-1500 stereoscopic microscope (Nikon, Tokyo, Japan). Based on diagnostic morphological characters from established taxonomic references [9,10,23], five species were tentatively assigned to the genus *Pedetontinus*, and nine species to the genus *Pedetontus*. After species identification, all tissue samples were preserved in absolute ethanol (−20 °C) and stored under controlled conditions at the Laboratory of Evolution and Molecular Ecology, Zhejiang Normal University. Genomic DNA was extracted from muscle tissues using the Ezup Column Animal Genomic DNA Purification Kit (Sangon Biotech, Shanghai, China), adhering strictly to the manufacturer's operational guidelines.

Table 1. Detailed Sample Information for the Fourteen Specimens.

Species	Sampling Localities	Geographic Coordinates	Accession No.
Pedetontinus songi	Taimushan, Fujian	27°07′27″ N, 120°11′05″ E	PX391408
Pedetontinus jinzhaiensis	Jinzhai, Anhui	31°18′13″ N, 115°40′38″ E	PX391406
Pedetontinus mengshanensis	Mengshan, Shandong	35°31′07″ N, 117°49′17″ E	PX391407
Pedetontinus tianmuensis	Chuzhou, Anhui	32°20′42″ N, 118°25′30″ E	PX391409
Pedetontinus yongjiaensis	Yongjia, Zhejiang	28°09′14″ N, 120°41′29″ E	PX391410
Pedetontus lanxiensis	Lanxi, Zhejiang	29°12′33″ N, 119°27′38″ E	PX391417
Pedetontus hainanensis	Wuzhishan, Hainan	18°51′43″ N, 109°37′33″ E	PX391416
Pedetontus formosa	Baxiandong, Taiwan	23°23′28″ N, 121°29′04″ E	PX391415
Pedetontus zhoui	Taimushan, Fujian	27°07′27″ N, 120°11′05″ E	PX391419
Pedetontus bawanglingensis	Bawangling, Hainan	19°03′49″ N, 109°10′14″ E	PX391411
Pedetontus dachendaoensis DCD	Dachendao, Zhejiang	28°28′20″ N, 121°54′06″ E	PX391414
Pedetontus cixiensis	Cixi, Zhejiang	30°10′18″ N, 121°15′39″ E	PX391412
Pedetontus dachendaoensis TT	Taizhou, Zhejiang	28°50′49″ N, 121°06′50″ E	PX391413
Pedetontus zhejiangensis TPS	Suzhou, Zhejiang	31°01′59″ N, 120°51′14″ E	PX391418

2.2. Sequencing and Assembly of the Mitochondrial Genome

Polymerase chain reaction (PCR) amplification of the *COI* gene fragment was performed using the universal insect primers LCO1490 and HCO2198 following genomic DNA extraction [59]. Species identification was conducted through sequence alignment against

the NCBI BLAST database (https://blast.ncbi.nlm.nih.gov/Blast.cgi, accessed on 30 April 2025). The complete mitochondrial genome was amplified using 13 pairs of species-specific primers designed by Zhang et al. [60], combined with Sanger sequencing technology. All PCR products were purified via gel electrophoresis prior to bidirectional sequencing (Sangon Biotech, Shanghai, China). Sequence assembly and verification were performed using the SeqMan Pro module within DNASTAR v6.0 software [61] to ensure high data accuracy.

2.3. Sequence Annotation and Analyses

tRNA identification and annotation were conducted using MITOS2 (https://usegalaxy.eu/, accessed on 15 May 2025) [62]. Comparative analyses of the *12S/16S rRNA* and 13 PCGs were conducted based on multiple sequence alignments generated by Clustal W [63,64]. Genetic distances were calculated utilizing the Kimura 2-parameter model in MEGA version 11 [65]. PhyloSuite v.1.2.3 [66] was utilized to compute AT content and assess relative synonymous codon usage across the fourteen mitochondrial genomes. The complete mitochondrial genomes (GenBank accession numbers: PX391406-PX391419) were visualized using CG View Server V1.0 (http://cgview.ca/, accessed on 18 May 2025) [67], and the resulting figures were subsequently refined with Adobe Illustrator 2021 [68]. RNA secondary structure prediction tools were employed to detect potential hairpin motifs (http://rna.tbi.univie.ac.at/, accessed on 20 May 2025) [69]. Nucleotide composition bias was quantified using standard deviation-based formulas: AT bias = (A − T)/(A + T) and GC bias = (G − C)/(G + C) [70].

2.4. Phylogenetic Analyses

To comprehensively elucidate the evolutionary relationships within Archaeognatha, this study integrated 14 newly sequenced mitochondrial genomes with 20 previously published mitochondrial genomes retrieved from the NCBI database [3,36,46,60,71–75], along with two mitochondrial genomes from Collembola [76] used as outgroups. The final dataset comprises a total of 36 species (Table S1), including one representative from Meinertellidae, 33 species from Machilidae and the selected outgroup taxa: *Podura aquatica* (NC_006075) and *Onychiurus orientalis* (NC_006074).

A standardized phylogenetic analysis pipeline was applied to the 13 PCGs using PhyloSuite v1.2.3 [66]. The workflow consisted of three main steps: (1) multiple sequence alignment using MAFFT v7 [77]; (2) trimming of highly variable regions using Gblocks v0.91b [78] to improve alignment accuracy; and (3) sequence assembly using integrated software tools [79].

Codon saturation was evaluated using DAMBE v7.3.11 [80], confirming the absence of substitution saturation, particularly at the third codon position. Phylogenetic reconstruction was conducted using both Bayesian inference (BI) and maximum likelihood (ML), based on nucleotide sequences from all three codon positions across the 13 PCGs [81,82]. Model selection was performed in PartitionFinder v2.2.1 [83] under the Bayesian Information Criterion (BIC) [84], resulting in an optimal data partitioning scheme and corresponding substitution models, as detailed in Table 2. Phylogenetic analyses was performed using two independent approaches: (1) maximum likelihood analysis implemented in IQ-TREE v2.0 [85], with 1000 ultrafast bootstrap replicates used to assess nodal support; and (2) Bayesian inference conducted in MrBayes v3.2 [86], involving 10 million generations of MCMC sampling, with the first 25% of samples discarded as burn-in to minimize initial state bias. The phylogenetic trees were visualized using FigTree v1.4 [87] and further refined in Adobe Illustrator [68] to enhance clarity and overall presentation quality.

Table 2. The best partitioning strategy for phylogenetic analyses, along with the associated alternative models, detailing the model names and the site classifications allocated to each partition.

Subset	Best Model	Partition Names
Partition_1	GTR + I + G	COII_codon1, COIII_codon1, ND3_codon1, Cytb_codon1, ATP6_codon1
Partition_2	GTR + I + G	COI_codon2, COIII_codon2, Cytb_codon2, ATP6_codon2, COII_codon2
Partition_3	GTR + G	ND3_codon3, COIII_codon3, Cytb_codon3, COI_codon3, COII_codon3
Partition_4	TIM + G	ND6_codon3, ND2_codon3, ATP8_codon3, ATP6_codon3
Partition_5	GTR + I + G	ND6_codon1, ATP8_codon2, ND2_codon1, ATP8_codon1
Partition_6	SYM + I + G	COI_codon1
Partition_7	GTR + I + G	ND5_codon1, ND4_codon1, ND1_codon1, ND4L_codon1
Partition_8	GTR + I + G	ND1_codon2, ND5_codon2, ND4_codon2, ND4L_codon2
Partition_9	TVM + G	ND5_codon3, ND4L_codon3, ND1_codon3, ND4_codon3
Partition_10	TVM + I + G	ND6_codon2, ND2_codon2, ND3_codon2

2.5. Estimation of Divergence Times

The selection of fossil calibration points is a crucial step in divergence times estimation [88–90]. To establish robust temporal references, we integrated data from peer-reviewed literature and the Paleobiology Database (https://paleobiodb.org/, accessed on 16 June 2025). According to the insect phylogeny proposed by Misof et al. [52], the Archaeognatha-Collembola cladogenic split was dated to approximately 479 million years ago (Mya) during the Early Ordovician radiation, which was implemented as a prior constraint for the root node age in our analysis. Four fossil calibration points were selected for this study: (1) *Dasyleptus lucasi* Brongniart, 1885 (order Archaeognatha), dated to approximately 298.9–303.7 Mya [51]. (2) *Machilis acuminata* (family Machilidae) dated to approximately 33.9–38.0 Mya [91]. (3) *Gigamachilis triassicus* (family Machilidae), dated to approximately 235–242 Mya [45]. (4) *Cretaceomachilis libanensis* (family Meinertellidae), dated to approximately 125.45–130.00 Mya [92]. Divergence times were estimated using MCMCTree within the PAML v4.8 software package [93], based on the BI phylogenetic tree topology. First, the nucleotide substitution rate was calculated using Baseml, and the gradient of branch lengths along with the associated Hessian matrix was obtained under a Bayesian framework. Subsequently, species divergence times were inferred using the approximate likelihood calculation method (usedata = 2). In the MCMCTree analysis, the following parameters were applied: the burn-in period of 1,000,000 iterations, with sampling every 1000 generations, resulting in the collection of 100,000 effective samples for downstream analyses. Optimization of MCMC chain convergence and mixing was verified using Tracer v1.7.1 [94]. All model parameters were assessed for effective sample size (ESS), showing that ESS values exceeded the recommended threshold of 200 for each parameter, confirming sufficient sampling efficiency and reliability of the estimates [95]. Estimated divergence time estimates across phylogenetic branches were visualized using FigTree v1.4 [87], and the resulting figures were further refined in Adobe Illustrator [68] to improve clarity and presentation quality.

2.6. Selection Pressure Analyses

The EasyCodeML v1.41 software [96] was employed to assess selective pressures acting on PCGs within the mitochondrial genomes of Archaeognatha. To investigate molecular evolutionary patterns of PCGs under different thermal regimes, populations of *Pd. silvestrii* from temperate regions (In proximity to 40° N), characterized by average winter temperatures below 0 °C, were designated as foreground branches representing the temperate group. In contrast, *Pd. hainanensis* and *Pd. bawanglingensis* from tropical regions (near

19° N), which experience average summer temperatures exceed 30 °C, were assigned as foreground branches representing the tropical regions group. Selection pressure analyses were carried out using three types of codon models—branch models, branch-site models, and clade models—to detect signatures of selection on specific lineages and sites. The branch model is employed to identify lineage-specific variations in evolutionary rates [97]. The branch-site model enables comparative analysis between a null model (Model Anull), which assumes only neutral and purifying selection, and an alternative model (Model A), thereby enabling the detection of positive selection on predefined foreground branches [98]. The clade model framework facilitates the identification of divergent selection pressures across distinct evolutionary lineages [99]. Additionally, a site model was employed to evaluate overall selective pressures without specifying foreground branches [100]. Model comparisons were conducted using likelihood ratio tests (LRTs) [101]. For statistical validation of adaptive evolution signals, the Bayesian empirical Bayes (BEB) approach was applied to estimate posterior probabilities at individual sites, with a threshold of $\geq$0.95 used to ensure reliable inference [102].

3. Results

3.1. Composition of Mitogenomes

All 14 mitochondrial genomes possess a double-stranded DNA structure, ranging in size from 14,625 bp (*Pn. jinzhaiensis*) to 15,808 bp (*Pd. bawanglingensis*) (Table S1; Figure S1). The control region could not be amplified in *Pn. jinzhaiensis*, and both the control region and *trnI* were not successfully amplified in *Pd. formosa*. Mitochondrial gene lengths, AT content and other relevant information are summarized in Table S2. The initiation and termination codons for each species are detailed in Table S3. The initiation codons are predominantly of the ATN type, however, GTG is also utilized as an initiation codon in several cases, such as in *COII* and *ND2*. With regard to stop codons, most PCGs utilize canonical termination signals (TAA or TAG). Incomplete stop codons (T or TA) were detected in *COI*, *COII*, *COIII*, *ND5*, and *ND4*. Relative synonymous codon usage (RSCU) is shown in Figure S2, and the corresponding codon usage frequencies are provided in Table S4. Codon usage analysis reveals that UUU, AUU, AUA, and UUA are the most frequently used codons, each occurring more than 200 times. In contrast, codons with G or C at the third nucleotide position exhibit lower usage frequencies. Notably, Long hairpin structures were identified between the *ND1* and *16S rRNA* genes across the mitochondrial genomes of 14 species within *Pedetontus* and *Pedetontinus*. These structures range in length from 42 to 76 bp, with an average of approximately 60 bp (Figure S3).

3.2. Genetic and Intergroup Genetic Distance Analyses

Genetic distances between *Pedetontinus* and *Pedetontus* species, based on the *COI* gene, are summarized in Table S5. Overall genetic divergences range from 1.5% to 23%, with a mean value of 16.98%. Intraspecific genetic divergence within *Pedetontinus* ranges from 7.4% to 14.2%. However, genetic divergence within *Pedetontus* is comparatively higher. Genetic divergences between *Pedetontus* from the southern China and those from the Northeast region all exceed 15%. The pairwise genetic distances between *Pd. formosa* and *Pd. zhoui* (collected from Taiwan and Fujian, respectively) and *Pedetontus* from Zhejiang (excluding *Pd. cixiensis*) ranged from 11.5% to 13.1%. Genetic divergences between *Pd. hainanensis* and other *Pedetontus* species are all consistently high, exceeding 20%. Similarly, genetic distances between *Pd. bawanglingensis* and other *Pedetontus* species also exceed 20%. Furthermore, the genetic divergence between *Pd. hainanensis* and *Pd. bawanglingensis* is

16.1%. Additionally, genetic distances between *Pd. cixiensis* and other *Pedetontus* species range from 17.2% to 21.5%.

Based on the genetic distance analysis, *Pd. cixiensis*, *Pd. hainanensis*, and *Pd. bawanglingensis* exhibited substantial genetic divergence from other species within the same genus. To further assess the intergeneric variation, a stratified genetic distance analysis was conducted. Taxa were reclassified into distinct groups based on two criteria: genus-level taxonomy and geographical distribution. Specifically, species belonging to the same genus and originating from the same geographic region were assigned to the same group, whereas those from different genera or different geographical regions were placed in separate groups. The grouping scheme is as follows: Group 1 included five samples of the genus *Pedetontinus* and its reference sequence (KJ754502); Group 2 consisted of *Pd. hainanensis* and *Pd. bawanglingensis*; Group 3 comprised *Pd. cixiensis*; Group 4 included six samples of *Pedetontus* from southern regions of China (excluding *Pd. cixiensis*, *Pd. hainanensis* and *Pd. bawanglingensis*) along with its reference sequence (NC_051491); and Group 5 contained six samples of *Pedetontus silvestrii* from northeast China and its reference sequence (NC_011717). Genetic distances among these groups were subsequently calculated, and the results are summarized in Table S6.

Following the inter-group genetic distance analysis of the five defined groups, the samples were further categorized into two major genera: *Pedetontus* and *Pedetontinus*, and the inter-generic genetic distance between these two genera was calculated. The results revealed that the genetic distance between Group 2 (*Pd. hainanensis* and *Pd. bawanglingensis*) and Group 3, 4 and 5 (other *Pedetontus* groups) all exceeded 20%. In contrast, the genetic divergence between the genera *Pedetontus* (excluding *Pd. hainanensis* and *Pd. bawanglingensis*) and *Pedetontinus* was 19.8%.

3.3. Phylogenetic Analyses of Archaeognatha

Phylogenetic reconstruction was conducted using both BI and ML approaches, yielding congruent topological structures (Figure 1). The monophyly of Archaeognatha was strongly supported. However, the phylogenetic analyses did not support the monophyly of the family Machilidae, as species previously assigned to the subfamily Petrobiellinae were recovered within Meinertellidae and formed a closely related sister group to this family. Furthermore, the monophyly of the subfamily Machilinae could not be confirmed, as *Trigoniophthalmus alternatus*, a species taxonomically classified within Machilinae, was positioned outside the clade containing other representative species from the same subfamily.

The phylogenetic tree generated in this study reveals that the genus *Pedetontinus* included in this analysis forms a robustly supported monophyletic clade, whereas the genus *Pedetontus* sampled here is not monophyly. Specifically, all sampled individuals of *Pd. silvestrii* form a distinct and well-supported clade, and the majority of *Pedetontus* specimens collected from Zhejiang (excluding *Pd. cixiensis*) also cluster within a separate monophyletic lineage. *Pd. formosa* and *Pd. zhoui* from South China formed a distinct clade that is clearly separated from the Zhejiang-derived *Pedetontus* samples, representing an independent evolutionary lineage. Phylogenetic analysis indicates that *Pd. formosa* and *Pd. zhoui* form a sister group to most of the *Pedetontus* samples from Zhejiang (except *Pd. cixiensis*), while *Pd. silvestrii* is recovered as the sister lineage to this clade. Furthermore, *Pd. hainanensis* and *Pd. bawanglingensis* are resolved outside the main clade comprising *Pedetontus* and *Pedetontinus*, occupying a relatively basal position, suggesting that these two taxa may represent early-diverging lineages within the subfamily.

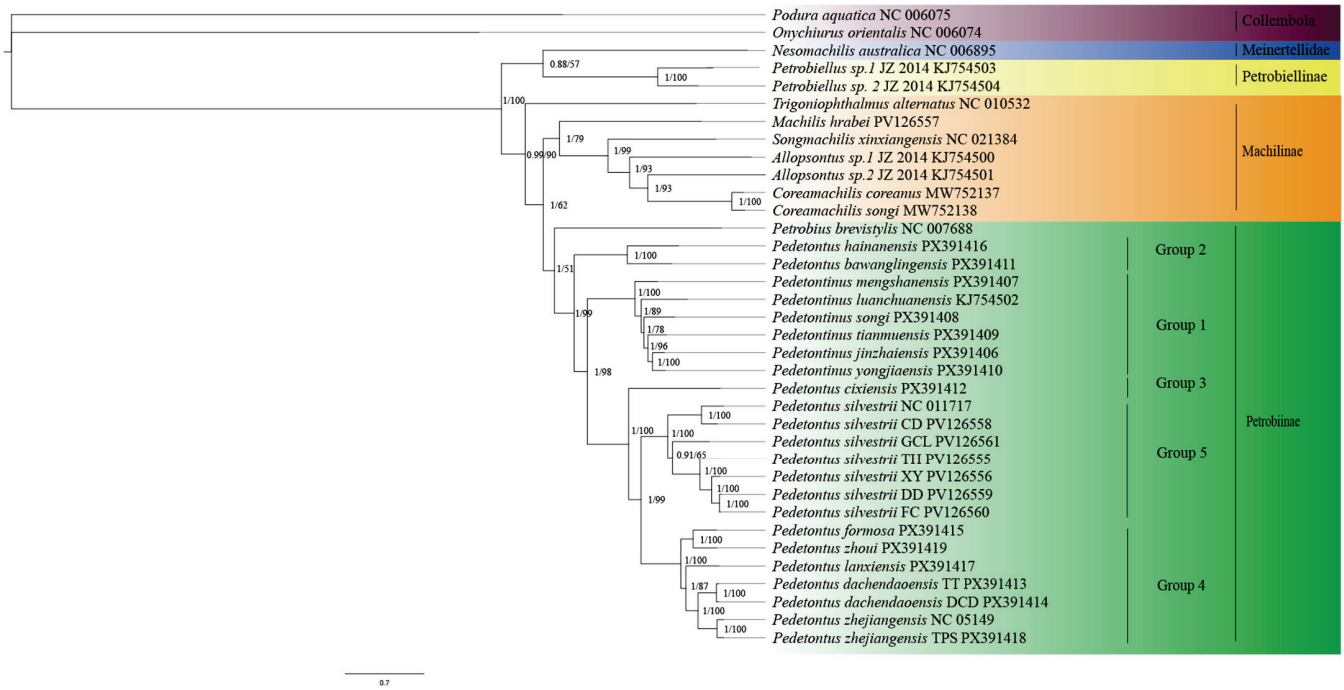


Figure 1. Phylogenetic relationships within Archaeognatha inferred through the analysis of 13 mitochondrial PCGs using ML and BI methods. Bootstrap values on the right side correspond to each branch, with posterior probabilities on the left.

3.4. Divergence Time Calculation

The chronogram, inferred from the BI phylogenetic tree, is presented in Figure 2. Phylogenetic analysis of Archaeognatha based on 13 mitochondrial PCGs reveals that the order originated during the Late Carboniferous period (301.15 Mya, 95% HPD: 298.88–303.67 Mya). *Trigoniophthalmus alternatus*, a member of the subfamily Machilinae, represents the earliest divergence from the main lineage, occurring in the Middle Triassic period (238.45 Mya, 95% HPD: 235–241.99 Mya). The split between the subfamilies Machilinae and Petrobiinae took place during the Jurassic period (140.64 Mya, 95% HPD: 94.65–222.39 Mya). *Pedetontus hainanensis* and *Pd. bawanglingensis* diverged from the main clade comprising the genera *Pedetontus* and *Pedetontinus* during the Early Cretaceous (106.93 Mya, 95% HPD: 70.46–170.92 Mya). The divergence between the genera *Pedetontus* and *Pedetontinus* occurred in the same geological period (92.1 Mya, 95% HPD: 60.61–145.97 Mya). *Pedetontus cixiensis* separated from the remaining members of the genus *Pedetontus* during the Late Cretaceous (73.69 Mya, 95% HPD: 46.24–114.85 Mya), followed by the divergence of *Pd. silvestrii* and *Pedetontus* populations from Zhejiang, Fujian, and Taiwan within the same epoch (62.06 Mya, 95% HPD: 38.68–98.34 Mya).

Moreover, our findings indicate that *Pedetontus* diverged earlier than *Pedetontinus*. The most recent common ancestor (MRCA) of *Pedetontus* originated during the Late Cretaceous (73.69 Mya, 95% HPD: 46.24–114.85 Mya), whereas the MRCA of *Pedetontinus* appeared in the Eocene (42.72 Mya, 95% HPD: 25.7–81.83 Mya). Divergence time analysis revealed three major diversification events during the Eocene: the origin of the MRCA of *Pedetontus silvestrii* at 44.94 Mya (95% HPD: 27.94–77.06 Mya), the divergence of the MRCA between the lineage comprising South China (*Pd. formosa* and *Pd. zhoui*) and Zhejiang populations (*Pd. lanxiensis*, *Pd. dachendaoensis* TT, *Pd. dachendaoensis* DCD, *Pd. zhejiangensis* TPS and *Pd. zhejiangensis* NC 051491) at 40.25 Mya (95% HPD: 26.17–69.29 Mya), and the emergence of the MRCA of *Pedetontus* from Zhejiang at 33.58 Mya (95% HPD: 21.28–58.81 Mya). The

MRCA of *Pd. formosa* and *Pd. zhoui* diverged later during the Oligocene (25.27 Mya, 95% HPD: 11.89–46.44 Mya).

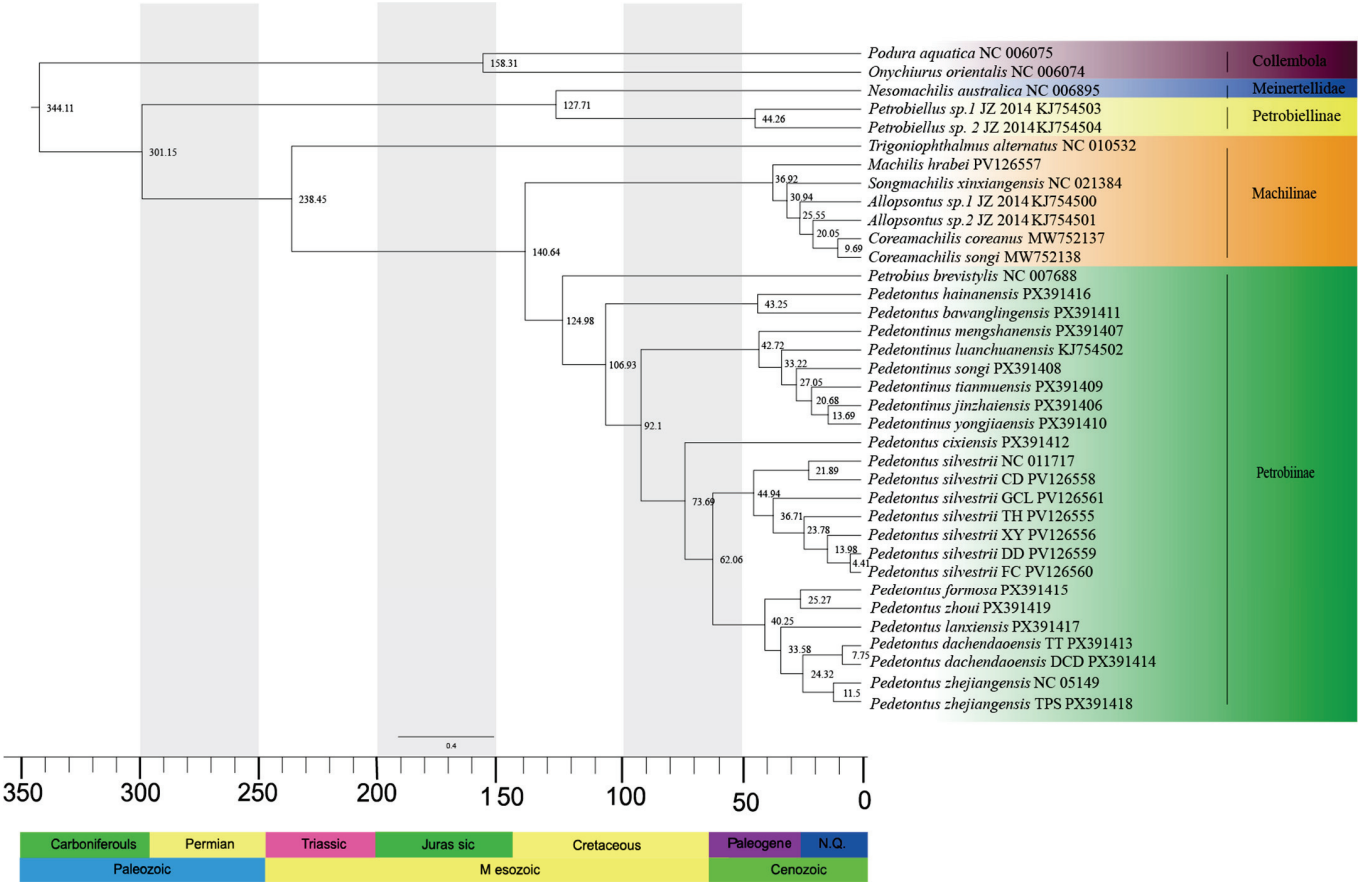


Figure 2. Time-calibrated phylogenetic tree of Archaeognatha inferred using the MCMCTree algorithm. Median divergence times are indicated at corresponding nodes. Stratigraphic age data are presented along the lower margin of the figure.

3.5. Positive Selection Analysis

The branch-site model was utilized to investigate selective pressures operating at the amino acid sites, based on aligned sequence data from 13 PCGs derived from 34 Archaeognatha species. When *Pedetontus silvestrii* were designated as the foreground branch, two amino acid sites were identified as potentially under positive selection, with statistically significant support ($p < 0.001$, BEB value ≥ 0.95), located at the 66th position of the *Cytb* gene and the 34th position of *ATP6* (Table 3). When *Pd. hainanensis* and *Pd. bawanglingensis* were used as foreground branches, six amino acid sites were found to be under positive selection, with statistically significant support ($p < 0.001$, BEB value ≥ 0.95), located at the 622nd position of the *Cytb* gene, the 499th position of *ATP6*, and the 623rd, 873rd, 1106th, and 1141st positions of *COI* (Table 4). Nevertheless, no significant signals of positive selection were detected using the branch model, site model, or evolutionary distinct branch model.

Table 3. Codon-based branch site modeling identified adaptive evolution signals by assigning *Pedetontus silvestrii* as the foreground lineage and utilizing remaining Archaeognatha species as reference clades. The symbol "*" indicates that the posterior probability for this site in the BEB analysis is ≥0.95, providing strong statistical evidence that the site may be under positive selection.

Branch Site Model (BSM)										
Model	**np**	**Ln L**	**Estimates of Parameters**					**Model Compared**	**LRT *p*-Value**	**Positive Sites**
Model A	71	−221,646.437857	Site class	0	1	2a	2b	Model A vs. Model A null	0.000884974	66 S 0.965 *, 1168 S 0.980 *
			Proportion	0.83698	0.15409	0.00754	0.00139			
			Background ω	0.05727	1.00000	0.05727	1.00000			
			Foreground ω	0.05727	1.00000	46.18276	46.18276			
Model A null	70	−221,651.964843								

Table 4. Codon-based branch site modeling identified adaptive evolution signals by assigning *Pedetontus hainanensis* and *Pd. bawanglingensis* as the foreground lineage and utilizing remaining Archaeognatha species as reference clades. The symbol "*" indicates that the posterior probability for this site in the BEB analysis is ≥0.95, providing strong statistical evidence that the site may be under positive selection.

Branch Site Model (BSM)										
Model	**np**	**Ln L**	**Estimates of Parameters**					**Model Compared**	**LRT *p*-Value**	**Positive Sites**
Model A	71	−221,635.143815	Site class	0	1	2a	2b	Model A vs. Model A null	0.000018027	622 F 0.953 *, 1633 Q 0.967 *, 2591 S 0.968 *, 2841 V 0.960 *, 3075 I 0.955 *, 3109 M 0.963 *
			Proportion	0.83368	0.15291	0.01133	0.00208			
			Background ω	0.05721	1.00000	0.05721	1.00000			
			Foreground ω	0.05721	1.00000	106.37636	106.37636			
Model A null	70	−221,644.337408								

4. Discussion

4.1. Special Structure of Mitogenomes from Pedetontus and Pedetontinus

Analysis revealed a long hairpin structure located between the *ND1* and *16S rRNA* genes across the 14 mitochondrial genomes of *Pedetontus* and *Pedetontinus*, which is consistent with the findings reported by Guan et al. [36]. Notably, such long hairpin structures have so far been observed exclusively in species belonging to the subfamilies Petrobiinae and Machilinae, but not in those within Petrobiellinae or Meinertellidae [36]. Therefore, we propose that this structural feature may be phylogenetically informative and could represent a shared derived character (synapomorphy) for Petrobiinae and Machilinae. However, its precise biological function and the underlying mechanism of formation remain unclear and require further investigation.

4.2. Analysis of Phylogenetic Tree Topology

Our phylogenetic reconstruction reveals the non-monophyly of Machilidae, challenging the morphological classification system that has been widely used for this taxon [31]. This incongruence stems from the closer phylogenetic relationship between the subfamily Petrobiellinae and the family Meinertellidae, rather than their affinities with other groups within Machilidae—a pattern consistent with findings from previous phylogenetic studies [3,36,46]. However, the interpretation of Petrobiellinae's phylogenetic position requires careful consideration of existing taxonomic uncertainties. As critically evaluated by Kaplin [103] and Mtow and Machida [104], the sequences of *Petrobiellus* used in our study and in previous analyses are taxonomically problematic. The sequences generated by Ma et al. may represent misidentified members of Meinertellidae rather than true *Petrobiellus* [3]. Therefore, while our analysis recovers the non-monophyly of Machilidae, the precise phylogenetic placement of Petrobiellinae should be interpreted not as a definitive conclusion but as a provisional hypothesis awaiting validation through future studies based on taxonomically verified voucher specimens.

Notably, *Petrobiellus* from Petrobiellinae exhibits morphological similarities to *Petrobius* from Petrobiinae, particularly in the underdeveloped distal jaw teeth with fused dental boundaries [4]. These morphological parallels may reflect either shared ancestry or convergent evolution [2,3]. However, molecular phylogenetic analyses indicate that these taxa are placed in distinct clades, with the two *Petrobiellus* species forming a monophyletic clade together with *Nesomachilis australica* from the family Meinertellidae. This finding, consistent with the observations of Kaplin [103] and Mtow and Machida [104], further suggests that there may be potential taxonomic inconsistencies or misidentifications within *Petrobiellus*, which warrant further investigation.

Although the monophyly of Meinertellidae has been supported by the studies of Zhang et al. and Montagna [2,45], only a single complete mitochondrial genome sequence from this family is currently available in the NCBI database [72]. Consequently, the present study included only one representative species from Meinertellidae, which limits the ability to comprehensively assess and validate the monophyletic status of this taxon. Nevertheless, several morphological characteristics provide evidence in support of the monophyly of Meinertellidae, including the absence of antennal scales, the lack of accessory reproductive structures, and the reduction in the size of abdominal plates [1].

Phylogenetic analyses further support the paraphyly of Machilinae, as evidenced by the placement of *T. alternatus* within Petrobiinae rather than among other Machilinae species. This finding aligns with the results reported by Guan et al. and Ma et al. [3,36]. Additionally, it has been demonstrated that the traditional classification of *Trigoniophthalmus*, which relies on ancestral morphological traits, has limited taxonomic accuracy and leads to

inconsistencies between phylogenetic and morphological classifications, as previously noted by Guan et al. [36]. Therefore, we recommend that the classification of the genus *Trigoniophthalmus* be reevaluated using an integrative approach that combines phylogenetic data with morphological evidence.

Within the phylogenetic framework, *Pedetontinus* as sampled here is robustly supported as a monophyletic group, in contrast to the paraphyletic structure observed in *Pedetontus* as represented here. This non-monophyletic pattern conflicts with the results of previous phylogenetic studies by Shen et al. and Cen et al., which inferred a monophyletic origin for *Pedetontus* [46,75]. We propose that this discrepancy may stem from the substantially expanded taxon sampling and broader geographical representation in our study, which includes specimens from multiple regions across southern, eastern, northern, and northeastern China. With regard to *Pd. silvestrii*, the sampling methodology employed in this study was consistent with that of Cen et al., and the topology of the reconstructed phylogenetic tree showed a high level of agreement with their results [46]. Notably, *Pd. cixiensis* collected from Cixi, Zhejiang Province, does not group within other specimens from Zhejiang but instead diverges outside the entire *Pedetontus* crown group, forming a distinct and elongated branch. Furthermore, the genetic distance between the *COI* gene of *Pd. cixiensis* and those of other *Pedetontus* specimens from Zhejiang exceeds 17%, indicating that this lineage may represent an early divergence event, which merits further investigation.

4.3. Divergence Time Estimation and Evolutionary Node Calibration

Divergence time estimation indicates that the family Machilidae originated during the Middle Triassic period (238.45 Mya, 95% HPD: 235–241.99 Mya), a result consistent with the findings reported by Montagna [45]. The divergence between the family Meinertellidae and the subfamily Petrobiellinae occurred during the Early Cretaceous (127.71 Mya, 95% HPD: 125.45–130 Mya), a timeframe that aligns with the fossil record of *Cretaceomachilis libanensis*, discovered in Early Cretaceous strata of Lebanon [92]. The earlier divergence of Machilidae relative to Meinertellidae is supported by morphological features, including the ovipositor, aedeagus, paragenitalia, coxal sac, and tarsus [2,3]. Moreover, the divergence time tree constructed by Cen et al. also supports this temporal pattern of diversification [46]. According to our analysis, the most recent common ancestor (MRCA) of Machilidae and Meinertellidae dates to the Early Cretaceous (127.71 Mya, 95% HPD: 125.45–130 Mya), which is notably later than previous estimates that placed this divergence at the Jurassic-Cretaceous boundary (approximately 146 Mya) [45,52]. We hypothesize that this discrepancy may stem from insufficient sampling of Meinertellidae in prior analysis, which could have affected the accuracy of the estimated divergence times. Inferred via divergence dating, the subfamilies Machilinae, Petrobiinae, and Petrobiellinae diverged sequentially during the Middle Triassic (approximately 238.45 Mya), Early Cretaceous (approximately 124.98 Mya), and Eocene (approximately 44.26 Mya), respectively. This temporal divergence pattern corresponds to the framework previously proposed by Cen et al. [46]. Notably, the estimated divergence time of the genus *Machilis* during the Eocene (36.92 Mya, 95% HPD: 34.33–38.14 Mya) is in close agreement with the fossil record of this genus preserved in Baltic Eocene amber [105].

The Mesozoic Era, a critical interval in Earth's evolutionary history, was characterized by major environmental changes that played a fundamental role in shaping modern insect communities [106]. Evidence indicates that the substantial rise in atmospheric carbon dioxide levels during the Cretaceous period maintained a prolonged warm climate. Together with the plate tectonic movements driven by the rifting of Gondwana, these factors synergistically promoted the reorganization of global vegetation distribution patterns [107,108]. Against this climatic and geological background, the adaptive radiation of bryophytes emerged as a pivotal event

in ecological evolution during the Cretaceous. Molecular phylogenetic studies indicate that epiphytic moss lineages underwent a phase of rapid diversification, giving rise to a broad spectrum of adaptive strategies [109]. The intensification of plant-insect coevolutionary interactions during this period further facilitated the diversification of multiple insect groups, including the genus-level differentiation within the order Archaeognatha. During the Cretaceous-Paleogene transition, the rapid diversification of numerous plant, animal, and fungal lineages triggered a major ecological transformation known as the "Cretaceous Terrestrial Revolution", which drove the evolutionary progression toward more complex and diverse insect-plant symbiotic systems [110]. Our phylogenetic analysis reveals that *Pedetontus* and *Pedetontinus* diverged from a common ancestral lineage in the late Mesozoic, a timeframe that closely aligns with a major phase of reorganization in the global biogeographic patterns of bryophytes [109]. Collectively, these findings highlight the profound impact of Mesozoic environmental changes on the evolutionary assembly of contemporary insect communities.

The MRCA of *Pd. formosa* and *Pd. zhoui* diverged during the late Oligocene (25.27 Mya, 95% HPD: 11.89–46.44 Mya). This molecular dating estimate appears inconsistent with the geological timeline of Taiwan Island's formation. Geological studies indicate that the fundamental topographic framework of Taiwan Island was established approximately 6.5 Mya, resulting from oblique plate interactions along the Luzon-Eurasian tectonic boundary [111]. Prior to this island formation, however, the region underwent significant tectonic evolution: continental rifting occurred during the Paleogene (39–50 Mya), followed by the opening of the South China Sea during the Oligocene to Middle Miocene (16–33 Mya) [112]. These tectonic processes likely contributed to the opening of the Taiwan Strait and induced localized crustal movements, which may have influenced biogeographic patterns and speciation events. Such dynamic geological settings could have provided diverse ecological niches for the ancestral populations of *Pd. formosa* and *Pd. zhoui*, thereby facilitating their divergence and adaptive evolutionary trajectories.

4.4. Genetic-Morphological Discrepancy in Pedetontus Taxonomy

Morphological methods have long served as the primary tools for species identification. Nevertheless, evolutionary relationships inferred from these approaches often exhibit substantial inconsistencies when compared with genetic evidence [113–115]. Due to the inherent limitations of traditional morphological identification systems in achieving accurate taxonomic classification, there is an increasing need for integrative frameworks that enable the systematic identification, refinement, and validation of diagnostic traits with improved discriminatory power. Phylogenetic and genetic distance analyses of *Pedetontus* have uncovered substantial taxonomic discrepancies within the genus. Comparative data indicate that the intergeneric genetic distance between *Pedetontus* and *Pedetontinus* was 19.7%, whereas the interspecific genetic distances between Group 2 (*Pd. hainanensis* and *Pd. bawanglingensis*) and other conspecific species exceeded 20%, ranging from 20.2% to 23.0%. Notably, the level of intrageneric genetic differentiation exceeds that typically observed between genera, providing strong support the hypothesis of a potential misclassification of *Pd. hainanensis* and *Pd. bawanglingensis* at the generic level. Phylogenetic reconstruction corroborates this conclusion, showing their phylogenetic divergence from congeneric *Pedetontus* species. Divergence time estimation further indicates that the lineage containing the Hainan population diverged approximately 106.93 Mya, significantly earlier than the divergence times of other *Pedetontus* species. Based on the molecular phylogenetic findings presented above, we propose an integrative taxonomic revision of *Pedetontus* to identify key morphological diagnostic characters suitable for genus-level classification. Furthermore, we recommend the development of a standardized and operationally robust framework for species identification that integrates morphological, molecular phylogenetic, and biogeographic evidence.

4.5. Positive Selection Pressure Analysis

Branch-site model analysis identified one site under positive selection in *Cytb* and an additional site in *ATP6* when *Pd. silvestrii* was designated as the foreground branch. *Cytb*, recognized as the major transmembrane component of complex III, is essential for ATP production [116]. As a core subunit of the mitochondrial respiratory chain, *Cytb* primarily mediates electron transfer from the substrate side to cytochrome *c*1. Its specialized energy-transducing form, cytochrome *b*T, is critically involved in coupling electron transport with proton gradient formation through the inner mitochondrial membrane, thereby serving as a key functional unit in oxidative phosphorylation and cellular energy conservation [117]. ATP synthase is also a core component of the mitochondrial respiratory chain, utilizes the proton motive force across the inner mitochondrial membrane to catalyze ATP synthesis from ADP and inorganic phosphate [118]. As a critical subunit of the enzyme, *ATP6* plays an essential role in oxidative phosphorylation [119].

Additionally, branch-site model analysis with *Pd. hainanensis* and *Pd. bawanglingensis* designated as foreground branches identified six positively selected sites: four in *COI*, one in *ATP6*, and one in *Cytb*. Complex IV catalyzes the final step of the electron transport chain by transferring electrons from reduced cytochrome c to oxygen, thereby reducing oxygen and generating a proton gradient [120]. The *COI* subunit is essential for initiating complex IV assembly and constitutes one of its catalytic core components [120,121].

It is noteworthy that in the analysis of positive selection sites under two distinct environmental conditions, both the *Cytb* and *ATP6* genes were identified. This finding indicates that these genes may have been subject to natural selection during both temperate and tropical environmental adaptation processes, suggesting their potential role in a shared adaptive mechanism in response to temperature-related selective pressures. In studies investigating other species' responses to temperate environments, mitochondrial genes such as *Cytb* and *ATP6* have exhibited significant signals of positive selection. Xu et al. identified 27 positively selected sites in Heptageniidae species in their study on cold adaptation, including two sites in the *Cytb* gene [56]. Hong et al. reported five amino acid sites under positive selection in Hylidae species inhabiting cold environments, including residues within the *Cytb* gene [122]. Ngatia et al. demonstrated evidence of positive selection acting on six genes—including *Cytb* and *ATP6*—in *Mammuthus primigenius* under cold stress conditions [123]. Collectively, these findings demonstrate that key mitochondrial genes associated with energy metabolism have undergone adaptive evolution during biological responses to low-temperature environments. Notably, while existing studies on positive selection have predominantly focused on temperate species, the present investigation into the adaptive evolutionary patterns of tropical species provides novel insights.

Overall, the PCGs of *Pedetontus* are functionally associated with energy metabolism and are subject to positive selection, potentially reflecting adaptive mechanisms that enable the species to meet energy demands and maintain normal physiological functions under temperate and tropical environmental stress.

5. Conclusions

This study involved the analysis of mitogenomes from 14 species representing the genera *Pedetontus* and *Pedetontinus*. Phylogenetic assessments employing ML and BI methodologies yielded the following findings: (1) the family Machilidae is non-monophyletic; (2) the subfamily Petrobiellinae and the family Meinertellidae form a single clade, and the subfamily Machilinae is also non-monophyletic; (3) within the subfamily Petrobiinae, *Pedetontinus* is monophyletic, whereas *Pedetontus* is non-monophyletic, with *Pd. hainanensis* and *Pd. bawanglingensis* diverging early from the main lineage. Divergence time estimation

indicates that the diversification of Petrobiinae occurred during the Mesozoic, leading to the emergence of the genera *Pedetontus* and *Pedetontinus*, a process potentially driven by the co-evolution between organisms and their environment. By integrating analyses of genetic distance, phylogenetic topology, and estimations of divergence timing, we propose a re-evaluation of the species status of *Pd. hainanensis* and *Pd. bawanglingensis*. Future research should aim to identify genus-level morphological diagnostic characters to refine the current taxonomic framework. Selection pressure analysis reveals that the mitochondrial PCGs of *Pedetontus* have undergone positive selection under both temperate and tropical environmental stress, likely reflecting adaptive responses to altered energy demands.

Supplementary Materials: The following supporting information can be downloaded at: https://www.mdpi.com/article/10.3390/insects16121194/s1, Figure S1: Circular genome maps illustrate the mitochondrial genomes of fourteen specimens representing the genera *Pedetontus* and *Pedetontinus*. Figure S2: Relative Synonymous Codon Usage (RSCU) patterns in 14 mitochondrial genomes. Figure S3: Inferred hairpin structures of 14 mitogenomes. The circle means the length between the *NDI* gene and *16S RNA* gene. Table S1: Species data employed in the construction of the phylogenetic tree. Table S2: The lengths of mitochondrial genes, AT content, AT skew and GC skew of 14 mitochondrial genomes. Table S3: Location of features of fourteen mitogenomes. Table S4: Comparative analysis of codon usage frequency profiles among 14 mitochondrial genomes. Table S5: Genetic distance analysis of the COI gene among species of *Pedetontinus* and *Pedetontus* is included in this study. Table S6: Pairwise genetic distance values among *Pedetontus* and *Pedetontinus* groups.

Author Contributions: Conceptualization, J.-Y.Z., D.-N.Y., W.C., K.B.S. and T.Y.; Methodology, W.C., T.Y. and J.-W.L.; Statistical analysis, W.C., T.Y. and J.-W.L.; Investigation, J.-Y.Z. and D.-N.Y.; Data curation, W.C., T.Y., J.-Y.Z., K.B.S. and D.-N.Y.; Writing—original draft preparation, W.C., J.-Y.Z. and D.-N.Y.; Writing—review and editing, W.C., T.Y., J.-Y.Z., K.B.S. and D.-N.Y.; Maps and graphics, W.C., J.-W.L. and T.Y.; Project administration, J.-Y.Z. and D.-N.Y.; funding acquisition, J.-Y.Z. All authors have read and agreed to the published version of the manuscript.

Funding: This work was supported by the Natural Science Foundation of Zhejiang Province (LY23C040002) and by the Natural Science Foundation of China (32470475). The funders had no role in the study design, data collection and analysis, decision to publish, or preparation of the manuscript. The publication costs of this study were supported by the National Undergraduate Training Program on Innovation and Entrepreneurship (202510345032).

Institutional Review Board Statement: All samples belong to non-protected invertebrate species, so no animal care protocol was needed.

Informed Consent Statement: Not applicable.

Data Availability Statement: Data to support this study are available from the National Center for Biotechnology Information (https://www.ncbi.nlm.nih.gov) (accessed on 25 July 2025). The GenBank numbers are PX391406-PX391419.

Acknowledgments: We gratefully acknowledge Jie-Hong Ji and Chen-Yang Shen for their invaluable assistance in sample acquisition. We also thank Chen-Yang Shen for providing essential morphological literature. Additionally, we are deeply grateful to three reviewers for their insightful comments and constructive feedback on this manuscript.

Conflicts of Interest: The authors declare no conflicts of interest.

References

1. Palacios–Martinez, I.; Jiménez-Ruiz, Y.; Otero-Ferre, P.; García-París, M. Systematics of the genus *Dilta* Strand, 1911 (Machilidae) in the Canary Islands (NW Africa, Spain) with comments on the phylogeny of Microcoryphia (Insecta). *Zool. Anz.* **2025**, *317*, 1–18. [CrossRef]

2. Zhang, W.; Li, H.; Shih, C.; Zhang, A.; Ren, D. Phylogenetic analyses with four new Cretaceous bristletails reveal inter-relationships of Archaeognatha and Gondwana origin of Meinertellidae. *Cladistics* **2018**, *34*, 384–406. [CrossRef]
3. Ma, Y.; He, K.; Yu, P.P.; Yu, D.N.; Cheng, X.F.; Zhang, J.Y. The complete mitochondrial genomes of three bristletails (Insecta: Archaeognatha): The paraphyly of Machilidae and insights into Archaeognathan phylogeny. *PLoS ONE* **2015**, *10*, e0117669. [CrossRef]
4. Sturm, H.; Bach, d.R.C. On the systematics of the Archaeognatha (Insecta). *Entomol. Gen.* **1993**, *18*, 55–90. [CrossRef]
5. Koch, M. Character evolution in the Archaeognatha: Consensus and conflict. *Entomol. Abh.* **2003**, *61*, 120–122.
6. Mendes, L.F.; Foottit, R.; Adler, P. Biodiversity of the thysanurans (Microcoryphia and Zygentoma). *Insect Biodivers. Sci. Soc.* **2018**, *2*, 155–198.
7. Matushkina, N.A.; Klass, K.-D. Male genitalia of Charimachilis (Insecta: Archaeognatha) and the status of archaeognathan "paleoforms". *Org. Divers. Evol.* **2020**, *20*, 253–266. [CrossRef]
8. Klass, K.; Matushkina, N. The exoskeleton of the male genitalic region in Archaeognatha, with hypotheses on the early evolution and the morphological interpretation of genitalia in insects. *Arthropod Syst. Phylogeny* **2018**, *76*, 235–294. [CrossRef]
9. Zhang, J.Y.; Song, D.X.; Zhou, K.Y. A new species of the genus *Pedetontinus* (Microcoryphia, Machilidae) from China. *Acta Zootaxonomica Sin.* **2005**, *30*, 549–554.
10. Yu, D.N.; Zhang, W.W.; Zhang, J.Y. Two new species of the genus *Pedetontus* (Microcoryphia, Machilidae) from China. *Acta Zootaxonomica Sin.* **2010**, *35*, 444–450.
11. Xue, L.; Yin, W. Two new species of Machilidae from the Tianmu Mountain, China (Microcoryphia). *Contrib. Shanghai Inst. Entomol.* **1991**, *10*, 77–86.
12. Zhang, J. A new record genus and species of Machilinae from China (Microcoryphia: Machilidae). *Jiangxi Plant Prot.* **2010**, *33*, 57–59.
13. Uchida, H. *Pedetontus* from Formosa: Thysanura: Machilidae. *Spec. Bull. Lepidopterol. Soc. Jpn.* **1965**, *1*, 249–252.
14. Zhang, J.Y.; Li, T. A new bristletail species of the genus *Pedetontinus* (Microcoryphia, Machilidae) from China. *Acta Zootaxonomica Sin.* **2009**, *34*, 203–206.
15. Zhang, J.; Zhou, K. Descriptions of one new genus and six new species of Machilidae (Insecta: Archaeognatha) from China: Morphological and molecular data. *J. Nat. Hist.* **2011**, *45*, 1131–1164. [CrossRef]
16. Song, Z.S. *Machilontus* (s. str.) *medogensis* Song & Huang, sp. nov. from Tibet, the northernmost record of the genus *Machilontus* Silvestri, 1912 and the first record of the family Meinertellidae (Insecta: Microcoryphia: Machiloidea) in China. *Zootaxa* **2011**, *2822*, 61–68. [CrossRef]
17. Silvestri, F. Note sui Machilidae. III. Descrizione di un nuovo genere e di sei nuove specie. *Redia* **1906**, *3*, 325–335.
18. Silvestri, F. Schwedisch-chinesiche wissenschaftliche Expedition nach den nordwestlichen Provinzen Chinas (38. Thysanura, Machilidae). *Ark. Zool.* **1934**, *27*, 1–7.
19. Silvestri, F. Descripzione di alcuni Machilidae (Thysanura) della China. *Notes Entomol. Chin. Du Mus. Heude Shanghai* **1936**, *3*, 103–115.
20. Silvestri, F. Contributto alla conoscenza dei Machilidae (Insecta, Thysanura) del Giappone. Bollettino del Laboratorio di Zoologia, generale e agraria della R. *Sc. Super. D'agricoltura Portici* **1943**, *32*, 283–306.
21. Mendes, L.F.; Gaju-Ricart, M.; de Roca, C.B.; Molero-Baltanás, R. On some Silvestri species of Machilidae (Microcoryphia, Insecta) which types are in the Muséum National d'Histoire Naturelle, Paris. *Pedobiologia* **2000**, *44*, 268–284. [CrossRef]
22. Li, P.; Yu, D.N.; Zhang, J.Y. One new species of the genus *Pedetontinus* (Microcoryphia, Machilidae) from China with morphological and molecular data. *Acta Zootaxon Sin.* **2012**, *37*, 740–746.
23. Kaplin, V. Description of a new species of the bristletail genus *Pedetontinus* Silv. (Thysanura, Machilidae) from China with a review of species of this genus. *Entomol. Rev.* **2015**, *95*, 73–86. [CrossRef]
24. Kaplin, V. A new species of the genus *Allopsontus* Silv. (Microcoryphia, Machilidae) from northwestern china. *Entomol. Rev.* **2016**, *96*, 126–131. [CrossRef]
25. Kaplin, V. A new species of bristletails of the genus *Silvestrichilis* Wygodzinsky, 1950 (Archaeognatha: Machilidae) from South China. *Far East. Entomol.* **2019**, *376*, 23–28. [CrossRef]
26. Huang, F.S.; Song, Z.S.; Liang, A.P. A new bristletail species of the genus *Allopsontus* Silvestri (Microcoryphia: Machilidae) from Shaanxi, China. *Orient. Insects* **2006**, *40*, 267–272. [CrossRef]
27. Deng, K.Z.; Zhang, J.Y.; Yu, D.N. A new species of the genus *Haslundichilis* (Microcoryphia, Machilidae) from China and redescription of *Haslundichilis hedini* (Silvestri). *Acta Zootaxonomica Sin.* **2011**, *36*, 882–887.
28. Shen, C.Y.; Wang, L.Y.; Wu, H.Y.; Zhang, J.Y. A new species of *Silvestrichilis* Wygodzinsky, 1950 (Insecta: Microcoryphia) from Wudang Mountain, Hubei, China, with the description of both sexes. *Zootaxa* **2025**, *5621*, 437–452. [CrossRef]

29. Chen, H.Y.; Yu, D.N.; Zhang, J.Y. One new species of the genus *Pedetontinus* (Microcoryphia, Machilidae) from China. *Acta Zootaxonomica Sin.* **2011**, *36*, 36–39.
30. Shen, C.Y.; Yang, T.; Ji, J.H.; Zhang, J.Y. Six New Species of Genus *Pedetontus Silvestri*, 1911 (Microcoryphia: Machilidae), from Southern China. *Insects* **2025**, *16*, 916. [CrossRef] [PubMed]
31. Kaplin, V. On the classification and phylogeny of the Machilidae (Thysanura, Microcoryphia). *Entomol. Rev.* **1985**, *64*, 117–131.
32. Ji, J.H.; Wu, H.Y.; Gao, Y.X.; Shen, C.Y.; Yang, Z.W.; Storey, K.B.; Yu, D.N.; Zhang, J.Y. Unusual genetic diversity within *Thereuopoda clunifera* (Wood, 1862) (Chilopoda: Scutigeromorpha) revealed by phylogeny and divergence times using mitochondrial genomes. *Insects* **2025**, *16*, 486. [CrossRef]
33. Tong, Y.; Wu, L.; Ayivi, S.P.G.; Storey, K.B.; Ma, Y.; Yu, D.N.; Zhang, J.Y. Cryptic species exist in *Vietnamella sinensis* Hsu, 1936 (Insecta: Ephemeroptera) from studies of complete mitochondrial genomes. *Insects* **2022**, *13*, 412. [CrossRef]
34. Guo, Z.Q.; Shen, C.Y.; Cheng, H.Y.; Chen, Y.X.; Wu, H.Y.; Storey, K.B.; Yu, D.N.; Zhang, J.Y. Mitogenome-Based phylogeny with divergence time estimates revealed the presence of cryptic species within Heptageniidae (Insecta, Ephemeroptera). *Insects* **2024**, *15*, 745. [CrossRef]
35. Ye, F.; Lan, X.E.; Zhu, W.B.; You, P. Mitochondrial genomes of praying mantises (Dictyoptera, Mantodea): Rearrangement, duplication, and reassignment of tRNA genes. *Sci. Rep.* **2016**, *6*, 25634. [CrossRef] [PubMed]
36. Guan, J.Y.; Shen, S.Q.; Zhang, Z.Y.; Xu, X.D.; Storey, K.B.; Yu, D.N.; Zhang, J.Y. Comparative mitogenomes of two *Coreamachilis* species (Microcoryphia: Machilidae) along with phylogenetic analyses of Microcoryphia. *Insects* **2021**, *12*, 795. [CrossRef] [PubMed]
37. Hong, M.Y.; Lee, E.M.; Jo, Y.H.; Park, H.C.; Kim, S.R.; Hwang, J.S.; Jin, B.R.; Kang, P.D.; Kim, K.-G.; Han, Y.S. Complete nucleotide sequence and organization of the mitogenome of the silk moth *Caligula boisduvalii* (Lepidoptera: Saturniidae) and comparison with other lepidopteran insects. *Gene* **2008**, *413*, 49–57. [CrossRef] [PubMed]
38. Fenn, J.; Cameron, S.; Whiting, M. The complete mitochondrial genome sequence of the Mormon cricket (*Anabrus simplex*: Tettigoniidae: Orthoptera) and an analysis of control region variability. *Insect Mol. Biol.* **2007**, *16*, 239–252. [CrossRef]
39. Clary, D.O.; Wolstenholme, D.R. The mitochondrial DNA molecule of *Drosophila yakuba*: Nucleotide sequence, gene organization, and genetic code. *J. Mol. Evol.* **1985**, *22*, 252–271. [CrossRef]
40. Regier, J.C.; Shultz, J.W.; Ganley, A.R.; Hussey, A.; Shi, D.; Ball, B.; Zwick, A.; Stajich, J.E.; Cummings, M.P.; Martin, J.W.; et al. Resolving arthropod phylogeny: Exploring phylogenetic signal within 41 kb of protein-coding nuclear gene sequence. *Syst. Biol.* **2008**, *57*, 920–938. [CrossRef]
41. Regier, J.C.; Shultz, J.W.; Zwick, A.; Hussey, A.; Ball, B.; Wetzer, R.; Martin, J.W.; Cunningham, C.W. Arthropod relationships revealed by phylogenomic analysis of nuclear protein-coding sequences. *Nature* **2010**, *463*, 1079–1083. [CrossRef]
42. Meusemann, K.; von Reumont, B.M.; Simon, S.; Roeding, F.; Strauss, S.; Kück, P.; Ebersberger, I.; Walzl, M.; Pass, G.; Breuers, S.; et al. A phylogenomic approach to resolve the arthropod tree of life. *Mol. Biol. Evol.* **2010**, *27*, 2451–2464. [CrossRef] [PubMed]
43. Von Reumont, B.M.; Meusemann, K.; Szucsich, N.U.; Dell'Ampio, E.; Gowri-Shankar, V.; Bartel, D.; Simon, S.; Letsch, H.O.; Stocsits, R.R.; Luan, Y.X.; et al. Can comprehensive background knowledge be incorporated into substitution models to improve phylogenetic analyses? A case study on major arthropod relationships. *BMC Evol. Biol.* **2009**, *9*, 119. [CrossRef] [PubMed]
44. Von Reumont, B.M.; Jenner, R.A.; Wills, M.A.; Dell'Ampio, E.; Pass, G.; Ebersberger, I.; Meyer, B.; Koenemann, S.; Iliffe, T.M.; Stamatakis, A.; et al. Pancrustacean phylogeny in the light of new phylogenomic data: Support for Remipedia as the possible sister group of Hexapoda. *Mol. Biol. Evol.* **2012**, *29*, 1031–1045. [CrossRef] [PubMed]
45. Montagna, M. Comment on phylogenetic analyses with four new Cretaceous bristletails reveal inter-relationships of Archaeognatha and Gondwana origin of Meinertellidae. *Cladistics* **2020**, *36*, 227–231. [CrossRef]
46. Cen, W.; Li, J.W.; He, J.T.; Chen, X.Y.; Li, L.Y.; Storey, K.B.; Yu, D.N.; Zhang, J.Y. Morpho-Molecular discordance and cryptic diversity in jumping Bristletails: A mitogenomic analysis of *Pedetontus silvestrii* (Insecta: Archaeognatha: Machilidae). *Insects* **2025**, *16*, 452. [CrossRef]
47. Marshall, D.C.; Hill, K.B.; Moulds, M.; Vanderpool, D.; Cooley, J.R.; Mohagan, A.B.; Simon, C. Inflation of molecular clock rates and dates: Molecular phylogenetics, biogeography, and diversification of a global cicada radiation from Australasia (Hemiptera: Cicadidae: Cicadettini). *Syst. Biol.* **2016**, *65*, 16–34. [CrossRef]
48. Shear, W.A.; Bonamo, P.M.; Grierson, J.D.; Rolfe, W.I.; Smith, E.L.; Norton, R.A. Early land animals in North America: Evidence from Devonian age arthropods from Gilboa, New York. *Science* **1984**, *224*, 492–494. [CrossRef]
49. Labandeira, C.C.; Beall, B.S.; Hueber, F.M. Early insect diversification: Evidence from a Lower Devonian bristletail from Québec. *Science* **1988**, *242*, 913–916. [CrossRef]
50. Rasnitsyn, A.P.; Aristov, D.S.; Gorochov, A.V.; Rowland, J.M.; Sinitshenkova, N.D. Important new insect fossils from Carrizo Arroyo and the Permo-Carboniferous faunal boundary. *N. M. Mus. Nat. Hist. Sci. Bull.* **2004**, *25*, 215–246.

51. Rasnitsyn, A.P. Taxonomy and morphology of *Dasyleptus* Brongniart, 1885, with description of a new species (Insecta: Machilida: Dasyleptidae). *Russ. Entomol. J.* **1999**, *8*, 145–154.
52. Misof, B.; Liu, S.; Meusemann, K.; Peters, R.S.; Donath, A.; Mayer, C.; Frandsen, P.B.; Ware, J.; Flouri, T.; Beutel, R.G.; et al. Phylogenomics resolves the timing and pattern of insect evolution. *Science* **2014**, *346*, 763–767. [CrossRef]
53. Ballard, J.W.O.; Kreitman, M. Is mitochondrial DNA a strictly neutral marker? *Trends. Ecol. Evol.* **1995**, *10*, 485–488. [CrossRef] [PubMed]
54. Cai, Y.T.; Li, Q.; Zhang, J.Y.; Storey, K.B.; Yu, D.N. Characterization of the mitochondrial genomes of two toads, *Anaxyrus americanus* (Anura: Bufonidae) and *Bufotes pewzowi* (Anura: Bufonidae), with phylogenetic and selection pressure analyses. *PeerJ* **2020**, *8*, e8901. [CrossRef]
55. Li, X.D.; Jiang, G.F.; Yan, L.Y.; Li, R.; Mu, Y.; Deng, W.A. Positive selection drove the adaptation of mitochondrial genes to the demands of flight and high-altitude environments in grasshoppers. *Front. Genet.* **2018**, *9*, 605. [CrossRef] [PubMed]
56. Xu, X.D.; Guan, J.Y.; Zhang, Z.Y.; Cao, Y.R.; Cai, Y.Y.; Storey, K.B.; Yu, D.N.; Zhang, J.Y. Insight into the phylogenetic relationships among three subfamilies within Heptageniidae (Insecta: Ephemeroptera) along with low-temperature selection pressure analyses using mitogenomes. *Insects* **2021**, *12*, 656. [CrossRef] [PubMed]
57. Feng, Y.F.; Cen, W.; Storey, K.B.; Liu, L.J.; Yu, D.N.; Zhang, J.Y. Comparative mitogenomic analysis of three *Chionea* species (Tipulomorpha: Limoniidae): Insights into phylogenetic relationships and selection pressure. *Insects* **2025**, *16*, 720. [CrossRef]
58. Faddeeva, A.; Studer, R.; Kraaijeveld, K.; Sie, D.; Ylstra, B.; Mariën, J.; op den Camp, H.; Datema, E.; Den Dunnen, J.T.; Van Straalen, N.; et al. Collembolan transcriptomes highlight molecular evolution of hexapods and provide clues on the adaptation to terrestrial life. *PLoS ONE* **2015**, *10*, e0130600. [CrossRef]
59. Folmer, O.; Black, M.; Hoeh, W.; Lutz, R.; Vrijenhoek, R. DNA primers for amplification of mitochondrial cytochrome c oxidase subunit I from diverse metazoan invertebrates. *Mol. Mar. Biol. Biotechnol.* **1994**, *3*, 294–299.
60. Zhang, J.Y.; Zhou, C.F.; Gai, Y.H.; Song, D.X.; Zhou, K.Y. The complete mitochondrial genome of *Parafronurus youi* (Insecta: Ephemeroptera) and phylogenetic position of the Ephemeroptera. *Gene* **2008**, *424*, 18–24. [CrossRef]
61. Burland, T.G. DNASTAR's Lasergene sequence analysis software. *Bioinform. Methods Protoc.* **2000**, *132*, 71–91.
62. Bernt, M.; Donath, A.; Jühling, F.; Externbrink, F.; Florentz, C.; Fritzsch, G.; Pütz, J.; Middendorf, M.; Stadler, P.F. MITOS: Improved de novo metazoan mitochondrial genome annotation. *Mol. Phylogenet. Evol.* **2013**, *69*, 313–319. [CrossRef] [PubMed]
63. Thompson, J.D.; Higgins, D.G.; Gibson, T.J. CLUSTAL W: Improving the sensitivity of progressive multiple sequence alignment through sequence weighting, position-specific gap penalties and weight matrix choice. *Nucleic Acids Res.* **1994**, *22*, 4673–4680. [CrossRef] [PubMed]
64. Donath, A.; Jühling, F.; Al-Arab, M.; Bernhart, S.H.; Reinhardt, F.; Stadler, P.F.; Middendorf, M.; Bernt, M. Improved annotation of protein-coding genes boundaries in metazoan mitochondrial genomes. *Nucleic Acids Res.* **2019**, *47*, 10543–10552. [CrossRef]
65. Tamura, K.; Stecher, G.; Kumar, S. MEGA11: Molecular evolutionary genetics analysis version 11. *Mol. Biol. Evol.* **2021**, *38*, 3022–3027. [CrossRef] [PubMed]
66. Zhang, D.; Gao, F.L.; Jakovlić, I.; Zou, H.; Zhang, J.; Li, W.X.; Wang, G.T. PhyloSuite: An integrated and scalable desktop platform for streamlined molecular sequence data management and evolutionary phylogenetics studies. *Mol. Ecol. Resour.* **2020**, *20*, 348–355. [CrossRef]
67. Grant, J.R.; Stothard, P. The CGView Server: A comparative genomics tool for circular genomes. *Nucleic Acids Res.* **2008**, *36*, W181–W184. [CrossRef]
68. Illustrator, A. Adobe Illustrator. 2021. Available online: https://www.adobe.com/products/illustrator.html#modal-hash (accessed on 2 July 2025).
69. Lorenz, R.; Bernhart, S.H.; Höner zu Siederdissen, C.; Tafer, H.; Flamm, C.; Stadler, P.F.; Hofacker, I.L. ViennaRNA package 2.0. algorithms. *Mol. Biol.* **2011**, *6*, 26.
70. Perna, N.T.; Kocher, T.D. Patterns of nucleotide composition at fourfold degenerate sites of animal mitochondrial genomes. *J. Mol. Evol.* **1995**, *41*, 353–358. [CrossRef]
71. He, K.; Zhang, J.Y.; Deng, K.Z.; Chen, Z. The complete mitochondrial genome of the bristletail *Songmachilis xinxiangensis* (Archaeognatha: Machilidae). *Mitochondr. DNA* **2013**, *24*, 99–101. [CrossRef]
72. Cameron, S.L.; Miller, K.B.; D'Haese, C.A.; Whiting, M.F.; Barker, S.C. Mitochondrial genome data alone are not enough to unambiguously resolve the relationships of Entognatha, Insecta and Crustacea sensu lato (Arthropoda). *Cladistics* **2004**, *20*, 534–557. [CrossRef]
73. Carapelli, A.; Liò, P.; Nardi, F.; Van der Wath, E.; Frati, F. Phylogenetic analysis of mitochondrial protein coding genes confirms the reciprocal paraphyly of Hexapoda and Crustacea. *BMC Evol. Biol.* **2007**, *7* (Suppl. S2), S8. [CrossRef] [PubMed]
74. Podsiadlowski, L. The mitochondrial genome of the bristletail *Petrobius brevistylis* (Archaeognatha: Machilidae). *Insect Mol. Biol.* **2006**, *15*, 253–258. [CrossRef]

75. Shen, S.Q.; Cai, Y.Y.; Xu, K.K.; Chen, Q.P.; Cao, S.S.; Yu, D.N.; Zhang, J.Y. The complete mitochondrial genome of *Pedetontus zhejiangensis* (Microcoryphia: Machilidae) and its phylogeny. *Mitochondr. DNA B* **2020**, *5*, 3143–3145. [CrossRef]
76. Cook, C.E.; Yue, Q.; Akam, M. Mitochondrial genomes suggest that hexapods and crustaceans are mutually paraphyletic. *Proc. R. Soc. B Biol. Sci.* **2005**, *272*, 1295–1304. [CrossRef]
77. Katoh, K.; Standley, D.M. MAFFT multiple sequence alignment software version 7: Improvements in performance and usability. *Mol. Biol. Evol.* **2013**, *30*, 772–780. [CrossRef] [PubMed]
78. Talavera, G.; Castresana, J. Improvement of phylogenies after removing divergent and ambiguously aligned blocks from protein sequence alignments. *Syst. Biol.* **2007**, *56*, 564–577. [CrossRef] [PubMed]
79. Castresana, J. Selection of conserved blocks from multiple alignments for their use in phylogenetic analysis. *Mol. Biol. Evol.* **2000**, *17*, 540–552. [CrossRef]
80. Xia, X.; Xie, Z. DAMBE: Software package for data analysis in molecular biology and evolution. *J. Hered.* **2001**, *92*, 371–373. [CrossRef]
81. Schrago, C.G.; Aguiar, B.O.; Mello, B. Comparative evaluation of maximum parsimony and Bayesian phylogenetic reconstruction using empirical morphological data. *J. Evol. Biol.* **2018**, *31*, 1477–1484. [CrossRef]
82. Reyes-Hernández, J.L.; Hansen, A.K.; Jenkins Shaw, J.; Solodovnikov, A. Phylogeny-based taxonomic revision and niche modelling of the rove beetle genus *Loncovilius* Germain, 1903 (Coleoptera: Staphylinidae: Staphylininae). *Zool. J. Linn. Soc.* **2024**, *202*, zlad143. [CrossRef]
83. Lanfear, R.; Calcott, B.; Ho, S.Y.; Guindon, S. PartitionFinder: Combined selection of partitioning schemes and substitution models for phylogenetic analyses. *Mol. Biol. Evol.* **2012**, *29*, 1695–1701. [CrossRef]
84. Vrieze, S.I. Model selection and psychological theory: A discussion of the differences between the Akaike information criterion (AIC) and the Bayesian information criterion (BIC). *Psychol. Methods* **2012**, *17*, 228. [CrossRef] [PubMed]
85. Minh, B.Q.; Schmidt, H.A.; Chernomor, O.; Schrempf, D.; Woodhams, M.D.; Von Haeseler, A.; Lanfear, R. IQ-TREE 2: New models and efficient methods for phylogenetic inference in the genomic era. *Mol. Biol. Evol.* **2020**, *37*, 1530–1534. [CrossRef] [PubMed]
86. Ronquist, F.; Teslenko, M.; Van Der Mark, P.; Ayres, D.L.; Darling, A.; Höhna, S.; Larget, B.; Liu, L.; Suchard, M.A.; Huelsenbeck, J.P. MrBayes 3.2: Efficient Bayesian phylogenetic inference and model choice across a large model space. *Syst. Biol.* **2012**, *61*, 539–542. [CrossRef]
87. Rambaut, A. FigTree Version 1.4.4. Available online: http://tree.bio.ed.ac.uk/software/figtree/ (accessed on 1 July 2025).
88. Near, T.J.; Sanderson, M.J. Assessing the quality of molecular divergence time estimates by fossil calibrations and fossil–based model selection. *Philos. Trans. R. Soc. London Ser. B Biol. Sci.* **2004**, *359*, 1477–1483. [CrossRef] [PubMed]
89. Yang, Z.; Rannala, B. Bayesian estimation of species divergence times under a molecular clock using multiple fossil calibrations with soft bounds. *Mol. Biol. Evol.* **2006**, *23*, 212–226. [CrossRef]
90. Püschel, H.P.; O'Reilly, J.E.; Pisani, D.; Donoghue, P.C. The impact of fossil stratigraphic ranges on tip-calibration, and the accuracy and precision of divergence time estimates. *Palaeontology* **2020**, *63*, 67–83. [CrossRef]
91. Keilbach, R. Bibliographie und Liste der Arten tierischer Einschlüsse in fossilen Harzen sowie ihrer Aufbewahrungsorte. *Deut. Entomol. Z.* **1982**, *29*, 129–286. [CrossRef]
92. Sturm, H.; Poinar Jr, G.O. *Cretaceomachilis libanensis*, the oldest known bristle-tail of the family Meinertellidae (Machiloidea, Archaeognatha, Insecta) from the Lebanese Amber. *Deut. Entomol. Z.* **1998**, *45*, 43–48. [CrossRef]
93. Yang, Z. PAML 4: Phylogenetic analysis by maximum likelihood. *Mol. Biol. Evol.* **2007**, *24*, 1586–1591. [CrossRef] [PubMed]
94. Rambaut, A.; Drummond, A.J.; Xie, D.; Baele, G.; Suchard, M.A. Posterior summarization in Bayesian phylogenetics using Tracer 1.7. *Syst. Biol.* **2018**, *67*, 901–904. [CrossRef]
95. Drummond, A.J.; Rambaut, A. BEAST: Bayesian evolutionary analysis by sampling trees. *BMC Evol. Biol.* **2007**, *7*, 214. [CrossRef] [PubMed]
96. Gao, F.; Chen, C.; Arab, D.A.; Du, Z.; He, Y.; Ho, S.Y. EasyCodeML: A visual tool for analysis of selection using CodeML. *Ecol. Evol.* **2019**, *9*, 3891–3898. [CrossRef]
97. Yang, Z. Likelihood ratio tests for detecting positive selection and application to primate lysozyme evolution. *Mol. Biol. Evol.* **1998**, *15*, 568–573. [CrossRef] [PubMed]
98. Zhang, J.; Nielsen, R.; Yang, Z. Evaluation of an improved branch-site likelihood method for detecting positive selection at the molecular level. *Mol. Biol. Evol.* **2005**, *22*, 2472–2479. [CrossRef]
99. Bielawski, J.P.; Yang, Z. A maximum likelihood method for detecting functional divergence at individual codon sites, with application to gene family evolution. *J. Mol. Evol.* **2004**, *59*, 121–132. [CrossRef]
100. Bielawski, J.P.; Yang, Z. Maximum likelihood methods for detecting adaptive evolution after gene duplication. *J. Struct. Funct. Genom.* **2003**, *3*, 201–212. [CrossRef]
101. Huelsenbeck, J.P.; Rannala, B. Phylogenetic methods come of age: Testing hypotheses in an evolutionary context. *Science* **1997**, *276*, 227–232. [CrossRef]

102. Yang, Z.; Wong, W.S.; Nielsen, R. Bayes empirical Bayes inference of amino acid sites under positive selection. *Mol. Biol. Evol.* **2005**, *22*, 1107–1118. [CrossRef]
103. Kaplin, V. A new species of bristletails of the genus *Petrobiellus* (Microcoryphia: Machilidae) from Sakhalin. *Zoosystematica Ross.* **2020**, *29*, 17–22. [CrossRef]
104. Mtow, S.; Machida, R. What are *Halomachilis akkesiensis* and *Halomachilis kojimai* described from Hokkaido, Japan? (Insecta: Archaeognatha: Machilidae). *Zootaxa* **2024**, *5543*, 445–450. [CrossRef]
105. Olfers, E.V. Die «Ur-Insekten» (Thysanura und Collembola im Bernstein). *Schr. K. Phys.-ökon. Ges. Königsb.* **1907**, *48*, 1–40.
106. Wang, B.; Xu, C.; Jarzembowski, E.A. Ecological radiations of insects in the Mesozoic. *Trends. Ecol. Evol.* **2022**, *37*, 529–540. [CrossRef] [PubMed]
107. Wang, Y.; Huang, C.; Sun, B.; Quan, C.; Wu, J.; Lin, Z. Paleo-CO_2 variation trends and the Cretaceous greenhouse climate. *Earth-Sci. Rev.* **2014**, *129*, 136–147. [CrossRef]
108. McLoughlin, S. The breakup history of Gondwana and its impact on pre-Cenozoic floristic provincialism. *Aust. J. Bot.* **2001**, *49*, 271–300. [CrossRef]
109. Laenen, B.; Shaw, B.; Schneider, H.; Goffinet, B.; Paradis, E.; Désamoré, A.; Heinrichs, J.; Villarreal, J.; Gradstein, S.; McDaniel, S. Extant diversity of bryophytes emerged from successive post-Mesozoic diversification bursts. *Nat. Commun.* **2014**, *5*, 5134. [CrossRef]
110. Benton, M.J. The origins of modern biodiversity on land. *Philos. Trans. R. Soc. B. Biol. Sci.* **2010**, *365*, 3667–3679. [CrossRef] [PubMed]
111. Huang, C.Y.; Yuan, P.B.; Tsao, S.-J. Temporal and spatial records of active arc-continent collision in Taiwan: A synthesis. *Geol. Soc. Am. Bull.* **2006**, *118*, 274–288. [CrossRef]
112. Li, C.F.; Xu, X.; Lin, J.; Sun, Z.; Zhu, J.; Yao, Y.; Zhao, X.; Liu, Q.; Kulhanek, D.K.; Wang, J. Ages and magnetic structures of the South China Sea constrained by deep tow magnetic surveys and IODP Expedition 349. *Geochem. Geophys. Geosyst.* **2014**, *15*, 4958–4983. [CrossRef]
113. Ashman, L.G.; Shin, S.; Zwick, A.; Ślipiński, A.; McKenna, D.D. The first phylogeny of Australasian Lamiinae longhorn beetles (Coleoptera: Cerambycidae) reveals poor tribal classification and a complex biogeographic history. *Syst. Entomol.* **2022**, *47*, 213–230. [CrossRef]
114. Decru, E.; Moelants, T.; De Gelas, K.; Vreven, E.; Verheyen, E.; Snoeks, J. Taxonomic challenges in freshwater fishes: A mismatch between morphology and DNA barcoding in fish of the north-eastern part of the Congo basin. *Mol. Ecol. Resour.* **2016**, *16*, 342–352. [CrossRef] [PubMed]
115. Hirano, T.; Kameda, Y.; Kimura, K.; Chiba, S. Substantial incongruence among the morphology, taxonomy, and molecular phylogeny of the land snails Aegista, Landouria, Trishoplita, and Pseudobuliminus (Pulmonata: Bradybaenidae) occurring in East Asia. *Mol. Phylogenet. Evol.* **2014**, *70*, 171–181. [CrossRef]
116. Andreu, A.L.; Hanna, M.G.; Reichmann, H.; Bruno, C.; Penn, A.S.; Tanji, K.; Pallotti, F.; Iwata, S.; Bonilla, E.; Lach, B. Exercise intolerance due to mutations in the cytochrome b gene of mitochondrial DNA. *N. Engl. J. Med.* **1999**, *341*, 1037–1044. [CrossRef] [PubMed]
117. Chance, B.; Wilson, D.; Dutton, P.; Erecińska, M. Energy-coupling mechanisms in mitochondria: Kinetic, spectroscopic, and thermodynamic properties of an energy-transducing form of cytochrome *b*. *Proc. Natl. Acad. Sci. USA* **1970**, *66*, 1175–1182. [CrossRef]
118. Davies, K.M.; Strauss, M.; Daum, B.; Kief, J.H.; Osiewacz, H.D.; Rycovska, A.; Zickermann, V.; Kühlbrandt, W. Macromolecular organization of ATP synthase and complex I in whole mitochondria. *Proc. Natl. Acad. Sci. USA* **2011**, *108*, 14121–14126. [CrossRef]
119. Del Dotto, V.; Musiani, F.; Baracca, A.; Solaini, G. Variants in human ATP synthase mitochondrial genes: Biochemical dysfunctions, associated diseases, and therapies. *Int. J. Mol. Sci.* **2024**, *25*, 2239. [CrossRef]
120. Lazarou, M.; Smith, S.M.; Thorburn, D.R.; Ryan, M.T.; McKenzie, M. Assembly of nuclear DNA-encoded subunits into mitochondrial complex IV, and their preferential integration into supercomplex forms in patient mitochondria. *FEBS J.* **2009**, *276*, 6701–6713. [CrossRef]
121. Bourens, M.; Barrientos, A. A CMC 1-knockout reveals translation-independent control of human mitochondrial complex IV biogenesis. *EMBO Rep.* **2017**, *18*, 477–494. [CrossRef]
122. Hong, Y.H.; Huang, H.M.; Wu, L.; Storey, K.B.; Zhang, J.Y.; Zhang, Y.P.; Yu, D.N. Characterization of two mitogenomes of *Hyla sanchiangensis* (Anura: Hylidae), with phylogenetic relationships and selection pressure analyses of Hylidae. *Animals* **2023**, *13*, 1593. [CrossRef]
123. Ngatia, J.N.; Lan, T.M.; Dinh, T.D.; Zhang, L.; Ahmed, A.K.; Xu, Y.C. Signals of positive selection in mitochondrial protein-coding genes of woolly mammoth: Adaptation to extreme environments? *Ecol. Evol.* **2019**, *9*, 6821–6832. [CrossRef] [PubMed]

Disclaimer/Publisher's Note: The statements, opinions and data contained in all publications are solely those of the individual author(s) and contributor(s) and not of MDPI and/or the editor(s). MDPI and/or the editor(s) disclaim responsibility for any injury to people or property resulting from any ideas, methods, instructions or products referred to in the content.

insects

MDPI

Article

High-Humidity Incubation Improves Post-Microinjection Viability and Larval Performance of CRISPR/Cas9-Edited *Helicoverpa armigera* Embryos

Jingyun Zhu [1,2], Hongran Li [1], Yan Peng [1], Minghui Jin [1], Kaikai Mao [3] and Yutao Xiao [1,*]

[1] Shenzhen Branch, Guangdong Laboratory of Lingnan Modern Agriculture, Key Laboratory of Gene Editing Technologies (Hainan), Ministry of Agriculture and Rural Affairs, Agricultural Genomics Institute at Shenzhen, Chinese Academy of Agricultural Sciences, Shenzhen 518000, China; jingyun_zhu@126.com (J.Z.); lihongran@caas.cn (H.L.); pengyan@caas.cn (Y.P.); jinminghui@caas.cn (M.J.)

[2] Key Laboratory of Integrated Pest Management on Tropical Crops of the Ministry of Agriculture and Rural Affairs, Environment and Plant Protection Institute, Chinese Academy of Tropical Agricultural Sciences, Haikou 571101, China

[3] Guangxi Key Laboratory of Agro-Environment and Agric-Products Safety, College of Agriculture, Guangxi University, Nanning 530004, China; kaikaimao@gxu.edu.cn

* Correspondence: xiaoyutao@caas.cn

Simple Summary: This study focused on solving a key gap in insect gene editing: while humidity affects normal insect egg hatching, its role in post-microinjection recovery of CRISPR/Cas9-edited *Helicoverpa armigera* (cotton bollworm) eggs remained unstudied. Lab-bred *H. armigera* eggs (laid within 2 h) were injected with CRISPR/Cas9 (targeting the *TRPA1* gene) or a control solution, then incubated at 50%, 65%, 80%, or 95% relative humidity (RH) for 48 h. Results showed 95% RH was optimal: eggs stayed plump (avoiding shriveling at lower RH), with 100-egg weight peaking at ~103 mg and hatching rate rising over 27.5% vs. RH $\leq$ 80%. Larvae from these eggs also developed faster and had heavier pupae, while gene editing efficiency remained unchanged across humidities. This 48-h 95% RH incubation protocol boosts post-injection viability of *H. armigera* eggs, offering practical support for efficient insect gene editing and a reference for other species.

Abstract: Gene editing technologies are playing an increasingly important role in the study of insect gene functions. Appropriate incubation humidity helps improve the hatching rate of insect eggs. However, to date, no study has evaluated the impact of humidity on the hatching rate of gene-edited eggs or the subsequent development of the larvae. Using the cotton bollworm *Helicoverpa armigera* (Lepidoptera: Noctuidae) as a model, we investigated the weight and hatching rate of microinjected eggs under different humidity conditions. We determined the larval development time and pupal weight and calculated the larval gene editing efficiency. The results showed that post-microinjection incubation under high humidity (RH = 95%) had a significant influence on CRISPR/Cas9 gene-edited eggs. The key research results indicate that, compared with the incubation environment with RH $\leq$ 80%, after 48 h of incubation under 95% RH, the hatching rate of *H. armigera* eggs increased by more than 27.5%, with higher egg saturation and greater egg weight; meanwhile, the larval developmental duration was shorter and the pupal weight was also greater. These results establish a humidity-regulated developmental recovery protocol for gene-edited insects, which provides theoretical and practical support for optimizing post-microinjection recovery processes in gene-edited insects.

Keywords: CRISPR/Cas9; high-humidity incubation; *Helicoverpa armigera*

1. Introduction

With the advancement of gene sequencing technologies, gene editing systems have emerged as a powerful tool in biological sciences and an essential approach for insect gene function studies [1–4]. Insect eggs often require specific pretreatments before editing, which typically vary between species. For species with soft eggs, freshly collected eggs can be placed directly onto double-sided adhesive tape on a microscope slide and injected. Eggs with a soft chorion but high internal pressure should be dried before injection, while thick-shelled eggs should be softened and dried prior to injection [5]. The timing of the injection of eggs is also crucial, and to reduce the occurrence of chimeras, most experiments require this operation to be performed within 2 h after egg laying. Studies have shown that the earlier the injection is performed, the higher the deletion frequency [3,6].

Environmental humidity plays a critical role in insects' growth and development, influencing their egg hatch, developmental rate, fecundity, and body coloration [7–11]. For *Halyomorpha halys*, low humidity reduces the survival rate of first-instar nymphs but exerts no effect on third- to fourth-instar nymphs. In contrast, high humidity enhances the survival rate of first-instar nymphs while decreasing that of third- to fourth-instar nymphs [7]. Low environmental humidity delays egg development in *Callosobruchus maculatus* [9], yet it does not have this effect on *Halyomorpha halys* [7]. Low-humidity environments in *Picromerus lewisi* can not only prolong the developmental duration of eggs and reduce their hatching rates but also shorten the adult lifespan [10]. Notably, distinct species—and even different immature stages of the same species—exhibit specific humidity tolerance ranges [12]. Maternal oviposition behaviors—such as selecting optimal laying sites and clustering eggs—play a critical role in protecting eggs against desiccation [13]. Additionally, egg survival can be enhanced when mothers provide adequate internal water reserves, increase hydrocarbon content in the eggshell [14], or coat the eggs with substances such as hydrogels [15–18]. The deposited egg is also capable of protecting itself against desiccation, the serosa and its cuticle make a significant contribution to the egg's drought resistance [19,20]. Notably, in *Aedes*, *Anopheles*, and *Culex* mosquitoes, the formation of dark eumelanin in the endochorion may further enhance the serosa's contribution to drought resistance [21]. Diapause also enhances drought resistance in *Aedes aegypti* eggs [22].

In most cases, eggs utilized for genetic editing are relatively fragile due to being laid at an early developmental stage prior to full maturation. The pretreatment and the injection process of eggs can also cause certain damage to the eggs. It is therefore imperative to enhance the hatching rate of eggs post injection. This study focuses on *H. armigera* and investigates the effects of different humidity conditions on the recovery process of eggs following microinjection. The results showed that early-stage humidity incubation not only had a significant impact on the weight of *H. armigera* eggs after microinjection but also affected the hatching rate, larval developmental duration, and pupal weight.

2. Materials and Methods

2.1. Insect Rearing

The cotton bollworm (*Helicoverpa armigera*) was collected from Xiajin, Shandong Province, China, in 2023. Adults trapped in the wild are paired individually. After multiple generations of breeding, the eggs laid by the offspring of these paired adults are used for experiments. Insects were reared under controlled laboratory conditions at 27 $\pm$ 1 °C,

75 ± 10% relative humidity, and a photoperiod of 14 h of light and 10 h of dark. Adult moths were provided with a 10% sucrose solution as an energy source.

2.2. sgRNA Design and Synthesis

A single sgRNA against *TRPA1* (Accession Number: XM_049838796) was designed using the sgRNAcas9 design tool (Table 1) (developed by independent researchers; available at BiooTools: http://www.biootools.com/, Nanjing, China) [23]. The sgRNA target sequences were checked in a search of the *H. armigera* genome using the sgRNAcas9 design tool, and no potential off-target sites were identified. A PCR-based approach was used to synthesize sgRNAs following the manufacturer's instructions (GeneArt Precision gRNA Synthesis Kit, Thermo Fisher Scientific, Waltham, MA, USA). The Cas9 protein GeneArt Platinum Cas9 Nuclease) was purchased from Thermo Fisher Scientific (Shanghai, China).

Table 1. sgRNA sequence.

Primer ID	Sequence
sgRNA-*TRPA1*	GGTGCCACAGCGCACGGTCCG

2.3. Microinjection of Embryos

Freshly laid eggs (within 2 h) were washed from gauze using 1% (*v*/*v*) sodium hypochlorite solution and rinsed with distilled water. The eggs were then stuck to a microscope slide with double-sided adhesive tape. One hundred eggs were affixed to each microscope slide.

About 2 nL of a mixture of sgRNA (300 ng/μL) and Cas9 protein (50 ng/μL) was injected into individual eggs using the CRISPR/Cas9 genome editing system as previously reported [24]. The Cas9 protein (GeneArt Platinum Cas9 Nuclease) was purchased from Thermo Fisher Scientific, mixture of sgRNAs and Cas9 protein was injected into individual eggs using the NanojectIII (Drummond Scientific, Broomall, PA, USA). Injected eggs were incubated in environments with a temperature of 25 ± 1 °C and separate humidity levels of 50%, 65%, 80%, and 95% for 48 h. After 48 h, the eggs were transferred to an environment with a temperature of 25 ± 1 °C and 80% humidity for further incubation. Temperature was maintained at 25 °C with relative humidity (RH) levels of 50%, 65%, 80%, and 95%, controlled by saturated salt solutions of NH_4NO_3-$NaNO_3$, $NaNO_2$, $(NH_4)_2SO_4$, and $Pb(NO_3)_2$, respectively, following the method described by Winston [25].

Eggs that were injected with a mixture of H_2O + Cas9 protein and non-injected eggs were treated as described above, serving as the experimental and control groups, respectively.

2.4. Measurement of Hatching Rate and 100-Egg Weight Under Experimental Conditions

Before egg attachment in Section 2.2, the total weight of each microscope slide and its double-sided tape was measured and recorded as G0. After attaching the eggs, the weight of the slide with the eggs was measured and recorded as G1. The initial weight of 100 eggs was calculated as G1 minus G0. After placing the slides in different humidity environments for 24 h, the weight of each slide was measured again and recorded as G3. The weight of the eggs after 24 h was calculated as G3 minus G0. The egg weight after 48 h was calculated using the same method. Each humidity condition was repeated four times.

The number of hatched eggs on each slide under different humidity conditions was recorded for subsequent experimental analysis. The hatching rate of the eggs is equal to the number of hatched larvae on each slide divided by 100, then multiplied by 100 (i.e., expressed as a percentage).

2.5. Observation and Measurement of Developmental Duration, Pupal Weight, and Pupation Rate

The hatched larvae described in Section 2.3 were individually transferred to artificial diets and reared under controlled conditions (27 ± 1 °C, 75 ± 10% relative humidity). Upon reaching the 2nd instar, 10 larvae per replicate were randomly selected for individual genomic DNA extraction and genotyping (Section 2.6). The remaining larvae were reared continuously: the number of successfully pupated individuals was recorded, and the developmental duration and pupal weight were measured.

2.6. Determination of Gene Editing Efficiency in Hatched Larvae

Primers used for mutation detecting were designed using Primer Premier 5 (Premier Biosoft International, Palo Alto, CA, USA) according to the sgRNA locations (Table 2). Genomic DNA was extracted with a Multisource Genomic DNA Miniprep Kit (Axygen, Corning Incorporated, Union City, CA, USA). PCR amplicons were analyzed via agarose gel electrophoresis. PCR products were recovered and cloned into T3 Vector and sequenced by Sangon Biotech (Shanghai, China).

Table 2. Primers used for mutation detecting.

Primer ID	Sequence
D-*TRPA1*-F	ATGGGTGCATCGCTAGAG
D-*TRPA1*-R	AGGAAGCGAGGACTTGCG

2.7. Data Analysis

A statistical comparison of the hundred-egg weight and egg hatching rate across different treatment groups was performed using Student's *t*-test. A one-way analysis of variance (ANOVA) was used to analyze differences among the hatching rate, 100-egg weight, pupation rate, pupation time, and pupal weight of *H. armigera* followed by separation of means using Fisher's protected least significant difference (LSD) test at $p = 0.05$. The experimental data were analyzed using the package IBM SPSS Statistics 22.0 (SPSS, Inc., Chicago, IL, USA).

3. Results

3.1. Hatching Rate and 100-Egg Weight

At 95% relative humidity, eggs remained plump and intact, while eggs incubated under other humidity conditions showed varying degrees of shriveling (Figure 1A). Incubation under different humidity conditions had a significant effect on egg weight (Wt, $F = 49.373$, df = 3, 12, $p < 0.0001$; Injected-*TRPA1* + cas9, $F = 31.425$, df = 3, 12, $p < 0.0001$; Injected-H_2O + cas9, $F = 42.026$, df = 3, 12, $p < 0.0001$). When the humidity was 95%, the weight of 100 eggs was the highest, reaching 103.25 mg, 101.00 mg, and 101.75 mg, respectively. At 50% humidity, the weight of 100 eggs was the lowest, measuring 50.75 mg, 33.00 mg, and 36.50 mg, respectively (Figure 1B). Under the same incubation conditions, there was no significant difference in egg weight between eggs injected with *TRPA1* + Cas9 and those injected with water + Cas9 (50%RH, $p = 0.508$; 65%RH, $p = 0.969$; 80%RH, $p = 0.480$; 95%RH, $p = 0.874$). In the 50% and 60% humidity environments, the egg weight of non-injected eggs was significantly higher than that of injected eggs (Wt vs. Injected-*TRPA1* + cas9: 50%RH, $p = 0.016$; 65%RH, $p = 0.014$; Wt vs. Injected-H2O + cas9: 50%RH, $p = 0.020$; 65%RH, $p = 0.015$).

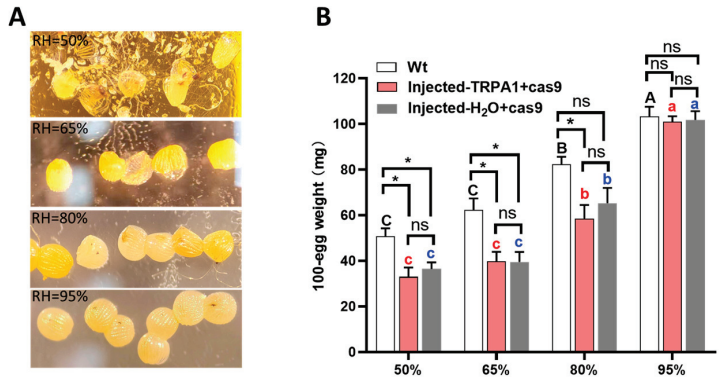


Figure 1. Egg weight of *H. armigera* after microinjection under different humidity incubation conditions: (**A**) *H. armigera* eggs injected with *TRPA1* + Cas9 after 48 h of incubation under different humidity levels; (**B**) weight per 100 eggs after 48 h of incubation under different humidity levels. Each humidity condition was replicated four times. Different letters in the figure indicate significant differences at $p < 0.05$ (one-way ANOVA). * represents values that were statistically significant at $p < 0.05$; ns indicates no significant difference at $p = 0.05$. The mean amounts are presented with the standard error of the mean (±SE).

Different incubation humidity conditions had a significant effect on the hatching rate of *H. armigera* eggs (Wt, F = 10.359, df = 3, 12, $p = 0.001$; Injected-*TRPA1* + cas9, F = 24.561, df = 3, 12, $p < 0.0001$; Injected-H2O + cas9, F = 24.270, df = 3, 12, $p < 0.0001$; Figure 2B). When the incubation humidity was 95%, the hatching rate of *H. armigera* eggs was the highest, Wt reaching 65.50%, Injected-*TRPA1* + cas9 reaching 48.25%, and Injected-H_2O + cas9 reaching 52.75%. There was no significant difference in the hatching rate of *H. armigera* eggs injected with *TRPA1* + Cas9 or water + Cas9 among the four humidity environments (50%RH, $p = 0.508$; 65%RH, $p = 0.969$; 80%RH, $p = 0.480$; 95%RH, $p = 0.874$; Figure 2B). The hatching rate of non-injected eggs after incubation at 50%, 65%, and 80% humidity was significantly higher than that of *TRPA1* + Cas9-injected (50%RH, $p = 0.006$; 65%RH, $p = 0.001$; 80%RH, $p = 0.001$) and H_2O + Cas9-injected (50%RH, $p = 0.006$; 65%RH, $p = 0.001$; 80%RH, $p = 0.003$; Figure 2B) eggs.

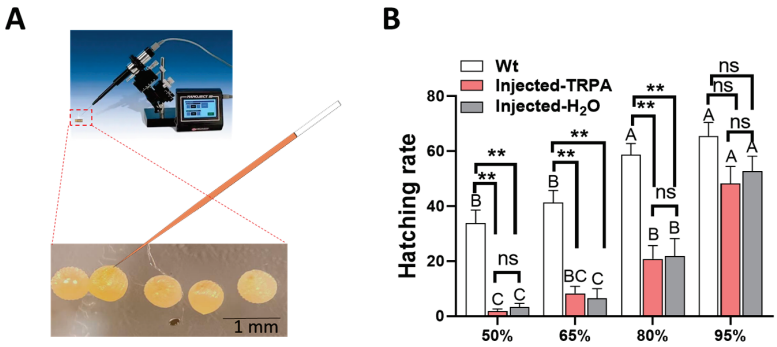


Figure 2. Hatching rate of *H. armigera* eggs after microinjection under different humidity incubation conditions: (**A**) diagram of the microinjection procedure; (**B**) hatching rates of eggs under different humidity conditions. Each humidity condition was replicated four times. Different letters in the figure indicate significant differences at $p < 0.05$ (one-way ANOVA). ** represents values that were statistically significant at $p < 0.01$; ns indicates no significant difference at $p = 0.05$. The mean amounts are presented with the standard error of the mean (±SE).

3.2. Developmental Duration, Pupal Weight, and Pupation Rate

Incubation under different humidity conditions significantly affected the developmental duration (F = 13.636, df = 3, 96, $p < 0.0001$; Figure 3A), pupal weight (F = 10.290, df = 3, 12,

$p < 0.001$; Figure 3B), and pupation rate (F = 5.033, df = 3, 12, $p = 0.017$; Figure 3C) of *H. armigera*.

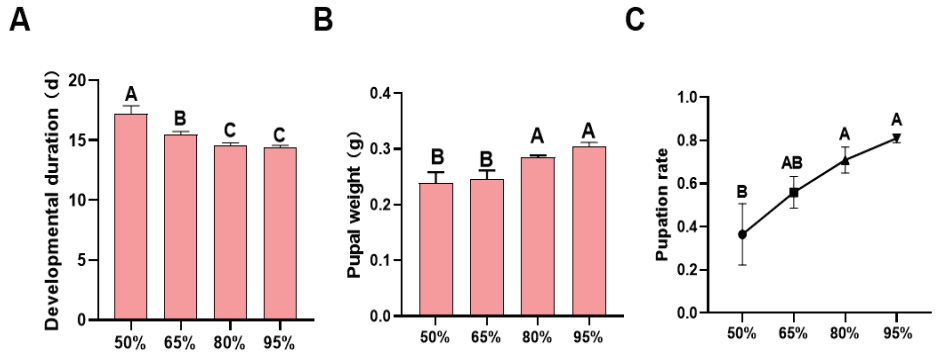


Figure 3. Larval performance of *H. armigera* larvae hatched after 48 h of incubation under different humidity conditions: (**A**) developmental duration; (**B**) pupal weight; (**C**) pupation rate. Different letters in the figure indicate significant differences at $p < 0.05$ (one-way ANOVA).

3.3. Gene Editing Efficiency in Hatched Larvae

There was no significant difference in the gene editing rate between eggs incubated under different humidity conditions (F = 1.778, df = 3, 12, $p = 0.205$; Figure 4).

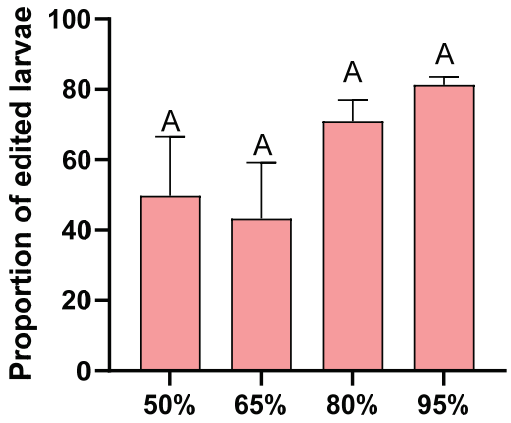


Figure 4. Proportion of successfully edited larvae under different humidity conditions. Each humidity condition was replicated four times. Different letters in the figure indicate significant differences at $p < 0.05$ (one-way ANOVA).

4. Discussion

Our experimental results show that the hundred-egg weight of *H. armigera* significantly decreases with decreasing humidity after microinjection (Figure 1). In a 50% humidity environment, the plumpness of *H. armigera* eggs decreases (Figure 1A), and the weight of 100 eggs is significantly lower than that in a 95% humidity environment (Figure 1B). This may be caused by a variety of factors. Bodily secretions, feces, hairs, and scales collectively form multiple defensive barriers on the egg surface [16,17,26]. These surface-based protective substances, however, are susceptible to damage by egg washing and egg disinfection. The serosa, an additional embryonic membrane that encloses the embryo and yolk and can protect the embryo from desiccation [19], can also be damaged by egg injection. The eggshell may become thinner during the pro-injection preparation process, reducing the egg's ability to retain water. Additionally, eggs may absorb water during the washing process; some species can even obtain sufficient water from the moisture of the air [27], and this absorbed water can be lost in a dry environment.

Humidity plays a critical role in the hatching rate of insect eggs [20,28–30]. Eggs maintained under excessively arid conditions may fail to hatch: in some instances, this is attributable to desiccation of the internal embryo; in other cases, it arises because the chorion itself hardens to a degree that precludes emergence of the immature insect [31]. Relative humidity also can affect egg hatching time; studies on blow flies have shown that higher relative humidity leads to shorter hatching durations [28]. High-humidity environments have varying effects on the hatching of eggs from different insect species. Studies on *Spodoptera exigua* have shown that higher humidity leads to a higher egg hatching rate [30]. In contrast, research on *Hypera postica* has indicated that excessively high humidity can reduce the hatching rate of its eggs [32]. We only investigated the impact of incubation in different humidity environments for 48 h on *H. armigera* eggs after microinjection, with the gene editing targeting a single locus (TRPA1). Our results showed that different humidity incubation conditions had a significant effect on the hatching rate of *H. armigera* eggs after gene editing; the higher the humidity, the higher the hatching rate (Figure 2B). Humidity plays a critical role in the recovery process of injected eggs. Compared to the control group, both the *TRPA1* + Cas9-injected and H_2O + Cas9-injected eggs exhibited significant reductions in both hundred-egg weight and hatching rate under low-humidity conditions. Eggs subjected to microinjection are more fragile and may therefore require higher humidity levels for successful development. This is consistent with the observed reduction in egg weight under low-humidity conditions. Our results are the first to demonstrate that humidity affects the hatching rate of eggs after microinjection targeting *TRPA1* in *H. armigera*.

Humidity influences larval development, and insects at different developmental stages exhibit varying humidity preferences. In *Halyomorpha halys*, early-instar nymphs are sensitive to drought, while later-instar nymphs are intolerant of high humidity [33]. Our study showed that early-stage humidity incubation had a significant impact on the growth and development of *H. armigera* larvae (Figure 3). The extended developmental period and decreased pupal weight may result from excessive desiccation of eggs incubated under low humidity, as varying degrees of water loss were observed at 80%, 65%, and 50% relative humidity (Figure 1). Due to their underdeveloped protective structures, early-stage eggs are particularly vulnerable to environmental stressors [34,35].

Many studies incubate insect eggs after injection in environments with approximately $70 \pm 10\%$ humidity [36,37]. Our research results indicate that in a humid environment below 80%, a certain proportion of *H. armigera* eggs can still hatch; however, the hatching rate is relatively low. To obtain gene knockout strains, it is necessary to increase the number of microinjected eggs, which will inevitably increase the usage of eggs and the workload. This study provides a strategy to improve the hatching rate of eggs after microinjection and enhance larval performance: by incubating the injected eggs under high humidity for two days. It should be noted that this strategy is currently based on experiments targeting the *TRPA1* locus in *H. armigera*, which limits the direct generalizability of our conclusions to other genes or insect taxa. Additionally, in the gene editing efficiency analysis, we genotyped 40 larvae per humidity condition but only counted edited and unedited individuals without distinguishing the presence of chimeras. This may compromise the accuracy of editing efficiency evaluation, and future studies should adopt more advanced methods (e.g., deep sequencing) to quantitatively analyze the chimerism level.

5. Conclusions

Our research results indicate that, compared with incubation in a low-humidity environment, the hatching rate and egg weight of *H. armigera* eggs incubated in an environment

with humidity greater than 80% for 48 h after microinjection are significantly higher. Without affecting editing efficiency, the larval developmental duration is shorter, and the pupal weight is greater. Our research findings provide guidance for the efficient editing of *H. armigera* eggs and may also serve as a preliminary reference for the incubation of edited eggs of other insect species, pending further verification to confirm whether these results can be broadly applicable across different genes and taxa.

Author Contributions: Conceptualization, Y.X.; methodology, J.Z. and H.L.; software, J.Z.; formal analysis, J.Z., Y.P., M.J. and K.M.; investigation, J.Z.; writing—original draft preparation, J.Z.; writing—review and editing, Y.P., M.J., K.M. and H.L.; visualization, Y.X.; supervision, Y.X.; project administration, Y.X.; funding acquisition, Y.X. and J.Z. All authors have read and agreed to the published version of the manuscript.

Funding: This work was supported by The National Natural Science Foundation of China (32372546), granted to Y.X., and the China Postdoctoral Science Foundation (No. 2022M723464), granted to J.Z.

Data Availability Statement: The original contributions presented in this study are included in the article. Further inquiries can be directed to the corresponding author.

Acknowledgments: The authors would like to thank all the editors and reviewers for the modifications and suggestions regarding the manuscript.

Conflicts of Interest: The authors declare no conflicts of interest.

References

1. William, R.; O'Brochta, D.A. Applications of genome editing in insects. *Curr. Opin. Insect Sci.* **2016**, *13*, 43–54. [CrossRef]
2. Gantz, V.M.; Akbari, O.S. Gene editing technologies and applications for insects. *Curr. Opin. Insect Sci.* **2018**, *28*, 66–72. [CrossRef]
3. Taning, C.N.T.; Van Eynde, B.; Yu, N.; Ma, S.; Smagghe, G. CRISPR/Cas9 in insects: Applications, best practices and biosafety concerns. *J. Insect Physiol.* **2017**, *98*, 245–257. [CrossRef]
4. Xu, J.; Xu, X.; Zhan, S.; Huang, Y. Genome editing in insects: *Current status* and challenges. *Natl. Sci. Rev.* **2019**, *6*, 399–401. [CrossRef]
5. Zhang, L.; Reed, R.D. A Practical Guide to CRISPR/Cas9 Genome Editing in Lepidoptera. In *Diversity and Evolution of Butterfly Wing Patterns*; Sekimura, T., Nijhout, H., Eds.; Springer: Singapore, 2017.
6. Li, X.; Fan, D.; Zhang, W.; Liu, G.; Zhang, L.; Zhao, L.; Fang, X.; Chen, L.; Dong, Y.; Chen, Y.; et al. Outbred genome sequencing and CRISPR/Cas9 gene editing in butterflies. *Nat. Commun.* **2015**, *6*, 8212. [CrossRef] [PubMed]
7. Khadka, A.; Hodges, A.C.; Leppla, N.C.; Tillman, P.G. The effects of relative humidity on *Halyomorpha halys* (Stål) (Hemiptera: Pentatomidae) egg hatch, nymph survival, and adult reproduction. *Fla. Entomol.* **2020**, *103*, 136–138. [CrossRef]
8. Yang, W.Q.; Li, X.; Meng, F.X.; Liu, T.X.; Zhang, S.Z. Effects of temperature, relative humidity, and photoperiod on life history of *Cotesia ruficrus* (Hymenoptera: Braconidae), an indigenous parasitoid of *Spodoptera frugiperda* (Lepidoptera: Noctuidae). *J. Econ. Entomol.* **2025**, *118*, 1133–1145. [CrossRef] [PubMed]
9. Aslam, A.; Jafir, M.; Wajid Javed, M.; Shehzad, M.; Zubair Chaudhary, M.; Aftab, M.; Muhammad Jafir, C. Effect of temperature and relative humidity on development of *Sitophilus oryzae* L. (coleoptera: Curculionidae). *J. Entomol. Zool. Stud.* **2017**, *5*, 85–90.
10. Ji, Y.T.; Xue, C.Z.; Wang, M.Q.; Xiang, M.; Li, P.; Li, Y.Y.; Mao, J.J.; Zhang, L.S. Effects of relative humidity on development of *Picromerus lewisi* Scott. *Chin. J. Biol. Control.* **2022**, *38*, 975–981.
11. Deruytter, D.; Coudron, C.L.; Claeys, J. Transporting *Tenebrio molitor* Eggs: The Effect of Temperature, Humidity and Time on the Hatch Rate. *Sustainability* **2023**, *15*, 6231. [CrossRef]
12. Prasad, K.V.H. Factors Affecting Growth and Metabolism of Insects. In *Insect Ecology: Concepts to Management*; Springer: Singapore, 2022.
13. Griese, E.; Dicke, M.; Hilker, M.; Fatouros, N.E. Plant response to butterfly eggs: Inducibility, severity and success of egg-killing leaf necrosis depends on plant genotype and egg clustering. *Sci. Rep.* **2017**, *7*, 7316. [CrossRef]
14. Urbanski, J.M.; Benoit, J.B.; Michaud, M.R.; Denlinger, D.L.; Armbruster, P. The molecular physiology of increased egg desiccation resistance during diapause in the invasive mosquito, *Aedes albopictus*. *Proc. Biol. Sci.* **2010**, *277*, 2683–2692. [CrossRef] [PubMed]
15. Finch, G.; Nandyal, S.; Perretta, C.; Davies, B.; Rosendale, A.J.; Holmes, C.J.; Gantz, J.D.; Spacht, D.E.; Bailey, S.T.; Chen, X.; et al. Multi-level analysis of reproduction in an *Antarctic midge* identifies female and male accessory gland products that are altered by larval stress and impact progeny viability. *Sci. Rep.* **2020**, *10*, 19791. [CrossRef]

16. Hilker, M.; Salem, H.; Fatouros, N.E. Adaptive plasticity of insect eggs in response to environmental challenges. *Annu. Rev. Entomol.* **2023**, *68*, 451–469. [CrossRef] [PubMed]
17. Matsushima, R.; Yokoi, T. Eggs in faeces: Defensive mechanisms and effects of faecal coating by a water scavenger beetle, *Coelostoma stultum* (Coleopterea: Hydrophilidae). *Sci. Nat.* **2023**, *110*, 29. [CrossRef]
18. Li, T.H.; Wang, X.; Desneux, N.; Wang, S.; Zang, L.S. Egg coverings in insects: Ecological adaptation to abiotic and biotic selective pressures. *Biol. Rev. Camb. Philos. Soc.* **2025**, *100*, 99–112. [CrossRef]
19. Jacobs Chris, G.C.; Rezende Gustavo, L.; Lamers Gerda, E.M.; van der Zee, M. The extraembryonic serosa protects the insect egg against desiccation. *Proc. Biol. Sci.* **2013**, *280*, 20131082. [CrossRef] [PubMed]
20. Vargas, H.C.; Farnesi, L.C.; Martins, A.J.; Valle, D.; Rezende, G.L. Serosal cuticle formation and distinct degrees of desiccation resistance in embryos of the mosquito vectors *Aedes aegypti*, *Anopheles aquasalis* and *Culex quinquefasciatus*. *J. Insect Physiol.* **2014**, *62*, 54–60. [CrossRef]
21. Farnesi, L.C.; Vargas, H.C.M.; Valle, D.; Rezende, G.L. Darker eggs of mosquitoes resist more to dry conditions: Melanin enhances serosal cuticle contribution in egg resistance to desiccation in *Aedes*, *Anopheles* and *Culex* vectors. *PLoS Negl. Trop. Dis.* **2017**, *11*, e0006063. [CrossRef]
22. Fischer, S.; De Majo, M.S.; Di Battista, C.; Campos, R.E. Effects of temperature and humidity on the survival and hatching response of diapausing and non-diapausing *Aedes aegypti* eggs. *J. Insect Physiol.* **2025**, *161*, 104726. [CrossRef]
23. Xie, S.; Shen, B.; Zhang, C.; Huang, X.; Zhang, Y. sgRNAcas9: A software package for designing CRISPR sgRNA and evaluating potential off-target cleavage sites. *PLoS ONE* **2014**, *9*, e100448. [CrossRef]
24. Jin, M.H.; Xiao, Y.T.; Cheng, Y.; Hu, J.; Xue, C.B.; Wu, K.M. Chromosomal deletions mediated by CRISPR/Cas9 in *Helicoverpa armigera*. *Insect Sci.* **2019**, *26*, 1029–1036. [CrossRef]
25. Winston, P.W.; Bates, D.H. Saturated solutions for the control of humidity in biological research. *Ecology* **1960**, *41*, 232–237. [CrossRef]
26. Fatouros, N.; Cusumano, A.; Bin, F.; Polaszek, A.; Van Lenteren, J. How to escape from insect egg parasitoids: A review of potential factors explaining parasitoid absence across the Insecta. *Proc. R. Soc. B* **2020**, *287*, 20200344. [CrossRef]
27. Gillott, C. *Entomology*, 3rd ed.; Springer: Dordrecht, The Netherlands, 2005.
28. Hans, K.R.; VanLaerhoven, S.L. Effects of relative humidity on egg hatching success of blow flies (Diptera: Calliphoridae). *Can. Soc. Forensic Sci.* **2024**, *57*, 215–223. [CrossRef]
29. Mitchaothai, J.; Lertpatarakomol, R.; Trairatapiwan, T.; Lukkananukool, A. Influence of Incubation Temperature and Relative Humidity on the Egg Hatchability Pattern of Two-Spotted (*Gryllus bimaculatus*) and House (*Acheta domesticus*) Crickets. *Animals* **2024**, *14*, 2176. [CrossRef]
30. Tang, J.; Cheng, Y.; Sappington, T.W.; Jiang, X.; Zhang, L.; Luo, L. Egg Hatch and Survival and Development of Beet Webworm (Lepidoptera: Crambidae) Larvae at Different Combinations of Temperature and Relative Humidity. *J. Econ. Entomol.* **2016**, *109*, 1603–1611. [CrossRef]
31. Wiggleswort, V.B. *The Principles of Insect Physiology*, 7th ed.; Chapman and Hall: London, UK, 1972.
32. Levi-Mourao, A.; Madeira, F.; Meseguer, R.; García, A.; Pons, X. Effects of Temperature and Relative Humidity on the Embryonic Development of *Hypera postica* Gyllenhal (Col.: Curculionidae). *Insects* **2021**, *12*, 250. [CrossRef]
33. Fisher, J.J.; Rijal, J.P.; Zalom, F.G. Temperature and humidity interact to influence brown marmorated stink bug (Hemiptera: Pentatomidae), survival. *Environ. Entomol.* **2021**, *50*, 390–398. [CrossRef] [PubMed]
34. Ofuya, T.I.; Reichmuth, C. Effect of relative humidity on the susceptibility of *Callosobruchus maculatus* (Fabricius) (Coleoptera: Bruchidae) to two modified atmospheres. *J. Stored Prod. Res.* **2001**, *38*, 139–146. [CrossRef]
35. Vargas, H.C.M.; Panfilio, K.A.; Roelofs, D.; Rezende, G.L. Increase in egg resistance to desiccation in springtails correlates with blastodermal cuticle formation: Eco-evolutionary implications for insect terrestrialization. *J. Exp. Zool. B Mol. Dev. Evol.* **2021**, *336*, 606–619. [CrossRef] [PubMed]
36. Li, M.; Bui, M.; Akbari, O.S. Embryo Microinjection and Transplantation Technique for *Nasonia vitripennis* Genome Manipulation. *J. Vis. Exp.* **2017**, *130*, 56990.
37. Salum, Y.M.; Yin, A.; Zaheer, U.; Liu, Y.; Guo, Y.; He, W. CRISPR/Cas9-Based Genome Editing of Fall Armyworm (*Spodoptera frugiperda*): Progress and Prospects. *Biomolecules* **2024**, *14*, 1074. [CrossRef] [PubMed]

Disclaimer/Publisher's Note: The statements, opinions and data contained in all publications are solely those of the individual author(s) and contributor(s) and not of MDPI and/or the editor(s). MDPI and/or the editor(s) disclaim responsibility for any injury to people or property resulting from any ideas, methods, instructions or products referred to in the content.

MDPI AG
Grosspeteranlage 5
4052 Basel
Switzerland
Tel.: +41 61 683 77 34

Insects Editorial Office
E-mail: insects@mdpi.com
www.mdpi.com/journal/insects



Disclaimer/Publisher's Note: The title and front matter of this reprint are at the discretion of the Guest Editors. The publisher is not responsible for their content or any associated concerns. The statements, opinions and data contained in all individual articles are solely those of the individual Editors and contributors and not of MDPI. MDPI disclaims responsibility for any injury to people or property resulting from any ideas, methods, instructions or products referred to in the content.





Academic Open
Access Publishing

mdpi.com

ISBN 978-3-7258-9234-1